RADAR
Systems and Components

BY

MEMBERS OF THE TECHNICAL STAFF OF
BELL TELEPHONE LABORATORIES

With an Introduction by

MERVIN J. KELLY

1949
D. VAN NOSTRAND COMPANY
TORONTO NEW YORK LONDON

Digitized by Google
Original from UNIVERSITY OF MICHIGAN
Generated on 2019-09-21 08:13 GMT / http://hdl.handle.net/2027/mdp.39015077775156
Public Domain, Google-digitized / http://www.hathitrust.org/access_use#pd-google

NEW YORK
D. Van Nostrand Company, Inc., 250 Fourth Avenue, New York 3
TORONTO
D. Van Nostrand Company (Canada), Ltd., 228 Bloor Street, Toronto
LONDON
Macmillan & Company, Ltd., St. Martin's Street, London, W.C. 2

COPYRIGHT, 1949
By
D. VAN NOSTRAND COMPANY, INC.

All Rights Reserved
This book, or any parts thereof, may not be reproduced in any form without written permission from the publishers.

PRINTED IN THE UNITED STATES OF AMERICA

Generated on 2019-09-21 08:14 GMT / http://hdl.handle.net/2027/mdp.39015077775156
Public Domain, Google-digitized / http://www.hathitrust.org/access_use#pd-google
Digitized by Google
Original from UNIVERSITY OF MICHIGAN

THE BELL TELEPHONE LABORATORIES SERIES

THEORY OF VIBRATING SYSTEMS AND SOUND. *By* IRVING B. CRANDALL.

CONTEMPORARY PHYSICS. *By* KARL K. DARROW. Second Edition.

SPEECH AND HEARING. *By* HARVEY FLETCHER.

PROBABILITY AND ITS ENGINEERING USES. *By* THORNTON C. FRY.

ELEMENTARY DIFFERENTIAL EQUATIONS. *By* THORNTON C. FRY. Second Edition.

TRANSMISSIONS CIRCUITS FOR TELEPHONIC COMMUNICATION. METHODS OF ANALYSIS AND DESIGN. *By* K. S. JOHNSON.

TRANSMISSION NETWORKS AND WAVE FILTERS. *By* T. E. SHEA.

ECONOMIC CONTROL OF QUALITY OF MANUFACTURED PRODUCT. *By* W. A. SHEWHART.

ELECTROMECHANICAL TRANSDUCERS AND WAVE FILTERS. *By* WARREN P. MASON. Second Edition.

RHOMBIC ANTENNA DESIGN. *By* A. E. HARPER.

POISSON'S EXPONENTIAL BINOMIAL LIMIT. *By* E. C. MOLINA.

ELECTROMAGNETIC WAVES. *By* S. A. SCHELKUNOFF.

NETWORK ANALYSIS AND FEEDBACK AMPLIFIER DESIGN. *By* HENDRIK W. BODE.

SERVOMECHANISMS. *By* LEROY A. MACCOLL.

QUARTZ CRYSTALS FOR ELECTRICAL CIRCUITS. *By* R. A. HEISING.

CAPACITORS—THEIR USE IN ELECTRONIC CIRCUITS. *By* M. BROTHERTON.

FOURIER INTEGRALS FOR PRACTICAL APPLICATIONS. *By* GEORGE A. CAMPBELL AND RONALD M. FOSTER.

VISIBLE SPEECH. *By* RALPH K. POTTER, GEORGE A. KOPP, AND HARRIET C. GREEN.

APPLIED MATHEMATICS FOR ENGINEERS AND SCIENTISTS. *By* S. A. SCHELKUNOFF.

EARTH CONDUCTION EFFECTS IN TRANSMISSION SYSTEMS. *By* ERLING D. SNUDE.

RADAR SYSTEMS AND COMPONENTS. *By* MEMBERS OF THE STAFF OF THE BELL TELEPHONE LABORATORIES; Introduction by M. J. KELLY.

THEORY AND DESIGN OF ELECTRON BEAMS. *By* J. R. PIERCE.

PUBLISHED BY D. VAN NOSTRAND COMPANY, INC.

Generated on 2019-09-21 08:15 GMT / http://hdl.handle.net/2027/mdp.39015077775156
Public Domain, Google-digitized / http://www.hathitrust.org/access_use#pd-google
Digitized by Google
Original from UNIVERSITY OF MICHIGAN

Foreword

ONE of the most striking phenomena of World War II was the speed, efficiency, and completeness with which the scientific resources of the United States were mobilized for the national defense. Without detracting in the slightest degree from the magnificent accomplishments of the armed services and of the country's industrial organizations, it is reasonable to believe that the technical superiority of the Allied nations may well have been the determining element in their victory.

Typical of the response of America's scientists and engineers to the nation's need was the work done in Bell Telephone Laboratories—the development organization of the Bell Telephone System and one of the nation's leading industrial laboratories. During the war years and in the period of preparedness immediately before Pearl Harbor, eighty per cent of the Bell Laboratories' manpower and equipment was assigned to the projects of the armed services. During that time the organization was approximately doubled in size, a growth which would have been exceeded had it not been for the danger of sacrificing quality in technological output.

Some 2,000 separate projects for the Army, Navy, and National Defense Research Committee were handled by the Laboratories at an expenditure of approximately $170,000,000. These projects were principally in the areas of communication, radar, sonar, the atomic bomb, battle announcing systems, mines, torpedoes, rockets, proximity fuses, and electrical gun directors. About one-half of the Laboratories' total effort was devoted to radar. Bell Laboratories shared with the Radiation Laboratory at Massachusetts Institute of Technology the responsibility for the bulk of research and development in this field in the United States.

At the war's end it was felt that the striking scientific advances achieved, particularly in the field of radar, should be recorded in detail so far as security considerations would permit and the pressure of other urgent business would allow. The papers appearing in this volume were therefore prepared and originally published in the Bell System Technical Journal. While the work described was directed towards radar development as its immediate objective, it has a broad application to the important new field of microwave transmission, and it is hoped that this book will be a useful tool for scientists and engineers working in that area.

M. J. KELLY

Generated on 2019-09-21 08:15 GMT / http://hdl.handle.net/2027/mdp.39015077775156
Public Domain, Google-digitized / http://www.hathitrust.org/access_use#pd-google
Digitized by Google
Original from UNIVERSITY OF MICHIGAN

Contents

	Page
Introduction	1

EARLY FIRE-CONTROL RADARS FOR NAVAL VESSELS

Introduction	9
Historical Background	9
Early Work	9
Application to Fire Control	10
Need for Higher Frequencies	11
Chart-Antenna Beam Width vs Aperture	12
Chart-Antenna Gain vs Aperture	12
Plate Modulation	13
First 500–700 MC Radar	13
The CXAS Radar	15
Antenna	16
Indicator and Controls	19
Transmitter-Receiver	19
Duplexing	19
Tuning Range	24
Advantage of Higher Frequency for Surface Targets	25
Table I—Characteristics of CXAS Radar	25
Performance of CXAS Radar	25
The Mark 1 Radar	26
The Mark 2 Radar	26
Coordination of Radar and Optics	27
The Mark 3 Radar	27
Indicators	28
Tracking Meters	28
Antennas	30
Antenna Lobe Switching	31
Table II—Antenna Characteristics of Radars Mark 3 and Mark 4	38
Accurate Range Measurement	39
Phase Shifters	39
The Two-speed Principle for Increased Accuracy	39
Range Indicator Presentation	39
Detailed Operating Principles	40
Transmitter	
The Multicavity Magnetron	43
Duplexing	
The TR Tube and TR Box	45
Receiver	46
Noise Figure	46
The "Lighthouse" Tube	46
Automatic Gain Control	46
The Mark 4 Radar	48
Two-plane Lobe Switching	48
First Demonstration of Three-coordinate Radar using Single Antenna	49
Application and Use of Mark 3 and Mark 4 Radars	52

THE MAGNETRON AS A GENERATOR OF CENTIMETER WAVES

Introduction	56
PART I—THE MAGNETRON OSCILLATOR	
1. General Description	58
1.1 Description	58

Digitized by Google
Original from UNIVERSITY OF MICHIGAN
Generated on 2019-09-21 08:15 GMT / http://hdl.handle.net/2027/mdp.39015077775156
Public Domain, Google-digitized / http://www.hathitrust.org/access_use#pd-google

Page

1.2 Analogy to Other Oscillators 59
1.3 Use of Equivalent Circuits 61
1.4 Electron Motions in Electric and Magnetic Fields 62
2. Types of Magnetron Oscillators 66
2.1 Definitions 66
2.2 The Negative Resistance Magnetron Oscillator—Type I 67
2.3 The Cyclotron Frequency Magnetron Oscillator—Type II 68
2.4 The Traveling Wave Magnetron Oscillator—Type III 70
3. The Electronic Mechanism 71
3.1 Electronic Interaction at Anode Gaps 71
3.2 The Interaction Field 77
3.3 The Traveling Wave Picture 78
3.4 Phase Focusing 81
3.5 Space Charge Configuration 82
3.6 Induction by the Space Charge Cloud 83
4. Conditions Relating Measurable Parameters 85
4.1 Necessary Conditions for Oscillation 85
4.2 The Performance Chart 87
4.3 The Electronic Efficiency 89
4.4 Scaling 91
4.5 Effect of Other Components in the Interaction Field 92
5. The RF Circuit of the Magnetron Oscillator 94
5.1 General Considerations 94
5.2 Simple Single Frequency Resonator 94
5.3 The Q Parameters 95
5.4 Energy Storage and Loss 96
5.5 Resonators with Distributed Constants 98
6. Resonator Systems 100
6.1 Two Coupled Resonators 100
6.2 The Multicavity Anode Structure 102
6.3 The Modes of the Resonator System 103
6.4 Higher Order Modes 109
7. Separation of Mode Frequencies 110
7.1 Necessity and Means 110
7.2 Strapping of the Resonator System 111
7.3 Asymmetries in Strapping 115
7.4 The "Rising Sun" Resonator System 116
8. Output Cirsuit and Load 121
8.1 Output Circuit 121
8.2 Load 123
9. Equivalent Circuit Theory 124
9.1 The Equivalent Circuit 124
9.2 The Rieke Diagram 127
9.3 Magnetron Circuit 128
9.4 Pulling Figure 132
10. Special Topics 134
10.1 Frequency Stabilization 134
10.2 Frequency Sensitive Loads 134
10.3 Magnetron Tuning 137
10.4 Electronic Effects on Frequency 140
10.5 Frequency Spectrum of a Pulsed Magnetron 141
10.6 Oscillation Buildup—Starting 142
10.7 Magnetron Cathodes 145
10.8 The Magnetic Circuit 148
10.9 Magnetron Measurements 148

PART II—DEVELOPMENTAL WORK ON THE MAGNETRON OSCILLATOR AT THE BELL TELEPHONE LABORATORIES, 1940–1945

11. General Remarks 153
12. Reproduction of the British Magnetron 159
13. Magnetrons for Wavelengths of 20 to 45 Centimeters 160
13.1 The 700 A-C Magnetrons 160
Table I. Magnetrons for Wavelengths of 20 to 45 Centimeters 163

Generated on 2019-09-21 08:15 GMT / http://hdl.handle.net/2027/mdp.39015077775156
Public Domain, Google-digitized / http://www.hathitrust.org/access_use#pd-google
Digitized by Google
Original from UNIVERSITY OF MICHIGAN

Page
13.2 The 728 A-J Magnetrons ... 165
13.3 The SJ23 Magnetron ... 168
13.4 The 4J21-30 Magnetrons ... 169
14. Tunable Magnetrons for Wavelengths of 20 to 45 Centimeters ... 174
14.1 General ... 174
14.2 The 4J42 Magnetron ... 176
14.3 The 4J51 Magnetron ... 177
14.4 The 5J26 Magnetron ... 178
15. Magnetrons for Wavelengths Near 10 Centimeters—Under 200 Kilowatts ... 184
15.1 The 706A-C and 714A Magnetrons ... 184
15.2 The 706AY-GY, 714AY, and 718AY-EY Magnetrons ... 187
Table II. Magnetrons for Wavelengths near 10 Centimeters ... 188
16. Magnetrons for Wavelengths Near 10 Centimeters—200 Kilowatts to 1 Megawatt ... 191
16.1 The 720 A-E Magnetrons ... 191
16.2 The 4J45-47 Magnetrons ... 196
17. Magnetrons for Wavelengths Near 3 Centimeters—Under 100 Kilowatts ... 196
17.1 The 725A and 730A Magnetrons ... 196
Table III. Magnetrons for Wavelengths near 3 Centimeters ... 202
17.2 The 2J48, 2J49, 2J50, and 2J53/725A Magnetrons ... 206
17.3 The 2J55 and 2J56 Magnetrons ... 207
18. Tunable Magnetrons for Wavelengths Near 3 Centimeters ... 208
18.1 The 2J51 Magnetron ... 208
19. Magnetrons for Wavelengths Near 3 Centimeters—100 to 300 Kilowatts ... 213
19.1 The 4J50, 4J52, and 4J78 Magnetrons ... 213
20. Magnetrons for Wavelengths Near 1 Centimeter ... 221
20.1 Preliminary Work ... 221
20.2 The 3J21 Magnetron ... 223
Table IV. The 3J21 Packaged Magnetron at 1.25 Centimeters ... 229
21. Magnetron Cathodes ... 231
22. Acknowledgments ... 236

HIGH-VACUUM OXIDE-CATHODE PULSE MODULATOR TUBES

Introduction ... 238
Tube Requirements ... 238
Design Considerations ... 239
The 701A Vacuum Tube ... 241
Table of Ratings of Tubes ... 244
The 715A Tube ... 244
The 715B Tube ... 249
The 5D21 Tube ... 250
The 426XQ Tube ... 253
The Chief Problems ... 254

COIL PULSERS FOR RADAR

History of Development ... 257
Non-Linear Coil Structures ... 258
Low-Level Pulser ... 259
Power Pulser ... 261
Operating Principles ... 261
Load Circuit ... 264
Magnetic Bias ... 265
Transformer Coupling ... 265
Pulse Shaping ... 266
Pulser Box ... 268
Acknowledgment ... 269

SPARK GAP SWITCHES FOR RADAR

Introduction ... 270
I. Rotary Spark Gap Switches for Low-Voltage Circuits ... 271

Generated on 2019-09-21 08:16 GMT / http://hdl.handle.net/2027/mdp.39015077775156
Public Domain, Google-digitized / http://www.hathitrust.org/access_use#pd-google
Digitized by Google
Original from UNIVERSITY OF MICHIGAN

Page

II. Fixed Gaps ... 275
(a) Triggering Gaps in Series ... 276
(b) The Hydrogen-Argon Aluminum Cathode Gap ... 279
(c) The Mercury Cathode Gap ... 287
(d) Starting and Operating Characteristics ... 290
(e) Dissipation and Switching Efficiency ... 298
(f) Development of Fixed Gaps for Manufacture ... 301
(g) Evaluation of the Fixed Gap as a Modulator Switch, *with table giving ratings* of W. E. Fixed Spark Gap Tubes ... 308

THE GAS-DISCHARGE TRANSMIT-RECEIVE SWITCH

Introduction ... 310
Requirements ... 310
Historical Background of TR Boxes ... 310
Method of operation ... 315
TR Boxes ... 315
The ATR ... 318
TR Box Performance ... 323
Receiver Protection ... 324
The Spike ... 325
The Flat ... 329
Direct Coupling ... 331
Receiver Self Protection ... 332
Leakage Power Measurement ... 333
High Level Loss ... 333
Recovery Time ... 333
Low Level Loss ... 337
The ATR Low Level Loss Component ... 340
TR Box Design Considerations ... 343
The Tube Design ... 345
Manufacturing and Testing ... 349
Acknowledgements ... 352
Appendix A: Analysis of the Idealized TR Box ... 353
The Low Level Transmission ... 355
High Level Operation ... 356
The Derived "g" Parameters ... 357
Off Resonance Analysis ... 357
Tabulation of Related Equations—Table I ... 358
Appendix B: Experimental Determinations of "g" Parameters of Windows ... 359
Appendix C: The ATR Box ... 360
Appendix D: The Analysis of Leakage Power Data ... 363

THE RADAR RECEIVER

Introduction ... 364
1. Radar Receiver Design Considerations ... 365
1.1 The Military Radar System ... 365
1.2 The Function of the Radar Receiver ... 366
1.21 Characteristics of the Radar Receiver Input Signal ... 368
1.22 Character of the Output of a Radar Receiver ... 371
1.3 Composition of the Radar Receiver ... 373
2. Radar Receiver Component Design ... 376
2.1 The Radar Receiver Input Circuit ... 376
2.11 Input Signal Characteristics ... 377
2.12 Input Circuit Noise Considerations ... 377
2.13 1000-Mc Radio-Frequency Amplifier Design ... 379
2.14 The Radar Converter ... 382
2.15 The Radar Receiver Beat Oscillator ... 391
2.16 Typical Radar Input Circuit Designs ... 395
2.2 The Radar Intermediate Frequency Amplifier ... 401
2.21 IF Amplifier Requirements ... 401
Band Width ... 401

Digitized by Google
Original from UNIVERSITY OF MICHIGAN
Generated on 2019-09-21 08:16 GMT / http://hdl.handle.net/2027/mdp.39015077775156
Public Domain, Google-digitized / http://www.hathitrust.org/access_use#pd-google

Page

Gain Characteristics ... 403
Intermediate Midband Frequency ... 404
The Second Detector ... 405
2.22 IF Amplifier Input Circuit Design ... 405
Table I—Principal Characteristics of IF Amplifier Tubes ... 408
2.23 Interstage Circuit Design ... 409
Table II—Interstage Band Width and Over-all Gain of Multistage IF Amplifiers ... 411
2.24 Second Detector Design ... 413
2.25 Typical Component Designs ... 413
2.3 The Radar Video Amplifier ... 419
2.31 Gain-Frequency Considerations ... 419
2.32 Gain-Amplitude Considerations ... 421
2.33 D-C Restoration Methods ... 423
2.34 Typical Radar Receiver Video Amplifier Circuits ... 425
2.4 The Radar Indicator ... 427
2.41 Classification of Radar Display Types ... 427
2.42 The Cathode-Ray Tube ... 432
Electrostatic Deflection Type ... 433
Magnetic Deflection Type ... 434
Characteristics of the Fluorescent Screen ... 435
2.43 Typical Radar Indicator Component Designs ... 437
2.5 The Radar Sweep Circuit ... 443
2.51 Function ... 443
2.52 The Timing Wave Form Generator ... 446
The Multivibrator ... 446
Typical Timing Wave Circuits ... 449
2.53 The Sweep Wave Form Generator ... 451
2.54 The Sweep Amplifier ... 454
2.6 Circuits for Radar Range and Bearing Measurement ... 459
2.61 Electronic Bearing Marker Circuits ... 460
2.62 Range Marker Circuits ... 462
Fixed Range Markers ... 462
Variable Range Marker Circuits ... 463
2.7 Automatic Frequency Control and Automatic Gain Control ... 470
2.71 Automatic Frequency Control ... 470
Function and Requirements ... 472
AFC Circuit Design Considerations ... 474
Typical AFC Circuit Designs ... 475
2.72 Automatic Gain Control ... 479
2.8 Radar Receiver Power Supplies ... 480
2.81 Primary Power Sources ... 480
2.82 Low Voltage Power Supplies ... 481
2.83 High Voltage Power Supplies ... 484
Conclusion ... 486

REFLEX OSCILLATORS

Symbols ... 488
I. Introduction ... 491
II. Electronic Admittance—Simple Theory ... 495
III. Power Production for Drift Angle of $(n + \frac{3}{4})$ Cycles ... 498
IV. Effect of Approximations ... 507
V. Special Drift Fields ... 508
VI. Electronic Gap Loading ... 510
VII. Electronic Tuning—Arbitrary Drift Angle ... 512
VIII. Hysteresis ... 521
IX. Effect of Load ... 540
A. Fixed Loads ... 541
B. Frequency Sensitive Loads—Long Line Effect ... 551
C. Effect of Short Mismatched Lines on Electronic Tuning ... 559
X. Variation of Power and Electronic Tuning with Frequency ... 565
XI. Noise Sidebands ... 570

Digitized by Google
Original from UNIVERSITY OF MICHIGAN
Generated on 2019-09-21 08:17 GMT / http://hdl.handle.net/2027/mdp.39015077775156
Public Domain, Google-digitized / http://www.hathitrust.org/access_use#pd-google

Page

XII. Build-up of Oscillation ... 573
XIII. Reflex Oscillator Development at the Bell Telephone Laboratories ... 578
A. Discussion of the Beating Oscillator Problem ... 578
B. A Reflex Oscillator with an External Resonator—The 707 ... 581
C. A Reflex Oscillator with an Integral Cavity—The 723 ... 586
D. A Reflex Oscillator Designed to Eliminate Hysteresis—The 2K29 ... 591
E. Broad Band Oscillators—The 2K25 ... 598
F. Thermally Tuned Reflex Oscillators—The 2K45 ... 605
G. An Oscillator with Wave-Guide Output—The 2K50 ... 625
H. A Millimeter-Range Oscillator—The 1464XQ ... 631
I. Oscillators for Pulsed Applications—The 2K23 and 2K54 ... 635
J. Scope of Development at the Bell Telephone Laboratories ... 648

APPENDICES

I. Resonators ... 650
II. Modulation Coefficient ... 657
III. Approximate Treatment of Bunching ... 667
IV. Drift Angle as a Function of Frequency and Voltage ... 671
V. Electronic Admittance—Non-simple Theory ... 672
VI. General Potential Variation in the Drift Space ... 684
VII. Ideal Drift Field ... 688
VIII. Electronic Gap Loading ... 691
IX. Losses in Grids ... 701
X. Starting of Pulsed Reflex Oscillators ... 702
XI. Thermal Tuning ... 705
Acknowledgments ... 708

DEVELOPMENT OF SILICON CRYSTAL RECTIFIERS FOR MICROWAVE RADAR RECEIVERS

Introduction ... 710
Definition of Crystal Rectifier ... 710
Organizations engaged in Military Research on Crystal Rectifiers ... 710
Role of Crystal Rectifiers in Early Microwave Research ... 711
Early Experimental Types of Crystal Rectifiers ... 711
Rectifier Inserts and Contact Points ... 713
Mounting Block for Use with Inserts ... 714
Development of Ceramic Cartridge Structure ... 716
History of Ceramic Cartridge ... 717
Steps in Preparation of Ceramic Cartridge ... 718
Adjustment of Crystal Rectifiers ... 719
Impregnating Compounds for Crystal Rectifiers ... 720
Shelf Aging of Crystal Rectifiers ... 721
Development of Shielded Rectifier Structure ... 722
Design Advantages of Shielded Rectifier Structure ... 722
Types, Applications, and Operating Characteristics of Crystal Rectifiers ... 724
Standard RMA Codes ... 725
Performance Factors When Used in Converters ... 726
Converter for Crystal Rectifiers ... 727
Operating Characteristics as Converters ... 727
Factors Determining Impedance of Converter Using Crystal Rectifiers ... 728
Power Handling Ability of Crystal Rectifiers ... 729
Direct Current Characteristics of Crystal Rectifiers ... 731
Processes for Preparing Crystal Rectifiers ... 731
Extent of Manufacture and Utilization of Crystal Rectifiers ... 739

CHARACTERISTICS OF VACUUM TUBES FOR RADAR IF AMPLIFIERS

1. Introduction ... 740
2. Amplification and Bandwidth ... 743
Table I—Characteristics of IF Amplifier Tubes ... 745
3. Input Conductance ... 750
4. Noise ... 752

Digitized by Google
Original from UNIVERSITY OF MICHIGAN
Generated on 2019-09-21 08:17 GMT / http://hdl.handle.net/2027/mdp.39015077775156
Public Domain, Google-digitized / http://www.hathitrust.org/access_use#pd-google

Page
5. Description of the Design of the W.E. 6AK5 Tube ... 756
5.1 Mechanical Description ... 756
5.2 Low Frequency Electrical Characteristics ... 759
5.3 Fixed Tuning ... 760
Table II—Characteristics and Ratings of the Type 6AK5 Vacuum Tube ... 761
6. Conclusion ... 761

RADAR ANTENNAS

Introduction ... 763
Part I—Electrical Principles ... 767
1. General ... 767
2. Transmission Principles ... 769
2.1 Gain and Effective Area of an Antenna ... 769
Definition of Gain ... 769
Definition of Effective Area ... 769
2.2 Relationship between Gain and Effective Area ... 770
2.3 The Ratio G/A for a Small Current Element ... 770
2.4 The General Transmission Formula ... 773
2.5 The Reradiation Formula ... 773
2.6 The Plane, Linearly Polarized Electromagnetic Wave ... 774
3. Wave Front Analysis ... 775
3.1 The Huygens Source ... 776
3.2 Gain and Effective Area of an Ideal Antenna ... 778
3.3 Gain and Effective Area of an Antenna with Aperture in a Plane and with Arbitrary Phase and Amplitude ... 779
3.4 The Significance of the Pattern of a Radar Antenna ... 780
3.5 Pattern in Terms of Antenna Wave Front ... 781
3.6 Pattern of an Ideal Rectangular Antenna ... 782
3.7 Effect on Pattern of Amplitude Taper ... 783
3.8 Effect on Pattern of Linear Phase Variation ... 784
3.9 Effect on Pattern of Square Law Phase Variation ... 785
3.10 Effect on Pattern of Cubic Phase Variation ... 787
3.11 Two General Methods ... 788
3.12 Arrays ... 789
3.13 Limitations to Wave Front Theory ... 789
4. Application of General Principles ... 790
Part II—Methods of Antenna Construction ... 790
5. General ... 790
6. Classification of Methods ... 791
7. Basic Design Formulation ... 793
7.1 Dimensions of the Aperture ... 793
7.2 Amplitude Distribution ... 794
7.3 Phase Control ... 794
8. Parabolic Antennas ... 794
8.1 Control of Phase ... 794
8.2 Control of Amplitude ... 796
8.3 Choice of Configuration ... 797
8.4 Feeds for Paraboloids ... 801
8.5 Parabolic Cylinders between Parallel Plates ... 803
8.6 Line Sources for Parabolic Cylinders ... 805
8.7 Tolerances in Parabolic Antennas ... 807
9. Metal Plate Lenses ... 809
9.1 Lens Antenna Configurations ... 812
9.2 Tolerances in Metal Plate Lenses ... 812
9.3 Advantages of Metal Plate Lenses ... 813
10. Cosecant Antennas ... 813
10.1 Cosecant Antennas based on the Paraboloid ... 814
10.2 Cylindrical Cosecant Antennas ... 817
11. Lobing ... 817
11.1 Lobe Switching ... 818
11.2 Conical Lobing ... 819
12. Rapid Scanning ... 819

Digitized by Google
Original from UNIVERSITY OF MICHIGAN
Generated on 2019-09-21 08:17 GMT / http://hdl.handle.net/2027/mdp.39015077775156
Public Domain, Google-digitized / http://www.hathitrust.org/access_use#pd-google

Page

12.1 Mechanical Scanning ... 820
12.2 Array Scanning ... 821
12.3 Optical Scanning ... 825
Part III—Military Radar Antennas Developed by the Bell Laboratories ... 827
13. General ... 827
14. Naval Shipborne Radar Antennas ... 829
14.1 The SE Antenna ... 829
14.2 The SL Antenna ... 829
14.3 The SJ Submarine Radar Antenna ... 834
14.4 The Modified SJ/Mark 27 Radar Antenna ... 837
14.5 The SH and Mark 16 Radar Antennas ... 837
14.6 Antennas for Early Fire-Control Radars ... 840
14.7 A Shipborne Anti-Aircraft Fire-Control Antenna ... 841
14.8 The Polyrod Fire-Control Antenna ... 843
14.9 The Rocking-Horse Fire-Control Antenna ... 844
14.10 The Mark 19 Radar Antenna ... 845
14.11 The Mark 28 Radar Antenna ... 848
14.12 A 3-cm Anti-Aircraft Radar Antenna ... 850
15. Land Based Radar Antennas ... 850
15.1 The SCR-545 Radar "Search" and "Track" Antennas ... 850
15.2 The AN/TPS-1A Portable Search Antenna ... 852
16. Airborne Radar Antennas ... 855
16.1 The AN/APS-4 Antenna ... 855
16.2 The SCR-520, SCR-717 and SCR-720 Antennas ... 856
16.3 The AN/APQ-7 Radar Bombsight Antenna ... 858

TECHNIQUES AND FACILITIES FOR MICROWAVE RADAR TESTING

Introduction ... 861
Requirements ... 862
Operation of Typical Radar ... 862
Types of Tests and Test Sets ... 862
Generality of Application ... 863
Broadbanding ... 865
Precision ... 865
Packaging—Size and Weight ... 865
Environmental Influences ... 865
Simplicity, Reliability, Accessibility ... 866
Ruggedness ... 866
Range Capability ... 867
Signal Generators ... 869
Types of Signals ... 869
Receiver Sensitivity ... 870
RF Oscillators ... 871
Some Design Principles ... 871
A Pulsed and FM Signal Generator ... 873
Signal Generator Designs ... 875
Frequency Measurement ... 875
Coaxial Wavemeters ... 877
Cylindrical Cavity Wavemeters ... 877
Linearity ... 878
Frequency Coverage ... 879
Guideposts ... 879
Couplings ... 879
Types of Detectors ... 879
Methods of Use ... 880
Drive and Scale ... 880
Effect of Temperature and Humidity ... 881
Calibration ... 881
Power Measurement ... 881
Measurement of Pulse Power ... 881
Thermistor Power Meters ... 882
Water Loads ... 883
Echo Boxes ... 883

Digitized by Google
Original from UNIVERSITY OF MICHIGAN
Generated on 2019-09-21 08:17 GMT / http://hdl.handle.net/2027/mdp.39015077775156
Public Domain, Google-digitized / http://www.hathitrust.org/access_use#pd-google

Page
Types and Uses ... 884
Q and Ring Time ... 888
Spectrum Analysis ... 888
Standing Wave Measurements ... 889
Theory ... 889
Devices ... 890
Directional Couplers ... 894
Auxiliaries and Components ... 899
RF Loads ... 899
Microwave Attenuators and Pads ... 899
RF Cables and Connectors ... 902
Oscilloscopes ... 902
Range Calibration ... 905
Computer Test Sets, etc. ... 907
Conclusion ... 907

HIGH Q RESONANT CAVITIES FOR MICROWAVE TESTING

Introduction ... 909
Definitions and Fundamental Formulas ... 910
Modes ... 910
The MS Factor ... 910
Fundamental Formulas ... 911
The Mode Chart ... 912
Choice of Operating Mode ... 914
Extraneous or Unwanted Modes ... 914
Methods of Minimizing Effects of Unwanted Modes ... 918
Cavity Couplings ... 920
Principle of Similitude ... 922
Application of Theory ... 922
Design Requirements ... 922
Determining the Theoretical Q Required ... 922
Finding the Cavity Dimensions ... 923
Selection of Operating Area on Mode Chart ... 924
Some Practical Considerations ... 926
Description of Echo Box Test Sets ... 926
End Plate Gaps ... 929
Back Cavity Effects ... 931
Cylinder Tolerances ... 931
Plating ... 932
Couplings ... 932
Drive Mechanism ... 932
Application of Similitude ... 933
Use of Cavities for Radar Testing ... 933
Uniformity Control and Expected Ringtime ... 934
Other Uses ... 934
Bibliography ... 935
Tables
1—Formulas for Cavity Resonators—Fields, Resonant Frequencies and Mode Shape Factors for Rectangular Prism, Circular Cylinder and Full Coaxial Facing page 911
2—Constants for Use in Computing the Resonant Frequencies of Circular Cylinders ... 913
3—Values of the Bessel Function Zero (r_{1_m}) for the First 180 Modes in a Circular Cylinder Resonator ... 919
4—Orifice Coupling of Wave Guide (*TE* 10 Mode) to Cylindrical Cavity (*TE* 0*mn* Mode) ... 921

END PLATE AND SIDE WALL CURRENTS IN CIRCULAR CYLINDER CAVITY RESONATOR

Introduction ... 936
End Plate:
Contour Lines ... 938

Digitized by Google
Original from UNIVERSITY OF MICHIGAN
Generated on 2019-09-21 08:18 GMT / http://hdl.handle.net/2027/mdp.39015077775156
Public Domain, Google-digitized / http://www.hathitrust.org/access_use#pd-google

Page
Current Streamlines ... 939
Current Distributions ... 940
Side Wall: Contour and Streamlines ... 941
Fig. 2—Plate Showing Side Wall Currents ... Facing page 943
Figs. 19 to 50—Plates Showing End Plate Currents ... 952 to 974
Integration of $\int_0^x J_l(x)/J_l'(x)\,dx$ ... 975
Tables of Above Integral ... 978 to 980
Tables of Bessel Functions $J_l(x)$ and $J_l'(x)$ ... 981 to 984

SOME RESULTS ON CYLINDRICAL CAVITY RESONATORS

Fig. 1—Formulas for Cavity Resonators ... 985
Approximation Formula for Number of Resonances in a Circular Cylinder ... 986
Minimum Volume of Circular Cylinder for Assigned Q ... 988
Limitation on Frequency Range of Tunable Cavity ... 995
The Elliptic Cylinder ... 998
Resonant Frequencies ... 1001
Table II—Fields ... 1002
Table III—Root Values of Radial Elliptic Cylinder Functions ... 1003
Resonator Q ... 1004
Full Cylindrical Coaxial Resonator ... 1006
Fins in a Cavity Resonator ... 1013
Bibliography ... 1017

Generated on 2019-09-21 08:18 GMT / http://hdl.handle.net/2027/mdp.39015077775156
Public Domain, Google-digitized / http://www.hathitrust.org/access_use#pd-google
Digitized by Google
Original from UNIVERSITY OF MICHIGAN

Introduction

By MERVIN J. KELLY

RADAR—RAdio Detection And Ranging—in the importance of its contribution to victory ranks high among the new weapons of World War II. It employs radio waves for the detection and accurate location of objects, fixed or moving. It can see farther than the eye, even under conditions most favorable to vision. It sees equally well by night and by day. Neither smoke, fog, clouds, nor rain diminishes its range or its resolution of objects. It can do more than see, however; it can also measure distance and angles. It continuously measures the distance to a fixed or moving object and the angles defining the direction of the object with such exactness that the information can be used to control the firing of guns, the directing of torpedoes, or the dropping of bombs.

Radar refers to no single instrument: it is a synthetic word which describes a function. Indeed, an individual radar set may weigh only a hundred pounds, have the size and shape of a small bomb, and be suited to installation in a fast airplane; or it may be a vast assemblage of equipment mounted in a truck and several trailers, have a giant antenna structure, and require a whole company of soldiers to operate it. It may be a three-ton equipment disposed above and below the deck of a battleship, or it may be two or three water-tight boxes on the deck and a small antenna on the mast of a landing barge. Although radars assume this great variety of form and size, they are all governed by the same basic principles and employ the same electronic and communication techniques. Their functioning elements have electron tubes in large number and great variety, interconnected by most complex communication-like circuits.

All radars embody a transmitter, an antenna, a receiver, and a video system. The transmitter generates the radio energy as pulses of suitable form and power. These are of the order of one microsecond in length, and are spaced uniformly in time, recurring at rates of several hundred a second. A single antenna usually serves both as a radiator of transmitted power and a receiver of energy returned, or "echoed," from the objects viewed. The pulses of power from the transmitter are fed to the antenna by a suitably terminated conductor, and the configuration of the antenna determines the form of the beam radiated. It assumes a pencil or vertical fan shape, for example, depending on the function of the particular system. The receiver accepts from the antenna the returning pulses, and amplifies and reshapes them in such a way that the video system can display the echo information in a variety of visible patterns, and supply it in electrical form for the direction of missiles.

Digitized by Google
Original from UNIVERSITY OF MICHIGAN
Generated on 2019-09-21 08:20 GMT / http://hdl.handle.net/2027/mdp.39015077775156
Public Domain, Google-digitized / http://www.hathitrust.org/access_use#pd-google

In consequence of its ability to see, radar played a great and increasingly important role in the conduct of the war on land, at sea, and in the air. It brought about profound changes in the pattern of warfare. Surprise has always been one of the most important elements in attack. In the past, it has been achieved by the deployment of forces in the darkness of night or under a covering of fog, cloud, or smoke. The early warning of enemy approach afforded by our ever-improving radar equipments and the increasingly effective techniques for their use deprived the enemy of the advantage of surprise attacks.

A new instrument of war, when properly applied by the combatants, changes the style of war but is not likely to become a decisive element in victory for either side. When one of the combatants moves more rapidly in developing the new instrument, however, and makes broader and more rapid use of it in his strategy of war, he then can make it an important and perhaps determining element in his victory. This is the pattern of radar's application in World War II.

In the years immediately before the war, radar was conceived and had its pioneering development in the military laboratories of England, Germany, our own country, and perhaps Japan. At the war's beginning, the radar technologies of Germany, England, and our country were at about the same level of development, while Japan's was decidedly inferior. As the war progressed, we advanced radar science with much greater speed than did our enemies. We applied radar to almost all sectors of warfare, and supplied our armed forces with a tremendous volume of specialized equipments suited to a wide variety of applications. Our armed forces made immediate and broad application of this equipment, and modified their strategy of war to great advantage as they increased their facility in the use of this new weapon.

Our enemies, advancing the technology at a slower pace, made available to their armed forces a substantially smaller volume of equipments, which were more limited in variety and of a lower level of effectiveness. As the war progressed, therefore, radar became an instrument of increasing advantage to us. It shortened the war, and made our victory possible at a lower cost in lives and material.

This great importance to victory was attained by radar because our country concentrated on it gigantic efforts in research, development, design, and production. In 1940 less than $25,000,000 was expended on technical and production effort for radar. Radar effort in all its phases expanded rapidly through out the war, however, and in 1945 reached the level or more than $1,000,000,000 annually.

There have been many technical workers in this field both in England and in this country. They have enjoyed full interchange of technical in-

Digitized by Google
Original from UNIVERSITY OF MICHIGAN
Generated on 2019-09-21 08:21 GMT / http://hdl.handle.net/2027/mdp.39015077775156
Public Domain, Google-digitized / http://www.hathitrust.org/access_use#pd-google

formation, so that each could use the information of the other as well as his own. In particular, Bell Laboratories worked very closely first with Army and Navy laboratories and later also with the Radiation Laboratory at Massachusetts Institute of Technology. In all cases there was freest interchange of technical material.

The laboratories of the Services were working in radar through the 1930's. When, in 1940, the national defense program was materially stepped up, the National Defense Research Committee set up the Radiation Laboratory at Massachusetts Institute of Technology to undertake a broader program of Government-sponsored research than had been possible with the limited facilities of the Services' laboratories. This organization built up its research staff and facilities and carried out a most important program of research and development work, particularly in the microwave field.

The Bell System played a larger part in the radar program, from research through production, than any other industrial organization. Through its manufacturing company—the Western Electric—it produced about half of all the radar made in the United States; and through its research organization—Bell Telephone Laboratories—it carried out a comparable portion of the research and development programs. As an outgrowth of this work of the Laboratories, some 900 million dollars worth of radar equipment was produced by the Western Electric Company, and at least 100 million dollars worth by other companies.*

Although Bell Telephone Laboratories carried on the development of some one hundred radar systems of which more than sixty were standardized and produced, its only publication concerned with complete radar systems is that of W. C. Tinus and W. H. C. Higgins, "Early Fire Control Radars for Navy Vessels." Here are described the first four fire-control radars developed in this country, Marks 1–4. The Laboratories initiated the research and development work leading directly to these equipments in 1938. This paper also recounts the fine work in progress under Dr. A. Hoyt Taylor at the Naval Research Laboratory on search radars operating in the 200-megacycle range. A full consideration of the outlook for radar development led Bell Telephone Laboratories to study systems for determining the exact position of a ship or plane in terms of the distance and angle from the radar, so that accurate gun fire might follow location by search radar at night. Its studies centered in the frequency range from 500 to 700 megacycles, which was adequately high for the purpose, and as high as electronic research had succeeded in providing even the minimum needs in electronic devices.

*For a more complete statement of early radar history and radar principles of operation and military applications, see "Radar—A Report of Science at War" released by the Joint Board on Scientific Information Policy 1946.

Digitized by Google
Original from UNIVERSITY OF MICHIGAN
Generated on 2019-09-21 08:22 GMT / http://hdl.handle.net/2027/mdp.39015077775156
Public Domain, Google-digitized / http://www.hathitrust.org/access_use#pd-google

The first of the standardized equipments were installed aboard a battleship in July, 1941, and quantity production was in progress by Pearl Harbor. The Marks 3 and 4 played most important parts in the night victories of our Navy in the Pacific in 1942 and 1943. Almost 1,000 of these equipments were manufactured and installed in our fleet, and were continuously modernized as the art advanced. They proved to be so sound basically and to have such high tactical value that almost 400 were still in the fleet at V-J Day, even though one advanced design of fire-control radar followed another in rapid succession throughout the war as our knowledge grew. Many of the features that continued to be essential in radar systems made their first appearance in these pioneer fire-control radars: the gas discharge "T-R" tube employed in duplexing, the resonant-cavity magnetron, and the close spaced power tetrode for pulsing are typical.

These pioneer systems so pleased the Navy that they placed their entire ship radar fire-control program with Bell Telephone Laboratories, and this responsibility continued throughout the war. A rapid advance in the art and science of radar fire control for ships was brought about by the co-operative programs of the Bureau of Ordance and Bell Telephone Laboratories.

As the capabilities of the early radars became known, large numbers of tactical applications of greatest variety developed. Each new tactical situation presented a new group of requirements: functional and physical. If the needs of this continuously expanding variety of systems with their more exacting requirements were to be met, there must be available an ever-increasing reservoir of fundamental knowledge of the electronics, the apparatus elements, and the circuits upon which radar systems depend for the prompt development of the particular device or system best suited to the special needs of each situation. New physical, as well as new functional, requirements frequently required new electronics, apparatus, and circuits. The maximum of freedom of choice was essential to success in meeting military needs *when required*.

Long experience in telephone systems development gave Bell Telephone Laboratories an early appreciation of the best procedures to adopt in the development of radar. Basic programs of broad coverage were under way in 1940, and they were continuously expanded. The leadership of Bell Laboratories in magnetrons, reflex oscillators, pulsing systems and their components, crystal rectifiers, intermediate-frequency amplifers, "T-R" boxes, waveguide circuit elements, and antennas owes much to foresight in programming and to emphasis. Most of the papers of this volume are concerned with contributions in these areas.

In "The Magnetron as a Generator of Centimeter Waves," Fisk, Hagstrom, and Hartman deal with the most important single device in the large family of radar systems. Without the resonant-cavity magnetron, radar

Digitized by Google
Original from UNIVERSITY OF MICHIGAN
Generated on 2019-09-21 08:22 GMT / http://hdl.handle.net/2027/mdp.39015077775156
Public Domain, Google-digitized / http://www.hathitrust.org/access_use#pd-google

would not have attained technical maturity during the war and become perhaps the war's most important single contribution to victory. It is still the only source of pulsed power with peak values of tens or hundreds of kilowatts in the frequency range from 1,000 to 30,000 megacycles. Denied these power levels in this frequency range, radar would have had limited application.

Although resonant cavities in association with a magnetron diode were already in the patent literature in 1940, their application to centimeter-wave pulsed-power generation was a British development. Their early embodiment of the generator was in a form whose basic features were continued throughout the extensive elaboration of types brought about through the war developments. The Tizard Mission brought one of the first of their operating units to America in September, 1940; it operated at 3,000 megacycles. Professor R. H. Fowler, Professor J. D. Cockcroft (both later knighted in recognition of their war contributions), and Dr. E. G. Bowen made a full disclosure of this important development to members of Bell Laboratories in early October. Within a few days after their disclosure, it was operated at our Whippany radar laboratories with a peak power output of the order of 10 kilowatts. On the day of these tests it was recognized that the resonant-cavity magnetron was a complete answer to the power needs of our fire-control radars. Marks 1 and 2 had power outputs from special triodes limited to a few kilowatts. Development of 700-mega ycle magnetrons of this type was at once undertaken. Samples with outputs of tens of kilowatts were made available for systems tests by December, 1940, and production was available by mid 1941. War speeds were the order of the day, even in the year before Pearl Harbor.

An extensive and ever-expanding integrated program of research, development, and design under Dr. Fisk's able leadership began immediately following the tests at Whippany in October. Our country's whole centimeter wave radar program relied chiefly on Dr. Fisk's group for magnetron development for more than a year—until the N.D.R.C. group at the Radiation Laboratory was organized and became effective. From that time, the research and development programs were shared by these groups in a coordinated program. The Fisk, Hagstrom, and Hartman paper is a splendid presentation of the major elements of the developments of Bell Laboratories.

Many methods of generating the pulses for driving the magnetron were proposed, and developments were carried out on most of them. Bell Laboratories developed three general types, and in each of the radar systems of its development selected for use that type best suited to the engineering requirements. In the type first developed, the pulse was generated at a low power level by a non-linear coil, and then amplified to the required level by vacuum tubes. To meet the requirements of pulse amplification,

Digitized by Google
Original from UNIVERSITY OF MICHIGAN
Generated on 2019-09-21 08:22 GMT / http://hdl.handle.net/2027/mdp.39015077775156
Public Domain, Google-digitized / http://www.hathitrust.org/access_use#pd-google

special vacuum tubes were made available. Our Laboratories developed the principal ones that were standardized by the Services for general radar use, but they were produced by several manufacturers. Mr. C. E. Fay describes these tubes and their uses in "High-Vacuum Oxide Cathode Pulse Modulator Tubes."

Another approach is to employ non-linear coils of sufficient power capacity to deliver directly to the magnetron the power required for its operation. Bell Laboratories developed such coils for peak powers in the range from 100 to 1,000 kilowatts, and for pulse widths from two tenths to one microsecond, and pulsing rates from 400 to 3,600 per second. This type of pulser was best suited to the requirements of the precision radars for fire control and, except for the early systems, was generally used. Mr. E. Peterson describes these power pulse coils and their applications in "Coil Pulsers for Radar."

Another interesting means of generating these high-energy pulses of extremely short duration is the spark gap. The Laboratories first studied gaps operating in air, and developed a rotary gap in which the time of breakdown was controlled mechanically. Such gaps were successfully adapted to a variety of radar systems. Demands for light weight and small volume led to the development of fixed gaps of the sealed-unit type. To make these sealed gaps reliable and uniform in operation throughout a long life, a number of interesting physical problems had to be solved. Success was achieved, and several sealed-gap units were developed by the Laboratories and standardized by the Services for general use. These developments are described by F. S. Goucher, J. R. Haynes, W. A. Depp, and E. J. Ryder in "Spark Gap Switches for Radar."

The successful employment of a single antenna in a radar system was realized by using a gas-discharge tube to perform the function of a switch; the antenna becoming available for transmission during one portion of the time "cycle" and for reception during the other. In our country, Bell Laboratories initiated the development of gas-discharge tubes for this function. A similar solution to the single antenna was developed independently in England. A number of the tubes developed by our Laboratories were standardized for general use by the Services, and produced by a number of manufacturers. A. L. Samuel, J. W. Clark, and W. W. Mumford describe these tubes and their uses in "The Gas-Discharge Transmit-Receive Switch."

Although the receivers of all radar systems have many characteristics in common, the performance requirements of each system place demands on its receiver that make its development difficult. Mr. L. W. Morrison in "The Radar Receiver" discusses the general problems of receiver design, and considers many of those individual to particular systems.

Digitized by Google
Original from UNIVERSITY OF MICHIGAN
Generated on 2019-09-21 08:22 GMT / http://hdl.handle.net/2027/mdp.39015077775156
Public Domain, Google-digitized / http://www.hathitrust.org/access_use#pd-google

The development of three of the apparatus elements of the radar receiver is described in three separate papers. Reflex oscillators are treated in a paper by J. R. Pierce and W. G. Shepherd. The beat oscillator of substantially all radar receivers for frequencies of 1,000 megacycles and higher was the single-cavity reflex oscillator tube; for lower frequencies of the microwave range, a special triode known as the lighthouse tube was generally used. The paper gives a broad exposition of the theory of the reflex oscillator and describes a number of typical tubes developed by Bell Laboratories. These tubes were standardized for general radar use by the services, and were produced in large quantities by the Western Electric Company.

The silicon-crystal point-contact rectifier was universally used in the frequency converter or first detector in superheterodyne radar receivers operating at frequencies of 1,000 megacycles and higher. Bell Laboratories began research on these units in about 1935. Research studies on waveguide transmission at that time developed a need for frequency converters in the centimeter-wave-length range, and the silicon-crystal point-contact rectifier was the best answer to the need. With this work as a background, the Laboratories rapidly expanded its efforts on all phases of the crystal converter in 1940, when its application to radar became evident. The history of the development is told in a paper by J. H. Scaff and R. S. Ohl, "Development of Silicon Crystal Rectifiers for Microwave Radar Receivers," which gives the characteristics and uses of a number of units developed by the Laboratories. These units were standardized for general use by the Services and were produced in very large volume by Western Electric Company and other manufacturers.

Vacuum tubes for intermediate-frequency amplifiers of the radar receiver are described in a paper by G. T. Ford. The amplification of the received radar signals was done at frequencies from 30 to 60 megacycles. Vacuum tubes of highest transconductance, low capacitances, high input resistance and good noise figure are necessary. Mr. Ford tells of the development and standardization of vacuum tubes to meet this need. Our final development, the 6AK5, was the most generally used intermediate-frequency amplifying tube. Many millions of them were employed. It was made by the Western Electric Company and several other manufacturers.

H. T. Friis and W. D. Lewis tell the story of radar antenna research and development in Bell Laboratories. The difference in functions of radar systems makes the antenna development of each a different problem. The solution frequently proved to be one of the most difficult as well as most interesting tasks in the development of the complete systems. Recourse to mathematical analysis was specially helpful here, and our mathematicians were an integral part of many of the research teams.

A radar system is a most complex equipment. Typical systems have from

Generated on 2019-09-21 08:23 GMT / http://hdl.handle.net/2027/mdp.39015077775156
Public Domain, Google-digitized / http://www.hathitrust.org/access_use#pd-google
Digitized by Google
Original from UNIVERSITY OF MICHIGAN

50 to 250 vacuum tubes associated with many times that number of electrical and electro-mechanical components of great variety. Nothwithstanding most careful design and high quality manufacture, it is easy for radar performance to become impaired under operating conditions. The range of coverage may fall to a fraction of the normal, or the accuracy of measurement may decrease by a large amount with nothing in the radar's performance to indicate it. There must be test facilities at the battlefronts which make testing and adjusting possible if the radar system is to operate with its normal coverage and accuracies.

E. I. Green, H. J. Fisher, and J. G. Ferguson in their paper "Techniques and Facilities for Microwave Radar Testing" tell a most interesting story. The variety and complexity of test sets approach that of the radar systems themselves. It was a challenge to the developer and designer to implement the many precision measurements that had to be made in the battle areas with sufficiently portable and rugged equipments, each having the facilities for making the largest number possible of different kinds of tests. Bell Laboratories and the Radiation Laboratory of the N.D.R.C. in a well co-ordinated program undertook substantially all of the development of test facilities for the Services.

In three separate papers, I. G. Wilson, J. P. Kinzer, and C. W. Schramm treat different phases of the problems of high-Q resonant cavities in microwave testing. These papers give a detailed picture of the complexity of a limited sector of the radar test problem, and afford some insight into the general complexity of the test equipment.

In this introduction I have attempted to supply historical perspective and to place the papers assembled in the volume into their proper relationship to the whole program of radar research and development. Each paper attempts to give full recognition of the assistance received from and the co-operation with other organizations. Since there was almost daily informal interchange of information between members of Bell Laboratories and those of other organizations, full acknowledgement cannot be made. Radar development, like substantially all of the war developments, was a most co-operative program. Scientists and engineers from all organizations involved in a program in our country and frequently those involved in England, Canada, and on occasion Australia and New Zealand, worked as a single unit; information flowed rapidly through informal as well as formal channels. We are pleased to express our debt generally to all engaged in the radar developments of the war period.

Generated on 2019-09-21 08:23 GMT / http://hdl.handle.net/2027/mdp.39015077775156
Public Domain, Google-digitized / http://www.hathitrust.org/access_use#pd-google
Digitized by Google
Original from UNIVERSITY OF MICHIGAN

Early Fire-Control Radars for Naval Vessels

By W. C. TINUS and W. H. C. HIGGINS

Introduction

FOR a number of years before the war a very intensive development effort was under way in the Army and Navy laboratories, and in several commercial laboratories, on the application of radio methods to the location of objects at a distance. The equipment which resulted was eventually called "Radar" equipment by the Navy and this term is now almost universally used. The urgent needs of the war have resulted in the very rapid development and extensive application of this new science during the last few years.

Radar equipments of many different types have been designed to perform specific functions on land and sea, and in the air. These equipments have had an important part in the winning of the war and the recent relaxation in secrecy regulations now permits publishing some of the story. In this present article a description of the Mark 3 and 4 Fire-Control Radars for Naval Vessels will be given, together with a little of the history that preceded their development.

Historical Background

When the Bell Telephone Laboratories began active radar development work early in 1938 an effort was made to set technical objectives for this work that would avoid duplication of the intensive work then under way in the Army and Navy laboratories, and that would advance the art toward the solution of some of the recognized basic problems. The general objectives were to increase the accuracy of radar measurement of location and to increase as much as possible the operating carrier frequency. The reasons for these objectives are discussed in the following paragraphs.

The state of the art at the time under discussion has been partially described in a recent paper by Maj. Gen. R. B. Colton.[1] The work he described and directed was carried out at the Signal Corps Laboratories at Fort Monmouth, New Jersey and was directed principally toward solving

[1] "Radar in the U. S. Army" by Maj. Gen. Roger B. Colton, published in the *Proceedings of the I. R. E.*, November, 1945.

Digitized by Google
Original from UNIVERSITY OF MICHIGAN
Generated on 2019-09-21 08:26 GMT / http://hdl.handle.net/2027/mdp.39015077775156
Public Domain, Google-digitized / http://www.hathitrust.org/access_use#pd-google

the ground forces' problems of aircraft warning and searchlight control. At the same time intensive work was being pursued at the Naval Research Laboratory at Anacostia, D. C. under the direction of Dr. A. H. Taylor, Dr. R. M. Page and Mr. L. C. Young. Their work was directed primarily toward developing radar equipment that would be useful aboard ship, and it was from them and from the engineers of the Navy Department that the principal inspiration and guidance for the work described in this paper were obtained.

The first military application in which radar equipment proved its usefulness was in the detection of approaching aircraft. For this kind of application the radar is not required to locate the approaching planes with very great accuracy and the experimental radars of 1938 and 1939 performed this function in quite a useful way. The fact that the first application of radar was a strictly defensive one may account in part for the great interest and support given radar work in England and in this country, while apparently much less radar work was done before the war by the scientists of Germany and Japan. Thus, when radar later became a powerful and versatile aid to offense, the enemy nations found themselves years behind in development.

Very early in their work the men of the Naval Research Laboratory recognized the potential ability of radar to help solve the fire-control problem. Since this problem determined the design of the radar systems to be described later in this paper a brief general discussion of fire control is given here. The term *fire control* refers broadly to the means by which a gun or other weapon is aimed and fused so that, when fired, the projectile will hit or burst near the intended target. A fire-control system includes two major parts: first, a locating device for determining the present position of the target; and second, a computing device which analyzes the present position data, computes the target's course and speed, and the position the target will occupy at the future time when the projectile arrives at that point, and finally furnishes the correct aiming and fusing information to the guns. A modern fire-control system does these things in a continuous manner so the guns remain correctly aimed and can be fired at any time during the engagement.

Before the war the present position of the target was ordinarily determined by optical instruments. Operators tracked the target by controlling their telescopes in such a way that the target remained on the crosshairs in their eyepieces. Thus the azimuth and elevation angles were found. Another operator measured the range to the target with an optical range finder, or indirectly estimated range from the angular extent of the target and its estimated size.

The accuracy of this optical system in determining azimuth and elevation

Digitized by Google
Original from UNIVERSITY OF MICHIGAN
Generated on 2019-09-21 08:26 GMT / http://hdl.handle.net/2027/mdp.39015077775156
Public Domain, Google-digitized / http://www.hathitrust.org/access_use#pd-google

angles is very good provided the target can be seen clearly. This proviso is a serious limitation under many typical operating conditions. It is frequently difficult to see a target at a range of several miles on account of haze even on a relatively clear day, and at night or in fog or smoke screen the usefulness of a telescope is almost nil. The optical range finder is subject to the same limitations as the telescope and in addition leaves much to be desired in the matter of accuracy and continuity of data even under the best visibility conditions. This is due to the fact that optical range finders are triangulation devices which inherently have accuracy limitations. The need for a long and very stable base line between the prisms of an optical range finder is difficult to meet aboard ship, and the principle of operation makes inevitable a rapidly decreasing accuracy with increasing range. Thus, as the effective range of guns increased, the need for more accurate means for measuring range became more acute.

In its earliest forms radar offered at once a potential means for measuring range with much better accuracy than that of the optical range finder. This was due to the different principle on which radar works. A pulse of radio frequency energy is sent out to the target and the echo signal is received back at the source. The velocity of the waves en route is the same as that of light, and is one of the basic physical constants. To measure range accurately with radar required only the development of techniques for producing short transmitted pulses and for measuring accurately the short intervals of time between the transmitted pulse and the returning echo pulse. Both of these were the kind of problems which yield readily to electronic solutions. The early work in Bell Telephone Laboratories thus included the production of shorter transmitted pulses than were being commonly used, and the development of improved range measuring means.

The second important general objective for the early work at Bell Telephone Laboratories was to devise equipment which would operate at frequencies much higher than had been previously used. The need for higher-frequency operation arose from the fact that for a given size of antenna the beam width decreases with increasing frequency while the gain increases. Narrow beams are required to obtain accurate angular data while increased gain is desirable since it obviously provides increased range for a given transmitter power and receiver noise figure. These factors are illustrated by the curves of Figs. 1A and 1B which show the relationship between beam width, antenna gain and antenna size expressed in wavelengths. The curve labeled "uniform illumination" yields maximum gain and minimum beam width for a given antenna size but produces unwanted side lobes of undesirable amplitude. For this reason the illumination is usually graded over the antenna aperture to reduce minor lobes. The gain

Digitized by Google
Original from UNIVERSITY OF MICHIGAN
Generated on 2019-09-21 08:26 GMT / http://hdl.handle.net/2027/mdp.39015077775156
Public Domain, Google-digitized / http://www.hathitrust.org/access_use#pd-google

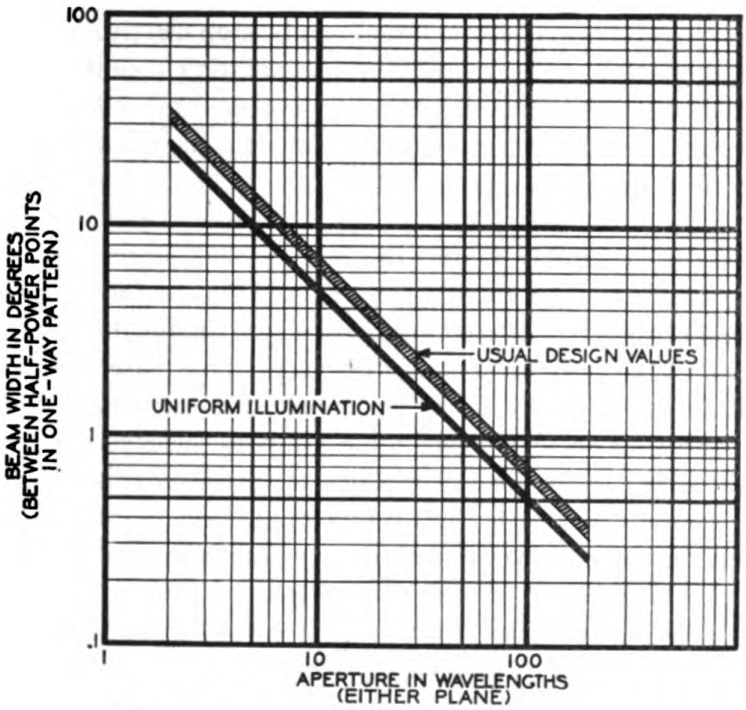

Fig. 1A—Antenna beam width vs. aperture

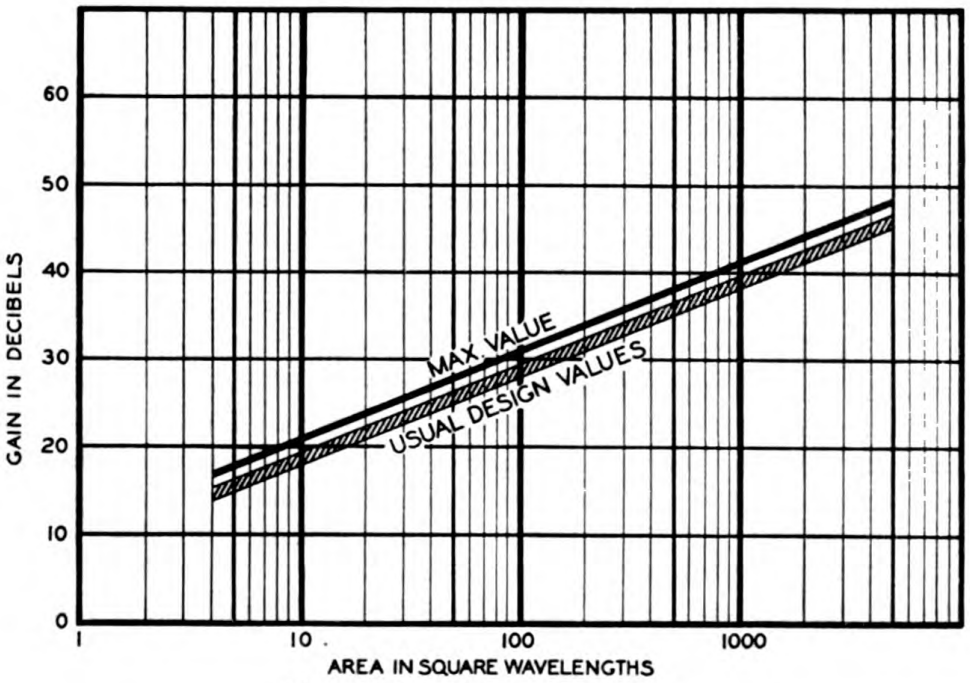

Fig. 1B—Antenna gain vs. aperture

and beam width obtained in this manner are shown by shaded area labelled *usual design values*. The need for higher frequency or shorter wavelength

Digitized by Google
Original from UNIVERSITY OF MICHIGAN
Generated on 2019-09-21 08:27 GMT / http://hdl.handle.net/2027/mdp.39015077775156
Public Domain, Google-digitized / http://www.hathitrust.org/access_use#pd-google

was apparent to all of the early experimenters since physical limitations restricted the size of antenna which could be installed conveniently aboard ship. However, development effort along these lines had previously been hampered by lack of suitable vacuum tubes.

In spite of the vacuum tube difficulties the Laboratories work was started in the range from 500 to 700 mcs, a region several times that then in use at the Army and Navy laboratories. The best tubes available were those of the *doorknob* type which have been described in the literature by A. L. Samuel[2] and are illustrated in Fig. 2. The smallest of these was used in the receiver input circuits and two of the middle sized ones were used in the tramsmitter oscillator. These triodes operated at quite high frequencies by virtue of the very small spacing between their electrodes, a feature which made them fragile and demanded the development of plate modulation. Earlier radars had generally used grid keyed oscillators, i.e., the plate voltage was applied to the oscillator continuously together with a high grid bias voltage. The bias was removed momentarily by the keyer to emit a pulse. In order to obtain a useful pulse output from the doorknob oscillator tubes it was found essential to remove all stress from them except during the pulse. This was accomplished by using a direct coupled pulse amplifier or modulator, effectively in series with the oscillator and the power supply. Here again in 1938 no really suitable tubes were available for the modulator service since it also demanded a highly intermittent duty. However, since the modulator duty did not require the tubes to operate at very high frequency it was possible to use rugged high-voltage triodes which had been designed for continuous service, and to obtain the required pulse current capacity by paralleling a number of tubes. The earliest radar modulators used in the Laboratories employed a group of Eimac 100-TH tubes. Later, in the CXAS and Mark 1 Radars, six tubes similar to the W. E. 356A were used in parallel.

After a great deal of laboratory work an experimental equipment was assembled and demonstrated to the Army and Navy in July 1939. This early radar was notable in that it operated at what was then considered a very high frequency and also in that it employed a single antenna only about 6 ft. square. The transmitter and receiver were connected to the common antenna by a *duplexing technique* to be described later, which had been applied at lower frequencies by engineers at the Naval Research Laboratory. The results of these first field tests were encouraging and both the Army and the Navy ordered one prototype model equipment to be known as the CXAS. This radar was to operate at 500 or 700 mcs and was to incorporate a number of new features which were designed to make it

[2] *Proceedings of I. R. E.*, Vol. 25, page 1243, 1937—"Negative Grid Triode Oscillator and Amplifier for Ultra High Frequencies." Digest in Oct. 1937 *B. S. T. J.*

Digitized by Google
Original from UNIVERSITY OF MICHIGAN
Generated on 2019-09-21 08:27 GMT / http://hdl.handle.net/2027/mdp.39015077775156
Public Domain, Google-digitized / http://www.hathitrust.org/access_use#pd-google

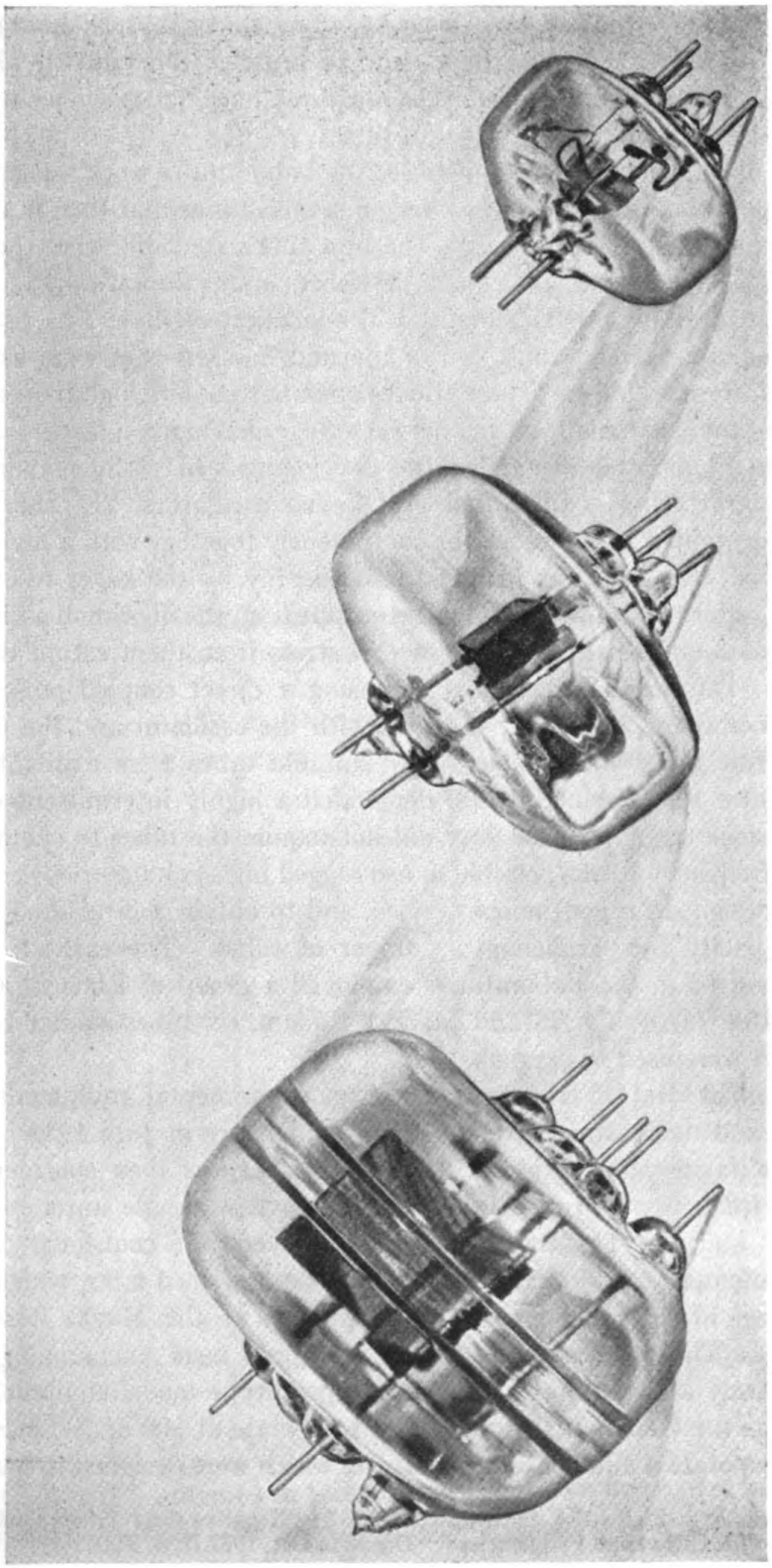

Fig. 2—Vacuum tubes for ultra-short waves

Digitized by Google
Original from UNIVERSITY OF MICHIGAN
Generated on 2019-09-21 08:27 GMT / http://hdl.handle.net/2027/mdp.39015077775156
Public Domain, Google-digitized / http://www.hathitrust.org/access_use#pd-google

convenient to operate and to provide a range accuracy that would be useful in fire control. Since this early radar is of cosiderable historical importance it will be described in some detail.

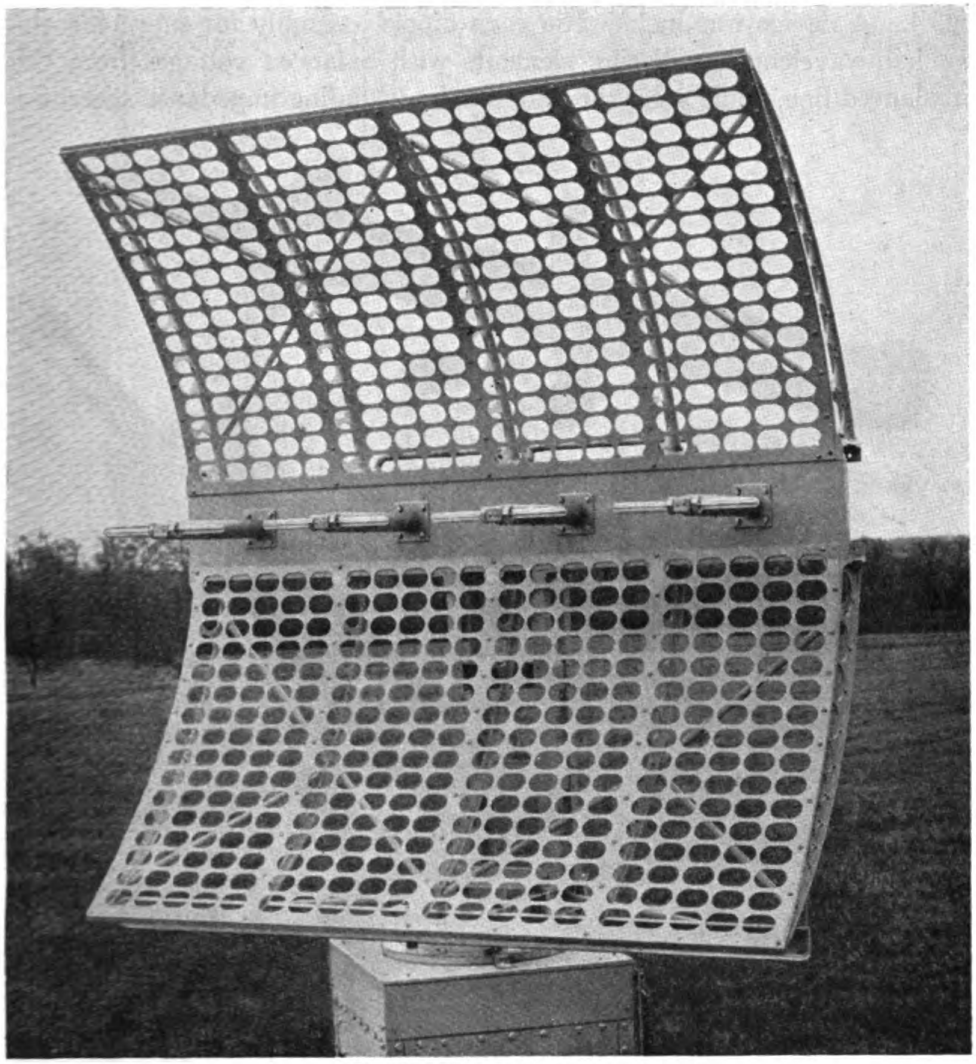

Fig. 3—CXAS—Antenna

The CXAS Radar

This equipment was divided into three major assemblies and the circuits were arranged so the three could be installed at some distance from each other. The antenna (see Fig. 3) consisted of a cylindrical parabolic reflector about 6 ft. square with an array of eight half-wavelength dipoles along the focal line. With shipboard use in mind the reflector was perforated to minimize wind resistance and the dipole and coaxial line feed

Digitized by Google
Original from UNIVERSITY OF MICHIGAN
Generated on 2019-09-21 08:28 GMT / http://hdl.handle.net/2027/mdp.39015077775156
Public Domain, Google-digitized / http://www.hathitrust.org/access_use#pd-google

system was made weatherproof, which was accomplished by making the line system pressure-tight and filling it with dry gas. The gas-line system was extended to include the radiating elements by covering the latter with pyrex test tubes sealed to the support with a packing gland as shown in Fig. 4. A device was included in each dipole assembly for supplying the two half-wavelength radiating elements with balanced voltages from the unbalanced line, while a coaxile line harness including impedance matching

Fig. 4—CXAS—Dipoles

transformers was used to connect the several dipole assemblies and provide a matched load to the single transmitter-receiver line. A schematic diagram of this arrangement is shown in Fig. 5. The contemplated use of this radar was for surface targets or low-flying planes and rotation was provided only in azimuth. A gas-tight rotary joint was developed to carry the $\frac{7}{8}''$ coaxial line through the azimuth axis (Fig. 6).

The operator's cathode ray oscillograph indicator and all of the essential

Digitized by Google
Original from UNIVERSITY OF MICHIGAN
Generated on 2019-09-21 08:28 GMT / http://hdl.handle.net/2027/mdp.39015077775156
Public Domain, Google-digitized / http://www.hathitrust.org/access_use#pd-google

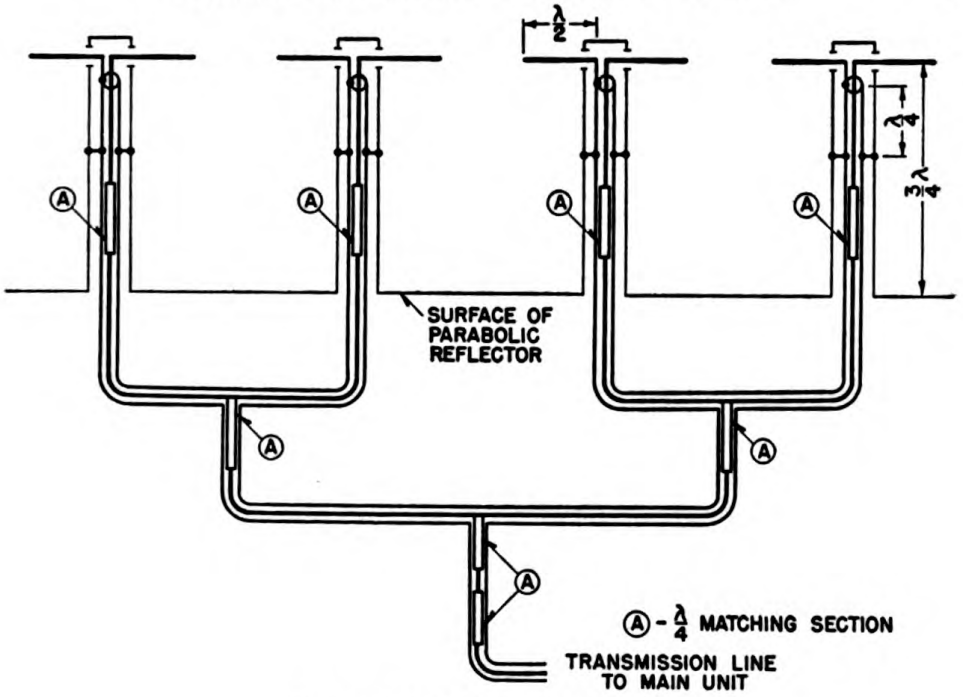

Fig. 5—CXAS—Antenna schematic

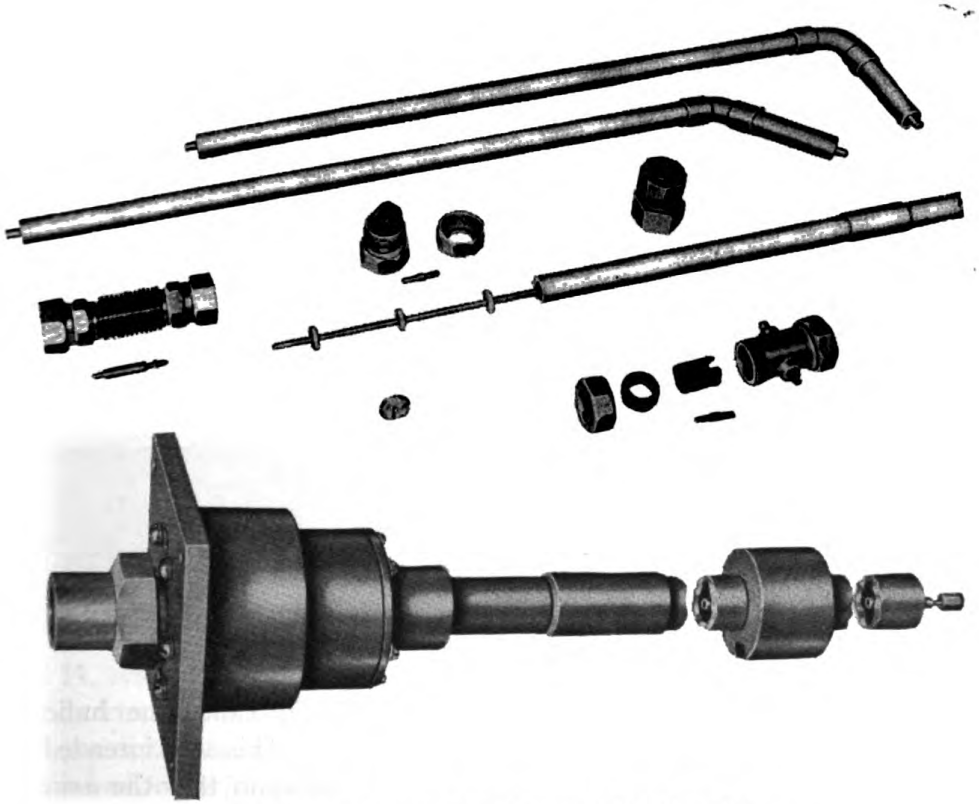

Fig. 6—CXAS—Rotary joint & transmission line fittings

Digitized by Google
Original from UNIVERSITY OF MICHIGAN
Generated on 2019-09-21 08:28 GMT / http://hdl.handle.net/2027/mdp.39015077775156
Public Domain, Google-digitized / http://www.hathitrust.org/access_use#pd-google

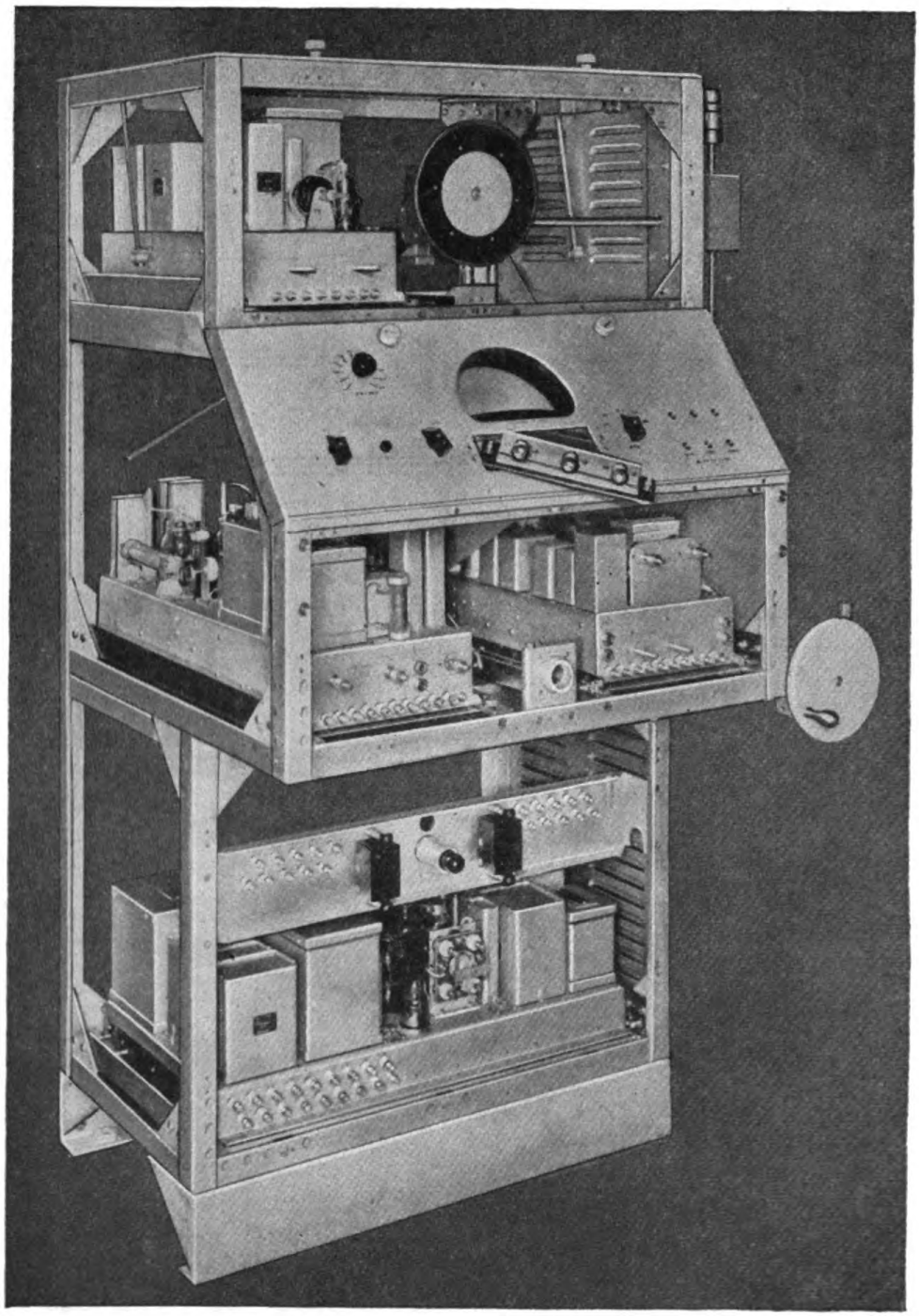

Fig. 7—CXAS—Indicator desk—covers removed

operating controls were combined into an assembly called the Indicator Desk, a photograph of which is shown in Fig. 7. This was intended for indoor mounting below the antenna in such a position that the azimuth

Digitized by Google
Original from UNIVERSITY OF MICHIGAN
Generated on 2019-09-21 08:28 GMT / http://hdl.handle.net/2027/mdp.39015077775156
Public Domain, Google-digitized / http://www.hathitrust.org/access_use#pd-google

hand wheel on the desk could be connected to the antenna turntable by a shaft. The indicator employed a 7″ cathode ray tube and displayed the radar signals by what is now known as a Class A sweep with a full scale of 100,000 yards. A pioneering feature of this indicator was the provision of a series of electronic range marks to increase the accuracy with which target range could be read. Earlier indicators had used a ruled mask for the range scale and had suffered in accuracy due to parallax, sweep non-linearity, drift of sweep position, etc. The CXAS provided sharp pulses to mark the 10,000-yard intervals along the sweep line, and smaller pulses to mark the intervening 2,000-yard intervals. This system was free from the errors of the ruled mask and permitted range readings accurate to ±200 yards throughout the 100,000-yard scale. Provision was also made to expand any desired 20,000-yard segment of the scale to fill the entire tube screen so that signals could be examined more closely. The ranges corresponding to the 10,000-yard intervals were designated by illuminated

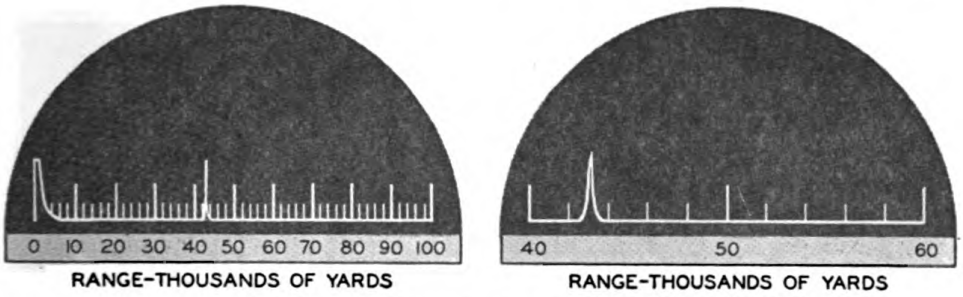

Fig. 8—CXAS—Range mark system

numerals located directly below the electronic scale. The presentation obtained with this arrangement is indicated in Fig. 8 which shows the electronic calibration marks, transmitted pulse, and an echo at 43,000 yards on both the full and expanded scales.

The third part of the CXAS equipment was an assembly known as the Transmitter-Receiver or Main Unit. It was designed to be unattended in normal operation and contained the Pulse Generator, Radio Receiver, Power Control Panel, Radio Transmitter, and H.V. Rectifier, which were all built as removable *drawer type* units. A side compartment in the Main Unit also housed the duplexing circuits, gas equipment for the transmission line, and some built-in test equipment, including a wavemeter and monitoring rectifier. The Main Unit and its sub-units are shown in Figs. 9 to 14, respectively. A single $\frac{7}{8}$″ coaxial transmission line provided connection from the Main Unit to the antenna.

In order to use a single antenna for both transmission and reception, means had to be provided to effectively disconnect the receiver during the

Digitized by Google
Original from UNIVERSITY OF MICHIGAN
Generated on 2019-09-21 08:29 GMT / http://hdl.handle.net/2027/mdp.39015077775156
Public Domain, Google-digitized / http://www.hathitrust.org/access_use#pd-google

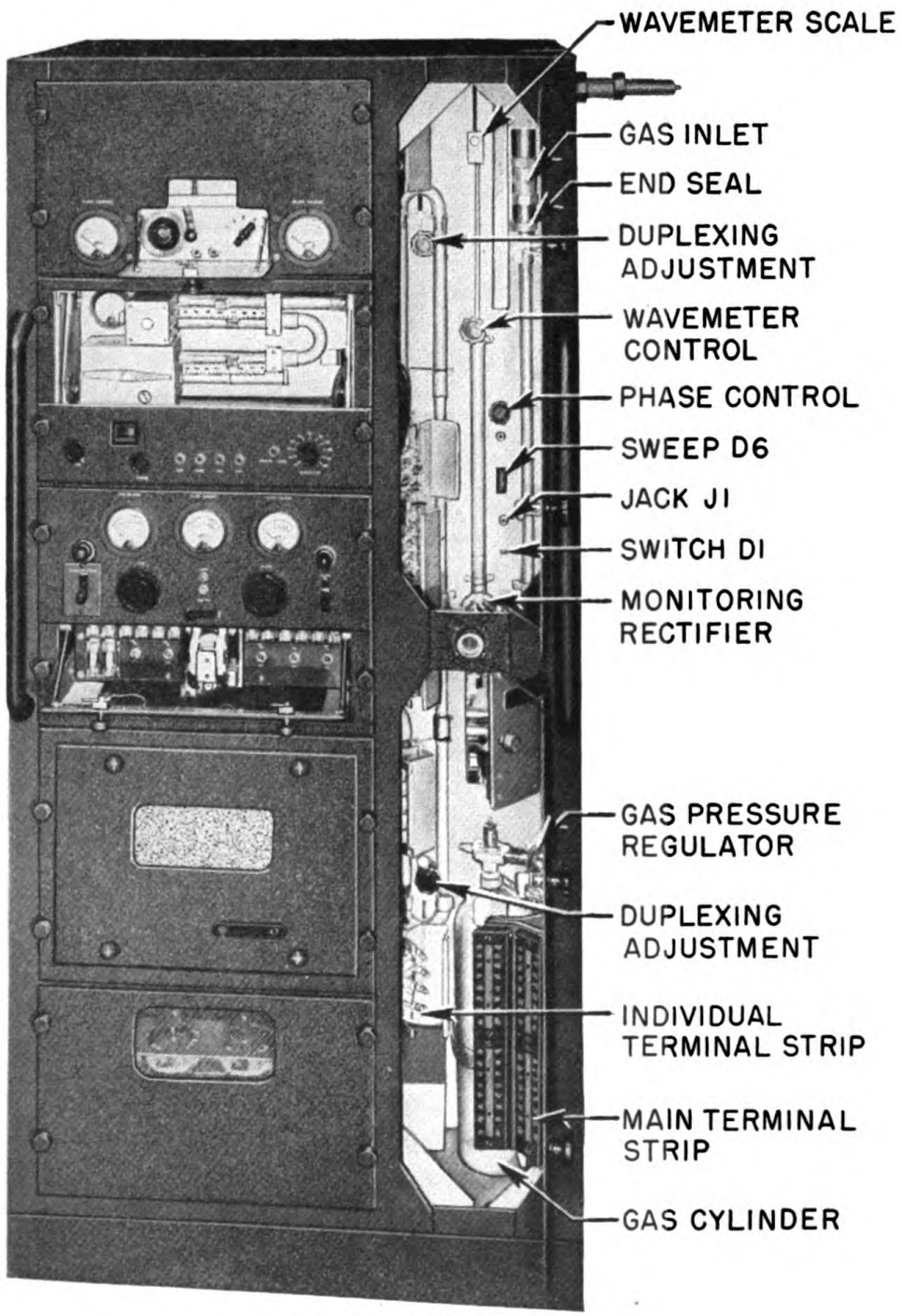

Fig. 9—CXAS—Main unit

transmitted pulse and to effectively disconnect the transmitter when the echo is received. If this were not done, a large part of the transmitted

Digitized by Google
Original from UNIVERSITY OF MICHIGAN
Generated on 2019-09-21 08:29 GMT / http://hdl.handle.net/2027/mdp.39015077775156
Public Domain, Google-digitized / http://www.hathitrust.org/access_use#pd-google

energy would be dissipated in the receiver. Also, the minute received energy would be partially lost in the transmitter output circuit thus reducing the maximum range. Because of the extremely short time intervals between transmitted and received pulses, ordinary switching methods cannot be used. A *duplexing technique* mentioned earlier was therefore developed to provide this function. In the CXAS Radar this switching was obtained by connecting the transmitter and receiver to the antenna transmission line through adjustable lengths of coaxial line which were preset for a given operating frequency to be effectively an odd multiple of

Fig. 10—CXAS—Modulation or pulse generator

one-quarter wavelength long. During the transmitted pulse, a small amount of the transmitted power overloaded the first tube in the receiver and provided a low impedance at that point. Due to the line length between receiver and junction point this low impedance is reflected as a high impedance at the junction point with the result that very little power is lost in the receiver line. At the end of the transmitted pulse the output impedance of the transmitter consists only of the small inductance of the output coupling loop and this impedance is reflected by proper choice of line length as a very high impedance at the junction joint with the receiver line. Thus, most of the received echo is directed to the receiver input

Digitized by Google
Original from UNIVERSITY OF MICHIGAN
Generated on 2019-09-21 08:29 GMT / http://hdl.handle.net/2027/mdp.39015077775156
Public Domain, Google-digitized / http://www.hathitrust.org/access_use#pd-google

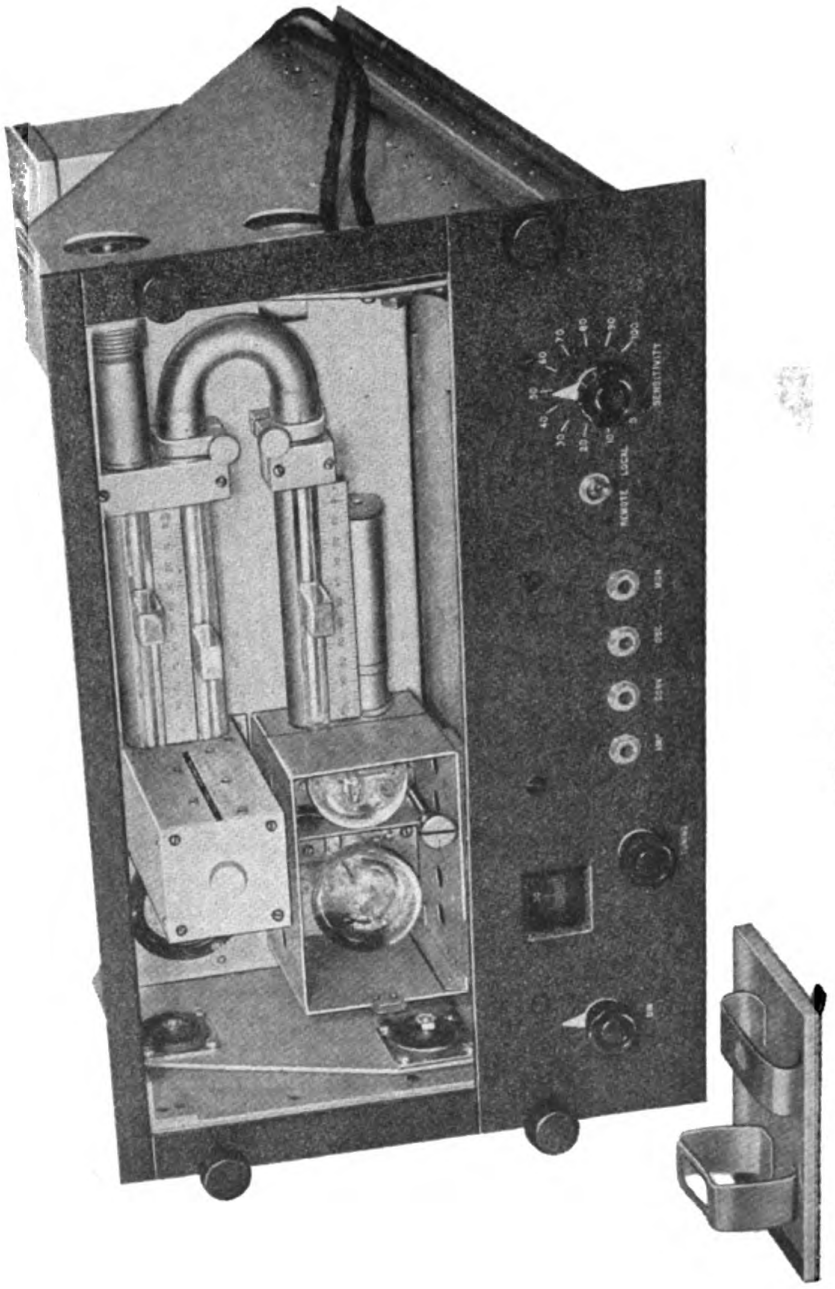

Fig. 11—CXAS—Receiver

Digitized by Google
Original from UNIVERSITY OF MICHIGAN
Generated on 2019-09-21 08:30 GMT / http://hdl.handle.net/2027/mdp.39015077775156
Public Domain, Google-digitized / http://www.hathitrust.org/access_use#pd-google

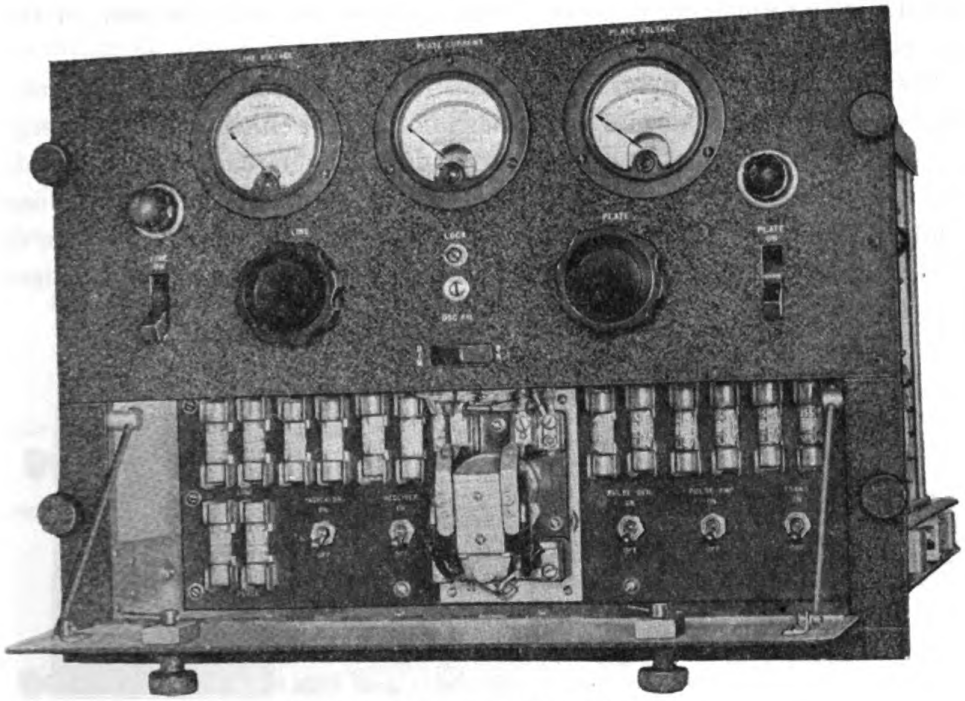

Fig. 12—CXAS—Power control panel

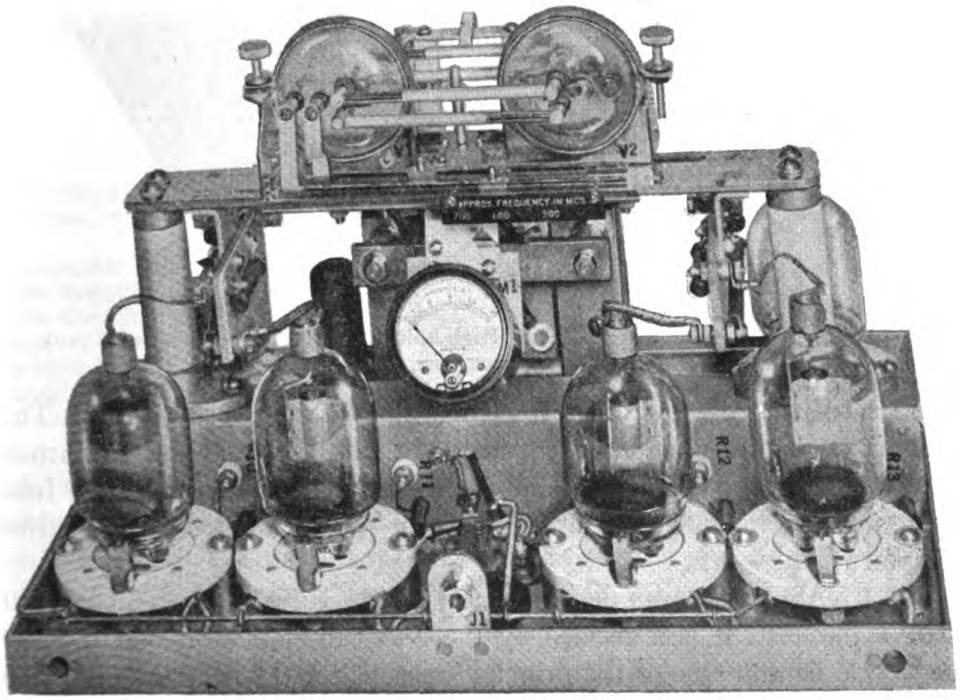

Fig. 13—CXAS—Transmitter

Digitized by Google
Original from UNIVERSITY OF MICHIGAN
Generated on 2019-09-21 08:30 GMT / http://hdl.handle.net/2027/mdp.39015077775156
Public Domain, Google-digitized / http://www.hathitrust.org/access_use#pd-google

circuit. The adjustable duplexing transmission lines may be seen in the side compartment of the Main Unit on Fig. 9.

The equipment just described could be operated over a small frequency band of about 40 megacycles in the neighborhood of either 700 or 500 megacycles. The transmitter, receiver, and duplexing circuits were tunable over the entire range, but it was necessary to set up the antenna for one band or the other. This was accomplished by installing the proper one of the two sets of dipoles furnished, and installing or omitting a set of wedges

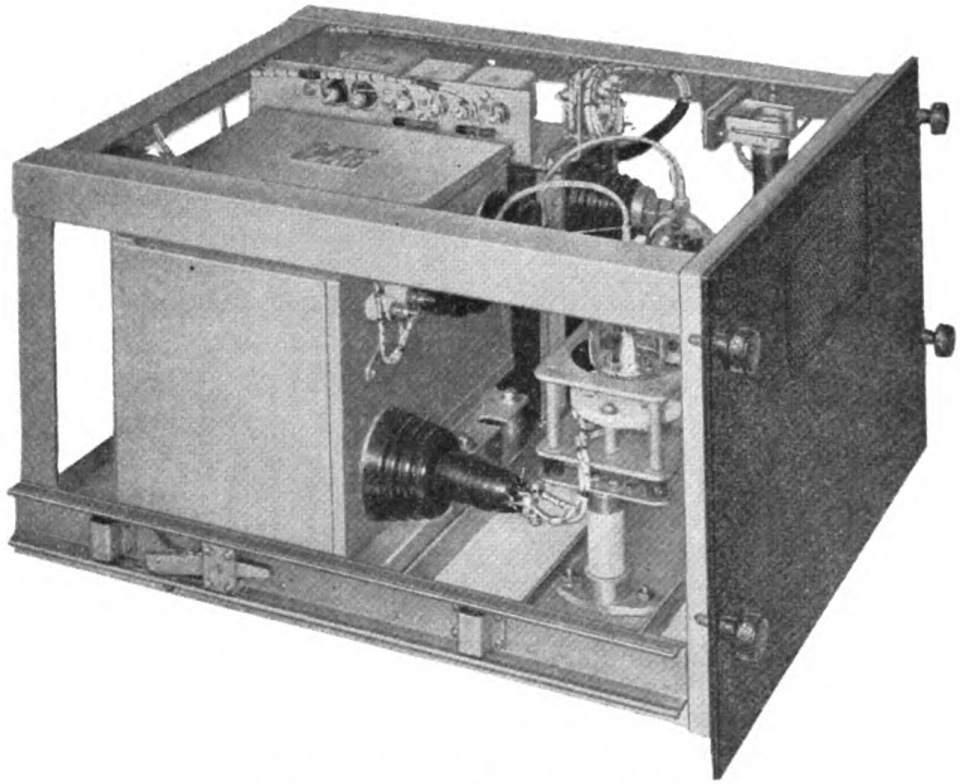

Fig. 14—CXAS—High voltage rectifier

which tilted the reflector wings to change the parabola focal length. This antenna set a precedent in design in that the dipoles and coaxial harness were designed for fairly broadband operation and were entirely free from field tuning adjustments which had been very troublesome in earlier equipment.

The CXAS Radar was demonstrated to the Navy in December 1940. After a few tests it was decided by the Navy to standardize on the 700-megacycle band. One of the principal reasons for this was that the tests had proved the superiority of shorter waves for surface target work; the

Digitized by Google
Original from UNIVERSITY OF MICHIGAN
Generated on 2019-09-21 08:31 GMT / http://hdl.handle.net/2027/mdp.39015077775156
Public Domain, Google-digitized / http://www.hathitrust.org/access_use#pd-google

CXAS having regularly out-performed much higher powered equipment operating at 100 or 200 megacycles for this service. The reason for this can best be uuderstood by reference to Fig. 15 which illustrates what happens when a radio beam is directed horizontally over water. The beam breaks up into an interference pattern of several rays due to reflection from the surface; the position of the lowest ray depending only upon the height of the antenna measured in wavelengths above the water. Since the mount-

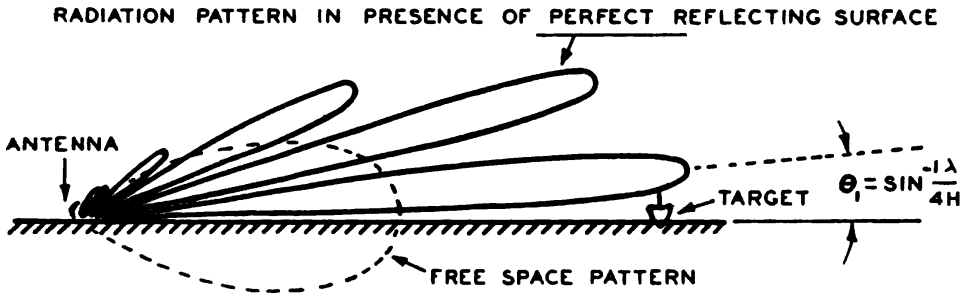

$$e = 2 \sin \left(2\pi \frac{H}{\lambda} \sin \theta\right) \times \left[\text{FREE SPACE ANTENNA PATTERN}\right]$$

WHERE H = ANTENNA HEIGHT

λ = WAVE LENGTH IN SAME UNITS AS H

θ = ELEVATION ANGLE IN DEGREES

e = RELATIVE FIELD STRENGTH

Fig. 15—Effect of surface reflection on elevation beam

TABLE I

Operating Frequency	Tunable 680–720 mcs.
Antenna	Dipole array of 8 half-wave radiators, reflector 6′ x 6′, beam width 12 degrees, gain 22 db.
Transmitter Pulse Power	Approximately 2 kw.
Pulse Repetition Rate	1640 PPS
Pulse Duration	Variable in 5 steps from 1 to 5 microseconds.
Receiver-Superheterodyne	1 mc bandwidth, 30 mc IF frequency.
Receiver Noise Figure	Approximately 24 db.
Range Calibration	Electronic marks at 10,000 and 2,000 yard intervals.

ing height available aboard ship is fixed, the use of shorter wavelengths made it possible to keep the lowest ray more nearly horizontal where it could intercept a target's superstructure at greater distance.

The principal characteristics of the CXAS Radar as set up for operation at 700 megacycles are given in Table I.

This equipment gave useful results on surface targets at ranges of 10 miles or more (depending on the size of the target) and the range accuracy

Generated on 2019-09-21 08:31 GMT / http://hdl.handle.net/2027/mdp.39015077775156
Public Domain, Google-digitized / http://www.hathitrust.org/access_use#pd-google
Digitized by Google
Original from UNIVERSITY OF MICHIGAN

of about ±200 yards was then considered very usable in surface target fire control. The target azimuth could also be determined to a precision of one or two degrees by rapidly swinging the antenna back and forth and observing the point which gave a maximum echo signal. This angular information was hardly good enough for fire control use. The equipment was also of some use against low flying aircraft as a means of getting better range data for fire control. Minor equipment difficulties were not entirely solved; in particular the doorknob triodes in the transmitter had a very short life under the high voltage pulse operating conditions. They had, of course, been designed originally for CW communication use and strenuous development effort to make them more suitable for the intermittent high power radar use had not been very successful.

The Mark 1 Radar

In spite of the obvious unsolved development problems the Navy immediately ordered 10 equipments, similar to the CXAS, for use in the Fleet. These were first called the FA Radio Ranging Equipment but the designation was later changed to Radar Mark 1. Several changes were made to better adapt the equipment for installation aboard ship, the principal one being a servo driven antenna pedestal of the amplidyne type which was furnished by the General Electric Company. The servo system eliminated the antenna drive shaft problem while retaining control from a handwheel on the control desk. The desk was also modified to provide dials reading both relative and true azimuth bearing, the latter being obtained by interconnection with the ships gyro compass system.

The first Mark 1 Radar was shipped by the Western Electric Company in June 1941 and installation on the USS Wichita was completed at the Brooklyn Navy Yard early in July 1941. This was the first fire control radar in our Fleet and the first of many thousands of radars of all types which the Western Electric Company was destined to build for the Navy in the following four years.

The Mark 2 Radar

While the ten Mark 1 radars were being built, development work was proceeding at top speed on major improvements designed to increase performance, eliminate operating troubles, and to make this new device fit better into the existing fire control situation aboard ship. The older optical devices were neatly integrated into a system, many features of which were automatic. For example, the gyro stabilized telescopes and optical range finder were assembled into a compact rotating armored box called a *director*, located high on the ship. Target data from the director was sent

Digitized by Google
Original from UNIVERSITY OF MICHIGAN
Generated on 2019-09-21 08:32 GMT / http://hdl.handle.net/2027/mdp.39015077775156
Public Domain, Google-digitized / http://www.hathitrust.org/access_use#pd-google

automatically by *synchro* data transmitters to the computer below decks, which solved the fire control problem and likewise transmitted automatically the correct information to the guns. For the new radar target locating device to fit into the existing system it was necessary to make its angle finding function operate more in the manner of the telescopes. Not only was it desired to determine target angles more accurately but it was necessary to track target position continuously and smoothly. Finally, to take care of the anticipated need for rapidly changing back and forth during an engagement from optical to radar data it became apparent that the same operators should handle both jobs. Thus it was decided that the system should provide the existing operators with oscilloscopes to supplement their telescopes, and to arrange them so either could be used as desired. Further to coordinate the data it became obvious that the radar antenna should be connected with the optics in such a way that the two were always pointed in the same direction. This would make it possible to leave the existing data transmission system alone and would avoid any break in data when changing from optics to radar or vice versa. For example, if a visible target disappeared behind a fog bank the telescope operator would simply move his head to look at his oscilloscope and data would continue to flow smoothly to the computer and to the guns.

Thus the engineers of the Navy decided the new radar device could be fitted into the existing fire control system. Any other decision would likely have required modification of many parts of the system, and would have delayed the extensive use of fire control radar by a matter of years. The Bell Telephone Laboratories were accordingly asked to modify and improve the radar design to make possible the coordination of optics and radar as just discussed. The new radar was to be called Mark 2 and was to be similar to the Mark 1 but modified to provide continuous tracking in azimuth with an accuracy of ± 15 minutes of arc, and continuous tracking in range with an accuracy of ± 50 yards. Further, the operator's oscilloscopes and controls were to be put into small units that could be mounted alongside of the telescopes in the director, and the antenna was to mount on the director. These requirements demanded some important forward steps in radar development which will be described in some detail. Before Radar Mark 2 got into production a much higher powered transmitter was developed and with this change the equipment was re-named Radar Mark 3.

The Mark 3 Radar

The general arrangement of apparatus for this radar differed from the Mark 1 principally in the indicators, which were designed to mount in the

Digitized by Google
Original from UNIVERSITY OF MICHIGAN
Generated on 2019-09-21 08:33 GMT / http://hdl.handle.net/2027/mdp.39015077775156
Public Domain, Google-digitized / http://www.hathitrust.org/access_use#pd-google

already crowded gun director. These indicators are shown in Figs. 16, 17 and 19. Fig. 16 shows the range operator's oscilloscope, called the Control and Indicator, which was located near the optical range finder. Adjacent to this unit was mounted the range unit, shown in Fig. 17 by means of which the operator could select the target to be followed and continuously

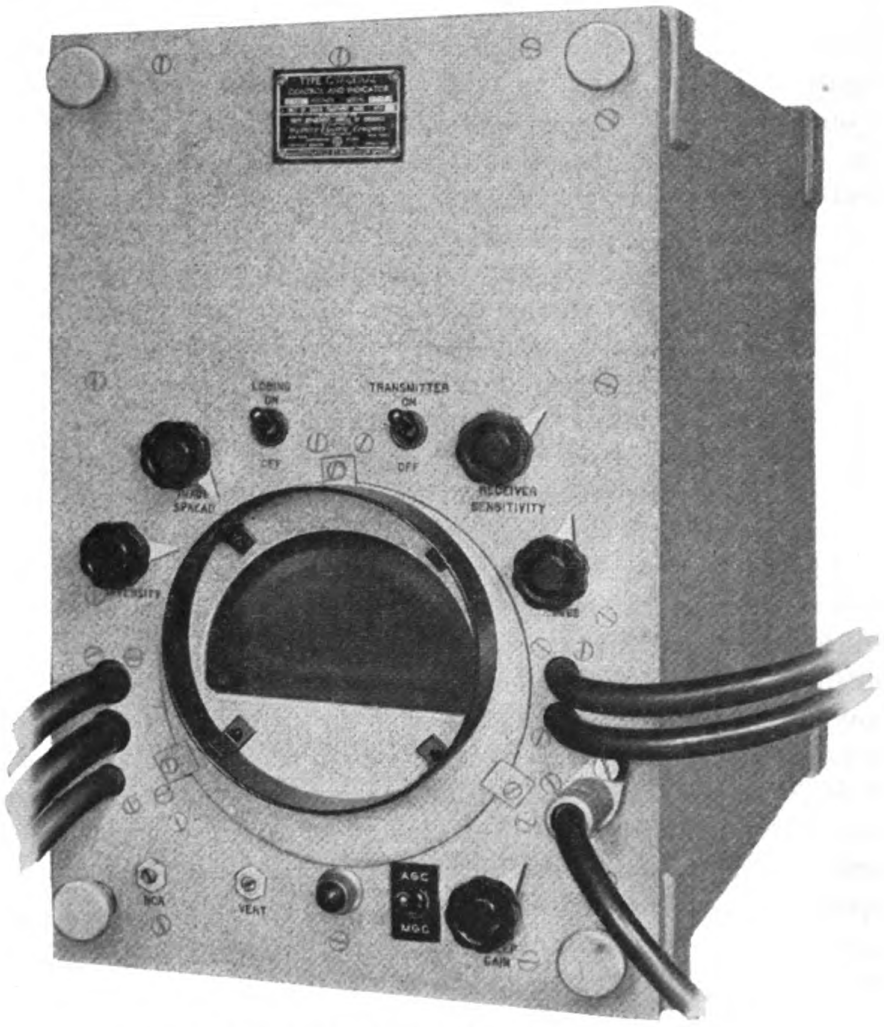

Fig. 16—Control & indicator—Radars Mark 2, 3 & 4

maintain accurate range readings. A typical installation of these two units is shown in Fig. 18. The third unit, shown in Fig. 19, is called a Train or Elevation Indicator and, in Radar Mark 3 (which was for surface fire only) this indicator was mounted adjacent to the Train (azimuth) Operator's telescope.

In addition to the Train Indicator, the azimuth operator was provided

Digitized by Google
Original from UNIVERSITY OF MICHIGAN
Generated on 2019-09-21 08:33 GMT / http://hdl.handle.net/2027/mdp.39015077775156
Public Domain, Google-digitized / http://www.hathitrust.org/access_use#pd-google

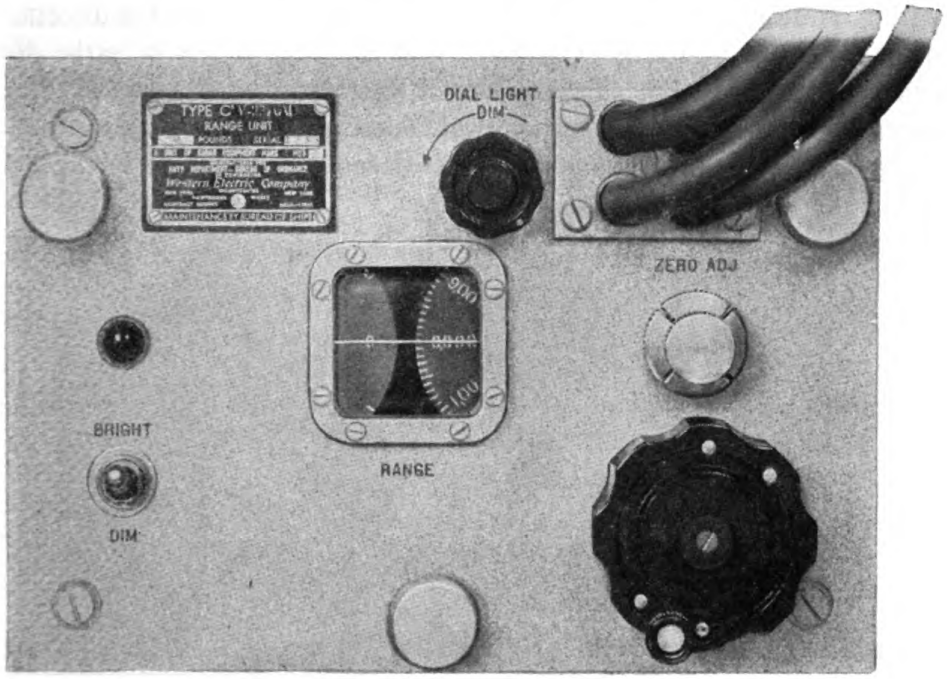

Fig. 17—Range unit—Radars Mark 2, 3 & 4

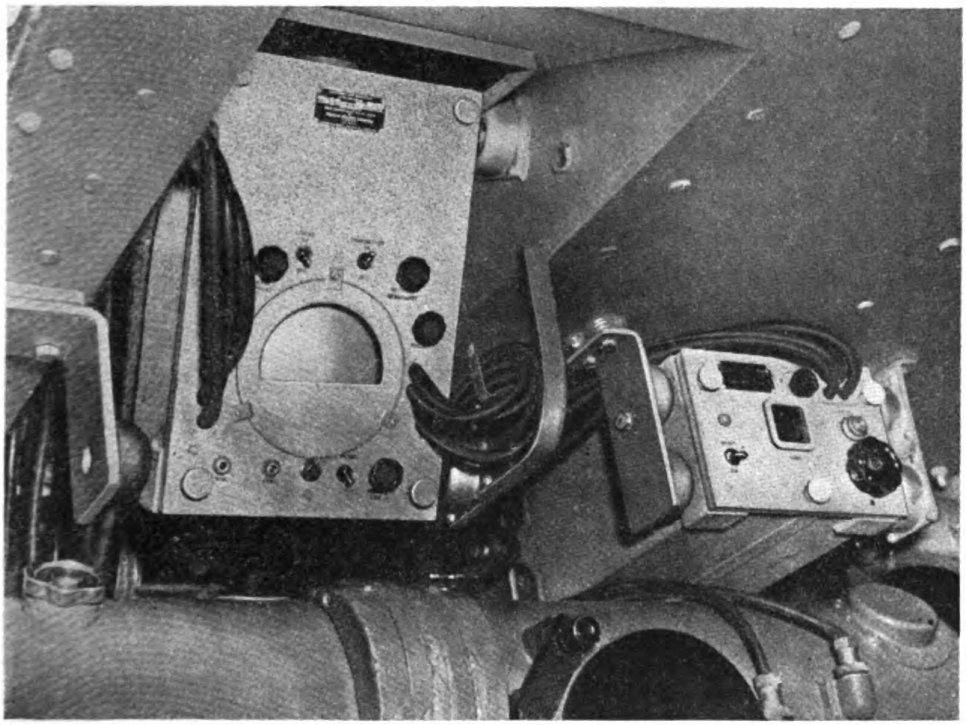

Fig. 18—Mark 3 Radar—Range operator's position on Cruiser Honolulu (Navy Photo 153-6-42)

Digitized by Google
Original from UNIVERSITY OF MICHIGAN
Generated on 2019-09-21 08:33 GMT / http://hdl.handle.net/2027/mdp.39015077775156
Public Domain, Google-digitized / http://www.hathitrust.org/access_use#pd-google

with a Train Meter of the zero center type which indicated the direction of deviation from true target position. One of these meters of early design can be seen in Fig. 38. Two meters of later design are shown in Fig. 39 mounted immediately below optical telescopes. The pulse generator, receiver, transmitter, rectifiers, etc., were located below decks in the Trans-

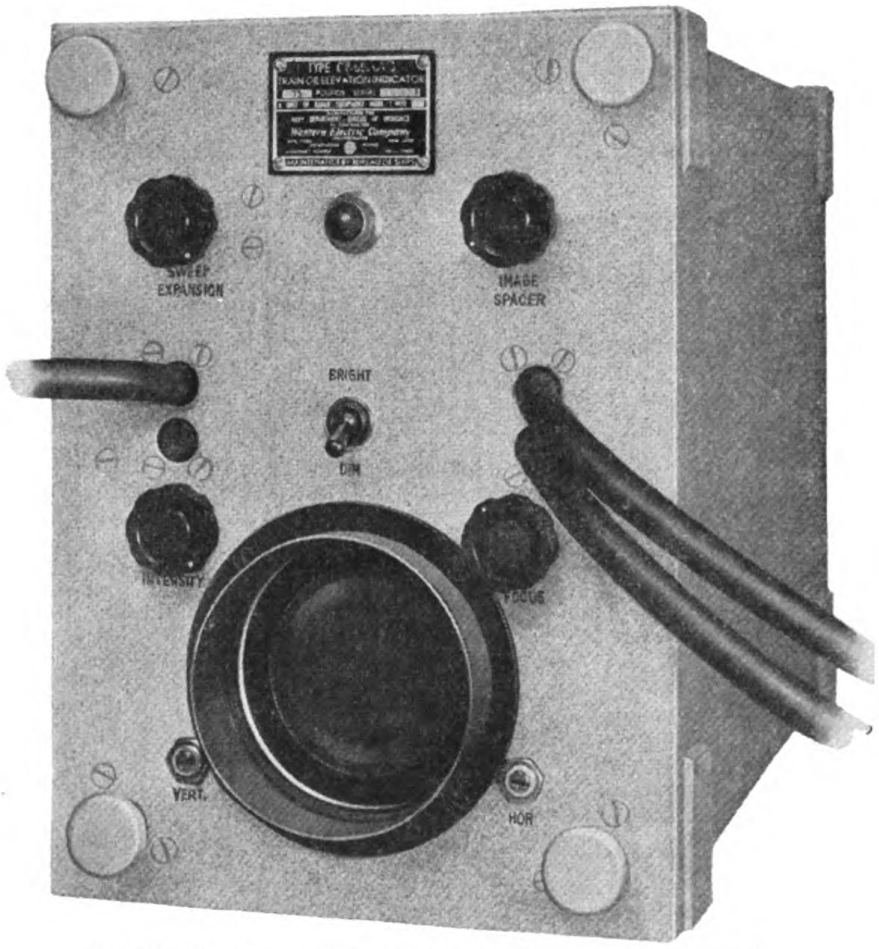

Fig. 19—Train or elevation indicator—Radars Mark 2, 3 & 4

mitter-Receiver, or Main Unit which was very similar in appearance to the Main Unit of Radar Mark 1 shown in Fig. 9.

Two types of antennas were provided for this radar: a 6 ft. by 6 ft. parabolic array similar to the Mark 1 antenna, and a 3 ft. by 12 ft. parabolic array. Either one or the other of these antennas was mounted on top of the gun director and rotated with it in azimuth. Both were provided with azimuth lobe switching to be described later. Because of the relatively narrow elevation beam of the 6 ft. by 6 ft. array, this antenna required gyro

Digitized by Google
Original from UNIVERSITY OF MICHIGAN
Generated on 2019-09-21 08:33 GMT / http://hdl.handle.net/2027/mdp.39015077775156
Public Domain, Google-digitized / http://www.hathitrust.org/access_use#pd-google

stabilization in elevation to take care of pitch and roll of the ship. Such stabilization was not required with the broad elevation beam obtained with the 3 ft. by 12 ft. antenna; and in addition, this wider antenna provided more accurate tracking due to the narrower antenna beam in azimuth. Installations of these antennas aboard ship are shown in Figs. 20 and 21 and 22, 23 and 24.

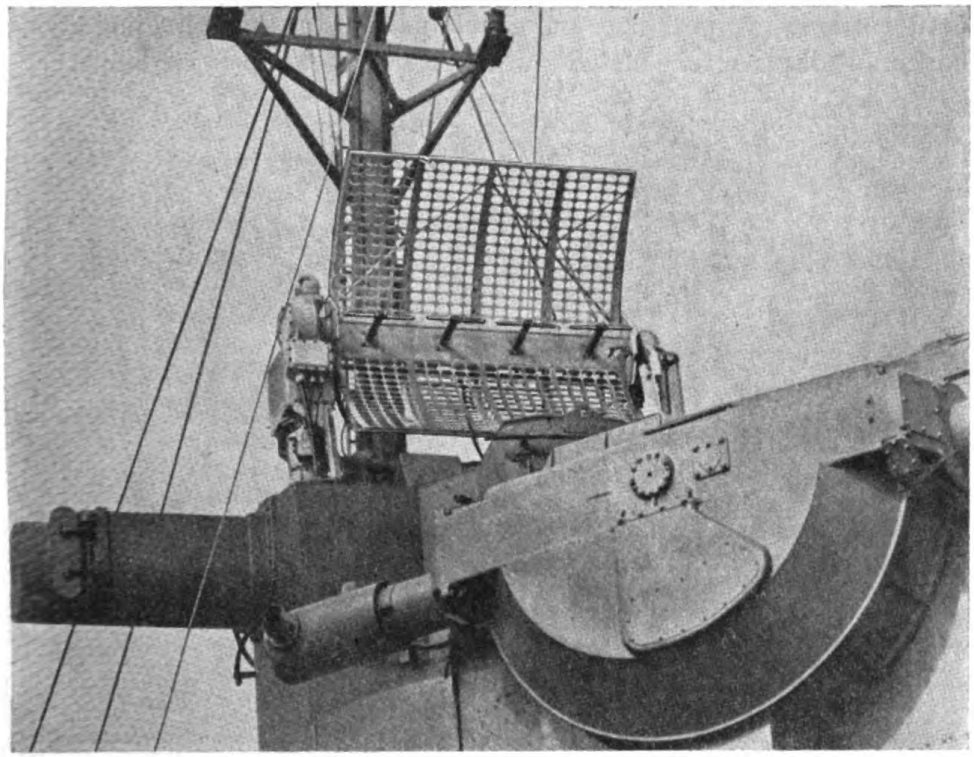

Fig. 20—Radar Mark 3 antenna (6′ x 6′) on Cruiser Honolulu (Navy Photo 144-6-42)

Antenna Lobe Switching

The problem of measuring angles accurately with a relatively broad radio beam has been faced many times in the radio direction finding art. The most successful attack has made use of the fact that while the nose of a radio antenna beam is blunt, the sides of the beam are relatively steep; i.e., while the rate of change of signal amplitude with angle is very low near the nose of the beam it becomes substantial down on the side of the beam. A very well known application of this principle is the airway radio range wherein two very broad overlapping beams define a narrow path by utilizing the points where the two overlap with equal intensity. A somewhat similar scheme in which the antenna beam is switched rapidly between two positions has been applied in radar, and in an early form was first used

Digitized by Google
Original from UNIVERSITY OF MICHIGAN
Generated on 2019-09-21 08:34 GMT / http://hdl.handle.net/2027/mdp.39015077775156
Public Domain, Google-digitized / http://www.hathitrust.org/access_use#pd-google

in this country by the Signal Corps in the work described by General Colton, to which reference has been made.

The use of two antenna beam (or lobe) positions to obtain more accurate radar angle data is referred to as *lobe switching* and the operating principle is illustrated in Fig. 25. The antenna beam is shown in two positions: position 1 being directed to the right, and position 2 to the left of the mechanical axis of the antenna. The antenna beam is caused to switch rapidly between these two positions, and simultaneous with this switching a small horizontal displacement of the indicator Class A sweep is introduced. In

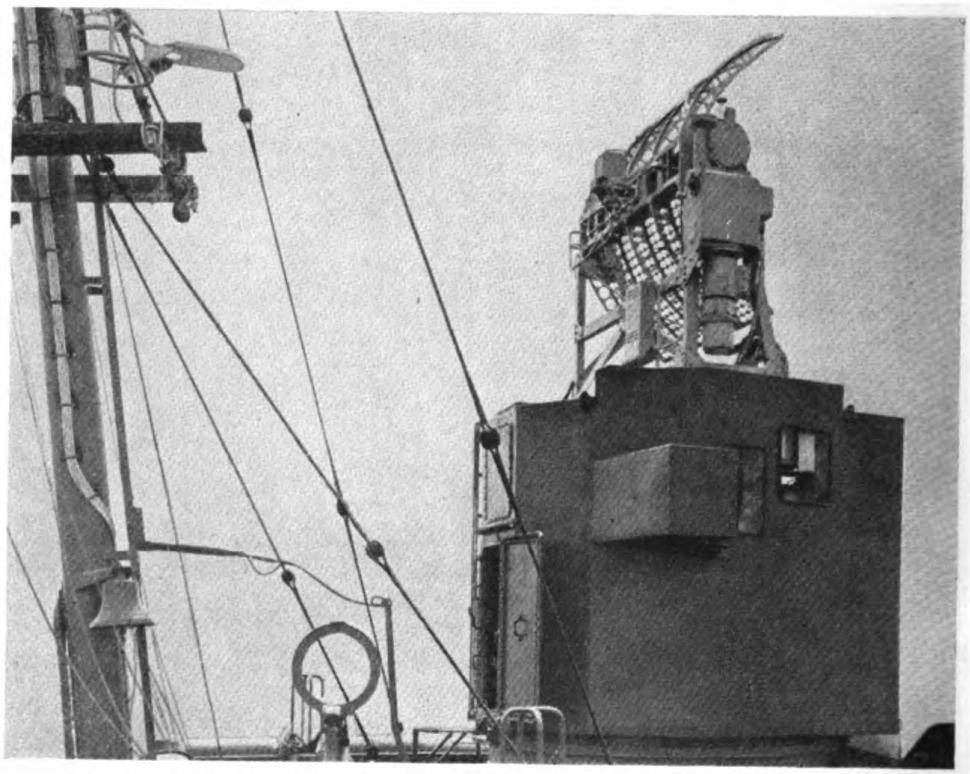

Fig. 21—Radar Mark 3 antenna on Destroyer Porter (Navy Photo 2711-42)

this manner the signals received in the two beam positions may be viewed separately. The speed of switching is made sufficiently high to minimize flicker and the effect of fading signals. It will be noted from this diagram that the signal strength received from target A is the same for both beam positions thereby producing equal "pip" heights on the indicator screen. However, for target B the signal amplitude is greater in position 1 than in position 2 and the "pip" amplitudes on the indicator differ correspondingly. If the operator wishes to track target B it is only necessary for him to rotate the antenna until the two "pips" are of equal amplitude. Smooth

Digitized by Google
Original from UNIVERSITY OF MICHIGAN
Generated on 2019-09-21 08:34 GMT / http://hdl.handle.net/2027/mdp.39015077775156
Public Domain, Google-digitized / http://www.hathitrust.org/access_use#pd-google

Generated on 2019-09-21 08:35 GMT / http://hdl.handle.net/2027/mdp.39015077775156
Public Domain, Google-digitized / http://www.hathitrust.org/access_use#pd-google

Digitized by Google

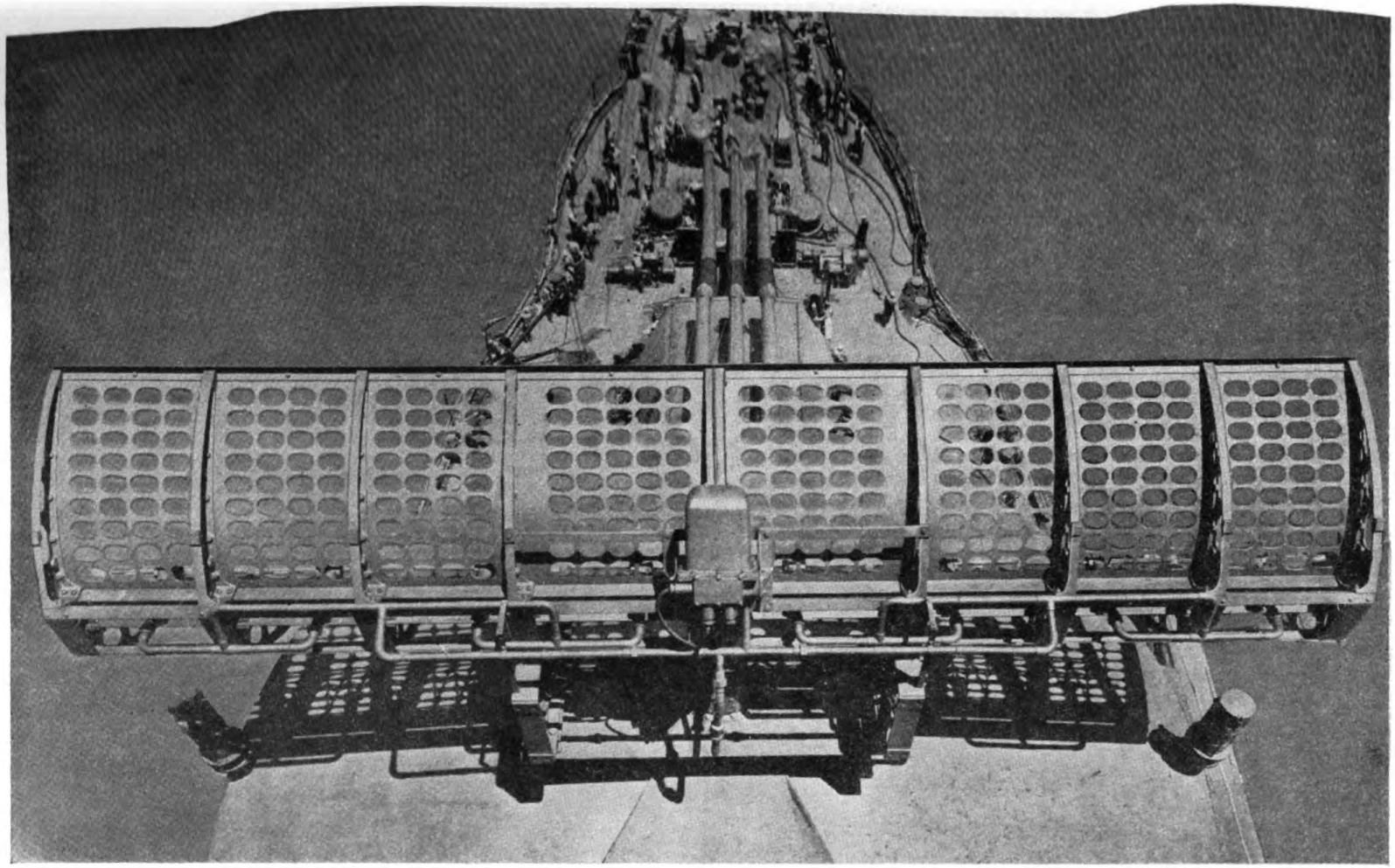

Fig. 22—Radar Mark 3 antenna (3′ x 12′) on Battleship Pennsylvania (Navy Photo 4273-42)

Original from UNIVERSITY OF MICHIGAN

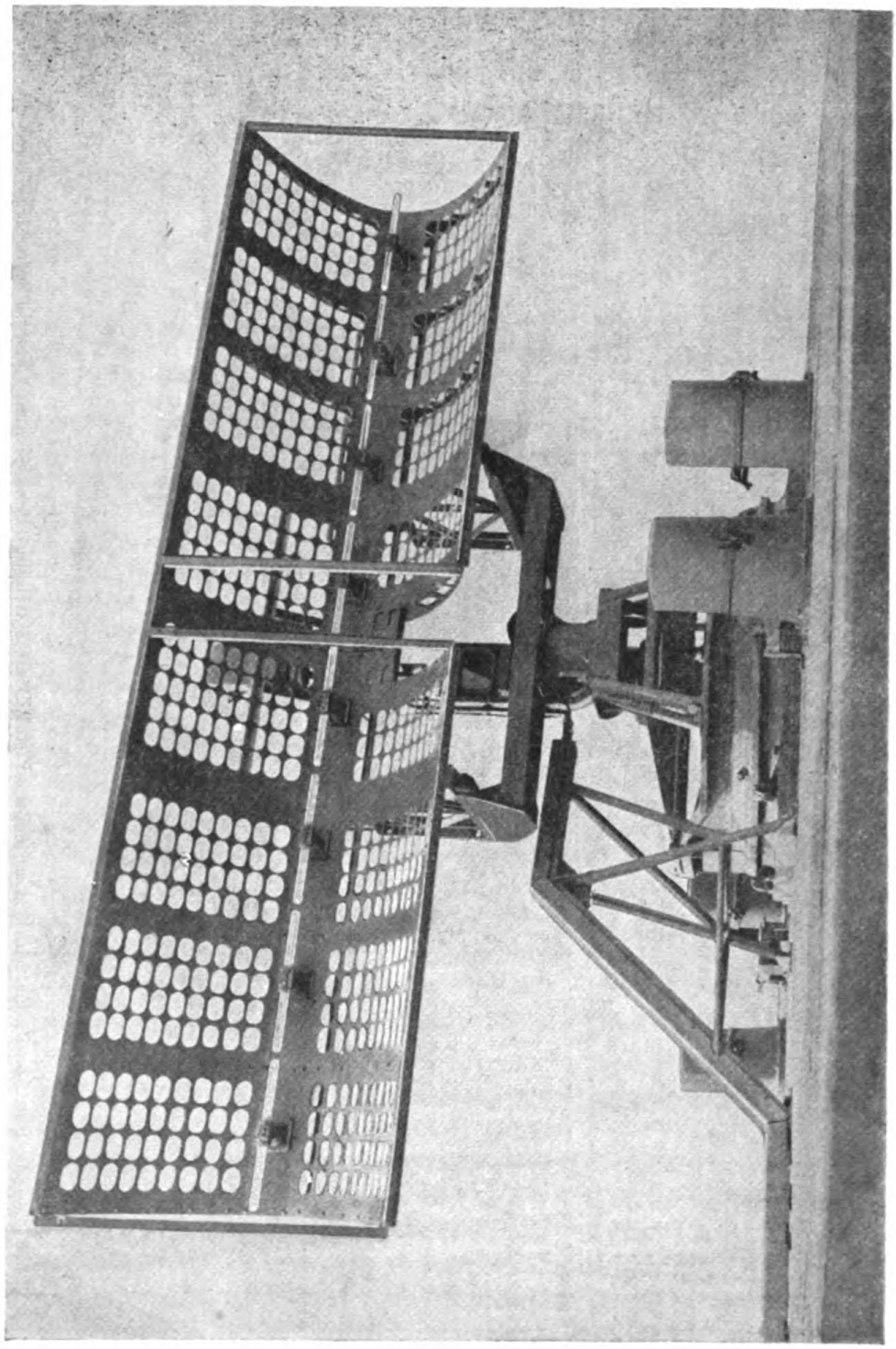

Fig. 23—Radar Mark 3 antenna (3′ x 12′) on Battleship New Jersey (Navy Photo 181812)

Generated on 2019-09-21 08:35 GMT / http://hdl.handle.net/2027/mdp.39015077775156
Public Domain, Google-digitized / http://www.hathitrust.org/access_use#pd-google
Digitized by Google
Original from UNIVERSITY OF MICHIGAN

flow of azimuth data will be obtained if the operator continuously maintains equal amplitude of the two "pips".

In the Signal Corps equipment to which reference has been made, separate antennas were used for transmission and reception with lobe switching

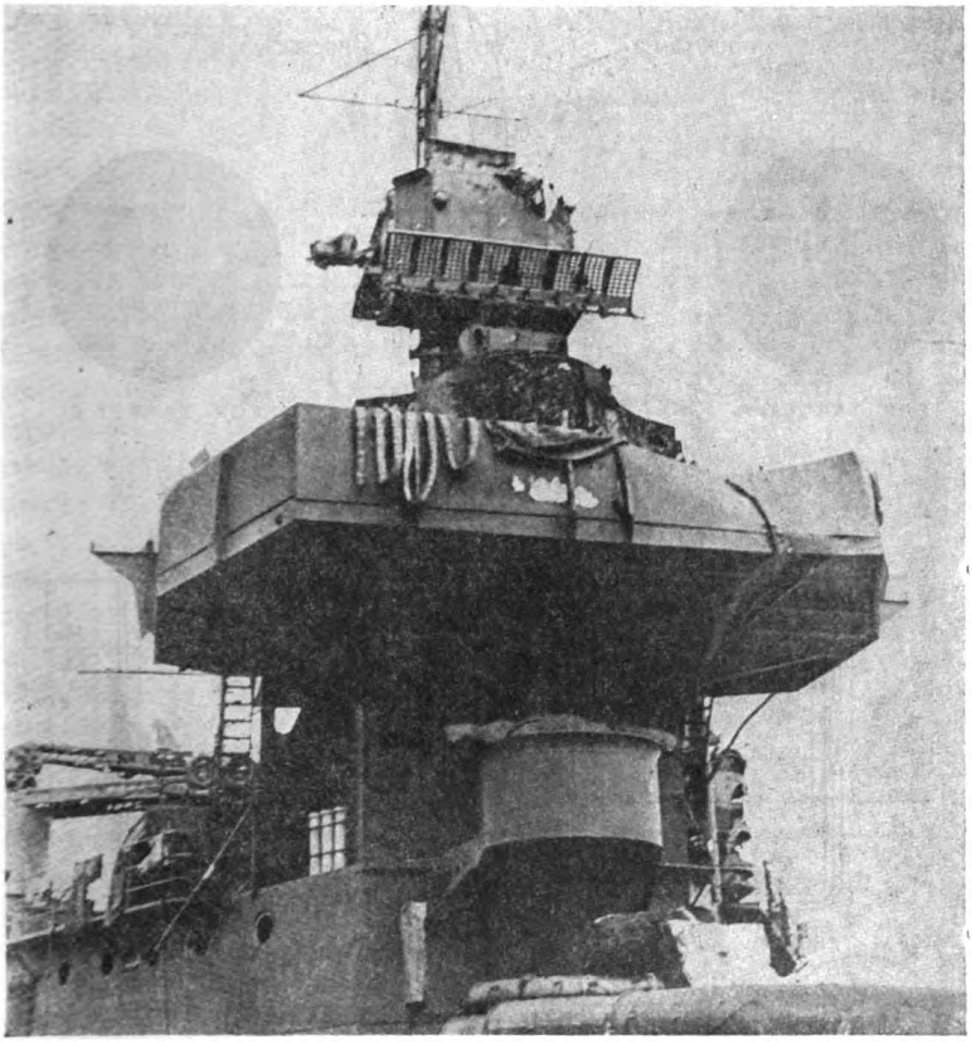

Fig. 24—Radar Mark 3 antenna (3′ x 12′) on Cruiser San Francisco after Pacific battle (Navy Photo 34133)

applied only to the receiving antenna. Space limitations aboard ship made it mandatory to accomplish all functions using a single antenna. This required the development of a lobe switching device capable of withstanding the high peak power during the transmitted pulse; a problem which had not been faced in the Signal Corps equipment. It was further desired to provide a weatherproof lobe switching device, free from radio

Digitized by Google
Original from UNIVERSITY OF MICHIGAN
Generated on 2019-09-21 08:35 GMT / http://hdl.handle.net/2027/mdp.39015077775156
Public Domain, Google-digitized / http://www.hathitrust.org/access_use#pd-google

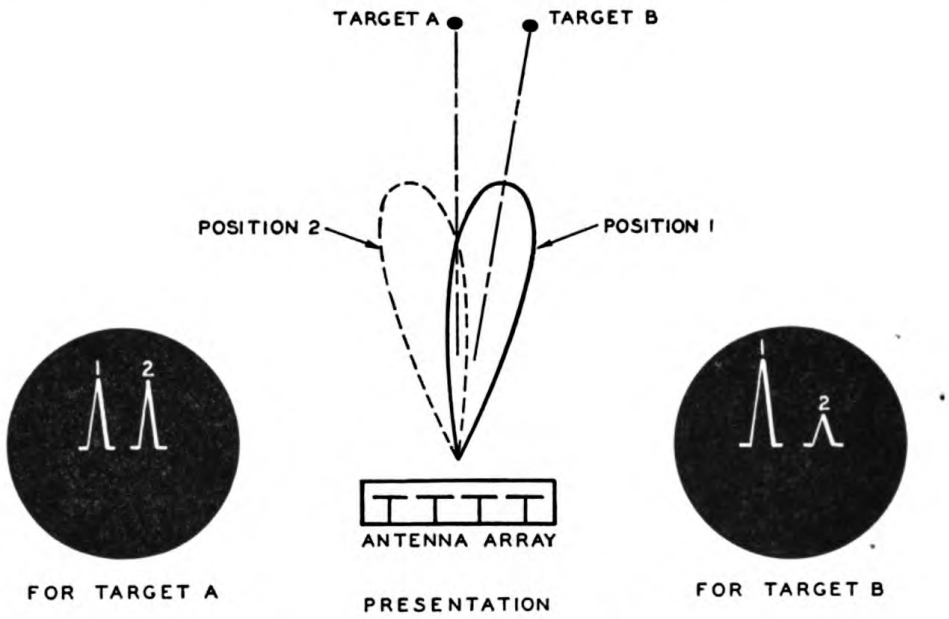

Fig. 25—Principle of lobe switching

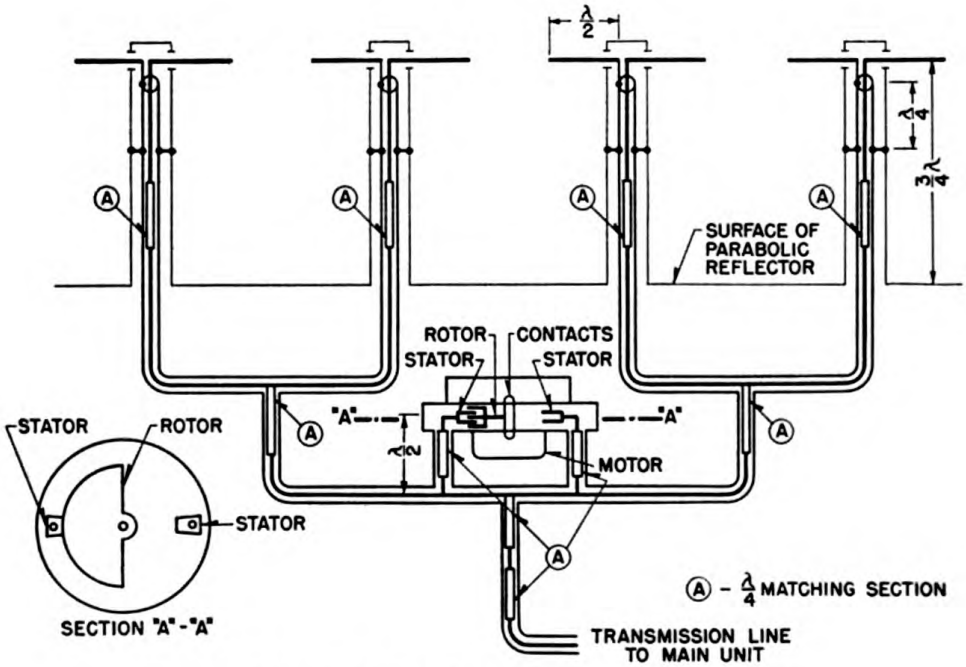

Fig. 26—Mark 2 & 3—Antenna schematic

frequency adjustments, in order to simplify operation and maintenance. The manner in which these objectives were met is described below.

To obtain lobe switching of the antenna beam, use was made of the fact

Digitized by Google
Original from UNIVERSITY OF MICHIGAN
Generated on 2019-09-21 08:36 GMT / http://hdl.handle.net/2027/mdp.39015077775156
Public Domain, Google-digitized / http://www.hathitrust.org/access_use#pd-google

that the beam position depends upon the relative phase of the excitation applied to the radiating elements of the array. If all elements are excited in phase, as in Radar Mark 1, the beam will be normal to the line of the array, while gradually increasing phase difference across the array will result in displacement of the beam. For small angles of beam shift, entirely satisfactory results may be obtained by shifting the phase of excitation applied to one-half of the array with respect to the other, and this expedient results in a much simpler phase shifting mechanism than would be required to obtain uniform phase change. This system was used in Radar Mark 3 and its application is illustrated schematically in Fig. 26. It will be seen that this array is identical to that used for Radar Mark 1 except for the central section of transmission line in which a lobe switching unit has been added. In this unit the phase of excitation to one-half of the array is retarded with respect to the other half by connecting a capacitive reactance alternately across one feed line or the other to obtain the two beam positions. Switching is accomplished by the use of a motor driven rotary capacitor shown in Section A-A. The rotor is a semicircular aluminum casting which is maintained at substantially ground potential by very close spacing to the grounded metal housing. The two stators are small metal plates which interleave with the rotor during approximately one-half revolution and are connected through half-wavelength coaxial lines to the antenna transmission lines. The purpose of the half-wavelength stub lines is to avoid physical limitations which would otherwise be encountered in connecting the rotary capacitor to the lines. Allowance is made in these stubs for end-loading caused by stray capacitance of the stator plates and supporting insulators. It will be seen that during nearly one-half revolution of the rotor one of the stators is engaged to shift the antenna beam in one direction while during the other half revolution the other stator is engaged to produce the other lobe position. The switching occurs during the small interval in which both stators are engaged by the rotor. Signals received during this interval are blanked out in the indicator. The rotor of the lobe switcher is driven at about 30 RPS by an induction motor mounted within a weatherproof housing. The motor shaft also carries cam operated contacts to produce image spacing on the indicators, control signals for the Train Meter, and blanking during the lobe switch interval. The entire unit is gas tight and is filled with dry gas through the transmission line.

The value of the lobe switching capacitor and its position along the feed line must satisfy two conditions: first, the phase shift must be such that the antenna beam will be displaced by the desired amount; and second, the impedance at the feed point must be such that equal division of power will be obtained in the two halves of the array. In the first Radar Mark 3 antenna (6 ft. by 6 ft. parabolic array) a beam displacement of about 3.0

Digitized by Google
Original from UNIVERSITY OF MICHIGAN
Generated on 2019-09-21 08:36 GMT / http://hdl.handle.net/2027/mdp.39015077775156
Public Domain, Google-digitized / http://www.hathitrust.org/access_use#pd-google

degrees was chosen as a suitable compromise between target angle sensitivity (steepness of beam) and reduction of signal amplitude "on target". This displacement required a phase shift of approximately 53 degrees between the two halves of the array. From transmission line theory it can be shown that this phase difference will be obtained with a capacitive reactance equal to the characteristic impedance of the feed line when connected at a point 0.176 wavelength from the feed point. It can also be shown that this condition satisfies the requirement for equal power division to the two halves of the array. A capacitor of the required value (about 3 micromicrofarads) can readily be built to withstand the peak transmitted power by proper condenser plate separation. A frequency variation of about 40 megacycles can be tolerated without materially affecting the antenna performance.

TABLE II.—*Antenna Characteristics*

	Radar Mark 3		Radar Mark 4
Dimensions	3′ x 12′	6′ x 6′	6′ x 7′
Apperture in Wavelengths			
Azimuth	8.5	4.25	4.25
Elevation	2.1	4.25	4.95
Beam Width in Degrees (between half power points in one way pattern)			
Azimuth	6	12	12
Elevation	30	14	12
Antenna Gain in db	22.0	22.0	22.5
Beam Shift in Degrees			
Azimuth	±1.5°	±3.0°	±3.0°
Elevation	—	—	±3.0°

A lobe switching unit similar to that described above was also applied to the 3 ft. by 12 ft. antenna. Pertinent information regarding beam widths and lobing angles for both antennas (together with information on the antenna for Radar Mark 4 to be described later) is given in Table II.

The effective beam widths as used in these radars were somewhat narrower than the values given above due to the square law characteristic of the second detector in the receiver, and the deflection sensitivity was such that the specified tracking accuracy of ±15 minutes of arc could readily be achieved. The "on target" position or axis of the antenna (lobe crossover) was carefully aligned with the optical telescopes at the time of installation so that either optics or radar angles could be used. The symmetrical design of the antenna made this alignment substantially independent of small changes in operating frequency.

To minimize target confusion the signals presented on the Train or Elevation Indicator (azimuth operator's oscilloscope) consisted only of

Generated on 2019-09-21 08:36 GMT / http://hdl.handle.net/2027/mdp.39015077775156
Public Domain, Google-digitized / http://www.hathitrust.org/access_use#pd-google
Digitized by Google
Original from UNIVERSITY OF MICHIGAN

those received from the target being tracked by the range operator, all others being blanked out in the indicator circuits.

Accurate Range Measurement

The second major problem which required solution to adapt radar to the fire control problem was the provision of means for accurate and continuous range tracking. It was obvious that what was required was some sort of electronic range mark on the indicator sweeps, the position of which could be varied by a rotary device whose motion could be used to transmit range information to a remote point over a synchro system. The range mark could then be aligned with the target "pip" on the oscilloscope. For accurate data transmission it was necessary to obtain a linear relationship between angular rotation of the range handwheel and corresponding range to the marker on the radar indicator screen.

One method which was first employed by the Signal Corps made use of the fact that the transmitted pulses were generated at a periodic rate from a sine wave oscillator of fixed frequency; the pulse being produced at a fixed point in each cycle. By transmitting this same sine wave through a linear phase shifter a new pulse could be generated whose position in time, relative to the transmitted pulse, could be varied by rotation of the phase shifter. In the Signal Corps equipment a special goniometer was used to produce the phase shift and the accuracy obtained was considered adequate for the intended purpose. However, non-linearity of the phase shifting device, though small, was much greater than could be tolerated in the Navy fire control system. A study indicated that large scale manufacture of special phase shifters, hand adjusted to meet the stringent accuracy requirements was out of the question. It was therefore decided that a two speed system be used, in which the phase shifter errors would be divided by the gear ratio to the high-speed unit in much the same way that accurate synchro information is transmitted by a "coarse" and a "fine" synchro. The manner in which this was worked out by Bell Telephone Laboratories and applied to Radars Mark 3 and 4 is described below.

The method of range measurement can perhaps best be understood by first examining the method of presentation used on the cathode ray tube indicator for the range operator. This presentation is shown in Fig. 27 in which it will be noted that a Class A sweep is used to display the transmitted pulse and received echoes. This horizontal sweep, however, differs from the simple sweep of earlier radars in several respects. First, the central portion of the sweep is expanded to permit more accurate viewing of signals appearing within this region; second, a downward deflection called the range "notch" is produced in the approximate center of the expanded section; and third, the circuits are so arranged that the notch

Digitized by Google
Original from UNIVERSITY OF MICHIGAN
Generated on 2019-09-21 08:37 GMT / http://hdl.handle.net/2027/mdp.39015077775156
Public Domain, Google-digitized / http://www.hathitrust.org/access_use#pd-google

remains centered as the range unit phase shifters are rotated thus causing all of the signals (rather than the notch) to move across the screen. Range measurement is made by rotating the range unit handcrank to place the desired signal in the center of the range notch on the indicator. This type of presentation has several advantages. It permits the full 100,000-yard range to be viewed at all times so that new targets may be immediately detected, and permits accurate viewing of the desired target in the expanded

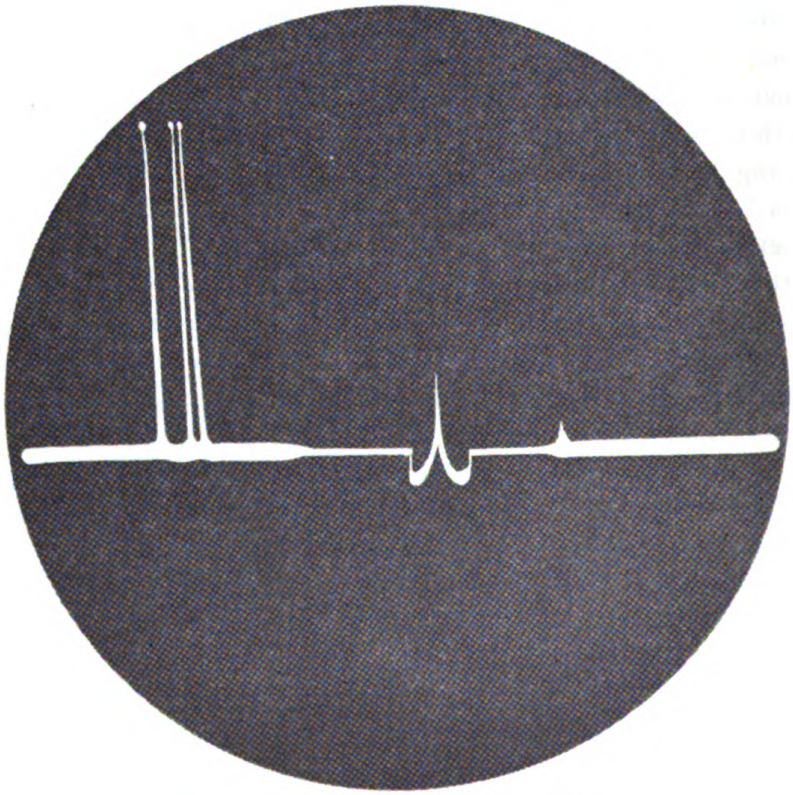

Fig. 27—Mark 3 & 4—Range presentation

center of the sweep where best focus is obtained. For smooth range tracking it is only necessary for the operator to rotate the range unit hand crank to keep the desired signal centered in the range notch.

A block diagram of the range measuring system, together with the circuits used to obtain the cathode ray indicator presentation described above, is shown in Fig. 28. A base or reference oscillator generates a sine wave of 1.639 kc, one cycle of which corresponds to a radar range of 100,000 yards. This wave, after amplification, is applied to a non-linear coil pulse generator[3] which generates short pulses (one positive and one negative pulse

[3] "Magnetic Generation of a group of Harmonics," E. Petersen, J. M. Manley, L. R. Wrathall—August 1937, *B. S. T. J.*, October 1937.

Digitized by Google
Original from UNIVERSITY OF MICHIGAN
Generated on 2019-09-21 08:37 GMT / http://hdl.handle.net/2027/mdp.39015077775156
Public Domain, Google-digitized / http://www.hathitrust.org/access_use#pd-google

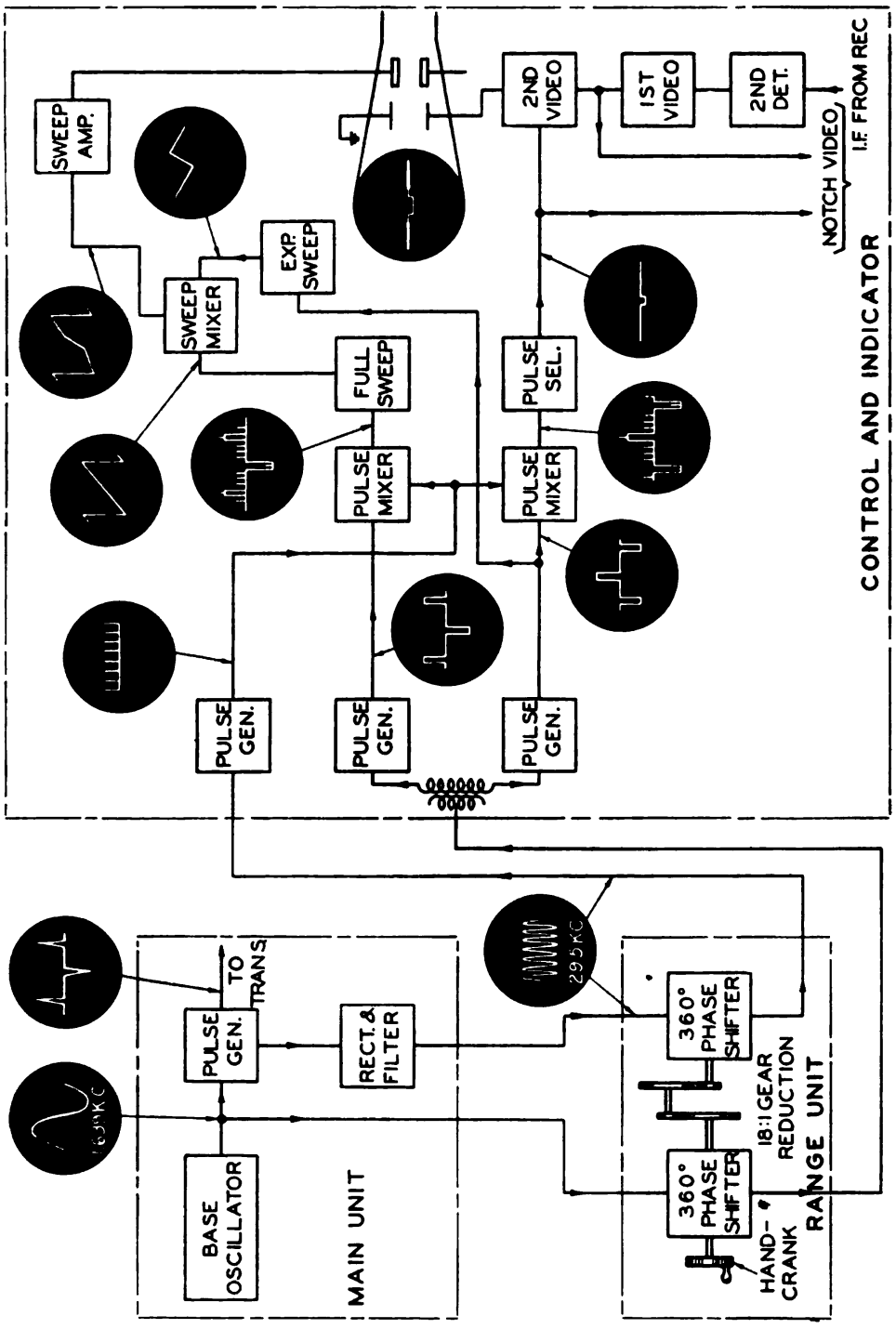

Fig. 28—Mark 3 & 4—Range measuring system

Generated on 2019-09-21 08:37 GMT / http://hdl.handle.net/2027/mdp.39015077775156
Public Domain, Google-digitized / http://www.hathitrust.org/access_use#pd-google
Digitized by Google
Original from UNIVERSITY OF MICHIGAN

per cycle); the positive pulses being used for keying the transmitter. These pulses are rich in odd harmonics of the base oscillator frequency. By rectifying these pulses to reverse the negative pulses, even harmonics of the base frequency are obtained and the 18th harmonic (29.5 kc) is selected by means of a filter. This harmonic frequency and the original base frequency are applied to two phase shifters whose shafts are geared together in the ratio of 18 to 1. Since one revolution of the one speed phase shifter corresponds to 100,000 yards, one revolution of the 18-speed unit corresponds to only 5550 yards with the result that range errors caused by non-linearity of this phase shifter are reduced by a factor of 18. The phase shifters employed are similar to those designed by Bell Telephone Laboratories for use in a phase measuring bridge[4] and are linear to within ± 1.5 degrees or about 0.4 per cent. The possible range error introduced by imperfections in the 18-speed phase shifter was therefore only 23 yards, well within the design requirements. It remains to be shown how this accurate range information was applied to the indicator.

The output of the 18-speed phase shifter in the range unit is connected to the Control and Indicator where the phase shifted sine wave is used to generate short, rectangular pulses of about 600 yards duration. One pulse is produced for each cycle of the 29.5 kc wave so that 18 of them occur during the 100,000-yard sweep interval. It is desired that only one of these pulses appear as a range notch on the indicator screen and this pulse is selected from the others by a pedestal pulse generated from the output of the one speed phase shifter. It will be noted that as the phase shifters are rotated by means of the range unit hand crank, the desired pulse from the 18-speed phase shifter will remain substantially centered on the one-speed pedestal pulse. After further shaping, the selected pulse is mixed with the received signals in the second video amplifier and is then applied to the vertical plates of the cathode ray indicator to form the "range notch". The range notch is also transmitted to the Train Indicator and Train Meter where it is used to prevent any signal from affecting those instruments except the one being tracked by the range operator.

Since it is desired to have the range notch appear in the center of the 100,000-yard sweep on the indicator, the sweep trigger pulse must occur 50,000 yards in advance of the notch. This trigger is obtained by selection of another pulse from the accurate phase shifter, this time using a one-speed pedestal produced by an input of reversed phase. The pulse thus selected is used as a trigger for starting a saw-tooth sweep wave with a duration corresponding to 100,000 yards radar range. Expansion of the center portion of this sweep is obtained by adding to this wave a second

[4] L. A. Meacham, U. S. Patent 2004613.

Digitized by Google
Original from UNIVERSITY OF MICHIGAN
Generated on 2019-09-21 08:37 GMT / http://hdl.handle.net/2027/mdp.39015077775156
Public Domain, Google-digitized / http://www.hathitrust.org/access_use#pd-google

saw-tooth wave having maximum rate of change in the center of the sweep; the latter being derived from the range notch selection pedestal. The combined sweep is then applied to the horizontal plates of the cathode ray tube. The return trace is blanked by applying to the control grid of the cathode ray tube a voltage obtained by differentiating the sweep waveform.

Transmitter

As mentioned earlier the transmitter oscillator tube problem was one of the major obstacles in the march of radar development to higher frequencies. Intense development effort on many possible types of tubes was underway in several laboratories in this country and abroad during 1939

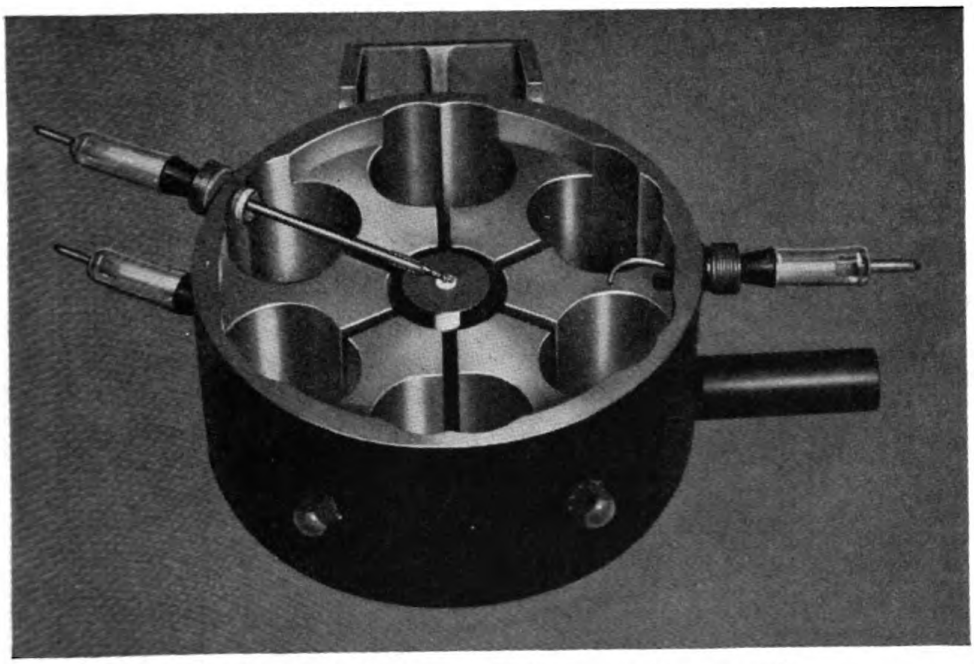

Fig. 29—W. E. 700-type magnetron—one side removed

and 1940. The first significant improvement came in England where work with multicavity magnetrons showed that this device was probably the answer to radar's need for a highly intermittent duty oscillator suitable for high power in the microwave region. A sample of this device was brought to this country by the Government and was tested in Bell Telephone Laboratories in October 1940. It produced pulses of several kilowatts at a frequency in the neighborhood of 3000 mc. A tremendous development of this device got under way immediately[5] and the multicavity magnetron

[5] "The Magnetron as a Generator of Centimeter Waves," J. B. Fisk, H. G. Hagstrum, and P. L. Hartman. See pp. 56 ff.

Digitized by Google
Original from UNIVERSITY OF MICHIGAN
Generated on 2019-09-21 08:37 GMT / http://hdl.handle.net/2027/mdp.39015077775156
Public Domain, Google-digitized / http://www.hathitrust.org/access_use#pd-google

became the key piece in the enormous development of radar equipment for still higher frequencies during the war. However, at the beginning of 1941 there were still many unsolved problems in 3000 mc radar other than that of the transmitter tube. On the other hand, the systems problems had been quite satisfactorily solved in the 700-mc region. The decision was therefore immediately made to extrapolate the British design down to

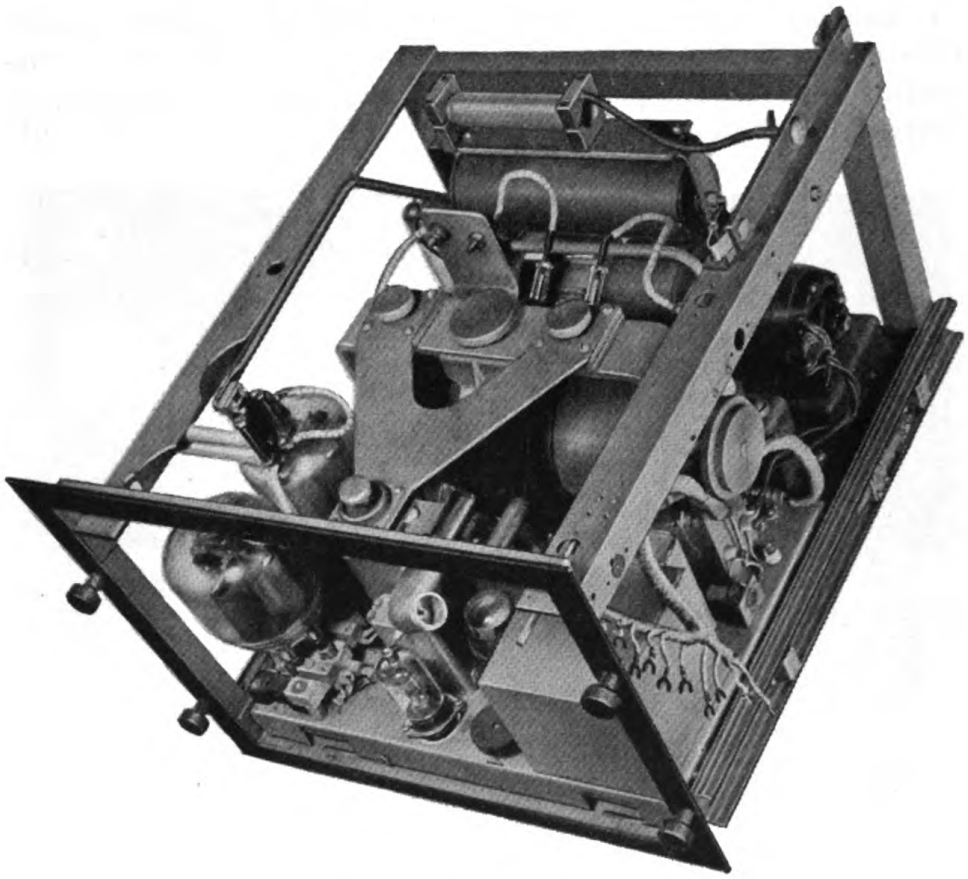

Fig. 30—Mark 3 & 4—transmitter

700 mc in order to obtain a higher powered and more satisfactory oscillator for the existing systems. This was done at top speed and a picture of the resulting tube is shown in Fig. 29. This was the first type of multi-cavity magnetron to go into production in this country. Concurrent with the design of the new magnetron the vacuum tube department of the Laboratories developed an improved tetrode modulator tube which was many times as efficient for radar pulse service as the triodes formerly used. This tube was designated W.E. 701-A.

A new transmitter using the magnetron and two of the new modulator

Digitized by Google
Original from UNIVERSITY OF MICHIGAN
Generated on 2019-09-21 08:38 GMT / http://hdl.handle.net/2027/mdp.39015077775156
Public Domain, Google-digitized / http://www.hathitrust.org/access_use#pd-google

tubes was rushed through development and produced in time to go with the first accurate fire control radars. This transmitter provided a peak power output of about 40 kw with a pulse duration of 2 microseconds. It resulted in a material increase in reliable range, with satisfactory tube life. The new transmitter, shown in Fig. 30, was made mechanically interchangeable with the old and was applied retroactively also to the Mark 1 Radars.

Duplexing

The use of the high-power transmitter required additional protection for the receiver during the transmitted pulse in order to prevent damage

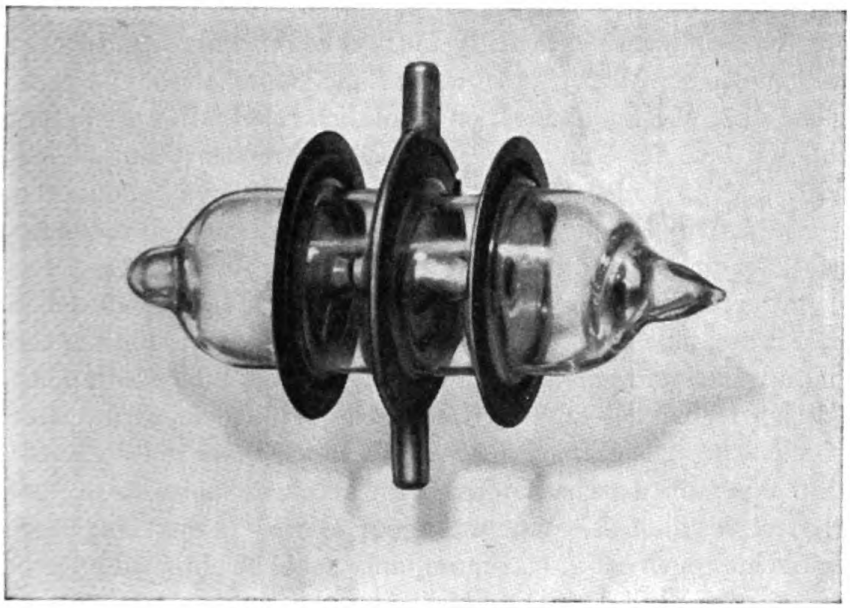

Fig. 31—W. E. 702—TR tube

and to permit the receiver to recover rapidly for reception of nearby echoes. The duplexing equipment was therefore modified to include a gas switching tube in the receiving transmission line. This was a refinement of the method used earlier by the Naval Research Laboratory.

The switching tube (W.E. 702A) was developed specifically for this purpose and is shown in Fig. 31. It was the first of the "TR" tubes of this general form and consists of a hydrogen-water vapor filled glass chamber with three copper electrodes.[6] This tube was mounted in the center of a half-wavelength coaxial line short circuited at each end, the outer conductor being connected to the outer electrodes and the center conductor

[6] "The Gas Discharge Transmit-Receive Switch," A. L. Samuel, J. W. Clark, and W. W. Mumford. See pp. 310 ff.

Digitized by Google
Original from UNIVERSITY OF MICHIGAN
Generated on 2019-09-21 08:38 GMT / http://hdl.handle.net/2027/mdp.39015077775156
Public Domain, Google-digitized / http://www.hathitrust.org/access_use#pd-google

to the middle electrode. Input and output connections were tapped on this half-wave line near the short circuited ends. During reception this assembly introduces negligible loss in the receiving line. However, during the transmitted pulse a small amount of the transmitted power ionizes the gas in the switching tube and effectively short-circuits the receiver line. This device, which in later forms came to be called a "T-R Box", is located near the receiver input and the length of line between it and the junction with the transmitter line can be adjusted to an odd multiple of quarter wavelengths to present the desired high impedance at that point during transmission.

Receiver

The receiver delivered with early Mark 3 equipments was identical to that used in Radar Mark 1. It was of the superheterodyne type employing one stage of RF amplification (doorknob tube), 316A oscillator tube, and doorknob first detector. The intermediate frequency amplifier had a bandwidth of about 1 megacycle at a midband frequency of about 30 megacycles. The second detector and video stages were located in the indicating equipment. A photograph of this receiver is shown in Fig. 11.

Since in microwave work the controlling noise is that produced in the receiver, it is desirable to reduce this noise to the theoretical limit of thermal agitation in the input circuit. However, in 1939 tube limitations and circuit design techniques at these frequencies resulted in performance far short of this goal. The amount by which the receiver noise exceeds the theoretical minimum has been termed the receiver "noise figure" and in this early receiver the noise figure was about 24 db. It was recognized that considerable improvement in maximum range could be obtained by reducing this receiver noise.

Shortly after first deliveries of Radar Mark 3 a new tube (GL-446 or "lighthouse" tube) was made available by the General Electric Company which showed promise of providing a substantial improvement in the receiver noise figure. An amplifier using this tube was accordingly designed by Bell Laboratories in which coaxial cavities were used for tuning elements. Two stages of amplification were used to replace the single "doorknob" tube stage previously employed. The new amplifier resulted in a reduction of the receiver noise figure to about 9 db and provided a marked improvement in maximum range capability of the radar. These amplifiers were manufactured and shipped to the Fleet for field installations on early equipments and were included in production on equipments shipped subsequently to availability of the amplifiers. A photograph of the receiver with the two amplifiers installed is shown in Fig. 32.

Another field modification provided automatic gain control of the signal

Digitized by Google
Original from UNIVERSITY OF MICHIGAN
Generated on 2019-09-21 08:39 GMT / http://hdl.handle.net/2027/mdp.39015077775156
Public Domain, Google-digitized / http://www.hathitrust.org/access_use#pd-google

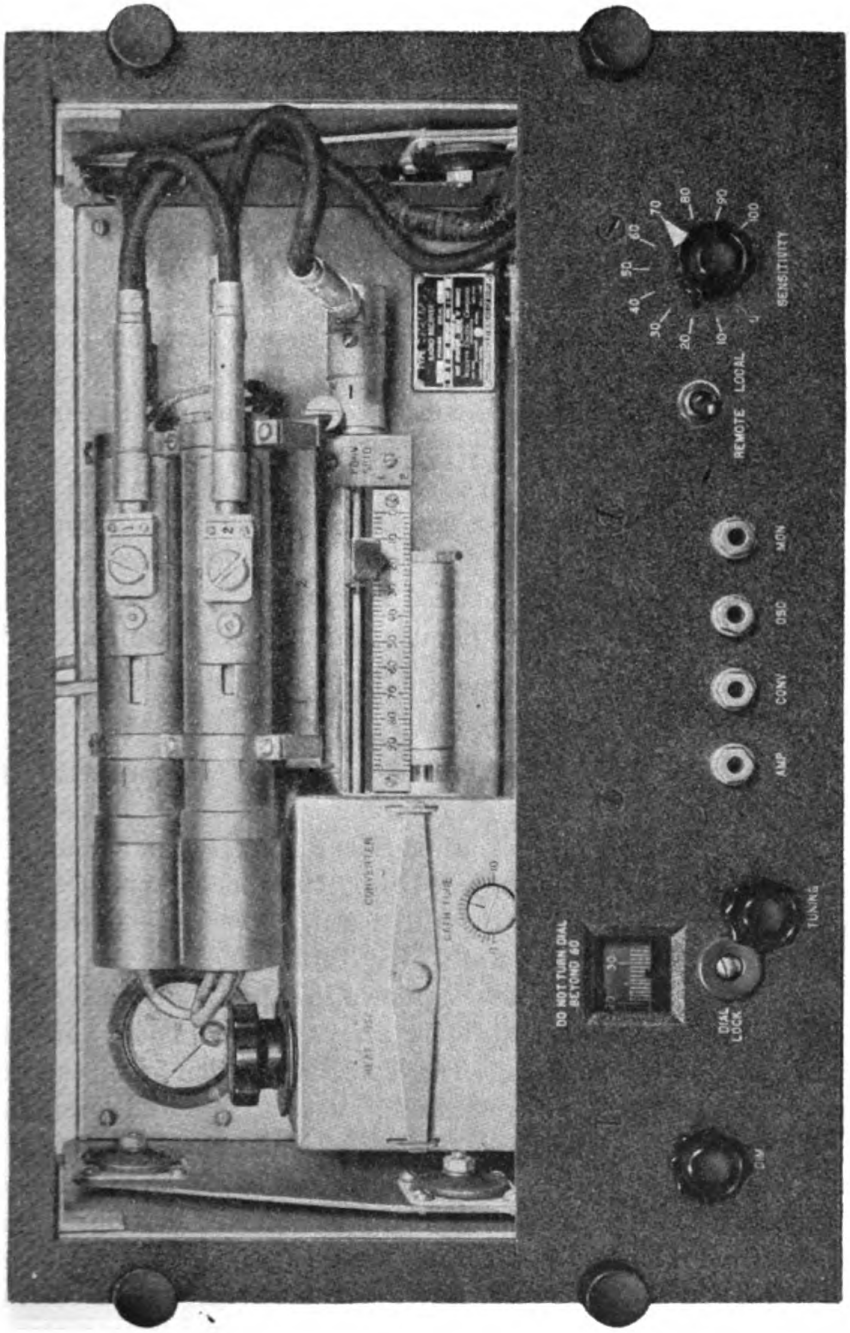

Fig. 32—Receiver—showing improved R. F. amplifier

Digitized by Google
Original from UNIVERSITY OF MICHIGAN
Generated on 2019-09-21 08:39 GMT / http://hdl.handle.net/2027/mdp.39015077775156
Public Domain, Google-digitized / http://www.hathitrust.org/access_use#pd-google

selected by the range operator. This was supplied in the form of an external unit which controlled the gain of the receiver IF amplifier to reduce signal fluctuations produced by fading.

The first production Mark 3 Radars were delivered to the Navy in October 1941, and the first two installations were completed on the main battery directors of the U.S.S. Philadelphia at the Brooklyn Navy Yard that month.

Radar Mark 4

During the development work on Radar Mark 3 the Navy pointed out the need for a fire control radar for use with the 5-inch Naval guns against enemy aircraft. The Bell Telephone Laboratories was therefore requested to further modify the radar design to meet this need. The anti-aircraft equipment was first designated FD, later becoming known as Radar Mark 4.

For antiaircraft fire control a new coordinate had to be added to the target-locating system; namely, elevation angle. Again it was desired that the additional information be obtained from the single antenna with a precision equal to that already obtained in azimuth. This problem was approached in a manner similar to that used for the Mark 3 antenna and is described below.

Two Plane Lobe Switching

In considering two plane lobe switching methods it appeared that the desired result could be obtained by mounting two 3 ft. x 6 ft. parabolic arrays one above the other. This arrangement was tried and resulted in the array shown in Fig. 33. It provided two plane lobe switching with an antenna only slightly larger than the 6 ft. x 6 ft. antenna used before and had comparable gain and beam width (see Table II).

A schematic diagram of the array is shown in Fig. 34. Here it will be seen that there are two horizontal dipole arrays, each mounted along the focal line of a cylindrical parabola. The dipoles are in four groups and the interconnecting harness is criss-crossed and joined to the feed line at the center. Symmetrically placed around the feed point are four stub lines connected to the lobe switcher stators. Here again a semi-circular rotor is used for the lobing shifting capacitor. It will be observed that during each quarter turn of the rotor two stator plates are engaged, and the sequence is such that the beam shifts left, up, right, and down during one rotation. A separate Indicator was provided for the Pointer (elevation operator). To avoid signal confusion on the two Indicators it is necessary to show only left-right signals on the Trainer's oscilloscope and up-down signals on the Pointer's oscilloscope. This is accomplished by means of cam operated contacts in the lobe switcher which blank the indicators during the required

Digitized by Google
Original from UNIVERSITY OF MICHIGAN
Generated on 2019-09-21 08:39 GMT / http://hdl.handle.net/2027/mdp.39015077775156
Public Domain, Google-digitized / http://www.hathitrust.org/access_use#pd-google

intervals. Other contacts on this assembly provide left-right and up-down image spacing.

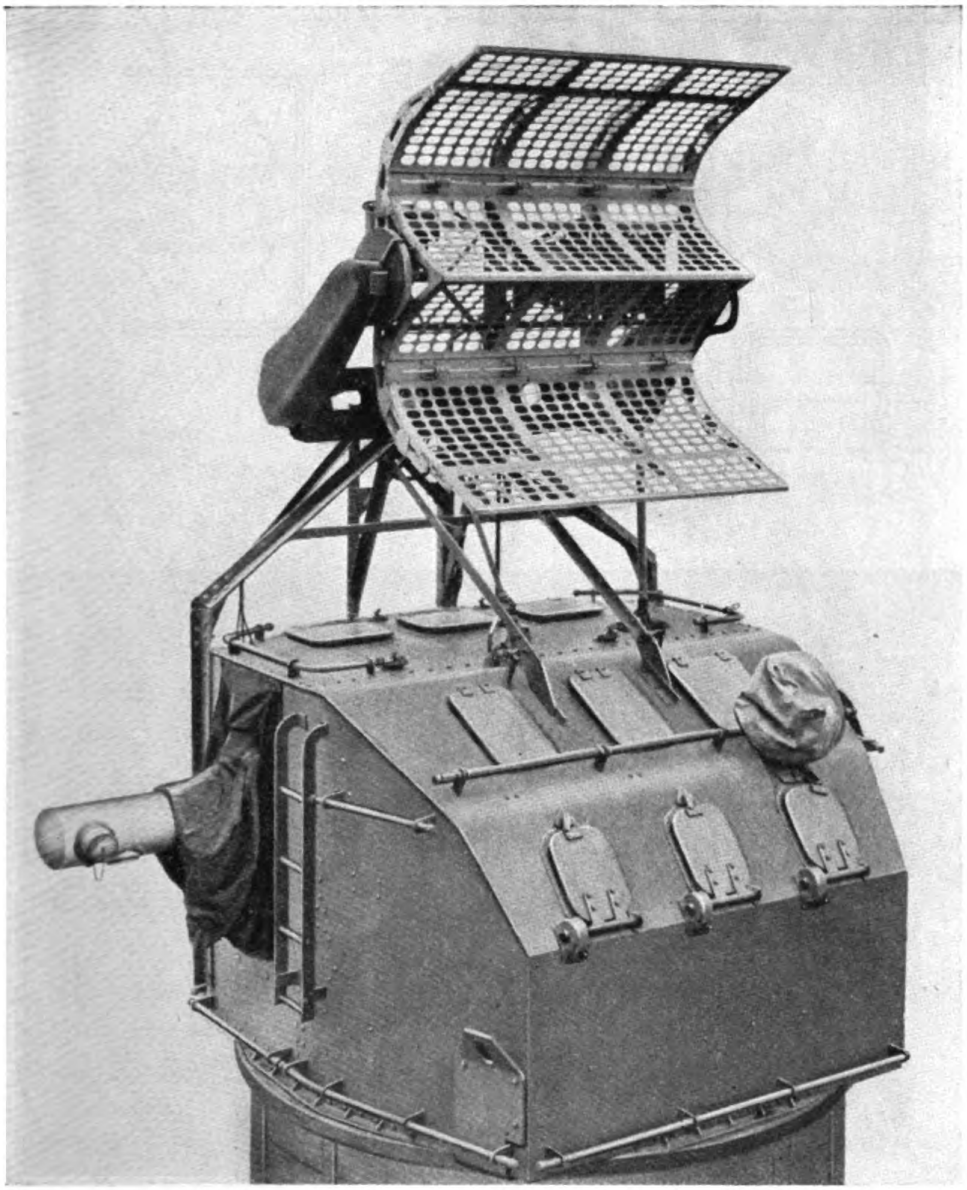

Fig. 33—Mark 4—antenna on gun director

Except for the new antenna and the additional Train or Elevation Indicator for the Pointer (elevation operator), this radar was identical to Radar Mark 3. The first demonstration of a development model of Radar Mark 4 was made at Atlantic Highlands, New Jersey, in September 1941 and this model was installed aboard the destroyer U.S.S. Roe the latter

Digitized by Google
Original from UNIVERSITY OF MICHIGAN
Generated on 2019-09-21 08:39 GMT / http://hdl.handle.net/2027/mdp.39015077775156
Public Domain, Google-digitized / http://www.hathitrust.org/access_use#pd-google

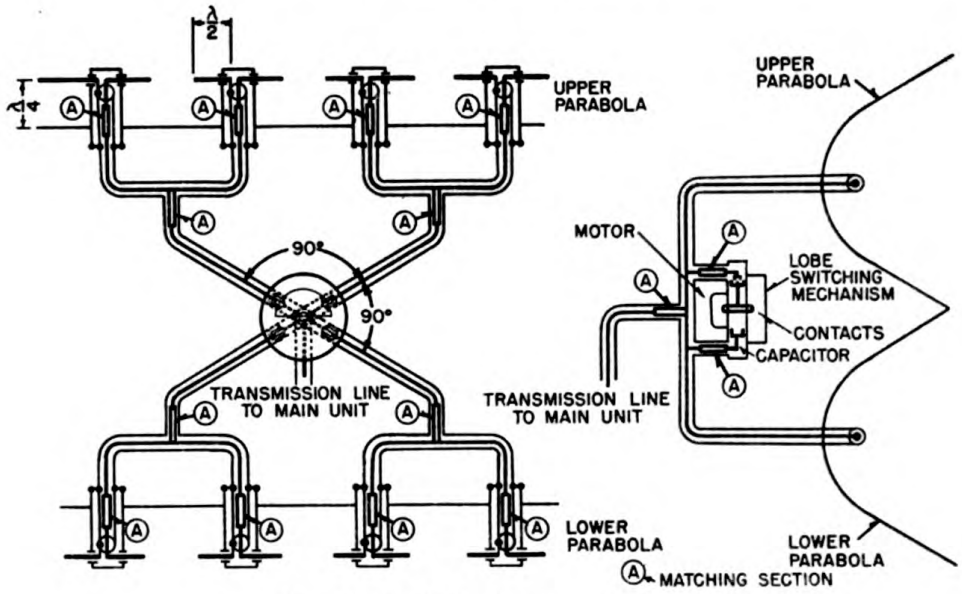

Fig. 34—Mark 4—Antenna schematic

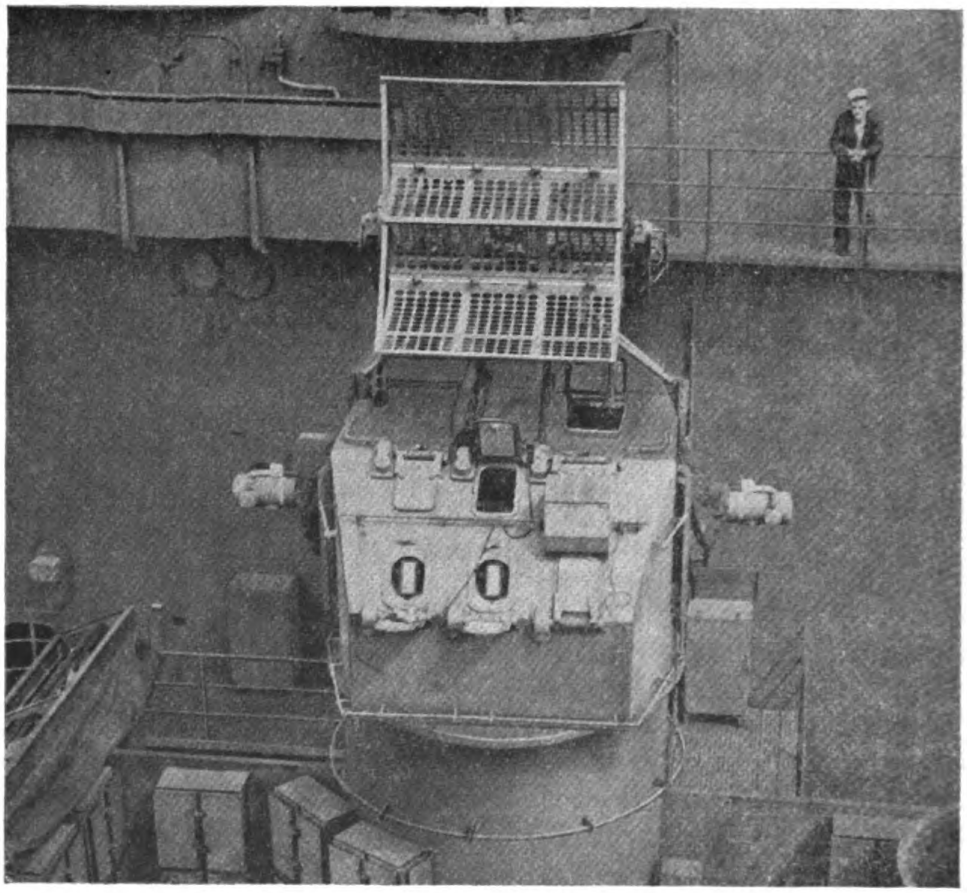

Fig. 35—Mark 4 antenna on Battleship Tennessee (Navy Photo 1908-43)

Digitized by Google
Original from UNIVERSITY OF MICHIGAN
Generated on 2019-09-21 08:40 GMT / http://hdl.handle.net/2027/mdp.39015077775156
Public Domain, Google-digitized / http://www.hathitrust.org/access_use#pd-google

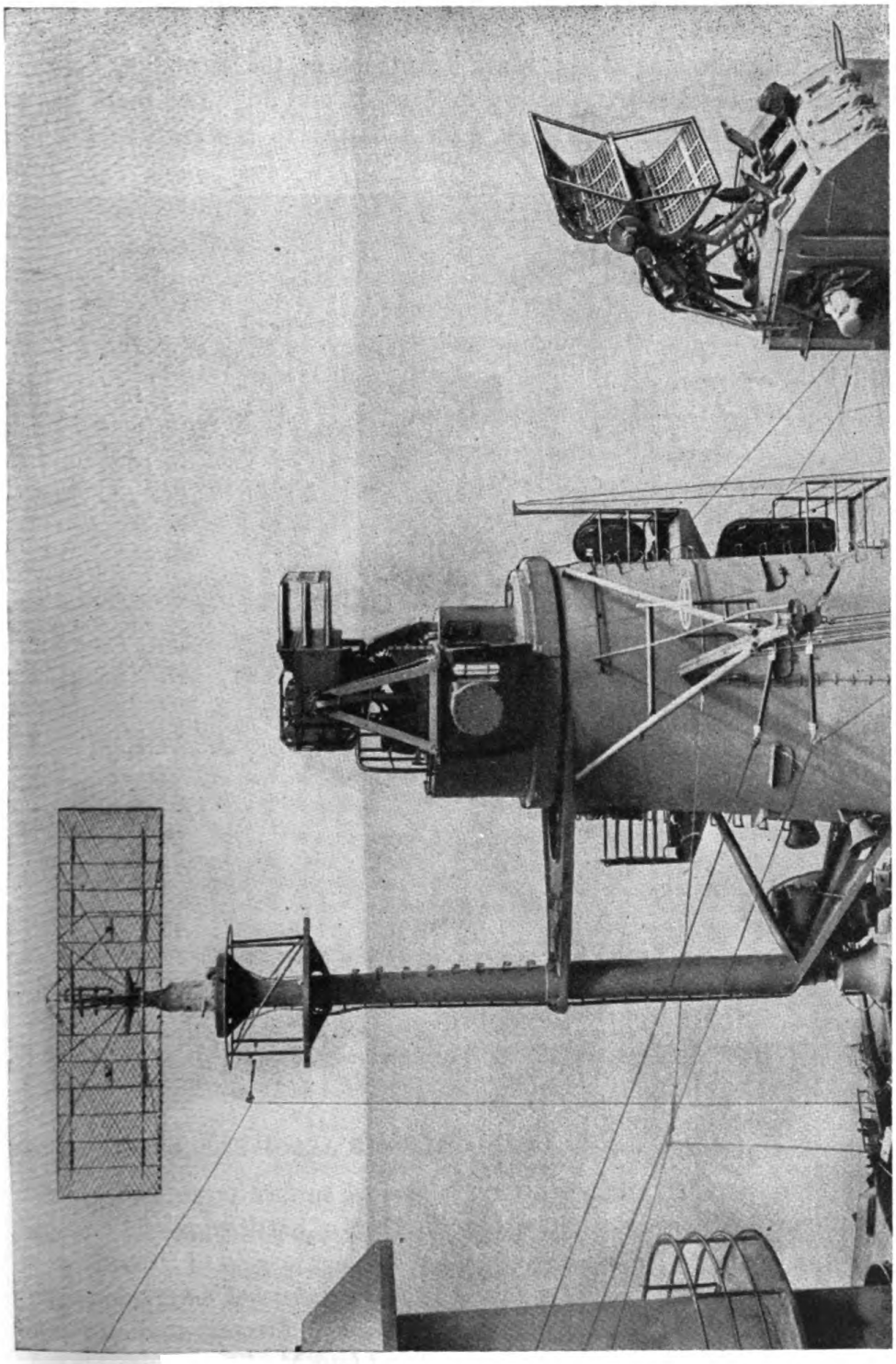

Fig. 36—Radar antennas on Battleship Tennessee (Navy Photo 1905-43)

Digitized by Google
Original from UNIVERSITY OF MICHIGAN
Generated on 2019-09-21 08:40 GMT / http://hdl.handle.net/2027/mdp.39015077775156
Public Domain, Google-digitized / http://www.hathitrust.org/access_use#pd-google

part of that month. Initial production deliveries of these radars were made in December 1941.

Typical installations of the Mark 4 Antenna on the secondary battery directors of a battleship are shown in Figs. 35 and 36. The main frame installation for Mark 3 and Mark 4 on a battleship is shown in Fig. 37

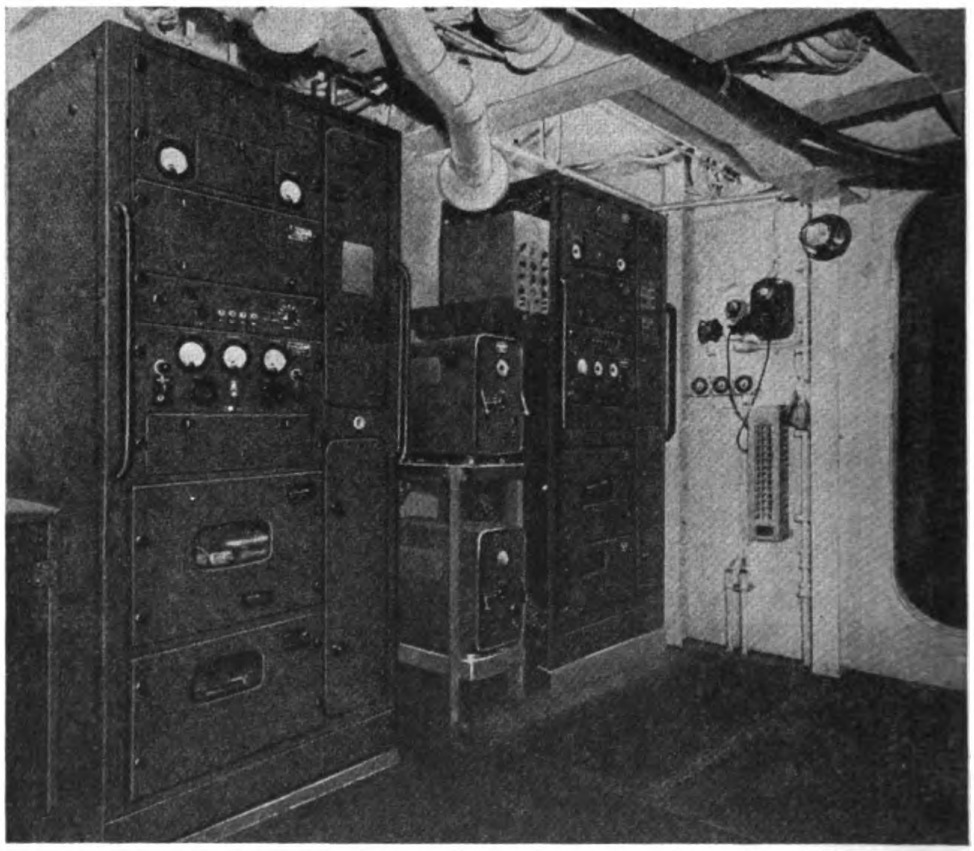

Fig. 37—Radars Mark 3 & 4—main units on Battleship New Jersey (Navy Photo 181809)

while typical installations of the train and elevation operator's units in the director are shown in Figs. 38 and 39.

Application and Use of Mark 3 and 4 Radars

The Mark 3 radars, designed for use against surface targets only, were generally installed on the main battery directors of battleships and cruisers. The Mark 4 radars for use against either surface targets or aircraft were generally installed on the secondary battery directors of battleships and cruisers, and on the one and only dual purpose director on destroyers. Thus a battleship usually had two Mark 3 and four Mark 4 equipments and a destroyer one Mark 4. Practically every ship in the fleet, of destroyer

Digitized by Google
Original from UNIVERSITY OF MICHIGAN
Generated on 2019-09-21 08:42 GMT / http://hdl.handle.net/2027/mdp.39015077775156
Public Domain, Google-digitized / http://www.hathitrust.org/access_use#pd-google

size or larger, was equipped with one or more of these equipments early in the war. A total of 139 Mark 3, and 670 Mark 4 radars were built, including those used ashore at schools. Although some of these equipments were replaced by more modern designs before the end of the war and some were lost in battle, there were still approximately 85 Mark 3 and 300 Mark 4

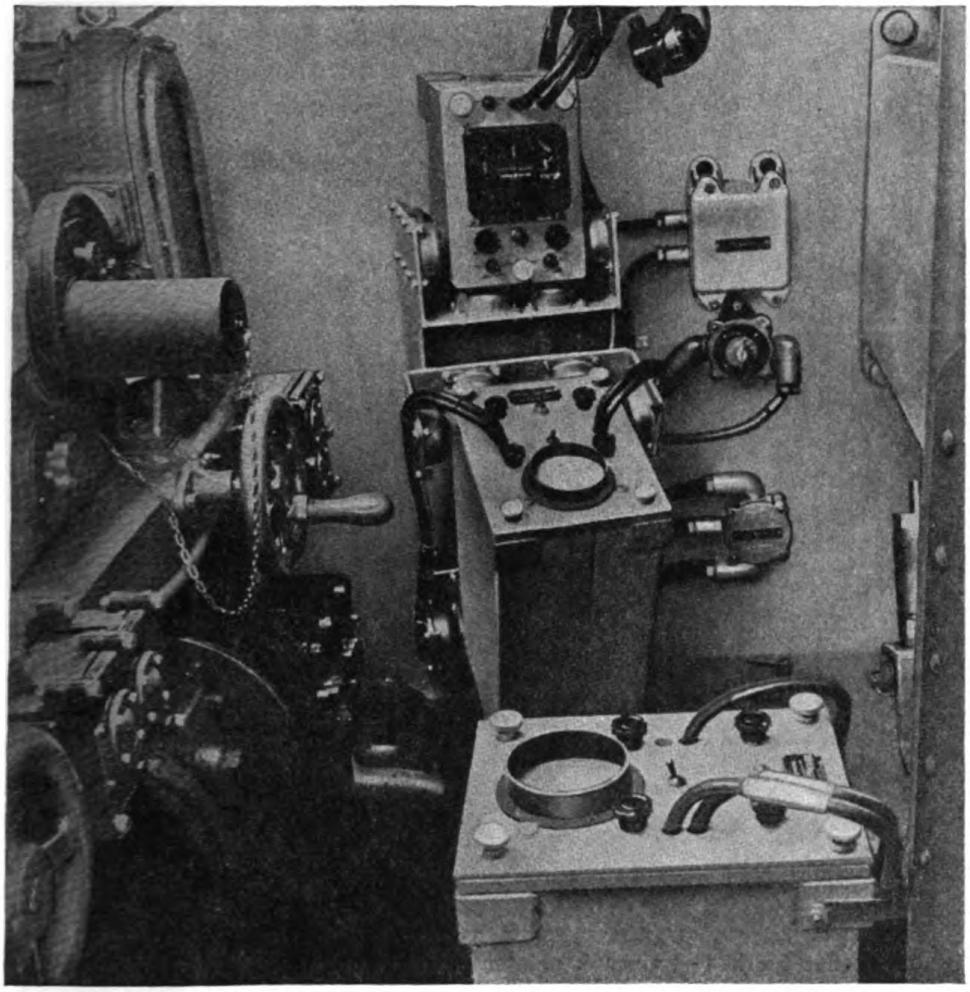

Fig. 38—Mark 4 Radar—trainer & pointer operators' positions on Aircraft Carrier Saratoga (Navy Photo 177347)

radars in service in the fleet on V-J day. The first four Mark 4's, Serial Nos. 1, 2, 3 and 5 installed on the battleship Washington were used until the middle of 1945, although newer designs had been going on all new vessels for more than a year.

These early equipments were the "guinea pigs" of fire control radar. They were the instruments with which our fleet learned to fight effectively

Digitized by Google
Original from UNIVERSITY OF MICHIGAN
Generated on 2019-09-21 08:42 GMT / http://hdl.handle.net/2027/mdp.39015077775156
Public Domain, Google-digitized / http://www.hathitrust.org/access_use#pd-google

at night and thereby gain a large advantage over the enemy whose radar was feeble and inaccurate. They played a part in every one of the early battles and most of the later ones in the Pacific. They controlled the cruiser Boise's guns in October 1942, when she blazed away at night at a vastly superior fleet in the Solomons and made the enemy pay 10 to 1 for the

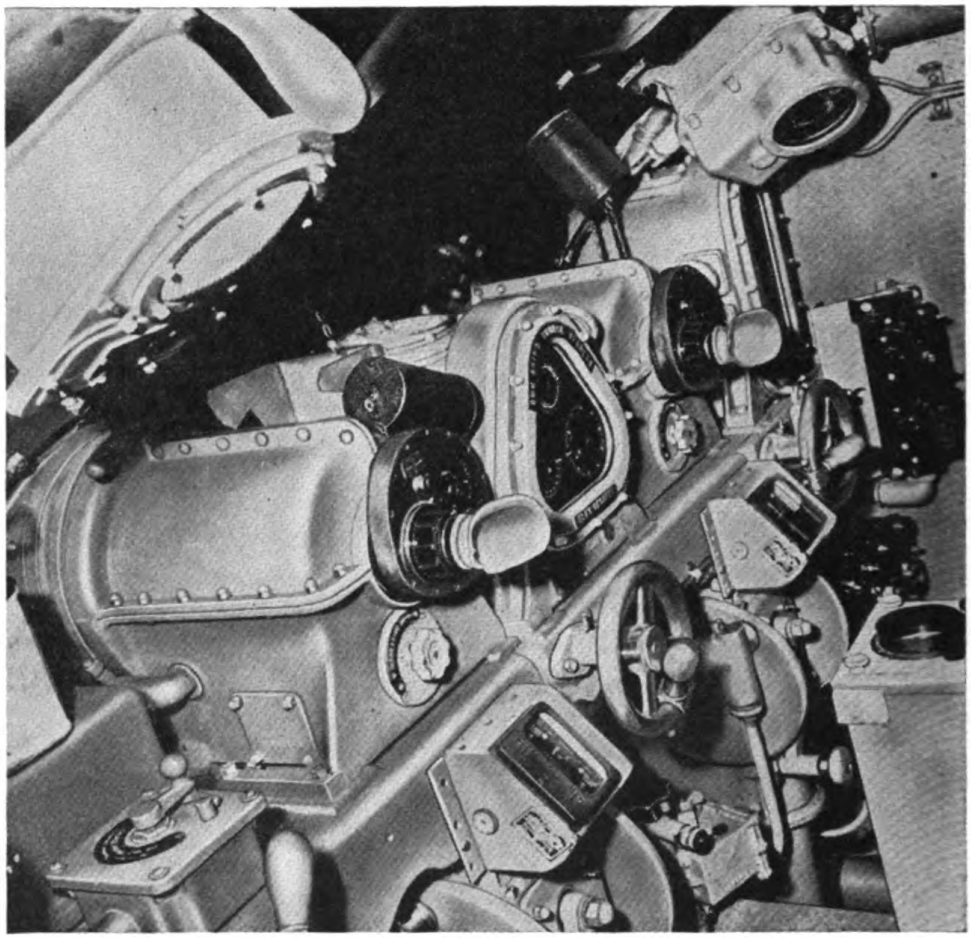

Fig. 39—Radar Mark 4—trainer & pointer operators' positions on Destroyer Barton (Navy Photo 181775)

damage they succeeded in doing. They were with the cruiser San Francisco on a night in November 1942, when a small U. S. force sank 27 enemy ships, almost completely destroying a large Japanese convoy bound for Guadalcanal when our hold there was at best precarious. The Mark 3 steered the big guns of the battleship South Dakota in the Solomons on the dark night of November 4, 1942, when she sank a major Japanese war vessel eight miles away with two salvos. Even in engagements in broad daylight when optics could be used for target angles these radars still played a vital

Digitized by Google
Original from UNIVERSITY OF MICHIGAN
Generated on 2019-09-21 08:42 GMT / http://hdl.handle.net/2027/mdp.39015077775156
Public Domain, Google-digitized / http://www.hathitrust.org/access_use#pd-google

part in furnishing accurate range which made 5″ gunfire against aircraft, for example, deadly at long range. Thus on October 16, 1942, when the South Dakota was attacked by planes she shot down an even 38 out of 38 attacking.

The rapid and widespread application of this rather complex electronic equipment was not accomplished without pain and confusion. It is beyond the scope of this paper to discuss the enormous problem of training in operation and maintenance that had to be solved, or of the tactical revolution in Naval warfare that fire-control radar produced. It is sufficient here to say that these and other problems were solved by heroic efforts of hundreds of officers and civilians in the Navy Department ashore and the thousands of officers and men of the fleet. Their problems were made more difficult by weaknesses in the equipment which were revealed by battle experience as the new science of radar got its baptism of fire. In every possible case the Laboratories attempted to remove the causes of recurring troubles by redesign and the furnishing of improvement kits of parts for installation in the fleet. The many lessons of experience learned from the Mark 3's and 4's were immediately applied in the design of the many more modern radars for the same and other types of service.

The authors of this paper wish to express their gratitude to the many Navy men with whom they have worked in connection with these equipments, and whose whole-hearted cooperation during difficult times made possible the successful development of these fire-control radars. They also wish to thank their colleagues in Bell Telephone Laboratories who worked as a team to make this important equipment possible, and the men of the Western Electric Company for their help on the many engineering problems which arose during production and use in the field. It is the hope of all who were concerned with this development that accurate radars, like other radars, will find peaceful use in a peaceful world, but it is also the determination of these engineers that as long as we need a Navy, we will try to provide it with radars as much superior to those of any possible enemy as they were in the recent war.

Generated on 2019-09-21 08:42 GMT / http://hdl.handle.net/2027/mdp.39015077775156
Public Domain, Google-digitized / http://www.hathitrust.org/access_use#pd-google
Digitized by Google
Original from UNIVERSITY OF MICHIGAN

The Magnetron as a Generator of Centimeter Waves

By J. B. FISK, H. D. HAGSTRUM, and P. L. HARTMAN

Introduction

LATE in the summer of 1940, a fire control radar operating at 700 megacycles per second was in an advanced state of development at the Bell Telephone Laboratories. The pulse power of this radar was generated by a pair of triodes operating near their upper limit of frequency. Even when driven to the point where tube life was short, the generator produced peak power in each pulse of only two kilowatts, a quantity usable but marginal. Although the triodes employed had not been designed for high voltage pulsed operation, they were the best available. This is an example of how development of radar in the centimeter wave region was circumscribed by the lack of a generator of adequate power and reasonable life expectancy. Moreover, the prospects of improvement of the triode as a power generator at these wavelengths and extension of its use to shorter wavelengths were not bright. Solution of the problem by means of power amplification was remote. A new source of centimeter wave power was urgently needed.

For the British, who were at war, the problem was even more urgent. They had undertaken a vigorous search for a new type of generator of sufficiently high power and frequency to make airborne radar practicable in the defense against enemy night bombers. They found a solution in the multiresonator magnetron oscillator, admirably suited to pulsed generation of centimeter waves of high power.

In the fall of 1940, an early model of this magnetron operating at ten centimeters was brought to the United States for examination. The first American test of its output power capabilities was made on October 6, 1940 in the Bell Telephone Laboratories' radio laboratory at Whippany, N. J. This test confirmed British information and demonstrated that a generator now existed which could supply several times the power that our triodes delivered and at a frequency four times as great. The most important restraint on the development of radar in the centimeter wavelength region had now been removed.

A number of pressing questions remained to be answered, however. Could the new magnetron be reproduced quickly and in quantity? Was its

Digitized by Google
Original from UNIVERSITY OF MICHIGAN
Generated on 2019-09-21 08:44 GMT / http://hdl.handle.net/2027/mdp.39015077775156
Public Domain, Google-digitized / http://www.hathitrust.org/access_use#pd-google

operating life satisfactory? Could its efficiency and output power be substantially increased? Could one construct similar magnetrons at forty centimeters, at three centimeters, even at one centimeter? Could the magnetron oscillator be tuned conveniently? One by one, during the war years, all of these questions have been answered in the affirmative. In many instances, but not without detours and delays, results have been better than expected or hoped for.

The British magnetron was first reproduced in America at the Bell Telephone Laboratories for use in its radar developments and those at the Radiation Laboratory of the National Defense Research Committee which was then being formed at the Massachusetts Institute of Technology. Since that time, extensive research and development work has been carried on in our Laboratories, in other industrial laboratories, and in the laboratories of the National Defense Research Committee. Several manufacturers have produced the resultant designs. Magnetron research and development were also carried on in Great Britain by governmental and industrial laboratories. There has been continuous interchange of information among all these laboratories through visits and written reports. Magnetron and radar developments have been greatly accelerated by this interchange.

Multicavity magnetron oscillators are now available for use as pulsed and continuous wave generators at wavelengths from approximately 0.5 to 50 centimeters. The upper limit of peak power is now about 100 kilowatts at 1 centimeter, 3 megawatts at 10 centimeters. Operating voltages may be less than 1 kilovolt or more than 40 kilovolts. The magnetic fields essential to operation range from 600 to 15,000 gauss. Tunable magnetrons now exist for many parts of the centimeter wave region. The tuning range for pulsed operation at high voltage is about $\pm 5\%$. It is as much as $\pm 20\%$ for low voltage magnetrons. Magnetrons may now be tuned electronically, making frequency modulation possible. Present magnetron cathodes are rugged and have long life. Even for high frequency magnetrons where current density requirements are most severe, research has made available rugged cathodes with adequate life. Magnetrons are built to withstand shock and vibration without change in characteristics. Designs have been compressed and in some cases the magnet has been incorporated in the magnetron structure in the interest of light weight for airborne radar equipments.

PART I of this paper is a general discussion of present knowledge concerning the magnetron oscillator. As such it is largely a discussion of what has come to be common knowledge among those who have carried out wartime developments. It brings together in one place results of work done by all the magnetron research groups including that at our Laboratories. PART I supplies the background necessary to understanding the

Digitized by Google
Original from UNIVERSITY OF MICHIGAN
Generated on 2019-09-21 08:44 GMT / http://hdl.handle.net/2027/mdp.39015077775156
Public Domain, Google-digitized / http://www.hathitrust.org/access_use#pd-google

discussion in PART II of the magnetrons developed at the Bell Laboratories during the war. More complete presentations of the experimental and theoretical work done on the magnetron during the war are soon to be published by other research groups.

The material written up during the war has appeared as secret or confidential reports issued by the British Committee on Valve Development (CVD Magnetron Reports), by the Radiation Laboratories at the Massachusetts Institute of Technology and at Columbia University, and by the participating industrial laboratories. No attempt has been made in PART I to indicate the specific sources of the work done since 1940. To fit the wartime development of magnetrons into the sequence of previous developments, specific references are made to publications appearing in the literature prior to 1940.

The nature and scope of PART II of the paper are discussed more fully in its introductory Section, 11. GENERAL REMARKS.

PART I

THE MAGNETRON OSCILLATOR

1. GENERAL DESCRIPTION

1.1 *Description:* The multicavity magnetron oscillator has three principal component parts: an electron interaction space, a multiple resonator system, and an output circuit. Each of these is illustrated schematically in Fig. 1. The electron interaction space is the region of cylindrical symmetry between the cathode and the multisegment anode. In this region electrons emitted from the cylindrical cathode move under the action of the DC radial electric field, the DC axial magnetic field, and the RF field set up by the resonator system between the anode segments. These electronic motions result in a net transfer of energy from the DC electric field to the RF field. The RF interaction field is the fringing electric field appearing between the anode segments, built up and maintained by the multicavity resonator in the anode block. RF energy fed into the resonator system by the electrons is delivered through the output circuit to the useful load. The output circuit shown in Fig. 1 consists of a loop, inductively coupled to one of the hole and slot cavities, feeding a coaxial line.

To operate such a magnetron oscillator, one must place it in a magnetic field of suitable strength and apply a voltage of proper magnitude to its cathode, driving the cathode negative with respect to the anode. This voltage may be constant or pulsed. In the latter case, the voltage is applied suddenly by a so-called pulser or modulator for short intervals, usually of about one microsecond duration at a repetition rate of about 1000 pulses per second. With suitable values of the operating parameters, the magnetron

Digitized by Google
Original from UNIVERSITY OF MICHIGAN
Generated on 2019-09-21 08:44 GMT / http://hdl.handle.net/2027/mdp.39015077775156
Public Domain, Google-digitized / http://www.hathitrust.org/access_use#pd-google

oscillates as a self excited oscillator whenever the DC voltage is applied. The energy available at the output circuit may be connected, as in a radar set, to an antenna or, as in a laboratory experimental setup, may be absorbed in a column of water.

1.2 *Analogy to Other Oscillators:* In its fundamental aspects, the magnetron oscillator is not unlike other and perhaps more familiar oscillators. In particular, instructive analogies may be drawn between the magnetron oscillator, the velocity variation oscillator, and the simple triode oscillator. In Fig. 2 are depicted schematically the parallelisms among these types of oscillators and a simplified equivalent lumped constant circuit.

In the triode of Fig. 2(a), as in the gap of the second cavity of the velocity variation tube of Fig. 2(b) and in the interaction space of the magnetron

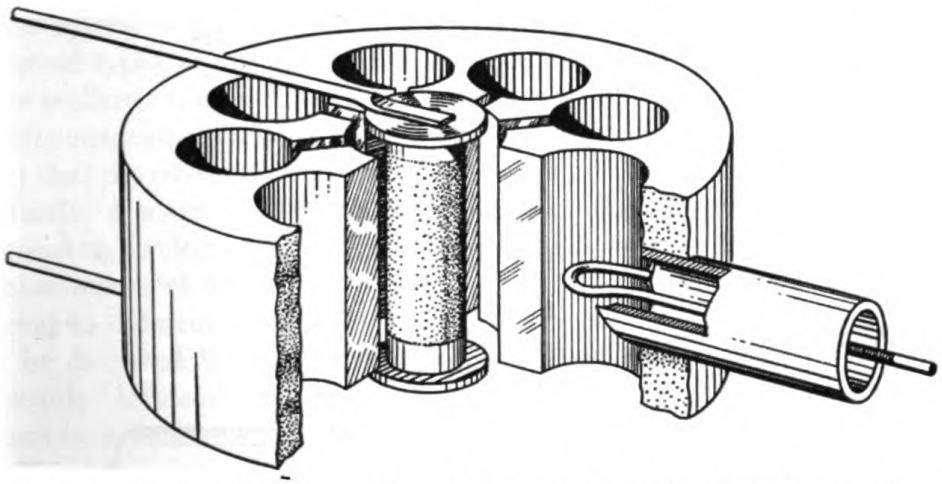

Fig. 1.—A schematic diagram designed to show the principal component parts of a centimeter wave magnetron oscillator. The resonator system and output circuit each represents one of several types used in magnetron construction.

oscillator of Fig. 2(c), electrons are driven against RF fields set up by the resonator or "tank circuit," to which they give up energy absorbed from the primary DC source. In each type of oscillator there is operative a mechanism of "bunching" which allows electrons to interact with the RF field primarily when the interaction will result in energy transfer *to* the RF field. In the triode oscillator this is accomplished by the grid, whose RF potential is supplied by the "tank circuit" in proper phase with respect to the RF potential on the anode. In the velocity variation oscillator, bunching is accomplished by variation of the electron velocities in the gap of the first cavity, followed by drift through the intervening space to the second gap. The first cavity is driven in proper phase by a feed back line from the second cavity. In the magnetron oscillator, as is to be described in detail later, electron interaction with the RF fields is such as to group the electrons into

Generated on 2019-09-21 08:44 GMT / http://hdl.handle.net/2027/mdp.39015077775156
Public Domain, Google-digitized / http://www.hathitrust.org/access_use#pd-google
Digitized by Google
Original from UNIVERSITY OF MICHIGAN

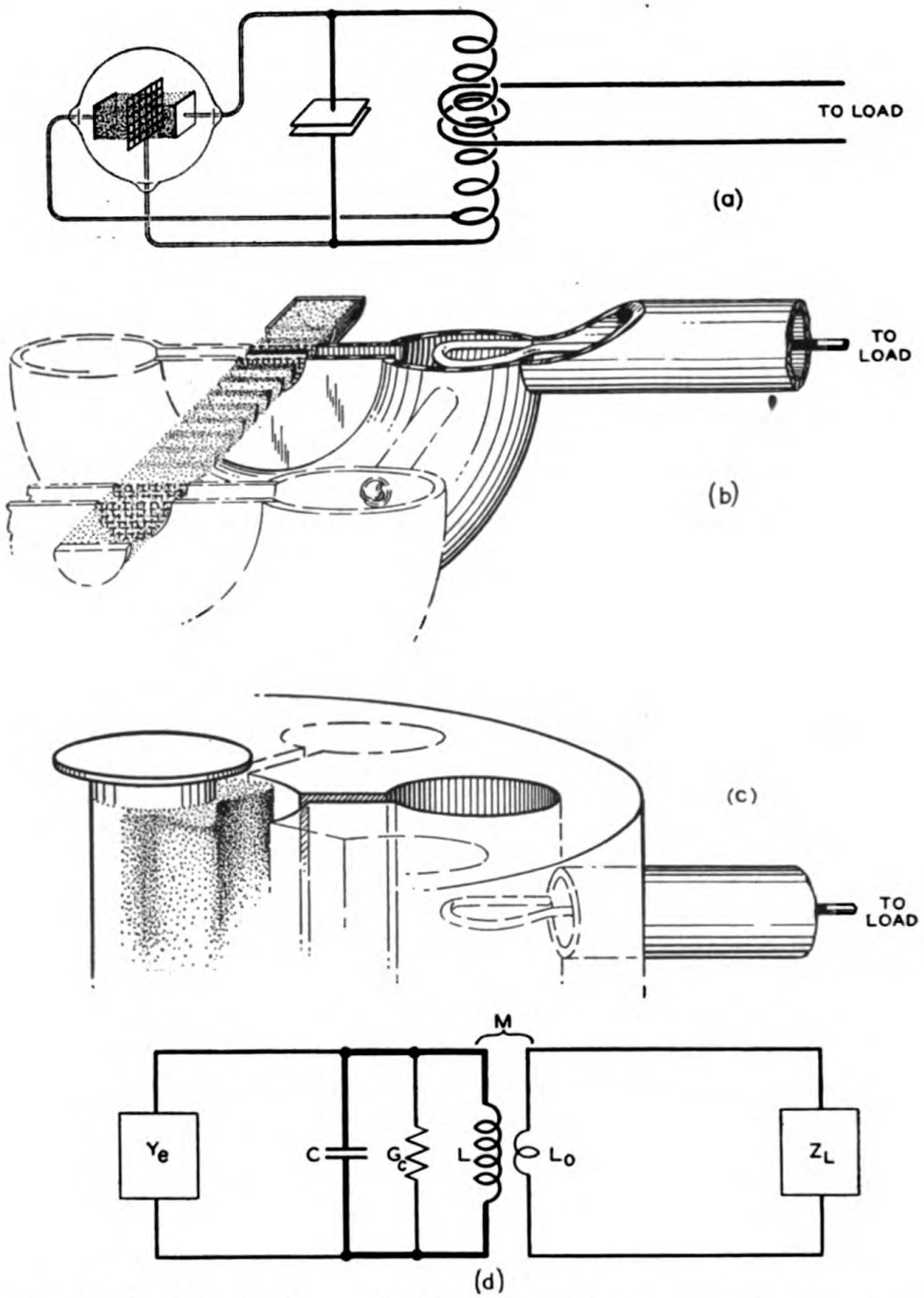

Fig. 2.—A schematic diagram depicting the parallelism among the conventional triode oscillator, the velocity variation oscillator, the centimeter wave magnetron and an equivalent lumped constant circuit. In the figure an attempt is made to align corresponding parts vertically above one another.

bunches or "spokes" which sweep past the gaps in the anode, in phase for favorable interaction with the RF fields across the gaps. The bunching field

Digitized by Google
Original from UNIVERSITY OF MICHIGAN
Generated on 2019-09-21 08:44 GMT / http://hdl.handle.net/2027/mdp.39015077775156
Public Domain, Google-digitized / http://www.hathitrust.org/access_use#pd-google

is thus the same field as that to which energy is transferred. In this sense the magnetron oscillator is perhaps more properly analogous to the reflex type of velocity variation oscillator, in which a single cavity is used both as "buncher" and "catcher"; the electrons, after traversing the gap once, are turned back in the proper phase in the drift space so as to pass through the gap again in the opposite direction.

Each type of oscillator has a resonator in which energy is stored and which synchronizes the flow of energy from the electrons into it by the means of self excitation. In each type, energy is extracted from the resonator by an output circuit at a rate which, under steady state conditions, equals that of influx from the electron interaction, minus the losses in the resonator itself.

1.3 *Use of Equivalent Circuits:* In many instances the understanding of electromagnetic oscillators is made easier and analytic treatment made possible by use of an equivalent circuit with lumped constants. Of several possible types, one of the simpler and more frequently used for the magnetron oscillator is shown in Fig. 2. This may appear in the case of the multicavity magnetron to be an oversimplification as it does not account for the fact that the resonant frequency of the magnetron resonator system is many valued. A magnetron resonator, being made up of a number of coupled resonating cavities, is capable of supporting several modes of oscillation. These modes of oscillation have different resonant frequencies and correspond to different configurations of the electromagnetic fields. By means to be discussed, however, magnetron resonators can be made to oscillate "cleanly" in one of these modes and may thus be represented for many purposes by a simple L-C circuit having a single resonance.

The output circuit of the oscillator is also amenable to treatment by equivalent lumped constant circuits which account for its behavior with accuracy. More general, four terminal network theory has also been applied in the study and design of impedance transformations in this part of the oscillator.

Finally, the electrons, which in a sense are connected to the circuit formed by the resonator and the load, may also be treated by circuit concepts. The electrons moving in the space between the cathode and anode, by virtue of their presence and motion, induce charge fluctuations on the anode segments. The time derivative of these fluctuations is equivalent to an RF current flowing into the anode from the interaction space. This current and the RF voltage on the anode, bearing a definite phase relationship, make possible the definition of an admittance called the average electronic admittance, $Y_e = G_e + jB_e$. Since the electrons are being driven against RF fields in the interaction space, this admittance looking into the electron stream has a negative conductance term. Unlike usual circuit admittances, the electronic admittance is nonlinear, being a function of the voltage

Digitized by Google
Original from UNIVERSITY OF MICHIGAN
Generated on 2019-09-21 08:44 GMT / http://hdl.handle.net/2027/mdp.39015077775156
Public Domain, Google-digitized / http://www.hathitrust.org/access_use#pd-google

amplitude of oscillation, V_{RF}, as well as of other parameters governing the electronic behavior of the oscillator, such as voltage and magnetic field. It is not known *a priori* but may be deduced from measurements on the operating oscillator and its circuit.

A necessary condition for oscillation, applicable to the magnetron as to any oscillator, is that, on breaking the circuit at any point, the sum of the admittances looking in the two directions is zero. Thus, if the circuit is broken at the junction of electrons and resonator, as is convenient, the electronic admittance, Y_e, looking from the circuit into the electron stream, must be the negative of the circuit admittance, Y_c, looking from the electron stream into the circuit.

With these remarks, of general applicability to all types of electromagnetic oscillators, the discussion will be continued for the centimeter wave magnetron oscillator in particular. As far as is possible, the electronic interaction space, resonator system, and output circuit of the device will be taken up in that order. The function and operation of each part will be described; then the principles of its design, and its relation to previous magnetron development will be indicated.

1.4 *Electron Motions in Electric and Magnetic Fields—The DC Magnetron:* Before beginning the discussion of the electronics of the magnetron oscillator, it is well to review briefly electron motions in various types and combinations of electric and magnetic fields, and the operation of the DC magnetron.[1]

An electron, of charge e and mass m, moving in an electric field of strength E, is acted upon by a force, independent of the electron's velocity, of strength eE, directed oppositely to the conventional direction of the field. If the field is constant and uniform, the motion of the electron is identical to that of a body moving in a uniform gravitational field.

An electron moving in a magnetic field of strength B, however, is acted upon by a force which depends on the magnitude of the electron's velocity, v, on the strength of the field, and on how the direction of motion is oriented with respect to the direction of the field. The force is directed normally to the plane of the velocity and magnetic field vectors and is of magnitude proportional to the velocity, the magnetic field, and the sine of the angle, θ, between them. Thus the force is the cross or vector product of $\vec{v}$ and $\vec{B}$,

$$\vec{F} = e[\vec{v} \times \vec{B}], \qquad F = Bev \sin \theta.$$

An electron moving parallel to a magnetic field ($\sin \theta = 0$) feels no force. One moving perpendicular to a uniform magnetic field ($\sin \theta = 1$) is con-

[1] The cylindrical DC magnetron was reported by A. W. Hull. Phys. Rev. 18, 31 (1921).

Digitized by Google
Original from UNIVERSITY OF MICHIGAN
Generated on 2019-09-21 08:44 GMT / http://hdl.handle.net/2027/mdp.39015077775156
Public Domain, Google-digitized / http://www.hathitrust.org/access_use#pd-google

strained to move in a circle by the magnetic force at right angles to its path. Since this force is balanced by the centrifugal force, the radius, ρ, of the circular path depends on the electron's momentum and the strength of the field; that is,

$$Bev = \frac{mv^2}{\rho},$$

yielding

$$\rho = \frac{mv}{eB}. \tag{1}$$

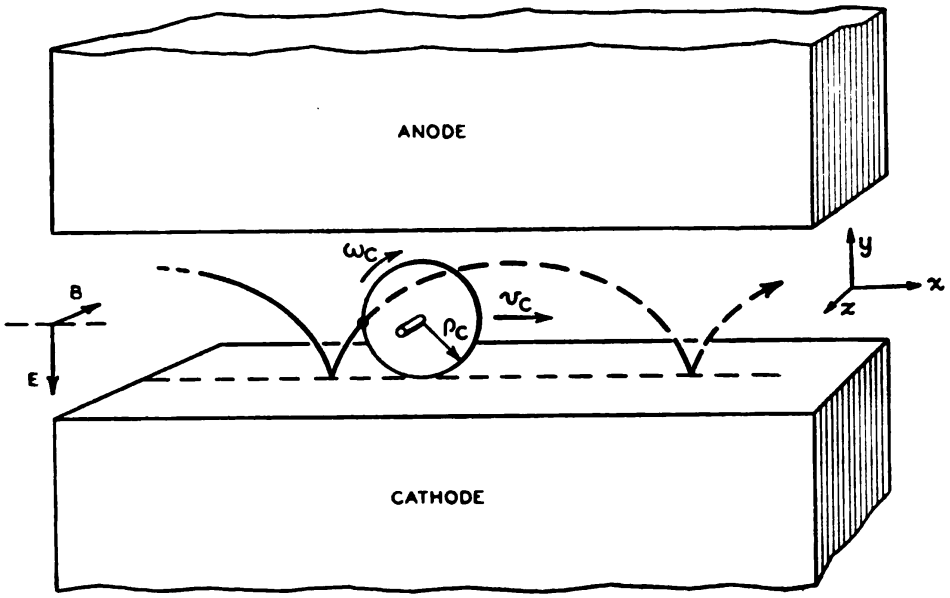

Fig. 3.—The cycloidal path of an electron which started from rest at the cathode in crossed electric and magnetic fields for the case of parallel plane electrodes. The mechanism of generation of the orbit by a point on the periphery of a rolling circle is depicted.

The time, T_c, required to traverse the circle is independent of the radius and hence of the velocity of the electron; $T_c = 2\pi\rho/v = 2\pi m/eB$. Thus, the angular frequency of traversing the circular path, the so-called cyclotron frequency, depends on the magnetic field alone and is given by,

$$\omega_c = 2\pi f_c = 2\pi\frac{1}{T_c} = \frac{e}{m}B. \tag{2}$$

In the magnetron, electron motion in crossed electric and magnetic fields is involved. Consider first such motion between two parallel plane electrodes, neglecting space charge. If, as in Fig. 3, the electric field is directed in the negative y direction and the magnetic field in the negative z direction, the equations of motion of the electron are:

Digitized by Google
Original from UNIVERSITY OF MICHIGAN
Generated on 2019-09-21 08:45 GMT / http://hdl.handle.net/2027/mdp.39015077775156
Public Domain, Google-digitized / http://www.hathitrust.org/access_use#pd-google

$$\left.\begin{aligned} \frac{d^2x}{dt^2} &= \frac{eB}{m}\frac{dy}{dt}, \\ \frac{d^2y}{dt^2} &= \frac{e}{m}\left(E - B\frac{dx}{dt}\right), \\ \frac{d^2z}{dt^2} &= 0. \end{aligned}\right\} \tag{3}$$

The particular case of most interest here is that for which the electron starts from rest at the origin. The equations of motion then yield a cycloidal orbit given by the parametric equations:

$$\left.\begin{aligned} x &= v_c t - \rho_c \sin \omega_c t = \rho_c(\omega_c t - \sin \omega_c t), \\ y &= \rho_c(1 - \cos \omega_c t), \end{aligned}\right\} \tag{4}$$

in which:

$$v_c = \frac{E}{B}, \tag{5}$$

$$\rho_c = \frac{m}{e}\frac{E}{B^2}, \tag{6}$$

$$\omega_c = \frac{e}{m}B. \tag{7}$$

This motion may be regarded as a combination of rectilinear motion of velocity v_c in the direction of the x axis, perpendicular to both E and B, and of motion in the xy plane about a circular path of radius ρ_c, at an angular frequency ω_c, the cyclotron frequency. Fig. 3 shows the resulting cycloidal path and its generation by a point on the periphery of the rolling circle. In the case of cylindrical geometry, it is often convenient to think in terms of the plane case.

In the case of cylindrical geometry with radial electric and axial magnetic fields, the electron orbit, neglecting space charge, approximates an epicycloid generated by rolling a circle around on the cylindrical cathode. The orbit is not exactly an epicycloid because the radial motion is not simple harmonic, which state of affairs arises from the variation of the DC electric field with radius. The approximation of the epicycloid to the actual path is a convenient one, however, because the radius of the rolling circle, its angular frequency of rotation, and the velocity of its center, for the epicycloid, all approximate those for the cycloid of the plane case. These approximations improve with increasing ratio of cathode to anode radii. Several electron orbits in a DC cylindrical magnetron are shown in Fig. 4 for several magnetic fields.

Digitized by Google
Original from UNIVERSITY OF MICHIGAN
Generated on 2019-09-21 08:45 GMT / http://hdl.handle.net/2027/mdp.39015077775156
Public Domain, Google-digitized / http://www.hathitrust.org/access_use#pd-google

It is clear from this simplified picture of the orbits in a DC cylindrical magnetron without space charge, that, at a given electric field, an electron orbit for a sufficiently strong magnetic field may miss the anode completely and return to the cathode. The critical magnetic field at which this is just possible is called the cut-off value, B_c. For a given voltage between cathode and anode, as the magnetic field is increased, the current normally passed by the device falls rather abruptly at B_c. A current versus magnetic field curve, together with electron orbits corresponding to four regions of the

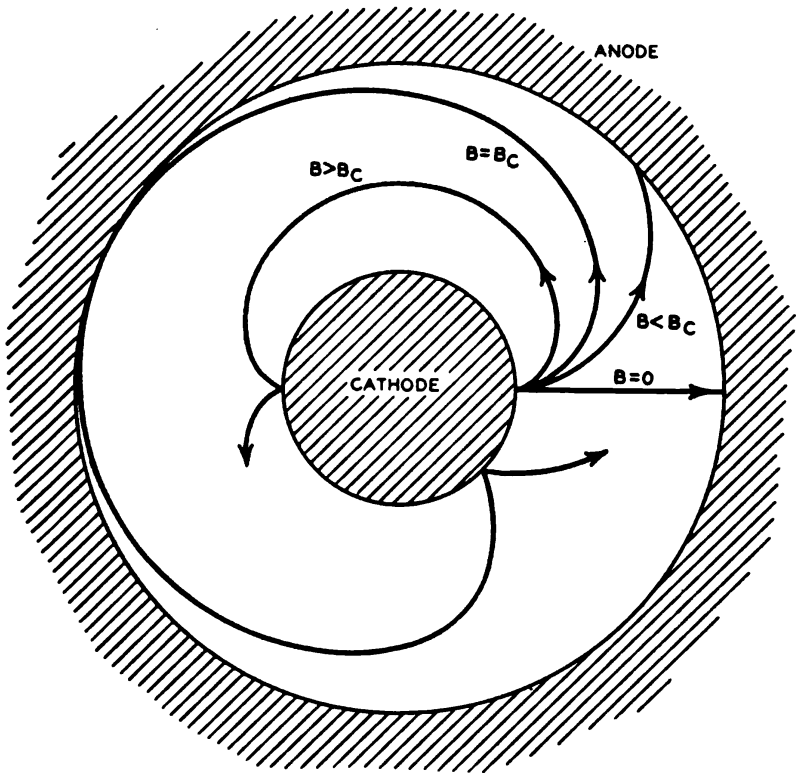

Fig. 4.—Electron paths in a cylindrical DC magnetron at several magnetic fields above and below the cut-off value, B_c. The electrons are assumed to be emitted from the cathode with zero initial velocity.

curve, is shown in Fig. 5. For the case of parallel plane electrodes, the cut-off relation between the critical anode potential, V_c, and magnetic field, B_c, and the electrode separation, d, for the parallel plane case, is obtained by equating the electrode separation to the diameter of the rolling circle. Thus,

$$d = 2\,\frac{m}{e}\left(\frac{V_c}{d}\right)\frac{1}{B_c^2},$$

from which

$$V_c = \frac{eB_c^2d^2}{2m}.$$

Digitized by Google
Original from UNIVERSITY OF MICHIGAN
Generated on 2019-09-21 08:45 GMT / http://hdl.handle.net/2027/mdp.39015077775156
Public Domain, Google-digitized / http://www.hathitrust.org/access_use#pd-google

For the cylindrical case, the relation may be shown to be

$$V_c = \frac{eB_c^2 r_a^2}{8m}\left[1 - \left(\frac{r_c}{r_a}\right)^2\right]^2, \tag{8}$$

in terms of cathode and anode radii, r_c and r_a.

2. Types of Magnetron Oscillators

2.1 *Definitions:* The DC magnetron may be converted into an oscillator, suitable for the generation of centimeter waves, by introducing RF fields into the anode-cathode region. This may be done by applying between anode

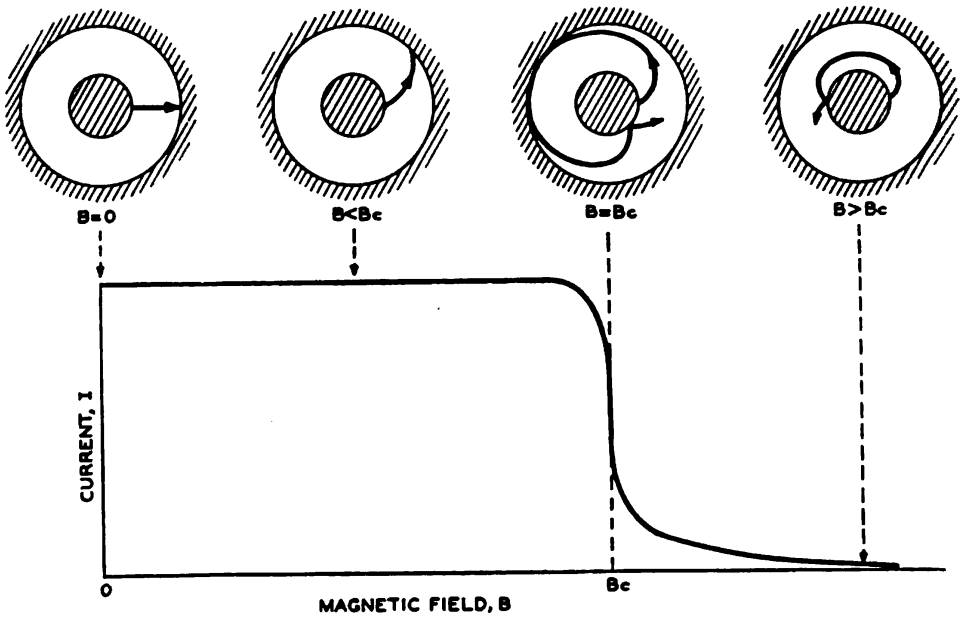

Fig. 5.—Variation of current passed by a cylindrical DC magnetron at constant voltage, plotted as a function of magnetic field. The orbits of electrons occurring at four different magnetic fields are shown above the corresponding regions of the current characteristic.

and cathode RF voltage from a resonant circuit, in which case the electrons interact with the superposed radial RF field. Or, it may be done by splitting the magnetron anode into two or more segments between which the RF voltage is applied. Then the electrons interact with the fringing RF fields existing between the segments. The problem of understanding the electronics of the multicavity magnetron oscillator is that of understanding how an electron, subject to the constraints placed upon its motion by the DC axial magnetic and DC radial electric fields, can move so as to interact favorably with the RF field; how an electron interacting unfavorably is rejected; and why, on the average, the electrons transfer more energy to the RF field than they take from it.

Generated on 2019-09-21 08:45 GMT / http://hdl.handle.net/2027/mdp.39015077775156
Public Domain, Google-digitized / http://www.hathitrust.org/access_use#pd-google
Digitized by Google
Original from UNIVERSITY OF MICHIGAN

On the basis of the nature of the electronic mechanism by means of which energy is transferred to the RF field, it is now convenient to distinguish three types of magnetron oscillators.[2] The *negative resistance magnetron oscillator* depends on the existence of a static negative resistance characteristic between the two halves of a split anode.[3] The *cyclotron frequency magnetron oscillator* operates by virtue of resonance between the period of RF oscillation and the period of the cycloidal motion of the electrons (rolling circle or cyclotron frequency).[4] The *traveling wave magnetron oscillator* depends upon resonance, that is, approximate equality, between the mean translational velocity of the electrons and the velocity of a traveling wave component of the RF interaction field.[5]

The magnetron oscillator with which this paper is primarily concerned is of the traveling wave type. The other magnetron types are discussed briefly for the sake of completeness and because an understanding of them enhances one's grasp of the entire subject and places the traveling wave magnetron oscillator in its proper historical perspective.

2.2 *The Negative Resistance Magnetron Oscillator—Type I:* In the negative resistance magnetron oscillator,[6] the anode is split parallel to the axis into two halves, between which the RF circuit is attached. The electrons emitted by the cathode must move under the combined action of the DC radial electric and DC axial magnetic fields together with the RF electric field existing between the two semicylinders forming the anode. The transit time from cathode to anode is not involved in the mechanism except that it must be small relative to the period of the RF oscillation. The static negative resistance characteristic arises from the fact that under certain conditions the allowable orbits for the majority of electrons terminate on the segment of lower potential, irrespective of the segment toward which they start. These electrons, being driven against the RF component of the field, give energy gained from the DC field to the RF field.

In Fig. 6 are shown the paths, plotted by Kilgore,[7] of two electrons starting initially toward opposite segments but both striking the segment of lower potential. Each path is completely traversed in a time during which

[2] The magnetron oscillator discussed by Hull, in which the magnet winding is coupled to the plate circuit, is not considered as it is essentially an audio frequency device. K. Okabe in his book, "Magnetron-Oscillations of Ultra Short Wavelengths" (Shokendo, 1937), distinguishes five types, but it is not clear just how his types C and E are to be identified.

[3] These oscillations have been called Habann, quasi-stationary, or dynatron oscillations, and correspond to Okabe's type D.

[4] These oscillations have been called electronic oscillations by Megaw, transit time oscillations of the first order by Herriger and Hülster, and correspond to Okabe's type A.

[5] These oscillations are the running wave type discussed by Posthumus, the transit time oscillations of higher order of Herriger and Hülster, and correspond to Okabe's type B.

[6] This type was disclosed by Habann, Zeit f. Hochfrequenz. 24, 115 and 135 (1924).

[7] G. R. Kilgore, Proc. I.R.E. 24, 1140 (1936).

Digitized by Google
Original from UNIVERSITY OF MICHIGAN
Generated on 2019-09-21 08:45 GMT / http://hdl.handle.net/2027/mdp.39015077775156
Public Domain, Google-digitized / http://www.hathitrust.org/access_use#pd-google

the RF field changes little. Thus it is possible by applying DC potential differences between the anode segments to measure a negative resistance between them. As can be seen from the orbits of Fig. 6, magnetic fields considerably above the cut-off value are used. With magnetrons of this type, power output up to 100 watts at 600 mc/s at an efficiency of 25% has been attained.[7] Oscillations of frequency as high as 1000 mc/s, (30 cm.) have been produced.[8] Because a large number of orbital loops are required, however, making $\omega \ll \frac{eB}{m}$, this type of magnetron oscillator demands the

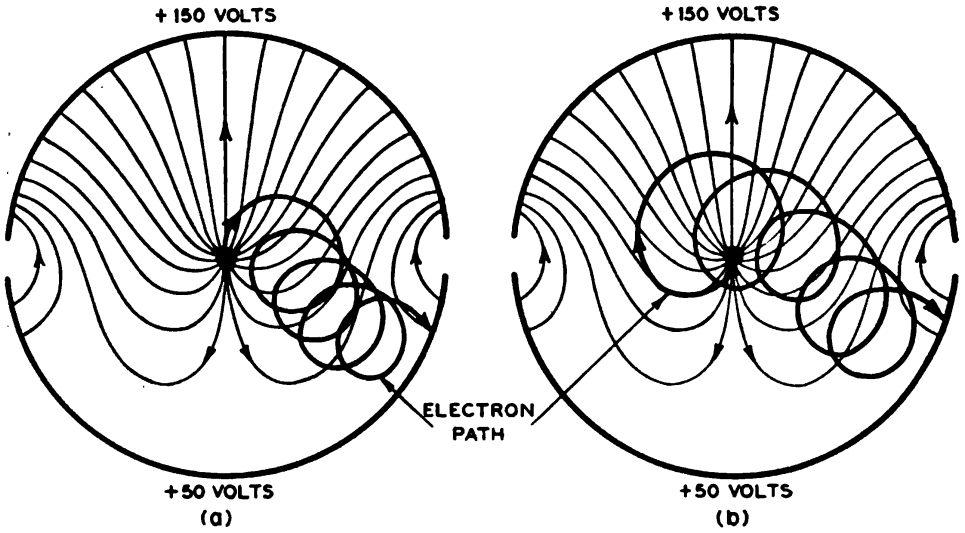

Fig. 6.—Electron paths plotted by Kilgore for the negative resistance magnetron oscillator, Type I. During the time the orbits shown are being executed, the cathode is at zero potential and the anode segments at the potentials indicated. Lines of electric force on an electron are plotted in this figure. The two orbits are those of electrons which start initially toward opposite anode segments. It should be noted that in either case the electron is driven to the segment of lower potential against the RF field component.

use of high magnetic field in the centimeter wave region and is thus less desirable than other types.

2.3 *The Cyclotron Frequency Magnetron Oscillator—Type II:* Not long after the invention of the DC magnetron, oscillations between anode and cathode were found to occur near the cut-off value of magnetic field.[9] These were found to be strongest for wavelengths obeying a relation of the form:

$$\lambda = \frac{\text{constant}}{B}. \tag{9}$$

[8] E. C. S. Megaw, Journ. I.E.E. (London) 72, 326 (1933).
[9] A. Zacek, Cos. Pro. Pest. Math. a Fys. (Prague) 53, 578 (1924). A summary appeared in Zeit. f. Hochfrequenz. 32, 172 (1928).

Digitized by Google
Original from UNIVERSITY OF MICHIGAN
Generated on 2019-09-21 08:45 GMT / http://hdl.handle.net/2027/mdp.39015077775156
Public Domain, Google-digitized / http://www.hathitrust.org/access_use#pd-google

Later, it was shown that the oscillation period is equal to the electron transit time from the vicinity of the cathode to the vicinity of the anode and back. This made it possible to calculate a value for the constant in the above equation in good agreement with experiment.[10] The oscillation frequency is that of the rotational component of the electronic motion, that is, approximately the cyclotron frequency of equation (7).

The mechanism must be explained in terms of electrons moving in the DC radial electric and axial magnetic fields and the superposed RF radial electric field. This may be done as follows: An electron leaving the cathode in such phase as to gain energy when moving from the cathode toward the anode will also gain energy during its return, striking the cathode with more energy than it had when it left. There, such an electron is stopped from further motion during which it would continue to absorb energy from the

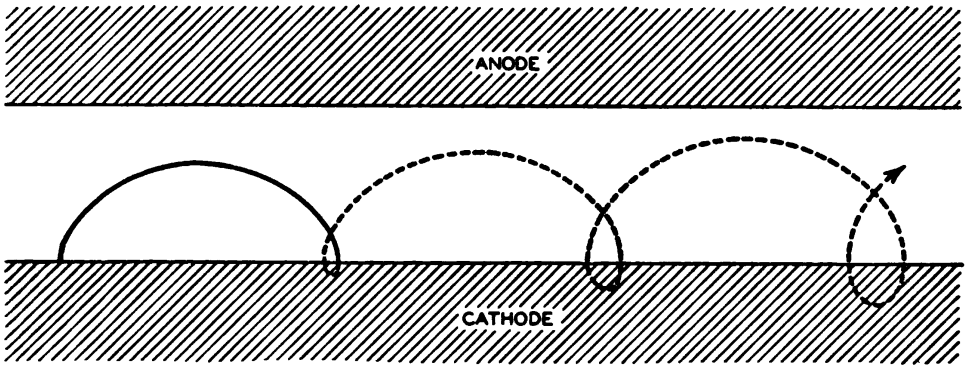

Fig. 7.—An approximate orbit of an electron which gains energy from the RF field in a cyclotron frequency or Type II magnetron oscillator, shown for the plane case. The orbit is continued as a dashed line indicating how it would be traversed were it not stopped by the cathode. The DC electric force on the electron is directed from cathode to anode.

RF field at the expense of the oscillation. The electron will execute an orbit something like that in Fig. 7 for the plane case. An electron leaving the cathode in the opposite phase, on the other hand, loses energy when moving toward the anode and again on its return toward the cathode. As is shown in Fig. 8, it reverses its direction after the first trip without reaching the cathode surface and starts over on a second loop of smaller amplitude, remaining in the same phase and continuing to lose energy to the field. This process continues until all the energy of the rotational component of the electron's motion has been absorbed by the RF field. If the electron is not removed at this stage, in its subsequent motion the rotational component will build up, extracting energy from the RF oscillation. Means such as tilting the magnetic field or placing electrodes at the ends of the tube have been used to remove the electrons from the interaction space when all the

[10] K. Okabe, Proc. I.R.E. 17, 652 (1929).

Digitized by Google
Original from UNIVERSITY OF MICHIGAN
Generated on 2019-09-21 08:45 GMT / http://hdl.handle.net/2027/mdp.39015077775156
Public Domain, Google-digitized / http://www.hathitrust.org/access_use#pd-google

rotational energy has been absorbed. It is possible to maintain the oscillations and extract energy from them because electrons which give energy to the field can do so over many cycles, whereas electrons of opposite phase can gain energy over only one cycle before they are removed.

Magnetrons oscillating in this manner have been built with split anodes.[10,11] Here the RF field with which the electron interacts is more tangential than radial but the criterion for oscillation is the same, namely, resonance between the field variations and the rotational component of the electron's motion. Operating efficiencies of 10 to 15% have been obtained. It was with a magnetron of this type having an anode diameter of 0.38 mm. that radiation of wavelength as low as 0.64 cm. was generated.[12]

The cyclotron frequency magnetron oscillator has been almost entirely superseded by the traveling wave magnetron oscillator as a generator of

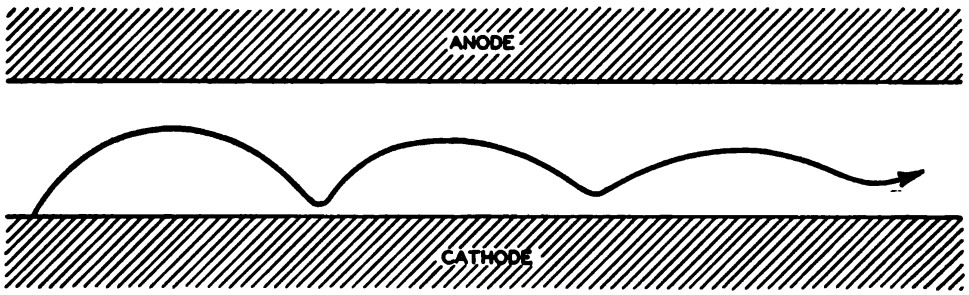

Fig. 8.—An approximate orbit of an electron which loses energy to the RF field in a cyclotron frequency or Type II magnetron oscillator, shown for the plane case. If the electron after losing all its rotational energy remains in the interaction space, it gains energy from the RF field, and its orbit builds up cycloidal scallops in a manner directly the reverse of that shown here. The DC electric force on the electron is directed from cathode to anode.

centimeter waves. In the main this is the result of the impossibility of removing electrons emitted from an extended cathode area from the interaction region at the proper stage in their orbits. This inherent drawback is not shared by the traveling wave magnetron oscillator which may be operated at higher efficiency without critical adjustment of orientation in the magnetic field or of the potential of auxiliary electrodes.

2.4 *The Traveling Wave Magnetron Oscillator—Type III:* Oscillations have been found to occur in the magnetron which are independent of any static negative resistance characteristic and which can occur at frequencies widely different from the cyclotron frequency. In 1935[13] the electronic mechanism of these oscillations was correctly interpreted as an inter-

[11] H. Yagi, Proc. I.R.E. 16, 715 (1928).
[12] C. E. Cleeton and N. H. Williams, Phys. Rev. 50, 1091 (1936).
[13] K. Posthumus, Wireless Engineer 12, 126 (1935).

Digitized by Google
Original from UNIVERSITY OF MICHIGAN
Generated on 2019-09-21 08:46 GMT / http://hdl.handle.net/2027/mdp.39015077775156
Public Domain, Google-digitized / http://www.hathitrust.org/access_use#pd-google

action of the electrons with the tangential component of a traveling wave whose velocity is approximately equal to the mean translational velocity of the electrons. Later[14] the role of the radial component of the rotating electric field in keeping the electrons in proper phase was recognized. Magnetrons of wavelength as short as 75 cm., operating at better than 50% efficiency, were built prior to 1940, but performance such as was later to be attained with this type of magnetron at much shorter wavelengths was not attained then, perhaps primarily because of the lack of a good resonator. It was a magnetron of this type which the British brought to the United States in 1940. The British magnetron was a 10 cm. oscillator, intended for pulsed operation, having a tank circuit consisting of eight resonators built into the anode block as shown in Fig. 1.[15]

3. The Electronic Mechanism

3.1 *Electronic Interaction at Anode Gaps:* The electrons in the interaction space of the magnetron oscillator are the agents which transfer energy from the DC field to the RF field. As such, they must move subject to the constraints imposed by the DC radial electric and DC axial magnetic fields, considering, for the moment, the RF fields to be small. Under these conditions, as has been seen for the DC cylindrical magnetron (see Fig. 4 for $B > B_c$), electrons follow approximately epicycloidal paths which progress around the cathode. The mean velocity of this progression, that of the center of the rolling circle, depends upon the relative strengths of the electric and magnetic fields [see equation (5) for the plane case]. By proper choice of DC voltage, V, between cathode and anode and of magnetic field, B, the mean angular velocity of the electrons may be set at any desired value.

The RF electric fields in the interaction space, with which the electrons moving as described above must interact, are the electric fields fringing from the slots in the anode surface. These fields are provided by the N coupled oscillating cavities of which the magnetron resonator system is composed. As will be discussed in more detail later, such a system of resonators may oscillate in a number of different modes in each of which the oscillations in adjacent resonators, and thus the fields appearing across adjacent anode slots, bear a definite phase relationship. For a system of N resonators it will be seen that the phase difference between adjacent resonators may assume the values $n\frac{2\pi}{N}$ radians, n being the integers 0, 1, 2, $\cdots$, $\frac{N}{2}$.

Adopting another point of view, one may consider the potentials placed upon the anode segments by the resonators. The variation of the potential

[14] F. Herriger and F. Hülster, Zeit. f. Hochfrequenz, 49, 123 (1937).

[15] The use of such internal resonators is reported in the literature by N. T. Alekseieff and D. E. Maliaroff, Journ. of Tech. Phys. (U.S.S.R.) 10, 1297 (1940); republished in English, Proc. I.R.E. 32, 136 (1944). A. L. Samuel has obtained U. S. Patent #2,063,342 Dec. 8, 1936, for a similar device.

Digitized by Google
Original from UNIVERSITY OF MICHIGAN
Generated on 2019-09-21 08:46 GMT / http://hdl.handle.net/2027/mdp.39015077775156
Public Domain, Google-digitized / http://www.hathitrust.org/access_use#pd-google

from one segment to the next depends upon the mode of oscillation of the system as a whole. The restriction on the phase difference stated above requires the sequence of anode segment potentials at any instant to contain

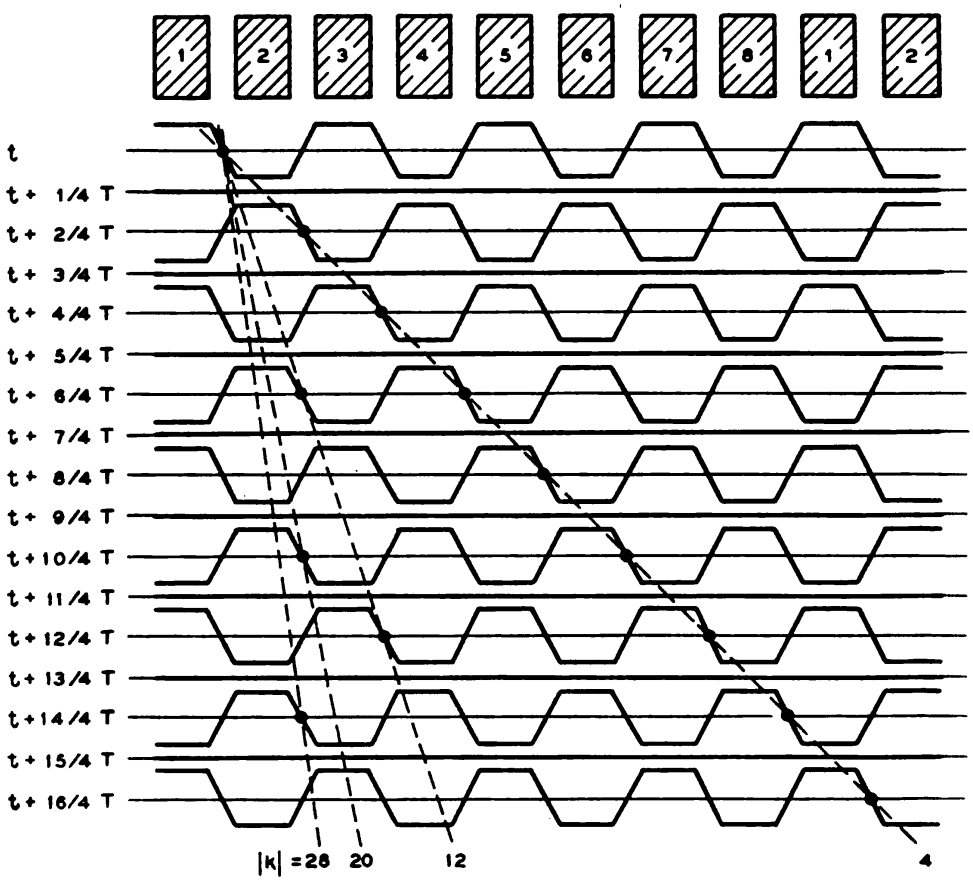

Fig. 9.—A plot showing the π mode anode potential wave at several instants in an eight resonator magnetron and the mean paths of electrons which interact favorably with the RF field. The plot is developed from the cylindrical case, the shaded rectangles at the top representing the anode segments. The anode potential variation is a standing wave, shown here for a sequence of instants one quarter period ($T/4$) apart. Note that the potential is constant across the anode surfaces and varies linearly between them. Electrons interacting favorably with the RF field cross the anode gaps when the field there is maximum retarding as indicated by the filled circles. The lines for $|k| = 4, 12, 20, 28, \cdots$ represent mean paths of electrons traveling with mean angular velocities $\frac{2\pi f}{4}, \frac{2\pi f}{12}, \frac{2\pi f}{20}, \frac{2\pi f}{28}, \cdots$ around in the interaction space. Since the field is a standing wave, it is clear that electrons possessing these velocities in either direction may interact favorably with the RF field.

n complete cycles in one traversal of the cylindrical anode, n still denoting the integers $0, 1, 2, \cdots, \frac{N}{2}$. In general, these anode potential waves may be standing waves or waves traveling around the anode structure in either direction with angular velocity $\frac{2\pi f}{n}$ radians per second, where f is the RF

Digitized by Google
Original from UNIVERSITY OF MICHIGAN
Generated on 2019-09-21 08:46 GMT / http://hdl.handle.net/2027/mdp.39015077775156
Public Domain, Google-digitized / http://www.hathitrust.org/access_use#pd-google

frequency. For the two modes in which adjacent resonators are in phase ($n = 0$) and π radians out of phase ($n = \frac{N}{2}$, the so-called π mode), however, only standing potential waves on the anode are possible. As examples of

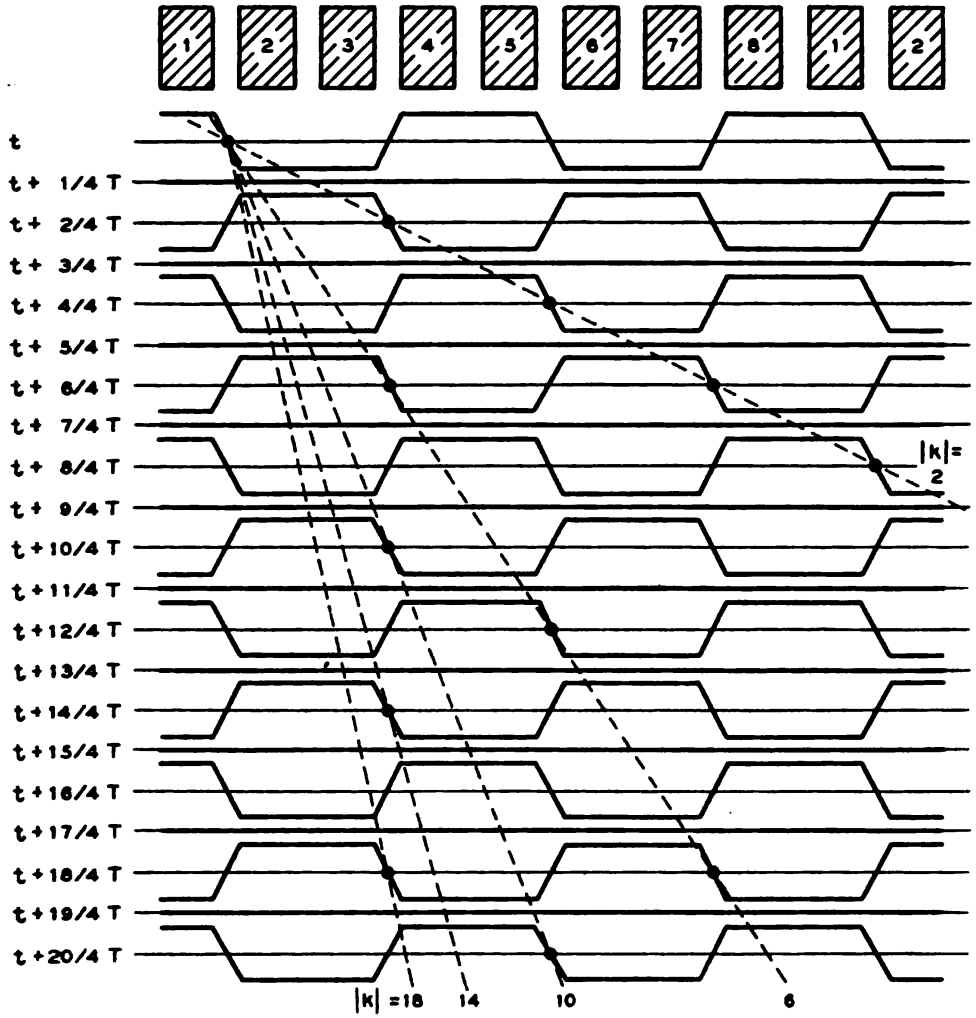

Fig. 10.—A plot similar to that of Fig. 9 for the standing wave component of anode potential of periodicity $n = 2$ in a magnetron having eight resonators. Electrons which interact favorably have mean angular velocities $\frac{2\pi f}{2}, \frac{2\pi f}{6}, \frac{2\pi f}{10}, \frac{2\pi f}{14}, \cdots$ in either direction in the interaction space.

standing and traveling anode potential waves in an anode structure having eight resonators ($N = 8$), the standing wave for $n = 4$ and standing and traveling waves for $n = 2$ are shown in Figs. 9, 10, and 11 respectively.

From what has been said about the RF field and the electronic motion in the interaction space of the magnetron oscillator of Type III, it is possible

Digitized by Google
Original from UNIVERSITY OF MICHIGAN
Generated on 2019-09-21 08:46 GMT / http://hdl.handle.net/2027/mdp.39015077775156
Public Domain, Google-digitized / http://www.hathitrust.org/access_use#pd-google

to understand its fundamental electronic mechanism. As in any oscillator, the criterion for oscillation is that more energy shall be transferred to the RF field by electrons driven against it than is taken from the RF field by electrons accelerated by it. This can be accomplished in the traveling wave

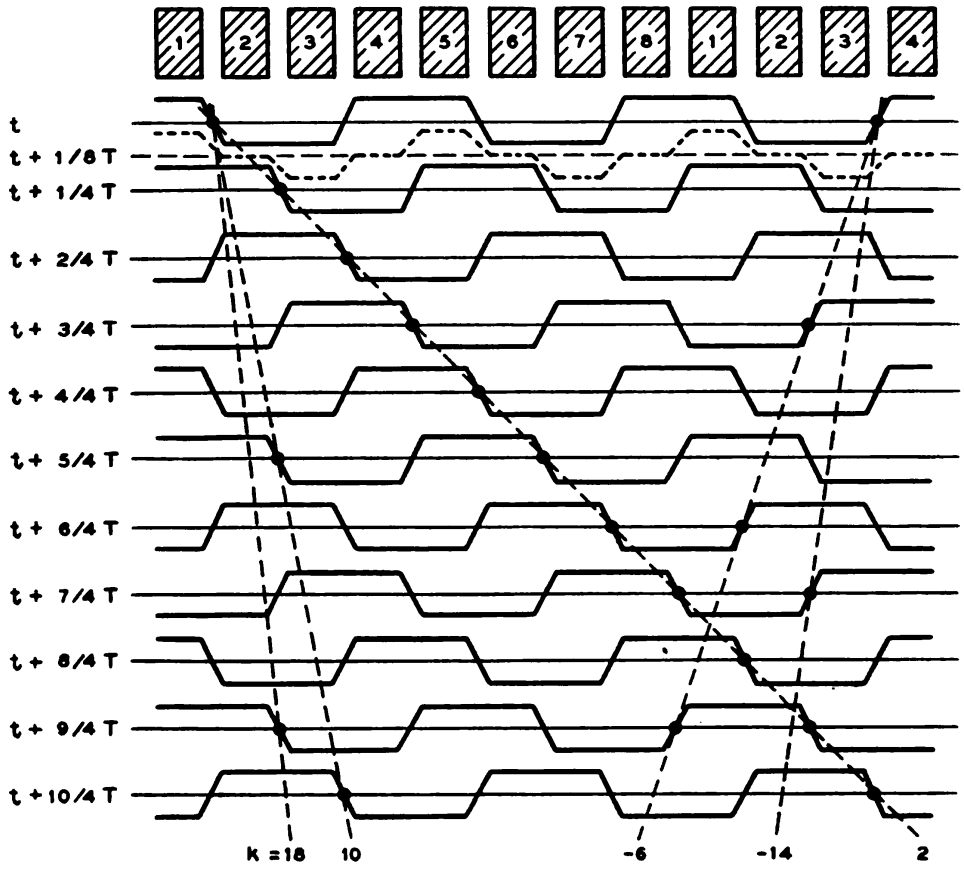

Fig. 11.—A plot similar to those of Figs. 9 and 10 for the rotating wave of anode potential of periodicity $n = 2$ in a magnetron having eight resonators [see equation (13) in the text]. The field at the instant $t + \frac{1}{8}T$ is plotted as a dashed line to show that the traveling wave does not preserve its shape at all instants. Whereas the wave travels in one direction with the angular velocity $\frac{2\pi f}{2}$, electrons which travel with velocities $\frac{2\pi f}{2}, \frac{2\pi f}{10}, \frac{2\pi f}{18}, \cdots$ in the same direction or with velocities $\frac{2\pi f}{6}, \frac{2\pi f}{14}, \cdots$ in the opposite direction interact favorably with the RF field. Directions of electron motion must now be distinguished. Electrons whose velocity is opposed to that of the rotating field are said to be driving a "reverse" mode.

magnetron oscillator only if the mean angular velocity of the electrons is such as to make them pass successive gaps in the anode at very nearly the same phase in the cycle of the RF field across the gaps. Then it is possible for an electron which leaves the cathode in such phase as to oppose the tangential component of the RF field across one anode gap, to continue to

Generated on 2019-09-21 08:47 GMT / http://hdl.handle.net/2027/mdp.39015077775156
Public Domain, Google-digitized / http://www.hathitrust.org/access_use#pd-google
Digitized by Google
Original from UNIVERSITY OF MICHIGAN

lose energy gained from the DC field to the RF field at successive gaps. Electrons which gain energy from the RF field are driven back into the cathode after only one orbital loop and are removed from further motion detrimental to the oscillation. This process of selection and rejection of electrons forms the groups of bunches, shown in Fig. 2(c), which sweep past the anode slots in phase to be retarded by the RF field component. The criterion that the electron drift velocity shall be such as to keep these bunches in proper phase is analogous to the condition that the drift angle in a velocity variation oscillator [Fig. 2(b)] be such as to cause the bunches to cross the gap of the second or "catcher" cavity in phase to lose energy to the RF field across the gap.

The condition placed upon the mean angular velocity of the electrons may be discussed more readily by reference to Figs. 9, 10, and 11. Consider first, however, only Fig. 9 for the standing potential wave of the $n = 4$ mode, and focus attention on an electron which crosses the gap between anode segments 1 and 2 at the instant t when the RF field is maximum retarding, that is, the potential on segment 1 is maximum and on segment 2 minimum. It is clear that this electron can cross the next gap in the same phase if the time required to reach it is $(|p| + \frac{1}{2})\ T$, in which p is any integer and T is the period of RF oscillation. In Fig. 9, four lines are drawn representing the mean paths of electrons moving with such velocities as to make $p = 0, 1, 2,$ and 3. Each line crosses a gap when the RF field is maximum retarding, that is, when the potential has the maximum negative slope at the center of the gap. As will be seen later, a more convenient parameter, to be called k, is that whose absolute magnitude, $|k|$, specifies the number of RF cycles required for the electron to move once around the interaction space. $\frac{|k|}{N}$ is then the number of cycles between crossings of successive anode gaps, which for the π mode of Fig. 9 must take on the values:

$$\frac{|k|}{N} = |p| + \frac{1}{2}, \qquad p = 0, \pm 1, \pm 2, \cdots,$$

or the values given by the more general expression, applicable to any mode:

$$\frac{|k|}{N} = |p| + \frac{n}{N}, \qquad p = 0, \pm 1, \pm 2, \cdots.$$

In this expression, $\frac{n}{N}$ is the phase difference between adjacent resonators, expressed as a fraction of a cycle. k may thus assume the values given by

$$\left.\begin{aligned} k &= n + pN, \\ p &= 0, \pm 1, \pm 2, \cdots. \end{aligned}\right\} \quad (10)$$

Digitized by Google
Original from UNIVERSITY OF MICHIGAN
Generated on 2019-09-21 08:47 GMT / http://hdl.handle.net/2027/mdp.39015077775156
Public Domain, Google-digitized / http://www.hathitrust.org/access_use#pd-google

The mean angular velocity which the electrons must possess is then given by

$$\frac{d\theta}{dt} = \frac{2\pi}{kT} = \frac{2\pi f}{k}, \tag{11}$$

in which θ is the azimuthal angle.

For the π mode ($n = \frac{N}{2}$) it is seen that the negative integers, p, give the same series of values for $|k|$ as do the positive integers including zero. The sequence is $|k| = 4, 12, 20, 28, \cdots$. Reference to Fig. 9 indicates that electrons may travel in either direction around the interaction space and interact favorably with the RF field, provided their mean angular velocity is given by equation (11) with values of k specified by equation (10). That this should be so is clear from the fact that the anode potential wave is a standing wave with respect to which direction has no meaning. Fig. 9 also makes clear how an electron moving with velocity different from that corresponding to the lines shown, will fall out of step with the field, and on the average be accelerated as much as it is retarded, thus effecting no net energy transfer.

In Figs. 10 and 11, diagrams for the $n = 2$ mode similar to that of Fig. 9 for the π mode are shown. Fig. 10 is for electronic interaction with a standing wave of periodicity $n = 2$ and Fig. 11 for a traveling wave of the same periodicity. Again, as in the case of the π mode, the values of k for favorable electronic interaction are given by equation (10).

The sequence of positive integral values of p (including zero) and the sequence of negative integral values of p do not each give the same sequence of values for $|k|$ as was the case for the π mode. For $p \geqq 0$, $|k| = 2, 10, 18, \cdots$, and for $p < 0$, $|k| = 6, 14, 22, \cdots$. For the standing potential wave (Fig. 10) each of these values of $|k|$ does specify the velocity of possible electron motion in *either* direction for favorable interaction with the field. For the traveling potential wave (Fig. 11), on the other hand, only the positive values of k ($p \geqq 0$) correspond to electron motion in the same direction as the traveling wave, the negative values of k ($p < 0$) corresponding to electron motion in the direction opposite to the traveling wave. The sign of k has significance. If the electrons are moving with velocities specified by equation (11) with the negative values of k from equation (10), and are thus moving counter to the traveling RF field wave, the electrons are said to be driving a "reverse" mode.

The actual electron orbits do not correspond to simple translation but, as has been discussed, to rotation superposed on translation. The epicycloid-like scallops in the orbit are of no significance to the fundamental electronic mechanism. It is the mean velocity of the electron motion around the interaction space, specified by the relative values of V and B, that is of importance. The magnetron may operate, for example, at such

Digitized by Google
Original from UNIVERSITY OF MICHIGAN
Generated on 2019-09-21 08:47 GMT / http://hdl.handle.net/2027/mdp.39015077775156
Public Domain, Google-digitized / http://www.hathitrust.org/access_use#pd-google

high magnetic field, provided V has the proper value, that the scallops became relatively small variations in an otherwise smooth orbit (see Fig. 18).

In the cylindrical magnetron, the radial variation of the DC electric field, resulting in a decrease in the mean angular velocity of the electrons as they approach the anode, would make it impossible for an electron to keep step with the fields across the anode gaps were not a mechanism of phase focusing operative. That such focusing is inherent in the interaction of electrons and fields will be seen later.

3.2 *The Interaction Field:* The electronic mechanism which has been discussed in terms of electron motions through the fields at the gaps in the multisegment anode, may also be discussed in terms of the traveling waves of which the RF interaction field may be considered to be composed. The RF interaction field corresponds to anode potential waves like those plotted in Figs. 9, 10, and 11. The interaction fields for the several modes of oscillation of the resonator system are thus to be distinguished by the number, n, of repeats of the field pattern around the interaction space. Since the potential at the anode radius is nearly constant across the faces of the anode segments and varies primarily across the slots, the azimuthal variation of the field cannot be purely sinusoidal but must involve higher order harmonics.

For a mode of angular frequency $\omega = 2\pi f$, corresponding to a phase difference between adjacent resonators of $n\frac{2\pi}{N}$, the anode potential wave is of periodicity n around the anode and may be written as a Fourier series of component waves traveling in opposite directions around the interaction space:

$$V_{RF} = \sum_k A_k e^{j(\omega t - k\theta + \gamma)} + \sum_k B_k e^{j(\omega t + k\theta + \delta)}, \qquad k = n + pN, \quad p = 0, \pm 1, \pm 2, \cdots. \tag{12}$$

Note that the summations are taken over all integral values of k given by equation (10).

The interaction field for any mode of periodicity n is thus represented by two oppositely traveling waves, whose fundamentals are moving with angular velocities $\frac{\omega}{n} = \frac{2\pi f}{n}$, and whose component amplitudes, A_k and B_k, in general are not equal. γ and δ are arbitrary phase constants. The expression (12) may be reduced to the form:

$$V_{RF} = \sum_k (A_k - B_k)\cos(\omega t - k\theta + \gamma) + \sum_k 2B_k \cos\left(\omega t + \frac{\gamma + \delta}{2}\right)\cos\left(k\theta - \frac{\gamma - \delta}{2}\right), \qquad k = n + pN, \quad p = 0, \pm 1, \pm 2, \cdots, \tag{13}$$

Digitized by Google
Original from UNIVERSITY OF MICHIGAN
Generated on 2019-09-21 08:47 GMT / http://hdl.handle.net/2027/mdp.39015077775156
Public Domain, Google-digitized / http://www.hathitrust.org/access_use#pd-google

which shows that the complete field pattern may be considered to consist of a rotating wave superposed on a standing wave, each having a fundamental component of periodicity n.

The fact that the periodicities, k, of the harmonics in the expressions (12) or (13) are those for which k has the values given by (10) may be determined from a Fourier analysis of the complete anode potential waves like those of Figs. 9, 10, and 11. Only those harmonics which specify the same pattern of potentials at the centers of the anode segments as the fundamental are admitted in the analysis.

As has been mentioned before, the complete field patterns for $n = 0$ and $n = \frac{N}{2}$ are standing waves. Thus for these modes of oscillation $A_k = B_k$ in the expressions (12) and (13). For the other modes, $n = 1, 2, 3, \cdots, \frac{N}{2} - 1$, the electrons may interact with the traveling field component of expression (13) or with the standing field components which, in case $A_k = B_k$, is the only component present (see Figs. 10 and 11 for the case $n = 2$, $N = 8$).

The terms in expressions (12) and (13) for which $|k| = n$ are the fundamental components; those for which $|k| \neq n$ are called the Hartree harmonics. The components of field strength corresponding to these harmonics in the interaction field pattern fall off in intensity from anode to cathode more rapidly the higher the value of k. The variation with radius is of the form $\left(\frac{r}{r_a}\right)^k$. Thus the farther from the anode one samples the field, the more like the fundamental sinusoidal pattern it appears.

For each value of k in expression (12), whether or not $A_k = B_k$, there are two oppositely traveling sinusoidal wave components of periodicity k. Since each requires k cycles of the RF oscillation to complete one trip around the interaction space, the linear velocity at the anode surface is $\frac{2\pi f r_a}{k}$ corresponding to an angular velocity of $\frac{2\pi f}{k}$. Thus, as seen in Fig. 11 for the nstant $t + T/8$, the change of shape of the total traveling wave indicates ihat the components of which it is composed travel with different velocities. n Fig. 23 are shown instantaneous RF interaction field patterns for the tndamental components ($p = 0$) of the $n = 1, 2, 3$, and 4 modes of an anode Iock having eight resonators.

3.3 *The Traveling Wave Picture:* It is instructive to discuss the operation of the Type III magnetron oscillator in terms of electron interaction with the traveling wave components present in the interaction field. This might at first appear to be difficult in view of the many components of several possible modes. By mode frequency separation, as discussed later, it is

Digitized by Google
Original from UNIVERSITY OF MICHIGAN
Generated on 2019-09-21 08:47 GMT / http://hdl.handle.net/2027/mdp.39015077775156
Public Domain, Google-digitized / http://www.hathitrust.org/access_use#pd-google

generally possible, however, to restrict oscillation to only one mode, usually the π mode. Further, the fact that the electronic motion in crossed DC electric and magnetic fields results in a mean drift of electrons around the interaction space, enables one to restrict his attention to a single traveling wave corresponding to the fundamental or a single Hartree harmonic of the field of this mode; for it is possible, in principle at least, by proper adjustment of V and B to equate the mean angular velocity of the electrons to the angular velocity, $\frac{2\pi f}{|k|}$, of *any* one of the traveling field components. When this is true, only the field of this component has an appreciable effect upon the electron's motion. With respect to the fields of the oppositely traveling component of the same harmonic (same k), and the components of all other harmonics (different k), the electron finds itself drifting rapidly through regions of accelerating and decelerating field with no net energy transfer. From the point of view of the electron, the fields of the other components vary so rapidly as to average out over any appreciable interval of time. The only exception to these statements occurs when a harmonic of periodicity k' of another mode of frequency f' has the same angular velocity as the harmonic of periodicity k, that is, when $\frac{2\pi f'}{|k'|} = \frac{2\pi f}{|k|}$. The effect on magnetron operation of this coincidence of angular velocities will be discussed further in a later section. In the calculation of electron motions, the restriction to the field of a single traveling wave component has been called the rotating field approximation.

The consideration of the electronic mechanism has thus been reduced to that of the motion of electrons under the combined influence of the radial DC electric field, the axial DC magnetic field, and a sinusoidal field wave traveling around the interaction space. From what has been said thus far it is clear that for energy to be transferred to the RF field it is necessary that the mean electron velocity very nearly equal that of the traveling wave. Then an electron leaving the cathode in such phase as to find itself moving in a region of decelerating tangential component of the RF field, may continue to move with this region and lose energy to the field. In contrast to the Type II magnetron oscillator, the energy transferred to the RF field in this case is the potential energy of the electron in the radial DC electric field. The energy in the rotational component of the motion remains practically unaffected and the electron orbit from cathode to anode looks something like that plotted in Fig. 12 for the case with plane electrodes. On the other hand, an electron which leaves the cathode in such phase as to gain energy in a region of accelerating tangential RF field, is removed at the cathode after only one cycle of the epicycloid-like motion. If this did not occur, the electron would continue to move with the field and absorb energy. An approxi-

Digitized by Google
Original from UNIVERSITY OF MICHIGAN
Generated on 2019-09-21 08:48 GMT / http://hdl.handle.net/2027/mdp.39015077775156
Public Domain, Google-digitized / http://www.hathitrust.org/access_use#pd-google

mate orbit is shown in Fig. 13. It is instructive to compare the orbits of the two categories of electrons in the traveling wave magnetron oscillator with the orbits of corresponding electrons in the cyclotron frequency type of magnetron oscillator (Figs. 7 and 8). In each case, it is the fact that "favorable" electrons may interact for a considerably longer time than "unfa-

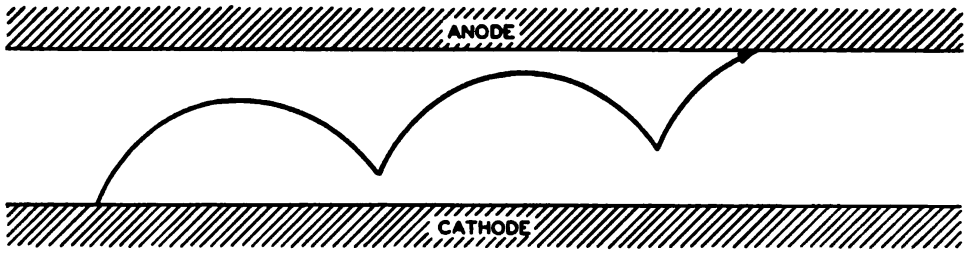

Fig. 12.—An approximate orbit of an electron which is losing energy to the RF field in a traveling wave or Type III magnetron oscillator, shown for the plane case. Here the energy loss is potential energy of the electron in the DC field. Compare this with the orbit in Fig. 8 where the energy loss is rotational energy of the electron. The DC electric force on the electron is directed from cathode to anode.

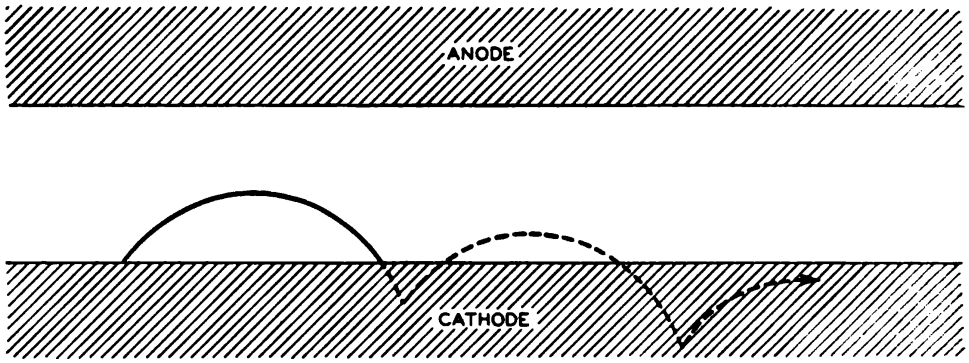

Fig. 13.—An approximate orbit of an electron which gains energy from the RF field in a traveling wave or Type III magnetron oscillator, shown for the plane case. The orbit is extended as a dashed line as though the cathode were not there. The energy gained is potential energy of the electron in the DC field. Compare this with the orbit in Fig. 7 where the energy increase is in the rotational energy of the electron. The DC electric force on the electron is directed from cathode to anode.

vorable" electrons which makes possible a net energy transfer between the DC and RF fields.

One may now compare the traveling wave picture of the electronic mechanism with that presented earlier in which the motion of electrons past the gaps in the anode structure is considered. An electron moving so that $\frac{|k|}{N} = |p| + \frac{n}{N}$ cycles of the RF oscillation elapses between its crossing of two successive anode gaps, is thus moving around the interaction space in synchronism with a traveling component of the *kth* harmonic of the inter-

Digitized by Google
Original from UNIVERSITY OF MICHIGAN
Generated on 2019-09-21 08:48 GMT / http://hdl.handle.net/2027/mdp.39015077775156
Public Domain, Google-digitized / http://www.hathitrust.org/access_use#pd-google

action field. Both points of view are of value. That involving the motion of electrons past the anode gaps is more fundamental physically. That in terms of a traveling wave component, on the other hand, is more convenient in calculations of electron orbits including space charge effects, where by transformation to a coordinate system rotating with the field it is possible to treat of motions in static fields.

3.4 *Phase Focusing:* It has been seen from two points of view how groups of electrons which move around the interaction space of the magnetron oscillator are formed by a process of selection and rejection of electrons by the tangential component of the RF field. However, space charge debunching and the discrepancy at all but one radius between the mean velocity of translation of the electrons and the velocity of the interaction field would tend to disperse these groups and prevent efficient interaction, were it not for the phase focusing provided by the radial component of the RF field.

The mechanism of the phase focusing may be discussed either in terms of the interaction of electrons with the actual fields existing at the anode gaps or in terms of the traveling wave picture of the electronic mechanism. The fundamental mechanism involved depends upon the effect of the radial component of the RF field in aiding or opposing the radial DC field in determining the mean drift velocity of the electron around the interaction space. If the radial RF field increases the net radial field in which the electron finds itself at any instant, the mean velocity of the electron increases as can be seen from equation (5) for the plane case. Similarly, a decrease in the net radial electric field, caused by the RF radial component, results in decreased electron translation velocity. These changes in the electron's velocity operate so as to keep the electron near the position in which it can interact most favorably with the tangential component of the RF field.

Consider an electron which crosses an anode gap at the instant the RF field there is maximum retarding, that is, an electron which is to be found on the plane marked M in Fig. 14 at this instant. It experiences about as great an increase of velocity by virtue of the radial component aiding the DC radial field before crossing the gap as decrease by virtue of the radial component opposing the DC radial field after crossing the gap. Another electron which is lagging behind the electron just considered is to be found opposite a positively charged anode segment, as at P in Fig. 14, when the RF field passes through its maximum value. Since the RF field component decreases with time after this instant, the effect of the radial component of the field on the electron's velocity after crossing the gap will be less than its effect before crossing the gap, the net effect being one of increasing the mean velocity of translation, bringing the electron more nearly into the proper phase. An electron which leads the electron first considered, on the other

Digitized by Google
Original from UNIVERSITY OF MICHIGAN
Generated on 2019-09-21 08:48 GMT / http://hdl.handle.net/2027/mdp.39015077775156
Public Domain, Google-digitized / http://www.hathitrust.org/access_use#pd-google

hand, will be found opposite the negatively charged anode segment beyond the gap when the RF field is maximum, and for it the net effect of the radial component is to reduce the mean velocity of the electron, bringing it also more nearly into the proper phase.

In discussing the mechanism of phase focusing from the traveling wave point of view, the field lines of Fig. 14 may be considered to be those of the traveling wave component with which the electrons are interacting. Then the whole field pattern indicated moves to the right as shown by the arrow above the plane of maximum retarding tangential field at *M*. An electron

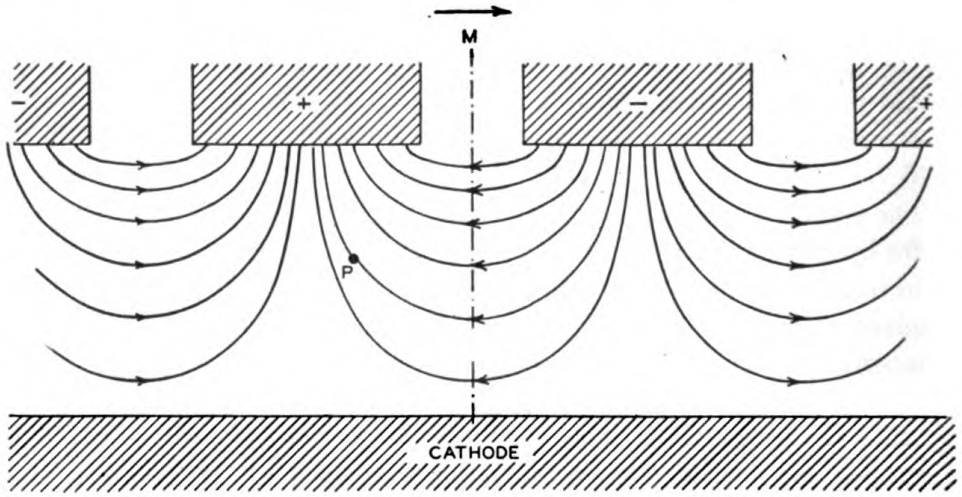

Fig. 14.—A plot of lines of electric force on an electron (drawn for the plane case) for the fundamental of the π mode. It is shown for the purpose of explaining the phase focusing property of the radial field component. The plane of maximum opposing force on the electron intersects that of the figure along the line *M*. The arrow shown above the line *M* indicates the direction of electron motion. The force on the electron due to the DC electric field is directed from cathode to anode. The force lines shown may be considered to be those of the total fundamental field component at the instant the field is maximum. Then an electron at the point *P* will cross the center of the anode gap after the instant of maximum retarding force. Or the lines shown may be considered to be those of the traveling component of the fundamental moving in the same direction as the electrons. In this case an electron at the point *P* is lagging behind the maximum of the retarding tangential field.

which falls behind the position *M* to the point *P*, for example, finds itself in a stronger net radial electric field which increases its mean translational velocity tending to bring it back to the position *M*. The reverse holds for an electron which runs ahead of the plane *M*.

3.5 *Space Charge Configuration:* The over-all picture of the electronic mechanism in the Type III magnetron oscillator thus presents a spoke-shaped space charge cloud of electrons wheeling around the cathode in synchronism with the anode potential wave, each spoke in a region of maximum retarding field. This picture of what is happening has been very handsomely confirmed by actual orbital calculations taking account of

Digitized by Google
Original from UNIVERSITY OF MICHIGAN
Generated on 2019-09-21 08:48 GMT / http://hdl.handle.net/2027/mdp.39015077775156
Public Domain, Google-digitized / http://www.hathitrust.org/access_use#pd-google

space charge. The calculations have been carried out by the so-called self consistent field method using the rotating field approximation mentioned earlier. In this method, orbits of electrons are calculated in an assumed field, and the space charge due to these electrons determined. The field calculated on the basis of this space charge distribution may then be compared with that assumed. This cycle of calculations is repeated, each time using the calculated field of the previous cycle as that in which the electrons move, until a field is obtained which is consistent with that used in calculating the electron orbits. This method will be recognized as that used in the calculation of electron orbits about the nucleus in atoms.

The result of one such calculation is shown in Fig. 15. The orbits of four electrons which were emitted from the cathode in different phases are plotted in a set of coordinates rotating with the RF field component. One electron is returned to the cathode, and the other three reach the anode. The boundaries of the space charge cloud are shown as dashed lines. The spoke-shaped structure is clear, and its position with respect to the rotating anode potential wave is as expected. The number of spokes of the cloud is equal to the periodicity of the component of the mode with which the electrons are interacting. In the case of Fig. 15 there are four spokes, since the magnetron is operating in the fundamental of the $n = 4$ mode ($k = 4$, $p = 0$).

3.6 *Induction by the Space Charge Cloud:* Another view of the mechanism by which the electrons drive the resonator system may be obtained by considering the effect of the space charge spokes in inducing current flow in the anode segments themselves. For example, the oscillation of the resonator block in its π mode corresponds to the periodic interchange of electric charge from each anode segment, around a resonating cavity to the next anode segment. This oscillation is maintained, much in the manner of a pendulum escapement drive, by the space charge spoke appearing in front of an anode segment at that instant in the oscillation cycle when it can aid in building up the net positive charge on the segment. At the same instant, the adjacent segments, being opposite a "gap" in the space charge wheel, may build up a negative charge.

The RF current, I_{RF}, induced in the anode structure, thus results from the motion of the spoke-shaped space charge cloud in the interaction space. It is not to be confused with the total circulating RF current in the resonator system. Whereas I_{RF} must be in a phase with the space charge cloud it need not be in phase with the RF voltage, V_{RF}, between the anode segments. In terms of the electron motions, this means that the spokes of the space charge cloud may lead or lag the maxima in the tangential field. In general, the electronic admittance defined by the ratio of I_{RF} to V_{RF} may thus include a susceptance as well as a conductance. The product of V_{RF} and the in-phase component of I_{RF}, integrated over a period of one cycle of RF

Digitized by Google
Original from UNIVERSITY OF MICHIGAN
Generated on 2019-09-21 08:48 GMT / http://hdl.handle.net/2027/mdp.39015077775156
Public Domain, Google-digitized / http://www.hathitrust.org/access_use#pd-google

oscillation, equals the energy per cycle which is delivered to the load. This amount of energy is twice that transferred in the half cycle during which the spokes of space charge move against the field from positions in front of one

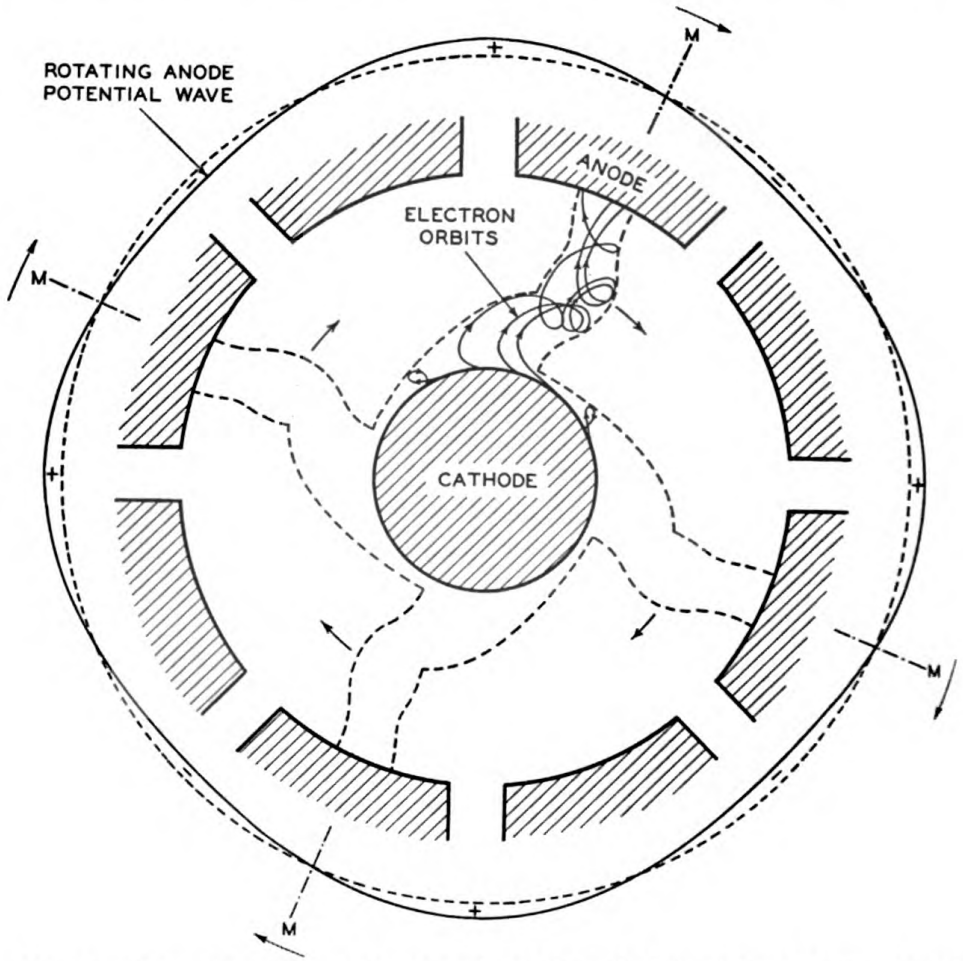

Fig. 15.—The orbits of four electrons which left the cathode in different phases, plotted n a coordinate system rotating with the anode potential wave. These orbits have been icalculated by the self consistent field method which includes space charge effects. In this frame of reference the orbits exhibit loops whereas in a stationary frame they would more nearly exhibit cusps. The dashed lines inclose the orbits of the electrons and hence delineate the boundaries of the space charge cloud which rotates around the cathode in synchronism with the anode potential wave. Planes of maximum retarding tangential field are represented by the lines *M* (see Fig. 14). This figure is reproduced by courtesy of the British Committee on Valve Development (CVD) and is taken from the CVD Magnetron Report No. 41.

set of alternate anode segments to similar positions in front of the adjacent anode segments.

In each spoke of the electron space charge cloud, individual electrons progress from cathode to anode. The DC current, I, passed by the magnetron is made up of electrons which strike the anode from the ends of the space charge spokes. Quite apart from its dependence on other parameters,

Digitized by Google
Original from UNIVERSITY OF MICHIGAN
Generated on 2019-09-21 08:49 GMT / http://hdl.handle.net/2027/mdp.39015077775156
Public Domain, Google-digitized / http://www.hathitrust.org/access_use#pd-google

this DC current is directly proportional to anode length, h. If the magnetron is driven at greater DC current, the space charge in the interaction space increases but the phase of its structure with respect to the traveling anode wave does not change to a first approximation. Thus both the in-phase and quadrature components of I_{RF} increase with no change in electronic admittance. The second order effects which do arise from small shifts in the phase of the rotating space charge structure are discussed in Section 10.4 *Electronic Effects on Frequency.*

4. Conditions Relating Measurable Parameters

4.1 *Necessary Conditions for Oscillation:* After having discussed the electron motions in the interaction space of the Type III magnetron oscillator, the viewpoint will now be changed to that looking from the outside in, so to speak, and it will be asked what conditions relating measurable parameters are imposed by the nature of the electronic mechanism. Beyond the geometrical parameters of cathode and anode radii, r_c and r_a, one can determine the DC voltage, V, applied between cathode and anode; the magnetic field B, in which the magnetron is placed; the DC current, I, drawn by the anode; the frequency of oscillation, f; and, from impedance measurements, the RF load, $Y_s = G_s + jB_s$, presented to the electrons by the resonator, output, and load.

Perhaps the most fundamental condition for oscillation of the traveling wave magnetron is that imposed by the requirement of synchronism between the electron drift and the RF field. As has been indicated, the angular velocity of a rotating component of a Hartree harmonic of the interaction field, of order k, is $\frac{2\pi f}{|k|}$. An approximate expression for the mean angular velocity of the electrons may be determined by neglecting the variation of electric field with radius and calculating the angular velocity midway between cathode and anode, thus:

$$\frac{v}{(r_a + r_c)/2} = \frac{E/B}{(r_a + r_c)/2} = \frac{V/(r_a - r_c)B}{(r_a + r_c)/2} = \frac{2V}{(r_a^2 - r_c^2)B}.$$

Equating this to the angular velocity $\frac{2\pi f}{|k|}$, one obtains the relation:

$$V = \frac{\pi f}{|k|} r_a^2 B \left[1 - \left(\frac{r_c}{r_a}\right)^2\right]. \tag{14}$$

In this derivation it should be recognized that the angular velocity $\frac{2\pi f}{|k|}$ may be considered either to be that of a traveling component of the RF field with which the electron interacts or the mean angular velocity which the

Digitized by Google
Original from UNIVERSITY OF MICHIGAN
Generated on 2019-09-21 08:49 GMT / http://hdl.handle.net/2027/mdp.39015077775156
Public Domain, Google-digitized / http://www.hathitrust.org/access_use#pd-google

electron must have to maintain proper phase with the total RF fields existing across the anode gaps.

Posthumus[13] derived an expression, assuming negligible cathode diameter, which is similar to equation (14). By the same method as that used above, Slater has derived an expression differing from (14) by a term which results from the use of a more accurate value for the electron's translational velocity at the midpoint between cathode and anode in cylindrical geometry. Slater's expression is:

$$V = \frac{\pi f}{|k|} r_a^2 B \left[1 - \left(\frac{r_c}{r_a}\right)^2\right] - 2\frac{m}{e}\left(\frac{\pi f r_a}{|k|}\right)^2 \left[1 - \left(\frac{r_c}{r_a}\right)^2\right]. \quad (15)$$

Hartree has derived an expression from a consideration of the conditions under which electrons are just able to reach the anode with infinitesimal amplitude of RF voltage in the k^{th} harmonic. It is:

$$V = \frac{\pi f}{|k|} r_a^2 B \left[1 - \left(\frac{r_c}{r_a}\right)^2\right] - 2\frac{m}{e}\left(\frac{\pi f r_a}{|k|}\right)^2. \quad (16)$$

In a sense this condition represents a cut-off relation for the oscillating magnetron analogous to Hull's cut-off relation for the DC magnetron [equation (8)].

Plotted on a V-B graph, the expressions (14), (15), and (16) represent parallel straight lines. The line of equation (14) passes through the origin; the so-called Hartree line of (16) is tangent to the DC cut-off parabola; the so-called Slater line of (15) lies above the Hartree line but below the line of expression (14). Each of the above expressions indicates that the electrons will drive a given harmonic of the RF interaction field in a type III magnetron oscillator only at values of DC voltage and magnetic field which bear a definite relation. This relation expresses the fact that V/B is very nearly constant [equation (14)].

In Fig. 16 are plotted as an illustration, the Hartree lines for the fundamentals ($p = 0$) of the $n = 1, 2, 3,$ and 4 modes and for the $k = -5$ harmonic ($p = -1$) of the $n = 3$ mode of a 10 cm. magnetron with eight resonators.[16]

[16] This magnetron, used as an illustrative example in Part I, has the following characteristics:

Number of resonators, N = 8.
Cathode radius, r_c = 0.3 cm.
Anode radius, r_a = 0.8 cm.
Anode length, h = 2.0 cm.
Anode to end cover distance = 0.6 cm.
Frequency (π mode), f = 2800 mc/s.
Wavelength (π mode), λ = 10.7 cm.
DC operating voltage, V = 16 kv.
Operating magnetic field, B = 1600 gauss.
Typical operating peak current, I = 20 amps.
Over-all efficiency, η = 42%.
Peak power output, P_o = 135 kw.
Pulse duration, τ = 1 microsecond.
Pulse repetition frequency = 1000 pps.

Digitized by Google
Original from UNIVERSITY OF MICHIGAN
Generated on 2019-09-21 08:49 GMT / http://hdl.handle.net/2027/mdp.39015077775156
Public Domain, Google-digitized / http://www.hathitrust.org/access_use#pd-google

Since the operating voltage is found to increase with increasing current, oscillation at a constant anode current takes place along a line, such as the Slater line for example, lying slightly above and parallel to the Hartree line (see Fig. 16). The separation of the operating line from the Hartree line increases with increasing DC current.

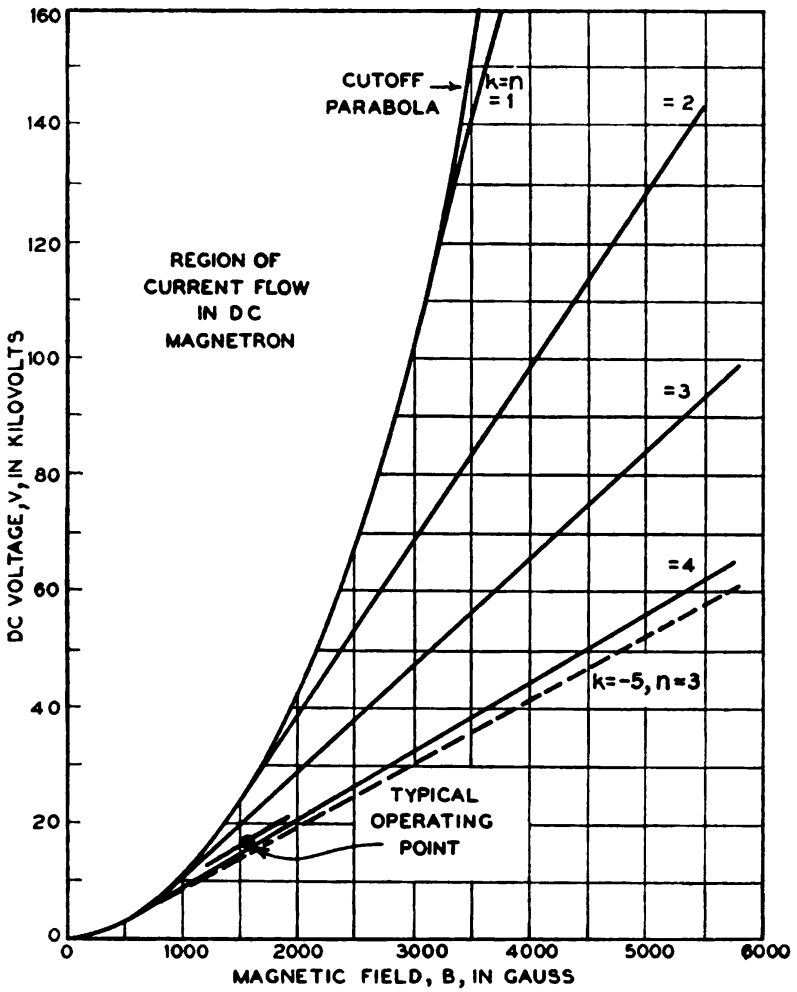

Fig. 16.—A *V-B* plot for a magnetron having eight resonators (see footnote 16) showing the cut-off parabola and Hartree lines for several rotating field components. The ranges of DC voltage and magnetic field have been extended considerably beyond values ever applied to such a magnetron to show the lines for the fundamentals of all of the modes. The typical operating point plotted is that specified in footnote 16 and plotted in Fig. 17.

The necessary conditions for oscillation discussed above have been of great value in the identification of the modes of operating magnetrons and as the starting point in the design of new magnetrons for given wavelength, magnetic field, and voltage.

4.2 ***The Performance Chart:*** Another fundamental performance char-

Digitized by Google
Original from UNIVERSITY OF MICHIGAN
Generated on 2019-09-21 08:50 GMT / http://hdl.handle.net/2027/mdp.39015077775156
Public Domain, Google-digitized / http://www.hathitrust.org/access_use#pd-google

acteristic of the operating magnetron is the *V-I* plot or performance chart. In Fig. 17 such a chart is plotted for the same magnetron[16] used as the example for Fig. 16. In it are plotted contours of constant magnetic field, RF power output, and over-all efficiency. The fact that the constant mag-

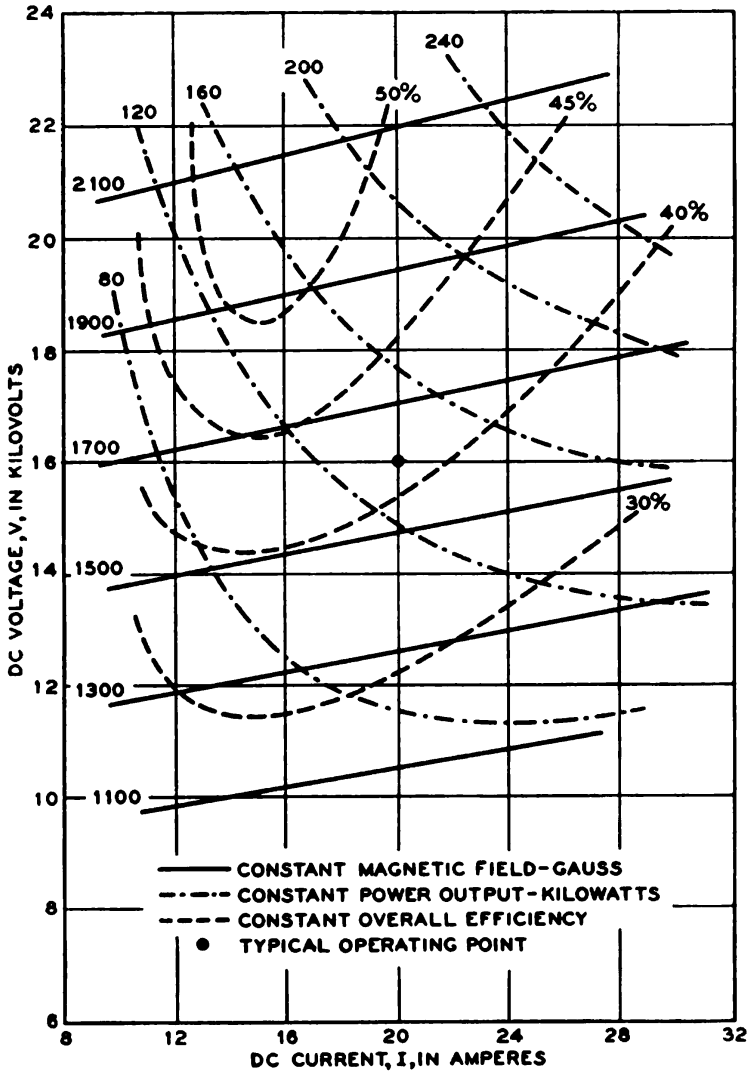

Fig. 17.—A *V-I* plot or performance chart for a magnetron having eight resonators (see footnote 16). Contours of constant magnetic field, power output, and over-all efficiency are shown. The typical operating point plotted is that specified in footnote 16 and plotted in Fig. 16.

netic field contours are nearly horizontal and spaced as they are is a manifestation of the oscillation conditions of equations (15) and (16). The increase of voltage with current is an effect, attributable to the space charge, quite independent of the condition of synchronism between field and elec-

Digitized by Google
Original from UNIVERSITY OF MICHIGAN
Generated on 2019-09-21 08:50 GMT / http://hdl.handle.net/2027/mdp.39015077775156
Public Domain, Google-digitized / http://www.hathitrust.org/access_use#pd-google

trons. For if the magnetron is to deliver more power at a given magnetic field, the induced RF current must increase. This entails increased space charge and a greater DC current flow. To maintain the increased space charge additional DC voltage is required.

4.3 *The Electronic Efficiency:* The performance chart also shows the not too surprising fact that more power may be drawn from the magnetron as the voltage and current are increased. More interesting are the increase of the over-all efficiency with voltage and the maximum through which the efficiency passes with increasing current. This variation of over-all efficiency, η, is to be attributed to changes in the electronic efficiency, η_e, since the other factor involved in the over-all efficiency, the circuit efficiency, η_c, is essentially constant over the diagram ($\eta = \eta_e\eta_c$).

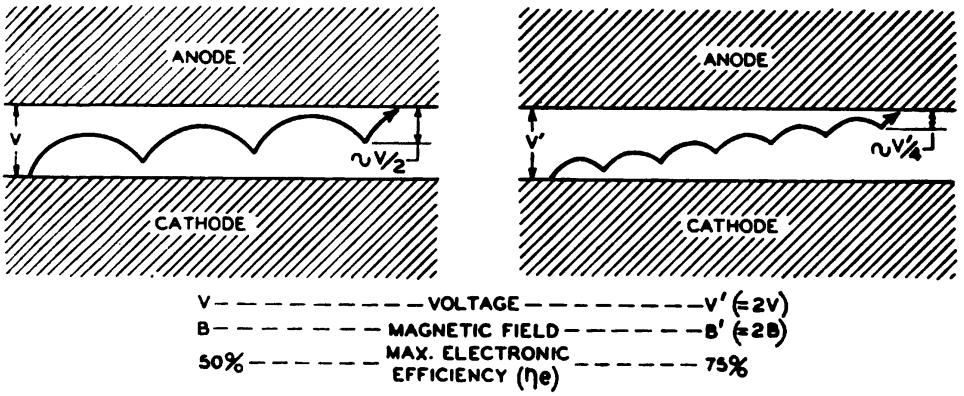

Fig. 18.—Approximate orbits of electrons which transfer energy to the RF field, plotted for operation of a plane magnetron at two different magnetic fields. It is shown how the relative kinetic energy gained beyond the last cusp and dissipated at the anode decreases as the magnetic field and voltage of operation are increased, resulting in increased efficiency of electronic conversion of energy from the DC field to the RF field. The two illustrative cases differ by a factor two in DC voltage and hence by the same factor in magnetic field and diameter of the rolling circle.

The increase of electronic efficiency with voltage, and hence magnetic field, may be explained by the picture of electron motions in the interaction space. The highest electronic efficiency is attained when the electrons reaching the anode do so with least kinetic energy. For the approximate orbit of Fig. 12, the energy lost at the anode per electron is that gained as kinetic energy beyond the last cusp. Bringing the last cusp closer to the anode, corresponding to a reduction of the amplitude of the rotational component of the electron motion, reduces the ratio of kinetic energy lost at the anode to the potential energy possessed by the electron at the cathode. Thus, according to equation (6) for the radius of the rolling circle, this fractional energy loss should vary as V/B^2 or, since V/B is approximately constant, as $1/B$, η_e increasing with B. In terms of the approximate electron orbits for a plane magnetron, Fig. 18 shows how increase in voltage

Digitized by Google
Original from UNIVERSITY OF MICHIGAN
Generated on 2019-09-21 08:50 GMT / http://hdl.handle.net/2027/mdp.39015077775156
Public Domain, Google-digitized / http://www.hathitrust.org/access_use#pd-google

and magnetic field increases the electronic efficiency. The dependence of electronic efficiency on B predicted by this simple picture is in accord with the dependence predicted by more sophisticated theories.

In all probability the decrease of electronic efficiency toward low and high currents is, in part at least, the result of decrease in the phase focusing action. This occurs as a result, on the one hand, of low RF field strength in the proper mode when the current and RF oscillation are small, and, on the other hand, as a result of space charge debunching when the current and space charge become very large. In addition, at low currents the leakage to the anode of electrons which are not effective in interaction with the RF field, assumes a more dominant role, reducing the effective electronic efficiency. These electrons are no doubt those emitted near or at the ends of the cathode.

Of importance to the motion of electrons near the ends of the interaction space, and thus to the electron leakage, are the configurations of the DC electric and magnetic fields there. These depend upon the geometry of the cathode ends and surrounding walls and of the magnetic pole pieces. The electrons are largely confined to the interaction space by the axial force, directed toward the center of the interaction space, produced by the non-uniformities in the electric and/or the magnetic fields. For uniform magnetic field, the desired focusing action on the electrons may be achieved by disks at cathode potential which are mounted at each of the cathode and extend beyond the cathode surface over the ends of the interaction space as may be seen in Fig. 1. In other cases, distortion of the magnetic field in the end spaces of the magnetron, in addition to cathode end disks, has been used to produce the same effect.

Although the dependence of operation of a magnetron oscillator on load is primarily a circuit problem, detailed discussion of which will be delayed until the RF circuit has been discussed, there is one feature of the dependence on load and circuit characteristics which may properly be discussed now. This is the dependence of the electronic efficiency, η_e, on the circuit conductance, G_s, presented to the electrons. The plot in Fig. 19 is a typical example and shows an optimum value of conductance, to each side of which η_e decreases. With decreasing G_s the RF voltage increases. Whereas initially the increase of V_{RF} with decreasing G_s increases the phase focusing properties, it results eventually in such strong RF field that electrons are drawn more or less directly to the anode where they arrive with considerable kinetic energy. On the other hand, the decrease in V_{RF} with increasing G_s eventually will result in an RF field too weak to produce the necessary amount of phase focusing. The value of G_s presented to the electrons depends not only upon the output circuit properties and load but also upon the parameters of the resonator itself. The dependence of electronic efficiency upon G_s is a

Digitized by Google
Original from UNIVERSITY OF MICHIGAN
Generated on 2019-09-21 08:50 GMT / http://hdl.handle.net/2027/mdp.39015077775156
Public Domain, Google-digitized / http://www.hathitrust.org/access_use#pd-google

good example of how intimately the electronics and circuit of the magnetron oscillator are associated.

4.4 *Scaling:* Once an efficient design has been achieved for a given wavelength, voltage, current, and magnetic field, one is interested in reproducing it at other values of these parameters. In doing this, use is made of the theory of scaling. For cases where the interaction space remains geometrically similar and the magnetron operates in the same mode, the same efficiency is presumably achieved when it is arranged that the electron orbits remain similar. Directly from dimensional arguments applied to Maxwell's equations for the electromagnetic field and to the equations of

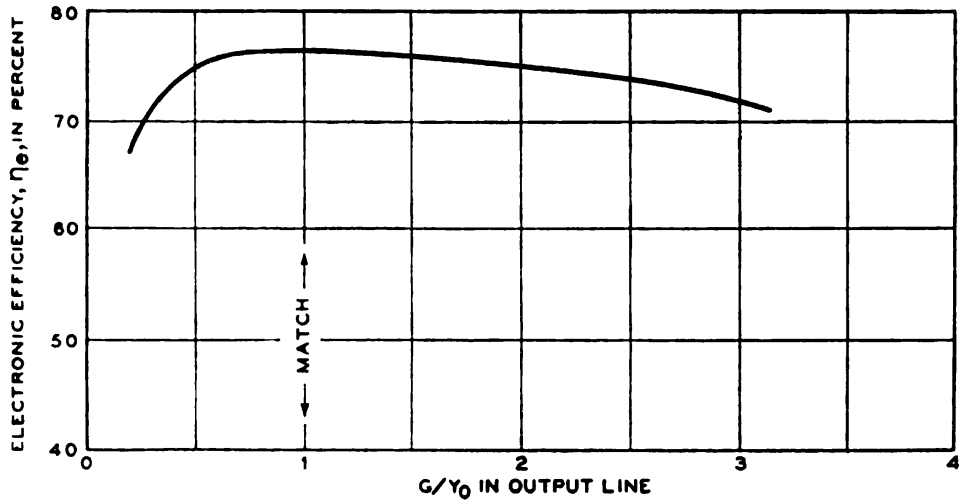

Fig. 19.—A plot of electronic efficiency as a function of load conductance. The conductance G/Y_0 in the output line is related to that presented by the circuit to the electrons, G_e, directly through the magnetron resonator and output circuits. The magnetron with which these data were obtained is a 3.2 cm. magnetron having sixteen resonators.

motion of the electrons, it can be shown that the orbits and operation will be equivalent for all conditions for which the loading and the quantities

$$\lambda B, \quad (\lambda/r_a)^2 V, \quad \text{and} \quad (\lambda^3/r_a^2 h) I$$

remain invariant.

It would perhaps be of interest to consider, as a simple example, the case for which all the linear dimensions of a given magnetron are changed by a factor α. The new resonant wavelength, λ', is equal to $\alpha\lambda$ since the new resonator is α times the size of the original, while the new frequency is $f' = f/\alpha$. The new anode radius, cathode radius, and anode length scale directly so that

$$r'_a = \alpha r_a, \; r'_c = \alpha r_c \text{ and } h' = \alpha h$$

Digitized by Google
Original from UNIVERSITY OF MICHIGAN
Generated on 2019-09-21 08:50 GMT / http://hdl.handle.net/2027/mdp.39015077775156
Public Domain, Google-digitized / http://www.hathitrust.org/access_use#pd-google

Since λB, $(\lambda/r_a)^2 V$, and $(\lambda^3/r_a^2 h)I$ must remain invariant,

$$\lambda' B' = \lambda B \text{ or } B' = B/\alpha,$$

$$(\lambda'/r'_a)^2\, V' = (\lambda/r_a)^2\, V \text{ or } V' = V,$$

and

$$(\lambda'^3/r'^2_a\, h')\, I' = (\lambda^3/r_a^2\, h)\, I \text{ or } I' = I.$$

Thus the magnetic field changes by $1/\alpha$ and the operating voltage and current remain unchanged.

The idea of scaling has been extended to magnetrons of varying r_c/r_a and N by the introduction of sets of reduced variables for V, B and I involving r_c/r_a and N, in terms of which the performance may be expressed independently of the exact nature of the magnetron.

4.5 *Effect of Other Components in the Interaction Field:* In the discussion of the traveling wave magnetron oscillator, it has been considered that the electrons interact with a single traveling RF field component, generally a component of the fundamental of the π mode. The justification for this, as has been stated, is that from the point of view of the electron the fields of all other Hartree harmonics of the π mode vary so rapidly that their effects average out over an appreciable number of RF cycles. This is generally true, as well, for the harmonics of other modes which may be excited. The fact has been mentioned that it is possible for the values of V and B for oscillation in the π mode very nearly to satisfy equation (16) for oscillations in a harmonic of another mode. Then the angular velocity, $\frac{2\pi f'}{|k'|}$, of the harmonic very nearly equals that of the π mode, $\frac{2\pi f}{N/2}$, and the Hartree line of the harmonic lies very close to that of the π mode (see Fig. 16). The effect of this situation on magnetron operation will be discussed in connection with the problem of "moding" in Section 10.6 *Oscillation Buildup—Starting.*

Of particular interest is the presence in the interaction space, in addition to the π mode field, of an RF field component which is independent of angle. Such a component appears, for example, as an inherent contamination in the interaction field of the so-called "rising sun" type resonator system to be described later. Generally, this component is of no concern because the electrons interact with the π mode component throughout a time interval covering several cycles, during which the effect of the contamination averages out. The exception to this occurs when the frequency of the rotational component of the electron motion, approximately the cyclotron frequency, resonates with the RF frequency as in a Type II magnetron. From equation (2) this occurs for the plane case when $f = c/\lambda = eB/2\pi m$, from which $\lambda B = 2\pi cm/e = 10{,}700$ gauss-cm. For a typical cylindrical case the constant is somewhat greater, being about 12,500 gauss-cm. When λB has this

Digitized by Google
Original from UNIVERSITY OF MICHIGAN
Generated on 2019-09-21 08:50 GMT / http://hdl.handle.net/2027/mdp.39015077775156
Public Domain, Google-digitized / http://www.hathitrust.org/access_use#pd-google

value, perturbation of the electron motion occurs, decreasing the efficiency of interaction with the traveling wave and manifesting itself on the perform-

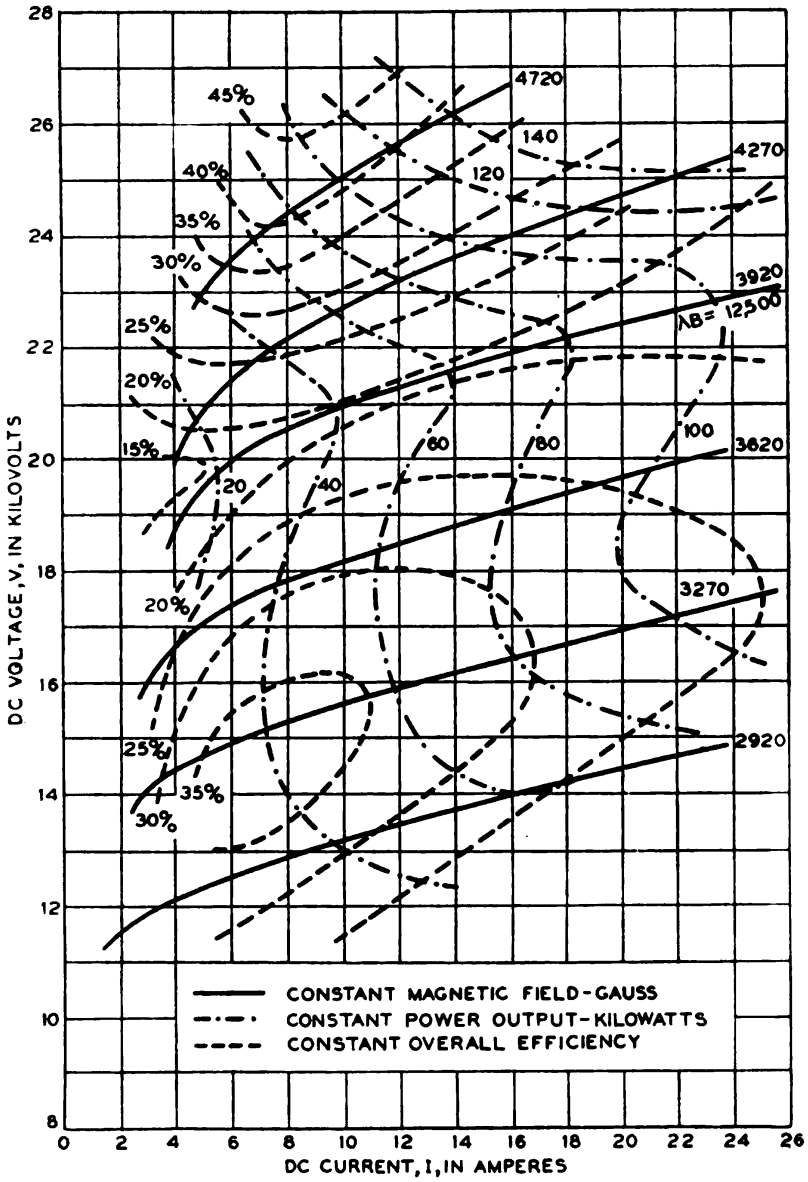

Fig. 20.—A performance chart for a magnetron which has present in its interaction field a contaminating component independent of azimuth. Note the efficiency "valley" appearing along the line $B = 3920$ gauss (compare with Fig. 17). The wavelength of the magnetron being 3.18 cm., λB along the efficiency "valley" is 12,500 gauss-cm. The data were obtained on a magnetron having a "rising sun" type resonator system and are reproduced here through the courtesy of the Columbia Radiation Laboratory.

ance chart as a "valley" in operating efficiency appearing along the constant B line for which $\lambda B = 12{,}500$ gauss-cm. In Fig. 20 is plotted the performance chart of a magnetron, having a "rising sun" type anode structure which

Digitized by Google
Original from UNIVERSITY OF MICHIGAN
Generated on 2019-09-21 08:51 GMT / http://hdl.handle.net/2027/mdp.39015077775156
Public Domain, Google-digitized / http://www.hathitrust.org/access_use#pd-google

exhibits this kind of behavior. In general, it would be preferable to operate this magnetron at magnetic fields above the "valley," but considerations having to do with available magnetic fields, in some cases may make it necessary to operate near the efficiency maximum at lower magnetic fields.

5. The RF Circuit of the Magnetron Oscillator

5.1 *General Considerations:* The discussion to this point has presented a picture of how the multicavity magnetron oscillator works from the point of view of its electronics; how in this respect it is related to other types of magnetron oscillators; and how, on the basis of the picture of the electronic mechanism, some of its fundamental operating characteristics are to be accounted for. In the same manner the RF circuit of the magnetron oscillator, comprising the resonator system, the output circuit, and the load, will be discussed. The importance of this part of the magnetron is apparent. It provides the RF fields with which the electrons interact. To do this, electromagnetic energy must be stored in the cavities of the resonator, which reservoir in turn is tapped to deliver energy through the output circuit to the useful load. The detailed manner in which these functions are performed has a bearing, not only on such circuit characteristics as circuit efficiency or on the effect of load on frequency, but, as has been seen, on the electronic efficiency as well. Furthermore, the circuit analysis of the magnetron oscillator enables one to explain the remaining important operating characteristic, the so-called Rieke diagram, which describes the operational dependence on load.

The type of resonator system used in the magnetron oscillator of concern here has already been indicated in Fig. 1. It is a resonator system comprising a number of cavities spaced equally about the cylindrical anode. This general shape is dictated by the slotted anode cylinder upon which the RF interaction field is set up. To be sure, other types of resonators have been devised which contrive to place π mode potentials on the anode segments of a cylindrical magnetron. Here, however, except for brief references, the discussion will concern itself with the multicavity resonator system of the general type shown in Fig. 1. Although the individual cavities have not been limited to hole and slot geometry like those shown in Fig. 1, and other features have been added, a resonator system consisting of a system of cavities, arranged around the anode in the manner of Fig. 1, has been used in the majority of magnetron oscillators developed for centimeter wave generation since 1940.

5.2 *Simple Single Frequency Resonator:* The fact that the magnetron resonator system has a number of cavities electromagnetically coupled together makes it multiresonant. What has been learned about the various modes and their electromagnetic field configurations, and how they may in a sense be controlled to improve magnetron operation must be discussed in some detail. Before this is done, however, it would be well to refresh one's memory as to the fundamental ideas concerned with a single electromagnetic

Digitized by Google
Original from UNIVERSITY OF MICHIGAN
Generated on 2019-09-21 08:51 GMT / http://hdl.handle.net/2027/mdp.39015077775156
Public Domain, Google-digitized / http://www.hathitrust.org/access_use#pd-google

resonator like one of the magnetron cavities.[17] This is important not only because the magnetron resonator system comprises a number of such cavities but also because the resonator system as a whole may under certain circumstances be considered to resonate at one frequency, in which case it behaves like a simple single frequency resonator.

Concerned with the simple electromagnetic resonator are the fundamental ideas of a natural frequency of resonance, of the rate of energy loss or the sharpness of resonance, and of the characteristic admittance or the energy storage capacity. The electromagnetic resonator, whether it has lumped or distributed constants, consists of a device in which energy is transferred between electric and magnetic fields cyclically in a manner entirely analogous to the transfer of energy between potential and kinetic in the simple swinging pendulum. Each of these oscillations, electromagnetic or mechanical, is described by a second order differential equation in terms of a parameter such as voltage or current on the one hand, and angular displacement of the pendelum bob on the other. The solutions represent simple harmonic oscillations, the one for the simple electrical circuit having the frequency,

$$f_0 = \frac{\omega_0}{2\pi} = \frac{1}{2\pi\sqrt{LC}}. \tag{17}$$

This occurs when the susceptances of the two components of the circuit, L and C, are equal, or when

$$\frac{1}{\omega_0 L} = \omega_0 C. \tag{18}$$

The fact that a finite time is required to transfer the energy between the electric and magnetic fields is a lumped constant circuit is not surprising since a finite time is required for a condenser to charge or discharge, and for a current to build up or decay in an inductance.

5.3 *The Q Parameters:* The type of oscillation of the simple L-C circuit discussed above is its natural or free oscillation, not constrained by the ap-

[17] In the next sections of this paper, material has been drawn from the theory of a single resonant circuit having either lumped or distributed constants, the theory of coupled circuits, and the theory of centimeter wave transmission in coaxial lines and wave guides, treatments of which are to be found in the following representative texts:

L. Page and N. I. Adams, *Principles of Electricity*, D. Van Nostrand Co., New York (1931).

E. A. Guilleman, *Communication Networks*, Vols. I and II, John Wiley and Sons, New York (1931).

J. G. Brainerd, G. Koehler, H. J. Reich, and L. F. Woodruff, *Ultra-High Frequency Techniques*, D. Van Nostrand Co., New York (1942).

J. C. Slater, *Microwave Transmission*, McGraw-Hill Book Co., New York (1942).

R. I. Sarbacher and W. A. Edson, *Hyper and Ultrahigh Frequency Engineering*, John Wiley and Sons, New York (1943).

S. A. Schelkunoff, *Electromagnetic Waves*, D. Van Nostrand Co., New York (1943).

Digitized by Google
Original from UNIVERSITY OF MICHIGAN
Generated on 2019-09-21 08:51 GMT / http://hdl.handle.net/2027/mdp.39015077775156
Public Domain, Google-digitized / http://www.hathitrust.org/access_use#pd-google

plication of any external driving force. It is the sort of oscillation the circuit would undergo were it left to itself after being excited or started initially. Such an oscillation, once started, does not continue indefinitely because the energy put into the circuit initially, dissipates itself in resistive losses in the circuit components and in a load which may be coupled electromagnetically to the circuit. The exponential rate at which the original energy is dissipated is a very important characteristic of the circuit. It is usually specified by a parameter Q, defined as 2π times the ratio of the energy stored in the circuit to the energy dissipated per cycle of the oscillation.[18] Thus a circuit always loses a certain fraction of its energy per cycle independent of how great this energy may be. In the exponential decay of oscillations in a resonator from which the drive has been removed, $Q/2\pi$ is the number of cycles of oscillation, required for the stored energy to decay to $1/e$ of its initial value. Similarly, in the buildup of oscillations in a resonator to which is fed a constant amount of energy per cycle, $Q/2\pi$ is the number of cycles required for the stored energy to buildup to $(1 - 1/e)$ of its final equilibrium value.

It is possible to define several types of Qs for a circuit, depending upon the nature of the energy dissipation being considered. If one considers only the energy lost in the resistance of the circuit components themselves, one defines the so-called unloaded Q, Q_0. If the circuit is coupled electromagnetically to a resistive load, the Q defined in terms of the energy dissipated in the load and internal resistance is called the loaded Q, Q_L. Finally, for some purposes it is convenient to consider the ratio of energy stored to that dissipated in the external load only. This defines the external Q, Q_{ext}. It is clear that both Q_L and Q_{ext} are functions of the degree of coupling between the oscillating circuit and the resistive load.

The Q parameters, however, tell one more than the rate at which energy is dissipated in a circuit oscillating at its natural frequency. The admittance of the circuit, measured as a function of the frequency of an external driving source, passes through a minimum at the natural frequency of oscillation of the circuit. The sharpness of the dip in the admittance curve is determined by the Q_L of the circuit in such a manner that the sharper the dip, the higher the Q_L. In passing through resonance the susceptance of the circuit changes sign from inductive for frequencies below the frequency of resonance, to capacitive, for frequencies above the frequency of resonance. The rate at which the susceptance varies with frequency is another measure of the sharpness of resonance and of the Q_L of the circuit.

5.4 *Energy Storage and Loss:* The remaining ideas concerned with a simple *L-C* circuit of lumped constants which should be mentioned here are the characteristic admittance of the circuit, the energy storage capacity,

[18] As will be seen in the subsequent discussion the factor 2π is included here so as to simplify the definition in terms of admittance.

Digitized by Google
Original from UNIVERSITY OF MICHIGAN
Generated on 2019-09-21 08:51 GMT / http://hdl.handle.net/2027/mdp.39015077775156
Public Domain, Google-digitized / http://www.hathitrust.org/access_use#pd-google

and how these are related to each other and to the concepts already mentioned. For this purpose it is convenient to consider the circuit shown in Fig. 31 (c). Across the terminals AB is connected the L-C circuit in which the resistive losses are represented by the circuit conductance G_c. The circuit is loaded by the admittance $Y_L'' = G_L'' + jB_L''$.

Looking into the circuit at the terminals AB one sees the admittance:

$$Y_s = G_c + jB_c + Y_L'' = G_c + \frac{1}{j\omega L} + j\omega C + Y_L''$$

which may be rewritten:

$$\begin{aligned} Y_s &= G_c + j\sqrt{\frac{C}{L}}\left(\frac{\omega}{\omega_0} - \frac{\omega_0}{\omega}\right) + Y_L'' \\ &\cong G_c + 2j\left(\frac{\omega - \omega_0}{\omega_0}\right) Y_{0c} + Y_L'', \end{aligned} \tag{19}$$

where $\omega_0 = \frac{1}{\sqrt{LC}}$ and $Y_{0c} = \sqrt{\frac{C}{L}}$.

The expression $\sqrt{\frac{C}{L}}$, having the dimensions of an admittance, is by definition the characteristic admittance of the circuit, Y_{0c}. Its relation to the energy stored in the circuit, and through this to the various Qs defined above, may be seen from the following: Using the root mean square value of voltage, the energy stored in the circuit is CV_{RF}^2. This can be reduced by the use of the definition of the resonant frequency and by differentiation of the expression (19) for the admittance, thus:

$$CV_{RF}^2 = \frac{Y_{0c}}{\omega_0} V_{RF}^2 = \frac{1}{2}\left|\frac{dB_c}{d\omega}\right|_{\omega=\omega_0} \cdot V_{RF}^2 . \tag{20}$$

Thus, at a given frequency ω_0, the energy stored in the circuit for unit voltage applied to it may be specified either by the characteristic admittance of the circuit, Y_{0c}, or by the rate of change of susceptance with frequency at the resonant frequency, $\left|\frac{dB_c}{d\omega}\right|_{\omega=\omega_0}$.

The loss of energy per cycle in the circuit itself, that is, in the shunt conductance G_c, is the power loss in the circuit divided by the frequency, $\frac{V_{RF}^2 G_c}{\omega_0/2\pi}$. From this and equation (20) the unloaded Q is seen to be:

$$Q_0 = 2\pi \frac{\frac{Y_{0c}}{\omega_0} V_{RF}^2}{\frac{V_{RF}^2 G_c}{\omega_0/2\pi}} = \frac{Y_{0c}}{G_c}. \tag{21}$$

Digitized by Google
Original from UNIVERSITY OF MICHIGAN
Generated on 2019-09-21 08:52 GMT / http://hdl.handle.net/2027/mdp.39015077775156
Public Domain, Google-digitized / http://www.hathitrust.org/access_use#pd-google

Similarly, for the loaded and external *Qs*:

$$Q_L = \frac{Y_{0c}}{(G_c + G_L'')}, \tag{22}$$

$$Q_{ext} = \frac{Y_{0c}}{G_L''}. \tag{23}$$

It follows that the *Qs* are related thus:

$$\frac{1}{Q_L} = \frac{1}{Q_0} + \frac{1}{Q_{ext}}. \tag{24}$$

The efficiency of the circuit, defined as the fraction of the energy which reaches the useful load is then:

$$\begin{aligned} \eta_c &= \frac{G_L'' V_{RF}^2}{G_L'' V_{RF}^2 + G_c V_{RF}^2} = \frac{G_L''}{G_L'' + G_c} \\ &= \frac{\frac{Y_0}{Q_{ext}}}{\frac{Y_0}{Q_{ext}} + \frac{Y_0}{Q_0}} = \frac{1}{1 + \frac{Q_{ext}}{Q_0}} = \frac{Q_L}{Q_{ext}}. \end{aligned} \tag{25}$$

5.5 *Resonators with Distributed Constants.* The individual cavities of the magnetron oscillator, however, are circuits in which the parameters are distributed and not lumped. They may be considered to be "strip-type" resonators, three forms of which generally used in magnetrons, are shown in Fig. 21 (a), (b), and (c). Type (a) has been called the slot type resonator; (b), the vane type, deriving its name from a common method of fabrication in which rectangular plates are disposed around and brazed to the inside of a cylindrical cavity; and (c), the hole and slot type resonator. The forms of these resonators, especially the parallel strip form of Fig. 21 (a), suggest that the resonators may be considered as sections of terminated transmission lines.

Voltage and current waves traveling down a section of uniform transmission line, terminated at one end by a short circuit and driven by a sinusoidal voltage at the other end, are reflected at the shorted end. The interference of the incident and reflected waves results in standing waves of voltage and current along the line. Since the voltage and current waves suffer phase changes on reflection differing by π radians, the corresponding standing waves are shifted by $\pi/2$ radians relative to one another. Thus the input admittance of the section of line is a periodic function of the distance, ℓ, to the shorted end. For a lossless line, this admittance is given by the expression:

$$Y = -jY_c \cot \frac{2\pi\ell}{\lambda} = -jY_0 \cot \frac{2\pi f\ell}{c}. \tag{26}$$

Digitized by Google
Original from UNIVERSITY OF MICHIGAN
Generated on 2019-09-21 08:52 GMT / http://hdl.handle.net/2027/mdp.39015077775156
Public Domain, Google-digitized / http://www.hathitrust.org/access_use#pd-google

In (26), Y_o is the characteristic admittance of the line. For a line of given length, this expression gives the input admittance as a function of frequency. When the frequency is $c/4\ell$, the line is a quarter wavelength long, and the

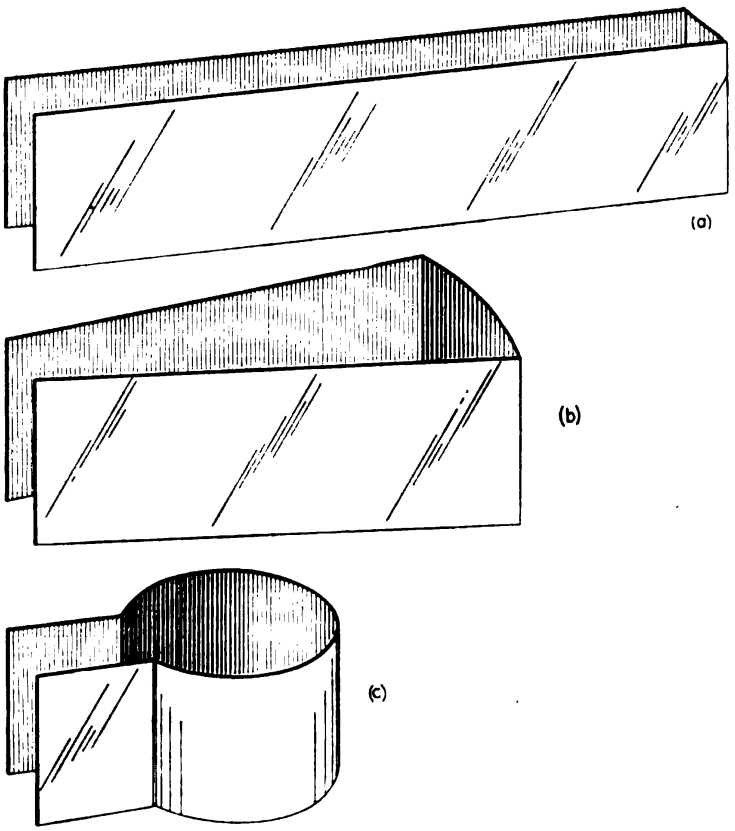

Fig. 21.—Three "strip type" cavities commonly used in magnetron resonator systems, each resonant at the frequency c/λ. Type (*a*) is essentially a quarter wavelength ($\lambda/4$) section of uniform transmission line. It should be noted how types (*b*) and (*c*) are physically shorter than type (*a*) by virtue of the greater relative capacitive loading near the open ends.

input admittance, if the line is lossless, is zero. In other words, the section of line resonates at this frequency.[19] In a quarter wavelength resonator of

[19] The frequency of resonance, $f = c/4\ell$, is the fundamental or lowest frequency of an infinite series of resonant frequencies for which the line length is $(2q - 1)\lambda/4$;

$$f_q = (2q - 1)c/4\ell, q = 1, 2, 3, \cdots.$$

These frequencies may be specified by considerations of the phase relationships which must

Digitized by Google
Original from UNIVERSITY OF MICHIGAN
Generated on 2019-09-21 08:52 GMT / http://hdl.handle.net/2027/mdp.39015077775156
Public Domain, Google-digitized / http://www.hathitrust.org/access_use#pd-google

uniform geometry, the voltage is maximum at the input end and the current is maximum at the shorted end, each varying sinusoidally to a node at the other end of the line.

The frequency of resonance of a section of terminated uniform line is thus determined by its length. If the geometry of the line is nonuniform, the frequency of resonance may be determined by the solution of Maxwell's equations with the appropriate boundary conditions. In general, this procedure is involved and tedious, however. One may get a reasonable idea of the values of ω_0 and Y_0 by assuming the half of the resonator near the open end to be capacitive only, the half near the closed end inductive only, and calculating C and L by application of elementary formulas to an equivalent parallel plate capacitance and a single turn sheet inductance of height h and proper cross sectional area. In the case of geometry like that of Fig. 21 (c), the division of the resonator on this basis is obvious.

A line of physical length ℓ', less than $\lambda/4$, may be made to resonate at the frequency c/λ by connecting across its input end a lumped capacitive susceptance, of magnitude, ωC, equal to that of the inductive susceptance of the line, $Y_0 \cot \frac{2\pi\ell'}{\lambda}$ [see equations (18) and (26)]. In like manner, resonators like those of Fig. 21 (b) and (c), whose physical length is less than $\lambda/4$, may be considered to be made up of an inductive section of uniform line across which additional capacitance has been inserted near the open end, bringing the frequency of resonance to c/λ. In Fig. 21, the three resonators of different physical lengths all resonate at the same frequency.

In addition to the resonant frequency of a resonator of distributed constants, one may define its Qs and characteristic admittance and link these to the rate of change of susceptance and energy storage capacity at resonance as was done for the circuit of lumped constants. Resonators of different geometry but of the same resonant frequency differ in characteristic admittance and loss conductance and hence in the Qs and the amount of energy which can be stored with unit voltage impressed across the input end. Of the resonator types shown in Fig. 21, the slot type has the largest admittance, the vane type, the smallest admittance, with the hole and slot type intermediate.

6. Resonator Systems

6.1 *Two Coupled Resonators:* The resonator system of the magnetron oscillator consists of a number of individual resonators of distributed parameters, machined into the anode block. As the simplest case of a system of coupled resonators, consider that having two resonators which are coupled

exist between oppositely traveling waves on a lossless line for constructive interference. These considerations are similar to those employed later in the discussion of the modes of oscillation of the magnetron resonator system as a whole.

Digitized by Google
Original from UNIVERSITY OF MICHIGAN
Generated on 2019-09-21 08:52 GMT / http://hdl.handle.net/2027/mdp.39015077775156
Public Domain, Google-digitized / http://www.hathitrust.org/access_use#pd-google

only by the mutual linkage of magnetic lines and which resonate at the same frequency, ω_0, when uncoupled.

When such a coupled system is shock excited it is observed that the oscillation amplitude in either of the circuits is modulated at a so-called beat frequency, ω_B. A fraction or all of the energy in the system, depending on the initial conditions, surges back and forth at this frequency between the circuits similar to the manner in which the energy of motion is exchanged between two coupled pendulums. The total energy in the system is constant, the beats differing in phase by $\pi/2$ radians between the circuits.

The observation of beats is a manifestation of the fact that the two coupled resonators form a complex system oscillating simultaneously in its two modes for which the frequencies are $(\omega_0 + \omega_B)$ and $(\omega_0 - \omega_B)$. The oscillation in either circuit results from the superposition of the two component oscillations in this manner:

$$A \cos (\omega_0 + \omega_B)\, t + B \cos [(\omega_0 - \omega_B)\, t + \delta] =$$

$$(A - B) \cos (\omega_0 + \omega_B)\, t + 2B \cos\left(\omega_B t - \frac{\delta}{2}\right) \cos\left(\omega_0 t + \frac{\delta}{2}\right), \tag{27}$$

with a similar expression for the case when $A < B$. The oscillation may be predominantly of one frequency, that is, almost entirely in one mode, if, for example, $A \gg B$. In general, the oscillation is a superposition of a steady oscillation in the predominant mode $[(\omega_0 + \omega_B)$ if $A > B]$ and an oscillation whose amplitude varies with the beat frequency, ω_B. In the special case, when the component oscillations are of equal intensity, $A = B$, the amplitude of the resultant oscillation in either circuit goes to *zero* periodically at the frequency ω_B. This represents the case for which all the energy present in the system is transferred back and forth between the circuits.

The frequency separation of the two modes arises from the coupled effect of the oscillation in each of the circuits on the oscillation in the other. Thus, in the mode of lower frequency, $(\omega_0 - \omega_B)$, the two circuits oscillate in phase and the self induction effect in each circuit is aided by the mutual induction, each circuit behaving as though it were oscillating freely with a greater value of self inductance and hence at lower frequency [equation (17)]. For the mode of higher frequency, $(\omega_0 + \omega_B)$, the reverse is true. Here the two circuits oscillate out of phase by π radians, the mutual induction opposing the self induction and the circuits oscillating as though uncoupled with a smaller value of self inductance and hence at higher frequency.

If instead of shock exciting the system of two coupled resonators it is forced to oscillate by applying to it a sinusoidal voltage of variable frequency, the admittance of the system is found to pass through minima at the mode frequencies $(\omega_0 + \omega_B)$ and $(\omega_0 - \omega_B)$. Thus it is possible to drive the system and store energy in either of the two modes. For each mode of

Generated on 2019-09-21 08:53 GMT / http://hdl.handle.net/2027/mdp.39015077775156
Public Domain, Google-digitized / http://www.hathitrust.org/access_use#pd-google
Digitized by Google
Original from UNIVERSITY OF MICHIGAN

the coupled circuit system, as for the simple single frequency resonator, Q parameters and a characteristic admittance may be defined which specify sharpness of resonance and energy storage capacity, respectively.

6.2 *The Multicavity Anode Structure:* As an introduction to the discussion of the multicavity resonator system of the magnetron oscillator having cylindrical symmetry, consider the system of a series of resonators machined side by side in a linear block as shown in Fig. 22. One may consider such a linear array either to be infinite in extent or to be terminated in some manner at the ends of a string of N identical resonators.

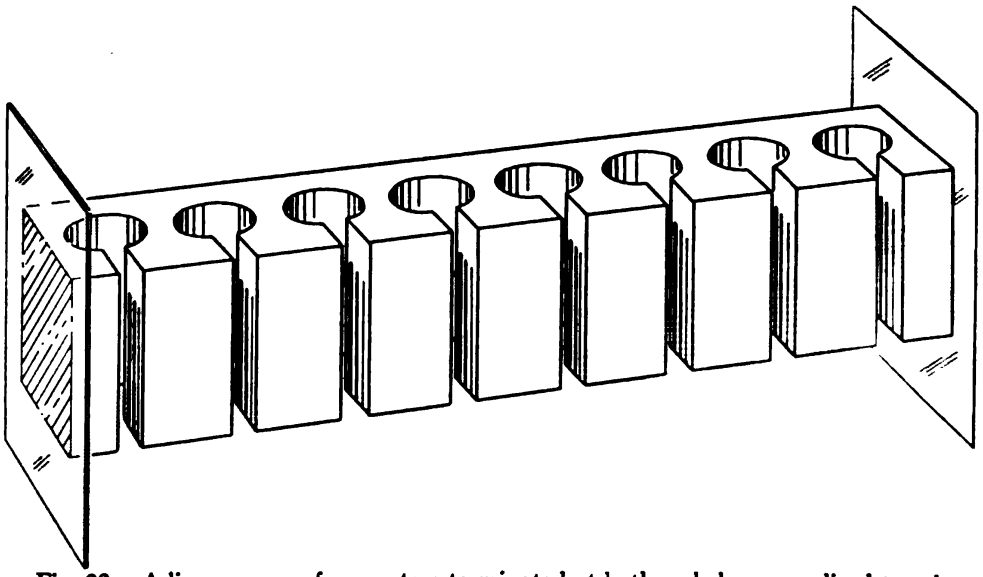

Fig. 22.—A linear array of resonators terminated at both ends by generalized terminations represented by planes. The figure is meant also to indicate the nature of the infinite array of resonators referred to in the text.

The oscillation in each resonator of the array of coupled resonators is specified by a differential equation in terms of a variable, such as current or voltage, the constants of the circuit itself, and the mutual interaction between the circuit and its neighbors. Each solution of the set of simultaneous differential equations for all the resonators involved corresponds to a definite phase shift between adjacent resonators. The allowed values of this phase shift depend upon the boundary conditions imposed on the string of resonators. If the block is infinitely long, all values of phase shift are allowed. In terms of the electromagnetic field pattern formed on the front surface of the block by the fringing fields of the individual resonators, this means that traveling wave solutions representing waves of any velocity, traveling over the surface of the block in directions normal to the slots, are possible. If the block is terminated, on the other hand, the boundary

Digitized by Google
Original from UNIVERSITY OF MICHIGAN
Generated on 2019-09-21 08:53 GMT / http://hdl.handle.net/2027/mdp.39015077775156
Public Domain, Google-digitized / http://www.hathitrust.org/access_use#pd-google

conditions restrict the phase shift between resonators to a set of specific values. These correspond to the traveling waves which on reflection at the terminations constructively interfere.

The cylindrical magnetron anode structure is a series of N resonators connected in a ring. It may be thought to be a section of a linear array of resonators rolled into a cylinder. The boundary condition imposed is that of connecting together the resonators at the ends of the string. Under these circumstances only those modes of oscillation are possible for which the total phase shift around the ring is $2\pi n$ radians, n being any integer including zero. The oscillations in adjacent cavities then differ in phase by $\frac{2\pi n}{N}$ radians. Again this means that only those waves traveling around the anode block which constructively interfere are possible solutions. These are waves which, after leaving an assumed starting point and traversing the anode once, arrive back in phase with the wave then leaving in the same direction. The anode potential waves and the RF interaction fields in the interaction space to which they correspond have already been discussed in connection with equations (12) and (13). In these electromagnetic field patterns, the electric and magnetic field components are displaced both in space and time phase by $\pi/2$ radians relative to one another, similar to the manner in which voltage and current on a terminated transmission line are related.

6.3 *The Modes of the Resonator System:* It has been seen that the modes of oscillation of a magnetron resonator system are characterized by definite values of the phase shift between adjacent resonators specified by $\frac{2\pi n}{N}$, in which the parameter n may assume only integral values including zero. Each such mode of oscillation has a frequency different from the frequency of any other mode and from the frequency of one of the N resonators oscillating freely and uncoupled from its neighbors. In the general case of N coupled resonators, as in the case of two coupled resonators previously discussed, the modes of oscillation have different frequencies because of the effect of the mutual coupling between the resonators. For $N = 2$, the oscillations in the two resonators are either in phase or π radians out of phase, the induction in one circuit by the other either directly adding to or subtracting from the self induction. In the case of the multiresonator system the mutual induction effect may bear phase relations to the self induction other than 0 and π radians. Thus not only the magnitude of the coupling but also this phase relationship determines the magnitude of the effect of the mutual induction and hence the amount of deviation of the

Digitized by Google
Original from UNIVERSITY OF MICHIGAN
Generated on 2019-09-21 08:53 GMT / http://hdl.handle.net/2027/mdp.39015077775156
Public Domain, Google-digitized / http://www.hathitrust.org/access_use#pd-google

mode frequency from that of a single uncoupled resonator. If the coupling between resonators were in some way gradually reduced, all mode frequencies would converge to the value for a single uncoupled resonator.

The complete anode potential wave for a mode specified by the parameter n has been given in equation (12). Each of its traveling components is represented by a fundamental of periodicity n and a series of so-called Hartree harmonics of periodicities $k = n + pN$, $p = 0, \pm 1, \pm 2, \cdots$. Any sinusoidal component for which the number of complete cycles around the anode is greater than $\frac{N}{2}$ is thus a harmonic of the complete field pattern for one of the modes whose fundamental is of periodicity $n = 1, 2, \cdots, \frac{N}{2}$. Physically distinguishable modes of oscillation exist only for the values of n less than or equal to $\frac{N}{2}$, including zero. However, this accounts for only $\frac{N}{2} + 1$ of the N modes of oscillation which one expects a system of N resonators to possess. The reason for this is that in general the frequency of a mode specified by the parameter n (except for the values 0 and $\frac{N}{2}$) is a double root for a perfectly symmetrical anode structure. The mode is thus a doublet and is said to be degenerate. One would expect this on mathematical grounds from the fact that the general solution of expression (12) has four arbitrary constants, whereas a singlet solution of the system of second order differential equations specifying the oscillations should have no more than two.

The nature of the degeneracy of the modes of the resonator system is perhaps most clearly seen by investigating what happens when the symmetry of the system is destroyed by the presence of a disturbance or perturbation at one point, a coupling loop in one of the cavities for example. Such a disturbance provides the additional boundary condition needed to remove the degeneracy.

Consider the effect of the perturbation on the nth mode. It represents an admittance shunted across the otherwise uniform closed ring of resonators. This shunt admittance may be represented by ϵY_0, ϵ being a complex number, taken to be small for simplicity, and Y_0 the characteristic admittance of the closed resonator system. In such a system, a potential wave incident upon the disturbance ϵY_0, having an amplitude a at the disturbance, breaks up into a reflected wave and a transmitted wave which, if ϵ is small, have the amplitudes $-\frac{\epsilon}{2} a$ and $\left(1 - \frac{\epsilon}{2}\right) a$, respectively [see equation (30)

Digitized by Google
Original from UNIVERSITY OF MICHIGAN
Generated on 2019-09-21 08:53 GMT / http://hdl.handle.net/2027/mdp.39015077775156
Public Domain, Google-digitized / http://www.hathitrust.org/access_use#pd-google

for the reflection coefficient on a transmission line]. In passing across the disturbance, a wave undergoes a small phase shift $\delta\phi(\omega)$. Since the total phase shift around the entire system must remain $2\pi n$, one may write: $\phi(\omega) + \delta\phi(\omega) = 2\pi n$, in which $\phi(\omega)$ is the phase shift around the system not including the disturbance. If there is no disturbance, $\omega = \omega_n$ (ω_n is used here for the ω_0 of the nth mode), $\delta\phi(\omega) = 0$, and $\phi(\omega_n) = 2\pi n$. For waves incident upon ϵY_0 from either direction, the respective amplitudes a and b at ϵY_0 must satisfy the equations:

$$a = \left[-\frac{\epsilon}{2} b + \left(1 - \frac{\epsilon}{2}\right) a\right] e^{j\phi(\omega)}$$

$$b = \left[-\frac{\epsilon}{2} a + \left(1 - \frac{\epsilon}{2}\right) b\right] e^{j\phi(\omega)}.$$

Writing $2\pi n - \left|\frac{\partial\phi}{\partial\omega}\right|_{\omega_n} \cdot (\omega - \omega_n)$ for $\phi(\omega) = 2\pi n - \delta\phi(\omega)$ in these equations and keeping only first order terms, one obtains the following pair of homogeneous linear equations for a and b:

$$\left[j\left|\frac{\partial\phi}{\partial\omega}\right|_{\omega_n} \cdot (\omega - \omega_n) - \frac{\epsilon}{2}\right] a - \frac{\epsilon}{2} b = 0$$

$$-\frac{\epsilon}{2} a + \left[j\left|\frac{\partial\phi}{\partial\omega}\right|_{\omega_n} \cdot (\omega - \omega_n) - \frac{\epsilon}{2}\right] b = 0.$$

These equations have a solution if and only if the determinant of the coefficients vanishes, that is, if:

$$j\left|\frac{\partial\phi}{\partial\omega}\right|_{\omega_n} \cdot (\omega - \omega_n)\left[j\left|\frac{\partial\phi}{\partial\omega}\right|_{\omega_n} \cdot (\omega - \omega_n) - \epsilon\right] = 0.$$

The two solutions are thus: $\omega = \omega_n$, for which $a = -b$, and $\omega = \omega_n - \frac{j\epsilon}{\left|\frac{\partial\phi}{\partial\omega}\right|_{\omega_n}}$ for which $a = b$.

From these facts concerning the amplitudes, namely, that at the disturbance ϵY_0 the amplitudes of the two oppositely traveling waves must either be equal or equal and opposite in sign for all time, one may conclude that the waves are of equal amplitude and that the standing waves resulting for each frequency must have a node at the disturbance for the $\omega = \omega_n$ solution and an antinode there for the $\omega = \omega_n - \frac{j\epsilon}{\left|\frac{\partial\phi}{\partial\omega}\right|_{\omega_n}}$ solution.

What this means in terms of the general solution for the degenerate mode

Digitized by Google
Original from UNIVERSITY OF MICHIGAN
Generated on 2019-09-21 08:54 GMT / http://hdl.handle.net/2027/mdp.39015077775156
Public Domain, Google-digitized / http://www.hathitrust.org/access_use#pd-google

of periodicity n of equation (13) may now be seen. Expression (13) may be rewritten in terms of θ measured from the disturbance ϵY_0 in this way:

$$V_{RF} = \sum_k (A_k - B_k) \cos(\omega t - k\theta + \gamma) + \sum_k 2B_k \cos\left(\frac{\gamma - \delta}{2}\right) \cos\left[\omega t + \left(\frac{\gamma + \delta}{2}\right)\right] \cos k\theta + \sum_k 2B_k \sin\left(\frac{\gamma - \delta}{2}\right) \cos\left[\omega t + \left(\frac{\gamma + \delta}{2}\right)\right] \sin k\theta. \quad (28)$$

When the degeneracy is removed, the first summation representing the traveling wave vanishes since the amplitudes A_k and B_k are equal for the reasons indicated. Furthermore, the second term involving cos $k\theta$ terms is then the component of the doublet whose frequency changes, and the third term involving sin $k\theta$ terms is the component of undeviated frequency. For the latter component the disturbance appears at a node and hence has no effect. The reverse holds for the cos $k\theta$ solution. For it, the frequency deviation depends on the magnitude of the disturbance through the quantity ϵ. The disturbance caused by the coupling loop in an actual magnetron resonator system is sometimes sufficient to split the components into distinguishable resonances.

Thus an unsymmetrical multicavity resonator system in general has two modes of different frequency for each value of n. With respect to the asymmetry as origin, one of these modes has a cosine-like field pattern, the other a sine-like field pattern. This is true for $n = 1, 2, \cdots, \frac{N}{2} - 1$, contributing $N - 2$ modes. The remaining two modes of the resonator system, for which $n = 0$ and $\frac{N}{2}$, are singlet modes even in the symmetrical anode. This may be seen from the analysis demonstrating the splitting of the nth mode into two components. For the $n = 0$ mode, since the anode potential wave is independent of azimuthal angle, the solution $\omega = \omega_n$ for which $a = -b$ represents the trivial case of zero amplitude at all points. Similarly, for the $n = \frac{N}{2}$ mode (the π mode) the $\omega = \omega_n - \frac{j\epsilon}{\left|\frac{\partial \phi}{\partial \omega}\right|_{\omega_n}}$ solution for which $a = b$ yields a cosine-like pattern giving zero potentials at each anode segment, an equally trivial case. Thus each of the N modes of the multicavity resonator system have been accounted for.

As an example, plots of the field configurations for the modes of a magnetron having eight resonators are shown in Fig. 23. For clarity, only the

Digitized by Google
Original from UNIVERSITY OF MICHIGAN
Generated on 2019-09-21 08:54 GMT / http://hdl.handle.net/2027/mdp.39015077775156
Public Domain, Google-digitized / http://www.hathitrust.org/access_use#pd-google

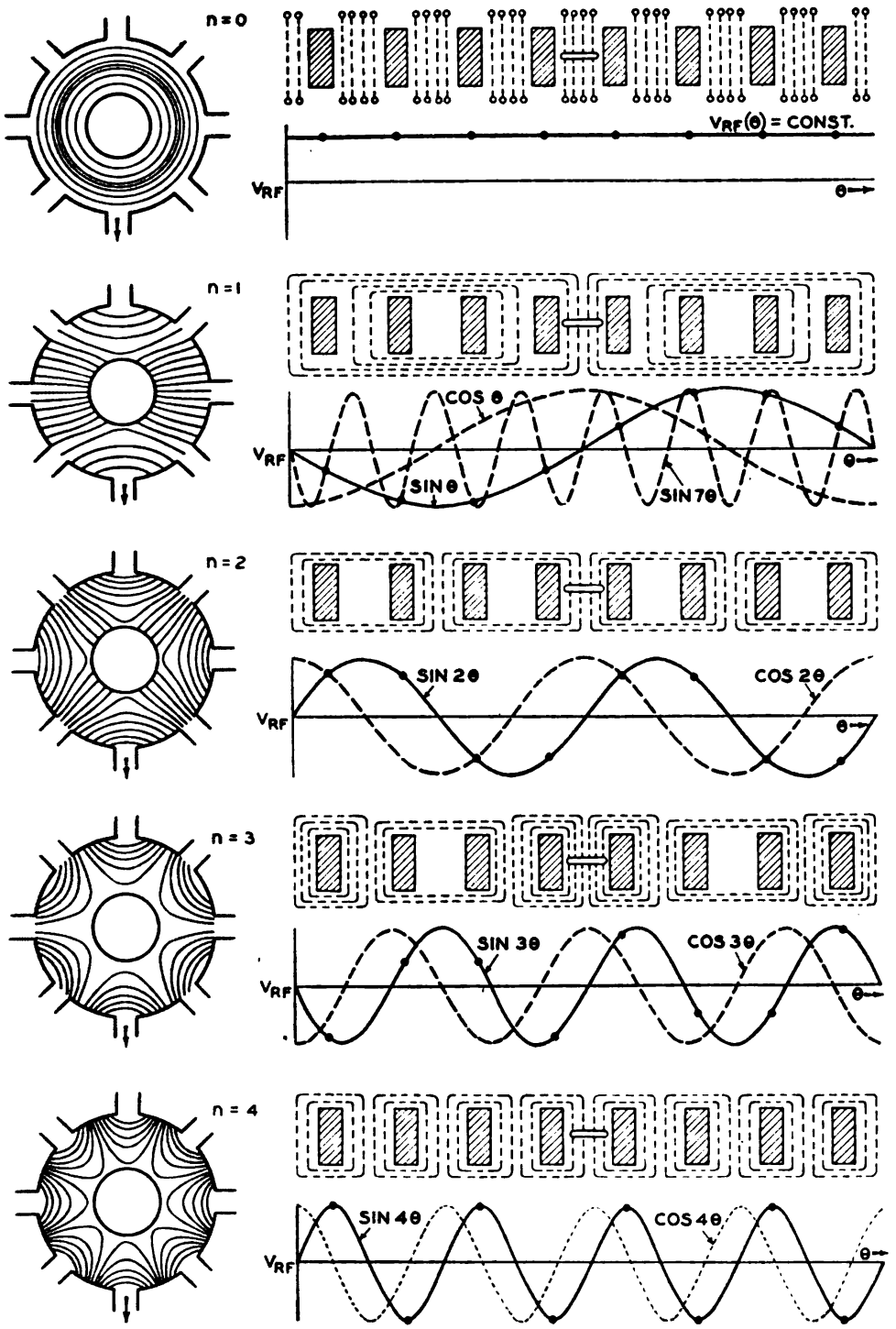

Fig. 23.—Configurations of electric fields, magnetic fields, and anode potentials for the $n = 0, 1, 2, 3$, and 4 modes of a resonator system having eight resonators. For each field pattern of periodicity n, the configuration of the electric lines of force in the magnetron interaction space is shown at the left, the configuration of the magnetic lines threading the resonators is shown at the upper right, and anode potential waves are shown at the lower

Digitized by Google
Original from UNIVERSITY OF MICHIGAN
Generated on 2019-09-21 08:54 GMT / http://hdl.handle.net/2027/mdp.39015077775156
Public Domain, Google-digitized / http://www.hathitrust.org/access_use#pd-google

electric field lines of the fundamental component ($p = 0$) of each mode are shown in the interaction space. Only the magnetic field lines are shown in the resonators. Below these is plotted the distribution in potential for each of the fundamentals, sin $n\theta$ and cos $n\theta$, $n = 0$, 1, 2, 3, and 4. For the $n = 0$ mode the magnetic flux threads through all the resonators in the same direction and returns through the interaction space. That all the segments are in phase and the interaction space field is independent of angle may be seen. That there is but one π mode is also seen from the fact that the cos 4θ term corresponds to zero potential on all the anode segments. The first Hartree harmonic for the $n = 1$ mode, namely that for which $p = 1$, having seven repeats ($k = 7$) or a total phase shift of 14π radians around the anode, is also plotted in Fig. 23 in addition to the fundamental. The fact that it yields the same variation of anode segment potential around the anode as the fundamental is apparent.

If the system of N resonators were shock excited it would oscillate in all of its modes simultaneously, producing beats in a manner analogous to but considerably more complicated than that for the system of two resonators already discussed. Furthermore, if the system were forced to oscillate by an external drive whose frequency can be varied, the admittance of the system would go through a minimum at each of the mode frequencies. With each such resonance there are associated values of the Qs, characteristic admittances, energy storage capacities, and the like.

The loading of the two modes of the same value of n by the output circuit of the magnetron depends on the position of the output loop relative to the respective standing wave patterns. If the output coupling loop forms

---

right. The interaction field plots represent only the fundamental components in each case. The higher harmonics would affect the fields as plotted most radically near the slots in the anode surface. The arrow shown in one of the slots in each case indicates the resonator which is coupled to the output circuit. The field lines in each plot are spaced correctly relative to one another but not relative to those in any other plot. In the plot of magnetic field lines in the resonator system (shown as dashed lines), the anode is developed from the cylindrical case, the anode segments being represented by the shaded rectangles. At the center is a representation of the output loop. The magnetic lines for the $n = 0$ mode thread through each resonator in the same direction and back through the interaction space in the opposite direction as indicated by the open circles at the ends of the lines. For each mode the magnetic lines are shown for the instant when RF current flow is maximum and all anode segments are at zero potential. In the plots of anode potential, the full lines represent the potential variations with azimuthal angle θ of the fundamental components sin $k\theta$, $k = n$. θ is measured from the position of the output coupling loop. The full circles on these curves indicate the potentials of the anode segments. The dashed lines represent the cos $k\theta$, $k = n$, modes. It should be noted that the cos 4θ configuration is trivial as it yields zero potential on each anode segment at all times. The cosine curves may also be taken to represent the azimuthal variation of magnetic field intensity which is in time quadrature with respect to the corresponding sine curves of potential. Similarly, the sine curves may represent magnetic field intensity corresponding to the cosine curves of potential. For the $n = 1$ mode the potential variation for the second Hartree harmonic ($n = 1$, $p = -1$) is also plotted (actually sin 7θ is plotted instead of sin -7θ for comparison with sin θ). It is to be noted that it corresponds to the same anode segment potentials as its fundamental.

Digitized by Google
Original from UNIVERSITY OF MICHIGAN
Generated on 2019-09-21 08:54 GMT / http://hdl.handle.net/2027/mdp.39015077775156
Public Domain, Google-digitized / http://www.hathitrust.org/access_use#pd-google

the asymmetry discussed above, one of the modes is strongly coupled and the other weakly coupled. The strongly coupled mode is that for which the anode potential wave is sine-like with respect to the cavity containing the output coupling loop as origin. In this mode the current and hence the magnetic flux in the output cavity is maximum. The fact that one of the modes of periodicity n is weakly coupled may be of significance in magnetron operation. As will be discussed later, oscillation in a loosely coupled mode, having a high Q by virtue of its being damped only by losses in the resonator system itself, may build up more rapidly under electron drive than that of the π mode. Then it is possible for the magnetron to oscillate either steadily under certain conditions, or intermittently, in an unwanted mode. For this reason it is usually necessary to provide a second asymmetry in the anode structure so as to shift the standing wave patterns of the two modes of same n most likely to offend and in this way to equalize their coupling to the output circuit.

6.4 *Higher Order Modes:* To this point in the discussion the RF circuit of the magnetron has been assumed to behave like a string of N lumped circuits coupled together in a ring, each circuit having only one natural frequency of resonance. This structure, as has been seen, has N modes of oscillation. Actually the multicavity resonator, since its constants are distributed, has an infinite number of modes of oscillation. They are to be distinguished by the nature of the variation of the RF field along the axis of the resonator system and radially in the individual resonators. Thus there may be nodal planes passing through the resonator system normal to its axis, or nodal cylinders, concentric with the axis of the system, passing through the resonators. The modes may be classified as symmetric or antisymmetric depending on whether the two ends of the system are in phase or π radians out of phase. The variation of RF voltage along the anode length is a circular sine or cosine function if the mode frequency is greater than the resonant frequency of the unstrapped resonator system and is a hyperbolic sine or cosine function if the mode frequency is less. The fundamental multiplet of N modes discussed above are symmetric modes corresponding either to no variation or to a hyperbolic cosine variation of RF voltage along the length. In these modes of the resonator system the cavities, considered as radial shorted transmission lines, resonate in their fundamental modes. Generally the frequencies of the higher order modes of the resonator system are quite far removed from those of the fundamental multiplet and only rarely need be considered.

6.5 *Other Types of Resonators:* As alluded to earlier, other types of magnetron resonators have been devised which can supply the proper alternate π mode potentials to the segments of a multisection anode. Two of these which have received some consideration by magnetron designers

Digitized by Google
Original from UNIVERSITY OF MICHIGAN
Generated on 2019-09-21 08:54 GMT / http://hdl.handle.net/2027/mdp.39015077775156
Public Domain, Google-digitized / http://www.hathitrust.org/access_use#pd-google

but which have not come into general use will be mentioned in passing. One, the so-called "serpentine" anode structure, consists of a single slot, cut into the anode body, which winds up and down the anode length and around the interaction space. It is essentially a "half-section" wave guide, closed on itself, oscillating in its fundamental at the cut-off wavelength. As one passes along the resonator, the field for this mode is uniform, but, by virtue of the geometrical arrangement, the field it supplies to the interaction space is π radians out of phase from gap to gap. Other modes correspond to integral numbers of wavelengths along the length of the "serpentine" resonator. The separation in frequency between the fundamental and the next highest harmonic generally is not as great as is desirable.

The other magnetron resonator system to be mentioned involves the use of a single toroidal cavity of rectangular cross section whose inner cylindrical surface has been removed. Across this opening are placed the anode segments, adjacent ones being connected to opposite sides. The fundamental of this cavity corresponds to the cut-off wavelength as in the "serpentine" structure. This cavity has been mentioned in the literature[20] and has received some attention during the war. It is most useful in low voltage CW magnetrons where the small interaction space makes possible a resonator with sufficiently great mode separation between the fundamental and the first harmonic.

7. Separation of Mode Frequencies

7.1 *Necessity and Means:* The frequencies of the modes of the magnetron resonator system near that of the π mode would ordinarily be closely grouped were not steps taken to separate them. Curve (a) of Fig. 25 shows the distribution of mode wavelengths for a typical 10 cm. resonator system like that of Fig. 1. It is not easy to account for the exact nature of this curve. By virtue of the fact that the mutual induction effects between circuits bear different phase relations to the self induction effects for different modes one would expect the mode frequencies to differ. However, the conditions at the ends of the resonator block, in which region the flux lines link the resonators, are extremely important and affect frequency in a way not completely explained as yet. That the end regions should have an effect is understandable since they contribute capacitance and inductance as does any other part of the resonating cavity in which there are electric and magnetic field lines. Furthermore, as might be expected, it has been demonstrated that the end conditions have a greater effect on mode frequency the lower the mode number n. This results from the fact that the field strength in a mode of periodicity n falls off inversely as rapidly as the nth power of the distance from the resonator block.

From the point of view of the electronics of the magnetron, one might

[20] This resonator is the so-called "turbator" discussed by F. Lüdi, Bull. Schweiz. Elektrotechn. Verein, Vol. 33, No. 23 (1942).

Digitized by Google
Original from UNIVERSITY OF MICHIGAN
Generated on 2019-09-21 08:55 GMT / http://hdl.handle.net/2027/mdp.39015077775156
Public Domain, Google-digitized / http://www.hathitrust.org/access_use#pd-google

think proximity of mode frequencies to be no problem because the different modes, even if of the same frequency, generally require different conditions relating the operating parameters V and B for oscillation [see relation (14)]. From the circuit point of view, however, close proximity of the mode frequencies is clearly undesirable, for under such conditions it is possible that a second mode may be excited by the electronically driven mode which is usually the π mode. The π mode oscillation, coupled to the second mode through some asymmetry in the resonator system, under these conditions sets up forced oscillations in the second mode. The interaction field pattern of the second mode then appears as a contamination of the π mode pattern, adversely affecting the electronic interaction with the π mode.

The mode frequency separation in magnetron resonator systems generally has been accomplished by two methods which bear an instructive relation to the means by which the mode frequencies of two coupled resonators may be separated. In the two resonator system, it is clear that the mode frequency separation can be increased by increasing the coupling since the difference in mode frequencies is brought about by the mutual coupling between the circuits, as has been explained. On the other hand, mode frequency separation may also be accomplished by detuning the individual resonators relative to one another. In either case the mode frequencies separate. Under shock excitation of the system, the beat frequency, equal to half the difference in the two mode frequencies, increases, corresponding to the greater rate of interchange of energy between one resonator and the other.

In the multicavity resonator system of the magnetron these means correspond, on the one hand, to the increase of coupling by conductive connections between the resonators, or so-called straps, and, on the other hand, to the use of cavities tuned alternately to different frequencies. This latter method has been used in the so-called "rising sun" anode structure to be discussed presently.

7.2 *Strapping of the Resonator System:* The idea of strapping a magnetron anode appeared in a British attempt to lock the oscillation of the resonator system into the π mode by connecting alternate anode segments together with wire straps. Although the number of modes of such a strapped structure is not changed, since its N-fold symmetry remains, the so-called "mode-locking straps" did succeed in separating the modes and making for easier oscillation in the π mode alone. The frequency separation of the modes is not infinite, however, because the straps are not of negligible length compared to a wavelength and thus have appreciable impedance between points on the structure to which they are connected. In most magnetron resonator systems today, straps of some form or other are employed.

In Fig. 24 are shown four types of strapping including the early British

Digitized by Google
Original from UNIVERSITY OF MICHIGAN
Generated on 2019-09-21 08:55 GMT / http://hdl.handle.net/2027/mdp.39015077775156
Public Domain, Google-digitized / http://www.hathitrust.org/access_use#pd-google

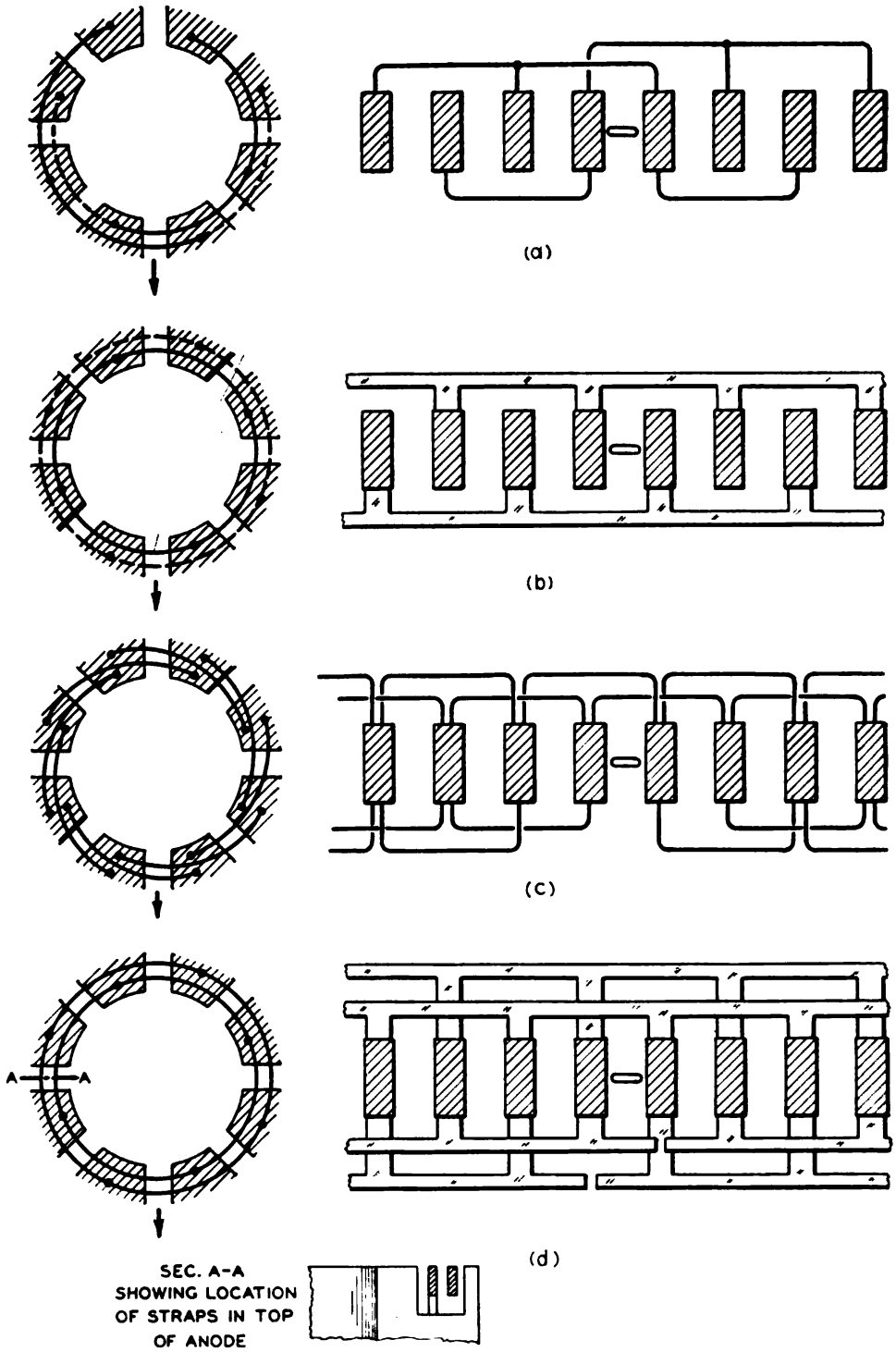

Fig. 24.—Schematic diagrams of four strapping schemes used in magnetron resonator systems. End views are shown on the left, and views rolled out as in Fig. 23 are shown on the right. (*a*) represents the early British type of unsymmetrical wire strapping, (*b*), a single ring type, (*c*), the so-called echelon type of wire strapping, and (*d*), the double ring type. In types (*a*) and (*b*) the straps on each end are at the same radius except where they overlap but are shown separated on the left-hand diagram for clarity. In types (*c*) and (*d*) the straps on the same end are at the same height and are shown as in the right-hand diagrams for clarity. The section *A*–*A* through type (*d*), shown below, indicates how the straps may be recessed into the resonator structure for shielding. The nature of the strap breaks introduced into types (*c*) and (*d*) are seen. In type (*c*) two links are removed and in type (*d*) actual breaks are made in the otherwise symmetrical rings. The breaks, shown here adjacent to the output coupling loop, are usually placed diametrically opposite.

Digitized by Google
Original from UNIVERSITY OF MICHIGAN
Generated on 2019-09-21 08:56 GMT / http://hdl.handle.net/2027/mdp.39015077775156
Public Domain, Google-digitized / http://www.hathitrust.org/access_use#pd-google

type. In Fig. 25 are shown the distributions of mode frequency for a typical resonator system unstrapped, and strapped with three of the types of strapping shown in Fig. 24.

It is possible to account, in quite simple terms, for the shift which takes place in the mode frequency distribution when the anode is strapped. For this purpose consider a double ring strapped system like that of Fig. 24 (d). The role of the straps in determining mode frequency depends upon the relative magnitudes of their shunt inductive and capacitive effects. The

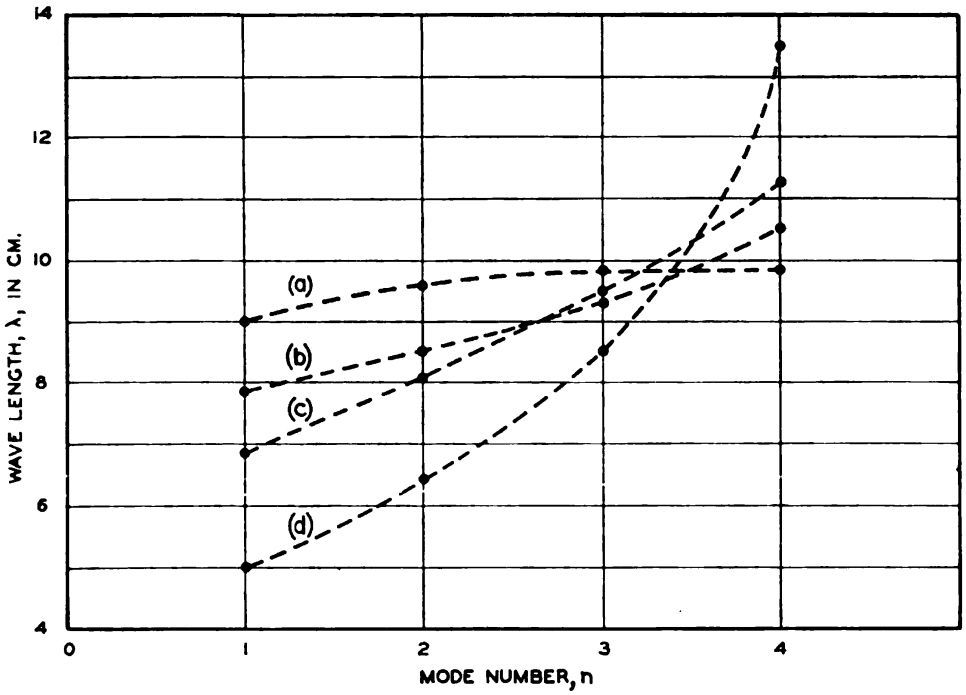

Fig. 25.—Plots of the variation of mode wavelength with mode number for a resonator system, unstrapped, or strapped in different ways. Curve (*a*) is for the unstrapped anode structure. Curve (*b*) is for the same structure strapped as shown in Fig. 24 (*a*), curve (*c*) for the same structure strapped as shown in Fig. 24 (*b*), and curve (*d*) for the same structure strapped as shown in Fig. 24 (*d*). It is to be noted how the wavelength increases for large *n* and decreases for small *n* as the "strength" of strapping is increased.

capacitive effect of the straps for any mode depends upon the amount of shunt capacitance added relative to that already present in the resonators and upon the positions in the system to which they are connected. This latter determines the average phase difference between the rings and thus their potential difference per unit RF voltage excitation. Similarly, the inductive effect of the straps depends upon the magnitude of their shunting inductance relative to that in the resonators. However, the important consideration concerning the points to which the straps are connected is the phase differences between points along the resonator system to which a

Digitized by Google
Original from UNIVERSITY OF MICHIGAN
Generated on 2019-09-21 08:56 GMT / http://hdl.handle.net/2027/mdp.39015077775156
Public Domain, Google-digitized / http://www.hathitrust.org/access_use#pd-google

given ring is connected. This determines the amount of current which the strap carries.

In the case of the π mode the two straps are π radians out of phase, each strap being connected to points which are in phase and at potential maxima [compare Figs. 23 and 24 (d)]. Their effect is predominantly capacitive. The only currents flowing in the straps are the charging currents of the strap capacitances. If a resonator system having a total capacitance C, a total inductance L, and a π mode angular frequency ω_0, is strapped by a strapping system which adds a total capacitance C_s to the resonator system, the new frequency is

$$\omega_0' = 1/\sqrt{L(C + C_s)} = \omega_0/\sqrt{1 + C_s/C}.$$

The change in frequency is thus specified by the so-called "strength" or "tightness" of the strapping implied in the ratio of strap to resonator capacitance.

For modes of lower periodicity, $n < N/2$, the average potential difference between the straps and thus their capacitive effect is less because the straps connect points on the resonator structure differing in phase by less than π radians. This corresponds to the shunting of a resonant line by a capacitance nearer the voltage node, at which point it would have no effect. On the other hand, a *given* ring now connects points on the anode whose potentials differ in phase. The ring thus provides additional conducting paths for the circulating RF currents in the resonator system. These paths are essentially shunt inductances across the resonators which reduce the over-all inductance of the resonator system, shifting the mode to shorter wavelength. As mode number decreases the two straps come closer together in potential but each strap connects points of greater potential difference. Thus the capacitive effect decreases, the currents carried by the straps and hence the inductive effect increase, resulting in a progressive depression of mode wavelength.

In Fig. 25 the curves (a), (b), (c), and (d) represent the progression from the unstrapped case, (a), through three successive cases of increasing strength of strapping. This increase in strength of strapping has resulted both in an increase of strap capacitance and a decrease of strap inductance as the increase of π mode wavelength and the decrease of mode wavelengths for smaller n demonstrates. It is accomplished by increasing both the inter-strap and strap-to-body capacitances as well as the cross sectional area of the straps.

The magnitude of the inductance of a strap depends on its physical length between the points on the anode structure to which it is connected. As this length increases, the strap inductance increases and hence has less effect as a shunt path. For this reason, the effectiveness of a given strapping scheme in producing separation of mode frequencies is reduced if the anode

Digitized by Google
Original from UNIVERSITY OF MICHIGAN
Generated on 2019-09-21 08:56 GMT / http://hdl.handle.net/2027/mdp.39015077775156
Public Domain, Google-digitized / http://www.hathitrust.org/access_use#pd-google

diameter is increased for higher voltage operation or to accommodate a greater number of resonators around the anode periphery.

Finally, it should be pointed out that the location of the straps at the ends of the anode structure causes their effectiveness to reduce with increasing anode length. As anode length is increased, the mode frequency distribution approaches that of the unstrapped resonator system of infinite length.

7.3 *Asymmetries in Strapping—Strap Breaks:* Of very great importance to the operation of a strapped resonator system is the degree of symmetry in the strapping system. The early British strapping is not symmetrical around the anode. The other three types shown in Fig. 24 are symmetrical except for breaks which are usually incorporated at least on one end of the anode. These asymmetries in the strapping provide the most convenient method of incorporating in the resonator system the additional asymmetry needed to orient the standing wave patterns of doublet modes with respect to the output circuit of the magnetron so as to equalize their loading. In addition, the strap asymmetries are arranged so as not to affect the symmetrical distributions of voltage and current in the resonator system for the π mode but to destroy such symmetry to an appreciable extent for other modes. For example, the destruction of the symmetry of the $n = 3$ mode pattern in a system of eight resonators by a single asymmetry in the strapping amounts to its contamination with a field component of periodicity corresponding to $n = 1$. Since the voltage and magnetic field values at which this contaminating component may be driven by the electrons are considerably farther removed from the π mode values than are those of the $n = 3$ mode, one has effectively converted the $n = 3$ mode into another mode less troublesome electronically.

In the echelon strapping of Fig. 24 (c) the asymmetry is produced by removal of two of the connecting links. The breaks in the strip or ring straps of Fig. 24 (d) are located as shown in the center of a link between two strap "feet". The break is thus at a current node in the strap for the π mode and has no effect on the pattern symmetry of this mode. For the other modes, however, the breaks appear at points where currents would normally flow and so represent sharp discontinuities in the structure for these modes.

In connection with strapped resonator systems there are two further points which should be mentioned. The first of these is the necessity in some cases of shielding the straps from the interaction space. The inner ring straps, mounted on the ends of the anode structure, present potentials to the interaction space which are independent of angle. This amounts to a perturbing $n = 0$ like component in the field pattern which is particularly strong near the ends of the anode and which affects magnetron operation adversely

Digitized by Google
Original from UNIVERSITY OF MICHIGAN
Generated on 2019-09-21 08:56 GMT / http://hdl.handle.net/2027/mdp.39015077775156
Public Domain, Google-digitized / http://www.hathitrust.org/access_use#pd-google

in the manner already discussed in Section 4.5 *Effect of Other Components in the Interaction Field.* It can be removed by shielding the straps as shown for the case of the double ring straps in the section A-A of Fig. 24 (d). The shields, being parts of the anode segments, maintain the proper potential distribution in the interaction space. The echelon straps of Fig. 24 (c), since they overlap, need not be shielded.

Secondly, the location of the straps at the ends of the resonator system has an effect on the amount of variation of RF voltage along the length of the anode in the π mode. For anodes of length approaching a half wavelength or greater, this may become great enough to warrant attention. It is instructive, in this connection, to consider the anode structure as being made up of two circular strip transmission lines, the straps at the ends of the structure, between which there are connected at intervals N "half-section" wave guides, the N resonators of the system. Since the resonant frequency of the system is less than that of an individual resonator, the resonators act as inductances connected across each set of straps and as wave guide connections between the sets of straps operating beyond cut-off, the RF voltage varying hyperbolically along their lengths. Since the two ends of the anode structure are in phase, the mode is symmetric about the median plane and the variation of RF voltage along the axis is expressed by the hyperbolic cosine.

7.4 *The "Rising Sun" Resonator System:* The second type of magnetron resonator system in which the mode frequencies may be separated sufficiently well to allow "clean" operation in the π mode is an unstrapped structure involving the use of resonant cavities of two sizes so arranged that adjacent cavities are alternately large and small. This resonator system, called the "rising sun" system, accomplishes mode frequency separation by a means analogous to the increase in separation of the mode frequencies of a system of two coupled resonators achieved by relative detuning of the individual resonators. At the Columbia Radiation Laboratory during a series of experiments with asymmetries in an unstrapped resonator system, designed to achieve good operation in a harmonic of one of its doublet modes rather than in the π mode, it was observed that as the natural frequencies of the two sets of resonators were separated the mode frequencies diverged in two groups as though each group corresponded to one of the two sets of resonators and that in this configuration the π mode was quite well separated from the other modes. Thus the system appeared to be well suited for π mode operation, providing a means of mode separation without the use of straps. As such it is particularly adaptable to use in magnetrons of short wavelength where straps become very small and extremely difficult to construct.

Digitized by Google
Original from UNIVERSITY OF MICHIGAN
Generated on 2019-09-21 08:56 GMT / http://hdl.handle.net/2027/mdp.39015077775156
Public Domain, Google-digitized / http://www.hathitrust.org/access_use#pd-google

A "rising sun" resonator system for $N = 18$ is shown in Fig. 26. The distribution of its mode frequencies is shown in Fig. 27, together with distributions for unstrapped and strapped eighteen resonator systems which have the same π mode frequency. It is seen that the modes of the "rising sun" resonator system arrange themselves into two groups or branches. Since the anodes are quite "long" (approximately $3\lambda/4$) the distribution for the unstrapped case having uniform resonator size [curve (a)] approximates the distribution for an anode of infinite length. It is reversed from the

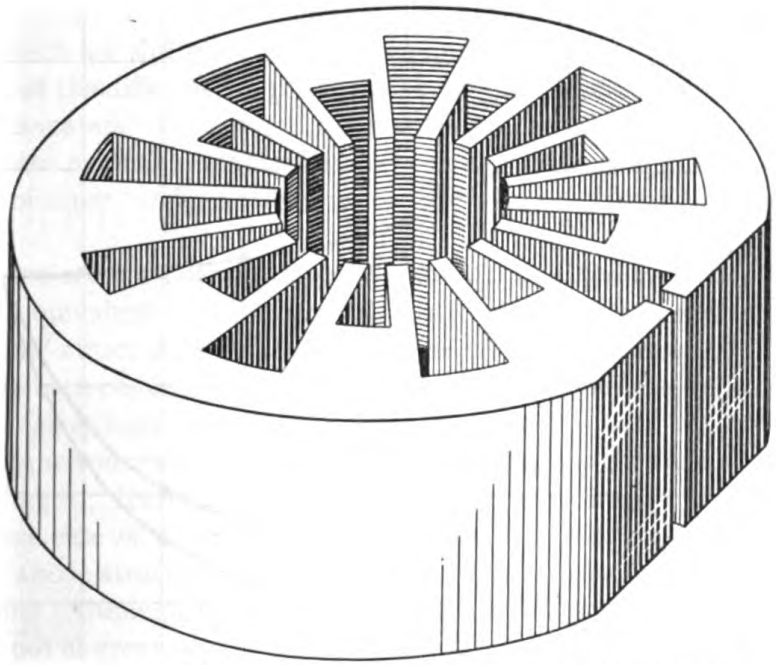

Fig. 26.—A so-called "rising sun" type resonator system having eighteen resonators. The slit at the "back" of the resonator in the right foreground is to be connected to the output circuit (compare Fig. 30).

unstrapped distribution of Fig. 25, curve (a), in which the end effects upon modes of small n are appreciable.

In the system of two coupled resonators, whether or not they are tuned individually to the same frequency, it has been seen that there are two mode frequencies corresponding to oscillations of the coupled system in which the resonators are in phase or π radians out of phase. In the "rising sun" system one observes two *groups* of mode frequencies corresponding to oscillations of the coupled *systems* of resonators in which corresponding

Digitized by Google
Original from UNIVERSITY OF MICHIGAN
Generated on 2019-09-21 08:56 GMT / http://hdl.handle.net/2027/mdp.39015077775156
Public Domain, Google-digitized / http://www.hathitrust.org/access_use#pd-google

modes of the component systems, that is, modes of the same pattern periodicity, add in phase or π radians out of phase. Thus the modes of a "rising sun" system having eighteen resonators corresponding to $n = 0, 1, 2, \cdots, 8$, and 9 are to be compounded of the two sets of modes for the large and

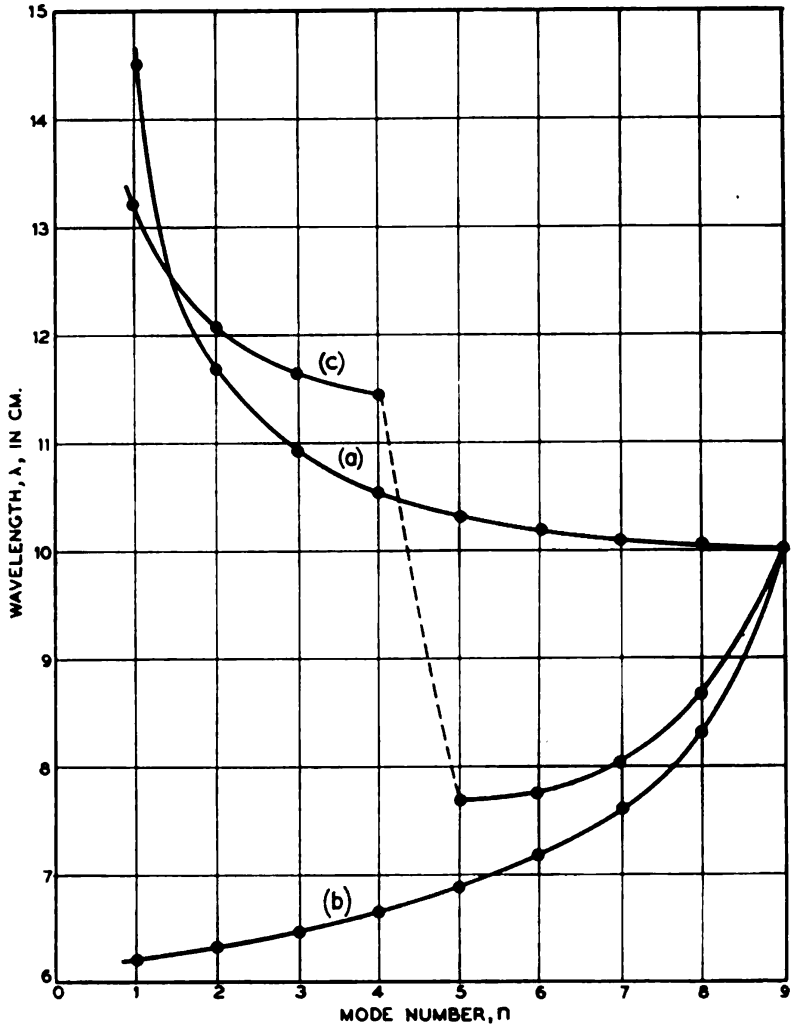

Fig. 27.—Plots of mode wavelength as a function of mode number for three different resonator systems of eighteen resonators having the same axial length and π mode wavelength. Curve (*a*) is for an unstrapped resonator system of identical resonators. Curve (*b*) is for a "heavily" strapped resonator system having identical resonators. Curve (*c*) is for a "rising sun" type resonator system having a ratio of resonator wavelengths of 1.8.

small resonators, each set including modes of periodicities $n' = 0, 1, 2, 3$, and 4. The two $n' = 0$ modes when added in phase give the $n = 0$ mode of the whole system but when added π radians out of phase give the $n = 9$ or π mode of the whole resonator system. This latter fact is perhaps made more clear by the observation that in the $n = 9$ or π mode all the large

Digitized by Google
Original from UNIVERSITY OF MICHIGAN
Generated on 2019-09-21 08:57 GMT / http://hdl.handle.net/2027/mdp.39015077775156
Public Domain, Google-digitized / http://www.hathitrust.org/access_use#pd-google

resonators are in phase and π radians out of phase with all the small resonators. Similarly the $n' = 1$ modes of the two component sets of resonators added in phase give the $n = 1$ mode, added π radians out of phase give the $n = 8$ mode. The $n' = 2$ modes yield the $n = 2$ and $n = 7$ modes of the total resonator, and so on. Modes of the component resonator systems of different periodicities do not add as they are uncoupled in the same sense as two modes of a resonator system with resonators all of the same size. The curve showing the distribution in mode frequency from $n = 0$ to $n = 4$ thus has the usual shape for increasing periodicity of the field pattern. The distribution in mode frequency for the remaining modes, however, is reversed in form and, as n goes from 9 down to 5, appears as a distribution should for which the mode periodicity increases. The two branches of the mode frequency distribution curve thus appear as approximate mirror images which are shifted relative to one another along the frequency scale by virtue of the difference in phase of the mutual coupling between the two sets of resonators. As far as frequency is concerned, the π mode of the total system has the characteristics of a mode whose field pattern is independent of angle, and its frequency is well separated from those of other modes.

As in the case of both unstrapped and strapped symmetrical resonator systems, equivalent circuits have also been devised and studied for the "rising sun" structure. Suffice it to say here concerning them that in each case it has been possible to explain and predict the mode frequency behavior to a surprising degree of accuracy.

As a magnetron resonator the "rising sun" system has both advantages and disadvantages. Its most obvious advantages are its lack of strapping with consequent ease of construction for short wavelengths and the ability to make an anode structure of any length with no penalty in mode frequency separation. Although the frequency separation of the π mode from other modes is not as great as is possible in strapped magnetrons, its independence of anode length and the fact that it can be realized at higher values of N are both important for high power magnetrons. Furthermore, the "rising sun" structure, having no strap losses, possesses an inherently higher unloaded Q than strapped resonator systems. This results in an improvement in circuit efficiency by a factor which may be as high as 1.2 at 1.25 cm. wavelength.

The major disadvantage of the "rising sun" resonator system is the presence in its π mode interaction field of a strong admixture of a component independent of angle. How this comes about may be seen from the following considerations: The π mode frequency of the composite resonator system lies somewhere between the free oscillation frequencies of the large and small resonators. When oscillating in the π mode, therefore, the large resonators are longer and the small resonators shorter than an equivalent

Digitized by Google
Original from UNIVERSITY OF MICHIGAN
Generated on 2019-09-21 08:57 GMT / http://hdl.handle.net/2027/mdp.39015077775156
Public Domain, Google-digitized / http://www.hathitrust.org/access_use#pd-google

quarter wavelength. Said another way, the electrical distance from the back of a large resonator to its opening in the anode, across the segment face, and to the back of the adjacent small resonator is an electrical half wavelength along which the voltage and current vary approximately sinusoidally. For this reason the maximum in the RF voltage and the corresponding current node do not appear at the mouth of either cavity but at a point (M of Fig. 28) somewhat inside the opening of the large cavity. This means that the electric field across the mouth of the larger cavity is greater than that across the mouth of the smaller cavity. The excess, since all the large cavities are in phase, adds up around the anode to form an electric field

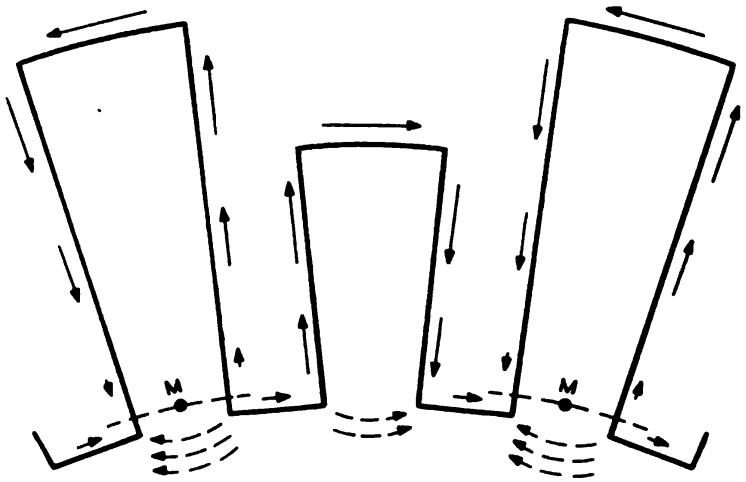

Fig. 28.—A diagram illustrating the origin of the component independent of angle in the π mode interaction field of the "rising sun" resonator system. The length of the arrow lying parallel to and just inside the resonator wall at any point is proportional to the magnitude of the RF current flowing there. The RF current node, and hence RF voltage maximum, occurs at M, inside the mouth of the larger cavity. Note that this gives rise to currents flowing in the faces of the anode segments which are in the same direction around the interaction space and that the RF field strength across the mouth of a larger cavity is greater than that across the mouth of a smaller cavity. This latter is indicated schematically by means of the dashed arrows.

component independent of angle like the $n = 0$ mode field in Fig. 23. Further, it is seen in Fig. 28 that at any instant there are currents flowing across the faces of the anode segments which are all in the same direction around the anode. With this net circumferential current is associated the unidirectional RF magnetic field component parallel to the axis shown also in Fig. 23.

The amount by which the two sets of mode frequencies of the "rising sun" structure are separated increases with increasing ratio of resonator sizes. Corresponding to this, the amount of $n = 0$ like component in the interaction field increases.

The presence of the component independent of angle in the interaction

Digitized by Google
Original from UNIVERSITY OF MICHIGAN
Generated on 2019-09-21 08:57 GMT / http://hdl.handle.net/2027/mdp.39015077775156
Public Domain, Google-digitized / http://www.hathitrust.org/access_use#pd-google

field is thus an inherent characteristic of the "rising sun" resonator system. One is faced with the problem of designing for sufficient mode separation without unduly increasing this component. How the presence of this component in the interaction field perturbs the electronic interaction with the π mode, resulting in a performance characteristic like that of Fig. 20, has already been discussed.

8. Output Circuit and Load

8.1 *Output Circuit:* In the general physical description of the centimeter wave magnetron whose constituent parts are shown in Fig. 1 there remains the discussion of the output circuit. The output circuit is the means of coupling the fields of the magnetron resonator to the load and as such it must contrive to induce a voltage across a coaxial line or a waveguide to which the load circuit is connected. Several types of coupling are involved in magnetron construction. These are illustrated schematically in Fig. 29. Here the resonator of the magnetron is represented by a simple L—C circuit and any transformer action of the output circuit between the resonator and the load is to be accounted for by the unspecified network T. The scheme of Fig. 29 (a) involves magnetic coupling, that of (b), electrostatic coupling, those of (c) and (d), two forms of direct coupling.

Type (a), it is clear, corresponds to the output coupling accomplished by a loop, like that shown in Fig. 1, feeding a coaxial line. The loop may be placed inside the cavity as in Fig. 1, may be placed above the resonator in the end space as in the case of the so-called "halo" loop, or may be placed with its plane parallel to the axis of the anode between the resonators in the end space. In each case the coupling is effected mainly by linking of magnetic lines of force by the loop. The coupling is not entirely magnetic, however. There is electrostatic induction in the loop by the anode segments near it, corresponding to coupling of type (b) of Fig. 29, and in the case of the third possible placement of the loop listed above, there is involved some direct coupling of the type (c) of Fig. 29 since the loop is terminated on an anode segment on which there is RF potential.

In most cases the coaxial line must expand in dimensions from the loop extremity, pass through the vacuum envelope, and be provided with a means of coupling to the coaxial load line of the system in which the magnetron is used. The output circuit from the loop to the smooth line of the system must provide the transformer action necessary to load the loop by an admittance which gives the desired Q [see equation (23)]. What this admittance must be is dependent, to be sure, on the size and position of the loop, that is, upon the degree to which it couples the magnetic lines in the resonator. Generally, the attempt is made to build the transformer

Digitized by Google
Original from UNIVERSITY OF MICHIGAN
Generated on 2019-09-21 08:57 GMT / http://hdl.handle.net/2027/mdp.39015077775156
Public Domain, Google-digitized / http://www.hathitrust.org/access_use#pd-google

into the magnetron, preferably inside the vacuum envelope where any large standing waves present are less likely to cause RF voltage breakdown.

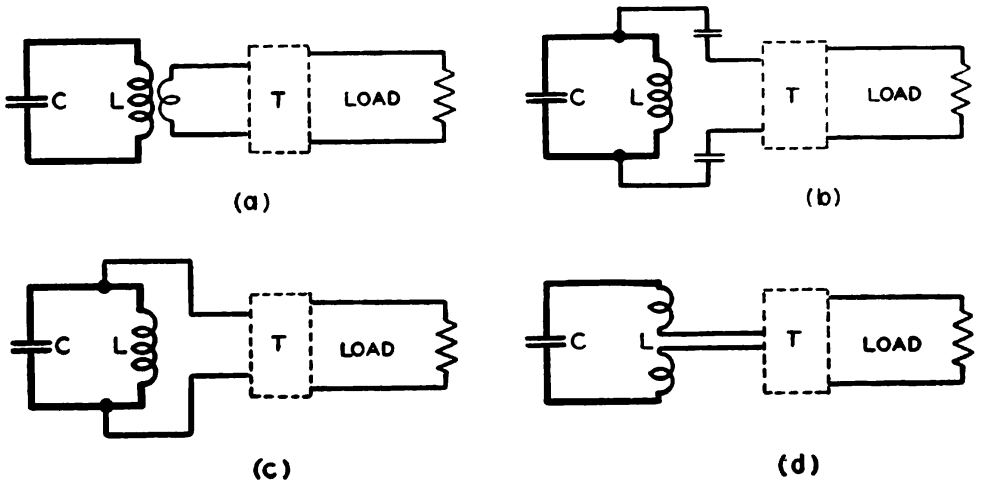

Fig. 29.—Schematic circuit diagrams representing four types of output couplings Type (*a*) is magnetic coupling, (*b*), electrostatic, (*c*) and (*d*), two forms of direct coupling. The unspecified network *T* represents the output circuit between the points where it couples to the resonator system and the load.

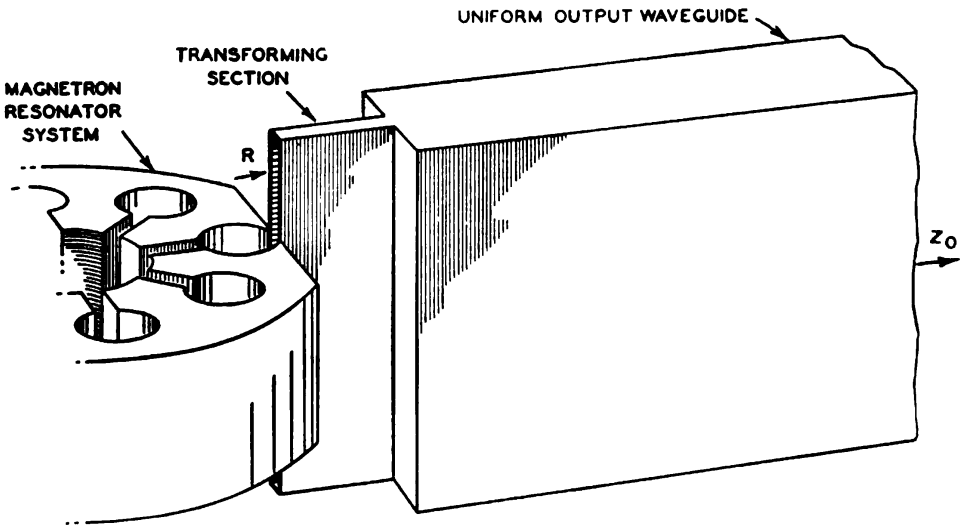

Fig. 30.—An example of a type of waveguide output circuit. It is representative of the type of coupling of Fig. 29 (*d*). Other types of resonator systems may be used (compare Fig. 26), and the transforming section, for example, may be of dumbbell-shaped cross section rather than of rectangular cross section as shown.

The type of magnetron output circuit represented schematically by Fig. 29 (d) is the so-called waveguide output. Here one of the resonators is broken into by means of a slit as shown in Fig. 30. Attached to this slit is a transforming section which feeds directly into the load waveguide. The im-

Digitized by Google
Original from UNIVERSITY OF MICHIGAN
Generated on 2019-09-21 08:58 GMT / http://hdl.handle.net/2027/mdp.39015077775156
Public Domain, Google-digitized / http://www.hathitrust.org/access_use#pd-google

pedance, R, at the resonator presented by the output circuit must be small. The characteristic impedance, Z_0, of the waveguide is large. The transformer usually consists of a quarter wavelength section of characteristic impedance equal to the geometric mean of R and Z_0, $\sqrt{RZ_0}$. The vacuum seal is made by a dielectric window in the waveguide. The quarter wave transformer section may be a parallel plate transmission line cut in the resonator block or may be a waveguide line of rectangular or dumb-bell shaped cross section. Here again, the specific amount of its transformer action must be adjusted, usually by variation of the small dimension, until it provides the proper value of Q_{ext}.

Another type of output circuit involves coupling a coaxial line directly onto the straps. This represents practically a pure case of the type of coupling shown in Fig. 29 (c).

8.2 *Load:* The load admittance which the output line presents to the output circuit of the magnetron oscillator depends upon the characteristic admittance, Y_0, of the line and upon the manner in which the line is terminated. In discussing the single resonator of the magnetron resonator system as a section of lossless transmission line terminated by a short circuit, the input admittance and its relation to the standing waves on the line were mentioned. Since the termination reflects all the energy incident upon it in the shorted line, the voltage standing wave ratio, σ, defined as the ratio of the maximum voltage to the minimum voltage along the line, is infinite. The input admittance of a shorted section of length ℓ has been given in equation (26).

In the general case in which the line is terminated by an admittance, Y_T, not all the energy incident upon the termination is reflected, the standing wave, whose position is determinated by the phase of Y_T, has a finite value of σ greater than unity, and the input admittance is given by the expression

$$Y = Y_0 \frac{Y_T + jY_0 \tan \frac{2\pi\ell}{\lambda}}{Y_0 + jY_T \tan \frac{2\pi\ell}{\lambda}}. \tag{29}$$

If the voltage reflection coefficient, $\vec{r}$, is defined at any point as the ratio of the complex voltage amplitudes of the reflected and incident waves, A_R and A_I,

$$\vec{r} = \rho e^{j\phi} = \frac{A_R}{A_I},$$

the standing wave ratio may be written

$$\sigma = \frac{|A_I| + |A_R|}{|A_I| - |A_R|} = \frac{1 + \rho}{1 - \rho},$$

Digitized by Google
Original from UNIVERSITY OF MICHIGAN
Generated on 2019-09-21 08:58 GMT / http://hdl.handle.net/2027/mdp.39015077775156
Public Domain, Google-digitized / http://www.hathitrust.org/access_use#pd-google

and the input admittance, Y, expressed as

$$Y = Y_0 \frac{1 - \vec{r}}{1 + \vec{r}}.$$

Conversely:

$$\vec{r} = \rho e^{j\phi} = \frac{\sigma - 1}{\sigma + 1} e^{j\phi} = \frac{1 - Y/Y_0}{1 + Y/Y_0}. \tag{30}$$

If the line is matched, that is, terminated in its characteristic admittance, $Y_T = Y_0$, it is clear that the input admittance, Y, is equal to Y_0, the voltage reflection coefficient, $\vec{r}$, is zero and the voltage standing wave ratio, σ, is unity.

These concepts are recalled here because they are used in specifying the magnetron load. The remaining point of interest with respect to admittance relationships on transmission lines is the transformation of admittance which occurs in going through a line of variable characteristics such as the output circuit of the magnetron. Such a section of nonuniform line may in general be considered as a lossless transducer, the admittance transformation through which is expressed as a bilinear form. In terms of the reflection coefficient $\vec{r}_2$ looking into the load at the output terminals of the transducer, the reflection coefficient $\vec{r}_1$, looking into the transducer at its input terminals may be written thus:

$$r_1 = e^{-j\vec{\alpha}_{12}} \frac{\beta_{12} + \vec{r}_2 e^{j\vec{\alpha}_{21}}}{1 + \beta_{12} \vec{r}_2 e^{j\vec{\alpha}_{21}}}. \tag{31}$$

In this expression the number β_{12} and the angles $\vec{\alpha}_{12}$ and $\vec{\alpha}_{21}$ are the three parameters completely describing the transducer, which for lossless transducers are real numbers.

9. Equivalent Circuit Theory

9.1 *The Equivalent Circuit:* From time to time in the discussion thus far, reference has been made to a lumped constant circuit or circuits which may be considered to be equivalent to the resonator system, output circuit, and load of the magnetron oscillator. One is now in a position to appreciate the justification for the use of such a simple, singly resonant circuit to represent as complex a device as the magnetron. As has been pointed out, this justification lies in the ability to separate the mode frequencies and to diminish sufficiently well, excitation of all modes except the π mode. Further, in the discussion of the equivalent circuit shown in Fig. 2, it was pointed out how the output circuit and the electronics may be treated by circuit analysis. This particular equivalent circuit will now

Digitized by Google
Original from UNIVERSITY OF MICHIGAN
Generated on 2019-09-21 08:58 GMT / http://hdl.handle.net/2027/mdp.39015077775156
Public Domain, Google-digitized / http://www.hathitrust.org/access_use#pd-google

be discussed in some detail. From an analysis of this circuit it will be explained how the power which the magnetron delivers and the frequency at which it oscillates depend upon the load attached to it.

Consider now the equivalent circuit shown in Fig. 2, or as repeated in Fig. 31 (a). Since the N cavities of which the magnetron resonator system is composed are essentially in parallel for the π mode, the C of the equivalent circuit is N times the capacitance and the L is $\frac{1}{N}$ times the inductance of a single cavity. G_e is the shunt conductance representing the series resistance

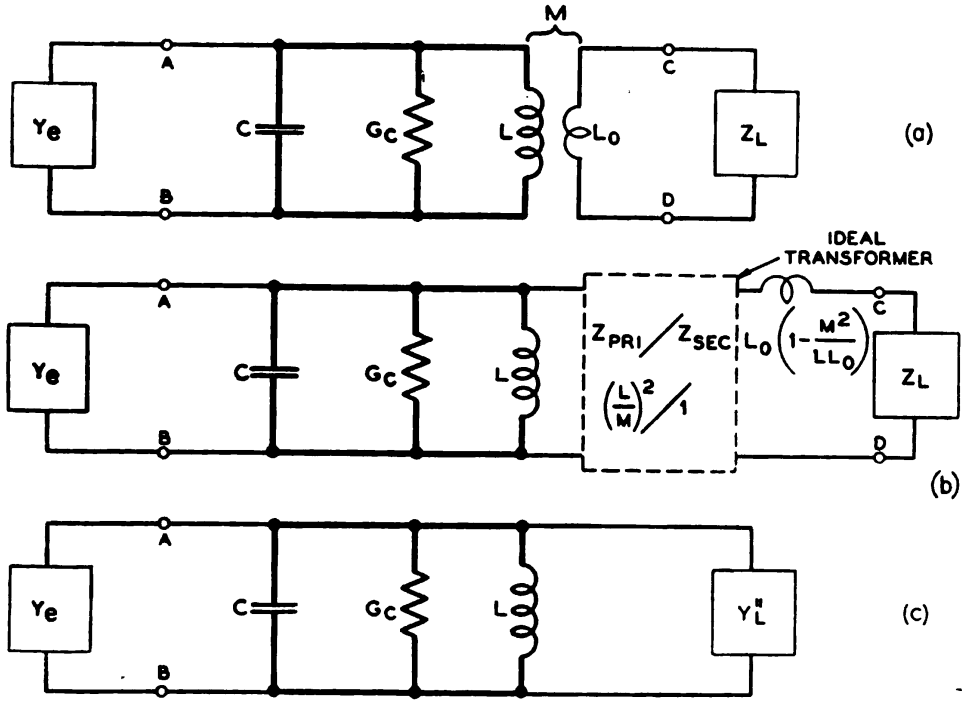

Fig. 31.—A diagram showing an equivalent RF circuit for the magnetron oscillator, (*a*), and how this circuit may be reduced in two steps, (*b*) and (*c*), to a simpler form.

in the copper walls of the resonator system, L_0, the inductance of the output loop which is coupled by the mutual inductance, M, to the lumped inductance of the equivalent resonating circuit. Z_L represents the impedance of the load at the loop terminals. Thus it represents the load impedance to which the magnetron is attached, transformed through the output circuit to the loop terminals.

The first step in understanding the circuit of Fig. 31 (a) is to reduce it to a simpler form. This is done in two steps as shown in Fig. 31. The inductances L and L_0, with mutual inductance M between them, form a transformer through which the impedances in the secondary circuit, $j\omega L_0$ and

Digitized by Google
Original from UNIVERSITY OF MICHIGAN
Generated on 2019-09-21 08:58 GMT / http://hdl.handle.net/2027/mdp.39015077775156
Public Domain, Google-digitized / http://www.hathitrust.org/access_use#pd-google

Z_L, are reflected into the primary circuit. It may be shown[21] that the circuit of Fig. 31 (b) is the equivalent of that of Fig. 31 (a). The coupling into the primary circuit is represented by an ideal transformer connected across the primary inductance L to the secondary winding of which are connected the load impedance Z_L and a reduced loop reactance

$$X_0 = j\omega L_0\left(1 - \frac{M^2}{LL_0}\right).$$

The ideal transformer effects a voltage transformation of $\frac{L}{M}$:1 or an admittance transformation of $\left(\frac{M}{L}\right)^2$:1 from its secondary to its primary terminals. Thus, the admittance, Y_L'', presented at the primary terminals of the ideal transformer, is

$$\begin{aligned} Y_L'' = G_L'' + jB_L'' &= \left(\frac{M}{L}\right)^2\left(\frac{1}{X_0 + Z_L}\right) \\ &= \left(\frac{M}{L}\right)^2 Y_L' = \left(\frac{M}{L}\right)^2 (G_L' + jB_L') \end{aligned} \tag{32}$$

in terms of the admittance Y_L' at the secondary terminals.

The equivalent circuit has now been reduced to that of Fig. 31 (c) used earlier in the discussion of a single resonator of the magnetron resonator system. Each of the quantities defined or derived for this circuit are now to be applied to the magnetron resonator system as a whole. These include the characteristic admittance of the resonator, Y_0, the unloaded, loaded, and external Qs given by the relations (21), (22) and (23), and the circuit efficiency, η_c, of equation (25).

Looking to the left at the terminals AB into the electron stream one sees the electronic admittance $Y_e = G_e + jB_e$. This is defined in terms of the current, I_{RF}, induced in the anode segments by the electrons moving in the interaction space, and the RF voltage, V_{RF}, appearing across the resonators, that is, across the terminals AB of Fig. 31 (c). Looking into the circuit at the terminals AB one sees the admittance Y_s.

This admittance by equations (19) and (32) is

$$\begin{aligned} Y_s &= G_c + j2Y_{0c}\frac{\omega - \omega_0}{\omega_0} + Y_L'' \\ &= G_c + j2Y_{0c}\frac{\omega - \omega_0}{\omega_0} + \left(\frac{M}{L}\right)^2 (G_L' + jB_L'). \end{aligned} \tag{33}$$

[21] See Guillemin, Communications Networks, Vol. II, p. 154.

Digitized by Google
Original from UNIVERSITY OF MICHIGAN
Generated on 2019-09-21 08:59 GMT / http://hdl.handle.net/2027/mdp.39015077775156
Public Domain, Google-digitized / http://www.hathitrust.org/access_use#pd-google

The condition for oscillation stated earlier requires that:

$$Y_e + Y_s = 0,$$

or:

$$G_e + jB_e + G_s + j2Y_{0c}\frac{\omega - \omega_0}{\omega_0} + \left(\frac{M}{L}\right)^2 (G'_L + jB'_L) = 0. \quad (34)$$

Separating real and imaginary parts, this reduces to the pair of equations:

$$\left.\begin{aligned} G_e + G_s = 0, \quad \text{or,} \quad G_e + G_c + \left(\frac{M}{L}\right)^2 G'_L = 0, \\ B_e + B_s = 0, \quad \text{or,} \quad B_e + 2Y_{0c}\frac{\omega - \omega_0}{\omega_0} + \left(\frac{M}{L}\right)^2 B'_L = 0. \end{aligned}\right\} \quad (35)$$

Since $\left(\frac{M}{L}\right)^2 G'_L$ is equal to G''_L, one may write the first of equations (35) in terms of the Qs defined by (21), (22), (23) and (24) thus:

$$-G_e = G_s = Y_{0c}\left(\frac{1}{Q_0} + \frac{1}{Q_{ext}}\right) = \sqrt{\frac{C}{L}}\frac{1}{Q_L}. \quad (36)$$

9.2 *The Rieke Diagram:* The electronic conductance and susceptance, being functions of the parameters such as V_{RF}, V, and B which govern the electronic behavior of the magnetron, are not known *a priori* except for the fact that they are undoubtedly slowly varying functions of frequency. The circuit conductance and susceptance are given by equation (33). Equations (35) state that the circuit conductance and susceptance must be the negative of the electronic conductance and susceptance respectively. It is from these relations that the behavior of the oscillator under changes of load is to be inferred.

Suppose now that one were to vary the load in such a way that only B'_L changes, G'_L remaining constant. Then, by the first of equations (35), G_e and hence G_s would not change. If, further, the frequency of oscillation changes such that

$$2Y_{0c}\frac{\Delta\omega}{\omega_0} + \left(\frac{M}{L}\right)^2 \Delta B'_L = 0, \quad (37)$$

by equations (35) B_e and hence B_s remain constant as well and the electronic operation of the magnetron involving the RF voltage, V_{RF}, is undisturbed. Since the power delivered by the magnetron is

$$P = -G_e V_{RF}^2 = G_s V_{RF}^2, \quad (38)$$

contours of constant G'_L on a plot of performance versus load, Fig. 32 (a), are thus contours of constant output power. Along any such constant

Digitized by Google
Original from UNIVERSITY OF MICHIGAN
Generated on 2019-09-21 08:59 GMT / http://hdl.handle.net/2027/mdp.39015077775156
Public Domain, Google-digitized / http://www.hathitrust.org/access_use#pd-google

power contour the frequency of the magnetron varies linearly with B'_L as equation (37) indicates. Hence any constant frequency contour on the diagram is obtainable from a neighboring contour of different frequency through translation in the direction of B'_L by an amount given by equation (37). The form of the contours of constant frequency depends upon the interdependence of the electronic parameters G_e and B_e. The fundamental electronic performance as a function of load is specified by the conductance G_e presented to the electrons at the anode slots, changes in load susceptance being compensated for by frequency changes and hence susceptance changes in the resonator. As G'_L is varied G_e, G_e, and the output power must vary as well. If B_e is independent of these changes the constant frequency contours will correspond to lines of constant B'_L. Actually it is found that B_e does depend to some extent on G_e, resulting in the constant frequency contours on the $G'_L - B'_L$ plot being approximately straight lines inclined to the constant B'_L lines at a small angle α as shown in Fig. 32 (a).

If the $G'_L - B'_L$ plane is transformed to the reflection coefficient or $\vec{r}$ plane on which the load characteristic is usually plotted, contours of constant G'_L or power become circles tangent to the circle $\rho = 1$ at the same point. Constant B'_L contours form the set of circles orthogonal to these. The contour of constant frequency of Fig. 32 (a) transforms to a circle which intersects all the contours of constant power at the angle α.

Fig. 32 (b) is thus the form of the characteristic depicting the dependence of magnetron performance on load, called the Rieke diagram, plotted for that point in the equivalent circuit where the admittance looking out into the load is $Y'_L = G'_L + jB'_L$. Between this point and a point in the smooth output line, with respect to which the load admittance is usually measured, there is the series reactance X_e and the output circuit of the magnetron, forming a transducer through which the reflection coefficient defining the load admittance may be transformed by the expression (31). In undergoing such a transformation the contours of constant power and frequency plotted on the $\vec{r}$ plane retain their general form although they may be rotated and expanded or contracted. Thus the general form of the Rieke diagram shown in Fig. 32 (b) should be the same as that experimentally determined and plotted on a reflection coefficient plane for a point in the output line. Fig. 33 is such a Rieke diagram and its resemblance to that of Fig. 32 (b) is apparent.

9.3 *Magnetron Circuit Parameters:* The fact that the circuit theory of the magnetron based on the simple equivalent circuit of Fig. 31 (a) explains the nature of the Rieke diagram so well is ample justification for its use. The parameters which specify the equivalent magnetron circuit may be

Generated on 2019-09-21 08:59 GMT / http://hdl.handle.net/2027/mdp.39015077775156
Public Domain, Google-digitized / http://www.hathitrust.org/access_use#pd-google
Digitized by Google
Original from UNIVERSITY OF MICHIGAN

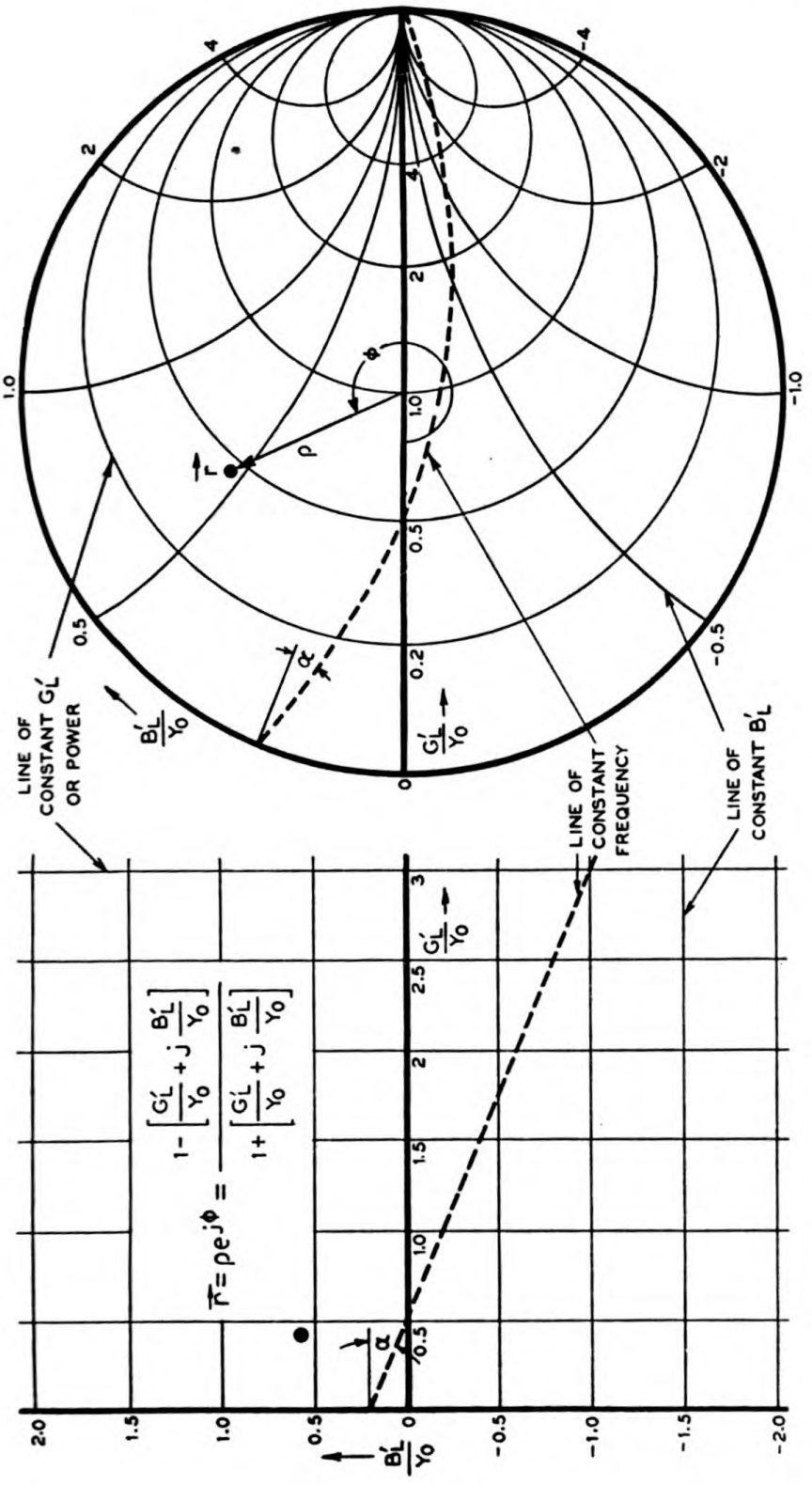
LINE OF CONSTANT G'L OR POWER
LINE OF CONSTANT FREQUENCY
LINE OF CONSTANT B'L
$\vec{r} = \rho e^{j\phi} = \dfrac{1 - \left[\frac{G'_L}{Y_0} + j\,\frac{B'_L}{Y_0}\right]}{1 + \left[\frac{G'_L}{Y_0} + j\,\frac{B'_L}{Y_0}\right]}$
$\frac{B'_L}{Y_0}$
$\frac{G'_L}{Y_0}$
(a)
(b)

Fig. 32.—Charts showing how the G'_L–B'_L plane of (*a*) transforms to the $\vec{r}$ plane of (*b*) under the bilinear transformation written out in the upper half of chart (*a*). A line of constant magnetron frequency is shown plotted on chart (*a*) and in its transformed position on chart (*b*). Note that all the straight lines of (*a*) becomes circles in (*b*) with angles of intersection preserved. Note also the transformation of the admittance point represented by the filled circle. The configuration of constant G'_L lines, corresponding to constant output power, and constant f lines shown on chart (*b*) is to be compared with the experimental Rieke diagram of Fig. 33.

Generated on 2019-09-21 08:59 GMT / http://hdl.handle.net/2027/mdp.39015077775156
Public Domain, Google-digitized / http://www.hathitrust.org/access_use#pd-google
Digitized by Google
Original from UNIVERSITY OF MICHIGAN

determined as a function of frequency by a measurement of the impedance Z_c looking into a non-oscillating magnetron through its output circuit and an independent measurement or calculation of one of the parameters such as C or Y_{0c}. The impedance Z_c in terms of the equivalent circuit is the impedance across the terminals CD in Fig. 31 (a) looking to the left with

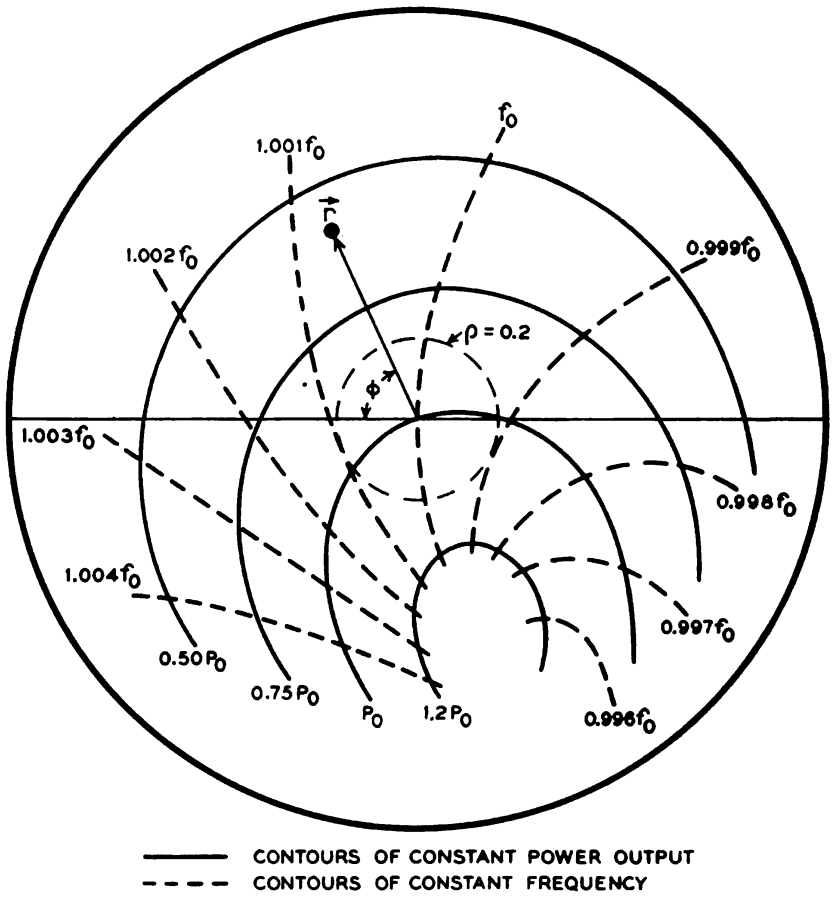

Fig. 33.—A typical experimental Rieke diagram for magnetrons in the centimeter wavelength range. The $\rho = 0.2$ circle indicates a pulling figure of $0.02 f_0 mc/s$ for this example. Present practice is to couple long wavelength magnetrons more tightly to the load and short wavelength magnetrons less tightly to the load than this. The rotation of the diagram from the position of the contours of chart (*b*) of Fig. 32 is attributable to the transformer action between the terminals of the ideal transformer of the circuit of Fig. 31 (*b*) and the point in the output line to which the experimental diagram is referred.

the terminals AB open circuited. From the circuit of Fig. 31 (b) this is seen to be

$$Z_c = j\omega L_0\left(1 - \frac{M^2}{LL_0}\right) + \left(\frac{M}{L}\right)^2\left[\frac{1}{G_c + j2Y_{0c}\dfrac{\omega - \omega_0}{\omega_0}}\right] \qquad (39)$$

Digitized by Google
Original from UNIVERSITY OF MICHIGAN
Generated on 2019-09-21 08:59 GMT / http://hdl.handle.net/2027/mdp.39015077775156
Public Domain, Google-digitized / http://www.hathitrust.org/access_use#pd-google

which, using equation (21), becomes

$$Z_e = jX_0 + \left(\frac{M}{L}\right)^2 \frac{1}{Y_{0e}} \left[\frac{1}{\frac{1}{Q_0} + j2\,\frac{\omega - \omega_0}{\omega_0}} \right] = R_e + jX_e \qquad (40)$$

The experimental data may be given in terms of the values of R_e and X_e plotted as functions of ω as shown in Fig. 34. The value of X_0 is deter-

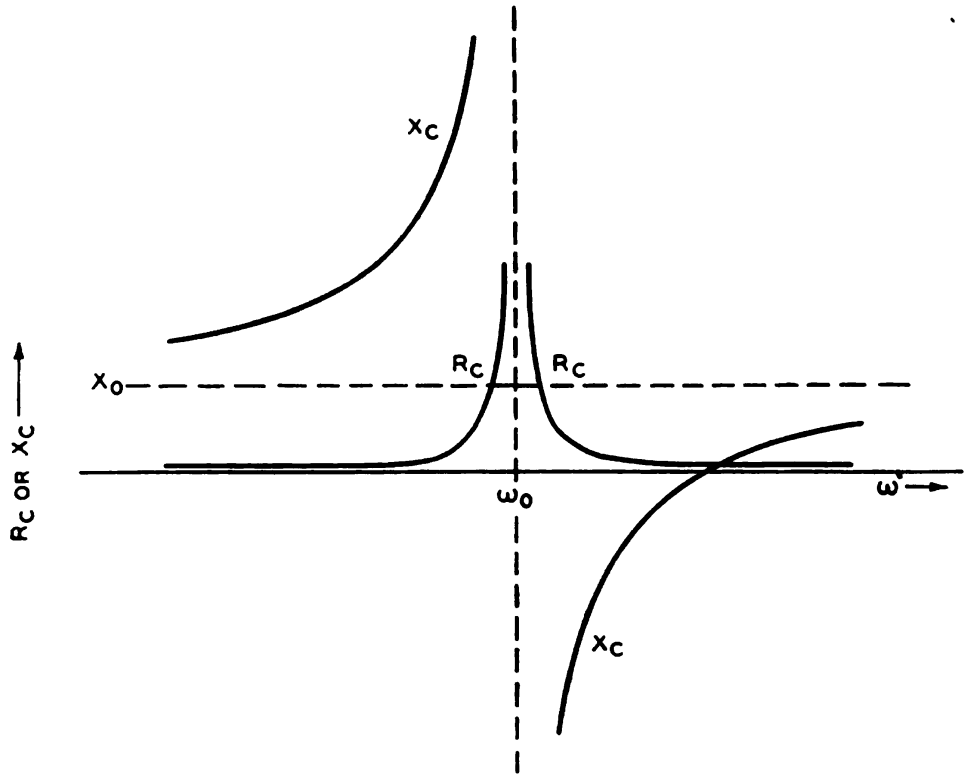

Fig. 34.—A plot of the resistive and reactive components of the impedance $Z_e = R_e + jX_e$, looking into a non-oscillating magnetron through its output circuit [terminals CD of Fig. 31 (*a*)]. Note the symmetry of the reactance about the point (ω_e, X_e) determining the value of X_e, the loop reactance.

mined by the fact that the reactance curve is antisymmetric about the point (X_0, ω_0). When X_0 has been determined one may determine the admittance, $\frac{1}{Z_e - jX_0}$, at the terminals of the ideal transformer of Fig. 31 (b). In terms of the circuit parameters this admittance is

$$\frac{1}{Z_e - jX_0} = \left(\frac{L}{M}\right)^2 Y_{0e} Q_0 + j2Y_{0e}\left(\frac{L}{M}\right)^2 \frac{\omega - \omega_0}{\omega_0}. \qquad (41)$$

Digitized by Google
Original from UNIVERSITY OF MICHIGAN
Generated on 2019-09-21 08:59 GMT / http://hdl.handle.net/2027/mdp.39015077775156
Public Domain, Google-digitized / http://www.hathitrust.org/access_use#pd-google

The conductance term, $\left(\frac{L}{M}\right)^2 Y_{0c}Q_0$, is independent of frequency and the susceptance term, $2Y_{0c}\left(\frac{L}{M}\right)^2 \frac{\omega - \omega_0}{\omega_0}$ varies linearly with frequency. If these quantities are plotted from experimental data as functions of ω, the values of Q_0 and $\left(\frac{L}{M}\right)^2 Y_{0c}$ may be determined. To determine the individual values of the factors in $\left(\frac{L}{M}\right)^2 Y_{0c}$ for a given magnetron, it is necessary to calculate or somehow to measure a value for $Y_{0c} = \sqrt{\frac{C}{L}} = \omega_0 C = \frac{1}{\omega_0 L}$. When used with ω_0 this yields values for L, C, and M. How this is done will not be explicitly discussed here. From the values of Q_0 and Y_{0c}, values of Q_L, Q_{ext}, and η_c may be calculated for any magnetron load G''_L by the relations (21), (22), (23), and (25). There are other methods of extracting the Q values from the experimental data than that presented above.

When values of the circuit parameters are available one can calculate the values of G_e and B_e from which G_e and B_e are obtained. From the output power the RF voltage is then calculable by equation (38), and from this and the electronic admittance the in-phase and quadrature components of the RF current may be obtained. Using the circuit efficiency, η_c, now determined as a function of load, one can obtain the dependence of the electronic efficiency, η_e, as a function of load conductance from experimental values of the over-all efficiency, η, measured along a constant frequency contour of a Rieke diagram ($\eta = \eta_e\eta_c$). The plot of Fig. 19 was obtained in this way. One is now in possession of values for each of the parameters upon which the electronics of the magnetron depends and may study the relations between them.

9.4 *Pulling Figure:* The Rieke diagram completely specifies the dependence upon load of the magnetron output power and frequency of operation. Nevertheless, it is convenient to be able to specify by a single parameter the dependence of operating frequency on load changes. The preceding discussion has shown that the changes in load conductance reflected into the resonant circuit of the magnetron, that is, specified at either the primary or secondary terminals of the ideal transformer of Fig. 31 (b), vary output power only. Further, if G_e and B_e are unrelated, load susceptance changes specified at the same points vary frequency only. Since G_e and B_e are in fact related, constant frequency contours on the $G'_L - B'_L$ plane, as has been seen, are inclined to constant B'_L lines at the angle α. Thus changes in B'_L are more effective by the factor $1/\cos\alpha$ in affecting frequency

Digitized by Google
Original from UNIVERSITY OF MICHIGAN
Generated on 2019-09-21 09:00 GMT / http://hdl.handle.net/2027/mdp.39015077775156
Public Domain, Google-digitized / http://www.hathitrust.org/access_use#pd-google

than equation (37) would indicate. The quantity calculated for $\frac{\Delta\omega}{\Delta B_L'}$ from equation (37) multiplied by the factor $1/\cos\alpha$ is a parameter which specifies the dependence of frequency on load. It may be specified at any value of load admittance Y_L', that is, for any position on the $\vec{r}$ plane. Generally, however, one considers the rate of change of frequency with susceptance at matched load, for which Y_L' is equal to the characteristic admittance Y_0' of the output line at the point in question. Using the parentheses $(\ )_0$ to indicate that the quantity enclosed is measured at the match point and incorporating the factor $1/\cos\alpha$, one obtains from (37):

$$\left(\frac{\Delta\omega}{\Delta B_L'}\right)_0 = \frac{1}{2}\left(\frac{M}{L}\right)^2 \frac{\omega_0}{Y_{0c}} \frac{1}{\cos\alpha}. \tag{42}$$

The quantity $\left(\frac{\Delta\omega}{\Delta B_L'}\right)_0$ as it stands is not a convenient one to measure. For this reason it is customary to specify the total excursion of frequency, $\Delta f = \frac{\Delta\omega}{2\pi}$, resulting from a standard variation in $\Delta B_L'$, namely, that obtained by the total possible phase variation of a standing wave of 1.5 voltage ratio in the line at the point in question. This is equivalent to traversing the $\rho = 0.2$ circle on the reflection coefficient plane, shown on Fig. 33. It can be shown that such a variation of load admittance results in a variation of susceptance of $\pm$ 0.41 times the characteristic admittance of the line, Y_0', corresponding to a total susceptance variation of 0.82 Y_0'. When determined in this way the total frequency excursion is called the pulling figure, *PF*. Hence by equation (42)

$$PF = \Delta f = \frac{\Delta\omega}{2\pi} = \frac{1}{2}\frac{2\pi f_0}{2\pi}\left(\frac{M}{L}\right)^2 \frac{.82 Y_0'}{Y_{0c}} \frac{1}{\cos\alpha}$$

$$= 0.41\, f_0 \frac{\left(\frac{M}{L}\right)^2 Y_0'}{Y_{0c}} \frac{1}{\cos\alpha}. \tag{43}$$

Since $Y_0' = (G_L')_0$, the quantity $\left(\frac{M}{L}\right)^2 Y_0'$ in this expression is recognized as $(G_L'')_0$, the load admittance at the primary terminals of the ideal transformer when the line is matched at the point in question, namely, the secondary terminals. Using this fact and equation (23) the pulling figure is seen to be:

$$PF = 0.41\, f_0 \frac{(G_L'')_0}{Y_{0c}} \frac{1}{\cos\alpha} = \frac{0.41\, f_0}{(Q_{ext})_0} \frac{1}{\cos\alpha}. \tag{44}$$

Digitized by Google
Original from UNIVERSITY OF MICHIGAN
Generated on 2019-09-21 09:00 GMT / http://hdl.handle.net/2027/mdp.39015077775156
Public Domain, Google-digitized / http://www.hathitrust.org/access_use#pd-google

Although this equation was derived for a specific point in the equivalent circuit, it is of general validity at any point in the output circuit or load line of the magnetron, provided the quantity $(Q_{ext})_0$ is properly interpreted as the external Q measured at match in the line at the same point.

10. Special Topics

10.1 *Frequency Stabilization:* The degree of stability of the operating frequency of the magnetron to load changes is specified by the external Q, as equation (44) indicates. The external Q, by equation (23), may be increased either by decreasing the load conductance, G_L'', or by increasing the circuit characteristic admittance, Y_{0c}. The first alternative may be accomplished by reduction of the coupling between the load and magnetron resonator system. Although this results in greater frequency stability, it entails a reduction in output power. Increase of the characteristic admittance of the magnetron resonator system, on the other hand, increases the energy storage capacity as indicated by equation (20) without appreciably changing the output power. Frequency stability may be increased in this way either by redesign of the magnetron resonator system or by coupling to it a tuned cavity of high unloaded Q. In the latter case, the degree of stabilization, defined as the ratio of energy stored in the combination of magnetron resonator system and stabilizing cavity to the energy stored in the magnetron resonator system alone, is the factor by which the external Q is increased and the pulling figure decreased. In actual practice the stabilizing cavity may be coupled into one of the magnetron resonator cavities or may be built into the output circuit.

10.2 *Frequency Sensitive Loads:* In the preceding sections it has been seen how the load admittance, among other parameters, determines the frequency at which the magnetron oscillates. If this load admittance is itself a function of frequency, it may be possible for the condition of oscillation to be satisfied at more than one frequency. This fact makes for an uncertainty of operation, which is to be avoided. Should the load fluctuate for example, as it does in many applications, the oscillation may jump discontinuously from one frequency to another. If the magnetron is pulsed, it may in certain circumstances oscillate at different frequencies on successive pulses. A tunable magnetron operating into a frequency sensitive load exhibits periodic gaps in its tuning characteristic in which the magnetron cannot be made to operate.

The discussion here will be limited to the specific type of frequency sensitive load consisting of a long line terminated in an admittance, assumed to be frequency insensitive, which differs from the characteristic admittance of the line. The input admittance of such a line is represented by a reflec-

Digitized by Google
Original from UNIVERSITY OF MICHIGAN
Generated on 2019-09-21 09:00 GMT / http://hdl.handle.net/2027/mdp.39015077775156
Public Domain, Google-digitized / http://www.hathitrust.org/access_use#pd-google

tion coefficient of amplitude, ρ, depending only on the termination [see equation (30)], and of phase, ϕ, depending only on the frequency, f, and the line length, ℓ. Thus:

$$\phi = \frac{2\pi\ell}{\lambda/2} = \frac{4\pi\ell f}{c},$$

from which

$$f = \frac{c\phi}{4\pi\ell}. \tag{45}$$

This equation expresses the linear relation between frequency and phase for the load, specified by the reflection coefficient, into which the magnetron operates. The heavy dashed lines in Fig. 35 represent this relation for two particular line lengths, ℓ_1 and ℓ_2, with ℓ_2 very much longer than ℓ_1. The difference in line length, $\ell_2 - \ell_1$, corresponds to an input phase difference of many times π radians. For the case in Fig. 35, however, this is chosen as an integral multiple of π so that the curve, plotted for the fundamental period 0 to π, will lie in the same range.

The variation of operating frequency of the magnetron with variable phase of the load reflection coefficient is a periodic function whose amplitude increases with increasing amplitude, ρ, of the reflection coefficient. This function may be determined graphically from a Rieke diagram of the magnetron, like that shown in Fig. 33, by traversing the appropriate circle concentric with the center of the diagram and plotting the frequency of operation against phase. In Fig. 35 are plotted such curves for two values of ρ corresponding to different terminations at the end of the long line.

A more detailed analysis of the condition of oscillation shows that it is possible for the magnetron to oscillate stably at those intersections of the magnetron and load frequency characteristics at which the slope of the load line is greater than the slope of the magnetron characteristic. Thus, as indicated in Fig. 35, oscillation may occur at only one frequency for the line of length ℓ_1 if $\rho = 0.2$ but at two frequencies if $\rho = 0.5$. In the latter case the middle intersection, indicated by an open circle, does not correspond to stable oscillation. For a line of length ℓ_2, on the other hand, two oscillation frequencies are possible at both $\rho = 0.2$ and $\rho = 0.5$. If in either case the line lengths ℓ_1 and ℓ_2 are increased by only an approximate quarter wavelength, corresponding to a phase change of $\pi/2$ radians, the light dashed lines labelled ℓ_1' and ℓ_2' in Fig. 35 represent the load characteristics, and oscillation can occur at only one frequency with ρ equal either to 0.2 or 0.5.

If one considers the relationships depicted in Fig. 35 it becomes clear that there are two critical relationships between ρ and ℓ. The first specifies the

Digitized by Google
Original from UNIVERSITY OF MICHIGAN
Generated on 2019-09-21 09:01 GMT / http://hdl.handle.net/2027/mdp.39015077775156
Public Domain, Google-digitized / http://www.hathitrust.org/access_use#pd-google

values of ρ and ℓ which if exceeded makes oscillation possible at more than one frequency at all phases of the load reflection coefficient. The second specifies the values of ρ and ℓ which must not be exceeded if oscillation is to be possible at only one frequency for all phases of the load reflection coefficient. This latter relation between ρ and ℓ is that for which the slope of the load line is equal to the slope of the magnetron characteristic at its point of inflection.

From what has been said it would appear that the use of long load lines is to be avoided if at all possible. If the magnetron is pulsed and the line

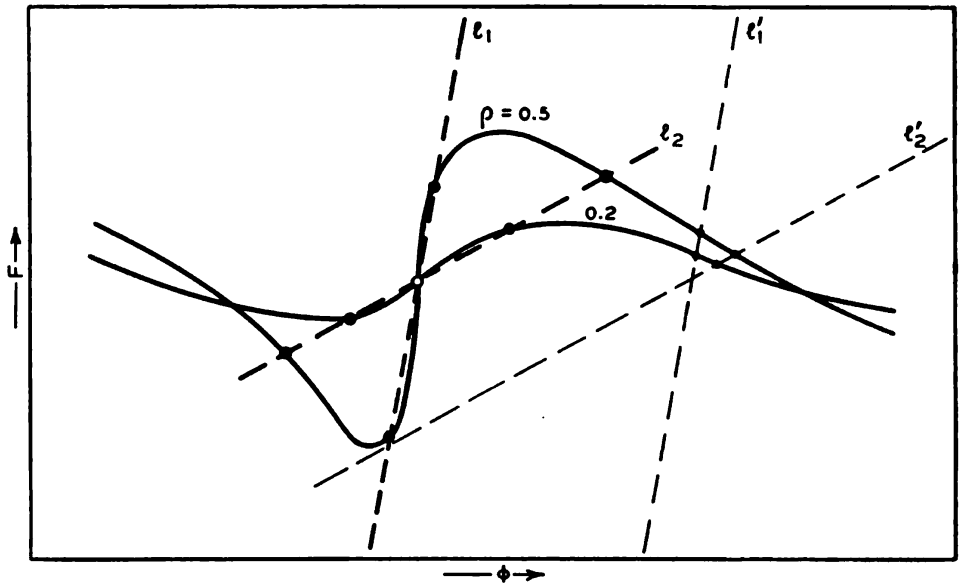

Fig. 35.—Plots of the frequency characteristics of a magnetron and a frequency sensitive load for two magnitudes of reflection coefficient, ρ, and two line lengths, ℓ. The ordinates are frequency and the abscissas are phase angle of the reflection coefficient in the fundamental period 0 to π radians. Stable oscillation occurs at the intersections indicated by filled circles. The open circle indicates a point of unstable operation for the three conditions $\rho = 0.5$ and $\ell = \ell_1$, $\rho = 0.5$ and $\ell = \ell_2$, and $\rho = 0.2$ and $\ell = \ell_3$. In addition, it indicates a point of stable operation for $\rho = 0.2$ and $\ell = \ell_2$. These four points are coalesced on the figure for simplicity. The lines ℓ_1' and ℓ_2' indicate how stable operation at both $\rho = 0.2$ and 0.5 may be attained by an increase of line length of approximately a quarter wavelength.

is sufficiently long, however, it is possible for the oscillation in a pulse to have been completed before any energy reflected from the termination has arrived back at the magnetron. Under these circumstances the magnetron operates into an effectively infinite line which presents its characteristic admittance to the magnetron output. For a pulse of one microsecond duration this would require a line length of about 150 meters. Usually such lengths are not possible or are undesirable by virtue of attenuation, and either the line is made sufficiently short or its length critically adjusted or the standing wave on it reduced so as to cause operation to occur at a single

Digitized by Google
Original from UNIVERSITY OF MICHIGAN
Generated on 2019-09-21 09:01 GMT / http://hdl.handle.net/2027/mdp.39015077775156
Public Domain, Google-digitized / http://www.hathitrust.org/access_use#pd-google

frequency. Studies have been made of the transient conditions prevailing near the beginning of a pulse when, in establishing the steady state, the successive reflections are returning to the magnetron and, as a consequence, its frequency is changing. Except in a limited region on the Rieke diagram where operation is completely uncertain, it has been shown that the magnetron will settle down to operation at one frequency dictated by the phase of the first reflection, even if oscillation at two frequencies by the previous analysis is possible. Gaps in the tuning curve of a tunable magnetron correspond to the periodic traversal of this uncertain region as the frequency is varied and the load reflection coefficient moves around a constant ρ circle on the Rieke diagram.

10.3 *Magnetron Tuning:* To tune the magnetron oscillator it is necessary to vary a susceptance somewhere in its circuit. It has already been observed how variation of load admittance when reflected into the resonator system as a susceptance change results in frequency pulling. Although for other reasons this variation is usually limited by output circuit design to the order of 0.1% of the operating frequency, it could be increased and used in special instances as a means of tuning the magnetron. Similarly the susceptance of a stabilizing cavity coupled into the resonator system may be varied by tuning the cavity. This method in general enables one to tune over a wider range than does variation of load susceptance since the resonator system is usually more tightly coupled to the stabilizing cavity than it is to the load.

The largest tuning ranges have been attained, however, when it has been arranged to vary one of the frequency determining parameters of the magnetron resonator itself. Schemes have been devised which alter primarily either the inductance or the capacitance of the resonant cavities. Variation of the inductance has been found more convenient at the shorter wavelengths and variation of the capacitance easier at longer wavelengths.

Variation of the inductance may be accomplished by the insertion of a conducting pin into each resonator where the RF magnetic lines of force are concentrated. In a system of hole and slot type resonators it is arranged to move the pins in and out along or near the axes of the holes. Such an arrangement is shown schematically in Fig. 36 (a). As the pins are inserted they reduce the volume available for the magnetic flux, thus reducing the inductance and increasing the frequency. Tuning ranges as great as $\pm 7\%$ of the mean frequency have been attained by this means. In spite of the fact that the ratio of strap to resonator capacitance remains nearly constant, the separation of mode frequencies, as might be expected, decreases with increasing frequency because of the increase in strap inductance resulting from increase of its electrical length. The effect is not so large,

Digitized by Google
Original from UNIVERSITY OF MICHIGAN
Generated on 2019-09-21 09:01 GMT / http://hdl.handle.net/2027/mdp.39015077775156
Public Domain, Google-digitized / http://www.hathitrust.org/access_use#pd-google

however, that with reasonable tightness of strapping difficult is encountered with mode frequency separation.

Variation of the capacitance may be accomplished by moving a member in the vicinity of the region of large distributed capacitance of the resonators. One such tuning scheme is that shown in Fig. 36 (b) in which a member shaped like a "cookie cutter" is moved in and out of annular grooves in one end of the resonator block, the other end of which is usually strapped. As the member is inserted the mode frequencies decrease. The frequency range available for π mode operation is limited by the fact that the frequencies of modes of smaller n, which are normally higher than that of the π mode, change faster and eventually cross the π mode frequency.

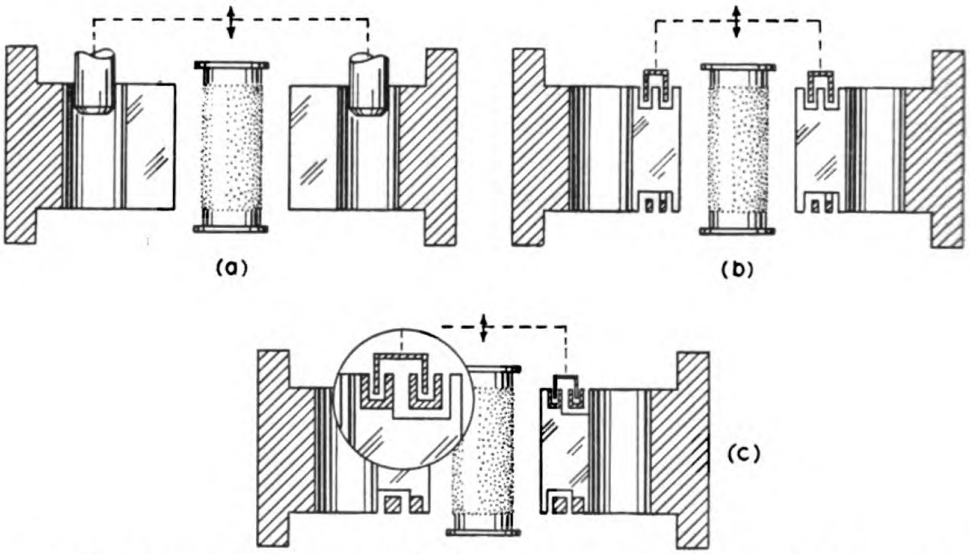

Fig. 36.—Schematic diagrams showing three types of tuning schemes which have been used in magnetron resonator systems. The views represent sections on a diametral plane through the anode structure. The cathode is shown in the center of each part of the figure. The resonators are of the hole and slot type. (*a*) shows the scheme involving variation of the inductance by means of tuning pins, (*b*), the scheme involving variation of resonator capacitance, and (*c*), that involving variation of strap capacitance. Each of the last two schemes is accomplished with a "cookie cutter" shaped member.

To understand what determines the frequency of resonance in any mode, it is sufficient to consider the inductances and capacitances present in the average sector of the resonator system across which there is a half wavelength azimuthal variation of RF potential with an extremum at either end. In the π mode of an $N = 8$ resonator system, one may thus consider one eighth of the system, namely, a single resonator; in the $n = 1$ mode, one may consider half of the resonator system. In the case of the half wavelength sector for the $n = 1$ mode, across which the potential varies monotonically (see Fig. 23), the four resonators may be considered as connected essen-

Digitized by Google
Original from UNIVERSITY OF MICHIGAN
Generated on 2019-09-21 09:06 GMT / http://hdl.handle.net/2027/mdp.39015077775156
Public Domain, Google-digitized / http://www.hathitrust.org/access_use#pd-google

tially in series, making up an equivalent resonator oscillating at the $n = 1$ mode frequency. If one considers further, for the sake of argument, that there is no coupling between resonators, all the modes would have the same frequency but the net inductance and capacitance of the equivalent resonator for each mode of periodicity n, would be proportional to $N/2n$ and $2n/N$, respectively. Thus for the $n = 1$ mode, the equivalent L is four times and the equivalent C is one quarter of the respective values for the π mode. The tuner capacitance added to the equivalent resonator for the $n = 1$ mode, on the other hand, may be considered to be approximately a series-parallel arrangement of capacitances each of which is that between the tuner and one anode segment, C_T: the two parallel capacitances at the positive anode segments connected in series through the tuner ring with the two parallel capacitances at the negative anode segments, the combination having a net capacitance C_T. For the π mode, the net tuner capacitance added per half wavelength potential variation is made up of two capacitances each of magnitude one half of that between the tuner and one anode segment, connected in series through the tuner; the net tuner capacitance is thus $C_T/4$.

By similar reasoning for any mode, one may conclude that the added tuner capacitance per half wavelength sector increases as n decreases, while the net resonator capacitance across which the tuner is shunted decreases as n decreases. In this way the increased effectiveness of the tuner in varying the mode frequencies of the low periodicity modes is accounted for. In actuality the resonators in the half wavelength variation of RF potential are not in simple series connection because of the phase relations between them; the approximation improves for smaller n. Also because of the phase relation between adjacent resonators, the adjacent tuner to segment capacitances are not charged to the same potential and so are not actually in simple parallel connection. Furthermore, the coupling between resonators is important. These considerations modify the above argument somewhat but do not affect the conclusions reached as to the trend of tuning for the different modes. In all the tuning schemes described, second order effects come in through change in the electrical lengths of the straps and tuner as the frequency is varied.

If one arranges to vary the characteristics of the straps by means of a movable tuning member as in the scheme of Fig. 36 (c), considerably greater tuning ranges may be achieved than by the means just described. In this instance, the straps are enlarged to channels of U-shaped cross section, in and out of which the tuning member of "cookie cutter" shape is driven The effect of insertion of the tuning member is to increase the capacitance per unit length of the strap system by increasing the interstrap capacitance and to decrease the inductance per unit length by effectively increasing the

Digitized by Google
Original from UNIVERSITY OF MICHIGAN
Generated on 2019-09-21 09:06 GMT / http://hdl.handle.net/2027/mdp.39015077775156
Public Domain, Google-digitized / http://www.hathitrust.org/access_use#pd-google

cross sectional area of the straps. The effects of these changes upon the mode frequencies may be seen from the considerations of the effect of straps on the mode frequencies of the unstrapped resonator system already discussed. The increase in strap capacitance increases the wavelength of the π mode; the decrease in strap inductance decreases the wavelength of modes of smaller n. As the tuning member is inserted, the mode frequencies separate, and no limitation on the range of operation in the π mode is imposed by interference from other modes. This means has been used for tuning ranges of better than $\pm 6\%$, but there is nothing inherent in the scheme to prevent its use for ranges considerably in excess of this value.

Tuning of the magnetron resonator system by any of the means described above alters its characteristic admittance, $Y_{0e} = \sqrt{\frac{C}{L}}$, and hence the stored energy. For fixed output coupling and load admittance this amounts to a variation of the effective loading as specified by the external Q. In some cases, attempts have been made to compensate for this by designing into the output circuit a frequency characteristic which keeps the external Q, and hence the pulling figure, more nearly independent of frequency.

Each of the tuning schemes described above is adaptable to precise and specific frequency adjustment or to frequency variation at a slow rate. For tuning over small ranges it is possible to vary the magnetron frequency electronically, enabling one to frequency modulate its output at a high rate. Of the schemes tried for this purpose there may be mentioned that in which an intensity modulated electron beam of a specific velocity is shot parallel to a superposed DC magnetic field through one of the magnetron resonators or a closely coupled auxiliary cavity.

Concerning the variation of magnetron operating frequency will be mentioned finally the shifts which are brought about by temperature variations of the resonator block. Since the resonator system is generally constructed entirely of copper, it expands or contracts uniformly with temperature and the frequency shifts are those attained by a uniform scaling of the resonator system by a very small factor. The temperature coefficient of frequency may readily be seen to equal the negative of the linear coefficient of thermal expansion of copper.

10.4 *Electronic Effects on Frequency:* In Section 3.6 *Induction by the Space Charge Cloud* it has been seen that the electrons moving in the interaction space of the magnetron oscillator contribute an admittance Y_e connected to the resonator system. The magnitude of the negative electronic conductance determines the energy delivered to the circuit and thus the amplitude of oscillation. The electronic susceptance, arising from the phase relation between the space charge spokes and the maximum of the tangential

Digitized by Google
Original from UNIVERSITY OF MICHIGAN
Generated on 2019-09-21 09:07 GMT / http://hdl.handle.net/2027/mdp.39015077775156
Public Domain, Google-digitized / http://www.hathitrust.org/access_use#pd-google

retarding field, affects the frequency of oscillation. Under equilibrium conditions the magnitude of the current, I_{RF}, induced in the anode segments, its phase relative to the RF voltage between the segments, and the operating frequency adjust themselves such that this admittance, $Y_e = I_{RF}/V_{RF}$, equals the circuit admittance Y_e. The induced RF current and its phase relative to the RF voltage both depend upon the parameters such as V and B, governing the electronic operation of the magnetron. The frequency change at constant load arising from changes in V or B when divided by the change in the DC current, I, drawn by the magnetron, is called the frequency "pushing" and is measured in mc/s per ampere.

A further effect of the electronic susceptance is the shift of the resonant frequency between the oscillating and non-oscillating conditions of the magnetron. In general the oscillating frequency is lower than the resonant frequency of the non-oscillating magnetron. Thus the electronic susceptance is capacitive with the space charge spokes moving somewhat ahead of the field maxima during oscillation. This shift in the resonant frequency is important in pulsed radar systems where the same antenna is used for both receiving and transmitting. An echo of the transmitted pulse on its return then encounters a high, off-resonance impedance at the magnetron which absorbs very little of the returned energy. Most of the received pulse energy is consequently made available to the receiver. For some magnetrons the shift off resonance is not sufficient and other means such as the use of the so-called ATR box are required to divert the received pulse energy into the receiver.

10.5 *Frequency Spectrum of a Pulsed Magnetron:* Only if a generator operates for an infinitely long time is its output "monochromatic", that is of a single frequency. The period of operation of a CW oscillator is generally long enough to make any deviations from this unobservable.

If, however, the oscillation is modulated as in the case of pulsed magnetrons for which the pulse duration is of the order of one microsecond, it is readily detectable that the output is "polychromatic" with the energy distributed throughout a band of frequencies. The plot of the distribution in frequency of the energy generated is called the frequency spectrum.

This state of affairs is perhaps made plausible if one considers pulsing the magnetron to be a very drastic means of amplitude modulating its output. Already, in connection with the case of two coupled circuits, it has been seen how amplitude modulation of an oscillating system in time has associated with it the distribution of the energy over more than one frequency. In an analogous but more complicated manner, a sinusoidal oscillation which is amplitude modulated by a nonsinusoidal pulse shape like that of Fig. 37 (a) is compounded of frequencies not now discrete but

Digitized by Google
Original from UNIVERSITY OF MICHIGAN
Generated on 2019-09-21 09:07 GMT / http://hdl.handle.net/2027/mdp.39015077775156
Public Domain, Google-digitized / http://www.hathitrust.org/access_use#pd-google

distributed continuously throughout a band, Fig. 37 (a′). The energy distributions in time and frequency are related mathematically by the Fourier transform.

The breadth of the frequency distribution is inversely proportional to the modulating pulse width as shown in Fig. 37. The spectrum widths of operating magnetrons may exceed the theoretical width by a factor of not more than two for reasons not altogether clear.

10.6 *Oscillation Buildup—Starting:* Of importance in the design and operation of pulsed magnetrons are the phenomena associated with the buildup of oscillation when the voltage is applied. Here will be discussed briefly what is known about the problem, the factors upon which the rate of buildup of oscillation in the circuit depends, how this is related to the rate

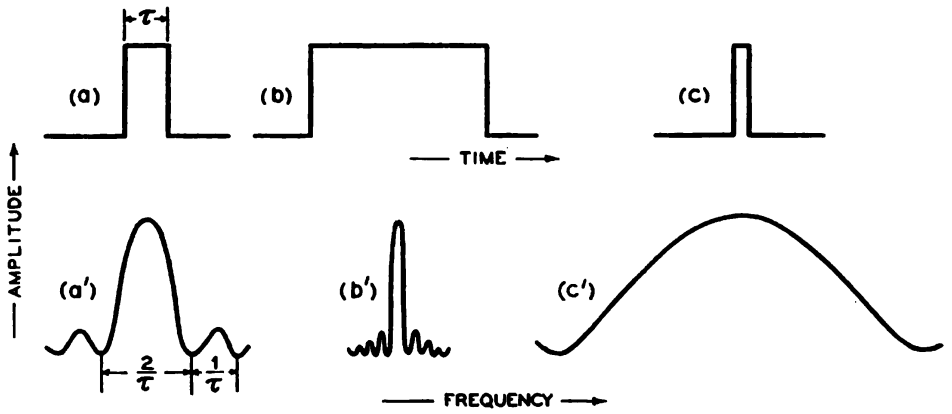

Fig. 37.—Plots of DC voltage pulse shapes (*a*), (*b*), and (*c*) and the frequency spectra (*a′*), (*b′*), and (*c′*) resulting from each, respectively. These are shown for the idealized case of perfectly rectangular voltage pulse shapes.

of voltage buildup and to pulser characteristics, and how these factors result in various types of magnetron starting behavior.

The rate of buildup of oscillation in the magnetron depends not only upon the circuit characteristics but also upon the electronic behavior with increasing DC and RF voltages. Because of the nonlinear nature of the electron interaction, the amount of energy fed to the circuit per cycle is dependent upon the amplitude of the oscillation. Considering the condition for oscillation given by the first of equations (35) and expanding it to include during buildup a term to account for the energy being stored in the resonators, one may derive a simple expression for the rate of increase of RF voltage amplitude. The energy stored in the circuit at any instant being $W = CV_{RF}^2$, the rate at which energy is being stored is $\frac{dW}{dt} = 2CV_{RF}\frac{dV_{RF}}{dt}$.

Digitized by Google
Original from UNIVERSITY OF MICHIGAN
Generated on 2019-09-21 09:07 GMT / http://hdl.handle.net/2027/mdp.39015077775156
Public Domain, Google-digitized / http://www.hathitrust.org/access_use#pd-google

This corresponds to a conductance term, G, obtained by equating $\frac{dW}{dt}$ and GV_{RF}^2:

$$G = 2C \frac{dV_{RF}}{dt} \frac{1}{V_{RF}}. \tag{46}$$

The necessary condition for oscillation during buildup is thus:

$$G_e(V_{RF}) + G_s + G = 0, \tag{47}$$

from which one obtains

$$G_e(V_{RF}) + G_s + 2 \frac{C}{V_{RF}} \frac{dV_{RF}}{dt} = 0. \tag{48}$$

Since oscillation in the magnetron does in fact build up, $|G_e(V_{RF})|$ must be greater than G_s when oscillation starts. When equilibrium is reached, $G_e(V_{RF}) + G_s = 0$. Thus $|G_e(V_{RF})|$ must be a decreasing function of V_{RF} crossing the value G_s at the operating point. By equation (48), V_{RF} thus builds up rapidly at first and then more slowly as $|G_e(V_{RF})|$ approaches G_s.

Increase in load, resulting in an increase of G_s, decreases the rate of oscillation buildup.[22] The dependence on the total resonator capacitance indicates that for magnetrons of different sizes related by a simple scale factor, G_e and G_s under such scaling presumably remaining invariant, the rate of buildup decreases with increasing wavelength. Unknown in relation (48) is, to be sure, the exact transient dependence of G_e on RF and DC voltages, magnetic field, and interaction space geometry. It is known, however, that an increase of cathode diameter, although it is accompanied by a decrease in electronic efficiency, does reduce the difficulty with "modding" resulting from failure to start in the π mode.

Associated with the rate of buildup of RF oscillation in determining magnetron starting behavior is the rate at which the DC voltage is applied. From the discussion of the electronics of the magnetron it is clear that oscillation is not possible at all values of V but only for a limited range near that which provides synchronism between the electron motion and the rotating field pattern. If the pulser can apply a voltage which rises to a value in this region and which can remain at substantially this value regardless of the current drawn, no difficulty is encountered. However, should the pulser regulation be such that to secure operation at a given voltage

[22] This is directly the opposite of the behavior with respect to load variations of a circuit being driven in such a way that a constant amount of energy is fed in per cycle, in which case the rate of buildup is inversely proportional to Q.

Digitized by Google
Original from UNIVERSITY OF MICHIGAN
Generated on 2019-09-21 09:07 GMT / http://hdl.handle.net/2027/mdp.39015077775156
Public Domain, Google-digitized / http://www.hathitrust.org/access_use#pd-google

and current it is necessary to apply a voltage which on no load would rise to a value considerably higher than the operating value, the rate at which the voltage passes through the range of possible operating values and the relation of this rate to that of RF buildup are extremely important. Should the pulse voltage rise so rapidly as to pass through the region where oscillation is possible before the RF oscillation can build up and cause the magnetron to pass current, which by modulator regulation keeps the DC voltage from rising further, the magnetron fails to start. Clearly, the more rapid the oscillation buildup the more rapid a voltage rise is permissible. Conversely, for a given rate of DC voltage rise, failure to start should appear at greater load and longer wavelength as relation (48) implies. Experience has corroborated both of these conclusions. It is also clear by equation (48) that the equalization of loading of the doublet modes of the same periodicity, which is achieved by proper location of strap asymmetries, equalizes their starting times and makes possible interference with π mode starting less likely.

When oscillation in the π mode fails, the magnetron may fail to oscillate at all or may oscillate in another mode for which the operating voltage in a harmonic is higher than but close to that of the π mode. In this case, as has been seen, $\frac{2\pi f'}{|k'|} > \frac{2\pi f}{N/2}$, and the Hartree line of the "second" or "primed" mode lies just above that of the π mode. This case in which oscillation in the π mode is skipped for oscillation in another mode represents the most common type of "moding" encountered in pulsed magnetrons. If, on the other hand, $\frac{2\pi f'}{|k'|} < \frac{2\pi f}{N/2}$, and the Hartree line of the harmonic of the "second" mode lies just below that of the π mode, as in Fig. 16, the magnetron is observed to oscillate first in the "second" mode before oscillation at low currents in the π mode commences. When the mode driven during the interval at the top of the pulse is the π mode, oscillation in the "second" mode occurs only momentarily on the rise and fall of each pulse as the voltage passes through the range of operating values for this mode.

The starting behavior of pulsed magnetrons may be shown by the so-called dynamic performance chart or *V-I* plot on which the course in time of the voltage and current is shown. In Fig. 38 are shown three *V-I* plots of this type. The initial current rise is the charging current of the cathode to anode capacitance. The current rise when oscillation commences is very rapid and is shown as a dashed line. After remaining for the major part of the pulse at the operating point, indicated in Fig. 38 by a large dot, the current and voltage fall during which they follow closely a constant *B* line of the static performance chart (see Fig. 17).

In Fig. 38 (a) is shown the dynamic *V-I* plot for normal operation in the

Digitized by Google
Original from UNIVERSITY OF MICHIGAN
Generated on 2019-09-21 09:07 GMT / http://hdl.handle.net/2027/mdp.39015077775156
Public Domain, Google-digitized / http://www.hathitrust.org/access_use#pd-google

π mode. In Fig. 38 (b) is shown a dynamic plot after the voltage control has been raised above the point of π mode failure. Here the magnetron does not oscillate at all. As seen in Fig. 38 (c), further increase of the voltage control of the pulser makes possible oscillation in the $k = -5$ ($p = -1$) harmonic of the $n = 3$ mode ($N = 8$). In both (b) and (c) of Fig. 38 it is of interest to note how the magnetron tries to oscillate in the π mode as the voltage at the end of the pulse falls through the range of permissible values. These attempts at oscillation are indicated by the magnetron drawing in this region small amounts of current which vary from pulse to pulse.

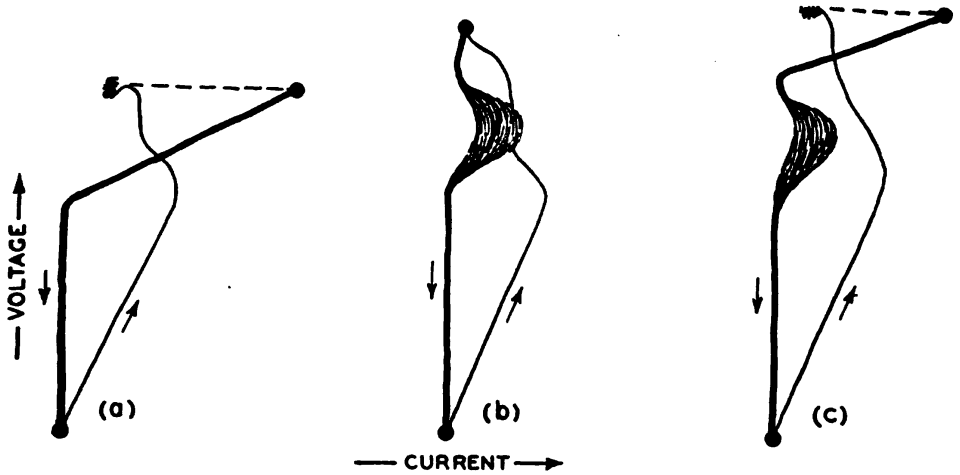

Fig. 38.—Three so-called dynamic V-I plots or dynamic performance charts illustrating the mode skip phenomenon. The plots are copies of presentations obtained with an oscilloscope whose vertical deflection is proportional to DC voltage and whose horizontal deflection is proportional to DC current. On any plot the heaviness of the lines is roughly inversely proportional to the rate at which the coordinates are traversed, and the large dot at the upper extremities represents the operating point at the top of the pulse. (*a*) shows shows normal operation in the π mode. (*b*) shows failure to oscillate in any mode, the π mode being skipped. (*c*) shows oscillation in a harmonic of a mode of smaller n.

10.7 *Magnetron Cathodes:* One important component part of the magnetron oscillator which to this point has not been discussed in detail, but which has been assumed present and operating satisfactorily, is the cathode. Its duty is to supply the electrons which serve as the intermediaries between the DC and RF fields. In terms of the usual requirements of vacuum tube cathodes, the number of electrons demanded of a magnetron cathode is little short of prodigious. Magnetron cathodes may be required to deliver current densities of the order of 50 amperes per square centimeter as contrasted with the 0.5 amperes per square centimeter emitted by oxide cathodes in high vacuum tubes normally.

How oxide surfaces are capable of emitting such enormous currents is

Digitized by Google
Original from UNIVERSITY OF MICHIGAN
Generated on 2019-09-21 09:08 GMT / http://hdl.handle.net/2027/mdp.39015077775156
Public Domain, Google-digitized / http://www.hathitrust.org/access_use#pd-google

not yet entirely clear. It is certain, however, that the RF oscillation in the magnetron is responsible for the fact that such currents may be attained. This is made evident experimentally by measuring the current that may be drawn when the magnetic field is reduced so that oscillation is impossible and comparing it with the current drawn during oscillation. At temperatures even in excess of the operating temperature such pulsed emission currents of excellent magnetrons may run as low as 1% of the currents flowing during oscillation. Furthermore, the fields at the cathode during these measurements may actually exceed those present during oscillation because of the absence of the dense space charge clouds in the interaction space.

In the process of phase selection of electrons, as previously discussed, those electrons starting from the cathode in a phase such as to gain energy from the RF field are removed from the interaction space and driven into the cathode. They impart to the cathode the energy they have gained, causing secondary electrons to be emitted and the cathode temperature to increase. In most magnetrons the amount of this returned energy is about 5% of the input, though in some cases it may become as high as 10%. This means that the average energy of back bombardment may run as high as 75 watts per square centimeter of cathode surface. This amount of energy must be dissipated under equilibrium conditions by radiation and conduction. In general, the short wavelength magnetrons are run with no heater power supplied to the cathode, the cathode temperature being maintained by back bombardment. In many cases, cathode overheating by this process is actually the limitation on the operating capabilities of the magnetron.

There is some experimental evidence that the large current drawn from the magnetron cathode is not primarily made up of secondary electrons but may result from an "enhanced" primary emission. This is supported by the fact that the secondary electrons emitted at the return to the cathode of the "out of phase" electrons are themselves, assuming negligible emission time, largely "out of phase" electrons later to return to the cathode. However, the emission of large numbers of secondary electrons may lead to an "enhanced" primary emission by a process not now understood. As possible processes may be mentioned field emission or an actual lowering of the cathode work function, each brought about by the fields in the cathode coating which result from the charge loss attendant upon the secondary emission. Ionic conduction or electrolytic action in the coating may also contribute in some manner to a lowered work function and to the "enhanced" emission, although such ionic processes would generally involve time intervals longer than a microsecond. The actual mechanism involved, however, is still speculative.

A word about the relation of magnetron scaling to magnetron cathode

Digitized by Google
Original from UNIVERSITY OF MICHIGAN
Generated on 2019-09-21 09:08 GMT / http://hdl.handle.net/2027/mdp.39015077775156
Public Domain, Google-digitized / http://www.hathitrust.org/access_use#pd-google

problems will here be in order. It has been seen earlier that, in scaling all magnetron dimensions by a factor α, the magnetic field changes by a factor $\frac{1}{\alpha}$ while the current and voltage remain unchanged. That this places severe requirements on the cathode may be seen by considering the scaling of a 10 cm. magnetron down to 1 cm. The operating current may be 20 amperes in both cases. If this corresponds to a current density of 5 amperes per sq. cm. at 10 cm., 500 amperes per sq.cm. will be required at 1 cm. What is more, the back bombardment in watts per sq. cm. is increased by a factor of 100. Both of these requirements are completely unreasonable and preclude direct scaling in this instance. Consequently, an attempt is made in such cases to decrease the current density by increasing both the cathode length and diameter. Increasing the latter usually involves increasing the anode diameter and the number of resonators. Even so, current densities may exceed 50 amperes per sq. cm., as stated earlier.

The pulsed magnetron cathode at the shorter wavelengths (less than 10 cm.) in the centimeter band is a limiting factor in magnetron design. In CW magnetrons the small size of the interaction space has made the cathode an important and difficult design problem throughout the centimeter wavelength region. Considerable effort has been expended in a number of laboratories not only to understand the physics of the operation of the magnetron cathode but to find suitable materials and constructional designs. It has become clear that a good magnetron cathode which will meet the special conditions of high current density and high voltage gradient and the considerable electron back bombardment are these: (1) sufficient primary emission to enable the magnetron to start and to supply a part of the required operating current; (2) sufficient secondary emission to supply the remainder (it may be practically all) of the required current density through whatever mechanism is involved; (3) sufficient active material to permit satisfactory life; (4) some mechanical means of holding the active material on the cathode surface; (5) sufficiently low electrical resistance of the coating to permit large bursts of current without undue local heating and high back bombardment without excessive coating temperature; and (6) satisfactory over-all heat dissipation characteristics, conductive and/or radiative, to keep evaporation of active material to a minimum.

In pulsed magnetrons of wavelength 10 cm. or greater it has generally been possible to use plain oxide coated cathodes. Nickel base material is generally used and the active material is the usual double carbonate coating (reduced to the oxides during activation). At wavelengths of 3 cm. and shorter the development of satisfactory pulsed magnetrons would have been impossible without the development of special cathodes. In the main,

Digitized by Google
Original from UNIVERSITY OF MICHIGAN
Generated on 2019-09-21 09:08 GMT / http://hdl.handle.net/2027/mdp.39015077775156
Public Domain, Google-digitized / http://www.hathitrust.org/access_use#pd-google

these have been aimed at meeting requirements (3) to (5) above. The constructions have made use of wire meshes and of sintered nickel matrices both to reduce the coating resistance and to hold sufficient material on the cathode in a manner such that it may be dispensed gradually during life.

10.8 *The Magnetic Circuit:* The magnetic field required for operation of the magnetron oscillator is generally obtained, except in laboratory experiments, by means of a permanent magnet. At long wavelengths and in early models at shorter wavelengths, the magnetron and permanent magnet are separable. Building the magnetic pole faces into the magnetron structure itself and attaching the magnetic material to it has made possible the reduction of the over-all magnet gap, and hence total magnet weight, as well as the use of mechanically superior axial cathode mountings. The resulting so-called "packaged" magnetron design has been used at shorter wavelengths where the magnetic fields are high but need not extend over a large area. The total magnet weight under these conditions is much less than that required in a separate magnet. Needless to say, the possession of good permanent magnet material and the work done on magnet design have contributed materially to the success of the centimeter wave magnetron.

10.9 *Magnetron Measurements:* The fundamental measurements made on the magnetron oscillator have already been discussed or alluded to where the performance characteristics of the magnetron and its circuit theory are described. Here will be described briefly the technique of measurement.

Magnetron measurements are of two general types. One is made on the oscillating magnetron and the other on the non-oscillating magnetron. The latter may be made at any stage in the fabrication of the magnetron after its anode structure and output circuit are completed. Figs. 39 and 40 illustrate schematically the apparatus employed in these tests.

Perhaps the best way of describing the techniques of magnetron measurements is to list all of the parameters, quantities, or characteristics associated with such measurements and for each to give the definition, method of measurement or calculation, or the way it is put together from other data, as the case may be. In any event, the list given below permits of ready reference. Although the text applies directly to pulsed magnetrons the simplifications for CW magnetrons are obvious.

The *DC magnetic field*, B, in which the magnetron operates is generally supplied in the laboratory by an electromagnet, the field in the gap generally being calibrated in terms of the current passed through the magnet coils.

The *peak DC voltage*, V, applied to the magnetron cathode is measured by means of a peak voltmeter or by observing a known fraction of the voltage

Digitized by Google
Original from UNIVERSITY OF MICHIGAN
Generated on 2019-09-21 09:08 GMT / http://hdl.handle.net/2027/mdp.39015077775156
Public Domain, Google-digitized / http://www.hathitrust.org/access_use#pd-google

pulse on the calibrated screen of an oscilloscope. In a simple but suitable peak voltmeter it is arranged to charge a condenser through a diode to the peak voltage which may then be measured with a high resistance DC voltmeter.

The *peak DC current*, I, drawn by the magnetron is measured by passing the current through a known resistance, usually one or two ohms, and determining the peak voltage developed across the resistance by means of a peak voltmeter or calibrated oscilloscope.

The *average DC current* drawn by the magnetron is the current measured on a DC meter connected in one leg of the pulsing circuit, as shown in Fig. 39.

The *pulse duration*, τ, as its name implies, is the length of the time during which the voltage, usually measured near the top of the pulse, is maintained across the magnetron. It may be determined from the pulse presentation on an oscilloscope having a calibrated sweep or it may be calculated as indicated below when other parameters are known.

The *pulse recurrence rate*, *pps*, is the repetition frequency at which the voltage pulse is applied and is determined by the frequency of the calibrated primary oscillator driving the pulser or modulator circuit.

The *duty cycle*, defined as the fraction of time the pulsed magnetron operates, may be determined as the ratio of average to peak DC current or as the product of the pulse duration and the pulse recurrence rate.

The *peak input power* is the product of the peak DC voltage and the peak DC current.

The *average input power* is the product of the peak input power and the duty cycle.

The *voltage and current pulse shapes* as observed with oscilloscopes are of importance in studying the spectrum and moding characteristics of the magnetron under test.

The *dynamic V-I plot*, or *dynamic performance chart*, is viewed on an oscilloscope in which at any instant the vertical deflection is proportional to peak DC voltage and the horizontal deflection proportional to peak DC current. Three such plots are shown on Fig. 38 and their usefulness is indicated in the corresponding text.

The *average output power* is the average centimeter wave power delivered to the useful load. The simplest and most foolproof method of measuring this power is to absorb the energy in a column of water. From a determination of the rate of water flow and its temperature rise the power may be calculated readily. The water column terminating the coaxial line or wave guide of the test apparatus is made reflectionless either by tapering it or preceding it by a quarter wavelength matching plate of proper dielectric constant, analogous to the optical quarter wave plate.

The *peak output power* may be calculated as the average output power divided by the duty cycle.

Digitized by Google
Original from UNIVERSITY OF MICHIGAN
Generated on 2019-09-21 09:08 GMT / http://hdl.handle.net/2027/mdp.39015077775156
Public Domain, Google-digitized / http://www.hathitrust.org/access_use#pd-google

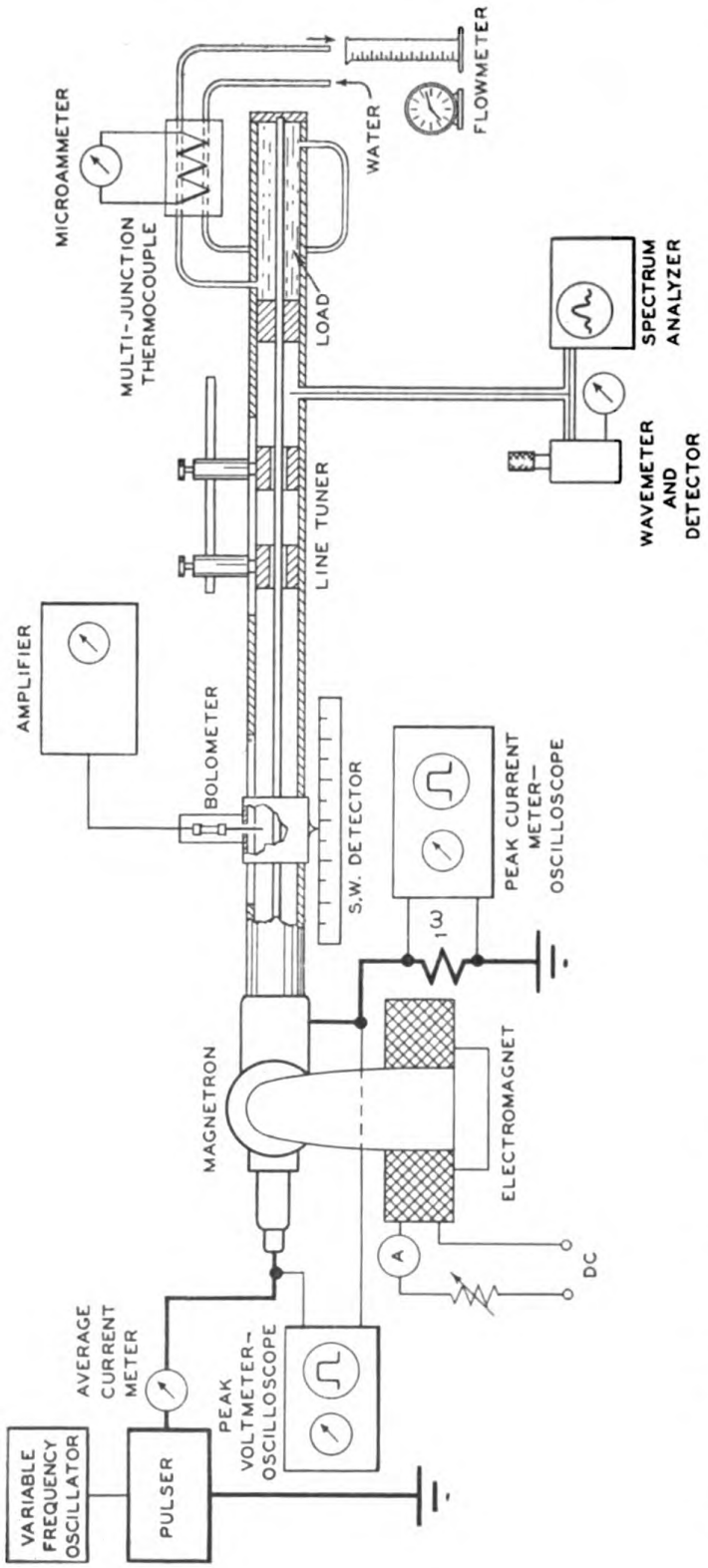

Fig. 39.—A schematic diagram showing the arrangement of apparatus generally used in making measurements on an operating magnetron in the laboratory.

Digitized by Google
Original from UNIVERSITY OF MICHIGAN
Generated on 2019-09-21 09:08 GMT / http://hdl.handle.net/2027/mdp.39015077775156
Public Domain, Google-digitized / http://www.hathitrust.org/access_use#pd-google

The *over-all efficiency* of operation is the ratio of the peak output to peak input powers or the ratio of average output to average input powers.

The *frequency of oscillation* of the magnetron is determined by feeding a small amount of the RF power into a calibrated variable frequency resonant cavity of high Q and by means of a detector observing the frequency at which the cavity absorbs or passes power.

The *load impedance* into which the magnetron operates is determined by measurement in the output line of the voltage standing wave and its phase with respect to some previously chosen reference point. This measurement is made with a *standing wave detector* in which it is arranged to move an electrostatic probe along a section of slotted line in which it samples the RF energy in the line. The energy picked up by the probe is detected after sufficient attenuation either by a crystal or by a small bolometer whose resistance is a function of the energy fed into it. The voltage standing wave

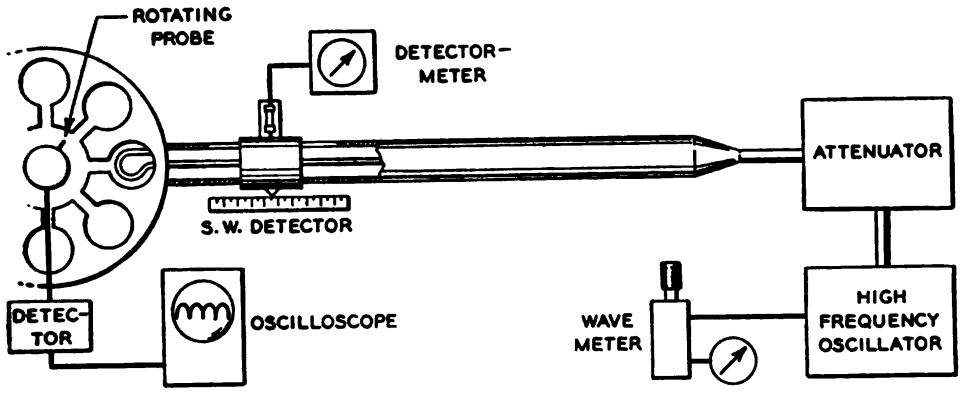

Fig. 40.—A schematic diagram showing the arrangement of apparatus used in making measurements on a non-oscillating magnetron or magnetron resonator block.

ratio and its phase may be translated into impedance, admittance, or reflection coefficient in the manner already discussed. The magnetron load impedance may be varied from the match presented by the terminating water column by means of a *line tuning section* or *tuner*. In one such line tuning section, two sleeves constituting in effect quarter wavelength lines of low characteristic impedance may be moved relative to one another to vary the magnitude, and moved together to vary the phase of the standing wave.

The *Rieke diagram*, is a plot of constant output power and frequency on a reflection coefficient plane. Its construction thus involves the measurement of output power, frequency, and load impedance as the line tuners are moved over a wide range of positions. The operating parameter maintained constant is usually chosen to be the peak DC current. Such a diagram is shown in Fig. 33.

Digitized by Google
Original from UNIVERSITY OF MICHIGAN
Generated on 2019-09-21 09:09 GMT / http://hdl.handle.net/2027/mdp.39015077775156
Public Domain, Google-digitized / http://www.hathitrust.org/access_use#pd-google

The *pulling figure, PF*, defined as the maximum frequency excursion of the magnetron as the load reflection coefficient traverses the $\rho = 0.2$ circle, may be obtained from the Rieke diagram. It may be measured directly by two simple wavemeter measurements taken at the frequency extrema occuring as the standing wave of 1.5 voltage ratio is moved up and down the line. Various types of *standing wave introducers* have been devised to produce a reflection coefficient of $\rho = 0.2$ for the specific measurement of pulling figure.

The *performance chart* is a plot of constant magnetic field, peak output power and over-all efficiency contours on a *V-I* plane. Its construction thus involves the measurement of peak DC voltage, peak DC current, and peak output power at several magnetic fields. Sometimes frequency, pushing figure, and spectrum appearance are also determined. Figs. 17 and 20 are examples of this chart.

The *frequency spectrum* is the distribution of energy with frequency for a pulsed magnetron and is displayed on a so-called *spectrum analyzer*. This analyzer is a very narrow band tunable radio receiver whose pass band is varied periodically twenty or so times per second over several *mc/s*. The response of the receiver to the frequency distribution of energy appears on an oscilloscope whose sweep is synchronized with the pass band frequency variation.

The *pushing figure* is the instantaneous frequency change in *mc/s* per ampere change in peak DC current at constant load. It may be obtained by measuring the frequency shift on a spectrum analyzer as the pulse current is changed by a known amount. The current change must be executed rapidly enough to avoid frequency shifts arising from temperature changes.

Impedance measurements on the non-oscillating magnetron involve the use of a variable frequency RF oscillator feeding power through an attenuator and a standing wave detector into the output circuit of the magnetron (see Fig. 40). These measurements determine as a function of frequency the impedance Z_e discussed in the text.

Mode frequencies are determined from the impedance measurements on the non-oscillating magnetron by noting the frequencies at which the input standing wave is observed to go through a minimum. They may also be determined by the observation of energy maxima with a pickup loop or probe placed in the resonator system.

Mode identification is made by observing the periodicity of RF field in the interaction space of the resonator system. This is done by sampling the field with a rotating RF probe placed in an axial cylinder corresponding to the cathode as shown in Fig. 40. The probe response is detected and displayed on an oscilloscope with sweep synchronized to the rotation of the probe.

Digitized by Google
Original from UNIVERSITY OF MICHIGAN
Generated on 2019-09-21 09:09 GMT / http://hdl.handle.net/2027/mdp.39015077775156
Public Domain, Google-digitized / http://www.hathitrust.org/access_use#pd-google

PART II

DEVELOPMENTAL WORK ON THE MAGNETRON OSCILLATOR AT THE BELL TELEPHONE LABORATORIES, 1940–1945

11. General Remarks

IN THE first part of this paper the fundamentals of the theory of the magnetron oscillator have been discussed. The objective has been to establish for the reader a general picture of the nature of the electronic mechanism and of the role played by the RF circuit and load.

In the second part of the paper is traced the research and development work done at the Bell Telephone Laboratories on the magnetron oscillator during the war years, 1940–1945. The effort was directed, for the most part, toward the development of magnetrons to meet definite radar needs.

Fifteen different types or families of magnetrons were developed at the Bell Laboratories during the war. Included among these are some 75 separate Western Electric Company or RMA code numbers. It has been found most convenient to discuss the work done on each type of magnetron as a unit, although, to be sure, there has been considerable interplay between projects. Something is said of the origin of each type, of the problems encountered in its development, and of the solution of these problems, in some cases involving studies and experiments of general interest. Special characteristics and general performance data for each type of magnetron discussed are given. Included also is a general discussion of the work done on magnetron cathodes, which, although carried out on specific magnetrons, has been of general applicability to all.

Before proceeding with the detailed discussion, it would be well for the reader to recognize the general scope of the work to be described and the general nature of the problems encountered. The work of the Bell Laboratories in the development of pulsed magnetrons for radar use has extended over practically the whole range of effort surveyed in the Introduction. Work has been done throughout the range of wavelengths from 45 cm. to 1 cm. and on magnetrons capable of developing over one megawatt peak RF power. It has included work on such features as tuning, coaxial and wave guide outputs, several types of resonator systems and strapping schemes, and on the incorporation of the magnetic circuit into the magnetron structure in so-called "packaged" types.

The scope of the developments to be described may be judged from Figs. 41, 42, 43, and 44. That part of a magnetron oscillator which perhaps best gives one an idea of size and wavelength range is the resonator block. In Fig. 41 is shown a series of resonator blocks ranging in resonant fre-

Generated on 2019-09-21 09:10 GMT / http://hdl.handle.net/2027/mdp.39015077775156
Public Domain, Google-digitized / http://www.hathitrust.org/access_use#pd-google
Digitized by Google
Original from UNIVERSITY OF MICHIGAN

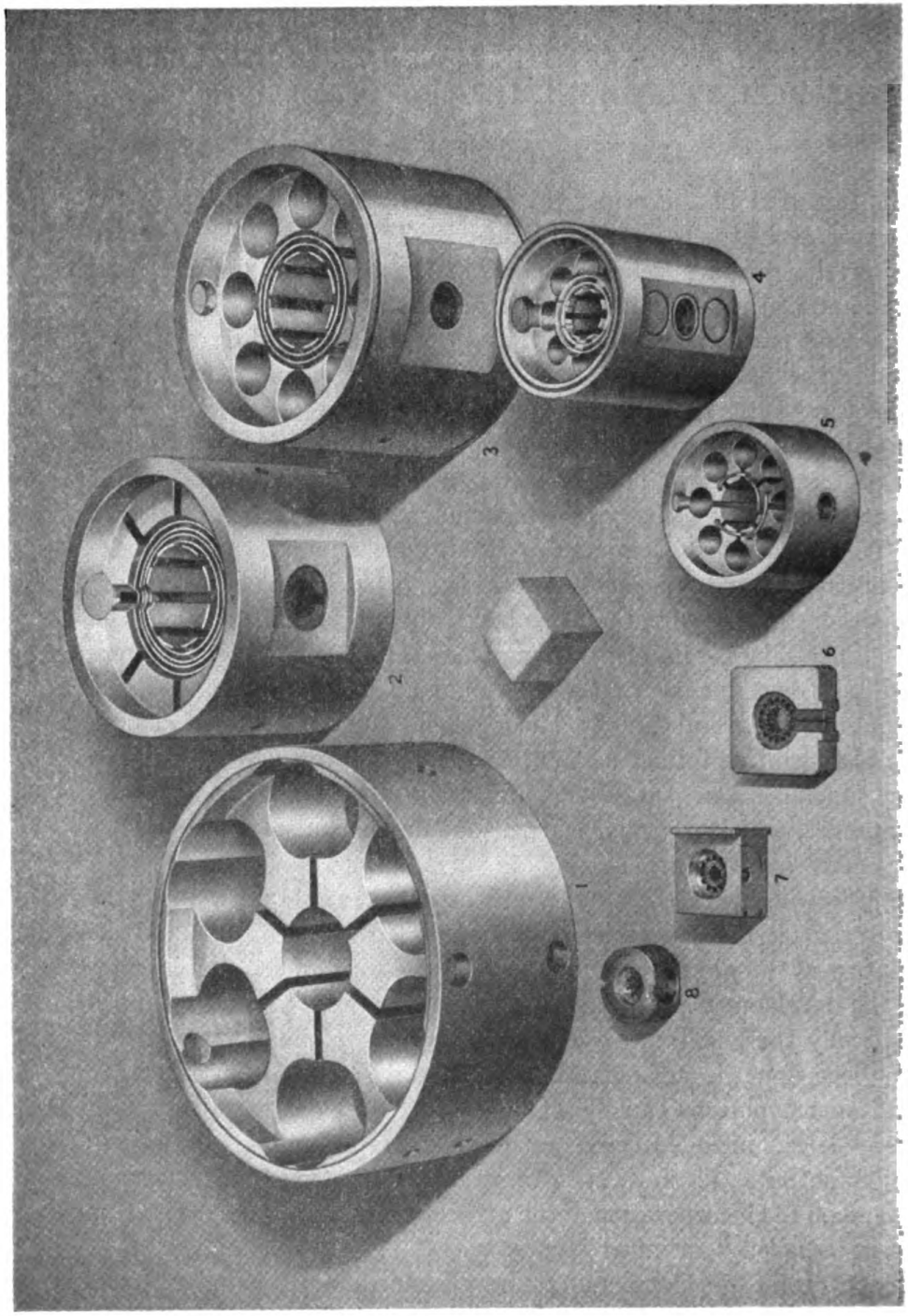

Fig. 41—Resonator blocks of centimeter wave magnetrons developed at the Bell Telephone Laboratories. From the largest to the smallest these resonator systems are those of: (1) the 700 A-D magnetrons of fixed frequencies near 700 mc/s; (2) the 5J26 magnetron, tunable over the frequency range 1220 to 1350 mc/s; (3) the 4J21-30 magnetrons of fixed frequencies near 1280 mc/s; (4) the 720A-E magnetrons of fixed frequencies near 2800 mc/s; (5) the 706AY-GY magnetrons of fixed frequencies near 3000 mc/s; (6) the 4J50 magnetron at 9375 mc/s; (7) the 725A magnetron at 9375 mc/s; and (8) the 3J21 magnetron at 24,000 mc/s. Note the hole and slot type resonators of (1), (3), (4), (5), (6), and (7), the slot type resonators of (2); and the vane type resonators of (8).

Digitized by Google
Original from UNIVERSITY OF MICHIGAN
Generated on 2019-09-21 09:10 GMT / http://hdl.handle.net/2027/mdp.39015077775156
Public Domain, Google-digitized / http://www.hathitrust.org/access_use#pd-google

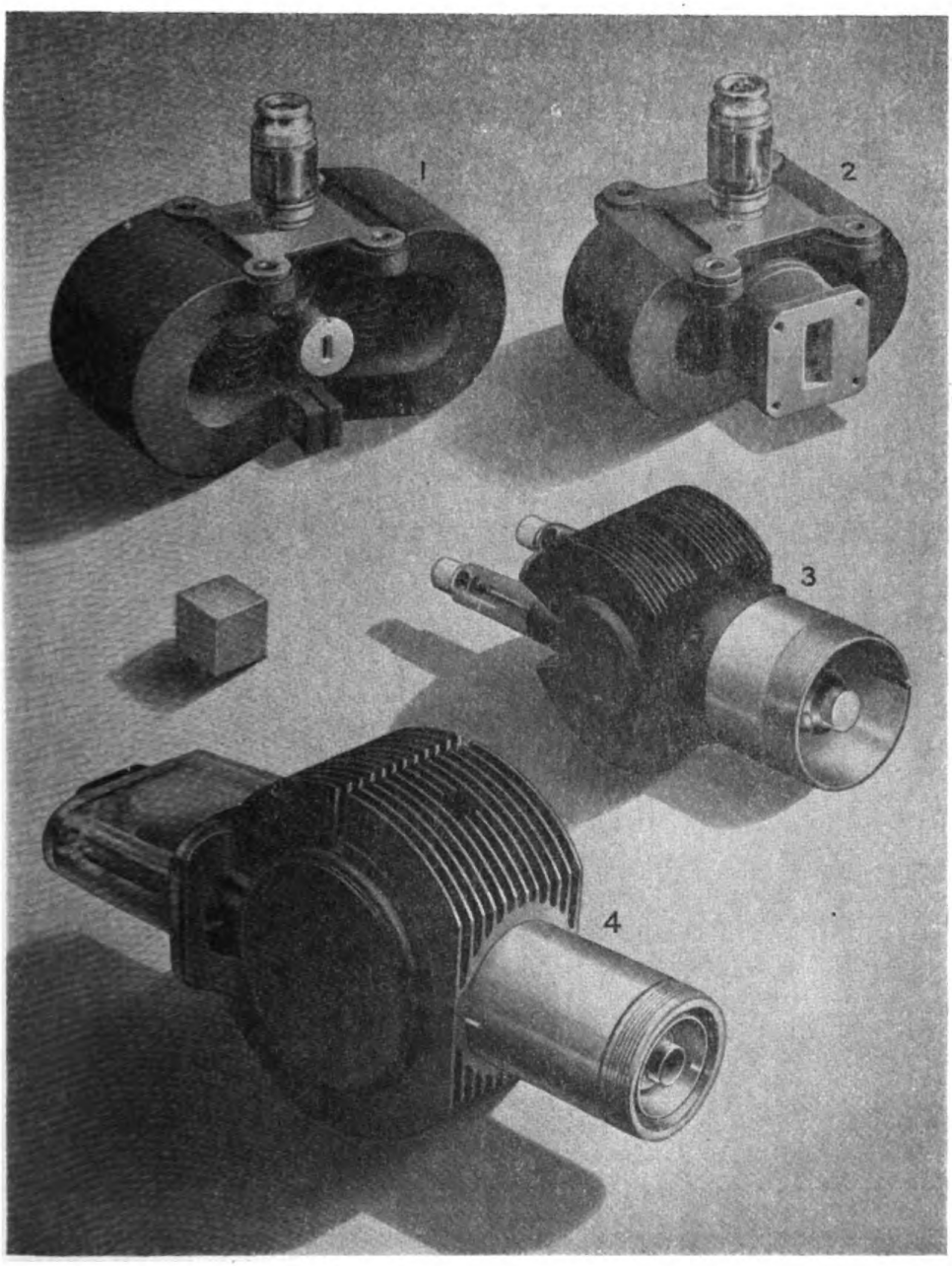

Fig. 42—Four fixed frequency magnetron oscillators. They are: (1) the 3J21 magnetron (60 kw., 24,000 mc/s); (2) the 4J52 magnetron (100 kw., 9375 mc/s); (3) the 720A-E magnetron (1000 kw., ~2800 mc/s); (4) the 4J21-30 magnetron (600 kw., ~1280 mc/s). Note the two types of output circuit, coaxial and waveguide; the use of packaged magnets; and the two types of input leads.

quency from 700 mc/s to 24,000 mc/s.[23] In Fig. 42 is shown the external view of four magnetrons of operating frequencies distributed over the range

[23] In this and other photographs of PART II either a one inch cube or a line of length one inch has been included for size reference.

Digitized by Google
Original from UNIVERSITY OF MICHIGAN
Generated on 2019-09-21 09:11 GMT / http://hdl.handle.net/2027/mdp.39015077775156
Public Domain, Google-digitized / http://www.hathitrust.org/access_use#pd-google

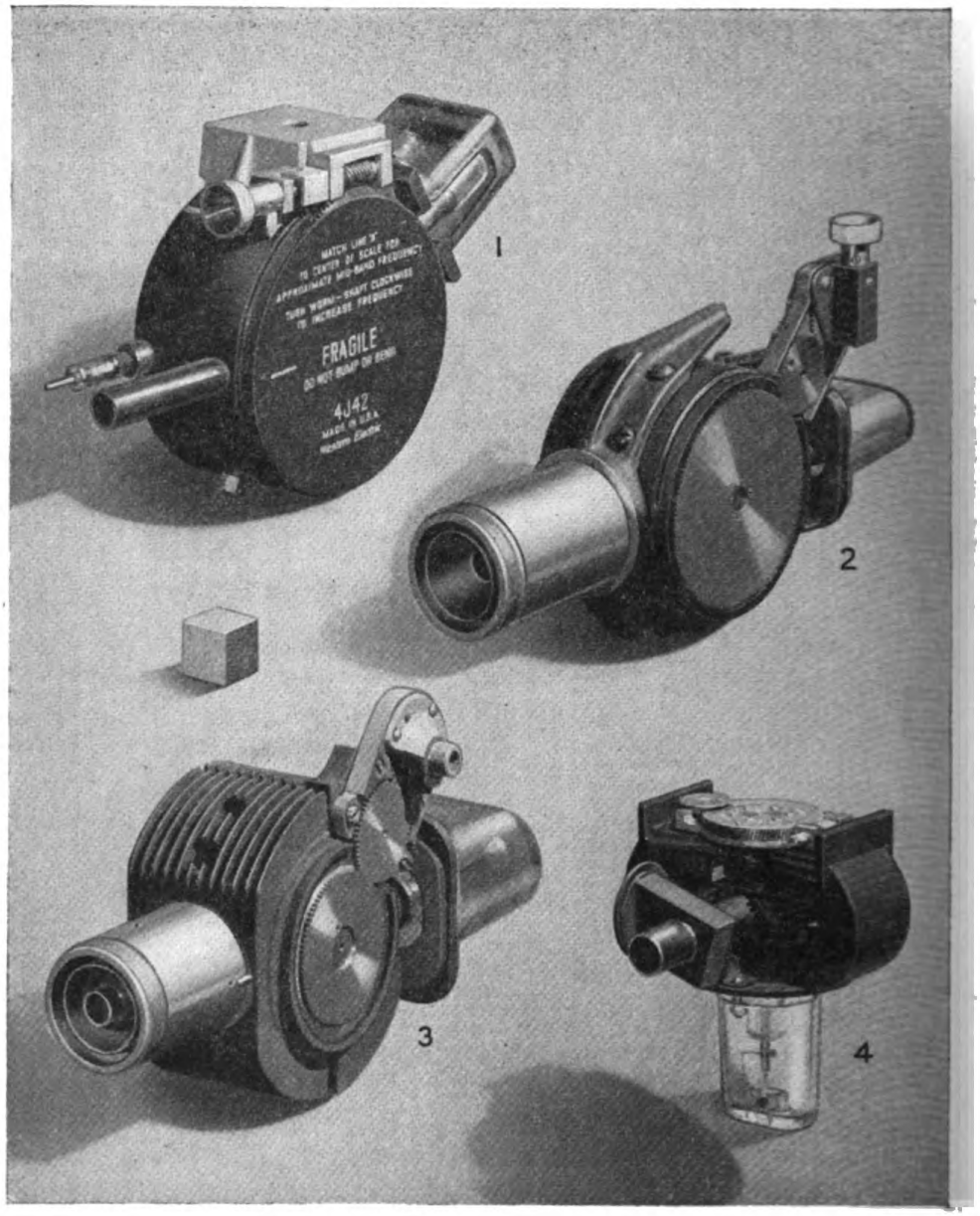

Fig. 43—Four tunable magnetron oscillators. They are: (1) the 4J42 magnetron (40 kw., 660 to 730 mc/s); (2) the 4J51 magnetron (275 kw., 900 to 970 mc/s); (3) the 5J26 magnetron (600 kw., 1220 to 1350 mc/s); and the 2J51 magnetron (55 kw., 8500 to 9600 mc/s).

in which work has been done. It illustrates both the coaxial and waveguide types of output circuits, the use or not of attached magnets, and the two types of input leads and cathode supports. In Fig. 43 is shown the group of tunable magnetrons developed as replacements for fixed frequency models with which they are electrically and mechanically inter-

Digitized by Google
Original from UNIVERSITY OF MICHIGAN
Generated on 2019-09-21 09:16 GMT / http://hdl.handle.net/2027/mdp.39015077775156
Public Domain, Google-digitized / http://www.hathitrust.org/access_use#pd-google

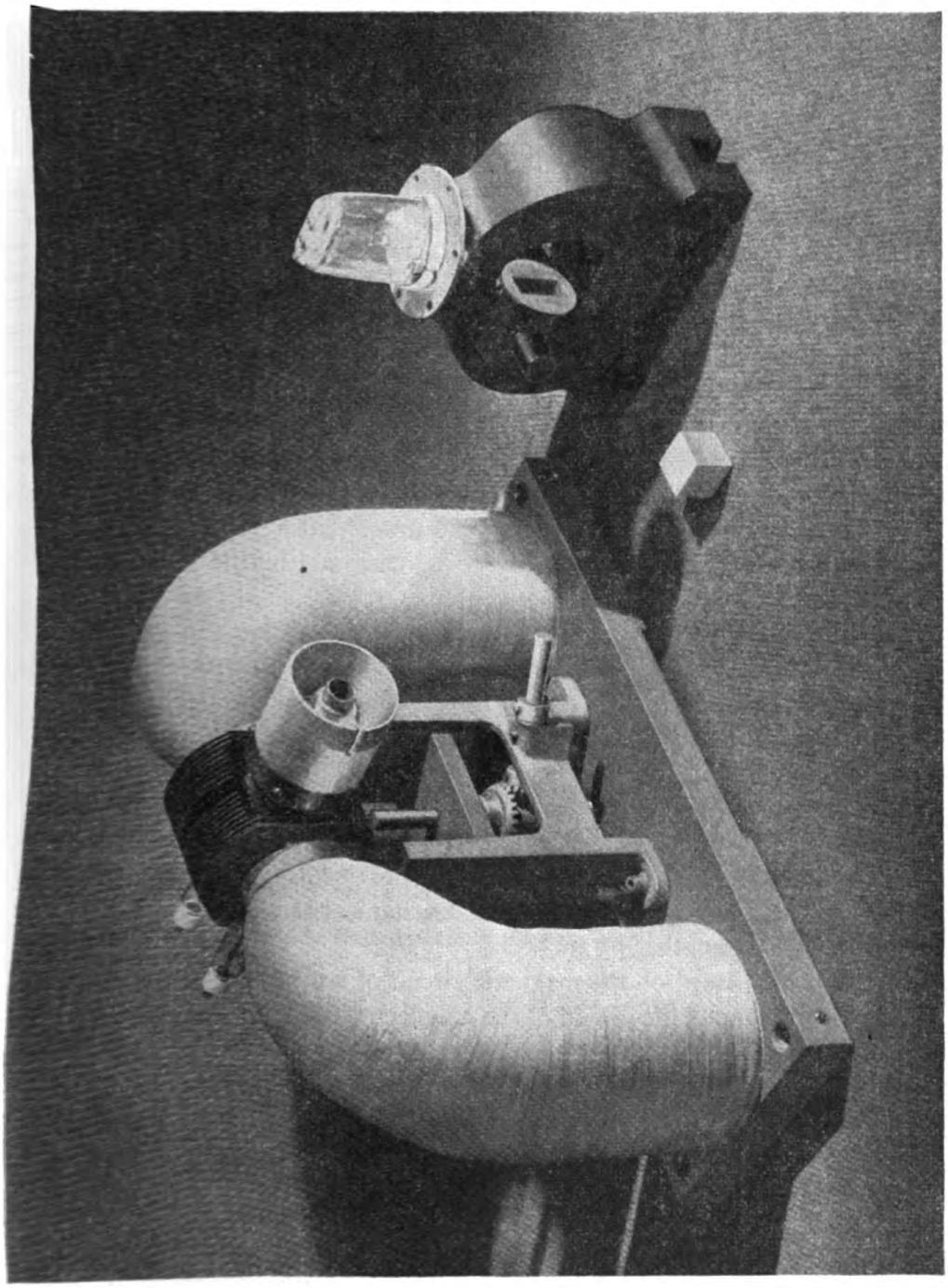

Fig. 44—The 720A-E (1000 kw., ~2800 mc/s) and the 725A (55 kw., 9375 mc/s) magnetrons, shown at the left and right respectively, each mounted in its magnet.

Digitized by Google
Original from UNIVERSITY OF MICHIGAN
Generated on 2019-09-21 09:16 GMT / http://hdl.handle.net/2027/mdp.39015077775156
Public Domain, Google-digitized / http://www.hathitrust.org/access_use#pd-google

changeable. Finally, in Fig. 44 are shown two magnetron oscillators, the 720A and 725A, mounted in their magnets. By comparison with Fig. 42, the space and weight saved by packaging may be seen. A fair comparison is that between the 725A and magnet of Fig. 44 and the 4J52, number 2 in Fig. 42. Both are 3.2 cm. models, the latter, moreover, being capable of generating higher power.

The designer of a magnetron oscillator is faced with a variety of tasks. If the magnetron is to be used in a specific application he has at his disposal data concerning the amount of power available to drive the magnetron, the nature of the pulsing if such is to be used, the frequency of operation, mechanical features having to do with form and weight, and an idea of what the user hopes or expects to obtain in the way of output power, frequency stability, and operating efficiency. It is the problem of magnetron design to arrange the resonator system, output circuit, cathode, magnetic circuit, and mechanical features to meet these requirements if possible.

In the design of the resonator system it must be arranged to achieve the proper frequency of operation, proper characteristics regarding modes, the proper size of interaction space, and other characteristics which have a bearing on the electronic operation. In special cases a tunable resonator system must be provided.

In the design of the output circuit it is necessary to arrange the type of coupling to the resonator system, the necessary impedance transformation from resonator to load, the type of external coupling, a vacuum seal, and generally to take into account the possibility of electrical breakdown when the power delivered is high.

In the design of the magnetron cathode, attention must be paid to its surface and how it is equipped to meet the rigorous demands made of it. The cathode mounting and input leads must be designed for proper geometry at the cathode ends, heat dissipation, mechanical strength, and DC voltage breakdown strength.

The requirements placed on the magnetic circuit of a magnetron must be borne in mind throughout the design of the magnetron itself. Considerable effort may be expended in arranging for the magnet gap, and hence the required magnet, to be as small as possible. In "packaged" magnetrons the magnet pole pieces, which are built into the magnetron structure, must be designed to produce a field of proper configuration and to make the necessary external magnets feasible.

Generally, the design of the mechanical features of a device as complicated as the multiresonator magnetron oscillator is extremely important and must provide for structural strength under a variety of conditions, as well as cooling facilities and external protection of relatively fragile parts.

Generated on 2019-09-21 09:16 GMT / http://hdl.handle.net/2027/mdp.39015077775156
Public Domain, Google-digitized / http://www.hathitrust.org/access_use#pd-google
Digitized by Google
Original from UNIVERSITY OF MICHIGAN

12. Reproduction of the British Magnetron

The problem undertaken at the Bell Telephone Laboratories immediately after the visit of the British delegation in October 1940 was the reproduction of the 10 cm. magnetron for study and for general radar use at the Bell Laboratories and the Radiation Laboratory at the Massachusetts Institute of Technology. The data available were contained in a drawing of a magnetron having six resonators and in an X-ray photograph of the magnetron used in the demonstration at the Whippany Laboratory, described in the Introduction. The X-ray photograph, reproduced in Fig. 45, showed a

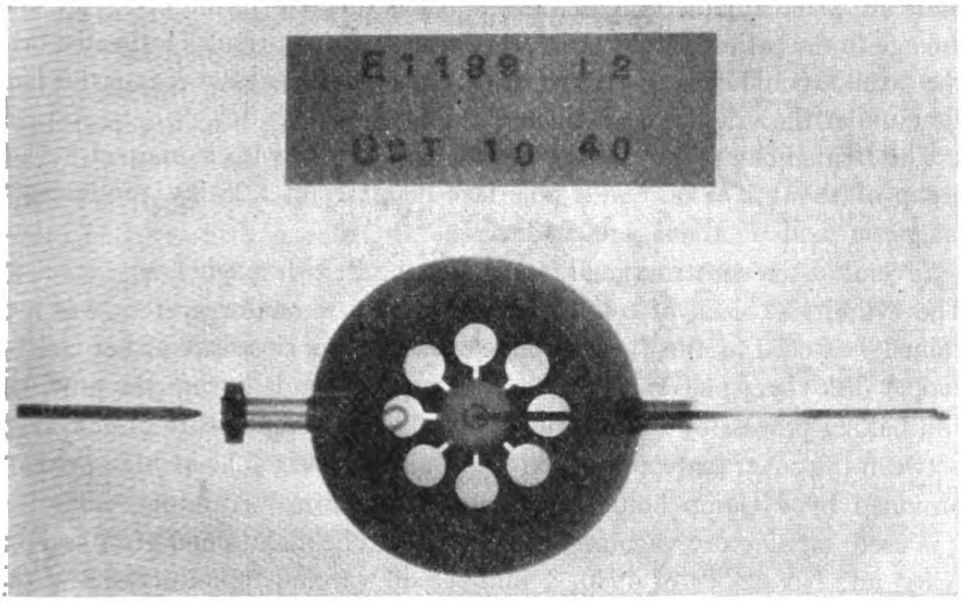

Fig. 45—An X-ray photograph of the 10 cm. magnetron oscillator brought to America by a British delegation in October 1940 and copied at the Bell Laboratories. It is the prototype of most magnetron oscillators in the centimeter wave region developed in Great Britain and the United States during the war.

resonator system having eight resonators. Since this arrangement was known to operate, it was adopted as the starting point for the work here.

In its first tests at Whippany, the British magnetron was pulse operated at about 10 kv. and 10 amps. peak current. The pulses were of 1 microsecond duration and recurred 1000 times per second. The magnetic field required was about 1100 gauss. The magnetron was loaded with a simple radiating antenna of unknown load impedance. Under these conditions the magnetron generated RF power estimated at the time to be greater than 10 kw.

The eight hole and slot type resonators of the British magnetron were spaced around an anode of 0.8 cm. radius. The resonator system, machined in a block of copper, was 2 cm. long. It was unstrapped, strapping

Digitized by Google
Original from UNIVERSITY OF MICHIGAN
Generated on 2019-09-21 09:17 GMT / http://hdl.handle.net/2027/mdp.39015077775156
Public Domain, Google-digitized / http://www.hathitrust.org/access_use#pd-google

not being known at the time, and in its general features was much like that shown schematically in Fig. 1.

The output circuit of the British magnetron was also similar to that of Fig. 1. It had no particular transformer properties designed into it. The vacuum seal, made of copper, glass, and tungsten, was incorporated in the output coaxial line in very much the same manner as that shown in Figs. 60 and 61.

The cathode was a plain, oxide coated, nickel cylinder, 0.3 cm. in radius. It had nickel end disks of 0.5 cm. radius and was mounted on radial leads passing through glass vacuum seals like those shown in Fig. 61. The leads are placed diametrally across the resonator hole to minimize RF flux linkage to the cathode structure. Preliminary British results indicated that the cathode could be activated properly and would possess a reasonable lifetime under the original operating conditions.

The British magnetron had been designed for use with a magnet having a gap of about 1.75 in. and a pole face diameter of 1.25 in., producing a magnetic field of about 1500 gauss.

Several of the constructional features of the British magnetron were new. The cylindrical block of copper into which the resonator system was machined was used as the vacuum envelope. It was closed at either end by copper disk cover plates. The vacuum seal was made during the pumping and baking process by the alloying at the baking temperature of gold rings between the cover plate and block. The alloying was done at high pressure provided by a clamp bolted across the magnetron. Although no getter was used, satisfactory vacuum conditions could be maintained after seal-off.

By mid-November of 1940, a number of working reproductions of the British magnetron had been supplied in our Laboratories and to the Radiation Laboratory at M. I. T., and a program of study of the magnetron oscillator commenced. The work thus started was continued, on the one hand, to put the new magnetron into production, and on the other hand, to attempt to understand it, improve upon it, and extend its range of usefulness.

13. Magnetrons for Wavelengths of 20 to 45 Centimeters

13.1 *The 700A-D Magnetrons:* After the British 10 cm. magnetron had been successfully reproduced and an emergency program of research and development of multicavity magnetron oscillators commenced, the question immediately was asked: Can a multicavity magnetron be designed to operate near 40 cm. in the pulsed radar set under development in the Whippany radio laboratory? Clearly there now existed the possibility of much greater power than was possible with triodes at this wavelength with reasonable

Digitized by Google
Original from UNIVERSITY OF MICHIGAN
Generated on 2019-09-21 09:17 GMT / http://hdl.handle.net/2027/mdp.39015077775156
Public Domain, Google-digitized / http://www.hathitrust.org/access_use#pd-google

life expectancy. The modulator of the radar set provided pulsed input power to the oscillator at about 12 kv. and up to 10 amps. peak current.[24]

The performance of the 10 cm. multicavity magnetrons appeared to make the development of such a generator at 40 cm. feasible. A straightforward enlargement of the 10 cm. magnetron by a factor of four was out of the question, however, as it resulted in a magnetron entirely too bulky, requiring a prohibitively large magnet. The development of the 700 mc/s magnetron oscillator thus involved departures from the British design. In particular it was found necessary to reduce the axial length of the resonator system to a considerably smaller fraction of a wavelength than in the 10 cm. design. The development involved design of the interaction space for maximum operating efficiency, the resonator system, for which both eight and six resonator structures were employed, and the output circuit for coupling into the existing radar system.

An early 700 mc/s multicavity magnetron design employed eight resonators of axial length less than one tenth wavelength; the 10 cm. design was about one fifth wavelength long. Operating models initially produced approximately 10 kw. of RF power near the desired frequency. It was found, however, that a smaller and lighter magnetron could be made to operate at the same voltage if the number of resonators were reduced from eight to six, permitting smaller anode and cathode radii [equation (16) in PART I]. The weight and over-all diameter was further reduced by use of elongated holes in the hole and slot resonators. This change resulted in the resonator system used in the 700A-D magnetrons (see Figs. 41 and 46). Each hole is made by boring two intersecting cylinders in the resonator block as may be seen in Fig. 46. No difficulty was encountered in achieving the desired frequency. The frequency differences between the four coded magnetrons near 700 mc/s were achieved by variation of the resonator slot width.

The separation of mode frequency between the $n = 3$ mode (π mode) and the nearest other mode is of the order of 3 per cent. Although this is small compared to that obtainable in strapped magnetrons, it is greater than that for the early unstrapped magnetrons near 10 cm. This is reflected in greater operating efficiency.

The cathode in the 700A-D magnetrons is supported, as in the British magnetron, by radial leads extending across the center of one of the hole and slot resonators. The cathode diameter was varied in an experiment designed to determine the value for maximum operating efficiency. Early experiments of this type involving measurements of output power and efficiency were quite crude and conclusions from their results were by no means as significant as those based on measurements of frequency. The primary

[24] This radar development is discussed in: W. C. Tinus and W. H. C. Higgins, "Early Fire-Control Radars for Naval Vessels." See pp. 9 ff.

Digitized by Google
Original from UNIVERSITY OF MICHIGAN
Generated on 2019-09-21 09:17 GMT / http://hdl.handle.net/2027/mdp.39015077775156
Public Domain, Google-digitized / http://www.hathitrust.org/access_use#pd-google

difficulty lay not in the actual measurement of power or voltage but in the fact that the magnetrons were not loaded in a reproducible fashion. It was considerably later that load impedance measurements were made and used in evaluating magnetron performance. In many early studies the effect of load on operation was not sufficiently disentangled from the effects of other things. In spite of these inadequacies, however, it was generally possible to distinguish a good design change from a bad one, and much of value was gained in early work.

The cathode diameter used in the 700A-D magnetrons is given in TABLE I along with other data on these and other magnetrons in the 20 to 45 cm.

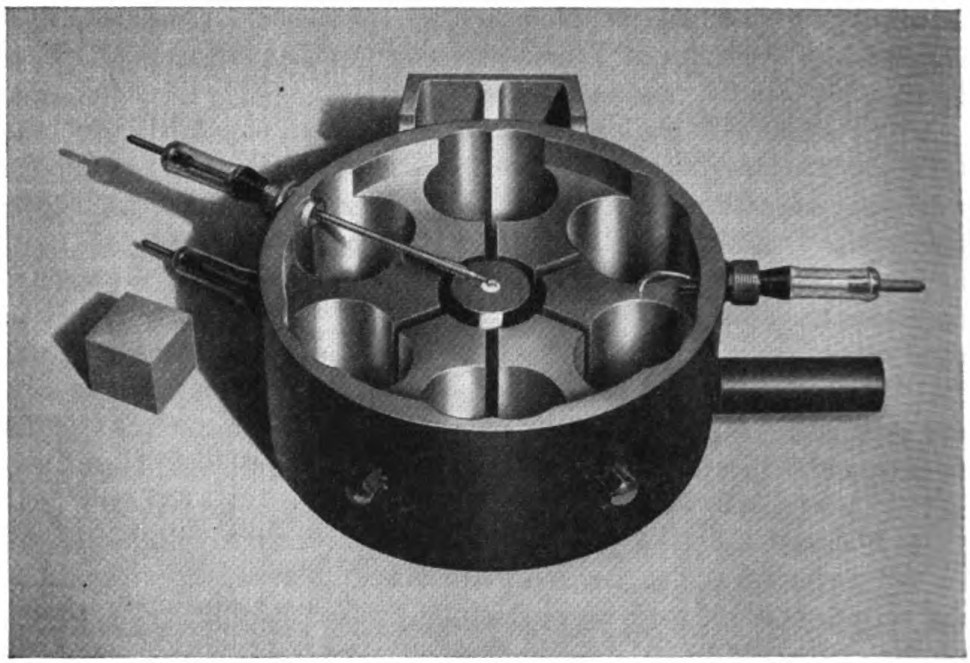

Fig. 46—An internal view of a 700A-D magnetron (40 kw., ~700 mc/s) showing the unstrapped resonator system of six hole and slot circuits, the cathode, the cathode end disks and support leads, and the output coupling loop and lead.

wavelength range. It should be noted that the optimized ratio r_c/r_a is 0.300 as compared to 0.375 in the British magnetron having eight resonators. Plain oxide coating is used on the cathode. Life expectancy is thousands of hours.

As may be seen in Fig. 46, the output coupling is accomplished by means of a loop in the end space of the structure. The loop is connected to an anode segment. It is driven by direct coupling to the anode segment and by coupling to the magnetic flux linking the two adjacent resonators. The output circuit was not designed to operate into a matched output line, however, and external impedance transformation must be incorporated into the load line.

Digitized by Google
Original from UNIVERSITY OF MICHIGAN
Generated on 2019-09-21 09:17 GMT / http://hdl.handle.net/2027/mdp.39015077775156
Public Domain, Google-digitized / http://www.hathitrust.org/access_use#pd-google

Generated on 2019-09-21 09:17 GMT / http://hdl.handle.net/2027/mdp.39015077775156
Public Domain, Google-digitized / http://www.hathitrust.org/access_use#pd-google

Digitized by Google

TABLE I

MAGNETRONS FOR WAVELENGTHS OF 20 TO 45 CENTIMETERS

	700A-D Unpackaged	728A-J Unpackaged			5J23 Unpackaged			4J21-25 Unpackaged			4J26-30 Unpackaged			4J42 Unpackaged Tunable	4J51 Unpackaged Tunable	5J26 Unpackaged Tunable	
N	6	8			8			8			8			6	8	8	
r_a (in.)	0.160	0.266			0.266			0.218			0.230			0.199	0.266	0.375	
r_c (in.)	0.689	0.687			0.709			0.582			0.612			0.689	0.687	0.687	
h (in.)	1.576	1.716			2.360			1.940			2.040			1.451	1.500	1.940	
Magnet gap (in.)	2.980	3.290			3.990			3.540			3.640			2.983	3.290	3.640	
Weight (lb.)	12.5	13.0			16.5			15.0			15.0			16.5	14.5	18.5	
Resonators	hole and slot	hole and slot			hole and slot			hole and slot			hole and slot			hole and slot	hole and slot	slot	
Unstrapped λ (cm.)	43.0	~26.0			~21.5			~18.0			~19.0			~38.0	~23.5	10.3	
Straps	none	double ring			echelon wire			double ring			double ring			wire	double ring	double channel	
λ (cm.)	43.0	32.1			28.6			22.8			24.0			43.0	32.1	23.4	
f (mc/s)	720–680	970–900			1056–1044			1350–1280			1280–1220			670 to 730	900 to 970	1220 to 1350	
Nearest mode	$n = 2$	$n = 3$			$n = 3$			$n = 3$			$n = 3$			$n = 1$	$n = 1$	$n = 3$	
λ separation (%)	−3	~−30			~−20			−20			−20			−16	+4	~−60	
Tuning	—	—			—			—			—			resonator capacitance	resonator capacitance	strap capacitance	
$\Delta\lambda$ (%)	—	—			—			—			--			10.2	7.5	10.3	
Tuner travel (in.)	—	—			—			—			—			0.100	0.080	0.154	
Q_e	>5000	~4500			~3200			2800			2800			1600→2500	3500→4500	700→1800	
Q_{ext}	~280	170			150			170			180			285	215	210	
η_e (%)	~95	~96			~95			94			94			87	95	82	
Output circuit	coaxial	coaxial			coaxial			coaxial			coaxial			coaxial	coaxial	coaxial	
V (kv.)	12	19.0	21.0	24.5	16.5	19.0	24.5	15.5	22.0	26.5	16.5	23.0	27.0	12.0	23.0	27	27
I (amps.)	10	19	20	28	20	24	33	25	40	48	25	40	46	9	20	46	46
B (gauss)	650	1000	1100	1200	800	900	1100	900	1200	1400	900	1200	1400	650	1100	1400	1400
τ (μs)	2	1	1	1	1	1.5	1	1.5	1	5	1.5	1	5	1.5	1	1	5
pps	1000	1000	1000	1000	2000	1000	1000	1000	1000	200	1000	1000	200	2000	1000	1000	200
P_o (kw.)	40	210	260	400	170	250	475	175	440	640	200	470	700	30	285	600	600
η (%)	33	58	62	58	55	55	59	45	50	50	48	51	56	28	62	48	48
η_o (%)	~35	~61	~65	~61	~58	~58	~62	48	53	53	51	54	60	32	65	58	58
PF (mc/s)	~1.2	2.5	2.5	2.5	3.0	3.0	3.0	3.4	3.4	3.4	3.0	3.0	3.0	1.2	1.9	3.0	3.0

Original from UNIVERSITY OF MICHIGAN

In mechanical construction the 700A-D magnetrons involved techniques like those described above. The input and output leads included copper to glass to tungsten seals much like those in the reproductions of the British magnetron. The end covers were sealed to the resonator body by means of the gold ring technique employed in the British magnetron.

The 700A-D magnetrons are limited in frequency to the four 10 mc/s bands between 680 and 720 mc/s, respectively. These magnetrons operate at 12 kv. and 8 amps. peak current input at a magnetic field of 650 gauss. Over-all efficiency ranges between 30 and 40%, which is better, as has been explained, than that attained with unstrapped 10 cm. magnetrons. Other data of interest are given in TABLE I.

One feature which is immediately apparent from the rated operating conditions of the 700A-D magnetrons is the fact that the ratings are not nearly as high as one might expect from the size of the magnetron. Back bombardment of the cathode at considerably greater input power could easily be handled. The difficulty lay in the fact that it was impossible to drive the magnetrons in the π mode to much greater currents than the rated currents. If the attempt is made to drive the magnetron harder it either refuses to oscillate at all or oscillates in another mode. This phenomenon has been the single deterrent in the development of higher power magnetrons at wavelengths greater than 20 cm. It is now recognized as a starting time phenomenon having to do with the rate at which oscillation builds up and the rate at which pulse voltage is applied (see Section 10.6 *Oscillation Buildup—Starting*). What has been done in studying the phenomenon and in magnetron design to circumvent it will be discussed in some detail in connection with the 5J26, the tunable replacement for the 4J21-30 series.

In quantity production the 700A-D magnetrons presented new problems, all of which arose because of its size. The oxide coated cathode, having a relatively large surface area, gave off a considerable quantity of gas during cathode activation. In as much as the massive copper anode could be outgassed only by a long baking process at temperatures below the softening point of the glass parts, difficulty with magnetrons "going soft" after seal-off was encountered initially.

The development of the 700A-D magnetrons was carried on simultaneously with early studies at 10 cm. and with the early attempts to produce power at 3 cm. A number of auxiliary experiments were undertaken which, although they were not a part of the specific magnetron development, contributed results of considerable value complementary to those obtained at the shorter wavelengths. In particular, these experiments had to do with the technique of measurement and of magnetron scaling.

Digitized by Google
Original from UNIVERSITY OF MICHIGAN
Generated on 2019-09-21 09:18 GMT / http://hdl.handle.net/2027/mdp.39015077775156
Public Domain, Google-digitized / http://www.hathitrust.org/access_use#pd-google

Before the invention of straps the 700A-D magnetrons were scaled to 10 cm. to explore the possibilities of a more efficient magnetron design at this wavelength. Straps were introduced before the completion of the experiment. The resultant strapped magnetron having six resonators was very efficient—60 per cent—but required a high magnetic field as can be seen by referring to equation (16) of PART I. Like other magnetrons, the 700A-D became much more efficient when strapped. At the normal test point the efficiency ranged around 50 per cent, while at higher magnetic field and voltage, 75 per cent over-all efficiency was achieved. The introduction of straps into the manufactured design was not undertaken.

One further experiment of interest arose during the development of the 700A-D magnetrons from the desire to measure the gas pressure in a sealed-off magnetron. The non-oscillating magnetron itself was used as an ionization manometer. With the magnetic field set at a high value above cutoff and under conditions of no RF oscillation, electrons which arrive at the anode can do so only after having lost energy by collision with a gas molecule. Under these conditions the anode current is directly proportional to the pressure.

Although by present standards the 700A-D magnetrons might appear somewhat crude and inadequate, they nevertheless have an important place in the story of wartime magnetron development. They filled an immediate need in the radar system for which they were designed, providing the U. S. Navy with a radar set which saw service in a number of crucial engagements. Furthermore, the development of the 700A-D magnetrons provided invaluable experience.

13.2 *The 728A-J Magnetrons:* The 728A-J magnetrons were developed for fire control and search radar systems to supersede those which had used the 700A-D magnetrons. In these new systems a magnetron generator was to be required which could deliver 200 kw. peak output power in the frequency range 920-970 mc/s (later extended to 900 mc/s).

In an early design, the resonator system had eight resonators and was strapped with wire straps in the early British configuration [see Fig. 24(a) of PART I]. The anode length was 4 cm., the same as was used in the 700 A-D, which on a wavelength basis was about 2/3 that used in the British 10 cm. magnetron. The first models were designed for operation at pulse voltages of about 27 kv. When, subsequently, it was decided to reduce this voltage, a redesign involving a reduction of size of the interaction space became necessary. Since more had been learned about the technique of strapping in the meantime, it was decided that straps of the double ring type [see Fig. 24(d) of PART I] should be used in the new design. At first, the straps were set on the ends of the anode structure projecting into the end spaces but were later recessed into channels cut into the copper resonator

Digitized by Google
Original from UNIVERSITY OF MICHIGAN
Generated on 2019-09-21 09:18 GMT / http://hdl.handle.net/2027/mdp.39015077775156
Public Domain, Google-digitized / http://www.hathitrust.org/access_use#pd-google

structure for the purpose of electrostatic shielding from electrons in the interaction region. The frequency range required was spanned by the use of anode structures having three different slot widths for the primary frequency separation, small additional frequency shifts being obtained by small distortions of the straps. Resonant frequencies of magnetron resonator systems were now being determined prior to sealing for pumping by measurements like those described in PART I, during which any necessary strap adjustment could be made.

The cathode was a plain, oxide coated, nickel cylinder much like that used in the 700A-D magnetrons. The heater inductance was considerably higher than that of any previous cathode assembly. It was found that sudden and severe transient conditions, such as those imposed by a momentary internal arc between cathode and anode, would cause relatively high voltages to develop between the cathode and the open end of the heater. This could break down the heater insulation and cause either open or short circuits. This difficulty was minimized by incorporating in the driving equipment a condenser across the heater and an RF choke in series with the heater. Before final design specifications were submitted, the input leads and cathode structure were completely redesigned to provide greater rigidity and strength. To withstand violent shock and vibration, the structure was designed to have as high frequencies of mechanical resonance as possible. The structure looked much like that to be seen in the 5J23 magnetron of Fig. 49. Direct mechanical injury to the input leads is prevented by the use of a heavy glass housing.

The output circuit in early experimental models was a coaxial type fed by a loop in one of the resonators. The central conductor was a tungsten rod to which the glass seal was made and to which the inner conductor of the load coaxial was clamped. When the resonator system was redesigned for lower voltage, a new design of output circuit was made in which was used a choke or contact-free load coupling like that designed for the 720A-E. This removed the possibility of stress being applied to the glass of the output seal at either the inner or outer conductors. Except for the critical dimensions determined by frequency, the output circuit is identical to that used on the 5J23 shown in the photograph of the cut-away model of Fig. 49.

In Fig. 47 is shown a schematic diagram of this type of coupling. On both inner and outer conductors an electrical short circuit is produced at the gap between magnetron and load coaxials by folded low impedance coaxial sections incorporated into the bodies of the conductors. In the outer conductor a half wavelength section folded once is employed. In the section shown at (a), the joint is made at the current node in the choke section by the outer of two cylinders which project from the load end of the coupler

Digitized by Google
Original from UNIVERSITY OF MICHIGAN
Generated on 2019-09-21 09:18 GMT / http://hdl.handle.net/2027/mdp.39015077775156
Public Domain, Google-digitized / http://www.hathitrust.org/access_use#pd-google

into the magnetron lead. In the partial section shown at (b), this outer cylinder is not used and the joint occurs at the end of the section where there is a current antinode. In this method there exists the greater possibility of sparking should the coupling not be clamped tightly. A folded quarter wavelength section is built into the inner conductor. If the wavelength is short enough, as in the 5J26 and the 720A-E (see Figs. 58 and 63), this section need not be folded, the inner post on the magnetron center conductor can be eliminated and replaced by a solid center conductor on the load side.

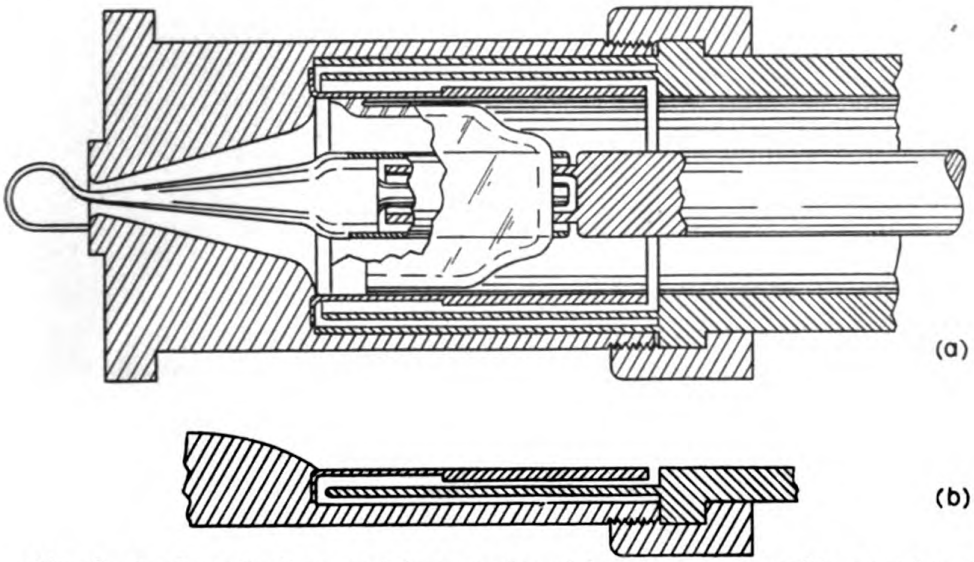

Fig. 47—A schematic diagram of the type of coaxial output circuit used in a number of magnetrons of wavelength 10 cm. or greater. Of particular interest are the means of contact-free or "choke" coupling employed in the inner and outer conductors, consisting of a folded concentric line section which presents zero impedance at the gap in the conductor. (a) and (b) represent two variations of the "choke" in the outer conductor as explained in the text.

The more recent designs of magnetrons for wavelengths greater than 10 cm. have some form of this coupling.

The impedance required at the output coupling to load the 728A-J magnetrons for sufficient power output necessitated a rather high standing wave in the output line. This standing wave was provided by a transformer built into the radar system to which the magnetron was attached. This caused no trouble since the output power was below the point where RF voltage breakdown in air in the line or coupling would occur. The press of time necessitated the adoption of this output circuit although "preplumbing" by incorporation inside the vacuum of the necessary transformer action for coupling directly to a matched load line would have been preferable. Such a design was executed but its completion came too late for its incorporation into the manufacturing specifications.

Generated on 2019-09-21 09:18 GMT / http://hdl.handle.net/2027/mdp.39015077775156
Public Domain, Google-digitized / http://www.hathitrust.org/access_use#pd-google
Digitized by Google
Original from UNIVERSITY OF MICHIGAN

Ten different magnetrons, coded the 728A-J, were put into manufacture. These covered the frequency range from 900 to 970 mc/s, a 7 mc/s range being allotted to each code type. The operating characteristics of the final design together with other pertinent data are tabulated in TABLE I. An external view of the magnetron is shown in Fig. 48. A maximum current limitation for satisfactory operation in the π mode was also encountered in this magnetron but at current values above the 20 ampere operating point

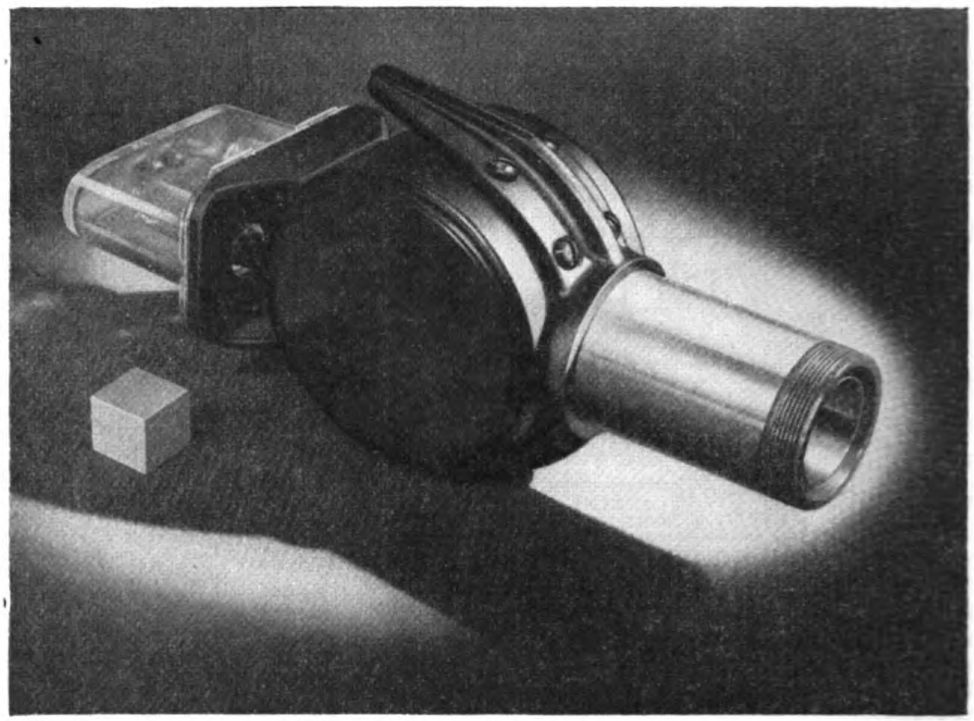

Fig. 48—An external view of a 728A-J magnetron (275 kw., ~930 mc/s). The concentric cylindrical sleeve to be seen inside the output circuit coupling, from which the magnetron is supported, is a part of the "choke" (see Fig. 47). Note the heavy glass protective housing over the input leads.

at which the required output power was attained. Because of the shorter wavelength, the current limitation was not as severe as that encountered in the 700A-D.

The 728A-J magnetrons were driven by a spark wheel, line type modulator. The greater tendency of the driving voltage to overshoot with this modulator, by virtue of the slowness of buildup of RF oscillation, was reduced by the use of a series resistance and capacitance network coupled across the magnetron input like that used earlier with 720A-E magnetrons at 10 cm.

13.3 *The 5J23 Magnetron:* The request for the Laboratories to develop

Digitized by Google
Original from UNIVERSITY OF MICHIGAN
Generated on 2019-09-21 09:18 GMT / http://hdl.handle.net/2027/mdp.39015077775156
Public Domain, Google-digitized / http://www.hathitrust.org/access_use#pd-google

a semiportable radar pack set and a searchlight control radar involved the design of a new magnetron in the frequency range 1050 to 1110 mc/s to operate at a maximum pulse voltage input of 25 kv. with power output of at least 200 kw. Since these requirements, except for frequency, were essentially those of the 728A-J magnetrons already under development, the new work closely paralleled that already in progress.

Because of the maximum current limitation being encountered in the development of longer wavelength magnetrons, a relatively longer anode was designed for the new magnetron, coded the 5J23, thus insuring satisfactory operation at higher current and input power. The resonator system was "heavily" strapped with echelon wire straps [see Fig. 24(c) in PART I]. Coarse frequency variation was accomplished by the use of straps at different heights above the surface of the anode block. Finer frequency adjustments were made in "pretuning" the structure, before sealing, by small displacements of the wire straps already in position.

Output circuit work on the 5J23 was done together with that on the 728 A-J magnetrons and went through the same series of developments. The output circuit used in the manufacturing design is identical with that of the 728A-J except for the dimensions critical to wavelength.

For operational reasons, only one magnetron, the 5J23, in the frequency range 1074 to 1086 mc/s, was coded. Fig. 49 shows a cut-away view of its internal structure. Performance characteristics and other data are to be found in TABLE I. Note that the 5J23, by virtue of its greater anode length and higher frequency, has a higher critical current, I_c, above which π mode operation fails, than do the 700A-D or 728A-J magnetrons.

13.4 *The 4J21-30 Magnetrons:* When development work on the 5J23 had just been completed, an international agreement on frequency allocation made the frequency range of the 5J23 unavailable for radar purposes at some future date. Consequently the work was to be redone for operation in the band 1220 to 1350 mc/s. The 5J23 and the equipment in which it was used were to continue in manufacture and be used in the period necessary for the development of the new equipment and magnetrons. In addition to the frequency change, power output demands on the magnetron were raised considerably, it being required that the new magnetrons produce at least 500 kw. output power. Although the maximum current limitation had seriously affected maximum output power capabilities of the magnetrons in this wavelength range, it appeared that the new high power demands were within reach by virtue of the higher frequency at which the new magnetrons were to operate.

The new assignment came just upon completion of the 5J23 and made it necessary to build or acquire new laboratory equipment, CW oscillators,

Digitized by Google
Original from UNIVERSITY OF MICHIGAN
Generated on 2019-09-21 09:18 GMT / http://hdl.handle.net/2027/mdp.39015077775156
Public Domain, Google-digitized / http://www.hathitrust.org/access_use#pd-google

wavemeters, output couplings, and loads. On the other hand, the new development did provide the opportunity to make use of new ideas and developments, some of which, although already completed, could not be used in magnetrons then in manufacture.

When work on this new series of magnetrons was commenced, the art of magnetron development had reached the stage where for the first time it was possible to make a reasonably satisfactory approach to the problem of a new design. The principles of magnetron scaling had been worked

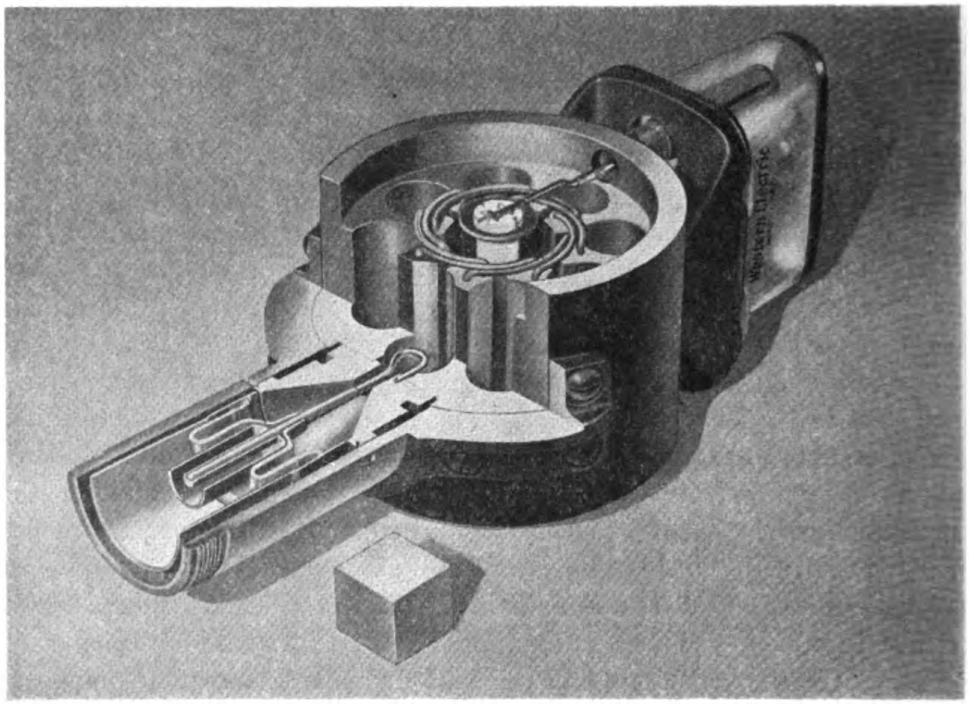

Fig. 49—A sectioned 5J23 magnetron (275 kw., ~1050 mc/s) showing, among other things, the echelon type of wire strapping and coaxial output circuit with contact-free load connector.

out and tested in detail, enabling one to make use of results obtained or verified at different frequencies. The mode frequency spectrum of a magnetron resonator system was now understood and the means of controlling it by strapping were in use. The problem of the output circuit was in hand. Magnetrons were being "preplumbed" and the problems of reproducibility were being solved. Furthermore, the method of studying each of these magnetron characteristics by CW measurements on resonator blocks and output circuit models had advanced to the point where it was possible to complete a design in detail before an operating magnetron had been constructed. Such a procedure was adopted for the new series of

Generated on 2019-09-21 09:19 GMT / http://hdl.handle.net/2027/mdp.39015077775156
Public Domain, Google-digitized / http://www.hathitrust.org/access_use#pd-google
Digitized by Google
Original from UNIVERSITY OF MICHIGAN

magnetrons, coded the 4J21-30, in the band 1220-1350 mc/s. A satisfactory resonator system giving proper operating voltage, π mode frequency, and mode frequency separation was designed prior to and incorporated in the first operating model. Similarly, a satisfactory output circuit for proper loading over the broad band of frequencies and the design of mechanical features involved in the cathode, cathode mount, cooling facilities, output circuit, straps, and resonator system were provided.

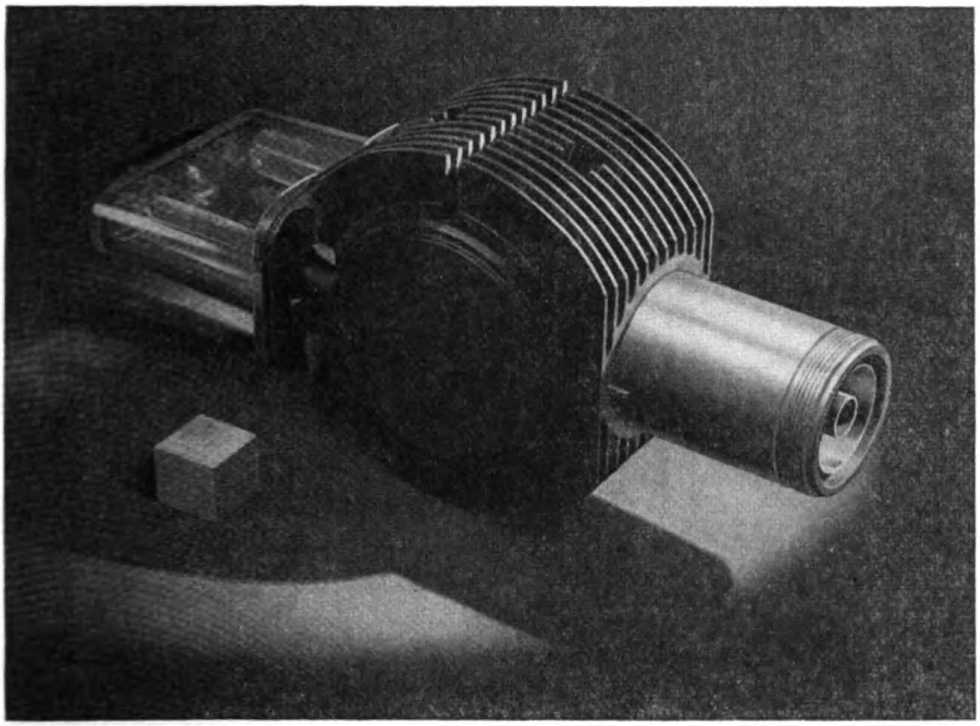

Fig. 50—An external view of the 4J28 magnetron (one of the 4J21-30 series, 600 kw., ~1280 mc/s). Note the cooling fins attached to the magnetron body.

The new interaction space and resonator system were scaled from a compromise between the 728A-J and the 5J23 designs. Shielded, double ring straps like those of the 728A-J were adopted. Two anode structures differing somewhat in resonator dimensions and size of interaction space were used, one for the short wavelength half of the band (4J21-25), the other for the long wavelength half of the band (4J26-30). The different frequencies within each of these groups were attained by the use of straps of different widths.

A single design of output circuit for the entire frequency range necessitated making the transformer properties as independent of frequency, or as broad band, as possible. The output circuit has three parts. At the outside of the

Digitized by Google
Original from UNIVERSITY OF MICHIGAN
Generated on 2019-09-21 09:19 GMT / http://hdl.handle.net/2027/mdp.39015077775156
Public Domain, Google-digitized / http://www.hathitrust.org/access_use#pd-google

magnetron is the choke or contact free coupling to the load coaxial. The general type of design used in previous magnetrons was followed here. The transformation from the load coaxial to the coaxial which breaks into the resonator at the coupling loop was made by use of a tapered line in which the characteristic impedance was kept constant. The proper loading was accomplished by adjustment of the loop size. It was found possible to achieve a sufficiently low loaded Q in this way within the bounds of a satisfactory geometrical arrangement. Each of these design procedures was

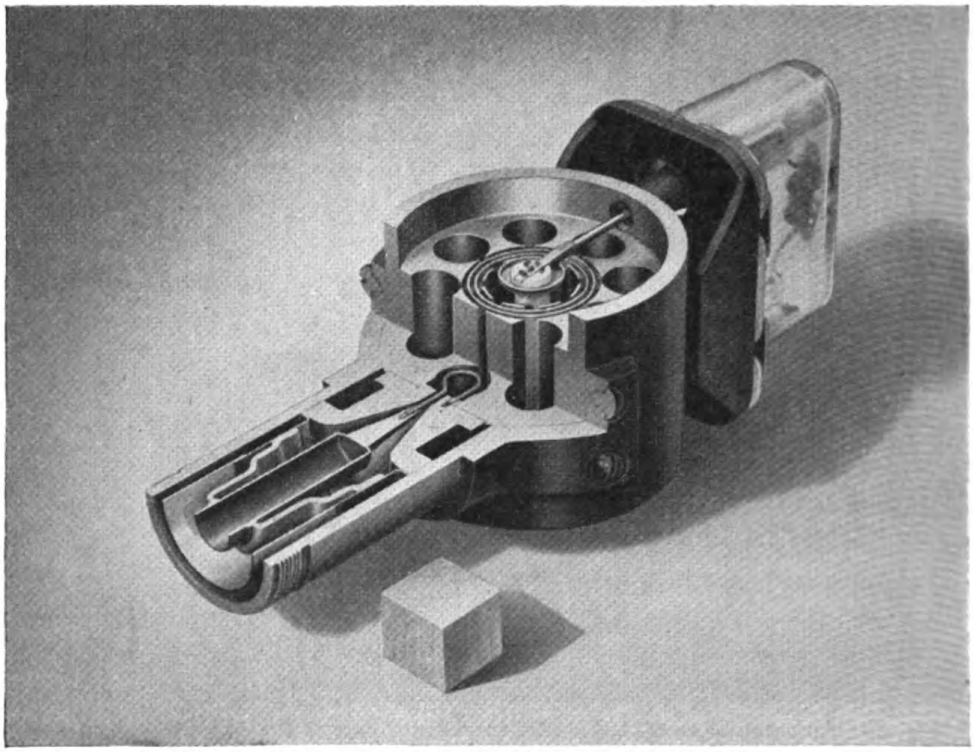

Fig. 51—An internal view of a 4J21-30 magnetron (600 kw., ~1280 mc/s). Of special interest are the recessed double ring straps and the output circuit in which the characteristic impedance of the coaxial line from loop to load is approximately constant.

carried out by CW measurement of impedance, looking into a model through the output circuit. Special models of the tapered line and choke coupler were also studied.

When operating magnetrons were constructed, except for minor changes, no redesign was necessary. The first working models performed satisfactorily at the required pulse voltage, current, magnetic field, power output, and pulling figure. It was possible to get more than 750 kw. output at better than 50 per cent efficiency from these magnetrons.

An external view of the final design may be seen in Fig. 50 and a photograph of a cut-away model in Fig. 51. Operational and other data are given

Digitized by Google
Original from UNIVERSITY OF MICHIGAN
Generated on 2019-09-21 09:19 GMT / http://hdl.handle.net/2027/mdp.39015077775156
Public Domain, Google-digitized / http://www.hathitrust.org/access_use#pd-google

in TABLE I. A typical performance chart of one of the series is shown in Fig. 52. The maximum current boundary limits the output to values well below those at which other factors, such as cathode dissipation, become restrictive.

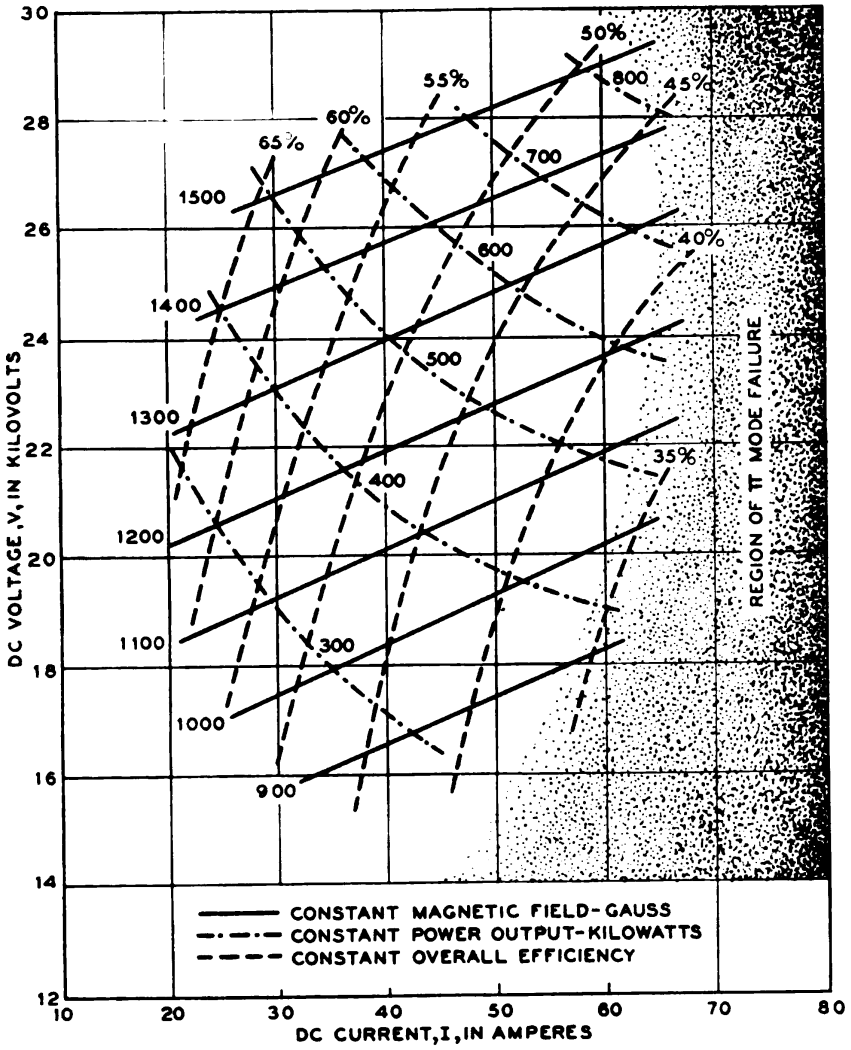

Fig. 52—A typical performance chart of a magnetron of the 4J21-25 series (~1315 mc/s).

During operation in the high power, spark gap, line type modulator with which the magnetron was to be used, it was found that the pulse voltage applied to the cathode input leads was sometimes sufficient to cause flash-over. If the arc persisted, vacuum failure from cracking or puncturing of the glass resulted. The external flash-over was accompanied by internal arcs between cathode and anode which were injurious to the life of the

Digitized by Google
Original from UNIVERSITY OF MICHIGAN
Generated on 2019-09-21 09:19 GMT / http://hdl.handle.net/2027/mdp.39015077775156
Public Domain, Google-digitized / http://www.hathitrust.org/access_use#pd-google

magnetron. To circumvent this difficulty, the input leads and their glass housing were redesigned. The glass of the leads was lengthened and folded to provide a greater surface distance over which the arc must strike. Although the redesign was limited somewhat by the space available in the transmitter unit, it was possible to make leads which could stand 60 cycle peak voltages of almost twice the normal pulse voltage applied to the magnetron. This step all but eliminated flash-over in operation. To take care of the occasional flash-over, a spark gap across which the breakdown could occur was added in the equipment.

The 4J21-30 magnetrons are illustrative of carefully designed non-tunable magnetrons of wavelengths 20 to 30 cm. developed at the Bell Laboratories. They were the first magnetrons designed here completely on the basis of CW impedance measurements.

14. Tunable Magnetrons for Wavelengths of 20 to 45 Centimeters

14.1 *General:* As fixed frequency magnetrons became available in the various frequency bands designated for radar use, the interest quite naturally turned to the development of tunable magnetrons. The operational reasons for this were to enable one to set the frequency of a radar system at will, thus avoiding interference between sets in a large group of aircraft on naval vessels, to enable one to vary the frequency at will from time to time or as the need arises to avoid jamming, and to permit the stocking of fewer magnetrons to cover a given frequency band.

Early work on tunable magnetrons at the Bell Laboratories was done with 10 cm. models. Although no such developments were carried to the stage of production, the ideas and techniques evolved were used at other frequencies. Somewhat later the Bell Laboratories committed itself to a program of development of tunable magnetrons for pulsed radar use in the 20 to 45 cm. wavelength range.

The program initially was not directed toward the goal of some particular magnetron of fixed specifications. Rather, it was the intention to explore the field of possible tuning methods and to find that one which appeared both electrically and mechanically to be best suited for large magnetrons. Work in this initial stage was done on anodes of the 4J21-30 series and may be divided into two main channels characterized by the degree of symmetry involved in the tuning scheme. In one, the tuning of the entire anode block is accomplished by modification of a single one of the resonators and may thus be characterized as unsymmetrical tuning. In the other, each resonator of the multiresonator block is tuned in a symmetrical fashion.

Among the unsymmetrical types studied were those employing an auxiliary loop in one resonator connected to a reactive element which could be either a

Generated on 2019-09-21 09:19 GMT / http://hdl.handle.net/2027/mdp.39015077775156
Public Domain, Google-digitized / http://www.hathitrust.org/access_use#pd-google
Digitized by Google
Original from UNIVERSITY OF MICHIGAN

coaxial line terminated in a plunger or a variable capacitance, or a coaxial to wave guide junction with movable plungers in the wave guide. Another form involved the deformation of one of the resonators itself to accommodate a prism shaped tuning element which was moved from outside the vacuum through a diaphragm arrangement.

Although considerable effort was expended in the study of unsymmetrical tuning schemes and much learned about them in the course of this work, they have two rather fundamental drawbacks which caused them to be replaced by the symmetrical types in which these defects could be eliminated. In the first place, it is difficult by this means to obtain the desired range of frequency change. Secondly, by virtue of asymmetry, operation in other modes is difficult to avoid except over rather narrow frequency ranges. Those types in which part of the tuning circuit is outside the vacuum envelope have the additional drawback of bringing high RF voltages into structures in air where very high standing waves are necessary and breakdown difficult to avoid.

It was found possible to circumvent each of these difficulties by using symmetrical tuners. Some such tuners were like those tried on 10 cm. models and involved spider-like straps connecting alternate segments to two common points on the axis of the tube. These points in turn were connected to the center and outer conductors of a coaxial line. After passing through a vacuum seal, this coaxial line connected to a reactor like those used in the unsymmetrical schemes.

In the general arrangement finally used, a tuning member was mounted in the end space. The structure included a vacuum diaphragm mounted in the end cover of the magnetron. The tuning was effected by variation of the capacitance between the resonator system and the tuning member.

In unstrapped magnetrons, the tuning was accomplished by moving a tuning member of the general shape of a "cookie cutter" in a single groove cut into the slotted portion of the anode structure. Later, this range was increased by using two slots and a tuning member having two concentric rings. This type of tuner was used on both the 4J42 and 4J51 magnetrons to be discussed. It is the first of the two types of tuning by variation of capacitance discussed in PART I of this paper. Considerable effort was expended to extend the frequency range of tuning by strapping the untuned end of the resonator system and by variations of the resonator dimensions on which relative mode frequencies depend. It was found possible to obtain a tuning range of better than ± 5 per cent, but it appears quite difficult to exceed this amount appreciably in high voltage magnetrons using this tuning means.

Digitized by Google
Original from UNIVERSITY OF MICHIGAN
Generated on 2019-09-21 09:20 GMT / http://hdl.handle.net/2027/mdp.39015077775156
Public Domain, Google-digitized / http://www.hathitrust.org/access_use#pd-google

In the strap tuning scheme, use was made of straps of channel or U-shaped cross section, inside which the double rimmed "cookie cutter" element is moved. The tuning arrangement of the 5J26 magnetron is of this type. It is the second of the two types of tuning by variation of capacitance discussed in PART I.

Quite early in this program of development it became apparent that the armed services would require all these tunable magnetrons to be mechanical and electrical replacements for existing fixed frequency magnetrons, interchangeable in all respects. This requirement, in addition to the facts of electrical design, indicated that the "cookie cutter" type of tuner represented the line of attack most likely to succeed. The capacitance in the anode structure or in the straps is the frequency determining circuit parameter most easily varied, as it is the most accessible in these large size magnetrons. The tuning element may be moved conveniently by a mechanism, compact in the axial dimension, mounted in the end space and cover of the magnetron. These are factors of prime importance in "unpackaged" magnetrons where over-all axial length is important. Magnetrons in this wavelength range are sufficiently large to make such a mechanical design feasible.

The magnetrons of wavelength 20 to 45 cm. for which tunable replacements were designed were: the 700A-D series (680-720 mc/s), the 728A-J series (900–970 mc/s), and the 4J21-30 series (1220-1350 mc/s). Although it was preferable to span the 4J21-30 band with one tunable replacement, the use of two tunable replacements, each covering half the band, would have been satisfactory had it been necessary. In the development of each of the tunable replacements, improvements and modernizations which could be incorporated within the limitations of mechanical and electrical interchangeability were made.

14.2 *The 4J42 Magnetron:* The tunable replacement for the 700A-D series is the 4J42. It covers an increased frequency band of 660 to 730 mc/s. The tuning is accomplished by variation of the intersegment capacitance of the anode structure itself, the first of the two capacitance tuning methods listed above. Frequency varies nearly linearly with displacement of the tuning member. The tuning range, although adequate for the purposes of the 4J42, is limited by interference of other modes as was discussed in PART I. In this respect it is not a great deal better than can be attained by unsymmetrical means. The advantages of symmetrical capacitance tuning enumerated above made it the logical choice nevertheless. A satisfactory tuning range of the π mode without interference from other modes was achieved by strapping the end of the magnetron opposite that at which the tuning mechanism is mounted. This necessitated changes in the resonator

Digitized by Google
Original from UNIVERSITY OF MICHIGAN
Generated on 2019-09-21 09:20 GMT / http://hdl.handle.net/2027/mdp.39015077775156
Public Domain, Google-digitized / http://www.hathitrust.org/access_use#pd-google

dimensions of the 700A-D magnetrons to obtain the frequency range desired. The cathode structure was improved, making use of later developments. Its diameter was changed from 0.8 cm. to 1.0 cm. in order to increase the maximum current to which operation in the π mode is possible. The anode diameter was retained; the operating conditions were not appreciably affected. It was necessary to retain the original form of output circuit.

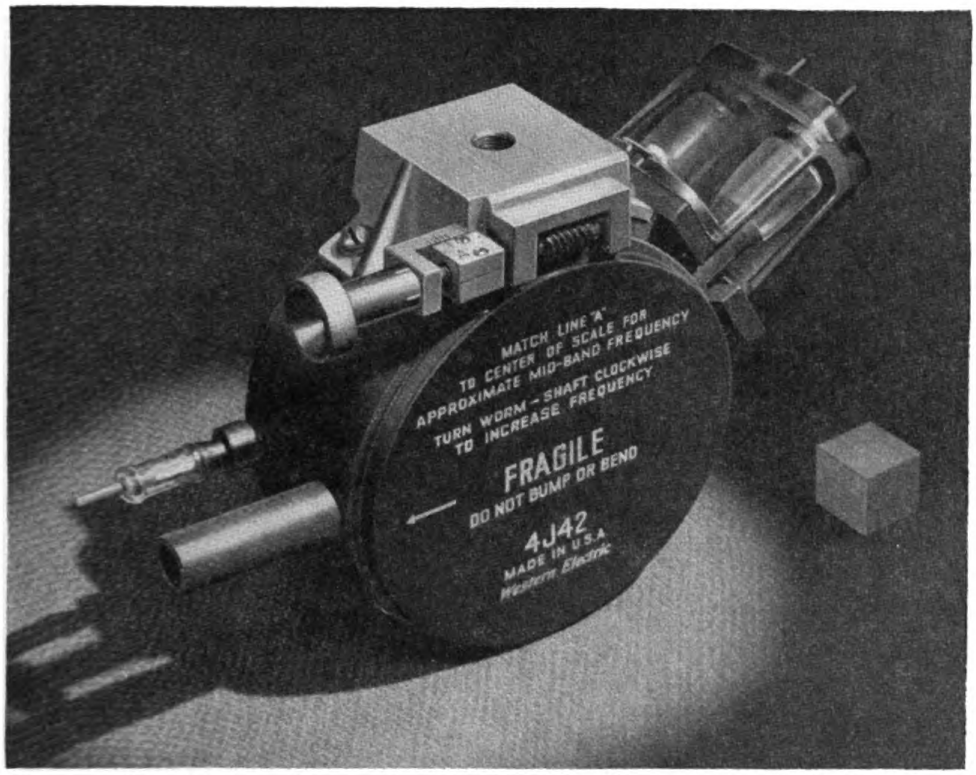

Fig. 53—The 4J42 tunable magnetron (40 kw., 660 to 730 mc/s)—the tunable replacement for the 700A-D magnetrons. The worm drive in the mounting bracket operates the tuning mechanism enclosed in the end cover of the magnetron. Note the improved input leads and protective housing (see Fig. 46).

In Fig. 53 is shown an external view of the 4J42. In TABLE I are given operational data and other characteristics. The performance of the 4J42 is as good or better than that of the corresponding magnetron in the 700A-D series.

14.3 *The 4J51 Magnetron:* The 728A-J series of fixed frequency magnetrons was replaced by the 4J51, covering the frequency band of 900 to 970 mc/s. An external view of the magnetron is shown in Fig. 54. As in the 4J42, the resonator system is a modification of that used in the fixed frequency prototype, strapped on the untuned end by double ring strapping. Satisfactory mode frequency separation is maintained by increasing the

Digitized by Google
Original from UNIVERSITY OF MICHIGAN
Generated on 2019-09-21 09:20 GMT / http://hdl.handle.net/2027/mdp.39015077775156
Public Domain, Google-digitized / http://www.hathitrust.org/access_use#pd-google

strap capacitance of the single pair of rings to approximately twice that of one pair in the 728A-J. The tuning scheme is the same as that used in the 4J42. It may be seen in the photograph of a cut-away model in Fig. 55.

The output circuit of the 4J51 incorporated the broad band transformer properties developed for the output circuit of the 4J21-30 series. This necessitated a larger loop size in the 4J51 than was used in the 728A-J.

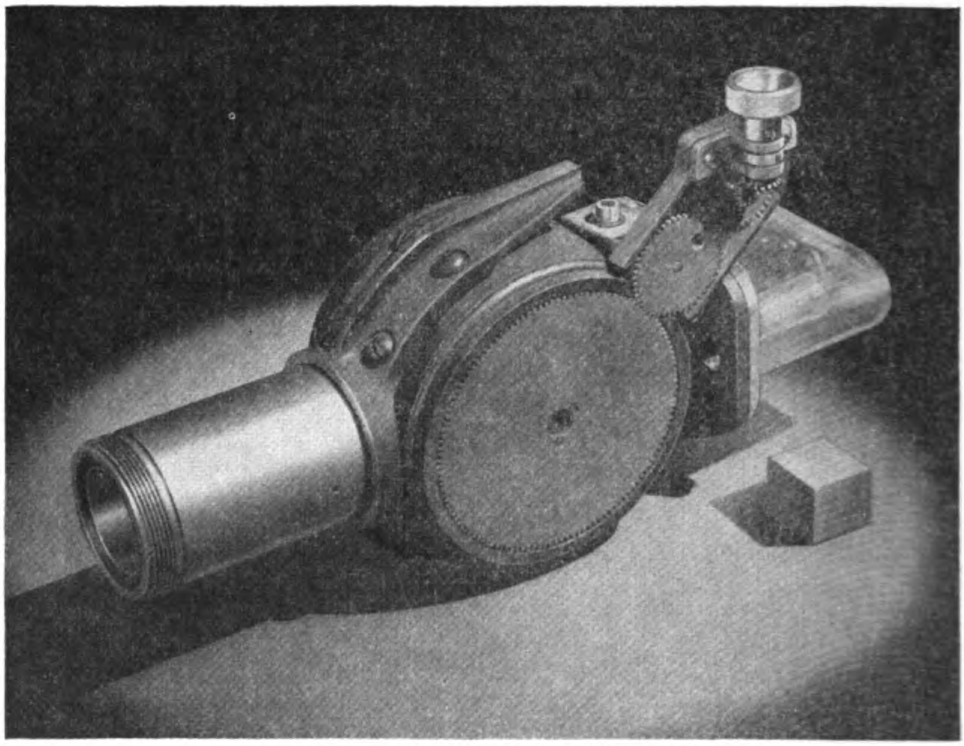

Fig. 54—The 4J51 tunable magnetron (275 kw., 900 to 970 mc/s)—the tunable replacement for the 728A-J magnetrons.

These features may be seen in Fig. 55. The output circuit was designed for coupling to a matched load line.

TABLE I includes relevant data on the 4J51 magnetron. In Fig. 56 are shown power output and mode frequency tuning curves for the magnetron. Fig. 56 may be taken as representative of the type of tunable magnetron in which the intersegment capacitance of the resonator system is varied. The frequency range is limited by the crossing of the π mode frequency curve by those of other modes. The power output is reduced appreciably at the crossing point of the $n = 3$ mode component. Throughout its tuning range, indicated in Fig. 56, the 4J51 magnetron operates as well or better than its fixed frequency predecessors.

14.4 *The 5J26 Magnetron:* Replacement of the 4J21-30 series of mag-

Digitized by Google
Original from UNIVERSITY OF MICHIGAN
Generated on 2019-09-21 09:20 GMT / http://hdl.handle.net/2027/mdp.39015077775156
Public Domain, Google-digitized / http://www.hathitrust.org/access_use#pd-google

netrons with a tunable equivalent necessitated a tuning range which was found to be unattainable with the scheme used in the 4J42 and 4J51 magnetrons. Two tunable replacements employing the "tuned segment" type of tuning, each spanning half the band, were constructed as "insurance" should the efforts to develop a single replacement having the required range fail. However, it was found that by tuning the straps as has been de-

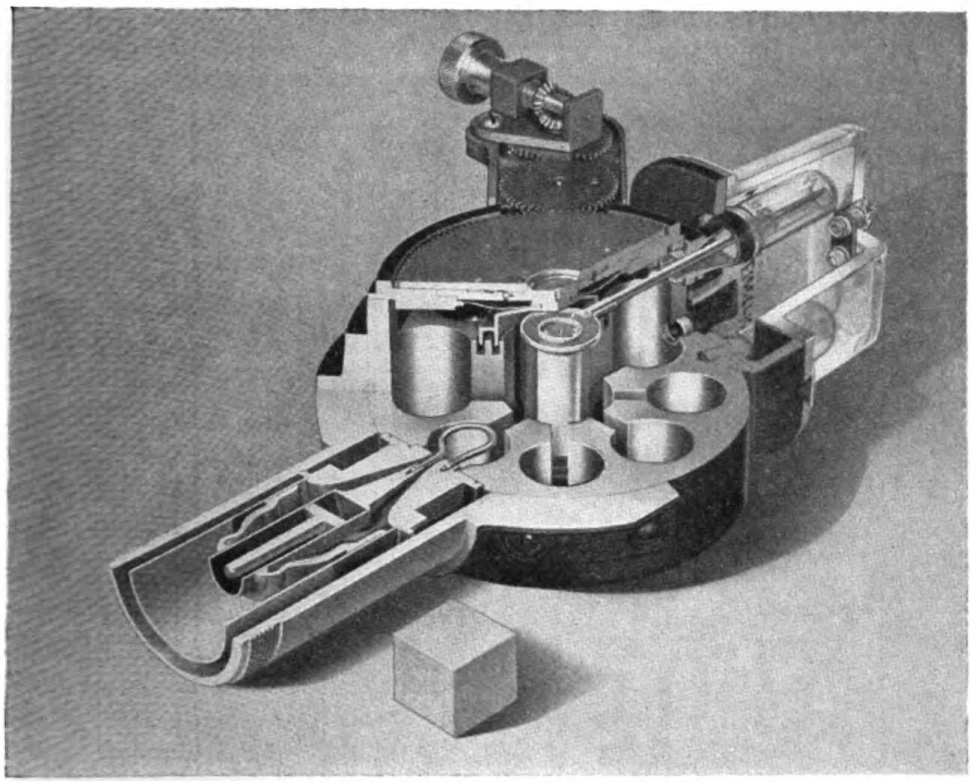

Fig. 55—A view of a cut-away 4J51 tunable magnetron (275 kw., 900 to 970 mc/s). Note the tuning member consisting of two concentric rings which are moved up and down in the grooves in the segments of the anode structure. The details of the tuning drive mechanism, including the flexible vacuum diaphragm, the axial screw, the nut and ball bearing, and the gear drive are to be seen. The resonator system is strapped on the end not seen in the figure.

scribed in PART I a single tunable magnetron for the entire 4J21-30 series covering the band from 1220 to 1350 mc/s could be provided. An external view of the resulting magnetron, coded the 5J26, is shown in Fig. 57 and an internal view in Fig. 58.

As can be seen in Fig. 58, the 5J26 magnetron includes radical departures in design in addition to the tuning scheme. Slot type resonators are used in the resonator system, and the anode and cathode diameters, as well as their ratio, are considerably larger than those used in previous designs for the same operating voltage and magnetic field. These features of the design

Digitized by Google
Original from UNIVERSITY OF MICHIGAN
Generated on 2019-09-21 09:20 GMT / http://hdl.handle.net/2027/mdp.39015077775156
Public Domain, Google-digitized / http://www.hathitrust.org/access_use#pd-google

resulted from a systematic study of the causes of and possible cures for the maximum current limitation encountered in long wavelength magnetrons. The difficulty had been particularly noticeable in the 4J21-30, which on

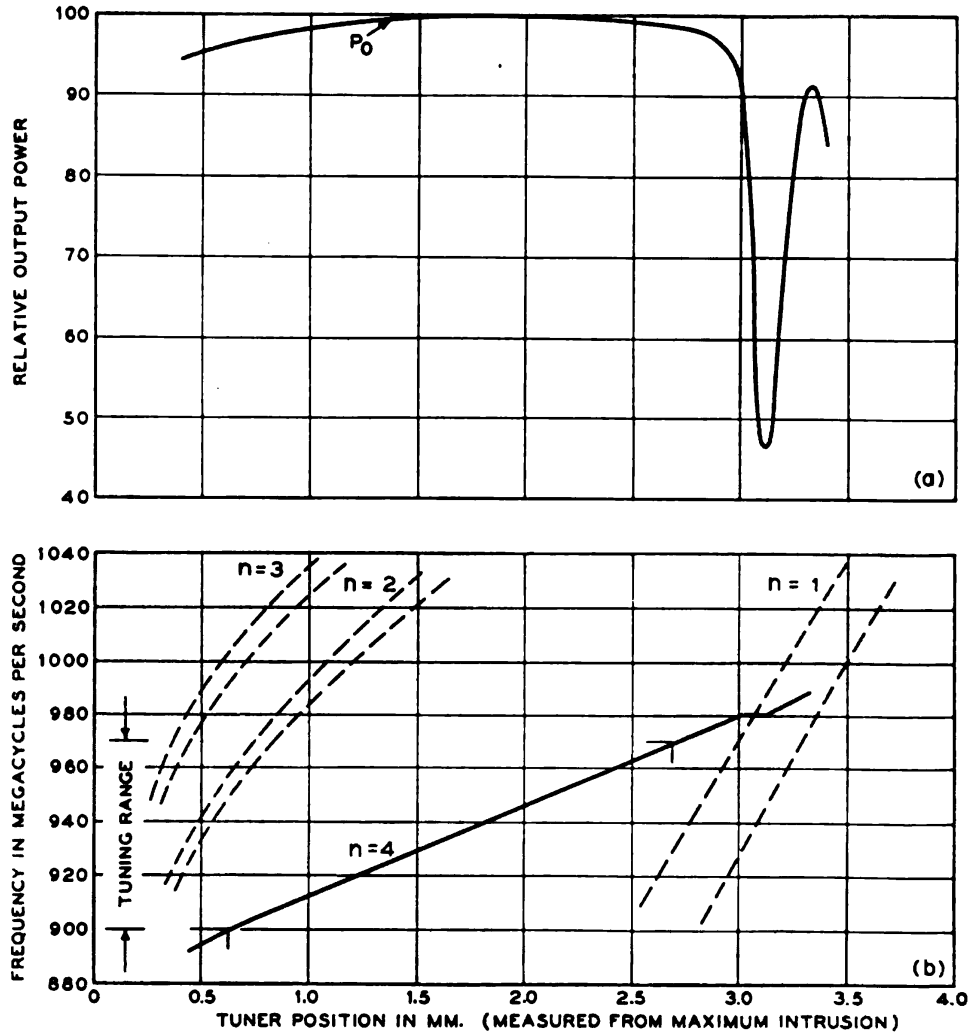

Fig. 56—Typical experimental curves of power output and mode frequency variation with tuner position in the 4J51 magnetron. The following points of interest are to be noted: the relatively more rapid tuning for modes of small n than for the π mode ($n = 4$); the drop in output power at the coincidence of the frequencies of the π mode and one of the components of the $n = 1$ mode; the limitation on the tuning range in the π mode imposed by the crossing of mode frequency curves of other modes; the fact that the $n = 1$, 2, and 3 modes are doublets and the π mode a singlet.

hard tube modulators were able to pass the required current before π mode failure with little margin. For some reason the performance of the early experimental models of the tunable replacement was considerably inferior in this respect and would not meet the specifications for which the magnetron was being designed. Thus a study of the phenomenon was imperative. It

Digitized by Google
Original from UNIVERSITY OF MICHIGAN
Generated on 2019-09-21 09:20 GMT / http://hdl.handle.net/2027/mdp.39015077775156
Public Domain, Google-digitized / http://www.hathitrust.org/access_use#pd-google

resulted in the 5J26 magnetron. It dictated the nature of the interaction space and resonator system and thus the cathode size and output coupling loop. Initial experiments were performed with a vane type resonator system [see Fig. 21(b)] having channel straps and an interaction space of approximately the size used in the 4J21-30 series.

From studies of dynamic *V-I* plots on the experimental tunable models and other magnetrons under a variety of operating conditions, it became clear that the phenomenon had to do with the rate of buildup of RF oscilla-

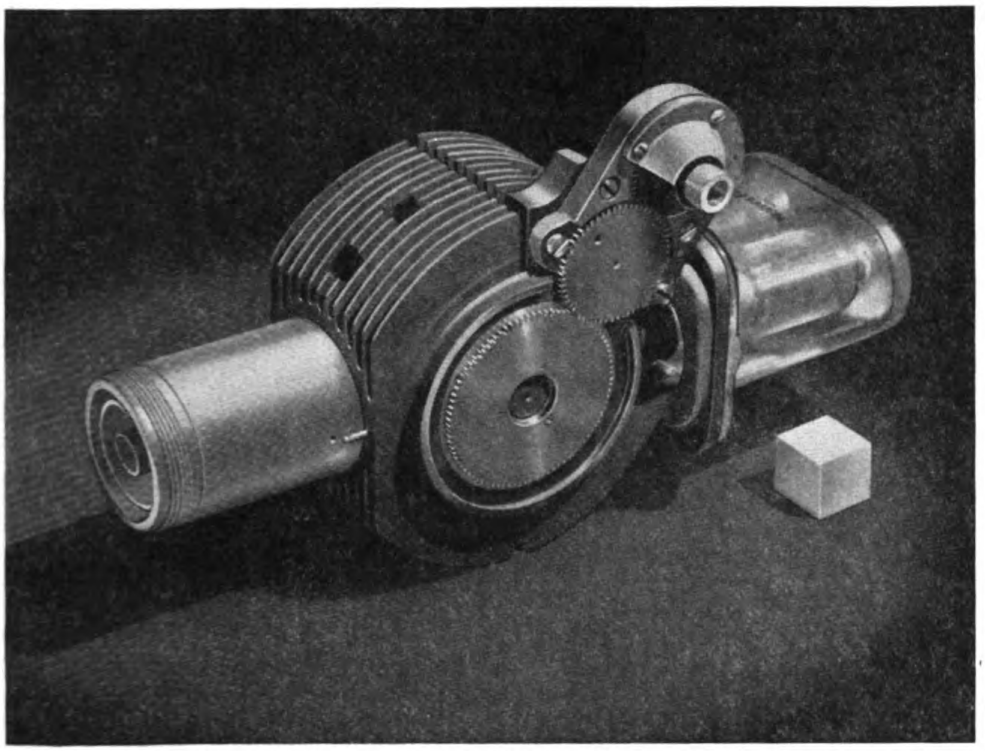

Fig. 57—The 5J26 tunable magnetron (600 kw., 1220 to 1350 mc/s)—the tunable replacement for the 4J21-30 magnetrons.

tion in the π mode and with the rate of rise of the applied DC voltage. The "mode skip" shown in the sequence of *V-I* plots of Fig. 38 and discussed in PART I is an example of the behavior of one of the experimental models used in this work when failure to oscillate in the π mode occurs.

Thus at constant magnetic field there appears to be a maximum DC voltage above which π mode oscillation is impossible. This voltage is presumably that beyond which the mean angular velocity of the electrons around the interaction space becomes enough greater than that of the traveling field component for the phase focusing to fail to maintain synchronism. The term "maximum current limitation" is thus in a sense a misnomer as Fig. 38(b) indicates. Here, π mode oscillation fails even to start and does not

Digitized by Google
Original from UNIVERSITY OF MICHIGAN
Generated on 2019-09-21 09:21 GMT / http://hdl.handle.net/2027/mdp.39015077775156
Public Domain, Google-digitized / http://www.hathitrust.org/access_use#pd-google

fail at a maximum current on each pulse. The point at which π mode oscillation fails thus has to do with the relation of the rate of rise of DC voltage through the range of permissible values to the rate of buildup of RF oscillation. As one attempts to drive the magnetron harder by applying greater peak voltages to it, the rate of voltage rise in this region becomes greater, finally exceeding that which the rate of RF voltage buildup will permit.

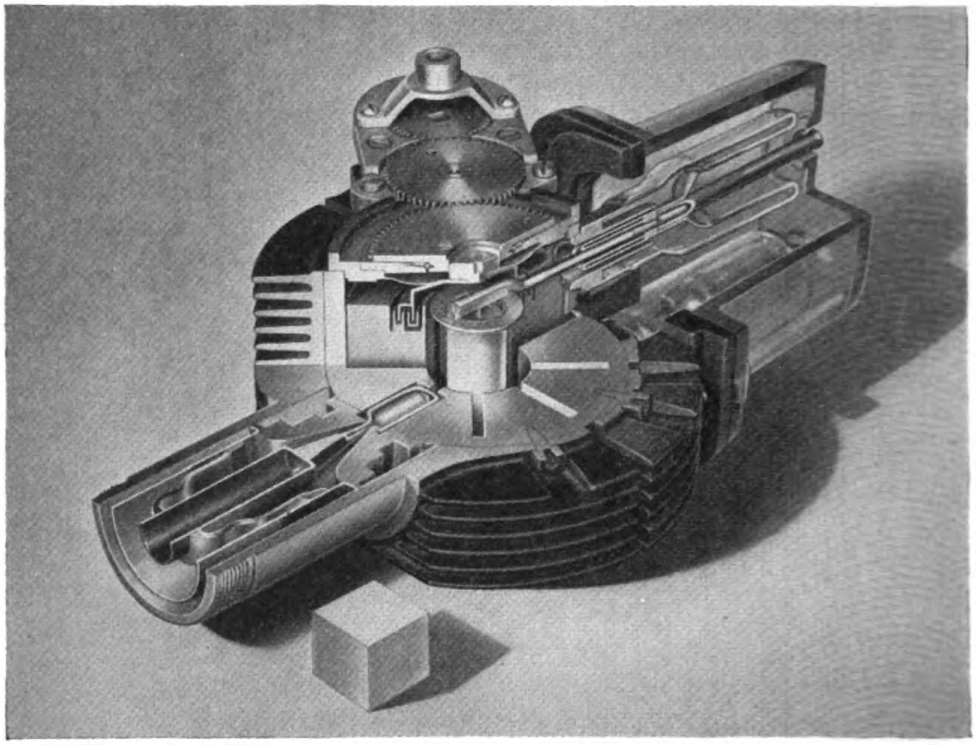

Fig. 58—A view of a sectioned 5J26 tunable magnetron (600 kw., 1220 to 1350 mc/s). Note that the tuning member, consisting of two concentric rings, is moved up and down inside the two recessed channel straps by a mechanism like that in the 4J51 magnetron (see Fig. 55). Compare the interaction space geometry and shape of resonators with those of the fixed frequency 4J21-30 magnetrons (Fig. 51), the changes having been made to achieve better starting characteristics as explained in the text. Note also the enlargement of the output resonator to accommodate the coupling loop, the RF chokes incorporated in the cathode support leads, and the large input lead construction to prevent external flashover.

The phenomenon of π mode failure was studied as a function of five parameters:

1. magnetic field, B;
2. frequency, f;
3. ratio of cathode to anode radii, $\frac{r_c}{r_a}$;
4. load conductance, G_s;
5. rate of DC voltage rise, $\frac{dV}{dt}$.

Digitized by Google
Original from UNIVERSITY OF MICHIGAN
Generated on 2019-09-21 09:21 GMT / http://hdl.handle.net/2027/mdp.39015077775156
Public Domain, Google-digitized / http://www.hathitrust.org/access_use#pd-google

The results were found to fit well into the picture of starting time behavior discussed in PART I. Thus, increase of frequency and decrease of load both result in a greater rate of RF voltage buildup and permit a greater rate of rise of DC voltage through the range where oscillation starts. The magnetron may thus be driven harder and more current passed. In agreement with these results, changes in the rate of voltage rise applied by the pulser, accomplished by changing its characteristics, also permitted oscillation to continue to higher current and voltage values. The dependence on B and r_c/r_a presumably are to be accounted for by the dependence of $G_e(V_{RF})$ on these quantities. It appears that $G_e(V_{RF})$ increases with both B and r_c/r_a.

Empirical relations of the critical current, I_c, and the electronic efficiency, η_e, at which π mode failure occurs, to the load conductance, G_s, were obtained.[25] Whereas I_c decreases with increasing G_s, η_e decreases.

Since the work was done at different frequencies and interaction space geometries, it was found convenient and instructive to express voltages, currents, and conductances as reduced variables of the type introduced by Slater, that is, as ratios to the voltage, V_o, and current, I_o, at the intersection of the Hartree line and the cutoff parabola, and the conductance, $G_o = \frac{I_o}{V_o}$, respectively. I_o and V_o may be determined from the expressions for the cut-off parabola and the Hartree line [expressions (8) and (16) of PART I, respectively]. Plotted in terms of the reduced variables I_c/I_o and G_s/G_o, it was found that the data relating I_c/I_o to G_s/G_o and η_e to G_s/G_o predicted approximately the same relationship independent of frequency and r_c/r_a. Thus, quite independent of the fundamental significance of these particular reduced variables to the functional dependence of the quantities involved, it appeared that they would be useful in the design of a new magnetron whose design parameters would lie in or near the range for which data were available.

The purpose of the work was to produce a tunable magnetron which would operate satisfactorily to currents in excess of those needed to meet the power output specifications. It was hoped to do this by redesign of the magnetron itself. This course rejected as unsatisfactory the alternative of limiting the rate of voltage rise on each equipment with which the magnetron would be used. The general goal of the proposed changes in magnetron design were to increase the rate of buildup of RF oscillation while at the same time keeping the electronic efficiency at a reasonably high value. These goals are not independent but oppose one another as has been seen. Thus, if r_c/r_a is increased, I_c increases, but η_e decreases. If G_s is increased to increase η_e, I_c drops. The hope of success in the venture lay in the prob-

[25] G_s was determined from the relation $G_s = \frac{Y_{oc}}{Q_L} = \frac{1}{\omega_L Q_L}$ [see equation (36) of PART I], using a calculated value for the total resonator inductance and the measured value of the loaded Q.

Digitized by Google
Original from UNIVERSITY OF MICHIGAN
Generated on 2019-09-21 09:21 GMT / http://hdl.handle.net/2027/mdp.39015077775156
Public Domain, Google-digitized / http://www.hathitrust.org/access_use#pd-google

ability that these effects do not exactly cancel one another and that a net improvement in performance could be effected.

The design of the 5J26 was accomplished in the following way: The slot type resonator was chosen as it possesses a low value of inductance needed to give a high value of G_s for a given value of loaded Q.[25] The number of resonators was chosen to be eight, the anode length of the 4J21-30 retained, and the design carried out at $Q_L = 150$ and $f = 1220$ mc/s. The empirical relations used were that relating I_o/I_o to G_s/G_o, that relating η_e to G_s/G_o, and the equation of a constant B line on the performance chart obtained for the 4J21-30. In addition to the definitions of G_s, V_o, I_o, and G_o, there were to be met the operating conditions of $V = 27$ kv., $I = 46$ amps., and $B = 1400$ gauss, as well as a maximum value for the over-all diameter of the resonator system dictated by interchangeability. The value of resonator inductance was calculated for a terminated parallel plate line. With the choice of $I_o = 60$ amps., the above mentioned conditions could be solved numerically to give a definite set of design parameters. The anode and cathode radii, resonator length, and thus unstrapped wavelength were determined. The straps were designed to achieve the proper frequency and to provide sufficient tuning range with the tuning means employed. The ratio r_c/r_a was determined as 0.546, considerably in excess of the value 0.375 in the 4J21-30 magnetrons.

The output circuit of the 5J26 magnetron was similar to that used in the other tunable magnetrons of long wavelength. It employed the broad band design of external coupling and transition section to the coupling loop. The size of the loop was dictated by the coupling required to provide a Q_L of approximately 150. It may be seen in Fig. 58.

The input leads of the 5J26 magnetron were of new design, incorporating chokes in the leads to prevent leakage of RF energy picked up on the cathode, and large size center conductor to minimize RF voltage breakdown on the input leads.

The significant design and operating data for the 5J26 magnetron are included in TABLE I. This magnetron design provided a single tunable replacement of superior performance for the entire 4J21-30 series. In Fig. 59 are shown curves of mode frequency tuning throughout the π mode tuning range, indicating that in the strap tuning method difficulties with mode frequency interference are avoided.

15. MAGNETRONS FOR WAVELENGTHS NEAR 10 CENTIMETERS—UNDER 200 KILOWATTS

15.1 *The 706A-C and 714A Magnetrons:* The work in the wavelength region near 10 cm., described in Section 12, was continued in the study of variations from the British design. For the most part these early studies

Digitized by Google
Original from UNIVERSITY OF MICHIGAN
Generated on 2019-09-21 09:21 GMT / http://hdl.handle.net/2027/mdp.39015077775156
Public Domain, Google-digitized / http://www.hathitrust.org/access_use#pd-google

had to do with the electron interaction space and the resonator system. Later, when driving equipment became available, life studies were started. In the main this work showed the British design to be a very nearly optimum as an unstrapped magnetron. Consequently the series of magnetrons

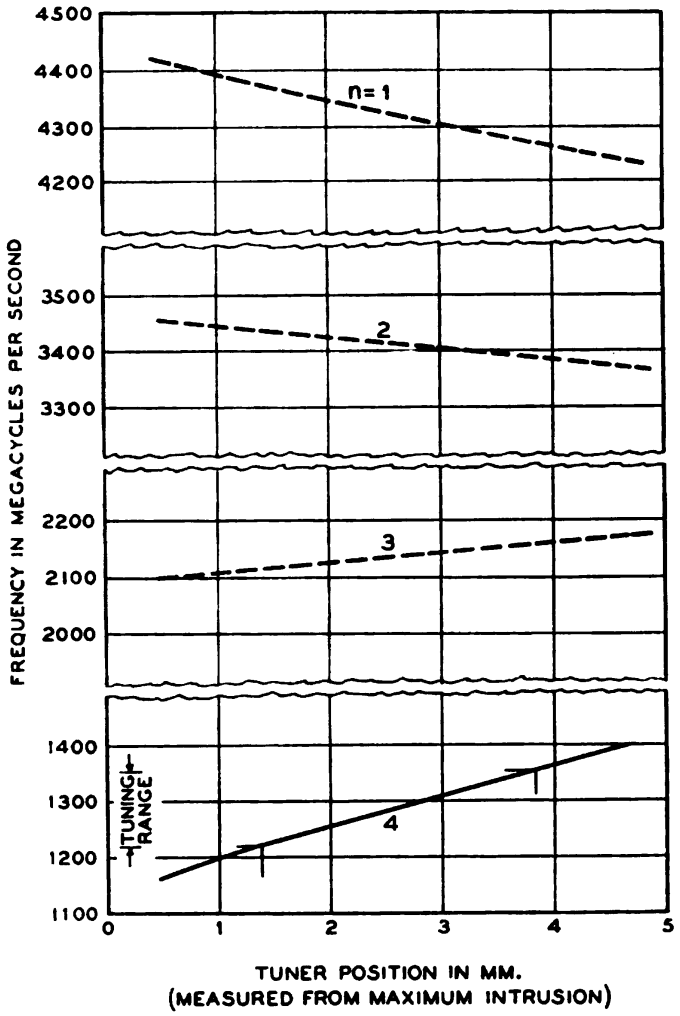

Fig. 59—Curves of mode frequency variation with tuner position in the 5J26 magnetron. The curve for $n = 4$ is experimental, those for $n = 1, 2$, and 3 have been calculated from an equivalent circuit theory of the resonator system (doublet structure not shown). Note the large mode frequency separation and the complete freedom of the π mode from interference by other modes (compare Fig. 56).

having wavelengths near 10 cm. which were coded for American manufacture were similar to the British prototype. The experiments and calculations which had been made constituted a body of valuable information to be used later in departing from the original design.

Digitized by Google
Original from UNIVERSITY OF MICHIGAN
Generated on 2019-09-21 09:21 GMT / http://hdl.handle.net/2027/mdp.39015077775156
Public Domain, Google-digitized / http://www.hathitrust.org/access_use#pd-google

The variations in the resonator system of the British magnetron were made primarily for the purpose of studying the parameters affecting frequency of operation. Magnetrons were built incorporating such variations as dimensional changes in the hole and slot resonators; the use of other forms of resonators such as slot resonators; and variations of factors affecting the coupling between adjacent resonators, as, for example, the volume of the end space region between the ends of the resonator system and the end covers of the magnetron. A series of magnetrons was built having from four to ten resonators, including odd numbers, but the majority of the experimentation was done with eight resonators as in the original system.

Besides affecting frequency, most of these resonator changes markedly affected the electronic operation as well. Undoubtedly this was the result of changes occurring in the mode frequency distribution. At the time, the significance of this distribution to magnetron operation was not fully appreciated nor, indeed, was it known for these magnetrons. As discussed in PART I in connection with curve (a) of Fig. 25, it was later found that the frequencies of several modes including the π mode were very nearly equal, making the electronic operation quite sensitive to the exact nature of the frequency distribution. This made the experiments difficult to interpret. None of the resonator systems, involving only changes in anode length and diameter with corresponding changes in the cathode, appeared to be appreciably better than that in the British magnetron.

In one rather important experiment the cathode diameter, and thus r_c/r_a, was varied to determine the value for optimum efficiency using the British anode dimensions. The result, confirmed later by comparison with British work, showed the original dimensions to be very nearly optimum.

Some variations of the output coupling to the resonator system were also tried. In one such variation the coupling loop was placed in the end space of the magnetron between two resonators. In this position the loop was coupled magnetically by the flux linking the two adjacent resonators, as well as directly by virtue of the fact that the end of the loop is fastened to the anode segment (see the discussion of output coupling in PART I). It will be recognized that this type of coupling is that used later in the 700A-D magnetrons. The output circuits in the first American 10 cm. magnetrons were like those in the British design.

The constructional techniques used in the British magnetron were followed with some variations. The most bothersome technique was that of making the vacuum seals between the end covers and the body of the magnetron. This was done by means of tin plated gold ring seals between the members. Little difficulty was encountered with this seal in production, however, and it was used throughout the production at the Western

Digitized by Google
Original from UNIVERSITY OF MICHIGAN
Generated on 2019-09-21 09:21 GMT / http://hdl.handle.net/2027/mdp.39015077775156
Public Domain, Google-digitized / http://www.hathitrust.org/access_use#pd-google

Electric Co. of 10 cm. magnetrons under 200 kw. output power.

The first unstrapped magnetrons coded for manufacture by the Western Electric Co. were the 706A-C for frequencies near 3060 mc/s (9.8 cm.). The frequency differences were achieved by small changes in the resonator slot widths. Another magnetron, the 714A, oscillating at 3300 mc/s (9.1 cm.) was also coded at this time. It differed from the others in having slightly smaller resonator holes. These magnetrons were used in some of the earliest American ship and airborne radar systems. A set of typical operating data is included in TABLE II.

The improvement in measured over-all efficiency to approximately 25 per cent was undoubtedly the result of improvements in the technique of operation and of measuring the output power. Unlike the measurement of frequency, for which good techniques were already available, the measurement of output power initially was crude and unreliable. At first, estimates of power were based on the heating of resistors to incandescence, with no assurance that all the power was being dissipated in this load. The production of corona has always been spectacular evidence of RF power. Later, when water load techniques were used, all the power could be absorbed and measured. Means of line tuning permitted the adjustment of the magnetron load impedance to the point of maximum output power even though the impedance itself was unknown.

Some preliminary studies of magnetron tuning were made as auxiliary experiments. With one or more extra coupling loops terminated externally in adjustable coaxial tuners, tuning ranges of 2 to 4 per cent were achieved.

15.2 *The 706AY-GY, 714AY, and 718AY-EY Magnetrons:* A significant improvement in the multiresonator magnetron was the method of strapping, used by the British as a means of achieving mode frequency separation (see discussion in PART I). When used in the resonator system of the 706A-C magnetrons, the early British "mode locking straps" increased the π mode wavelength from 9.8 cm. to 10.7 cm. and resulted in an increase in operating efficiency by about a factor of two with much more freedom from "moding" difficulties. Here was a really worthwhile advance and no time was lost in making use of it. The resultant strapped magnetron, oscillating at 10.7 cm. wavelength, was used directly as the basis for a new family of magnetrons of wavelength near this value. These were coded as the 718AY-EY series. The cathode, output circuit, and general mechanical features of the 706A-C were adopted essentially without change. Experiments like those done on the original British design, when repeated on strapped magnetrons, indicated the design parameters still to be close to optimum. The cathodes used were plain, oxide coated, nickel cylinders.

Generated on 2019-09-21 09:22 GMT / http://hdl.handle.net/2027/mdp.39015077775156
Public Domain, Google-digitized / http://www.hathitrust.org/access_use#pd-google
Digitized by Google
Original from UNIVERSITY OF MICHIGAN

Generated on 2019-09-21 09:22 GMT / http://hdl.handle.net/2027/mdp.39015077775156
Public Domain, Google-digitized / http://www.hathitrust.org/access_use#pd-google

Digitized by Google

TABLE II

MAGNETRONS FOR WAVELENGTHS NEAR 10 CENTIMETERS

	706A-C Unpackaged	714A Unpackaged	706AY-GY Unpackaged			714AY Unpackaged			718AY-EY Unpackaged			720A-E Unpackaged			4J45-47 Unpackaged		
N	8	8	8			8			8			8			8		
r_a (in.)	0.119	0.119	0.110			0.100			0.119			0.107			0.107		
r_c (in.)	0.315	0.315	0.295			0.270			0.315			0.283			0.283		
h (in.)	0.788	0.788	0.788			0.788			0.788			1.576			1.576		
Magnet gap (in.)	1.480	1.480	1.490			1.490			1.490			2.750			2.750		
Weight (lb.)	2.1	2.1	2.1			2.1			2.1			4.9			4.9		
Resonators	hole and slot	hole and slot	hole and slot			hole and slot			hole and slot			hole and slot			hole and slot		
Unstrapped λ (cm.)	9.8	9.1	~8.9			~8.3			9.8			~8.0			~8.0		
Straps	none	none	British wire			British wire			British wire			double ring			double ring		
λ (cm.)	9.8	9.1	9.8			9.1			10.7			10.7			10.7		
f (mc/s)	3100–3019	3320–3280	3100–2914			3320–3280			2890–2720			2890–2720			2855–2750		
Nearest mode	$n = 3$	$n = 3$	$n = 3$			$n = 3$			$n = 3$			$n = 3$			$n = 3$		
λ separation (%)	−1	−1	−11			−11			−11			−10			−10		
Q_0	>1500	>1500	~1000			~1000			~1000			1500			1500		
Q_{ext}	<100	<100	~120			~120			~120			130			130		
η_c (%)	~93	~93	~89			~89			~89			93			93		
Output circuit	coaxial	coaxial	coaxial			coaxial			coaxial			coaxial			coaxial		
V (kv.)	11.0	11.0	11.4	18.5	20.9	11.6	17.7	19.5	11.9	17.9	20.0	21.0	24.0	27.0	21.0	27.0	23.0
I (amps.)	12.5	12.5	12.5	16	20	12.5	16	20	12.5	16	20	45	53	65	45	65	45
B (gauss)	1300	1300	1300	1900	2100	1500	2100	2250	1300	1800	1950	2300	2600	2900	2300	2900	2550
τ (μs)	1	1	1	1	1	1	1	1	1	1	1	1	1	1	1	1	5
pps	1000	1000	2000	1000	1000	2000	1000	1000	2000	1000	1000	1000	650	500	1000	500	120
P_0 (kw.)	25	22	40	146	206	40	125	165	45	136	193	550	800	1100	550	1100	650
η (%)	18	16	28	49	49	28	47	42	30	47	48	58	63	63	58	63	63
η_e (%)	~19	~17	~31	~55	~55	~31	~53	~47	~34	~53	~54	62	68	68	62	68	68
PF (mc/s)	~15	~16	11	11	11	12	12	12	11	11	11	10	10	10	10	10	10

Original from UNIVERSITY OF MICHIGAN

No particular precautions were taken to protect the active coating. Even so, lives both in the laboratory and in the field were shown to be well over 2000 hours. Much later, the mechanical structure of the cathode and its support was improved and a heavy glass protective housing designed to cover the input leads. The performance chart of Fig. 17 in PART I is that of one of the 718AY-EY series. Other data concerning these magnetrons are given in TABLE II.

Quite early in the study of the multicavity magnetron it had been realized that the mode frequency distribution of the resonator system is very important to efficient operation. Evidence had accumulated which indicated that something needed to be done to suppress all but one mode of oscillation. Attempts at influencing mode frequency separation were made in which fluxbarriers or partitions, either complete or partial, were used in the end spaces of the resonator system. These included what was essentially the distortion of the structure into the form of the so-called "serpentine" mentioned in PART I. Although striking changes in operation were produced, supporting the basic contention that there are more ways of doing a thing wrong than right, worthwhile improvements were not achieved.

Following the confirmation, here and elsewhere, of the British results with strapping and the coding of the series of 718AY-EY magnetrons, intensive work was started in the general investigation of the modes of the magnetron resonator system and their relation to the various possible methods for strapping. This work involved the determination of the mode patterns for mode identification, the technique for which was consequently developed. Various strapping schemes were devised, built into magnetron resonator systems, and studied. Among these were the echelon strapping also used by the British, single and double ring strapped systems, and diametral straps which were adaptable to external tuning of the magnetron. The importance of strap shielding and strap assymmetries discussed earlier were brought out in these studies. The effects of end space volume and anode length on mode frequency distribution for given strapping systems were also studied.

Strapping made possible greater tuning ranges with tunable magnetrons. Efficient magnetrons having broken echelon strapping on one end and diametral straps on the other, connected through a glass seal to an external coaxial tuner were built. Tuning ranges of over ± 5 per cent were achieved in this way. There was no demand at the time for tunable magnetrons.

Following the introduction of the 718AY-EY magnetrons, their properties were reproduced at an extended range near the wavelengths of the 706A-C and at the wavelength of the 714A. The designs for these were arrived at by scaling the 718AY-EY to the appropriate wavelengths. The principles

Generated on 2019-09-21 09:22 GMT / http://hdl.handle.net/2027/mdp.39015077775156
Public Domain, Google-digitized / http://www.hathitrust.org/access_use#pd-google
Digitized by Google
Original from UNIVERSITY OF MICHIGAN

of scaling discussed in PART I had been studied in connection with the extension of magnetron frequencies into the 20 to 45 cm. and 3 cm. wavelength ranges and were fairly well understood by this time. These new strapped magnetrons were coded as the 706AY-GY and the 714AY. The frequency variation over the 706AY-GY band was accomplished by variation of the resonator slot width. The characteristics of these magnetrons, apart from frequency, are essentially the same as those of the 718AY-EY series (see TABLE II). External and internal views of the 706AY-GY type are shown in Figs. 60 and 61. The strapping scheme to be seen in Fig. 61 is the early British system depicted schematically in Fig. 24(a).

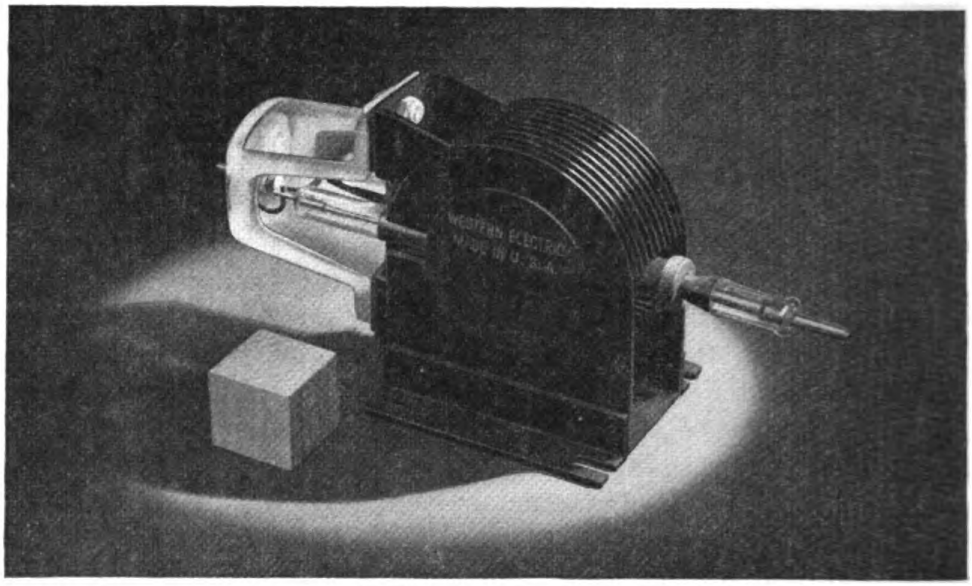

Fig. 60—An external view of a 706AY-GY magnetron (150 kw., ~3000 mc/s).

The means of fabricating the anode block in manufacture is also of interest. This had to be inexpensive and fast. As worked out by Western Electric engineers, it consisted of boring the interaction space hole first and turning the end spaces into the solid copper block. This was followed by two operations in a multiple spindle drill press in which the eight resonator holes are drilled to size. Following this, a broach consisting of eight tapered series of projecting cutting edges, spaced equally around the main shaft, was drawn through the interaction space hole, cutting the eight slots to size in a single operation.

Although more powerful magnetrons were subsequently developed, these 10 cm. magnetrons of power output below 200 kw. are still considered to be highly satisfactory designs. Together with similar designs in Great Britain, they have been produced by several manufacturers in large quantity and

Digitized by Google
Original from UNIVERSITY OF MICHIGAN
Generated on 2019-09-21 09:22 GMT / http://hdl.handle.net/2027/mdp.39015077775156
Public Domain, Google-digitized / http://www.hathitrust.org/access_use#pd-google

have seen extensive use in many forms of pulsed radar systems. They have also served as the basis for much of the subsequent magnetron design work.

16. Magnetrons for Wavelength near 10 Centimeters—200 Kilowatts to 1 Megawatt

16.1 *The 720A-E Magnetrons:* A natural outgrowth of the early magnetron experimentation was the effort to generate higher power. Since the earliest magnetrons were unstrapped there was much to be hoped for in

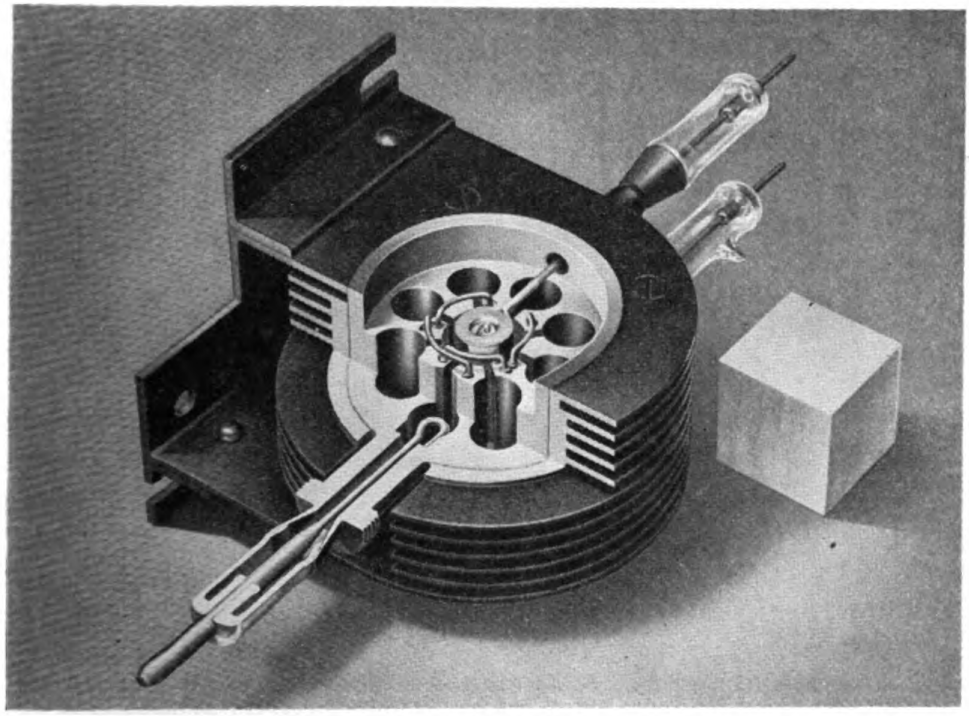

Fig. 61—An internal view of a 706AY-GY magnetron (150 kw., ~3000 mc/s). Note the type of wire strapping [compare Fig. 24(a)] and the simple coaxial output circuit.

improved efficiency. Higher power magnetrons would have to be designed to operate at voltages above 20 kv. and currents of greater than 50 amps. To accomplish these objectives, the interaction space was enlarged, in some designs involving a greater number of resonators, and the anode length increased by two or even three times. Although it was possible to develop over 200 kw. with magnetrons of eight, ten, and twelve resonators, efficiencies were poor, seldom exceeding 20 per cent at maximum loading. This was even poorer than unstrapped 10 cm. magnetrons like the 706A-C. The reduction in mode frequency separation attendant upon increases in anode length and number of resonators was later found to be the cause.

Following their first use in the 718AY-EY magnetrons, straps were in-

Digitized by Google
Original from UNIVERSITY OF MICHIGAN
Generated on 2019-09-21 09:22 GMT / http://hdl.handle.net/2027/mdp.39015077775156
Public Domain, Google-digitized / http://www.hathitrust.org/access_use#pd-google

corporated in the high power designs with immediate improvement in performance. The output circuits used were simple loop to coaxial lead combinations like those in use on the 706A-C.

Radar needs for higher power near 10 cm. had developed to the point of a specific requirement for a magnetron of not less than 350 kw. output. Since it was believed that the best one could obtain from the 718AY-EY was 250 kw. even at the risk of shortened cathode life, the requirement made necessary a new design. In the work on higher power magnetrons, better than 300 kw. had been obtained at efficiencies greater than 50 per cent at maximum loading with what was essentially a double length 718AY-EY

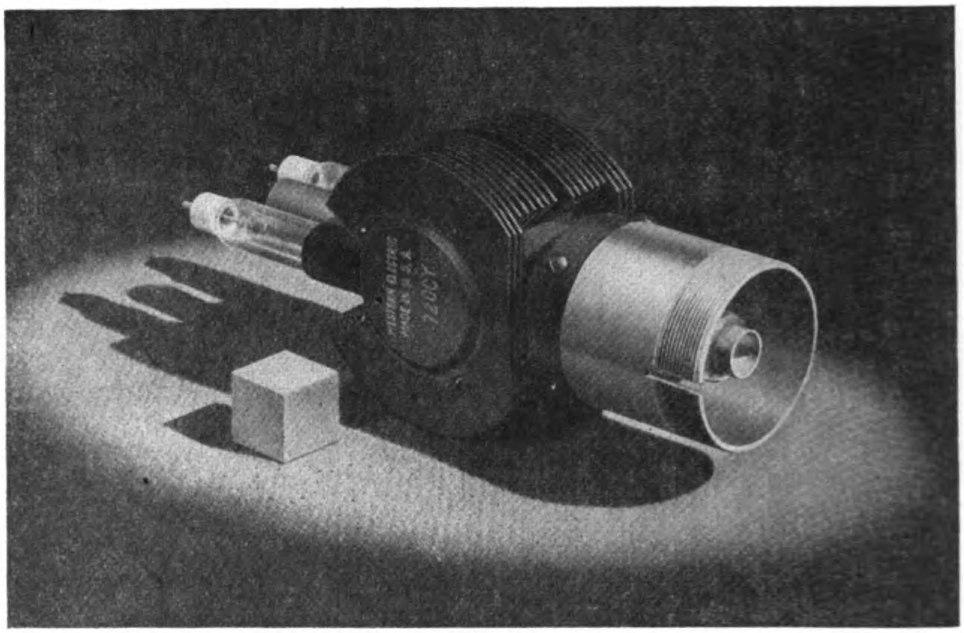

Fig. 62—An external view of a 720A-E magnetron (1000 kw., ~2800 mc/s).

type. Thus it appeared that the new power requirement could be met with such a design. The press of time made it necessary to concentrate further efforts on improving this design, with not much if any time to be devoted to further experimentation along other lines. The chief drawback of the double length magnetron was the large magnet it required. Several months later an equally efficient magnetron, shorter, and having a larger number of circuit elements might have been produced, but the original program had advanced beyond the stage at which it could be changed. The improvements in design of the double length 718AY-EY type magnetron resulted in the 720A-E series.

An external view of the 720A-E magnetron is shown in Fig. 62. A cutaway model is shown in Fig. 63 in which may be seen the nature of the

Digitized by Google
Original from UNIVERSITY OF MICHIGAN
Generated on 2019-09-21 09:23 GMT / http://hdl.handle.net/2027/mdp.39015077775156
Public Domain, Google-digitized / http://www.hathitrust.org/access_use#pd-google

resonator system, straps, cathode, and output circuit. In TABLE II are given dimensions and other data concerning these magnetrons.

The resonator system has eight hole and slot type cavities. Its anode length is 4 cm., double that of the 706AY-GY. It is strapped with double ring shielded straps of special design which could be stamped out of sheet copper and oven brazed in position in a wide ledge trepanned around the interaction space into the ends of the anode block. These straps were easier to control in dimensions than the echelon straps, used in early experimental models, which had made necessary the development of a pretuning

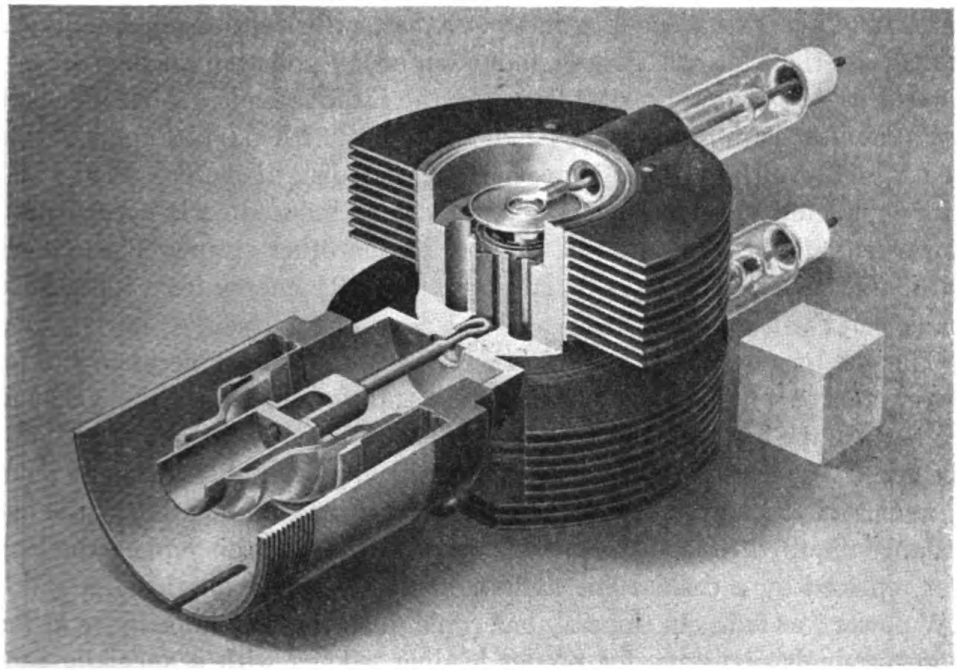

Fig. 63—A view of a cut-away 720A-E magnetron (1000 kw., ~2800 mc/s) showing the large cathode end disks and the impedance transformer sections in the output circuit.

technique. The large number of wire straps used had made it impossible to predict from visual inspection that a given anode would eventually oscillate at a specified wavelength. The straps were adjusted manually to bring the frequency of resonance determined before sealing and pumping into the required range. These heavily strapped models operated at efficiencies up to 65 per cent, but their initial operating wavelengths were near 13 cm. The high operating efficiency was achieved at the required wavelength by scaling the structure. The increase in magnetic field required by the scaling was achieved without increase in magnet size by incorporation of steel disks in the end covers of the magnetron. The new stamped straps required considerably less manipulation during pretuning than the echelon straps.

Generated on 2019-09-21 09:23 GMT / http://hdl.handle.net/2027/mdp.39015077775156
Public Domain, Google-digitized / http://www.hathitrust.org/access_use#pd-google
Digitized by Google
Original from UNIVERSITY OF MICHIGAN

The five wavelength groups of the 720A-E employ straps of different height.

The cathode was similar to that of the 706AY-GY but longer and with different end disk design. The surface was a plain oxide coating on the nickel cylinder base. Adequate life under the most stringent of its operating conditions was obtained (see TABLE II). The radical departure in cathode end disk design was necessitated by the pickup of RF energy by the cathode. This was aggravated by the length of the cathode. An end disk of conventional size, being closer to the inner strap than to the outer strap, is more influenced by its potential. Since the inner straps are π radians out of phase and the cathode approximately a half wavelength long, conditions were quite right for considerable induction of RF potential on the cathode. Considerable RF power was radiated by the cathode leads. Measurements on a non-oscillating magnetron indicated that cathode pickup could be neutralized very nearly by increasing the end disk diameter. If the end disk completely covered both straps, the charge induced on it by one strap was essentially balanced by that induced by the other strap. The 720A-E with large cathode end disks radiates very little RF energy from its cathode leads.

The greater power which the 720A-E produced made it necessary to redesign the output circuit to include the transformer inside the vacuum. Voltages in the external transformer had been sufficiently high to break down the line. The redesign was carried out empirically by a substitution method. A replica of the output circuit was constructed and terminated in the impedance required to load the magnetron properly. In this replica the loop was replaced by a coaxial line and standing wave detector through which CW power was fed. In this way one could determine the impedance at the loop terminals necessary for proper loading. Then with a specially constructed output circuit, in which the dimensions between the glass seal and the loop terminals could be varied, the dimensional changes necessary to achieve the required impedance at the loop with match in the output load coaxial was determined. The dimensions determined in this way provided the final design. The 720A-E was one of the early "preplumbed" magnetrons.

A coaxial lead coupling using chokes instead of contacts was developed for the output circuit and used not only at 10 cm. but on all the later magnetrons of longer wavelength as has been described. The centrifugal glass seal at the outer conductor is to be noted (see Fig. 63). The original tungsten center conductor to which an external "thimble" was soldered (similar to that in the 5J23, see Fig. 49) was replaced by a Kovar cup to which the glass was sealed directly. Greater strength, better cooling, and elimination

Generated on 2019-09-21 09:23 GMT / http://hdl.handle.net/2027/mdp.39015077775156
Public Domain, Google-digitized / http://www.hathitrust.org/access_use#pd-google
Digitized by Google
Original from UNIVERSITY OF MICHIGAN

of the high voltage gradient in air which had existed at the small diameter tungsten rod resulted.

In Fig. 64 is shown a typical performance chart for the 720A-E series. Other performance data are given in TABLE II. In Fig. 44 is shown one of the 720A-E magnetrons mounted in its magnet.

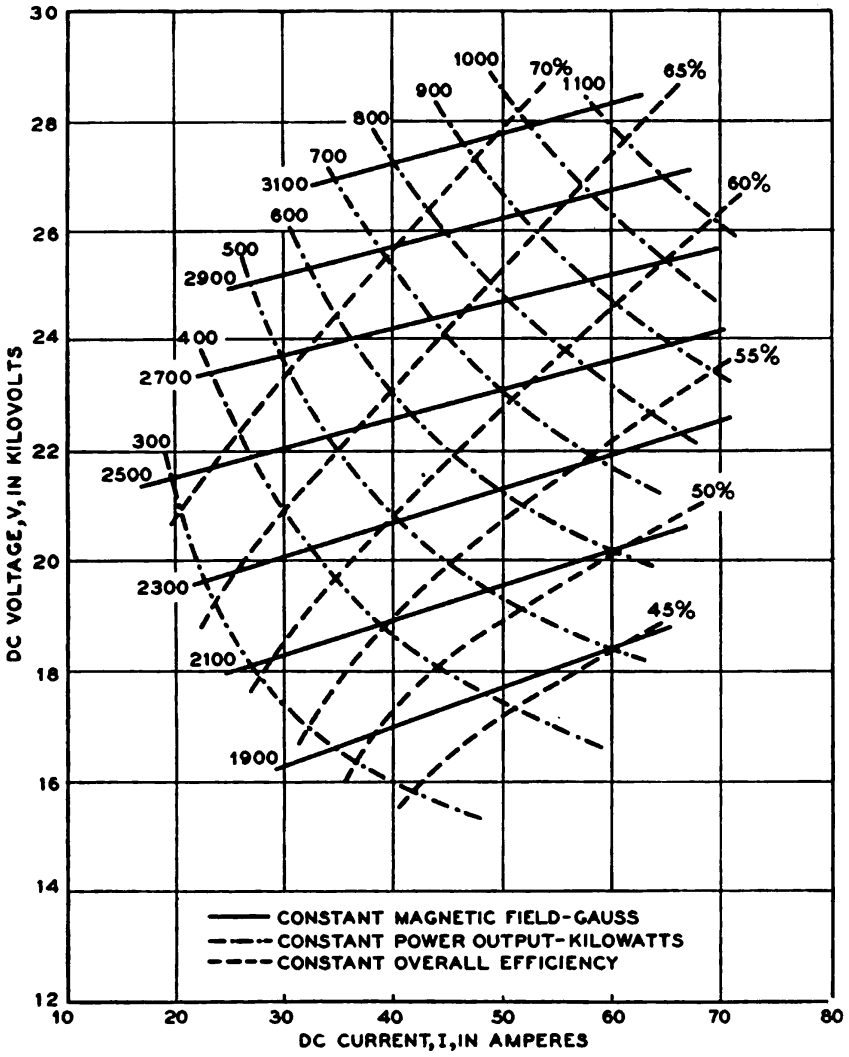

Fig. 64—A typical performance chart of the 720A-E magnetrons (~2800 mc/s).

In the use of the 720A-E on line type modulators the difficulty with what was then called voltage "overshoot" was first encountered. It is the result of the finite buildup time for the RF oscillation during which the pulse voltage rises to values higher than required for π mode operation. It is particularly aggravated on line type modulators for which the magnetron, before it oscillates and draws current, presents a mismatch to the line network causing the voltage to rise to a much higher value. The difficulty was

Digitized by Google
Original from UNIVERSITY OF MICHIGAN
Generated on 2019-09-21 09:23 GMT / http://hdl.handle.net/2027/mdp.39015077775156
Public Domain, Google-digitized / http://www.hathitrust.org/access_use#pd-google

circumvented by connecting across the modulator network a condenser in series with a resistance equal to the characteristic impedance of the network. The condenser is of low impedance for rapid voltage changes, terminating the network properly during the voltage rise. The condenser, however, stores some energy which must be dissipated at the end of the pulse. The discharge of this energy through the magnetron causes very weak oscillations to occur following the main pulse. This condition somewhat lengthens the interval of time following the pulse during which the radar receiver may not detect an echo.

16.2 *The 4J45-47 Magnetrons:* For the extension of radar range it had been found desirable to use pulses of longer duration with consequent increase in total energy radiated per pulse. As indicated in PART I, the longer the pulse, the narrower the frequency spectrum. A long pulse consequently makes possible a narrower receiver band width, an improved receiver signal to noise ratio, and greater range. Although it was necessary to reduce the peak power somewhat in operating the 720A-E at a pulse length of 5 microseconds, a substantial increase in range could still be effected. The Radiation Laboratory at M. I. T. proposed to use 720A-E type magnetrons on long pulse operation and performed many tests of these magnetrons under these conditions. Many 720A-E magnetrons performed satisfactorily under these long pulse conditions. However, arcing both internally between cathode and anode and externally across the input leads deteriorated the performance and made the life expectancy of the magnetron questionable.

To meet the new demands a new series of magnetrons, the 4J45-47 was developed by making two design changes in the 720A-E. The plain, oxide coated cathode was replaced with a cathode of the "mesh" type to be described in Section 21. MAGNETRON CATHODES. The "mesh" cathode proved to be more rugged, involved less arcing, was longer lived, and required a minimum of changes in internal structure.

External arcing at the input leads was minimized by lengthening the glass section, accomplished by increasing the over-all lead length and shortening the metal section of the lead at the magnetron body, and by enclosing the leads in housings filled with a silicone anticorona compound. These changes were limited by the requirement of interchangeability with the 720A-E.

The modified 720B-D magnetrons were coded the 4J45-47. Operating characteristics are given in TABLE II. These magnetrons were used with long pulses and in the usual service for which the 720A-E had been designed.

17. MAGNETRONS FOR WAVELENGTHS NEAR 3 CENTIMETERS—UNDER 100 KILOWATTS

17.1 *The 725A and 730A Magnetrons:* As the antenna size of a radar is reduced, it is necessary to reduce the operating wavelength to maintain

Digitized by Google
Original from UNIVERSITY OF MICHIGAN
Generated on 2019-09-21 09:23 GMT / http://hdl.handle.net/2027/mdp.39015077775156
Public Domain, Google-digitized / http://www.hathitrust.org/access_use#pd-google

the same width of radiated beam and resolving power. To meet the needs for aircraft and submarine radar and other applications in which antenna size must be small, shorter wavelength magnetrons were essential. The development of magnetrons of frequency near 10,000 mc/s (3 cm. wavelength) was part of the expanding program of magnetron research and development which grew out of the earliest experiments. The work was concentrated at 3.2 cm., roughly a factor of three below the initial 10 cm. work. From the earliest 3 cm. magnetron developments was evolved an efficient 3.2 cm. magnetron, the 725A, requiring roughly the same driving conditions as were used in the first 10 cm. magnetron applications.

An operating 3 cm. magnetron was built in the summer of 1941. The crude techniques then in use in the 10 cm. wavelength range were adapted to the 3 cm. range, and 5 kw. peak power from this magnetron was measured in a coaxial water load. This design involved an unstrapped resonator system having eighteen quarter wavelength slots. The choice of so many resonators was made in order that large cathode and anode dimensions could be used, later shown to be unreasonable for the voltage range employed. In addition the design suffered from a confusion of many modes of the resonator system and from an inadequate output circuit.

A later design, similar in some respects to one upon which work was done at the M. I. T. Radiation Laboratory, made use of a resonator system having twelve slots. This design operated in a mode other than the π mode, probably that for which $n = 3$ or $n = 4$. The M. I. T. version, the 2J21, was the first 3 cm. magnetron to be manufactured in quantity. Its power output was about 15 kw., generated at an efficiency of from 12 to 15 per cent. Many variations of this design were made without major success in an attempt to obtain efficient and reliable operation.

Prior to the introduction of straps, attempts were made to adapt 10 cm. magnetron designs to 3 cm. While none came up to the 10 cm. operating efficiencies, one such, having an unstrapped resonator system of eight hole and slot resonators, was used extensively in systems experimental work in our Laboratories.

By this time it was realized that some fundamental reason existed for the failure of these 3 cm. magnetrons to reach efficiencies comparable with those obtained at 10 cm. The resonator systems were unstrapped at 3 cm., and they operated in a mode other than the π mode. However, this did not fully explain their failure. Attempts were made to operate strapped 3 cm. magnetrons in the π mode, but they still did not result in the desired or expected improvements. The trouble lay not only in the mode frequency distribution of the resonator system but also in the size of the interaction space. Prior to this time, 3 cm. magnetrons were made with larger inter-

Digitized by Google
Original from UNIVERSITY OF MICHIGAN
Generated on 2019-09-21 09:23 GMT / http://hdl.handle.net/2027/mdp.39015077775156
Public Domain, Google-digitized / http://www.hathitrust.org/access_use#pd-google

action spaces than direct scaling from 10 cm. would indicate. This had been done to achieve greater cathode size and smaller operating magnetic field. It appeared that 3 cm. magnetrons had been suitable only for operation at high voltage and high magnetic field and were being operated far below their range of maximum efficiency or even of reasonable operation. A decisive step forward was taken when a strapped magnetron was built which was rigorously scaled, according to the scaling principles discussed in PART I, from 10 cm. designs of the same operating voltage and current as that desired at 3 cm.

The first such magnetrons were scaled from the 10.7 cm. strapped magnetrons having eight resonators, the 718AY-EY, with only minor changes being made in the resonators for mechanical reasons. The results obtained were very encouraging although they were erratic for a variety of reasons. Mechanical construction was difficult and not reproducible before newer tools and techniques for making and assembling small parts were introduced. Output circuit variations in many cases completely masked good electronic operation, and it was not until a carefully considered and executed study of the output circuit design was instituted that consistent results were obtained. However, the results were such that it was decided to shift all emphasis in 3 cm. magnetron development at the Bell Laboratories to strapped designs scaled from 10 cm. magnetrons.

This was by no means an easy decision to make. For example, it meant the use of very small parts and clearances, of order 0.010 in., and very close tolerances. That such a magnetron would be feasible for large scale production was by no means obvious. A cathode, 0.100 in. or less in diameter, which must deliver a considerably higher current density than any previous magnetron cathode, would be necessary. Whether such a cathode, at the expected operating conditions, would have any appreciable life was not known. Furthermore, a scaled 3 cm. magnetron would require a much higher magnetic field than previous 3 cm. designs, a demand which might increase the magnet weight.

On the other hand, it was possible that the improved electronic efficiency of the scaled magnetron would result in less rigorous treatment of the cathode in spite of its small size. In spite of the increase in magnetic field, the decrease in anode length of the scaled magnetron made possible the reduction of the magnet gap to a point where it was conceivable that no greater magnetomotive force and size of magnet would be required than in previous 3 cm. designs. Greater stability and freedom from mode troubles could be expected.

Early strapped magnetrons having eight resonators had anode diameters of order 0.175 in. and cathode diameters of order 0.065 in. Magnetrons of

Digitized by Google
Original from UNIVERSITY OF MICHIGAN
Generated on 2019-09-21 09:24 GMT / http://hdl.handle.net/2027/mdp.39015077775156
Public Domain, Google-digitized / http://www.hathitrust.org/access_use#pd-google

over-all efficiency better than 45 per cent at a pulling figure of 15 mc/s were made.

The cathode life in these magnetrons was very short—10 to 30 hours. Reduction of the severity of the demands made of the cathode was necessary. Strapped magnetrons having twelve resonators and larger cathodes were designed and a few built with promising results.

The 3 cm. magnetron development program was later broadened by the inclusion of personnel from the NDRC Radiation Laboratories at the Massachusetts Institute of Technology and at Columbia University. Effort on magnetrons having twelve resonators was expanded and prosecuted vigorously along with the work on the eight resonator types. Somewhat later the effort was concentrated solely on the twelve resonator magnetron. The design which was made shortly thereafter became, with only minor changes, the 725A.

Experience gained with previous magnetrons at all wavelengths enabled one to design a mechanically feasible resonator system with proper strapping to give the desired RF characteristics and π mode resonant frequency. The interaction space, on the basis of previous work and Hartree's oscillation condition, was designed to meet the specification of 12 kv. and 12 amps. input. The design was complicated both mechanically and electrically by the requirement of interchangeability with the 2J21. Thus good operation at 10 kv. and 10 amps. input was necessary.

The resonator system of the 725A is machined into a separable "anode insert" which, when completed, is brazed into position in the so-called "shell" carrying the leads and cooling fins. The straps are placed in a channel for shielding from the interaction space and are broken on one end.

The first cathodes were the ordinary, nickel sleeve type with double carbonate coating sprayed onto its surface. Not long after the start of the 3 cm. magnetron development, it was recognized that the cathode development problem would be a large part of the over-all project. Indeed, the 725A proved to be an excellent magnetron for cathode development work. Many of the cathode improvements and new designs developed for it have been used successfully in other magnetrons. The cathode as finally developed for the 725A was a nickel blank, complete with end disks and heater chamber turned out of nickel rod. Over the cylindrical portion was welded or sintered a fine nickel mesh in the interstices of which the active coating was applied. This is shown in Fig. 79 and will be described more fully with other cathode developments in Section 21. MAGNETRON CATHODES. Under normal operating conditions the cathode heater is turned off, the necessary heat being provided by electron back bombardment.

Considerable effort was expended in the design of a satisfactory and repro-

Generated on 2019-09-21 09:24 GMT / http://hdl.handle.net/2027/mdp.39015077775156
Public Domain, Google-digitized / http://www.hathitrust.org/access_use#pd-google
Digitized by Google
Original from UNIVERSITY OF MICHIGAN

ducible output circuit for the 725A. The requirement of interchangeability with the 2J21 restricted the output wave guide flange in its position relative to the axis of the anode and the mounting flange. Previous 3 cm. magnetrons having hole and slot resonators utilized coaxial output circuits coupled to the resonator system by a loop located in the median plane of one of the resonators as in Fig. 1. Although it was recognized that a wave guide output for a small magnetron of this type would be more elegant and reproducible than a coaxial output, difficulty in twisting the plane of polarization from the resonator to the output wave guide flange, involved in the interchangeability requirement, and the lack of experience with such outputs made necessary the choice of an output for the final design similar to the original. To obviate the removal of a large portion of one resonator to accommodate the output and to make the loop easily accessible for inspection and adjustment, it was placed in the end space directly over the circular hole of one of the resonators. This so-called "halo" type loop is shown in Fig. 66. The coaxial line was terminated, as in previous 3 cm. magnetrons, in a junction to wave guide, fabricated as part of the magnetron. The output circuit was designed around a matched junction which, it was hoped, would have the best electrical breakdown strength at the reduced pressures of high altitude operation, would be frequency insensitive, and would avoid adjustment of the junction on individual magnetrons. The entire antenna of the junction was enclosed in the vacuum envelope of the magnetron as may be seen in Fig. 66.

The method of attack on the output circuit problem from this point on may be summarized as follows: First, a matched junction from coaxial to wave guide such that it could be applied to the final over-all design, had to be achieved. Then, for a given choice of loop size and position relative to the resonator, it was necessary to obtain the transformer properties of the coaxial line immediately adjacent to the loop so that the proper over-all coupling from magnetron resonator to wave guide load was achieved. Here again the mechanical restriction on the distance between the resonator and wave guide axes was found to be cumbersome. Two loop sizes were tried, that requiring the higher standing wave in the coaxial transformer to couple it properly being later discarded. At any given stage in the development, the procedure consisted of finding the impedance to be presented to the loop by the coaxial output. This was done by transforming through the entire output circuit to the loop terminals, the impedance needed in the output wave guide for proper loading, using the transformer parameters measured on a simulated output circuit. This impedance at the loop terminals was obtained by variation of the transformer properties of the coaxial line between the loop terminals and the coaxial to wave guide junction. The

Generated on 2019-09-21 09:24 GMT / http://hdl.handle.net/2027/mdp.39015077775156
Public Domain, Google-digitized / http://www.hathitrust.org/access_use#pd-google
Digitized by Google
Original from UNIVERSITY OF MICHIGAN

change of diameter of the coaxial center conductor at a critical distance from the loop terminals is to be seen in Fig. 66. The height of the output loop above the resonator end surface was a convenient variable upon which the over-all output coupling depended. This was not without disadvantages, however, since its value for reproducibility had to be held to within 0.001 in. Its nominal height above the anode is 0.011 in.

While the scaling of 10 cm. magnetrons to 3 cm. demanded higher magnetic fields than had previously been used at 3 cm., the magnet size was

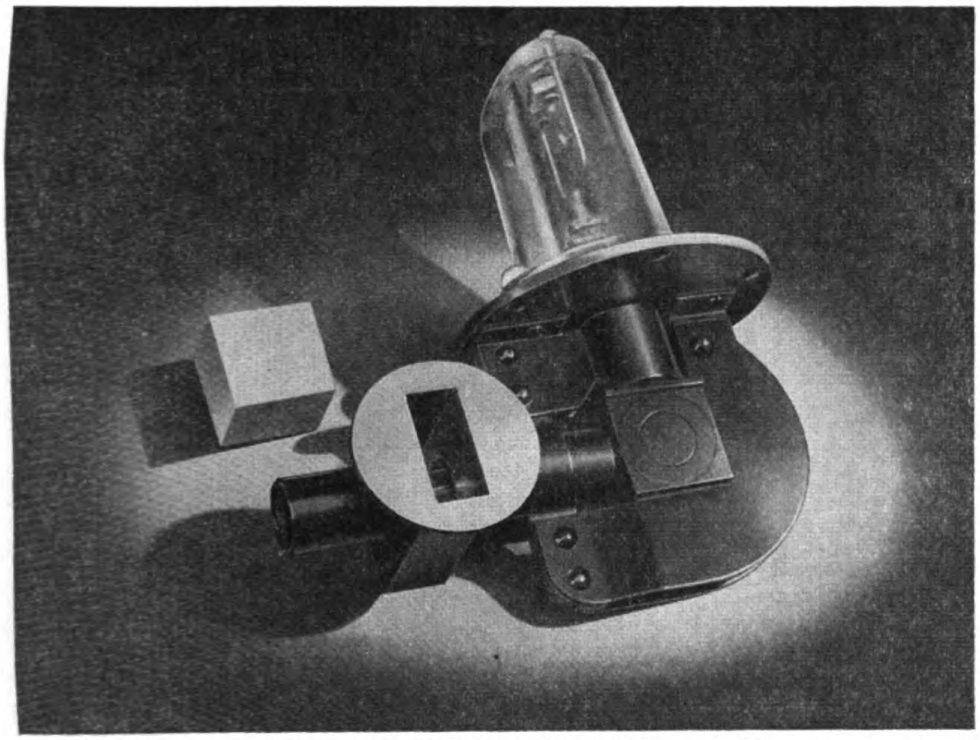

Fig. 65—An external view of the 725A magnetron (55 kw., 9375 mc/s), showing the attached coaxial to wave guide junction in the output circuit.

kept down by the reduction of the magnet gap made possible in the scaling of anode length. A further reduction in effective magnet gap was made by the inclusion of steel disks in the end covers of the magnetron. With these changes, the magnetomotive force required to supply the field for the 725A was almost identical to that required by the 2J21 and no extensive magnet redesign was necessary.

The requirement of interchangeability with the 2J21 made it necessary to place the input and output leads of the 725A at right angles (see Fig. 65). Along with the 725A, there was developed a version, coded the 730A, with input leads mounted directly opposite to the output in a so-called "straight

Generated on 2019-09-21 09:24 GMT / http://hdl.handle.net/2027/mdp.39015077775156
Public Domain, Google-digitized / http://www.hathitrust.org/access_use#pd-google
Digitized by Google
Original from UNIVERSITY OF MICHIGAN

Generated on 2019-09-21 09:24 GMT / http://hdl.handle.net/2027/mdp.39015077775156
Public Domain, Google-digitized / http://www.hathitrust.org/access_use#pd-google

Digitized by Google

TABLE III

MAGNETRONS FOR WAVELENGTHS NEAR 3 CENTIMETERS

	725A, 730A Unpackaged			2J48-50 Unpackaged			2J55-56 Packaged	2J51 Packaged Tunable			4J50, 4J78 Packaged			4J52 Packaged	
N	12			12			12	12			16			16	
r_a (in.)	0.051			0.051			0.062	0.062			0.104			0.104	
r_c (in.)	0.102			0.102			0.125	0.125			0.159			0.159	
h (in.)	0.250			0.250			0.250	0.250			0.250			0.250	
Magnet gap (in.)	0.625			0.625			0.384	0.384			0.380			0.380	
Weight (lb.)	1.5,1.1			1.5			3.8	4.6			9.5			5.5	
Resonators	hole and slot			hole and slot			hole and slot	hole and slot			hole and slot			hole and slot	
Unstrapped λ (cm.)	2.3			~2.3			~2.3	~2.6			2.46			2.46	
Straps	double ring			double ring			double ring	double ring			double ring			double ring	
λ (cm.)	3.2			3.22, 3.3, 3.4			3.2, 3.24	3.33			3.2, 3.3			3.2	
f (mc/s)	9375 ± 30			9315 ± 5, 9080 ± 80, 8825 ± 75			9375 ± 30, 9245 ± 55	8500 to 9600			9375 ± 30, 9080 ± 80			9375 ± 30	
Nearest mode	$n = 5$			$n = 5$			$n = 5$	$n = 5$			$n = 7$			$n = 7$	
λ separation (%)	−16			−16			~−16	~−16			−14			−14	
Tuning	—			—			—	resonator inductance			—			—	
$\Delta\lambda$ (%)	—			—			—	12.1			—			—	
Tuner travel (in.)	—			—			—	0.110			—			—	
Q_0	680			680			680	630–460			850			850	
$Q_{ext.}$	280			280			290	290			350			350	
η_c (%)	71			71			70	65			71			71	
Output circuit	coaxial-wave guide			coaxial-wave guide			coaxial-wave guide	coaxial-wave guide			wave guide			wave guide	
V (kv.)	10.0	12.0	13.0	10.0	12.0	13.0	12.0	11.0	12.0	14.3	22.0	22.0	22.0	15.0	15.0
I (amps.)	10	10	12	10	10	12	12	11	12	14	27	27	27	15	13.5
B (gauss)	4500	5400	5650	4500	5400	5650	3350	3050	3350	4000	6900	6900	6900	4950	4950
τ (μs)	1	1	1	1	1	1	1	1	1	1	1	2	5	1	5.5
pps	1000	1000	1000	1000	1000	1000	1000	1000	1000	1000	1000	500	200	1000	200
P_0 (kw.)	31	44	56	31	44	56	50	33	40	60	280	280	280	110	95
η (%)	31	37	36	31	37	36	35	27	28	30	47	47	47	49	47
η_0 (%)	44	52	51	44	52	51	50	42	43	46	66	66	66	69	66
PF (mc/s)	13.5	13.5	13.5	13.5	13.5	13.5	12	12	12	12	12	12	12	12	12

Original from UNIVERSITY OF MICHIGAN

through" design. Experimental models were released for systems tests and the need developed for such magnetrons to be used in some special radar systems. The 730A is identical to the 725A except for external mechanical details. An external view is shown in Fig. 67.

Details of the final design of the 725A (and 730A except for the mechanical differences noted) may be seen in Fig. 66. Data on these magnetrons and their performance are given in TABLE III. A typical performance chart

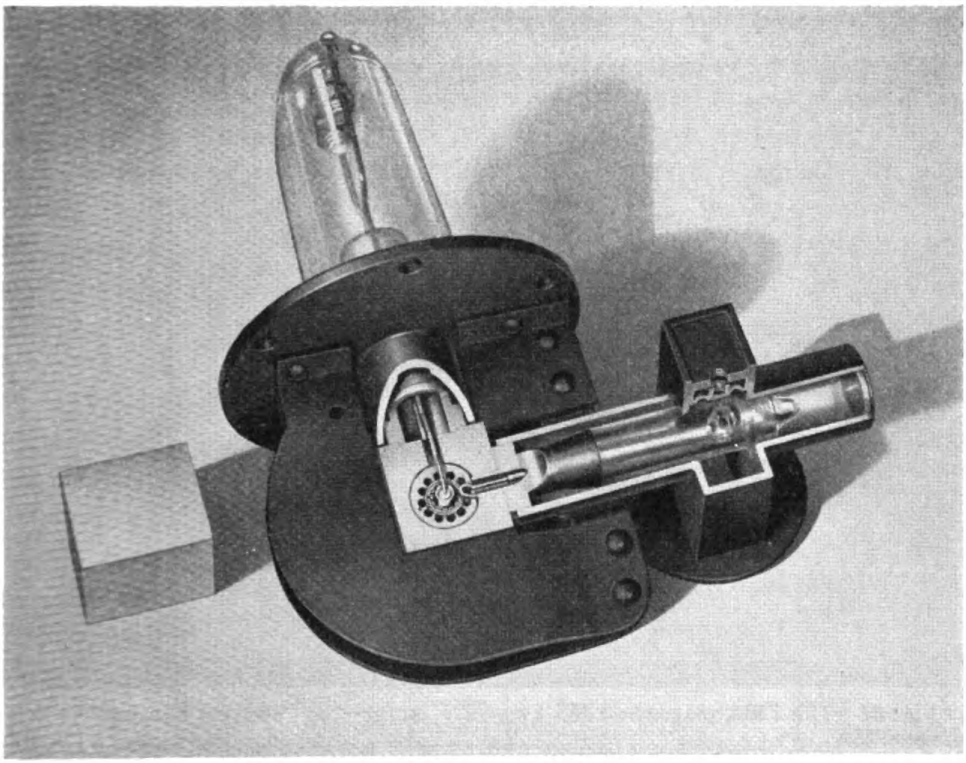

Fig. 66—A view of a cut-away 725A magnetron (55 kw., 9375 mc/s). Note the breaks in the double ring straps, the so-called "halo" loop above the hole of the output resonator, the step in the center conductor of the output coaxial providing the necessary impedance transformation, and the details of the coaxial to wave guide junction.

is shown in Fig. 68. Experience has indicated that it is entirely adequate for 150 kw. input at duty cycles up to 0.001 and, with later cathode designs, at pulse lengths up to 5μs. The RF spectrum is satisfactory even under rather extreme conditions of mechanical vibration and shock, and the operation under a variety of conditions is remarkably free from "moding". Difficulties have been encountered in attempts to push its power input with 5μs pulses much above 175 kw. although with short pulses at lenient duty cycle operation with as much as 300 kw. peak input power has been achieved.

Generated on 2019-09-21 09:24 GMT / http://hdl.handle.net/2027/mdp.39015077775156
Public Domain, Google-digitized / http://www.hathitrust.org/access_use#pd-google
Digitized by Google
Original from UNIVERSITY OF MICHIGAN

Many difficulties were encountered in the early stages of production above those of training personnel to handle small parts and to perform new types of operations. Maintenance of cathode centering through all operations had to be rigidly supervised since off-center cathodes resulted in poor operation. The size and position of the output loop were very sensitive variables directly affecting output power and pulling figure. The latter were also marked functions of variables in the transformer of the output circuit. It was found, for example, that variations in the glass, and particularly in the bead supporting the center conductor, were causing considerable

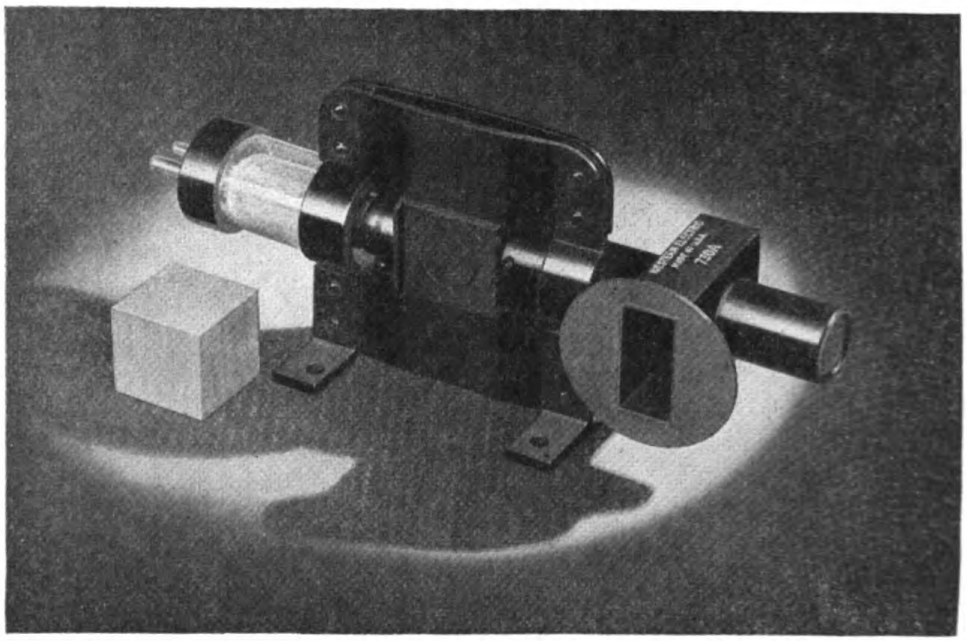

Fig. 67—The 730A magnetron (55 kw., 9375 mc/s)—the "straight through" version of the 725A.

spread in characteristics. Closer tolerance on the glass, involving the use of a molded bead, greatly improved this situation.

With the very narrow limits specified for the operating frequency of the magnetron, it was essential that the anode pretuning be done very precisely. Here, considerable difficulty was encountered with a pretuning arrangement in which the indication of resonance depended on the equivalent line length of the output circuit between the anode block and the detector in the wave guide. Variability in this electrical length caused the actual resonance to vary over a considerably wider range than the required 9375 $\pm$ 30 mc/s. By use of a detector connected at the output loop it was possible to reduce the percentage of magnetrons eliminated for being outside the frequency

Generated on 2019-09-21 09:25 GMT / http://hdl.handle.net/2027/mdp.39015077775156
Public Domain, Google-digitized / http://www.hathitrust.org/access_use#pd-google
Digitized by Google
Original from UNIVERSITY OF MICHIGAN

limits at final test from more than 50 per cent to less than 1 per cent. At one point in the development, when it appeared that the frequency spread could not easily be reduced, a tuning screw mechanism was designed with which the frequency of the resonator system could be varied by movement

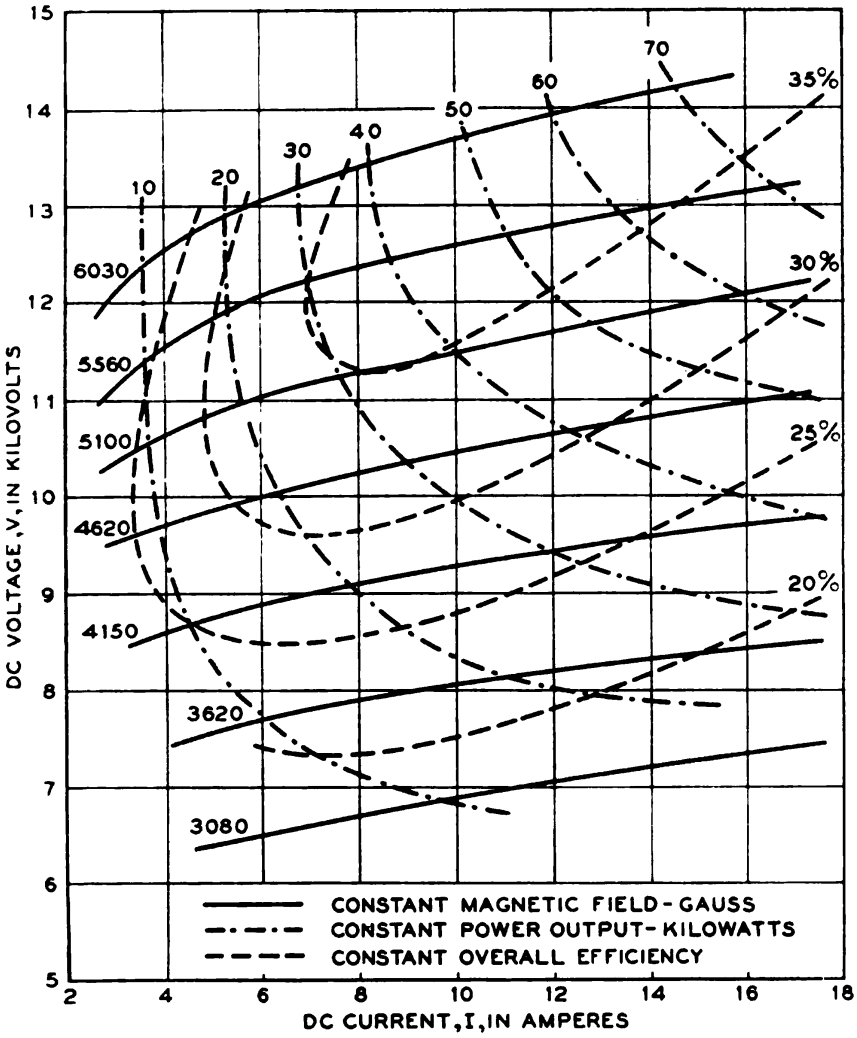

Fig. 68—A typical performance chart of the 725A and 730A magnetrons (9375 mc/s).

of a plug through the side wall of one resonator and which could be adjusted from outside the vacuum envelope at the final acceptance test. Although the mechanism was built, tested, and found to operate satisfactorily, the improvement of the pretuning technique made its adoption unnecessary.

During the initial stages of production it was verified that the pulling figure of the 725A and 730A could be adjusted within limits by variation of the position of the end plate shorting the wave guide section into which the

Digitized by Google
Original from UNIVERSITY OF MICHIGAN
Generated on 2019-09-21 09:32 GMT / http://hdl.handle.net/2027/mdp.39015077775156
Public Domain, Google-digitized / http://www.hathitrust.org/access_use#pd-google

coaxial output circuit of these magnetrons is terminated. It is possible by a displacement of 0.040 in. of the whole end plate to effect about a 6 mc/s change in pulling figure near the value of 15 mc/s. An end plate consisting of a convoluted diaphragm was constructed which could be adjusted at final test if necessary. By this means it was possible to make the adjustment without disturbing the airtight seal needed in some pressurized installations. The adjustable end plate is to be seen in the cutaway model of Fig. 66.

Despite initial difficulties, it was possible in the first nine months of production to increase the yield of shippable magnetrons meeting all the test specifications from a very low initial figure to over 85 per cent of all those completed and reaching final acceptance tests. Although subsequent tightening of the test specifications, such as the increase of pulse length at test from 1μs at 1000 pps to 2 μs at 325 pps, caused temporary setbacks in the percentage yield, it was nevertheless increased until it ran consistently better than 95 per cent.

Although better magnetrons have since been built in the 3 cm. wavelength range, the 725A occupies a special place in magnetron development at these wavelengths. It represents the first high efficiency, π mode, strapped magnetron for 3 cm. operation, and as such has served as the prototype of most of the subsequent 3 cm. magnetron developments in the United States and Great Britain.

The 725A was manufactured by the Western Electric Co. in this country and the Northern Electric Co. of Canada. The Raytheon Mfg. Co. used Bell Laboratories' design information to produce a 725A magnetron but redesigned the resonator system to use a vane type more adapted to their manufacturing practice. The total number of 725A magnetrons produced in these three plants was over 300,000, indicating the extent to which it was used during the war.

17.2 *The 2J48, 2J49, 2J50, and 2J53/725A Magnetrons:* Following completion of the 725A magnetron at 3.2 cm., requests were made for three similar magnetrons. These were to have the same characteristics as the 725A, differing only in their frequencies of operation.

The 2J48 is an exact duplicate of the 725A but has a narrower spread in frequency, $\pm$ 5 mc/s, around a mean value of 60 mc/s lower than the nominal 725A frequency of 9375 mc/s. The 2J48 was never manufactured by the Western Electric Co.

The 2J49 and 2J50 are 725A types operating at 3.3 cm. and 3.4 cm., respectively. These new wavelengths were met by a new resonator design involving larger resonator holes than in the 725A. The nominal wavelength of the new design was 3.35 cm., tuned either into the 3.3 cm. or the 3.4 cm. band by strap manipulation.

Generated on 2019-09-21 09:32 GMT / http://hdl.handle.net/2027/mdp.39015077775156
Public Domain, Google-digitized / http://www.hathitrust.org/access_use#pd-google
Digitized by Google
Original from UNIVERSITY OF MICHIGAN

In an effort to get high power from the 725A magnetron operating on long pulses, considerable work was done to build a cathode for a power input of 225 kw. While a few thousand such magnetrons were made and tested at the higher test condition, entirely satisfactory operation was never achieved. Magnetrons tested at 225 kw. input were coded the 2J53/725A but after the first production run were not manufactured again. The 4J50 and 4J52 magnetrons are now available for this range of operating conditions.

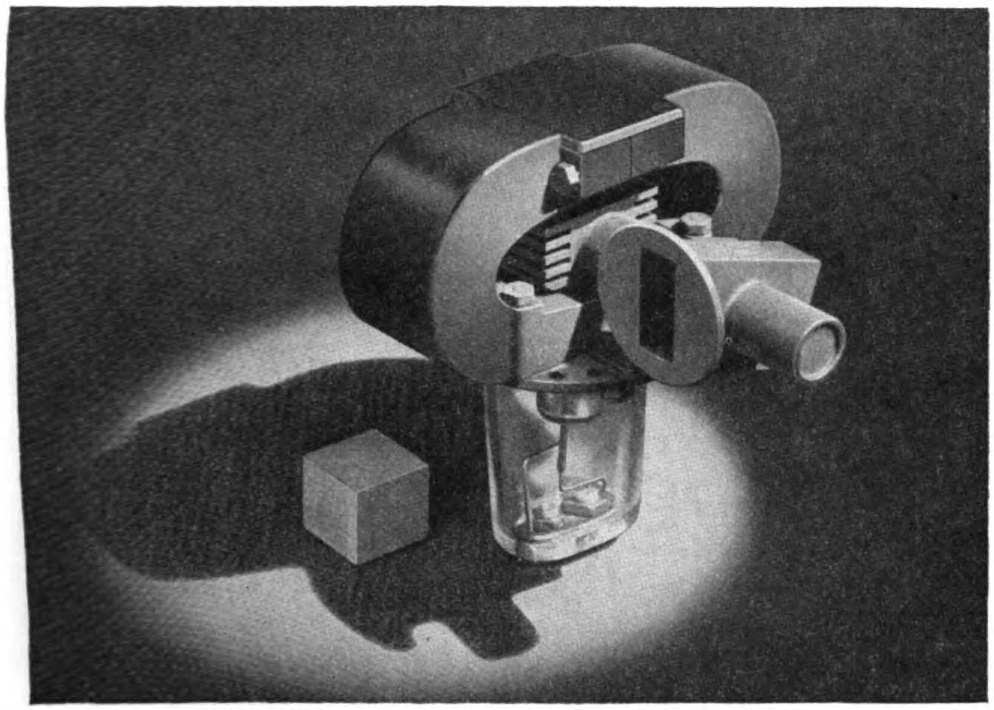

Fig. 69—The 2J55 magnetron (55 kw., 9375 mc/s)—the "packaged" version of the 725A. Compare with the size of the 725A and its magnet shown in Fig. 44.

17.3 *The 2J55 and 2J56 Magnetrons:* The 2J55 and 2J56 are by-products of the development of a tunable 3 cm. magnetron, the 2J51, described below. The 2J51 design, being "packaged" and thus lighter and more compact than the 725A and its magnet, with which it is interchangeable, was ideally suited for conversion into a fixed frequency, "packaged", 3 cm. magnetron. The only design changes required were those associated with the removal of the tuning mechanism and the change in dimensions of the resonator system needed to bring the wavelength to the proper value. The two magnetrons designed in this way for operation at the wavelengths 3.2 and 3.25 cm. were coded the 2J55 and 2J56, respectively. Each weighs 3 lbs. 12 oz. as compared to the weight of 11 lbs. 2 oz. of the 725A magnetron and its magnet.

Generated on 2019-09-21 09:33 GMT / http://hdl.handle.net/2027/mdp.39015077775156
Public Domain, Google-digitized / http://www.hathitrust.org/access_use#pd-google
Digitized by Google
Original from UNIVERSITY OF MICHIGAN

A photograph of the 2J55 magnetron is shown in Fig. 69 and operating data are included in TABLE III.

18. TUNABLE MAGNETRONS FOR WAVELENGTHS NEAR 3 CENTIMETERS

18.1 *The 2J51 Magnetron:* As in the 20 to 45 cm. wavelength region, the demand arose for tunable magnetron replacements when fixed frequency magnetrons had become available in the 3 cm. band. A significant step toward satisfying this demand was taken at the NDRC Radiation Labora-

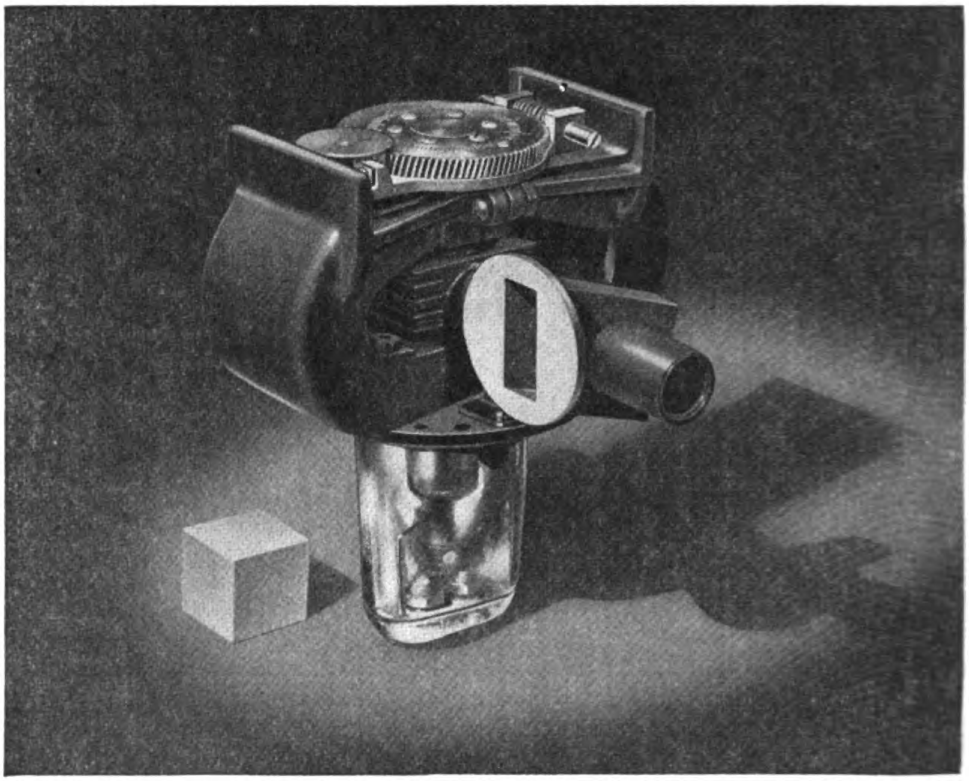

Fig. 70—An external view of the 2J51, tunable, "packaged" magnetron (55 kw., 8500 to 9600 mc/s).

tory at Columbia University in 1943 when a tuned, "packaged" magnetron was built around a 725A anode structure and output circuit. The tuning scheme used was that of variation of resonator inductance, as discussed in PART I, by a so-called tuning head consisting of a set of pins which project into the holes of the resonator system. The mechanism for driving the tuning head is contained inside one of the magnet pole pieces. The other pole piece carries the axial cathode mount. Two magnets are clamped to opposite sides of the pole pieces in the usual "packaged" construction. These and other details are shown in the photographs in Fig. 70 and 71 of complete and cutaway models of the magnetron, coded the 2J51, as it was put into production at the Western Electric Co.

Generated on 2019-09-21 09:33 GMT / http://hdl.handle.net/2027/mdp.39015077775156
Public Domain, Google-digitized / http://www.hathitrust.org/access_use#pd-google
Digitized by Google
Original from UNIVERSITY OF MICHIGAN

From the inception of the project until the bulk of the work of developing the tunable 3 cm. magnetron was transferred to the Bell Laboratories, a number of problems had been encountered and solved at the Columbia Laboratory. It had been shown that tuning a 725A type magnetron was

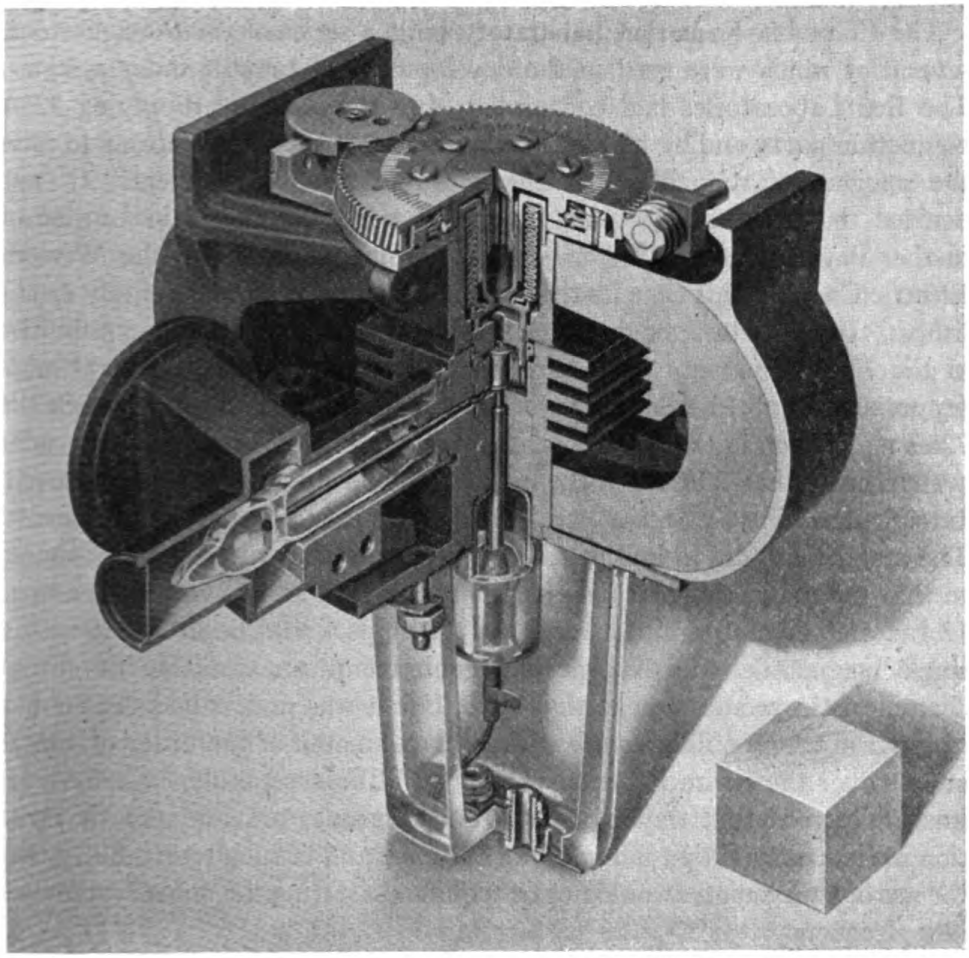

Fig. 71—A view of a sectioned 2J51, tunable, "packaged" magnetron (55 kw., 8500 to 9600 mc/s). Features of interest to be seen are: the tuning pins, the drive mechanism and vacuum bellows, the axial cathode mount, the glass bead support of the center conductor of the coaxial output line, and the sheathed permanent magnet construction.

feasible by the means chosen. The range of wavelength from 3.13 to 3.53 cm. could easily be spanned. The variation in frequency was found to be very nearly linear with position of the tuning pins. It was shown how a spurious resonance of the pin structure occurring within the frequency range could be displaced so as to cause no difficulty. Although no work of revision had been done on the 725A output circuit used in the tunable magnetron, it was demonstrated that tolerably "flat" characteristics of

Digitized by Google
Original from UNIVERSITY OF MICHIGAN
Generated on 2019-09-21 09:33 GMT / http://hdl.handle.net/2027/mdp.39015077775156
Public Domain, Google-digitized / http://www.hathitrust.org/access_use#pd-google

output power and pulling figure against frequency could be obtained with it. The fundamental mechanical problems of "packaging" the magnetron and providing facilities for driving the tuning head were shown to be feasible and a smooth working and resettable driving mechanism designed and constructed.

The Columbia Radiation Laboratory built a series of these magnetrons, several of which were used in the development of tunable radar systems. The Bell Laboratories had cooperated from the start by supplying 725A magnetron parts, and by making anode inserts of special dimensions to raise the maximum attainable wavelength of the resonator system. It was decided that the Bell Laboratories should take over the main burden of further development of the magnetron for manufacture by the Western Electric Co. By this time its specifications had been quite definitely established. It was to be a magnetron with the general power output capabilities of the 725A, tunable over the frequency range from 8500 to 9600 mc/s (approximately 3.13 to 3.53 cm.). It was to be interchangeable with the 725A magnetron in the sense that it could be installed directly in any radar system using the 725A when the magnetron and its magnet were removed. Interchangeability, as usual, was one of the most annoying requirements. The magnetron was to be "packaged" and provided with magnetic shunts so that the magnetic fields necessary for operation at 10 kv. and 10 amps., 12 kv. and 12 amps., and 14 kv. and 14 amps. could be attained with a single magnet design. No specific requirements on variation of output characteristics were made at that time, but it was understood that only a magnetron whose pulling figure varied by an amount of the order of 3 mc/s or less over the entire frequency band would be acceptable. Similarly, it was understood that the tuning mechanism should provide smooth variation in frequency with a minimum of backlash and of such resettability that the use of a wavemeter would not be required in setting the radar system to a new frequency.

During the course of the development at the Bell Laboratories it became necessary to redesign the magnetron in a number of important respects. The requirement that the magnetron operate at 14 kv. and 14 amps. demanded a magnetic field for which the magnet weight would be prohibitive. Consequently, anode and cathode radii were scaled from those of the 725A magnetron by the factor 1.2. The larger cathode resulting from this redesign made easier the problem of attaining the maximum of 200 kw. peak input power required by the specifications. However, it caused a recurrence of the difficulty with a resonance of the tuning pin structure appearing in the 8500 to 9600 mc/s range. This had been found at the Columbia Laboratory to be a resonance of the capacitance between the pins and anode structure

Digitized by Google
Original from UNIVERSITY OF MICHIGAN
Generated on 2019-09-21 09:33 GMT / http://hdl.handle.net/2027/mdp.39015077775156
Public Domain, Google-digitized / http://www.hathitrust.org/access_use#pd-google

with the inductance of the end space region through which the pins project from the magnet pole piece into the resonators. As before, the frequency of this resonance was removed by filling the end space with a copper ring or collar.

In the course of study of this resonance and of output circuit characteristics, an extensive program of testing of non-oscillating experimental models, whether operable or not, was carried out to supplement the data of oscillation tests. From these measurements, three important types of data were obtained, namely, the variation of pulling figure with frequency, the amount of RF energy loss introduced by the insertion of the tuning pins, and the variation of frequency with position of the tuning head. The first of these data, combined with measurements of the output circuit transformer characteristics made on simulated and adjustable models, yielded a complete understanding of the functioning of the output circuit. The effect of coupling loop size and of the variation of the dimensions of the coaxial to wave guide junction on the performance of the magnetron over the frequency range were determined. Although other designs of output circuits of the general 725A type were experimented with, it was possible to adjust the parameters of the original 725A output circuit to give a reasonably flat characteristic with frequency. In Fig. 72 are shown the variation of pulling figure and Q_{ext} over the frequency band.

The variation of unloaded Q with frequency, obtained in the above mentioned non-oscillating tests, indicated that stainless steel pins or even such pins copper plated to a considerable thickness were unsatisfactory. It was found that under the heat treatment occurring during brazing operations the copper plate and steel diffused through each other so as to increase markedly the surface resistance of the pins. Copper sheathed pins were found to be satisfactory. Solid copper was finally used as it was found to possess sufficient strength under mechanical shock test. Even so, as Fig. 72 indicates, the Q_0 of the resonator system falls off with increasing frequency and pin penetration.

Determination of the variation of frequency with position of the tuning pins dictated the design of the drive mechanism to provide the necessary range of motion. It was found that, with a pin diameter of 0.064 in. moving in resonator holes of 0.088 in. diameter, the frequency band could be spanned in a total travel of 0.110 in. Fig. 72 shows the nearly linear relationship between frequency and pin penetration.

The drive mechanism of the early Columbia models was redesigned to make possible its fabrication by a single brazing operation in a jig and to provide a sleeve rather than a thread bearing. The backlash achieved in the final design is such that one may reset the tuning head for a given frequency

Digitized by Google
Original from UNIVERSITY OF MICHIGAN
Generated on 2019-09-21 09:33 GMT / http://hdl.handle.net/2027/mdp.39015077775156
Public Domain, Google-digitized / http://www.hathitrust.org/access_use#pd-google

to within 1 mc/s which corresponds to a displacement of the pins of 0.0001 in. and to 0.1 turn of the worm wheel drive. The tuning mechanism is provided with a positive stop at each end of the tuning range. The frequency band is covered in five revolutions of the main drive screw and gear. A flexible vacuum envelope is provided by means of sylphon bellows. Details of the design may be seen in the sectioned model shown in Fig. 71.

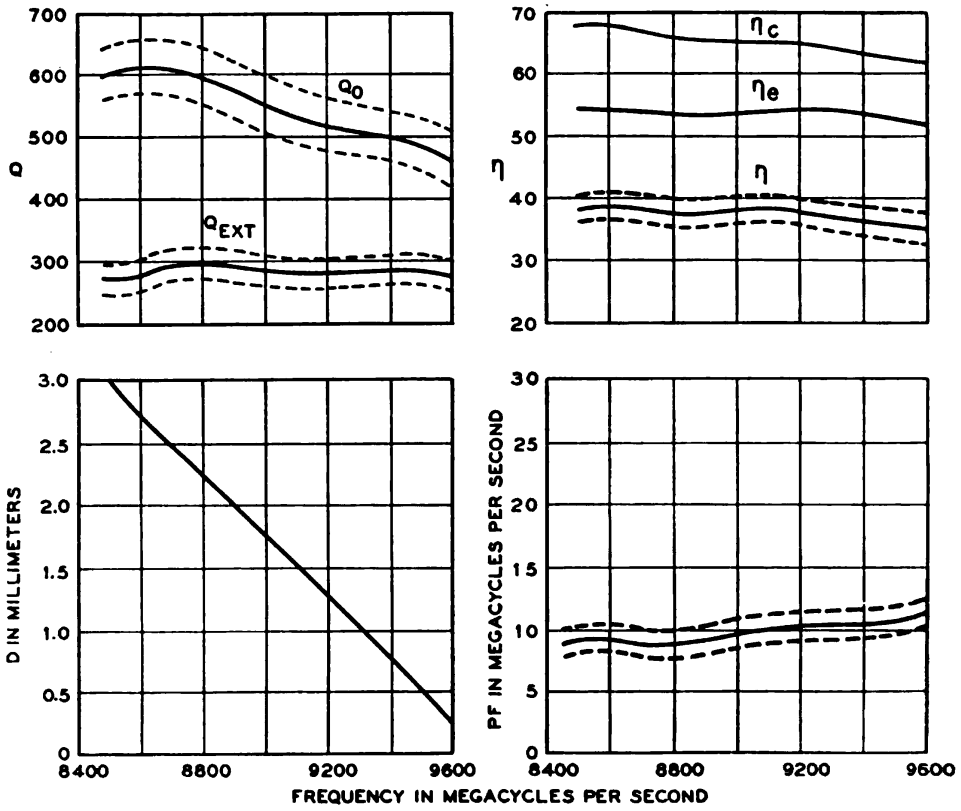

Fig. 72—Smoothed characteristics of the 2J51 tunable magnetron (55 kw., 8500 to 9600 mc/s) throughout its frequency band. Shown is the dependence upon frequency of the unloaded Q, Q_0; of the external Q, Q_{ext}; of the circuit efficiency, η_c; of the electronic efficiency, η_e; of the over-all efficiency, η; and of the pulling figure , PF. Also shown is the dependence of the operating frequency upon position of the tuning pins, D, measured from the position of maximum intrusion. The dashed lines on either side of the experimental curves indicate the range of possible variation of the data. The curves for η_c and η_e have been determined from the experimental results by the use of equation (25) of PART I and the relation $\eta = \eta_e \eta_c$.

The elimination of radial cathode support leads and the use of the magnetic pole pieces as the end covers of the magnetron body made possible a large reduction in the magnet gap and magnetomotive force required to produce the necessary magnetic field. Because of the requirement of interchangeability with the 725A magnetron, a very awkward V-shape magnet design in which the leakage flux was tremendous could not be avoided.

Digitized by Google
Original from UNIVERSITY OF MICHIGAN
Generated on 2019-09-21 09:33 GMT / http://hdl.handle.net/2027/mdp.39015077775156
Public Domain, Google-digitized / http://www.hathitrust.org/access_use#pd-google

Fortunately, before production commenced, relaxation of the interchangeability requirements made a change in the magnet form possible, and the much more efficient U-shape of those shown in Fig. 70 was adopted.

In performance, the 2J51 magnetron is essentially a 725A capable of operating over a 12 per cent frequency band. TABLE III gives two sets of operating conditions available through the use of the magnetic shunts. Fig. 72 shows several circuit characteristics of the magnetron over the frequency band. Also shown is the variation in over-all operating efficiency. The slight drop in efficiency observed as the frequency increases is due primarily to the decrease in Q_0. The electronic efficiency increases slightly with increasing frequency. The performance chart of the magnetron at its intermediate magnetic field is very similar to that of the 725A at the same field value, as shown in Fig. 68. The performance of the 2J51, when connected to a long, mismatched line exhibits a periodicity in power output, pulling figure, and frequency variation as the tuning is changed. This is expected in such a case because of the resulting changes occurring in the electrical length of the line with changing frequency. If the mismatch is sufficiently great, the condition may exist in which periodic regions of the frequency spectrum are completely unattainable, as discussed in section 10.2 *Frequency Sensitive Loads.*

The 2J51 represents an attempt to design considerable versatility into one magnetron. As has been described in the discussion of the 2J55 and 2J56, the development of the 2J51 provided the opportunity to make available "packaged" magnetrons of fixed wavelengths near 3 cm. by the omission of the tuning mechanism.

19. MAGNETRONS FOR WAVELENGTHS NEAR 3 CENTIMETERS—100 TO 300 KILOWATTS

19.1. *The 4J50, 4J52, and 4J78 Magnetrons:* In the later stages of development of the 725A, it had been demonstrated that a high efficiency scaled magnetron of wavelength near 3 cm. was feasible. It also had become evident that, freed from the hampering restrictions on input power and mechanical interchangeability, a magnetron of considerably greater output power capabilities could be made. The achievement of a magnetron design capable of delivering at least 200 kw. output power at a duty cycle of 0.001 or greater was set as a first objective. This was achieved with a good margin. During its entire course, the program was actively participated in by members of the Radiation Laboratory at M. I. T. working in residence at the Bell Laboratories.

The objective of 200 kw. peak output power at the factory test was not considered to be the maximum obtainable from a 3 cm. magnetron but

Digitized by Google
Original from UNIVERSITY OF MICHIGAN
Generated on 2019-09-21 09:34 GMT / http://hdl.handle.net/2027/mdp.39015077775156
Public Domain, Google-digitized / http://www.hathitrust.org/access_use#pd-google

was largely determined by the state of development of systems and components when the work began. It was desirable to produce a magnetron which, while marking a very substantial gain over the 725A in power output, should at the same time be of reasonable weight, air-cooled, and capable of operation with a pulser of modest dimensions and of working into the system components in existence or under development.

The design began with the choice of a resonator system having sixteen resonators. The anode diameter was chosen for an operating voltage range of 20 to 25 kv. The increase in number of resonators from twelve to sixteen and operation at higher voltage necessitated a considerable increase in cathode diameter over that of the 725A. The length of the anode was left as before because it was felt that the desired increase in total cathode emission would be available from the increase in cathode area and that the magnet weight ought to be kept as low as possible.

Experimental models incorporating these design changes were built in the 725A type structure with radial cathode mount, "halo" coupling loop and coaxial output terminating in a junction to wave guide. The performance of these early models was satisfactory. Operating efficiency better than that of the 725A mgnetron was achieved over the range of currents from 4 to 40 amps.

However, it was easily to be seen that the 725A type structure was by no means the ideal for a 3 cm. magnetron of increased output power. The output circuit was marginal in its power handling capabilities; it could transmit no more than 300 kw. Furthermore, the opportunity presented itself of eliminating other troublesome features such as the "halo" loop and the coaxial to wave guide junction by designing a wave guide output whose critical dimensions are machined to size. The type of cathode structure of the 725A was limited in its heat dissipation in comparison with the axial type of cathode mount made possible by the use of magnet "packaging". In addition, the axial type cathode mount is superior from the standpoints of DC voltage breakdown and economy of space. Considerations of weight also favored the "packaged" structure, in which the magnet pole pieces form an integral part of the magnetron structure. Many of these first experimental models suffered from a drooping voltage-current characteristic at constant magnetic field in the region of low currents. This effect and its attendant loss of operating efficiency became progressively worse as the magnetron was operated. It was hoped that the parasitic electron emission from the cathode end disks, believed from experiments with non-emissive coating materials to be responsible for the effect, could be eliminated or reduced in an axially mounted cathode.

Accordingly, an entirely new design was undertaken, built around the

Generated on 2019-09-21 09:34 GMT / http://hdl.handle.net/2027/mdp.39015077775156
Public Domain, Google-digitized / http://www.hathitrust.org/access_use#pd-google
Digitized by Google
Original from UNIVERSITY OF MICHIGAN

sixteen resonator anode structure used in the early work but including the features of "packaging," axial cathode mount, and wave guide output. A number of vexing but nevertheless interesting problems was encountered. Principal among these were the tendency to operate in another mode under certain conditions and the problem of obtaining satisfactory magnetic field uniformity in a design which necessitated the removal of a considerable portion of the center of the magnet pole piece to accommodate the axial cathode mount. Each of these difficulties was surmounted as is described in the detailed discussion later. The resonator system was redesigned quite late in the development to take advantage of the possibility of operating at a lower electronic conductance and hence higher RF voltage for the same output power. The advantages of this step were a reduction in the tendency of the magnetron to "mode" and an increase in unloaded Q.

The development program briefly sketched above resulted in three coded magnetrons, the 4J50, 4J52, and 4J78. The 4J50 and 4J78 magnetrons, identical except for frequency, were built with magnets large enough to permit operation near the maximum power capabilities of the design and with larger input leads to withstand the higher DC voltage required. The 4J52 magnetron, although incorporating the same internal design as the other models, was built with smaller magnets for operation at a set of conditions easily attainable with the higher power design but beyond the reach of the 725A. Developmental work on all three magnetrons was conducted simultaneously.

In the 4J50 magnetron a hole and slot resonator system was adopted. The remarkable freedom of the 725A magnetron from "moding" difficulties had made it appear desirable to retain as large a mode frequency separation as possible. Equivalent circuit theory indicated that to do this the increase in the number of resonators from twelve to sixteen would necessitate about twice the strap capacitance of the 725A. This would have required extremely wide straps for which the recess channel in the anode structure would be very difficult to trepan. For this reason the resonator system was strapped less heavily; the $n = 8$ and $n = 7$ mode frequencies differed by 19 per cent rather than 25 per cent as in the 725A.

In none of the early models built into 725A type structures was any "moding" or "misfiring" observed. When axial cathode and wave guide output were introduced, however, "moding" was experienced both in those with no strap breaks and those with the usual double break at one end of the anode. By enlarging the cathode diameter such that the ratio of cathode to anode radii increased from 0.60 to 0.66, the difficulty was removed in models with broken straps, but it was not possible to eliminate it in those with unbroken straps. Decreasing the r_c/r_a ratio increased the tendency to "mode."

Digitized by Google
Original from UNIVERSITY OF MICHIGAN
Generated on 2019-09-21 09:34 GMT / http://hdl.handle.net/2027/mdp.39015077775156
Public Domain, Google-digitized / http://www.hathitrust.org/access_use#pd-google

It might be surmised that the trouble in the unbroken strap case was due to a component of $n = 7$ which did not couple to the output circuit. The phenomenon was studied in an operating magnetron with small electrostatic probes built into several resonators. The $n = 7$ components were identified, their relative intensities being approximately those expected. It is of some interest to note that the "moding" encountered here differed from that seen in magnetrons of longer wavelength. The magnetron seemed invariably to start in the π mode, falling into oscillation in the $n = 7$ mode more rapidly as loading increased. As might be expected from this behavior, the mode boundary on a performance chart is little affected by the rate of rise of the pulse as it had been in other magnetrons. Later evidence made it appear that the change in the operating voltage of the $n = 7$ mode brought about by the redesign of the resonator system was a decided improvement.

The necessity of using strap breaks led to an unforeseen difficulty. Under the influence of RF electric forces, the overhanging ends of the straps at the strap breaks moved together and shorted, causing failure after only a few hours of operation. The trouble was eliminated by removing the overhanging portions of the straps with no noticeably harmful effects.

In a 3 cm. magnetron, strapped as heavily as the 4J50, circuit losses become very important in determining the over-all efficiency. A noticeable improvement in unloaded Q was effected when an atmosphere of prepurified N_2 was substituted for the CO_2-alcohol mixture which had previously been used to prevent oxidation during the final brazing. The CO_2-alcohol method had been abandoned for another reason, namely, that chemical analysis showed carbon deposited on the steel pole-pieces underneath the copper plating.

If one determines the circuit efficiency for matched load by impedance measurements on a non-oscillating magnetron [see equation (25) of PART I], one may then calculate its value for any load. From measurements of over-all efficiency as a function of load conductance, the dependence of the electronic efficiency on this conductance may be determined. The curve of Fig. 19 was obtained in this way for the 4J50. The fact that the electronic efficiency, as seen in Fig. 19 is practically independent of load, that is to say, of electronic conductance, together with some observations of the load sensitivity of the "moding" in the 4J52; led to consideration of a new design for the resonator system. It was found invariably that the boundary for mode change in the 4J52 magnetron moved to higher currents as the load impedance was changed to values further removed from the frequency sink and power maximum in any direction on the Rieke diagram. This suggests that, as the circuit conductance [G_e of equation (36)] is

Digitized by Google
Original from UNIVERSITY OF MICHIGAN
Generated on 2019-09-21 09:34 GMT / http://hdl.handle.net/2027/mdp.39015077775156
Public Domain, Google-digitized / http://www.hathitrust.org/access_use#pd-google

increased, the decrease in RF voltage in the π mode places that mode at a disadvantage in competition with the $n = 7$ mode.

As a result of these considerations, a new resonator system was designed in which the electronic conductance at the normal operating point was to be two thirds of that in the first design. To maintain the pulling figure invariant, it was necessary to reduce the total resonator capacitance. Although all of this capacitance could not be removed from the straps without reducing the mode frequency separation too drastically, a good proportion of it could be. From this, one might expect a gain in unloaded Q since the straps are the lossiest part of the circuit.

The new resonator system is more satisfactory than the old. Mechanically, it is neater in that the outer strap does not extend into the holes of the hole and slot resonators. A definite increase in over-all efficiency attributable to a greater Q_e was observed. The mode separation is 17 per cent, much greater than the expected value. An analysis of data on the $n = 8$, 7, and 6 mode wave lengths, by means of equivalent circuit theory, indicated that this is due to the straps being effectively shorter although their physical length is unchanged in the new design. This is plausible, however, for in the new design the outer strap is connected at a higher voltage point along the resonator.

The cathode structure of the 4J50, 4J52, and 4J78 magnetrons represents a radical departure from previous designs. It was desirable from the production standpoint to be able to build the cathode structure completely as a subassembly before mounting it in the magnetron. This entailed making holes in the magnet pole pieces large enough for the cathode to pass through; these holes were, in fact, made of the same diameter as the anode (0.319 in.). Since no radial cathode support leads were required, it was possible to reduce the end spaces to a height of 0.065 in., making the magnet pole gap 0.380 in. It was recognized that the large hole to gap ratio would result in two bad effects: first, a loss of magnetic field and, second, an antibarreling of the magnetic field which results in an axial force acting on the electrons, directed away from the center of the interaction space. Both of these difficulties were surmounted by the use of cathode end structures made of high Curie temperature permendur (50 per cent iron, 50 per cent cobalt).

The permendur pieces, toroidal in shape, are mounted at the two ends of the cathode (see Figs. 75 and 78). Their cross section and location, necessary for a nearly uniform field over 80 per cent of the gap and a focusing field over the remainder, were determined in electrolytic tank experiments. Since the permendur pieces fill up a part of the hole in the magnet pole piece and have a separation less than the pole gap, they contribute substantially

Digitized by Google
Original from UNIVERSITY OF MICHIGAN
Generated on 2019-09-21 09:34 GMT / http://hdl.handle.net/2027/mdp.39015077775156
Public Domain, Google-digitized / http://www.hathitrust.org/access_use#pd-google

to the magnetic field in the anode-cathode region. The effective gap is reduced from 0.380 in. to 0.340 in. by their presence, resulting in about a 20 per cent decrease in magnet weight. While their primary function is magnetic, the permendur pieces also serve as normal cathode end disks preventing electrons from reaching the pole pieces. Their smooth contour gives a good DC voltage breakdown condition between anode and cathode. Finally, they are mounted in such a way that there is some thermal isolation from the cathode and that the migration path from cathode to external surface of the permendur is quite long. These features discourage electron emission from the cathode end structures.

Almost any degree of cooling may be obtained with an axially mounted cathode without the attendant disadvantages of the heavy tungsten leads which fill up the end spaces of a magnetron having radial cathode mounting. An upper limit to the cooling is set by the fact that the cathode must be raised to 1050°C in activation, using a heater which can be contained within the cathode sleeve without encroaching too much upon its wall thickness. The high temperature needed during activation sets certain limits upon the materials which may be used in the cathode structure. Since the cathode is mounted from one end only (this being dictated by assembly considerations), mechanical strength is exceedingly important. A cathode, once off center, is subjected to magnetic forces on the permendur ends which tend to pull it further off center. Fortunately, measurement at the magnetic fields used in normal operation shows that these forces are only of the order of one pound for a cathode position 0.015 in. off the axis, increasing to about 3.5 pounds when the permendur is in contact with the wall.

The first cathode surfaces used in these magnetrons were of the "mesh" type. Later, the newly developed, sintered nickel matrix type was used. More recently, considerations of strength have led to the introduction of molybdenum cathodes. The cathode assembly is brazed into a hollow metal cone in the base of which is a receptacle type heater and cathode connection. Because of the length of the supporting structure and the relatively high temperature at which it operates, there is considerable expansion and resultant motion of the cathode in the axial direction. The cathode is offset when cold to correct for this expansion. Performance is not very sensitive to cathode location, but in extreme cases of misalignment moding difficulties may be aggravated. The cathode structure is to be seen in Fig. 78 and is shown mounted in the magnetron in Fig. 75. Attention should be called to the external cathode input lead which is of heavy glass and Kovar construction sufficiently rugged to make unnecessary any protective housing.

In the wave guide output designed for the 4J50 magnetron, the necessary

Digitized by Google
Original from UNIVERSITY OF MICHIGAN
Generated on 2019-09-21 09:35 GMT / http://hdl.handle.net/2027/mdp.39015077775156
Public Domain, Google-digitized / http://www.hathitrust.org/access_use#pd-google

impedance transformation is accomplished by a quarter wavelength section opening directly into the output wave guide at one end and into the outside wall of one resonator at the other (see Fig. 30 and discussion in PART I). The small height of the resonator system from pole piece to pole piece makes it necessary to use a loaded line, in this case of H-shape cross section. The nature of the output circuit may be seen in the photograph of a cutaway model of the 4J52 in Fig. 75.

The transformation from the wave guide impedance of about 400 ohms through the iris formed by the junction of the H-shape and rectangular wave guides and through the $\lambda/4$ section inserts a resistance of about 2 ohms in series with the resonator to which the output circuit is connected. End effects make the desired transformer length differ slightly from $\lambda/4$. The length necessary to give a pure resistance at the input end was determined by measurements in a 10 cm. model with which the distance from the rectangular wave guide to the first voltage minimum in the H-section could be measured.

The vacuum seal in the wave guide output circuit was made at a circular window sealed in a Kovar cup, mounted between choke couplings as seen in Fig. 75. The diameter of the window and its thickness were chosen so that the reflection coefficient of the window would be quite low over a broad band of wavelengths near 3 cm. Insertion of a dielectric such as the glass window into the wave guide line increases the capacitance per unit length of the line. Compensation for this to bring the characteristic impedance back to the normal value is done by increasing the inductance per unit length over the same region. This may be accomplished by reduction of the long dimension of the wave guide resulting in a nearly square cross section. The circular opening, preferable for glass sealing, is a compromise, the critical diameter being determined by experiment. The relatively large size of the window makes it capable of withstanding RF voltage breakdown even at very high power.

Control of the output coupling is most readily effected by varying the width of the slot in the H-section. The over-all transformation properties of the H-section have been analyzed theoretically and the results confirmed by measurements on output circuit models. By means of this analysis it is possible to estimate fairly well the effect of changes in the slot width upon the pulling figure. To hold the latter within production limits of $\pm$ 2 mc/s, the slot must be held to $\pm$0.001 in.

The output circuit of the magnetron is formed by building up the assembly from sections in what has been called a "sandwich" type construction. The resonator system and the central portion of the output H-section are machined into one slab of copper. The "sides" of the H-section are

Digitized by Google
Original from UNIVERSITY OF MICHIGAN
Generated on 2019-09-21 09:35 GMT / http://hdl.handle.net/2027/mdp.39015077775156
Public Domain, Google-digitized / http://www.hathitrust.org/access_use#pd-google

milled into this piece on either end. This center slab is "capped" on each end by a slab of copper, in which are contained the magnet pole pieces and appropriate surfaces on which to build the rest of the magnetron. Some of the details of this structure may be seen in the cutaway model of Fig. 75.

Despite the large impedance transformations involved, the output circuit is quite frequency insensitive. As it appeared that these magnetrons might be made tunable, considerable attention was paid to this characteristic. Numerous tests of the output circuit and its component parts were

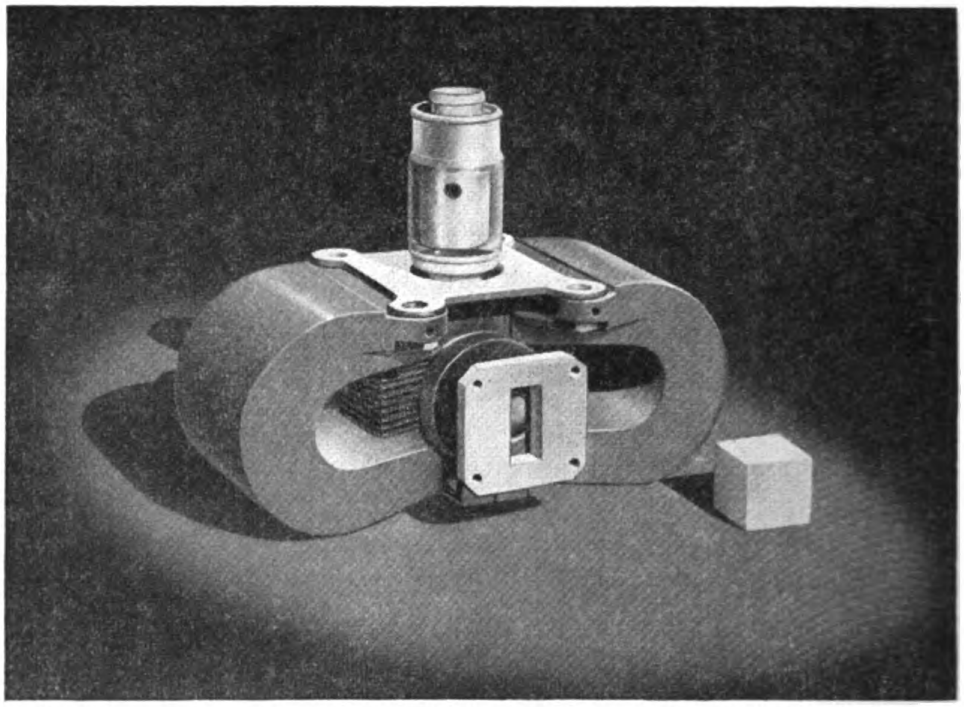

Fig. 73—An external view of the 4J50 "packaged" magnetron (280 kw., 9375 mc/s). Note the circular glass window in the wave guide output circuit and rugged axial input lead which requires no external protecting boot.

made over the 8500–9600 mc/s band. The iris and quarter wave length guide section were studied theoretically in this regard as well. The transformer properties of the window and choke coupling combination is the most frequency sensitive part of the entire output circuit. By adjustment of the distance from the H-section to the window, it was found possible to cancel some of the sensitivity of the two parts.

External views of the 4J50 (4J78) and the 4J52 magnetrons are shown in Figs. 73 and 74 respectively. The internal view of the 4J52 is shown in Fig. 75.

Except for magnet size and cathode supporting structure all three of

Generated on 2019-09-21 09:35 GMT / http://hdl.handle.net/2027/mdp.39015077775156
Public Domain, Google-digitized / http://www.hathitrust.org/access_use#pd-google
Digitized by Google
Original from UNIVERSITY OF MICHIGAN

these magnetrons are essentially identical. Geometrical and performance data are given in Table III. As may be seen, these magnetrons represent an increase in power capabilities by a sizable factor over the 725A. The 4J52 magnetron has been used extensively under the severe conditions of 5 μs pulse duration, a repetition rate of 200 pulses per second, 15 kv. and 15 amps. input. Under these conditions it has not been possible to eliminate entirely a tendency to arc, although good performance is obtained.

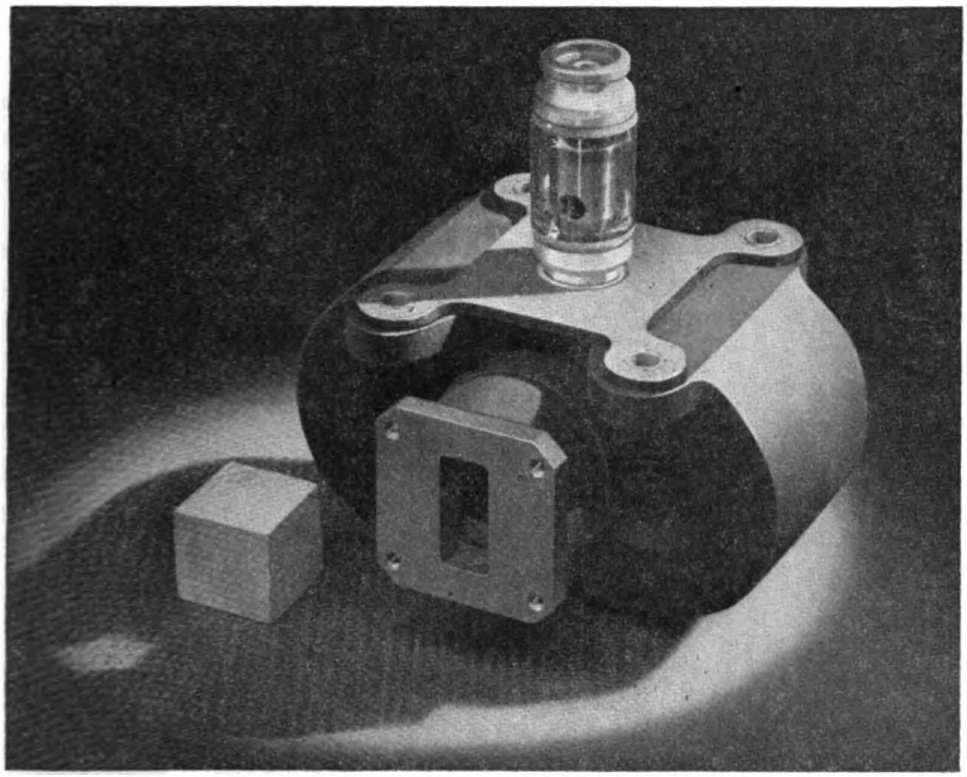

Fig. 74—The 4J52 "packaged" magnetron (100 kw., 9375 mc/s).

In most respects these magnetrons represent the optimum achieved in magnetron design for wavelengths near 3 cm. during the war. Largely because of the lack of hampering electrical and mechanical restrictions, it was possible to make use of all the latest and best techniques in the design of each of its parts. Thus each possesses the desirable features of "packaging," axial cathode mount, wave guide output, and high efficiency at low pulling figure.

20. Magnetrons for Wavelengths near 1 Centimeter

20.1 *Preliminary Work:* Intensive work on magnetrons for wavelengths near 1 cm. began when a joint program with the Radiation Laboratory at

Digitized by Google
Original from UNIVERSITY OF MICHIGAN
Generated on 2019-09-21 09:35 GMT / http://hdl.handle.net/2027/mdp.39015077775156
Public Domain, Google-digitized / http://www.hathitrust.org/access_use#pd-google

Columbia University was undertaken to prepare for manufacture a variation of a magnetron developed there. Prior to this, some work primarily of an exploratory nature had been done in our Laboratories. When it had been demonstrated that scaling from the 10 cm. range yielded an efficient 3 cm. magnetron, similar attempts were made in scaling to wavelengths of 1 to 2 cm. Magnetrons of such wavelengths, obtained by scaling from eight

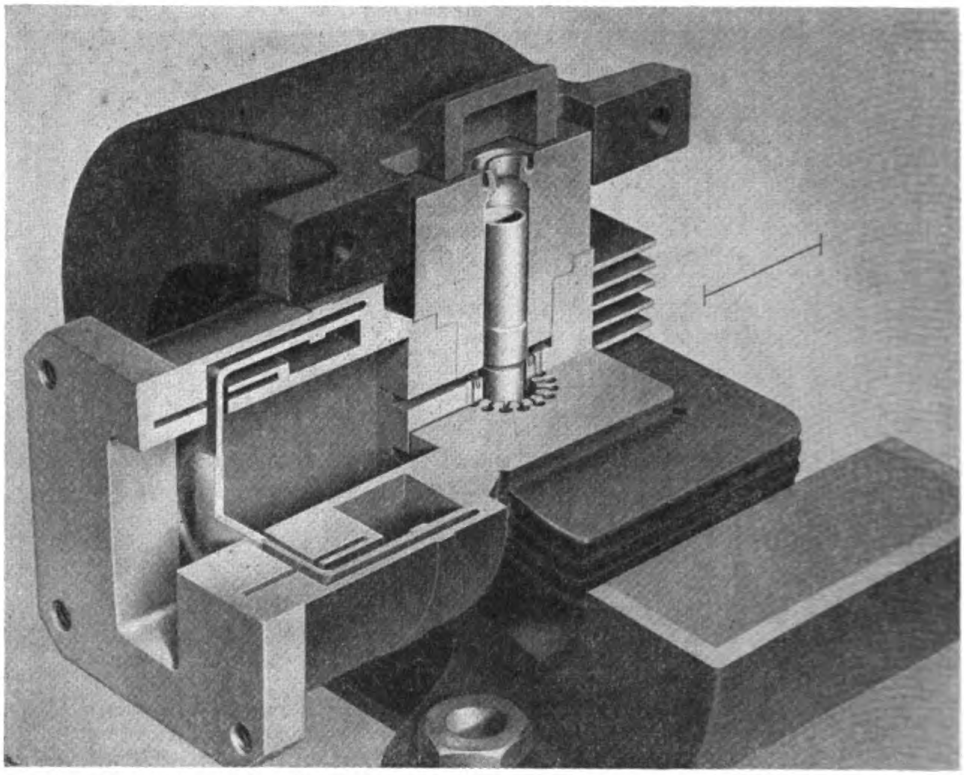

Fig. 75—A view of a cut-away 4J52 "packaged" magnetron (100 kw., 9375 mc/s) which in internal details is essentially like the 4J50 magnetron (280 kw., 9375 mc/s). Of special interest are: the axial cathode construction including permendur end pieces and radiative extension; the quarter wavelength transformer of H-shape cross section (between the output resonator and the line wave guide); and the wave guide window construction with associated chokes.

resonator, 10 cm. models like the 706A-C, were unstrapped while others were strapped with the early British type of strapping and with double ring type strapping. Others were made by scaling from twelve resonator, 3 cm. models and were strapped with both double and single ring straps. The output circuits used were of the loop and coaxial type.

Although some of these magnetrons were faulty, primarily in their output circuits, the majority oscillated. One magnetron of the unstrapped eight resonator variety, the most successful type, was operated over a consider-

Digitized by Google
Original from UNIVERSITY OF MICHIGAN
Generated on 2019-09-21 09:40 GMT / http://hdl.handle.net/2027/mdp.39015077775156
Public Domain, Google-digitized / http://www.hathitrust.org/access_use#pd-google

able period in our Laboratories. Although no magnetron was developed for manufacture from this work, the experience gained was very useful in the concurrent work at 3 cm. where a similar development program of small magnetrons was under way. Specific developments in this category which should be mentioned are: the use of inserts in which the magnetron resonator system is machined, separable from the rest of the magnetron structure; the use of a double lead cathode input seal to reduce over-all thickness; assembly tools for cathode and strap alignment; and the work with small oxide coated cathodes. The work was discontinued here because of extensive commitments for work at 3 cm. and because an active and successful program of development of magnetrons near 1 cm. wavelength was under way at Columbia University.

The work at the Columbia Radiation Laboratory from the start had been concentrated on magnetrons of very short wavelength. The first Columbia magnetron that was reasonably successful was unstrapped, having a vane type resonator system. It was manufactured in small quantities as the 3J30. Later, the "rising sun" resonator system was discovered as a means of obtaining mode frequency separation. The small scale manufacture was then shifted to the new anode structure, the new magnetron being the 3J31. It was a satisfactory magnetron operating at about 14 kv. and 14 amps., in a magnetic field of 7200 gauss, at a pulling figure of approximately 25 mc/s, and a power output of about 35 kw. The magnetic field was obtained by an external, separable magnet. The cathode was supported by the conventional radial leads.

In addition to the work on the "rising sun" structure, work had continued at the Columbia Laboratory on strapped resonator systems for use at wavelengths near 1 cm. Performance of these magnetrons was quite comparable to that of the "rising sun" variety.

20.2. *The 3J21 Magnetron:* The Bell Laboratories undertook, in collaboration with the Columbia Laboratory, to design a "packaged" version of the 3J31 magnetron for manufacture by the Western Electric Co. At the time, it had not been decided whether the new magnetron should have a strapped or a "rising sun" resonator system. Considerations having primarily to do with manufacturing techniques indicated the latter to be preferable although the former would have been possible. Accordingly, work was started on a "packaged", "rising sun" magnetron to oscillate at 1.25 cm. wavelength (24,000 mc/s). It was to have wave guide output like the Columbia model and axial cathode mount dictated by the "packaged" construction. Operating conditions were to be 15 kv., 15 amps., a pulling figure of 25 mc/s, and as much peak power as could be obtained. It was coded the 3J21.

Generated on 2019-09-21 09:41 GMT / http://hdl.handle.net/2027/mdp.39015077775156
Public Domain, Google-digitized / http://www.hathitrust.org/access_use#pd-google
Digitized by Google
Original from UNIVERSITY OF MICHIGAN

In the development of the 3J21, the "rising sun" resonator system used by the Columbia Laboratory was adopted practically without change. The ratio of the natural frequencies of the large and small resonators is approximately 1.8. The anode diameter is 0.160 in. and the anode length 0.190 in. The structure is fabricated by the so-called "hubbing" technique,[26] which had been brought to a high state of development at the Columbia Laboratory for the purpose. In this technique, a hardened steel die or hub, machined to be the "negative" of the desired contour, is forced by high hydraulic pressure (of order 250,000 lb./sq. in.) into a copper blank. The hubbed blank, after trimming and turning to size, becomes the resonator system and body of the magnetron. The proper contour to receive the wave guide output circuit is then bored.

The cathode of the 3J21 magnetron has a diameter of 0.096 in. and a length of active coating of 0.165 in. At 15 amps. peak current, the current density at the cathode surface is about 50 amps./sq. cm.—a considerably higher value than that in magnetrons of longer wavelength. Furthermore, the back bombardment of the cathode in this magnetron is about 10 per cent of the input power as compared to the 3 to 6 per cent in longer wavelength magnetrons. For these reasons, the cathode was one of the severest problems of the whole design.

The first axially mounted cathodes were supported on Kovar tubes sealed to the input glass structure. The heater lead was carried down the center of this tube through a glass bead in the input end. The structure resembled that of the 2J51 seen in Fig. 71. Since the hole through the magnetic pole piece was initially 0.100 in. and the cathode end disks 0.130 in. in diameter, the cathode was assembled onto its support after the Kovar tubing was in place. However, in quantity production the cathode could better be assembled as a unit before attachment to the outer glass and pole piece structures. At the expense of magnetic field strength and uniformity, the hole in the pole piece was enlarged to accommodate the entire cathode structure. No ill effects were observed and no special features such as the permendur cathode end structures of the 4J50 magnetron were found necessary.

The problem of the dissipation of the considerable heat of back bombardment was complicated by the necessity of activating the cathode at a temperature of 1050°C. The requirements of heat dissipation and activation oppose one another, one calling for low thermal impedance of the cathode

[26] The technique is here called "hubbing" rather than hobbing for two reasons: The term hobbing has a meaning in machine practice quite apart from the technique in question. The term hubbing is used for processes in which the interior of a piece is removed by forcing a member into it. It presumably arose from the early practice of making axle holes by forcing a hardened steel member through the wrought iron wheel hub. Furthermore, it has an analogous usage in coining.

Digitized by Google
Original from UNIVERSITY OF MICHIGAN
Generated on 2019-09-21 09:41 GMT / http://hdl.handle.net/2027/mdp.39015077775156
Public Domain, Google-digitized / http://www.hathitrust.org/access_use#pd-google

support, the other, high. To meet each requirement satisfactorily with the first cathode structure was found very difficult if not impossible.

A major step forward was taken in the design of the so-called "soldering iron" cathode in which the heater element is placed in a larger part of the cathode lead, heat being conducted to the cathode surface through a solid rod. The cathode itself is solid, making for greater rigidity and lower thermal impedance. The heater element is placed where it may be made considerably larger and more rugged than if placed inside the cathode, whose diameter is 0.096 in. A view of the 3J21 magnetron cathode structure is to be seen in Fig. 78. The heater is contained within the section of larger diameter immediately adjacent to the cathode.

The "soldering iron" cathode presented more difficult problems of heat conduction and dissipation than the older design. For an operating temperature of 800°C at the cathode surface, it is necessary to heat the heater chamber to about 1000°C, whereas the necessary activation temperature of 1050°C requires the temperature of the heater chamber to be about 1300°C. As a result, rather careful design to provide the proper balance between heat losses by conduction and radiation was necessary. Radiation losses, which are the more important type, are increased by extending the cathode rod considerably beyond the active surface, as seen in Fig. 78. The cathode should also have good thermal conducting properties in this extension, throughout the main cathode body, heater chamber, and support. Under normal operating conditions the heater is turned off, cathode heat being supplied solely by back bombardment.

It is apparent that a cathode design of this type calls for a careful choice of materials. They must be highly refractory as well as of good thermal conductivity and structural strength. Copper, silver, and nickel do not meet all of these requirements. The first cathodes of promise were turned from solid stock of so-called machinable molybdenum, complete with cathode end disks and heater chamber. The heater end was brazed to a Kovar detail, subsequently welded to the support cone of the type developed for the 4J52 magnetron. However, molybdenum machines poorly. The tolerances on size did not permit of large scale production of precision molybdenum parts. Consequently it was proposed to make the cathode of tungsten rod which could be ground to shape even on a production basis. The cathode end disks were to be punched or turned from molybdenum or Kovar and brazed to the tungsten rod. The tungsten rod extends into a hollow molybdenum heater chamber, the dimensions of which are not critical. Inside the heater chamber the heater coil encloses the protruding tungsten rod so that better heat conductivity from the heater to the cathode is provided. The heater is brazed to the cathode at one end in the braze between the tungsten and molybdenum. The other end is spot welded to

Digitized by Google
Original from UNIVERSITY OF MICHIGAN
Generated on 2019-09-21 09:41 GMT / http://hdl.handle.net/2027/mdp.39015077775156
Public Domain, Google-digitized / http://www.hathitrust.org/access_use#pd-google

a heavy central support lead inside the Kovar cone through a hole provided in the cone. The input end of the heater chamber is flared to accommodate the Kovar support cone to which it is brazed. All of the materials are thus of good structural strength. The tungsten and molybdenum are good thermal conductors, the Kovar not. Some parts of the cathode were grit blasted to increase their radiative emissivity.

The total axial motion of the cathode by thermal expansion from cold start to operation is 0.008 in. The cathode is offset axially by this amount when installed.

The cathode surface consists of a nickel matrix base, like that developed for the 725A magnetron, into which the active coating is impregnated. Attempts were made to increase the thermal conductivity through the 0.008 in. thickness of matrix. Larger particle size was used. Ball milling the nickel powder before sintering resulted in more dense particles. A later improvement was effected by making the matrix oversize by a mil or two, impregnating it with the active coating, and then compressing it to size in a mold. This procedure also resulted in a surface far superior in smoothness and regularity to that previously obtained.

The first output circuit used in the 3J21 magnetron, like that in the Columbia model, involved a quarter wave length transforming section of low characteristic impedance (about 20 ohms), extending from an iris in the "back" of one of tbe large resonators directly into the output wave guide. This section was 0.350 in. high and about 0.0125 in. wide. It was made by milling a slot into solid bar stock, the top of which was closed by brazing on a copper plate. A quarter wavelength section of this line was brazed between the anode body and the output wave guide piece which carried the choke joints and wave guide window seal. This latter piece was fabricated by hubbing a rectangular wave guide in a copper cylinder into which the circular choke was later turned. The wave guide window consisted of a circular glass disk sealed into a Kovar cup like that used in the 4J50 magnetron (compare Figs. 77 and 75). In the 3J21, as in the 4J50, the external choke facing the wave guide window and a short section of wave guide were later incorporated as part of the magnetron.

Holding the pulling figure of the operating magnetron to a specified value presented a serious problem. The problem was one of securing uniformity of the narrow transformer section and, to some extent, of the resonator to which it is attached. A variation of 1 mil in the width of this transformer produced 3 mc/s change in the pulling figure. Even with an improved mechanical design, the spread in output characteristics was uncomfortably large. Part of the difficulty resulted from the formation of solder fillets in the transformer section during brazing, the size of which could not easily be controlled. A rigid inspection of both electrical and mechanical

Digitized by Google
Original from UNIVERSITY OF MICHIGAN
Generated on 2019-09-21 09:41 GMT / http://hdl.handle.net/2027/mdp.39015077775156
Public Domain, Google-digitized / http://www.hathitrust.org/access_use#pd-google

properties of each magnetron before sealing and pumping was an absolute necessity to insure reproducibility. The use of an iris coupling between the resonator and the wave guide presented a possible solution. However, the iris required would be too large to be placed directly at the back of the resonator. It was proposed to put a hubbed rectangular resonant iris at the back of the resonator and a decoupling iris a half wave length distant in the wave guide. This construction provided a resonant cavity between the two irises in which the storage of energy would provide some degree of frequency stabilization. The structure of this output circuit may be seen in the photograph of a cutaway model in Fig. 77. Both higher efficiency of

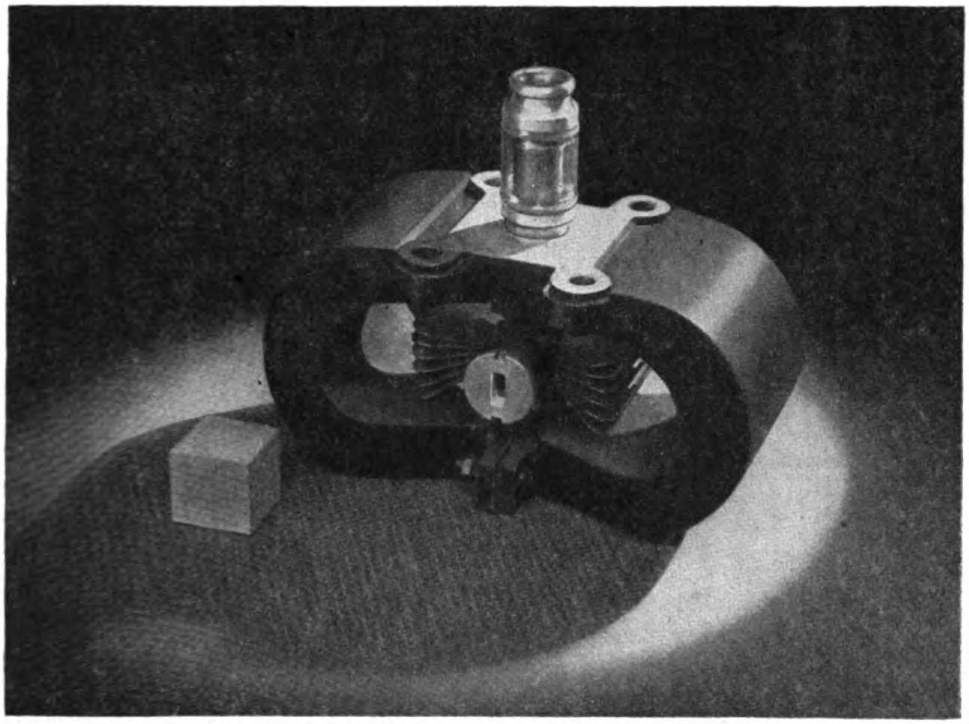

Fig. 76—An external view of the 3J21 "packaged" magnetron (60 kw., 24,000 mc/s).

operation and lower pulling figure than obtained with the earlier circuits resulted. As average values, an increase in over-all efficiency from 24 to 28 per cent and a drop in pulling figure from 25 to 18 mc/s may be cited.

The RF voltage breakdown strength of the wave guide window was marginal. A new design developed at the Columbia and M. I. T. Laboratories, incorporating a larger window and "streamlined" wave guide contours adjacent to it, was modified slightly and used in the 3J21.

The magnetic pole gap was made 0.290 in. This was as small as was felt practical. This and other steps were taken in an effort to save as much as possible on magnet weight.

The mechanical problems connected with the fabrication of the 3J21

Digitized by Google
Original from UNIVERSITY OF MICHIGAN
Generated on 2019-09-21 09:41 GMT / http://hdl.handle.net/2027/mdp.39015077775156
Public Domain, Google-digitized / http://www.hathitrust.org/access_use#pd-google

magnetron resulted largely from the small tolerances it was found necessary to impose. The tolerance allowed on radial location of the cathode was ±0.002 in.; on transformer slot width (when this output was used), ±0.0005 in.; and on dimensions of the anode structure, ±0.001 in. Deformations, such as those produced by placing a magnetron with slightly misaligned pole pieces on a strong magnet, had to be carefully avoided. The importance

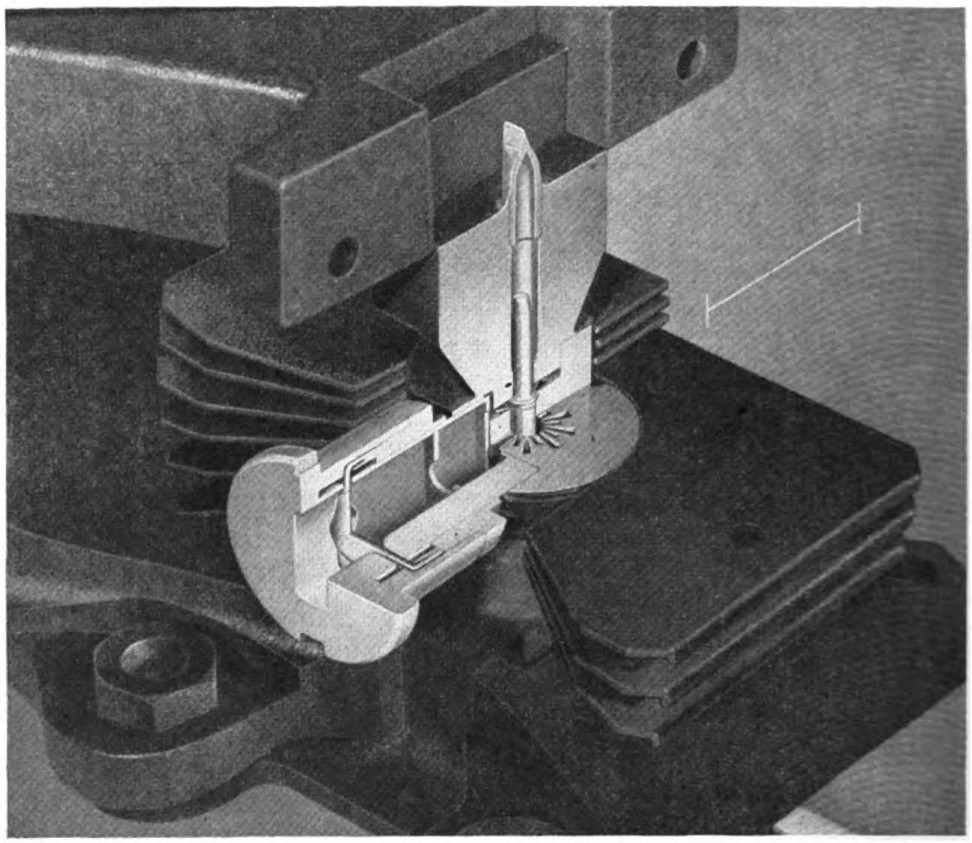

Fig. 77—An internal view of the 3J21 "packaged" magnetron (60 kw., 24,000 mc/s). Note the "rising sun" resonator system, the stabilizing cavity in the wave guide output between a rectangular resonant iris at the "back" of the output resonator and a circular decoupling iris a half wavelength distant, and the beveling of the wave guide edges adjacent to the wave guide window.

of cathode alignment, for example, may be seen from the fact that across the anode-cathode space, which in the 3J21 is only 0.032 in., there is an operating voltage gradient of 165 kv./in. This gradient is doubled in the region where the cathode support passes through the hole in the pole piece, at which point there is a nominal clearance of 0.015 in. Thus the elimination of small burrs and small radii was essential.

An external view of the 3J21 magnetron is shown in Fig. 76, an internal view in Fig. 77. Operational and other data are to be found in TABLE IV.

Digitized by Google
Original from UNIVERSITY OF MICHIGAN
Generated on 2019-09-21 09:41 GMT / http://hdl.handle.net/2027/mdp.39015077775156
Public Domain, Google-digitized / http://www.hathitrust.org/access_use#pd-google

The principal operational problems encountered in the 3J21 magnetron were the occurrence of so-called "gassy tubes" and some difficulties with "moding." Despite numerous precautions taken during fabrication, gas, identified spectroscopically as hydrogen, was evolved during operation in a discouragingly large number of magnetrons during the developmental work. By the use of a zirconium getter attached to the cathode support cone the difficulty could be circumvented. Also it had been found possible

TABLE IV
THE 3J21 PACKAGED MAGNETRON AT 1.25 CENTIMETERS

N	18	
r_c (in.)	0.048	
r_a (in.)	0.080	
h (in.)	0.186	
Magnet gap (in.)	0.290	
Weight (lb.)	6.6	
Resonator system	"rising sun"	
Resonators	vane type	
Resonator λ ratio	1.8	
λ (cm.)	1.25	
f (mc/s)	23986 ± 240	
Nearest modes	$n = 4$, $n = 8$	
λ separation (%)	+25, −10	
Q_0	1400	
Q_{ext}	580	
η_e (%)	70	
Output circuit	wave guide with $\lambda/2$ stabilizing cavity	
Stabilization factor	2	
V (kv.)	15.0	15.0
I (amps.)	15	15
B (gauss)	8000	8000
τ (μs)	0.5	0.25
pps	1000	2000
P_0 (kw.)	60	60
η (%)	26	26
η_c (%)	37	37
PF (mc/s)	17	17

to "clean up" a gassy tube temporarily by running the cathode very hot. This led to a pumping cycle which greatly reduced the occurrence of hydrogen.

Considerable effort was expended in attempting to track down the source of the hydrogen evolution. The iron pole pieces were found to be the major offender, but some hydrogen was evolved from other parts including the cathode. Cleaning and plating solutions release atomic hydrogen which readily permeates the iron pole pieces and other parts. Various

Digitized by Google
Original from UNIVERSITY OF MICHIGAN
Generated on 2019-09-21 09:41 GMT / http://hdl.handle.net/2027/mdp.39015077775156
Public Domain, Google-digitized / http://www.hathitrust.org/access_use#pd-google

methods of treating the parts, such as preglowing in vacuum, were used. These largely eliminated the difficulty.

An interesting feature of the problem was the relatively infrequent occurrence of hydrogen in magnetrons built at the Western Electric Co. The reason for this was finally traced to the precaution, prescribed by the safety engineers, that the sintering of the copper plate on the pole pieces be done in an atmosphere of 95 per cent nitrogen and only 5 per cent hydrogen. All sintering and brazing operations in our Laboratories had been done in a 100 per cent hydrogen atmosphere. Pole pieces sintered in the predominantly nitrogen atmosphere were found to be nearly as free of hydrogen as the vacuum preglowed parts. However, the use of the zirconium getter was continued in models built at the Laboratories as added insurance against recurrence of the difficulty.

The other operational fault of the 3J21 magnetron was a tendency to oscillate in a mode other than the π mode under certain circumstances. Examination of a large number of magnetrons, opened after operation, showed that the only observable causes were resonator distortion, the presence of brazing flux or other foreign material, and off-center cathode location. As in other magnetrons, the tendency to "mode" was greater when heavily loaded or when operated with a sharply rising voltage pulse. Western Electric engineers concluded, as the result of an extended study of magnetrons in which the cathode position was changed during operation by flexing the input lead, that a cathode position 2 to 3 mils off center toward the output resonator was desirable. A tool was developed with which a permanent change in cathode location could be made on operating magnetrons. By its use many "mody" magnetrons were reclaimed.

An interesting phenomenon, discovered during the development of the 3J21 magnetron, is that known as the "cold start." Whereas most magnetrons may be started with difficulty with a cold cathode, the 3J21 was found to start readily under these conditions over several discrete bands of magnetic field intensity. Although the phenomenon is not well understood, some correlation with the work of Posthumus[13] has been made.

In making tests on the 3J21 magnetron at a duty cycle of 0.001 and a pulse duration of 0.1 μs, the cathode was found to operate at a considerably higher temperature than at 0.5 μs pulse duration and the same duty cycle and average input power. This behavior has since been observed in the 725A and 4J52 magnetrons. It is thought to result from unfavorable conditions during the periods of rise and fall of the voltage pulse, which become a greater percentage of the total pulse duration as the pulse duration is reduced. The effect presumably would not appear if the pulse shape were truly rectangular. With present modulators, however, it

Generated on 2019-09-21 09:42 GMT / http://hdl.handle.net/2027/mdp.39015077775156
Public Domain, Google-digitized / http://www.hathitrust.org/access_use#pd-google
Digitized by Google
Original from UNIVERSITY OF MICHIGAN

presents a lower limit on pulse duration which may be employed and further complicates the cathode cooling problem.

21. Magnetron Cathodes

From the start of its work with centimeter wave magnetrons, the Bell Laboratories has been engaged in an extensive program of magnetron cathode testing and design. The range of cathode size is illustrated in Fig. 78. The largest cathode, shown at the extreme left, is that of the 5J26 magnetron, operating at about 23 cm., the smallest, that of the 3J21 magnetron operating near 1 cm. The range of operating conditions to be met, as well as the magnitude of the problem at shorter wavelengths, is illustrated by these two extremes. The cathode of the 3J21 magnetron, although its surface area is only 0.31 sq. cm., is called upon to deliver peak currents comparable to those demanded of the cathode of the 5J26, having a surface area of 17.1 sq. cm. The ratio of current densities is 25 to 1. The peak back bombardment of the two cathodes is comparable. Other cathodes shown in Fig. 78 operate under conditions intermediate between these extremes. Needless to say, the 5J26 cathode is operated quite conservatively, the 3J21 cathode under extremely severe conditions.

Little difficulty with cathodes has been experienced in pulsed magnetrons above 10 cm. wavelength. For the most part they are plain, nickel sleeves coated with active material. The highest emission density (10.1 amps./cm.^{2}) used successfully with this type of cathode was in the 720A-E, which operated satisfactorily at 1 μs but was not satisfactory at 5 μs. The operation at 5 μs required a modification of the cathode as described. When the simple sprayed cathode was tried in developmental models of the 725A magnetron, the life at 1 μs was of order 10 hours. At the high emission density required (approximately 30 amps./cm.^{2}) the active coating was rapidly lost as a result of arcs, and frequently the nickel support itself was fused and vaporized.

The problem of arcing to the cathode surface in small magnetrons was soon recognized as the most important cathode problem. It prevented steady operation and hastened destruction of the cathode surface and the end of useful magnetron life. All of these cathodes were found to require an initial break-in period during which the arcing is particularly violent. As the input voltage and current are gradually increased, the violent arcing gradually subsides. The tendency to arc at any time subsequent to this initial period depends on the nature of the cathode surface, but beyond that, it depends also on the operating conditions to which the magnetron is subjected. Increase in power input, either as increased voltage or current, or both, rapidly increases the frequency of arcs. Similarly, increased pulse

Digitized by Google
Original from UNIVERSITY OF MICHIGAN
Generated on 2019-09-21 09:42 GMT / http://hdl.handle.net/2027/mdp.39015077775156
Public Domain, Google-digitized / http://www.hathitrust.org/access_use#pd-google

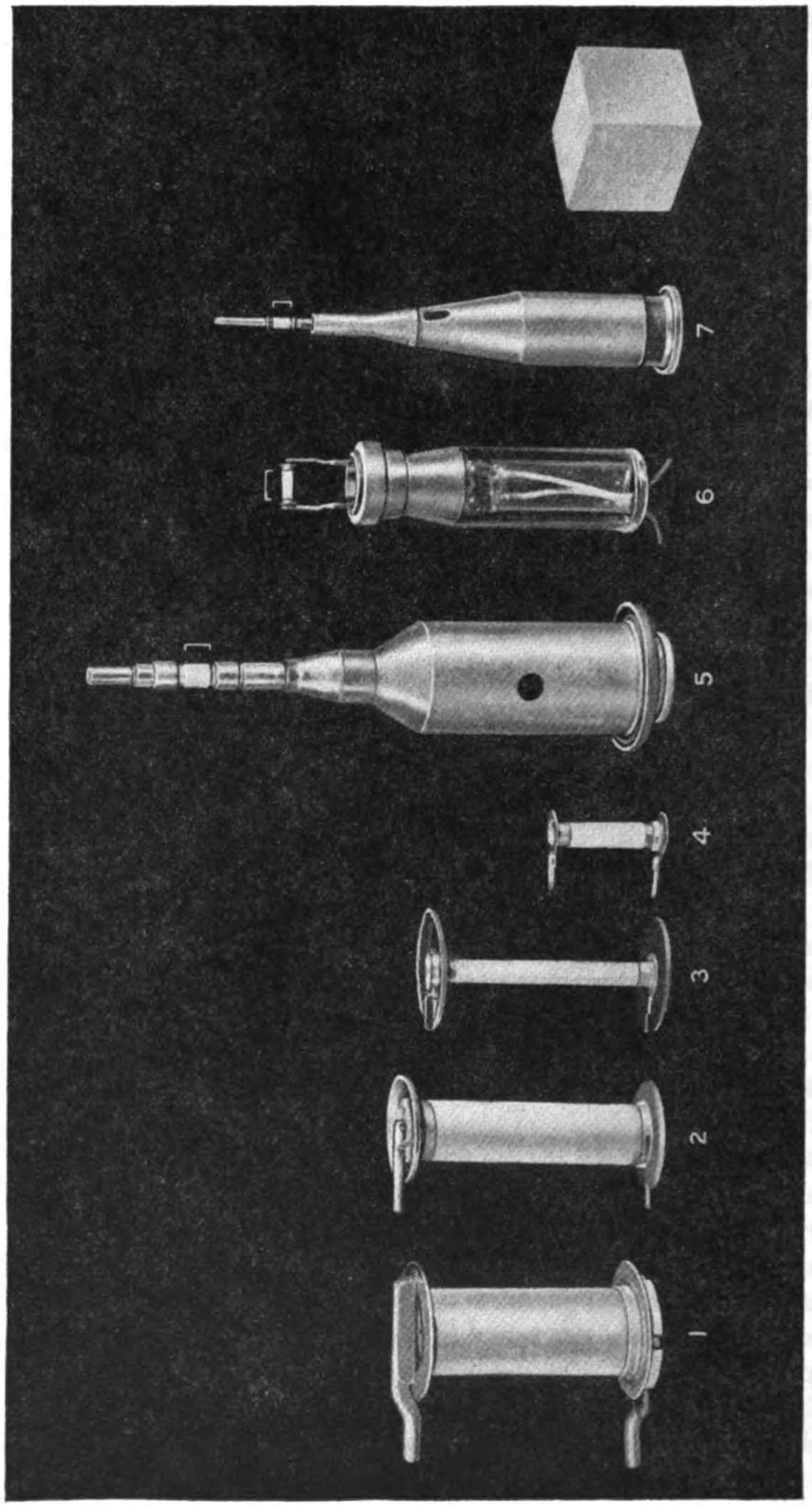

Fig. 78—A group of cathode structures for centimeter wave magnetrons. From left to right they are: (1) the 5J26 cathode—oxide coating on roughened nickel base; (2) the 4J21-30 cathode—oxide coating on roughened nickel base; (3) the 720A-E cathode—metallized, oxide coating on nickel wire mesh base; (4) the 706AY-GY cathode—oxide coating on smooth nickel base; (5) the 4J50 cathode and support structure—oxide coating on sintered, nickel powder, matrix base; (6) the 725A cathode and support leads—oxide coating on sintered, nickel powder, matrix base; and (7) the 3J21 cathode and support structure—oxide coating on sintered, nickel powder, matrix base. The active cathode portion in each of the structures (5), (6), and (7) is indicated by a bracket.

Generated on 2019-09-21 09:42 GMT / http://hdl.handle.net/2027/mdp.39015077775156
Public Domain, Google-digitized / http://www.hathitrust.org/access_use#pd-google
Digitized by Google
Original from UNIVERSITY OF MICHIGAN

length makes the arcing much worse; in the 725A for example, changing the pulse length from 1 μs to 2 μs may increase the arcing rate by a factor of 10 to 20. A decrease in recurrence rates with some types of cathodes also causes a noticeable increase in the rate of arcing.

In the great majority of cases, magnetron cathodes have employed coatings of the ordinary strontium and barium carbonates as the source of primary and secondary electrons. All-metal, secondary emitting cathodes with primary emitting, starter cathodes have been tried in some laboratories with some success but have not yet come into general use. The efforts at the Bell Laboratories have been directed toward developing and improving the oxide coated cathode along lines making it more nearly possible to satisfy requirements (3), (4), (5), and (6) listed in Section 10.7 *Magnetron Cathodes* of PART I without impairing the ability to meet requirements (1) and (2).

Most of the cathode developments were made in connection with the 725A. This magnetron served as a convenient "laboratory" or "proving ground" for magnetron cathode studies. Its cathode is small enough and the demands made upon it stringent enough to make apparent any cathode weaknesses and any improvements which may be made. A large number of life racks were kept in constant operation for 725A magnetron life tests over a long period of time under various conditions in which the cathodes were generally run to destruction.

Attempts were made to make the data reproducible by controlling the activation, by controlling the initial break-in of the operating magnetron, and by devising means of quantitatively determining some measure of the adequacy of any given cathode. The last of these items involved the development of an automatic counter which registers the number of arcs or bursts of arcs which cause the current to exceed a predetermined value. By recording the accumulated number of arcs at intervals throughout the life of the magnetron, it is possible to get a picture of the arcing pattern with life. Such counters have done much to put the life testing and initial break-in of magnetrons on a semi-quantitative basis. The smoothed curves shown in Fig. 80 were obtained through the use of these counters.

Early attempts at building a cathode upon which sufficient active material may be held, made at both the M. I. T. Radiation Laboratory and the Bell Laboratories, involved winding coated cathodes with nickel wire to provide a reservoir of active material under the wires. In this manner, the material was protected from direct arcing effects, allowing the active material to migrate slowly to the outside surface of the wires. This general idea was greatly improved upon when the wire winding was replaced by a woven nickel mesh into the interstices of which the active material was packed. The

Digitized by Google
Original from UNIVERSITY OF MICHIGAN
Generated on 2019-09-21 09:42 GMT / http://hdl.handle.net/2027/mdp.39015077775156
Public Domain, Google-digitized / http://www.hathitrust.org/access_use#pd-google

nickel mesh, being spot welded or sintered directly to the nickel base, formed a part of the cathode foundation, helping to reduce the coating resistance. It was found that arcs, rather than striking directly to the active material, tended to strike to the nickel wires. In spite of this fact, sudden bursts of current in arcing would erupt some of the active material from the cathode.

The mesh used in the 725A cathode is made of 6 mil nickel wire woven with 75 wires to the inch. The radial thickness of the mesh on the cathode is 10 mils. The average amount of active double carbonate mixture which the cathode holds is 23 mg. per sq. cm. The mesh cathode is shown in Fig. 79 in three stages of its fabrication. With this cathode, it was possible to

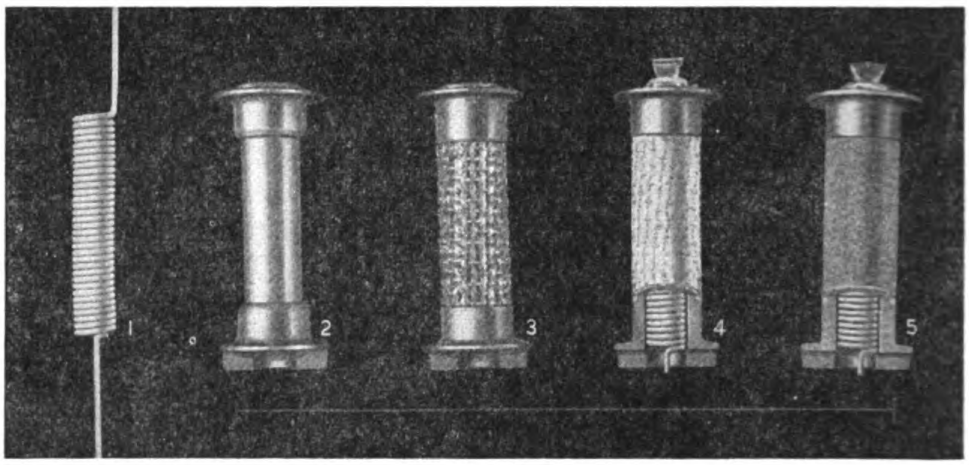

Fig. 79—725A cathode construction. Shown are: (1) the heater element; (2) the machined nickel cathode blank; (3) the cathode blank with the nickel wire mesh, welded or sintered in place; (4) the mesh type cathode with oxide coating applied, cut away to show heater element in place; (5) the more recent cathode with sintered, nickel powder, matrix base (uncoated).

produce 725A magnetrons having a guaranteed life at rated operating conditions of at least 500 hours, the average value being considerably higher. The arcing characteristic of the mesh cathode, excluding the initial break-in period, is shown in Fig. 80. The abrupt failure is typical of magnetron cathodes. At shorter pulse lengths failure occurs considerably later but in the same abrupt fashion. The life curve of the early type of cathode consisting of an oxide coated nickel cylinder, if plotted with the data on other cathodes in Fig. 80, would be crowded very close to the axis of zero hours.

Even with cathodes of mesh construction, operation of the magnetron was generally inadequate at 5 μs pulse duration. Furthermore, considerable break-in time was necessary before stable operation at 1 μs pulse duration was achieved. Some of the first mesh cathodes used in the 725A,

Generated on 2019-09-21 09:42 GMT / http://hdl.handle.net/2027/mdp.39015077775156
Public Domain, Google-digitized / http://www.hathitrust.org/access_use#pd-google
Digitized by Google
Original from UNIVERSITY OF MICHIGAN

for example, took as long as 45 minutes of intense arcing during gradual increase of input voltage and current before satisfactory operation was attained. It seemed unlikely that the arcing during the break-in period could be completely eliminated, but it was found that improvements in cathode construction which made steady operation at higher current possible also reduced the time of initial break-in to attain these conditions.

It appeared that the resistance of the cathode coating might be lowered by distributing nickel more uniformly throughout the coating. Accord-

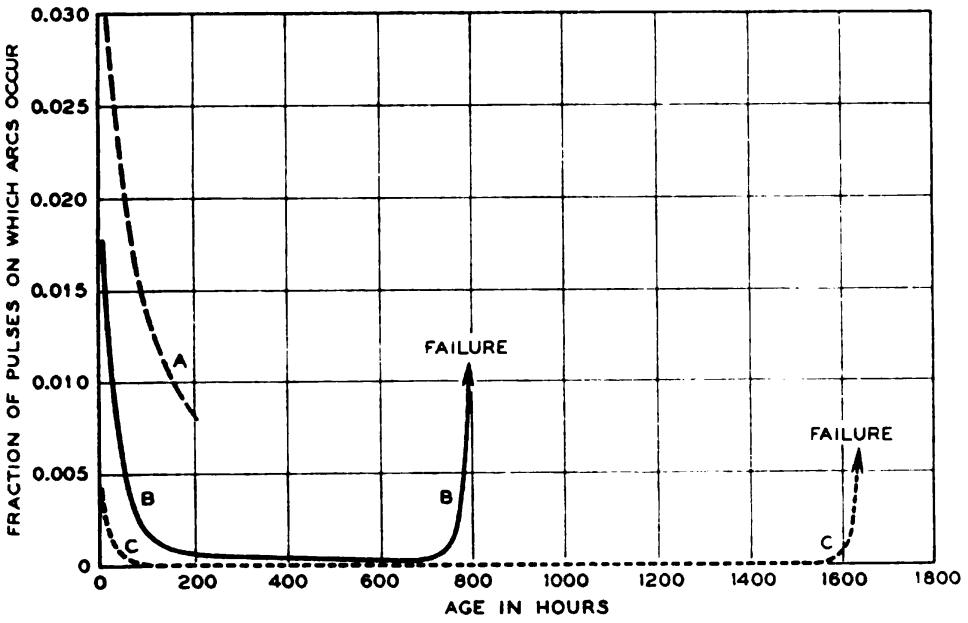

Fig. 80—Curves of arcing during life for 725A magnetrons, having various types of cathodes, operating at 5.7μs pulse duration, 165 pulses per second, and 210 kw. peak power input. It is to be emphasized that these conditions are considerably more stringent than the normal operating conditions. Curve (a) is for a cathode having oxide coating on a nickel wire mesh base; curve (b), metallized coating on a nickel wire mesh base; curve (c), either plain oxide or metallized coating on a sintered, nickel powder, matrix base.

ingly, mesh cathodes were coated with a mixture of double carbonates in which was distributed a fine nickel powder of high purity having an average particle size of 2 microns. The carbonate particle size is between 1 and 2 microns. The amount, found not to be critical, was 55 per cent by weight of the combined dry ingredients of the coating mixture. Although this reduced the amount of active material present on the cathode surface, as seen in Fig. 80 it resulted in a cathode having considerably improved arcing characteristics with considerably longer useful life. This cathode construction was adopted finally for the 725A production and was also utilized in the 10 cm. high power magnetrons, the 4J45–47, for operation at 5 μs pulse duration.

Generated on 2019-09-21 09:42 GMT / http://hdl.handle.net/2027/mdp.39015077775156
Public Domain, Google-digitized / http://www.hathitrust.org/access_use#pd-google
Digitized by Google
Original from UNIVERSITY OF MICHIGAN

The next step in the development was the replacement of the nickel mesh by a sintered matrix of coarse nickel powder (see Fig. 79). The average particle size was 55 microns. The active material is packed into this matrix in much the same manner as in the mesh cathode. Little difference was observed in the addition of fine nickel powder to the active coating in this type of cathode. The matrix cathode has the best life characteristic of any yet devised for the magnetron oscillator. Its life characteristic is shown in Fig. 80 with those of the earlier types.

The sintered matrix type of cathode has been used extensively in the 4J50 and 4J52 magnetrons at 3 cm. and in the 3J21 magnetron at 1 cm. In these cathodes, it was important to have high heat dissipation. This was achieved by designing a high thermal conductivity support and providing considerable radiating area immediately adjacent to the cathode surface by extending the cathode, as shown in Figs. 75 and 77, into the pole piece opposite that carrying the cathode mount.

22. Acknowledgments

During the war, the interchange of ideas and results among authorized persons concerned with magnetrons has been rapid and effective. Because of this it would be difficult to trace the origins of much of the general material presented in PART I and no attempt has been made to do so. It must be clear that the results reported have involved the efforts of many people. In the Bell Laboratories, the authors were members of a group which, as the work progressed, grew to a considerable size. In the early stages they were joined by G. E. Moore and W. B. Hebenstreit, later by N. Wax, L. M. Field, A. T. Nordsieck, and R. D. Fracassi. Other members of the Technical Staff in the magnetron group were A. J. Ahearn, H. W. Allison, B. B. Cahoon, C. J. Calbick, M. S. Glass, R. K. Hansen, J. G. Potter, R. Rudin, H. G. Wehe, A. E. Whitcomb, and C. M. Witcher, as well as several technical assistants.

The NDRC Radiation Laboratories at the Massachusetts Institute of Technology and at Columbia University generously supplied personnel for several cooperative projects and information on new results. In the 725A development, A. T. Nordsieck, then of Columbia, took part. L. R. Walker of M. I. T. contributed not only to the development of the 725A but took part in the development of the 4J50, 4J52, and 4J78. Other M. I. T. Staff Members in residence from time to time were F. Hutchinson, E. Everhart, and D. B. Bowen. The developments of the 2J51 and the 3J21 were effected jointly with the Columbia Laboratory.

Prof. J. C. Slater, first as a member of the M. I. T. Radiation Laboratory and later as a member of the Bell Laboratories, made numerous studies in our Laboratories and consulted generally on magnetron problems.

Digitized by Google
Original from UNIVERSITY OF MICHIGAN
Generated on 2019-09-21 09:43 GMT / http://hdl.handle.net/2027/mdp.39015077775156
Public Domain, Google-digitized / http://www.hathitrust.org/access_use#pd-google

Mechanical design, as well as constructional work and preparation of the detailed specifications for manufacture, was carried out by V. L. Ronci, D. P. Barry, F. H. Best, J. E. Clark, D. A. S. Hale, J. P. Laico and their associates, including T. Aamodt, C. J. Altio, D. I. Baker, C. Blazier, R. H. Griest, F. B. Henderson, W. Knoop, W. J. Leveridge, J. B. Little, C. Maggs, J. A. Miller, H. W. Soderstrom, and F. W. Stubner.

Permanent magnets were designed by P. P. Cioffi of the magnetics group in the Physical Research Department. Numerous physico-chemical problems were solved by L. A. Wooten and his associates of the Chemical Department. The work of J. B. Johnson and J. R. Pierce in allied fields contributed to that described in this paper. In addition, many users of magnetrons for radar purposes throughout the Laboratories collaborated by conducting tests of magnetrons used in radar equipments. We wish to acknowledge the support and advice of M. J. Kelly and J. R. Wilson under whose general direction the work proceeded.

Finally, the authors wish to thank L. M. Field, W. B. Hebenstreit, G. E. Moore, A. T. Nordsieck, and N. Wax, who have read parts of the paper critically.

Generated on 2019-09-21 09:43 GMT / http://hdl.handle.net/2027/mdp.39015077775156
Public Domain, Google-digitized / http://www.hathitrust.org/access_use#pd-google
Digitized by Google
Original from UNIVERSITY OF MICHIGAN

High-Vacuum Oxide-Cathode Pulse Modulator Tubes

By C. E. FAY

Introduction

IN PRACTICALLY all pulsed oscillators such as those used in radar, some means must be provided to apply the pulse voltage to the oscillator circuit. In many early radars, a high-vacuum modulator was used for this purpose. The pulse was generated at low power level and then amplified by means of one or more stages employing high vacuum tubes. The final stage was required to block, or cut off the d-c supply voltage with no pulse applied, and to permit as much as possible of the d-c voltage to appear on the oscillator during the pulse. Since most radar oscillators operate at pulse voltages of from 5 to 20 kv and require currents of several amperes during the pulse, the requirements of the modulator tubes are quite severe. Standard transmitting[1] tubes were used at first, the higher power tubes having the necessary voltage rating and having in general a fair amount of cathode emission. Tubes were operated in parallel to provide the required amount of current. Practically all of these tubes were of the thoriated tungsten filament type. For example an early army radar, the SCR268,[2] employed 8 tubes in parallel having a total filament power of 1040 watts to provide a pulse current of about 10 amperes. The use of such equipment in portable or airborne service would be obviously impractical because of the large power consumption, bulk, and weight. In an attempt to provide tubes more suited to this type of service, those described in this paper were developed.

Tube Requirements

The function of the high-vacuum modulator tube essentially is to act as a switch to turn the pulse on and off at the transmitter in response to a control signal. The best device for this purpose will be the one which requires the least signal power for control and which allows the transfer of power with the least loss, from the transmitter power source to the oscillator.

If the oscillator must be supplied with a pulse of voltage E_p and current I_p,* or power E_pI_p, then the voltage which must be supplied by the transmitter power supply will be $E_b = E_p + e_p$, Fig. 1, if e_p represents the voltage

* It is assumed here that the pulse is rectangular in shape. This is usually the desired shape and is fairly well approximated in most cases.

Digitized by Google
Original from UNIVERSITY OF MICHIGAN
Generated on 2019-09-22 05:37 GMT / http://hdl.handle.net/2027/mdp.39015077775156
Public Domain, Google-digitized / http://www.hathitrust.org/access_use#pd-google

drop in the modulator tubes necessary to allow current I_p to pass. The plate efficiency of the modulator is then simply $\frac{E_p}{E_b}$ and the power dissipated in the modulator tube plate is $I_p e_p$ during a pulse. The average power dissipated in the plate is then $I_p e_p$ multiplied by pulse length and by pulse frequency. The heat storage capability of the plate is ordinarily great enough that the average power is all that needs consideration.

The conditions imposed on the modulator tube are somewhat analogous to those of a class C amplifier at low frequency. The main difference is that the angle of operation is very small, and there is usually no appreciable backswing of plate voltage since the load is essentially a resistance. Typical

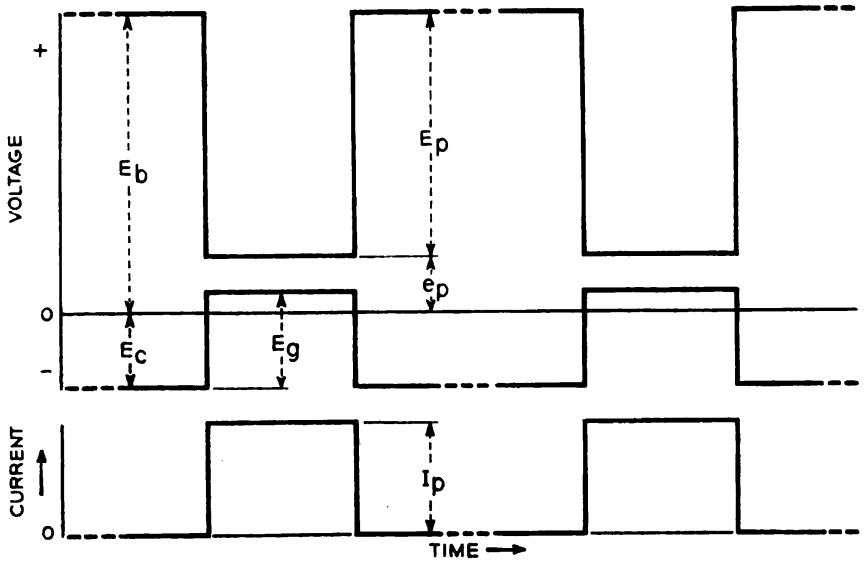

Fig. 1—Current and voltage relations in a pulse modulator tube.

modulator circuits are shown in Fig. 2. It is sometimes found desirable to employ a shunt inductance across the oscillator in the interest of a sharp cutoff of the pulse on the oscillator, particularly where capacitances to ground of various circuit components are appreciable. This results in an additional current demand on the modulator tube since the current through the inductance must also be supplied. The oscillator is often coupled to the modulator circuit by means of a transformer in order that desirable impedances are realized in each circuit.

Design Considerations

It was apparent on first consideration of the high-vacuum modulator problem that use of oxide coated cathodes would be of enormous advantage

Generated on 2019-09-22 05:37 GMT / http://hdl.handle.net/2027/mdp.39015077775156
Public Domain, Google-digitized / http://www.hathitrust.org/access_use#pd-google
Digitized by Google
Original from UNIVERSITY OF MICHIGAN

in keeping power requirements down. Heretofore the use of oxide cathodes in high voltage power tubes had been found very difficult, particularly where filamentary cathodes were employed. Any spark or momentary discharge in operation usually resulted in the burning out of the relatively fragile filaments. This result was caused mainly by the fact that a considerable amount of energy was of necessity available from the power supply equipment. However, in pulse service it is possible to limit the amount of energy available so that a momentary tube breakdown will not result in damage to a reasonably rugged equipotential cathode. Also, in the interest

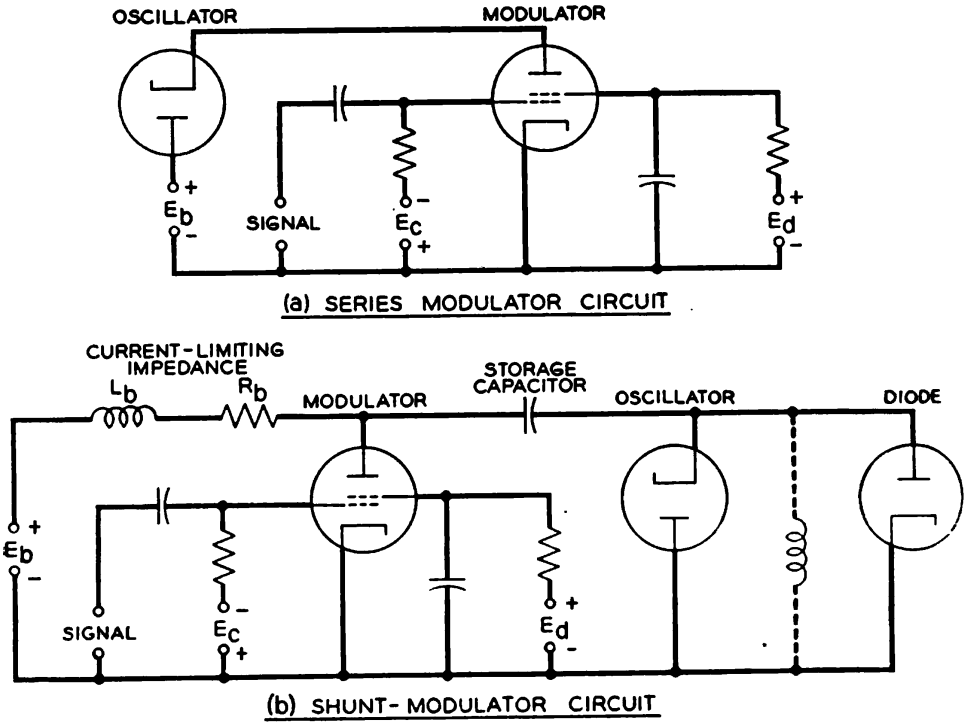

(a) SERIES MODULATOR CIRCUIT

(b) SHUNT-MODULATOR CIRCUIT

Fig. 2—Typical pulse modulator circuits.

of conserving control power it is desirable to build high perveance tubes which require very close control-grid to cathode spacings. This is much more easily accomplished with rigid cathode structures rather than filamentary cathodes, especially for service conditions under which extreme shock and vibration may be encountered.

Conservation of drive power requires that the modulator tube have high power-gain. This is most easily provided in the tetrode which provides a high over-all amplification factor with reasonable drive characteristics. Lining up the control-grid and screen-grid wires is of course advantageous in the interest of minimizing screen dissipation and getting the largest possible portion of the cathode current to the plate. The control-grid to

Generated on 2019-09-22 05:38 GMT / http://hdl.handle.net/2027/mdp.39015077775156
Public Domain, Google-digitized / http://www.hathitrust.org/access_use#pd-google
Digitized by Google
Original from UNIVERSITY OF MICHIGAN

plate capacitance is of little importance as long as it does not store much energy, there being little chance for oscillation in such a circuit. While it is desirable to operate with as low a minimum plate voltage as possible, it is of little additional advantage to bring the plate voltage below the screen voltage if the screen voltage is about 1000 volts and the supply voltage 15 kv. It was therefore thought permissible to increase plate to screen spacing beyond the optimum for best characteristics in the interest of high voltage and screen dissipation ratings.

The insulation in the tube between plate and other electrodes must be capable of withstanding the full supply voltage plus a comfortable margin. This dictates that if internal insulators are used they must have long path and that the bulb must have sufficient length to prevent flash-over externally.

The 701A Vacuum Tube

At the time of this development a tube was very urgently needed for a Navy radar application.[3] Since speed was of prime importance it was decided to take parts of a standard oxide-cathode beam-power tetrode, Western Electric 350A, and mount them in a structure capable of withstanding the required voltage; 12 kv in this case. Accordingly a cruciform structure was designed in which four sets of 350A electrodes were mounted on ceramic members attached to a molded glass dish-stem as shown in Figure 3. The four cathodes have a total coated area of approximately 14 square centimeters. A molybdenum plate of cruciform section mounted from a lead-in at the top of the bulb was used. This construction eliminated internal insulators between plate and grids other than the bulb. The control-grid of the 350A is normally gold plated to inhibit primary emission. This feature was retained in the 701A and the screen-grid also gold plated. The plate to screen-grid spacing was increased over that normally used in the 350A in order to allow somewhat better cooling of the grids and to allow greater clearance for high voltage reasons. This made the characteristics depart from good "beam tube" performance but at the high voltage condition of operation this was of little consequence. Characteristic curves of the 701A indicating performance under both high voltage and low voltage conditions are shown in Fig. 4. Since no experience was available at the time of this development to indicate what currents could safely be drawn from the cathodes under pulse conditions, the matter of rating these tubes was mainly guesswork since time was not available to await the outcome of life tests under various conditions. The ratings put on the 701A are as shown in Table I.

For the immediate application in hand, which required 12 ampere pulses at about 10 kv, it was decided to specify two 701A tubes operating in paral-

Generated on 2019-09-22 05:38 GMT / http://hdl.handle.net/2027/mdp.39015077775156
Public Domain, Google-digitized / http://www.hathitrust.org/access_use#pd-google
Digitized by Google
Original from UNIVERSITY OF MICHIGAN

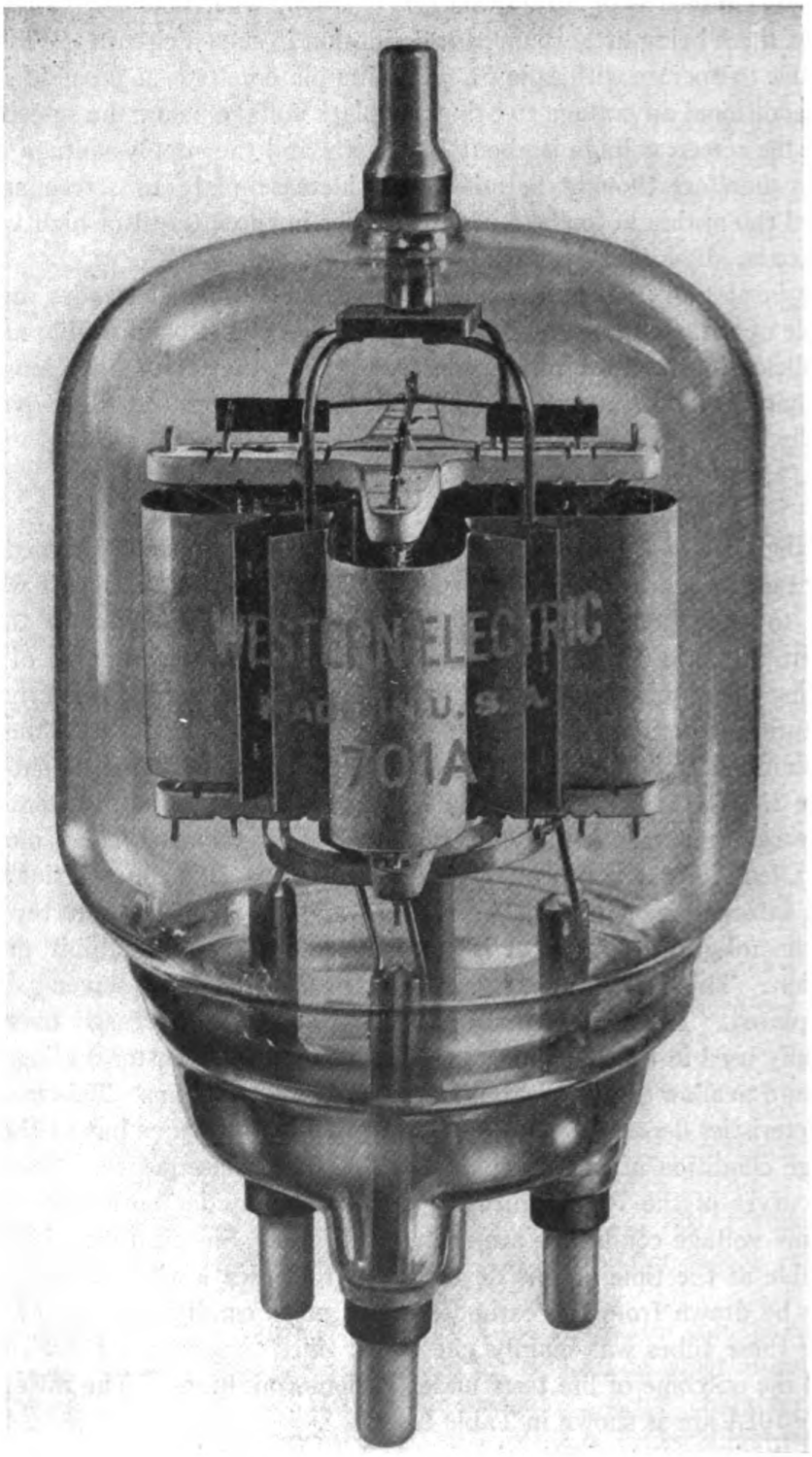

Fig. 3—The 701A vacuum tube.

Digitized by Google
Original from UNIVERSITY OF MICHIGAN
Generated on 2019-09-22 05:38 GMT / http://hdl.handle.net/2027/mdp.39015077775156
Public Domain, Google-digitized / http://www.hathitrust.org/access_use#pd-google

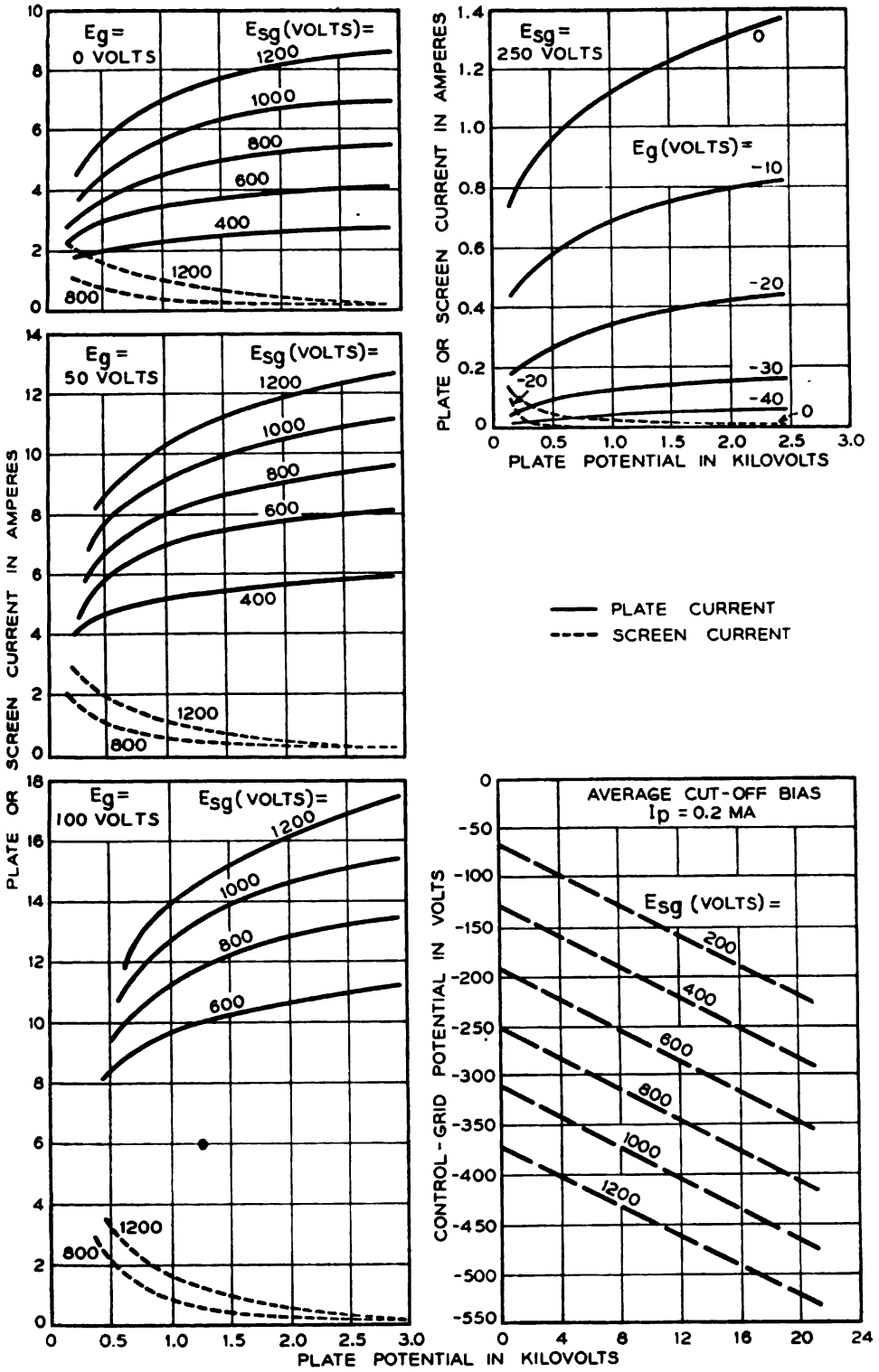

Fig. 4—Characteristics of the 701A vacuum tube.

Digitized by Google
Original from UNIVERSITY OF MICHIGAN
Generated on 2019-09-22 05:38 GMT / http://hdl.handle.net/2027/mdp.39015077775156
Public Domain, Google-digitized / http://www.hathitrust.org/access_use#pd-google

lel. The pulse in this case was trapezoidal having a base width of about 4μ seconds and a top width of about 1.75 μ seconds; repetition rate was 1600 per second. When the tubes were operated under these conditions there was customarily some sparking within the tube in the first few minutes and then it apparently "aged in," and operated satisfactorily. At the rated heater voltage, the cathodes operated at about 800°C (brightness). This temperature would normally provide a cathode life of more than 1000 hours. Life tests in the laboratory indicated satisfactory performance for about 2000 hours. Reports from the Navy were difficult to obtain but those which were obtained indicated similar results. End of life was caused by both loss of cathode emission and by primary grid emission. Mechanically the tube proved to be reasonably rugged for normal service. However, shocks sustained in shipment of tubes caused mechanical misalignment in some cases, indicating a need for a more rugged structure for use in the armed services.

TABLE I
TABLE OF RATINGS OF OXIDE-CATHODE PULSE MODULATOR TUBES

Tube	Heater Voltage	Heater Current	Peak Plate Voltage	Peak Screen Voltage	Peak Plate Current	Plate Dissipation	Screen Dissipation	Max. Duty Cycle for Peak Plate Current	Capacitances		
									C_{in}	C_{out}	C_{gp}
	Volts	*Amperes*	*KV*	*KV*	*Amperes*	*Watts*	*Watts*		*mmf*		
701A	8	7.5	12.5	1.2	10	100	15	0.005	56	11.5	3.2
715A	27	2.15	14	1.2	10	60	8	0.002	35	7	1.2
715B	26	2.10	15	1.25	15	60	8	0.001	35	7	1.2
5D21	26	2.10	20	1.25	15	60	8	0.001	35	7	1.2
426XQ	8	7.5	25	1.5	20	150	15	0.001	46	7.5	0.6

THE 715A TUBE

The advent of airborne radar made the development of high power lightweight transmitters an urgent requirement. In this case long life was somewhat subordinate to lightweight and small dimensions. Ruggedness was also a requirement. The electronic properties of the 701A tube were well suited for airborne radar but the large bulk was an extreme disadvantage. Work was begun on a tube using the same cathodes as the 701A but having a simpler and more rugged mechanical structure. Out of this evolved the 715A tube. In this tube the cathodes were placed side by side and enveloped by a single control-grid, screen-grid and plate. In order to provide the necessary ruggedness and to keep the grids cool, heavier grid wires were used and they were wound on very heavy supports of high heat-

Generated on 2019-09-22 05:38 GMT / http://hdl.handle.net/2027/mdp.39015077775156
Public Domain, Google-digitized / http://www.hathitrust.org/access_use#pd-google
Digitized by Google
Original from UNIVERSITY OF MICHIGAN

conductivity material. Both grids were gold plated as in the 701A. All electrodes were mounted between two specially shaped ceramic insulators which provided a relatively long path between plate and grids. This structure is shown in Fig. 5. Heat radiating fins were attached to the ends

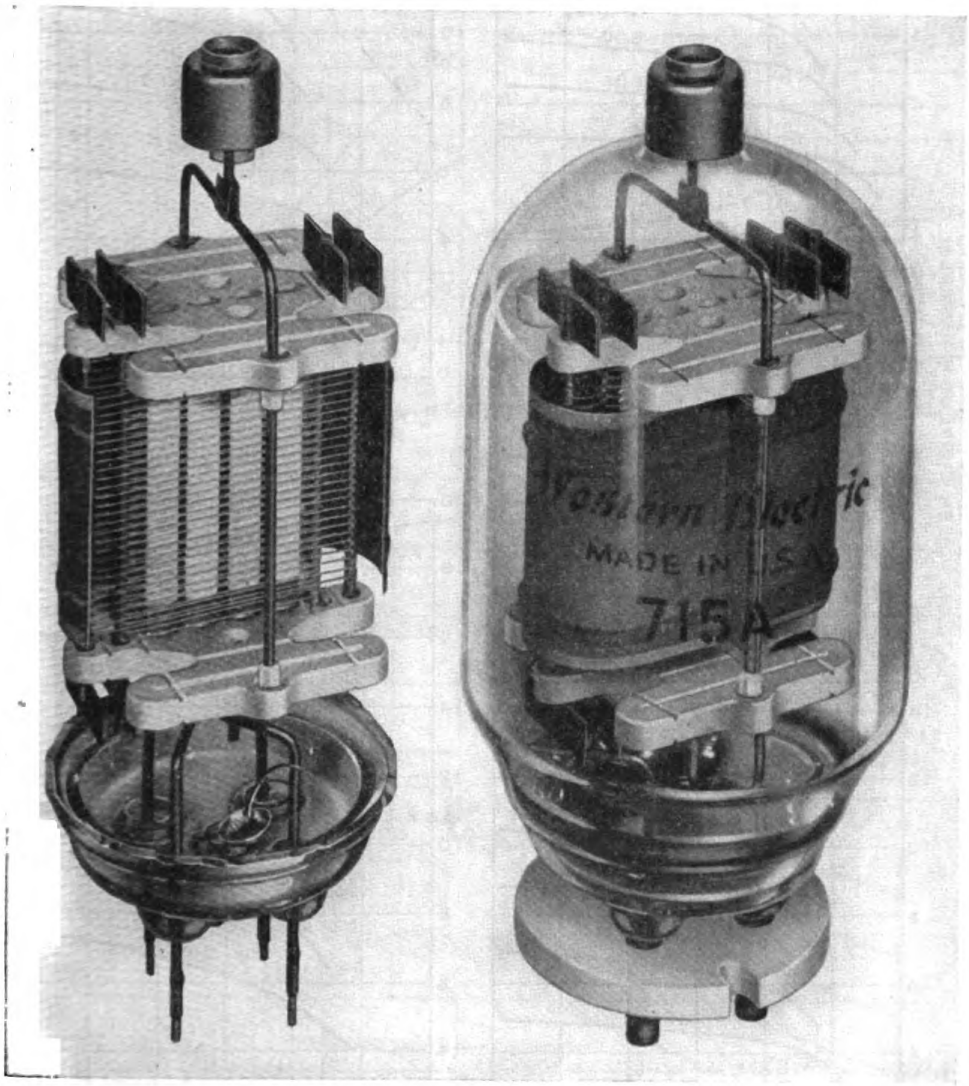

Fig. 5—The 715A vacuum tube.

of the control-grid and screen-grid supports. The plate is molybdenum with zirconium coating on its outside surface. This coating was employed to increase the thermal emissivity of the plate in the interest of a low operating temperature. It also serves to absorb some gas. The cathode, heater and grid terminals of the tube were brought out in the moulded-glass 4-Pin

Digitized by Google
Original from UNIVERSITY OF MICHIGAN
Generated on 2019-09-22 05:39 GMT / http://hdl.handle.net/2027/mdp.39015077775156
Public Domain, Google-digitized / http://www.hathitrust.org/access_use#pd-google

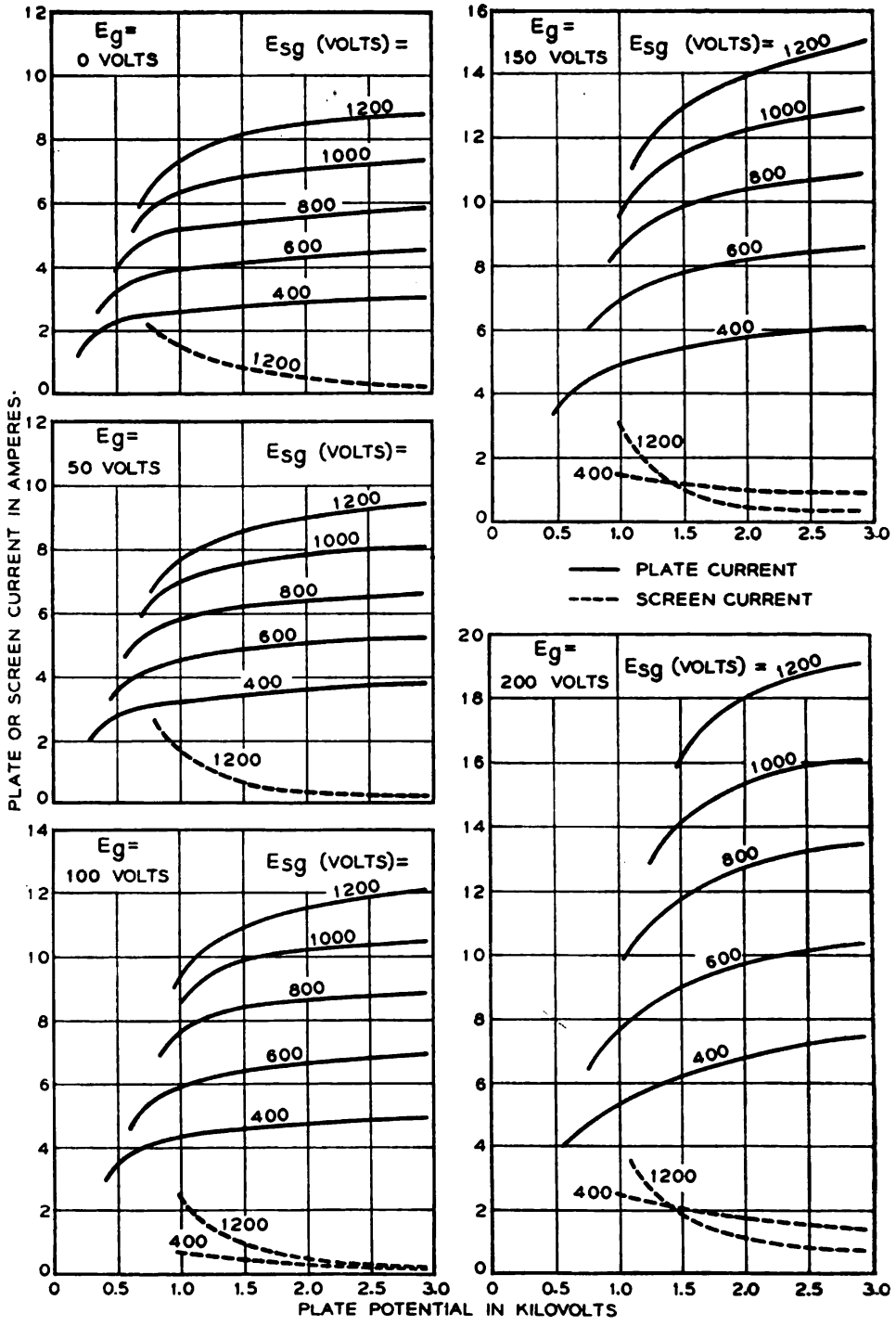

Fig. 6—Characteristics of the 715A vacuum tube.

base, and the plate terminal out the top of the bulb. This provided a very rigid structure which could stand extreme shock and vibration condi-

Digitized by Google
Original from UNIVERSITY OF MICHIGAN
Generated on 2019-09-22 05:39 GMT / http://hdl.handle.net/2027/mdp.39015077775156
Public Domain, Google-digitized / http://www.hathitrust.org/access_use#pd-google

tions. Although this structure sacrificed something in electronic performance over the 701A it still was quite satisfactory as a pulse modulator.

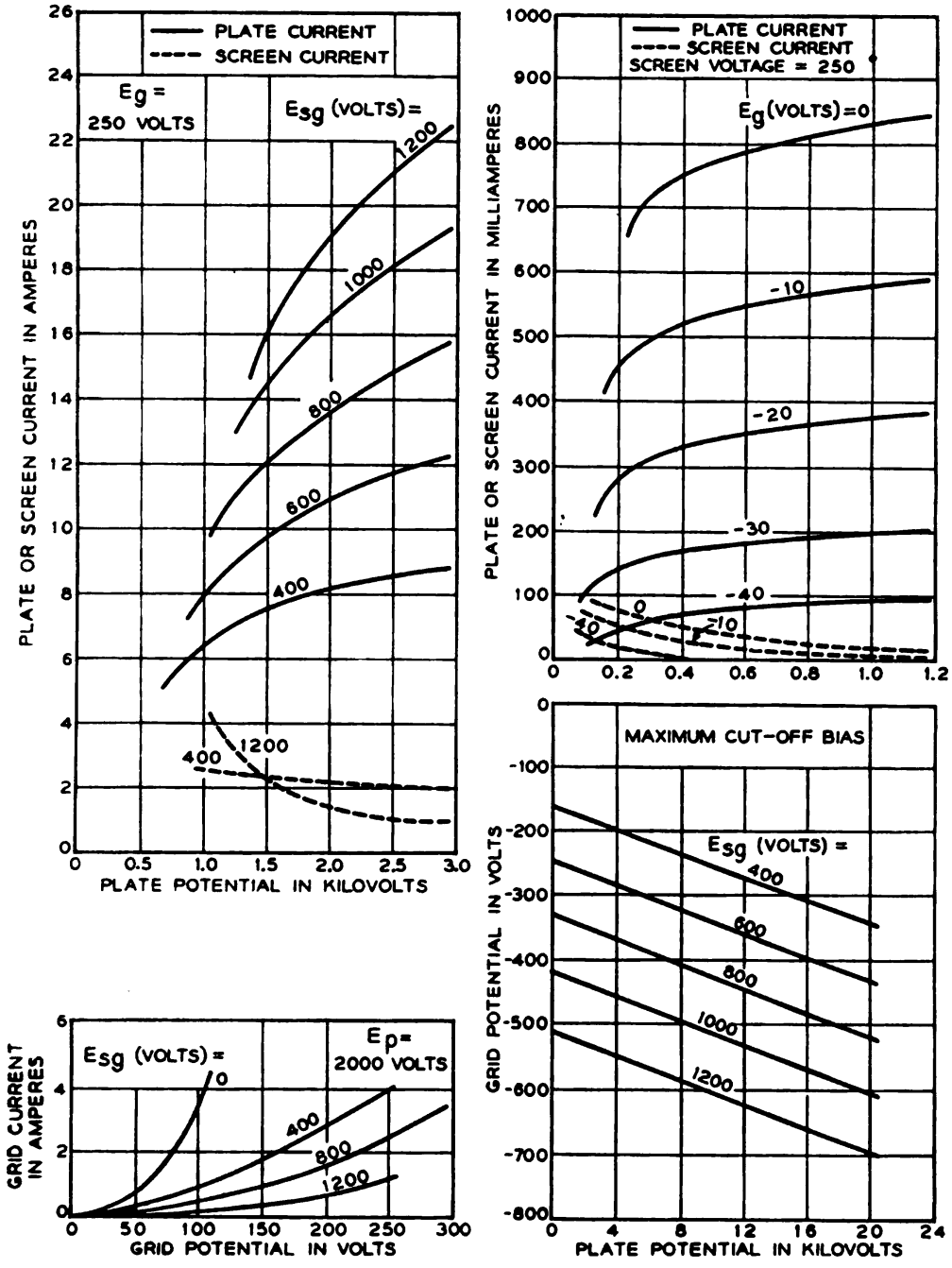

FIG. 6 (Continued)

The characteristics of the 715A tube applicable to both high voltage and low voltage operation are shown in Fig. 6. It was found that in spite of

Digitized by Google
Original from UNIVERSITY OF MICHIGAN
Generated on 2019-09-22 05:39 GMT / http://hdl.handle.net/2027/mdp.39015077775156
Public Domain, Google-digitized / http://www.hathitrust.org/access_use#pd-google

the internal ceramic insulators, satisfactory operation could be obtained at voltages as high as 15 kv. Since the 715A was designed primarily for airborne applications it was found desirable to design the heater to operate directly from the aircraft's storage battery which was a 24 volt battery.

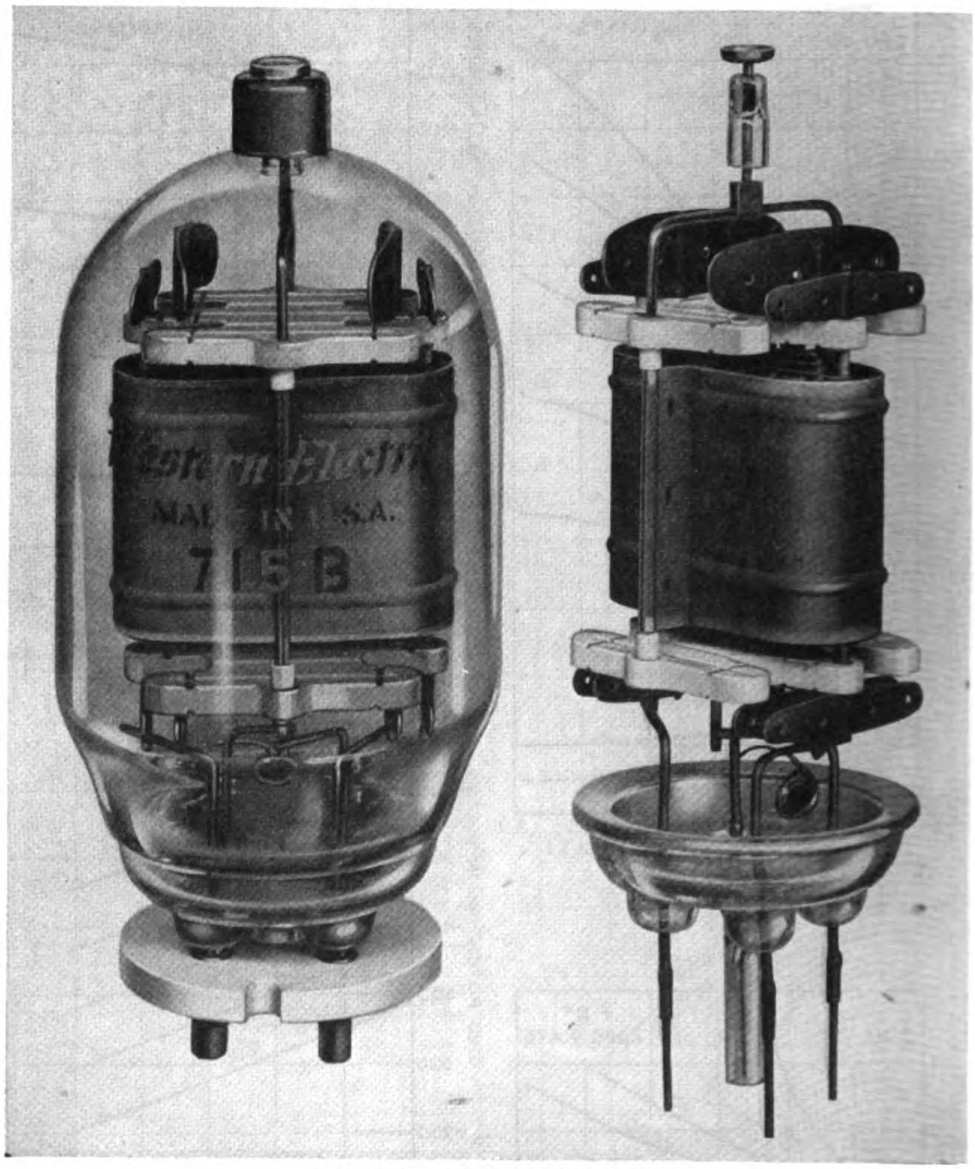

Fig. 7—The 715B vacuum tube.

It was also desirable that the equipment be operable when the charging generator was not running, at which point the voltage might be as low as 22 volts, and also when the generator was charging and the voltage as high as 28.5 volts. This required a compromise in the design of the heater which

Digitized by Google
Original from UNIVERSITY OF MICHIGAN
Generated on 2019-09-22 05:40 GMT / http://hdl.handle.net/2027/mdp.39015077775156
Public Domain, Google-digitized / http://www.hathitrust.org/access_use#pd-google

resulted in operation of the cathode at somewhat higher than normal temperature under rated conditions. The ratings of the 715A tube are given in Table I.

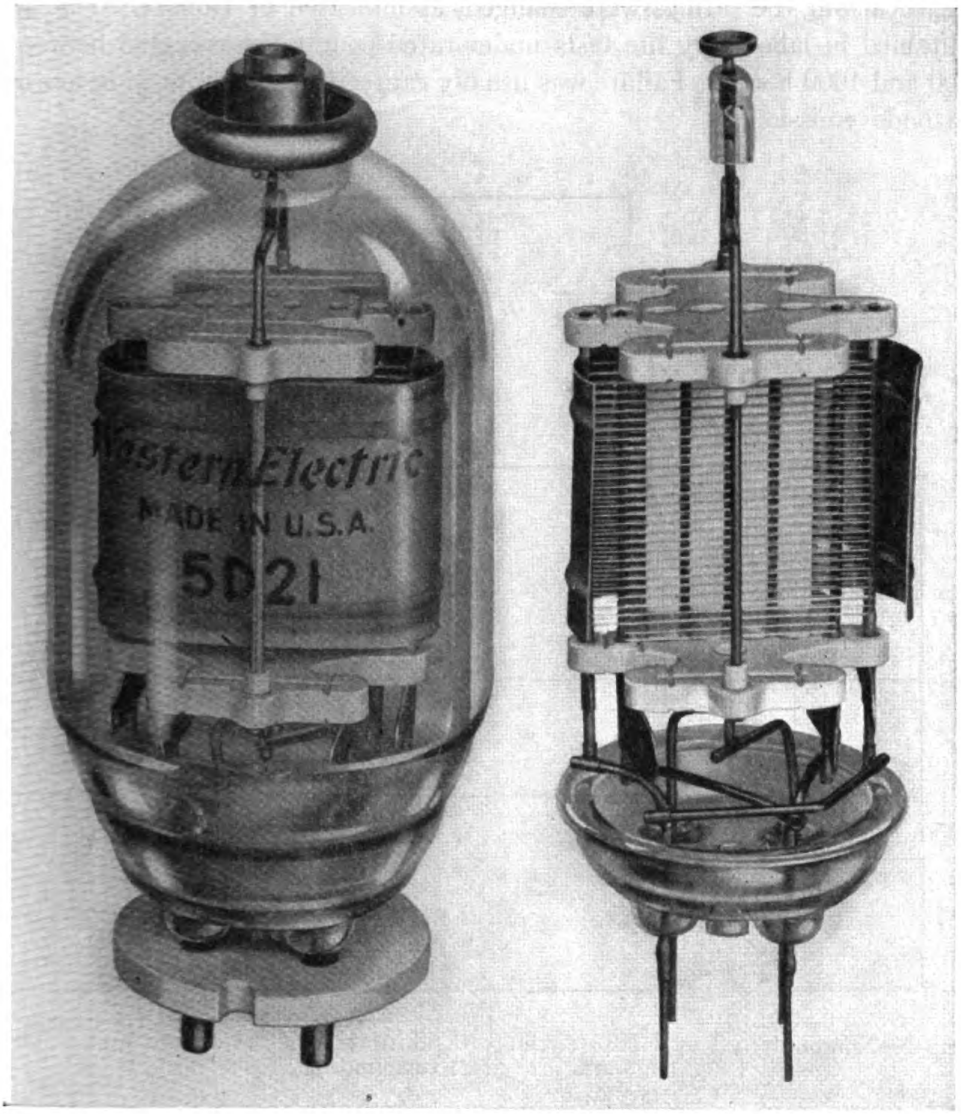

Fig. 8—The 5D21 vacuum tube.

The 715B Tube

Some applications developed which required a peak pulse current slightly greater and of longer duration than that for which the 715A was rated. Meanwhile more experience with the 715A and improvements in processing techniques indicated that a higher peak current rating was justifiable providing the grid temperatures were not increased.

Digitized by Google
Original from UNIVERSITY OF MICHIGAN
Generated on 2019-09-22 05:40 GMT / http://hdl.handle.net/2027/mdp.39015077775156
Public Domain, Google-digitized / http://www.hathitrust.org/access_use#pd-google

The 715B tube is essentially the same structure as the 715A except that larger radiating fins are attached to the ends of the grid support wires. Figure 7 shows the structure of the 715B tube. The characteristics were identical but the ratings were changed, as indicated in Table I. The life obtained in laboratory life tests under rated conditions averaged between 500 and 1000 hours. Failure was usually caused by grid emission or loss of cathode emission.

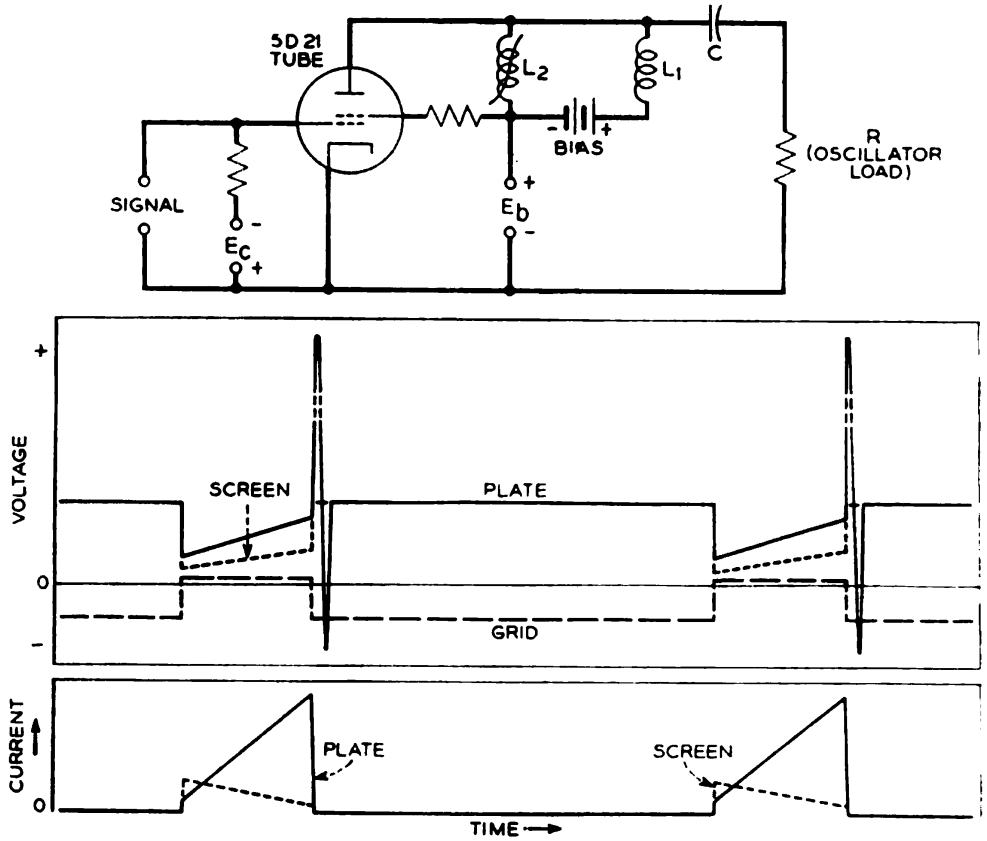

Fig. 9—Non-linear coil modulator circuit with illustration of the current and voltage relations in the 5D21 vacuum tube.

The 5D21 Tube

In response to the demand for further improvement of this structure in its ability to withstand higher voltage, the 5D21 tube was developed, Fig. 8. It is of the same family as the 715A and 715B. It was found that higher voltages could be used if the grid cooling radiators were removed from the top end of the tube. The cooling of the grid was maintained by providing copper wire connections from the bottom ends of the grid support wires to the base seals. This and the use of a specially designed plate terminal cap enabled the voltage rating to be raised to 20 KV.

Digitized by Google
Original from UNIVERSITY OF MICHIGAN
Generated on 2019-09-22 05:40 GMT / http://hdl.handle.net/2027/mdp.39015077775156
Public Domain, Google-digitized / http://www.hathitrust.org/access_use#pd-google

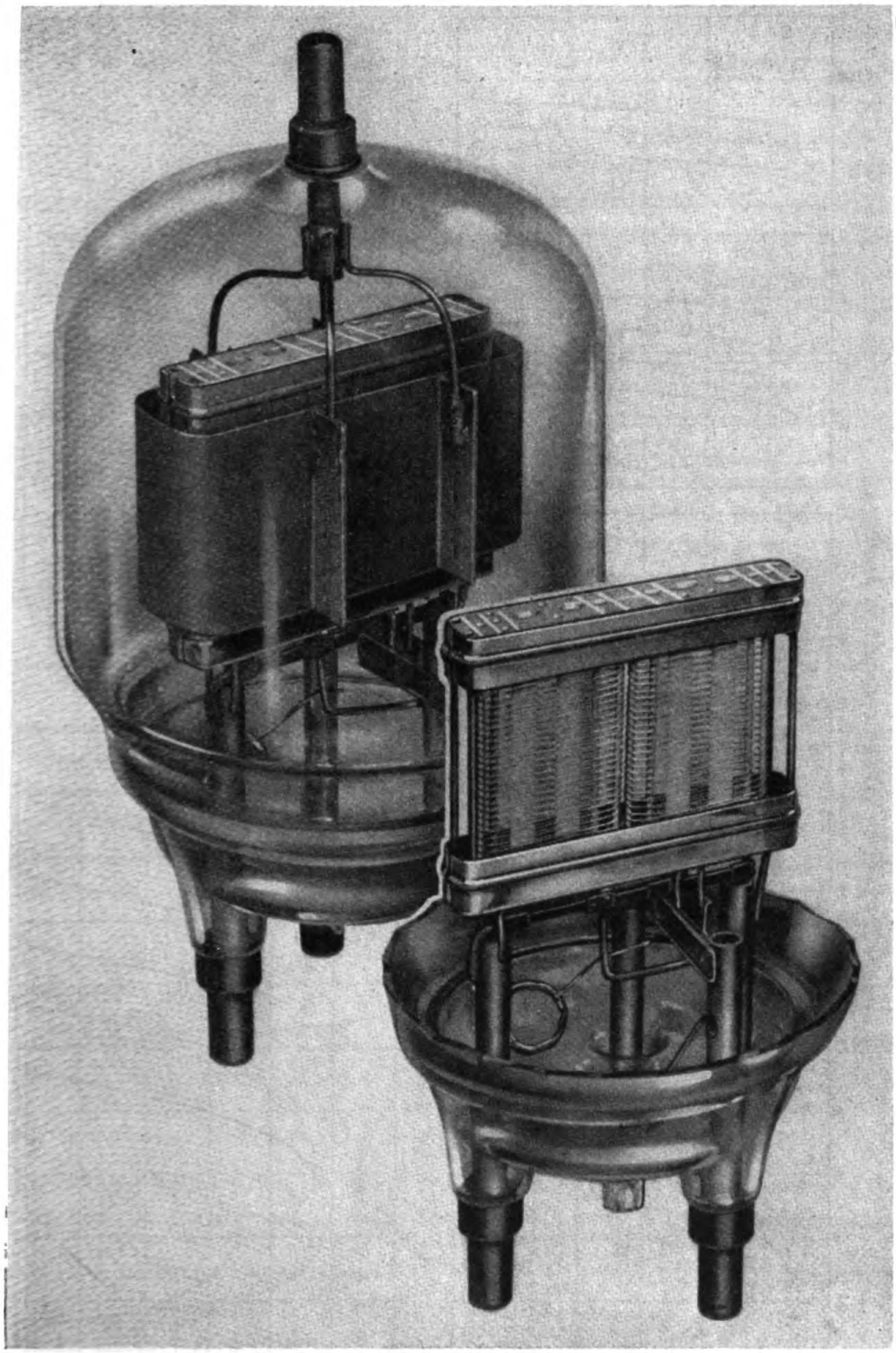

Fig. 10—The experimental 426XQ vacuum tube.

The 5D21 tube also found application as the control tube in non-linear coil type modulators.[4] Here the function of the tube was to permit passage

Digitized by Google
Original from UNIVERSITY OF MICHIGAN
Generated on 2019-09-22 05:40 GMT / http://hdl.handle.net/2027/mdp.39015077775156
Public Domain, Google-digitized / http://www.hathitrust.org/access_use#pd-google

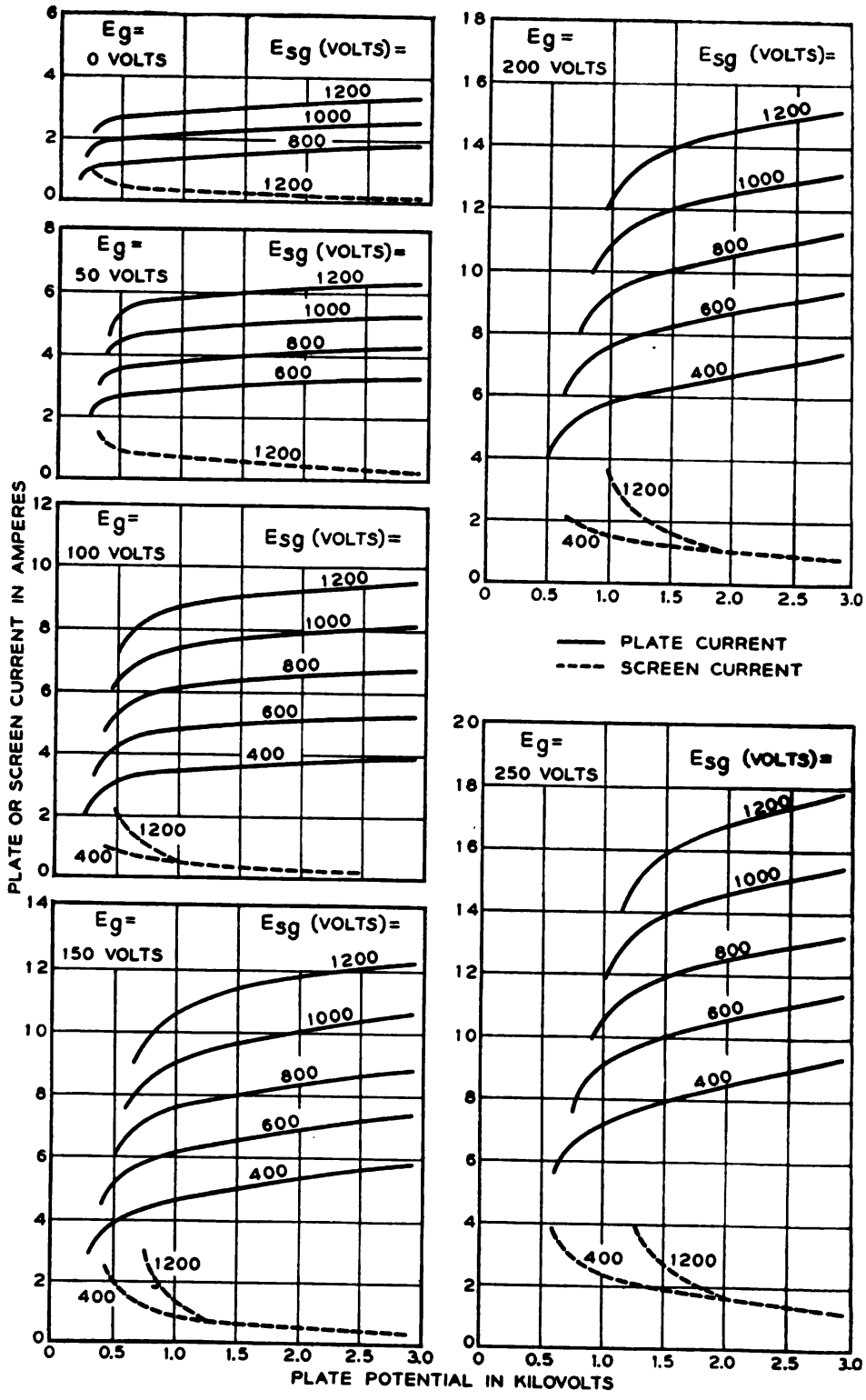

Fig. 11—Characteristics of the 426XQ vacuum tube.

Digitized by Google
Original from UNIVERSITY OF MICHIGAN
Generated on 2019-09-22 05:40 GMT / http://hdl.handle.net/2027/mdp.39015077775156
Public Domain, Google-digitized / http://www.hathitrust.org/access_use#pd-google

of a moderately high current through an inductance and then suddenly to cut off the current and withstand the resulting voltage which built up across the circuit. A schematic of this type of circuit is shown in Fig. 9. In this circuit the tube is required to pass about two amperes peak plate current which builds up over a period of about 150 microseconds. The d-c. voltage under these conditions is about 1000 to 4000 volts and the screen voltage may be obtained from the same source through series resistance. The grid is driven only slightly positive. Screen-grid dissipation is one of the limiting factors in this type operation. Primary emission from the screen

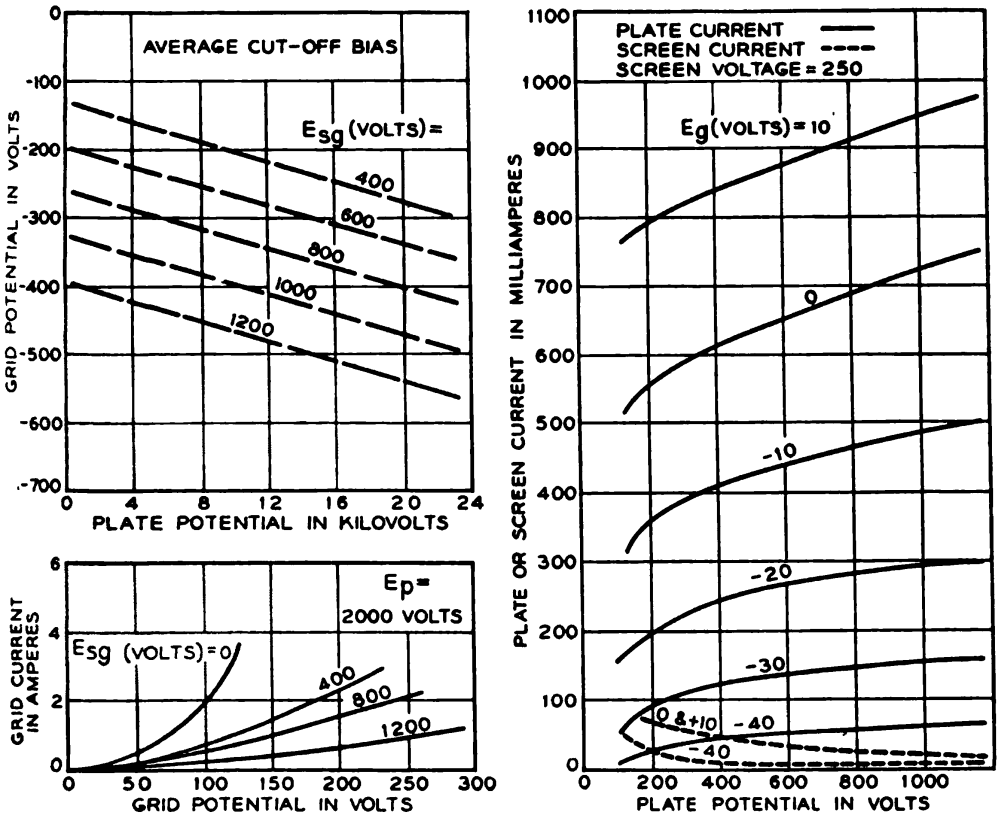

FIG. 11 (Continued)

grid, being present when the plate rises to its very high potential, tends to discharge the circuit prematurely, the energy wasted appearing as heat at the plate.

THE 426XQ TUBE

Since there was considerable demand for tubes capable of operating at voltages as high as 25 KV, a tube was developed to operate at this voltage. The limit of the 5D21–715B type structure seemed to have been reached at about 20 KV. It was also desirable to increase the current rating of the

Digitized by Google
Original from UNIVERSITY OF MICHIGAN
Generated on 2019-09-22 05:41 GMT / http://hdl.handle.net/2027/mdp.39015077775156
Public Domain, Google-digitized / http://www.hathitrust.org/access_use#pd-google

tube since in a laboratory test equipment a pulse power of 1.5 to 2 megawatts was needed. The laboratory number 426XQ tube shown in Fig. 10 was the result. Four of these tubes in parallel were capable of providing pulses of about 1.75 megawatts. In the 426XQ tube, the bulb used on the 701A was employed and the plate supported entirely from its terminal in this bulb. The same four cathodes were used, but were spaced farther apart than in the 715-type tube. Two separate control-grids and two screen-grids were used, each pair encompassing two cathodes. This allowed a reduction of dissipation per grid compared to the 715-type, otherwise similar techniques were employed. The characteristics are shown in Fig. 11.

The tentative ratings applied to the 426XQ are given in Table I. The allowable peak plate current was increased for this tube because the technique of processing had improved so that a higher level of cathode activity was consistently realized. Also the greater spacing between cathodes and use of two sets of grids resulted in better grid cooling. The tube was not used in any radar equipment, because by the time it was available the trend in radar equipment was toward small, compact apparatus in which spark gap and transmission line modulators[5] found considerable application. The 426XQ proved very satisfactory in laboratory test equipment. One set of these tubes operated for somewhat more than 2000 hours.

The Chief Problems

The difficulties experienced with this series of oxide-cathode pulse modulator tubes can be divided into three general classifications, namely: sparking, cathode emission, and grid emission.

The sparking in these tubes can roughly be divided into two types, which may be called inter-electrode sparking and cathode sparking. Inter-electrode sparking is a discharge between two electrodes of the tube caused by the momentary breakdown of the insulation between them or by a gas discharge. If the breakdown of insulation is caused by light deposited films, the resultant discharge usually causes removal of the film and cures the trouble automatically, provided no other damage is done to the tube. Gas discharges from isolated pockets may be initiated by the high fields or by bombardment by stray electrons. If these pockets are not numerous they are usually dissipated after a few minutes of tube operation such that further sparking is very intermittent and probably not of sufficient intensity to interfere with operation. The gas so released is ordinarily taken up by the getter in the tube so that operation is not subsequently impaired.

Cathode sparking may be caused by positive ion bombardment of the cathode or by poor adherence of cathode material when subject to electro-

Generated on 2019-09-22 05:41 GMT / http://hdl.handle.net/2027/mdp.39015077775156
Public Domain, Google-digitized / http://www.hathitrust.org/access_use#pd-google
Digitized by Google
Original from UNIVERSITY OF MICHIGAN

static fields. This type of sparking usually does not clear up and when it becomes serious the tube must be replaced.[6] It can be aggravated by sparking in the oscillator part of the radar system. There is some evidence to indicate that very high rates of rise of the pulse current drawn from the cathode may tend to produce cathode sparking. At rates of rise in excess of about 50 amperes per microsecond per square centimeter of cathode area a tendency for increased sparking has been noticed.

Cathode emission, here as in any other tube, is governed by cathode temperature and other considerations such as quantity and kind of gas in the tube, the core material, coating material, and techniques of processing. No attempt will be made to consider these factors in this paper as they are sufficiently complex that no very clear cut dissertation can be given. Standard core materials and coatings were employed with good results. It was found that the double carbonates (Ba, Sr) were less subject to sparking than the triple carbonates (Ba, Sr, Ca). The cleanliness and previous treatment of the other parts of the tube seemed to be the major factor in determining the level of emission obtained.

Primary grid emission, or thermionic emission from the control-grid and screen-grid, was one of the most difficult problems in the development and production of these tubes. Many trials were made using different materials and coatings on the grids, but from all considerations gold was found to be the most satisfactory. The grids in all the tubes described here are gold plated or gold clad molybdenum. It is not considered that the use of molybdenum for the core material is necessary, it being used here mainly because it seemed to be the most economical material that had sufficient stiffness to maintain grid alignment. Materials that tend to alloy with gold easily are not suitable as it was found that gold alloys were not as good as pure gold on the grid surface. The limitation involved in the use of gold is that the temperature of the grid must be kept low enough that evaporation of gold is not serious. This temperature limit is probably about 700°C. If gold is evaporated, the grid soon loses its coating and primary emission builds up rapidly. Also, the cathode emission seems to be poisoned by the gold vapor.[7]

Acknowledgment

The author wishes particularly to acknowledge the contributions of his immediate associates, Messrs. H. L. Downing, J. W. West, and J. E. Wolfe in the development of this series of tubes. Many others also made important contributions. We are also indebted to the M.I.T. Radiation Laboratory for data from life tests which they conducted on many of these tubes.

Generated on 2019-09-22 05:41 GMT / http://hdl.handle.net/2027/mdp.39015077775156
Public Domain, Google-digitized / http://www.hathitrust.org/access_use#pd-google
Digitized by Google
Original from UNIVERSITY OF MICHIGAN

References

1. R. Colton, Radar in the U. S. Army, *Proc. I.R.E.*, Vol. 33, pp. 740–750, November 1945.
2. The SCR-268 Radar, Editorial, *Electronics*, Vol. 18, pp. 100–109, Sept. 1945.
3. W. C. Tinus and W. H. C. Higgins, Early Fire-Control Radar for Naval Vessels. See pp. 9 ff.
4. E. Peterson, Coil Pulsers for Radar. See pp. 257 ff.
5. F. S. Goucher, J. R. Haynes, W. A. Depp, and E. J. Ryder, Spark Gap Switches for Radar. See pp. 270 ff.
6. E. A. Coomes, The Pulsed Properties of Oxide Cathodes, *Jour. Applied Phys.*, Vol. 17, pp. 647–654, August 1946.
7. J. Rothstein, The Poisoning of Oxide Cathodes by Gold, (Abstract) *Phys. Rev.* Vol. 69, 1st/15th June 1946, p. 693.

Generated on 2019-09-22 05:41 GMT / http://hdl.handle.net/2027/mdp.39015077775156
Public Domain, Google-digitized / http://www.hathitrust.org/access_use#pd-google
Digitized by Google
Original from UNIVERSITY OF MICHIGAN

Coil Pulsers for Radar

By E. PETERSON

RADAR systems in current use radiate short bursts of energy developed by pulsing a high-frequency generator, usually a magnetron. One means of developing the requisite impulses employs a non-linear coil and is termed a coil pulser. Such pulsers are found in substantial numbers among the Navy's complement of precision radars. Most fire control radars on surface vessels are equipped with them, and all modern radar installations on submarines are so equipped for search and for torpedo control.

History of Development

Coil pulsers had their origin in the magnetic harmonic generators first built for the telephone plant. Multi-channel carrier telephone systems in general use throughout the Bell System require numbers of carriers, harmonically related in frequency. These are derived from non-linear coil circuits[1] which convert energy supplied by a sine wave input into regularly spaced, sharply peaked pulses.

When development was started on precision radars, one of these circuits generating a power peak of a few hundred watts, several microseconds in duration, was adapted to the purpose.[2] Its output was shaped and amplified by vacuum tubes of sufficient power to key or modulate the ultra-high-frequency generator of the radar transmitter. All early fire-control radars were made up in this way; hundreds are still in use.

The next development of pulsers for fire-control radars was directed toward higher-powered pulses, shorter in duration for good range resolution. These had to be provided by a small package pulser, small enough and rugged enough to mount integrally with the magnetron and the antenna. The power rectifier was to be located at any convenient distance, and the rectified voltage had to be low enough to permit the use of standard low-voltage cables. These requirements put high vacuum tubes at a disadvantage in handling the finally developed pulses. Pulse transformers had not attained their present state of perfection in dealing with short pulses at this early stage and the pulser therefore had to work the magnetron directly.

[1] Magnetic Generation of a Group of Harmonics, by Peterson, Manley and Wrathall, *B.S.T.J.*, vol. XVI, p. 437, 1937.

[2] Fire-Control Radars, by Tinus and Higgins. See pp. 9 ff.

Digitized by Google
Original from UNIVERSITY OF MICHIGAN
Generated on 2019-09-22 05:45 GMT / http://hdl.handle.net/2027/mdp.39015077775156
Public Domain, Google-digitized / http://www.hathitrust.org/access_use#pd-google

One arrangement developed by W. Shockley to meet these requirements used a thyratron as a switch to generate pulses. High vacuum tubes were used at low voltages for comparatively long-time intervals in the driving circuit. Deficiencies of the thyratrons available at that time prevented the generation of pulse powers as high as required. With the earlier experience on low-level coil pulsers in mind, it was natural to think of using a non-linear coil for switching pulses at high level, in place of the thyratron. Much development was required to arrive at suitable circuits embodying the basic ideas, to build non-linear coils capable of withstanding high voltages, to proportion the circuit elements for efficient operation at specified powers and pulse durations, and to shape the output pulse to the desired flat-topped form.

This development resulted in a power pulser mounted in an oil-filled steel box, with associated high vacuum tubes of the sturdiest sort mounted externally, operated from a 1200 volt d-c. supply. It was suitable for installation integral with the antenna, and rugged enough to withstand gun blast and shock. Life of the pulser box components is long, and performance stable with time and temperature. The time of pulse emission is linked precisely to the input wave, practically independent of voltage and frequency variations over a suitable range. Such precision timing, or freedom from jitter, permits starting the indicator equipment in advance of the pulse emission time so that target ranges may be accurately measured. The power rectifier voltage is much lower than that of the pulse applied to the magnetron, and the pulser works directly into the magnetron without requiring an intermediary pulse transformer.

Subsequent developments left unchanged the general form of the circuit and its mounting, but were devoted to achieving various pulse widths, powers, and pulsing rates to suit different applications. Pulse widths covered a range from two-tenths to over one microsecond, peak powers ranged from 100 to 1000 kw, and pulsing rates ranged from 400 to 3600 pulses per second.

Non-Linear Coil Structures

An idea of the general form and makeup of non-linear coils used in various radar developments can be had from the photograph of Fig. 1. All cores shown there are made of molybdenum permalloy tape, one mil thick. Insulation is electroplated on the tape in a silicic acid bath, and the tape is wound in ring form. After the standard magnetic anneal of 1000°C in hydrogen, the coating of insulation a fraction of a mil thick adheres firmly to the tape.

The smallest coil shown in Fig. 1 seen just in front of the oil filled container in which it is mounted is used for low-power pulse generation. Its core weighing 7 grams is wound on an isolantite form.

Digitized by Google
Original from UNIVERSITY OF MICHIGAN
Generated on 2019-09-22 05:45 GMT / http://hdl.handle.net/2027/mdp.39015077775156
Public Domain, Google-digitized / http://www.hathitrust.org/access_use#pd-google

The two larger coils shown are used in power pulsers. Their cores are made up of self-supporting rings. The smaller coil has a core weight of one kilogram and is used at voltages up to 25 kv. for the generation of power peaks of the order of 100–250 kw. Phenol fibre is used to support and position the core and winding. The larger core has a weight of 13 kg. and is used at a voltage of 40 kv. in a pulser generating power peaks of one megawatt. Glass-bonded mica and built-up mica are used for support and

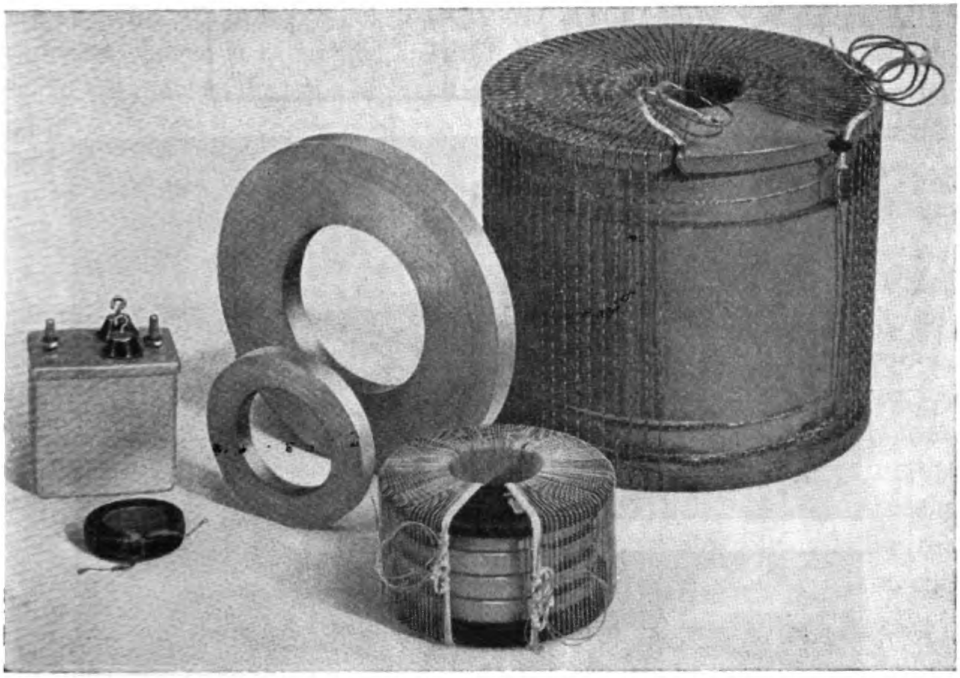

Fig. 1—Non-linear coils used in various radar transmitters. The smallest coil at the left, seen in front of its container, is used for low power pulse generation. The two larger coils are used in power pulsers developing 200 KW and 1000 KW peaks, respectively. The core rings of molybdenum permalloy tape are assembled into the coils shown.

positioning of the core rings and windings. The coils are assembled with other passive elements of the pulser network and the whole immersed in oil.

Operating principles of the two types of pulser circuits in which these coils are used are now to be discussed.

Low-Level Pulser

A schematic of the circuit used for developing low-power pulses is shown in Fig. 2a. Sinusoidal driving current (i_1) is introduced from the left, and a sharply peaked wave (i_2) is developed in the right-hand mesh. A resonant circuit (L_1C_1) serves to prevent dissipation of the generated pulse in the input mesh, and to tune out the input reactance at the driving frequency.

Generated on 2019-09-22 05:45 GMT / http://hdl.handle.net/2027/mdp.39015077775156
Public Domain, Google-digitized / http://www.hathitrust.org/access_use#pd-google
Digitized by Google
Original from UNIVERSITY OF MICHIGAN

Capacitance and resistance elements (C_2R_2) in conjunction with the non-linear coil (L_2) make up the output mesh.

A complete cycle of the input wave is depicted in Fig. 2c, placed to correspond with the *B-H* loop of the non-linear core shown above it in Fig. 2b.

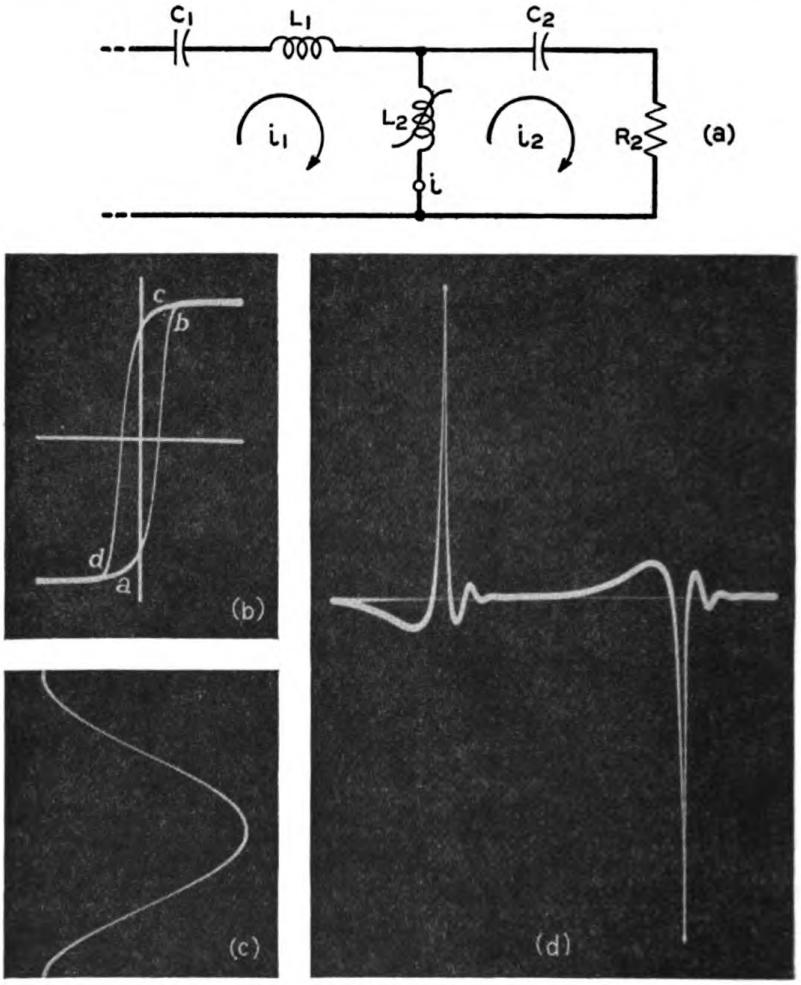

Fig. 2—Low-level coil pulser.

(a) Circuit diagram showing input tuning C_1L_1, non-linear coil L_2, output condenser C_2, and load resistor R_2.

(b) *B-H* loop of non-linear coil, with letters marking transitions between permeable and saturable regions.

(c) Sinusoidal input current wave scaled and placed to correspond with the horizontal scale of Fig. 2b.

(d) Pulsed output wave, i_2 as ordinate; i_1 as abscissa.

Action of the circuit is now to be followed throughout a cycle, starting with the input wave at its maximum negative excursion, condenser C_2 uncharged, and the core in its lower saturation region. Here the slope of the *B-H* loop and the corresponding differential permeability and inductance are

Digitized by Google
Original from UNIVERSITY OF MICHIGAN
Generated on 2019-09-22 05:46 GMT / http://hdl.handle.net/2027/mdp.39015077775156
Public Domain, Google-digitized / http://www.hathitrust.org/access_use#pd-google

small. Hence the voltage drop across the coil is small. Little current flows in the output mesh, and practically all the input current flows through the coil. Matters are much different during the next interval in which the increase of current in L_2 brings the core into the permeable region *a-b*. Here the differential permeability is large so that part of the input current is diverted to the output mesh, charging the output condenser until upper saturation is reached at *b*. There the coil inductance falls to a low value, switching most of the condenser voltage across the load resistance. A current pulse accordingly develops in the output mesh lasting until the condenser charge is exhausted. The form of the current pulse shown in Fig. 2d approaches that of a highly damped sinusoid, and the pulse duration and magnitude are functions of the three elements of the discharge mesh. During the next half-period of the input wave, the same situation develops as in the first half-period, except that the corresponding currents and voltages throughout are reversed in sign.

According to this description the non-linear coil acts like a switch which automatically shifts the inductance from relatively high to relatively low values at specific coil currents. When the core is driven well into saturation, as is the case here, the ratio of these two inductances can be made large, usually in the neighborhood of several thousand. One feature of its action important from the efficiency standpoint is that the pulse occurs for the most part in the saturation region, where the contribution to eddy loss is small. The principal core loss occurs in the permeable region while the output condenser is charging, when variation of current through the coil occurs at a relatively slow rate.

In low-level radar applications the pulser output feeds a vacuum tube amplifier biased so that pulses of just one polarity are passed, the other oppositely poled pulse being cut off.

Since the range sweep of the radar receiver is initiated prior to pulse emission, the pulse should occur at a time linked precisely to the input wave. Otherwise the received pulse would be blurred introducing an uncertainty in measuring target range. No blurring (jitter) is visible with normal coil pulser operation. To get a measure of any variations which might be associated with core magnetization, tests were performed on a communication circuit in which jitter occurring at an audio rate would show up as noise. Measurements with a sensitive noise meter indicate the corresponding variation of pulse emission time to be smaller than 10^{-9} second.

Power Pulser

Operating Principles

The power pulser has the same type of discharge circuit as the low-level pulser just discussed. It differs in using a d-c. rather than an a-c. power

Digitized by Google
Original from UNIVERSITY OF MICHIGAN
Generated on 2019-09-22 05:46 GMT / http://hdl.handle.net/2027/mdp.39015077775156
Public Domain, Google-digitized / http://www.hathitrust.org/access_use#pd-google

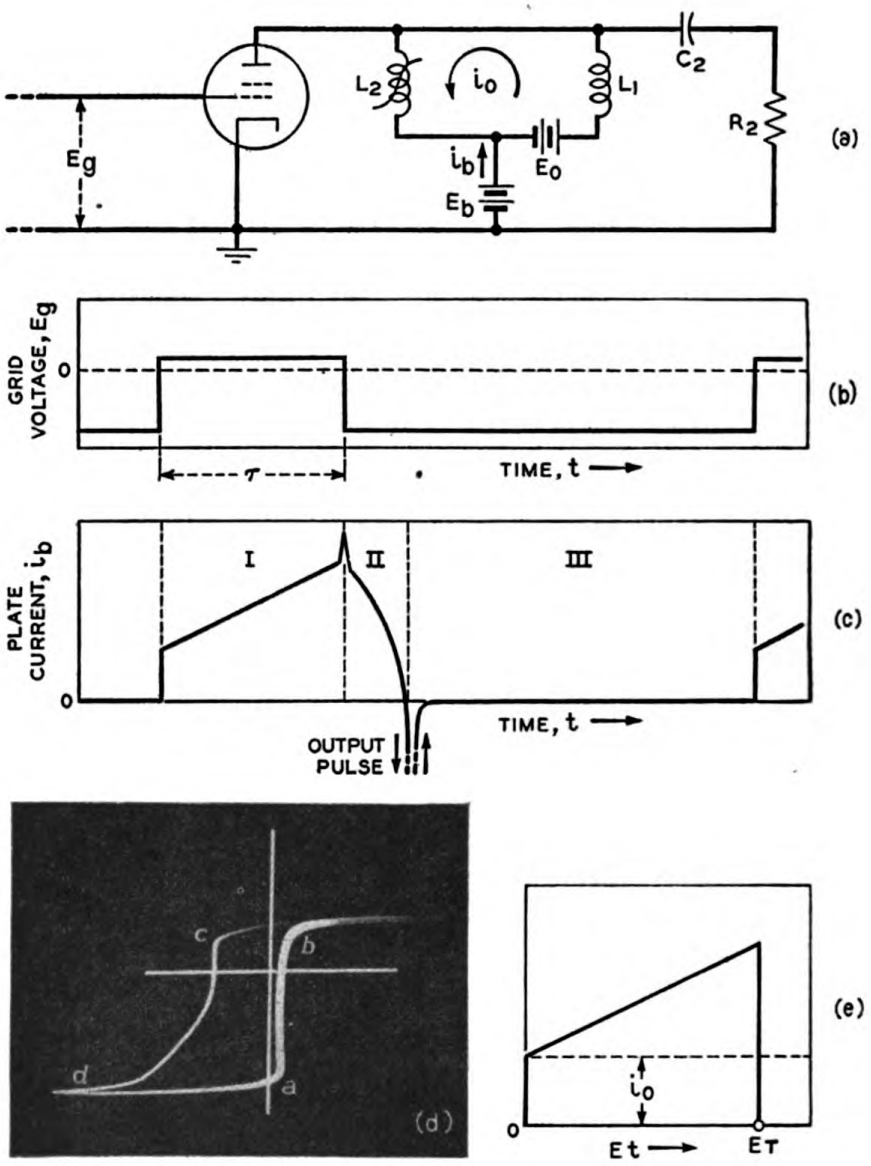

Fig. 3—Power pulser.

(a) Simplified circuit diagram showing charging tube at left, bias supply E_0, plate power supply E_b, linear coil L_1, non-linear coil L_2, output condenser C_2, and load resistor R_2.

(b) Rectangular wave of grid voltage impressed upon the tetrode of Fig. 3a. The tube conducts during the time τ in each cycle, and is cut off outside that interval.

(c) Plate current wave (i_b) corresponding to time scale of (b). During interval *I*, current is drawn through the paralleled inductors and the charging tube. At the end of this interval the tube is cut off and remains so until the start of the next cycle. During II, the magnetically stored energy is transferred to the condenser through R_2. At the same time the non-linear coil is brought toward saturation. During III saturation is reached; energy stored in C_2 is transferred to the load resistor through L_2 in a short pulse.

(d) *B-H* loop of non-linear coil used in the circuit of (a). Letters mark the most important transitions. During interval I magnetization proceeds from the lower left through *a* up to *b*; during II magnetization decreases past *c* down to *d*, and during III it extends far beyond the limits of the Figure to the left, returning to the neighborhood of *d* upon completion of the output pulse.

(e) Plot of current in linear coil during charging interval I against the product of coil voltage and time. Enclosed area represents energy stored in the linear coil. The rectangular area under the dashed line drawn through i_0 represents that part of the stored energy which varies with bias current.

Digitized by Google
Original from UNIVERSITY OF MICHIGAN
Generated on 2019-09-22 05:46 GMT / http://hdl.handle.net/2027/mdp.39015077775156
Public Domain, Google-digitized / http://www.hathitrust.org/access_use#pd-google

source, and in charging the load condenser by a free, rather than by a forced oscillation. Energy for the free oscillation is taken from the d-c. source in a preliminary operation, in which energy is stored in a linear inductor. This preliminary operation consists in closing a d-c. path from the plate power supply through the linear inductor by means of a high vacuum tube, permitting current to build up with time. After a predetermined time has elapsed, the tube circuit is opened, the d-c. path is thereby interrupted, and energy stored in the inductor transfers to the load condenser. In this way the voltage to which the load condenser is charged can be made many times greater than the voltage of the plate power supply. The simplified circuit of Fig. 3(a) will serve to bring out salient operating features. Conduction of the tetrode at the left is controlled by a rectangular wave of grid voltage (Fig. 3b) developed by a multivibrator (not shown) which swings the grid from a potential below cutoff to one just above cathode potential. The plate power source E_b feeds two inductors in parallel, L_1 being linear, and L_2 non-linear. A small biasing voltage E_0 drives polarizing current i_0 through the two inductors in series.

The preliminary operation which serves to transfer energy from the main power source to the inductors is initiated when the tetrode grid is driven positive. Current from the main source builds up through the paralleled inductors and the tetrode as indicated on Fig. 3c, interval *I*. The region in which the non-linear coil works may be seen from the hysteresis loop of Fig. 3d. Its operating point is displaced to the left of the origin near *d* by the bias current. When the tetrode conducts, current in the non-linear coil rises rapidly at first in the lower saturation region until *a* is reached. The rise thereafter is comparatively small and slow in traversing the permeable region *a-b*, while at the same time current builds up in the linear coil at a much greater and practically uniform rate. When the core of L_2 reaches saturation near *b* its inductance again drops, preventing further rise of current in L_1. At this time the tetrode is driven below cutoff and remains out of the picture until the start of the next cycle.

The second interval, in which energy is transferred from the linear inductor to the load condenser, starts with the cutoff of tetrode current. This transfer is effected in an oscillation with frequency determined mainly by the paralleled inductors and the load condenser. In this interval II of Fig. 3c, current through the non-linear coil falls suddenly at first from *b* to *c* and then more slowly from *c* to *d*. The rate of change in region *c-d* is much greater than that in *a-b* as indicated by the fainter trace in Fig. 3d, so that eddy currents in the core are increased and the slope of the descending branch of the loop reduced correspondingly. Thus some of the energy previously stored in the linear inductor is used up in completing the magnetization cycle and this part, consequently, is not available for transfer to the load

Digitized by Google
Original from UNIVERSITY OF MICHIGAN
Generated on 2019-09-22 05:46 GMT / http://hdl.handle.net/2027/mdp.39015077775156
Public Domain, Google-digitized / http://www.hathitrust.org/access_use#pd-google

condenser. The maximum voltage to which C_2 is charged in this interval is made much greater than that of the d-c. power source (E_b). The ratio of these two voltages depends upon the ratio of the inductance charging time in the preceding interval to the oscillation period. Both factors can be varied over wide limits, and step-up ratios of roughly ten to twenty are generally used.

The third interval starts with magnetization of the non-linear core near point *d* on the loop, where the inductance again drops. This situation is precisely the same as that previously described for the low-power pulser. As a result the condenser discharges through the load resistance at the time indicated in Fig. 3c, driving the core far into saturation with a field of the order of a hundred oersteds. This field extends too far to the left of point *d* to be shown in Fig. 3(d). Here the differential permeability approaches unity, and the correspondingly low inductance permits a rapid build-up of pulse current. Evidently but one pulse is produced each time the tetrode conducts, and the number of pulses produced per second is changed simply by varying the input frequency without requiring any circuit change, power dissipations permitting.

Energy storage in the linear coil depends upon its inductance, upon the bias current, and upon the peak current reached during the tetrode conduction interval. A plot of the current in L_1 against the product of time and of voltage across the coil permits this energy to be represented as an area (Fig. 3e). Evidently a given area can be made up by varying the relative sizes of its component triangle and rectangle, only the latter varying with bias current. If for example the bias is reduced to zero, the rectangle would vanish and the peak current would have to be increased to attain the original amount of stored energy. The higher maximum current requires more cathode emission of the tetrode and leads to greater plate power dissipation. Thus in addition to determining the energy stored, the amount of bias is one of the factors determining power dissipation capacity and emission which must be provided in the driving tube or tubes. Additional factors enter to make a bias corresponding to *d* (Fig. 3d) the most favorable from an efficiency standpoint.

The operating principles developed above in terms of a simplified circuit have been applied to a number of practical circuit forms which are described in the sections following.

Load Circuit

In radar applications the useful load is a magnetron which takes the place of the linear resistance previously considered. Since the magnetron viewed at its input terminals acts essentially like a negatively biased rectifier, additional means must provide for the flow of condenser charging current in a

Digitized by Google
Original from UNIVERSITY OF MICHIGAN
Generated on 2019-09-22 05:46 GMT / http://hdl.handle.net/2027/mdp.39015077775156
Public Domain, Google-digitized / http://www.hathitrust.org/access_use#pd-google

direction opposite to that of the discharge pulse. This takes the form of a suitably poled diode shunted around the magnetron input terminals. After the main discharge pulse is completed, reactive elements are left with some little energy which tends to redistribute throughout the network. In course of redistribution, additional pulses of lower energy may occur shortly after the main pulse is completed. This tendency is a harmful one if the after-pulses are large, since echoes from short-range targets are obscured. Suppression of after-pulses is assisted by shunting around the diode-magnetron a linear inductance known as a clipping choke. This added inductance slows down the rate at which energy is redistributed, and permits the diode to fulfill its second function of dissipating the greater part of the residual energy. The shunting inductor, too, is made to fill a second function. Through provision of a bifilar winding, it passes heating current to the filament of the magnetron, thereby eliminating the need for high-voltage insulation otherwise required in the filament transformer.

Magnetic Bias

Several arrangements have been worked out for supplying various amounts of bias, some of them using a separate source, others being self-biased.[3] In general the use of external bias leads to a lower demand on the driving tetrode and is associated with pulse production at best efficiency. Circuits dispensing with an external bias source are that much more convenient in use, where the added tube demand and the lower efficiency corresponding can be handled without undue increase of the tube complement. In general the energy delivered to the magnetron is roughly 25 to 55 per cent of the plate energy input, with the higher figure applying to the higher outputs and external bias.

Transformer Coupling

In some cases it is convenient to equip the non-linear coil with primary and secondary windings providing voltage transformation or isolation to avoid adding a transformer for that purpose. The first case arises in the higher-powered pulsers, where the load condenser has to be charged to a voltage greater than the driving tetrode can withstand. For the Western Electric 5D21 tubes customarily used, voltage breakdown occurs near 20 kv, while condenser voltages in certain of the pulsers reach 30 and 40 kv. This situation calls for a step-up ratio from primary to secondary to fit the required potentials. The need for isolation may be illustrated by reference to Fig. 3a where the bias battery E_0 is shown maintained at the plate supply potential above ground. To avoid the resulting insulation problems in a

[3] One widely used circuit using a small amount of self-bias was developed by L. G. Kersta and E. E. Crump.

Digitized by Google
Original from UNIVERSITY OF MICHIGAN
Generated on 2019-09-22 05:46 GMT / http://hdl.handle.net/2027/mdp.39015077775156
Public Domain, Google-digitized / http://www.hathitrust.org/access_use#pd-google

rectifier built to supply bias, a secondary winding is readily provided on the non-linear coil for connection to the linear coil and to the bias rectifier, which can then be maintained with one side at ground potential.

In either case whenever coupled windings are employed, the inside winding is invariably made to carry the discharge pulse. This provision results in minimum saturation inductance, since the inner winding is brought as close to the magnetic core as the voltage breakdown strength of the intervening dielectric permits. This winding is disposed as uniformly as possible around the core to avoid leakage which would add to the saturation inductance, and so limit the rate of current build-up in the pulse. The other winding can then be disposed with generous spacings, and with partial core coverage if desired.

Pulse Shaping

The oscillation frequency of the magnetron is determined primarily by its internal structure, although it is to some extent a function of the impressed potential. Departure of the driving wave from perfectly rectangular form permits the oscillation frequency to vary during the pulse, to an extent depending upon the size and duration of the departure and upon the characteristics of the magnetron.[4] Frequency modulation thus produced disperses energy over the spectrum. With the receiver band width limited to reduce noise and interference, one effect of this spreading of energy over the spectrum is to cut down the strength of the observed echo. For this reason, other things being equal, rectangularity must be approximated well enough to make the wasted energy a small fraction of that usefully employed.

It is convenient to regard the rectangular wave as synthesized by a series of harmonically related sine waves of appropriate magnitudes. The fundamental component according to this concept has a half period equal to the duration of the pulse, and the other components, progressively smaller in amplitude, have frequencies which are odd harmonics of the fundamental. In the low-power pulser with its rounded discharge wave the harmonic waves are quite small in amplitude. To approach the flat-topped discharge wave necessary in the power pulsers, harmonic components must be built up. This can be done by providing additional resonances in the discharge circuit at the wanted harmonic frequencies.

With the close spacing between circuit elements and their proximity to the pulser box walls, parasitic capacitances of appreciable magnitude add to those normally present. These involve dielectrics of low loss and, since the circuit elements and connecting wires are firmly fixed in position, they are fairly well reproduced. They can be used, therefore, in conjunction

[4] The Magnetron as a Generator of Centimeter Waves, by Fisk, Hagstrum, and Hartman. See pp. 56 ff.

Digitized by Google
Original from UNIVERSITY OF MICHIGAN
Generated on 2019-09-22 05:47 GMT / http://hdl.handle.net/2027/mdp.39015077775156
Public Domain, Google-digitized / http://www.hathitrust.org/access_use#pd-google

with added reactors of small size to provide harmonic resonances needed to shape the discharge pulse. These help to bring up the third and fifth, and in some cases higher harmonics.

Results after shaping are shown in Fig. 4 for two extremes of pulse width. The shorter pulse, roughly a quarter microsecond in average duration,

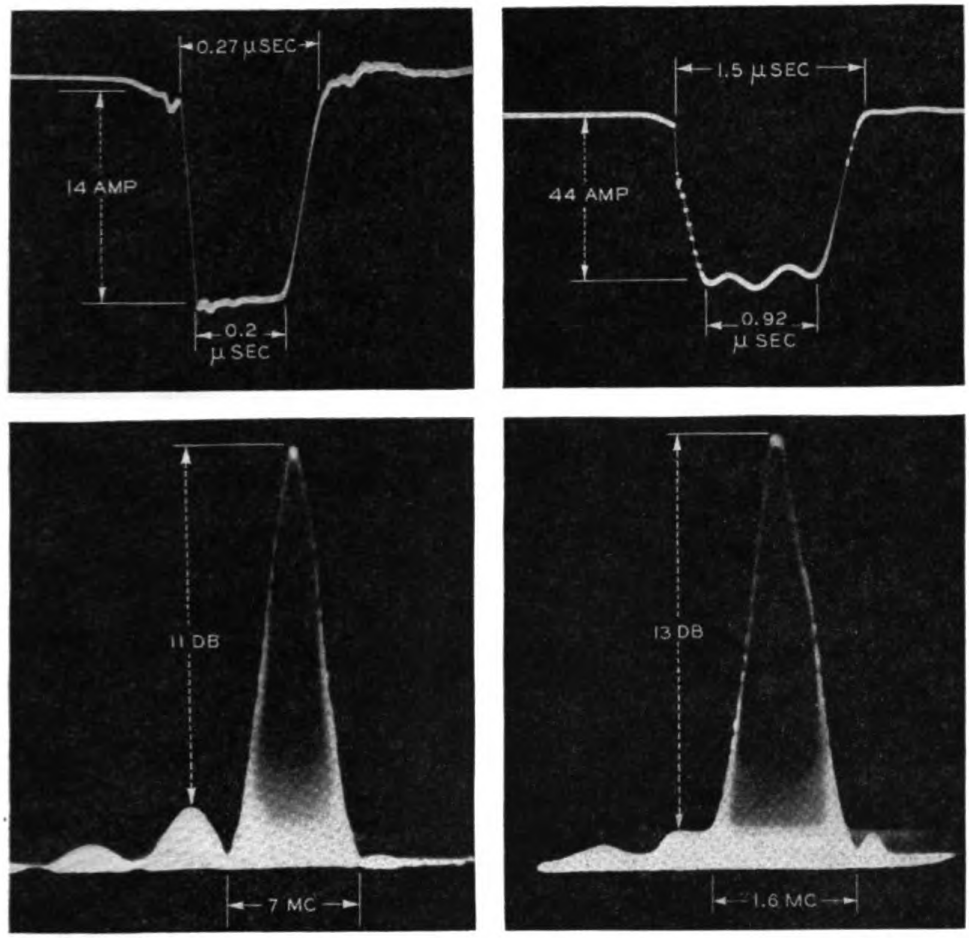

Fig. 4—Shaped magnetron current pulses, together with the radio frequency spectrograms corresponding. Pulse at upper left indicates presence of high harmonics; pulse at upper right shows strong fifth harmonic and little at higher harmonics. The band width of the main energy lobe, and the dispersion of energy outside that band in both cases indicate negligibly small effect attributable to frequency modulation.

evidences the presence of fairly high harmonics. The wider pulse, roughly one and a quarter microseconds in average duration, has a strong fifth harmonic and some even harmonics as well.[5] Below each pulse is shown a spectrogram of the corresponding magnetron high-frequency output, which

[5] Magnetron currents are shown rather than voltages, since current is a far more sensitive indicator of performance.

Digitized by Google
Original from UNIVERSITY OF MICHIGAN
Generated on 2019-09-22 05:47 GMT / http://hdl.handle.net/2027/mdp.39015077775156
Public Domain, Google-digitized / http://www.hathitrust.org/access_use#pd-google

represents energy as a function of frequency. Different magnetrons are used with the two pulses; their operating frequencies and power capacities differ widely. Apparently frequency modulation exists in both cases to a small extent indicated by the departure of each spectrogram from symmetry about a vertical axis. Detailed study, however, shows that the band

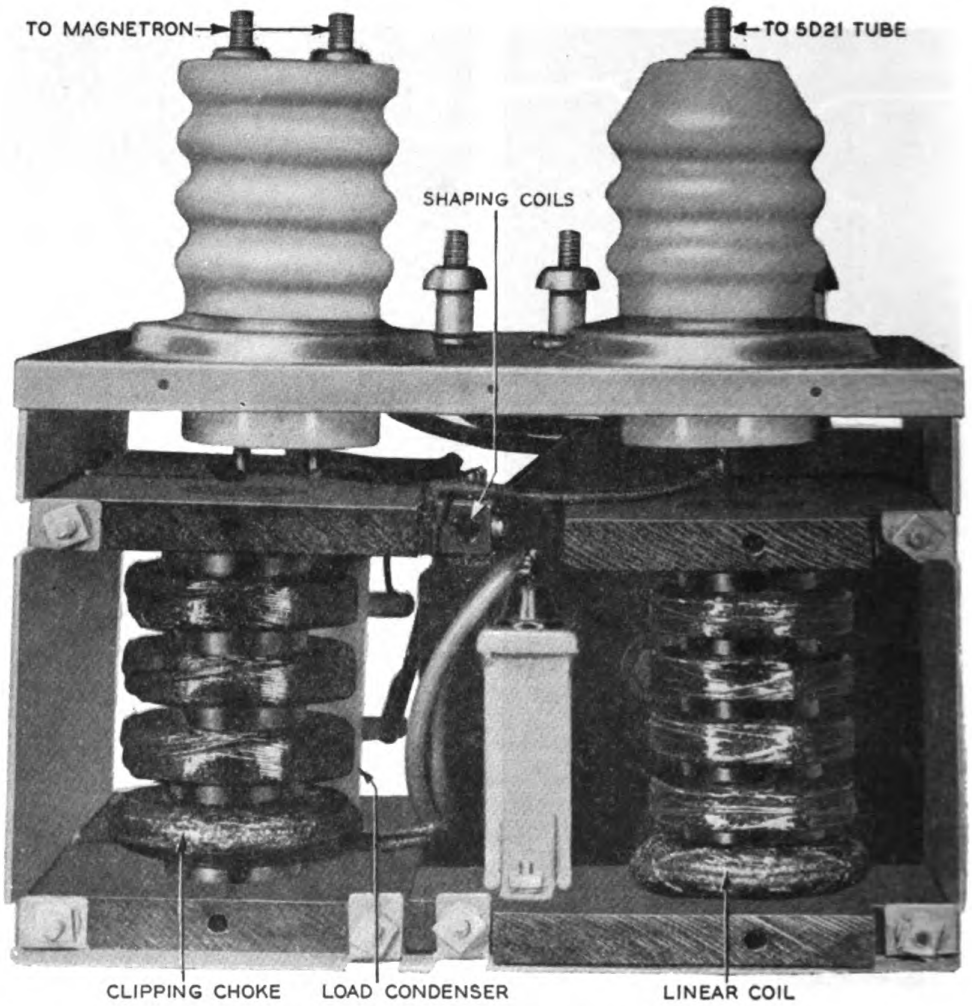

Fig. 5—Typical power pulser network.

width of the main energy lobe differs inappreciably from that with zero frequency modulation, and that the dispersion of energy attributable to frequency modulation is negligibly small. The pulses shown therefore provide satisfactory performance with their respective magnetrons.

Pulser Box

The form in which the typical power pulser network appears is shown in Fig. 5. Power peaks generated by the particular network shown are of the

Digitized by Google
Original from UNIVERSITY OF MICHIGAN
Generated on 2019-09-22 05:47 GMT / http://hdl.handle.net/2027/mdp.39015077775156
Public Domain, Google-digitized / http://www.hathitrust.org/access_use#pd-google

order of 150 kw, with pulse durations of the order of a half microsecond. The non-linear coil here is similar to the one kilogram model pictured in Fig. 1; it is mounted on a panel back of the linear inductor indicated on the Figure. The two larger insulators are used to support high-voltage terminals, the double terminal at the left connecting to the cathode and heater of the magnetron and the single terminal at the right connecting to the tetrode plate. The smaller terminals provide lower-voltage connections including those to the plate power supply of 1000–1500 volts, the bias source where required, and the heating power supply for the magnetron. In use the network is sealed into a closely fitting oil-filled container.

Acknowledgment

The development of coil pulsers was a cooperative enterprise involving a number of different groups in the Laboratories. Design and engineering of the research models were the work of J. M. Manley, P. A. Reiling, L. R. Wrathall, W. R. Bennett, L. W. Hussey and E. M. Roschke. Magnetic cores were developed under the direction of R. M. Bozorth and E. E. Schumacher. Production models were engineered under the direction of F. J. Given. The achievement of successful coil pulsers, moreover, owes much to the efforts of W. H. Doherty and his radar development group.

Generated on 2019-09-22 05:47 GMT / http://hdl.handle.net/2027/mdp.39015077775156
Public Domain, Google-digitized / http://www.hathitrust.org/access_use#pd-google
Digitized by Google
Original from UNIVERSITY OF MICHIGAN

Spark Gap Switches for Radar

By F. S. GOUCHER, J. R. HAYNES, W. A. DEPP and E. J. RYDER

Introduction

AN ESSENTIAL feature of radar is the generation, by means of an oscillator, of high-energy pulses of short duration, repeated many times a second. The energy for these pulses is furnished to the oscillator from a power supply in a variety of ways. One of the most widely used of these is the "line type modulator" in which a pulse-forming network made up of a series of condensers and inductances is charged from the power supply through a choke and is then discharged by a switch so that a substantially constant current will flow for a predetermined short time through the primary of a pulse transformer coupled to the oscillator. This switch is, therefore, an essential component of this type of modulator.

To meet the pulsing requirements of radar as it developed during the war, this line modulator switch was required to withstand thousands of volts between pulses and to carry hundreds of amperes for the pulse duration which was of the order of microseconds. Also, the switching operation had to be repeated from a few hundred to a few thousand times a second for a total operating time of hundreds of hours. Furthermore, the dissipation of energy within the switch had to be very small in comparison with the energy delivered to the oscillator for efficient operation.

The switch which had the widest application in this type of modulator was that employing an electric spark. Of over 50,000 radars of various types manufactured by the Western Electric Co. during the war, over half employed the electric spark in switching. One form of this switch was a rotary spark gap, operating in air, in which the timing of breakdown was controlled mechanically. These gaps were successfully adapted to a variety of radar types including airborne radar. However the demands for a more compact and lighter weight switch capable of operating at lower voltages for airborne radar led to the development of fixed sealed unit type gaps which, when connected in series, can be broken down electrically in a simple circuit.

Many problems had to be solved in the development of these switches. They required a considerable amount of study, and with the aid of new techniques developed during the war, a number of significant measurements have been made which have extended our knowledge of sparks generally. It is the object of this paper to describe the results of some of these studies,

Digitized by Google
Original from UNIVERSITY OF MICHIGAN
Generated on 2019-09-22 05:47 GMT / http://hdl.handle.net/2027/mdp.39015077775156
Public Domain, Google-digitized / http://www.hathitrust.org/access_use#pd-google

as well as to describe the essential characteristics of a variety of spark gap switches which were used in such numbers that they may be considered as an important contribution to the war effort.

I. Rotary Spark Gap Switches For Low Voltage Circuits

Rotary gaps were used successfully as switches in some of the earlier radar systems developed by Bell Telephone Laboratories. The switching voltages in the modulator circuits were relatively high, being in excess of 20 kilovolts. No trouble was encountered in switching at the required pulsing rates nor in obtaining satisfactorily long life. Fortunately the sparks tend to move about the electrode surfaces uniformly and the rate of erosion is such that with tungsten or molybdenum electrodes a uniformly small change in electrode dimensions is achieved which in no way interferes with satisfactory operation over long periods of time.

A difficulty was encountered, however, when the switching voltage was reduced to lower values, as required for applications in which the power supply voltages were limited. The gaps failed to break down regularly.

A particular application in which this difficulty was encountered was one in which the power supply was limited to 4 kilovolts, and in which 80 ampere pulses of one microsecond duration were required every 600 microseconds. The modulator circuit used was that shown schematically in Fig. 1 (a). The pulse-forming network includes the condenser elements which are charged through the choke and discharged by the spark gap designed to break down at the required pulsing rate of 1600 per second. The load is the primary of a pulse transformer coupled to a magnetron and is closely equivalent to a 50-ohm resistance. The constants of the circuit are such that following the discharge of the network it is recharged sinusoidally along the solid line of Fig. 1 (b) to a peak value of approximately 8000 volts in 600×10^{-6} seconds, at which point breakdown must again occur and the operation be repeated. The dashed line is the approximate path of the charging voltage wave when breakdown at the peak fails to occur.

A rotary spark gap was designed to meet these pulsing conditions. In this gap there are four fixed and four moving electrodes as indicated in Fig. 1 (a). These electrodes are tungsten rods 3 mm in diameter and about 15 mm in length mounted with their axes parallel and so spaced that the moving electrodes pass very close to the fixed electrodes with an overlap of about one-half their length. The speed of the moving electrodes is such that in the region of near approach the maximum gradients are those indicated in Fig. 1 (c). The solid curve shows the gradients when breakdown takes place at the required time and the dashed curve the gradients when breakdown fails to occur. Although the latter greatly exceed the normal

Digitized by Google
Original from UNIVERSITY OF MICHIGAN
Generated on 2019-09-22 05:49 GMT / http://hdl.handle.net/2027/mdp.39015077775156
Public Domain, Google-digitized / http://www.hathitrust.org/access_use#pd-google

dielectric strength of air, sparking failed to take place a large fraction of the time.

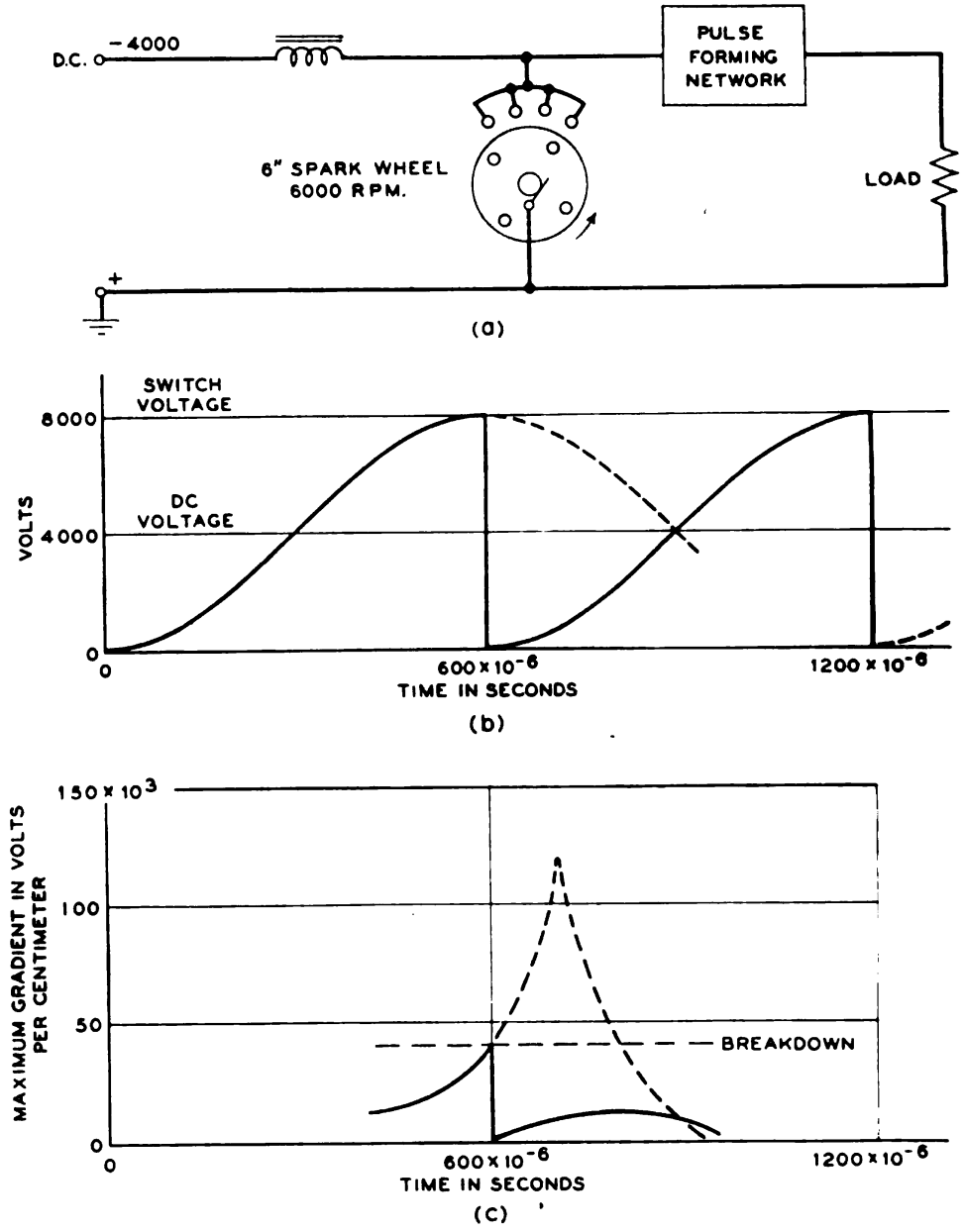

Fig. 1—(a) Line modulator circuit with rotary spark gap switch, (b) switch voltage vs. time, (c) maximum voltage gradient between electrodes vs. time.

Experiment indicated that this was caused by spark delay time, as irradiation of the cathodes by means of an ultra-violet lamp produced 100%

Digitized by Google
Original from UNIVERSITY OF MICHIGAN
Generated on 2019-09-22 06:13 GMT / http://hdl.handle.net/2027/mdp.39015077775156
Public Domain, Google-digitized / http://www.hathitrust.org/access_use#pd-google

breakdown. This method of reducing spark delay time was not practical, however, and other means were sought. A solution was found through a rediscovery of the efficacy of corona prior to breakdown which came about through the introduction of a properly placed sharp edge on the cathode. Although this edge was apart from the sparking area of the cathode, 100% breakdown of the gaps was obtained and spark delay time so reduced

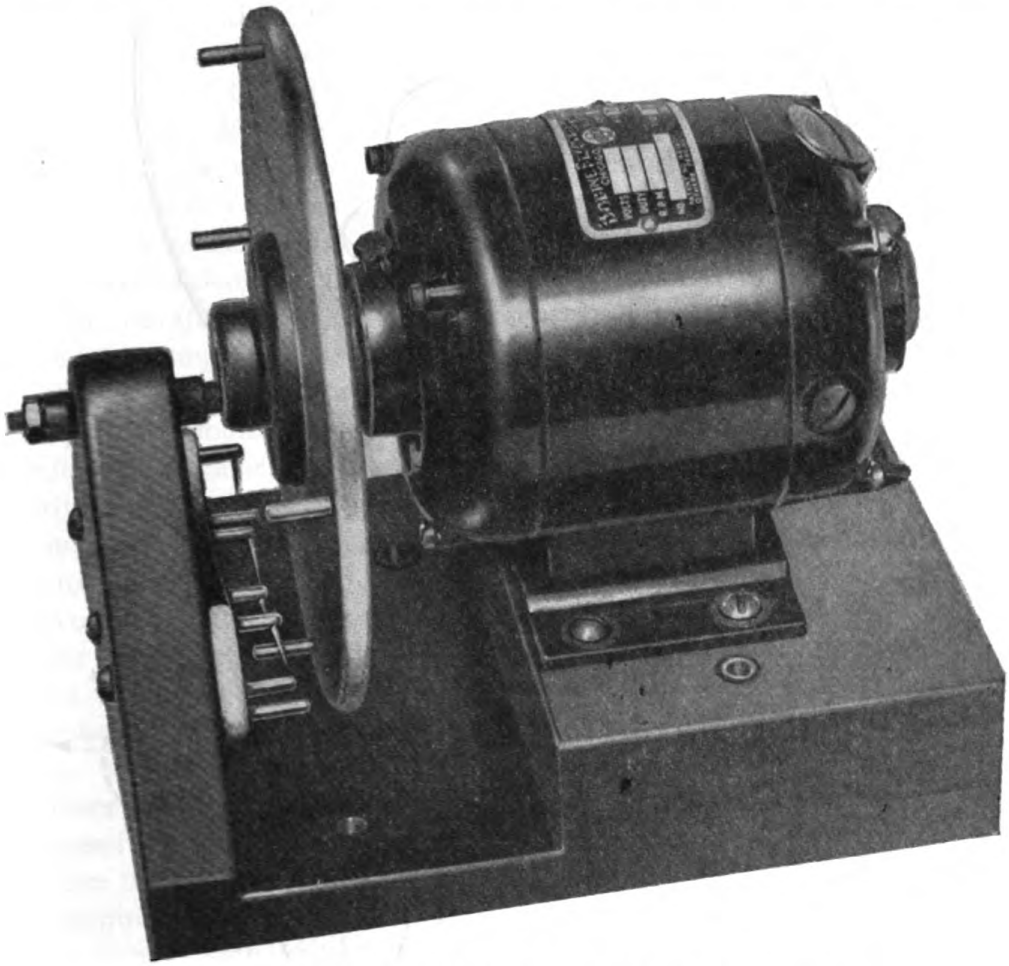

FIG. 2—Experimental model of rotary gap showing corona points.

that mechanical limitations alone controlled the variation in time of breakdown.

The essential features of the gap as finally developed for this project are shown in the photograph of an experimental model, Fig. 2, and in the perspective drawing and accompanying diagram, Fig. 3. The electrodes are of tungsten as in the earlier design, and corona points are introduced by the addition of the rods holding sharp metal points mounted on the same metal

Digitized by Google
Original from UNIVERSITY OF MICHIGAN
Generated on 2019-09-22 06:13 GMT / http://hdl.handle.net/2027/mdp.39015077775156
Public Domain, Google-digitized / http://www.hathitrust.org/access_use#pd-google

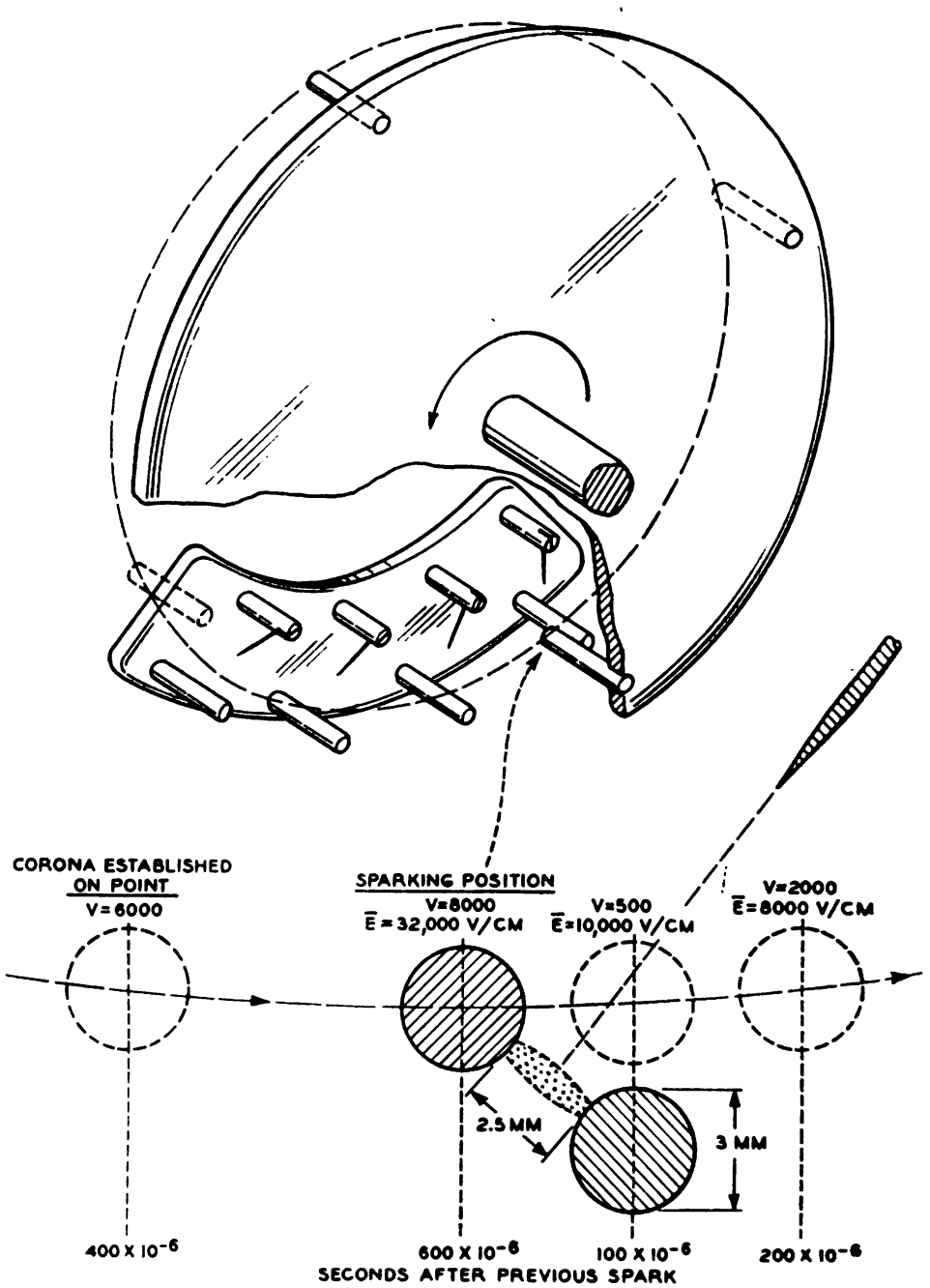

Fig. 3—Above, perspective drawing of rotary gap showing arrangement of corona points. Below, diagram showing voltage (V), and mean voltage gradient ($\bar{E}$) at various times in the spark-over region.

base as the fixed electrodes. The moving electrodes pass between the fixed electrodes and their associated corona points. This arrangement is clarified in the diagram which is a section through a plane normal to the electrode

Digitized by Google
Original from UNIVERSITY OF MICHIGAN
Generated on 2019-09-22 06:14 GMT / http://hdl.handle.net/2027/mdp.39015077775156
Public Domain, Google-digitized / http://www.hathitrust.org/access_use#pd-google

axes and passing through the region of overlap. The shaded areas are for the sparking position as indicated and the location of the corona point is shown to scale. Experiment shows that when the moving electrode has reached the position corresponding to 400×10^{-6} seconds after the previous spark, corona is established on the point. Thus the cathode is irradiated for 200×10^{-6} seconds prior to breakdown.

No serious erosion problem was encountered when these gaps were operated for many hundreds of hours in air. No deterioration of the points was observed when their locations were properly adjusted so as to avoid sparking over to them. The cathode erosion rate is so low that appreciable flats were produced only after a hundred hours of operation. The anode erosion was estimated to be less than one-tenth of that of the cathode, and was doubtless associated with a small amount of reverse current shown to be present. The magnitude of the cathode erosion rate for tungsten in air is about twenty-five fold less than that for tungsten in hydrogen under the same conditions which indicates that oxygen plays an important and somewhat unexpected role in making practical the operation of these gaps.

There was, however, a serious corrosion problem when these gaps were adapted to airborne radar because of the necessity for sealing the modulator unit in a container capable of maintaining atmospheric pressure at high altitudes. Spark discharges in air are attended by the formation of both ozone and oxides of nitrogen, the latter combining with moisture to form nitrous and nitric acids. These reached such concentrations under continuous operation in the container that they were damaging to all enclosed equipment because of their corrosive action. A solution for this was arrived at after considerable study on the part of the Chemical Department. This consisted of the use of a copper impregnated activated carbon as an absorbent. With this absorbent a life of 500 hours was shown to be possible.

Over 10,000 rotary gap switches of this type were manufactured and used successfully in both ship and airborne radars. However, under the urge to reduce the weight of all possible components used in airborne radar and even to eliminate the necessity for pressurizing, the development of glass-enclosed fixed gaps as switches was diligently pursued.

The authors would like to acknowledge the cooperation of Mr. N. I. Hall of the Whippany Laboratories whose responsibility it was to engineer and develop these rotary gap switches for manufacture.

II. Fixed Gaps

Preliminary experiment indicated that a series of fixed gaps could be made to operate satisfactorily as a modulator switch. A study was therefore made to determine the most suitable gas atmosphere, electrode material and gap design for use in sealed gaps. This led to the development of a unit

Digitized by Google
Original from UNIVERSITY OF MICHIGAN
Generated on 2019-09-22 06:14 GMT / http://hdl.handle.net/2027/mdp.39015077775156
Public Domain, Google-digitized / http://www.hathitrust.org/access_use#pd-google

type gap, two or more of which could be operated in series. The first unit type gap had an aluminum cathode and a hydrogen-argon gas atmosphere. Later, under the urge for higher peak powers, mercury cathode gaps were developed. Details of this study and development will be discussed in this section.

(a) *Triggering Gaps in Series*

An alternative to a rotary gap in which the timing of spark breakdown is controlled mechanically was the use of a fixed gap, the breakdown of which is controlled electrically. One method of accomplishing this was to use a third electrode to which an impulse voltage was applied periodically at double the frequency of the resonant charging circuit. This voltage breaks down one gap with a discharge of energy furnished by the trigger circuit, which in turn causes a breakdown of the main gap, either through a modification of the field in this gap or through the addition of ions which reduce its breakdown voltage. This type of gap, however, required a strong air blast to de-ionize the gaps and, because of this, its use obviously presented no great improvement over the rotary gap. It was well known that the rate of de-ionization is greater the smaller the gap, so an attempt was made to trigger without air blast a number of smaller gaps which when connected in series would withstand the full switch voltage as employed in the rotary gap.

The arrangement used was that shown in Fig. 4. Six tungsten pins, 3 mm in diameter, were mounted with their axes parallel and spaced to give five 0.5 mm gaps. The switch voltage was divided by means of equal high resistances connected across the gaps, and a highly damped bi-directional trigger pulse was applied to the four middle pins through capacity coupling as shown. Corona points were also connected in such a way that the cathode of each of the gaps is irradiated in order to reduce the spark delay time.

By an appropriate adjustment of the circuit elements it was demonstrated that this series of gaps could be broken down by the trigger pulse and de-ionized with sufficient rapidity so that no air blast was required.

Although no attempt will be made here to elucidate the detailed steps in the triggering of the five gaps just described, we can get a qualitative idea of the process by considering a simple two-gap and three-gap circuit which, it turned out, was all that was required for the various applications of fixed gaps as they were eventually developed.

In the two-gap circuit, Fig. 5 (a), if the first half cycle of the trigger pulse and the switch voltage are both positive, gap 1 will break down when the potential at the mid point, due to the sum of the switch voltage and that of the trigger, is equal to the gap breakdown voltage, which for the moment we shall consider as singly valued. This effectively shorts gap 1 and throws the full switch voltage across gap 2 which in turn will break down provided this

Generated on 2019-09-22 06:14 GMT / http://hdl.handle.net/2027/mdp.39015077775156
Public Domain, Google-digitized / http://www.hathitrust.org/access_use#pd-google
Digitized by Google
Original from UNIVERSITY OF MICHIGAN

switch voltage is equal to or greater than the breakdown voltage of one gap. The gaps will operate for all switch voltages up to a value equal to twice the breakdown voltage of one gap when both gaps will break down without the addition of trigger. This, then, is the maximum operating voltage and the ratio of maximum to minimum operating voltage is two to one on the basis of this simple picture.

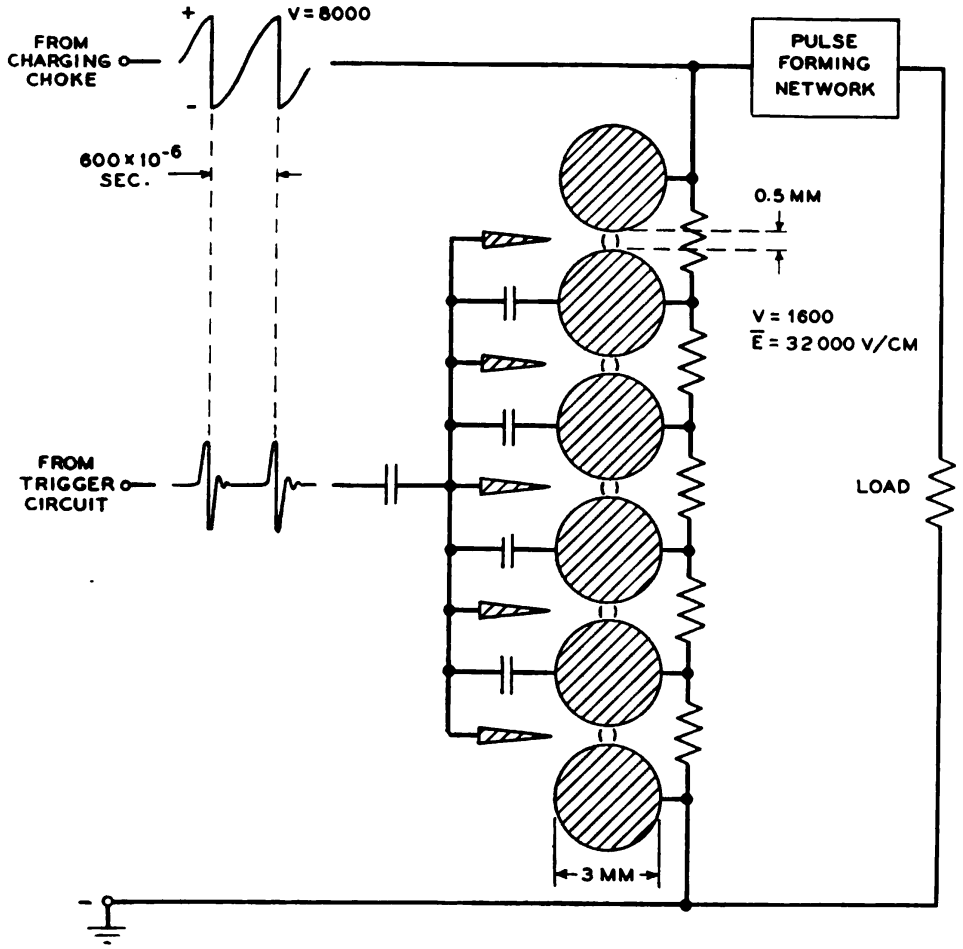

Fig. 4—Line modulator circuit with fixed gap switch composed of five 0.5 mm. air gaps triggered electrically.

In the case of the three-gap circuit, Fig. 5 (b), gaps 1 and 2 may be broken down by the simultaneous application of a trigger pulse through capacity coupling. The circuit elements can be so chosen that gap 1 first breaks down leaving enough trigger on gap 2, over and above that furnished by the switch voltage, to break it down. The full switch voltage is then applied across gap 3 and it will break down for values of switch voltage in excess of the

Digitized by Google
Original from UNIVERSITY OF MICHIGAN
Generated on 2019-09-22 06:14 GMT / http://hdl.handle.net/2027/mdp.39015077775156
Public Domain, Google-digitized / http://www.hathitrust.org/access_use#pd-google

single gap breakdown voltage. In this case the switch voltage may be increased to a value three times that of the breakdown of one gap before the three gaps can break down without addition of trigger. Thus the ratio of maximum to minimum operating voltage is three to one. Ideally this ratio may be increased by the addition of more gaps.

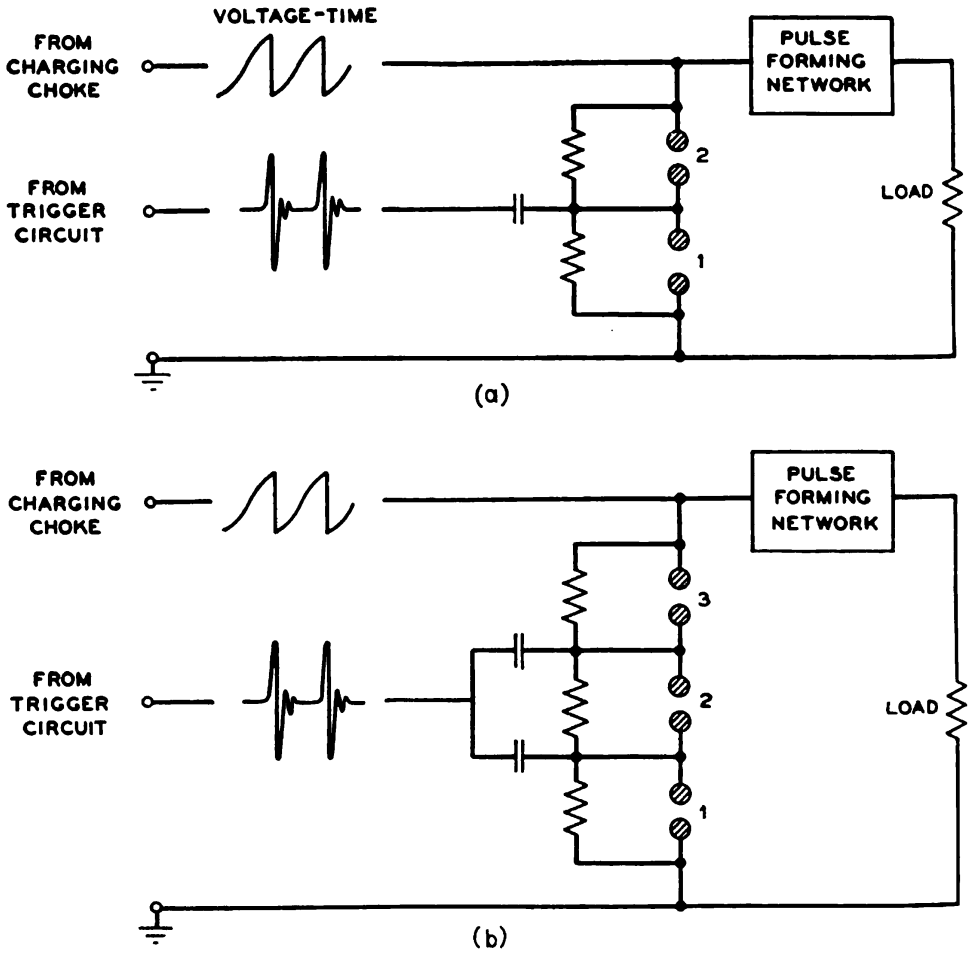

Fig. 5—Line modulator circuit (a) using two fixed gaps as switch, (b) using three fixed gaps as switch.

The operating characteristics of actual gaps do not conform exactly to this simple picture as we shall see later. This is because the breakdown voltage of a gap is not singly valued but depends on a variety of conditions such as rate of rise of applied voltage, pulsing rate, and the energy of the pulse, as well as the type of gap employed. However, we may regard it as a qualitatively correct picture of the operating characteristics of series gaps.

A more complete description of operating characteristics will be given in a

Generated on 2019-09-22 06:14 GMT / http://hdl.handle.net/2027/mdp.39015077775156
Public Domain, Google-digitized / http://www.hathitrust.org/access_use#pd-google
Digitized by Google
Original from UNIVERSITY OF MICHIGAN

later section, but, in view of the fact that the gap itself plays an important part in these characteristics, it seems desirable to describe first the gap types with which we have to deal.

(b) *The Hydrogen-Argon Aluminum Cathode Gap*

Following the successful triggering of fixed gaps in air without the use of air blast for their de-ionization, experiments were undertaken with sealed gaps in various gas atmospheres using simple rod electrodes having their axes parallel. A large number of gases were tested and the conclusion reached that hydrogen was the most satisfactory because of its high de-ionization rate. With it fewer and wider gaps were required to meet a given pulsing condition. Three 4 mm. gaps in hydrogen at pressures somewhat less than atmospheric were approximately equivalent to the five 0.5 mm. gaps in air already referred to. Thus, from this point of view, the use of hydrogen would very greatly simplify the problem of making practical gaps.

The spark in hydrogen, particularly with relatively small peak currents, was, however, unsatisfactory in that it terminated in a high-pressure glow with a high cathode drop rather than the low drop required for efficient switching. The addition of about 25% argon corrected this and about this proportion was used successfully in the gaps with which we are concerned in this report.

Although the required operating conditions were met with this gas mixture, cathode erosion or sputtering was so excessive with all readily available cathode materials that this factor appeared as the chief obstacle in the way of making practical gaps. The sputtered material was deposited on all surfaces in the form of a fine powder which eventually destroyed the insulation, thereby limiting the useful life of the gaps to a few hours.[1]

A promising lead was, however, obtained in the case of aluminum cathodes. It was observed that some of the sputtered material deposited on the anodes opposite the cathodes from which it was removed. This deposit was reasonably compact and smooth, which suggested the possibility of reducing by gap design the extent of harmful scattering. This might be achieved by increasing the amount of sputtered cathode material which is deposited on the anode or returned to the cathode within the sparking area.

The tube, Fig. 6, was an early attempt in this direction. This tube had three 4 mm. gaps between flat electrodes, the cathode surfaces having raised portions to confine the sparking within their areas. The gaps were

[1] At about this time we learned that the British had developed sealed gaps triggered by means of an auxiliary electrode and known as "Trigatrons." These were high pressure gaps containing argon with a small amount of oxygen to reduce sputtering of the electrodes. The life of these gaps was determined by the time required to clean up this oxygen. Though these were tried it was decided to follow an independent development avoiding if possible all clean up effects.

Digitized by Google
Original from UNIVERSITY OF MICHIGAN
Generated on 2019-09-22 06:14 GMT / http://hdl.handle.net/2027/mdp.39015077775156
Public Domain, Google-digitized / http://www.hathitrust.org/access_use#pd-google

operated successfully for somewhat over 100 hours before enough scattered material accumulated to interfere with gap insulation. A uniform spark distribution was maintained throughout this time and measurement showed that aluminum was removed quite uniformly from the raised portion of the cathode to a depth of only a fraction of a millimeter. An equally thick

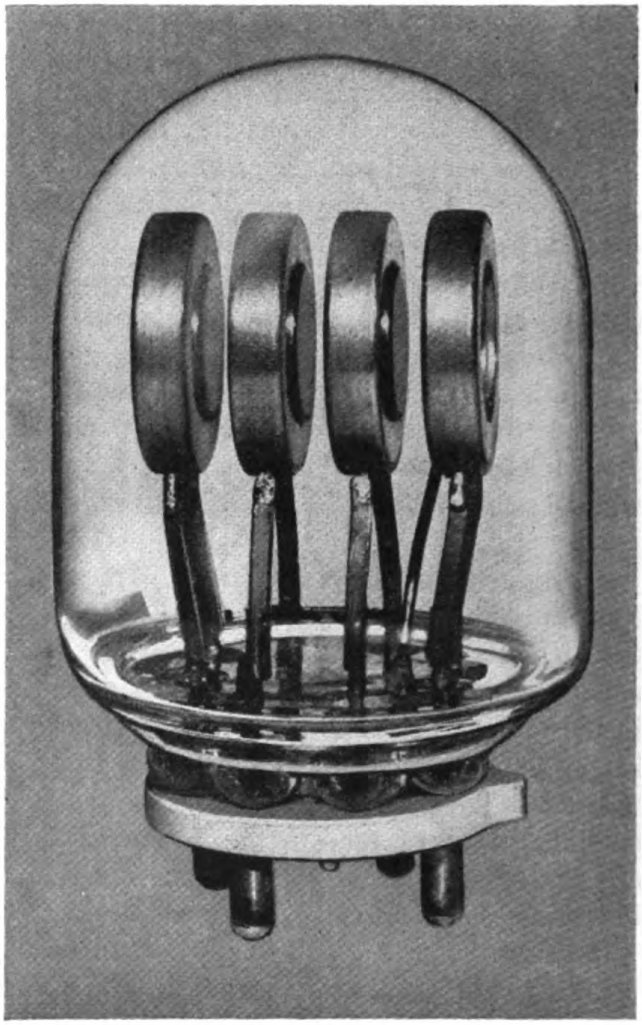

Fig. 6—Three gap tube having aluminum electrodes and a hydrogen-argon atmosphere ——actual size.

though somewhat rougher deposit was formed on the opposing anode surface, thereby retaining the gap spacing very satisfactorily. About 30 milligrams of loose material were scattered throughout the tube.

A more drastic but also more successful design change was introduced by making three separately enclosed gaps, one of which is shown in the photo-

Digitized by Google
Original from UNIVERSITY OF MICHIGAN
Generated on 2019-09-22 06:15 GMT / http://hdl.handle.net/2027/mdp.39015077775156
Public Domain, Google-digitized / http://www.hathitrust.org/access_use#pd-google

graph and radiograph, Fig. 7. In these gaps the sparking area of the cathode was hemispherical in shape, partly surrounding a spherical anode. These gaps were operating successfully at the end of 1000 hours. The scattered material was deposited on only a portion of the glass envelope of

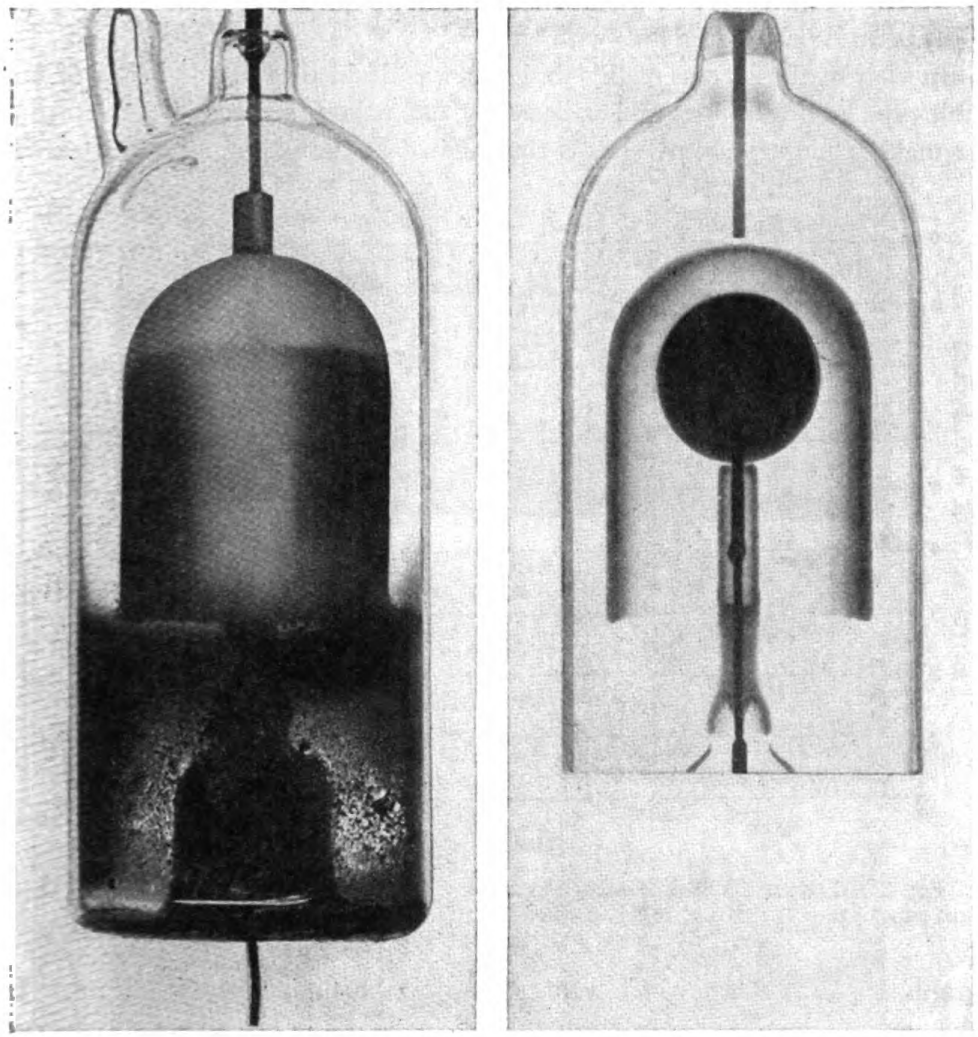

Fig. 7—Photograph and radiograph—actual size—of the first unit type gap having a re-entrant aluminum cathode, a spherical aluminum anode and a hydrogen-argon gas atmosphere, after operating 1000 hours with a 40 ampere pulse of one microsecond duration repeated 1660 times a second.

each gap, as shown in the photograph. The extent of the material removed from the cathode and deposited on the anode, as shown in the radiograph, was such as to cause no marked change in gap spacing. Furthermore, the operating range remained substantially constant throughout the 1000 hours of operation as shown in Fig. 8. This was an important observation since it

Digitized by Google
Original from UNIVERSITY OF MICHIGAN
Generated on 2019-09-22 06:15 GMT / http://hdl.handle.net/2027/mdp.39015077775156
Public Domain, Google-digitized / http://www.hathitrust.org/access_use#pd-google

indicated that there is no gas clean-up effect associated with gap operation, a fact that was later proved by careful measurement of gas pressure before and after operating gaps of this type. A section through the anode of this gap, Fig. 9 (a), shows that the anode deposit is not compact but assumes the form of a coral-like structure. This low-density deposit must, however, be electrically equivalent to a compact surface as shown by the constancy of the operating characteristics with time.

In view of the success of this design it was decided to develop gaps of the unit type having anodes well enclosed by the cathode surfaces. An attempt to make a more practical gap is that shown in the photograph and radio-

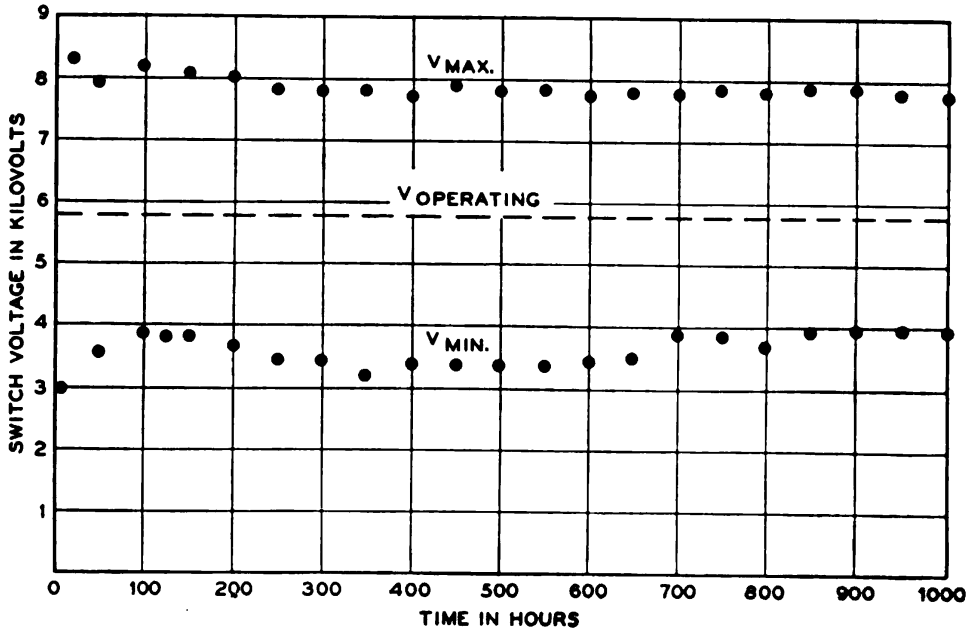

Fig. 8—Maximum and minimum operating voltages as a function of time, for three unit gaps of the type shown in Fig. 7, when operated in series.

graph, Fig. 10, both of which were taken after 750 hours operating time. In this gap the anode is an aluminum rod rounded at the end mounted concentrically with the enclosing cathode which has a hemispherical closed end. The corona point was added to facilitate starting. Because of the higher anode gradient the sparking was confined to the end region of the tube as indicated in the radiograph, and for this reason we have designated this design an "end sparking tube". A section through the anode, Fig. 9 (b), shows a deposit which in this case is compact due to the fact that the moving spark is confined to a smaller area than in the previous tube, Fig. 7 (a). It is to be noted also that the scattered material is less in extent than that

Generated on 2019-09-22 06:15 GMT / http://hdl.handle.net/2027/mdp.39015077775156
Public Domain, Google-digitized / http://www.hathitrust.org/access_use#pd-google
Digitized by Google
Original from UNIVERSITY OF MICHIGAN

obtained with the first design, pointing to a more effective trapping of the sputtered material.

Weight loss measurements made under a variety of pulsing conditions show that though the rate of cathode erosion is somewhat dependent on the

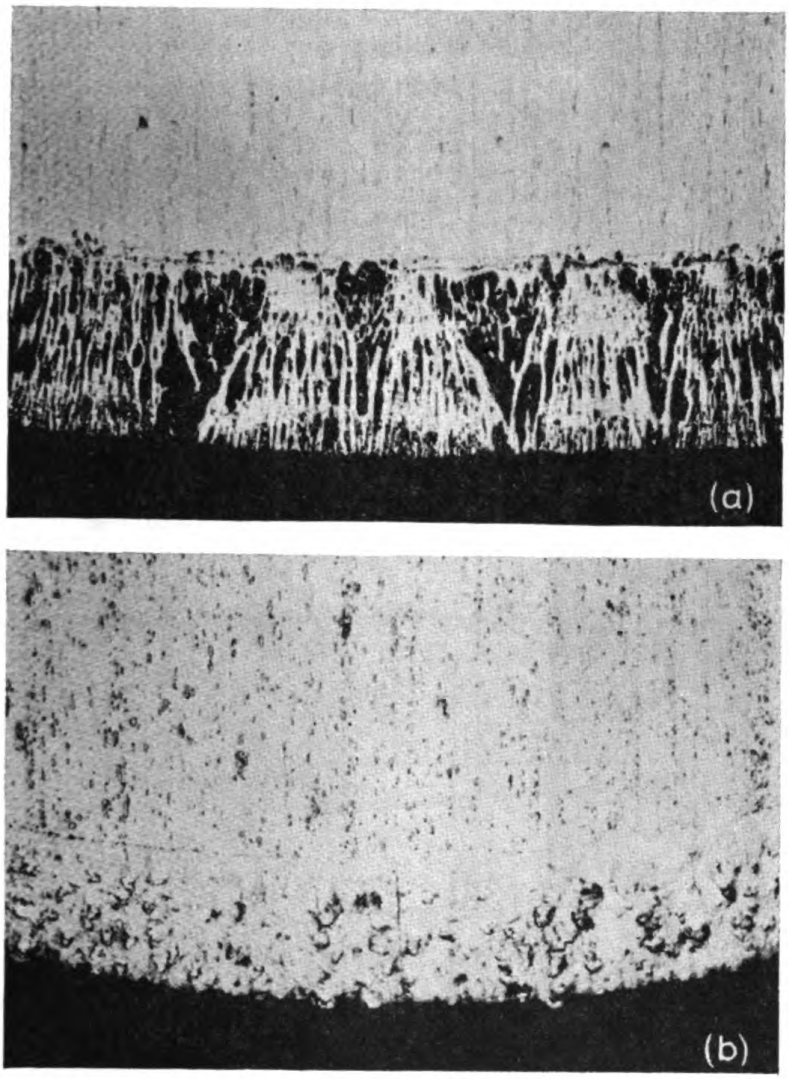

Fig. 9—Photomicrographs (×50) of sections showing anode deposits for (a) unit gap shown in Fig. 7, (b) unit gap shown in Fig. 10.

pulse duration, it depends to a much greater extent on gap design. Erosion rate measurements in terms of grams per coulomb are shown in Fig. 11 for the two gap designs there indicated and for pulse durations varying from one to five microseconds. It is clear that the open gap type of design in which the cathode is small leads to a loss which is at least five fold greater than

Digitized by Google
Original from UNIVERSITY OF MICHIGAN
Generated on 2019-09-22 06:15 GMT / http://hdl.handle.net/2027/mdp.39015077775156
Public Domain, Google-digitized / http://www.hathitrust.org/access_use#pd-google

that of the "end sparking" type of gap. The smaller loss in the case of the latter shows that much more material returns to the cathode for resputtering

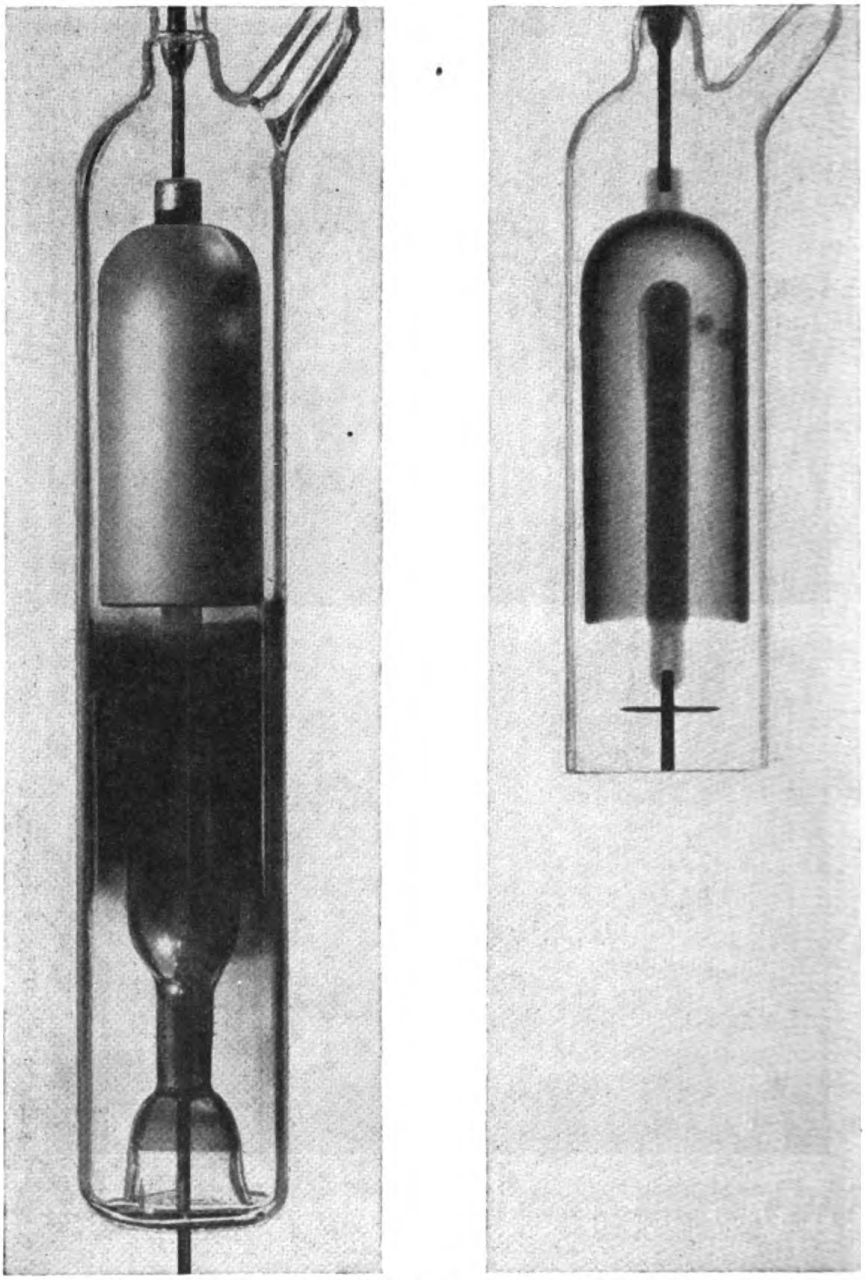

Fig. 10—Photograph and radiograph—actual size—of end sparking unit gap, after operating 700 hours with a 65-ampere pulse of one microsecond duration and repeated 1660 times a second.

than in the case of the former and supports the use of the unit type gap in which this process can be utilized. A cylindrical cathode enclosing a rod

Digitized by Google
Original from UNIVERSITY OF MICHIGAN
Generated on 2019-09-22 06:15 GMT / http://hdl.handle.net/2027/mdp.39015077775156
Public Domain, Google-digitized / http://www.hathitrust.org/access_use#pd-google

anode also behaves in this way and its erosion rate differs but little from the "end sparking" type of tube; in fact, the practical gaps to be described in II-(f) are essentially of this type.

With these facts in mind it would appear that gaps could be designed to meet a variety of pulsing conditions if the total number of ampere hours for a pre-assigned life were known, for the electrode areas could be so adjusted that the changes in gap spacing would be as small as required. Analysis of the gradients associated with the end sparking type of gap shows that there

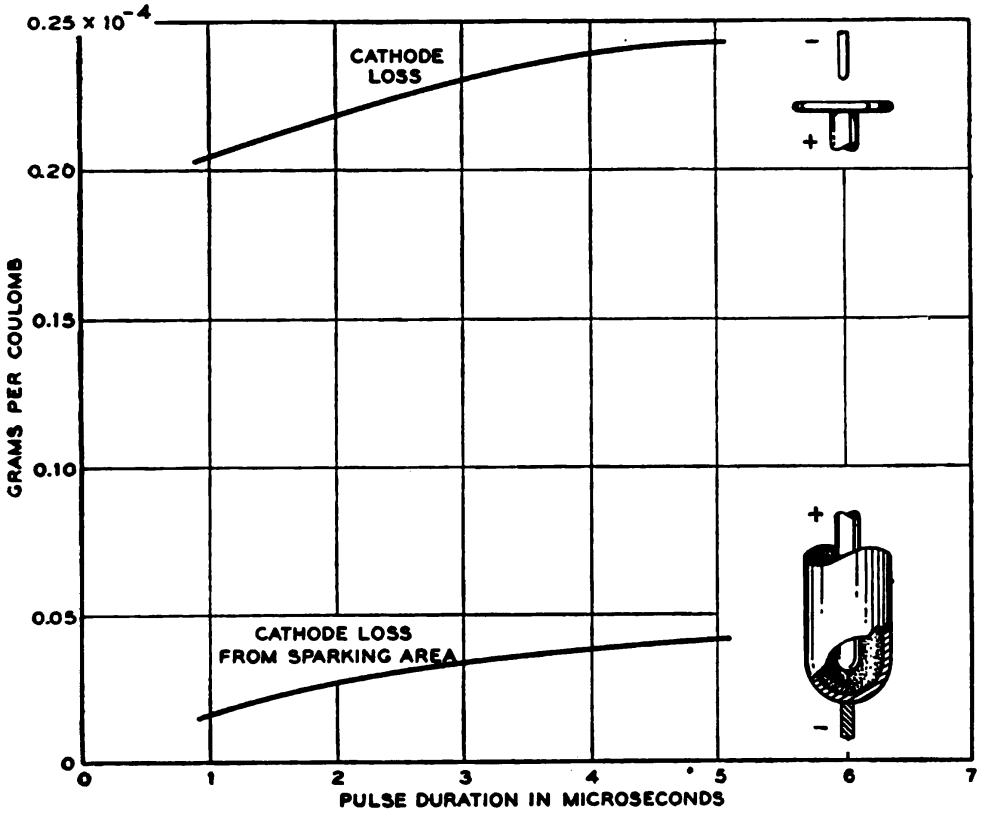

Fig. 11—Cathode loss, in grams per coulomb, as a function of pulse duration showing effect of gap design.

can be a considerable build-up on the anode before there is much change in the maximum gradient which determines the spark-over voltage.

Experience with gaps designed for a variety of pulsing conditions showed that substantial anode build-ups could be tolerated without interfering with operating conditions, but not as much as theory would predict for an unexpected factor had a controlling influence on gap life. This factor was the failure of the spark to keep moving under certain conditions with the result that spikes were grown on the anode which introduced a rapid deterioration

Digitized by Google
Original from UNIVERSITY OF MICHIGAN
Generated on 2019-09-22 06:15 GMT / http://hdl.handle.net/2027/mdp.39015077775156
Public Domain, Google-digitized / http://www.hathitrust.org/access_use#pd-google

of the operating range due to an increase in anode gradient and also in part to a decrease in gap spacing.

Both the relatively large anode build-up, which may be tolerated without interference with gap operation, and the nature of spike growth, which limited useful life, are illustrated in the radiographs, Fig. 12. It is to be noted that the spike is almost of uniform cross section along its length and radiographs made at various stages of its formation show that growth takes place

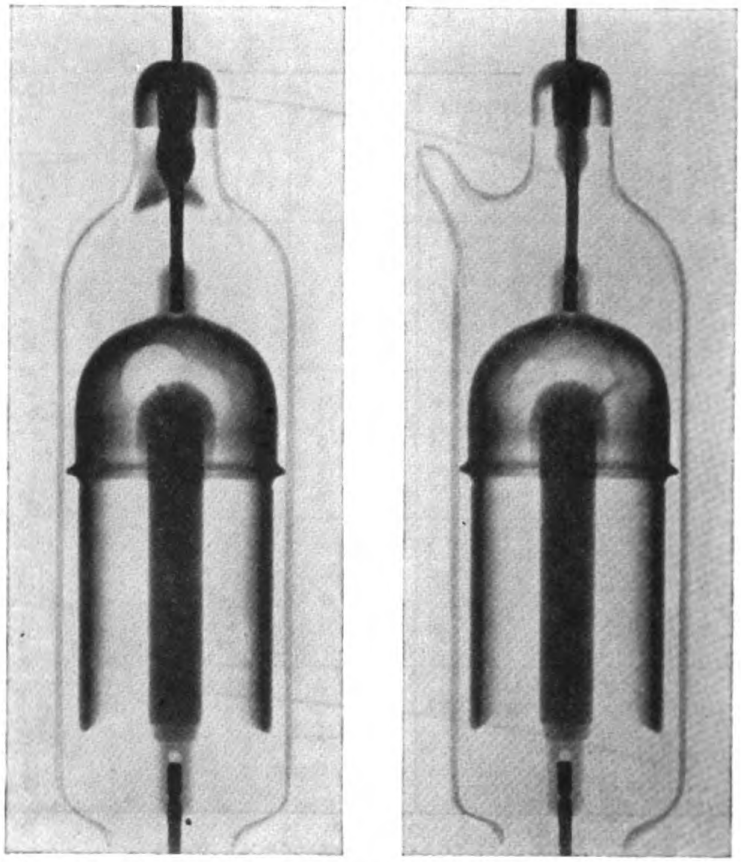

Fig. 12—Radiographs showing two views of the uniform deposit and subsequent spike growth on the anode of an end sparking unit gap.

at its end. This indicates a high concentration of negative ions in the vapor prior to deposit on the anode.

Life test data in which the pulse repetition rate was kept constant at 200 per second are shown in Fig. 13 for gaps having a fixed spacing but in which the peak current is varied (a), and for gaps having a variety of spacings but in which the peak current is kept constant (b). The life is measured in terms of hours to the beginning of spike growth. Both "end sparking" and "side sparking" tubes were employed in the tests. These data clearly show that

Digitized by Google
Original from UNIVERSITY OF MICHIGAN
Generated on 2019-09-22 06:16 GMT / http://hdl.handle.net/2027/mdp.39015077775156
Public Domain, Google-digitized / http://www.hathitrust.org/access_use#pd-google

if lives longer than 500 are to be obtained, there is a limiting peak current of about 70 amperes with gap spacings of 250 mils or with a peak current of 70 amperes there is a minimum spacing of 250 mils. Similar data were obtained indicating a different critical spacing for other pulsing conditions.

This factor of a critical gap spacing imposed an important restriction on gap design for it was desirable to make gap spacing as small as possible for any given project. This follows because of gap size and weight, also—as

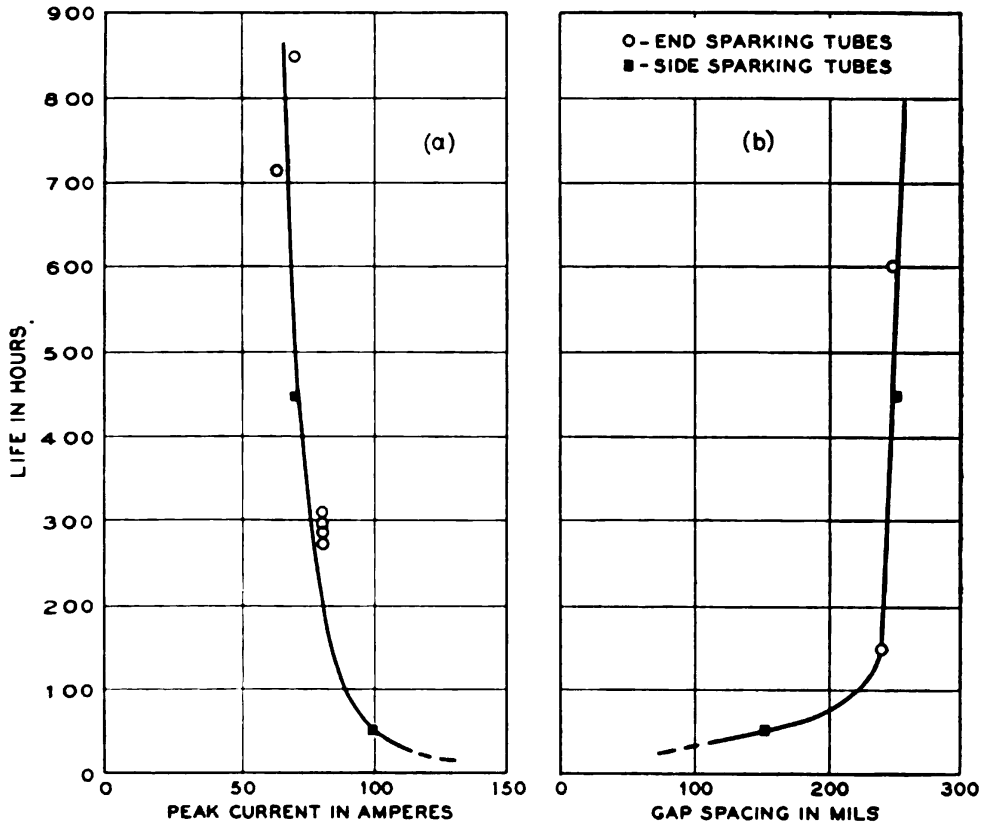

Fig. 13—Life in hours measured to the beginning of spike growth obtained with 5-microsecond pulses repeated 200 times a second (a) for a 60-mil gap and various peak currents, (b) for a fixed peak current of 70 amperes and various gap spacings.

we shall see in II-(e)—because of switching efficiency. This led to the development of a variety of unit gaps as described in II-(f).

(c) *The Mercury Cathode Gap*

Early in the study of the aluminum cathode gap it was realized that the sputtering difficulty might be largely if not entirely eliminated through the use of mercury as a cathode and the suppression of reverse current to avoid sputtering of the anode. It was shown that simple mercury pool cathode

Digitized by Google
Original from UNIVERSITY OF MICHIGAN
Generated on 2019-09-22 06:16 GMT / http://hdl.handle.net/2027/mdp.39015077775156
Public Domain, Google-digitized / http://www.hathitrust.org/access_use#pd-google

gaps could switch peak powers in the megawatt range for long periods of time with stable operating characteristics. Under the urge for still highe powers than those which were handled by the aluminum cathode gaps experiments were undertaken to develop a mercury cathode type of gap

The main difficulty in the way of using mercury as a cathode is a mechanical one, as the conditions of operation of spark gap switches, particularly for

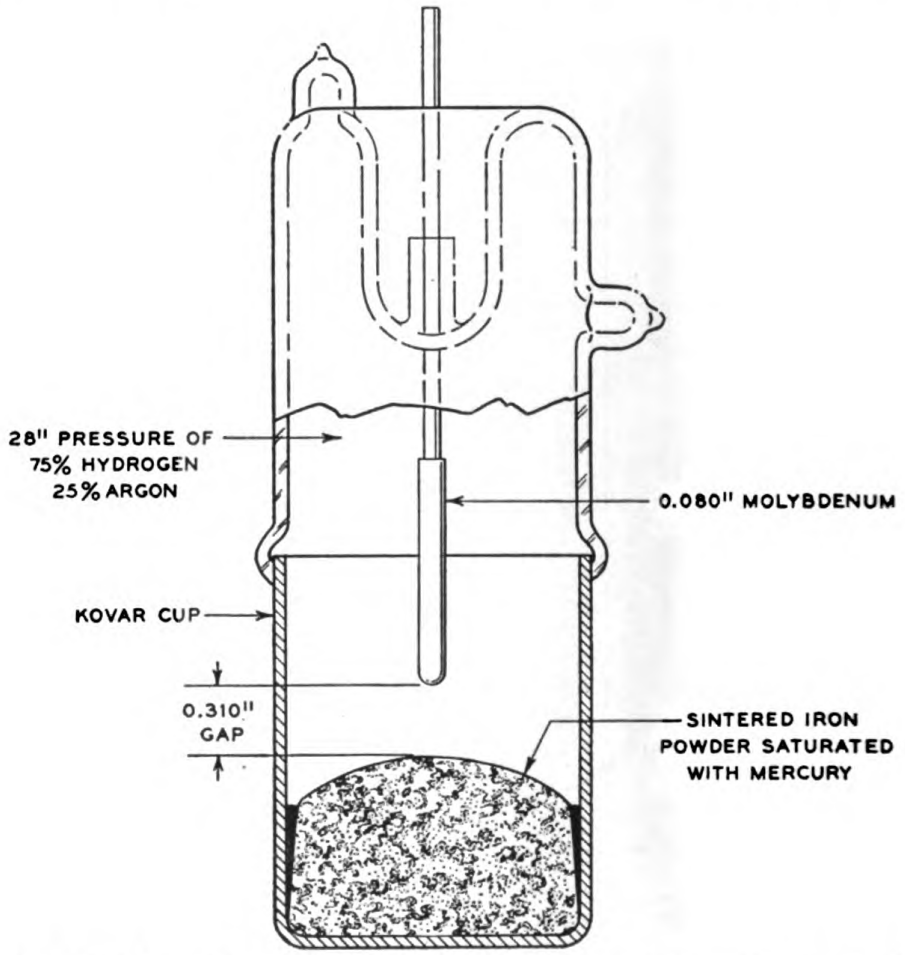

Fig. 14—Schematic drawing of an iron sponge mercury cathode unit gap—actual size.

airborne radar, demand that the sparking surface be rendered substantially quiescent. Preliminary experiments were made with metal baffles as damping agents and with metal wicks to furnish a mercury sparking surface. The latter led to the development of a sintered iron sponge saturated with mercury as the best means of obtaining a satisfactory cathode.

The constructional details of one of the earliest tubes of this type are given in the sketch, Fig. 14. The sintered iron sponge, a cross section of which is

Generated on 2019-09-22 06:16 GMT / http://hdl.handle.net/2027/mdp.39015077775156
Public Domain, Google-digitized / http://www.hathitrust.org/access_use#pd-google
Digitized by Google
Original from UNIVERSITY OF MICHIGAN

shown in the photomicrograph Fig. 15, is about 60% porous. It was prepared by pressing iron powder in the Kovar cup and sintering in a hydrogen atmosphere. A special heat treatment to remove oxide made it possible to fill all pores of the sponge with mercury and to supply a mercury film on its surface. Under sparking conditions mercury from this film is evaporated and is condensed on the tube walls, eventually returning to the cathode. Due to capillary action the film is continuously replenished. This film protects the iron sponge from sputtering provided that there is sufficient

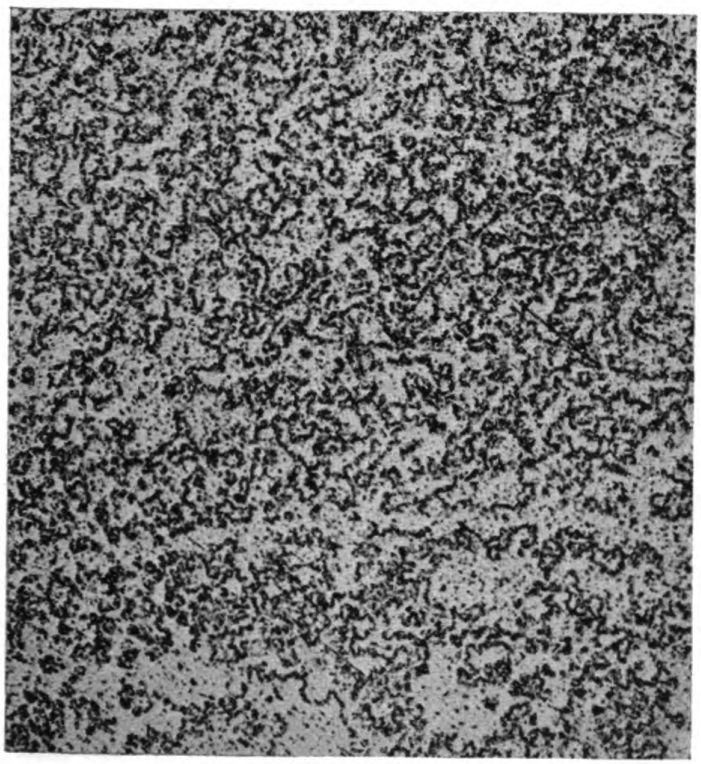

Fig. 15—Photomicrograph (×15) of a section through a sintered iron sponge showing porosity.

cooling of the cathode to maintain the mercury film at a temperature below its boiling point.

These gaps are not temperature sensitive as are most electronic devices containing mercury. This is because the mercury vapor plays no essential role in the spark discharge, as indicated by the fact that dissipation measurements—discussed in II-(e)—show its dependence on the hydrogen-argon rather than on the nature of the cathode material. With adequate cathode cooling gaps of this type operate satisfactorily over a range of ambient temperature at least from −50°C to over 100°C. Practical gaps constructed

Digitized by Google
Original from UNIVERSITY OF MICHIGAN
Generated on 2019-09-22 06:26 GMT / http://hdl.handle.net/2027/mdp.39015077775156
Public Domain, Google-digitized / http://www.hathitrust.org/access_use#pd-google

with iron-sponge mercury cathodes were developed to the manufacturing stage, as discussed in II-(f).

In addition to being capable of switching higher peak powers than aluminum cathode gaps, the mercury cathode gaps can be designed to have superior operating characteristics. Through the use of small radius anodes not possible with the aluminum cathode gaps, a wider operating range and much less time "jitter" can be attained. The small anodes build up corona at voltages less than those of breakdown, thus furnishing radiation prior to breakdown. For special applications, gaps have been developed having a range approaching 3 to 1 in a two-gap circuit, capable of switching 10 megawatts peak power, for many hundreds of hours, and having a time "jitter" of less than 0.02 microseconds at the operating voltage.[2, 3]

(d) *Starting and Operating Characteristics*

It has already been stated in II-(a) that starting and operating characteristics of series gaps cannot be interpreted simply because, under the circuit conditions of rapidly varying voltage, the breakdown voltage of a spark gap is not singly valued. Because of spark formation time the minimum voltage at which a spark gap will break down increases as the rate of rise of the voltage across it increases. Further, due to spark delay time, the voltage across the gap at breakdown is usually still higher than this minimum value. It is therefore impossible to designate a unique breakdown voltage of a spark gap when the voltage across it is increasing with time. It is, however, possible to find a practical minimum and maximum breakdown voltage for a particular rate of rise of voltage. The difference between this maximum and minimum value is a measure of the maximum spark delay time. It is for the purpose of reducing this spark delay time that corona points (or radium) are introduced, and it will be shown that the value of both spark delay time and spark formation time have an important bearing on the operational characteristics of fixed gaps.

In addition to rate of voltage rise, the breakdown voltage of a spark gap depends on the amount of ionization in the gap due to a previous spark. When a spark discharge stops, a column of highly ionized gas is left in the gap. Although this column is rapidly de-ionized by recombination and diffusion of ions, a lower breakdown voltage is found for many microseconds in consequence of this residual ionization. The minimum value of the breakdown voltage of the gap is therefore a function of the time

[2] F. S. Goucher, J. R. Haynes and E. J. Ryder, High Power Series Gaps Having Sintered Iron Sponge-Mercury Cathode, P.B. 19640, U. S. Department of Commerce, Office of the Publication Board.

[3] J. R. Dillinger, Operation of Sintered Iron Sponge-Mercury Cathode Type Series Gaps at S.C.I., A.E.W. and 5 Microsecond Conditions, P.B. 13270, U. S. Department of Commerce, Office of the Publication Board.

Digitized by Google
Original from UNIVERSITY OF MICHIGAN
Generated on 2019-09-22 06:26 GMT / http://hdl.handle.net/2027/mdp.39015077775156
Public Domain, Google-digitized / http://www.hathitrust.org/access_use#pd-google

after the spark ceases and is called the re-ignition voltage of the gap. It will be shown that this re-ignition voltage determines to a large extent the starting voltage of the fixed gaps.

Before describing the sequence of events required for starting and operating, it is desirable to define our terms more precisely than we have defined them up to this point. The minimum operating voltage is the lowest switch voltage at which the tubes will continue to break down 100% of the time under the action of the trigger pulse, and the maximum operating voltage is that higher switch voltage at which spontaneous breakdown of the series of gaps never occurs. Thus the operating range of voltage is that which includes those voltages existing across the series of gaps, at the time of application of trigger pulse, for which the tubes always break down under the action of the trigger pulse but never before. Starting voltage is defined as the minimum value of d-c voltage at which a series of gaps can be made to break down under the action of the trigger pulse. Starting thus differs fundamentally from operating in that while operating demands that the series of gaps always breaks down under the application of the trigger pulse, starting requires only that the gaps break down once in many trigger pulses occurring in a fraction of a minute. Thus, a starting voltage is always lower than the minimum operating voltage. However, due to the doubling of the switch voltage when starting occurs, the d-c power supply voltage required to start may be higher than the d-c power supply voltage at the minimum.

The results of a quantitative oscillographic analysis of starting and operating characteristics of a pair of preproduction W. E. 1B22 tubes[4] are now presented in detail, for they are qualitatively representative of all spark gaps. These tubes operate in a two-gap circuit, a schematic of which is shown in Fig. 5 (a). The analysis is carried out by an examination of the voltage-time wave which occurs at the point of application of the trigger pulse, the midpoint of the two gaps. It will help in understanding the oscillograms[5] which follow if it is borne in mind that the voltage across gap 1 is the voltage shown on the oscillogram with respect to ground or "O" voltage, while the voltage across gap 2 is the voltage shown on the oscillogram with respect to the switch voltage.

The sequence required for starting is shown in Fig. 16 (a). Just before the application of the trigger pulse the voltage at the midpoint of the two gaps is half that of the applied d-c by virtue of the resistance divider. When the trigger pulse is applied, the voltage rises to A (3.8 kv) which is the minimum breakdown voltage for these tubes with voltage rates of rise encountered in the trigger pulse. Gap 1, therefore, may break down at A

[4] These tubes contain both corona points and radium to reduce spark delay time (see II-(e)).

[5] The time scales of these oscillograms are expanded in regions of very rapidly reversing voltage in order to make clear the sequence of events.

Digitized by Google
Original from UNIVERSITY OF MICHIGAN
Generated on 2019-09-22 06:26 GMT / http://hdl.handle.net/2027/mdp.39015077775156
Public Domain, Google-digitized / http://www.hathitrust.org/access_use#pd-google

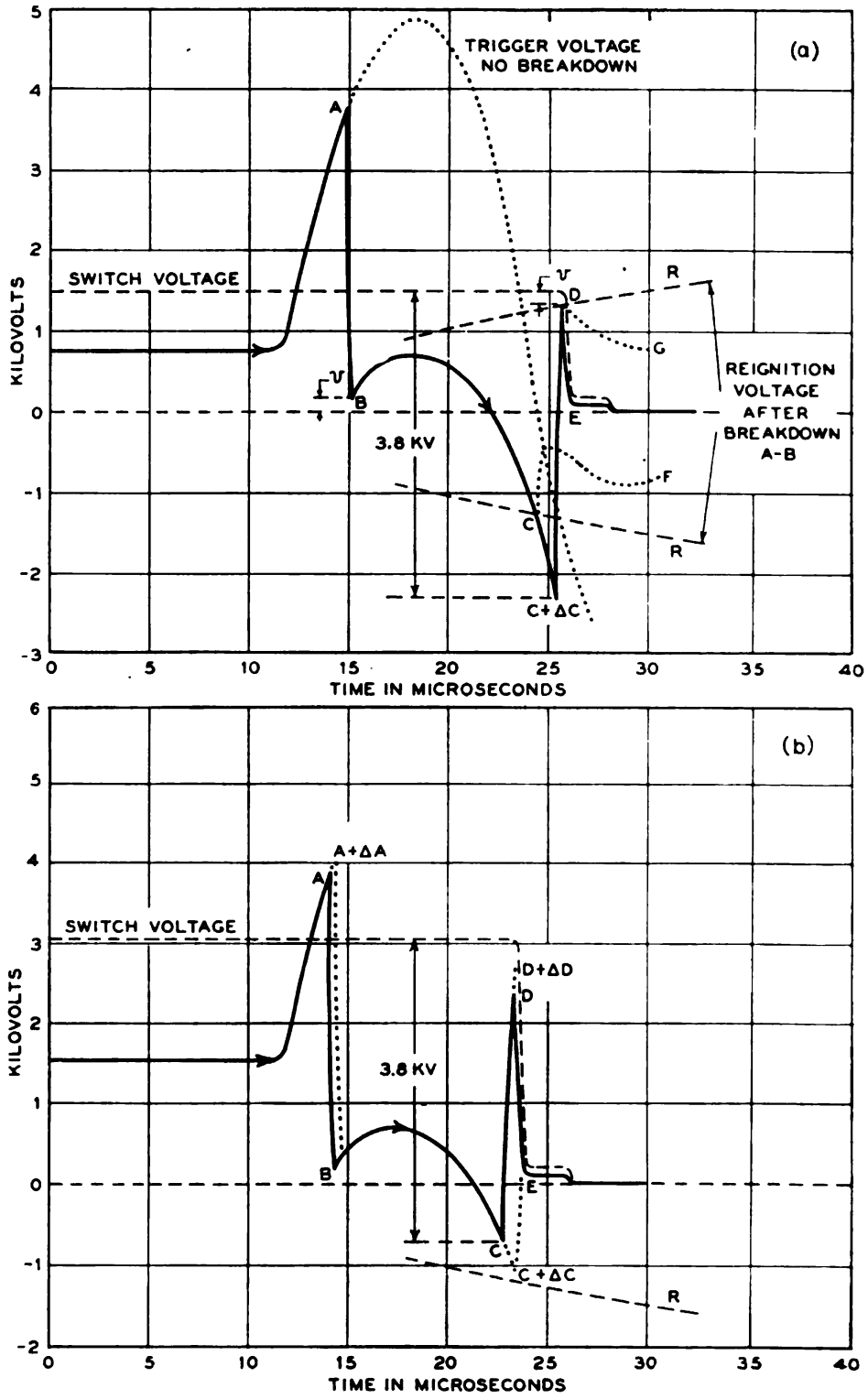

Fig. 16—Oscillographic traces of voltage vs. time as measured at the mid-point of a two-gap circuit during breakdown of 1B22 tubes, (a) for starting, (b) for operation at minimum switch voltage.

Digitized by Google
Original from UNIVERSITY OF MICHIGAN
Generated on 2019-09-22 06:27 GMT / http://hdl.handle.net/2027/mdp.39015077775156
Public Domain, Google-digitized / http://www.hathitrust.org/access_use#pd-google

passing a low-energy spark supplied by the trigger circuit. In consequence of this, the voltage drops sharply to B and then the discharge stops since the voltage (v) remaining is insufficient to maintain the discharge. This voltage, called the extinguishing voltage, is about 0.2 kv for these low energy sparks. Gap 1 is now ionized and has the independently measured re-ignition voltage characteristics, R, as shown. Under the action of the trigger pulse the voltage then proceeds to $C + \Delta C$ when gap 2 may break down since it has the minimum required voltage across it (3.8 kv). When this occurs, the voltage rises sharply to D, which falls short of the switch voltage by the amount of the extinguishing voltage (v). At this point gap 1 may re-ignite. If this occurs both gaps are simultaneously conducting and the switch voltage drops to L while passing the high-current pulse of energy from the network. This sequence occurs relatively infrequently.

Because of spark delay time, instead of breaking down at A, gap 1 may break down at some higher voltage, or not at all. Instead of gap 2 breaking down at $C + \Delta C$, gap 1 may break down in the reverse direction at any voltage higher than C, its re-ignition voltage, and is only prevented from doing so by spark delay time. Also, because of this delay time, gap 1 will usually fail to re-ignite at D, its re-ignition voltage, and since D is also the extinguishing voltage (v) for gap 2, the potential will drop to G under control of the trigger pulse. If any one of these things occurs the gaps will not start on that particular application of trigger pulse. However, since the pulses are applied at the rate of many hundred a second, it is usually only a fraction of a second until the desired sequence is obtained.

From the conditions essential for the consummation of each of the three steps necessary for starting, it follows that the starting switch voltage V_{dc} must be equal to $A - (R + \Delta C)$ or $v + R$, whichever is the greater. Since R, the re-ignition voltage, increases with time, $A - (R + \Delta C)$ decreases while $v + R$ increases with time. A minimum for V_{dc} will, therefore, be obtained when the period of the trigger voltage wave is such that when gap 2 breaks down,

$$A - (R + \Delta C) = v + R, \tag{1}$$

and since also for this minimum

$$V_{dc} = A - (R + \Delta C) \tag{2}$$

we get

$$V_{dc} = \frac{A - \Delta C + v}{2}. \tag{3}$$

By substituting the observed constant values of A, ΔC and v in (3) we get $V_{dc} = 1.5$ kv, which is the value of switch voltage depicted in the diagram. This diagram is, therefore, that for optimum period of the trigger voltage

Digitized by Google
Original from UNIVERSITY OF MICHIGAN
Generated on 2019-09-22 06:27 GMT / http://hdl.handle.net/2027/mdp.39015077775156
Public Domain, Google-digitized / http://www.hathitrust.org/access_use#pd-google

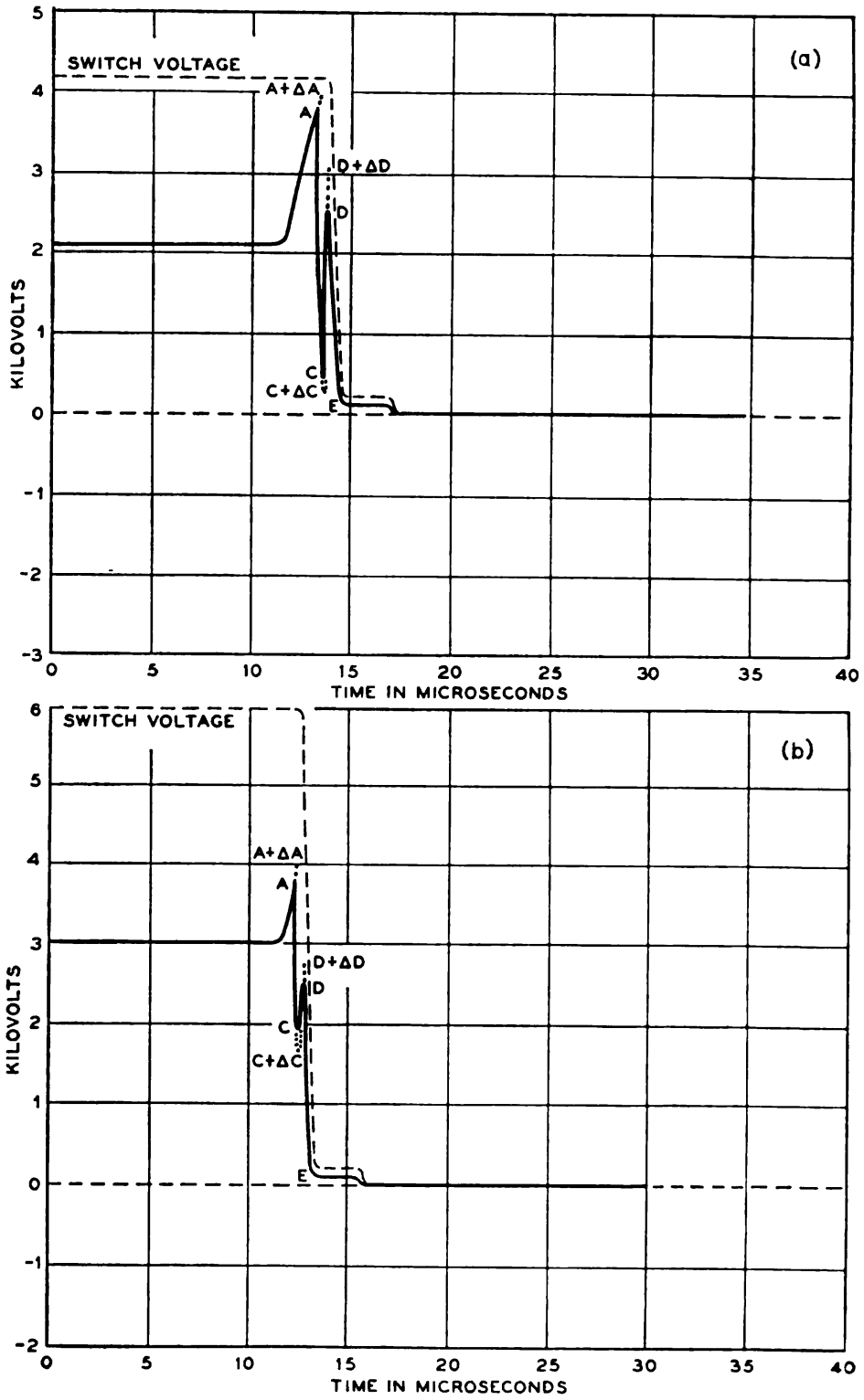

Fig. 17—Oscillographic traces of voltage vs. time as measured at the mid-point of a two-gap circuit during breakdown of 1B22 tubes (a) for normal operating switch voltage (b) for operation at maximum switch voltage.

Generated on 2019-09-22 06:27 GMT / http://hdl.handle.net/2027/mdp.39015077775156
Public Domain, Google-digitized / http://www.hathitrust.org/access_use#pd-google
Digitized by Google
Original from UNIVERSITY OF MICHIGAN

wave. That this is actually a minimum was demonstrated experimentally by varying the period of the trigger pulse. V_{dc} increased for pulse periods both greater than and less than that shown in the diagram. The increase was small and so is of no great practical interest, but it does confirm the prediction made on the basis of the above analysis.

After the tubes have started the switch voltage is nearly double the d-c voltage, and the tubes will operate continuously if the switch voltage is above the minimum operating voltage. The sequence of events near the minimum operating voltage is shown in Fig. 16 (b). During operation the spark delay time is much less than during starting, as indicated by a smaller value of ΔA and ΔC. There are reasons for believing that this is due primarily to the higher electrode temperature, but is doubtless aided by residual ionization left over by the high-energy sparks now passing. As a consequence the first gap always breaks down at voltages intermediate between A and $A + \Delta A$. Gap 2 always breaks down at voltages between C and $C + \Delta C$, below the re-ignition voltage of gap 1, and gap 1 always re-ignites at voltages between D and $D + \Delta D$ allowing the main pulse of current to current to pass at a voltage E. However, if the switch voltage is decreased, $C + \Delta C$ will occasionally cross the re-ignition voltage characteristic R of gap 1. Gap 1 can then re-ignite and thus the gaps will not fire on the application of that trigger pulse. A second way in which the gaps can miss is by failure of gap 1 to re-ignite at D. Even though either of one of these events occurs only once in many thousands of pulses, a minimum operating voltage is established.

Of course, no spark gap tubes are designed to operate very close to their minimum operating voltage. A margin of safety is always maintained. The characteristics of these tubes with a switch voltage at a practical operating voltage is shown in Fig. 17 (a). Gap 1 breaks down between A and $A + \Delta A$ and before gap 1 is extinguished gap 2 breaks down between C and $C + \Delta C$. Since in this case both gaps are conducting simultaneously, the main pulse passes without re-ignition of gap 1. The voltage at the midpoint of the two discharges rises to a value between D and $D + \Delta D$, due to the rapid change of spark impedance. This sequence always takes place since ample margin is provided.

If the switch voltage has been increased to a value near the maximum operating voltage, the voltage-time characteristic shown in Fig. 17 (b) results. Exactly the same sequence occurs as before. However, if the voltage be slightly increased above the value shown, the gaps can break down spontaneously during the network charging cycle and before the application of the trigger pulse, even though the value of A is some 20% greater than the charging voltage applied to the gap. This is the expected effect of spark formation time on minimum breakdown voltage since the rate of rise of

Digitized by Google
Original from UNIVERSITY OF MICHIGAN
Generated on 2019-09-22 06:27 GMT / http://hdl.handle.net/2027/mdp.39015077775156
Public Domain, Google-digitized / http://www.hathitrust.org/access_use#pd-google

trigger voltage is far higher than that of the network charging voltage. When spontaneous breakdown occurs, because of circuit conditions, both the rate of rise of the voltage of the network charging cycle and its peak value are increased. Since the switch voltage arrives at a higher value in a shorter time, spontaneous breakdown is most likely to occur again. The effect is cumulative so that, after a few increasingly frequent cycles, an arc is established. It is clear that this arcing must never be allowed to occur in the operating range.

These characteristics were taken while using a current pulse of 0.75 μs duration at a repetition rate of 1000 per second and a 30-ohm resistance load.

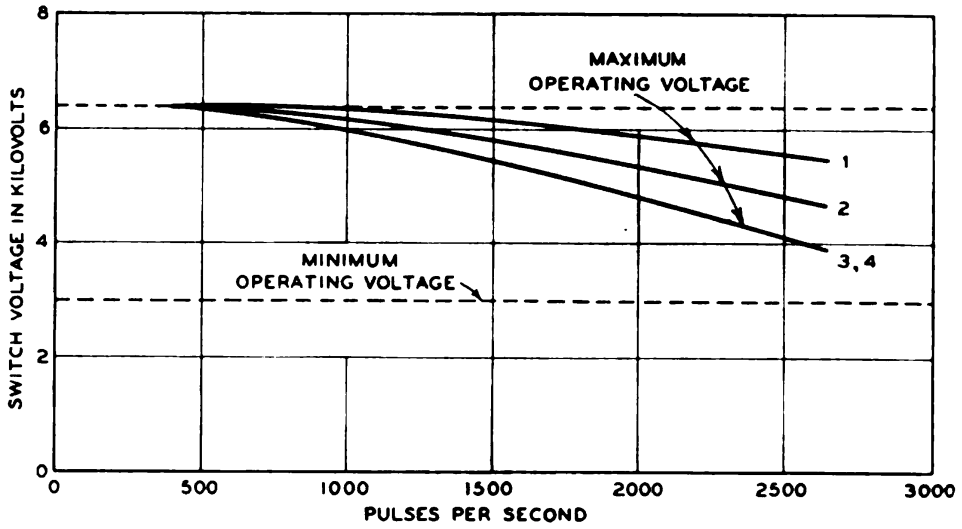

Fig. 18—Maximum operating voltage of 1B22 tubes in a two-gap circuit as affected by pulse repetition rate for a variety of pulsing conditions as follows:

Curve	Pulse Duration in Microseconds	Load in Ohms
1	0.75	55
2	0.75	30
3	0.75	15
4	1.50	30

This produced a peak current at the maximum operating voltage closely equal to the switch voltage divided by twice the resistance load, or about 100 amperes. Under these conditions, due to the relatively low pulse repetition rate, there is little residual ionization in the gaps at the time of the next pulse, so that the gaps have nearly recovered their maximum breakdown voltage. However, as the pulse rate is increased, thus decreasing the time between pulses, the value of switch voltage at which the gaps break down spontaneously is found to decrease due to residual ionization. Thus the maximum operating voltage is a function of the pulse repetition rate.

The decrease of the maximum operating voltage as a function of pulse rate, for these tubes, is shown in Fig. 18 for a variety of pulsing conditions.

Generated on 2019-09-22 06:28 GMT / http://hdl.handle.net/2027/mdp.39015077775156
Public Domain, Google-digitized / http://www.hathitrust.org/access_use#pd-google
Digitized by Google
Original from UNIVERSITY OF MICHIGAN

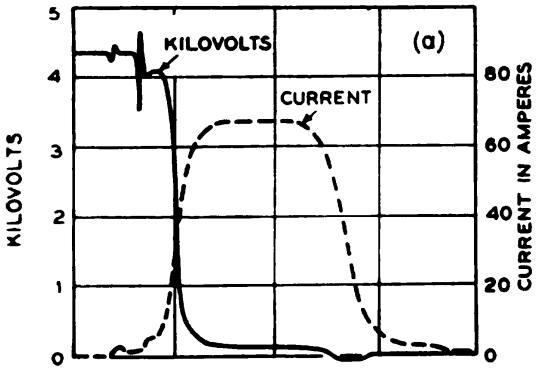

(a) Voltage vs. time and current vs. time for 0.75-microsecond pulse.

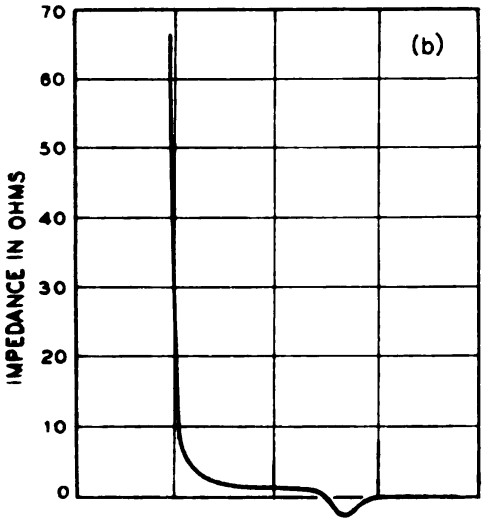

(b) Impedance vs. time.

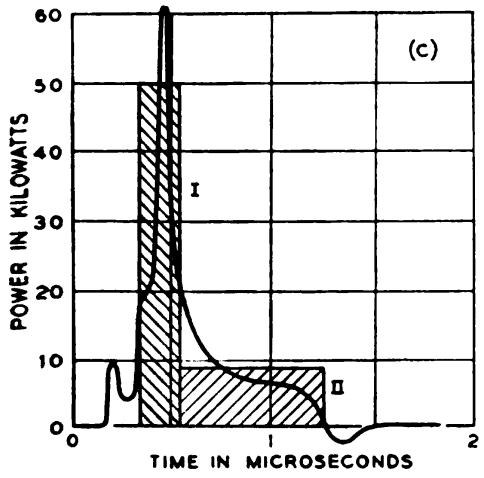

(c) Instantaneous power dissipated in gaps vs. time—solid trace from oscillographic, shaded areas from calorimetric measurements.

Fig. 19—Pulse characteristics of two 1B22 tubes operated in series.

Generated on 2019-09-22 06:28 GMT / http://hdl.handle.net/2027/mdp.39015077775156
Public Domain, Google-digitized / http://www.hathitrust.org/access_use#pd-google
Digitized by Google
Original from UNIVERSITY OF MICHIGAN

Curve 2 was obtained with the 0.75 μs pulse and a 30-ohm load. It will be observed that the maximum operating voltage decreases with pulse rate in the expected manner.

If the peak current of the pulse be decreased, fewer ions are produced in the spark and so at any given time after the pulse one would expect less residual ionization in the gaps. Curve 1 was obtained by keeping the pulse duration the same as before but increasing the load resistance to 55 ohms. Thus the current at a given switch voltage was reduced to 30/55 of its former value. It will be seen that, as predicted, the drop of maximum operating voltage with increased pulse repetition rate is less.

Conversely, if the current is increased the opposite effect is produced. Curve 3 was obtained by decreasing the load resistance to 15 ohms while keeping the pulse duration constant. This gives twice the peak current at the same switch voltage as that of Curve 2 with a resultant increased residual ionization and a decrease of maximum operating voltage at the higher pulse repetition rates.

If, instead of doubling the current, the pulse duration be doubled, a similar increase in residual ionization is produced. Curve 4 was obtained by doubling the pulse duration (1.5 μs) and using a 30-ohm load. Thus, while the current is the same as Curve 2, the current pulse has twice the duration. It will be observed that for these pulses, doubling the time of pulse is the equivalent of doubling the current.

One might expect that the minimum operating voltage would also decrease as the pulse repetition rate is increased. However, experimentally it is found that, for these tubes, the minimum operating voltage is nearly constant and, therefore, independent of residual ionization. This result is produced largely because the maximum breakdown voltage of the gaps at the extremely high rate of voltage-time change encountered in triggering at the minimum is little affected by this amount of residual ionization.

Since the minimum is nearly constant the operating range of voltage of these tubes is a decreasing function of the pulse repetition rate, current, and pulse duration. This is in general true of all fixed spark gaps; however, the amount of decrease of operating range depends on the spark gap spacing, gas atmosphere and geometry of the electrodes.

(e) *Dissipation and Switching Efficiency*

In II-(d) we considered the voltage-time relationships leading to the simultaneous breakdown of series gaps. In this subsection we will consider the voltage and current relationships with time during this breakdown, and their bearing on spark dissipation and switching efficiency.

In Fig. 19 (a) are shown a voltage-time and current-time trace obtained oscillographically with a pair of 1B22 gaps. The voltage is measured across

Digitized by Google
Original from UNIVERSITY OF MICHIGAN
Generated on 2019-09-22 06:29 GMT / http://hdl.handle.net/2027/mdp.39015077775156
Public Domain, Google-digitized / http://www.hathitrust.org/access_use#pd-google

both gaps and corresponds to the dotted traces shown for switch voltage in Fig. 17 (a). The current pulse is shown in proper time relationship with the voltage trace. Similar traces are obtained for any pulse duration and peak current. These, then, may be considered as typical of all pulses produced by spark switching with these gaps.

In Fig. 19 (b) is plotted the impedance of both gaps with time, from which we see that the impedance of this switch falls rapidly in a small fraction of a microsecond to an average value of only a few ohms while the main current pulse is passing. The tail of the trace showing a negative impedance is due not to the gaps but to inductance inherent in their leads.

The solid trace, Fig. 19 (c), shows the product of voltage and current in kilowatts plotted against time. The integrated area of this plot corresponds to the dissipation per pulse of both gaps. This area is independent of the pulse repetition rate, enabling one to determine the gap dissipation for any project by multiplying the loss per pulse by the repetition rate.

This area can be divided into two parts as suggested by the two shaded blocks I and II. The first part corresponds to the energy dissipated initially by the trigger and then by the pulse forming network in the brief transient period when the voltage across and the current through the gaps are changing rapidly. The former is comparatively small and usually can be neglected. The latter attains a maximum value of power when the impedance of the gaps approximates that of the load. The second so-called steady state part, corresponding to block II, represents the energy lost during the main pulse when the impedance of the gaps is low and comparatively constant. Its value will depend on both the pulsing conditions and the gaps themselves.

A calorimetric study was made of the dissipation of gaps as affected by various parameters. This method was superior to the oscillographic approach in that it afforded greater accuracy and ease of measurement. The curve, Fig. 20, shows observations in terms of joules per pulse per gap obtained calorimetrically with the 1B22 type tube as a function of pulse duration in microseconds. The peak current in all cases was 70 amperes and the trigger energy was included. It is clear that for pulse durations greater than 0.5 microseconds the dissipation D in joules per pulse per gap is given by

$$D = A + Bt \tag{1}$$

where A is the intercept of the extrapolated solid straight line through the observed points and where B is the slope of this line. The shaded blocks I and II of Fig. 19 (c) were obtained from values of the two terms A and Bt, respectively, showing graphically the agreement between the calorimetric and the oscillographic methods.

As a result of calorimetric measurements on a wide variety of gaps having either aluminum or mercury cathodes and operated under a wide variety of

Digitized by Google
Original from UNIVERSITY OF MICHIGAN
Generated on 2019-09-22 06:29 GMT / http://hdl.handle.net/2027/mdp.39015077775156
Public Domain, Google-digitized / http://www.hathitrust.org/access_use#pd-google

pulsing conditions, we have been able to establish an empirical formula for the dissipation D in joules per pulse per gap in terms of these gap parameters and pulsing conditions as follows:

$$D = 5.7(10)^{-7} I_p S + [40 + 3.9(10)^{-2} p^{0.4} S] I_p t. \quad (2)$$

Here I_p is the peak current in amperes, S the gap spacing in mils, p the gas pressure of hydrogen-argon in inches of mercury, and t is the duration in seconds of an idealized square-top wave equivalent in ampere-seconds to the actual current wave. This formula holds for either aluminum or mercury cathodes and is independent of gap design. It is modified only slightly when pure hydrogen is substituted for the hydrogen-argon mixture, the constant $3.9(10)^{-2}$ becoming $3.1(10)^{-2}$. It is based on many measurements in which the parameters covered the following ranges:

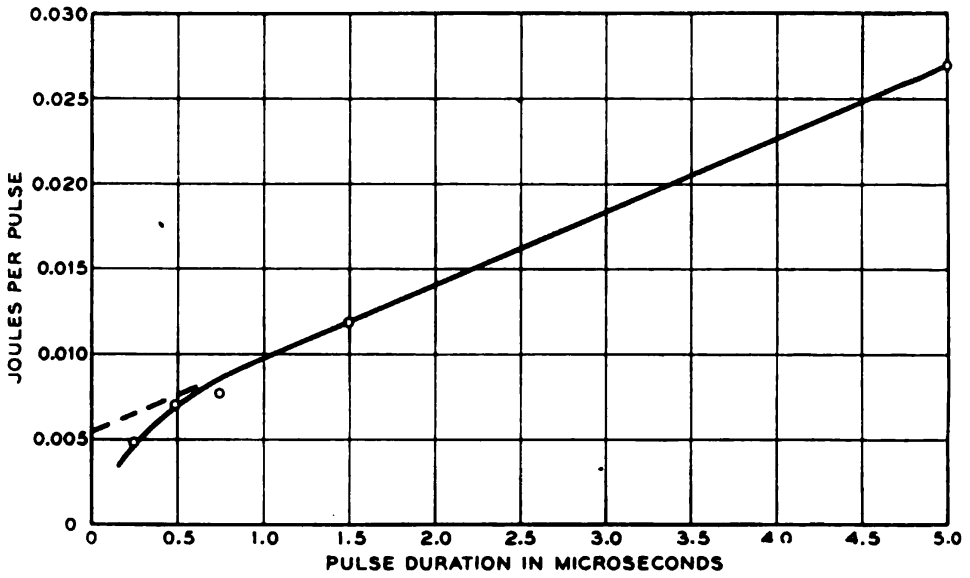

Fig. 20—Dissipation per gap per pulse vs. pulse duration for 1B22 gaps operated in series with a peak current of 70 amperes.

Parameter	Range
S	40–350 mils
p	28–50" Hg.
t	1–6 × 10^{-6} seconds
I_p	45–1070 amperes

After calculating the value of D from Equation (2) the dissipation in watts per gap for any project is obtained by multiplying by the pulse repetition rate. This equation does not include the trigger energy dissipated which usually

Digitized by Google
Original from UNIVERSITY OF MICHIGAN
Generated on 2019-09-22 06:29 GMT / http://hdl.handle.net/2027/mdp.39015077775156
Public Domain, Google-digitized / http://www.hathitrust.org/access_use#pd-google

can be neglected but which can be measured independently and added if so desired.

It is to be noted that the first or transient term of the formula is unaffected by pulse duration and argon content and depends at least to a first approximation on only the peak current and length of spark. The numerical constant includes the time of this transient, the average gradient during this period, and a factor to reduce the peak current to an average value. The portion of the second or steady state term within the brackets represents the average voltage across a gap when it is highly conducting and is approaching the characteristics of a steady arc. This average voltage is separated into two parts. The first part, 40 volts, is the sum of the cathode and anode drops arising from space charges at the electrodes. The second part is the voltage drop along the positive column which has a pressure dependent uniform gradient and which is of the order of 100 volts per cm. It is only this gradient which is perceptibly altered when argon is added to the hydrogen.

From this formula it is possible to calculate the switching efficiency for any design of gap and set of pulsing conditions within the specified range of parameters covered by the formula. Calculation shows that with three gaps in series the switching efficiency in all projects was at least 90%, whereas with two gaps in series it was in most cases as high as 96%.

(f) *Development of Fixed Gaps for Manufacture*

The designs of the fixed gaps for manufacture were dictated by the requirements of particular modulators. Under the code number of each of the gaps a brief description is given of the electrical and mechanical requirements which had to be met.

W.E. 1B22

The 1B22 fixed gap tube is an aluminum cathode type with a hydrogen-argon filling. An exterior and a cross-sectional view are shown in Fig. 21. This fixed gap tube was developed for the modulator of an airborne radar known initially as ASH and later an AN/APS-4. In this modulator two tubes are used in series to switch a peak power of about 105 kilowatts into a W.E. 725A magnetron. It was desirable that the peak voltage in the modulator section be kept fairly low so that the circuit would perform satisfactorily at high altitude even when the pressurizing container was damaged. Furthermore, the equipment was to be very compact and light in weight.

In order to meet the requirements of this radar, two tubes were used in series with a peak switching voltage of 4 kilovolts. They were required to pass a current pulse of 67 amperes for 0.75 microseconds at two repetition

Digitized by Google
Original from UNIVERSITY OF MICHIGAN
Generated on 2019-09-22 06:29 GMT / http://hdl.handle.net/2027/mdp.39015077775156
Public Domain, Google-digitized / http://www.hathitrust.org/access_use#pd-google

rates, one of 600, the other of 1000 pulses per second. They were also to operate for short periods at 2.25 microseconds and 330 pulses per second. The main problems in the design of such a tube were those of obtaining an adequate service life and a sufficiently low starting voltage.

As pointed out in II-(b), the life of an aluminum cathode gap of this type is critically dependent upon the anode-cathode spacing. For this tube a

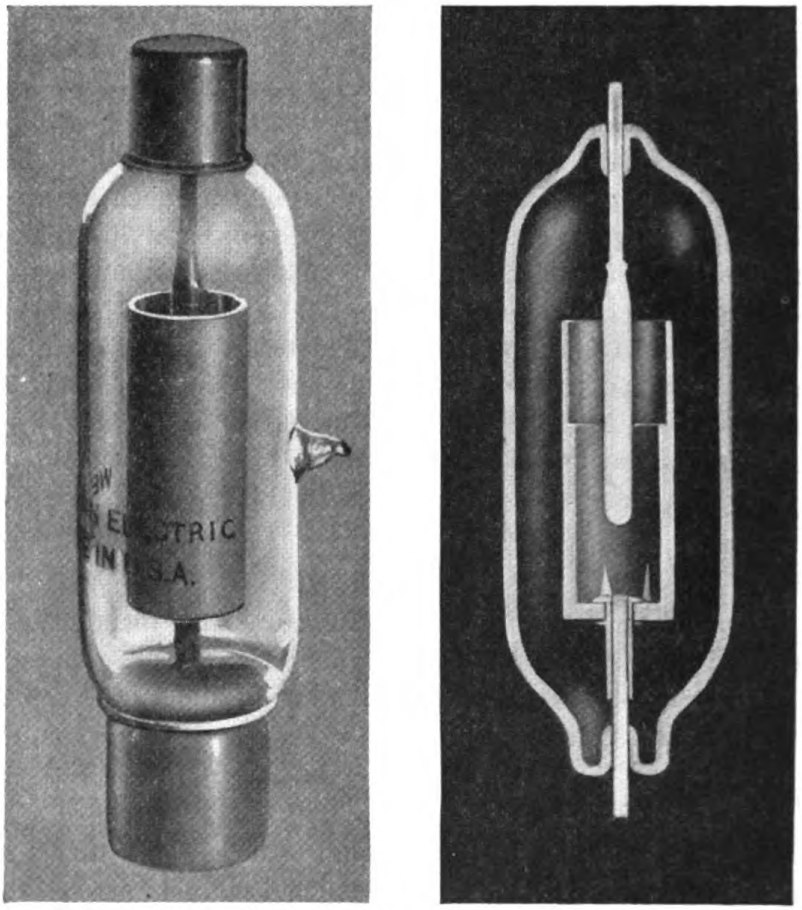

Fig. 21—Western Electric 1B22 spark gap tube.

spacing of approximately 150 mils was selected, the gas pressure being 20 inches of 75% hydrogen and 25% argon. This gave a life of about 500 hours for the 0.75 microsecond pulse, and a much shorter life for the 2.25 microsecond pulse. However, since the latter pulse duration is used only a small part of the time, the service life proved to be adequate. In order to obtain the maximum life from each tube, it was necessary that the anode and the cathode depart no more than a few mils from concentricity. Otherwise the sparking would not be uniformly distributed radially, leading to a

Digitized by Google
Original from UNIVERSITY OF MICHIGAN
Generated on 2019-09-22 06:32 GMT / http://hdl.handle.net/2027/mdp.39015077775156
Public Domain, Google-digitized / http://www.hathitrust.org/access_use#pd-google

non-uniform anode build-up and a shortened life. Furthermore, in order to prevent failure of the tube, due to sputtered material destroying the insulation of the interior glass walls, the inside diameter of the cathode was enlarged near the open end, thus confining the sparking to the deeper portion of the cathode cylinder.

As discussed in II-(d) the starting voltage of a pair of fixed gap tubes is particularly important. The operating voltage of the tubes in this case is approximately 4 kilovolts which is derived from the resonant charging of the pulse shaping network condensers from a high voltage supply of about 2.2 kilovolts. The open circuit voltage of this supply is about 2.7 kilovolts. This, then, is the voltage available for starting the gaps. In order to make the gaps start at a voltage well below this value, corona points were introduced at the end of the cathode opposite the end of the anode, a small quantity of radium was also introduced in this region, and the anode diameter was reduced to the lowest value consistent with long life. The effectiveness of the corona points and the radium was reduced by the sputtered material during the life of the tube, but the irregular deposition of this sputtered material favored the production of corona and actually reduced the starting voltage to a lower value than that for a new tube.

The tube was designed for fuse clip mounting but it was found that the acceleration imparted to the tube when it was snapped into heavy clips was greater than that encountered in flying service. Accordingly, a special mounting was devised so that the tube would not be broken when being installed in the radar set. By the end of the war these tubes had been installed in approximately 15,000 radar equipments.

W.E. 1B29

The 1B29 fixed gap tube is similar in constructional details to the 1B22 except that it is smaller, the gap spacing being only 90 mils. An exterior and a cross-sectional view of the tube are shown in Fig. 22.

The gaps were designed to switch 2.8 kilovolts and to pass a peak current of about 27 amperes for 0.75 microseconds at a repetition rate of 2000 pulses per second. The main design problems were those of adequate life and stability of tube drop during conduction.

The small size of these gaps resulted in a life of only 300 hours which was, however, quite adequate for this application. As pointed out in II-(b) the argon was added to the hydrogen to ensure a uniform low impedance on sparking. The extremely small peak current required an increase in the amount of argon to 50% instead of the usual 25%.

In mechanical construction, the 1B29 is essentially a scaled-down 1B22. Because of the smaller size of the tube, no new problems existed in making it rugged.

Digitized by Google
Original from UNIVERSITY OF MICHIGAN
Generated on 2019-09-22 06:32 GMT / http://hdl.handle.net/2027/mdp.39015077775156
Public Domain, Google-digitized / http://www.hathitrust.org/access_use#pd-google

Sufficient tubes were manufactured to supply approximately 3000 radar equipments.

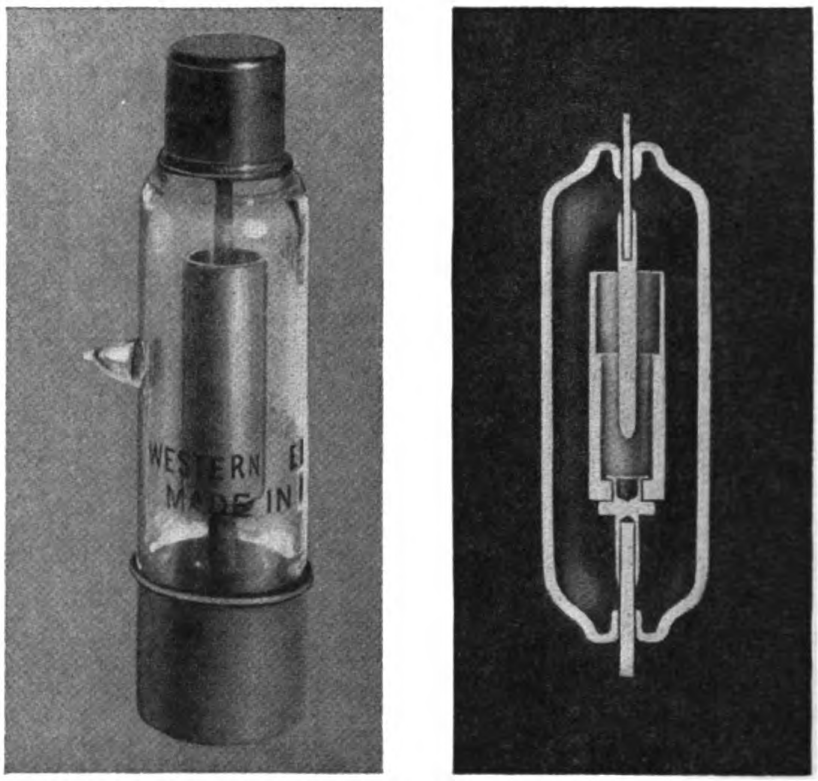

Fig. 22—Western Electric 1B29 spark gap tube.

W.E. 1B31

The 1B31 fixed gap was also an aluminum cathode gap, with a gap spacing of 300 mils and 24 inches of 75% hydrogen and 25% argon. An exterior and a cross-sectional view are shown in Figure 23. This gap was developed for an airborne radar. This modulator was required to furnish a peak power of 230 kilowatts to a W.E. 2J53 magnetron. The modulator was also to provide a range of pulse durations and repetition rates extending from 0.25 microseconds at 1600 pulses per second to 5.0 microseconds at 200 pulses per second.

In order to meet these requirements, two 1B31 tubes were used with a peak switch voltage of 8 kilovolts and a peak current of 75 amperes. By using a 300 mil spacing, a life greater than 500 hours was obtained at 200 pulses per second, 5 microseconds and 75 amperes. The other operating conditions were less severe from the life standpoint.

The wide spacing used meant a considerable increase in the size of the cath-

Generated on 2019-09-22 06:33 GMT / http://hdl.handle.net/2027/mdp.39015077775156
Public Domain, Google-digitized / http://www.hathitrust.org/access_use#pd-google
Digitized by Google
Original from UNIVERSITY OF MICHIGAN

ode over the previous designs. To make this tube rugged, both electrodes were supported from large diameter kovar-to-glass seals. During assembly the cathode end of the tube was open so that a tool could be inserted to hold the anode concentric with respect to the cathode, while its supporting member was sealed to the glass. A cup was then brazed in to cover the cathode opening.

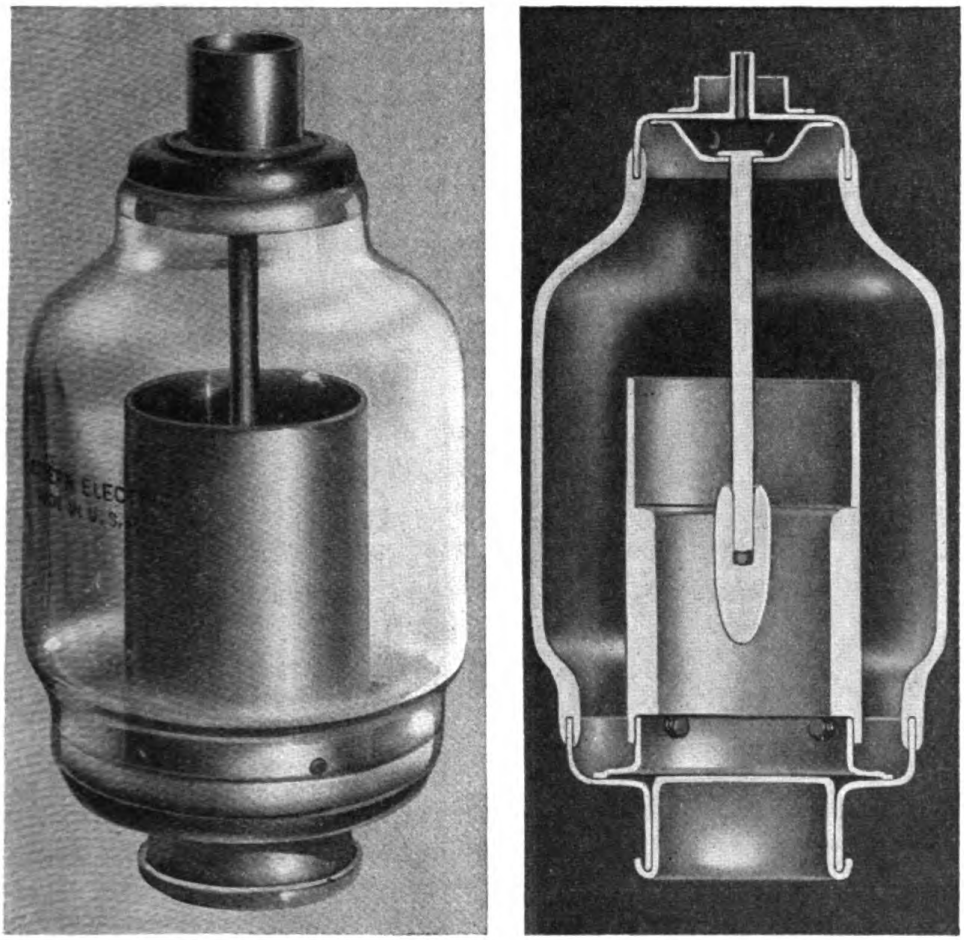

Fig. 23—Western Electric 1B31 spark gap tube.

Several hundred models of this tube were made in the laboratory and performed satisfactorily in the circuit. Due to circuit design changes, however, these tubes did not go into large scale manufacture.

W.E. 1B42

The 1B42 fixed gap tube departs considerably in design from the 1B22 and 1B29 in that mercury instead of aluminum was used as cathode. Its

Digitized by Google
Original from UNIVERSITY OF MICHIGAN
Generated on 2019-09-22 06:33 GMT / http://hdl.handle.net/2027/mdp.39015077775156
Public Domain, Google-digitized / http://www.hathitrust.org/access_use#pd-google

construction is illustrated in Fig. 24. This tube was developed for radars which were for long range search on shipboard. In these modulators three tubes were used in series to switch a peak power of 0.8 megawatts and 1.4

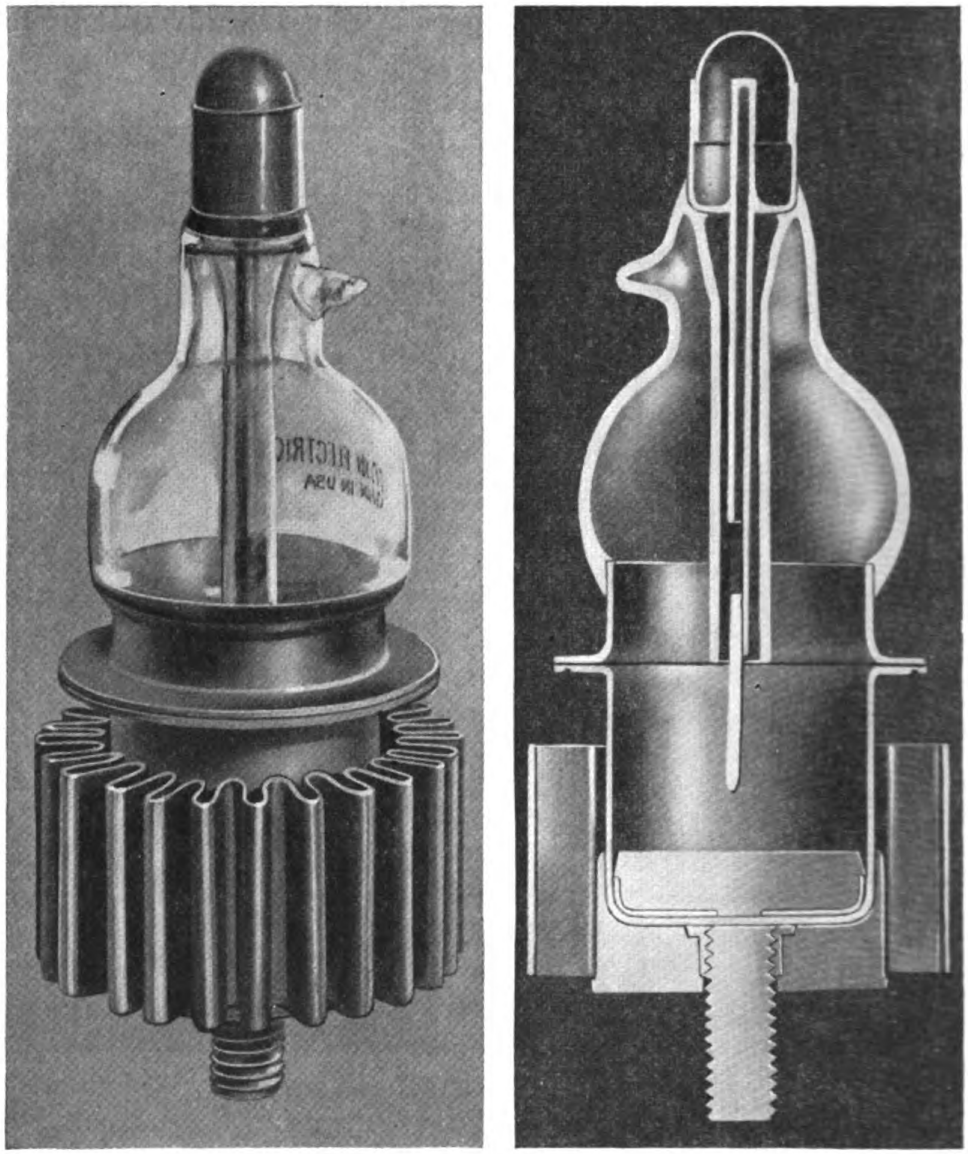

Fig. 24—Western Electric 1B42 spark gap tube.

megawatts, respectively, into high power triode oscillators. These modulators were to be capable of operation at either half or full power. The equipment was to be capable of withstanding the shock and vibration normally encountered on shipboard.

The series of gaps was required to operate with peak switch voltages

Digitized by Google
Original from UNIVERSITY OF MICHIGAN
Generated on 2019-09-22 06:33 GMT / http://hdl.handle.net/2027/mdp.39015077775156
Public Domain, Google-digitized / http://www.hathitrust.org/access_use#pd-google

varying from 10.5 to 17.1 kilovolts, and to pass a maximum current of 200 amperes for 6 microseconds at a repetition rate of 180 pulses per second. They were also required to operate with 1.5 microsecond pulses at 600 pulses per second. The main electrical design problems were those of obtaining a wide voltage operating range and an adequate life with large peak currents and long pulses.

As discussed in II-(c), the use of an iron sponge mercury cathode with a molybdenum rod anode provided a wide voltage operating range as well as a long life with 200 ampere, 6 microsecond pulses. The mercury sponge cathode also met the vibration and shock requirements of shipboard operation.

In order to secure good wetting of the sintered sponge, which was essential to a long life, a special construction, as shown in Fig. 24, was used. The sponge was sintered directly into the bottom of a Kovar cup which had six radial vanes welded into it. These served to anchor the sintered material as well as to conduct the heat away from the center of the cathode. After the anode assembly and glass envelope were attached to the upper Kovar flange, the two sub-assemblies were welded together by means of a single ring weld. This allowed a minimum of handling of the sintered material and eliminated all glass work after the sintered material was inside the tube.

The processing of the tube consisted of first evacuating and then of heating the lower portion to 800°C while passing purified hydrogen through the tube. After the sponge had partially cooled, the mercury was introduced and wetting took place instantly.

Since the temperature of the center of the sponge must be kept below the boiling point of mercury, in addition to the internal vanes described, the Kovar cup was soldered into a block of copper to which was attached a folded copper radiator.

Several hundred models of the tube were made in the laboratory and delivered to the Navy and to equipment manufacturers. Full manufacturing information was turned over to the Navy which in turn issued a contract for the procurement of several thousand tubes.

Ratings

The ratings of the four different models of spark gap tubes developed by the Laboratories are summarized in Table 1. In order to permit the use of these gaps under a wide variety of operating conditions, yet prevent the simultaneous application of the maximum values of peak current, pulse duration, and repetition rate, a special system of rating was evolved. In addition to placing a maximum value on each of these three quantities a maximum value was also placed on the product of any two of these quan-

Digitized by Google
Original from UNIVERSITY OF MICHIGAN
Generated on 2019-09-22 06:33 GMT / http://hdl.handle.net/2027/mdp.39015077775156
Public Domain, Google-digitized / http://www.hathitrust.org/access_use#pd-google

tities. For instance, one of these products would prevent the use of very high peak currents along with very long pulses, a combination which would give a very short life, especially with aluminum cathode gaps. Or another product would prevent the use of the tube at both high peak currents and high repetition rates, a condition which would not allow adequate deionization between pulses. The later types of gaps were rated in this manner.

(g) *Evaluation of the Fixed Gap as a Modulator Switch*

In order to compare the performance of fixed gaps in radar modulators with that of other switching devices, as well as to assess their future possibilities, we may consider them with respect to the following points.

TABLE I
RATINGS OF W. E. FIXED SPARK GAP TUBES

Tube Type	Repetition Rate—pps		Peak Current a Max.	Pulse Duration μs Max.	Micro-Coulombs per Pulse Max.	Operating Voltage Range—2 gap Ckt. kv		Operating Voltage Range—3 gap Ckt. kv		Peak Trigger Voltage 3 gap Ckt. kv Nominal	Peak Trigger Voltage 3 gap Ckt. kv Nominal	Voltage Required for Starting kV	
	Min.	Max.				Min.	Max.	Min.	Max.			2 gap Ckt. Min.	3 gap Ckt. Min.
1B29	500	2100	30	0.75	—	2.6	3.0	—	—	3.0	—	1.9	—
1B22	300	1100	75	0.75	—	3.8	5.4	—	—	5.0	—	2.5	—
1B31	200	1600	300	5.0	375	7.3	9.2	—	—	8.0	—	6.1	—
1B42	160	1500	300	6.1	1280	9.0	11.4	10.5	17.1	10.0	15.0	6.5	8.5

(More complete information on the above tubes is contained in the JAN Specifications for individual tubes.)

1) *Peak current*—The present coded tubes cover a range of currents from 20 amperes to 300 amperes. Experimental tubes have been tested up to 1000 amperes, and indications are that even larger currents are possible.
2) *Switch voltage*—The present tubes cover a range from 2.6 to 17.1 kilovolts. Experimental tubes have been tested up to 30 kilovolts.
3) *Peak power output*—With the limits of peak currents and voltages on the present tubes, power outputs of 25 kilowatts to 2.2 megawatts are possible. Experimental tubes were made which were capable of furnishing 15 megawatts. Much larger power outputs seem possible.
4) *Pulse duration*—The maximum range of pulse durations covered by any of the present tubes is from 0.25 to 6 microseconds. For pulses shorter than 0.25 microseconds the efficiency of these tubes would decrease rapidly. Pulse durations much greater than 6 microseconds, however, could probably be used if proper attention is given to cooling.

Generated on 2019-09-22 06:33 GMT / http://hdl.handle.net/2027/mdp.39015077775156
Public Domain, Google-digitized / http://www.hathitrust.org/access_use#pd-google
Digitized by Google
Original from UNIVERSITY OF MICHIGAN

5) *Pulse repetition rate*—A range of 160 to 2100 pulses per second has been covered by coded tubes. Experimental tubes with very short gaps have been tested up to 10,000 pulses per second. However, the design of tubes for practical operation in this region would entail considerable effort.
6) *Operating voltage range*—Although a given set of tubes may exhibit a wide range of operating voltage on a laboratory test, the rated range must be considerably less because of manufacturing variations and changes during life. However, since most radar modulators operate at a fixed power level, this limitation is not a serious one.
7) *Trigger requirements*—The spark gap tubes require a high-voltage low-current trigger supply. While this is more difficult to obtain than the low-voltage supplies required by some other modulators, it caused no real difficulty in practice.
8) *Time jitter*—Although the time jitter of coded tubes is of the order of one microsecond, experimental tubes have been made which have, at the operating voltage, a jitter of the order of one hundredth of a microsecond.
9) *Efficiency*—The switching efficiency for all of the past applications of fixed gaps has been in the range of 90 to 96 percent, which makes the fixed gap one of the most efficient switching devices for radar.
10) *Simplicity of manufacture*—Since the unit type of fixed gap has only two elements of simple geometry, its manufacture is relatively easy.
11) *Dependability*—The dependability of the fixed gap has been demonstrated by its satisfactory performance in its extensive application.

Acknowledgments

The authors wish to acknowledge the valuable help given by many who cooperated in this project. In particular, they would like to thank Dr. S. B. Ingram for his criticisms and suggestions in regard to the development of coded sealed gaps. Also, we are especially indebted to Messrs. H. W. Weinhart and C. Depew for their invaluable help in the design and construction of the large variety of gaps required for this development.

Generated on 2019-09-22 06:34 GMT / http://hdl.handle.net/2027/mdp.39015077775156
Public Domain, Google-digitized / http://www.hathitrust.org/access_use#pd-google
Digitized by Google
Original from UNIVERSITY OF MICHIGAN

The Gas-Discharge Transmit-Receive Switch

By A. L. SAMUEL, J. W. CLARK and W. W. MUMFORD

THE gas-discharge transmit-receive switch has become an accepted part of every modern radar set. Indeed, without such a device, an efficient single-antenna micro-wave radar would be nearly impossible. Many of the early radar sets made in this country employed separate antennae for the transmitter and receiver. The advantages of single antenna operation are so apparent as hardly to require discussion. The saving in space or, if the same space is to be occupied, the increase in gain and directivity of a large single antenna is, of course, apparent. But even more important, perhaps, is the tremendous simplification in tracking offered by a single antenna, particularly where a very rapid complex scanning motion is desired.

The fact that the receiver needs to be operative only during periods between the transmitting pulses makes single antenna operation possible if four conditions are satisfied. These are: (1) the receiver must not absorb too large a fraction of the transmitter power during the transmitting period, (2) the receiver must not be permanently damaged by that portion of the transmitter power which it does absorb, (3) the receiver must recover its sensitivity after any possible overload during the transmitting pulse in a time interval shorter than the interval required by the reflected pulse to arrive back to the receiver from the nearest target, and (4) the transmitter must not absorb too large a fraction of the received power. At frequencies of the order of 700 megacycles and at low power levels these conditions are not impossible of attainment without recourse to any special switching mechanism other than that provided automatically by the usual circuit components. Conditions (1) and (2) can be met by designing the receiver in such a way that the change in input impedance as a result of overload will cause most of the available input power to the receiver to be reflected. Condition (3) requires careful attention to the time constants of all those receiver circuits which are subject to overload. Condition (4) fortunately is automatically satisfied by most transmitters, again as a result of the large mismatch reflections which occur at the connections to the transmitter's "tank" circuit when the transmitter is not operating. The United States Navy Mark 1 radar was operated on this basis.

The speed with which the transmit-receive switch must operate rules out all consideration of mechanical devices, at least for all but the longest range

Digitized by Google
Original from UNIVERSITY OF MICHIGAN
Generated on 2019-09-22 06:35 GMT / http://hdl.handle.net/2027/mdp.39015077775156
Public Domain, Google-digitized / http://www.hathitrust.org/access_use#pd-google

"early warning" equipment. For example, the go and return time to a target at 500 feet distance requires approximately one microsecond. Switching times must, therefore, be measured in microseconds. Since these short time intervals would at first sight seem to be too small to permit the use of gaseous discharge devices, some work was done on the use of specially designed vacuum diodes. It is possible to employ balancing circuits (sometimes called hybrid circuits) to achieve single antenna operation, but such circuits require critical balancing adjustments and they dissipate a large part of the available power in non-useful balancing loads. The need for a still different approach to the duplexing problem was clearly indicated.

Spark discharges either in air or in enclosed gaps bridged across parallel wire transmission lines were used in some of the early experimental long-wave radar sets. Dr. Robert M. Page of the Naval Research Laboratory was one of the pioneers in this work. These devices were only moderately satisfactory because of their erratic behavior and because of electrode wear. However, it was observed that the recovery time of such discharges was not as long as might be expected on the basis of a simple ionization and deionization explanation of their operation. This led to the investigation of the use of low-pressure gas discharges. These very early gas-discharge "switches" were actually much more in the nature of "lightning protectors", their principal function being to limit the power delivered to the receiver during the transmitting pulse in a gross sort of way, with considerable reliance on impedance changes at the receiver and on the rugged overload capabilities of the first tube in the receiver.

The trend toward shorter wavelengths and the desire for better protection led to the development of a partially evacuated gas-discharge tube located in a relatively high Q resonant cavity. In England, cavity type duplex tubes were made by inserting gas in a then current type (Sutton Tube) of local oscillator tube. These devices were called TR boxes (abbreviation for transmit-receive) by the English, a designation which has continued. It is a curious coincidence that some of the earliest cavity type duplex tubes made in this country at the Bell Telephone Laboratories were also constructed by inserting gas in an American type local oscillator tube (the 712A vacuum tube). This tube (later coded the 709A vacuum tube) was tested in an operative system which was subsequently demonstrated to the Army with such satisfactory results that the tube was adopted without change for several radar systems. The 709A vacuum tube and its associated cavity are shown in Fig. 1.

A similar structure, known as the 702A and shown in Fig. 2 (together with the 709A tube) was used for longer wavelengths. The need for these tubes was so very great that no time was allowed for their improvement before production was undertaken by the Western Electric Company.

Digitized by Google
Original from UNIVERSITY OF MICHIGAN
Generated on 2019-09-22 06:35 GMT / http://hdl.handle.net/2027/mdp.39015077775156
Public Domain, Google-digitized / http://www.hathitrust.org/access_use#pd-google

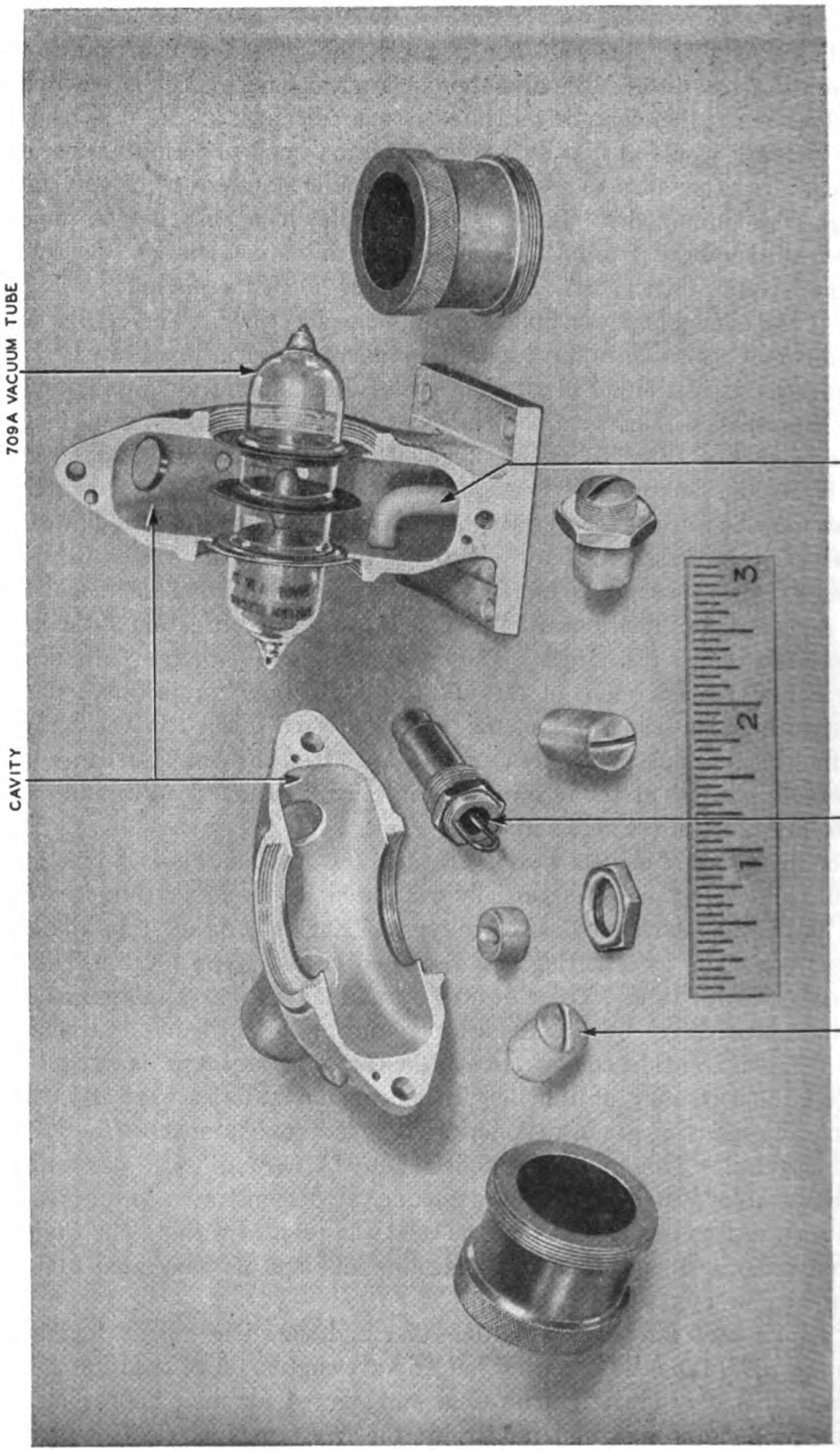

Fig. 1—The 709A vacuum tube and its associated cavity

Digitized by Google
Original from UNIVERSITY OF MICHIGAN
Generated on 2019-09-22 06:35 GMT / http://hdl.handle.net/2027/mdp.39015077775156
Public Domain, Google-digitized / http://www.hathitrust.org/access_use#pd-google

The radar on the U.S.S. Boise in the battle off Savo Island on October 11–12, 1942 employed a 702A vacuum tube.

Three developments soon led to the need for much improved TR boxes. One of these was the rapid progress which was being made in increasing the peak output power from the magnetron. The second was improvements in the silicon point contact rectifier, the so-called crystal detector, which increased its reliability and convenience and at the same time reduced its conversion loss and noise figure as compared with the vacuum tube converter. The third was the development of still higher frequency systems to

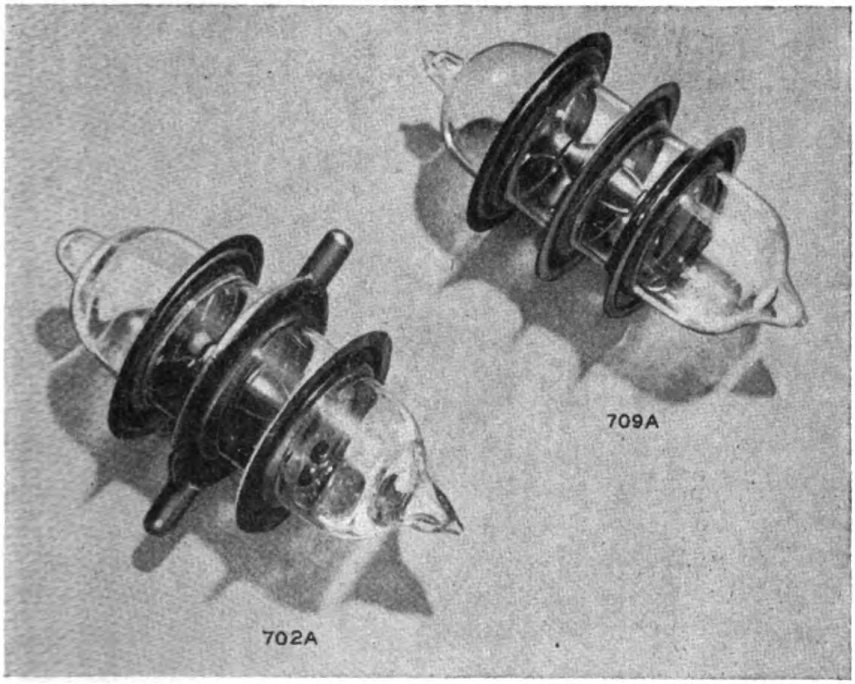

Fig. 2—The 702A and 709A vacuum tubes

achieve either greater antenna directivity or smaller size. Since satisfactory vacuum tube converters were not available for these frequencies, the silicon rectifier had to be used. Unfortunately the silicon rectifier, as then available, was subject to permanent damage if subjected to but very small amounts of power as compared with the magnetron power levels.

An active program of work was initiated at the Bell Telephone Laboratories to obtain designs of TR boxes offering adequate protection for contact rectifiers at any power levels then available or contemplated. Three tubes were developed, the 721A, 724B and 1B23 vacuum tubes shown in Fig. 3. These tubes are used at frequencies in the vicinity of 3000 megacycles, 10,000 megacycles, and 1000 megacycles respectively. They are all of the

Digitized by Google
Original from UNIVERSITY OF MICHIGAN
Generated on 2019-09-22 06:35 GMT / http://hdl.handle.net/2027/mdp.39015077775156
Public Domain, Google-digitized / http://www.hathitrust.org/access_use#pd-google

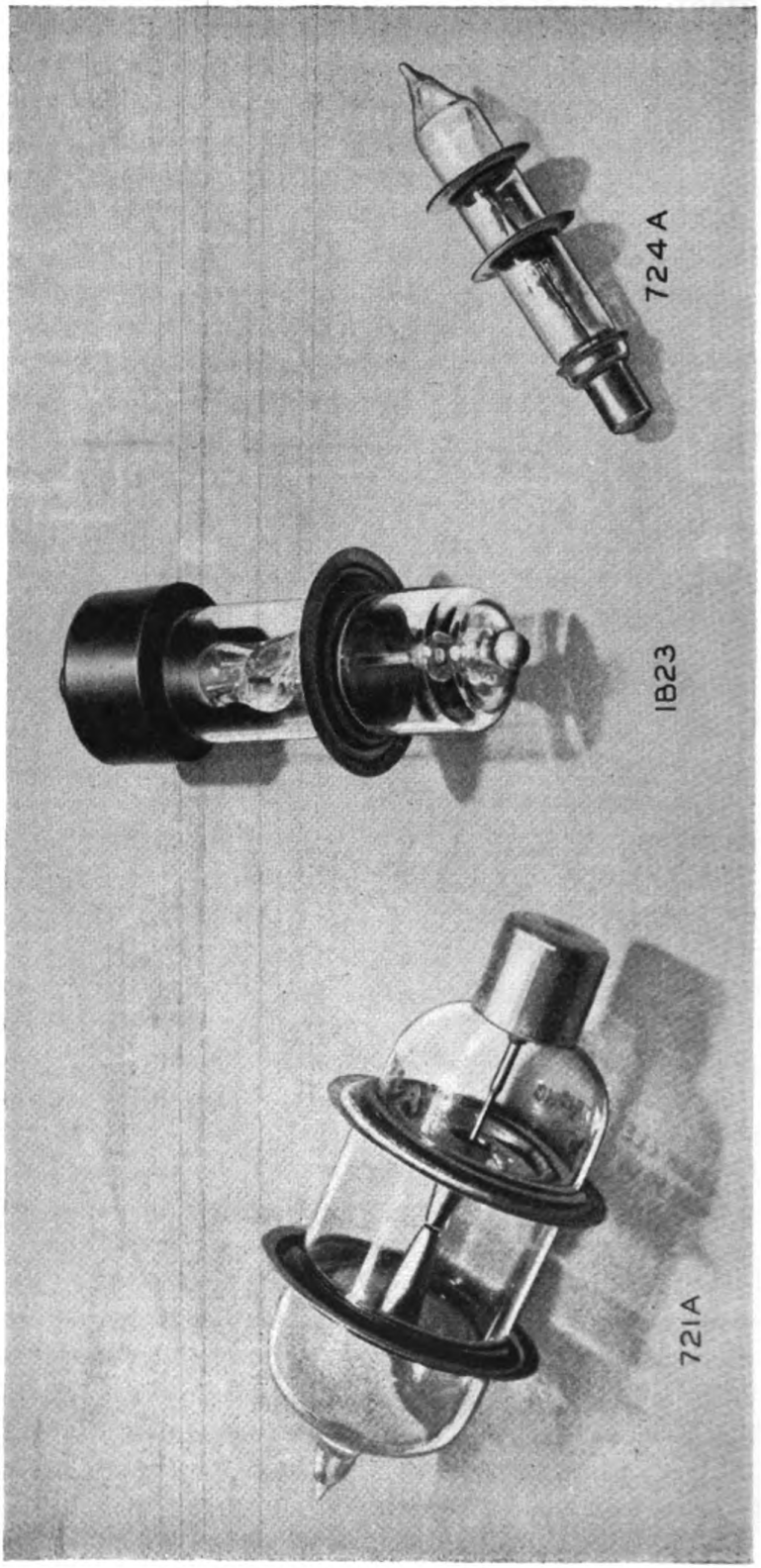

Fig. 3—The 721A, 724B and 1B23 vacuum tube

Digitized by Google
Original from UNIVERSITY OF MICHIGAN
Generated on 2019-09-22 06:35 GMT / http://hdl.handle.net/2027/mdp.39015077775156
Public Domain, Google-digitized / http://www.hathitrust.org/access_use#pd-google

separate cavity type in which contact through the vacuum envelope is made by means of thin copper discs. More recently other designs of tubes have appeared in which the entire cavity is evacuated. Over 400,000 tubes of the three types discussed in this paper were manufactured in 1944 alone and substantially all of the American-made radars which saw active service employed one or more of these tubes.

The TR tubes used in American radars are, of course, no more essential than are the magnetrons, the beating oscillators, and the many other special parts which go to make up the modern radar. Nevertheless it is interesting to note that the 721A tube was an essential part of the radar equipment on almost every major ship in the United States Fleet, that the 724B tube was an essential part of the bombing equipment on nearly every bomber used against Japan, including the planes which carried the atomic bombs, and that the capture of Okinawa, to name a single case, would have been much more expensive in men's lives without equipment depending upon the 1B23 tube.

Method of Operation

The 709A tube as shown in Fig. 1 was operated in what has come to be known as a shunt branching circuit. Its operation can be explained in terms of Fig. 4. During transmission, energy flows from the transmitter along the coaxial line toward the antenna. Some of this energy enters the branch leading to the receiver where it encounters the TR box. This consists of a resonant cavity with a pair of spark gap electrodes arranged so that the maximum resonant voltage is built up across the gap. Since the voltage across the gap is then limited by the discharge voltage and the voltage applied to the receiver is still further reduced by an equivalent step-down ratio of the output coupling in the resonant cavity, the receiver input power is held to a small value. The power dissipated in the gas discharge, and therefore abstracted from the transmitted signal is kept small by the impedance mismatch. The discharge itself takes the form of a small pale blue glow between the electrodes. The effect of the discharge is to place a low impedance (predominantly resistive) across the maximum impedance point of the cavity. This results in the appearance of a still lower apparent impedance across the input to the cavity. If the length L_1 is an odd number of quarter wavelengths, the apparent impedance of the receiver branch at the branching point becomes very high in comparison with the impedance of the antenna and is therefore unable to abstract much power from the line.

At the end of the transmitting period, the conductance of the gas discharge falls rapidly to a very low value since the small received voltages will be insufficient to maintain the discharge. Signals arriving at the antenna can then be transmitted through the TR box to the receiver. However,

Digitized by Google
Original from UNIVERSITY OF MICHIGAN
Generated on 2019-09-22 06:35 GMT / http://hdl.handle.net/2027/mdp.39015077775156
Public Domain, Google-digitized / http://www.hathitrust.org/access_use#pd-google

in the circuit shown in Fig. 4, the receiver is still bridged by the transmitter. It is a fortunate fact that the internal impedance of many magnetrons (the most common type of transmitting tube) becomes very low when they are in the inoperative condition so that the tube is nearly the equivalent of a short circuit. By adjusting the length L_2, until this equivalent short circuit position is an odd number of quarter wavelengths from the junction point "B", the shunting impedance at "B" can be made very high so that only a small part of the received energy is lost. In the event that this change of impedance of the transmitter is not sufficient, a second TR switch commonly known as an ATR, may be introduced to perform this function as will be described later. During the receiving period, some loss will occur in the TR box resonant cavity as a result of the inherent resistive and dielectric losses. An additional loss will occur immediately after the

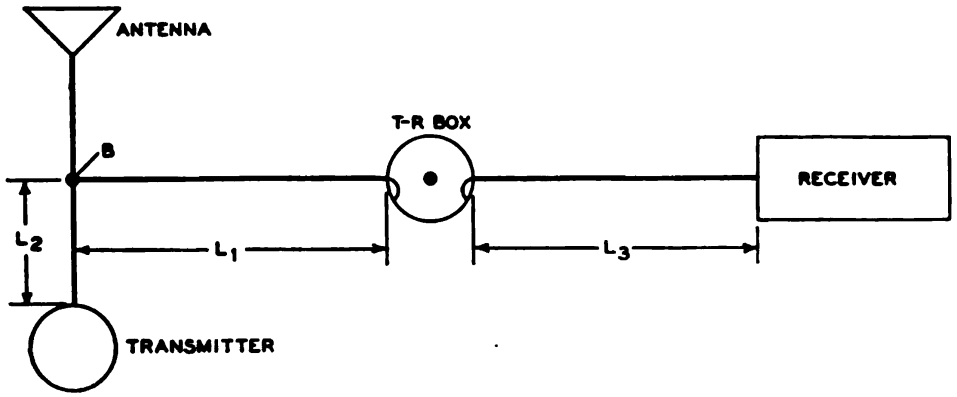

Fig. 4—The elements of a shunt branching circuit

transmitting period because of the loss producing particles (free electrons) which remain for a time in the discharge gap. The combined losses must be kept small so as not to impair the performance of the system.

Most modern radars employ series branching circuits instead of the shunt branching circuit just described. A coaxial line example of such a system (from the SCR-545) employing the 721A tube is shown in Fig. 5. As shown in Fig. 6 the cavity is coupled to the coaxial line by means of a window which can be slid along on a slot in the outer conductor of the coaxial line leading from the transmitter to the antenna. Fig. 7 is an exploded view of the cavity. Such a cavity is in effect in series with the line as the currents existing in the outer conductor of the coaxial line are interrupted by the window. During the transmitting period the low impedance at this window limits the voltage across it to a small value and prevents serious loss of transmitter power.

Reception in the series branching circuit of Fig. 5 is achieved by adjusting

Generated on 2019-09-22 06:36 GMT / http://hdl.handle.net/2027/mdp.39015077775156
Public Domain, Google-digitized / http://www.hathitrust.org/access_use#pd-google
Digitized by Google
Original from UNIVERSITY OF MICHIGAN

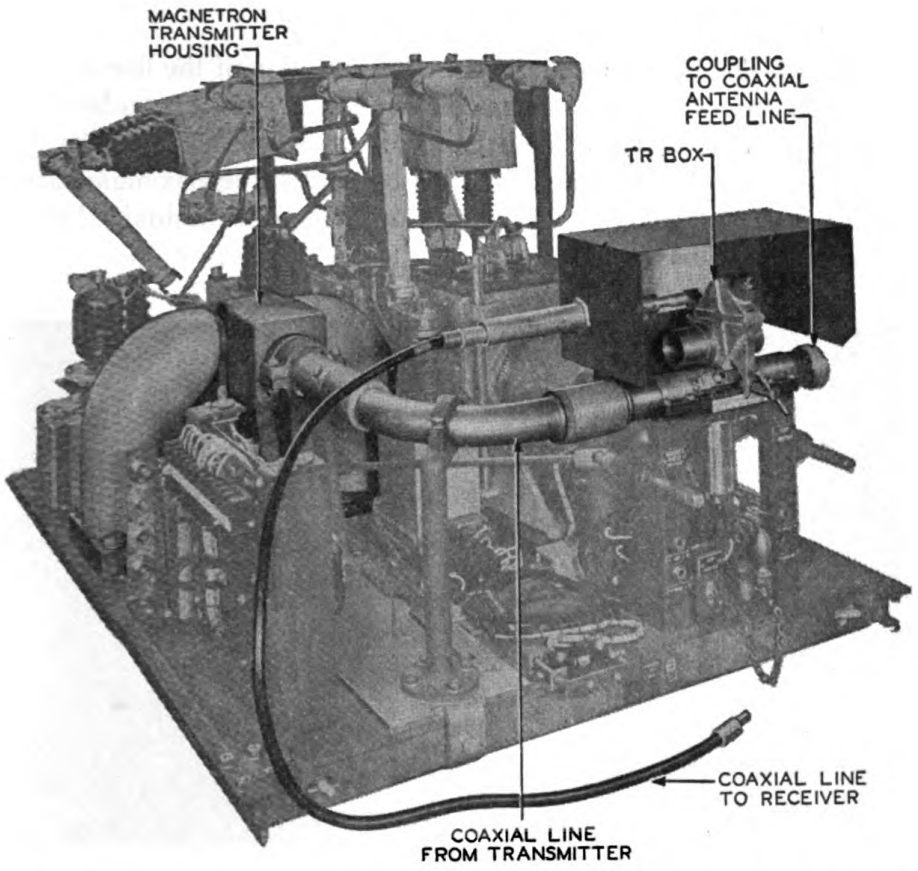

Fig. 5—The series branching circuit employing the 721A tube used in the SCR545

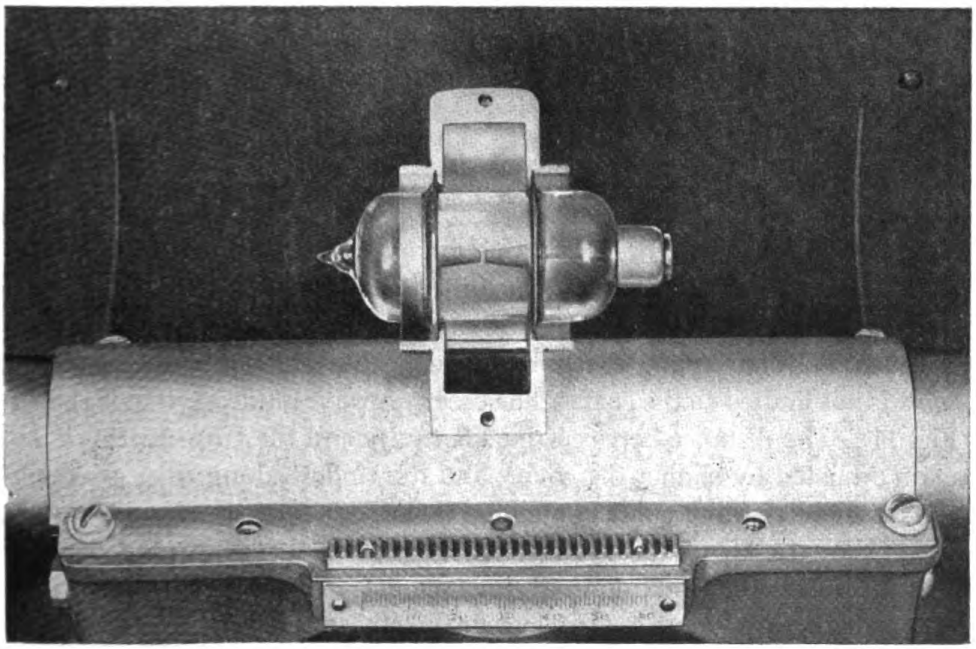

Fig. 6—Closeup view of the cavity shown in Fig. 5, partly disassembled to show coupling window

Digitized by Google
Original from UNIVERSITY OF MICHIGAN
Generated on 2019-09-22 06:36 GMT / http://hdl.handle.net/2027/mdp.39015077775156
Public Domain, Google-digitized / http://www.hathitrust.org/access_use#pd-google

the position of the TR cavity along the slotted section of the line until the window is located the correct distance from the transmitting tube. This now corresponds to an even number of quarter wavelengths between the equivalent short-circuit plane and the junction, so that the maximum current is caused to enter the cavity. The output to the receiver is obtained from a small coupling loop in the TR cavity.

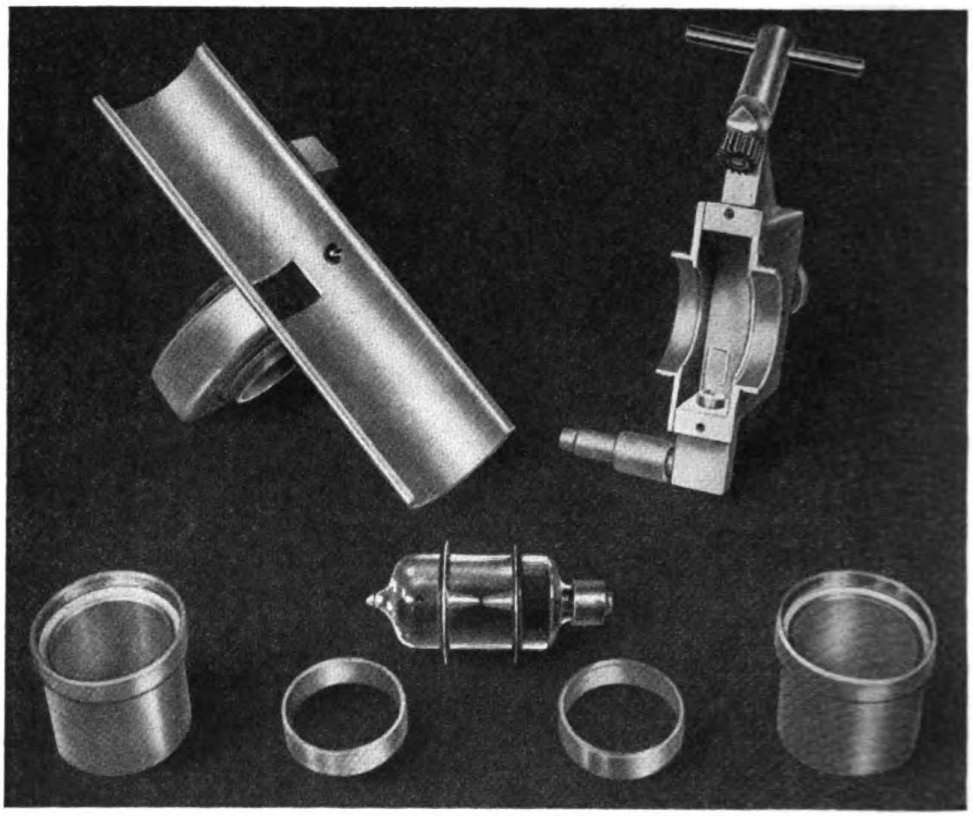

Fig. 7—Exploded view of the cavity of Fig. 6

A similar coaxial line series branching circuit using the 1B23 is shown in Fig. 8. The method of inserting the tube in the cavity is shown in Fig. 9 while Fig. 10 is an exploded view showing the details.

This method of coupling a resonant cavity to a transmission line by a window is not limited to the coaxial line case. A wave guide system is shown in Fig. 11. The distance between the TR cavity and the transmitting tube is again adjusted by sliding the cavity and its window along over a section of the rectangular wave guide containing a slot.

The ATR. In all of the systems so far described use is made of the impedance mismatch conditions at the magnetron or other transmitting tube terminals to prevent serious loss during the receiving period. If the

Digitized by Google
Original from UNIVERSITY OF MICHIGAN
Generated on 2019-09-22 06:36 GMT / http://hdl.handle.net/2027/mdp.39015077775156
Public Domain, Google-digitized / http://www.hathitrust.org/access_use#pd-google

magnetron "cold" impedance does not differ greatly from the surge impedance of the transmission line used, it may not be possible to avoid loss of reflected signal into the transmitter line. Also in some cases, an unreasonable amount of adjustment must be provided in the position of the TR cavity with respect to the transmitter to make up for large variations which may be encountered in transmitter "cold" impedance. Both difficulties

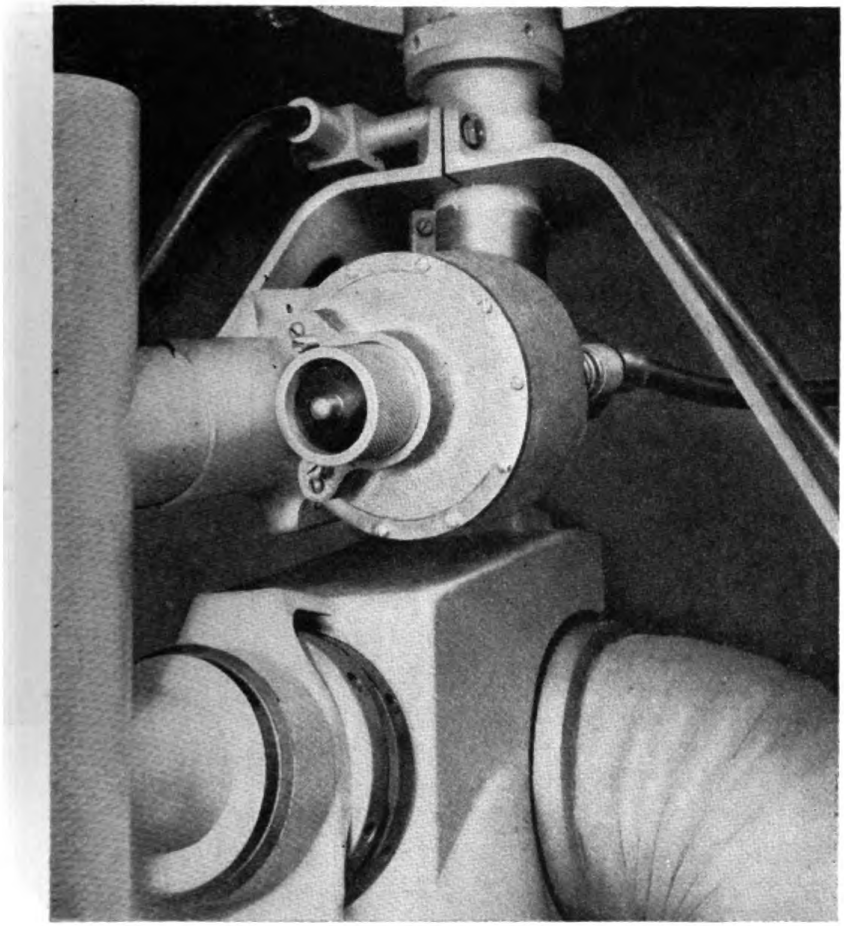

Fig. 8—Series branching circuit using the 1B23 vacuum tube

may be avoided by the use of a second gas discharge tube located between the transmitter and the TR and at an odd number of quarter wavelengths from the TR junction. This second tube is referred to as the anti-T-R tube (usually abbreviated to ATR), or sometimes as the RT tube. The use of an ATR tube was not found to be necessary in most of the systems which employed the 721A tube.

With the advent of still higher frequency systems, for which the 724B tube was designed, the "cold" impedance difficulties just mentioned made

Digitized by Google
Original from UNIVERSITY OF MICHIGAN
Generated on 2019-09-22 06:43 GMT / http://hdl.handle.net/2027/mdp.39015077775156
Public Domain, Google-digitized / http://www.hathitrust.org/access_use#pd-google

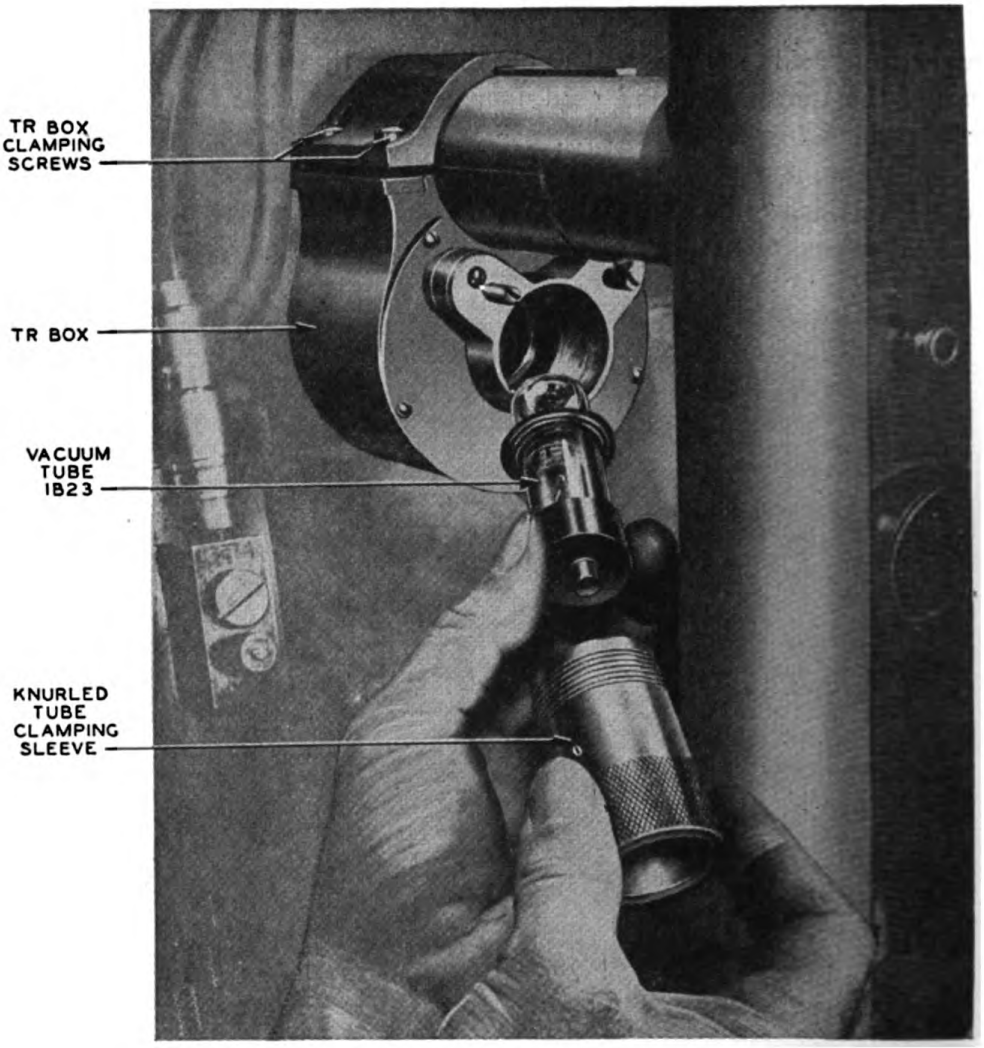

Fig. 9—Method of inserting the 1B23 into the circuit

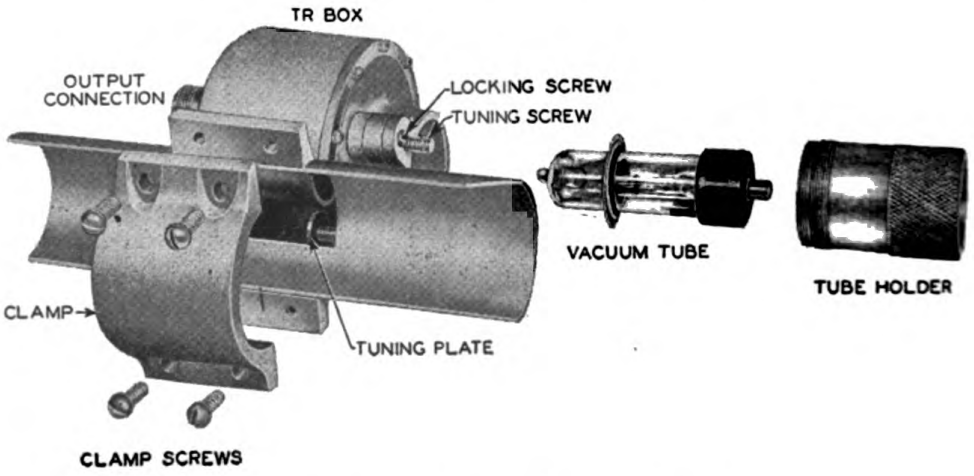

Fig. 10—Exploded view of the 1B23 cavity

Digitized by Google
Original from UNIVERSITY OF MICHIGAN
Generated on 2019-09-22 06:43 GMT / http://hdl.handle.net/2027/mdp.39015077775156
Public Domain, Google-digitized / http://www.hathitrust.org/access_use#pd-google

it seem advisable to employ an ATR tube. The general arrangements of the circuit elements in one of these systems is shown in Fig. 12. The main wave guide section is shown removed from the rest of the equipment

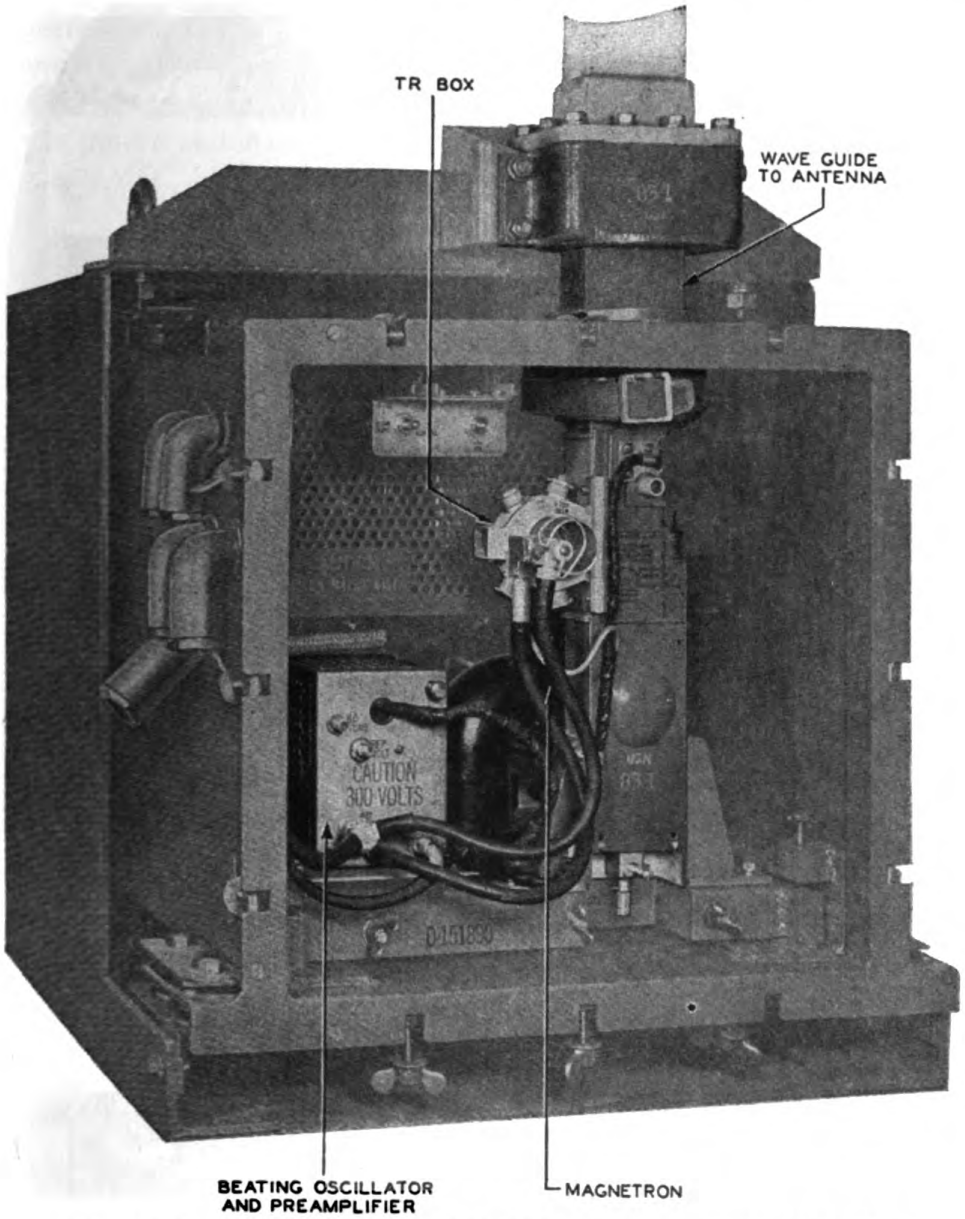

Fig. 11—The wave guide system of the SL radar employing the 721A tube

in Fig. 13 while Fig. 14 is an exploded view revealing the details of the cavity construction. The two cavities are, of course, coupled to the wave guide by means of windows. The wave guide branch leading to the receiver is in

Digitized by Google
Original from UNIVERSITY OF MICHIGAN
Generated on 2019-09-22 06:43 GMT / http://hdl.handle.net/2027/mdp.39015077775156
Public Domain, Google-digitized / http://www.hathitrust.org/access_use#pd-google

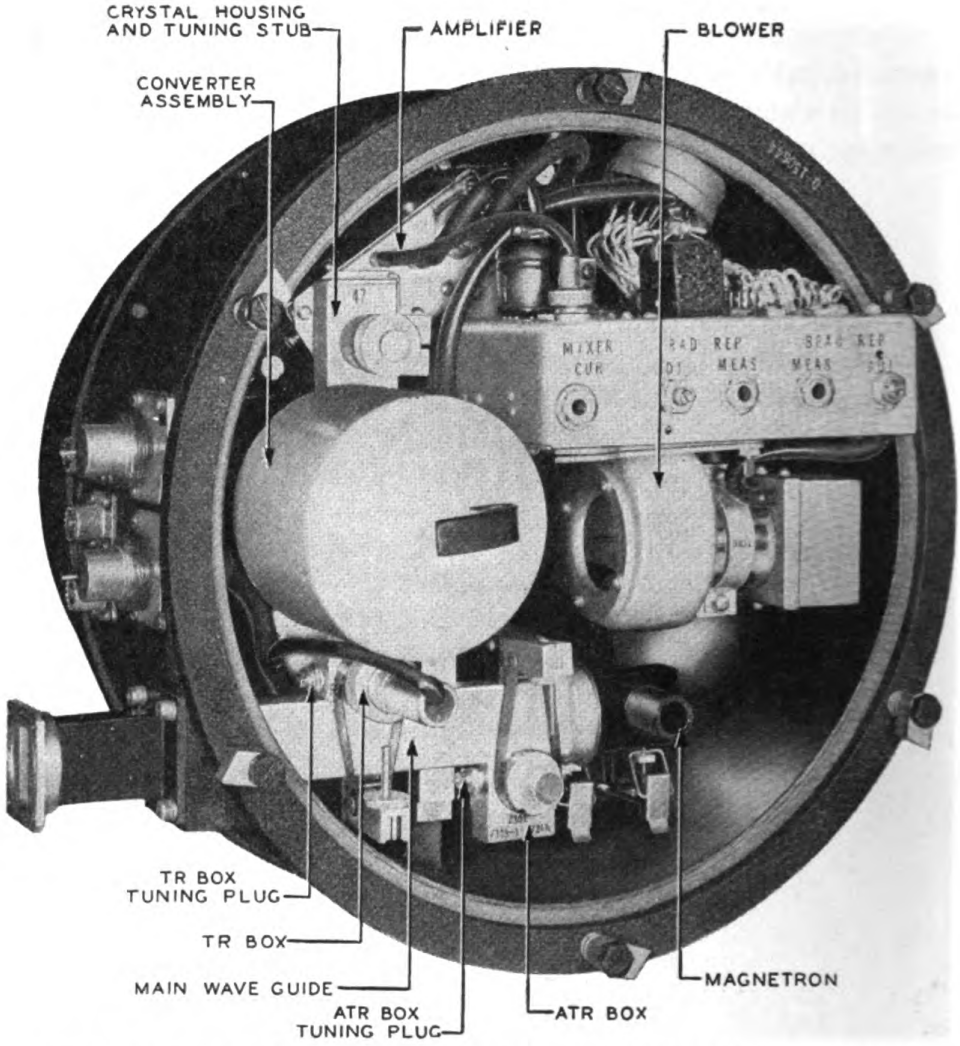

Fig. 12—A general view of a wave guide system employing a 724B tube in the TR box and a second 724B tube in the ATR

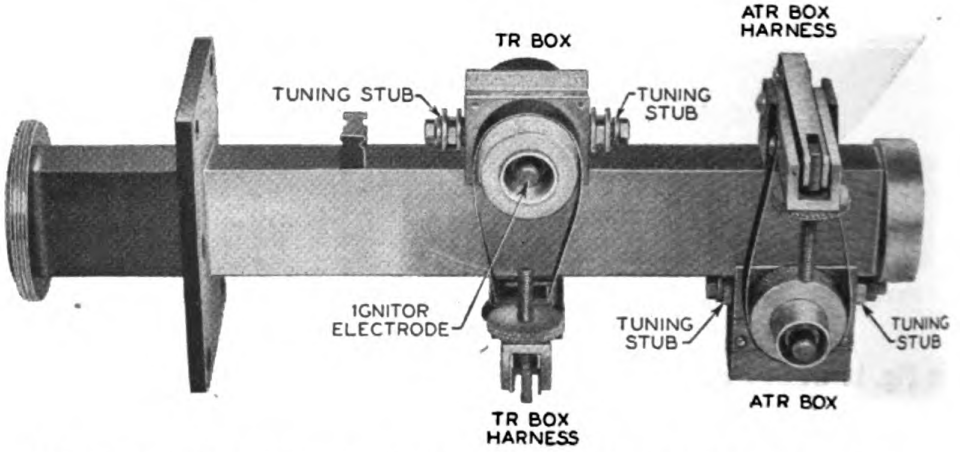

Fig. 13—The main wave guide of Fig. 12 removed from the rest of the equipment

Digitized by Google
Original from UNIVERSITY OF MICHIGAN
Generated on 2019-09-22 06:43 GMT / http://hdl.handle.net/2027/mdp.39015077775156
Public Domain, Google-digitized / http://www.hathitrust.org/access_use#pd-google

turn coupled to the TR cavity by another window. The input and output windows of the TR cavity are adjusted in size to provide an impedance match to the line during the receiving period. The window to the ATR is, however, adjusted so that it presents a high impedance, that is much greater than the surge impedance, during the receiving period. This high impedance is effectively in series with the magnetron impedance. The resulting high impedance is located at an odd number of quarter wavelengths from the TR and so presents a very low impedance in series with the receiving branch.

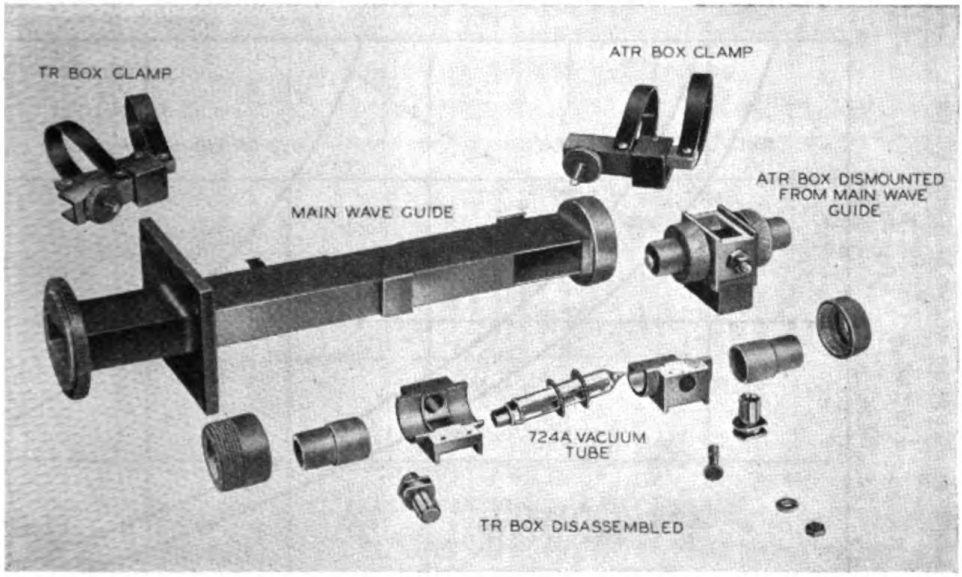

Fig. 14—An exploded view of Fig. 13

Both the TR box and the ATR box must be tuned to resonance at the magnetron frequency. Broad-band ATR boxes using very low Q circuits have been designed which require no adjustment over a 5% band. Such boxes, which obviously are very advantageous in tunable systems, do not use the copper-disc-seal tubes which form the principal subject matter of the present paper, and will not be discussed further.

TR Box Performance

The performance of a TR box can be described in terms of four parameters which are related to the four duplexing requirements mentioned earlier. These parameters are respectively: (1) the high level loss, which is the transmitting power loss in the TR tube; (2) the leakage power, which is the amount of transmitter power which reaches the receiver; (3) the recovery time, which measures the rate at which the TR box recovers its low level

Generated on 2019-09-22 06:43 GMT / http://hdl.handle.net/2027/mdp.39015077775156
Public Domain, Google-digitized / http://www.hathitrust.org/access_use#pd-google
Digitized by Google
Original from UNIVERSITY OF MICHIGAN

behavior after the termination of the transmitting period; and (4) the low-level loss, which describes the loss of the received signal including (a) the loss in the TR box itself and (b) the loss in the transmitting branch. These parameters are interrelated and conflicting. For example, the interdependence of the leakage power and the low-level loss may be computed on the basis of a somewhat idealized TR box as is done in Appendix A and the results presented in the form of the curves of Fig. 15. It is customary to design the cavities for matched input conditions ($\sigma = 1$), for obvious reasons, and for a low-level loss of one to two db. The relationship between the transmitting power dissipated in the TR tube and the low-level loss is shown

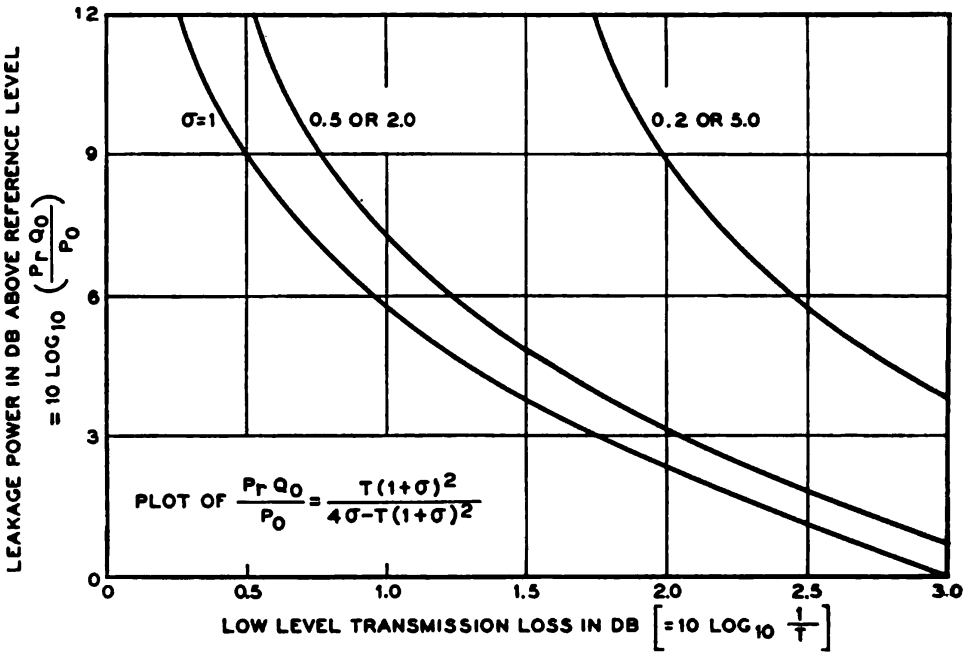

Fig. 15—The variation in leakage power with the low level loss adjustment.

in Fig. 16. This curve may also be used to determine the effect of the low-level loss adjustment of a TR cavity on the recovery time characteristic since recovery time depends upon the gas discharge power rather than upon the transmitter power per se. In spite of this interdependence, it will be convenient to consider the different operating parameters separately in the sections to follow. The receiver protection aspect will be considered first.

Receiver Protection. The receiver protection problem is complicated by the fact that power reaches the receiver through the TR box by three different mechanisms. As shown in Fig. 17, the observed leakage power pattern is composed of three parts known respectively as the spike, the normal flat leakage and the direct coupling. The spike is the result of the transient

Digitized by Google
Original from UNIVERSITY OF MICHIGAN
Generated on 2019-09-22 06:44 GMT / http://hdl.handle.net/2027/mdp.39015077775156
Public Domain, Google-digitized / http://www.hathitrust.org/access_use#pd-google

condition existing at the beginning of each pulse. Normal leakage power can be thought of as due to the finite voltage drop across the gas discharge while the direct coupling is that component of the leakage power which would be present if the voltage drop across the discharge were zero.

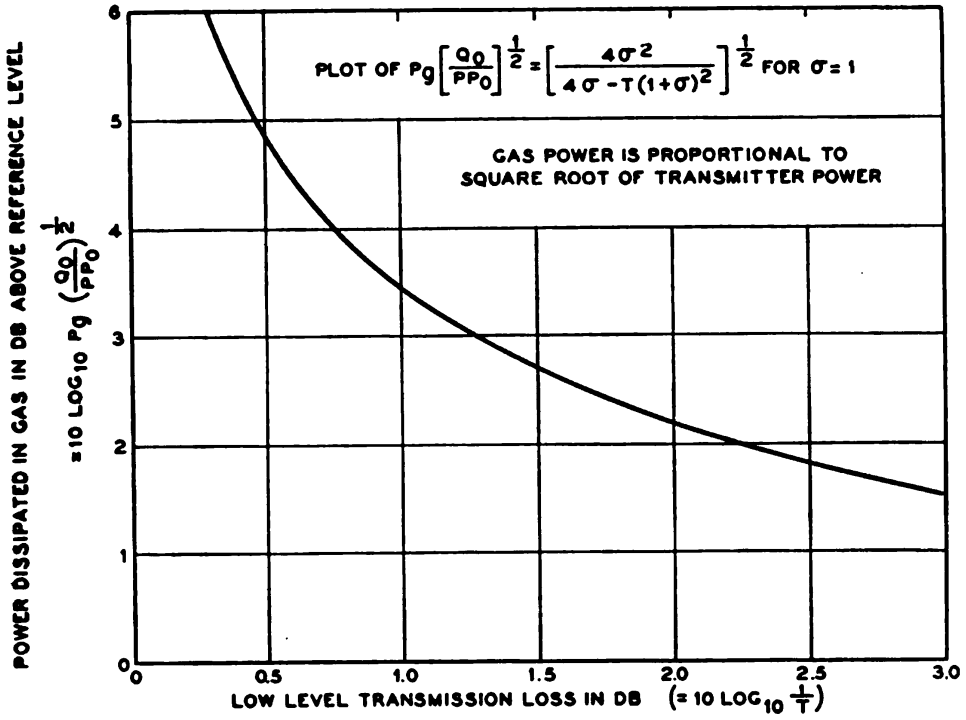

Fig. 16—The variation in gas discharge power with the low level loss adjustment

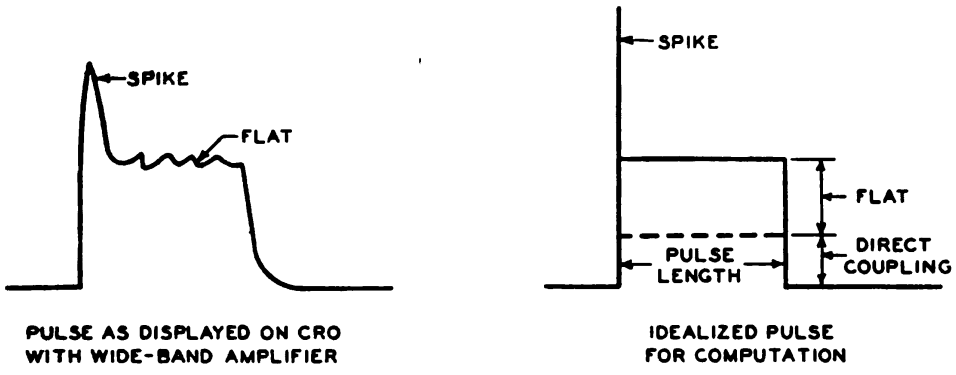

Fig. 17—The shape of the leakage power pulse

The Spike. Because of the rapid rate of rise and fall of the spike, the observable deflection on an oscilloscope is dependent upon the bandwidth of the video amplifier and upon the energy in the spike. Although an

Digitized by Google
Original from UNIVERSITY OF MICHIGAN
Generated on 2019-09-22 06:44 GMT / http://hdl.handle.net/2027/mdp.39015077775156
Public Domain, Google-digitized / http://www.hathitrust.org/access_use#pd-google

observation of the true shape of the spike has not yet been made, the duration is estimated to be of the order of 10^{-9} seconds, a time interval that is probably short compared with the thermal time constant of the contact on a converter crystal. However, it is possible to measure the energy content of the spike, and such measurements indicate that this energy is fairly independent of the length of the pulse and of the transmitted power level, although it is definitely dependent upon the steepness of the wave front of the transmitted pulse. The spike clearly represents energy transfer through the TR box during the period required to establish the discharge conditions which exist during the flat. The energy contained in the spike varies between a few hundredths of an erg to perhaps one erg per pulse, depending upon a variety of factors. By way of comparison, the conventional crystal rectifiers are proof tested in manufacture with a single spike of 0.3 erg to 5.0 ergs, depending upon the crystal type. It is generally believed that the spike is more damaging than the flat in most radar systems.

The energy in the spike is found to depend upon the repetition rate of the transmitting pulses, presumably because of residual ionization in the gas discharge gap. At low repetition rates (that is less than roughly 1,000 pulses per second), the spike energy may be materially decreased by a d-c glow discharge near the radio frequency gap. This discharge provides a continuous supply of ions and free electrons and so aids in establishing the desired condition in the r-f discharge path. A discharge is supplied in all the standard TR tubes. An auxiliary electrode called the "igniter" or "keep-alive" is used as the cathode, with the back or inside portion of one of the high frequency electrodes acting as the anode. A small amount of radioactive material is placed in the tube to insure that the igniter discharge starts on the application of the igniter voltage. Fig. 18 is a plot of the way in which the spike energy varies with the repetition rate both with and without an igniter discharge. Igniter oscillations sometimes occur as a result of the negative resistance characteristics of the igniter discharge. This causes a cyclic variation in the number of free electrons and ions with a resulting fluctuation in the spike energy. Inadequate protection may result from such oscillations. It is customary to mount a current limiting resistance very close to the igniter cap to minimize the effects of these undesirable oscillations. When such oscillations still occur they are usually evidence of an insufficiently high igniter voltage or of tube failure. The margin of safety in the igniter operation may be increased by increasing the discharge current but at the expense of greatly reduced tube life.

When a radar system is first turned on, the first pulse occurs without the benefit of residual ions in the discharge, and for the first few pulses the spike energy may easily reach dangerously high values. While the magnitude of this "turn on" effect is greatly reduced by the presence of the igniter

Digitized by Google
Original from UNIVERSITY OF MICHIGAN
Generated on 2019-09-22 06:44 GMT / http://hdl.handle.net/2027/mdp.39015077775156
Public Domain, Google-digitized / http://www.hathitrust.org/access_use#pd-google

discharge, it is customary to provide a "crystal gate" in the form of a shutter which isolates the crystal from the TR box until after stable transmitting conditions have been reached and until the TR tube discharge has been established. The need for this additional turn-on protection is somewhat greater with the 724B than it is with the 721A tube. Another important function of the "crystal gate" is to prevent the crystal in an idle radar from being damaged by energy from other radars operating nearby.

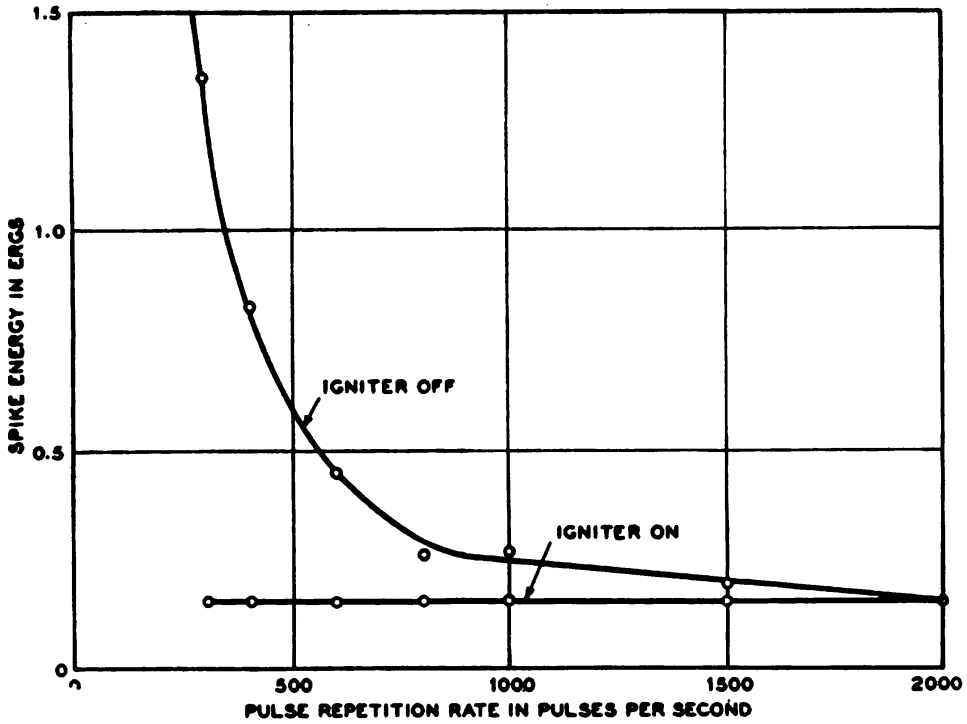

Fig. 18—The dependence of spike on the repetition rate for the 724B tube in a cavity adjusted for a 1.5 db low level loss and for a transmitter power level of 8 kw peak

The energy in the spike is a function of the effective size of the input and output coupling windows of the TR box. A convenient method of presenting this effect is to plot the spike energy as a function of the low-level transmission loss of the cavity which also depends upon the window sizes. Fig. 19 is such a plot for the 724B tube*. Comparing these experimental data with the computed flat power curve of Fig. 15, one notes that the spike energy varies at a more rapid rate than does the flat power. In both cases, the leakage decreases as the low-level loss increases and crystal protection can be purchased at the expense of receiver sensitivity.

* Based on data taken at the M.I.T. Radiation Laboratories by F. L. McMillan. Jr. and J. B. Wiesner.

Digitized by Google
Original from UNIVERSITY OF MICHIGAN
Generated on 2019-09-22 06:44 GMT / http://hdl.handle.net/2027/mdp.39015077775156
Public Domain, Google-digitized / http://www.hathitrust.org/access_use#pd-google

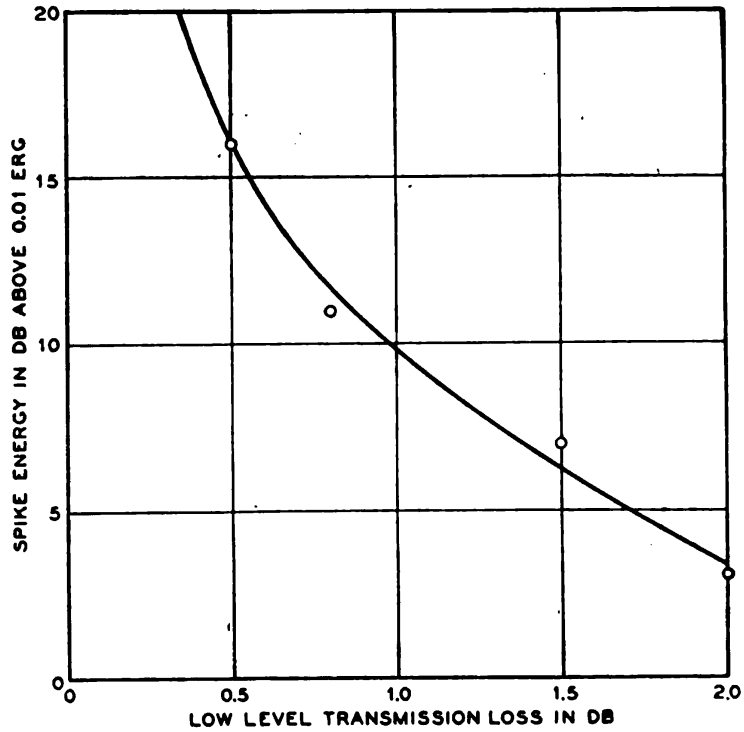

Fig. 19—The variation in spike energy with the low level loss adjustment ($\sigma = 1$) for the 724B. This experimental curve for the spike energy should be compared with the idealized flat power curves of Fig. 15

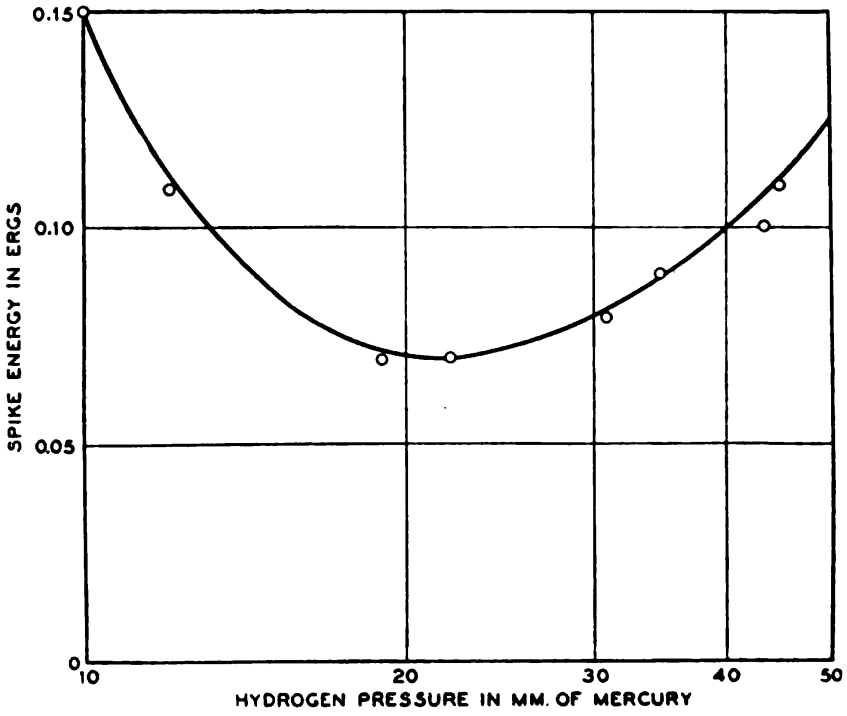

Fig. 20—The effect of gas pressure on the spike energy for the 724B

Digitized by Google
Original from UNIVERSITY OF MICHIGAN
Generated on 2019-09-22 06:44 GMT / http://hdl.handle.net/2027/mdp.39015077775156
Public Domain, Google-digitized / http://www.hathitrust.org/access_use#pd-google

The way in which the spike energy varies with pressure of the gas in the TR tube is illustrated in Fig. 20. These data were obtained on the 724B tube structure. Other factors, yet to be discussed, prevent the use of the exact optimum pressure as determined on the basis of the spike energy only.

The Flat. The more or less flat portion of the leakage power is in reality the result of two different mechanisms of energy transfer, one of which is reasonably independent of the transmitter power level. It is this portion only with which we will now be concerned. This flat power is critically dependent on the chemical constitution and pressure of the gas within the TR tube. It can be thought of as being the power transmitted by the TR

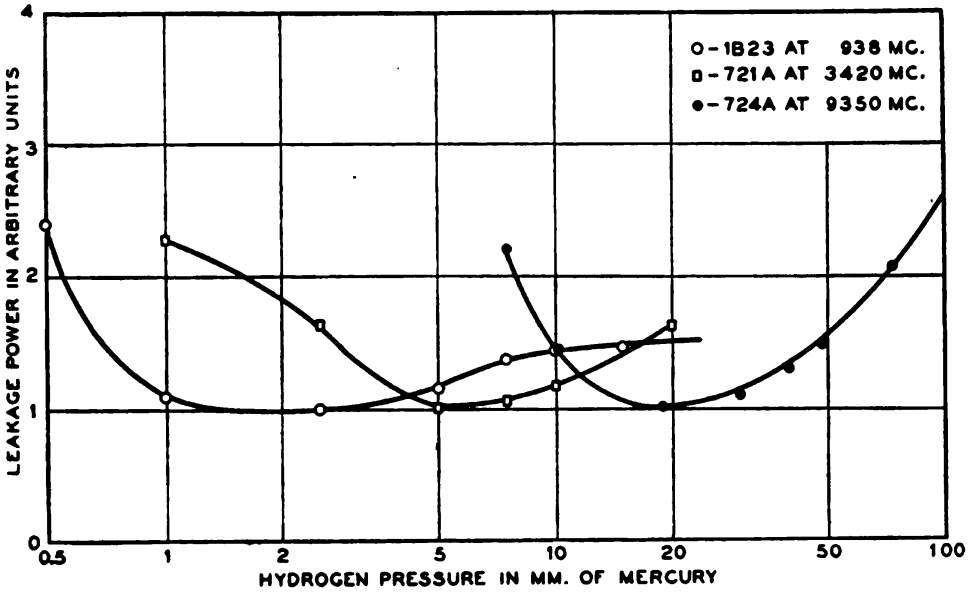

Fig. 21—Experimental curves showing the relationship between flat leakage power and gas pressure, taken with a c-w oscillator

box by virtue of the fact that the voltage drop across the gas discharge is not zero. The constancy of the flat power in spite of variations in the transmitter power level is presumably related to the similar phenomenon of a nearly constant voltage drop across a d-c gas discharge independent of the discharge current. Because of this constancy, the gas discharge parameter P_0, shown in Fig. 15, can be assumed to be a constant more-or-less independent of the transmitter power level. Reasonable values of P_0 for cavity design purposes are 20 volt-amperes for the 721A tube and 10 volt-amperes for the 724B tube. Corresponding values of the Q_0 parameters needed in interpreting Fig. 15 are 2500 for the 721A tube and 1500 for the 724B tube. Using these values the flat leakage power for a TR box using a 721A tube

Digitized by Google
Original from UNIVERSITY OF MICHIGAN
Generated on 2019-09-22 06:45 GMT / http://hdl.handle.net/2027/mdp.39015077775156
Public Domain, Google-digitized / http://www.hathitrust.org/access_use#pd-google

and having a low-level loss of 1 db would be 30 milliwatts. The corresponding flat leakage power for the 724B tube in a 1.5 db box would be 16 milliwatts. Actual measured values are usually somewhat less than these figures. As most crystals will withstand flat powers very much greater than this amount, the flat power is normally of much less importance than the spike in contributing to converter crystal failure.

Since the flat portion of the leakage power represents quasi-steady-state conditions, it is possible to simulate it for purposes of study by the use of a C.W. oscillator. Fig. 21 contains three experimental curves taken at

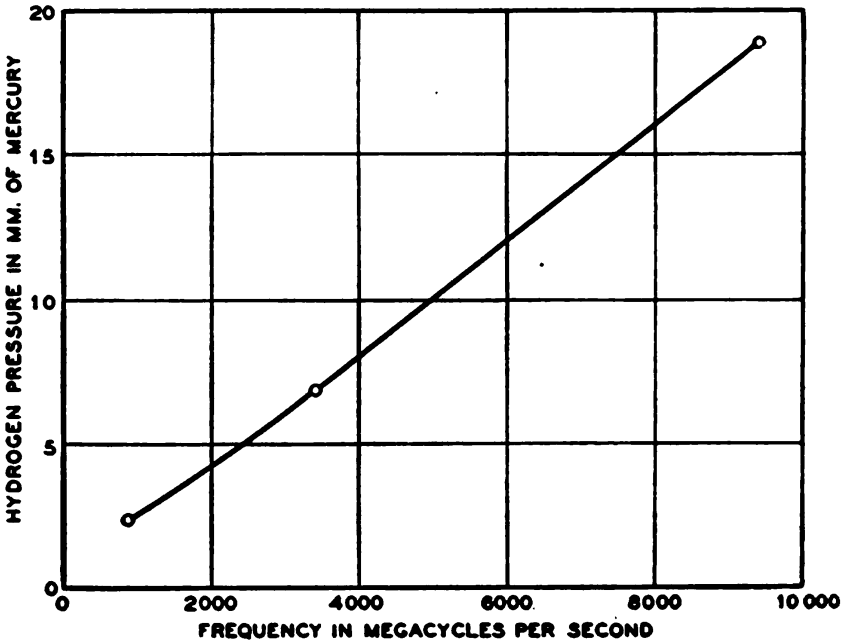

Fig. 22—The pressure for minimum leakage power as a function of frequency

three different frequencies showing the relationship between the flat leakage power and gas pressure. These curves were all taken with tubes filled with hydrogen only. Fig. 22 shows that the pressure for minimum flat leakage is proportional to the frequency. This simple law probably does not apply at frequencies much less than 1000 mc.

Water vapor is used in commercial TR tubes to improve the recovery time, as will be discussed later. The variation in flat leakage power with partial water vapor pressure as measured on a 721A type of tube containing both hydrogen and water is shown in Fig. 23. These data were taken in a radar system.

In this connection, it is of interest to note that the characteristics of the gas discharge in the TR box must of necessity be quite different from those that obtain at lower frequencies. Simple calculations indicate that the

Generated on 2019-09-22 06:45 GMT / http://hdl.handle.net/2027/mdp.39015077775156
Public Domain, Google-digitized / http://www.hathitrust.org/access_use#pd-google
Digitized by Google
Original from UNIVERSITY OF MICHIGAN

mean free path of an electron is in general of the same order as the distance between the electrodes but that very few electrons are able to reach the electrodes because of the very rapid reversals in the r-f field. Electrons therefore oscillate rapidly to and fro, losing energy to the neutral gas molecules and to positive ions through occasional collisions The positive ions do not contribute in any substantial way to the discharge current because of their large mass and correspondingly low velocity. The r-f voltage drop across the discharge is maintained at a relatively low value by the formation of more ions and free electrons by collisions between electrons and neutral

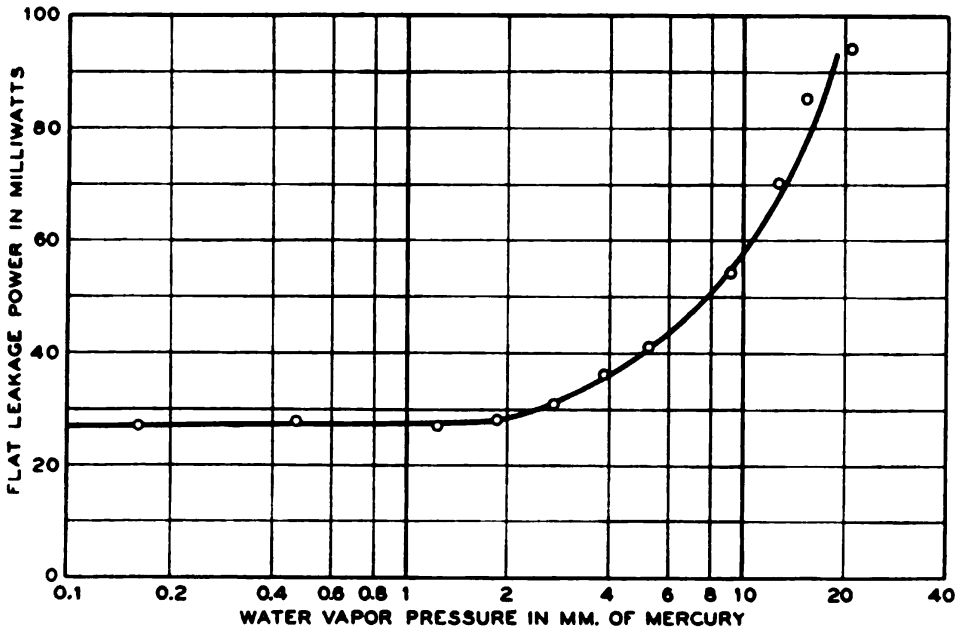

Fig. 23—The effect on leakage power of the addition of water vapor to 20 mm of hydrogen in the 721A type tube

molecules as soon as this voltage rises above some critical value. Measurements indicate that the voltage drop across the r-f gap is of the order of 80 to 100 volts for a typical TR tube. The variation in voltage drop with gap length may be inferred from the flat power measurements recorded in Fig. 24.

Direct Coupling. At very high transmitter power levels a third component of leakage power is observed which is directly proportional to the transmitter power. This component is usually called "direct coupling". It is due to the transmission of power through the cavity in modes which do not have voltage maxima at the gas discharge gap. It can therefore be observed even when the gap in the tube is short circuited. In fact measurements made under such short-circuited gap conditions yield results com-

Digitized by Google
Original from UNIVERSITY OF MICHIGAN
Generated on 2019-09-22 06:45 GMT / http://hdl.handle.net/2027/mdp.39015077775156
Public Domain, Google-digitized / http://www.hathitrust.org/access_use#pd-google

parable to the values observed for actual tubes. The direct coupling component of the total flat power and the gas discharge limited component are found to be additive. Direct coupling power is logically measured in terms of db below the transmitter power level and for the usual TR box is of the order of 60 to 70 db. An abnormal form of direct coupling which may reach dangerous values can occur under certain improper operating conditions when the magnetron produces an appreciable amount of power at other than the normal operating frequency. Some of these spurious frequencies may be in the vicinity of the resonant frequencies for these "direct coupling"

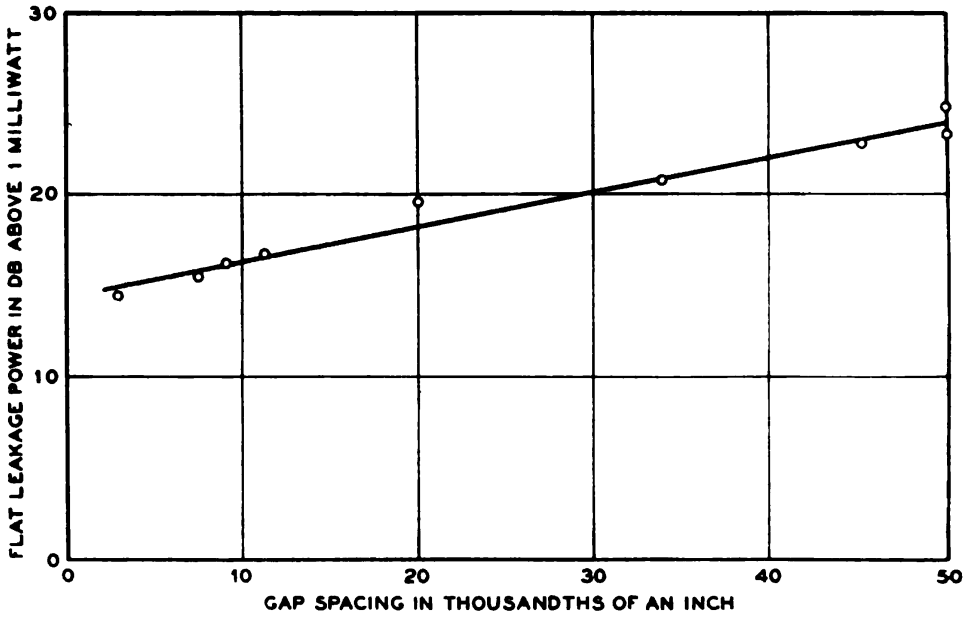

Fig. 24—The variation in flat leakage power with gap length, measured at 3000 megacycles

modes in the TR box and so be transmitted without much attenuation. Normally, direct coupling is of interest only in very high power systems.

Receiver Self-Protection. The fact was mentioned earlier that a receiver can provide itself with a certain amount of self-protection as a result of its change of impedance with level. This effect is still of use even in systems employing TR boxes. Unfortunately the apparent source impedance at the TR box output terminals is different for the different components of the leakage power so that the self-protection feature cannot be utilized for all components simultaneously. The matter is further complicated by the fact that the converter crystals themselves vary greatly in their impedance and in their variation of impedance with power level. The best designed converters as far as crystal protection is concerned are usually those which

Generated on 2019-09-22 06:45 GMT / http://hdl.handle.net/2027/mdp.39015077775156
Public Domain, Google-digitized / http://www.hathitrust.org/access_use#pd-google
Digitized by Google
Original from UNIVERSITY OF MICHIGAN

provide a certain amount of self-protection against the spike. It has been estimated that this self-protection seldom exceeds 2 db in practice.

Leakage Power Measurement. The c-w method of measuring the flat power has already been mentioned. Spike energy and direct coupling must, of course, be measured under normal high level operating conditions. Relative measurements of the spike can be made with an oscilloscope, acting ballistically, and the factors which affect the spikes can be studied in this manner. A correlation between the relative spike energies and the degree of crystal protection can be obtained by trial and from this correlation the operating conditions for adequate protection can be determined. Most of the early studies were made in this way. It is possible to deduce absolute values for spike energy, flat power, and direct coupling from measurements made when all three are present because of the different ways in which these parameters vary with the recurrence rate, pulse length and transmitter power. The method of doing this is outlined in appendix D.

A more precise method of measuring the spike energy involves the cancellation of the flat power by a signal of adjustable phase and amplitude obtained from the high-level transmission line. The average spike power is then measured directly and energy per spike computed. Most of the spike data quoted earlier were obtained in this fashion.

High-Level Loss. The power dissipated in the TR box as a result of the gas discharge is not ordinarily a large enough fraction of the total transmitter power to be of any concern. Using the P_0 values previously quoted, it is possible to compute the gas discharge power by the use of Fig. 16. At a line power of 100 kw and a low-level loss of 1 db the gas power in the 721A tube is 63 watts. The corresponding figure for a 1.5 db box using the 724B tube is 47 watts. For these cases the high-level loss is therefore less than 0.005 db. Low as this fraction is in db it still may be high enough to affect the life of the TR tube, as discussed in a later section. No trouble of this sort is ordinarily encountered with the 724B or 721A tubes. The chief cause of failure of the 1B23 is from loss of Q and this in turn is caused by the sputtering action of the high-frequency discharge.

Recovery Time. As mentioned earlier a TR box must recover its low-level properties at the end of the transmitting pulse in a very short period of time. The actual "recovery time" is in fact several orders of magnitude smaller than the deionization times of the usual gas discharge so that a quite different mechanism must be involved. While an exact theory of the recovery is beyond the scope of the present paper, a qualitative picture of the recovery process may be of interest.

During the transmitting period the free electrons provide almost all of the discharge current, and are replenished by electron-molecule collisions. At

Digitized by Google
Original from UNIVERSITY OF MICHIGAN
Generated on 2019-09-22 06:45 GMT / http://hdl.handle.net/2027/mdp.39015077775156
Public Domain, Google-digitized / http://www.hathitrust.org/access_use#pd-google

the end of the transmitting period these electrons may migrate from the discharge region, they may recombine with the positive ions, or they may be captured by molecules to form negative ions. Negative ion formation by attachment effectively removes an electron from the discharge because of the great increase in mass. It is an experimental fact that those gases which readily form such ions (of which water vapor is the most common) are the gases which exhibit good recovery in a TR box. This process is

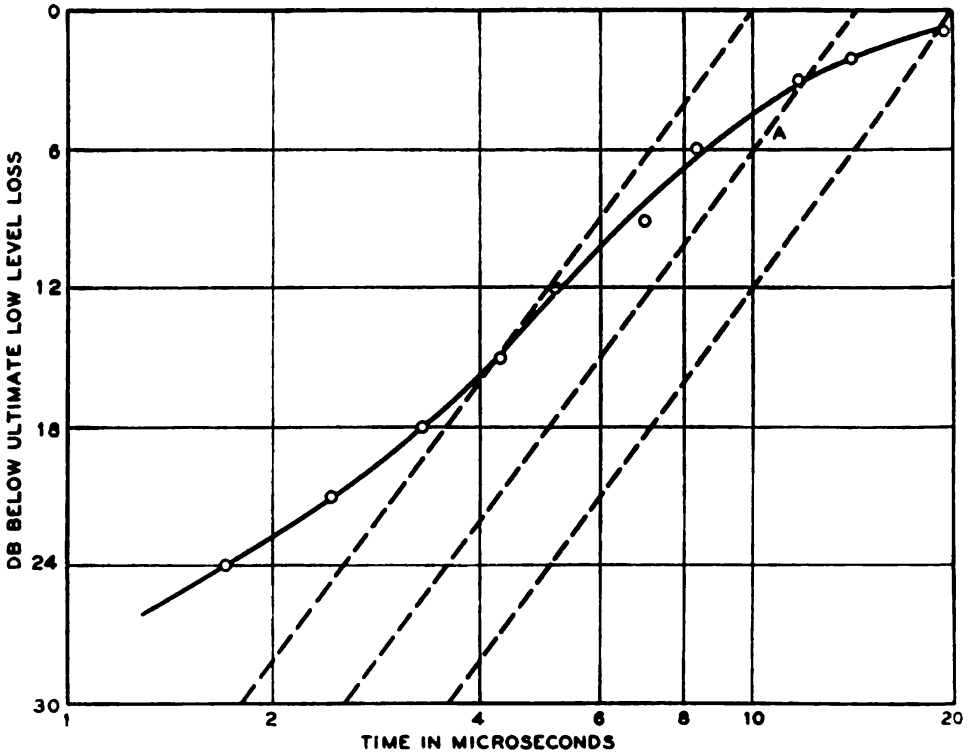

Fig. 25—A typical recovery time characteristic for the 721A tube in a TR cavity adjusted to 1.5 db low level loss with a transmitter power level of 100 kw peak

not deionization in the ordinary sense and it can take place at a surprisingly rapid rate.

Of course, immediately upon the termination of the transmitting pulse, the cloud of free electrons will cause an extremely high loss to any reflected signal but the loss will rapidly decrease to some limiting value set by the fixed losses in the TR cavity itself.

A typical recovery curve for the 721A tube is shown in Fig. 25. This curve has a particularly fortunate shape in that the variation in loss with distance, or more correctly with time, is at approximately the same rate as the variation in the reflected signal level with distance for a target of fixed size. The importance of this can be understood by considering the way in

Digitized by Google
Original from UNIVERSITY OF MICHIGAN
Generated on 2019-09-22 06:45 GMT / http://hdl.handle.net/2027/mdp.39015077775156
Public Domain, Google-digitized / http://www.hathitrust.org/access_use#pd-google

which the reflected signal intensity varies as an object of fixed size approaches a radar set from a great distance. Such an object as seen by a given radar set may be represented on Fig. 25 by a straight line having a slope of 12 db per factor of two in distance. Several such lines are shown. Considering line A it will be observed that this target can first be seen at a distance corresponding to 12 microseconds. Since this target line always remains below the TR recovery line for times shorter than that at the intersection point, an object once seen will remain in view continuously as it approaches

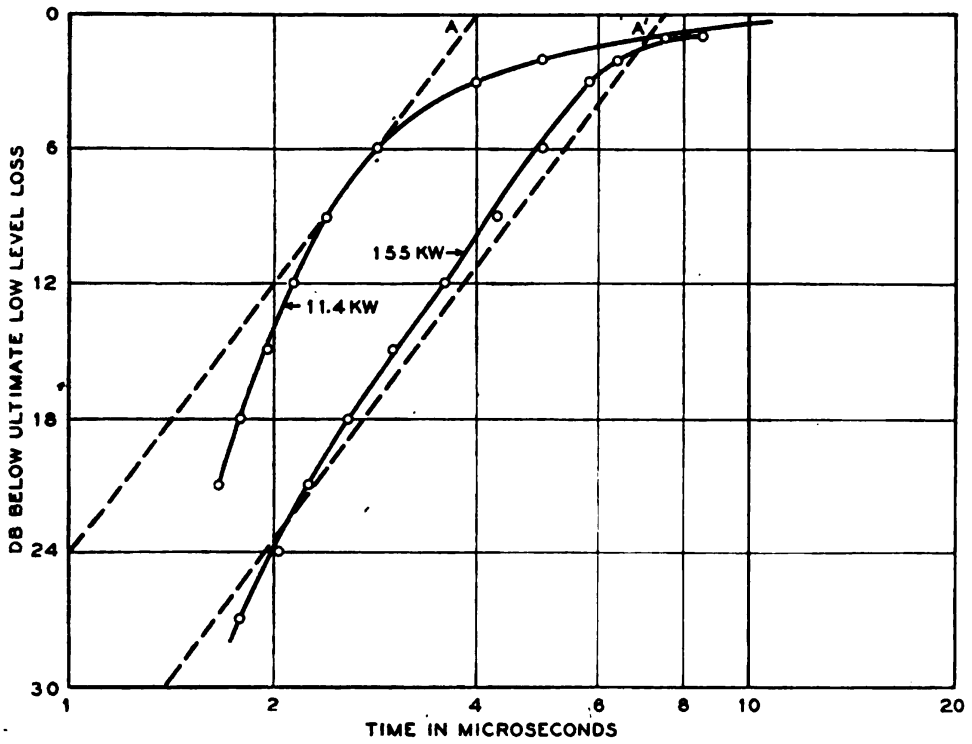

Fig. 26—The recovery time characteristic at two different transmitter power levels for the 724B tube in a 1.5 db TR box

the transmitter even in spite of the poor recovery characteristics of the TR box. A certain amount of sensitivity-time-control action is actually provided. The recovery time characteristic frequently does not necessarily set a lower limit on the effective range of a radar system although it always sets a limit on the smallest effective target size which can be observed.

The recovery time characteristic is critically related to the transmitter output power level as shown by the data for a 724B tube shown in Fig. 26. When the recovery time curves for two different power levels are compared, the target line which is just detectable at a power level of 11.4 kw is shown as the line marked A Contrasting with the 721A behavior this target would be visible only at one point and would then be lost from sight as it approached

Generated on 2019-09-22 06:46 GMT / http://hdl.handle.net/2027/mdp.39015077775156
Public Domain, Google-digitized / http://www.hathitrust.org/access_use#pd-google
Digitized by Google
Original from UNIVERSITY OF MICHIGAN

the transmitter. This same target is represented on the plot as line A' for a transmitter output power of 155 kw, that is being displaced vertically by approximately 12 db to take account of the difference in transmitter power. At this higher power level the target would be visible at a much greater distance (corresponding to 7 microseconds elapsed time) and would remain in view until the target distance corresponded to 2.1 microseconds time. In this case an increase in power by 12 db resulted in an increase in range by a factor of 2.8. While this would indicate that an increase in range can be obtained by increasing the transmitter power, it should not be inferred that an increase in the near-range sensitivity will always result from an increase in power. At any specified range there appears to be a unique value of transmitter power output beyond which the loss in TR box recovery more than offsets any increase in range due to higher output powers. While accurate figures are not available for the 721A tube, there is some evidence that an output power of 100 kw is already too large for ranges corresponding to elapsed times of 10 microseconds or less. Under these conditions improved operation results from a decrease in the transmitter power level. Such an effect has never been observed by the writers with the 724B tube, probably because the transmitter powers available in its operating frequency range have usually been somewhat less than that available with the 721A tube.

It should be noted, at this point, that the recovery time does not depend upon the transmitter power only, but rather upon the gas discharge power which is a function of both the transmitter power and the low-level loss adjustment of the TR box as shown by Fig. 16. A very great improvement in near range sensitivity can usually be obtained by increasing the transmitter power level and at the same time increasing the low-level loss adjustment of the cavity to limit the gas power to a value for which the recovery time is satisfactory. This of course increases the ultimate low-level loss and so adversely affects the long-range sensitivity.

The dependence of the recovery time on the ambient temperature for the 721A tube is shown in Fig. 27. The 724B tube is much less temperature dependent. This variation in recovery time with temperature is caused by the reduction in water vapor pressure through condensation, as shown by the identity of the recovery curve for a standard 721A tube at −186° C. with a special tube filled with hydrogen only.

With continued life the water vapor content of the tube decreases with the corresponding change in the recovery time characteristic. Fig. 28 shows the effect with the 721A tube. The dependence of the recovery time on the water vapor content in the 724B tube is shown in Fig. 29. Comparing this curve with Fig. 27, it will be observed that the loss of water vapor has much less effect on the recovery characteristics of the 724B tube than on the

Digitized by Google
Original from UNIVERSITY OF MICHIGAN
Generated on 2019-09-22 06:57 GMT / http://hdl.handle.net/2027/mdp.39015077775156
Public Domain, Google-digitized / http://www.hathitrust.org/access_use#pd-google

721A tube. It should be noted, however, that the 724B tube frequently reaches the end of its useful life as a result of its failure to provide adequate receiver protection before serious loss of recovery occurs.

The ATR, if one is used, can also contribute to poor recovery as may be seen by referring to Fig. 30. These data are not necessarily representative since it is possible to adjust the length of line between the magnetron

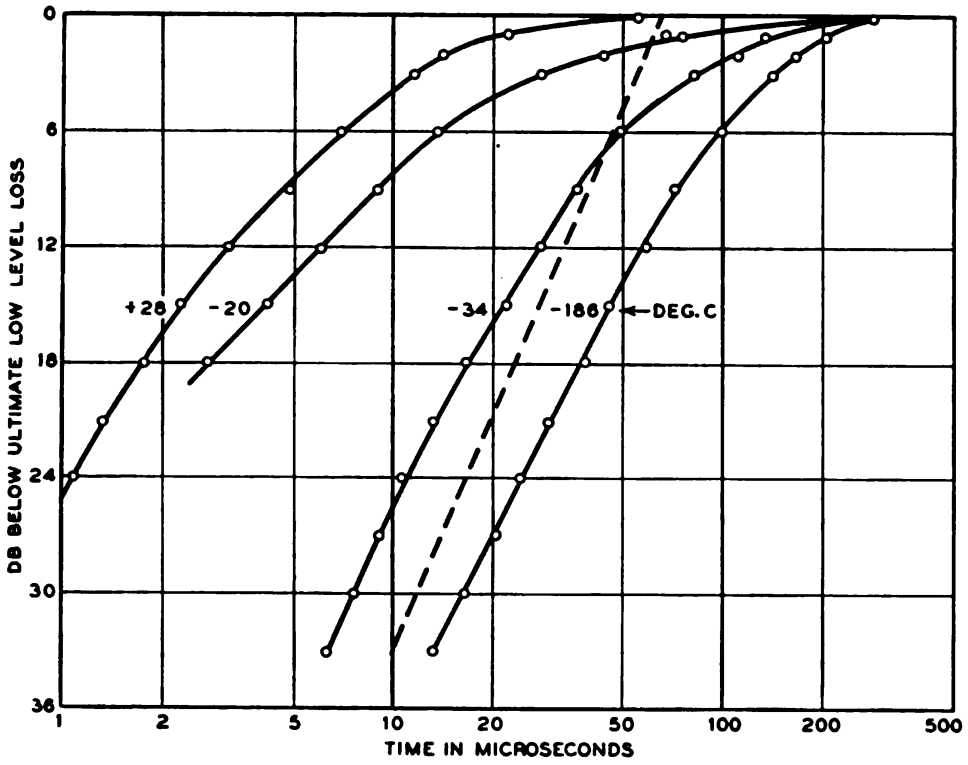

Fig. 27—The dependence of the recovery time on the ambient temperature for the 721A tube

and the ATR junction so as to minimize the effect. Nevertheless the effect is important and should not be overlooked.

Low-Level Loss. An analysis of the low-level loss must take into account two components of loss, the first resulting from power loss in the TR cavity itself and the second resulting from the fact that some power will always be absorbed by the transmitting branch of the system.

The relationships existing between the low-level loss adjustment of a TR box and its other performance characteristics have already been discussed. One aspect of the problem, not previously considered, has to do with the dependence of the performance on the Q of the cavity. This is clearly shown in Fig. 15 which has already been referred to in a different connection. From this aspect, at least, the higher the Q of the tube and its associated cavity the

Digitized by Google
Original from UNIVERSITY OF MICHIGAN
Generated on 2019-09-22 06:58 GMT / http://hdl.handle.net/2027/mdp.39015077775156
Public Domain, Google-digitized / http://www.hathitrust.org/access_use#pd-google

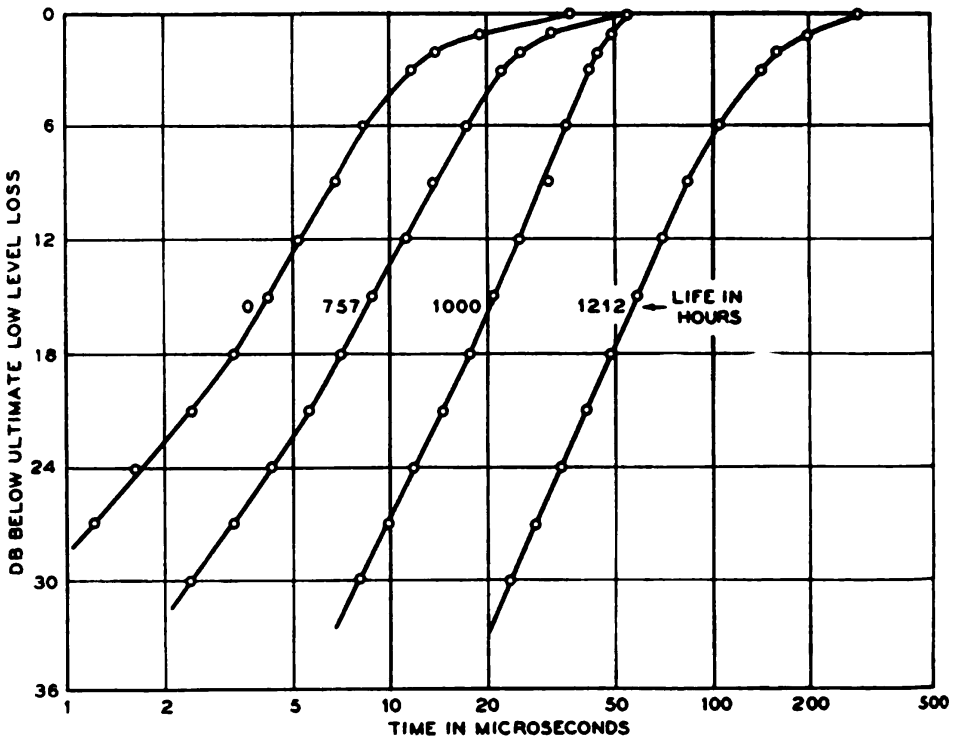

Fig. 28—The variation in recovery time with life for a typical 721A tube

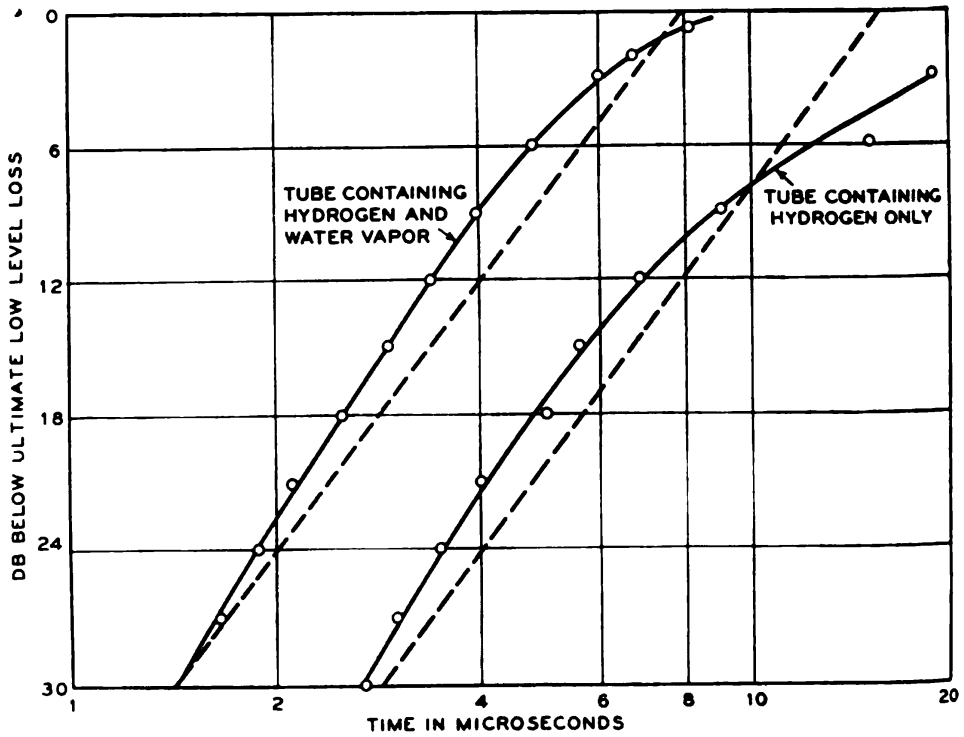

Fig. 29—The variation in recovery time with gas content for the 724B tube

Digitized by Google
Original from UNIVERSITY OF MICHIGAN
Generated on 2019-09-22 06:58 GMT / http://hdl.handle.net/2027/mdp.39015077775156
Public Domain, Google-digitized / http://www.hathitrust.org/access_use#pd-google

better the over-all performance of the system.* Any basic improvement in Q can be reflected either in a lowering of the leakage power or in a reduction of the low-level loss, as may be desired.

Variations in the Q between tubes used in a given cavity of fixed design, are, however, seen as variations in the low-level loss only and have no

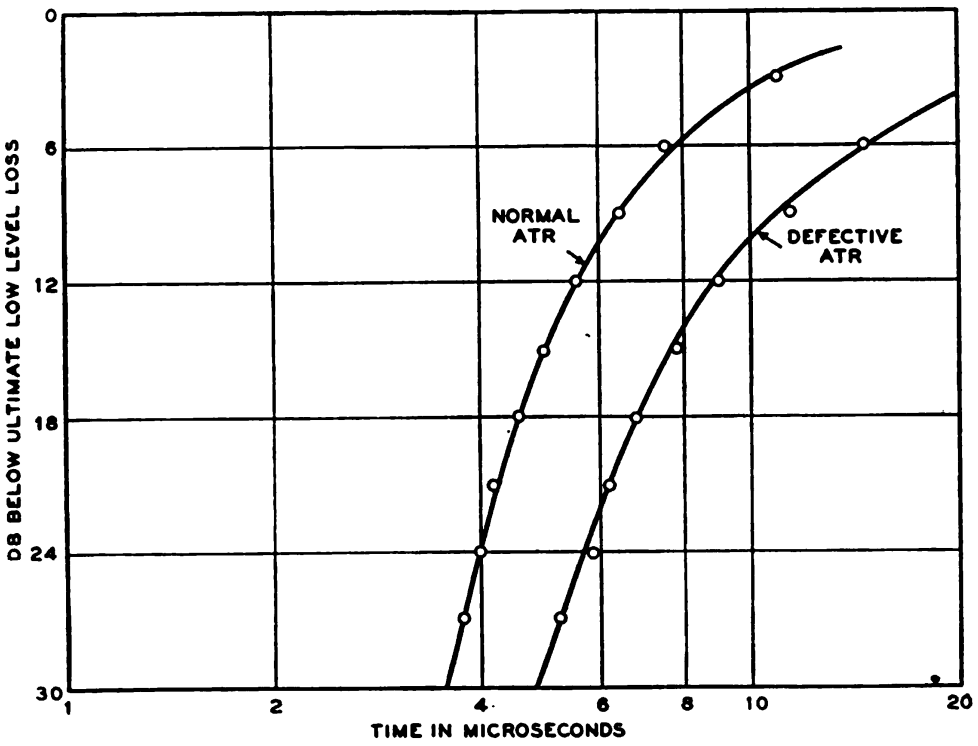

Fig. 30—The ATR recovery effect

noticeable effect on the leakage power. This may be understood by reference to the equations derived in appendix A. The performance of a somewhat idealized TR box may be expressed in terms of three design parameters δ_0, δ_1 and δ_2 which relate respectively to the properties of the cavity, its input coupling, and its output coupling; and in terms of a gas discharge parameter P_0. In terms of these new parameters the in-tune low-level tansmission of a TR box is given as a power ratio by

$$T = \frac{4\delta_1\delta_2}{[\delta_0 + \delta_1 + \delta_2]^2}. \qquad (12)\dagger$$

* As explained later in this section, band width limitations set an upper limit to the permissible Q.

† Numbered equations in the text correspond with the numbers used in the appendices.

Digitized by Google
Original from UNIVERSITY OF MICHIGAN
Generated on 2019-09-22 06:58 GMT / http://hdl.handle.net/2027/mdp.39015077775156
Public Domain, Google-digitized / http://www.hathitrust.org/access_use#pd-google

The input standing wave ratio on the input line is given by

$$\sigma = \frac{\delta_1}{\delta_0 + \delta_2}. \tag{13}$$

The leakage power is similarly given by

$$P_r = P_0 \delta_2 \tag{14}$$

while the gas-discharge power in terms of these parameters and the power in the transmitting line (P) is given by

$$P_g \doteq (P P_0 \delta_1)^{1/2} \tag{19}$$

The parameters δ_1 and δ_2 are properties of the input and output coupling as they are geometrically related to the cavity and are substantially independent of the Q of the cavity. The parameter δ_0 is, however, the reciprocal of the intrinsic or unloaded cavity Q. Equation 12 is seen to depend upon δ_0 but equations (14) and (19) do not. The effect of variations in Q is thus demonstrated.

The over-all performance is also affected by the relative values of δ_1 and δ_2. In view of the dependence of P_r on δ_2 directly and on δ_1 indirectly through the fact that P_0 is not entirely independent of P_g, it is advantageous to adjust the values of δ_1 and δ_2 so that the input standing wave ratio (σ of equation 13) is unity. Such a condition is also very desirable for system reasons as well. When this condition is met, equation (12) reduces to

$$T = \frac{\delta_2}{\delta_1}.$$

The curve marked $\sigma = 1$ of Fig. 15 and the curve of Fig. 16 were plotted on this basis. It should be noted that matched input requires that the input window be larger than the output window.

TR boxes are unfortunately not always operated in the in-tune condition, and they must also pass a band of frequencies as fixed by the narrowness of the transmitter pulse. For these reasons the Q must not be set at too high a value. The additional low-level loss which results from off-tune operation may be computed from equation 28 of appendix A.

Incidentally, it is an experimental fact that the leakage power and the gas-discharge power are not materially altered by small departures from the in-tune adjustment, presumably because of the very low effective Q of the gas discharge.

The ATR Low-Level Loss Component. The component of low-level loss which results from losses of power to the transmitting branch depends very greatly upon the "cold impedance" of the magnetron or other transmitting tube and upon the properties of an ATR box if one is used. As shown in

Digitized by Google
Original from UNIVERSITY OF MICHIGAN
Generated on 2019-09-22 06:59 GMT / http://hdl.handle.net/2027/mdp.39015077775156
Public Domain, Google-digitized / http://www.hathitrust.org/access_use#pd-google

appendix C the loss chargeable to the ATR and the associated transmitting arm can be expressed as a factor F given by

$$F = \frac{4}{(2 + G)^2 + B^2} \tag{33}$$

where G and B are respectively the conductance and susceptance of this branch in units of the surge admittance of the transmission line. Since

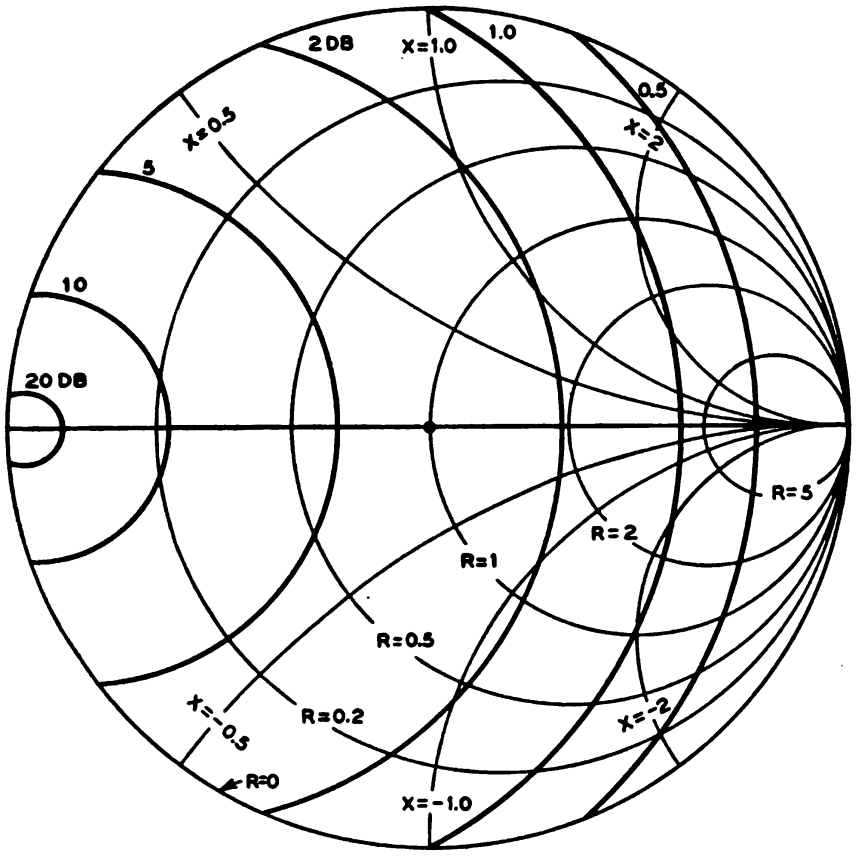

Fig. 31—Curves for constant ATR loss in db as a function of the impedance of the transmitting branch

curves for constant values of F appear on the reflection coefficient plane (Smith transmission line chart) as circles this presentation is very convenient. Fig. 31 is such a plot (impedance circles rather than admittance circles are shown).

If now an ATR is introduced having a resistive component of impedance the range of values of G and B is restricted so that a minimum value of F exists for any random value of the magnetron impedance. With variations in the magnetron cold impedance or in the effective length of line between the magnetron and the ATR junction the value of F will vary between this

Digitized by Google
Original from UNIVERSITY OF MICHIGAN
Generated on 2019-09-22 06:59 GMT / http://hdl.handle.net/2027/mdp.39015077775156
Public Domain, Google-digitized / http://www.hathitrust.org/access_use#pd-google

minimum value and some maximum value which may approach unity. For example if the ATR is adjusted to have the same gas-discharge power as that in a TR adjusted for a transmission of T, its low-level in-tune input impedance will be

$$Z = \frac{1}{1 - T}. \tag{38}$$

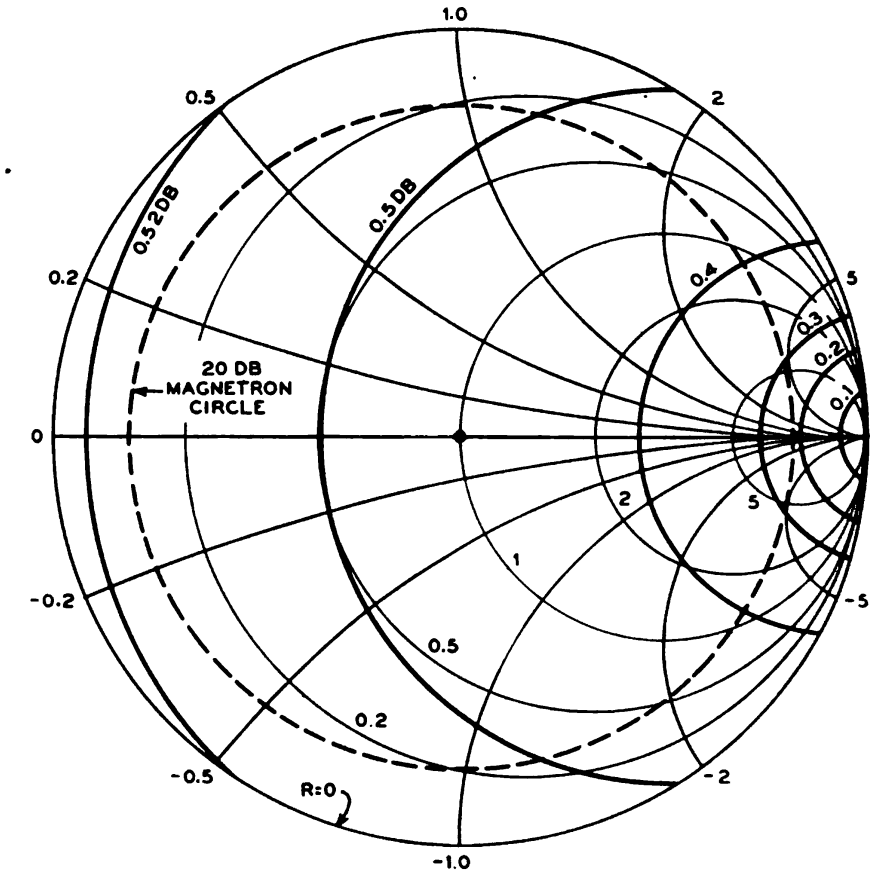

Fig. 32—The ATR low level loss as a function of the magnetron impedance with an ATR adjusted to an impedance of 8 + j0

Actually since the gas-discharge power is usually not the limiting factor in the design it is possible to adjust the ATR to have an input impedance of 8 or 9 (in terms of the line characteristic impedance), corresponding to a TR low-level transmission of the order of 1/2 db ($T = 0.89$) and yielding an ATR loss of approximately 1/2 db.

Since the exact value of the impedance of the magnetron branch is not necessarily known it is convenient to show the dependence of the loss factor F for any given ATR on the magnetron impedance by a plot somewhat

Digitized by Google
Original from UNIVERSITY OF MICHIGAN
Generated on 2019-09-22 06:59 GMT / http://hdl.handle.net/2027/mdp.39015077775156
Public Domain, Google-digitized / http://www.hathitrust.org/access_use#pd-google

similar to Fig. 31 but transformed to the magnetron side of the ATR junction. This may be done by subtracting the ATR impedance from the values read off of Fig. 31 corresponding to desired values of F and replotting these on the reflection coefficient plane. As an example, the in-tune value of Z for one typical 724B ATR cavity is $8 + j0$. Points lying on the $R = 8$ circle on Fig. 31 will then lie on the magnetron $R = 0$ circle, the region inside being distorted and expanded to fill the entire positive R region on the reflection plane. The results are shown in Fig. 32. From this plot it is evident that the maximum possible low-level loss chargeable to the transmitting branch would be slightly more than 0.52 db and that this would occur only for a restricted range in the value of magnetron impedance. As a matter of practical interest the "cold impedance" of the usual magnetron is such as to give at most a 20-db standing wave. This restricts the possible range in impedance values to the area on Fig. 32 within the dotted circle, thus limiting the maximum loss to slightly less than 0.52 db, and imposing a minimum loss limit of 0.22 db.

This type of analysis may be extended to consider the ATR loss during the recovery period if desired although the problem becomes rather complicated as a result of the simultaneous variation in input impedance of both the TR and the ATR.

TR Box Design Considerations

The desired electrical properties for a TR box can of course be achieved in a variety of different physical structures. A construction technique which separates the gas-discharge tube from the rest of the TR box cavity offers many advantages. In the first place the cost of the entire device is kept low by reason of the fact that it is not necessary to transmit the tuning motion through the vacuum-tight tube enclosure. The replacement cost is also greatly reduced since the more complicated part of the TR box is a permanent part of the equipment. Then, the same tube structure can be used for a variety of different types of equipment operating in different wavelength bands and requiring different amounts of receiver protection by the use of different size cavities and different size coupling windows. This greatly simplifies the problem of maintaining replacement stocks. An additional factor, which was of importance during the early days of the war, is that the design of such a tube can be frozen at an early stage, before all the possible circuit aspects of the TR problem have been solved since changes in the external parts of the TR box can be made independent of the design of the replaceable tube element. The widespread use of the 721A and 724B vacuum tube is, in a sense, proof of the essential soundness of the arguments for the external cavity type of construction.

Digitized by Google
Original from UNIVERSITY OF MICHIGAN
Generated on 2019-09-22 06:59 GMT / http://hdl.handle.net/2027/mdp.39015077775156
Public Domain, Google-digitized / http://www.hathitrust.org/access_use#pd-google

The chief difficulty to be overcome in the design of a separate cavity type of TR box has to do with the need for a low-loss contact between the internal portions of the tube and the external cavity. A copper-disc sealing technique, developed at the Bell Laboratories in connection with the construction of water cooled tubes* and later superseded by the now conventional Housekeeper seal, had previously been applied at ultra-high frequencies in the design of oscillators and amplifiers. This technique makes possible very satisfactory high-frequency connections by simply clamping the external portion of the disc between machined surfaces. The flexibility of the copper discs is sufficient to compensate for minor machining errors and for differential thermal expansions while the relative softness of the copper insures a continuous contact around the entire periphery. The goodness of contact provided by these contacts is evidenced by the fact that Q's of 4000 and greater are obtained at 3000 megacycles with discs of the 721A type. This technique was therefore adopted for the 721A tube and the 724B tube and for one electrode of the 1B23 tube. The second high-frequency electrode of the 1B23 was made in the form of a rod terminating in a ball for convenience in replacing tubes since the accompanying loss of Q can be tolerated in the frequency range where this tube is used.

In an external cavity type of TR box the over-all goodness of the design is largely determined by the design of the gas-discharge tube. It is the tube designer's responsibility to determine the optimum shape and size for the copper discs and for the glass tube envelope and to determine the optimum gas composition and pressure, with due consideration being given to such matters as mechanical ruggedness, manufactureability and freedom from undesirable ambient temperature, pressure and humidity effects.

With the copper-disc type of tube the system designer has at his disposal the ability to vary the design of the external cavity, and to arrive at any specific compromise between the various conflicting performance criteria which he feels to be the best for his particular application. For example, in systems employing vacuum tube converters it is customary to adjust the TR box for a low-level loss of 1 db or somewhat less since receiver protection is of minor interest while in systems employing crystal converters it is customary to fix the low-level loss at 1.5 db or sometimes as high as 2.0 db. Certain cavities, notably the one shown in Fig. 5, have to be designed to have an extended tuning range, in this case achieved by a piston tuner with, however, some loss in Q, while other cavities, the one shown in Fig. 11 being typical, do not require this same tuning range and a different tuning mechanism (in this case, tuning plugs) can be employed.

An extreme example, illustrating the advantages to the system designer

* W. Wilson, "A New Type of High-Power Tube," *B. S. T. J.*, vol. 1, p. 4, July 1922.

Digitized by Google
Original from UNIVERSITY OF MICHIGAN
Generated on 2019-09-22 06:59 GMT / http://hdl.handle.net/2027/mdp.39015077775156
Public Domain, Google-digitized / http://www.hathitrust.org/access_use#pd-google

of the external cavity type of tube, is that of certain radar systems which were required to be capable of receiving signals on occasion at a frequency differing from their normal tuning. This was done by a solenoid-operated plunger which could be preset to alter the tuning of the cavity by the desired amount whenever the solenoid was energized.

The Tube Design

The 702A and 709A vacuum tubes, as previously mentioned, were put into service with little or no consideration of their real suitability. With these stop-gap designs in production the basic design problem was given serious consideration, with separate studies being made of the mechanical design considerations as they relate to the size and shape of the discs and glass of the tube, and of the gas filling.

The exact shape of the disc is determined first by the total tuning range which is to be required of the tube, and second by the necessity for maintaining the Q of the structure as high as possible. It has been shown that in a spherical resonator with coaxial cones the maximum Q occurs when the cone half-angle is nine degrees. The copper-disc tube can only roughly approximate the ideal spherical resonator; nevertheless it appears desirable to use cones of this angle. The disc spacings and diameters are so chosen that the tube resonates at the shortest wavelength at which it is to be used in a "square" cavity; i.e., one in which the inside diameter approximately equals the height. Such a cavity is about the closest practical approach to a sphere. The glass diameter is made as large as mechanical considerations permit so it is as far as possible removed from the region of high electric field intensity.

The experimental results of Fig. 24, previously noted, indicate that the leakage power of a TR box decreases as the gap spacing decreases; thus one is tempted to make the gap extremely small. Too small a gap is very troublesome, however, since such a gap has an unreasonably rapid variation of resonant frequency with gap separation, making the tuning extremely subject to change as a result of dimensional variations due to processing or to temperature changes. Accordingly one chooses a compromise gap separation. The electrode radius at the gap must be large enough to permit the radio frequency glow discharge to dissipate the required power without excessive spreading, and must be determined by experiment.

Rather than attempting to hold all of the mechanical variations in the tube (including glass thickness) to the necessary tolerances to insure the desired uniformity in tuning, the tubes are pretuned before exhaust by deforming the copper discs. The tubes are placed in a special cavity and the disc inside the envelope distorted by a tool until resonance is obtained at a speci-

Generated on 2019-09-22 06:59 GMT / http://hdl.handle.net/2027/mdp.39015077775156
Public Domain, Google-digitized / http://www.hathitrust.org/access_use#pd-google
Digitized by Google
Original from UNIVERSITY OF MICHIGAN

fied frequency. It is quite easy to tune tubes in this way so that they are uniform to within ± 0.25%.

Unless the tube is properly designed, changes in ambient temperature may seriously affect its resonant frequency. The part of the disc which is inside the glass envelope may be considered as a diaphragm supported around its periphery by the glass which has a temperature coefficient of expansion negligibly small compared to that of the copper. An increase in temperature, which causes the copper to expand, will force the cone tip to move toward or away from the gap, depending on the initial slope of the nearly flat portion of the disc. The temperature coefficient of frequency may be either positive or negative, and will have extreme variations in magnitude from tube to tube if consideration is not given in disc design to avoid such difficulties.

A cavity made wholly of copper will have a fractional change in wavelength with temperature the same as the fractional change in length of copper (approximately fourteen parts in a million per degree centigrade). As the temperature increases, the frequency decreases. At a frequency of 1000 mc, the approximate temperature coefficient of frequency is −.014 megacycles per degree centigrade; at 3000 mc it is −.042 mc/°C; and at 10,000 mc it is −.14 mc/°C. Magnetrons normally have temperature coefficients of about these magnitudes. The ideal TR tube would have the same coefficient as the magnetron; practically speaking, any coefficient between zero and twice the value for copper is satisfactory.

It is practical to make a copper disc structure which has the required temperature coefficient. Fig. 33, which is a cross-section of a 721A tube, shows how temperature compensation within the tube is effected. The disc is slanted away from the center portion of the tube, so that as temperature rises the cone is carried away from the gap. At the same time the cone itself expands; the net effect is to increase the gap between the two cone tips. The angle of the slanted part of the disc must be such that the gap increases with temperature at the same rate that it would in an all-copper cavity. If this condition is fulfilled, the net result of the expansion of all the tube parts, and of the cavity itself, will be the same as if it were all made of copper. This result is achieved by an experimental series of successive approximations. A number of models are built until the angles are found which give the desired temperature coefficient of frequency.

The gas content of the tube was the subject of considerable study. As stated in the section on Recovery Time, gases which readily form negative ions are invariably the most satisfactory from that viewpoint. Gases of low ionization voltage, such as the rare gases, give excellent protection but usually have extremely poor recovery. The choice of a TR gas must of necessity be a compromise between the two requirements. Some otherwise

Generated on 2019-09-22 07:00 GMT / http://hdl.handle.net/2027/mdp.39015077775156
Public Domain, Google-digitized / http://www.hathitrust.org/access_use#pd-google
Digitized by Google
Original from UNIVERSITY OF MICHIGAN

satisfactory gases are not useful because of other characteristics. HCl is an excellent TR gas, but is very corrosive. Freon, a common refrigerant, is excellent but is unstable. In general, no gas which contains a solid elementary constituent is a satisfactory TR gas. The most satisfactory gas found was water vapor. It is cheap, stable, and easy to handle. Water vapor alone is not safe to use at a low temperature, so a small amount of hydrogen is added to ensure adequate protection when the water vapor is frozen out.

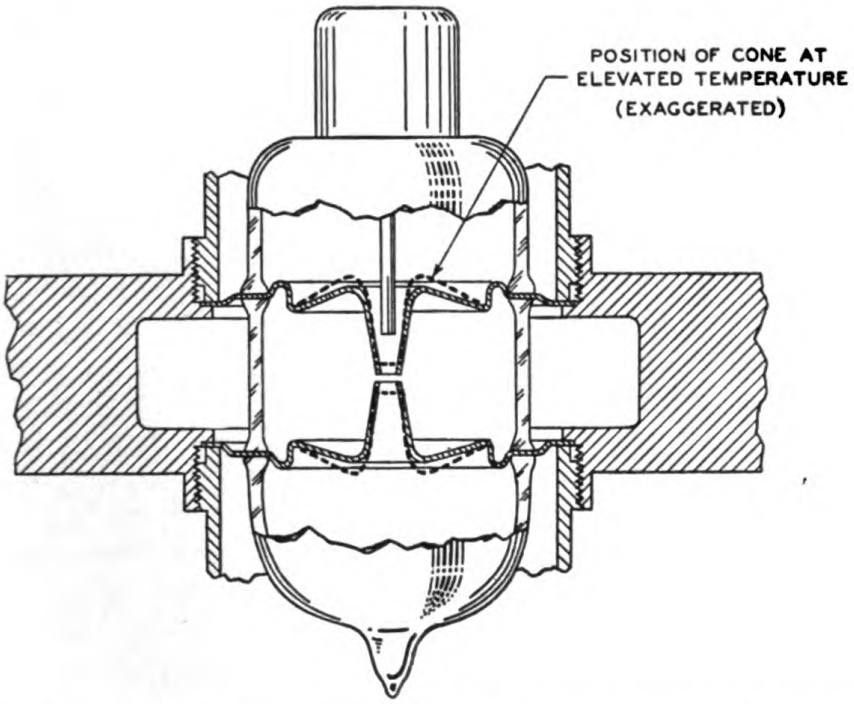

Fig. 33—Cross section of a 721A TR Tube, showing the special shape of the temperature compensated discs

The life of a TR box is in general determined by the gas volume. The radio-frequency discharge consumes no gas except at extremely high power levels; the igniter discharge accounts for the greater part of the loss of the gas initially placed in the tube. Reduction of the water vapor to hydrogen by formation of copper oxide on copper parts of the tube seems to be the principal process which goes on. This change results in no change in total pressure until the water vapor is exhausted; thereafter sputtering becomes more important and accounts for a fairly rapid hydrogen clean-up. The life of a TR tube is determined by the igniter current, which is maintained at a value as small as possible consistent with adequate spike protection, and by the volume of the tube.

Digitized by Google
Original from UNIVERSITY OF MICHIGAN
Generated on 2019-09-22 07:00 GMT / http://hdl.handle.net/2027/mdp.39015077775156
Public Domain, Google-digitized / http://www.hathitrust.org/access_use#pd-google

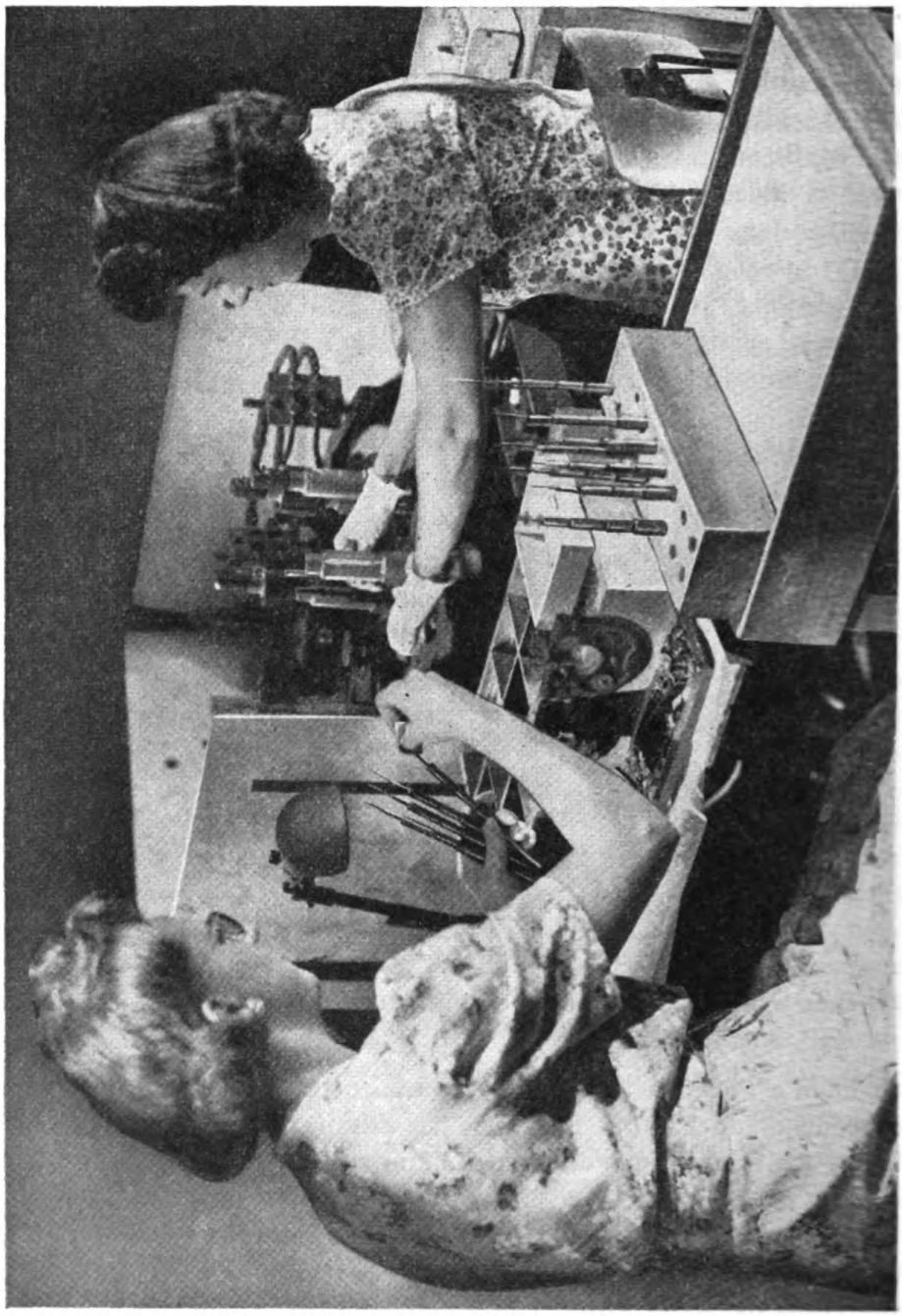

Fig. 34—Setup for making 724B copper to-glass disc seal

Digitized by Google
Original from UNIVERSITY OF MICHIGAN
Generated on 2019-09-22 07:00 GMT / http://hdl.handle.net/2027/mdp.39015077775156
Public Domain, Google-digitized / http://www.hathitrust.org/access_use#pd-google

The lack of water vapor in a tube which has been operated for some hundreds of hours may manifest itself by a failure in either protection or recovery time. The operating frequency determines which failure becomes important first; at long wavelength it is likely to be recovery, while at shorter wavelength the spike protection is likely to fail first.

The life of a TR tube operated without igniter is very much longer. This may be understood from the picture given above under "recovery," of the state of affairs existing in the radio-frequency discharge. Electrons do not completely traverse the gap, but oscillate about some mean position, while the positive ions hardly move at all. Thus there is little more interaction between the metal electrodes and the gas molecules with the R.F. discharge on than with it off. A few 721A's have been operated without igniter for as long as 5000 hours with no measurable change in either protection or recovery. This experiment was done at a transmitter power level of 250 kw. peak power. The best life that can be expected with the igniter operating at 100 microamperes is 500 hours, at which time the recovery time is badly deteriorated. In order to maximize the life of the tube, the initial gas filling consists of a minimum amount of hydrogen and as much water vapor as may be introduced without causing excessive leakage power (see Figs. 20 and 23).

Manufacturing and Testing

Some interesting problems occur in the manufacture of copper-disc seal TR tubes which are quite different from those encountered in the construction of more conventional tubes. The copper-disc seals are usually made by high-frequency induction heating. Close control of the spacing between discs must be maintained during the bulb-making operation in which the discs are fused to the glass parts of the tube. One way of accomplishing this is shown in Fig. 34, which depicts a machine setup for making the 724B TR tube. The parts are held by lavite forms which support and locate them during the bulb-making process. The seal is made possible by a correct choice of copper thickness. The copper disc is stressed due to forces set up by the different expansion coefficients of the glass and the copper, and if too thick will pull the seal apart. If too thin, the copper itself will tear. Nevertheless, a properly designed copper-disc seal is very strong; the copper-disc seal TR tubes will pass the JAN1-a* mechanical and thermal shock tests for glass tubes without any difficulty.

The electrical pretuning operation, referred to earlier, comes right in the middle of the manufacturing process. Before the igniter is sealed in, the bulb is placed in a special pretuning cavity. The setup includes an oscillator

* Joint Army-Navy Specification for electron tubes.

Digitized by Google
Original from UNIVERSITY OF MICHIGAN
Generated on 2019-09-22 07:00 GMT / http://hdl.handle.net/2027/mdp.39015077775156
Public Domain, Google-digitized / http://www.hathitrust.org/access_use#pd-google

of appropriate frequency range, a wavemeter, and some device for indicating resonance. The part inside the glass of one of the copper discs is bent, by gentle tapping, until the resonant frequency of the bulb in the special cavity is within the required tolerance (which may be as small as 0.25%) of the pretuning frequency.

No heat treatment of any kind is used in the pumping of TR tubes. It is obviously unnecessary to subject the tubes to the usual baking, the principal purpose of which is to remove water vapor film from the tube parts. On

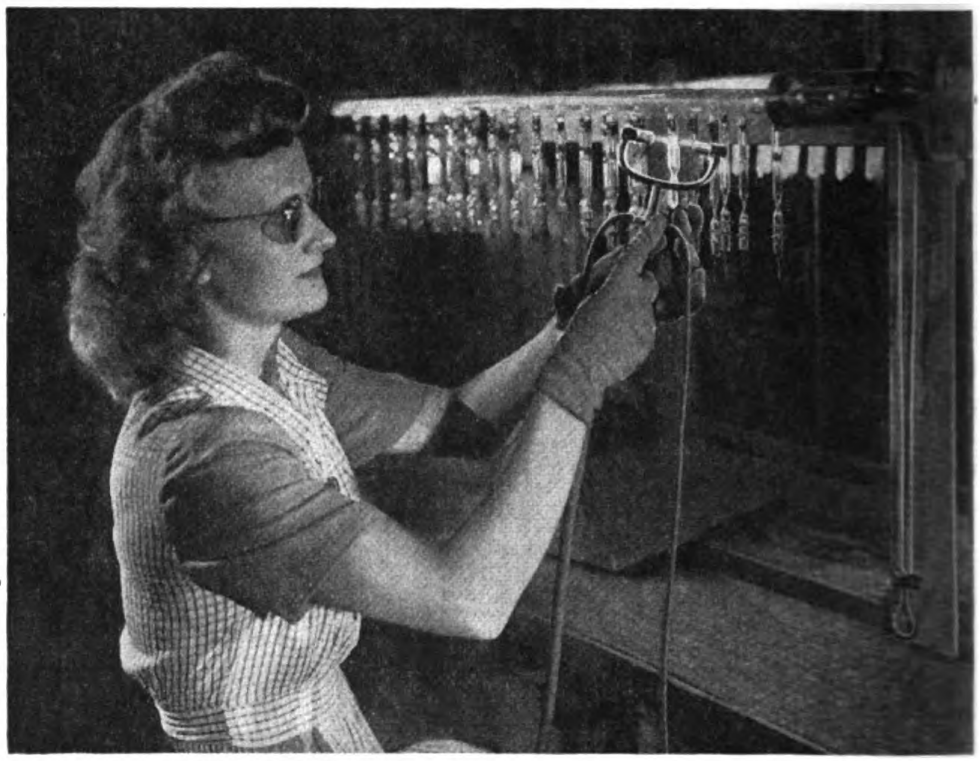

Fig. 35—Pump Station for the 724B Vacuum Tube

the contrary, it is difficult to control the water vapor pressure in tubes which have been baked as the parts absorb a surprising quantity of water. The tubes are filled to fairly high pressure, so a diffusion pump is not necessary. Fig. 35 shows a pump station used in production of the 724B.

The test procedure for TR tubes must verify that each individual tube will fulfill its fourfold function of protecting the crystal, of recovering rapidly, and of introducing neither excessive high-level loss nor excessive low-level loss. The tuning of each tube must be verified, and it must pass mechanical and dimensional tests. Fortunately a tube which is otherwise sound will never introduce excessive high-level loss, so no specific test is required.

The protection test may be made either with a c-w oscillator of suffi-

Digitized by Google
Original from UNIVERSITY OF MICHIGAN
Generated on 2019-09-22 07:00 GMT / http://hdl.handle.net/2027/mdp.39015077775156
Public Domain, Google-digitized / http://www.hathitrust.org/access_use#pd-google

ciently high level to ionize the TR tube gap, or with a magnetron in the equivalent of a radar microwave head. The high-level test bench used for the 724B is shown in Fig. 36. This bench uses a radar microwave head fitted to special plumbing. In either case, the leakage power is measured at a specified R.F. level. For production testing, an actual measurement of recovery time is not used. Instead a test which measures the quantity of

Fig. 36—High Level Test Bench for the 724B Vacuum Tube

water vapor in the tube in a relative way has been developed. This test involves touching some part of the tube envelope with a piece of carbon dioxide ice, so that most of the water vapor is frozen out forming a small spot of ice on the inside of the tube. Only the hydrogen remains, and the resulting change in either the leakage power or the igniter arc drop is indicative of the quantity of hydrogen and of water vapor in the tube. Careful correlation must be made between this simple dry-ice test and absolute recovery time measurements; experience has shown the dry-ice test to be reliable and in the hands of a skilled operator very informative.

Low-level loss and tuning are checked at such low level that the gas does

Digitized by Google
Original from UNIVERSITY OF MICHIGAN
Generated on 2019-09-22 07:01 GMT / http://hdl.handle.net/2027/mdp.39015077775156
Public Domain, Google-digitized / http://www.hathitrust.org/access_use#pd-google

not ionize in a cavity of restricted tuning range. Every tube must resonate within the range of the tuning adjustment, and the transmission loss through the test cavity must not be excessive.

Two additional tests are made at the time the d-c igniter characteristics are checked. One, igniter interaction, is important in the 721A, the 10 cm. TR tube. This tube has rather large openings in its cone tips, so that if the igniter electrode is sealed in too close to the cone tip, the glow discharge which surrounds it may extend out into the gap. Such a defective tube will show igniter interaction; the low-level loss through it will be more when the igniter arc is on than when it is off. Normal tubes do not show this effect.

The 724B 3 cm. TR tube has such a tiny opening in its cone tip that igniter interaction does not occur. The tube is more subject to igniter oscillations, perhaps because it is filled to a higher gas pressure. The consequences of these oscillations was explained in the section on The Spike. Igniter oscillations are usually due to an improper gas filling, and are detected by means of a cathode ray oscilloscope.

The above tests are made on each tube as it comes off the production line. Some additional tests are made on selected samples to insure that the quality is being maintained. Selected tubes are subjected to mechanical shock tests and to temperature variation tests to verify both their resistance to thermal changes and that their temperature coefficient of frequency is not excessive. Absolute recovery time, Q, and leakage power tests are made on these tubes, and some are set aside for life testing. By all these tests the important electrical properties of the tube are under constant scrutiny and the danger of shipping defective tubes is minimized. The importance of adequate testing can hardly be over-emphasized, as a defective TR tube may render a whole radar system inoperative.

Acknowledgements

Because of the very close liaison maintained during the war period between various industrial and governmental laboratories, the developments described in this paper were carried on with the constant advice and criticism of many individuals. It is not therefore possible to assign credit to specific individuals for any particular aspect of the work with any certainty. The authors would be remiss, however, were they not to call attention to the many contributions made at the M.I.T. Radiation Laboratory particularly by members of the group under the direction of Dr. J. R. Zacharias and later Dr. A. G. Hill. Colonel J. W. McRae assisted in the early formulation of the TR problem and Captain A. Eugene Anderson did much of the original development work on the 724B tube while at the Bell Laboratories and was later involved in the formulation of test methods and test limits in connection with his Signal Corps work. Mr. C. F. Crandell of the Southwestern

Digitized by Google
Original from UNIVERSITY OF MICHIGAN
Generated on 2019-09-22 07:01 GMT / http://hdl.handle.net/2027/mdp.39015077775156
Public Domain, Google-digitized / http://www.hathitrust.org/access_use#pd-google

Bell Telephone Company, while at the Bell Laboratories, was responsible for the construction of test equipment and for most of the recovery time measurements reported in this paper. At various periods during the development work Messrs. A. B. Crawford, V. C. Rideout, G. M. Eberhardt and J. P. Schafer were closely associated with the measurement of the system performance of TR tubes. Mr. R. M. Purinton of the Bureau of Ships deserves much credit for his encouragement and assistance in the standardization program which led to the adoption of the 721A and 724B tube designs by all manufacturers. The Thermionics Branch of the Evans Signal Laboratory provided the bulk of the electrical standardization, calibration and engineering service associated with these tubes and assisted in the development of improved test methods. The magnificent production job done by the Western Electric Company and by other manufacturers, particularly by the Sylvania Electric Products Inc. in making these tubes available to the armed services also deserves mention. Perhaps the final mention should go to the many circuit design engineers both within the Bell Laboratories and elsewhere who handled the many difficult problems relating to the design and use of TR cavities in actual radar systems.

APPENDIX A

Analysis of the Idealized TR Box

Schelkunoff has shown* that the impedance of a resonant cavity can be represented in terms of its resonant frequencies as

$$Z = \sum_a \frac{Z_a}{j\left(\frac{\omega}{\omega_a} - \frac{\omega_a}{\omega}\right) + \frac{1}{Q_a}} \tag{1}$$

or in the vicinity of any single resonance as

$$Z = Z_1 + \frac{Z_n}{j\left(\frac{\omega}{\omega_n} - \frac{\omega_n}{\omega}\right) + \frac{1}{Q_n}}. \tag{2}$$

Under most conditions the Z_1 term is negligibly small. We are therefore justified in thinking of the generalized resonant cavity used as a TR switch as a shunt resonant circuit to which are coupled input and output circuits. For the moment we will consider (1) that these external circuits are resistive only, (2) that the Z_1 in equation (2) is zero; and (3) we will restrict the analysis to the in tune condition.

When the cavity is excited by energy supplied from the input circuit there exists in the cavity a certain amount of reactive power which will be

* S. A. Schelkunoff, "Representation of Impedance Functions in Terms of Resonant Frequencies," *Proc. I.R.E.*, vol. 32, pp. 83–90, February (1944).

Digitized by Google
Original from UNIVERSITY OF MICHIGAN
Generated on 2019-09-22 07:06 GMT / http://hdl.handle.net/2027/mdp.39015077775156
Public Domain, Google-digitized / http://www.hathitrust.org/access_use#pd-google

designated by the symbol P_0. Of this power, a certain fraction δ_0 is dissipated as losses in the cavity itself where

$$\delta_0 = \frac{1}{Q_0}. \tag{3}$$

The symbol Q_0 with the subscript is further defined as the intrinsic Q, that is, the Q without external loading, to differentiate it from the more general Q_L which is the measured Q when the cavity is loaded down by external coupling. It should be noted that this definition of δ differs from the logarithmic decrement by a factor π.

When coupled to the external circuits the loaded δ is increased. On the assumption that the loading effects of the input and output irises are independent we can write

$$\delta_L = \delta_0 + \delta_1 + \delta_2 \tag{4}$$

where δ_L is the loaded δ, and δ_1 and δ_2 are respectively the input and output loadings. Physically the assumption underlying this expression is that the distribution of electromagnetic fields within the cavity is not seriously altered by the input and output coupling devices. This assumption should certainly be valid as long as the absolute values of the δ's are very small compared to unity. Since the δ's usually encountered are of the order of 10^{-3} or less, the assumption seems to be justified.

Equation (4) may be written

$$\frac{1}{Q_L} = \frac{1}{Q_0} + \delta_1 + \delta_2 \tag{5}$$

The values of δ_1 and δ_2 evidently depend upon the ratio of the apparent series resistance which the external coupling introduces into the resonant cavity to the effective reactance of the cavity, that is,

$$\delta_1 = \frac{k_1^2 R_1}{X} \tag{6}$$

where k_1 is the transformation ratio of the input coupling device, R_1 is the resistance of the input circuit and X is the cavity reactance. Similarly

$$\delta_2 = \frac{k_2^2 R_2}{X}. \tag{7}$$

The values of the δ's may be equally well considered as the ratios of the coupled conductance to the shunt susceptance of the cavity considered as a shunt resonant circuit so that equations (6) and (7) become

$$\delta_1 = \frac{G_1}{k_1^2 B} \tag{8}$$

Digitized by Google
Original from UNIVERSITY OF MICHIGAN
Generated on 2019-09-22 07:07 GMT / http://hdl.handle.net/2027/mdp.39015077775156
Public Domain, Google-digitized / http://www.hathitrust.org/access_use#pd-google

and

$$\delta_2 = \frac{G_2}{k_2^2 B} \tag{9}$$

when the R's and X are replaced by their reciprocals and transformed from a shunt to a series circuit.

The equivalent circuit is shown in Fig. 37, where for convenience everything is referred to the cavity and the sources for receiving and transmitting are represented by constant current generators, I and I_m respectively.

The Low-Level Transmission. We are now in a position to express the low-level transmission of the cavity. For this purpose we will assume that

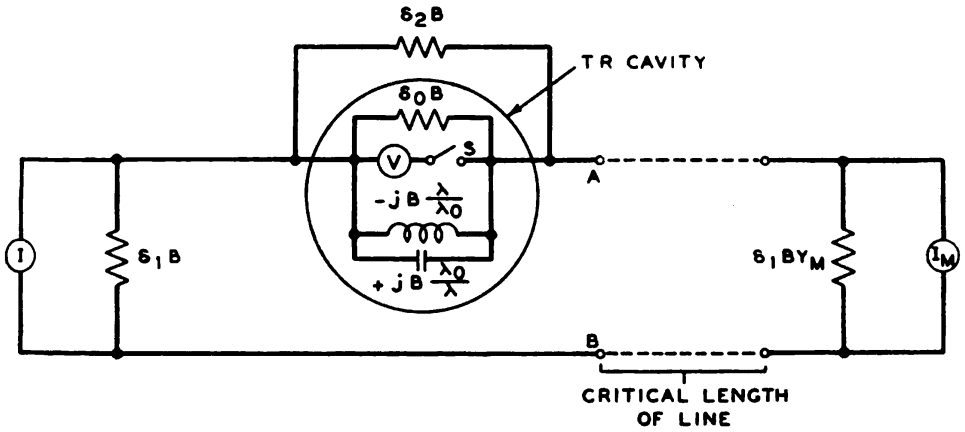

Fig. 37—Equivalent circuit of a system referred to the TR cavity

the admittance of the transmitting branch at plane AB is infinite. The available power is given by

$$P_{\text{avail}} = \frac{I^2}{4\delta_1 B}. \tag{10}$$

while the power actually going into the load is given by

$$P_{\text{out}} = \frac{I^2 \delta_2 B}{(\delta_0 + \delta_1 + \delta_2)^2 B^2} \tag{11}$$

the power transmission ratio defined as T is given by

$$T = \frac{4\delta_1 \delta_2}{(\delta_0 + \delta_1 + \delta_2)^2}. \tag{12}$$

One additional expression is desired. This is the ratio of cavity input resistance to the resistance of the input circuit. This is evidently the reciprocal of the conductance ratio and is given by

$$\sigma = \frac{\delta_1}{\delta_0 + \delta_2}. \tag{13}$$

Digitized by Google
Original from UNIVERSITY OF MICHIGAN
Generated on 2019-09-22 07:07 GMT / http://hdl.handle.net/2027/mdp.39015077775156
Public Domain, Google-digitized / http://www.hathitrust.org/access_use#pd-google

The symbol σ is used to call attention to the fact that the in tune impedance ratio is numerically equal to the voltage standing wave ratio on the input line.

The low-level behavior of the cavity is thus defined by three equations.

$$\delta_L = \delta_0 + \delta_1 + \delta_2 \tag{4}$$

$$T = \frac{4\delta_1 \delta_2}{(\delta_0 + \delta_1 + \delta_2)^2} \tag{12}$$

$$\sigma = \frac{\delta_1}{\delta_0 + \delta_2}. \tag{13}$$

High-Level Operation. The high-level performance of the cavity containing a gas discharge can be expressed directly in terms of our original definitions. Fig. 37 still applies, the transmitter admittance changing to its operating value which is assumed to be $\delta_1 B$ at the plane AB. When the gas discharge becomes conducting, the switch S is closed, the value of the reactive power in the cavity (P_0) is set by the character of the discharge and the leakage power is given by

$$P_r = P_0 \delta_2. \tag{14}$$

A constant value of P_0 is equivalent to a constant value of V in the figure. The power dissipated in the cavity walls, the gas discharge and in the output circuit must evidently be given by

$$P_1 = \frac{I_m V}{2} = (P P_0 \delta_1)^{1/2} \tag{15}$$

if $$V << I_m/\delta_1 B.$$

Of this power an amount called the excitation power

$$P_e = P_0 \delta_0 \tag{16}$$

is lost in the cavity walls. The net loss of power in the gas discharge is given by

$$P_g = P_1 - P_r - P_e \tag{17}$$

or

$$P_g = (P\, P_0 \delta_1)^{1/2} - P_0(\delta_0 + \delta_2). \tag{18}$$

Since the last term is usually very small compared to the first term, we may write

$$P_g \doteq (P\, P_0 \delta_1)^{1/2}. \tag{19}$$

Digitized by Google
Original from UNIVERSITY OF MICHIGAN
Generated on 2019-09-22 07:07 GMT / http://hdl.handle.net/2027/mdp.39015077775156
Public Domain, Google-digitized / http://www.hathitrust.org/access_use#pd-google

This equation was used for plotting Fig. 16, where δ_1 is replaced by its equivalent in terms of σ, Q_0 and T.

The Derived g Parameters. For some purposes it is convenient to eliminate δ_0 from the expressions for T and σ. This may be done by defining

$$g_1 = \frac{\delta_1}{\delta_0} \tag{20}$$

and

$$g_2 = \frac{\delta_2}{\delta_0}. \tag{21}$$

Introducing these new parameters the equations become

$$\frac{Q_0}{Q_L} = 1 + g_1 + g_2 \tag{22}$$

$$T = \frac{4g_1 g_2}{(1 + g_1 + g_2)^2} \tag{23}$$

$$\sigma = \frac{g_1}{1 + g_2} \tag{24}$$

$$P_r = P_e g_2 \tag{25}$$

$$P_g = (PP_e g_1)^{1/2} \tag{26}$$

The g parameters are particularly useful in defining the behavior of a tube and cavity combination when δ_0 is a fixed quantity while the effects of changes of δ_0 are more clearly shown when the δ parameters are used. The g parameters may be determined experimentally, using equations (21) and (22) without knowing the value of δ_0, that is of Q_0. On the other hand the g's are altered if a tube is replaced by one giving a different Q value while the δ's are intrinsic properties of the coupling mechanisms and remain fixed as long as the cavity and the tube tune at the same frequency and have the same effective reactance.

Tabulation of Related Equations. In the interest of completeness a number of the more important combinations of the basic equations are listed in Table 1. Some of these are of interest for measurement purposes while others apply particularly to actual system conditions.

Off-Resonance Analysis. The analysis can be extended to predict the transmission when the cavity is detuned from resonance by introducing the necessary susceptance term in equation (11) above and solving for T. This gives for the absolute value (neglecting phase)

$$T = \frac{4\delta_1 \delta_2}{[\delta_0 + \delta_1 + \delta_2]^2 + \left[\frac{\omega}{\omega_0} - \frac{\omega_0}{\omega}\right]^2} \tag{27}$$

Digitized by Google
Original from UNIVERSITY OF MICHIGAN
Generated on 2019-09-22 07:07 GMT / http://hdl.handle.net/2027/mdp.39015077775156
Public Domain, Google-digitized / http://www.hathitrust.org/access_use#pd-google

TABLE 1.—*Relations between Cavity Parameters*

	Quantity	Symbol	General Expressions		Special Cases	
			In terms of δ's & Q_0	In terms of σ, T, & Q_0	TR case $\sigma = 1$	ATR case $T = 0$
Low level parameters	Input standing wave ratio	σ	$\dfrac{\delta_1}{\delta_0 + \delta_2}$	σ	1	$\dfrac{Q_0}{Q_L} - 1$
	Low Level Transmission	T	$\dfrac{4\delta_1\delta_2}{(\delta_0 + \delta_1 + \delta_2)^2}$	$\dfrac{4\sigma}{(1+\sigma)^2}\left[1 - (1+\sigma)\dfrac{Q_L}{Q_0}\right]$	$1 - 2\dfrac{Q_L}{Q_0}$	0
	Q ratio	$\dfrac{Q_0}{Q_L}$	$(\delta_0 + \delta_1 + \delta_2)Q_0$	$\dfrac{4\sigma(1+\sigma)}{4\sigma - (1+\sigma)^2 T}$	$\dfrac{2}{1-T}$	$1 + \sigma$
	Input δ	δ_1	δ_1	$\dfrac{4\sigma^2}{[4\sigma - (1+\sigma)^2 T]Q_0}$	$\dfrac{1}{(1-T)Q_0}$	$\dfrac{\sigma}{Q_0}$
	Output δ	δ_2	δ_2	$\dfrac{(1+\sigma)^2 T}{[4\sigma - (1+\sigma)^2 T]Q_0}$	$\dfrac{T}{(1-T)Q_0}$	0
High level parameters	Leakage power	P_r	$P_0\delta_2$	$\dfrac{P_0(1+\sigma)^2 T}{Q_0[4\sigma - (1+\sigma)^2 T]}$	$\dfrac{P_0 T}{Q_0(1-T)}$	0
	Gas discharge power	P_g	$[PP_0\delta_1]^{\frac{1}{2}} - P_0(\delta_0 + \delta_2)$	$\dfrac{2\sigma}{1+\sigma}\left[\dfrac{PP_r}{T}\right]^{\frac{1}{2}} - \dfrac{4P_r\sigma}{T(1+\sigma)^2}$	$\left[\dfrac{PP_0}{(1-T)Q_0}\right]^{\frac{1}{2}} - \dfrac{P_0}{(1-T)Q_0}$	$\left[\dfrac{PP_0\sigma}{Q_0}\right]^{\frac{1}{2}} - \dfrac{P_0}{Q_0}$

Generated on 2019-09-22 07:08 GMT / http://hdl.handle.net/2027/mdp.39015077775156
Public Domain, Google-digitized / http://www.hathitrust.org/access_use#pd-google
Digitized by Google
Original from UNIVERSITY OF MICHIGAN

where ω_0 and ω are respectively the resonant angular frequency and the operating angular frequency.

This may be rewritten as

$$T = \frac{T_0}{1 + Q_L^2\left[\frac{\omega}{\omega_0} - \frac{\omega_0}{\omega}\right]^2} \tag{28}$$

where T_0 is the in tune transmission and Q_L is the loaded Q, if one assumes that the δ's and Q_L remain unchanged for small departures from the resonant wavelength.

The input impedance of the cavity in terms of the input line impedance is then

$$Z = \frac{\delta_1}{j\left[\frac{\omega}{\omega_0} - \frac{\omega_0}{\omega}\right] + \delta_0 + \delta_2}. \tag{29}$$

The effect of other resonant modes which have been neglected in this analysis may be included by the addition of a term (σ_1) in equation (29) giving

$$Z = \sigma_1 + \frac{\delta_1}{j\left[\frac{\omega}{\omega_0} - \frac{\omega_0}{\omega}\right] + \delta_0 + \delta_2}. \tag{30}$$

Equation (30) and equation (2) are identical except for terminology.

APPENDIX B

Experimental Determination of "g" Parameters of Windows

The derived g-parameters which express the electrical size of a window between a resonant cavity and a surge impedance line were defined in Equations 20 and 21 of Appendix A. Numerical values of these parameters may be of some interest, together with their relation to physical dimensions of the windows. The 721A test cavity was used for an experimental determination of the relation between window width and "g." This cavity is $2\frac{1}{16}$ inches inside diameter, and is coupled by means of windows to two $\frac{9}{16}$ diameter coaxial lines. The width of the windows may be adjusted by rotating the coaxial lines so as partially to close the openings. The insertion loss through the cavity was measured at 3100 mc. by means of a superheterodyne receiver which included a calibrated attenuator in its intermediate frequency section. The windows were carefully maintained geometrically equal. In this case,

$$g = \frac{T^{1/2}}{2(1 - T^{1/2})}$$

Digitized by Google
Original from UNIVERSITY OF MICHIGAN
Generated on 2019-09-22 07:08 GMT / http://hdl.handle.net/2027/mdp.39015077775156
Public Domain, Google-digitized / http://www.hathitrust.org/access_use#pd-google

which follows immediately from equation 23 of Appendix A on the assumption that $g_1 = g_2$. Fig. 38 shows the results; g proves to be proportional to the fifth power of the window width, over a very large range of values of g. A knowledge of this relationship permits one, with the aid of equations 23, 24, 25, 26, and 27 of Appendix A to calculate the window size

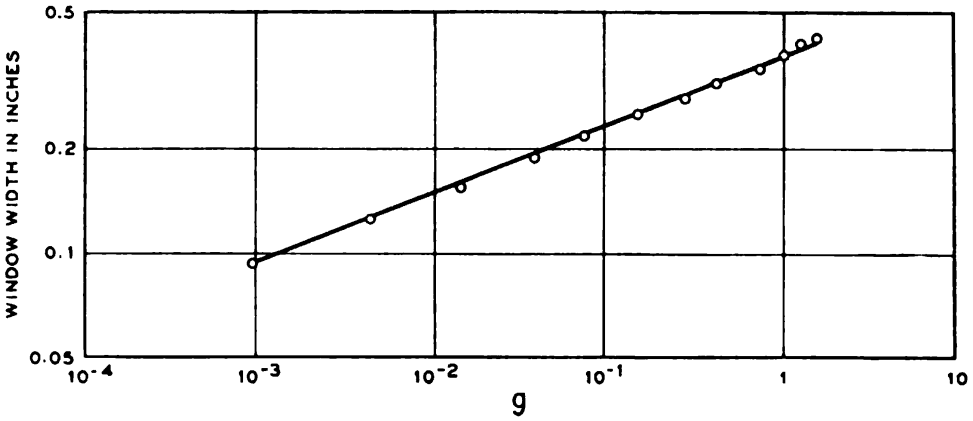

Fig. 38—The relationship between window conductance (g) and window width for the 721A test cavity

necessary to give any desired conditions of match, insertion loss, and leakage power.

APPENDIX C

The ATR Box

The value of the input impedance of the ATR is given by equation 29 with δ_2 equal to zero so that

$$Z = \frac{\delta_1}{j\left[\frac{\omega}{\omega_0} - \frac{\omega_0}{\omega}\right] + \delta_0} \tag{31}$$

which reduces to

$$Z = \frac{\delta_1}{\delta_0} \tag{32}$$

for the in tune case. This impedance is in series with the magnetron branch and hence restricts the possible range in values for the impedance at plane AB. Defining as F the fraction of the available power which is not absorbed by the ATR, then from Fig. 39 with the admittance of the receiver branch assumed to be $\delta_1 B$,

$$F = \frac{4}{(2 + G)^2 + B^2}, \tag{33}$$

Digitized by Google
Original from UNIVERSITY OF MICHIGAN
Generated on 2019-09-22 07:08 GMT / http://hdl.handle.net/2027/mdp.39015077775156
Public Domain, Google-digitized / http://www.hathitrust.org/access_use#pd-google

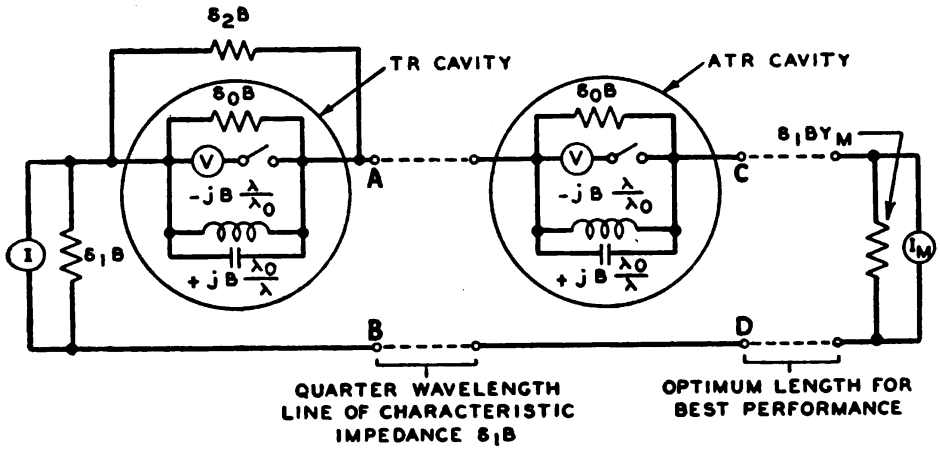

Fig. 39—Equivalent circuit of a system including an ATR

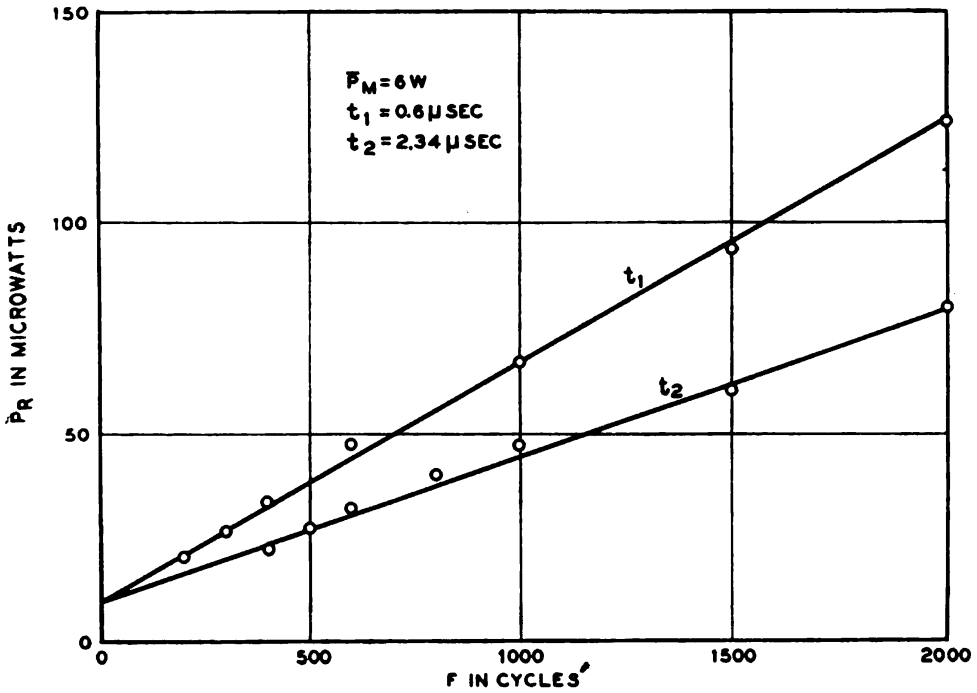

Fig. 40—Average leakage power as a function of repetition rate for two different values o pulse duration for 724B tube

where

$$G - jB = \frac{1}{(Z_m + Z)} \tag{34}$$

and Z_m is the impedance of the transmitter referred to the cavity and measured at the plane CD. The worst condition will occur when $Z_m = 0$. Under these conditions but assuming that the ATR is in tune

$$F = \frac{4}{(2 + G)^2}, \tag{35}$$

Digitized by Google
Original from UNIVERSITY OF MICHIGAN
Generated on 2019-09-22 07:08 GMT / http://hdl.handle.net/2027/mdp.39015077775156
Public Domain, Google-digitized / http://www.hathitrust.org/access_use#pd-google

But now G is the reciprocal of the Z of equation (32) so that

$$F = \frac{4\delta_1^2}{[2\delta_1 + \delta_0]^2}. \tag{36}$$

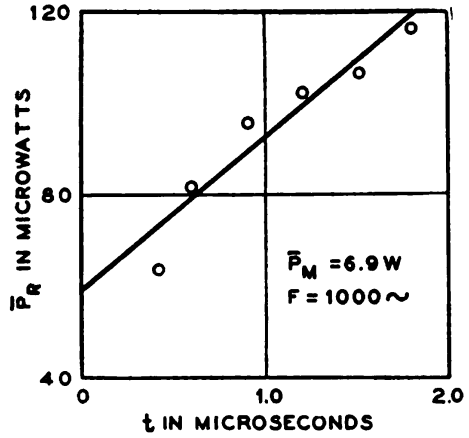

Fig. 41—Average leakage power as a function of pulse duration for the 724B tube

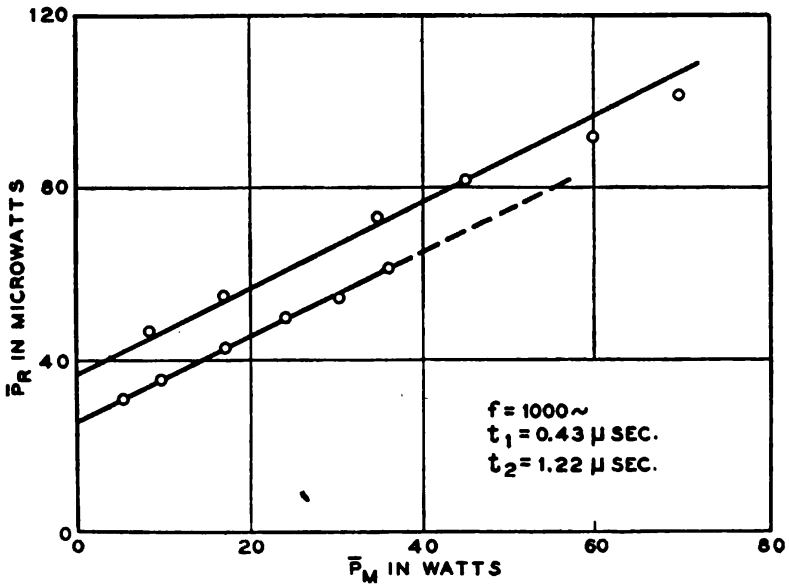

Fig. 42—Average leakage power as a function of average magnetron power for two different values of pulse duration for the 724B tube

This equation is analogous to equation (12) of Appendix A. At high levels the gas discharge power will be given by equation (19) as for the TR

$$P_g = [P\, P_0\, \delta_1]^{1/2} \tag{19}$$

Digitized by Google
Original from UNIVERSITY OF MICHIGAN
Generated on 2019-09-22 07:09 GMT / http://hdl.handle.net/2027/mdp.39015077775156
Public Domain, Google-digitized / http://www.hathitrust.org/access_use#pd-google

If the ATR and the TR are designed to have the same value of P_θ then the values of δ_1 and δ_0 must be the same so that a relationship will exist between F and T given by

$$F = \frac{4}{(3 - T)^2} \tag{37}$$

The input impedance Z to an ATR adjusted to the same gas discharge power of a TR with a transmission of T is given by

$$Z = \frac{1}{1 - T}. \tag{38}$$

APPENDIX D

The Analysis of Leakage Power Data

The section on receiver protection described the three components of leakage power which were referred to as spike, flat, and direct coupling. One may write down at once the following simple expression for leakage power:

$$\bar{P}_R = E_s f + P_F t + \bar{P}_M T_D \tag{39}$$

where $\bar{P}_R$ is average leakage power
E_s is energy in a single spike
f is pulse repetition frequency
P_F is flat power
t is pulse duration
$\bar{P}_M$ is average magnetron power (averaged over the recurrence period) and
T_D is direct coupling insertion loss.

Experimental curves verifying the linear relationships indicated by this simple equation are shown in Figs. 40, 41, and 42. It is a straightforward operation to deduce numerical values for the three TR box leakage parameters from the slopes and intercepts of these curves.

Equation (39) was written on the assumption that gas-limited flat power and direct coupling power add linearly. If instead we assume that a phase angle θ exists between the two currents, we find:

$$\bar{P}_R = E_s f + P_F t + T_D \bar{P}_M + 2\sqrt{P_F t T_D \bar{P}_M} \cos\theta \tag{40}$$

This of course is identical with equation (39) except for the cos θ term. If cos θ is not zero, we no longer expect a linear variation of $\bar{P}_R$ with f, t, or $\bar{P}_M$; the experimental curves demonstrate quite clearly that cos θ must vanish, hence θ must equal 90°.

Generated on 2019-09-22 07:09 GMT / http://hdl.handle.net/2027/mdp.39015077775156
Public Domain, Google-digitized / http://www.hathitrust.org/access_use#pd-google
Digitized by Google
Original from UNIVERSITY OF MICHIGAN

The Radar Receiver

By L. W. MORRISON, JR.

Introduction

THE spectacular development of radar during World War II remains an outstanding achievement in the history of communications and the allied electronic sciences. With military necessity furnishing the required driving force and through the full interchange of technical knowledge among all interested workers in this field, it has been possible to extend our visual senses far beyond the horizons considered quite inelastic only a few years ago. The potentialities of radar in the peacetime world and the future application of radar design principles and techniques to the communications and allied fields justify a review of some further details of this wartime development.

The performance and design aspects of radar receivers will be considered in this paper. For this purpose, the radar receiver will be defined as that assemblage of components within the radar system which is required to detect, amplify, and present the desired information as gathered at the radar location. The input signals to the radar receiver consist of radio-frequency pulses containing information regarding the area under observation by the radar system, together with coordinate data defining further characteristics of this observed area. The output of the radar receiver is most commonly an optical presentation of this composite information, but in certain applications the output is further converted into electrical or mechanical signals for specific use. In general, the output of a radar receiver is presented in a form capable of immediate analysis and use.

Though the functional boundaries of the radar receiver are by the above definition quite distinct, the exact detailed composition of the receiver and the specific component designs are influenced by a considerable number of factors. The successful performance of a radar receiver is dependent to a large degree on the nicety with which these individual components are assembled into the system as a whole.

A study of the principal factors which influence the design of the radar receiver is presented in the following sections, followed by a more detailed exposition of the principal design aspects of the various components associated within the receiver. Illustrative equipment descriptions are included

Digitized by Google
Original from UNIVERSITY OF MICHIGAN
Generated on 2019-09-22 07:11 GMT / http://hdl.handle.net/2027/mdp.39015077775156
Public Domain, Google-digitized / http://www.hathitrust.org/access_use#pd-google

where military security permits. All of the specific equipment examples presented here have been chosen from radar systems that have been developed within the Bell Telephone Laboratories and manufactured for the services by the Western Electric Company. This latter limitation excludes many interesting experimental developments which have not been produced in quantity and which have not, therefore, been substantially employed by the services during the war period.

It should be observed that the rapid development and successful employment of radar systems during World War II have come about through the cooperation and coordination of various governmental and military agencies, many research and development organizations, and countless individual workers. It is, therefore, an impossible task to assign individual credit for the details of the development which is here described. Radar has reached its present state of development through the efforts of many, not only those employed specifically on radar projects during the war years, but also those technical workers in the communications and allied fields in the years prior to the war who so adequately supplied the firm basic foundation upon which to build.

1. Radar Receiver Design Considerations

1.1 *The Military Radar System*

The specific use and area of operation of the radar system are two basic factors which exercise a profound influence on the receiver design. It is, therefore, pertinent to consider some common classifications of radar systems as employed during the war years.

A convenient functional classification of military radar systems may be made as follows:

A. *Search or Navigation*

This classification may include warning of the presence of enemy surface vessels or aircraft, navigation by location of landmarks, and reconnaissance.

B. *Missile Control*

This function includes radar systems to control gunfire and release bombs or missiles.

C. *Aircraft Interception*

This classification may be considered as an airborne combination of search and missile control, but is separated here because of the special radar design problems encountered.

As the detailed electrical performance requirements are primarily in-

Digitized by Google
Original from UNIVERSITY OF MICHIGAN
Generated on 2019-09-22 07:11 GMT / http://hdl.handle.net/2027/mdp.39015077775156
Public Domain, Google-digitized / http://www.hathitrust.org/access_use#pd-google

fluenced by the above functional classification of radar systems, the mechanical equipment design or arrangement is likewise considerably influenced by the area of use of the radar system. As an illustration of this factor, radar systems may be alternatively classified according to the area of operation as follows:

A. *Ground Equipment*

The equipment design of a ground radar system must include provisions for portability, protection against damage in movement over rough terrain, and for operation under extreme weather conditions.

B. *Naval Surface Vessel Equipment*

Radar equipment employed on surface vessels is subject to extreme atmospheric corrosive conditions, severe shock from gunfire and, in some cases, partial immersion in sea water. Large naval vessel installations often involve extreme distances between the location of the various components of the radar system.

C. *Airborne Equipment*

Mechanical equipment features for aircraft use must include provision for operation over rapidly fluctuating conditions of temperature and atmospheric pressure. Vibration conditions coupled with strict weight requirements result in many additional problems from the equipment designer's standpoint.

Figures 1, 2, and 3 indicate typical radar equipments employed on the ground, sea, and air, some component designs of which will be reviewed in later sections of this paper.

1.2 *The Function of the Radar Receiver*

The basic function of a radar receiver is to translate and present the information received at the radar location in a desirable form. This requires that the receiver contain provisions to enable:

A. Conversion of the received signals, originally of a microwave frequency character, to signals in a frequency region more convenient to utilize.
B. Amplification of the extremely low energy signals as received to amplitudes useful to the observer.
C. Correlation of all other available pertinent data with the received microwave signals to allow determination of the complete coordinates and other desired characteristics of the target under observation.

Digitized by Google
Original from UNIVERSITY OF MICHIGAN
Generated on 2019-09-22 07:11 GMT / http://hdl.handle.net/2027/mdp.39015077775156
Public Domain, Google-digitized / http://www.hathitrust.org/access_use#pd-google

Fig. 1.—Radar Equipment—Mark 20. This mobile equipment operating at 1000 mc is employed for searchlight control purposes.

Digitized by Google
Original from UNIVERSITY OF MICHIGAN
Generated on 2019-09-22 07:11 GMT / http://hdl.handle.net/2027/mdp.39015077775156
Public Domain, Google-digitized / http://www.hathitrust.org/access_use#pd-google

D. Presentation of all desired information to the observer in a form capable of immediate analysis and use.

With these functional requirements in mind, it is in order to examine the character of the information available at the input and that required at the output terminals of a radar receiver.

1.21 *Characteristics of the Radar Receiver Input Signal*

In general, the signal radiated by the radar transmitting antenna and received by the receiving antenna consists of intermittent pulses of energy

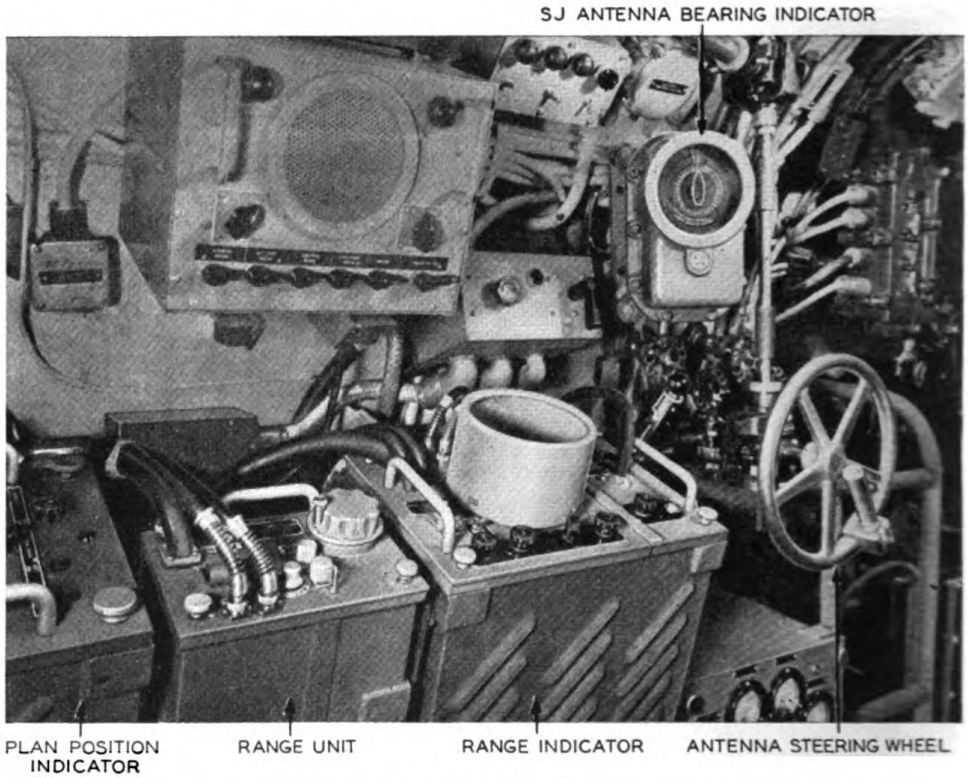

Fig. 2.—SJ Submarine Radar. Operating position of radar equipment in conning tower of U. S. Navy submarine.

at microwave frequencies. The methods employed in the generation and propagation of these radar microwave signals have been described elsewhere.[1, 2] For our purpose, it suffices to state that microwave frequencies extending from 700 mc to 10,000 mc are commonly employed. Pulse widths of 0.5 microsecond to 5 microseconds at repetition rates extending from 100 pps to 2000 pps are encountered in modern military radar systems, the

[1] "The Magnetron as a Generator of Centimeter Waves," J. B. Fisk, H. D. Hagstrum and P. L. Hartman. See pp. 56 ff.

[2] "Radar Antennas," H. T. Friis and W. D. Lewis. See pp. 763 f.

Digitized by Google
Original from UNIVERSITY OF MICHIGAN
Generated on 2019-09-22 07:11 GMT / http://hdl.handle.net/2027/mdp.39015077775156
Public Domain, Google-digitized / http://www.hathitrust.org/access_use#pd-google

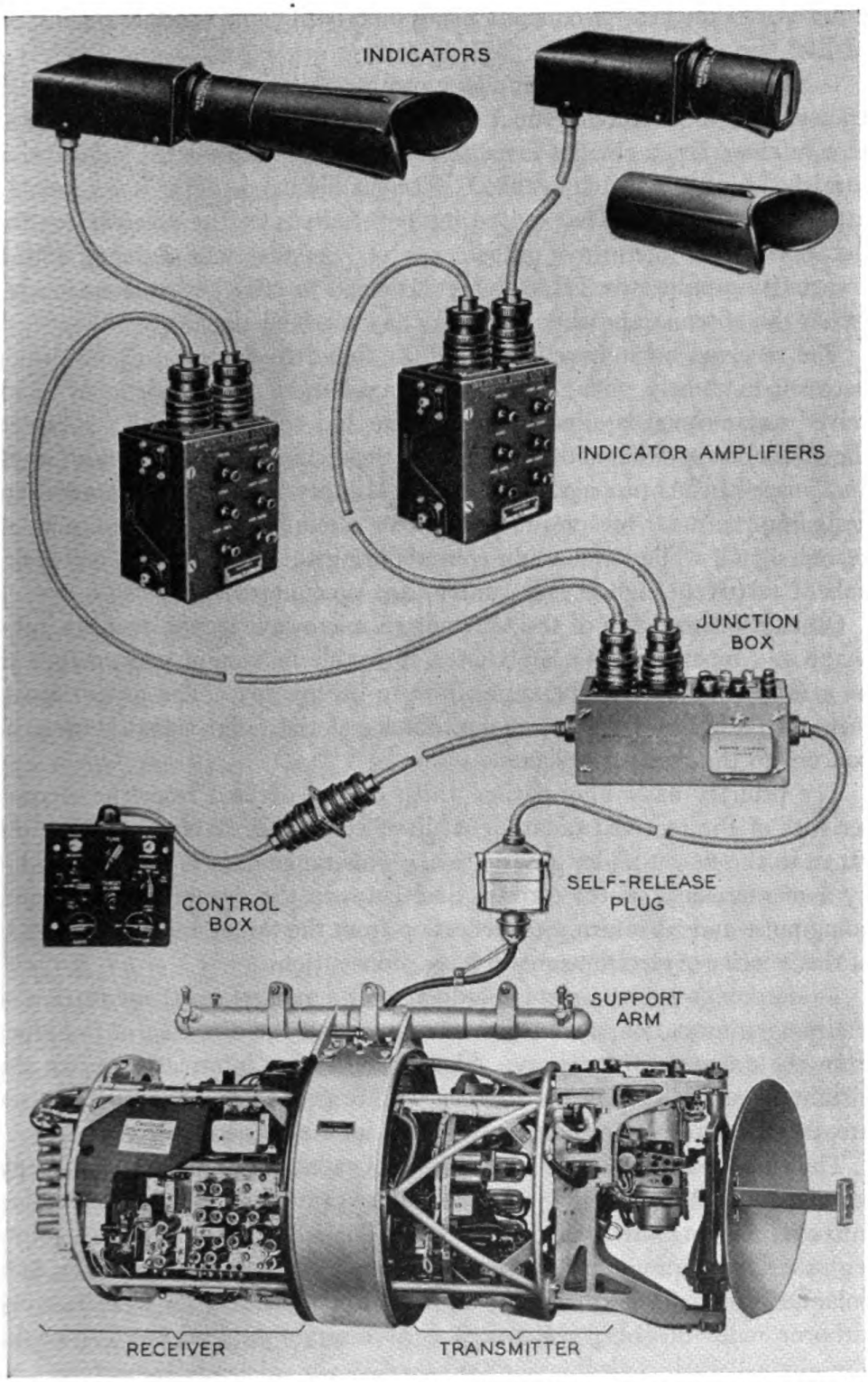

Fig. 3.—Components of Lightweight AN/APS-4. Airborne search and interception radar equipment.

Digitized by Google
Original from UNIVERSITY OF MICHIGAN
Generated on 2019-09-22 07:12 GMT / http://hdl.handle.net/2027/mdp.39015077775156
Public Domain, Google-digitized / http://www.hathitrust.org/access_use#pd-google

exact choice of these parameters being dictated by the specific application of each type of equipment.

It has been customary to employ a common antenna system for both the transmitting and receiving functions, the necessary protection of the sensitive receiver input circuits from the high power transmitted pulse being furnished by a TR switch or tube.[3] The gas discharge TR switch assembly attenuates the energy fed to the input terminals of the receiver for the duration of the microwave outgoing pulse. At the time of decay of this transmitting pulse, the TR switch is arranged to offer low attenuation between the antenna and the receiver to any received signal.

The received microwave signal will be found to fluctuate in amplitude between extremely wide limits. This amplitude characteristic of a received radar signal is affected by the size and composition of the target, the power of the radiated outgoing pulse, the distance or range to the target, and miscellaneous propagation effects. Military requirements necessitate designing the radar receiver to perform successfully with the minimum received signal, while not unduly compromising this performance when signals of relatively high energy content are encountered.

Other characteristics of the transmitted microwave signal, such as pulse shape and repetition rate, are chosen to enable maximum performance to be attained for the specific application to be covered. The proper treatment of these miscellaneous characteristics of the radar signal is of basic concern to the receiver designer.

The primary basic information which can be derived from the characteristics of the received radar signal itself consists of data concerning the range to the target under observation. This range data is made available by a measurement of the elapsed time between the departure of the outgoing pulse and its return after reflection from the target and consideration of the velocity of electromagnetic wave propagation.

To determine the complete coordinates of a radar target, correlation of the range information, as determined above, and the direction of radiation from the antenna is necessary. Signals containing information as to the instantaneous attitude of the antenna with respect to chosen reference axes are, therefore, to be considered as essential inputs to the radar receiver.

Though the natural coordinate system of radar is of a polar form, many specific applications of radar systems require conversion of this information into other forms more convenient of use. For example, while in gun-pointing radar applications, it is desirable to present the final information in a polar coordinate form, corresponding to the aiming axes of the guns in many airborne radar bombing systems, it is necessary that the presentation be

[3] "The Gas-Discharge Transmit-Receive Switch," A. L. Samuel, J. W. Clark and W. W. Mumford. See pp. 310 ff.

Digitized by Google
Original from UNIVERSITY OF MICHIGAN
Generated on 2019-09-22 07:12 GMT / http://hdl.handle.net/2027/mdp.39015077775156
Public Domain, Google-digitized / http://www.hathitrust.org/access_use#pd-google

made in terms of rectangular or other convenient coordinate systems referred to the ground itself. In certain applications, the characteristics of the display or presentation device requires that coordinate conversion functions be included within the radar receiver. The conversion and proper presentation of all radar system coordinate information will, therefore, be considered a necessary function of the radar receiver.

Additional forms of radar receiver input signals encountered are those primarily associated with the specific application of the radar system. Reference coordinate axes data obtained from compasses or gyroscopes are among the most common of these. In gun-fire control and bombing applications a considerable quantity of computed data must be accepted by the receiver. These data may include predicted quantities which must be presented in addition to the usual received present-time radar information. In the case of airborne radar systems, provision must be included to properly display navigational beacon and identification signals. The beacon is operated by the radar transmitter in the aircraft and returns a coded signal at a frequency slightly removed from the normal radar band. All aircraft radar receivers are required to adequately detect and properly display this information. It has also become common practice to require provision within the radar receiver for display of interrogator-response signals as employed for military identification purposes. The identification equipment (IFF) proper is not a radar system component and, therefore, it will not be considered here.

1.22 *Character of the Output of a Radar Receiver*

The output of a radar receiver is required to be available to the observer in a form which will permit immediate analysis and use of a maximum of the received information. The consideration of some additional characteristics of the radar information available and the military applications will furnish a basis for choice of presentation means in the receiver.

Because of the inherent pace of the constantly changing tactical military scene, the basic requirements imposed upon the radar presentation device are severe. For example, the use of radar in an aircraft, or on the ground or sea directed against aircraft involves a process of obtaining information on targets having relative velocities upward of 500 feet per second. If the radar system under consideration is being employed to furnish data for the release of bombs or to direct gunfire, a fraction of a second represents dimensions comparable to the target size. Such considerations adequately emphasize the extreme importance of retaining the "immediacy" characteristic of the information through the presentation device.

Another factor influencing the design of the presentation components in a radar receiver is found in consideration of the extreme complexity of the

Digitized by Google
Original from UNIVERSITY OF MICHIGAN
Generated on 2019-09-22 07:12 GMT / http://hdl.handle.net/2027/mdp.39015077775156
Public Domain, Google-digitized / http://www.hathitrust.org/access_use#pd-google

received radar information. This complexity is created out of the comparatively limited resolution available and from the military need for presentation of detailed information concerning large areas during small time intervals.

The effect of limited resolution on the choice of presentation means of a radar receiver can be appreciated by considering the following. The microwave pulse employed in modern radar systems has a duration in time corresponding in linear range dimensions of hundreds of feet, while the beam width of commonly employed radar antenna systems likewise includes hundreds of feet of target at useful ranges. Thus, the inherent radio-frequency "resolution" is limiting to an extent that, while it usually enables one to determine the coordinates of the centroid of the target, it will not furnish adequate information as regards the exact size or shape characteristics of the target. The radar response of an area of military interest is a function of electrical conductivity and other related characteristics, rather than of the military importance of the target. These factors indicate strongly that the human observer must be required to supply a certain function of interpretation, and that the chosen radar presentation means should be such that this is possible. An effective illustration of this situation is found in the descriptive term "navigation by constellation" which was common among the radar operators in the long-range bombing forces. Here the navigation to and the orientation with respect to the military objective was often possible only through the interpretation of strong radar responses from known landmarks. Offset bombing, where the bombing radar operator carried out his observations on a satisfactory radar target in the vicinity of the final objective and introduced the known offset coordinates in the computed release point so as to strike the military objective, was found to be a successful method of partially overcoming this basic limitation of World War II radar equipments.

Modern warfare is concerned with rapid movement and extremely large area operations. The display of continuous information regarding these large areas is a basic military requirement of the modern radar system. For specific military applications the radar viewpoint may often be restricted to selected limited areas with increased demands on detail and on reproduction of changing information during small time intervals.

The above considerations have led to a choice of presentation means for the military radar system which is of an optical nature and has the essential characteristics of motion pictures. Such a display of complex information, in general, allows the observer to concentrate his attention at any time on any desired region of interest, to orient himself with respect to the broad features of the complete area, and to be cognizant of changes in the scene as they occur.

Digitized by Google
Original from UNIVERSITY OF MICHIGAN
Generated on 2019-09-22 07:12 GMT / http://hdl.handle.net/2027/mdp.39015077775156
Public Domain, Google-digitized / http://www.hathitrust.org/access_use#pd-google

The cathode-ray tube has been most universally employed as the display device in the modern radar system. The incoming electrical information from the various receiver inputs is here electronically converted into a visual form capable of being modified over small intervals of time as the change in the radar scene occurs. Multiple presentations having various map-scale factors are found in many modern radar systems to enable detailed examination of a small magnified target area, while retaining the ability to observe the broad area features at will.

The use of radar for the purpose of control of gunfire, release of bombs, or steering of a vessel or aircraft requires that essentially continuous coordinate information be transmitted from the radar observer to the device under his control. This is usually accomplished through the registration of mechanical or projected electronic markers upon the visual radar display, this process of successive alignment furnishing the required information to the controlled device. In the case where automatic means of maintaining coincidence between marker and target are employed it should be observed that the original selection of the target and the initial coincidence adjustment still remains a matter for interpretation on the part of the human operator, and here again the visual radar display form is desirable.

The presentation means of a radar receiver has, therefore, been chosen to allow complete display of the data as quickly as it is received and in a form most convenient to the understanding of the human operator. In a broad sense, the radar system output terminal conditions and requirements are similar to those encountered for any communication system i.e. to supply the human observer with all the information available to the system in a form which will permit maximum usefulness with a minimum of delay.

1.3 *Composition of the Radar Receiver*

For convenience in the discussion to follow, the generalized radar receiver will be partitioned as shown in Figure 4. This particular choice of component division is somewhat arbitrary, but is chosen because of its functional simplicity. Mechanical, and in some cases electrical, conditions encountered in any particular radar system design often indicate physical arrangements which will differ considerably from the arrangement illustrated.

The converter component of the radar receiver has, as its primary function, the conversion of the received microwave signal to an intermediate frequency region where further amplification and discrimination is possible. The converter consists of a beating oscillator operating in the microwave frequency region and a nonlinear element, which at the higher radar frequencies consists of a point-contact crystal element. At the lower radar

Digitized by Google
Original from UNIVERSITY OF MICHIGAN
Generated on 2019-09-22 07:13 GMT / http://hdl.handle.net/2027/mdp.39015077775156
Public Domain, Google-digitized / http://www.hathitrust.org/access_use#pd-google

frequencies it is customary to employ vacuum tube radio-frequency amplifiers preceding the converter element, and in these cases, similar vacuum tubes are employed as the nonlinear element. The output frequency of the converter commonly ranges from 30 mc to 100 mc. Because of the comparative difficulties experienced in the transmission of microwave energy over transmission lines or waveguides as contrasted with the problem at the lower intermediate frequency region, it is standard practice to locate the converter in close proximity to the antenna and transmitter portions of the radar system.

The intermediate frequency (IF) amplifier and associated second detector unit following the converter in Fig. 4 is required to obtain the necessary

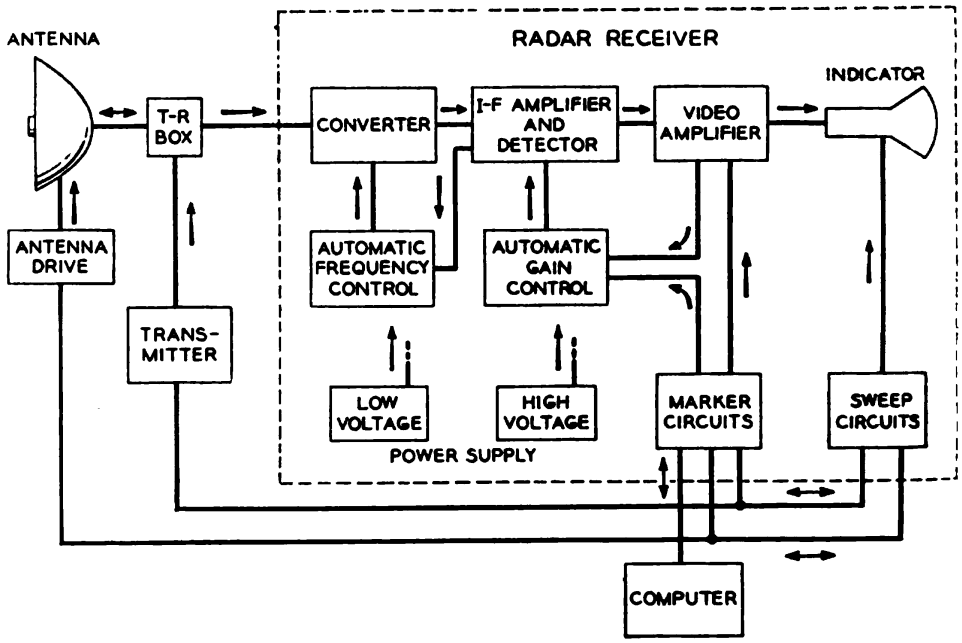

Fig. 4.—Schematic diagram of principal components of a military radar receiver.

amplification to the wanted signal, to supply discrimination against unwanted signals, and to finally convert the desired signal to a video form for presentation purposes. The usual gain required of a modern radar intermediate amplifier is of the order of 100 db. The band width of the IF amplifier is usually chosen between 1 mc and 10 mc depending on the specific radar system requirements. The techniques of construction developed for high gain radar IF amplifiers have resulted in compact component designs which are complete units in themselves, capable of being integrated into various radar systems.

The video amplifier characteristics are dependent to a large degree on the particular type of display system associated with it. Its primary func-

Digitized by Google
Original from UNIVERSITY OF MICHIGAN
Generated on 2019-09-22 07:13 GMT / http://hdl.handle.net/2027/mdp.39015077775156
Public Domain, Google-digitized / http://www.hathitrust.org/access_use#pd-google

tion is to amplify the video signal output of the second detector, together with some other signals to be impressed on the cathode-ray tube. In this field the principles of design follow closely those developed for television prior to the war. Band widths of the order of 1 mc to 5 mc are commonly employed and output voltages ranging from 10 volts to 250 volts are required by the cathode-ray tube. Controllable nonlinear amplitude-gain characteristics are occasionally included in these video circuits to enhance the contrast or improve the apparent signal-to-noise performance.

The display device universally employed in modern military radar systems is the cathode-ray tube. The electro-optical response characteristics of this device may be chosen over quite wide limits to suit the specific needs of a particular system. In slow scanning systems, use of long time-decay optical characteristics of the sensitive screen is found to be advantageous, while in other cases of high-speed scanning, shorter persistence-type screens are employed. Screen diameters commonly employed range from 2″ to 12″ with a wide variety of color characteristics available to fit the detailed requirement of the radar system. A variety of radar presentation forms are employed to display most conveniently the received information for the specific application at hand. These display types differ primarily in the manner in which the radar field coordinates are presented. The deflection methods employed may be of an electrostatic or magnetic nature with combinations of each occasionally encountered.

The sweep circuit components of the radar receiver generate the electrical time wave forms necessary to display the received data properly. Here again the television art has supplied a technical background for these specialized electronic circuits. The great number of display types employed, requiring varied wave forms, has resulted in the development of a myriad of specialized sweep circuits whose apparent complexity is the result of varied combinations of elemental electronic circuits.

The range and time-marker circuits are required to interpret the coordinate data available to the receiver and to prepare this data for display in the desired form. Here again, television techniques have been employed and enlarged upon as the radar systems became more complex. A large number of specialized electronic circuit forms has resulted.

The automatic frequency control (AFC) and automatic gain control (AGC) components of a radar receiver have a function not unlike those elements found in most radio-communication systems. The automatic adjustments of the tuning and gain of the radar receiver has contributed greatly to the successful employment of radar under practical military conditions and have now become practically indispensable in the art. The circuit designs follow, in general, the techniques previously employed in radio communications though it will be observed that the character of the signal

Digitized by Google
Original from UNIVERSITY OF MICHIGAN
Generated on 2019-09-22 07:13 GMT / http://hdl.handle.net/2027/mdp.39015077775156
Public Domain, Google-digitized / http://www.hathitrust.org/access_use#pd-google

and the close association of the receiver and the transmitter in the radar system introduces some additional new considerations.

The power supply components are shown divided into two types "low voltage" and "high voltage." This is a convenience which is desirable because of the different design problems encountered and the quite different equipment and circuits employed. The low d-c voltages required for the operation of the electronic components of a radar system vary from 100 volts to 500 volts with both polarities with respect to ground often required. The cathode-ray tube and "keep alive" circuits of the TR tube require voltages from 1000 to 7000 volts usually at low current. The voltage regulation of these power supply components to permit stable radar system operation under the extreme and variable military operating conditions encountered presents a problem of considerable magnitude to the radar receiver designer.

2. Radar Receiver Component Design

2.1 *The Radar Receiver Input Circuit*

The conversion of the received microwave radar signal to a lower frequency region where more efficient amplification is possible represents an extremely important function of the radar receiver. The basic military requirement of radar, that of providing the greatest possible useful sensitivity, depends fundamentally on the efficient handling of the low-energy microwave received signal in the input of the radar receiver. The microwave character of the received signal and the extremely low amplitudes encountered contribute to the difficulties of radar input circuit design.

The techniques of microwave transmission available to the communications engineer have but recently been developed and are at this time still extremely limited in comparison to those methods commonly employed at the normal radio frequencies. Even short physical connections required between elements in the microwave region become "electrically long," a matter of several wavelengths in the usual case, and here the design problem becomes acute. Network element of inductance, capcitance, and resistance are not available in the form so efficiently employed at the lower frequencies. Waveguides and cavities at radar frequencies replace them, and the design of selective frequency networks in the microwave region becomes a matter of precise arrangement and control of complex mechanical forms.

Suitable means for vacuum tube amplification at frequencies above 1000 mc have not been available to date; this represents another extremely restricting situation for the radar receiver designer.

Generated on 2019-09-22 07:13 GMT / http://hdl.handle.net/2027/mdp.39015077775156
Public Domain, Google-digitized / http://www.hathitrust.org/access_use#pd-google
Digitized by Google
Original from UNIVERSITY OF MICHIGAN

2.11 *Input Signal Characteristics*

The low amplitude of the signal at the input terminals of the radar receiver requires that this signal be efficiently utilized. The power of the received signal at this point under somewhat idealized free space assumptions is given by the following:

$$P_R = \frac{G^2 P A_e^2}{16\pi^3 D^4}$$

Where G = Power gain of common transmitting and receiving antenna
P = Transmitted power of radar system
$A\epsilon$ = Equivalent flat plate area of target (This represents an equivalent flat plate normal to the incident beam which reradiates all impinging energy)
D = Range to the target.

The two following sample computations are illustrative of the military radar system conditions:

1. Naval Vessel Search Radar System
   Frequency = 3000 mc
   Target range = 25 nautical miles
   Target-Destroyer (Effective flat plate area = 0.03 sq meter at 3000 mc)
   (This value has been determined from a study of target response with military radar systems)
   Power gain of Antenna = 30 db
   Transmitter Peak Power = 100 kw
   Received Peak Power = 13×10^{-14} watts
2. Airborne Search Radar System
   Frequency = 10,000 mc
   Target Range = 70 nautical miles
   Target-Destroyer (Effective flat plate area = 0.2 sq meters at 10,000 mc)
   Power Gain of Antenna = 30 db
   Transmitter Peak Power = 100 kw
   Received Peak Power = 11×10^{-14} watts

A reduction of the available received signal power, as computed above, is to be expected in practice due to multiple path effects and absorption and refraction effects over the propagation path.

2.12 *Input Circuit Noise Considerations*

While it is possible to conceive of providing sufficient gain within a radar receiver to meet any desired sensitivity requirement, this sensitivity cannot usefully be employed beyond certain limits as determined by the amplitude

Digitized by Google
Original from UNIVERSITY OF MICHIGAN
Generated on 2019-09-22 07:13 GMT / http://hdl.handle.net/2027/mdp.39015077775156
Public Domain, Google-digitized / http://www.hathitrust.org/access_use#pd-google

of the noise disturbances at the input terminals of the receiver. Noise disturbances may be defined as the resultant unwanted interfering electrical energy at the point under consideration and includes contributions due to atmospheric disturbances, unwanted radiation from adjacent electrical equipment, microphonic disturbances, and noise due to vacuum tubes and thermal agitation. At microwave frequencies we are usually concerned only with the thermal agitation and tube noise contribution. Atmospheric disturbances at radar frequencies are negligible and microphonic and electrical interferences from adjacent electrical equipment can, by proper and sufficient engineering, be reduced to any desired level.

It has been shown[4,5] that the thermal noise (Johnson noise) voltage which appears at the input terminals of a radio or radar receiver is determined by the value of the resistance component of the generator impedance at this point. For maximum transfer of signal power the load termination is required to be equal to the internal impedance of the generator and for this condition the total thermal noise power delivered to the load is given by

$$P_N = KTB \text{ (watts)}$$

where:

K = Boltzman's constant = 1.38×10^{-23} Joule/degree abs.

T = Absolute temperature in degrees

B = Bandwidth under consideration in cycles per second; and the signal-to-noise ratio is given by

$$\frac{P_S}{P_N} = \frac{P_S}{KTB} \text{ (a numeric)}$$

where P_S = maximum available signal power.

If the signal generator referred to is followed by any 4-terminal network representative of a converter element, an amplifier, or a passive network, the effective signal-to-noise ratio at the output terminals of the network will be modified. To obtain a measure of this effect we may assign a figure of merit, F, to the network called the "noise figure" of the network and define this as the ratio of the available signal-to-noise ratio at the signal generator terminals to the available signal-to-noise ratio at the output terminal of the network.

This may be written as:

$$F = \frac{P_S}{P_N} \frac{P_{S_2}}{P_{N_2}} = \frac{P_{N_2}}{KTBG} \text{ (a numeric)}$$

[4] "The Absolute Sensitivity of Radio Receivers," D. O. North, *R. C. A. Review*, Vol. VI, January 1942.

[5] "Noise Figures of Radio Receivers," H. T. Friis, *Proc. I. R. E.*, Vol. 32, No. 7, July 1944.

Digitized by Google
Original from UNIVERSITY OF MICHIGAN
Generated on 2019-09-22 07:14 GMT / http://hdl.handle.net/2027/mdp.39015077775156
Public Domain, Google-digitized / http://www.hathitrust.org/access_use#pd-google

where:

$$G = \frac{P_{S_2}}{P_S}, \text{ by definition the "gain" of the network.}$$

or we may write:

$$P_{N_2} = FKTBG \text{ watts.}$$

It is common practice to express F in decibels given by the relation $10 \log_{10} F$.

For the case of two generalized networks in tandem following the signal generator and having the same effective bandwidth we may similarly write:

$$P_{n_{out}} = F_a G_a G_b KTB + (F_b - 1) G_b KTB$$

$$= \left(F_a + \frac{F_b - 1}{G_a}\right) G_a G_b \, KTB \text{ watts.}$$

where the subscripts refer to networks a and b.

The effective noise figure of such a system is given by:

$$F_{system} = \left(F_a + \frac{F_b - 1}{G_a}\right)$$

This expression indicates the importance of the gain of the first network in the over-all system noise performance.

As an illustration, a noise figure of 11 db and a loss of 6 db may be considered as acceptable performance for a typical silicon crystal converter operating at 3000 mc. If the following input circuit of the IF amplifier has an effective noise performance represented by a noise figure of 5db , the over-all system noise figure will be found to be 13 db. The reduction in system performance due to the noise contribution of the input stage of the IF amplifier here is approximately 2 db. If the system performance must be improved by increasing the power of radiation, the importance of this secondary noise contribution is apparent.

A comparison of the noise figures of a point-contact crystal converter element and the GL-2C40 Lighthouse vacuum tube used as an amplifier and as a converter element is given in Fig. 5. At frequencies below 1000 mc there is a definite advantage in employing a vacuum tube as a radio-frequency (RF) amplifier preceding the nonlinear element.

2.13 *1000* MC *Radio-Frequency Amplifier Design*

In the design of military radar systems for the 1000 mc operating range the GL-2C40 vacuum tube has been employed rather universally in converter circuits.[6] The essential design features of this special purpose triode

[6] "The Lighthouse Tube," E. D. McArthur and E. F. Peterson, *Proc. of National Electronics Conference*, Vol. I, 1944.

Digitized by Google
Original from UNIVERSITY OF MICHIGAN
Generated on 2019-09-22 07:14 GMT / http://hdl.handle.net/2027/mdp.39015077775156
Public Domain, Google-digitized / http://www.hathitrust.org/access_use#pd-google

are illustrated in Fig. 6. The basic advantage of the GL-2C40 tube for use at high frequencies is found in its construction, whereby the tube elements are arranged to form an integral portion of the external circuit with a minimum of mechanical disturbance. At these frequencies external coupling circuits of the transmission line type are usually employed. This tube when operated at an anode potential of 250 volts has a mutual conductance of approximately 6000 micromhos and an amplification factor of 35. It has been customary to employ one or two stages of RF amplification associated

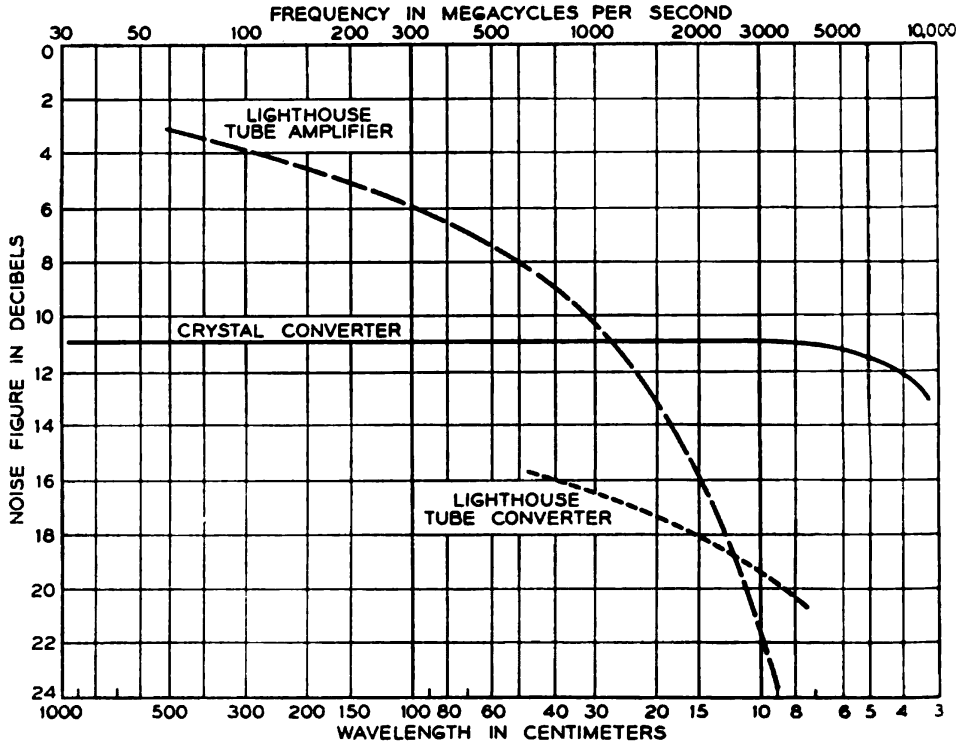
FREQUENCY IN MEGACYCLES PER SECOND
30 50 100 200 300 500 1000 2000 3000 5000 10,000
NOISE FIGURE IN DECIBELS
0 2 4 6 8 10 12 14 16 18 20 22 24
LIGHTHOUSE TUBE AMPLIFIER
CRYSTAL CONVERTER
LIGHTHOUSE TUBE CONVERTER
1000 500 300 200 150 100 80 60 40 30 20 15 10 8 6 5 4 3
WAVELENGTH IN CENTIMETERS

Fig. 5.—Comparison of noise figures for point-contact silicon crystal rectifier and GL2C40 vacuum tube.

with the nonlinear element and a beating oscillator using this same tube. The reduced performance of the GL-2C40 tube as a converter element as indicated in Fig. 5 is not of importance, if sufficient gain is provided prior to the actual conversion process, and the ability of this vacuum tube to operate at higher levels is a positive advantage.

The electrical circuit design techniques employed in this frequency region are based on the use of transmission line elements in place of the more or less orthodox lumped element configurations at the lower frequencies. The difficulties experienced in practical designs of radar converters of this type revolve about successfully terminating and satisfactorily isolating each stage so that confusing and inefficient interaction effects are minimized.

Digitized by Google
Original from UNIVERSITY OF MICHIGAN
Generated on 2019-09-22 07:14 GMT / http://hdl.handle.net/2027/mdp.39015077775156
Public Domain, Google-digitized / http://www.hathitrust.org/access_use#pd-google

The simplified schematic of a typical radio-frequency amplifier which employs a GL-2C40 vacuum tube operating at approximately 1000 mc is given in Fig. 7, together with an outline of the mechanical arrangement of the tuning elements. This amplifier is of the tuned-grid, tuned-plate type

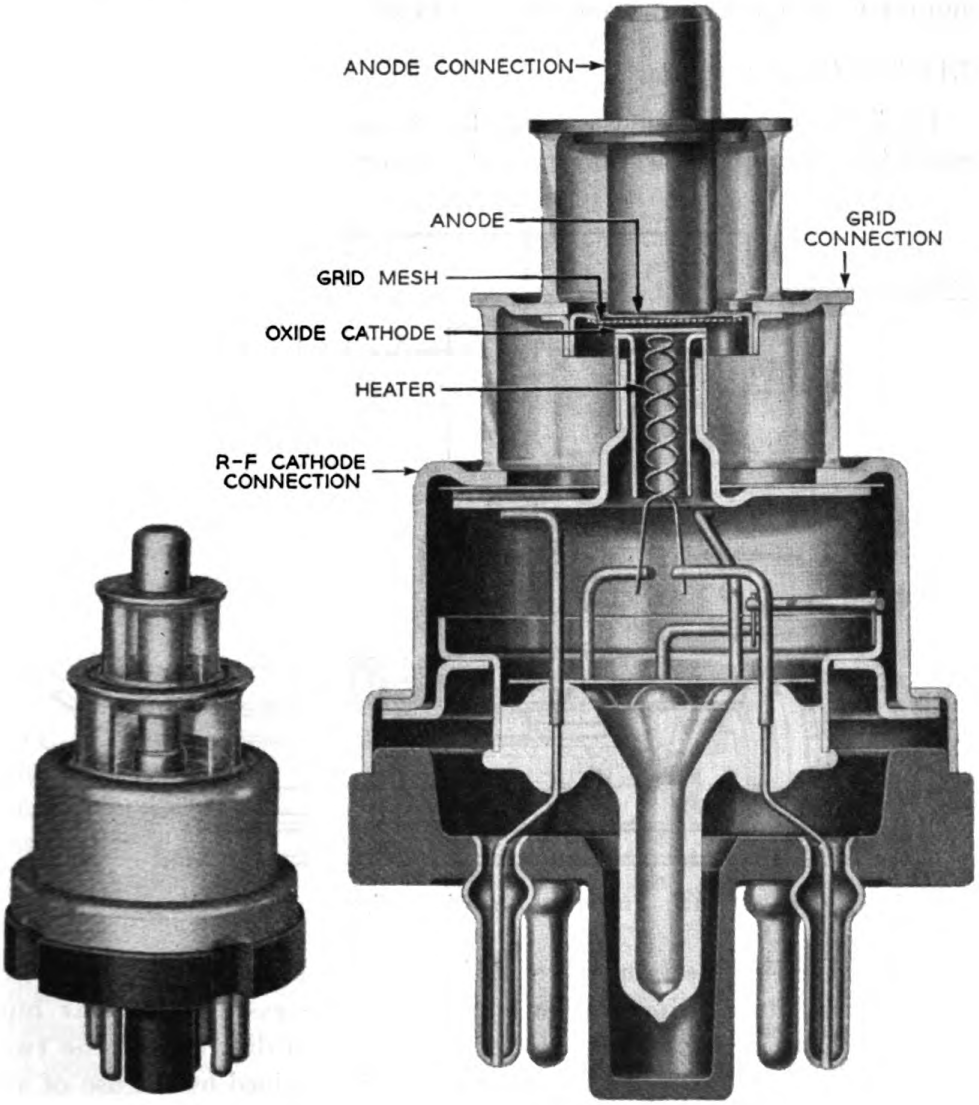

Fig. 6.—Constructional Features of the GL-2C40 (Lighthouse) vacuum tube.

of circuit where the input and output circuits consist of coaxial transmission line elements tuned by sliding plunger or ring elements, and is so constructed to include the GL-2C40 tube as an integral part of the tuning structure. The input coupling to the amplifier is achieved by means of a probe extend-

Digitized by Google
Original from UNIVERSITY OF MICHIGAN
Generated on 2019-09-22 07:14 GMT / http://hdl.handle.net/2027/mdp.39015077775156
Public Domain, Google-digitized / http://www.hathitrust.org/access_use#pd-google

ing into the input or grid cavity and is proportioned for operating out of a 50-ohm impedance cable connection to the radar antenna system. The output coupling is obtained from a coupling loop located in the region between the grid and plate concentric sleeves. The gain of this RF amplifier design is 12 db when operating at a frequency of approximately 1000 mc and the noise figure of this component is 14 db.

2.14 *The Radar Converter*

The basic converter is illustrated in Fig. 8 and may be defined as a device which has two input pairs and one output pair of terminals and is charac-

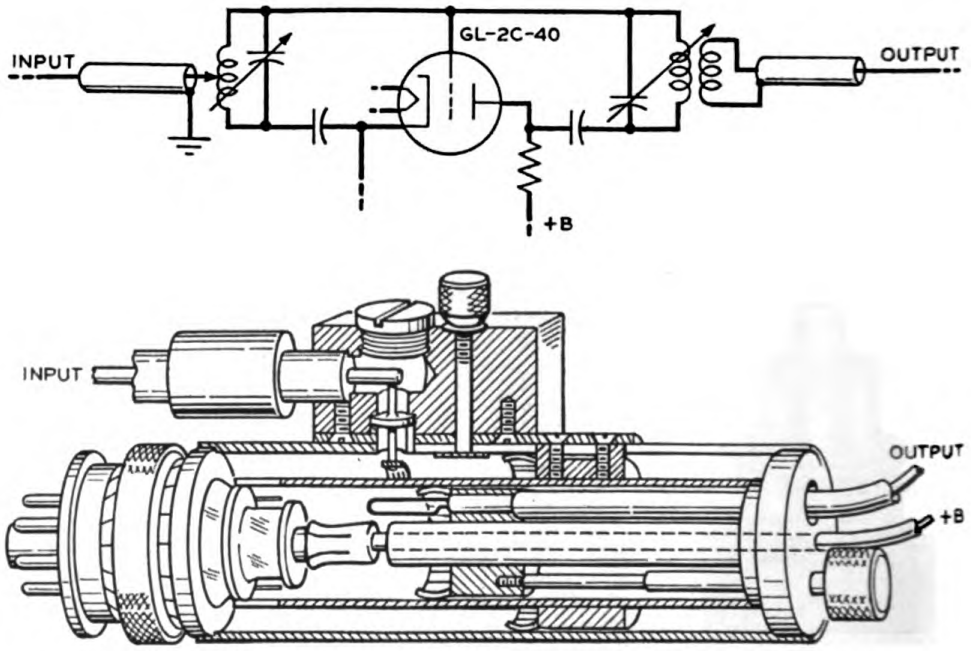

Fig. 7.—1000-mc Radio Frequency Amplifier. Simplified schematic diagram.

terized further by the property of delivering an output signal, which, in terms of amplitude of one of the input signals, is essentially linear but which has an output frequency related to the sum or difference of the two input frequencies. This frequency conversion is obtained by the use of an element which has a nonlinear voltage-current relationship and upon which is impressed the two input signals. The desired sum or difference frequency signal is then selected and utilized as the wanted signal output.

The basic configuration of the converter shown in Fig. 8 employs a nonlinear element with network coupling means to provide efficient transfer of signal power into and out of the component and a beating oscillator with its associated coupling network to supply the required additional input fre-

Digitized by Google
Original from UNIVERSITY OF MICHIGAN
Generated on 2019-09-22 07:14 GMT / http://hdl.handle.net/2027/mdp.39015077775156
Public Domain, Google-digitized / http://www.hathitrust.org/access_use#pd-google

quency. One or more of the networks involved may, of course, be arranged alternatively in a parallel configuration if desired. The nonlinear element may be a vacuum tube with properly chosen operating conditions or a point-contact silicon crystal rectifier. The beating oscillator in the modern military radar converter employs special types of vacuum tubes such as the GL-2C40 type previously mentioned or the single-cavity velocity modulated types[7] at the higher radar frequencies.

A typical voltage-current characteristic of a point-contact silicon rectifier is shown in Fig. 9. This nonlinear characteristic may be expressed mathematically as a power series with coefficients whose amplitude decreases quite rapidly with the order of the associated term. If two sinusoidal voltages represented by frequency f_1 and f_2 are simultaneously impressed

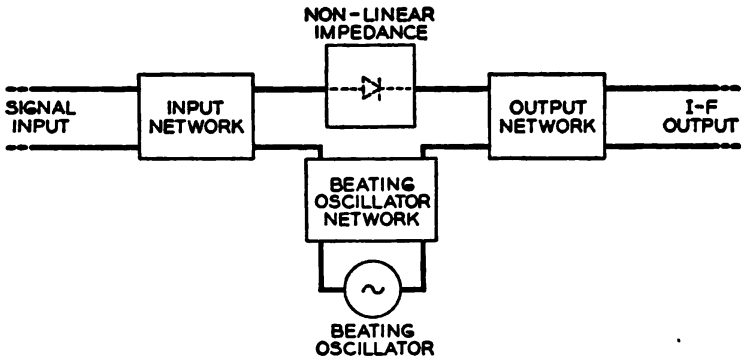

Fig. 8.—Basic configuration of a radar converter.

upon such a nonlinear element, the resultant current flowing in the output impedance will produce output signals of the form $nf_1 \pm mf_2$ where n and m are integers including zero. The effective amplitude of each of these modulation products is related to the magnitude of the power series coefficients. In the radar converter under consideration f_1 may represent the received signal frequency and f_2 represents the beat oscillator frequency. The difference terms of the above expression are of the greatest importance here because the desired output signal frequency has been chosen at a low value as compared with the input received radar signal. The selection of the wanted first-order difference term is accomplished by the frequency selectivity characteristics of the converter output coupling network and the following IF amplifier.

A major design problem encountered in the practical development of microwave radar converters is one concerning the design of the coupling networks. The previously referred to limitations of microwave network

[7] "Reflex Oscillators," J. R. Pierce and W. G. Shepherd. See pp. 488 ff.

Digitized by Google
Original from UNIVERSITY OF MICHIGAN
Generated on 2019-09-22 07:14 GMT / http://hdl.handle.net/2027/mdp.39015077775156
Public Domain, Google-digitized / http://www.hathitrust.org/access_use#pd-google

techniques and the difficulty in maintaining precise control of each element over the required band of frequencies are the fundamental problems of the radar converter designer. The network problem here is concerned with realizing the desired frequency conversion with a minimum of dissipation of the useful signal. This implies that coupling of the nonlinear element to the input and output terminals must be achieved in such a fashion that matched impedance conditions result for the signals in their respective frequency regions. Since the output signal has been shown to appear as a

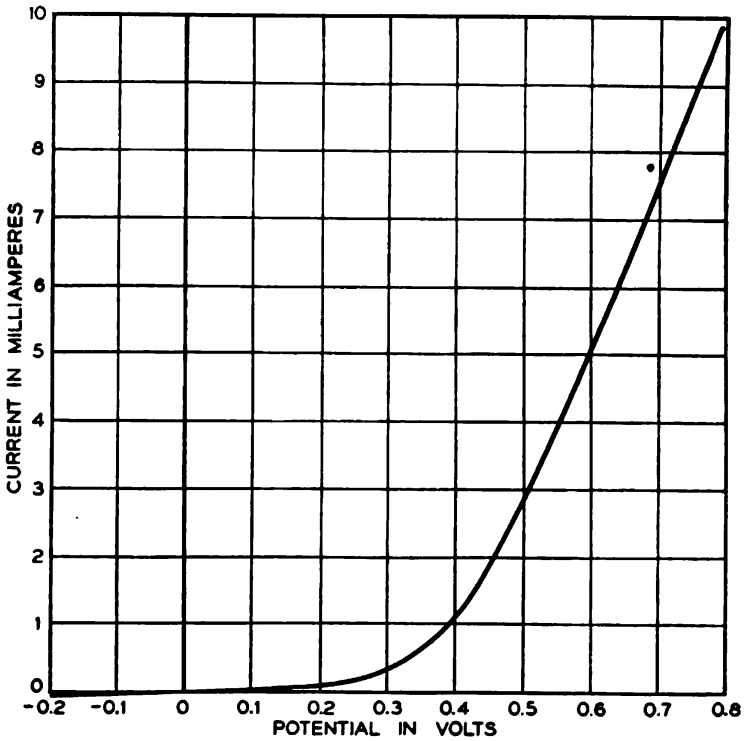

Fig. 9.—Typical voltage-current characteristic of a point-contact silicon crystal rectifier.

number of energy concentrations extending over a wide frequency range, it would appear that an efficient design of output coupling network would involve optimizing the impedance relationships over this wide-frequency band. Several factors tend to simplify this problem by restricting the output frequency band which must be considered in a practical radar converter design. First, the greatest amount of energy is found to be present in the lower order modulation products because of the rapid reduction in amplitude of the higher order terms in the equivalent expression for the nonlinear element. This results in a concentration of energy at the input, output, and beat oscillator frequencies and their respective second harmonic regions. Second, the ratio of f_1 to f_2 in a microwave radar converter is of necessity

Digitized by Google
Original from UNIVERSITY OF MICHIGAN
Generated on 2019-09-22 07:15 GMT / http://hdl.handle.net/2027/mdp.39015077775156
Public Domain, Google-digitized / http://www.hathitrust.org/access_use#pd-google

essentially equal to one, this factor also contributing to a narrowing of the frequency regions of interest to those around the input, the beat oscillator, and the output values. The third factor, which is of assistance to the converter designer, is the effective separation of the input and output circuits by the loss of the nonlinear element. Where a vacuum tube is employed as the nonlinear element, the interaction of these circuits may be made quite negligible and, in the case of the crystal rectifier the inherent loss of this element, which may be of the order of 6 db and undesirable from a radar system performance standpoint, does simplify the converter network design.

It has been found in practice that it is sufficient to consider the impedance conditions at the internal terminals of the converter networks in the frequency regions which include $f_1, f_1 - f_2, f_1 + f_2$ and $2f_2 - f_1$.

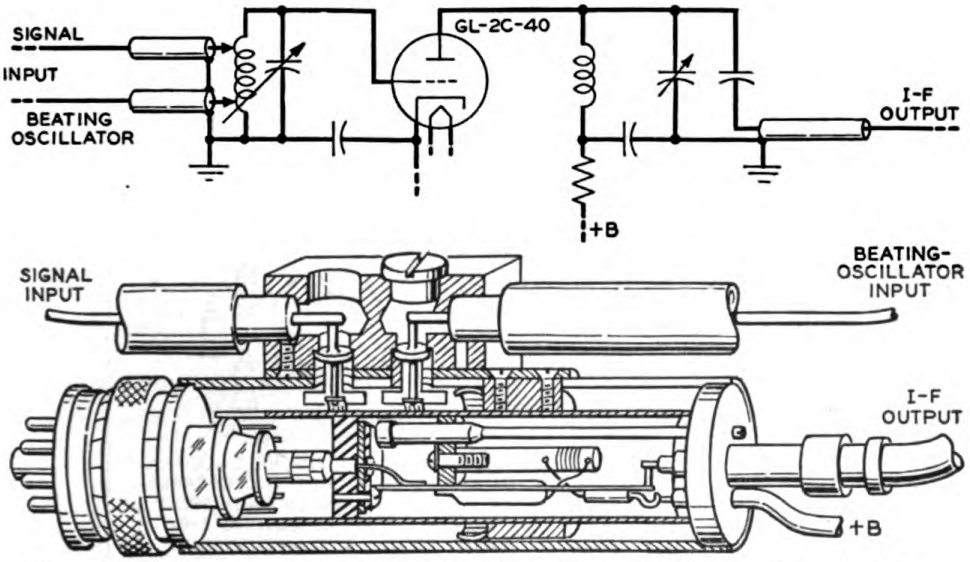

Fig. 10.—1000-mc Vacuum Tube Radar Converter. Simplified schematic diagram.

The matter of efficient transfer of power from the local beating oscillator to the nonlinear element is of secondary importance generally because of the relatively large amount of power available. This condition is advantageous allowing mismatch loss in this branch to effectively minimize the unwanted interaction effects with input and output circuits.

Figure 10 illustrates the schematic and certain constructional features of a vacuum-tube converter which has an operating frequency of approximately 1000 mc. The similarity of circuit and mechanical arrangement to that of the radio-frequency amplifier unit, shown in Fig. 7, is apparent. In the case of the GL-2C40 converter the two input frequencies are similarly probe coupled to the grid-cathode circuit, maintaining optimum impedance conditions for the signal input and locating the beat oscillator probe so as

Generated on 2019-09-22 07:15 GMT / http://hdl.handle.net/2027/mdp.39015077775156
Public Domain, Google-digitized / http://www.hathitrust.org/access_use#pd-google
Digitized by Google
Original from UNIVERSITY OF MICHIGAN

to effect an impedance mismatch and thus reduce the interaction between this circuit and the input circuit. The output coupling network, in this case operating at 60 mc, consists of an inductive impedance tuned with a variable condenser. The output of this converter is fed into the following IF amplifier by means of a 75-ohm coaxial transmission line. The loss of this converter unit, defined as the ratio of the power of the wanted 60-mc output signal to the signal power impressed upon the input terminal, is

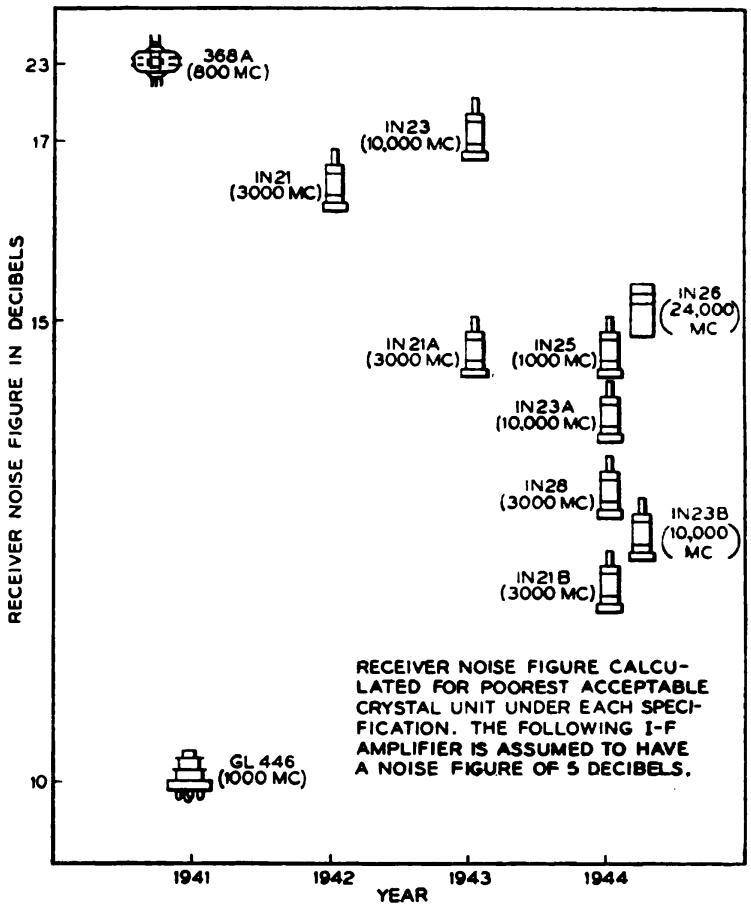

Fig. 11.—Chronological development of point-contact silicon crystal rectifiers and associated receiver noise performance.

approximately 6 db. The noise figure of a typical unit of this type is approximately 20 db, this value being of secondary importance since sufficient gain is provided in the associated radio-frequency amplifier.

At the higher radar frequencies the noise performance characteristics of silicon crystal-point contact rectifiers are considerably better than that of vacuum tubes available during the past war years. Figure 11 outlines the chronological developments of these units with respect to the receiver noise

Digitized by Google
Original from UNIVERSITY OF MICHIGAN
Generated on 2019-09-22 07:15 GMT / http://hdl.handle.net/2027/mdp.39015077775156
Public Domain, Google-digitized / http://www.hathitrust.org/access_use#pd-google

performance. The performance of two types of vacuum tubes are included for comparison purposes. The development details of the silicon crystal unit have been discussed elsewhere.[8] This development, together with the corresponding magnetron and reflex oscillator studies, assumes a status of major importance in the progress of the development of military radar equipment during World War II, allowing the designers to extend the frequency of operation upward with increased system performance resulting.

It is sufficient to limit our attention to the frequency region 3000 mc and above in the consideration of the silicon crystal converter. It is apparent that the absence of suitable vacuum tube radio-frequency amplifiers in this region imposes a strict requirement on the efficiency of conversion of this component.

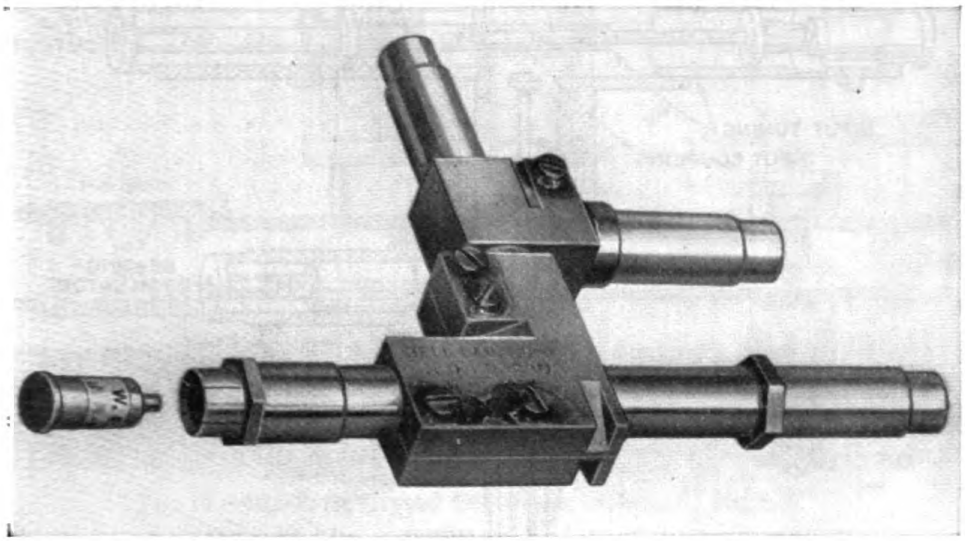

Fig. 12.—3000-mc Crystal Converter of an early design.

Historically, one of the first of the microwave converters of the silicon crystal type, operating at 3000 mc and which was employed in military radar equipment, is shown in Fig. 12 together with an illustration of the mechanical arrangement[9] in Fig. 13. In this early model the silicon crystal element was mounted in a cartridge type unit, a method which proved quite satisfactory and was followed for the remainder of the war years. The input tuning circuit of the converter here illustrated consists of a coaxial transmission line element having a length of approximately three-quarters of a wavelength and adjustable to enable fine control of tuning. The nonlinear ele-

[8] "Development of Silicon Crystal Rectifiers for Microwave Radar Receivers." See pp. 710 ff.

[9] "Microwave Converters," C. F. Edwards, To be published in a forthcoming issue of *Proceedings I.R.E.*

Digitized by Google
Original from UNIVERSITY OF MICHIGAN
Generated on 2019-09-22 07:15 GMT / http://hdl.handle.net/2027/mdp.39015077775156
Public Domain, Google-digitized / http://www.hathitrust.org/access_use#pd-google

ment is located at the high-impedance end of this transmission line, while the other end is essentially short-circuited at the input frequency by means of a small by-pass condenser element built into the IF output transmission line. The input line is coupled into this tuned circuit by means of a variable coupling probe and the local beat oscillator in turn is similarly coupled to the input line. The point of coupling of the beat frequency oscillator input is so arranged as to introduce an effective mismatch and thus provide adequate isolation of this and the input circuit. The output circuit of this converter includes the by-pass condenser previously referred to, together with the input transformer of the first IF amplifier stage. The average loss of a

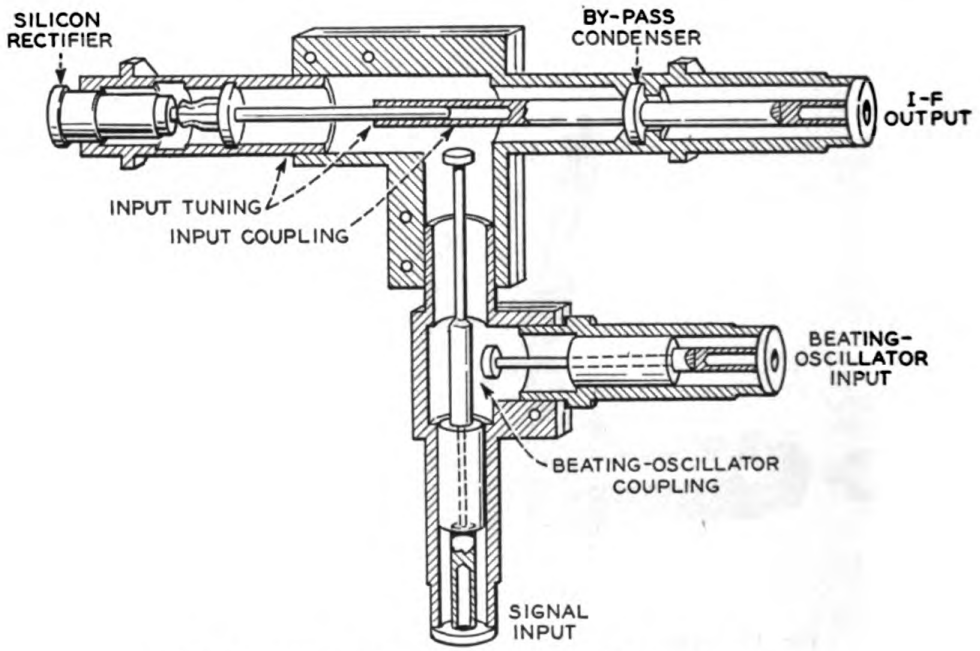

Fig. 13.—3000-mc Crystal Converter. Schematic diagram.

3000-mc crystal converter of this type was 6 db and a noise figure of 11 db was realized.

Another design of crystal converter which was developed during the early part of the war, and whose basic form was employed in many military radar equipments operating in the region of 10,000 mc, is shown in Fig. 14. Here the silicon crystal cartridge is positioned within the waveguide with its axis parallel to the E vector plane and at a point approximately one-quarter of a wavelength from the short circuiting piston which terminates this assembly. The IF output is obtained from the coaxial line mounting structure shown which offers a low impedance to the input frequency by virtue of its equivalence to a one-half wavelength element with a short circuit at the far end.

Generated on 2019-09-22 07:15 GMT / http://hdl.handle.net/2027/mdp.39015077775156
Public Domain, Google-digitized / http://www.hathitrust.org/access_use#pd-google
Digitized by Google
Original from UNIVERSITY OF MICHIGAN

The dielectric supporting rings shown form an RF by-pass element minimizing the loss of input signal power in the IF output network. In this design the beating oscillator energy is introduced into the waveguide by mounting the reflex oscillator tubes adjacent to the waveguide in such a fashion that the output probe is inserted into the waveguide cavity at a point removed by an odd one-quarter of a wavelength from the face of the TR output iris. This assures reflection of the local oscillator energy which travels toward the TR tube directing it toward the crystal element. The degree of coupling of the reflex oscillator circuit is varied by adjustment of the distance that the probe is inserted within the waveguide. For airborne applications an additional oscillator tube is included for beacon reception. This basic form

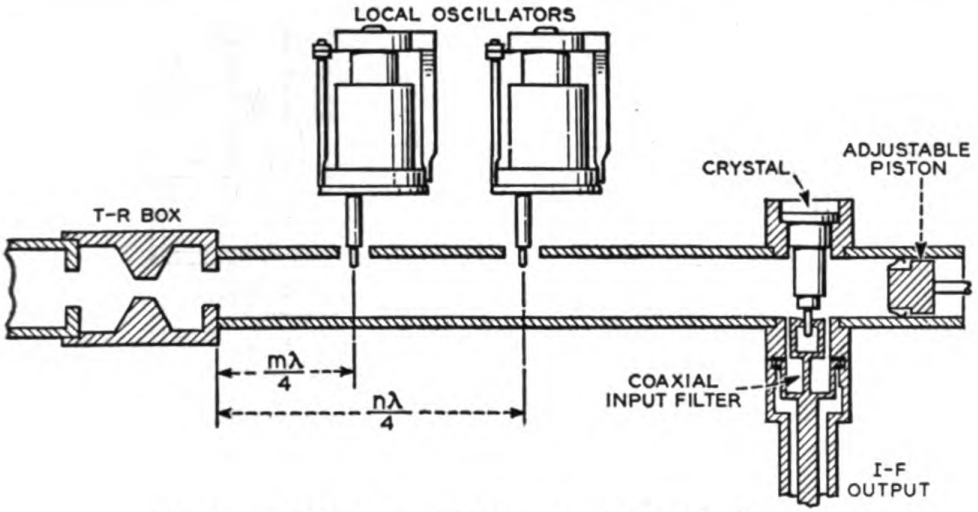

Fig. 14.—10,000-mc Crystal Converter. Schematic diagram.

of radar converter was employed in large numbers in the military airborne radar field during World War II.

A third type of crystal converter design which was developed in the latter period of the war is illustrated in Fig. 15. A basic difference in this structure is found in the use of a waveguide hybrid junction often referred to as a "magic tee." This junction has an electrical performance characteristic at microwaves similar to that of the hybrid coil common to low frequency communication circuits, i.e., a 4-pair terminal network with an internal configuration such that power applied to any one pair of terminals will appear equally at two other pairs of terminals, but will not be available at the remaining pair of terminals. Referring to Fig. 15, it should be noted that power applied to the input waveguide will appear equally in the output branches but is balanced out of the beat oscillator branch. In a similar fashion, the beat oscillator power will appear equally in the two output

Digitized by Google
Original from UNIVERSITY OF MICHIGAN
Generated on 2019-09-22 07:16 GMT / http://hdl.handle.net/2027/mdp.39015077775156
Public Domain, Google-digitized / http://www.hathitrust.org/access_use#pd-google

branches but will not appear in the input waveguide. Certain impedance matching adjustments are obtained through the use of the matching rods positioned as shown.

The method of insertion of the crystal cartridge into the waveguide in this

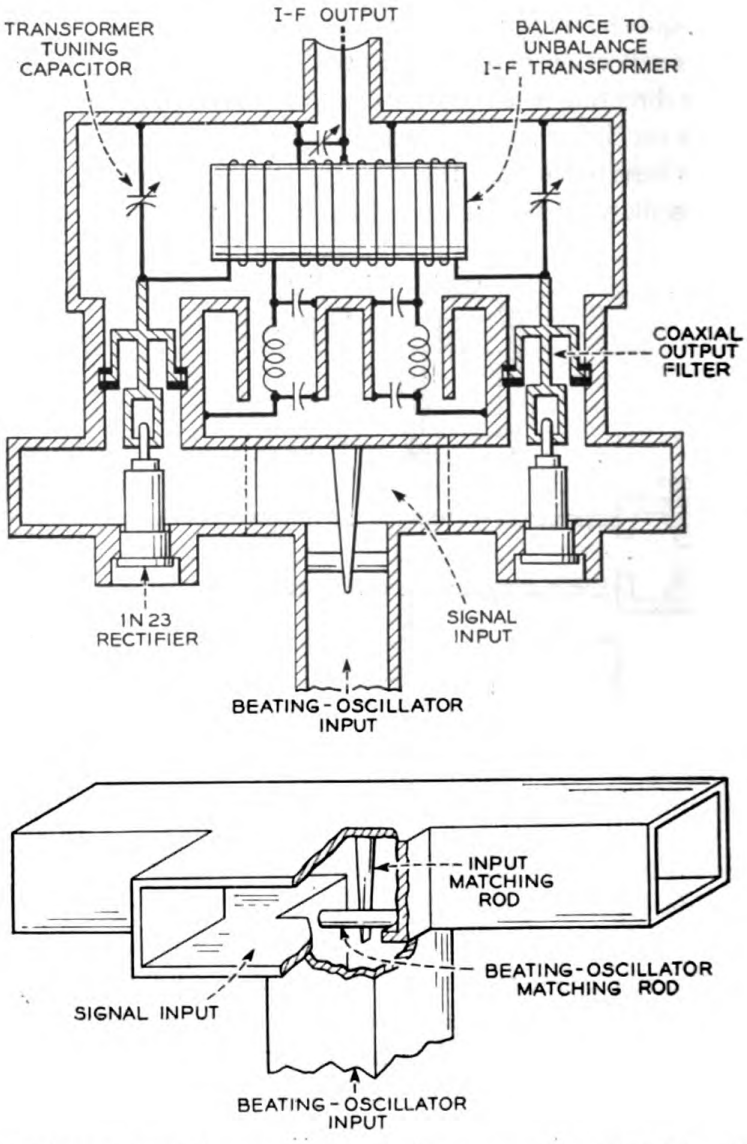

Fig. 15.—Balanced crystal converter employing wave-guide hybrid junction.

design follows the scheme employed in the converter just described. However, here two crystal elements are employed in a balanced form which necessitates a balanced-to-unbalanced impedance transformation of the IF output signal for transmission over a coaxial line to the input stage of the IF amplifier. The degree of balance obtainable here is necessarily a func-

Digitized by Google
Original from UNIVERSITY OF MICHIGAN
Generated on 2019-09-22 07:16 GMT / http://hdl.handle.net/2027/mdp.39015077775156
Public Domain, Google-digitized / http://www.hathitrust.org/access_use#pd-google

tion of the similarity of the crystal elements as well as the other elements shown. In practice, no particular difficulty was experienced in maintenance of sufficient balance with the improved production control of crystals during the latter part of the war program.

The advantages of the balanced radar converter here described are twofold. First, the signal power dissipation in the beating oscillator branch is reduced to a minimum and conversely the beating oscillator power fed back into the antenna and reradiated is reduced. Second, the noise sidebands, which are associated with the output frequency of the reflex oscillator, are reduced effectively in the IF output branch by the degree of balance available. This local oscillator noise sideband contribution is normally responsible for a definite degradation of the over-all radar receiver noise performance and hence, the use of a balanced converter will contribute to improved performance. An additional advantage of the balanced converter is the minimizing of signal branch impedance variation effects on the beating oscillator load impedance and, therefore, its frequency. The variation of the antenna impedance during the scanning cycle has in this design little effect on the tuning of the receiver.

2.15 *The Radar Receiver Beat Oscillator*

For microwave radar receiver purposes the selection of the local beat oscillator within the converter assembly has been essentially limited to two types of tubes, both of which were developed during the past war period. For radar systems operating at frequencies of 1000 mc and lower, the GL-2C40 lighthouse triode has served quite satisfactorily, while at frequencies above 1000 mc, the single-cavity reflex oscillator tube has been extensively employed. Both of these tube types have adequate power output and frequency stability characteristics to meet the normal radar system requirements.

Some of the desirable characteristics of a beat oscillator tube for use in military radar receivers can be listed as follows:

A. At least 20 milliwatts of useful output power is desirable. In the case of the silicon crystal rectifier element, the applied power is limited to approximately 1 mw; however, the availability of additional oscillator power enables the converter designer to effectively isolate the beat oscillator and signal branches by simple inpedance mismatch means.

B. The frequency stability of the ideal beat oscillator tube must be inherently good, or convenient means to automatically control this frequency must be provided. The maximum allowable radar receiver frequency variation due to all causes is of the order of 1 mc. In terms of the beating oscillator frequencies employed in the radar systems of the past war, this represents an allowable oscillator frequency variation

Digitized by Google
Original from UNIVERSITY OF MICHIGAN
Generated on 2019-09-22 07:16 GMT / http://hdl.handle.net/2027/mdp.39015077775156
Public Domain, Google-digitized / http://www.hathitrust.org/access_use#pd-google

from all causes of from 0.1% to .01%. The possible influencing factors include temperature, atmospheric pressure, supply voltage, and load impedance variations with time, and mechanical shock and vibration.

C. It is extremely desirable that frequency control of the beat oscillator be available by remote electrical means. The use of automatic tuning control of a military radar receiver has proved a necessity during the past war and, as will be discussed in a later section, the rates of change of frequency encountered are found to be quite great. This requires essentially that an electrical control method of continuously adjusting the beat oscillator frequency be employed to obtain satisfactory receiver performance.

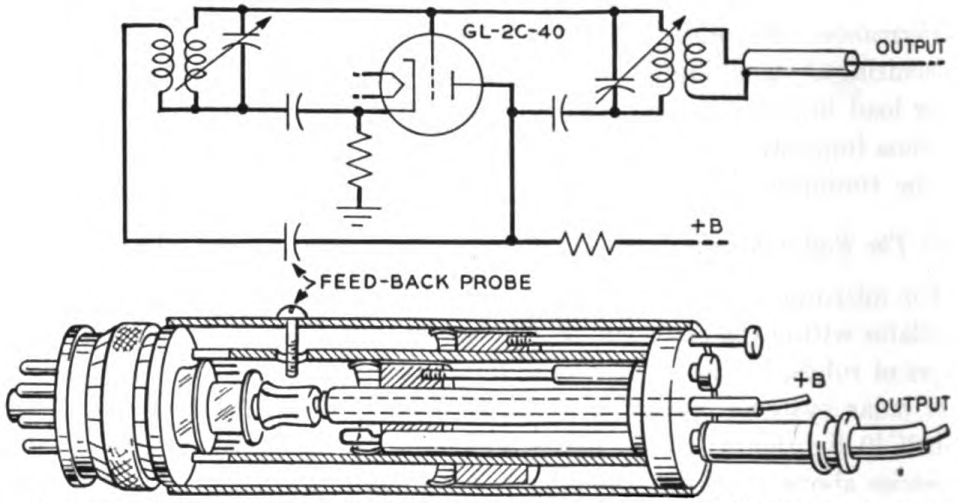

Fig. 16.—1000-mc Radar local beat oscillator employing GL-2C40 vacuum tube—schematic diagram.

D. It is desirable that the output of the beating oscillator tube be free from noise. In the usual radar system, if the output frequency of the beat oscillator is modulated with noise, a reduction in receiver performance will result. As previously discussed, the development of the balanced converter has provided the converter designer with some relief from this noise source and in this case this requirement assumes less importance.

A beat oscillator arrangement utilizing the GL-2C40 lighthouse tube, as developed for a military radar system operating in the 1000 mc region, is indicated in Figure 16. This assembly is quite similar mechanically to the RF and converter components employed in this frequency region and described previously. The positive feedback necessary to sustain oscillation is provided by means of a feedback coupling probe as shown. The oscillator output is available by means of a pick-up loop inserted into the

Digitized by Google
Original from UNIVERSITY OF MICHIGAN
Generated on 2019-09-22 07:16 GMT / http://hdl.handle.net/2027/mdp.39015077775156
Public Domain, Google-digitized / http://www.hathitrust.org/access_use#pd-google

plate-grid cavity and thence to the output coaxial line. The frequency stability of this particular design has been quite satisfactory due to the considerable development effort expended on the mechanical design features of this assembly.

Another radar receiver beating oscillator which has been extensively employed in military equipment designs operating at 3000 mc and higher during the past war period is the reflex velocity-modulated oscillator. The 2K25 type, which is a typical single-cavity reflex oscillator for operation in the 10,000-mc region, is illustrated in Fig. 17. The general principle of operation is quite straightforward, but the complete theory of operation is exceedingly complex and has been described in detail elsewhere.[10] A beam of electrons of relatively uniform velocity and density is projected from a cathode surface toward a cavity space defined in part by two grids and then toward a repeller electrode beyond. The presence of the oscillatory potential between the two cavity grids acts to impart initial velocities to the electron stream in accordance with the cavity radio-frequency potentials existing at the time of crossing of this gap. Under certain operating conditions between these grids and the repeller electrode, which is maintained at a negative potential, "bunching" of electrons occur and upon the return of the electrons to the cavity region under the retarding influence of the repeller electrode, a certain amount of power may be extracted and utilized externally. As might be expected from this cycle of events, the optimum operating conditions necessary for reinforcement of oscillation within the cavity are related to the time required to return the electrons to the cavity with reference to the instantaneous oscillatory radio-frequency potential of the cavity. Thus, numerous modes of oscillation are found in this type of reflex velocity-modulated oscillator which are related to each other by integral numbers of periods of the oscillatory frequency and the transit time of the electrons. In the practical application of the reflex oscillator the number of useful modes are limited to perhaps two or three, the external power output available at the additional theoretical modes being reduced by dissipative conditions within the oscillatory system. The relation of repeller potential to the appearance of these modes is illustrated in Fig. 18 for the case of a 2K25-type oscillator. It should be observed here that the frequency at the maximum power output condition for each mode is the same, i.e. the frequency associated with the cavity dimensions for that series of modes. The cavity dimensions of the reflex oscillator tube are varied by the application of external mechanical pressure regulated by an adjustable tuning strut as shown in Fig. 17. The power for external use is obtained from a coupling loop located within the cavity region and transmitted through the base by means of a coaxial lead.

[10] Pierce and Shepherd, Loc. Cit.

Digitized by Google
Original from UNIVERSITY OF MICHIGAN
Generated on 2019-09-22 07:16 GMT / http://hdl.handle.net/2027/mdp.39015077775156
Public Domain, Google-digitized / http://www.hathitrust.org/access_use#pd-google

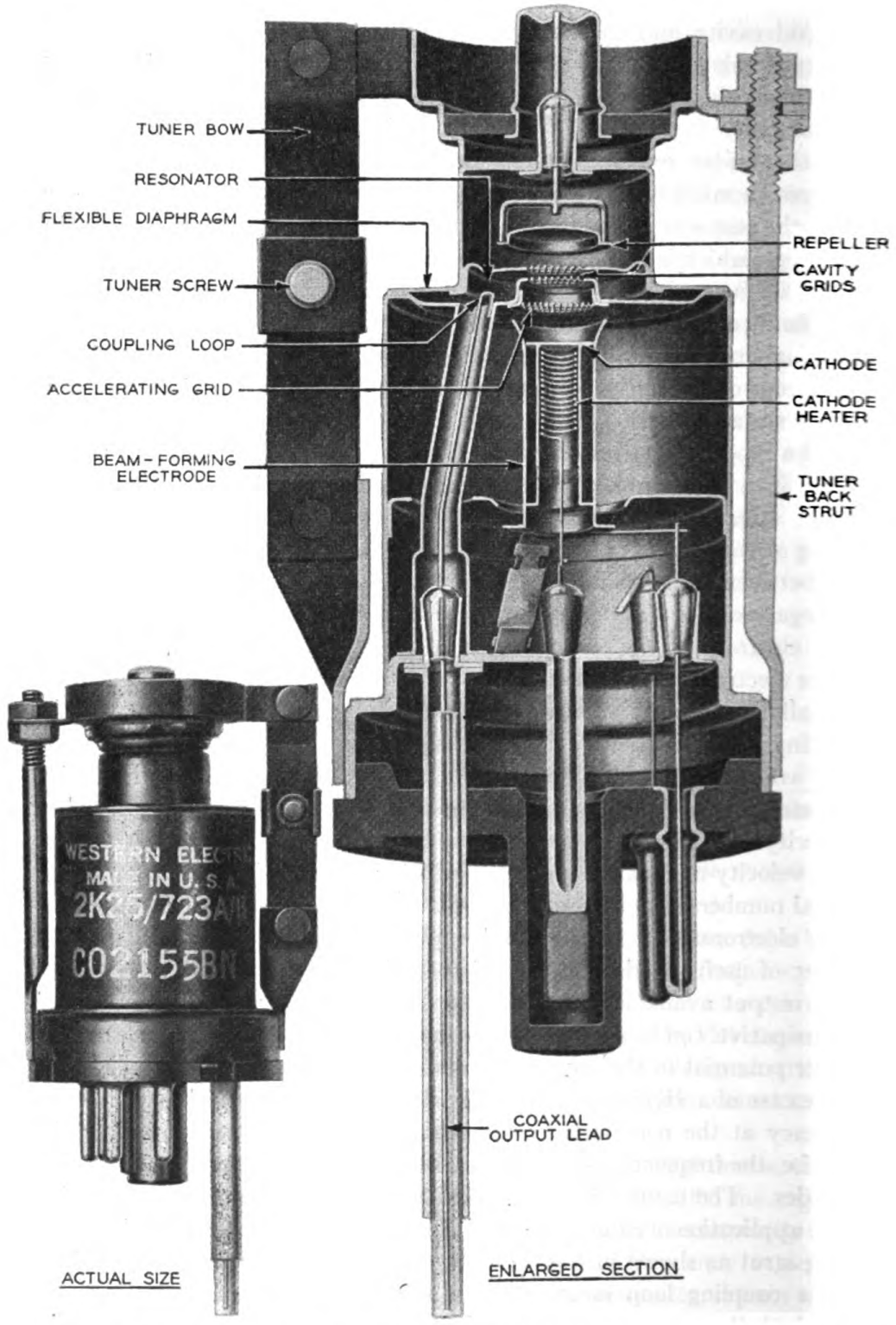

Fig. 17.—Constructional details of the type 2K25 single-cavity reflex oscillator for use at 10,000 mc.

Digitized by Google
Original from UNIVERSITY OF MICHIGAN
Generated on 2019-09-22 07:17 GMT / http://hdl.handle.net/2027/mdp.39015077775156
Public Domain, Google-digitized / http://www.hathitrust.org/access_use#pd-google

The single-cavity velocity-modulated oscillator is admirably suited to electrical remote control of its oscillation frequency by means of the potential applied to the repeller element, thus lending itself to automatic frequency control in a simple manner. Figure 19 indicates the frequency and power output versus repeller voltage characteristic of a typical 2K25 10,000-mc reflex oscillator when operating at a normal mode previously shown in Fig. 18. It is customary to define the electronic tuning range of a reflex oscillator as that range of frequencies over which the power output exceeds

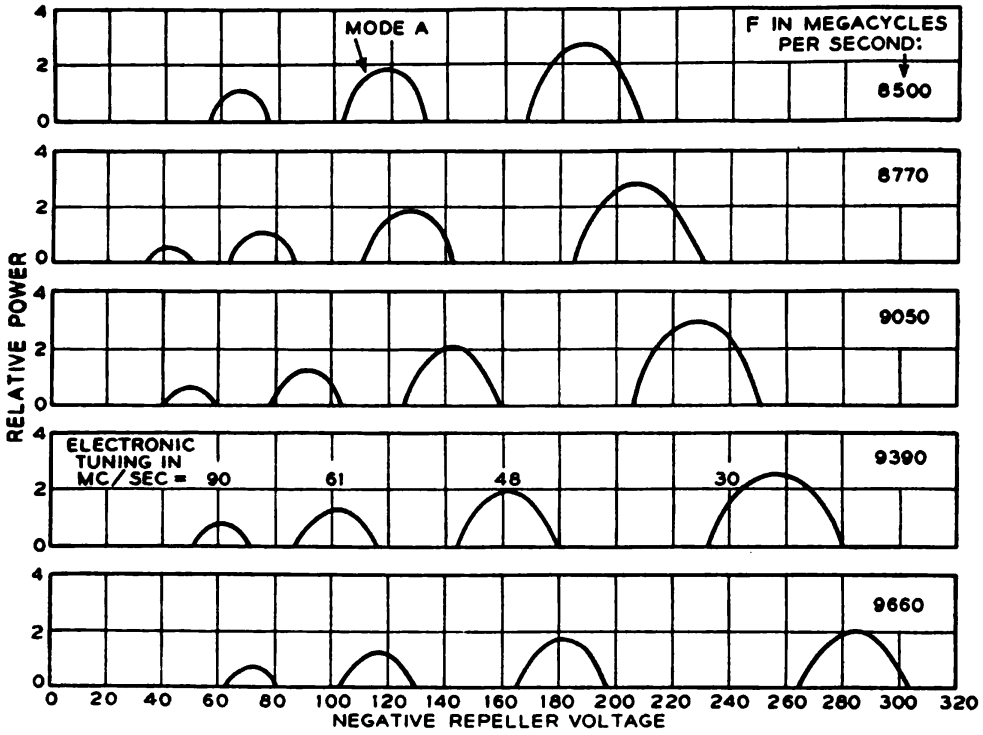

Fig. 18.—Typical output power modes vs. repeller voltage for a 2K25 type reflex oscillator.

50% of the maximum power output. The tube whose characteristic is illustrated in Fig. 19 would accordingly have an electronic tuning range of 53 mc.

2.16 *Typical Radar Input Circuit Designs*

An example of a radar receiver input circuit operating in the 1000-mc frequency range is shown in its final mechanical form in Fig. 20. This particular design was employed in several military ground radar systems including the Mark-20 Searchlight Control equipment of Fig. 1, and in modified form in several naval fire control systems. It consists of two stages of radio-frequency amplification, a converter stage, and a local beating

Digitized by Google
Original from UNIVERSITY OF MICHIGAN
Generated on 2019-09-22 07:17 GMT / http://hdl.handle.net/2027/mdp.39015077775156
Public Domain, Google-digitized / http://www.hathitrust.org/access_use#pd-google

oscillator all of which employ the GL-2C40 lighthouse tube. This particular equipment example has been developed in the form of a sliding drawer to assure ease of maintenance but with no sacrifice in rigidity of mechanical assembly so necessary in this type of equipment. Further mechanical details of the cavity and tube structures of each component are shown in Fig. 21 and are generally similar to the examples previously described. These cavity structures are heavily silver-plated to assure good electrical and thermal conductivity. The problem of adequate conduction of heat from the GL-2C40 vacuum tube under the severe ambient temperatures

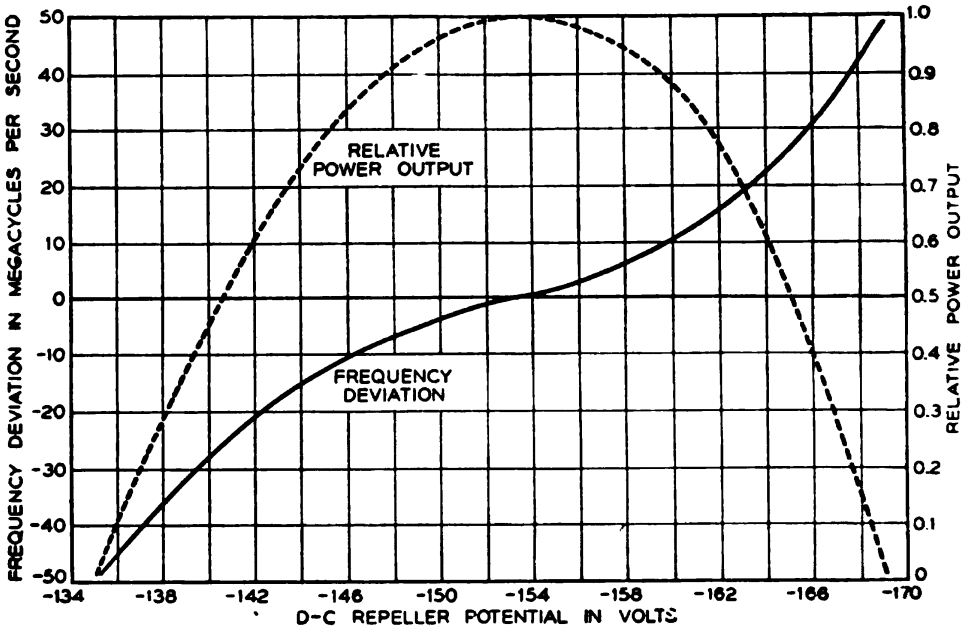

Fig. 19.—Power output and frequency deviation vs. repeller voltage for 2K25-type reflex oscillator.

encountered in military service is extremely important. Positive locking devices are provided for all adjustments in this mechanical design.

Figure 22 indicates the schematic diagram of this design. It may be observed that separation filters are employed extensively to assure negligible interaction effects between the various stages through the common power supply connections.

The over-all performance of this particular design of a radar receiver input circuit is as follows:

Input Frequency	1000 mc
Output Intermediate Frequency	60 mc
Over-all Band Width	5 mc
Over-all Gain	18 db
Over-all Noise Figure	14 db
Input Impedance	50 ohms
Output IF Impedance	75 ohms

Digitized by Google
Original from UNIVERSITY OF MICHIGAN
Generated on 2019-09-22 07:17 GMT / http://hdl.handle.net/2027/mdp.39015077775156
Public Domain, Google-digitized / http://www.hathitrust.org/access_use#pd-google

The above performance is representative of the limits which all manufactured units are required to meet and also indicates the field performance which must be maintained for satisfactory military service. Under laboratory conditions and with a certain compromise of stability and ease of

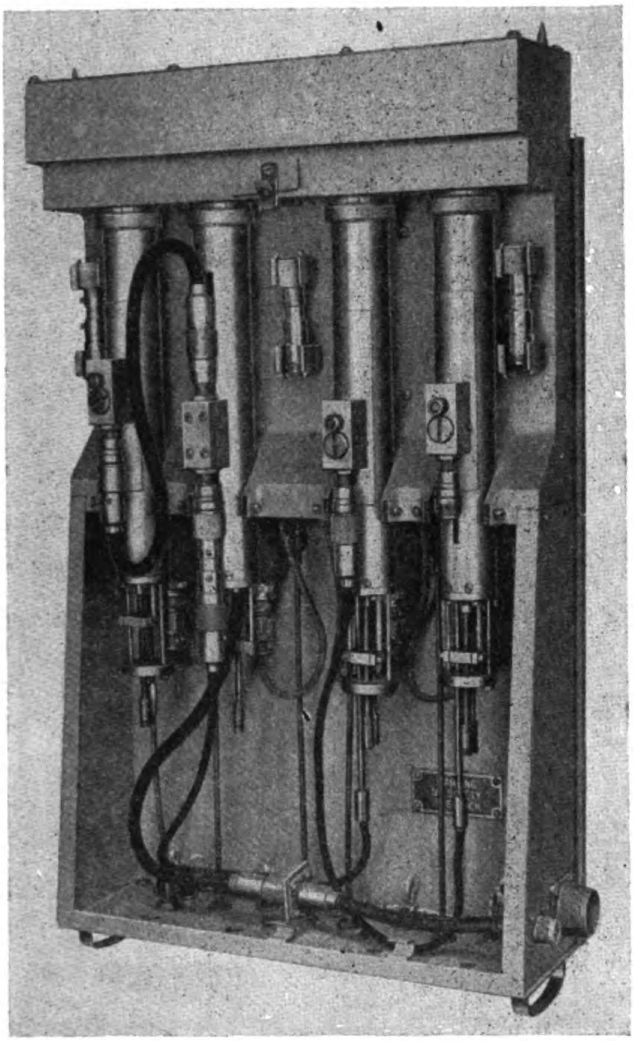

Fig. 20.—1000-mc Radar receiver input circuit design, including two stages of radio frequency amplification, converter, and beat oscillator.

adjustment, improved performance over the figures given here can be expected.

The design for manufacture of a converter assembly typical of airborne equipment methods is illustrated in Fig. 23. Here the equipment design reflects the fundamental requirement of radar equipment for aircraft—that of providing compact units of sufficient rigidity with a minimum of weight. This particular converter unit was employed in the AN/APS-4 Airborne

Digitized by Google
Original from UNIVERSITY OF MICHIGAN
Generated on 2019-09-22 07:17 GMT / http://hdl.handle.net/2027/mdp.39015077775156
Public Domain, Google-digitized / http://www.hathitrust.org/access_use#pd-google

Search and Interception radar equipment shown in Fig. 3 and operates within the 10,000-mc frequency band. The automatic frequency control

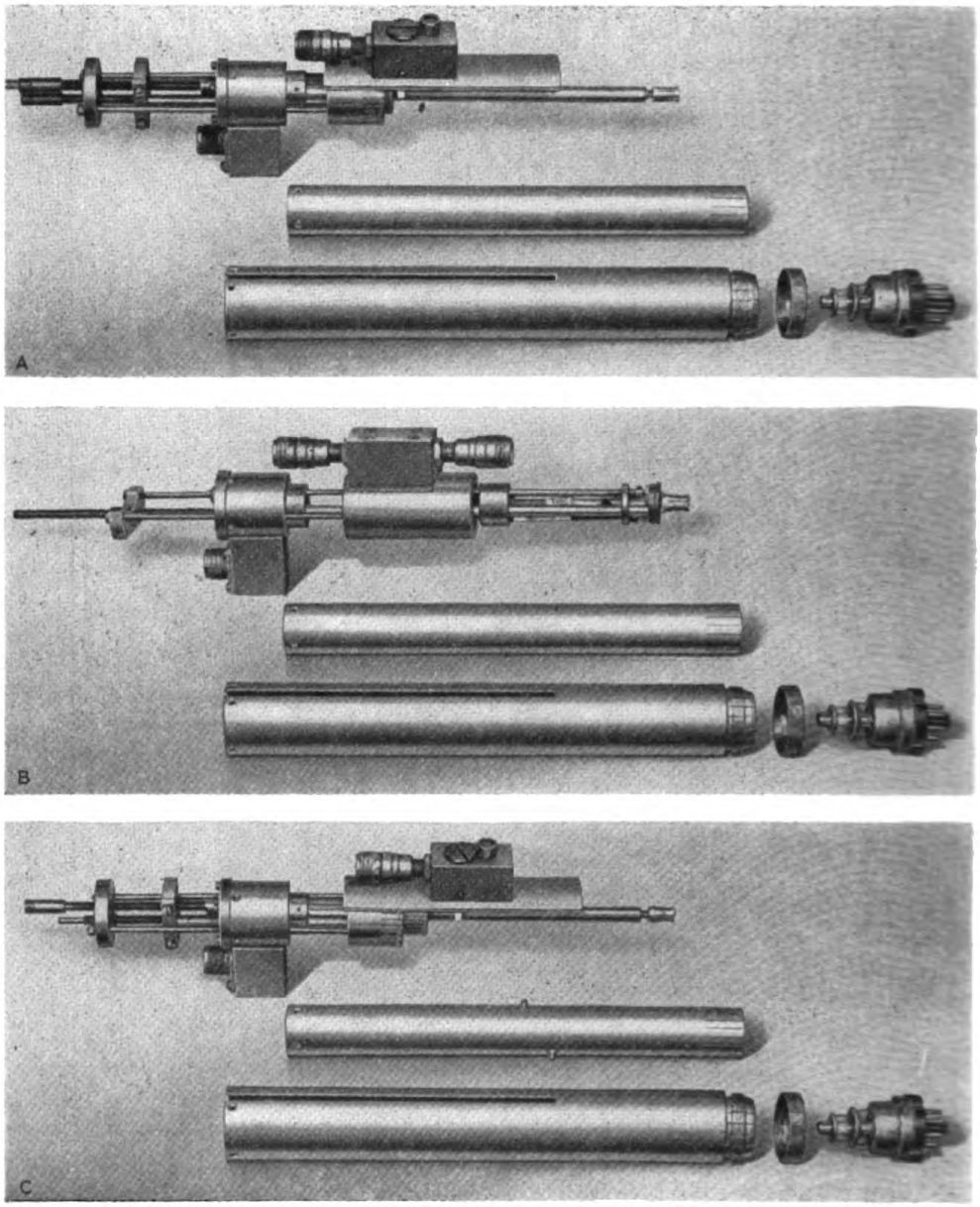

Fig. 21.—Mechanical details of cavity structures employed in 1000 mc radar receiver input circuit.

circuit and two *IF* preamplifier stages are also included here as an integral part of the converter assembly.

The schematic diagram of the converter portion of this assembly is given in Fig. 24. It should be observed that the basic arrangement of the crystal

Digitized by Google
Original from UNIVERSITY OF MICHIGAN
Generated on 2019-09-22 07:17 GMT / http://hdl.handle.net/2027/mdp.39015077775156
Public Domain, Google-digitized / http://www.hathitrust.org/access_use#pd-google

converter is similar to a form described in a previous section. The signal in this example is introduced into the converter section of the waveguide through an iris following the TR tube. Two 2K25 reflex oscillator tubes are mounted upon this waveguide with their output probes extending into the guide proper. The crystal cartridge is located near the end of the waveguide with an adjustable piston terminating the guide. A waveguide to

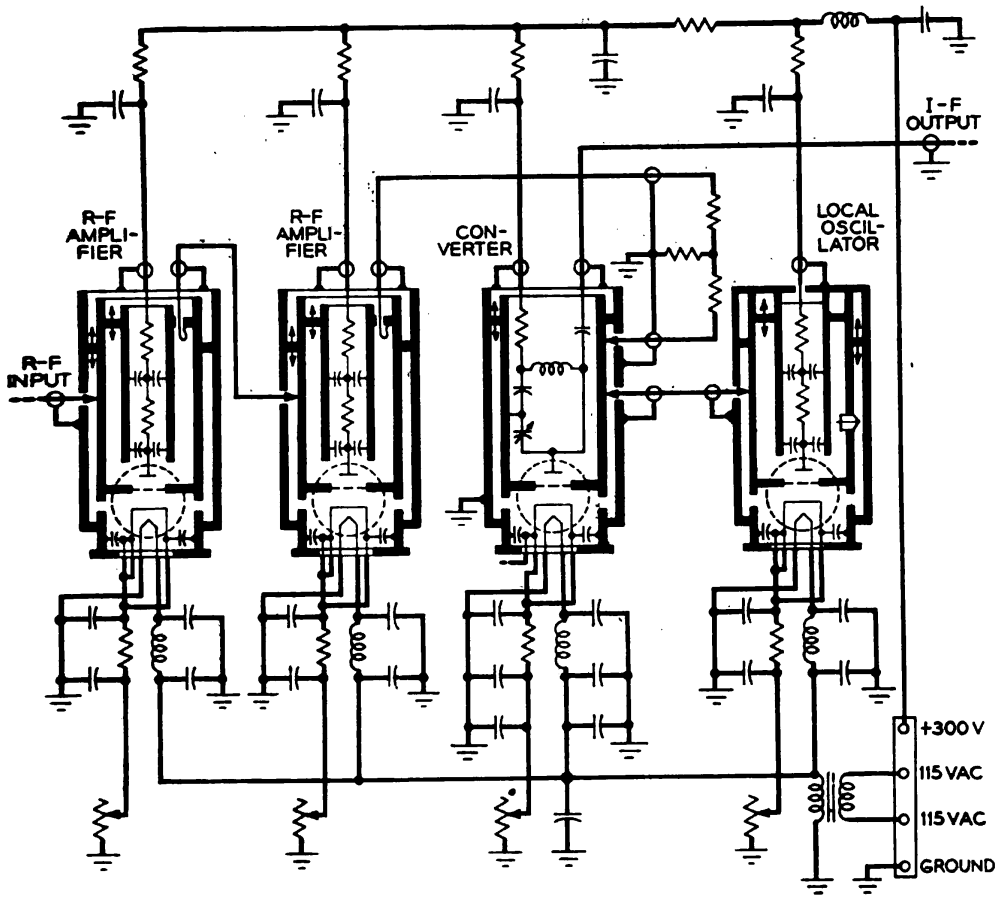

Fig. 22.—1000-mc Radar Receiver Input Circuit. Schematic diagram.

coaxial transforming section employs the crystal as an extension of its axial element with an adjustable capacitance element for tuning purposes.

It will be observed here that a shutter is included in this design, whereby the crystal element can be isolated from the signal input end of the waveguide. This is a most necessary device on all radar converters employing crystal converter elements to prevent accidental overload of the crystal. When the transmitter is not in operation and accordingly the TR tube "keep alive" is not energized, there is a possibility of subjecting the crystal element to signals of sufficient amplitude to destroy its characteristic. These over-

Generated on 2019-09-22 07:17 GMT / http://hdl.handle.net/2027/mdp.39015077775156
Public Domain, Google-digitized / http://www.hathitrust.org/access_use#pd-google
Digitized by Google
Original from UNIVERSITY OF MICHIGAN

load signals may occur as the result of direct pick-up of an adjacent radar system or in certain cases atmospheric discharges. To prevent this a mechanical shutter is inserted into the converter which offers effective attenuation to any signal input. This shutter is withdrawn only if the proper TR "keep alive" voltage is available.

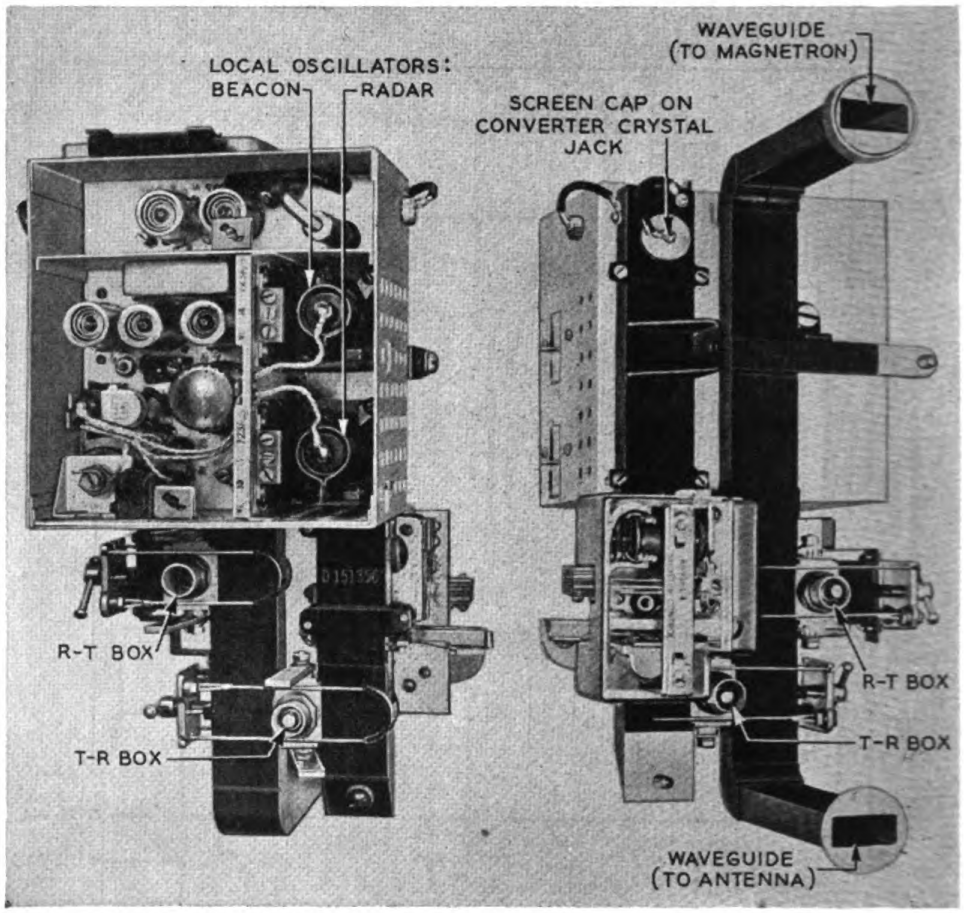

Fig. 23.—10,000-mc Converter and IF preamplifier assembly for AN/APS-4 airborne radar equipment.

The performance characteristics of this converter and IF preamplifier unit is as follows:

Radar Frequency	10,000 mc
IF Frequency	60 mc
Conversion Loss	6.5 db
Noise Figure of IF Preamplifier	4.5 db
Noise Figure of Converter	8.6 db
Noise Figure of Converter and Preamplifier	11.9 db
IF Band Width	4 mc

These values are representative of the performance under conditions of average crystals and average IF input tubes.

Generated on 2019-09-22 07:18 GMT / http://hdl.handle.net/2027/mdp.39015077775156
Public Domain, Google-digitized / http://www.hathitrust.org/access_use#pd-google
Digitized by Google
Original from UNIVERSITY OF MICHIGAN

2.2 *The Radar Intermediate Frequency Amplifier*

The intermediate frequency (IF) amplifier component of the radar receiver has as its function the selection and amplification of the received signal following its conversion to the intermediate frequency. The further conversion of the IF signal to a video form suitable for use in the display device is usually included as an integral part of the IF amplifier and will, therefore, be considered here as an additional function of this component.

2.21 IF *Amplifier Requirements—Band Width*

The frequency-selectivity characteristic of the radar receiver is determined effectively by the IF amplifier, since the preceding converter and other microwave components offer little or no selectivity. The receiver

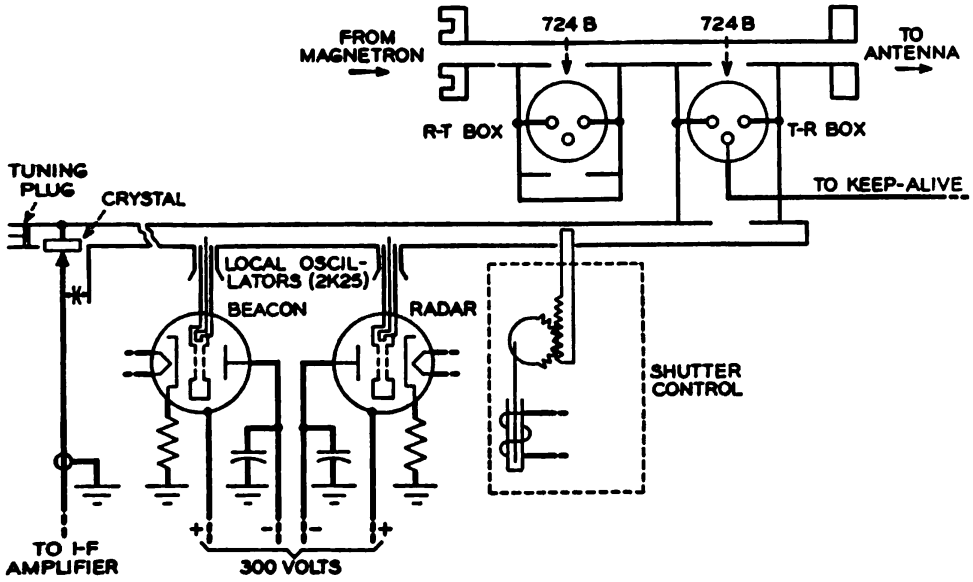

Fig. 24.—Schematic diagram of 10,000-mc AN/APS-4 converter unit.

band width required to adequately transmit the wanted signal, while restricting the noise contributions, is an extremely important factor in the radar system design and represents, therefore, a basic consideration in the design of the IF amplifier.

The receiver band width required to adequately transmit the basic received pulse information can be determined by a consideration of the frequency-energy characteristics of a radar pulse. The microwave pulse is created by the sudden application of a high-energy pulse to the magnetron microwave generator. It has been found sufficient to treat this output envelope as a simple rectangular pulse in band width computations. Figure 25 indicates the amplitude, time, and frequency relationships which exist for an idealized rectangular radar pulse envelope. It may be observed

Digitized by Google
Original from UNIVERSITY OF MICHIGAN
Generated on 2019-09-22 07:18 GMT / http://hdl.handle.net/2027/mdp.39015077775156
Public Domain, Google-digitized / http://www.hathitrust.org/access_use#pd-google

that approximately 75% of the energy contained in the idealized original pulse will be available after transmission through a band-pass structure of band width dimension of $\frac{1}{\tau}$ cycles per second. A further doubling of the band width to $\frac{2}{\tau}$ cycles per second will increase the available energy by only about 15%. In the case of the practical radar-pulse envelope which usually is characterized by a trapezoidal form with finite rise and decay intervals, the energy contained at frequencies outside of a $\frac{1}{\tau}$ band is reduced somewhat over the idealized case illustrated in Fig. 25.

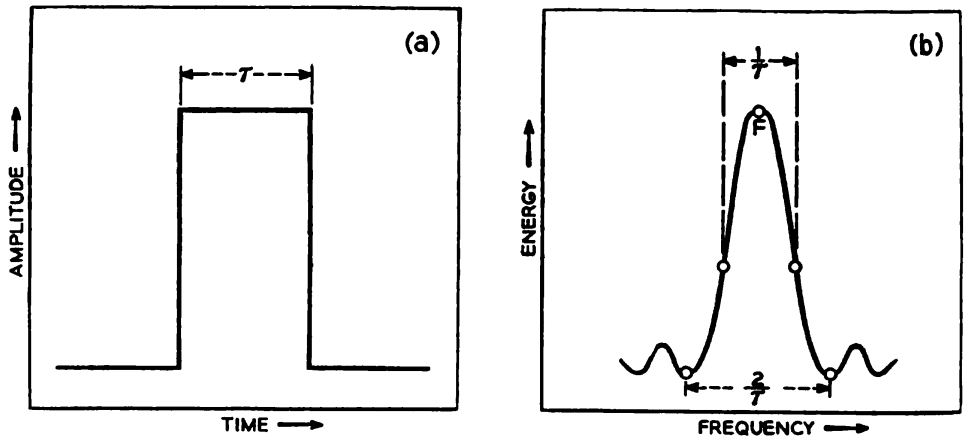

Fig. 25.—Amplitude-time and energy-frequency relationships for a rectangular radar pulse envelope.

The signal-to-noise ratio of the radar receiver is dependent on the over-all receiver band width as indicated in the previous section of this paper. It is extremely important then to restrict the IF band width as much as possible, consistent with adequate transmission of the signal itself. The final band width choice is that value where a further increase would result in a noise increase greater than the corresponding signal improvement and where a band width reduction would diminish the signal by a greater increment than the noise. The exact determination of the optimum radar receiver band width must be carried out using the final display device in making the signal-to-noise comparisons. If the radar system is to be employed for search purposes where echo presence is the primary measure of the performance of the equipment, the optimum over-all receiver band width has been found to be of the order of $\frac{1}{\tau}$ cycles per second resulting in an IF amplifier band width of $\frac{2}{\tau}$ cycles per second to adequately transmit the double-

Digitized by Google
Original from UNIVERSITY OF MICHIGAN
Generated on 2019-09-22 07:18 GMT / http://hdl.handle.net/2027/mdp.39015077775156
Public Domain, Google-digitized / http://www.hathitrust.org/access_use#pd-google

sideband signal at this point. In the case of fire-control radar equipments, where precision range measurement is required, it is desirable to determine the range by reference to the leading or lagging edge of the radar received pulse. Here the optimum band width may be considerably greater than the value indicated above for a simple search system to assure a minimum rise time of the displayed pulse and an accordingly more precise determination of the position of the pulse. Additional factors which influence the radar receiver band width value in a particular system design involve the frequency stability of the microwave generator and the local beating oscillator, the sensitivity characteristics of the automatic frequency control system, the frequency stability characteristics of the IF amplifier itself, and finally the desire to permit ease of tuning by the radar operator.

The phase distortion introduced by the IF amplifier is of secondary interest in the case of radar systems. The faithful reproduction of all characteristics of the received radar pulse is usually not of extreme importance, since with few exceptions the criterion of presence is all important. The detailed form of the transmission characteristic is likewise not extremely critical, the usual "rounded" IF transmission characteristic, however, contributing somewhat to ease in tuning the radar receiver.

Gain Characteristics

A consideration of the converted input signal levels encountered and the video output level desired indicates the IF amplifier gain requirement. The input signal to the IF amplifier is determined by the type of converter employed and the presence or not of radio-frequency amplification preceding the IF section and the absolute noise power resulting. The video level at the second detector must be maintained at a sufficiently high level so that microphonic disturbances within the remaining video components are negligible and low enough to assure satisfactory detection without serious overload effects. Undesired feedback at the IF frequency also tends to limit the practical gain which can be introduced into the IF amplifier. In the military radar systems of the past war period the usual maximum gain associated with the IF amplifier was of the order of 110 db with a maximum detector output level of approximately 1 volt rms of input circuit noise. The extreme variation of the level of the desired radar signal makes necessary that provision for a large gain control variation be included in the IF amplifier design. This gain control often involves automatic, as well as manual, adjustment and commonly a gain variation range of the order of 80 db is required.

Another consideration which enters into the IF amplifier design and is associated with gain features, is the behavior of the amplifier in the presence of extremely large radar signals or enemy "jamming" signals. Optimum

Digitized by Google
Original from UNIVERSITY OF MICHIGAN
Generated on 2019-09-22 07:18 GMT / http://hdl.handle.net/2027/mdp.39015077775156
Public Domain, Google-digitized / http://www.hathitrust.org/access_use#pd-google

protection against complete "blocking" of the IF amplifier under these conditions involves the use of extremely small-valued filter or by-pass elements which are associated with the grid and cathode circuits to present very short time constants and, accordingly, assure recovery of the amplifier in fractions of a microsecond after overloading by a large pulse signal. The gain control method is also chosen to minimize possible overloading by reducing the gain of the amplifier at a point as far forward in the radar receiver chain as possible.

Intermediate Midband Frequency

The choice of the intermediate frequency for a radar receiver is essentially a compromise between the need for reduction of unwanted external interference and noise, and the desire to realize maximum performance in terms of gain and noise figure.

The tendency to employ a high IF midband value arises from a consideration of the character of the certain local beating oscillator noise sidebands. As mentioned previously, the noise sideband output decreases as the frequency interval from the oscillator frequency is increased and it is apparent that a high value for the IF will be advantageous. In the case of balanced converters where the oscillator noise sidebands are reduced by the circuit balance, this factor assumes less importance. A moderately high IF is also advantageous in the elimination of the IF signal from the final detected video output which must be accomplished by the use of low-pass filters. The automatic frequency-control problem is somewhat simplified by the use of a high IF. The wider separation of the desired tuning point and the image response and the reduction of interfering TR pulse energy is a positive help in the performance of the automatic frequency-control circuits and will be discussed in detail in a later section.

There are also a number of factors which indicate that a low value of midband IF may be desirable. The noise figure of the input stage of the IF amplifier is generally better at a low frequency, though this improvement tends to be quite small for the band widths employed in the military radar system. A more important advantage of a low IF value is found in the improvement of the absolute frequency stability of the IF transmission characteristic under the influence of variations of tube and circuit capacitance.

Intermediate midband frequencies of 30 mc and 60 mc have been employed in the majority of military radar systems developed in the United States during World War II. In general, 30 mc has been employed quite extensively in naval and ground radar equipments for fire control where radar pulse widths of the order of one microsecond are used. For airborne radar equipments with the emphasis on compactness, weight, and the trend toward higher microwave transmission frequencies, 60 mc has proven to be an extremely popular intermediate frequency value.

Digitized by Google
Original from UNIVERSITY OF MICHIGAN
Generated on 2019-09-22 07:18 GMT / http://hdl.handle.net/2027/mdp.39015077775156
Public Domain, Google-digitized / http://www.hathitrust.org/access_use#pd-google

The Second Detector

The final conversion of the IF signal to a video form is accomplished by simple detection. This process is usually associated with the IF amplifier because of the relative ease by which the video signal can be transmitted to the following display circuits, usually physically removed from the IF amplifier, as compared with the transmission problem which exists at the intermediate frequency.

Two types of second detector circuits which are commonly employed in radar receiver design are the linear diode rectifier and the plate circuit detector, both similar in form to those employed in prewar television practice. Several factors must be considered in the choice of the second detector operating characteristic. Linear detection of the signal is desirable from the standpoint of realizing the greatest possible visibility of weak radar signals in the presence of noise of comparable amplitude. In the case of lobing radar signals where bearing determinations are made by comparison of the return signal amplitude for two bearing conditions of the antenna radiation, the characteristic of the second detector enters to affect the sensitivity of azimuth response in two ways. The lobing sensitivity is increased by the use of a square law detector, however, the presence of a "jamming" signal of the CW type which may be located off axis can introduce a false bearing indication, which is not present when a purely linear detector is employed. In general, the linear detector has been employed in most radar systems developed during the past war period.

The detailed circuit design of the IF amplifier can be conveniently separated into three quite distinct parts. These include the input circuit design, the interstage arrangement, and the design of the second detector circuit.

2.22 IF *Amplifier Input Circuit Design*

The primary consideration in the IF amplifier input circuit design is the effect of this stage on the over-all receiver noise figure. As indicated previously, this over-all receiver noise figure is dependent on the performance characteristics of the first or input IF amplifier stage to a degree dependent on the loss of the converter stage preceding it. In the military radar field, employing microwave frequencies of 3000 mc and greater, the crystal converter is universally employed and the over-all noise performance is determined largely by the IF input stage. The use of high-gain pentodes in the IF amplifier assures that noise contributions from the following stages are negligible.

Figure 26 represents an equivalent input circuit of the IF amplifier convenient for discussion of the noise performance of this circuit. Here the noise contribution, exclusive of the signal source, is observed to be composed of two sources, one due to shot noise of the first IF stage referred to the grid

Digitized by Google
Original from UNIVERSITY OF MICHIGAN
Generated on 2019-09-22 07:19 GMT / http://hdl.handle.net/2027/mdp.39015077775156
Public Domain, Google-digitized / http://www.hathitrust.org/access_use#pd-google

circuit and a second noise source related to active grid loading effects.[11]

The optimum IF amplifier input circuit design involves primarily the selection of impedance transformation means which results in the maximum over-all signal-to-noise performance for the radar receiver. It can be shown that this optimum value of impedance transformation is not that value which

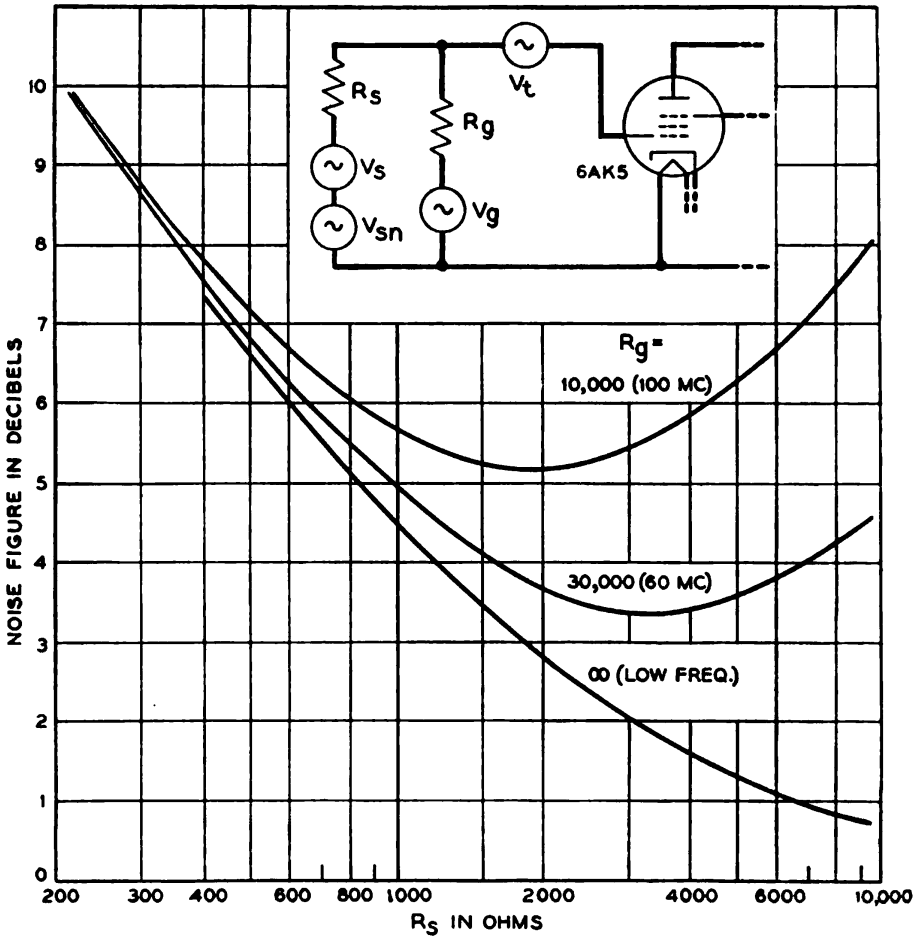

Fig. 26.—Simplified equivalent input circuit of an intermediate frequency amplifier and noise-figure vs signal source impedance.

maximizes the signal but rather is a condition where a definite signal mismatch obtains. This may be understood by an inspection of the characteristics of the two fictitious noise sources illustrated. The shot noise contribution of the vacuum tube employed in the input IF amplifier stage is here represented by the series noise generator V_T. Under conditions of shorted grid this is the only effective noise contribution, and this procedure offers a simple method for determination of the magnitude of this effect.

[11] "Considerations in the Design of a Radar IF Amplifier," Andrew L. Hopper and Stewart E. Miller, *Proc. I. R. E.*, November 1947.

Digitized by Google
Original from UNIVERSITY OF MICHIGAN
Generated on 2019-09-22 07:19 GMT / http://hdl.handle.net/2027/mdp.39015077775156
Public Domain, Google-digitized / http://www.hathitrust.org/access_use#pd-google

The additional noise contribution under the condition where an impedance is placed in the grid circuit is shown by the noise generator V_G. This noise source is related to the active grid loading. The resistance R_G represents this effective loading which is due to transit time and tube lead inductance effects and, therefore, has a value which is associated with the frequency of operation and the particular design of tube employed. At very low frequencies, $R_G \rightarrow \infty$, the shot noise effects are entirely controlling, and the optimum IF amplifier input grid circuit condition for minimum noise figure is that condition where the impedance of the signal source approaches an infinite impedance. As the frequency of operation is increased, R_G assumes a finite decreasing value and the optimum signal source impedance is given by the relationship illustrated in Fig. 26. It should be noted that the frequency values associated with the above characteristic are indicative of the performance of the 6AK5 pentode, one of the most satisfactory of available tubes for this purpose. It should be observed that the input IF amplifier stage noise figure is independent of the impedance of the signal source providing that a perfect or lossless transformer can be employed to achieve the optinum impedance transformation indicated.

The realization of proper impedance transformation characteristic in the radar IF amplifier input circuit is basically a network problem. The input grid impedance which can be maintained over the desired band of frequencies is limited by the total capacitance present in the grid circuit. For narrow IF band widths, particularly at the lower frequencies, the realizable impedance at the grid may be in excess of the active grid loading value and here the noise performance indicated in Fig. 26 may be realized. However, for wide IF band widths at normal radar IF midband values the maximum grid circuit impedance which can be achieved under the limitation of the grid circuit capacitance will be less than the value associated with the active grid loading and the noise figure obtained will be somewhat higher than the optimum shown. This restrictive design condition is referred to as "band width limited." In modern military radar receivers this condition normally obtains.

To achieve the maximum input coupling network efficiency it is extremely desirable to minimize all parasitic capacitances under control of the designer and to employ the most effective network arrangement available. The double-tuned transformer and autotransformer networks are commonly employed for this purpose. Any loss in the impedance transforming network will result in further degradation of the noise performance, since this loss is effective in reducing the signal energy while having no effect on the tube noise level. The magnitude of the impedance transformation ratio required in a typical radar design case for optimum noise figure is approximately seven times, where a crystal converter of the type shown in Fig. 14

Digitized by Google
Original from UNIVERSITY OF MICHIGAN
Generated on 2019-09-22 07:19 GMT / http://hdl.handle.net/2027/mdp.39015077775156
Public Domain, Google-digitized / http://www.hathitrust.org/access_use#pd-google

is employed, and the optimum grid impedance at 60 mc as shown in Fig. 26 is approximately 3000 ohms.

The vacuum tube employed in an input stage of an IF amplifier should have the following characteristics to achieve the optimum performance. The tube should be capable of providing sufficient gain to assure that the noise contribution of the following stages is negligible. The input conductance of the selected tube at the intermediate frequency should be as low as possible indicating generally that physical size should be small to assure small transit time effects and low lead inductance values. The noise output of the tube itself should be a minimum, this characteristic being somewhat controllable by proper emission characteristics. The characteristics of the most desirable of the vacuum tubes available to the radar receiver designer during the past war period for IF amplifier purposes is given in Table I.

TABLE I.—*Principal Characteristics of IF Amplifier Tubes*

Type	Heater Power Watts	Plate Current ma	Total Power Consumption Watts	Nominal Transconductance Micromhos	Interelectrode Capacitances Micromicrofarads		Band Merit B_e mc
					Control Grid to Heater, Cathode, Screen Suppressor Grid	Plate to Heater, Cathode, Screen, Suppressor Grid	
6AC7	2.84	10	4.7	9000	11	5	89
6AG7	4.10	30	9.6	11000	13	7.5	85
6AG5	1.89	7.2	3.0	5100	6.5	1.8	95
717A	1.10	7.5	2.3	4000	4.9	3.8	73
6AK5	1.10	7.5	2.3	5000	3.9	2.8	117

The development of the 6AK5 pentode was the direct result of the necessity for improved radar IF amplifier performance, and details of this development and the performance of this tube have been described elsewhere.[12]

The noise present in a pentode is greater than in a triode, primarily due to the presence of additional grid structures. Because of this fact, a number of attempts have been made to employ triodes in the input stage of the IF amplifier. To prevent oscillation due to large positive feed-back present through the plate-to-grid interelectrode capacitance, neutralization methods have been employed. For moderate IF band widths at 60 mc such experimental designs have shown an improvement in noise figure of slightly more than 1 db over the pentode design; however, the criticalness of the neutralization scheme and the difficulties in extending the performance to wider IF band widths has not allowed this design to be adopted extensively to military radar equipment during the past war period.

[12] "Characteristics of Vacuum Tubes for Radar Intermediate Frequency Amplifiers." See pp. 740 ff.

Generated on 2019-09-22 07:19 GMT / http://hdl.handle.net/2027/mdp.39015077775156
Public Domain, Google-digitized / http://www.hathitrust.org/access_use#pd-google
Digitized by Google
Original from UNIVERSITY OF MICHIGAN

2.23 *Interstage Circuit Design*

The design of the IF amplifier interstage circuit is basically concerned with achieving the greatest possible gain per stage while not compromising the frequency characteristic and stability, or complicating the structure to an extent where it will be difficult to realize the designed measure of performance under military operating conditions. The problem can be resolved into the choice of the vacuum tube and the selection of an interstage coupling network.

The gain of a pentode operated into a 2-terminal parallel resonant network which exhibits a maximum impedance R_o at resonance is given by $G_m R_o$ under the restriction $R_o << R_p$. If a band width ΔF is defined as that band of frequencies where the magnitude of the impedance Z of the network is equal to or greater than $\frac{R_o}{\sqrt{2}}$ it can be shown that

$$\Delta F = \frac{1}{2\pi R_0 C}.$$

The gain-band width product of an amplifier stage is a measure of performance of the stage and serves as a criterion for tube performance if a standard load impedance as above is adopted. Then the band merit B_o for this condition will be given by

$$B_0 = \Delta F G_m R_0 = \frac{1}{2\pi R_0 C} (G_m R_0) = \frac{G_m}{2\pi C}.$$

The band merit B_0 of a tube has the dimensions of frequency and may be interpreted as the frequency at which the voltage gain of the vacuum tube is at unity with a plate load impedance restricted solely by the sum of the plate and grid tube capacitances. The ideal IF amplifier vacuum tube will exhibit a high band merit figure, stable operating characteristics over the life of the tube, uniform characteristics during the production period, small size for compact amplifier use and for resulting mechanical rigidity, and finally low-power consumption, desirable from both the power supply standpoint and heat dissipation considerations. The actual types of vacuum tubes generally employed for radar IF amplifiers during the past military program in order of their availability were the 6AC7, 717A, and finally the 6AK5. The improvement in performance achieved through this succession of developments can be observed by reference to Table I and the band merit and power consumption figures for these tube types.

Figure 27 illustrates three types of interstage coupling networks which have been commonly employed in radar IF amplifiers for military purposes. The synchronous single-tuned network design has an advantage of simplicity of construction and permits relatively simple realignment procedures under

Digitized by Google
Original from UNIVERSITY OF MICHIGAN
Generated on 2019-09-22 07:19 GMT / http://hdl.handle.net/2027/mdp.39015077775156
Public Domain, Google-digitized / http://www.hathitrust.org/access_use#pd-google

the limited resources of military field conditions. This type of interstage has been employed quite widely in radar equipments designed during World War II. To achieve the maximum gain per stage it is necessary to restrict the total shunt capacitance of the interstage circuit to the unavoidable elements due to tube and circuit arrangement. Additional capacitance contributions are avoided by the use of a variable inductance element adjustable through the use of movable magnetic cores to resonate the network to the desired midband IF value. The shunt resistance element is chosen to achieve the desired band width.

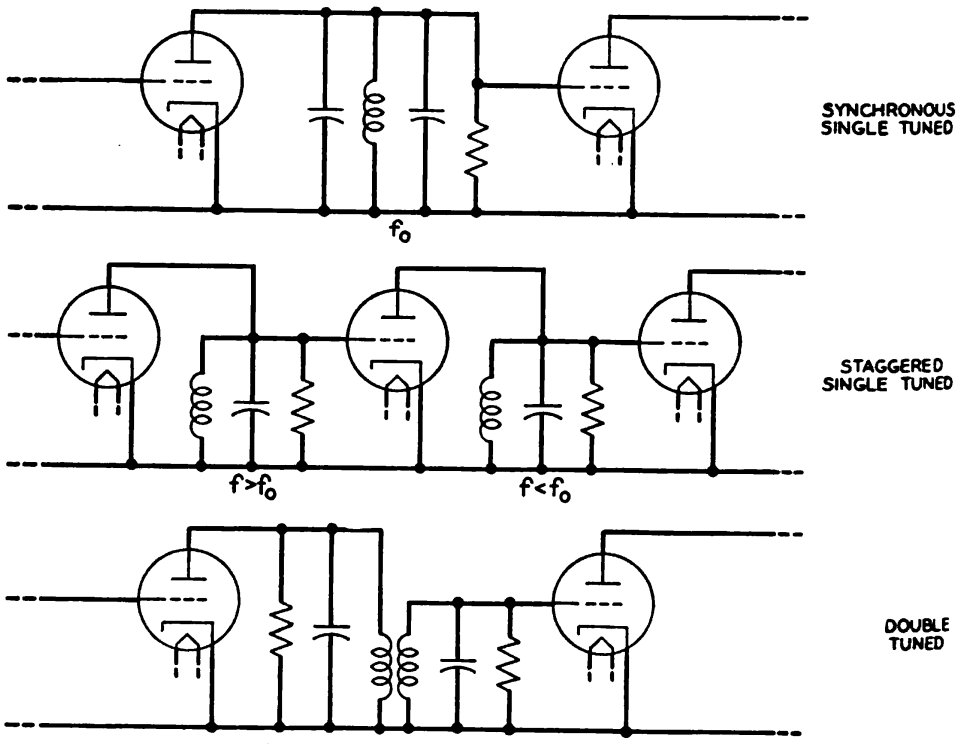

Fig. 27.—Typical IF Amplifier Interstage Circuits. Simplified schematics.

The band width required of each individual interstage circuit of a multistage amplifier of this type to meet an over-all band width requirement of B cycles is given by

$$B = \Delta F \sqrt{2^{1/N} - 1}$$

where ΔF represents the band width of the individual interstage network, defined as the band over which the response is within 3 db of the midband IF value, and N is the number of interstage circuits employed. As the individual interstage band width is increased to achieve the desired over-all value, the gain per stage is reduced and a greater number of stages is required

Digitized by Google
Original from UNIVERSITY OF MICHIGAN
Generated on 2019-09-22 07:20 GMT / http://hdl.handle.net/2027/mdp.39015077775156
Public Domain, Google-digitized / http://www.hathitrust.org/access_use#pd-google

to meet the over-all gain requirement. The over-all gain of a multistage amplifier employing synchronous single-tuned interstage networks is given by

$$G_0 = \left(\frac{G_m\sqrt{2^{1/N}-1}}{2\pi C_T B}\right)^N$$

where C_T represents the total interstage shunt capacitance and B is the over-all band width requirement. Table II presents the individual interstage band widths and the maximum over-all gain obtainable for multistage IF amplifiers having a 5 mc over-all band width requirement. Here the use of the 6AK5 pentode is assumed and the total interstage shunt capacitance is assumed to be 12 micromicrofarads. It should be observed that unavoidable misalignment of circuits, aging of tubes, and other such effects all tend to reduce the idealized computed performance under the practical military radar conditions and must be considered thoroughly in the design.

TABLE II.—*Interstage Band Width and Over-all Gain of Multistage IF Amplifiers*

No. of Amplifier Stages	Synchronous Single-Tuned Interstage		Double-Tuned Interstage	
	Interstage Band Width mc	Over-all Gain db	Interstage Band Width mc	Over-all Gain db
1	5	24	5.0	27
2	7.8	37	6.2	47
4	11.5	61	7.6	87
6	14.3	80	8.6	125
8	16.6	96	9.3	162
10	18.7	110	9.8	198

The double-tuned interstage network configuration shown in Fig. 27 is a somewhat more efficient circuit form than the single-tuned variety just discussed, and because of this improved performance has been employed to about the same extent as the synchronous single-tuned type during the past war. Its performance advantage lies in the basic fact that the transmission response curve for this structure has a flat-top characteristic resulting in a slower rate of over-all band width reduction as these circuits are cascaded. The ability to separate the output plate and the input grid circuit capacitances and the elimination of the plate-to-grid coupling capacitor with its additional parasitic capacitance to ground results in a greater gain-per-stage performance. In this structure the resonant frequency of both primary and secondary circuits corresponds to the midband IF and the conditions of equal Q of primary and secondary circuits and critical coupling are assumed. These conditions result in a smooth flat-topped response characteristic having optimum gain performance. The relationship between the individual inter-

Digitized by Google
Original from UNIVERSITY OF MICHIGAN
Generated on 2019-09-22 07:20 GMT / http://hdl.handle.net/2027/mdp.39015077775156
Public Domain, Google-digitized / http://www.hathitrust.org/access_use#pd-google

stage band width and the over-all band width of a multistage amplifier employing double-tuned interstage circuits is given by

$$B = \Delta F \sqrt[4]{4(2^{1/N} - 1)}$$

which is illustrated in Table II together with the corresponding over-all gain of multistage IF amplifiers of this design.

The third type of interstage network arrangement illustrated in Fig. 27 represents a method employed to realize improved performance of the single-tuned interstage network type by resonating alternate interstages at frequencies above and below the desired midband IF value. This stagger-tuned interstage design permits greater gain per stage together with an increased over-all band width for each pair of amplifier stages over that obtained with the synchronous single-tuned design. In the case of IF amplifiers having six or more stages a variation of this stagger-tuned method can be employed where three successive interstages are considered as a design unit and the individual interstage resonances are adjusted below, above, and centered at the midband IF respectively. To afford a measure of the improved performance of a stagger-tuned IF amplifier we may consider the relative performance of a 6-stage IF amplifier of 5 mc over-all band width employing the 6AK5 vacuum tube. An individual interstage band width of 7.2 mc and an over-all gain of 116 db will result from the use of stagger-tuned interstage circuits while reference to Table II indicates the synchronous single-tuned design would have an over-all gain of only 80 db while the double-tuned design would result in an over-all gain of 125 db. The use of a triple stagger-tuned design would produce a 6-stage amplifier having approximately the same gain performance as the double-tuned example above.

The choice of the interstage network configuration to be employed in a radar IF amplifier must be made considering the circuit efficiency, the gain-frequency stability behavior, and with due regard for the ever-present problem of maintenance of performance under the field conditions of modern warfare. From a standpoint of circuit efficiency alone, it has been shown that the synchronous single-tuned interstage network is decidedly inferior to the more complex forms, but the obvious simplicity of construction of this type and the possibility of adjustment and realignment with simple methods available in the field is a strong recommendation for its adoption in military radar IF amplifiers. The double-tuned circuit has a considerable advantage in circuit performance over the case above, but some portion of this increased efficiency must be sacrificed since it is impractical to construct this network with adjustable elements. Here the normal variations in interstage capacitance with replacement of vacuum tubes or aging effects must not be allowed to reduce the over-all amplifier performance below the design limit. The solution to this problem must be achieved by design of each interstage circuit

Generated on 2019-09-22 07:20 GMT / http://hdl.handle.net/2027/mdp.39015077775156
Public Domain, Google-digitized / http://www.hathitrust.org/access_use#pd-google
Digitized by Google
Original from UNIVERSITY OF MICHIGAN

to obtain a somewhat wider band under average tube conditions so that under subnormal but acceptable tube conditions the over-all performance of the amplifier is still within requirements. The use of stagger-tuned interstage designs will also result in increased performance over the basic synchronous single-tuned variety, but the maintenance of the over-all performance of a radar IF amplifier of this type involves relatively complex measurements not always possible under military conditions.

2.24 *Second Detector Design*

The final conversion of the IF signal to the video form, as required by the following radar display device, is accomplished by simple detection or rectification. For this purpose either a diode rectifier or a triode operating as plate circuit detector is usually employed. The second detector design follows the practices generally developed for television receivers prior to the war. The diode second detector method has the advantage of simplicity with no plate supply voltage being required, but the performance of such a detector is somewhat limited for the frequencies employed in radar systems. The linearity of rectification of a diode depends on maintaining a high load impedance relative to the internal impedance of the tube. The external load impedance is limited, by the presence of tube and parasitic circuit capacitance and the video band width required, to somewhat less than 1000 ohms for the typical radar case. The internal impedance of the usual available diode is of the order of several hundred ohms so that the linearity of detection suffers. The low value of the diode load resistance is also reflected in the termination of the last IF amplifier stage and affects the gain of this stage.

The plate circuit detector often employed consists of a triode operated near plate current cutoff. Here the detector load impedance is effectively isolated from the plate circuit of the last IF amplifier stage. The linearity that can be obtained from this type of second detector is essentially the same as with the usual diode detector.

The polarity of the detected video output signal may be chosen of either sign by proper circuit arrangement for convenience in the video amplifying and limiting circuits which follow. It is desirable to reduce the amplitude of the IF signal which appears at the output of the second detector to prevent overload and interference in the video amplifier following. This is accomplished commonly by the inclusion of a low-pass filter of simple form in the output circuit of the second detector.

2.25 *Typical Component Designs*

In the military radar system design it has been observed that a maximum video output signal of the order of one volt of noise is desirable as a design

Digitized by Google
Original from UNIVERSITY OF MICHIGAN
Generated on 2019-09-22 07:20 GMT / http://hdl.handle.net/2027/mdp.39015077775156
Public Domain, Google-digitized / http://www.hathitrust.org/access_use#pd-google

objective resulting in an over-all gain requirement of the order of 110 db. If the radar system employs RF amplification, the entire IF amplification may be provided in one unit. However, in radar systems operating above 1000 mc it has proved advantageous to provide the total IF gain required in two separate amplifier sections. The IF preamplifier assembly is commonly designed to be mounted adjacent to the crystal converter located in the transmitter portion of the radar system and usually consists of two stages of IF amplification. The main IF amplifier is usually located at some distance from the preamplifier, commonly associated with the indicator components of the radar receiver. The main IF amplifier assembly includes the second detector circuit and occasionally one stage of video amplification is included.

The IF preamplifier location as described above is quire desirable, eliminating the need for a long transmission line connecting the IF output circuit of the crystal converter to the input stage of the IF amplifier. As has been discussed previously, the impedance transformation employed in the IF input stage is chosen to realize optimum signal-to-noise performance. The output impedance of the crystal converter is normally of the order of 400 ohms. To assure negligible impedance reflection losses in this circuit, any connecting cable employed would have to be designed to present a characteristic impedance of this order of magnitude which is inconvenient. The practical solution as employed in past military radar systems is obtained by locating the IF preamplifier in close proximity to the converter. The absence of long leads at this IF input stage is also advantageous in reducing the interference pickup into this low signal level point. After moderate amplification the output of the IF preamplifier is usually fed over a 75-ohm coaxial transmission line to the main IF amplifier.

Figure 28 illustrates the converter and IF preamplifier assembly as employed on the AN/APQ-13 and AN/APQ-7 airborne radar bombing equipments operating at 10,000 mc. The local oscillator and silicon crystal converter are arranged in a manner similar to a basic type previously described in this paper. The IF output of the crystal converter is introduced directly into the preamplifier assembly without exposure. This preamplifier is arranged to offer two stages of amplification employing the 717A pentode and using a double-tuned input, interstage, and output network. Figure 29 indicates the circuit arrangement. The gain of this IF preamplifier is 30 db and an IF band width of 6 mc is provided. The output transformer network is arranged to operate into a 75-ohm coaxial transmission line. It should be observed that provision is here included to disable the preamplifier by application of a positive pulse to the cathode circuit of the second amplifier tube. This feature reduces the gain of the IF preamplifier during the short interval coincident with the outgoing radar pulse, which assures that the TR tube

Digitized by Google
Original from UNIVERSITY OF MICHIGAN
Generated on 2019-09-22 07:20 GMT / http://hdl.handle.net/2027/mdp.39015077775156
Public Domain, Google-digitized / http://www.hathitrust.org/access_use#pd-google

"spike" which precedes conduction will be attenuated and, therefore, less interfering with AFC operation. Further details of this effect will be discussed in a later section of this paper.

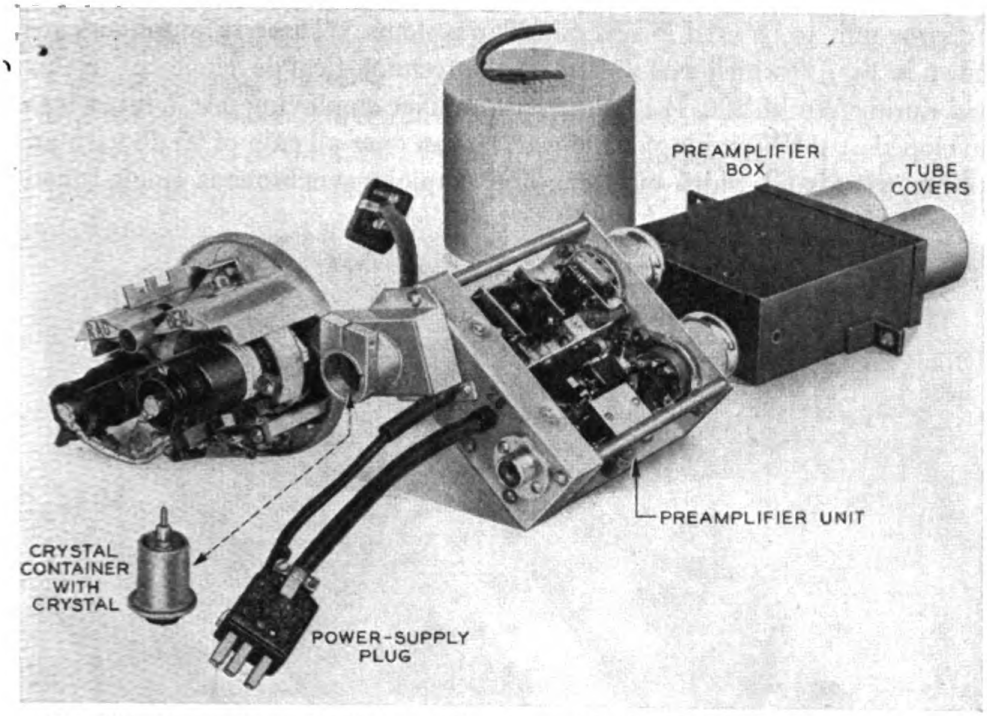

Fig. 28.—Converter and IF preamplifier assembly for AN/APQ-13 and AN/APQ-7 airborne radar bombing equipments.

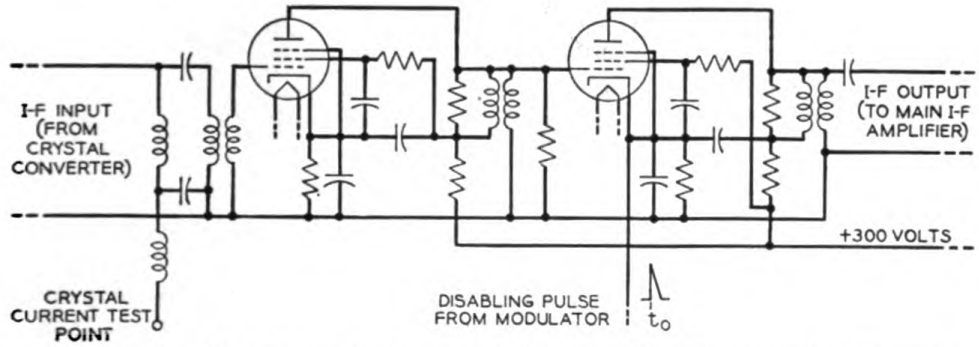

Fig. 29.—Simplified schematic diagram of IF preamplifier component of Figure 28.

Another example of equipment design of an airborne radar converter and preamplifier assembly has been illustrated previously in Fig. 23. In this design the 6AK5 tube is employed and single-tuned interstages and autotransformer input and output networks are employed; however, the general arrangement is quite similar to the design previously described.

The remainder of the IF amplifier gain required is of the order of 80 to

Digitized by Google
Original from UNIVERSITY OF MICHIGAN
Generated on 2019-09-22 07:20 GMT / http://hdl.handle.net/2027/mdp.39015077775156
Public Domain, Google-digitized / http://www.hathitrust.org/access_use#pd-google

100 db which is usually provided in a main IF amplifier that can be located conveniently within the receiver indicator portion of the radar system. The main IF amplifier is commonly designed as a complete shielded unit, required by the high-gain concentration and desirable from the standpoint of allowing the same unit to be used in several radar systems. Three IF amplifiers are shown in Fig. 30 which well illustrates the technological development in this field during World War II. The first amplifier employing 6AC7 tubes was developed at the beginning of the war, has an over-all gain of 95 db with an approximate band width of 2 mc, and employs synchronous single-tuned

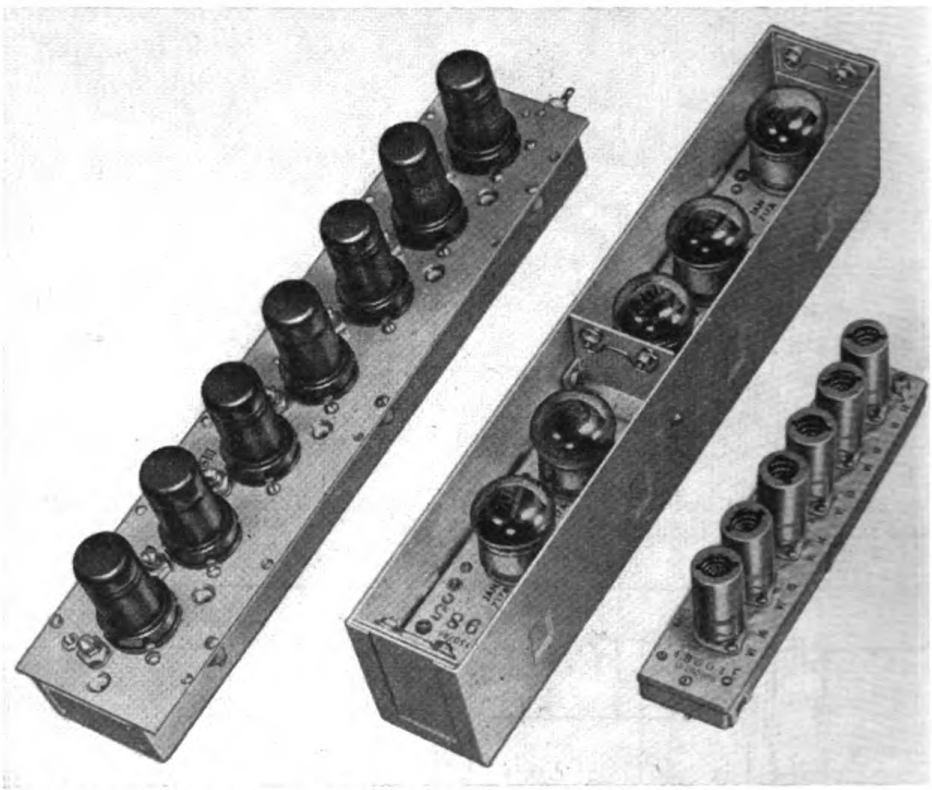

Fig. 30.—Typical IF amplifier equipment designs for military radar applications.

interstage networks. This design was employed extensively in early military radar equipments for land, sea, and air use. It has a total power consumption of 31 watts and weighs 2 pounds 4 ounces. The second amplifier illustrated was developed early in the war primarily for airborne search and interception radar systems and employs 717A pentodes with a double-tuned and single-tuned interstage combination of networks to produce a gain of 85 db with an over-all band width of 4 mc. The total power consumption is 11 watts and the weight here has been reduced to 1 pound 14 ounces. This design of IF amplifier with minor modifications was employed on the major-

Digitized by Google
Original from UNIVERSITY OF MICHIGAN
Generated on 2019-09-22 07:21 GMT / http://hdl.handle.net/2027/mdp.39015077775156
Public Domain, Google-digitized / http://www.hathitrust.org/access_use#pd-google

ity of airborne bombing radar equipments produced by the Western Electric Company during World War II. The third IF amplifier design illustrated was developed somewhat later in the radar program for specific application to the AN/APS-4 light-weight airborne search and interception radar equipment. This amplifier employs 6AK5 tubes with synchronous single-tuned interstage coupling networks realizing an over-all gain of 100 db for a band width of 2 mc. The power consumption here is 14.5 watts and the weight has been reduced to 9 ounces. This amplifier design has been employed in a number of airborne radar equipments during the later period of the past war.

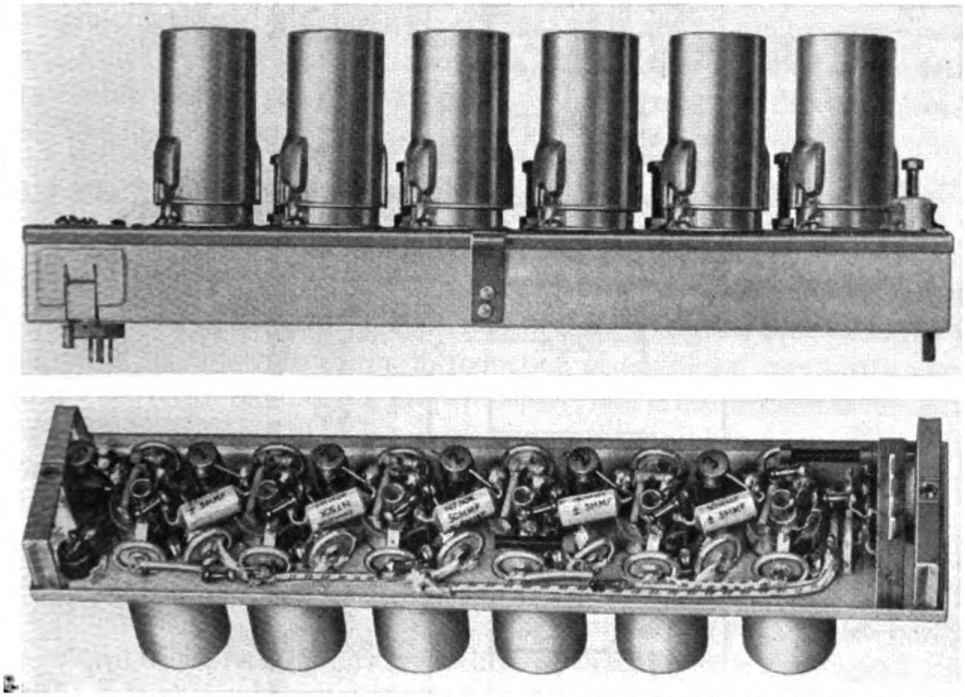

Fig. 31.—IF amplifier design as employed in AN/APS-4 airborne radar equipment.

Figure 31 illustrates further mechanical constructional details of the 6AK5 amplifier described above, and the schematic circuit arrangement is given in Fig. 32. Five stages of amplification and a second detector of a modified plate circuit type is included. A positive polarity video output is obtained from the cathode of the second detector and a single-section video low-pass filter attenuates the IF signal which appears at the detector output. A variable gain control voltage is applied to the plate circuits of the first three stages of the amplifier.

The mechanical arrangement of the components of this amplifier has been devised with a view to achieving optimum frequency and gain stability.

Generated on 2019-09-22 07:21 GMT / http://hdl.handle.net/2027/mdp.39015077775156
Public Domain, Google-digitized / http://www.hathitrust.org/access_use#pd-google
Digitized by Google
Original from UNIVERSITY OF MICHIGAN

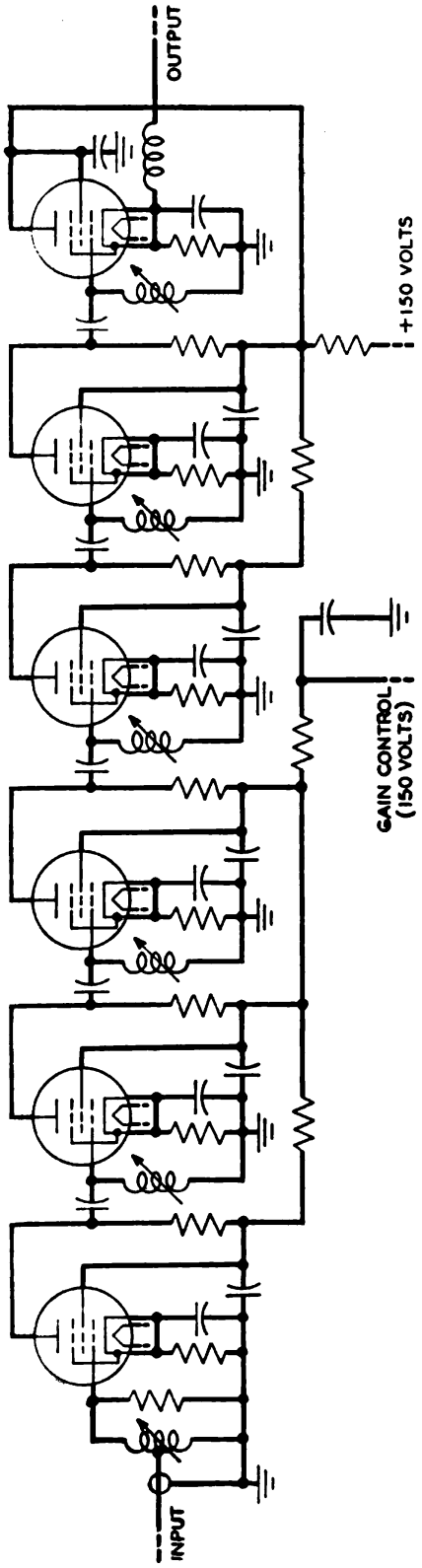

Fig. 32.—Simplified schematic diagram of 60-mc IF amplifier for AN/APS-4 radar.

Generated on 2019-09-22 07:21 GMT / http://hdl.handle.net/2027/mdp.39015077775156
Public Domain, Google-digitized / http://www.hathitrust.org/access_use#pd-google
Digitized by Google
Original from UNIVERSITY OF MICHIGAN

This equipment design features short and rigid connections and the use of silvered-mica button-type by-pass elements which are mechanically anchored in slots cut into the chassis and soldered in place. The entire unit is arranged to plug into a multipin socket which supplies all power and receives the video signal output. The IF signal input is arranged for plug-in connection at the opposite end of the chassis.

The adjustable inductance elements shown are wound on forms having an approximate diameter of $\frac{1}{4}''$ and the small variation in inductance required to compensate for circuit variations is achieved by the use of tuning screws as illustrated. These coils are adjusted in manufacture by a comparison technique employing factory standards of the same form. The completed amplifier is aligned with mean capacitance tubes and all tuning screws locked and sealed. Sufficient design margin of gain has been included in this design to enable meeting the radar system gain requirements with a complete set of "low-limit" tubes.

2.3 *The Radar Video Amplifier*

The video amplifier of the radar receiver, which follows the IF amplifier and second detector, has as its function the final preparation of the received and detected signal for display. This process involves amplification of the signal in its now video form, introduction of additional coordinate signals and wave forms required for proper display, and often includes modification of the original amplitude characteristics of the signal itself to enhance the presentation. The radar video signal is quite similar in many respects to the television video signal and the circuit technology, therefore, parallels the television art in many respects. Two characteristics of the radar video signal result, however, in somewhat less stringent demands on the radar video amplifier design. The lowest frequency of concern in radar video practice is related to the repetition rate which rarely is found to be less than 250 pps., while it is customary to design television systems to adequately transmit signals of the order of 1 cps. The requirement of faithful reproduction of the radar pulse shape is usually of secondary importance; the quality of presence alone usually sufficing to meet the radar system design objective. In certain fire-control radar systems, however, the radar system band width must be adequate to reproduce the received pulse to an exactness of the order maintained in standard television practice. In general these somewhat reduced transmission requirements for radar purposes result in a desirable economy of circuit elements and power consumption.

2.31 *Gain-Frequency Considerations*

The limiting performance of a video amplifier can conveniently be evaluated by a consideration of the transmission problem at the extremities of the

Digitized by Google
Original from UNIVERSITY OF MICHIGAN
Generated on 2019-09-22 07:22 GMT / http://hdl.handle.net/2027/mdp.39015077775156
Public Domain, Google-digitized / http://www.hathitrust.org/access_use#pd-google

video band of frequencies. At high frequencies the gain-frequency characteristic of a video amplifier stage employing pentodes as illustrated in Fig. 33 is given by

$$\frac{g_m R_L}{\sqrt{1 + f^2/f_H^2}}$$

where f_H represents the frequency at which the relative gain has been reduced 3 db over the value achieved at the video midband region. This cut-off frequency relationship is similar in form to that encountered in the radar IF

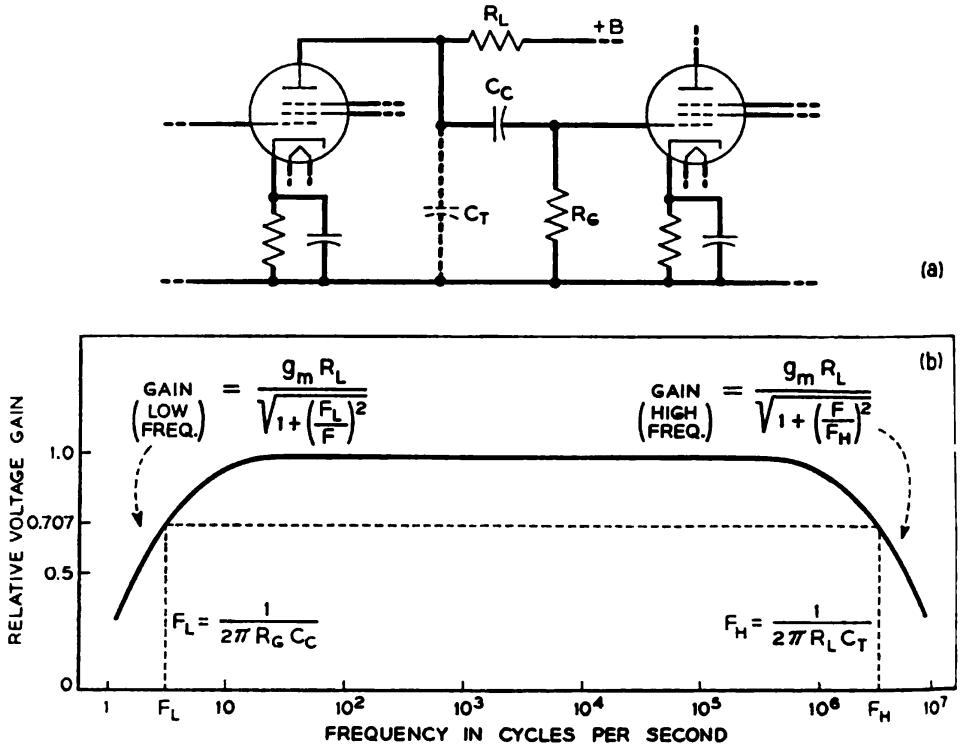

Fig. 33.—Radar video amplifier gain vs. frequency relationships.

amplifier design previously reviewed. In the video amplifier design the vacuum tube band merit B_o again determines the limiting performance of the amplifier, but since the associated video interstage circuit elements contribute considerably to the total circuit parasitic capacitance by reason of their large physical size, the effective band merit of a vacuum tube for video purposes must be considered in terms of the total tube and circuit capacitances. The additional consideration in vacuum tube choice for radar video amplifiers is one of load capacity, since the output signal voltage required for indicator use may range upward to several hundred volts.

In a somewhat analogous manner to the relationships discussed in the

Digitized by Google
Original from UNIVERSITY OF MICHIGAN
Generated on 2019-09-22 07:22 GMT / http://hdl.handle.net/2027/mdp.39015077775156
Public Domain, Google-digitized / http://www.hathitrust.org/access_use#pd-google

design of IF amplifier interstage networks, the video amplifier performance at high frequencies can be improved by the use of more complex 2- and 4-terminal interstage networks. In military radar systems, however, the added performance realized is more than offset by the undesirability of the additional circuit elements required and the more complex maintenance problems that arise, so that usually only the simple resistance-coupled interstage design is encountered in radar systems.

At the low-frequency extreme of the video band the gain performance of the simple video amplifier is related to the product of the series interstage plate-grid coupling capacitance and the input resistance of the following grid circuit. The low-frequency cut-off of a video amplifier is again defined as the frequency where the gain has fallen 3 db over the value at midband frequencies and is given by $f_L = \frac{1}{2\pi R_G C_c}$. The highest value of R_G that can be employed is related to the grid current characteristics of the vacuum tube chosen. The use of a large value of C_c is undesirable for two reasons. First, the interstage shunt parasitic capacitance increases as a physically larger condenser is employed, which results in poorer high video frequency performance. Second, the use of large coupling capacitances is undesirable from the standpoint of increase in susceptibility to blocking or paralysis in the presence of large signals or enemy jamming. The low-frequency gain response can be improved by certain proportioning of the plate, screen, and cathode by-pass elements also resulting in somewhat less possibility of undesirable feedback through the common power supply impedance.

In certain military radar system designs, multistage negative feedback video amplifiers have been employed. Here considerably greater transmission band width may be realized with the simple interstage network design and an order of improvement in stability results. The feedback amplifier design in these cases usually involves common cathode feedback impedance between the first and third stages.

2.32 *Gain-Amplitude Considerations*

The use of nonlinear gain versus amplitude characteristics in a video amplifier is a condition peculiar to the radar system and represents a considerable departure from established television practice. The factors that indicate the desirability of this treatment of the signal involve the behavior of the amplifier under the extreme range of received radar and jamming signals encountered and the electro-optical characteristics of certain radar indicator cathode-ray tubes.

Definite amplitude limiting of the video radar signal is commonly included in military radar systems. By introducing amplitude limiting at an early part of the video amplifier, complete amplifier paralysis is avoided when

Digitized by Google
Original from UNIVERSITY OF MICHIGAN
Generated on 2019-09-22 07:22 GMT / http://hdl.handle.net/2027/mdp.39015077775156
Public Domain, Google-digitized / http://www.hathitrust.org/access_use#pd-google

extremely large overloading signals are encountered. These signals may represent strong radar return echoes from objects in the vicinity of the radar antenna or may be due to enemy jamming signals. The ability of the radar receiver to recover in a short time following such serious overloading is an extremely important design consideration. In the case of jamming signals of a continuous-wave or long-pulse form, their effectiveness can be minimized by the inclusion of a high-pass network at the input of the video amplifier.

In the case of radar systems which employ intensity modulated displays of the B, C, and PPI forms the maximum useful brightness that can be attained is limited by "blooming," a phenomenon in which the cathode-ray tube spot on the fluorescent screen undergoes a sudden defocussing when the brightness is increased beyond a critical value. In addition, halation effects are quite pronounced in these long-persistence cascade layer screens and contribute to an undesired masking effect when large areas of extreme brightness are encountered. In these cases it is extremely important to limit the maximum amplitude of the signal that can be impressed upon the indicator. The usual radar video amplifier includes an amplitude limiting stage located early in the amplifier chain whose operating conditions are such as to be driven to plate current cut-off by signals which exceed a preselected amplitude.

The range of useful brightness of the cascade screen radar indicator is severely limited in comparison with the extreme amplitude range of the received radar signals. As has been discussed, the maximum useful brightness has been seen to be limited by halation and defocussing effects while the minimum brightness threshold is controlled by halation and ambient viewing conditions. These limitations of the viewing tube result in a criticalness of adjustment required of the radar operator to achieve the optimum performance of the radar system. In an effort to improve the general reproduction efficiency of the military radar system, several circuit forms have been devised whereby the amplitude of the indicator signal is related to the received radar signal in a nonlinear fashion. In certain instances two parallel amplifier paths have been provided where one path operates in a normal fashion until overload is reached when the second transmission path, designed to properly transmit the higher amplitude signals, becomes effective. In this manner two relatively linear amplification regions are provided with a step or amplitude limiting region interposed. Such a nonlinear circuit arrangement has been referred to as "duo-tone", indicative of the two reproduction regions employed. Another video nonlinear characteristic which was employed in a certain airborne radar bombing equipment developed toward the end of the war was of a logarithmic form realized by a two-path amplifier design. In general this nonlinear treatment of the radar signal amplitude has proven capable of reducing the critical adjust-

Digitized by Google
Original from UNIVERSITY OF MICHIGAN
Generated on 2019-09-22 07:22 GMT / http://hdl.handle.net/2027/mdp.39015077775156
Public Domain, Google-digitized / http://www.hathitrust.org/access_use#pd-google

ment which has in the past been required of the radar indicator and in this respect has contributed some measure of improved performance under military operating conditions.

2.33 *D-c Restoration Methods*

It is pertinent to examine the exact form of the video signal encountered at the output of the video amplifier as it exists available for indicator use. The presence of series coupling condensers in the video amplifier has removed the d-c component from the signal as detected and, therefore, the average value of the signal is zero. In this form the amplitude of the positive and negative signal excursions are dependent on the form of the signal itself. If such a signal is impressed upon an indicator of the intensity modulated type the average brightness of the scene will remain constant, and the presence of several large amplitude signals will tend to drive any accompanying weak signals below the useful reproduction threshold and effectively fail to reproduce them. In the case of an A-type display where the video signal deflection modulates the beam, the no-signal base line will assume a position on the screen dependent on the video signal form. For these applications it is required that the d-c component be restored to the signal before display. In many other parts of the radar system d-c restoration is required to enable utilizing to the fullest extent the load capabilities of vacuum tubes under the conditions of varying duty cycles of the impressed wave forms. In sweep circuit design a considerable economy of power is achieved by operating the amplifier tubes at or near plate current cut-off for no-signal conditions. Through the medium of d-c restoration, the signal excursions are confined to positive regions only and then regardless of the duty cycle the signal range of amplitude impressed upon the tube is maintained within desired limits.

Figure 34 illustrates three circuit forms which are employed to "reinsert" the d-c component of an a-c video signal. The diode restorer commonly employed in radar systems is shown in Fig. 34a. The impressed input wave, assumed to have an average value of zero as shown, will cause the diode to conduct whenever the signal polarity is negative. During this diode conducting period the condenser C will be charged rapidly, the full effective negative peak signal voltage appearing across its terminals. During the following positive excursion of the signal this voltage difference will be applied effectively in series with the signal. The time constant RC is chosen large with respect to the period of the signal repetition rate and thus maintains this additive bias for the remainder of the signal cycle. Since the effective time constant during the diode conducting period is extremely small valued, limited only by the conductive internal resistance of the diode itself, an extremely small negative excursion time will suffice to

Digitized by Google
Original from UNIVERSITY OF MICHIGAN
Generated on 2019-09-22 07:22 GMT / http://hdl.handle.net/2027/mdp.39015077775156
Public Domain, Google-digitized / http://www.hathitrust.org/access_use#pd-google

restore the grid circuit to reference zero potential. This particular d-c restorer circuit form is referred to as a positive restorer, indicative of the final polarity of the restored signal. A simple reversal of the diode elements will reverse the polarity of the restored signal.

Figure 34b illustrates the usual radar circuit form of a negative d-c restorer where the diode is eliminated, the normal vacuum tube grid circuit

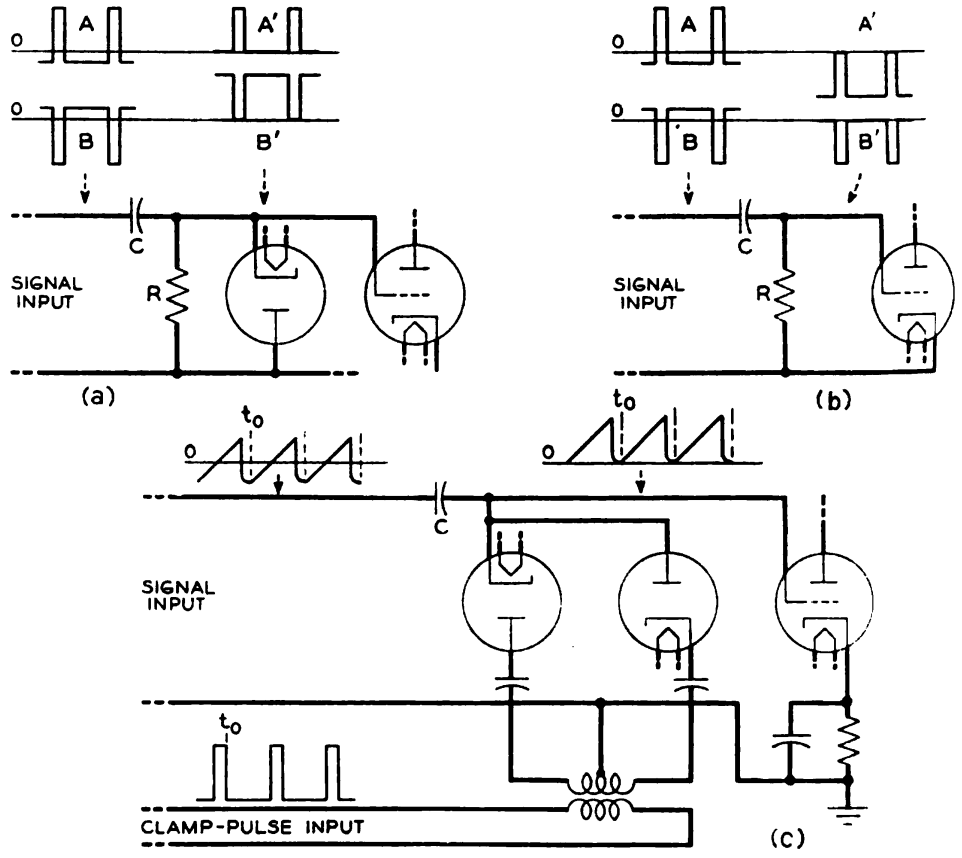

Fig. 34.—Typical D-c Restorer Circuit Forms. Simplified schematic diagrams.

serving here to fulfill this function. Here again an impressed signal form having an average value of zero is assumed, and a negative polarity restored signal is desired at the grid of the amplifier tube. During periods of positive excursions of the input signal the vacuum tube grid will conduct since it is normally operated at zero bias. The series condenser C is accordingly charged relative to the positive signal peak amplitude and this value of potential will be additively combined with the signal during negative excursions in a similar manner to the diode restorer action just described.

A third form of d-c restoration is known as a clamper or synchronized d-c restorer and is illustrated in Fig. 34c. Here a diode bridge circuit

Digitized by Google
Original from UNIVERSITY OF MICHIGAN
Generated on 2019-09-22 07:22 GMT / http://hdl.handle.net/2027/mdp.39015077775156
Public Domain, Google-digitized / http://www.hathitrust.org/access_use#pd-google

is arranged to be normally nonconductive except during the application of a clamping pulse bias introduced as shown. During this clamping interval, the grid circuit point of the condenser is re-established to reference potential by the low impedance of the conducting diode circuit. At the time of decay of the clamping pulse wave forms the operation of this circuit follows the principles of the d-c restorer types just described. This circuit has been employed less extensively than the preceding simple d-c restorer methods because of the relatively more complex arrangement, but has an advantage in that the impressed signal may be clamped to a convenient reference potential at any particular repetitive point in the cycle.

2.34 *Typical Radar Receiver Video Amplifier Circuits*

The radar receiver video amplifier signal output is required to modulate the indicator by either position or intensity change. In the A type of display the video signal is usually impressed upon a pair of vertical deflection plates of an electrostatic type of cathode-ray tube to present the amplitude characteristics of the signal while the range to the target is displayed as the horizontal coordinate. The maximum video signal amplitude required here to deflect the beam satisfactorily is usually of the order of several hundreds of volts. In the case of B, C, and PPI forms of display the radar video signal is required to intensity modulate the cathode-ray tube. Here a maximum video signal amplitude of 50 volts is commonly required by the radar indicator.

In certain military radar system applications it is desirable to locate the indicator component at some distance from the main radar receiver and video amplifier assemblies. This requirement is commonly encountered in large naval vessel installations where the main radar components may be located below deck and the indicator mounted as a part of the gun pointing mechanism. In such cases video amplifier designs employing video transformer coupling between the output amplifier stage and a coaxial transmission line and between the line and the indicator circuit proper, have proven to be entirely successful.

The development of video pulse transformers for radar purposes represents a considerable advance in the art of communication transformer design. The greatly improved wide frequency band performance of these components is the result of the employment of improved magnetic core materials such as supermalloy having relative permeabilities upward of four times that available in the permalloy materials, improved techniques of coil winding distribution, and the use of additional network elements in the final configuration. Figure 35 illustrates the constructional features of such a video pulse output transformer which has a band width extending

Digitized by Google
Original from UNIVERSITY OF MICHIGAN
Generated on 2019-09-22 07:23 GMT / http://hdl.handle.net/2027/mdp.39015077775156
Public Domain, Google-digitized / http://www.hathitrust.org/access_use#pd-google

from 100 cycles to 7 megacycles as employed in a naval fire-control radar equipment.

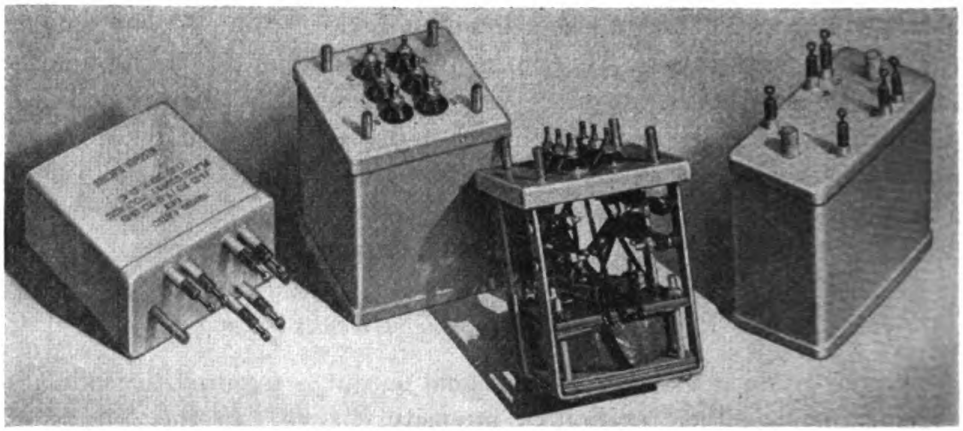

Fig. 35.—Typical designs of radar receiver video frequency transformers.

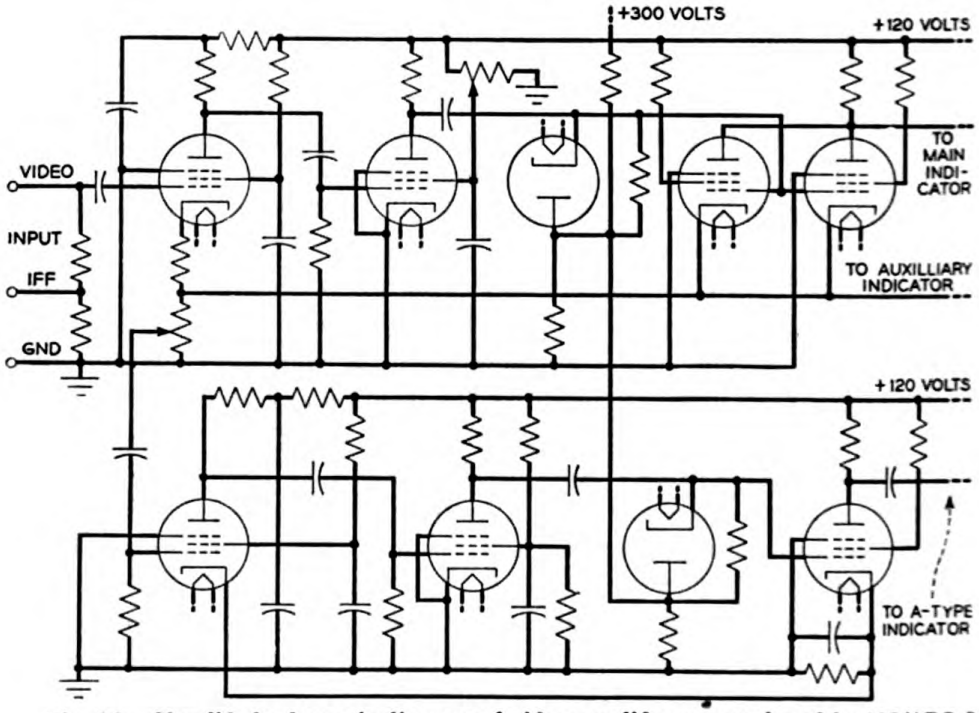

Fig. 36.—Simplified schematic diagram of video amplifiers as employed in AN/APQ-7 airborne radar equipment.

Figure 36 illustrates a video amplifier circuit arrangement as developed for the AN/APQ-7 radar bombing equipment during the latter period of the past war. This system employed two GPI type indicators, one of which was located at a remote station of the aircraft and included also an

Digitized by Google
Original from UNIVERSITY OF MICHIGAN
Generated on 2019-09-22 07:23 GMT / http://hdl.handle.net/2027/mdp.39015077775156
Public Domain, Google-digitized / http://www.hathitrust.org/access_use#pd-google

A-type indicator which was employed for certain conveniences in operation and maintenance of the equipment. This circuit design includes a main video amplifier for the ground plan indication and a separate amplifier for the A-type display, both of which are of the negative feedback type. The limiting amplifier is included as the second stage with negative d-c restoration included in this grid circuit and diode d-c restoration at the grid of the last stage. To provide sufficient output signal level with the wide video band width required it was necessary to employ two 6AG7 tubes in parallel in the final output stage of the main video amplifier. The local indicator is fed from the plate circuit while the remote navigator's display is fed by means of a low impedance coaxial transmission line. The video gain control is essentially an adjustment of the video amplitude limiting level, the actual signal amplitude being previously adjusted by the IF amplifier gain control. The over-all gain of the main video amplifier is approximately 32 db with a band width of approximately 5 mc. The over-all gain of the A-type display amplifier circuit is approximately 43 db with a useful band width of approximately 6 mc.

2.4 *The Radar Indicator*

The radar indicator assumes a position of extreme importance in the components of the radar receiver. Here with a few specific exceptions all of the electrical information which has been obtained regarding the area under observation is finally correlated and converted into an optical display for use by the radar observer. In the discussion thus far, only the received radar microwave signal properly selected, amplified, and finally converted to the video form has been discussed in detail. The preparation of the additional coordinate and reference data necessary to properly present the complete scene is reviewed in the following sections. In this section the characteristics of the presentation will be reviewed from the standpoint of the requirements imposed by the various radar applications. The electro-optical characteristics of the display device are also discussed.

2.41 *Classification of Radar Display Types*

The number and types of display methods which have been developed for military radar systems during World War II are the result of the varied specific applications to which radar has been subjected. These types of displays are in general related directly to the functional classification of military radar systems previously discussed. It is of interest to consider at this time the various types of indicators which have become common in the radar field. Figure 37 illustrates the basic characteristics of the most important types of radar presentations.

Basically the three coordinates which determine the position of the target

Digitized by Google
Original from UNIVERSITY OF MICHIGAN
Generated on 2019-09-22 07:23 GMT / http://hdl.handle.net/2027/mdp.39015077775156
Public Domain, Google-digitized / http://www.hathitrust.org/access_use#pd-google

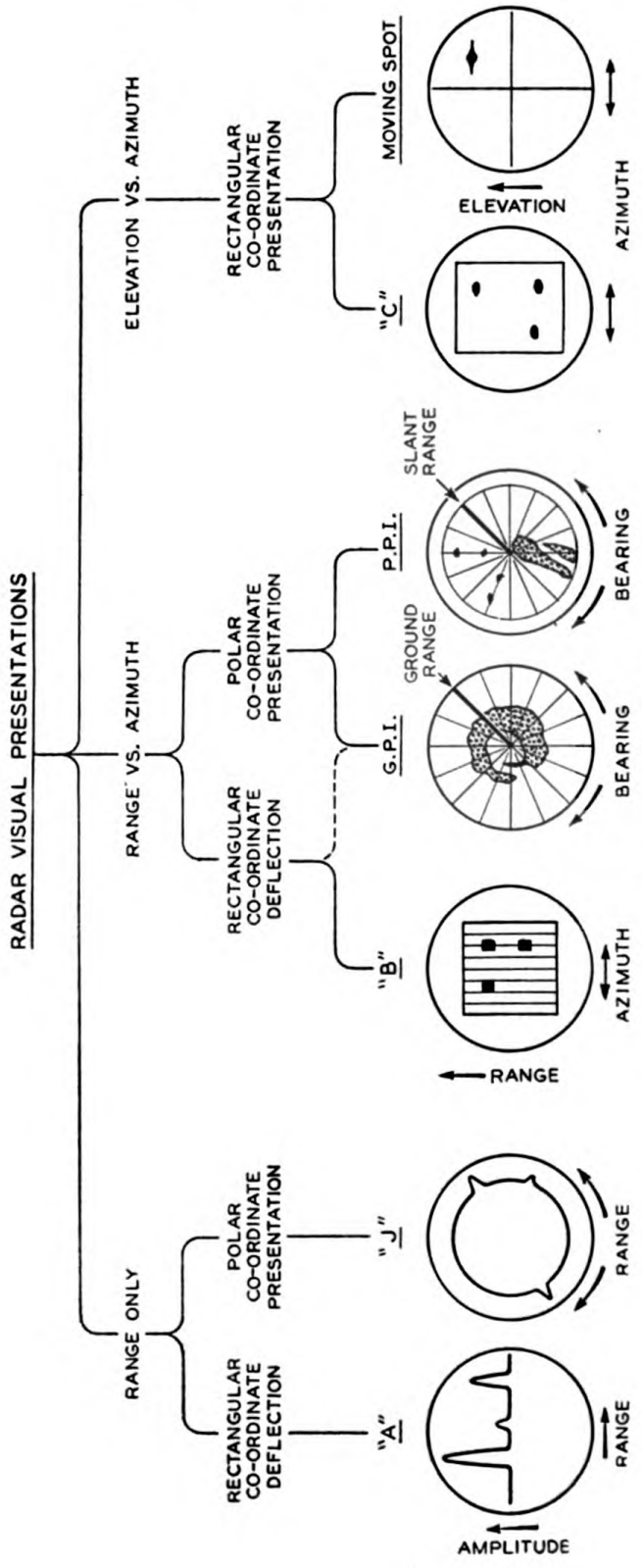

Fig. 37.—Typical military radar display types.

Digitized by Google
Original from UNIVERSITY OF MICHIGAN
Generated on 2019-09-22 07:23 GMT / http://hdl.handle.net/2027/mdp.39015077775156
Public Domain, Google-digitized / http://www.hathitrust.org/access_use#pd-google

in space and which are determinable from a single radar observation location are the range to the target, azimuth angle with respect to a chosen direction axis, and elevation angle as measured from a convenient reference plane. The classification of radar displays shown in Fig. 37 results from the fact that the only available and convenient display device has the property of resolving only two such coordinates simultaneously. The radar display problem is then one of selecting the most important two coordinates for the specific radar application and choosing the presentation means accordingly. For example, if the radar system under consideration is to be employed on a surface naval vessel against similar naval vessel targets, it follows that elevation angle radar information is redundant and, therefore, type-A or B display patterns are quite satisfactory and are in fact the typical presentations which have been universally employed for surface target fire-control applications. The basic A-type indicator presents range-only data, but for fire-control purposes a modified form is often employed with lobe switching by which accurate training of the radar antenna is possible and bearing information is thus secondarily obtained.

For airborne radar search and bombing applications the presentation is concerned with targets, one coordinate of which is known by other than radar means. Since all targets of interest are in this case located on the ground plane, the relative location of which is determinable by reference to the altimeter and a gyroscopic artificial horizon within the aircraft, it is sufficient here to present all information as a 2-dimensional map. The presence of targets and to some extent their composition is observable as an intensity modulation of the field of view. For this type of application the PPI or its more exact successor the GPI form of presentation is extensively employed.

For military radar applications where fire-control information is desired pertaining to targets which are not confined to a definite plane all three determinable coordinates must be known and, therefore, presented to the radar observer. In certain instances this requirement has been fulfilled by the use of multiple displays each presenting the information regarding one or two coordinates and in cases where gun training is accomplished through separate operators for each coordinate axis, range, bearing, and elevation, this method has proven entirely satisfactory. During World War II the fast moving and highly maneuverable aircraft target has required a more direct and, therefore, faster system of gun pointing. In these cases, the operator has been provided with a display which electronically duplicates a sighting telescope and which merely requires the operator to position the gun (and associated radar antenna) until the target image is centered. To introduce a measure of range to the target the size or form of the target "spot" is often varied in accordance with the range data. For defense against low-level aircraft attacks this admittedly crude range information

Digitized by Google
Original from UNIVERSITY OF MICHIGAN
Generated on 2019-09-22 07:23 GMT / http://hdl.handle.net/2027/mdp.39015077775156
Public Domain, Google-digitized / http://www.hathitrust.org/access_use#pd-google

has proven quite satisfactory. Similar presentation methods developed for airborne aircraft interception radar equipments have employed, in addition, separate instruments to notify the pilot or gunner at the time when the range to the target was proper for firing of the guns. Another variation in method of obtaining accurate range information simultaneous with the elevation and azimuth data is through the employment of automatic range tracking. In this case after identification and selection of the target has been made and the initial coincidence accomplished, the operator is then free to track in elevation and azimuth with the automatic tracking device continuing to furnish the changing range data to the gun.

Figure 37 indicates the fact that included in these display forms are variations which are a function of the deflection coordinates peculiar to the display device itself. The factors which determine this choice are related to the required form of the presentation from the standpoint of military use, the characteristics of the particular display device available and the mechanical form of the antenna scanning system.

It should be observed that a number of minor variations in the exact presentation is available to the radar system designer within the general classification indicated in Fig. 37. As mentioned previously, the A-type display may be modified to indicate azimuthal pointing errors. In this case, sometimes referred to as a K-type display, the radar system employs an antenna capable of producing two beams of radiation, available one at a time, with azimuthal bearings differing by the order of the beam width. Two signals, each of which is associated with one position of the radiated beam, are displayed in the basic A-type form with one slightly displaced in the range coordinate with respect to the other. By "steering" the antenna until the amplitude response of the desired target appears equal for each image, the target bearing is determined as the direction line bisecting the two antenna lobes.

It is often desirable to limit the display to a small area or to a small selected range interval to enable magnification of this particular portion of the scene. The accurate measurement of range for fire-control purposes can be accomplished on a conveniently small indicator screen by expanding only a selected small range interval of interest. The loss of information at other ranges under these conditions is unimportant. In certain airborne applications it is desirable to present large area information for navigational purposes, but at the time of starting the radar bombing attack the area of interest is limited to a narrow sector extending outward from the plane in the direction of the attack. Here a selected sector may be expanded with a probable increase in accuracy of individual target identification and final bombing accuracy.

In the "range only" classification of Fig. 37 the J-type of display has an

Digitized by Google
Original from UNIVERSITY OF MICHIGAN
Generated on 2019-09-22 07:24 GMT / http://hdl.handle.net/2027/mdp.39015077775156
Public Domain, Google-digitized / http://www.hathitrust.org/access_use#pd-google

advantage of expansion of the range information by a factor of approximately three times for the same size screen. The A and J types are employed extensively in fire-control radar equipments.

In the range versus azimuth class of radar presentations the B scan historically preceded the other forms shown. Its application was found originally in airborne radar systems for interception purposes. It was commonly employed in conjunction with an auxiliary C-type indicator for target elevation determination. The B type of display suffers from a distortion due to the reproduction of polar coordinate information directly on a rectangular coordinate field. This particular form of distortion is not of major importance where only a few isolated aircraft targets are to be displayed, and in the case of guiding an aircraft to intercept the target the relative expansion of the azimuth scale at short ranges may be a slight advantage. When the B type of presentation is employed for navigation and observation of ground features this inherent field distortion becomes very objectionable when map comparisons of the radar image are required. The B type of display has also been employed extensively on narrow sector rapid scanning naval fire-control radar systems.

The plan position indicator (PPI) type of display was developed to overcome the objectionable distortion of the B-type display and to afford a method of presenting a 360° azimuthal pattern when rotating antenna structures were employed. This form of display essentially replaced the B-type display for aircraft search radar systems and has been since universally employed for ground and naval vessel search systems. Here the linear range trace on the screen is directed outward from the center of the tube, its radial position being synchronized with the instantaneous bearing of the scanning antenna. The map presentation is exact for ground and naval vessel radar locations and for low-flying aircraft radar systems the distortion is negligible, since the slant radar range to the target at low altitudes is essentially comparable to the range as measured on the ground plane. As the altitude of a radar equipped aircraft is increased, the map distortion of the simple form of PPI display also becomes quite objectionable and several modified forms of this display can be employed to improve the presentation. One of these involves delaying the time of start of the linear range sweep by a time interval corresponding to the propagation time of the radar pulse to the ground and return. In this manner a simple but desirable improvement in display is realized. As the military requirements during the later period of the past war became more exacting with the emphasis on high-altitude radar bombing, the remaining distortion of the delayed PPI presentation was found undesirable, and the necessity for accurate map display directly beneath the aircraft resulted in the development of the ground plan indicator (GPI). In this type of display the range trace is deflected as a

Digitized by Google
Original from UNIVERSITY OF MICHIGAN
Generated on 2019-09-22 07:24 GMT / http://hdl.handle.net/2027/mdp.39015077775156
Public Domain, Google-digitized / http://www.hathitrust.org/access_use#pd-google

nonlinear function of time; its exact time function being dependent on the altitude of the aircraft. The altitude information is obtained from the aircraft altimeter and may be manually or automatically introduced into the radar receiver to produce the proper form of sweep function. These modified forms of PPI presentation were employed extensively in the large bombing through overcast radar program which attained a status of major importance toward the later portion of World War II.

The elevation versus azimuth classification of display forms is essentially restricted to fire-control and aircraft interception radar applications. As previously noted, the C-type display was developed early in the military radar program and has somewhat the same characteristics as the B scan in terms of the distortion which results in the display of polar coordinate data in a rectangular coordinate field without proper mathematical conversion. In the case of aircraft interception radar applications, this type of display is quite satisfactory and has been employed quite extensively for this purpose.

The moving spot (MS) form of radar display is usually associated with a radar system in which conical scanning or lobing is employed. Here the source of radiation of the antenna is arranged and rotated so as to provide a beam whose path describes a cone. If the target is located on the axis of this cone of radiation the signal response will be essentially constant for all instantaneous positions of the beam. If the target is positioned to one side of the cone's axis the received radar signal will be modulated at the frequency of the conical scanning process and the degree of modulation will be related to the angle between the conical axis and the bearing toward the target. This modulation information is utilized within the radar receiver to position an optical image on the face of the indicator screen in accordance with the direction of the target. In radar systems employing this form of indication the observer positions his radar antenna, and accordingly the associated weapon, to center the target image on the indicator. Mechanical or electronic cross hairs are employed as the reference axis. A measure of range to target information is often introduced into this form of display by assigning an arbitrary but distinctive size or shape to the target spot which can be varied in accordance with the range to the target being observed.

2.42 *The Cathode-Ray Tube*

The cathode-ray tube is without serious competition as the ideal radar indicator, primarily because of its unique high-frequency electro-optical response characteristic. Since the radar presentation requirements are not unlike those encountered in television practice, it is natural that the cathode-ray tube development for radar purposes should have progressed along simi-

Digitized by Google
Original from UNIVERSITY OF MICHIGAN
Generated on 2019-09-22 07:24 GMT / http://hdl.handle.net/2027/mdp.39015077775156
Public Domain, Google-digitized / http://www.hathitrust.org/access_use#pd-google

lar lines originally established by prewar television. Two general types of cathode-ray tubes have been commonly employed in the military radar program, electrostatic and magnetic, these classifications being indicative of the deflection and focussing method employed.

Electrostatic Deflection Type

A typical form of electrostatic-type of cathode-ray tube suitable for radar indicator purposes is shown in Fig. 38. In this tube type the electrons emitted from an indirectly heated cathode surface are initially formed into a beam by passage through an aperture which serves as a beam density or ultimate brightness control element. Following this, the electrons proceed through another aperture which is maintained at a positive potential with respect to the cathode. This first anode together with the following second anode forms an electron lens system which focuses the beam on the fluores-

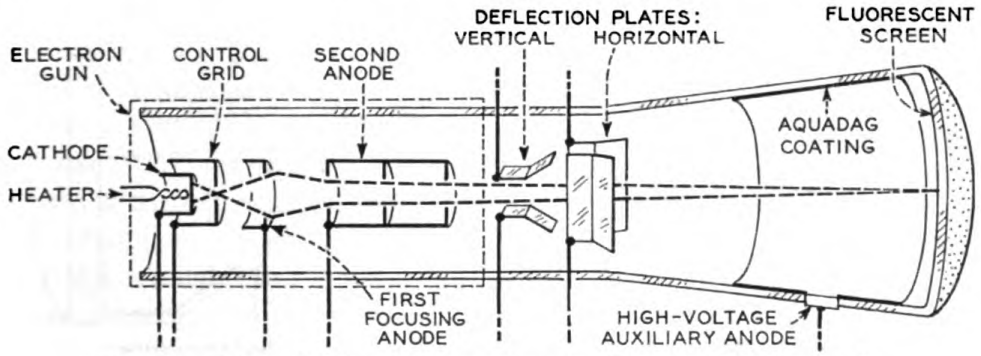

Fig. 38.—Schematic diagram of an electrostatic type cathode-ray tube.

cent screen surface. The relative potentials of these elements serve to enable focussing of the beam by electrical means. The deflection of the beam for scanning purposes is here accomplished by the introduction of an electric field formed by the application of potential across the deflection plates shown. Two pairs of plates enable separate horizontal and vertical deflection to be employed. The plates are formed as shown to enable obtaining the maximum deflection per unit of electrical potential applied without interference with the beam under large deflection conditions. The high-voltage auxiliary anode is provided in certain tube types to further accelerate the beam after deflection without an appreciable reduction of deflection sensitivity and results in an image of increased brightness.

To realize optimum performance of an electrostatic-type cathode-ray tube several precautions must be observed. Serious defocussing of the beam as it is deflected will result if the average potential of the pair of deflection, plates is allowed to vary substantially from the value present at the second anode. To minimize this effect, balanced sweep deflection amplifiers are

Generated on 2019-09-22 07:24 GMT / http://hdl.handle.net/2027/mdp.39015077775156
Public Domain, Google-digitized / http://www.hathitrust.org/access_use#pd-google
Digitized by Google
Original from UNIVERSITY OF MICHIGAN

commonly employed in radar receivers employing electrostatic deflection, and the second anode is maintained at the average potential of these deflection plates. Astigmatism, the selective focussing in one direction on the screen at the expense of focus in the other, results from the mechanical limitations whereby the electric fields of the two pairs of deflection plates cannot be made effective at the same point within the tube. Some improvement can be realized in this respect by operating the pairs of deflecting plates at slightly different average potentials.

The limitation in deflection response at high frequencies is a function of the total deflection circuit capacitance. To eliminate the blocking condensers with their considerable parasitic capacitance to ground it is common radar indicator practice to operate the deflection plates directly from the

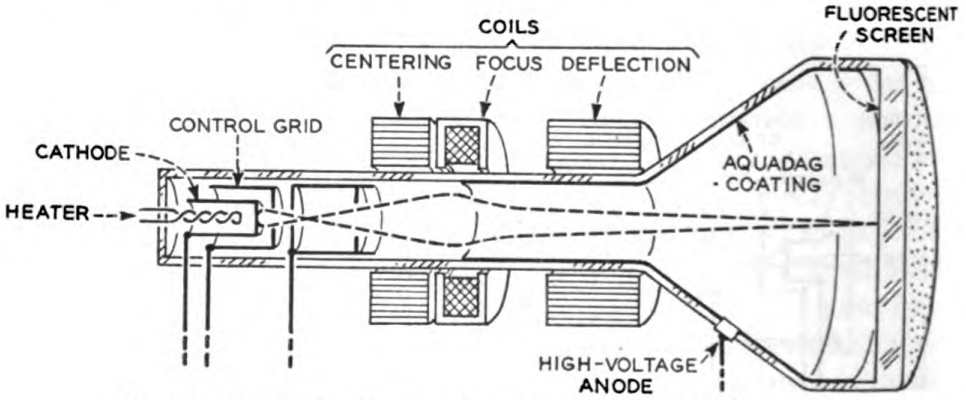

Fig. 39.—Schematic diagram of a magnetic type cathode-ray tube.

plates of the sweep amplifier tubes and then accordingly operate the cathode of the cathode-ray tube at a high negative potential.

Magnetic Deflection Type

A typical form of a magnetic-type cathode-ray tube is illustrated in Fig. 39. In this tube the electron gun structure comprises a heater, cathode, control grid, and second or screen grid which, together with the second anode, usually formed by an aquadag coating within the glass envelope and which is maintained at a high positive potential, roughly delineates the beam. The second grid in this case serves to shield the control grid from the high potential second anode and results in an improved control grid characteristic. The beam of electrons is focussed through the use of a magnetic field located as shown in Fig. 39, and produced by direct current flow through a coil or by a permanent magnet structure. The centering of the beam upon the screen under no deflection conditions is accomplished by the use of a distorting field commonly introduced as a part of the deflection coil and focussing assembly. The deflection of the beam for a rectangular coor-

Generated on 2019-09-22 07:24 GMT / http://hdl.handle.net/2027/mdp.39015077775156
Public Domain, Google-digitized / http://www.hathitrust.org/access_use#pd-google
Digitized by Google
Original from UNIVERSITY OF MICHIGAN

dinate display system is here accomplished by magnetic deflection fields perpendicularly disposed and produced by a pair of deflection coils located at the junction of the neck and bulb as shown. In the polar form of display (PPI) usually only one deflection coil is employed for the production of the radial sweep, the angular deflection being produced by rotation of this coil about the neck of the cathode-ray tube in synchronism with the rotation of the antenna.

It is of interest to compare the relative characteristics of the electrostatic and the magnetic-type of cathode-ray tubes from the standpoint of their application to radar indicators. The electrostatic-type of cathode-ray tube has a distinct advantage of lighter total weight for the tube itself and the associated deflection circuits required, which in the case of airborne radar equipment design is an important factor in its favor. In general, it is desirable to present a large radar display field. For the larger diameter cathode-ray tubes the magnetic-type tube has an advantage of shorter over-all length which has proven an important equipment design factor for airborne radar equipment where the available operating space is severely limited. The magnetic-type cathode-ray tube requires weighty focussing and deflecting assemblies and large power supplies to furnish the heavy deflection current required, but because of the higher anode voltages which may be employed here, the screen brightness achieved is considerably greater than that available in the usual electrostatic type of cathode-ray tube. If the anode potential of an electrostatic type of cathode-ray tube is increased and hence the screen brightness, the deflection sensitivity is seriously impaired and a difficult deflection amplifier design results. From a deflection point of view, it is possible to achieve somewhat better performance in reproducing extremely high-speed sweeps by employing an electrostatic-type of indicator which has somewhat less serious parasitic elements which act to limit the high-frequency response. The final choice of type of cathode-ray tube for the radar indicator is dependent on the specific detailed considerations of the system in hand. No general and fast rules governing this decision are evident.

Characteristics of the Fluorescent Screen

The fluorescent screen of the cathode-ray tube upon which the final radar information is converted into the desired visual form consists of a deposit of certain materials which exhibits fluorescence when bombarded with a high-velocity electron stream. Phosphorescence, the continued emission of visible light after bombardment has ceased, is also a property of all of these screen materials. These screen materials, referred to as "phosphors", have characteristics dependent on their physical form as well as their chemical composition.

Digitized by Google
Original from UNIVERSITY OF MICHIGAN
Generated on 2019-09-22 07:24 GMT / http://hdl.handle.net/2027/mdp.39015077775156
Public Domain, Google-digitized / http://www.hathitrust.org/access_use#pd-google

Two general types of phosphors have been commonly employed in military radar systems classified according to their phosphorescence characteristics. The medium persistence class of phosphors exhibit decay times of the order of milliseconds and are composed of a single layer of Willemite (zinc orthosilicate). This type of screen exhibits a green luminous response and is employed extensively in reproducing high-speed wave forms such as encountered in high-speed scanning systems, and for general A-type presentation purposes. The visible light output decays to the order of 1% of its initial value in approximately 50 milliseconds after electron excitation ceases. For photographic purposes other phosphor compositions of the same persistence class whose useful light output has a higher actinic value are commonly employed.

The long-persistence phosphors are composed of two layers of screen material which combination exhibits sustained phosphorescence, the visible light output decaying very slowly after cessation of bombardment. The double layer or cascade screen consists of an innermost layer subject to the direct influence of the electron stream which is composed of a silver activated zinc sulphide and a second layer adjacent to the glass envelope which consists of copper activated zinc cadmium sulphide. The first-named material fluoresces with an extremely brilliant blue light under bombardment and exhibits a rather rapid decay characteristic. The second layer is in turn excited by the blue radiation from the first layer and responds with a yellow visible emission which persists for a matter of several seconds after excitation ceases. The initial blue flash is appreciably absorbed by the second phosphor layer, but usually further optical attenuation is required to prevent eyestrain and degradation of night vision of the observer. This is commonly provided by the use of an amber optical filter placed over the screen face. The long-persistence characteristics available in this type of tube have proven invaluable in military radar systems which feature slow antenna scanning. In many of these systems the time between successive scans of the target may be of the order of a second or more and only through the use of the cascade-type long-persistence tube can the image be retained for this period of nonexcitation. Another property of the long persistence class of cathode-ray tube screens which is of advantage for radar purposes is an accumulative increase in brightness with successive scans of the target. Since the target image is usually repetitive as regards position on the screen, the image brightness will increase with successive scans while because of the random character of noise no such increase in noise image will result, and a small but evident signal-to-noise improvement obtains. The long-persistence type of screen characteristic is employed in the majority of military radar indicators of the B, C, and PPI-types.

Another general characteristic of the cathode-ray tube screen which influ-

Digitized by Google
Original from UNIVERSITY OF MICHIGAN
Generated on 2019-09-22 07:25 GMT / http://hdl.handle.net/2027/mdp.39015077775156
Public Domain, Google-digitized / http://www.hathitrust.org/access_use#pd-google

ences the over-all system performance is the range of useful brightness available. The extreme variation in the radar response of targets in an area under observation has been discussed previously. The inability of the cathode-ray tube screen to convert this extreme range of electrical signals to a correspondingly large optical brightness range has been a restriction on the performance of military radar systems. Isolated measurements of the useful brightness range available in a cascade screen cathode-ray tube indi-

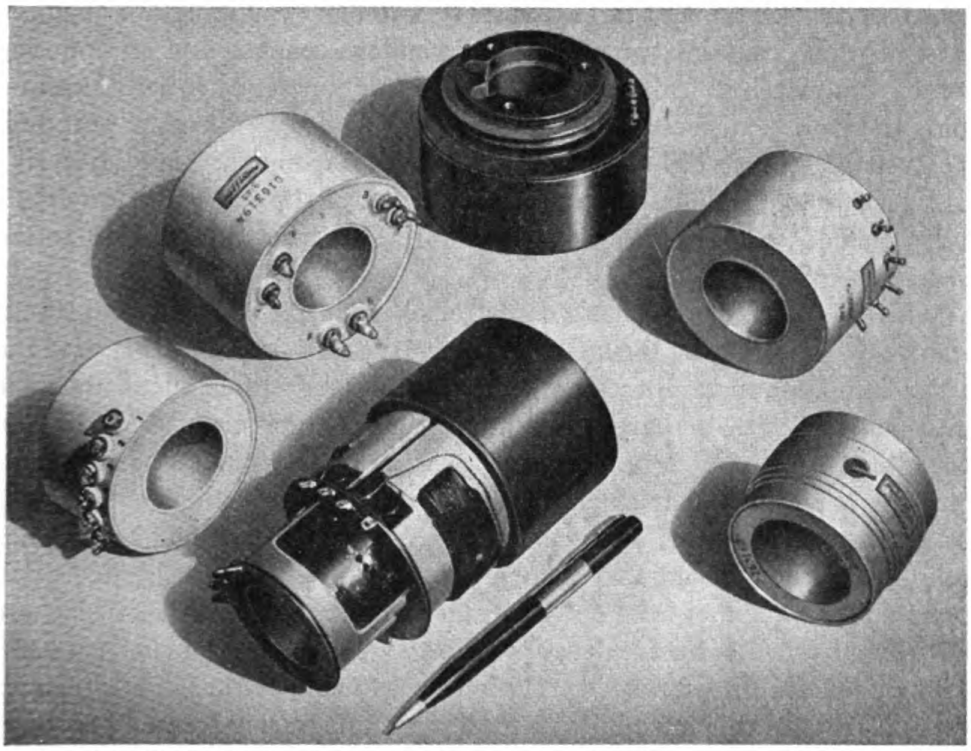

Fig. 40.—Typical magnetic focus and deflection coil designs as developed for military radar purposes.

cates that it is of the order of 10 to 1. The development of the logarithmic video amplifier and "duo-tone" is an attempt to improve this situation. In general this limited useful brightness range of the radar indicator results in a critical adjustment of the operating region of the indicator tube. In a practical military radar system operating under wartime conditions the inclusion of such a critical adjustment always effectively results in a reduction of performance from the optimum achieved in the laboratory.

2.43 *Typical Radar Indicator Component Designs*

Figure 40 illustrates a few typical component designs of magnetic deflection and focus coil structures developed for specific military radar applica-

Digitized by Google
Original from UNIVERSITY OF MICHIGAN
Generated on 2019-09-22 07:25 GMT / http://hdl.handle.net/2027/mdp.39015077775156
Public Domain, Google-digitized / http://www.hathitrust.org/access_use#pd-google

tions during the past war. The deflection coils illustrated include both air and permalloy core structures as used in rectangular and polar types of displays. Where the radar system involves extremely short time interval sweep wave forms, the maximum inductance which can be employed in the deflection coil is limited by the power supply voltages available, and in these indicator designs the air-core type of deflecting coil is usually employed. Where the sweep wave form is relatively slower the permalloy core types have been extensively employed with an effective improvement in deflection sensitivity. For the PPI form of display a toroidal coil structure has been devised which contains two distributed windings connected in an opposing sense. The internal leakage flux of such a structure is essentially uniform and, therefore, satisfactory for magnetic cathode-ray deflection purposes. The usual PPI type coil structure is arranged to mount within a large ring ball bearing to enable rotation around the neck of the tube with provisions being included on the coil housing for slip rings to afford connection to the deflection coil proper.

With the increased emphasis on extremely accurate radar presentations, which developed during the later war years especially in connection with the radar bombing program, the design and manufacturing tolerances allowable in connection with the large scale production of these magnetic deflection coils were severely reduced. Figure 41 illustrates the constructional details of a deflection coil as employed in the AN/APQ-7 radar bombing equipment. The presentation in this instance is of the GPI type employing rectangular coordinate deflection and extremely fast sweep wave forms. This deflection coil structure employs accurately formed open air-core windings which are initially adjusted and cemented to concentric phenol plastic cylinder forms. This design features a vernier rotation adjustment of the horizontal and vertical pairs of coil assemblies to meet a manufacturing scanning requirement of $90° \pm 0.5°$.

Two examples of focussing and centering structures for magnetic-type cathode-ray tube radar indicators are included in Figure 40. The focus coil consists of a simple winding located axially about the neck of the tube with a shielding magnetic structure containing an annular air-gap which restricts the external field to a region including the cathode-ray tube electron beam. This structure is designed to produce a uniform magnetic field distribution in the complete area of the beam to avoid defocussing effects. In certain early-design airborne radar equipment applications where the equipment was subjected to extreme variations in ambient temperature over short periods of operation some difficulty in maintaining optimum focus was experienced. This defocussing, due to the change in coil resistance with ambient temperature and in part to dissipation in the winding proper, is minimized in the designs shown by the introduction of a varistor element

Digitized by Google
Original from UNIVERSITY OF MICHIGAN
Generated on 2019-09-22 07:25 GMT / http://hdl.handle.net/2027/mdp.39015077775156
Public Domain, Google-digitized / http://www.hathitrust.org/access_use#pd-google

mounted in close proximity to the winding whose resistance temperature characteristic was chosen to compensate for similar characteristics of the winding proper. The beam centering structure included in the designs shown employs two pairs of coils arranged upon a closed magnetic core structure adjacent to the focus winding. The perpendicularly disposed magnetic fields are produced by direct current in the same fashion as discussed in connection with the deflection coil assembly.

Figure 42 illustrates the operation of a permanent magnet type of focussing and centering structure developed during the war and which was em-

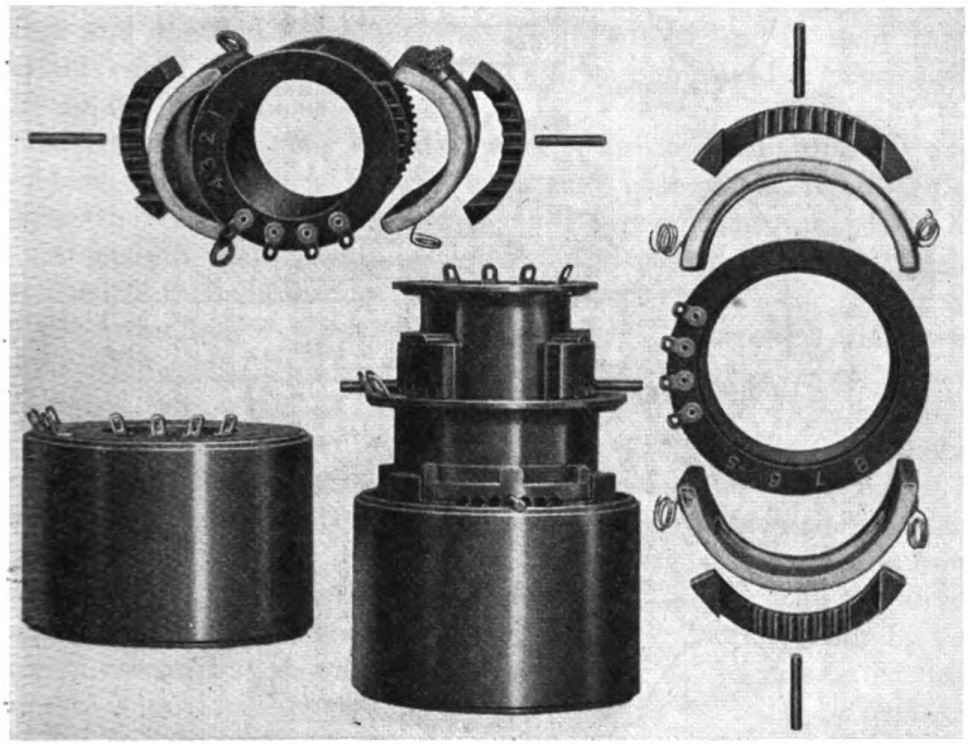

Fig. 41.—Constructional details—deflection coil design for AN/APQ-7 radar bombing equipment.

ployed extensively in airborne radar applications. Here a permanent ring magnet is equipped with a variable internal mechanical magnetic shunt whereby the focussing magnet field can be varied as shown. The centering of the beam is accomplished by means of a centering ring located as shown capable of being mechanically controlled along two perpendicular paths. Mechanical linkage arrangements provide location of the focus and centering adjustment controls on the indicator panel convenient to the operator. The permanent magnet type structure has the advantage of maintenance of proper focus and centering under conditions of extreme variations in ambient temperature. Similar permanent magnetic type structures have been em-

Digitized by Google
Original from UNIVERSITY OF MICHIGAN
Generated on 2019-09-22 07:25 GMT / http://hdl.handle.net/2027/mdp.39015077775156
Public Domain, Google-digitized / http://www.hathitrust.org/access_use#pd-google

ployed to permanently deflect the beam for off-center displays such as the B-type and certain modified sector scanning PPI forms. Here the ampli-

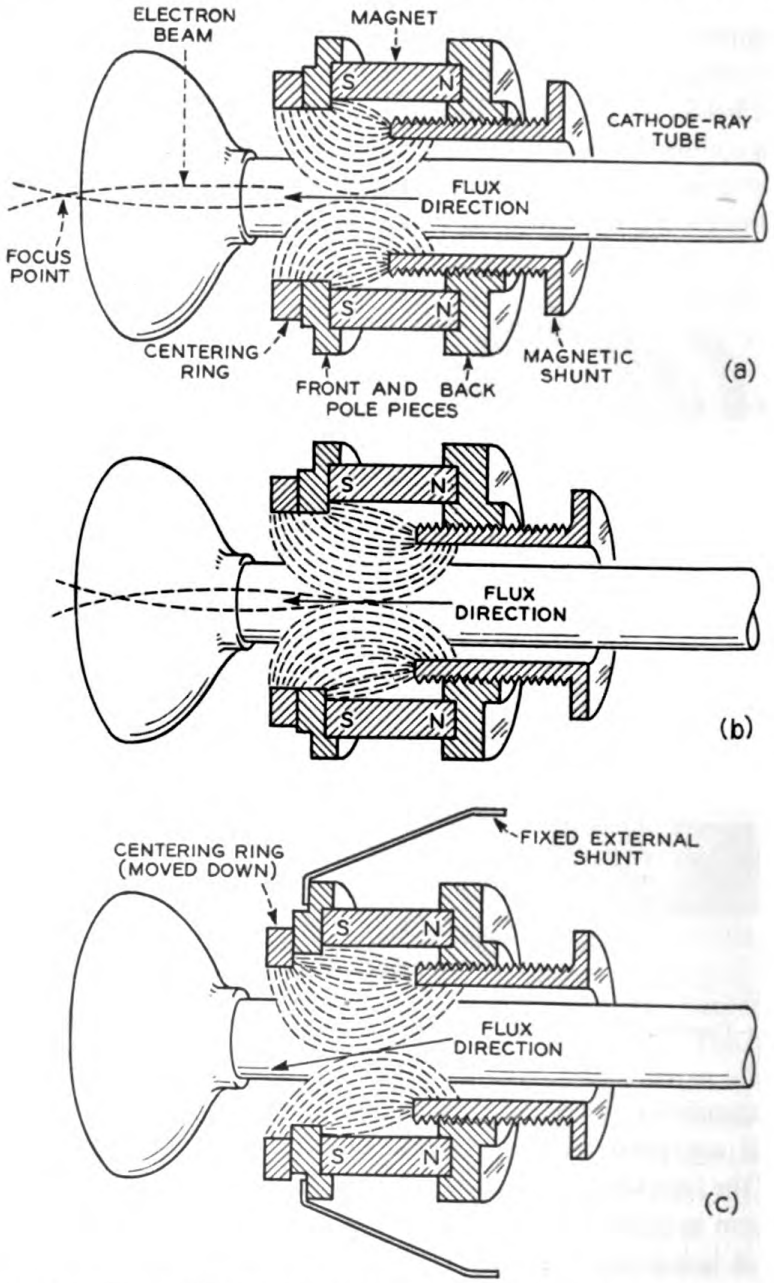

Fig. 42.—Operational diagram of permanent magnet type of focussing and centering structure for radar indicator.

tude of deflection required is approximately equal to the radius of the screen and this precludes the use of the usual beam centering structure located near the gun structure portion of the neck of the tube. To prevent physical

Digitized by Google
Original from UNIVERSITY OF MICHIGAN
Generated on 2019-09-22 07:25 GMT / http://hdl.handle.net/2027/mdp.39015077775156
Public Domain, Google-digitized / http://www.hathitrust.org/access_use#pd-google

interference by the neck of the tube with the deflected beam such off-center display deflecting structures are mounted close to the junction of the neck and bulb of the cathode-ray tube.

As indicated previously the blue-flash characteristic of the excitation of the first layer of the cascade-type screen is usually reduced in intensity through the use of an optical filter placed between the screen of the cathode-ray tube and the observer. These optical screens are usually constructed of an amber-colored transparent plastic whose particular optical transmission characteristics are chosen in accordance with the particular phosphor and speed of scanning employed. It is common practice to engrave general range and direction reference lines on such screens, and in many cases variable edge lighting of these engraved screens is employed to enhance the display.

In certain applications of radar, namely, airborne reconnaissance and bombing operations, it is desirable to obtain a photographic record of the display to be used for training, briefing, or damage assessment purposes. It is customary in these cases to employ a stop-frame moving picture camera attached to the indicator and exposed periodically as desired. Figure 43 indicates the design of a radar indicator viewing attachment which was employed in connection with an airborne bombing radar equipment toward the end of the past war. In this design a partially silvered mirror is located at a 45° angle with respect to the axis of the cathode-ray tube. An illuminated image of an adjustable course marker located below the mirror is observed superimposed upon the radar presentation with negligible parallax distortion. A portion of the light of the radar image is also reflected from the surface of the partially silvered mirror, and together with the direct image of the course marker is available for photographic recording by the camera mounted as shown. Automatic exposure at any preselected time interval is provided, the exact exposure time being controlled by impulses derived from the azimuthal scanning mechanism of the radar antenna. The photographic recording of radar displays has become a matter of prime importance in the modern military operations and has added another consideration for the military radar indicator designer.

Figure 44 indicates an equipment arrangement of a PPI indicator as employed in the AN/APQ-13 radar bombing system. In this system the indicator is designed for convenient overhead mounting in the restricted radar operating space available in modern bombing aircraft. The deflection coil in this equipment is rotated about the neck of the 5″ diameter long-persistence cathode-ray tube by a geared selsyn motor energized from a similar selsyn unit mechanically linked to the rotating radar antenna. Permanent magnet focussing and centering is employed in this particular indicator. Figure 45 illustrates a somewhat similar packaging arrangement for

Digitized by Google
Original from UNIVERSITY OF MICHIGAN
Generated on 2019-09-22 07:26 GMT / http://hdl.handle.net/2027/mdp.39015077775156
Public Domain, Google-digitized / http://www.hathitrust.org/access_use#pd-google

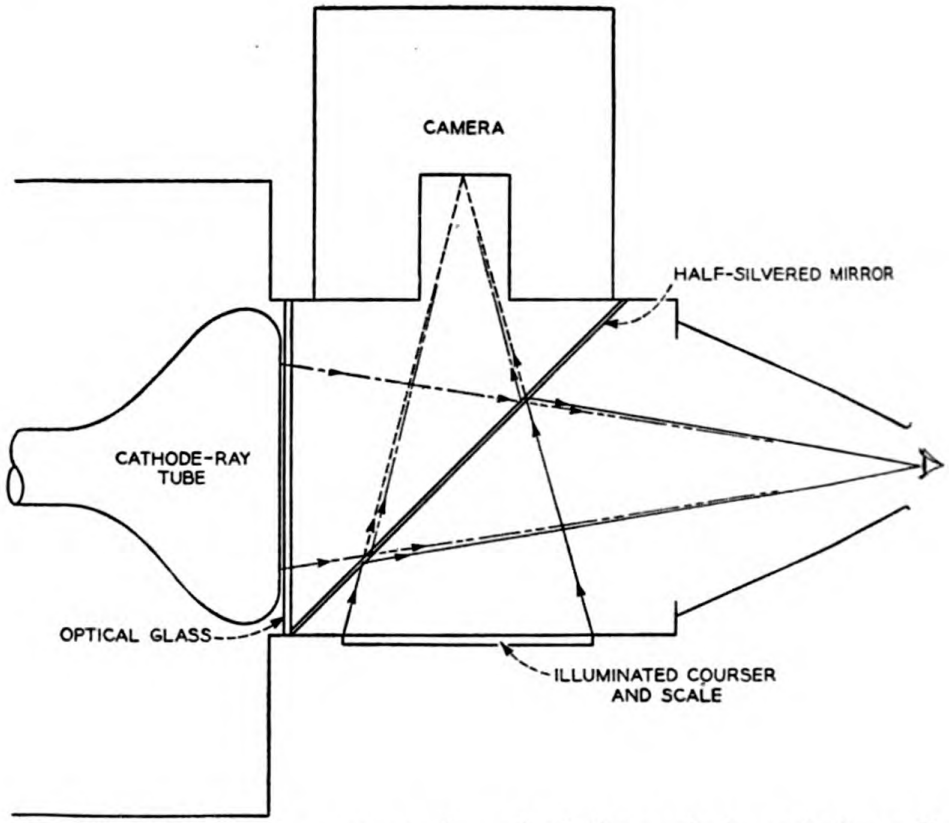

Fig. 43.—Mechanical arrangement of a radar indicator viewing and photographic attachment for AN/APQ-7 radar bombing equipment.

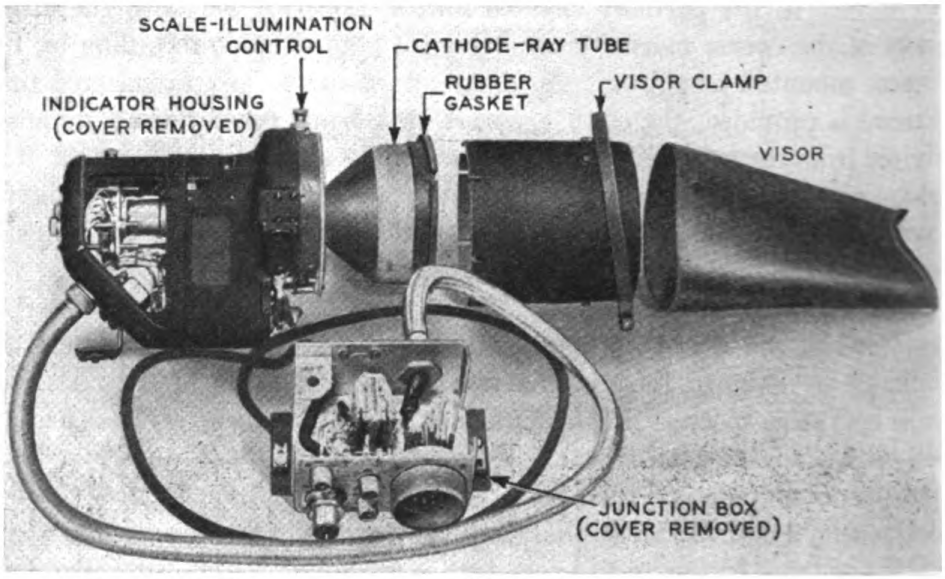

Fig. 44.—Indicator design for AN/APQ-13 radar bombing equipment.

Digitized by Google
Original from UNIVERSITY OF MICHIGAN
Generated on 2019-09-22 07:26 GMT / http://hdl.handle.net/2027/mdp.39015077775156
Public Domain, Google-digitized / http://www.hathitrust.org/access_use#pd-google

an airborne radar low-altitude bombing equipment as employed extensively during the past war. Here the display employed is of the B variety utilizing a 5″ long-persistence cathode-ray tube. The focussing and centering magnetic fields here are produced by coils located as shown. The azimuth sweep voltage is obtained by means of a potentiometer mechanically geared to the sector scanning antenna. The permanent off axis deflection of the zero range line of the B display is here obtained by the use of a permanent magnet yoke mounted at the junction of the neck and bulb of the cathode-ray tube.

Figure 46 illustrates a typical form of an A-type indicator as developed for the SH Naval and Mark 16 mobile fire-control radar equipments. This unit includes provision for receiver tuning and video limiting adjustment convenient to the observer. The SH and Mark 16 radar systems employ

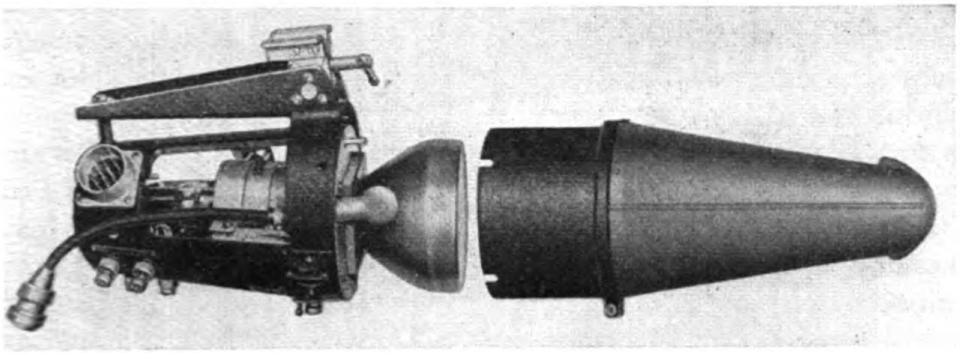

Fig. 45.—Mechanical design of AN/APQ-5 type B radar indicator.

both lobing of the antenna for precise azimuth bearing determination and also continuous rotation of the antenna for general search purposes. The indicator shown in Fig. 46 is employed when the lobing system is in operation and features a precision range sweep as well as the full range display. The equipment design here reflects the severe mechanical requirements which must be satisfied for electronic equipment which is to be employed on naval vessels or for trailer mobile ground service.

2.5 *The Radar Sweep Circuit*

2.51 *Function*

The sweep circuit components of a radar receiver are required to generate the specific voltage or current wave forms necessary to properly display the radar-received information in the desired form. These wave forms must also be actuated by or related to the various coordinate or computed types of data furnished to the radar receiver. The actual detailed configuration of the circuit employed for this purpose is dependent on the form of the input

Generated on 2019-09-22 07:27 GMT / http://hdl.handle.net/2027/mdp.39015077775156
Public Domain, Google-digitized / http://www.hathitrust.org/access_use#pd-google
Digitized by Google
Original from UNIVERSITY OF MICHIGAN

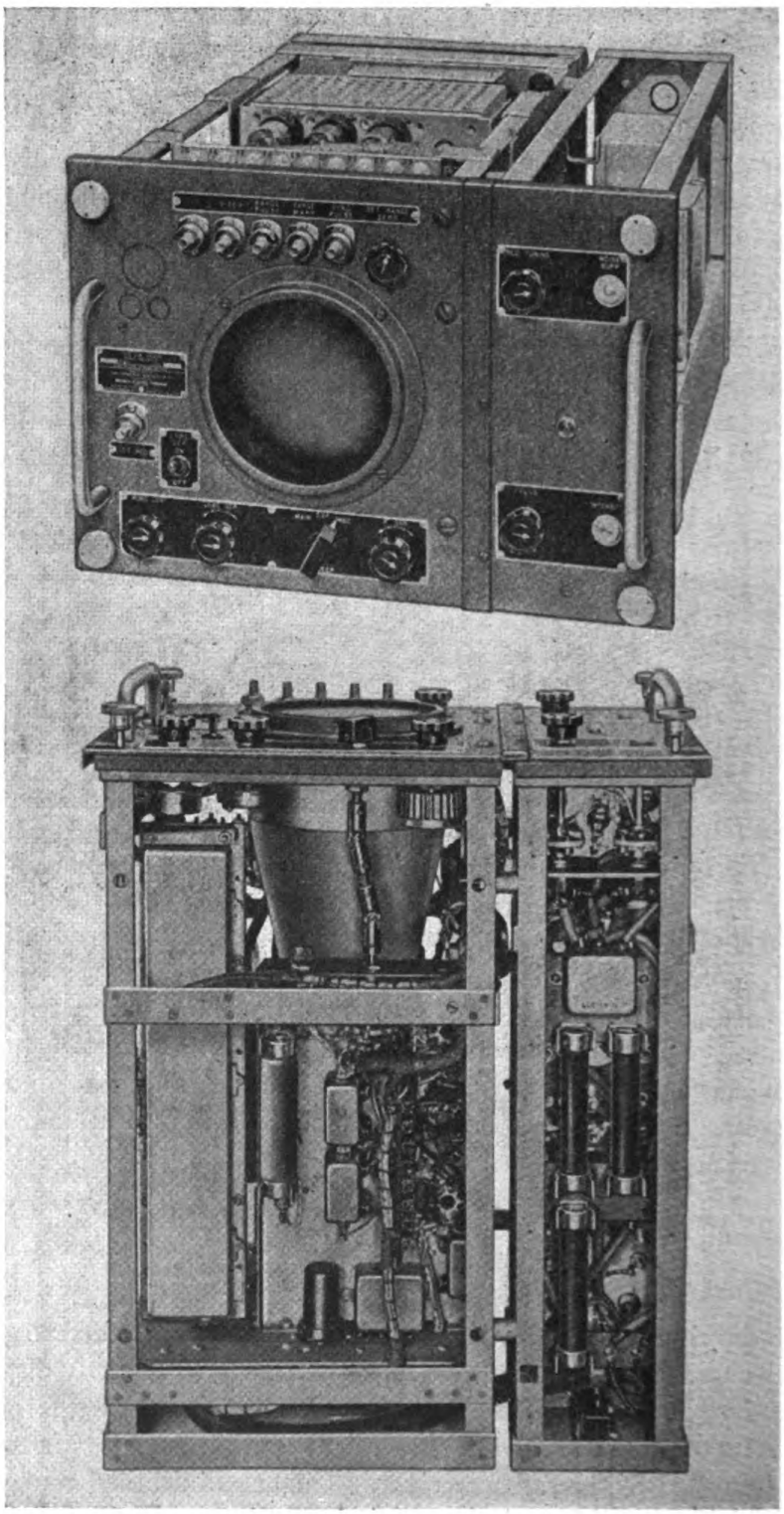

Fig. 46.—A-type indicator design for SH Naval radar equipment.

Digitized by Google
Original from UNIVERSITY OF MICHIGAN
Generated on 2019-09-22 07:27 GMT / http://hdl.handle.net/2027/mdp.39015077775156
Public Domain, Google-digitized / http://www.hathitrust.org/access_use#pd-google

information available and upon the indicator deflection methods to be employed.

The sweep deflection problems may be separated into two quite distinct categories dependent on the speeds of operation involved. The slow-speed deflection systems originate with the required deflection of the beam of the indicator cathode-ray tube in accordance with the instantaneous position of the axis of propagation of the antenna structure. Since the antenna structures with which we are concerned at radar frequencies are of comparatively large dimensions, their motional velocities are extremely limited and accordingly the electrical information describing these slow mechanical changes contains only low-frequency components. The deflection problem associated with this information, in general, offers little difficulty to the radar receiver designer. Commonly employed methods of slow-speed sweep deflection include the use of potentiometers, selsyn generators or variable capacitors mechanically linked to the deflection axes of the antenna structure and associated circuits of relatively simple form whereby the electrical changes in the characteristics of these devices are more or less directly impressed upon the proper deflection axis of the indicator. In the case of the PPI form of display, it is quite common to synchronize the rotation of the deflection coil about the axis of the cathode-ray tube with the azimuth bearing of the antenna through the use of selsyn motors or servo mechanisms. In general, slow-speed sweep deflection problems are associated with bearing coordinate data only.

The determination of range to the target, on the other hand, requires high-speed scanning whereby the time interval encompassing the time of propagation and return of the radar pulse over the selected range interval must be completely displayed upon the indicator screen. The total time interval available to deflect the beam for range measurement purposes may extend from 2500 microseconds which represents a range measurement of approximately 240 miles down to perhaps 6 microseconds representing an expanded interval of approximately 1000 yards useful in certain fire-control applications. Here, with extremely small times available for deflection purposes, the radar receiver designer is faced with difficult circuit design problems where the usual negligible parasitic circuit elements now severely restrict the circuit performance. In the following discussion, therefore, emphasis will be placed upon the design factors involved in the development of high-speed radar sweep wave forms.

The radar sweep circuit can be considered as providing the following functions:

1. Generation of time wave forms.
2. Generation of display sweep wave forms.
3. Amplification of sweep wave forms.

Digitized by Google
Original from UNIVERSITY OF MICHIGAN
Generated on 2019-09-22 07:27 GMT / http://hdl.handle.net/2027/mdp.39015077775156
Public Domain, Google-digitized / http://www.hathitrust.org/access_use#pd-google

2.52 *The Timing Wave Form Generator*

The generation of the timing wave forms consists of the preparation of specific voltage wave forms for use in the following sweep generator in accordance with timing information available at the radar receiver input. These timing data may consist of a pulse coincident or related to the outgoing radar microwave pulse serving as a reference for range display or, in the case of direction sweeps, may consist of signals related to the instantaneous position of the antenna.

The basic wave forms employed in this connection consist of rectangular pulses where the duration of the pulse may be controlled to serve as a measure of time, extremely short-duration pulses useful as time markers, and various combinations of these. In general, these wave forms are characterized by their nonsinusoidal form. The generation of these nonsinusoidal wave forms is accomplished by a number of specialized electronic circuits, which though apparently quite complex can be resolved generally into a combination of relatively simple basic circuit forms.

The Multivibrator

The "trigger" or multivibrator circuit was developed nearly thirty years ago and provides the fundamental circuits for the sweep circuit designer. Figure 47a illustrates a simple historical form of a trigger circuit which is of the Eccles-Jordan type. The essential current-voltage relationship which characterizes this circuit and all circuits employed for this purpose is a negative resistance characteristic which exists over a limited portion of the operating range of the device. In the case of the electronic circuit shown in Fig. 47a this negative-resistance characteristic is bounded by two stable limiting conditions. Referring to the trigger circuit of Fig. 47a, the chronological order of operation can be described as follows: Assume V_1 is conducting a somewhat larger current than V_2 so that the potential at the plate of V_1 is lower than the corresponding point at V_2 due to the voltage drop across the plate resistor R_1. This condition further implies that the grid potential of V_2 as determined by the connection from the plate of V_1 through the coupling resistor R_3 is lower than that at the grid of V_1. Similarly the grid potential of V_1 is at a higher positive potential, due to its connection with the plate of V_2. The action is cumulative and results in stablizing the circuit under the condition where the plate current of V_2 is entirely cut off and the voltage drop across V_1 is less than the grid bias voltage E_c.

If now a voltage is impressed across the input terminals of either a positive or negative form, the circuit will be driven away from this stable equilibrium condition as follows. Assume now that a large positive pulse be applied to the circuit shown. The tube V_1 which is operating in a conducting con-

Digitized by Google
Original from UNIVERSITY OF MICHIGAN
Generated on 2019-09-22 07:27 GMT / http://hdl.handle.net/2027/mdp.39015077775156
Public Domain, Google-digitized / http://www.hathitrust.org/access_use#pd-google

dition will not be affected but the grid of V_2 will be raised in potential by the amplitude of the enabling pulse. The plate current flow in V_2 under this influence will reduce the plate potential of V_2 and accordingly will tend to decrease the positive bias of V_1. The accompanying plate current reduction of V_1 will increase its plate potential and this will result in increasing the grid potential of V_2 through the coupling resistance R_3. Again the cumulative effect will be to abruptly cut off the plate current of V_1 and operate V_2. Thus an abrupt switching of this electronic circuit results when a single enabling pulse is impressed upon it. The wave form across one of the plate

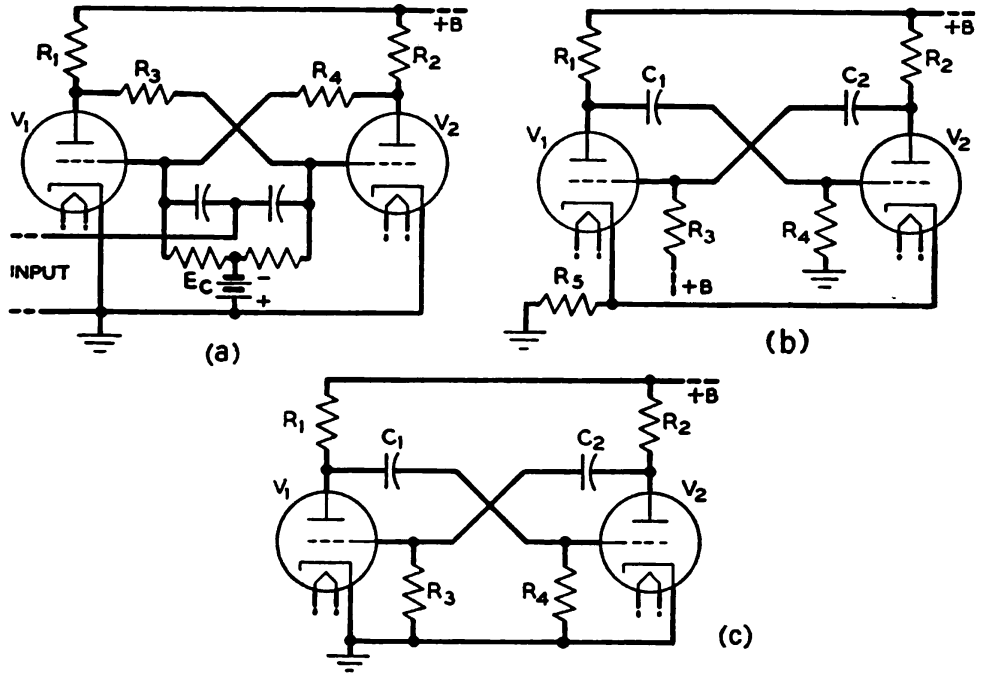

Fig. 47.—Basic Multivibrator Circuit Forms.

resistances is of a rectangular form whose duration is determined by the time interval which exists between the two applied excitation pulses.

A basic modification of the fundamental trigger circuit which has been found most useful in radar sweep circuit is given in Fig. 47b. Here the original circuit form has been modified so as to permit a complete cycle of operation upon excitation by a single actuating pulse. The duration of the cycle is here internally controlled by the arrangement and value of the circuit elements. This form of multivibrator is characterized by having one stable equilibrium condition and is known as a "one shot" type.

The chronological order of operation of this circuit type may be considered as follows: V_1 is normally conducting heavily because of the large positive grid potential impressed upon it by the plate supply battery and the connec-

Digitized by Google
Original from UNIVERSITY OF MICHIGAN
Generated on 2019-09-22 07:27 GMT / http://hdl.handle.net/2027/mdp.39015077775156
Public Domain, Google-digitized / http://www.hathitrust.org/access_use#pd-google

tion through R_3. The plate current of V_1 flowing through the common cathode resistor R_5 results in a large effective bias applied to V_2 which continues to maintain V_2 in a cut-off condition. If a negative pulse of relatively short duration is impressed upon the grid of V_1 this tube will be driven toward cut-off with an attendant increase in the plate potential of V_1. This positive increase in voltage will be impressed upon the grid of V_2 causing V_2 to conduct plate current. The resulting decrease in the potential at the plate of V_2 further decreases the grid potential of V_1 through the coupling condenser C_2. This action progresses until V_1 is driven beyond plate current cut-off and V_2 is conducting. This condition remains as long as the discharge of the condenser C_2 through R_3 will maintain the grid of V_1 at a net negative potential. When the condenser C_2 has discharged sufficiently to allow the grid of V_1 to increase above the cut-off value, V_1 will again conduct and the resultant action will reduce and eventually cut off the plate current of V_2. The duration of the cycle of operation is here shown to be dependent on the time constant of the circuit R_3 C_2 and may accordingly be controlled as desired by proper selection of these elements. The return of the grid of V_1 to a very high positive voltage point in the circuit has a definite advantage which may be considered as follows: A variation of the grid voltage of V_1 required to cut off the plate current will influence the time duration of the cycle of operation. Here the time rate of change of the grid voltage has been made extremely large by the choice of the return to the high-voltage supply. Thus, an order of magnitude increase in the duration stability of the circuit is achieved.

A further modification of the trigger circuit furnishes the third general type of multivibrator employed in the radar receiver field. This circuit form, called the "free-running" type, has the property of presenting two unstable limiting conditions and accordingly will produce sustained oscillations of a nonsinusoidal form. Figure 47c illustrates this circuit arrangement. The essential circuit change over that given in Fig. 47b, is seen to be the elimination of the stable equilibrium condition of V_1 by the absence of a positive potential on the grid of V_1.

In the free-running type of multivibrator shown, the duration of operation of a particular tube is related to the time of discharge of the coupling condenser and the grid resistance associated with the tube. If a different time constant is chosen for each tube circuit, an unsymmetrical wave form, i.e.—a pulse-to-no-pulse interval ratio other than one, can be produced. In general, the free-running multivibrator is seldom used in this basic form because of the limited repetition-rate stability of this circuit. It is customary, however, to trigger this free-running type of multivibrator with short-duration pulses having a slightly higher repetition-rate than that determined by the multivibrator circuit constants. In this manner the repetition-rate may be

Digitized by Google
Original from UNIVERSITY OF MICHIGAN
Generated on 2019-09-22 07:27 GMT / http://hdl.handle.net/2027/mdp.39015077775156
Public Domain, Google-digitized / http://www.hathitrust.org/access_use#pd-google

externally controlled as desired. It is also possible to synchronize this particular form of circuit at a submultiple of the externally available trigger repetition frequency.

Pentodes and other now available multi-element vacuum tubes, where the multivibrator interstage coupling involves additional control elements, are commonly employed in the modern radar receiver. Wave forms other than the basic rectangular pulse forms appearing at the plate terminals of the multivibrator circuit are available at various other points in the circuit and are often employed in specific applications.

One other basic form of pulse producing electronic circuits is known as the "blocking-oscillator" type: two typical examples of which are illustrated in Fig. 48. Here the positive feedback of energy required to produce the multivibrator characteristic is realized through the use of a single vacuum

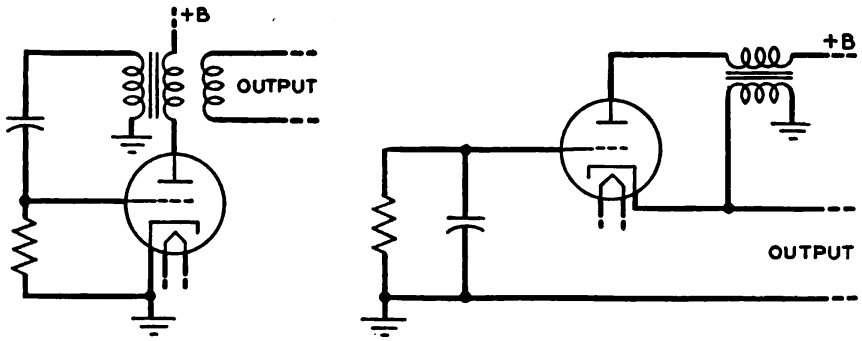

Fig. 48.—Typical Blocking-Oscillator Circuit Forms.

tube and a transformer feedback circuit. This form may be described as an oscillatory vacuum tube circuit where the grid circuit is so arranged to be driven negative after one or more cycles of operation. This results in an intermittent oscillation and the production of nonsinusoidal wave forms similar to those produced by the general multivibrator circuits previously described. The basic advantage of the blocking oscillator circuit form is one of economy of vacuum tubes and attendant power supply reduction.

Typical Timing Wave Circuits

The practical military equipment requirements of World War II with the emphasis on compactness and low-power consumption has resulted in the development of a myriad of specialized circuits which reflect the ingenuity of the electronic circuit designer and the basic flexibility of the modern vacuum tube. In general, however, these circuit developments are quite similar operationally to the basic forms here described.

Figure 49 illustrates a typical circuit arrangement of the sweep timing portion of a PPI indicator as employed in a naval search radar equipment.

Digitized by Google
Original from UNIVERSITY OF MICHIGAN
Generated on 2019-09-22 07:28 GMT / http://hdl.handle.net/2027/mdp.39015077775156
Public Domain, Google-digitized / http://www.hathitrust.org/access_use#pd-google

In this particular radar system the transmitting magnetron is pulsed from a free-running modulator and, therefore, the controlling timing reference pulse for sweep purposes must be obtained from the modulator circuit. In many other military radar systems it has proven desirable to time both the transmitter modulator and the receiver sweep circuits from a common controllable repetition frequency source. As shown in Fig. 49, a positive synchronizing pulse as obtained from the transmitting modulator is delivered to the radar receiver for range timing reference and here applied to the "clipper" portion of the timing circuit. It was considered here desirable to clip or limit the timing pulse to gain freedom from timing instability, due to possible amplitude variations and to eliminate any possible negative excursions of the timing pulse which might cause faulty operation of the following multivibrator circuit. The multivibrator shown is a modified form of the "one-

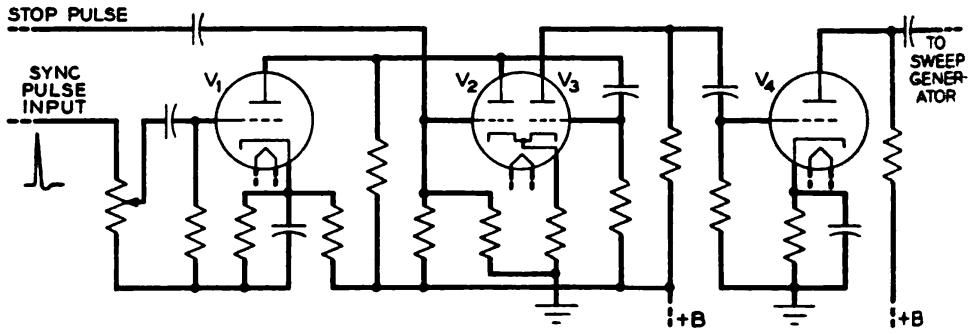

Fig. 49.—Radar Sweep Timing Circuit. Simplified schematic diagram.

shot" type described previously. The grid of V_3 is normally maintained at a positive potential through its connection to the positive plate supply source and accordingly V_2 is normally cut off.

Upon application of the positive synchronization pulse to V_1 and the resultant lowering of the plate potential of V_1 the grid of V_3 is driven below cut-off decreasing the voltage drop across the common cathode resistance and causing V_2 to conduct. This condition will be maintained until the coupling condenser has discharged sufficiently to permit V_3 to again conduct. In the circuit here described, however, this controlling time constant has been selected to be somewhat larger than the total period of the sweep rate and the termination of the sweep timing pulse is accomplished by an external stop pulse applied as shown. This stop pulse is developed in the following sweep amplifier circuits not here shown and is controlled directly by the deflection current. Details of this stop-pulse timing and generation is given in a later section.

The output of this timing circuit shown here then is observed to consist of a rectangular pulse whose leading edge is related to the time of the cut-

Digitized by Google
Original from UNIVERSITY OF MICHIGAN
Generated on 2019-09-22 07:28 GMT / http://hdl.handle.net/2027/mdp.39015077775156
Public Domain, Google-digitized / http://www.hathitrust.org/access_use#pd-google

going radar pulse and whose duration has been controlled by the limits of deflection desired on the radar indicator tube. This form of sweep circuit is known as a "start-stop" type and has proven extremely satisfactory as employed in a number of military radar equipments designed during the past war period.

2.53 *The Sweep Wave Form Generator*

The sweep wave form generator is required to generate the specific voltage or current time functions required to properly deflect the electron beam of the cathode-ray display device. The timing of the interval of this sweep wave form is provided by the timing or synchronizing circuits just described.

In general, it has been required that the range sweep wave form amplitude be essentially a linear function of time over the range interval under observation. During the latter portion of the war, certain airborne applications of radar did require that a specific nonlinear wave form be employed, but the commonly employed displays (A, B, C, and PPI) are usually operated with linear range deflection sweep circuits.

The basic method of obtaining a sweep voltage wave form which increases with time is illustrated in Fig. 50a. In this circuit V_1 is normally operating at little or no bias and, therefore, due to the large voltage drop across the plate resistor R, the plate potential of V_1 is considerably lower than the plate supply voltage B. If a negative rectangular pulse is applied to the grid of V_1 the tube will be abruptly driven to cut-off and, due to the current flow through the condenser C, the plate potential will rise exponentially as indicated to eventually assume the value of the supply voltage B. At the time of end of the negative driving pulse, V_1 will again conduct and the potential at the plate of V_1 will be abruptly reduced as shown.

There are several methods employed in radar sweep circuits to improve the linearity versus time of the fundamental exponential sweep wave form. The first of these takes advantage of the fact that the initial rise of the exponential wave form in the limit is a linear function of time. By using only a small portion of the wave form shown and supplying later amplification to produce the desired deflection, a simple improvement results. This form of linear sweep generation represents the original and by far the most common of the types employed in military radar systems during the past war.

Figure 50b illustrates a method of improving the linearity of the sweep wave form whereby the exponential wave form generated by the basic condenser charging operation is modified through the use of feedback. As shown here the asymptotic value of the exponential charging voltage has been increased by a factor of $(\mu + 1)$ and the effective time constant of the charging circuit has likewise been increased by the same factor. The use of an amplifier in the feedback circuit having an effective gain of 50 would

Digitized by Google
Original from UNIVERSITY OF MICHIGAN
Generated on 2019-09-22 07:28 GMT / http://hdl.handle.net/2027/mdp.39015077775156
Public Domain, Google-digitized / http://www.hathitrust.org/access_use#pd-google

result in an improvement in linearity comparable with the circuit of Fig. 50a, where the plate supply voltage was increased by the same factor.

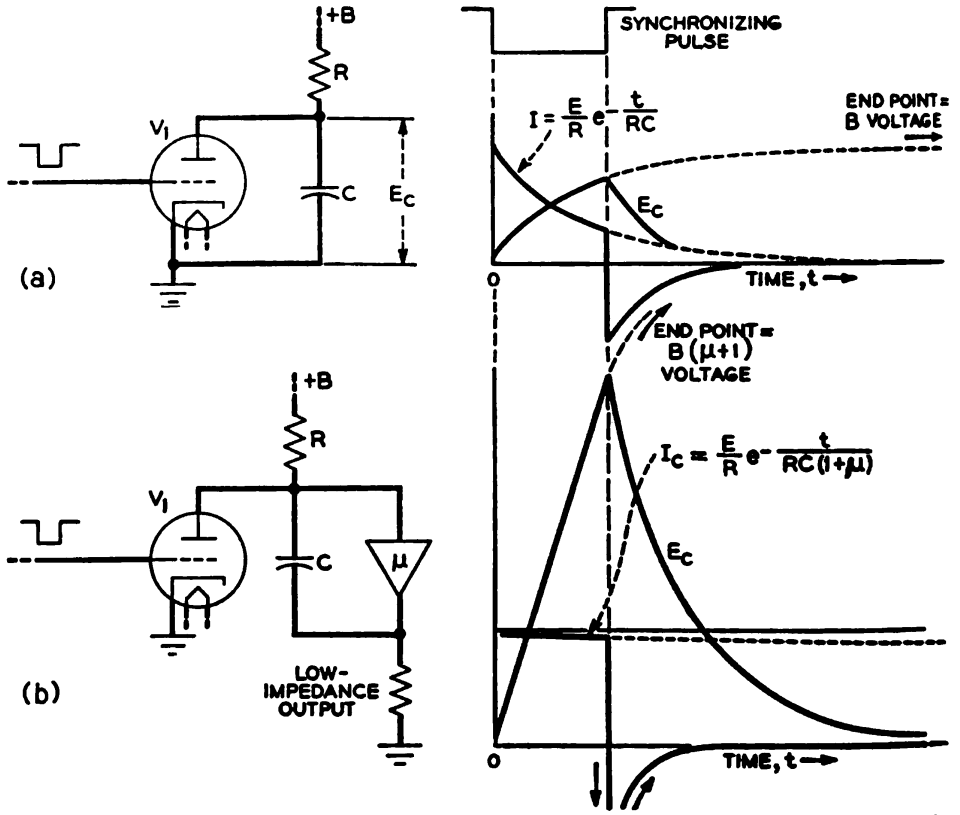

Fig. 50.—Radar sweep generation circuits—basic form and modified by negative feedback to improve linearity.

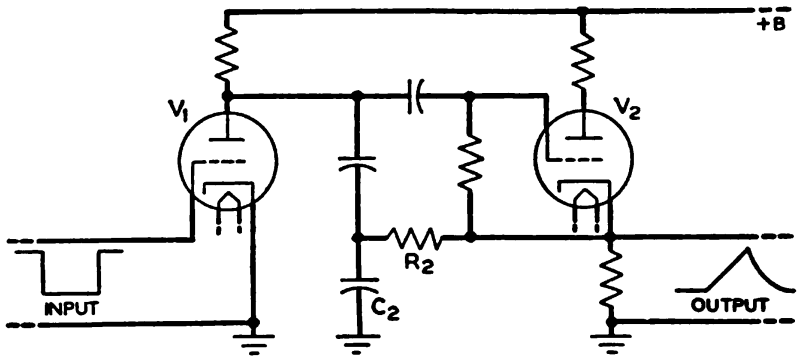

Fig. 51.—Circuit employed to improve linearity of sweep wave form by integration method.

A further method of improving the linearity of the generated sweep wave form is illustrated in Fig. 51 where an additional correction voltage is superimposed on the exponential sweep wave form. This correction voltage is

Digitized by Google
Original from UNIVERSITY OF MICHIGAN
Generated on 2019-09-22 07:28 GMT / http://hdl.handle.net/2027/mdp.39015077775156
Public Domain, Google-digitized / http://www.hathitrust.org/access_use#pd-google

derived by integration of the sweep wave form as impressed upon the elements R_2, C_2 and the voltage appearing across C_2 is effectively superimposed upon the output wave form. As employed on an airborne bombing radar equipment, a circuit similar to that shown in Fig. 51, was employed where a residual nonlinearity of less than 0.5% was achieved and maintained under severe military operating conditions.

In certain instances it is desirable to generate a sweep wave form which has a specific nonlinear time characteristic. An illustration of one such case as applied to airborne radar is given in Fig. 52. Here the airborne radar display was required to present a nondistorted ground plan which in

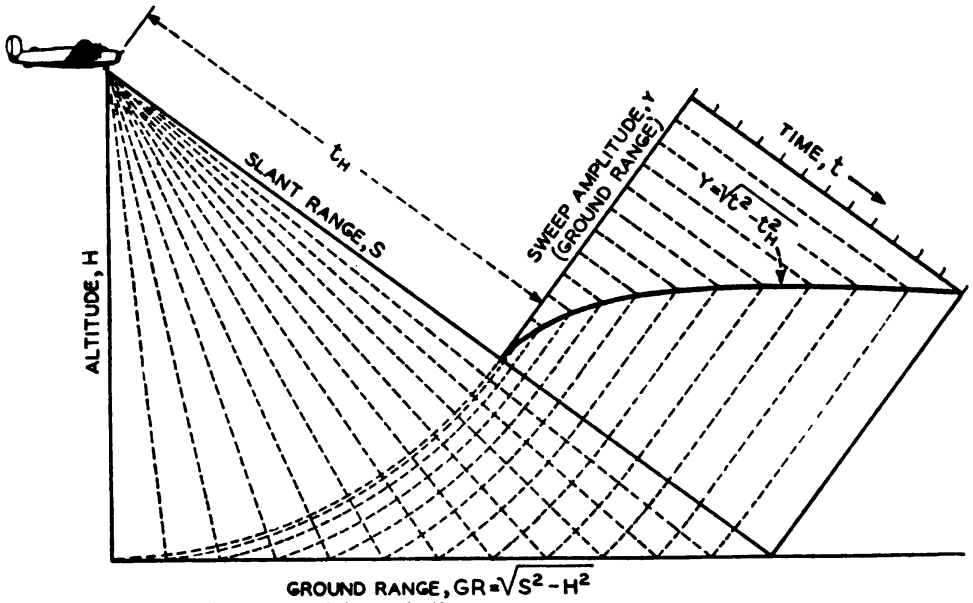

Fig. 52.—Development of hyperbolic sweep wave form for true ground plan radar presentation.

turn required that the range sweep wave form be of a hyperbolic form. The start of the display sweep must be delayed in time corresponding to the time of propagation and return of the radar pulse between the aircraft and the ground. This delay may be produced by the use of a multivibrator of a convenient form, actuated by a pulse coincident with the outgoing radar pulse, and where the duration of the multivibrator pulse is controlled either manually or automatically by reference to the aircraft's altimeter.

The hyperbolic sweep wave form illustrated may be approximated mathematically as the sum of a linear and a series of exponential terms. In this particular application, it was found sufficient to consider a linear and two additional exponential terms only to satisfy these specific requirements. Figure 53 indicates the method employed to generate this specific wave form. As indicated, the desired theoretical hyperbolic sweep function has

Digitized by Google
Original from UNIVERSITY OF MICHIGAN
Generated on 2019-09-22 07:28 GMT / http://hdl.handle.net/2027/mdp.39015077775156
Public Domain, Google-digitized / http://www.hathitrust.org/access_use#pd-google

an infinite starting slope which cannot be provided with the practical limitations of frequency band width and power available so that here the actual delay used was chosen as 0.9 H, resulting in evident but acceptable distortion in the display in the area directly beneath the aircraft. Figure 53b indicates the fundamental circuit method of generating this wave form. The linear term is generated across the capacitance C_0 and the series current flowing through the additional elements R_1, C_1 and R_2, C_2 supplies the two

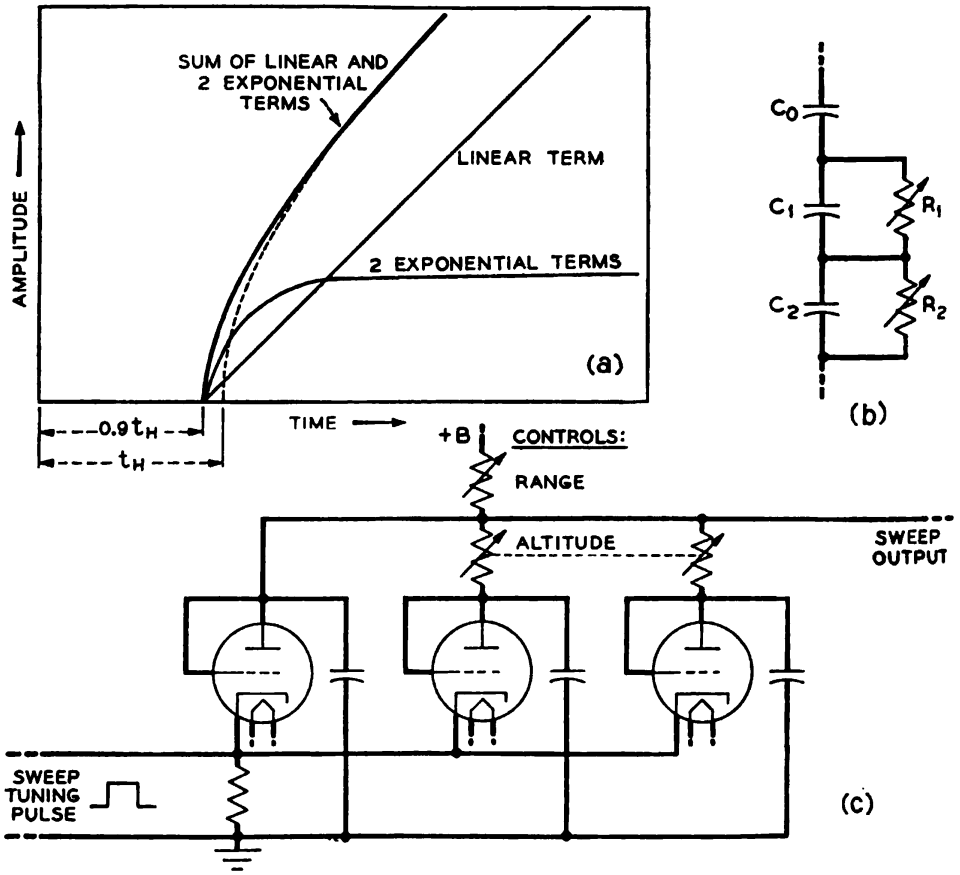

Fig. 53.—Hyperbolic sweep wave form generation—simplified schematic diagram.

additional exponential voltage wave forms. The resistances R_1 and R_2 are required to be variable, their value being determined by the altitude of the aircraft. The practical form of the circuit employed is outlined in Fig. 53c, which includes the additional resistor required to enable modifying the rate of rise of the sweep wave form in accordance with the selected interval of ranges to be displayed.

2.54 *The Sweep Amplifier*

The remaining portion of the radar sweep circuit is concerned with the amplification of the properly timed and generated sweep wave forms to

Digitized by Google
Original from UNIVERSITY OF MICHIGAN
Generated on 2019-09-22 07:28 GMT / http://hdl.handle.net/2027/mdp.39015077775156
Public Domain, Google-digitized / http://www.hathitrust.org/access_use#pd-google

assure adequate deflection voltage or current for display purposes. The sweep amplifier for range deflection purposes is essentially a specialized form of video amplifier which must be capable of wide band transmission to adequately reproduce the short time sweep wave forms and whose output characteristics are such as to properly supply the high voltage or current signals as required by the radar display system. Two general sweep amplifier design problems are presented for the two basic radar indicator types. The

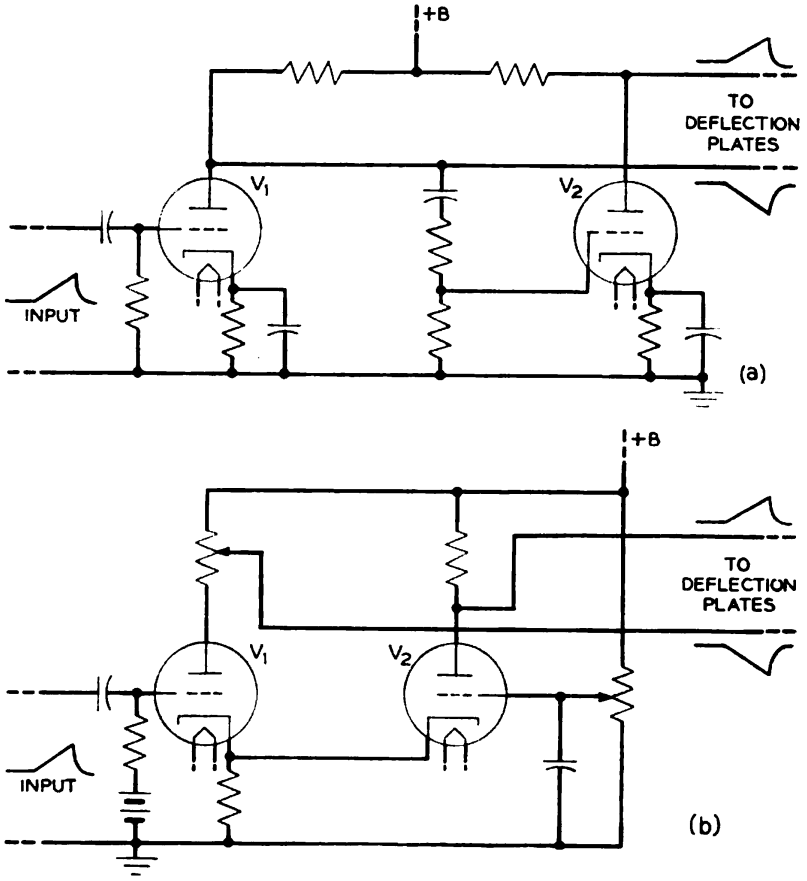

Fig. 54.—Range sweep amplifier circuit schematics for electrostatic-type radar displays.

electrostatic type cathode-ray tube generally requires a balanced to ground deflection signal of moderately high amplitude while the magnetic type cathode-ray tube requires a large deflection current for its operation.

Figure 54a illustrates a simplified schematic of a range sweep deflection amplifier to be employed with an electrostatic type-A radar display. Here the previously generated sweep wave form is impressed upon the grid of V_1 and after amplification a portion of the signal of opposite polarity and of amplitude comparable with the input signal at the grid of V_1 is applied to the grid of V_2. The plate circuit of each tube is connected directly to the deflection plate of the electrostatic cathode-ray tube. In this instance,

Digitized by Google
Original from UNIVERSITY OF MICHIGAN
Generated on 2019-09-22 07:29 GMT / http://hdl.handle.net/2027/mdp.39015077775156
Public Domain, Google-digitized / http://www.hathitrust.org/access_use#pd-google

the average potential of the horizontal plates of the indicator is maintained at a value determined by the d-c plate potentials and, as indicated previously, this same potential should be applied to the second anode of the cathode-ray tube to avoid defocussing effects. Another variation of a phase inverter amplifier which is commonly employed in radar sweep circuits is illustrated schematically in Fig. 54b. In this instance, a common cathode impedance is employed to accomplish similar excitation of the balanced output tubes. If one grid is excited the plate current flow of this

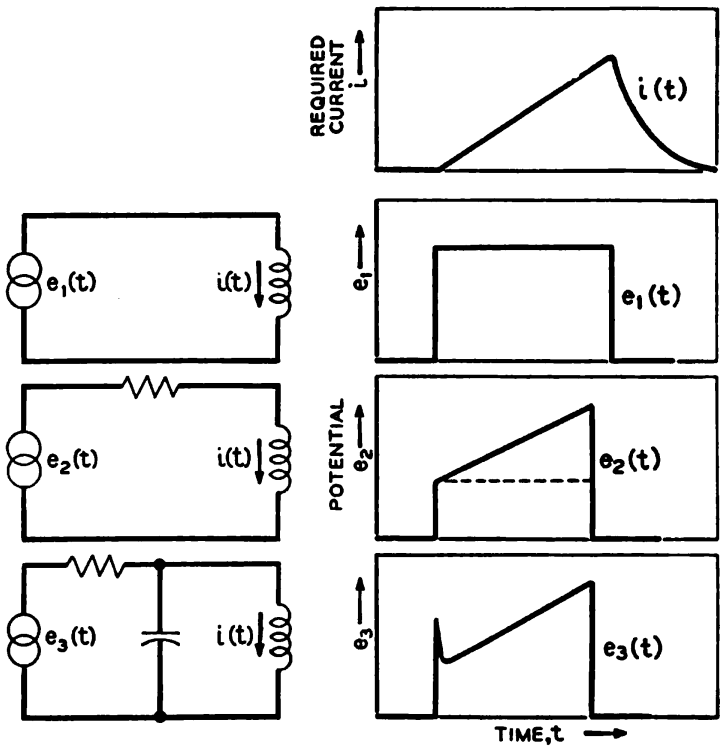

Fig. 55.—Voltage-current-time relationships for magnetic deflection structures.

tube through the cathode resistance serves to excite the second tube and a balanced output sweep signal voltage will result. The values of the plate resistors in this form of circuit are of unequal values and must be adjusted to produce the desired balanced output. The additional control illustrated in the grid circuit of V_2 may be employed to serve as a d-c positioning control.

The sweep amplifier design considerations involved for the magnetic deflection type of cathode-ray tube radar indicator are somewhat more involved, due primarily to the character of the amplifier load impedance. In the case of magnetic deflection the final flux density, and accordingly the sweep current through the deflection coil, is required to be proportional to

Generated on 2019-09-22 07:29 GMT / http://hdl.handle.net/2027/mdp.39015077775156
Public Domain, Google-digitized / http://www.hathitrust.org/access_use#pd-google
Digitized by Google
Original from UNIVERSITY OF MICHIGAN

the deflection time function desired. If a linear deflection function is assumed, as shown in Fig. 55, producing a linear sweep, the necessary form of the applied voltage wave will vary depending on the inductance, the resistance and the parasitic capacitance of the coil circuit. These conditions are illustrated in Fig. 55. It is entirely possible to generate sweep voltage functions of the forms indicated here for application to a linear amplifier and deflection coil circuits and in fact such an approach was employed in early military radar designs of World War II. It has, however, proven more convenient to employ negative feedback amplifiers whereby the deflection coil current output is maintained proportional to the applied voltage at the input of the sweep amplifier. In this manner, a sweep generator voltage wave form can be employed which has the characteristics desired of the final deflection.

A simplified schematic of a feedback sweep amplifier to be employed in connection with a magnetic deflection radar indicator is shown in Fig. 56. In this example the impressed sweep wave form voltage having the essential characteristics of the desired deflection time function is impressed upon the grid of V_1. This sweep form is amplified and the deflection coil current of the output stage which flows through the 80-ohm cathode resistance common to the first and third stages produces a voltage drop proportional to this current which is effectively applied between the cathode and grid of the first stage thus completing the negative feedback loop. If sufficient forward gain and adequate feedback is provided, the deflection coil current can be made to assume the essential characteristics of the original impressed voltage sweep wave form. It should be observed that the grid of the third stage is biased negatively beyond plate current cut-off to insure that the deflection coil current has an initial value of zero before the start of the sweep. If this condition is not observed, the zero range point on the indicator will be a function of the d-c current of the output stage and in the case of a PPI form of display, the zero range region will assume the characteristics of an open circle and map distortion at the short ranges will result. In this amplifier circuit, application of the sweep signal to the grid of V_3 will not result in deflection current flow until the tube is driven above cut-off. During this time the feedback is not effective and the over-all gain of the amplifier is at its maximum value. Due to the inductive characteristics of the amplifier load impedance, the initial rise in current will be delayed slightly with respect to the applied voltage and accordingly a further delay of the feedback voltage is introduced by the use of a time constant in the common feedback network. The result is a delaying of the applied feedback voltage with a corresponding period of maximum gain of the amplifier which tends to produce a sharp increase in deflection coil current at the time of the

Generated on 2019-09-22 07:29 GMT / http://hdl.handle.net/2027/mdp.39015077775156
Public Domain, Google-digitized / http://www.hathitrust.org/access_use#pd-google
Digitized by Google
Original from UNIVERSITY OF MICHIGAN

start of the sweep. After this short interval of time, the feedback becomes effective and the output current and input voltage correspondence obtains.

It is essential in this type of circuit that the feedback be determined entirely by the deflection coil current if optimum operation is to be obtained. It should be observed that this condition requires that the screen current which also normally flows through the feedback impedance does not con-

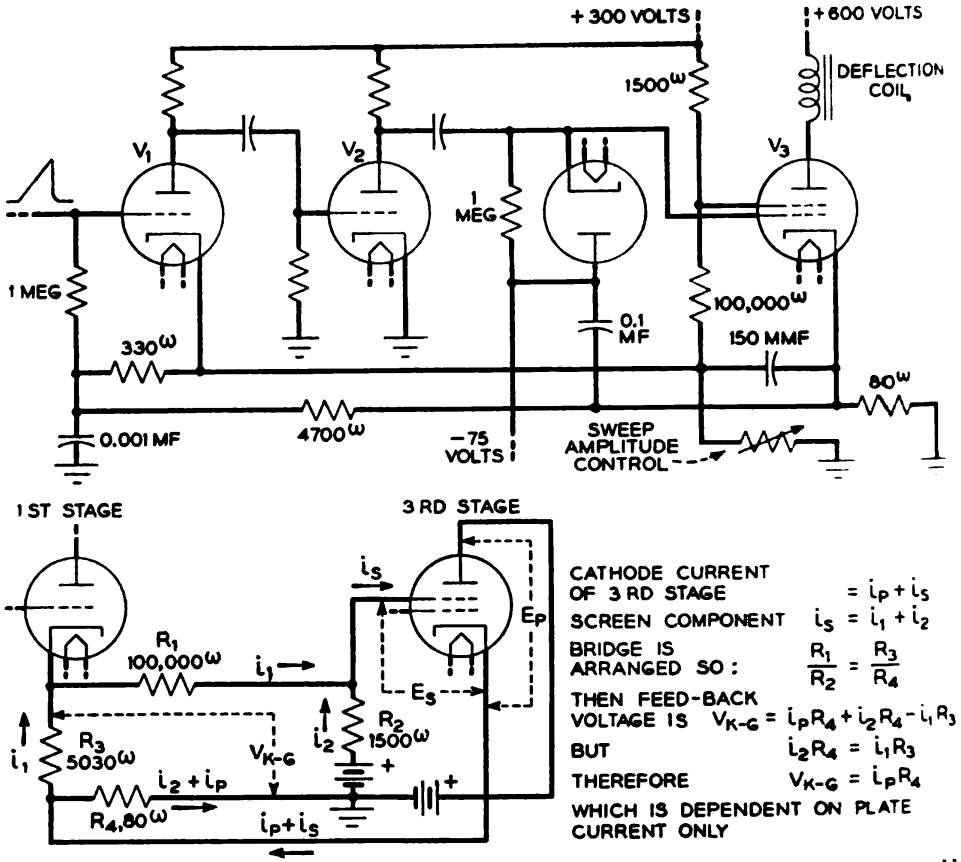

Fig. 56.—Radar range sweep amplifier employing negative feedback and screen grid bridge circuit—simplified schematic.

tribute to the net feedback. Figure 56 illustrates the bridge circuit which has been devised to accomplish this. A voltage from the screen of the third stage is directly applied to the cathode of the first stage, this voltage being equal in magnitude and of opposite polarity to that which appears across the feedback impedance due to the third stage screen current flow. This bridge circuit operation is independent of the absolute screen voltage value.

To insure identical starting potential conditions regardless of the duration of the range sweeps in use, d-c restoration is employed in the grid circuit of the last stage. The action here is similar to the operation described previously in connection with video amplifier design. The delay inherent in

Digitized by Google
Original from UNIVERSITY OF MICHIGAN
Generated on 2019-09-22 07:29 GMT / http://hdl.handle.net/2027/mdp.39015077775156
Public Domain, Google-digitized / http://www.hathitrust.org/access_use#pd-google

the magnetic deflection circuits must be carefully considered in the overall radar receiver design, if the display is required to reproduce short-range information. In such cases, it is customary to insert delay networks in the video channel introducing a delay to the received signal equal to that present in the indicator deflection system, or to "pre-pulse" the deflection circuits prior to the time of the outgoing radar pulse.

It is desirable from a power consumption and display appearance standpoint to limit the range deflection of the radar indicator only to that amplitude required to adequately fulfull the display requirements. A method commonly employed is indicated in Fig. 57. Here a measure of the current flow through the deflection coil, and accordingly the amplitude of the deflection of the cathode-ray tube beam upon the screen, is obtained from the feedback voltage of the sweep amplifier. This voltage is impressed upon a

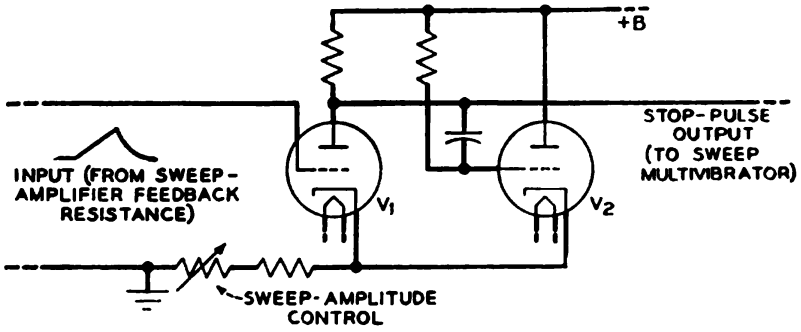

Fig. 57.—Range sweep stop pulser circuit for limiting sweep deflection.

"sweep-stop" pulser which upon rising to a preselected value corresponding to the desired sweep amplitude is caused to trigger this circuit. The output pulse of this circuit is then employed to operate the sweep limiter portion of the sweep timing multivibrator previously described, thus terminating the sweep timing pulse proper.

2.6 *Circuits for Radar Range and Bearing Measurement*

In this review of radar receiver design principles only the presentation of the received radar signal in a form convenient to the observer has been considered. To fully utilize the complete radar information available, determination of the complete coordinates is necessary with an exactness which is determined by the specific use of the data and by the capabilities of the radar system itself. This section will be devoted to a review of the methods employed to generate electronic markers necessary for the determination of range and azimuth and elevation angles. These markers include both the fixed variety, whereby the approximate coordinates of a radar target can be determined by inspection, and steerable markers by

Generated on 2019-09-22 07:29 GMT / http://hdl.handle.net/2027/mdp.39015077775156
Public Domain, Google-digitized / http://www.hathitrust.org/access_use#pd-google
Digitized by Google
Original from UNIVERSITY OF MICHIGAN

which means precise coordinate data necessary for most military applications are determinable. As indicated previously, the optical filters commonly employed over the screen of the radar indicator often serve as a medium for display of range, azimuth or elevation coordinate markings: however, these methods are seldom completely satisfactory in military fire-control radar systems because of errors introduced by the ever-present size or position variations in the electronic display field. Their use has been strictly limited to search or reconnaisance radar systems.

2.61 *Electronic Bearing Marker Circuits*

The bearing marker methods reviewed here are applicable generally to both azimuth and elevation angle determination. A method of azimuth or elevation bearing determination which can be associated with a lobing antenna system and an A-type indicator has been mentioned previously. This method remains an extremely precise system which has the desirable advantage of simplicity. During the latter part of the war, automatic tracking was applied to this method where the actual comparison of the lobes of the selected target signals was carried out electronically and the resultant antenna steering information utilized as the final bearing data. In a strict sense, however, only an indication of error in antenna training is observable to the operator on the radar equipment proper. The exact bearing data must be obtained from a measurement of the position of the antenna itself.

In the case of the continuous scanning systems employing B, C, or PPI presentations, it is common practice to provide a steerable electronic marker which can be superimposed upon the display field and by which means relatively exact azimuth and elevation angles can be determined by target and marker coincidence. This electronic marker method has the advantage that it is subject to the same size and position display field distortion influences as the received pulse signal, thus eliminating this source of error.

A circuit arrangement which has been employed in connection with a naval vessel radar search system to brighten a selected and variable range trace of the PPI indicator to serve as an electronic azimuth marker is given in Fig. 58. In this example the rotating antenna structure is equipped with a small permanent magnet pole piece whose cyclic excursions past a sealed magnetic reed relay cause a pair of contacts to close indicating coincidence. The relay structure is likewise mounted on a ring which can be rotated with respect to the scanning axis of the antenna. The relative bearing of a target is thus determinable by a knowledge of the angular position of the relay capsule with respect to the lubber line of the vessel. The circuit of Fig. 58 produces one brightened range trace for each revolution of the antenna upon closure of the bearing marker relay contacts and is ar-

Digitized by Google
Original from UNIVERSITY OF MICHIGAN
Generated on 2019-09-22 07:30 GMT / http://hdl.handle.net/2027/mdp.39015077775156
Public Domain, Google-digitized / http://www.hathitrust.org/access_use#pd-google

ranged to be unaffected by any subsequent chatter or false switch closures. The pedestal generator which includes vacuum tubes V_1 and V_2 which are normally operated below plate current cutoff produces upon closure of the bearing marker switch contact a rectangular negative pulse having a duration of 10,000 microseconds. This pulse operation is independent of additional chatter effects following the initial contact closure. The following single-cycle bearing mark multivibrator is normally held inoperative by the bias voltage developed on the cathode of V_3. The grid of V_3 is continuously excited with the range sweep start pulses of an amplitude insufficient to actuate this multivibrator circuit. The presence of the 10,000-microsecond pedestal is sufficient, however, to allow the following range sweep

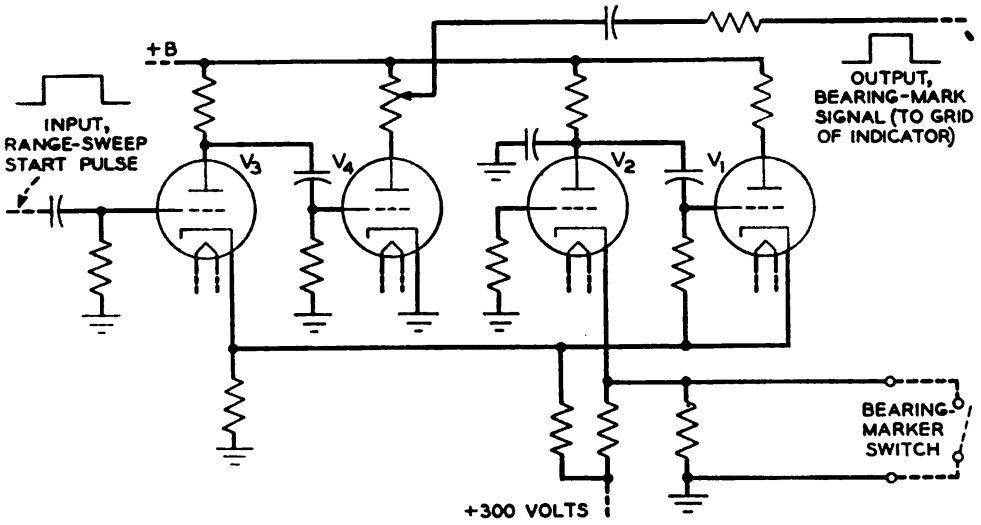

Fig. 58.—Electronic azimuth bearing marker circuit—simplified schematic.

start pulse to operate the multivibrator. The output of this circuit is then a 550-microsecond pulse which represents a time slightly longer than the maximum range to be displayed (60,000 yards) but shorter than the period of the sweep repetition rate. This positive 550-microsecond pulse is applied to the modulating grid of the PPI indicator tube through an adjustable trace brightness control element.

Another convenient azimuth display method which has been extensively employed in naval and airborne radar systems involves the use of "true North" presentations. Here the PPI azimuth indication is presented in terms of a compass reference, the actual instantaneous position of the range trace on the screen representing the compass direction of the antenna beam. In the indicator previously illustrated in Fig. 44 the compass information is introduced by means of a differential synchro inserted in the antenna-indicator synchronizing connections whose angular displacement is pro-

Generated on 2019-09-22 07:30 GMT / http://hdl.handle.net/2027/mdp.39015077775156
Public Domain, Google-digitized / http://www.hathitrust.org/access_use#pd-google
Digitized by Google
Original from UNIVERSITY OF MICHIGAN

portional to the instantaneous heading of the aircraft. In the SL radar indicator shown in Fig. 61 the compass information is introduced by means of a mechanical differential rotation of the indicator deflection coil proportional to the angular position of the compass repeater mechanism.

2.62 *Range Marker Circuits—Fixed Range Markers*

A simplified schematic diagram of a convenient fixed range mark generator circuit which has been extensively employed on airborne radar search systems is given in Fig. 59. Here the radar system requires 1- and 5-statute mile fixed range markers. The sweep start multivibrator pulse is applied to the grid of V_1 as shown. In the absence of a signal, this tube

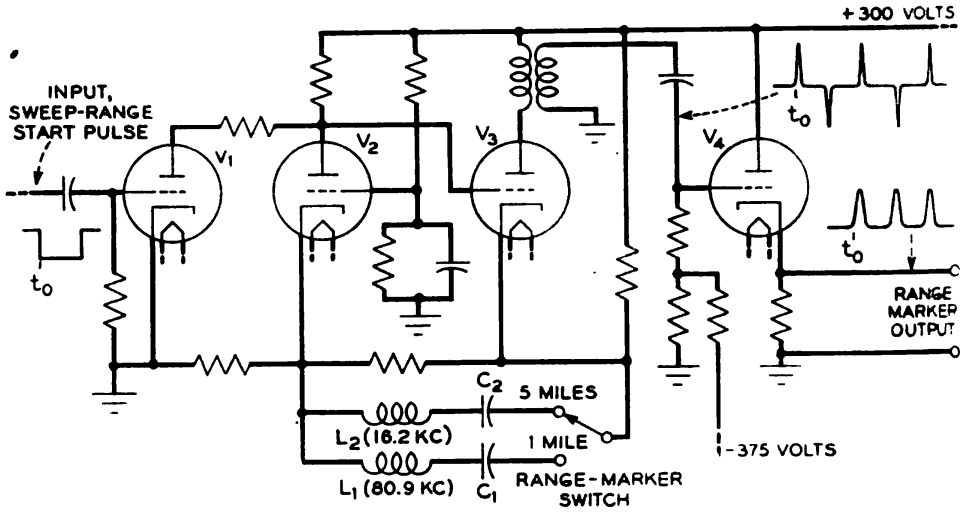

Fig. 59.—Fixed range marker circuit—simplified schematic.

operates at effectively zero bias, and because of the large plate current flow reduces the effective plate potential of V_2 and the grid potential of V_3 to a low value. Since the cathode of V_3 is subject to a large positive potential, this tube is cut off and the oscillatory circuit shown is inoperative. Upon application of the negative start pulse, V_1 is cut off for the duration of this pulse and the attendant rise in the V_3 grid potential permits the oscillator circuit to function. The series resonant elements $L_1 C_1$ and $L_2 C_2$ determine the frequency of oscillation by providing a high value of positive feedback at the series resonant frequency. The output of V_3 which consists of approximate sinusoidal pulses is differentiated by means of the air-core transformer shown. The differentiated pulses are then applied to a cathode follower amplifier stage biased to cut off where the output is limited to the desired positive fixed range mark pulses for indicator display. By careful choice of circuit elements and equipment arrangement, this simple circuit form has

Generated on 2019-09-22 07:31 GMT / http://hdl.handle.net/2027/mdp.39015077775156
Public Domain, Google-digitized / http://www.hathitrust.org/access_use#pd-google
Digitized by Google
Original from UNIVERSITY OF MICHIGAN

produced an entirely satisfactory range marker signal for radar search systems.

Variable Range Marker Circuits

Variable range marker circuits are employed where more precise range information is required for missile control applications of radar. Here the observer may position the electronic range mark to obtain coincidence with the selected target, and from an associated calibration of this positioning control, determine the range coordinate. For search or reconnaissance purposes it is often desirable to determine range with somewhat more accuracy than is afforded by the display of fixed markers, and for this purpose,

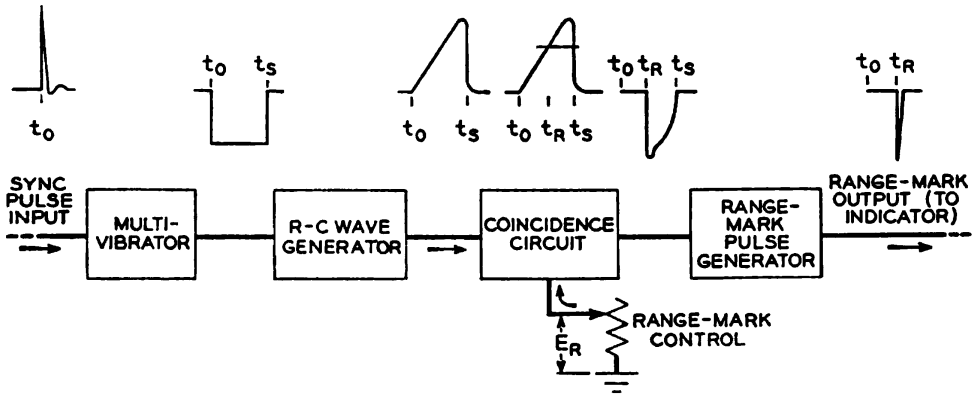

Fig. 60.—Variable range marker circuit of moderate precision—simplified schematic.

several designs of moderate precision variable range marker circuits have been developed and employed during the past war period.

Figure 60 illustrates the circuit operation of a variable range mark generator of moderate precision. This circuit operation depends on a pulse obtained from the transmitting modulator to serve as the zero time or range reference. This is applied to a single-cycle multivibrator which produces a rectangular pulse whose leading edge is coincident with the time of the synchronizing pulse and whose duration is somewhat greater than the maximum range measurement required. A saw-toothed voltage wave form is generated in the following RC wave generator by means similar to the sweep wave form generation described in a previous section of this paper. The coincidence circuit which follows consists of a vacuum tube biased below cut-off whose exact cut-off bias is determined by the range mark potentiometer setting. This coincidence circuit is thus inoperative until the saw-toothed input signal has reached the value of the cut-off voltage, at which time this circuit functions and produces a sharp decrease in its plate potential. The effective time delay which is here produced with respect

Digitized by Google
Original from UNIVERSITY OF MICHIGAN
Generated on 2019-09-22 07:31 GMT / http://hdl.handle.net/2027/mdp.39015077775156
Public Domain, Google-digitized / http://www.hathitrust.org/access_use#pd-google

to the time of the synchronizing pulse is observed to be a function of the rate of change of the saw-toothed wave form and the setting of the range control potentiometer which may be calibrated directly in units of range to the target. The following range mark generator differentiates this coincidence circuit output wave form and furnishes the desired amplification. Zero range calibration is here provided by employing a sample of the zero time reference pulse and introducing this voltage into the range control circuit.

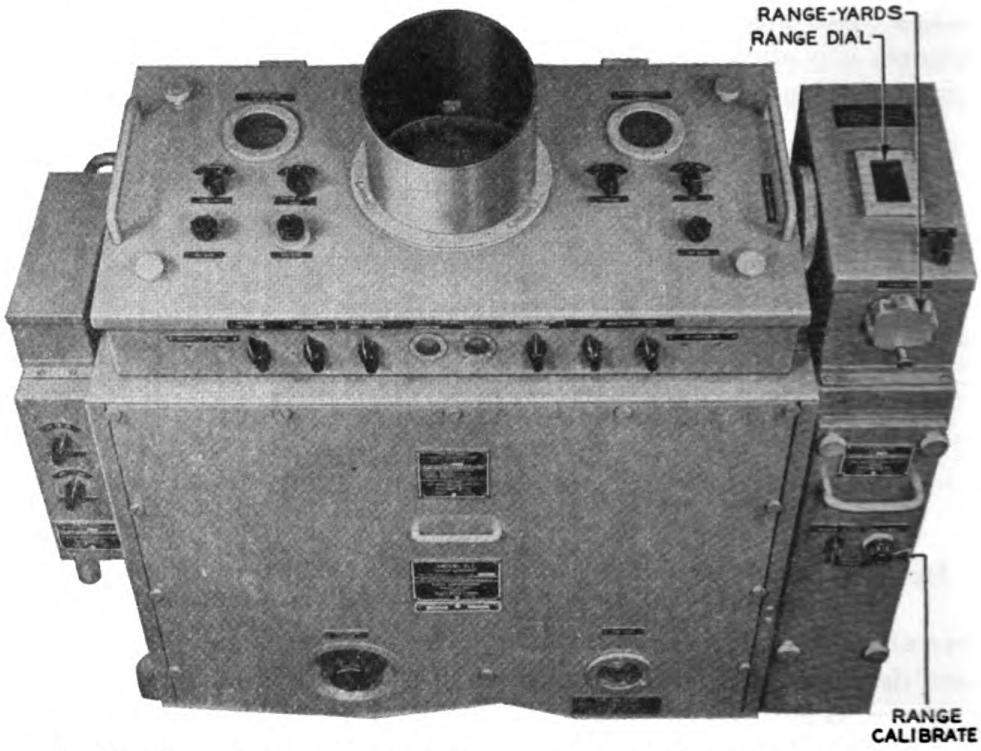

Fig. 61.—Transmitter-receiver-indicator assembly as designed for SL-Naval Search Radar equipment.

Figure 61 illustrates the transmitter-indicator assembly of the SL naval vessel search radar system. This system employs a PPI display with available range sweeps of 5, 25 and 60 nautical miles. The assembly shown to the right of the main unit contains a variable range marker circuit of the type just described. This range mark is positioned by means of the control located toward the top of this unit and its calibration is observable through a window located on the top panel. Here a maximum measuring range interval of 40,000 yards is available. In this application, the RC elements of the wave generator are enclosed within an oven and maintained at a constant temperature by thermostatic means. The accuracy achieved in this example, without recourse to calibration means involving targets at known

Generated on 2019-09-22 07:31 GMT / http://hdl.handle.net/2027/mdp.39015077775156
Public Domain, Google-digitized / http://www.hathitrust.org/access_use#pd-google
Digitized by Google
Original from UNIVERSITY OF MICHIGAN

range, is ± 200 yards at the maximum range with an accuracy of ± 100 yards for targets within 5 nautical miles.

For more precise determination of range than is afforded in the circuit just described, two methods have been extensively employed. The first method involves the production of a known time delay by actual measurement of the time of propagation of an acoustical wave through a liquid medium. Here the physical length of path is varied to produce the variable delay. The second method involves the phase shifting of a known precise sinusoidal frequency standard which bears a fixed phase relationship to the time of the outgoing radar pulse.

The "liquid delay tank" variable range unit over-all operation may be observed by reference to Fig. 62. The zero time range reference is obtained in the form of a pulse coincident with the outgoing radar pulse. This pulse actuates the one-cycle multivibrator shown to produce a sharp high-ampli-

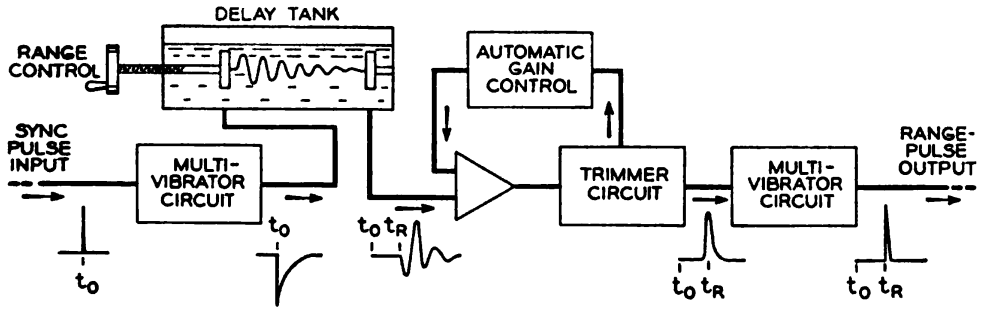

Fig. 62.—Liquid delay tank type of precision variable range unit—block diagram of operation.

tude output pulse, here relatively independent of amplitude and form characteristics of the synchronizing pulse and which is applied directly to the delay tank. This delay tank consists of a suitable container filled with a mixture of iron-free ethylene glycol and water so composed as to produce a zero temperature-velocity coefficient at 135°F, at which temperature the liquid is maintained by thermostatically controlled electrical heaters. In this temperature region the temperature-velocity characteristic is such as to produce a decrease of velocity of 0.1% for a temperature variation of 14°F. Located at one end of this tank is a quartz crystal, approximately $\frac{7}{8}''$ square and 0.040″ in thickness, mounted securely on a brass plate which serves as one electrode and which is immersed in the liquid. A similar crystal element is attached to a lead-screw carriage and located so that the face of this crystal is parallel to the fixed crystal. The distance between the crystal faces can be varied by rotation of the lead screw. The sharp voltage wave applied to the transmitting crystal causes it to oscillate in a damped vibration at its natural frequency for longitudinal waves which in this case

Digitized by Google
Original from UNIVERSITY OF MICHIGAN
Generated on 2019-09-22 07:31 GMT / http://hdl.handle.net/2027/mdp.39015077775156
Public Domain, Google-digitized / http://www.hathitrust.org/access_use#pd-google

is of the order of 1.4 megacycles. The mounting plate and surrounding liquid serves to highly dampen this oscillation. A short vibrational wave train is projected through the liquid toward the receiving crystal. The amplitude of this disturbance is only slightly attenuated by viscous dissipation for the maximum path length here employed. The large area of the crystal relative to the wave length results in a highly directive radiation and is reflected in a parallelism requirement for the crystal faces of the order of .01″. The voltage developed across the receiving crystal upon application of this delayed acoustical wave consists of a main response followed by minor disturbances due to re-reflections between the crystals.

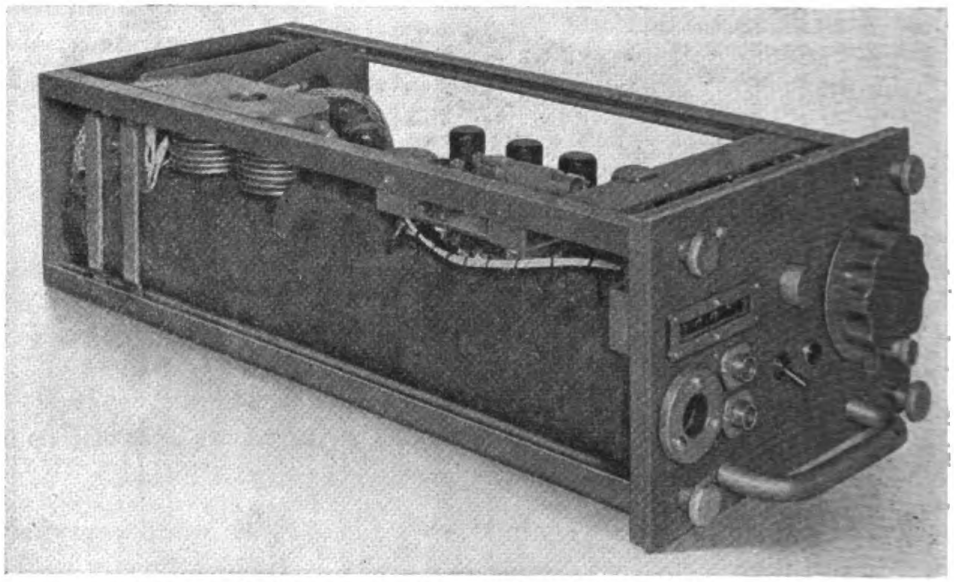

Fig. 63.—Liquid delay tank type of precision variable range unit.

The following amplifier shown in Fig. 62 is required to increase the .005-volt received signal to approximately 20 volts. This gain supplied is controllable by means of an automatic gain control circuit so as to provide a relatively constant amplitude of the first response signal. The following trimmer circuit consists of a pentode operating below cutoff such that a signal of at least 20 volts is required for plate current flow. Since the AGC circuit operates to adjust the gain of the amplifier to this condition, only the first and highest response peak is transmitted to the final range pulse multivibrator circuit where a sharp narrow rectangular pulse is produced to be employed in the following indicator circuit.

Figure 63 is a photograph of the liquid-tank type of variable range unit as developed and manufactured early in the past war and employed extensively in naval fire-control radar systems. This unit includes provision for a

Digitized by Google
Original from UNIVERSITY OF MICHIGAN
Generated on 2019-09-22 07:32 GMT / http://hdl.handle.net/2027/mdp.39015077775156
Public Domain, Google-digitized / http://www.hathitrust.org/access_use#pd-google

maximum range measurement of 40,000 yards with an accuracy of ± 40 yards at this range under normal field operating conditions.

The use of the liquid range unit is practically restricted to ground and naval vessel application because of its weight and the problems of handling these critical liquids. Another variable range unit development was initiated to meet the same accuracy requirements as above, but to be more suitable for aircraft and other extreme ambient applications. The phase-shifting type of variable range unit whose operation is illustrated in Fig. 64 was the result of this effort.

The input start-stop single-cycle multivibrator circuit produces a rectangular pulse output wave form whose leading edge is coincident with the time of the outgoing radar pulse and whose duration encompasses the maximum range time to be measured, in this example 270 microseconds.

The timing wave generator and associated phase shifting circuit is shown schematically in Fig. 65. The resonant frequency of the oscillatory circuit is 81.955 kc which period represents an equivalent radar range interval of 2000 yards. An initial d-c current of approximately 10 ma is present in the $L_1 C_1$ circuit in the absence of input start signals. Upon application of the negatively poled rectangular start-stop pulse V_1 and V_2 are abruptly driven to cutoff and the energy associated with the magnetic field of L_1 produces local current flow and oscillation at a frequency determined by $L_1 C_1$. The initial circuit conditions here are the same as the zero voltage condition for each cycle of a sustained oscillation and the behavior of the oscillatory system is the same as for the case of sustained oscillation. The absolute average potential of the oscillation is maintained constant regardless of the magnitude of the duty cycle. Positive feedback of the timing wave is included in the V_3 cathode connection in such a manner that uniform amplitude of the timing period throughout the active period results. The purpose of the remaining circuits shown in Fig. 65 consisting of V_3, V_4 and V_5 is to produce four output timing wave voltages whose relative phases differ by 90°. These voltages are to be later combined in such a manner that continuous phase shift of the output timing wave results. Two quadrature voltages are here produced by the use of LR and CR networks so proportioned that $\omega L_2 = \frac{1}{\omega C_2} = R_2$ at 81.955 kc. The desired four timing wave outputs are produced by the use of the phase inverter stages V_4 and V_5.

The method here employed to combine four quadrature voltages to enable continuous relative phase shift of the resultant output is illustrated in Fig. 66. This phase shifter capacitor consists of four quadrant shaped stator sectors which are equal in area and shape and which are mounted parallel to a ring stator as shown. A carefully shaped eccentric dielectric vane rotor

Digitized by Google
Original from UNIVERSITY OF MICHIGAN
Generated on 2019-09-22 07:32 GMT / http://hdl.handle.net/2027/mdp.39015077775156
Public Domain, Google-digitized / http://www.hathitrust.org/access_use#pd-google

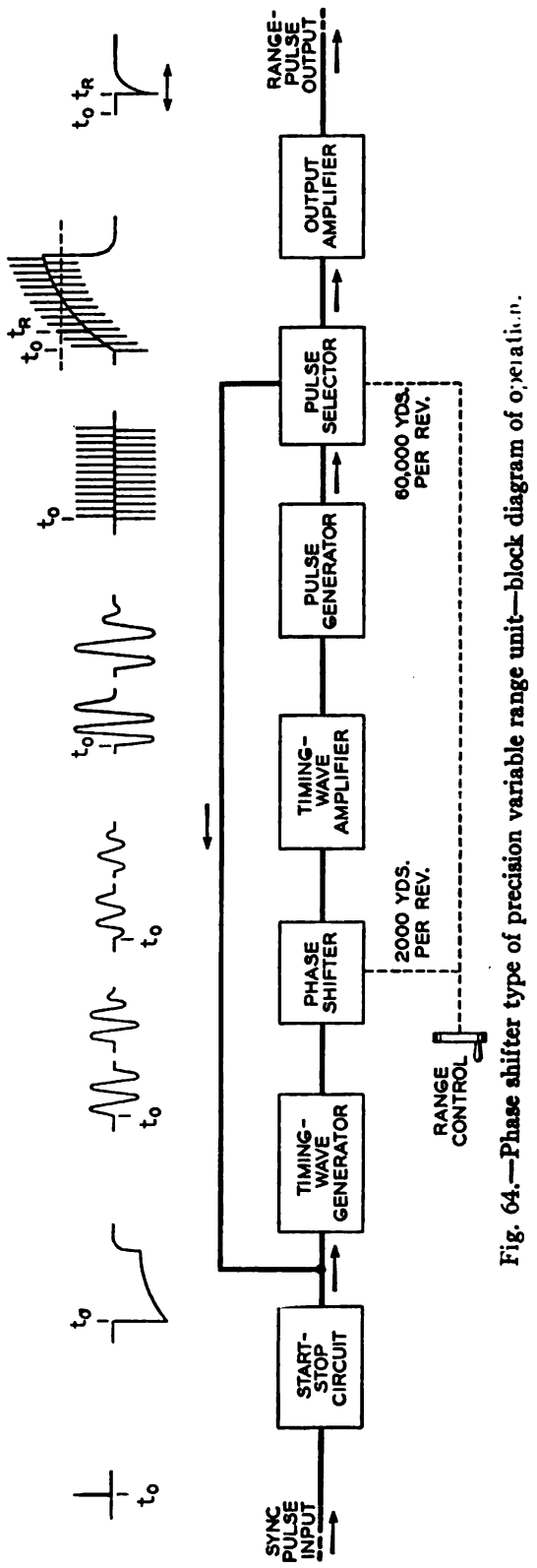

Fig. 64.—Phase shifter type of precision variable range unit—block diagram of operation.

Digitized by Google
Original from UNIVERSITY OF MICHIGAN
Generated on 2019-09-22 07:32 GMT / http://hdl.handle.net/2027/mdp.39015077775156
Public Domain, Google-digitized / http://www.hathitrust.org/access_use#pd-google

is provided whose rotation between the stator elements affects each quadrant stator capacitance in a like manner. As illustrated the resultant output voltage which appears from the ring stator to ground has a phase shift relative to any applied wave which varies linearly with angular displacement of the condenser shaft.

The function of the following amplifier shown in Fig. 64 is to provide a high-impedance termination for the phase-shifting condenser, and to provide increased amplitude of the timing wave. The pulse generator which follows limits or clips the applied timing wave, and differentiates the re-

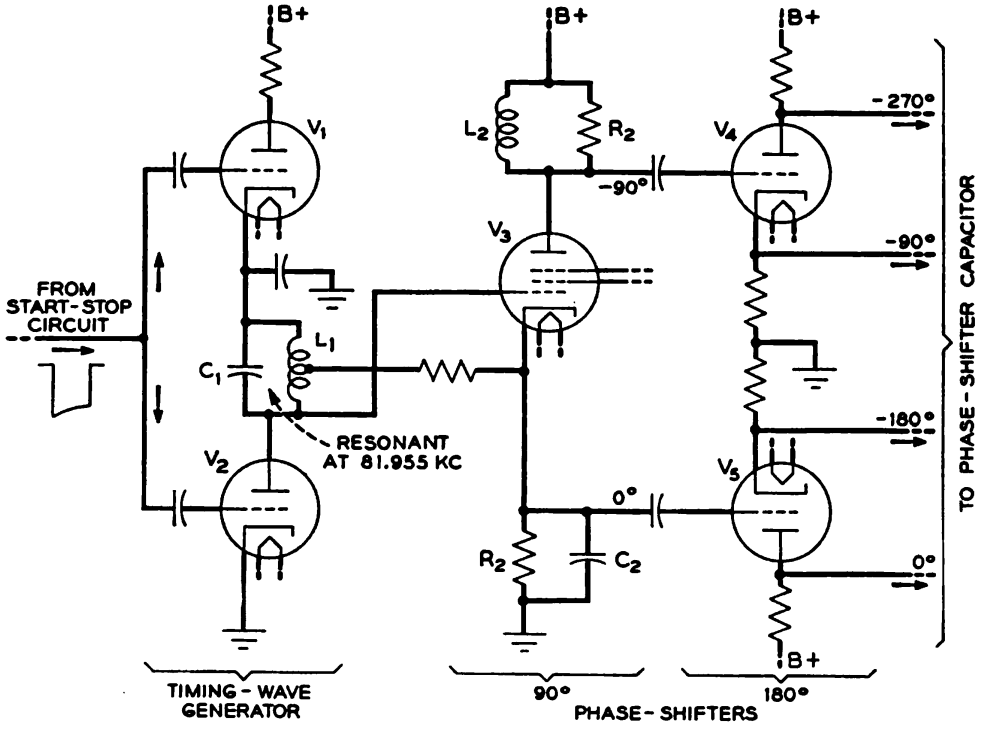

Fig. 65.—Timing wave generator circuit of phase shifter type range unit.

sultant wave form. The output here consists of trains of alternate positive and negative timing pulses.

The pulse selector component shown in Fig. 64 enables obtaining delay intervals greater than 12.2 microseconds the value associated with 360° phase shift of the timing wave. An increasing exponential saw-toothed wave form is generated starting at zero time reference by an RC circuit having a time constant of the order of 800 microseconds. The timing pulses are applied additively with this exponential to the grid of a vacuum tube operating below cutoff, its exact value of bias being determined by the setting of a potentiometer control. At the time that the grid signal amplitude exceeds this critical cut-off bias value, this tube conducts abruptly as

Generated on 2019-09-22 07:32 GMT / http://hdl.handle.net/2027/mdp.39015077775156
Public Domain, Google-digitized / http://www.hathitrust.org/access_use#pd-google
Digitized by Google
Original from UNIVERSITY OF MICHIGAN

shown and an output pulse is produced whose position on a time scale is determined by the additive phase shift of the timing wave and the setting of the pulse selector potentiometer. By mechanically gearing the potentiometer and phase-shifting condenser, the final rotation of the control shaft will result in an output pulse whose delay will increase uniformly and correspond to 2000 yards per revolution of the control. Further amplification is furnished in the output amplifier shown.

Figure 67 illustrates the final equipment features of a phase-shifting type of variable range unit as developed for naval vessel radar system application. It will be observed that this unit is mechanically interchangeable with the liquid range unit shown in Fig. 63.

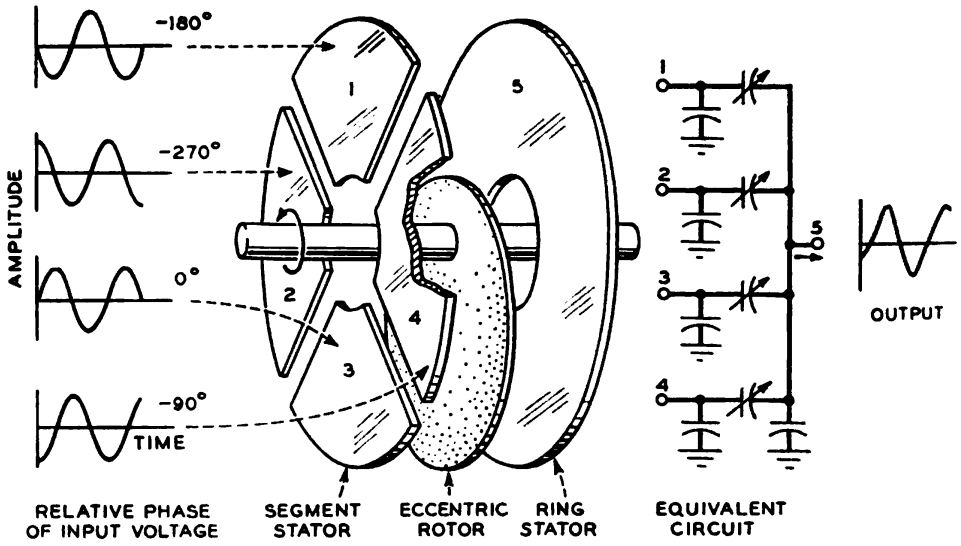

Fig. 66.—Schematic outline of operation of phase shifter condenser.

In this model, the parallel resonant timing wave oscillatory circuit is maintained at a constant temperature by employing an electrically heated oven. Measurements made on this design indicate that the range shift error to be expected for a "warm-up" period of 6 minutes was .003% or 15 yards at 45,000 yards range. After 6 minutes time, thermal equilibrium is reached and the total range error will be less than 20 yards at 45,000 yards range. The unit here illustrated has been universally employed in the majority of naval vessel fire-control radar systems of the past war and these basic circuit principles have served for range measurement in other applications including precision radar bombing.

2.7 *Automatic Frequency Control and Automatic Gain Control*

2.71 *Automatic Frequency Control*

The automatic frequency control (AFC) of the local beating oscillator to

Digitized by Google
Original from UNIVERSITY OF MICHIGAN
Generated on 2019-09-22 07:32 GMT / http://hdl.handle.net/2027/mdp.39015077775156
Public Domain, Google-digitized / http://www.hathitrust.org/access_use#pd-google

assure correct tuning of the radar receiver has become an extremely important feature of the military radar system and the successful solution of

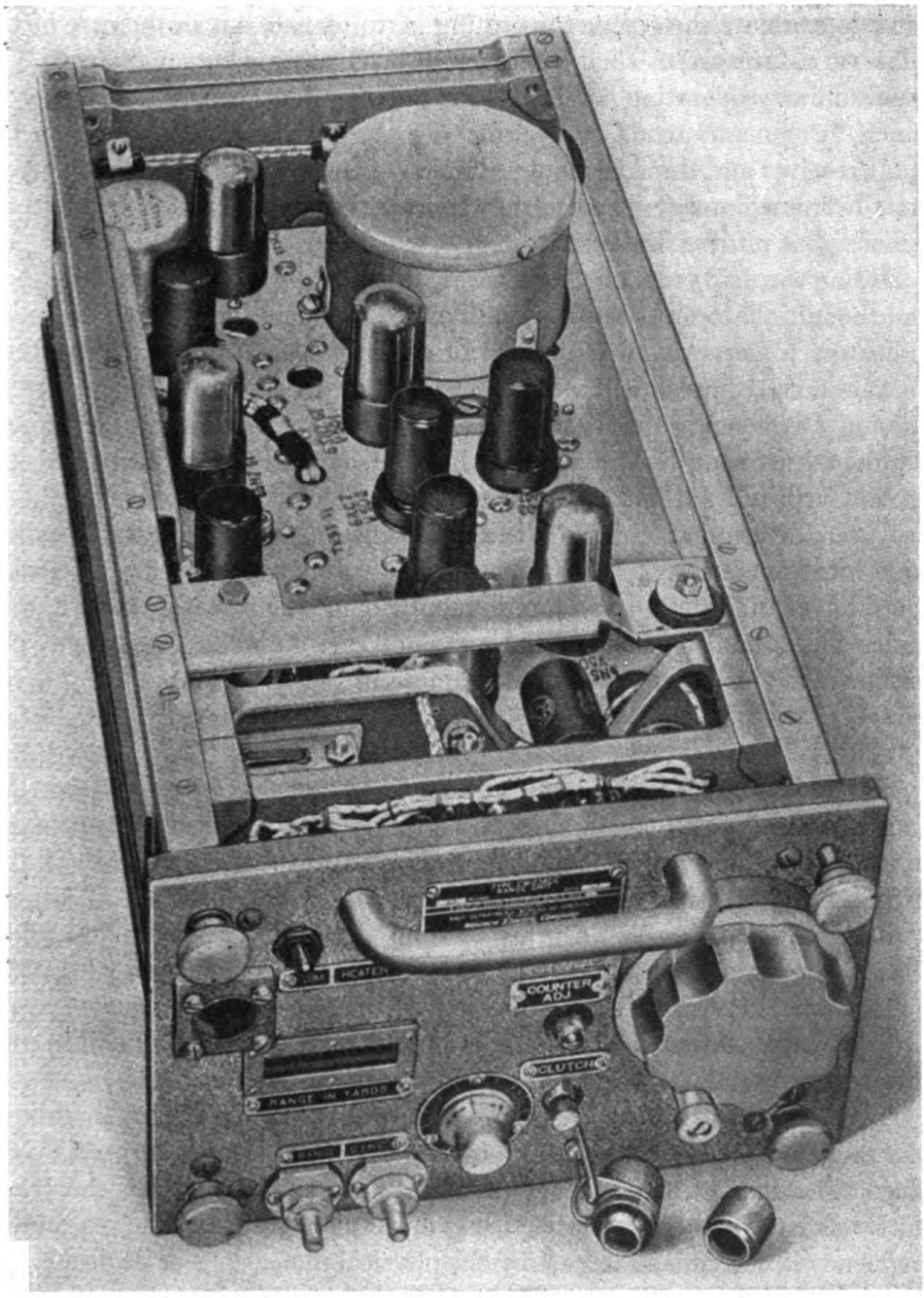

Fig. 67.—Precision variable range unit of the continuous phase shifter type.

this problem has contributed greatly to the practical success of radar during World War II, by assuring consistent optimum system performance under

Digitized by Google
Original from UNIVERSITY OF MICHIGAN
Generated on 2019-09-22 07:33 GMT / http://hdl.handle.net/2027/mdp.39015077775156
Public Domain, Google-digitized / http://www.hathitrust.org/access_use#pd-google

severe military field conditions. In the case of the usual radio-communication system, some knowledge of character and extent of the information which is being transmitted is available to the receiving location which may serve to evaluate the receiver operating performance, but in the case of the military radar system such reference data is not always available. The usual military operating conditions for radar systems are extremely severe which, in general, tends to degrade the performance. Mistuning of the radar receiver and the attendant reduction of the performance of the system must be immediately evident to the operator even under conditions where no radar signal returns are present.

During the first years of the past war, this tuning problem was recognized and the initial attempts at solution involved the inclusion of receiver tuning indicators to serve as an indication of adjustment. As the radar systems became more complex and with the trend toward the use of higher transmission frequencies the necessity for completely automatic continuous tuning adjustment of the receiver became increasingly evident and the present types of automatic frequency control devices were developed. It has been determined that in the specific case of airborne radar bombing equipment operating at 10,000 mc that the automatic frequency control of the receiver tuning is an absolute necessity, since the radar operator cannot under the normal military operating conditions maintain the system performance in this regard to a small fraction of the optimum.

Functions and Requirements

The basic reference for a radar automatic frequency control system must be the transmitter frequency since it is required that the receiver be properly tuned under the condition where no radar return signals are available. Either the frequency of the transmitter magnetron or the local beating oscillator frequency may be adjusted from an electrical error signal whose characteristics are related to the tuning point. Magnetrons whose frequency was conveniently controllable by remote electrical means were not then available so that the later method has been universally applied in military radar systems developed during the past war period.

It is pertinent to review the nature and extent of the frequency instability of a radar system to derive the requirements to be imposed upon an AFC device. The sources of frequency instability are associated with the transmitter as well as the receiver elements of a radar system. The magnetron frequency is determined in part by the physical dimensions of its oscillatory cavity structure, and as would be expected, ambient temperature and pressure conditions exert a decided influence. For example, a typical thermal coefficient of frequency for a magnetron may be as high as 200 kilocycles per degree Centigrade which over the range of ambient temperatures

Digitized by Google
Original from UNIVERSITY OF MICHIGAN
Generated on 2019-09-22 07:33 GMT / http://hdl.handle.net/2027/mdp.39015077775156
Public Domain, Google-digitized / http://www.hathitrust.org/access_use#pd-google

to be considered important for military equipment may result in a frequency shift of 20 mc from the time the equipment is turned on until thermal equilibrium is established. The magnetron frequency is extremely sensitive to its terminating load impedance. This termination in a radar equipment is composed of the antenna, the interconnecting RF transmission line, and the duplexing devices. The typical radar antenna system employs rotating joints or connecting devices to enable transfer of RF power to the antenna proper while it is mechanically operated over its scanning cycle. These connections cannot be made to present an entirely uniform impedance over their entire mechanical operating range and thus introduce variable impedance irregularities to the magnetron generator. The frequency of these impedance variations may range from a fraction of a cycle per second to perhaps 60 cps. The input impedance of the antenna proper is dependent on the extent and character of nearby obstructions in the radiation path. The characteristics and form of the radome employed to protect the antenna contribute to the variable impedance characteristics of the antenna and thus influence the magnetron frequency. An additional instability in magnetron operation which is introduced through power supply variations within the modulator and transmitter portion of the system must also be considered in the detailed design of the AFC system.

The receiver itself is responsible for a major contribution to the frequency instability characteristics of the radar system. The local beat oscillator frequency is critically dependent on the physical dimensions of its oscillatory structure and on the supply voltages. The effects of temperature and atmospheric pressure on the frequency of a reflex oscillator of the types previously described is considerable. For example, a thermal coefficient of 0.25 mc per degree Centigrade, typical of the 10,000-mc tubes, will produce a total excursion of perhaps 25 mc over the range of ambients experienced in military equipment. In the case of supply voltage variations, a 5-mc frequency shift will result for a 1% change in anode and repeller potential for a typical 10,000-mc reflex oscillator. Another source of receiver frequency instability is associated with the shift of the IF amplifier frequency selectivity characteristic with tube aging and operating conditions.

If the operating requirements for an AFC system are now reviewed from a consideration of these factors, it will be observed that for a radar system operating at the higher frequencies a total effective frequency change of perhaps as much as 50 mc may be encountered whose rate of change, in general, will be relatively slow and may be classified generally as effects due to "warm up". In addition fast variations of frequency will be present whose rates of frequency change may extend from 1 mc per second per second to 1000 mc per second per second. At the lower radar frequencies

Digitized by Google
Original from UNIVERSITY OF MICHIGAN
Generated on 2019-09-22 07:33 GMT / http://hdl.handle.net/2027/mdp.39015077775156
Public Domain, Google-digitized / http://www.hathitrust.org/access_use#pd-google

these frequency variations will be somewhat lower with an attendant reduction of the range of operation required of the AFC circuit.

AFC Circuit Design Considerations

To obtain a measure of the basic frequency reference for AFC purposes the direct approach is evident. A sufficiently attenuated sample of the outgoing radar pulse may be obtained from the transmitter and after sepa-

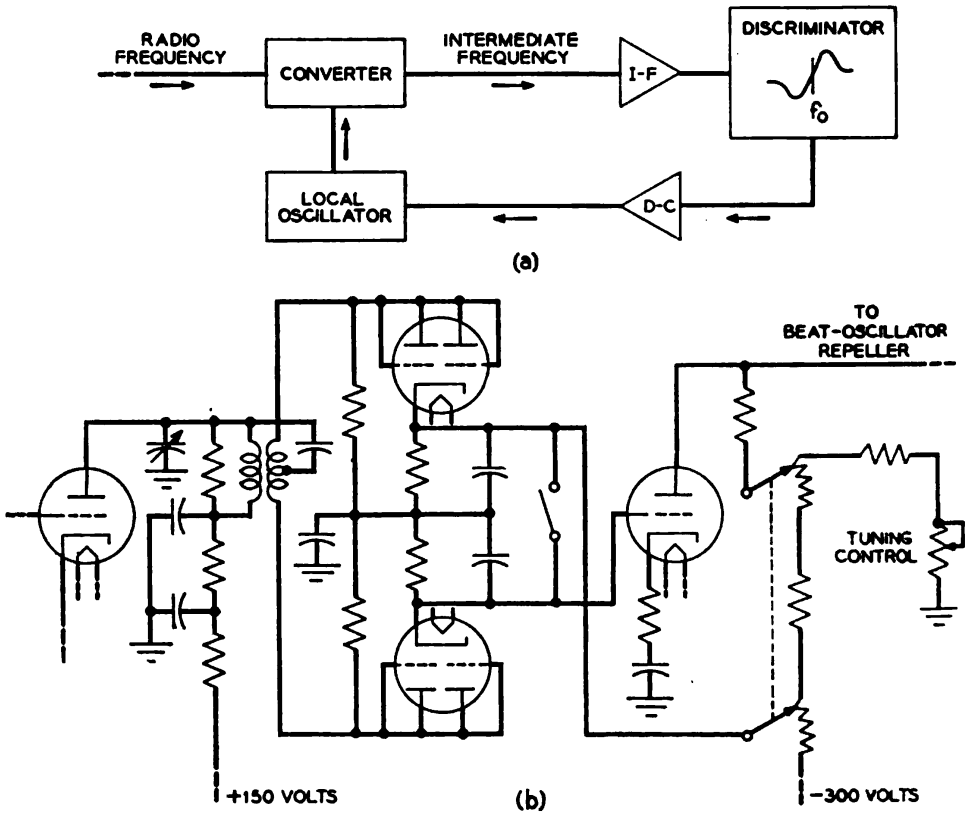

Fig. 68.—Radar AFC system—block diagram and circuit arrangement.

rate conversion but, under the influence of the regular receiver beat oscillator, may be employed as a true sample of the outgoing signal as it exists with the normal receiver IF channel. The separate AFC converter method has been employed in some military radar equipment but has the disadvantage that additional conversion components are required. A second method is more economical of equipment and has been extensively employed during the past war period, but this later type of AFC circuit has limitations which are imposed on it by the character of the IF signal as normally available in a radar receiver. Figure 68a illustrated the essential elements of such an AFC system for a radar receiver. It will be here observed that a

Generated on 2019-09-22 07:33 GMT / http://hdl.handle.net/2027/mdp.39015077775156
Public Domain, Google-digitized / http://www.hathitrust.org/access_use#pd-google
Digitized by Google
Original from UNIVERSITY OF MICHIGAN

sample of the IF signal after normal conversion and some amplification is applied to a frequency sensitive discriminator circuit and the resulting error signal is employed to readjust the beat oscillator frequency. The outgoing radar pulse is normally attenuated effectively by the TR circuit, and thus the remaining signal available for AFC purposes is due to inherent leakage of the TR elements. As previously indicated, the frequency spectrum of the output "spike" of the TR device extends over a wide frequency range, due primarily to the small finite delay in the breakdown of the TR tube. The energy frequency distribution characteristic of this spike is to a large degree independent of the magnetron frequency and, therefore, must be considered as an undesirable masking signal and accordingly reduced to a noninterfering level. As previously indicated this is usually accomplished by disabling one or more of the IF amplifier input stages for a short time interval coincident with the outgoing radar pulse.

With a signal available which is related to the frequency of the outgoing pulse, the remainder of the AFC design is concerned with the utilization of this information to accomplish the automatic tuning of the radar receiver. To determine the frequency gain characteristic of the discriminator circuit it is pertinent to examine the frequency repeller potential relationship of the local beat oscillator. This relationship for a 2K25-type reflex oscillator operating at 10,000 mc shown in Fig. 19 is approximately 2 mc/volt and is representative of the tubes of this type. This quantity provides an indication of the "loop gain" required for a satisfactory AFC circuit.

Typical AFC Circuit Designs

Figure 68b illustrates the essential elements of a radar AFC discriminator and amplifier circuit. This consists of an input circuit which is required to furnish the means for frequency measurement, rectifier elements to convert this frequency deviation information to a proportional voltage error signal, followed by an amplifier to increase the amplitude of this signal to the required level to adequately control the frequency of the local beat oscillator.

The operation of the discriminator input circuit may be observed by reference to the vector diagram of Fig. 69a. The input circuit, essentially a double-tuned transformer having a low value of mutual inductance, serves to couple the AFC rectifier to the preceding IF amplifier tube. The resonance frequency of both primary and secondary circuits is maintained at the desired midband IF tuning point, in this example, 60 mc. The output of the balanced secondary winding of this input network is applied to a balanced rectifier shown in the vector diagram as E_1 and E_1'. In addition a portion of the IF signal voltage which appears across the primary winding is also applied to each element of the balanced rectifier. At resonance, the primary and secondary voltages assume a quadrature relationship as indi-

Digitized by Google
Original from UNIVERSITY OF MICHIGAN
Generated on 2019-09-22 07:33 GMT / http://hdl.handle.net/2027/mdp.39015077775156
Public Domain, Google-digitized / http://www.hathitrust.org/access_use#pd-google

cated. The vector relationships for frequencies above and below this resonance, as shown, result in an amplitude change across the rectifier circuit. Figure 69b illustrates a typical rectified voltage versus frequency characteristic of such an array. The location of the actual crossover zero voltage point is determined only by the resonance of the secondary circuit over the limited range under consideration here. The primary resonance contributes essentially only to the symmetry of the voltage output versus frequency characteristic. The introduction of the time constant elements in the detector output circuit integrates the pulse output and are chosen with due regard

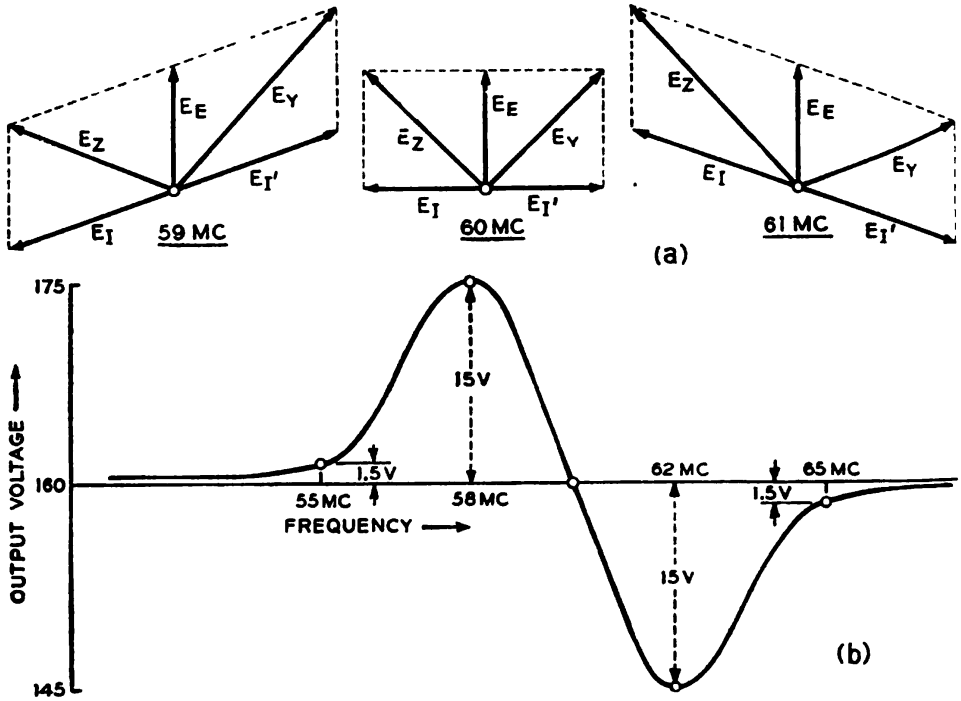

Fig. 69.—Operation of the AFC circuit—vector relationships in input circuit and output voltage vs. frequency characteristic.

to the maximum frequency rate of change which this circuit must control. The d-c amplifier shown is normally biased to operate at maximum gain consistent with stability, to produce the maximum sensitivity to frequency change and to accordingly achieve the least threshold deviation from the ideal tuning condition. Provision for disabling the AFC circuit is included to enable initial manual adjustment of the beat oscillator repeller potential. With the circuit shown here, failure of the AFC circuit proper will result in the return of the repeller potential to that value originally selected by initial tuning and further manual control may be used.

It is often convenient to describe the effectiveness of an AFC circuit in terms of its "pull in" range and its "hold in" characteristics. "Pull in"

Digitized by Google
Original from UNIVERSITY OF MICHIGAN
Generated on 2019-09-22 07:34 GMT / http://hdl.handle.net/2027/mdp.39015077775156
Public Domain, Google-digitized / http://www.hathitrust.org/access_use#pd-google

will be defined as the ability of the AFC circuit to restore proper tuning conditions with sudden application of the signal. The "hold in" characteristic of the AFC system will be defined as the ability of the circuit to maintain proper tuning conditions as slow changes occur in the frequency of the control signal. In the AN/APS-4 airborne radar equipment previously referred to, which employs an AFC circuit similar to the form here described, the "pull in" range is approximately ± 5 mc from the 60-mc midband value and the "hold in" range includes the entire tuning range of the reflex oscillator employed which is of the order of ± 40 mc. This example will maintain the tuning within 0.5 mc of the desired tuning point over the range of conditions encountered in wartime aircraft applications.

In some applications use has been made of a frequency scanning process whereby the AFC output voltage, in the absence of a suitable controlling signal within the IF band, is caused to vary periodically in a saw-tooth fashion thus causing the local beat oscillator frequency to vary, sweeping across the complete tuning range of the receiver. When the desired signal frequency is produced the AFC then functions in the normal manner. This form of circuit was employed in certain radar equipments developed during the early part of the war and a somewhat similar oscillatory AFC circuit has been employed in connection with later developed thermally tuned reflex oscillators and reported elsewhere.[13]

An automatic frequency control unit designed in connection with the AN/APQ-7 radar bombing equipment which operates at 10,000 mc is illustrated in Fig. 70 and Fig. 71. The basic operation of this equipment example is similar to the d-c amplifier type previously described but includes certain modifications important for this particular application. In this circuit the plate potential of the first IF stage of the AFC unit is obtained as a positive pulse from the transmitting modulator thus enabling the AFC circuit only during the short interval of time encompassing the outgoing radar pulse. This arrangement assures that no detuning of the receiver will result from spurious or nearby signals after the radar pulse has been transmitted. The rectifier elements here consist of triodes operating near plate current cut-off which results in improved linearity of detection. The d-c amplifier portion of this AFC circuit is arranged somewhat differently from the example previously discussed, including in this case balancing controls to account for tube and circuit variations. At the condition of resonance, in this case 60 mc, the voltages applied to each grid of the amplifier are equal and the net repeller potential is determined entirely by the manual control value. The overall output range of voltage for this circuit is ± 20 volts, which in this application represents a ± 40-mc frequency change for the associated

[13] "Considerations in the Design of Centimeter-Wave Radar Receivers", Stewart E. Miller, *Proc. I. R. E.*, Vol. 35, No. 4, April, 1947.

Digitized by Google
Original from UNIVERSITY OF MICHIGAN
Generated on 2019-09-22 07:34 GMT / http://hdl.handle.net/2027/mdp.39015077775156
Public Domain, Google-digitized / http://www.hathitrust.org/access_use#pd-google

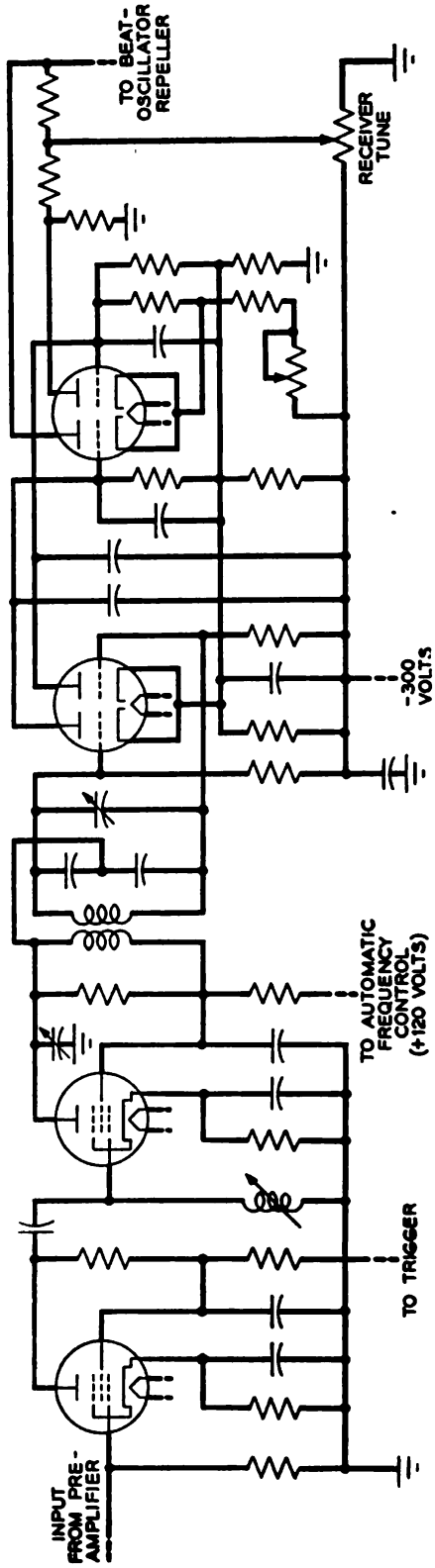

Fig. 70.—AFC circuit schematic for AN/APQ-7 radar system.

Digitized by Google
Original from UNIVERSITY OF MICHIGAN
Generated on 2019-09-22 07:34 GMT / http://hdl.handle.net/2027/mdp.39015077775156
Public Domain, Google-digitized / http://www.hathitrust.org/access_use#pd-google

reflex oscillator. Variations in the amplitude of the controlling signal are of less importance by virtue of the biasing action of this d-c amplifier circuit. The performance of this design includes maintenance of the tuning point of this receiver to within ± 0.25 mc of the center of the IF band which in this case is 60 mc.

2.72 *Automatic Gain Control*

Automatic gain control (AGC) of a selected radar signal is often required in military radar systems employed for fire control or aircraft interception purposes. In the case of the common search radar system, AGC is seldom required. The radar receiver AGC function is quite similar to that required of this circuit in the usual radio communication system, i.e., automatic am-

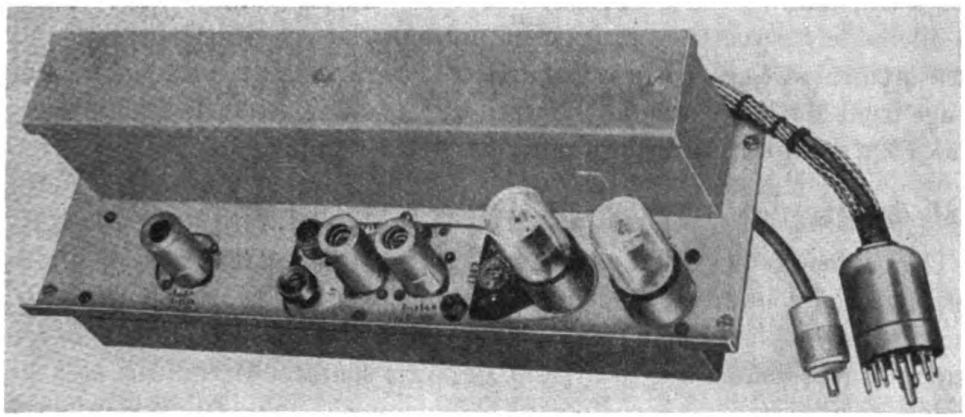

Fig. 71.—AFC component design as employed in AN/APQ-7 airborne radar system.

plitude stabilization of the desired signal. For the radar receiver case, however, the desired signal must be selected on a time interval basis.

In the usual type of automatic tracking radar system, the target is selected by manual alignment of a range and/or bearing "gate". This gating process is essentially a modulation process by which the complete received radar pulse signals are modulated with a rectangular pulse synchronized with the outgoing radar pulse. The modulating pulse or gate has a finite amplitude only over the time interval under observation. In this manner all received information, except that occurring during the selected time interval, is effectively rejected and the automatic gain control circuit operation is entirely defined by the data present during this time interval.

The remainder of the automatic gain control circuit is concerned with the measurement of the amplitude of the selected signal, usually by a peak voltage measurement, the averaging of this measurement over a convenient time interval, and the production of a suitable gain control voltage to be impressed upon the radar receiver IF or video amplifier circuit. The detailed

Digitized by Google
Original from UNIVERSITY OF MICHIGAN
Generated on 2019-09-22 07:34 GMT / http://hdl.handle.net/2027/mdp.39015077775156
Public Domain, Google-digitized / http://www.hathitrust.org/access_use#pd-google

AGC circuit design is dependent to a major extent upon the dynamic characteristics of the associated automatic tracking device. The subject of automatic tracking design principles cannot be reviewed here and accordingly more detailed AGC design consideration must also await inclusion in such a future report.

2.8 *Radar Receiver Power Supplies*

The remaining components of the radar receiver to be here reviewed consist of the power supplies necessary to produce the various d-c potentials as required for the operation of the electronic components of the receiver. The principal design problems associated with these components arise from the relatively poor stability characteristics of the prime sources of power available at the military scene and the rather severe output voltage requirements to adequately serve the precision nature of radar reception, display, and measurement. The supply voltages necessary for a military radar receiver range from low bias potentials upward to 5000 volts for cathode-ray tubes and TR application with both polarities often required.

2.81 *Primary Power Sources*

The characteristics of the primary source of power available for the military radar system are dependent on the area of use of the equipment. In the case of mobile ground radar installations, the gasoline engine driven generator represents the typical primary power source. In the case of large mobile radar systems it is customary to employ 115-volt—60-cycle primary power, while in certain more portable designs 115-volt—400-cycle primary power has proven satisfactory. The frequency and output voltage of a gasoline engine driven alternator cannot be maintained within the narrow limits desired by the radar receiver and here the major burden of precise voltage regulation must be carried by the electronic regulated power supply within the radar receiver.

For naval vessel radar installations 115–230-volt—60-cycle primary power is commonly available on the larger vessels. For PT and similar smaller craft, certain radar installations have been employed operating from 24–48 volts direct current with motor generator sets supplying 60-cycle or 400-cycle power for the radar system. In the case of undersea craft, the storage battery is employed as a primary source of power and motor generator sets are employed to obtain 115 volts, 60 cycles in most instances.

The primary source of power for aircraft radar purposes is either a low voltage (27 volts) d-c generator driven by the aircraft engine or an alternator similarly driven. If d-c power is available, an additional motor generator set may be employed to furnish the 115-volt—400 to 800-cycle power for the radar equipment use. Voltage regulators of the carbon pile compres-

Digitized by Google
Original from UNIVERSITY OF MICHIGAN
Generated on 2019-09-22 07:34 GMT / http://hdl.handle.net/2027/mdp.39015077775156
Public Domain, Google-digitized / http://www.hathitrust.org/access_use#pd-google

sion or electronic types are usually employed here, resulting in a nominal ± 3% voltage stabilization. The extreme variable electrical loads imposed upon the aircraft power system by electrically operated gun turrets and other combat equipment result in increased emphasis being placed on adequate regulation capabilities of the radar receiver power supplies. In addition, the ever-present requirement of minimum weight for aircraft equipment results in motor generator designs employing a minimum of magnetic material and usually results in a variation in output voltage wave shape with load. This factor must also be considered in the detailed design of the aircraft radar receiver power supplies.

During the initial airborne radar development program, the power frequencies in common use were 400 cps and 800 cps. The British use of direct coupled aircraft engine driven alternators produced variable frequency output voltages ranging from 1200–2400 cps dependent on the engine speed. In connection with the electronic warfare standardization program for equipment to be used jointly by our allies, the aircraft radar system was required to operate over the entire range of power frequencies extending from 400 cps to 2400 cps. All of the airborne radar equipment developed during the later half of World War II was designed to meet these variable power frequency requirements.

2.82 *Low Voltage Power Supplies*

The electronic regulated power supply has been universally employed to furnish the stable low voltages as required by the radar receiver. Here the output voltages required extend from 50 volts to 600 volts with maximum direct current required extending upward to 500 ma.

The basic electrical circuit arrangement of such a power supply is shown in Fig. 72. In this circuit, the regulating element consists of a variable series impedance, furnished in the form of a vacuum tube and resistance combination, whose magnitude may be controlled electrically from an error signal associated with the output voltage of the power supply and a reference voltage. The control circuit consists of a bridge network which includes a constant voltage gas-discharge tube as one element. A d-c amplifier is connected across the output terminals of this bridge circuit and serves to amplify the error signal for use in the regulating element. If the output voltage of the power supply varies from the desired value for any cause, the error signal appears at the output terminals of the bridge circuit, due to the effective unbalance of this circuit at all voltage levels except the reference value. The error signal after sufficient amplification is impressed upon the grid of the series regulating tube with a polarity such that a corrective impedance variation results. The degree of regulation obtainable is a function of the loop gain provided and the absolute stability of the output voltage

Digitized by Google
Original from UNIVERSITY OF MICHIGAN
Generated on 2019-09-22 07:35 GMT / http://hdl.handle.net/2027/mdp.39015077775156
Public Domain, Google-digitized / http://www.hathitrust.org/access_use#pd-google

is determined primarily by the constancy of the reference voltage derived by the use of the gas-discharge tube. By incorporating wide frequency band characteristics to the loop gain elements, the maximum rate of change of regulation can be extended, and this circuit becomes very effective in reducing the fundamental and harmonics of the primary supply voltage. The effective impedance of a radar receiver power supply of this type is of the order of one ohm, a factor of extreme importance in reducing the unwanted interaction between the various receiver components by coupling due to this common impedance. Other variations in circuit arrangement for regulated power supplies are occasionally employed, the most common of which involves the use of a vacuum tube as a shunt regulating element as contrasted with the series arrangement shown here. In certain low-current

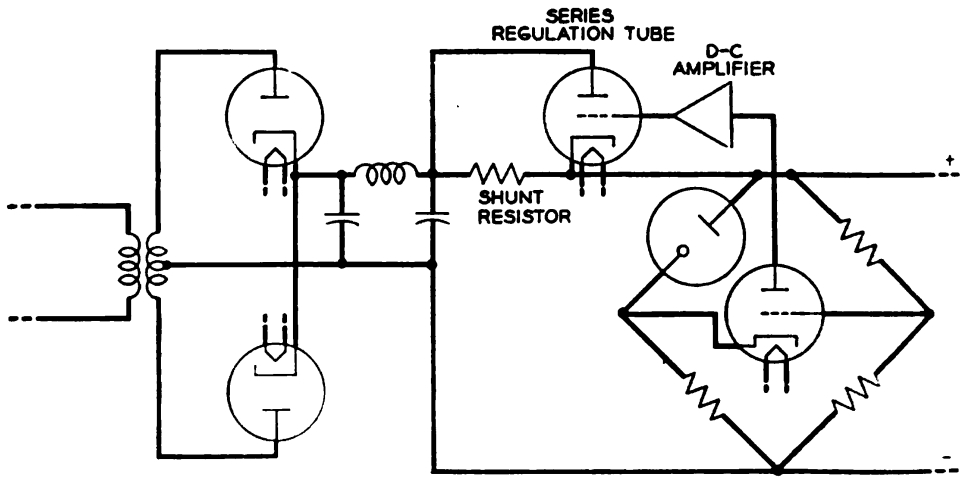

Fig. 72.—Simplified circuit schematic of low-voltage power supply—Series regulation type.

applications the use of gas-discharge tubes of constant voltage characteristics are occasionally employed in a shunt circuit configuration.

Figure 73 illustrates the equipment arrangement of a radar receiver power supply as employed for an airborne radar bombing system. In this example is included one non-regulated and three regulated rectifier power supplies with output voltages of +600, +300, +120 and −300 volts available for the radar receiver. The forced ventilation feature shown here is required to prevent extreme temperature rise of the components under high altitude conditions in the presence of considerable heat dissipation by the rectifier and series regulating circuits. Each power supply is designed as a separable subchassis within the over-all enclosure to provide for ease in manufacture and testing of the unit. The weight of this complete unit as installed in a military aircraft is approximately 50 pounds.

Generated on 2019-09-22 07:35 GMT / http://hdl.handle.net/2027/mdp.39015077775156
Public Domain, Google-digitized / http://www.hathitrust.org/access_use#pd-google
Digitized by Google
Original from UNIVERSITY OF MICHIGAN

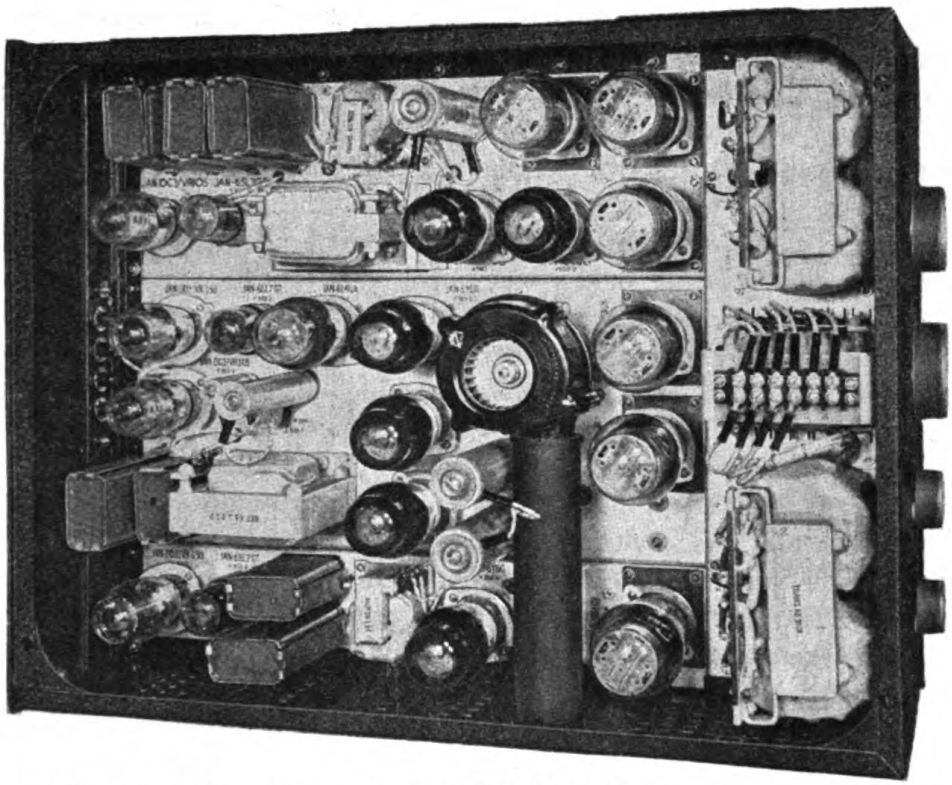

Fig. 73.—Low-voltage power supply for AN/APQ-7 airborne radar system—Mechanical features.

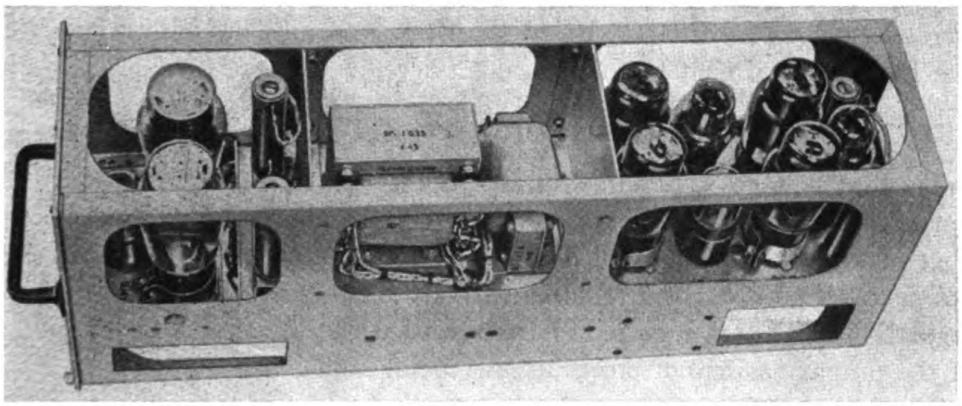

Fig. 74.—Low-voltage power supply for AN/APQ-5 low altitude radar bombing equipment.

Figure 74 indicates the mechanical design features of a typical airborne radar receiver power supply of the series regulated type as employed in the AN/APQ-5 radar bombing equipment. This example illustrates the emphasis which is placed on compactness and lightweight construction of airborne radar components.

Digitized by Google
Original from UNIVERSITY OF MICHIGAN
Generated on 2019-09-22 07:35 GMT / http://hdl.handle.net/2027/mdp.39015077775156
Public Domain, Google-digitized / http://www.hathitrust.org/access_use#pd-google

To obtain the maximum dependable performance from the various power transformers and coils employed in the radar receiver power supplies under the severe military field conditions, a considerable development program was carried on throughout the past war. At the beginning of this program the only available method of insuring adequate transformer winding insulation under extreme humidity conditions involved the sealing of the structure in a metal container. For aircraft service, where weight is of prime concern, this added weight could not be tolerated so that here an open type of structure was extensively employed, with the protection to the winding being furnished in the form of several coats of varnish followed by an enamel overcoat. With the increased emphasis on high-altitude operation of military aircraft and the rapid temperature and pressure changes involved, a development program was instituted to improve the open-type transformer sealing process. The result of this program has produced the Flexseal process whereby the service life of this type of power transformer has been increased as much as ten times that obtained with the varnish process formerly employed. This process involves a multiple-dip varnish coating method where the varnish is thickened by the addition of talc, a very fine low-gravity wettable inert filler. This process results in the formation of a relatively thick plastic shell which completely surrounds the transformer structure. One of the features of this process is found in its simplicity, whereby no special equipment was required to carry out the procedure, an important factor during a wartime production program. Figure 75 illustrates a number of typical open-type power transformers which were employed on various military radar projects, all of which incorporate the Flexseal treatment for improved service life.

2.83 *High Voltage Power Supplies*

The high voltage, as required for radar receiver cathode-ray tube indicator purposes, varies from 2000 volts to 5000 volts, and for the TR tube keep-alive potentials of the order of 1000 volts must be provided. In these cases, however, the d-c current requirements are quite small and generally no regulation means are required for stabilization of the voltage, the stability of the primary source of power usually being sufficient.

The design problems encountered in this type of power supply are concerned primarily with the requirements of reliability of operation under severe military operating conditions, and further require that only circuit elements having well-defined factors of safety be employed in such applications.

Figure 76 illustrates a number of typical high-voltage transformer designs which have been employed in military radar systems during the past war period. Both air insulated and oil immersed types of structures are shown.

Digitized by Google
Original from UNIVERSITY OF MICHIGAN
Generated on 2019-09-22 07:35 GMT / http://hdl.handle.net/2027/mdp.39015077775156
Public Domain, Google-digitized / http://www.hathitrust.org/access_use#pd-google

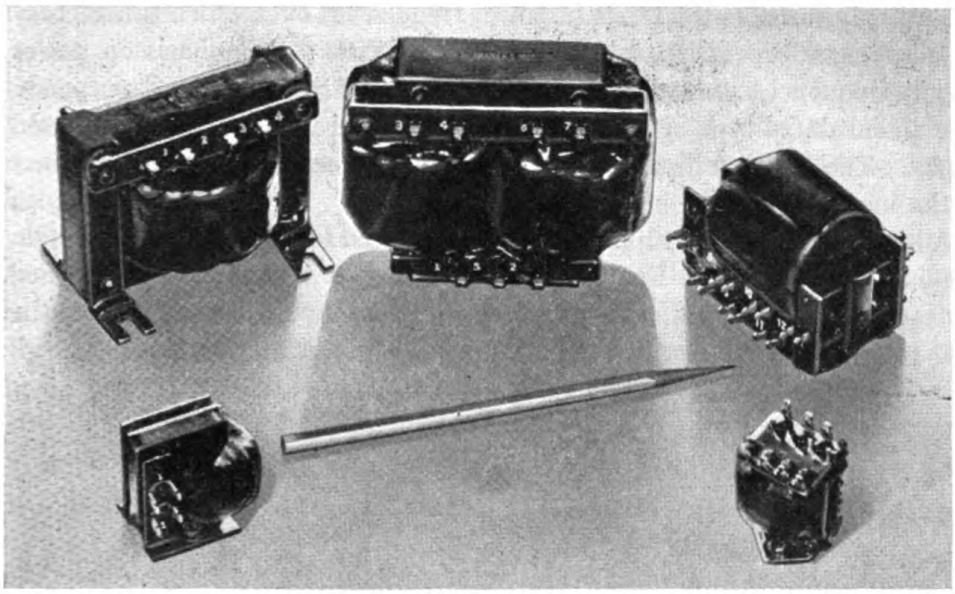

Fig. 75.—Flexseal treated open-core type power transformers as developed for airborne radar application.

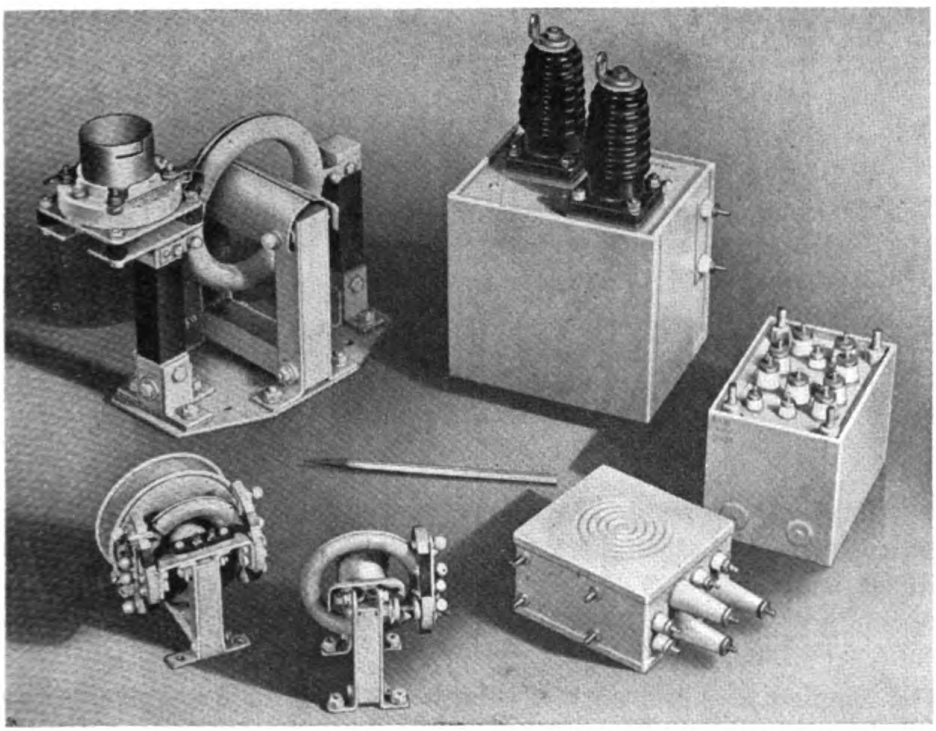

Fig. 76.—Power transformer designs for high voltage radar power supply application—Air-insulated and oil-filled types are included.

The use of air insulation in a high-voltage transformer results in a relatively low coupling coefficient between primary and secondary windings and

Digitized by Google
Original from UNIVERSITY OF MICHIGAN
Generated on 2019-09-22 07:35 GMT / http://hdl.handle.net/2027/mdp.39015077775156
Public Domain, Google-digitized / http://www.hathitrust.org/access_use#pd-google

accordingly restricts the range of power frequencies over which satisfactory regulation and operation can be expected. With the emphasis on power supply frequencies extending from 400 cps to 2400 cps for aircraft purposes, this air insulated type of structure was abandoned in favor of oil immersed types. The primary disadvantage of the oil immersed type of transformer is the increased weight of the unit.

A high-voltage power supply design as produced for airborne radar system application is shown in Fig. 77. In this example +4900 volts is supplied for cathode-ray tube indicator purposes and −1000 volts is available for the TR tube keep-alive circuit. This unit employs an air insulated type of

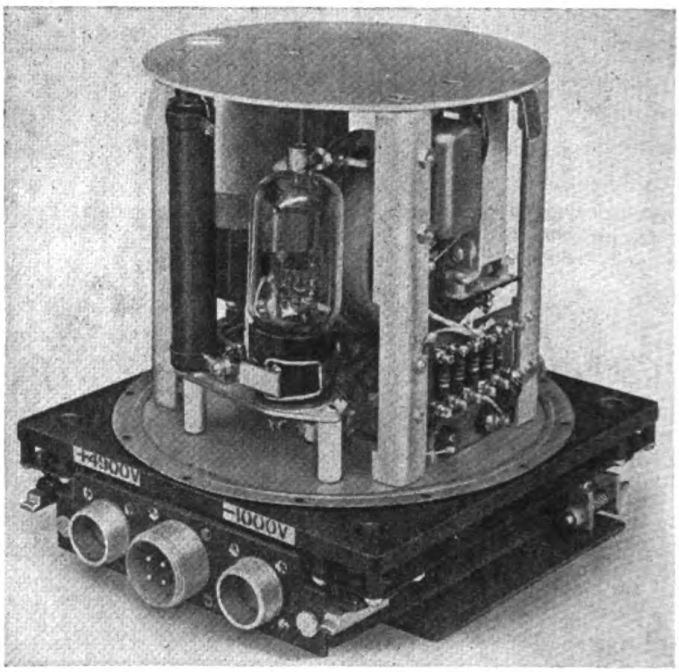

Fig. 77.—High-voltage power supply for airborne radar receiver application—pressurized type.

high-voltage transformer and by the use of a hermetically sealed enclosure operated at sea-level atmospheric pressure, satisfactory performance at high altitudes is realized.

Conclusion

The complete technical story of radar is of a magnitude comparable to a detailed report of the military campaigns of this past global war. During this period, the Bell Telephone Laboratories developed for manufacture more than 70 specialized radar systems for the Armed Services. It has been possible here only to review the major technical considerations which in-

Digitized by Google
Original from UNIVERSITY OF MICHIGAN
Generated on 2019-09-22 07:36 GMT / http://hdl.handle.net/2027/mdp.39015077775156
Public Domain, Google-digitized / http://www.hathitrust.org/access_use#pd-google

fluence design of a military radar receiver and to present a few radar circuit and equipment illustrations of the specialized technology that has resulted. It is a tribute to the ingenuity and industry of the workers in the radar field that this technology, developed under extremely accelerated and difficult conditions, will have a permanent value in future communication systems design.

The material used in this paper represents the concrete contributions of countless individual workers within and without the Bell Telephone Laboratories. The equipment products illustrated are the product of concentrated effort on the part of the staff of the Western Electric Company who produced these specialized and complex radar systems in quantities and within schedules necessary for the successful prosecution of the war. It is regrettable that it is an impossible task to assign individual credit for these specific military radar contributions.

Generated on 2019-09-22 07:36 GMT / http://hdl.handle.net/2027/mdp.39015077775156
Public Domain, Google-digitized / http://www.hathitrust.org/access_use#pd-google
Digitized by Google
Original from UNIVERSITY OF MICHIGAN

Reflex Oscillators

By J. R. PIERCE and W. G. SHEPHERD

SYMBOLS

A	A measure of frequency deviation (9.20).
B	Bandwidth (Appendix 10 only, (j-3)).
B	Susceptance
B_1	Reduced susceptance (9.7).
B_e	Electronic susceptance.
C	Capacitance
C	Heat capacity (k-1).
D	Reduced gap spacing (10.3).
E_0	Retarding field in drift space.
F	Drift effectiveness factor (5.4).
G	Conductance
G_1, G_2	Reduced conductances (9.6), (9.12).
G_B	Gap conductance of loaded resonator.
G_e	Electronic conductance.
G_L	Conductance at gap due to load.
G_R	Conductance at gap due to resonator loss.
H	Efficiency parameter (3.7).
H_m	Maximum value of H for a given resonator loss.
I	Radio-frequency current.
I_2	Current induced in circuit by convection current returning across gap.
I_0	D-C beam current.
K	Resonator loss parameter (3.9).
K	Radiation loss in watts/(degree Kelvin)^4 (k-2).
L	Inductance.
M	Characteristic admittance (a-8).
M_L	Characteristic admittance of line.
M_M	Short line admittance parameter (9.38).
N	Drift time in cycles.
N	Length of line in wavelengths (Section IX only).
N	Transformer voltage ratio.
P	Power.
Q	Equation (a-10).
Q_E	External Q (a-11).
Q_0	Unloaded Q (a-12).
R	Surface resistance (a-2).
S	Scaling factor (9.17).
T	Temperature.
V	Radio-frequency voltage.
V	Potential in drift space (Appendix VI only).
V_0	D-C beam voltage at gap.
V_R	The repeller is at a potential ($-V_R$) with respect to the cathode.
W	Work, energy (Appendix I).
W	Reduced radian frequency (10.5).
X	Bunching parameter (2.9).
Y	Admittance.
Y_C	Circuit admittance.
Y_e	Electronic admittance.
Y_L	Load admittance.
Y_R	Resonator admittance.
Z	Impedance.
Z_L	Load impedance.

Digitized by Google
Original from UNIVERSITY OF MICHIGAN
Generated on 2019-09-23 04:15 GMT / http://hdl.handle.net/2027/mdp.39015077775156
Public Domain, Google-digitized / http://www.hathitrust.org/access_use#pd-google

a Distance between grid wire centers.
d Separation between grid planes or tubes forming gap.
e Electronic charge (1.59×10^{-19} Coulombs).
f Frequency.
f Factor relating to effective grid voltage (b-37).
i Radio-frequency convection current.
i_2 Radio-frequency convection current returning across gap (c 4).
$(i_2)_f$ Fundamental component of i_2.
j $\sqrt{-1}$
k Boltzman's constant (1.37×10^{23} joules/degree K).
k Conduction loss watts/degree C (k-14).
l Length.
m Mutual inductance.
m Electronic mass (9.03 x 10^{-31} gram sevens).
n Repeller mode number. The number of cycles drift is $n + \frac{1}{4}$ for "optimum drift".
p Reduced power (9.5).
r Radius of grid wire, radius of tubes forming gap.
t Time, seconds.
u_0 D-C velocity of electrons.
v Total velocity (Appendix VIII only).
v Instantaneous gap voltage
w Real part of frequency (12.1).
x Coordinate along beam.
y A rectangular coordinate normal to x.
y Half-separation of planes forming symmetrical gap.
y_e Magnitude of small signal electronic admittance.
z A rectangular coordinate normal to x (Appendix II).
z A variable of integration (Appendix VI).
α Negative coefficient of the imaginary part of frequency (12.1).
β Modulation coefficient.
β_a Average value of modulation coefficient.
β_0 Modulation coefficient on axis.
β_r Modulation coefficient at radius r from axis.
β_s Root mean squared value of modulation coefficient.
β_y Modulation coefficient at distance y from axis.
γ $\gamma = \omega/u_0$.
ϵ Dielectric constant of space (8.85 x 10^{-14} farads/cm).
θ Drift angle in radians.
θ_g Gap transit angle in radians.
λ Wavelength in centimeters.
ϕ A phase angle.
Φ Reduced potential (g-13).
σ Voltage standing wave ratio.
τ Transit time.
τ Time constant of thermal tuner.
τ_H Cycling time on heating.
τ_C Cycling time on cooling.
ψ Magnetic flux linkage.
ω Radian frequency.

Generated on 2019-09-23 04:16 GMT / http://hdl.handle.net/2027/mdp.39015077775156
Public Domain, Google-digitized / http://www.hathitrust.org/access_use#pd-google
Digitized by Google
Original from UNIVERSITY OF MICHIGAN

THE reflex oscillator is a form of long-transit-time tube which has distinct advantages as a low power source at high frequencies. It may be light in weight, need have no magnetic focusing field, and can be made to operate at comparatively low voltages. A single closed resonator is used, so that tuning is very simple. Because the whole resonator is at the same dc voltage, high frequency by-pass difficulties are obviated.

The frequency of oscillation can be changed by several tens of megacycles by varying the repeller voltage ("electronic tuning"). This is very advantageous when the reflex oscillator is used as a beating oscillator. The electronic tuning can be used as a vernier frequency adjustment to the manual tuning adjustment or can be used to give an all-electrical automatic frequency-control. Electronic tuning also makes reflex oscillators serve well as frequency modulated sources in low power transmitters.

The single resonator tuning property makes it possible to construct oscillators whose mechanical tuning is wholly electronically controlled. Such control is achieved by making the mechanical motion which tunes the cavity subject to the thermal expansion of an element heated by electron bombardment.

The efficiency of the reflex oscillator is generally low. The wide use of the 707B, the 723A, the 726A and subsequent Western Electric tubes shows that this defect is outweighed by the advantages already mentioned.

Generated on 2019-09-23 04:17 GMT / http://hdl.handle.net/2027/mdp.39015077775156
Public Domain, Google-digitized / http://www.hathitrust.org/access_use#pd-google
Digitized by Google
Original from UNIVERSITY OF MICHIGAN

The first part of this paper attempts to give a broad exposition of the theory of the reflex oscillator. This theoretical material provides a background for understanding particular problems arising in reflex oscillator design and operation. The second part of the paper describes a number of typical tubes designed at the Bell Telephone Laboratories and endeavors to show the relation between theory and practice.

The theoretical work is presented first because reflex oscillators vary so widely in construction that theoretical results serve better than experimental results as a basis for generalization about their properties. While the reflex oscillator is simple in the sense that some sort of theory about it can be worked out, in practice there are many phenomena which are not included in such a theory. This leaves one in some doubt as to how well any simplified theory should apply. Multiple transits of electrons, different drift times for different electron paths and space charge in the repeller region are some factors not ordinarily taken into account which, nevertheless, can be quite important. There are other effects which are difficult to evaluate, such as distribution of current density in the beam, loss of electrons on grids or on the edges of apertures and dynamic focusing. If we could provide a theory including all such known effects, we would have a tremendous number of more or less adjustable constants, and it would not be hard to fit a large body of data to such a theory, correct or incorrect.

At present it appears that the theory of reflex oscillators is important in that it gives a semi-quantitative insight into the behavior of reflex oscillators and a guide to their design. The extent to which the present theory or an extended theory will fit actual data in all respects remains to be seen.

The writers thus regard the theory presented here as a guide in evaluating the capabilities of reflex oscillators, in designing such oscillators and in understanding the properties of such tubes as are described in the second part of this paper, rather than as an accurate quantitative tool. Therefore, the exposition consists of a description of the theory of the reflex oscillator and some simple calculations concerning it, with the more complicated mathematical work relegated to a series of chapters called appendices. It is hoped that this so organizes the mathematical work as to make it assimilable and useful, and at the same time enables the casual reader to obtain a clear idea of the scope of the theory.

I. Introduction

An idealized reflex oscillator is shown schematically in Fig. 1. It has, of course, a resonant circuit or "resonator."[1] This may consist of a pair of grids forming the "capacitance" of the circuit and a single turn toroidal

[1] For a discussion of resonators, see Appendix I. It is suggested that the reader consult this before continuing with the main work in order to obtain an understanding of the circuit philosophy used and a knowledge of the symbols employed.

Digitized by Google
Original from UNIVERSITY OF MICHIGAN
Generated on 2019-09-23 04:17 GMT / http://hdl.handle.net/2027/mdp.39015077775156
Public Domain, Google-digitized / http://www.hathitrust.org/access_use#pd-google

coil forming the "inductance" of the circuit. Such a resonator behaves just as do other resonant circuits. Power may be derived from it by means of a coupling loop linking the magnetic field of the single turn coil. An electron stream of uniform current density leaves the cathode and is shot across the "gap" between the two grids, traversing the radio-frequency field in this gap in a fraction of a cycle. In crossing the gap the electron stream is velocity modulated; that is, electrons crossing at different times gain

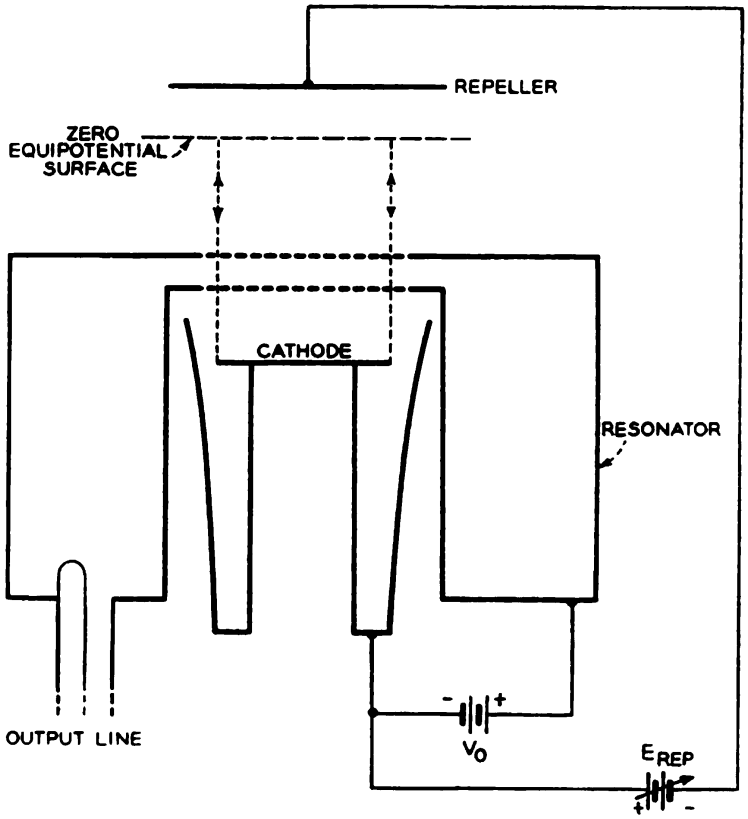

Fig. 1.—An idealized reflex oscillator with grids, shown in cross-section.

different amounts of kinetic energy from the radio-frequency voltage across the gap.[2] The velocity modulated electron stream is shot toward a negative repeller electrode which sends it back across the gap. In the "drift space" between the gap and the repeller the electron stream becomes "bunched" and the bunches of electrons passing through the radio frequency field in the gap on the return transit can give up power to the circuit if they are returned in the proper phase.

[2] The most energy any electron gains is βV electron volts, where V is the peak radio frequency voltage across the gap and β is the "modulation coefficient" or "gap factor", and is always less than unity. β depends on gap configuration and transit angle across the gap, and is discussed in Appendix II.

Digitized by Google
Original from UNIVERSITY OF MICHIGAN
Generated on 2019-09-23 04:18 GMT / http://hdl.handle.net/2027/mdp.39015077775156
Public Domain, Google-digitized / http://www.hathitrust.org/access_use#pd-google

The vital features of the reflex oscillator are the bunching which takes place in the velocity modulated electron stream in the retarding field between the gap and the repeller and the control of the returning phase of the bunches provided by the adjustment of the repeller voltage. The analogy of Fig. 2 explains the cause of the bunching. The retarding drift field may

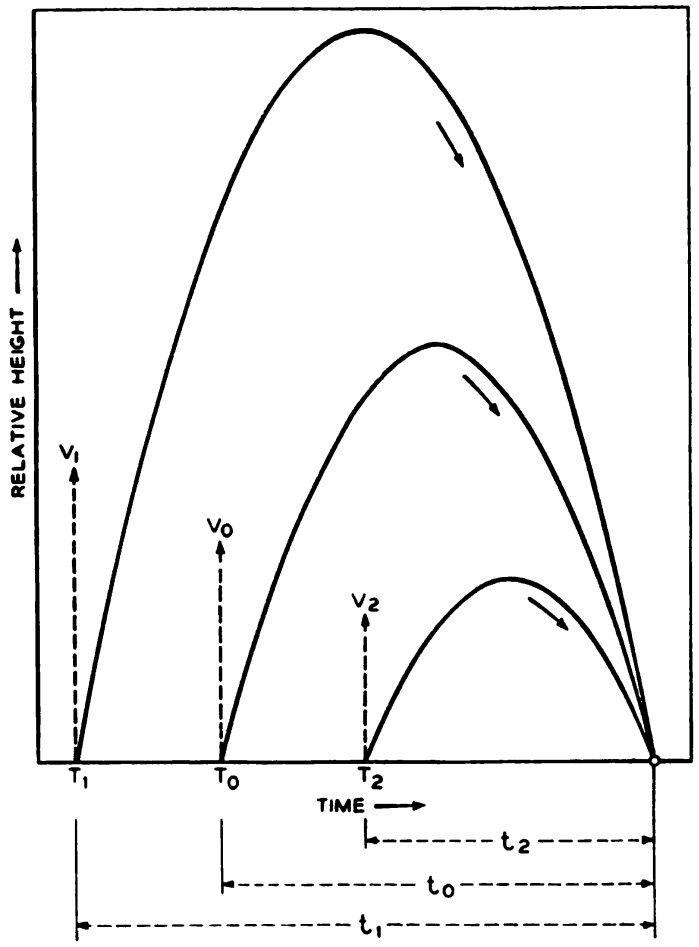

Fig. 2.—The motion of electrons in the repeller space of a reflex oscillator may be likened to that of balls thrown upward at different times. In this figure, height is plotted vs time. If a ball is thrown upward with a large velocity of V_1 at a time T_1, another with a smaller velocity at a later time T_0 and a third with a still smaller velocity at a still later time T_2 the three balls can be made to fall back to the initial level at the same time.

be likened to the gravitational field of the earth. The drift time is analogous to the time a ball thrown upwards takes to return. If the ball is thrown upward with some medium speed v_0, it will return in some time t_0. If it is thrown upward with a low speed v_1 smaller than v_0, the ball will return in some time t_1 smaller than t_0. If the ball is thrown up with a speed v_2 greater than v_0, it returns in some time t_2 greater than t_0. Now imagine three balls thrown upward in succession, evenly spaced but with large,

Digitized by Google
Original from UNIVERSITY OF MICHIGAN
Generated on 2019-09-23 04:18 GMT / http://hdl.handle.net/2027/mdp.39015077775156
Public Domain, Google-digitized / http://www.hathitrust.org/access_use#pd-google

medium, and small velocities, respectively.[8] As the ball first thrown up takes a longer time to return than the second, and the third takes a shorter time to return than the second, when the balls return the time intervals between arrivals will be less than between their departures. Thus time-position "bunching" occurs when the projection velocity with which a uniform stream of particles enters a retarding field is progressively decreased.

Figure 3 demonstrates such bunching as it actually takes place in the retarding field of a reflex oscillator. An electron crossing the gap at phase A

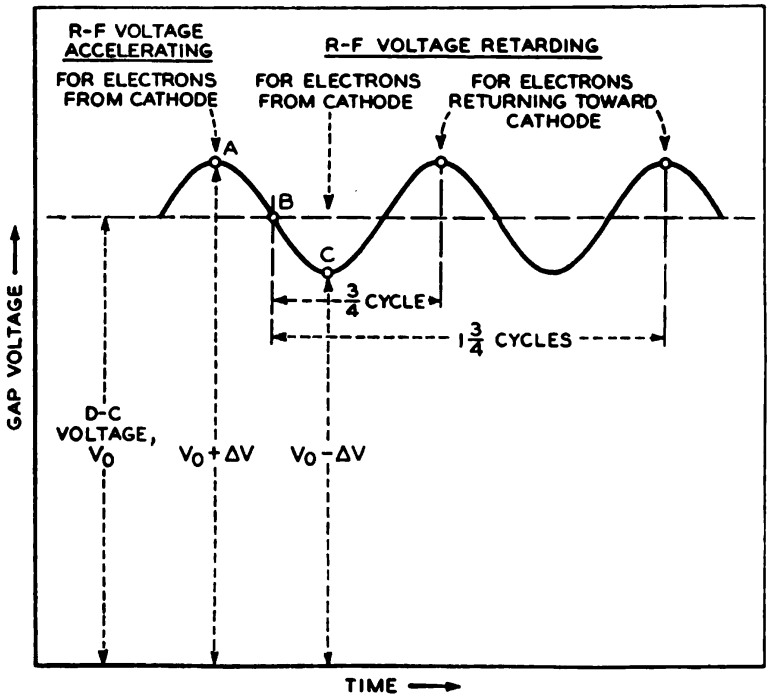

Fig. 3.—The drift time for transfer of energy from the bunched electron stream to the resonator can be deduced from a plot of gap voltage vs time.

is equivalent to the first ball since its velocity suffers a maximum increase, an electron crossing at phase B corresponds to the ball of velocity v_0 where for the electron V_0 corresponds to the d.c. injection velocity, and finally an electron crossing at phase C corresponds to the third ball since it has suffered a maximum decrease in its velocity. The electrons tend to bunch about the electron crossing at phase B. To a first order in this process no energy is taken from the cavity since as many electrons give up energy as absorb it.

The next step in the process is to bring back the grouped electrons in such a phase that they give the maximum energy to the r.f. field. Now, $\frac{3}{4}$ of a cycle after the gap voltage in a reflex oscillator such as that shown in Fig. 1 is changing most rapidly from accelerating to retarding for electrons

[8] The reader is not advised to try this experimentally unless he has juggling experience.

Digitized by Google
Original from UNIVERSITY OF MICHIGAN
Generated on 2019-09-23 04:19 GMT / http://hdl.handle.net/2027/mdp.39015077775156
Public Domain, Google-digitized / http://www.hathitrust.org/access_use#pd-google

going from the cathode, it has a maximum retarding value for electrons returning through the gap. This is true also for $1\frac{3}{4}$ cycles, $2\frac{3}{4}$ cycles, $n + \frac{3}{4}$ cycles. Hence as Fig. 3 shows if the time electrons spend in the drift space is $n + \frac{3}{4}$ cycles, the electron bunches will return at such time as to give up energy to the resonator most effectively.

II. Electronic Admittance—Simple Theory

In Appendix III an approximate calculation is made of the fundamental component of the current in the electron stream returning through the gap of a reflex oscillator when the current is caused by velocity modulation and drift action in a uniform retarding field. The restrictive assumptions are as follows:

(1) The radio-frequency voltage across the gap is a small fraction of the d-c accelerating voltage.

(2) Space charge is neglected. Amongst other things this assumes no interaction between incoming and outgoing streams and is probably the most serious departure from the actual state of affairs.

(3) Variations of modulation coefficient for various electron paths are neglected.

(4) All sidewise deflections are neglected.

(5) Thermal velocities are neglected.

(6) The electron flow is treated as a uniform distribution of charge.

(7) Only two gap transits are allowed.

An expression for the current induced in the circuit (β times the electron convection current) is

$$i = 2I_0\beta J_1\left(\frac{\beta V\theta}{2V_0}\right)e^{j(\omega t-\theta)}. \tag{2.1}$$

Here the current is taken as positive if the beam in its second transit across the gap absorbs energy from the resonator. The voltage across the gap at the time the stream returns referred to the same phase reference as the current is $v = Ve^{-j(\omega t-\pi/2)}$. Hence the admittance appearing in shunt with the gaps will be

$$Y_e = \frac{2I_0\beta}{V}J_1\left(\frac{\beta V\theta}{2V_0}\right)e^{j((\pi/2)-\theta)}. \tag{2.2}$$

For small values of V approaching zero this becomes

$$Y_{ee} = \frac{I_0\beta^2\theta}{2V_0}e^{j((\pi/2)-\theta)} = y_e e^{j((\pi/2)-\theta)} \tag{2.3}$$

$$y_e = \frac{I_0\beta^2\theta}{2V_0}. \tag{2.4}$$

Digitized by Google
Original from UNIVERSITY OF MICHIGAN
Generated on 2019-09-23 04:19 GMT / http://hdl.handle.net/2027/mdp.39015077775156
Public Domain, Google-digitized / http://www.hathitrust.org/access_use#pd-google

Here we define Y_{ss} as the small signal value of the admittance, and y_s as the magnitude of this quantity. If we plot the function Y_{ss} in a complex admittance plane it takes the form of a geometric spiral as shown in Fig. 4.

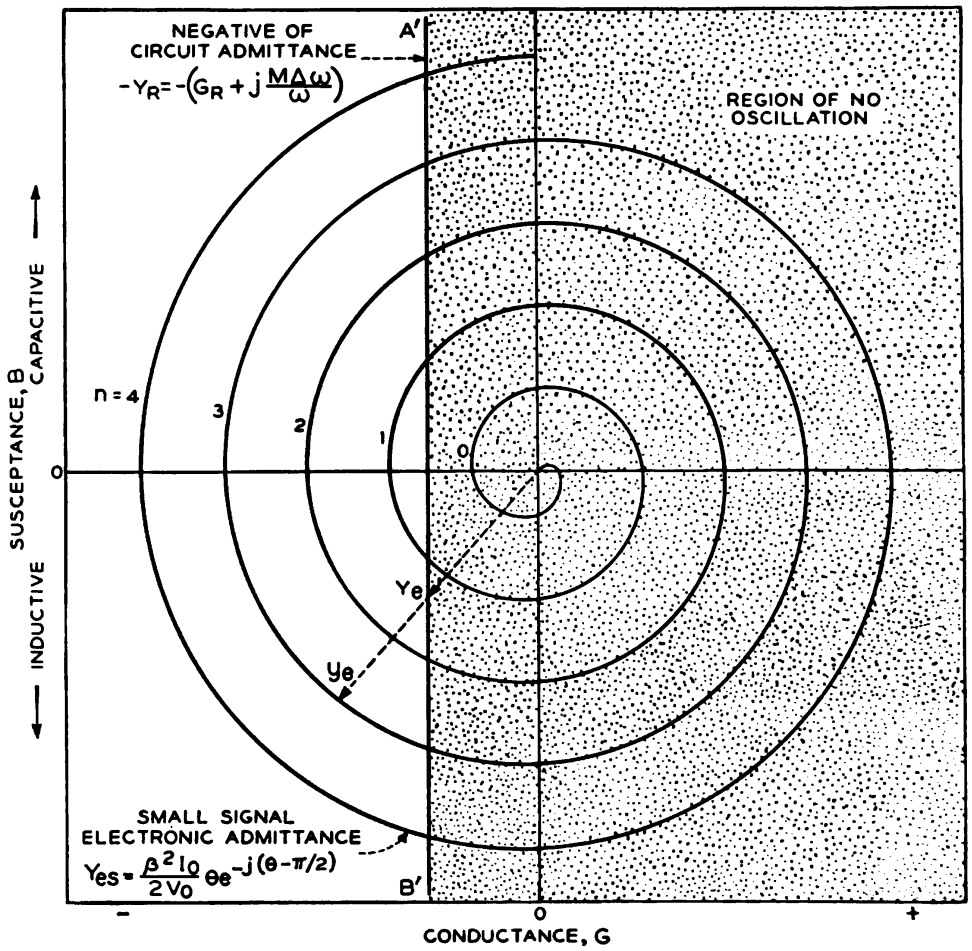

Fig. 4.—The negative of the circuit admittance (the heavy vertical line) and the small signal electronic admittance (the spiral) are shown in a plot of susceptance vs conductance. Each position along the circuit admittance line corresponds to a certain frequency. Each position along the spiral corresponds to a certain drift angle.

Such a presentation is very helpful in acquiring a qualitative understanding of the operation of a reflex oscillator.

In Appendix I it is shown that the admittance of the resonant circuit in the neighborhood of resonance is very nearly

$$Y_R = G_R + j2M\Delta\omega/\omega \tag{2.5}$$

where G_R is a constant. The negative of such an admittance has been plotted in Fig. 4 as the vertical line $A'B'$. Vertical position on this line is

Digitized by Google
Original from UNIVERSITY OF MICHIGAN
Generated on 2019-09-23 04:20 GMT / http://hdl.handle.net/2027/mdp.39015077775156
Public Domain, Google-digitized / http://www.hathitrust.org/access_use#pd-google

proportional to the frequency at which the resonator is driven. The condition for stable oscillation is

$$Y_R + Y_e = 0. \tag{2.6}$$

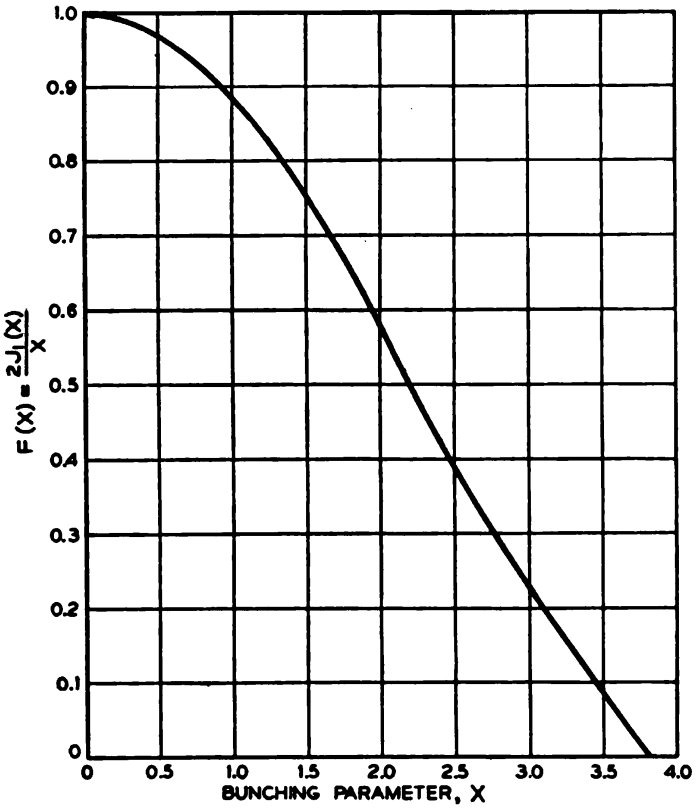

Fig. 5.—Relative amplitude of electronic admittance vs the bunching parameter X The bunching parameter increases linearly with radio frequency gap voltage so that this curve shows the reduction in magnitude of electronic admittance with increasing voltage.

We may rewrite (2.2) for any given value of θ as

$$Y_e = y_e F(V) e^{j((\pi/2)-\theta)} \tag{2.7}$$

where

$$F(V) = \frac{2J_1 \dfrac{(\beta V\theta)}{(2V_0)}}{\dfrac{\beta V\theta}{2V_0}} = \frac{2J_1(X)}{X}. \tag{2.8}$$

The quantity

$$X = \frac{\beta V\theta}{2V_0} \tag{2.9}$$

is called the bunching parameter. A plot of the function $F(V)$ vs X is shown in Fig. 5. For any given value of θ and for fixed operating conditions

Digitized by Google
Original from UNIVERSITY OF MICHIGAN
Generated on 2019-09-23 04:20 GMT / http://hdl.handle.net/2027/mdp.39015077775156
Public Domain, Google-digitized / http://www.hathitrust.org/access_use#pd-google

it is a function of V only and its action is clearly to reduce the small signal value of the admittance until condition (2.6) is satisfied. It will be observed that this function affects the magnitude only and not the phase of the admittance.

Thus, as indicated in Fig. 4, when oscillation starts the admittance is given by the radius vector of magnitude y_s, terminating on the spiral, and as the oscillation builds up this vector shrinks until in accordance with (12.6) it terminates on the circuit-admittance line $A'B'$, which is the locus of vectors $(-Y_E)$. The electronic admittance vector may be rotated by a change in the repeller voltage which changes the value of θ. This changes the vertical intercept on line $A'B'$, and since the imaginary component of the circuit admittance, that is the height along $A'B'$, is proportional to frequency, this means that the frequency of oscillation changes. It is this property which is known as electronic tuning.

Oscillation will cease when the admittance vector has rotated to an angle such that it terminates on the intersection of the spiral and the circuit-admittance line $A'B'$. It will be observed that the greater is the number of cycles of drift the greater is the electronic tuning to extinction. While it is not as apparent from this diagram, it is also true that the greater the number of cycles of drift the greater the electronic tuning to intermediate power points. Vertical lines farther to the left correspond to heavier loads, and from this it is apparent that the electronic tuning to extinction decreases with the loading. By sufficient loading it is possible to prevent some repeller modes (i.e. oscillations of some n values) from occurring. Since losses in the resonant cavity of the oscillator represent some loading, some modes of low n value will not occur even in the absence of external loading.

III. Power Production for Drift Angle of $(n + \frac{3}{4})$ Cycles

Now, from equation (2.2) it may be seen that Y_s will be real and negative for $\theta = \theta_n = (n + \frac{3}{4})2\pi$. Because θ also appears in the argument of the Bessel function this value of θ is not exactly the value to make the real component of Y_s a maximum. However, for the reasonably large values of n encountered in practical oscillators this is a justifiable approximation. Suppose, then, we consider the case of $n + \frac{3}{4}$ cycles drift, calling this an optimum drift time. Using the value of n as a parameter we plot the magnitude of the radio-frequency electron current in the electron stream returning across the gap given by equation (2.1) as a function of the radio-frequency voltage across the gap. This variation is shown in Fig. 6. As might be expected, the greater the number of cycles the electrons drift in the drift space, the lower is the radio-frequency gap voltage required to produce a given amount of bunching and hence a given radio frequency electron current. It may be seen from Fig. 6 that as the radio-frequency gap voltage

Digitized by Google
Original from UNIVERSITY OF MICHIGAN
Generated on 2019-09-23 04:20 GMT / http://hdl.handle.net/2027/mdp.39015077775156
Public Domain, Google-digitized / http://www.hathitrust.org/access_use#pd-google

is increased, the radio-frequency electron current gradually increases until a maximum value is reached, representing as complete bunching as is possible, after which the current decreases with increasing gap voltage. The maximum value of the current is approximately the same for various drift times, but occurs at smaller gap voltages for longer drift times.

The radio-frequency power produced is the voltage times the current. As the given maximum current occurs at higher voltages for shorter drift

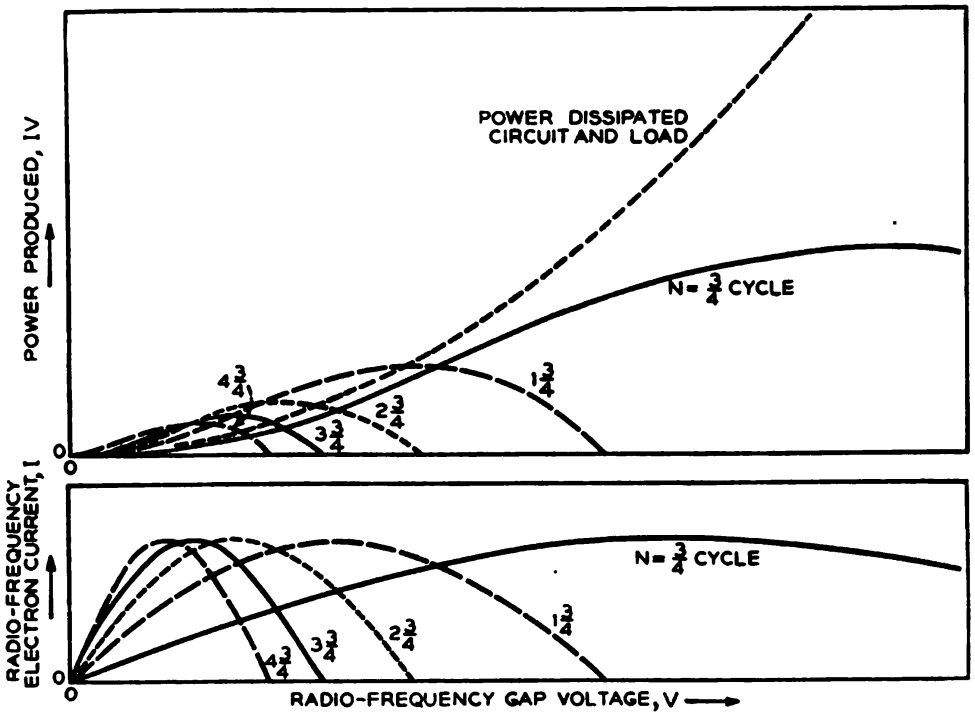

Fig. 6.—Radio frequency electron convection current I and the radio frequency power given up by the electron stream can be plotted vs the radio frequency gap voltage V for various drift times measured in cycles. Maximum current occurs at higher voltage for shorter drift times. For a given number of cycles drift, maximum power occurs at a higher gap voltage than that for maximum current. If the power produced for a given drift time is higher at low voltages than the power dissipated in the circuit and load (dashed curve), the tube will oscillate and the amplitude will adjust itself to the point at which the power dissipation and the power production curves cross.

times, the maximum power produced will be greater for shorter drift times. This is clearly brought out in the plots of power vs. voltage shown in Fig. 6.

The power dissipated in the circuits and load will vary as the square of the radio-frequency voltage. Part of this power will go into the load coupled with the circuit and part into unavoidable circuit losses. A typical curve of power into the circuit and load vs. radio-frequency voltage is shown in Fig. 6. Steady oscillation will take place at the voltage for which the power production curve crosses the power dissipation curve. For instance, in Fig. 6 the power dissipation curve crosses the power production curve for

Digitized by Google
Original from UNIVERSITY OF MICHIGAN
Generated on 2019-09-23 04:20 GMT / http://hdl.handle.net/2027/mdp.39015077775156
Public Domain, Google-digitized / http://www.hathitrust.org/access_use#pd-google

$1\frac{3}{4}$ cycles drift at the maximum or hump of the curve. This means that the circuit impedance for the dissipation curve shown is such as to result in maximum production of power for $1\frac{3}{4}$ cycles drift. For $2\frac{3}{4}$ cycles drift and for longer drifts, the power dissipation curve crosses the power production curves to the right of the maximum and hence the particular circuit loading shown does not result in maximum power production for these longer drift times. This is an example of operation with lighter than optimum load. The power dissipation curve might cross the power production curve to the left of the maximum, representing a condition of too heavy loading for production of maximum power output. The power dissipation curve in Fig. 6 lies always above the power production curve for a drift of $\frac{3}{4}$ cycles. This means that the oscillator for which the curves are drawn, if loaded to give the power dissipation curve shown, would not oscillate with the short drift time of $\frac{3}{4}$ cycles, corresponding to a very negative repeller voltage.

In general, the conclusions reached by examining Fig. 6 are borne out in practice. The longer the drift time, that is, the less negative the repeller, the lower is the power output. For very negative repeller voltages, however, corresponding to very short drift times, the power either falls off. which means that most of the available power is dissipated in circuit losses, or the oscillator fails to operate at all because, for all gap voltages, the power dissipated in circuit losses is greater than the power produced by the electron stream.

Having examined the situation qualitatively, we want to make a somewhat more quantitative investigation, and to take some account of circuit losses. In the course of this we will find two parameters are very important. One is the parameter X previously defined by equation (2.9), which expresses the amount of bunching the beam has undergone. In considering a given tube with a given drift time, the important thing to remember about X is that it is proportional to the *r-f* gap voltage V. For $\theta = \theta_n$ expression (2.2) is a pure conductance and we can express the power produced by the electron stream as one half the square of the peak *r-f* voltage times the circuit conductance which for stable oscillation is equal to the negative of the electronic conductance given by (2.2). This may be written with the aid of (2.9) as

$$P = 2(I_0V_0/\theta_n)XJ_1(X). \tag{3.1}$$

Suppose we take into account the resonator losses but not the power lost in the output circuit, which in a well designed oscillator should be small. If the resonator has a shunt resonant conductance (including electronic loading) of G_R, the power dissipated in the resonator is

$$P_R = V^2G_R/2, \tag{3.2}$$

Digitized by Google
Original from UNIVERSITY OF MICHIGAN
Generated on 2019-09-23 04:23 GMT / http://hdl.handle.net/2027/mdp.39015077775156
Public Domain, Google-digitized / http://www.hathitrust.org/access_use#pd-google

Then the power output for θ_n is

$$P = 2(I_0V_0/\theta_n)XJ_1(X) - V^2G_R/2. \tag{3.3}$$

The efficiency, η, is given by

$$\eta = \frac{P}{P_{DC}} = \frac{2}{\theta}\left[XJ_1(X) - \frac{G_R\theta_n V^2}{4I_0V_0}\right]. \tag{3.4}$$

From (2.4) and (2.9)

$$\frac{\theta_n V^2}{2I_0V_0} = \frac{1}{y_e}X^2. \tag{3.5}$$

Hence we may write

$$\eta = \frac{1}{(n + 3/4)}\frac{1}{\pi}\left[XJ_1(X) - \frac{G_R}{y_e}\frac{X^2}{2}\right]. \tag{3.6}$$

Let us write $\eta = \frac{H}{N}$ where $N = (n + \frac{3}{4})$. We may now make a generalized examination of the effect of losses on the efficiency by examining the function

$$H = (1/\pi)[XJ_1(X) - (G_R/y_e)X^2/2]. \tag{3.7}$$

Thus, the efficiency for $\theta = \theta_n$ is inversely proportional to the number of cycles drift and is propotional to a factor H which is a function of X and of the ratio G_R/y_e, that is, the ratio of resonator loss conductance to small signal electronic conductance.[4] For $n + \frac{3}{4}$ cycles drift, the small signal electronic conductance is equal to the small signal electronic admittance.

For a given value of G_R/y_e there is an optimum value of X for which H has a maximum H_m. We can obtain this by differentiating (3.7) with respect to X and setting the derivative equal to zero, giving

$$\begin{aligned} XJ_0(X) - (G_R/y_e)X &= 0 \\ J_0(X) &= (G_R/y_e). \end{aligned} \tag{3.8}$$

If we put values from this into (3.7) we can obtain H_m as a function of G_R/y_e. This is plotted in Fig. 7. The considerable loss of efficiency for values of G_R/y_e as low as .1 or .2 is noteworthy. It is also interesting to note that for G_R/y_e equal to $\frac{1}{3}$, the fractional change in power is equal to the fractional change in resonator resistance, and for G_R/y_e greater than $\frac{1}{3}$, the fractional power change is greater than the fractional change in resonator resistance. This helps to explain the fall in power after turn-on in some tubes, for an increase in temperature can increase resonator resistance considerably.

[4] An electronic damping term discussed in Appendix VIII should be included in resonator losses. The electrical loss in grids is discussed briefly in Appendix IX.

Digitized by Google
Original from UNIVERSITY OF MICHIGAN
Generated on 2019-09-23 04:23 GMT / http://hdl.handle.net/2027/mdp.39015077775156
Public Domain, Google-digitized / http://www.hathitrust.org/access_use#pd-google

In the expression for the admittance, the drift angle, θ, appears as a factor. This factor plays a double role in that it determines the phase of the admittance but also in a completely independent manner it determines, in part, the magnitude of the admittance. θ as it has appeared in the foregoing analysis, which was developed on the basis of a linear retarding field, is the actual drift angle in radians. As will be shown in a later section, certain special repeller fields may give effective drift action for a given angle greater than the same angle in a linear field. Such values of effective drift angle may have fractional optimum values although the phase must still be such as to give within the approximations we have been using a pure conductance at optimum. In order to generalize the following work we will speak of an effective drift time in cycles, $N_E = FN$, where N is the actual drift time in cycles, $n + \frac{3}{4}$, and F is the number of times this drift is more effective than the drift in a linear field.

Suppose we have a tube of given β^2, I_0, V_0 and resonator loss G_E and wish to find the optimum effective drift time, FN, and determine the effect on the efficiency of varying FN. It will be recalled that for very low losses we may expect more power output the fewer the number of cycles drift. However the resonator losses may cut heavily into the generated power, for short drift angles. With short drift angles the optimum load conductance becomes small compared to the loss conductance so that although the generated power is high only a small fraction goes to the useful load. There is, therefore, an optimum value which can be obtained using the data of Fig. 7. We define a parameter

$$K = \frac{2V_0}{\beta^2 I_0} G_E \tag{3.9}$$

which compares the resonator loss conductance with the small signal electronic admittance per radian of drift angle. Then in terms of K, $\frac{G_E}{y_e} = \frac{K}{\theta}$. Hence, for a fixed value of K, various values of $\theta = 2\pi FN$ define values of $\frac{G_E}{y_e}$. When one uses these values in connection with Fig. 7 he determines the corresponding values of H_m and hence the efficiency, $\eta = \frac{H_m}{FN}$. These values of η are plotted against FN as in Fig. 8 with values of K as a parameter. In this plot K is a measure of the lossiness of the tube. The optimum drift angle for any degree of lossiness is evident as the maximum of one of these curves.

The maximum power outputs in various repeller modes, $n = 0, 1$ etc. and the repeller voltages for these various power outputs correspond to discrete values of n and FN lying along a curve for a particular value of K.

Digitized by Google
Original from UNIVERSITY OF MICHIGAN
Generated on 2019-09-23 04:23 GMT / http://hdl.handle.net/2027/mdp.39015077775156
Public Domain, Google-digitized / http://www.hathitrust.org/access_use#pd-google

Thus, the curves illustrate the variation of power from mode to mode as the repeller voltage is changed over a wide range.

Changes in resonator loss or differences in loss between individual tubes of the same type correspond to passing from a curve for one value of K to a curve for another value of K.

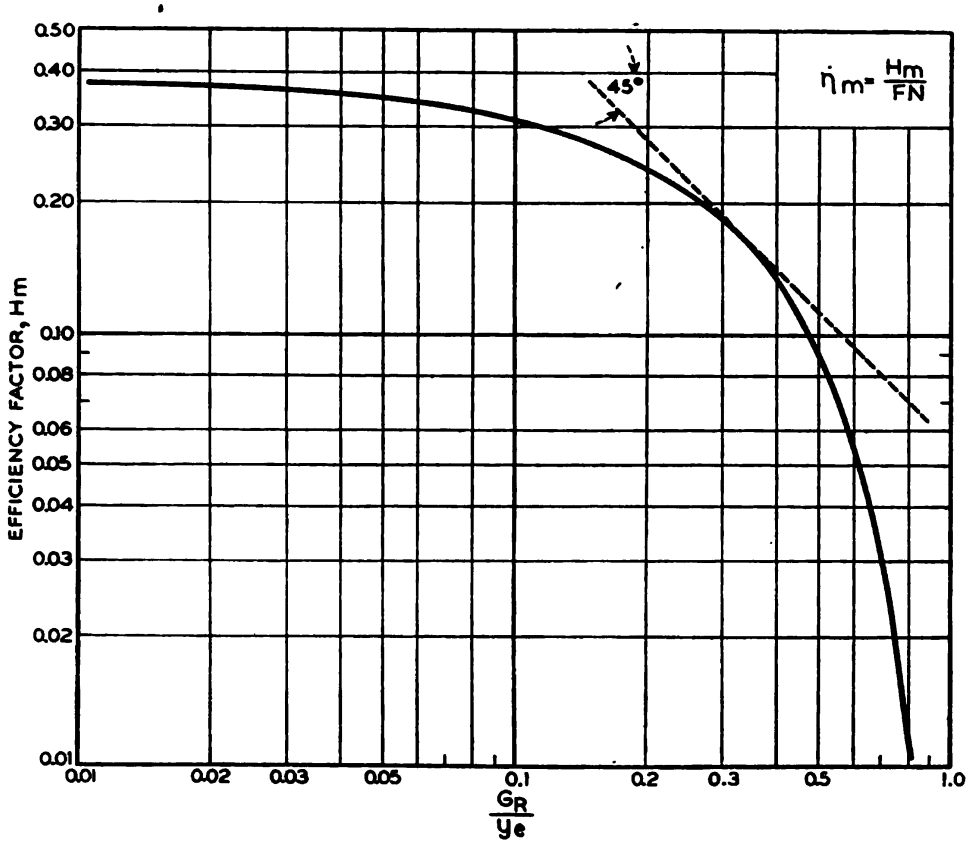

Fig. 7.—Efficiency factor H_m vs the ratio of resonator loss conductance to the small signal electronic admittance. Efficiency changes rapidly with load as the loss conductance approaches in magnitude the small signal electronic admittance. The efficiency is inversely proportional to the number of cycles drift.

It will be observed from this that although, from an efficiency standpoint, it is desirable to work at low values of drift time such low drift times lead to an output strongly sensitive to changes in resonator losses.

Perhaps the most important question which the user of the oscillator may ask with regard to power production for optimum drift is; what effect does the external load have upon the performance? If we couple lightly to the oscillator the *r-f* voltage generated will be high but the power will not be extracted. If we couple too heavily the voltage will be low, the beam will not be efficiently modulated and the power output will be low. There is

Digitized by Google
Original from UNIVERSITY OF MICHIGAN
Generated on 2019-09-23 04:23 GMT / http://hdl.handle.net/2027/mdp.39015077775156
Public Domain, Google-digitized / http://www.hathitrust.org/access_use#pd-google

apparently an optimum loading. Best output is not obtained when the external load matches the generator impedance as in the case of an amplifier.

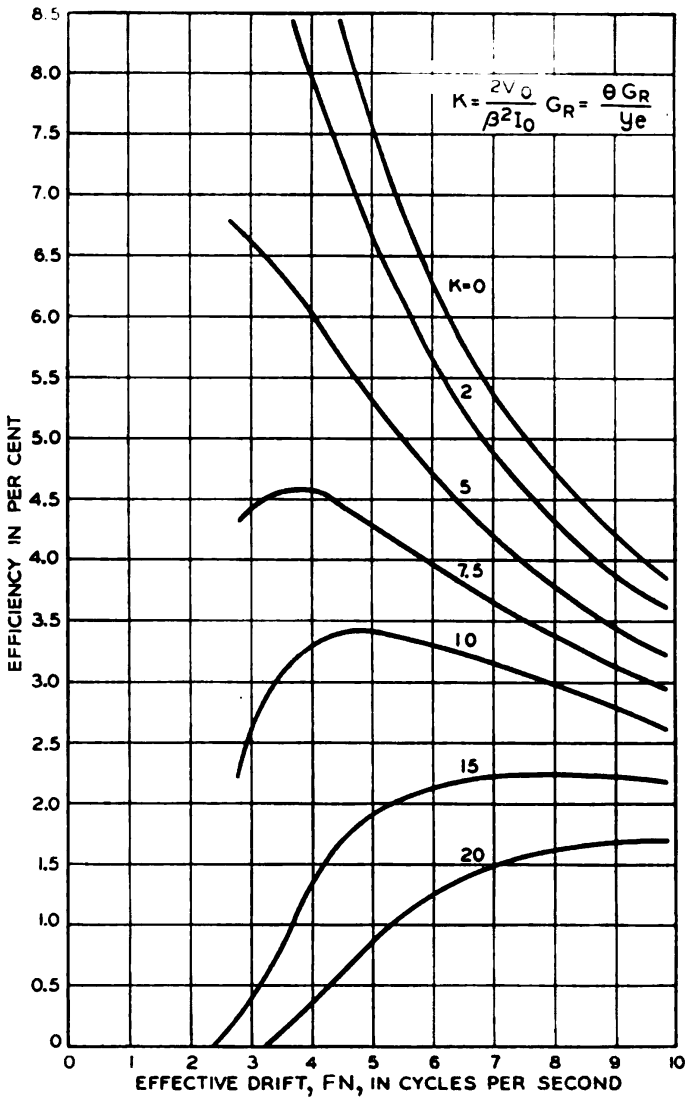

Fig. 8.—Efficiency in per cent vs the effective cycles drift for various values of a parameter K which is proportional to resonator loss. These curves indicate how the power output differs for various repeller modes for a given loss. Optimum power operating points will be represented by points along one of these curves. For a very low loss resonator, the power is highest for short drift times and decreases rapidly for higher repeller modes. Where there is more loss, the power varies less rapidly from mode to mode.

We return to equation (3.7) for H and assume that we are given various values of $\frac{G_R}{y_e}$. With these values as parameters we ask what variation in efficiency may be expected as we vary the ratio of the load conductance, G_L, to the small signal admittance, y_e. When $\frac{G_L}{y_e} + \frac{G_R}{y_e} = 1$ oscillation

Digitized by Google
Original from UNIVERSITY OF MICHIGAN
Generated on 2019-09-23 04:23 GMT / http://hdl.handle.net/2027/mdp.39015077775156
Public Domain, Google-digitized / http://www.hathitrust.org/access_use#pd-google

will just start and no power output will be obtained. We can state the general condition for stable operation as $Y_e + Y_C = 0$, where Y_C is the vector sum of the load and circuit admittances. For the optimum drift time this becomes

$$\frac{G_C}{y_e} = \frac{2J_1(X)}{X} \tag{3.10}$$

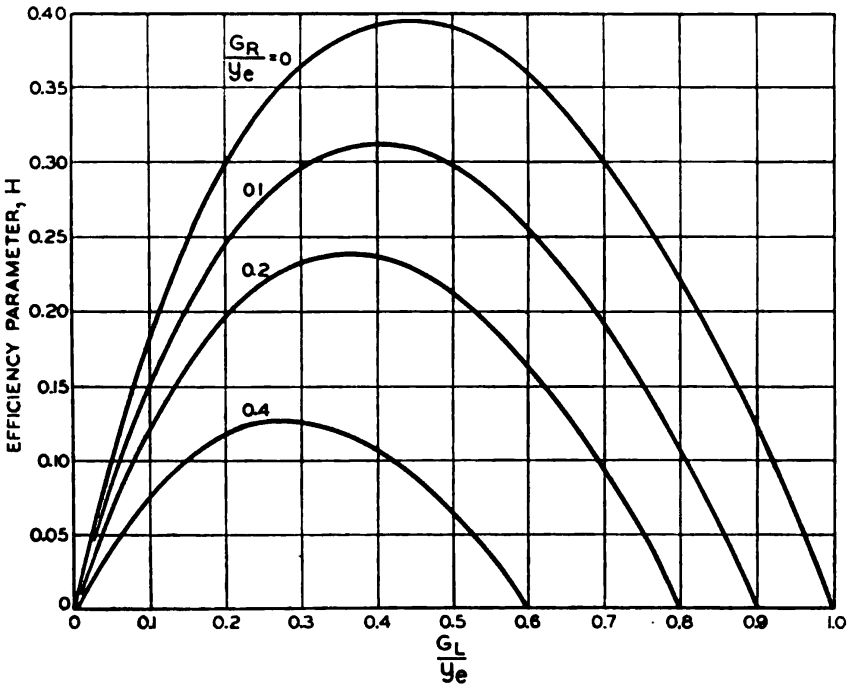

Fig. 9.—Efficiency parameter H vs the ratio of load conductance to the magnitude of the small signal electronic admittance. Curves are for various ratios of resonator loss conductance to small signal electronic admittance. The curves are of similar shapes and indicate that the tube will cease oscillating ($H = 0$) when loaded by a conductance about twice as large as that for optimum power.

where

$$\frac{G_C}{y_e} = \frac{G_L + G_R}{y_e}. \tag{3.11}$$

Hence for a given value of $\frac{G_R}{y_e}$ we may assume values for $\frac{G_L}{y_e}$ between zero and $1 - \frac{G_R}{y_e}$ and these in (3.11) will define values of X. These values of X substituted in (3.7) will define values of H which we then plot against the assumed values for $\frac{G_L}{y_e}$, as in Fig. 9. Thus we have the desired function of the variation of efficiency factor against load.

Digitized by Google
Original from UNIVERSITY OF MICHIGAN
Generated on 2019-09-23 04:24 GMT / http://hdl.handle.net/2027/mdp.39015077775156
Public Domain, Google-digitized / http://www.hathitrust.org/access_use#pd-google

From the curves of Fig. 9 it can be seen that the maximum efficiency is obtained when the external conductance is made equal to approximately half the available small signal conductance; i.e. $\frac{1}{2}(y_e - G_R)$. This can be seen more clearly in the plot of Fig. 10. Equation (3.8) gives the condition for maximum efficiency as

$$\frac{G_R}{y_e} = J_0(X).$$

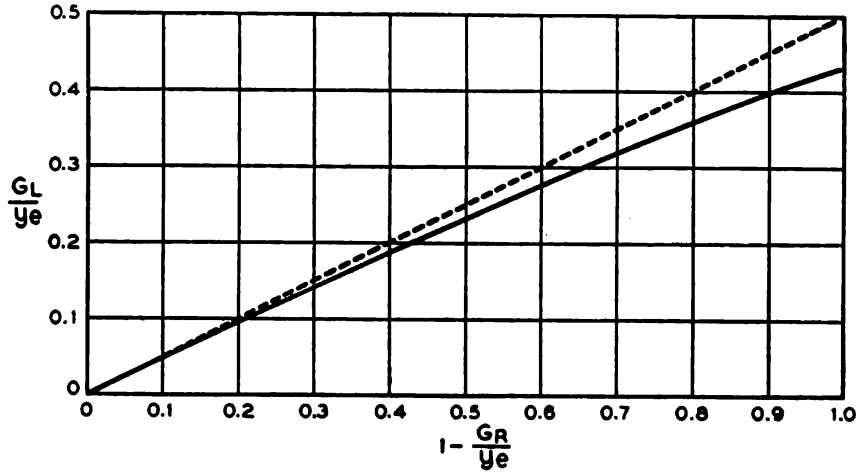

Fig. 10.—The abscissa measures the fractional excess of electronic negative conductance over resonator loss conductance. The ordinate is the load conductance as a fraction of electronic negative conductance. The tube will go out of oscillation for a load conductance such that the ordinate is equal to the abscissa. The load conductance for optimum power output is given by the solid line. The dashed line represents a load conductance half as great as that required to stop oscillation.

If we assume various values for $\frac{G_R}{y_e}$ these define values of X_0 which when substituted in

$$\frac{G_L}{y_e} = \frac{G_C}{y_e} - \frac{G_R}{y_e} = \frac{2J_1(X_0)}{X_0} - J_0(X_0) \tag{3.12}$$

give the value of the external load for optimum power. We plot these data against the available conductance

$$\left(1 - \frac{G_R}{y_e}\right) = 1 - J_0(X) \tag{3.13}$$

as shown in Fig. 10.

In Fig. 10 there is also shown a line through the origin of slope 1/2. It can thus be seen that the optimum load conductance is slightly less than half the available small signal or starting conductance. This relation is independent of the repeller mode, i.e. of the value FN. This does not mean

Digitized by Google
Original from UNIVERSITY OF MICHIGAN
Generated on 2019-09-23 04:24 GMT / http://hdl.handle.net/2027/mdp.39015077775156
Public Domain, Google-digitized / http://www.hathitrust.org/access_use#pd-google

that the load conductance is independent of the mode, since we have expressed all our conductances in terms of y_e, the small signal conductance, and this of course depends on the mode. What it does say is that, regardless of the mode, if the generator is coupled to the load conductance for maximum output, then, if that conductance is slightly more than doubled oscillation will stop. It is this fact which should be borne in mind by the circuit designer. If greater margin of safety against "pull out" is desired it can be obtained only at the sacrifice of efficiency.

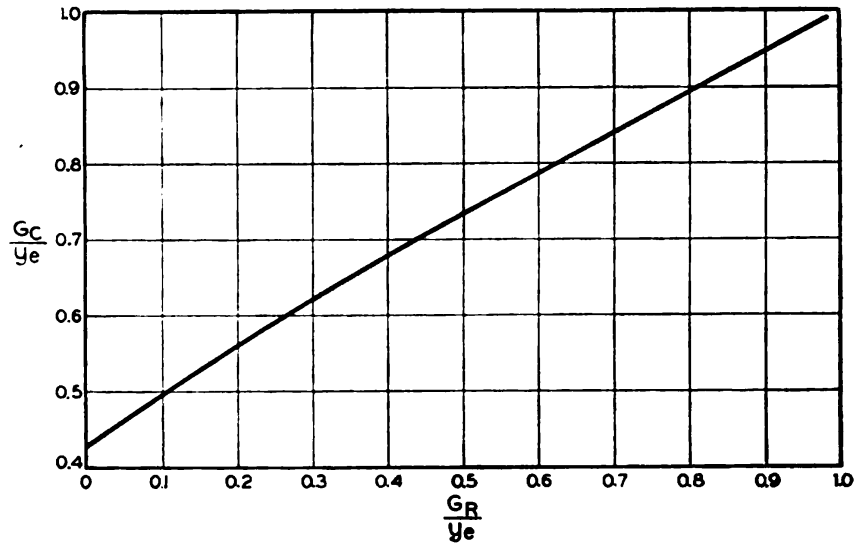

Fig. 11.—The ratio of total circuit conductance for optimum power to small signal electronic admittance, vs the ratio of resonator loss conductance to small signal electronic admittance.

An equivalent plot for the data of Fig. 10, which will be of later use, is shown in Fig. 11. This gives the value of $\frac{G_c}{y_e}$ for best output for various values of $\frac{G_R}{y_e}$.

IV. Effect of Approximations

The analysis presented in Section II is misleading in some respects. For instance, for a lossless resonator and $N = \frac{3}{4}$ cycles, the predicted efficiency is 53%. However, our simple theory tells us that to get this efficiency, the radio-frequency gap voltage V multiplied by the modulation coefficient β (that is, the energy change an electron suffers in passing the gap) is $1.018V_0$. This means that (a) some electrons would be stopped and would not pass the gap (b) many other electrons would not be able to pass the gap against a retarding field after returning from drift region (c) some electrons would

Digitized by Google
Original from UNIVERSITY OF MICHIGAN
Generated on 2019-09-23 04:24 GMT / http://hdl.handle.net/2027/mdp.39015077775156
Public Domain, Google-digitized / http://www.hathitrust.org/access_use#pd-google

cross the gap so slowly that for them β would be very small and their effect on the circuit would also be small (d) there might be considerable loading of the resonator due to transit time effects in the gap. Of course, it is not justifiable to apply the small signal theory in any event, since it was derived on the assumption that βV is small compared with V_0.

In Appendix IV there is presented a treatment by R. M. Ryder of these Laboratories in which it is not assumed that $\beta V \ll V_0$. This work does not, however, take into account variation of β with electron speed or the possibility of electrons being turned back at the gap.

For drift angles of $1\frac{3}{4}$ cycles and greater, the results of Ryder's analysis are almost indistinguishable from those given by the simple theory, as may be seen by examining Figs. 128–135 of the Appendix. His curves approach the curves given by the simple theory for large values of n.

For small values of n, and particularly for $\frac{3}{4}$ cycles drift, Ryder's work shows that optimum power is obtained with a drift angle somewhat different from $n + \frac{3}{4}$ cycles. Also, Fig. 131 shows that the phase of the electronic admittance actually varies somewhat with amplitude, and Fig. 130 shows that its magnitude does not actually pass through zero as the amplitude is increased.

The reader is also referred to a paper by A. E. Harrison.[5]

The reader may feel at this point somewhat uneasy about application of the theory to practice. In most practical reflex oscillators, however, the value of n is 2 or greater, so that the theory should apply fairly well. There are, however, so many accidental variables in practical tubes that it is well to reiterate that the theory serves primarily as a guide, and one should not expect quantitative agreement between experiment and theory. This will be apparent in later sections, where in a few instances the writers have made quantitative calculations.

V. Special Drift Fields

In the foregoing sections a theory for a reflex oscillator has been developed on the assumption that the repeller field is a uniform retarding electrostatic field. Such a situation rarely occurs in practice, partly because of the difficulty of achieving such a field and partly because such a field may not return the electron stream in the manner desired. In an effort to get some information concerning actual drift fields, we may extend the simple theory already presented to include such fields by redefining X as

$$X = \beta V F \theta / 2V_0. \tag{5.1}$$

Here the factor F is included. As defined in Section *III* this is the factor which relates the effectiveness of a given drift field in bunching a velocity

[5] A. E. Harrison, "Graphical Methods for Analysis of Velocity Modulation Bunching," *Proc. I.R.E.*, 33.1, pp. 20–32, June 1945.

Digitized by Google
Original from UNIVERSITY OF MICHIGAN
Generated on 2019-09-23 04:24 GMT / http://hdl.handle.net/2027/mdp.39015077775156
Public Domain, Google-digitized / http://www.hathitrust.org/access_use#pd-google

modulated electron stream with the bunching effectiveness of a field with the same drift angle θ but with a linear variation of potential with distance. Suppose, for instance, that the variation of transit time, τ, with energy gained in crossing the gap V is for a given field

$$\partial\tau/\partial V \tag{5.2}$$

and for a linear potential variation and the same drift angle

$$(\partial\tau/\partial V)_1. \tag{5.3}$$

Then the factor F is defined as

$$F = (\partial\tau/\partial V)/(\partial\tau/\partial V)_1. \tag{5.4}$$

In appendix V, F is evaluated in terms of the variation of potential with distance.

The efficiency is dependent on the effectiveness of the drift action rather than on the total number of cycles drift except of course for the phase requirements. Thus, for a nonlinear potential variation in the drift space we should have instead of (3.7)

$$\eta = H/FN. \tag{5.5}$$

In the investigation of drift action, one procedure is to assume a given drift field and try to evaluate the drift action. Another is to try to find a field which will produce some desirable kind of drift action. As a matter of fact, it is easy to find the best possible drift field (from the point of view of efficiency) under certain assumptions.

The derivation of the optimum drift field, which is given in appendix VII, hinges on the fact that the time an electron takes to return depends only on the speed with which it is injected into the drift field. Further, the variation in modulation coefficient for electrons returning with different speeds is neglected. With these provisos, the optimum drift field is found to be one in which electrons passing the gap when the gap voltage is decelerating take π radians to return, and electrons which pass the gap when the voltage is accelerating take 2π radians to return, as illustrated graphically in Fig. 136, Appendix VII. A graph of potential vs. distance from gap to achieve such an ideal drift action is shown in Fig. 137 and the general appearance of electrodes which would achieve such a potential distribution approximately is shown in Fig. 138.

With such an ideal drift field, the efficiency of an oscillator with a lossless resonator is

$$\eta_i = (2/\pi)(\beta V/V_0). \tag{5.6}$$

Digitized by Google
Original from UNIVERSITY OF MICHIGAN
Generated on 2019-09-23 04:24 GMT / http://hdl.handle.net/2027/mdp.39015077775156
Public Domain, Google-digitized / http://www.hathitrust.org/access_use#pd-google

For a linear potential variation in the drift space, at the optimum *r-f* gap voltage, according to the approximate theory presented in Section III the efficiency for a lossless resonator is

$$\eta = (.520)(\beta V/V_0). \tag{5.7}$$

Comparing, we find an improvement in efficiency for the ideal drift field in the ratio

$$\eta_i/\eta = 1.23, \tag{5.8}$$

or only about 20%. Thus, the linear drift field is quite effective. The ideal drift field does have one advantage; the bunching is optimum for all gap voltages or, for a given gap voltage, for all modulation coefficients since ideally an infinitesimal *a-c* voltage will change the transit time from π to 2π and completely bunch the beam. This should tend to make the efficiency high despite variations in β over various parts of the electron flow. The limitation imposed by the fact that electrons cannot return across the gap against a high voltage if they have been slowed up in their first transit across the gap remains.

This last mentioned limitation is subject to amelioration. In one type of reflex oscillator which has been brought to our attention the electrons cross the gap the first time in a region in which the modulation coefficient is small. If the gap has mesh grids, a hole may be punched in the grids and a beam of smaller diameter than the hole focussed through it. Then the beam may be allowed to expand and recross a narrow portion of the gap, where the modulation coefficient is large. Thus, in the first crossing no electrons lose much energy (because β is small) and in the second crossing all can cross the gap where βV is large and hence can give up a large portion of their energy.

VI. Electronic Gap Loading

So far, attention has been concentrated largely on electronic phenomena in the drift or repeller region. To the long transit time across the gap there has been ascribed merely a reduction in the effect of the voltage on the electron stream by the modulation coefficient β. Actually, the long transit across the gap can give rise to other effects.

One of the most obvious of these other effects is the production of an electronic conductance across the gap. If it is positive, such a conductance acts just as does the resonator loss conductance in reducing the power output. Petrie, Strachey and Wallis of Standard Telephones and Cables have treated this matter in an interesting and rather general way. Their work, in a slightly modified form, appears in Appendix VIII, to which the reader is referred for details.

Digitized by Google
Original from UNIVERSITY OF MICHIGAN
Generated on 2019-09-23 04:25 GMT / http://hdl.handle.net/2027/mdp.39015077775156
Public Domain, Google-digitized / http://www.hathitrust.org/access_use#pd-google

The work tells us that, considering longitudinal fields only, the electron flow produces a small signal conductance component across the gap

$$G_{eL} = \frac{I_0}{4V_0}\frac{\partial\beta^2}{\partial\gamma} \tag{6.1}$$

$$\gamma = \frac{\omega}{u_0}. \tag{6.2}$$

Here β is the modulation coefficient and u_0 is the electron speed. I_0 and V_0 are beam current and beam voltage. If the gap has a length d, the transit angle across it is $\theta_g = \gamma d$ and (6.1) may be rewritten

$$G_{eL} = -\frac{I_0\theta_g}{4V_0}\frac{\partial\beta^2}{\partial\theta_g}. \tag{6.3}$$

It is interesting to compare this conductance with the magnitude of the small-signal electronic admittance, y_e. In doing so, we should note that the current crosses the gap twice, and on each crossing produces an electronic conductance. Thus, the appropriate comparison between loss conductance and electronic admittance is $2G_{eL}/y_e$. Using (6.3) we obtain

$$2G_{eL}/y_e = -\frac{\theta_g}{\theta}\frac{1}{\beta^2}\frac{\partial\beta^2}{\partial\theta_g}. \tag{6.4}$$

Usually, the drift angle θ is much larger than the gap transit angle θ_g. Further, if we examine the curves for modulation coefficient β which are given in Appendix II, we find that $(\partial\beta^2/\partial\theta_g)/\beta^2$ will not be very large. Thus, we conclude that in general the total loss conductance for longitudinal fields will be small compared with the electronic admittance. An example in Appendix VIII gives $(2G_{eL}/y_e)$ as about 1/10. It seems that this effect will probably be less important than various errors in the theory of the reflex oscillator.

Even though this electronic gap loading is not very large, it may be interesting to consider it further. We note, for instance, that the conductance G_{eL} is positive when β^2 decreases as gap transit angle increases. For parallel fine grids this is so from $\theta_g = 0$ to $\theta_g = 2\pi$ (see Fig. 119 of Appendix II). At $\theta_g = 2\pi$, where $\beta = 0$, $\partial\beta^2/\partial\theta_g = 0$, and the gap loading is zero. In a region beyond $\theta_g = 2\pi$, $\partial\beta^2/\partial\theta_g$ becomes positive and the gap conductance is negative. Thus, for some transit angles a single gap can act to produce oscillations. For still larger values of θ_g, G_{eL} alternates between positive and negative. Gap transit angles of greater than 2π are of course of little interest in connection with reflex oscillators, as for such transit angles β is very small.

For narrow gaps with large apertures rather than fine grids, $\partial\beta^2/\partial\theta_g$

Digitized by Google
Original from UNIVERSITY OF MICHIGAN
Generated on 2019-09-23 04:25 GMT / http://hdl.handle.net/2027/mdp.39015077775156
Public Domain, Google-digitized / http://www.hathitrust.org/access_use#pd-google

never becomes very negative and may remain positive and the gap loading conductance due to longitudinal fields be always positive. In such gaps, however, transverse fields can have important effects, and (6.3) no longer gives the total gap conductance. Transverse fields act to throw electrons approaching the gap outward or inward, into stronger or weaker longitudinal fields, and in this manner the transverse fields can either cause the electrons to give up part of their forward velocity, transferring energy to the resonator, or to pick up forward velocity, taking energy from the resonator. An analysis of the effect of transverse fields is given in Appendix VIII, and this is applied in calculating the total conductance, due both to longitudinal and to transverse fields, of a short gap between cylinders with a uniform current density over the aperture. It is found that the transverse fields contribute a minor part of the total conductance, and that this contribution may be either positive or negative, but that the total gap conductance is always positive (see Appendix VIII, Fig. 140).

The electron flow across the gap produces a susceptive component of admittance. This susceptive component is in general more difficult to calculate than the conductive component. It is not very important; it serves to affect the frequency of oscillation slightly but not nearly so much as a small change in repeller voltage.

Besides such direct gap loading, the velocity modulation and drift action within a gap of fine grids actually produce a small bunching of the electron stream. In other words, the electron stream leaving such a gap is not only velocity modulated but it has a small density modulation as well. This convection current will persist (if space-charge debunching is not serious) and, as the electrons return across the gap, it will constitute a source of electronic admittance. We find however, that in typical cases (see Appendix VIII, (h59)–(h63)), this effect is small, and it is almost entirely absent in gaps with coarse grids or large apertures.

Secondary electrons produced when beam electrons strike grid wires and grid frames or gap edges constitute another source of gap loading. It has been alleged that if the frames supporting the grids or the tubes forming a gap have opposed parallel surfaces of width comparable to or larger than the gap spacing, large electron currents can be produced through secondary emission, the *r-f* field driving electrons back and forth between the opposed surfaces. It would seem that this phenomenon could take place only at quite high *r-f* levels, for an electron would probably require of the order of 100 volts energy to produce more than one secondary in striking materials of which gaps are usually constructed.

VII. Electronic Tuning—Arbitrary Drift Angle

So far, the "on tune" oscillation of reflex oscillators has been considered except for a brief discussion in Section II, and we have had to deal only with

Digitized by Google
Original from UNIVERSITY OF MICHIGAN
Generated on 2019-09-23 04:25 GMT / http://hdl.handle.net/2027/mdp.39015077775156
Public Domain, Google-digitized / http://www.hathitrust.org/access_use#pd-google

real admittances (conductances). In this section the steady state operation in the case of complex circuit and electronic admittances will be discussed. The general condition for oscillation states that, breaking the circuit at any point the sum of the admittances looking in the two directions is zero. Particularly, the electronic admittance Y_e looking from the circuit to the electron stream, must be minus the circuit admittance Y_C, looking from the electron stream to the circuit. Here electronic admittance is used in the sense of an admittance averaged over a cycle of oscillation and fulfilling the above condition.

It is particularly useful to consider the junction of the electron stream and the circuit because the electronic admittance Y_e and the circuit admittance Y_C have very different properties, and if conditions are considered elsewhere these properties are somewhat mixed and full advantage cannot be taken of their difference.

The average electronic admittance with which we are concerned is a function chiefly of the amplitude of oscillation. Usually its magnitude decreases with increasing amplitude of oscillation, and its phase may vary as well, although this is a large signal effect not shown by the simple theory. In reflex oscillators the phase may be controlled by changing the repeller voltage. The phase and magnitude of the electronic admittance also vary with frequency. Usually, however, the rate of change with frequency is slow compared with that of the circuit admittance in the vicinity of any one resonant mode. By neglecting this change of electronic admittance with frequency in the following work, and concentrating our attention on the variation with amplitude and repeller voltage, we will emphasize the important aspects without serious error. However, the variation of electronic admittance with frequency should be kept in mind in considering behavior over frequency ranges of several per cent.[6]

The circuit admittance is, of course, independent of amplitude and is a rapidly varying function of frequency. It is partly dependent on what is commonly thought of as the resonator or resonant circuit of the oscillator, but is also profoundly affected by the load, which of course forms a part of the circuit seen from the electron stream. The behavior of the oscillator is determined, then, by the electronic admittance, the resonant circuit and the load. The behavior due to circuit and load effects applies generally to all oscillators, and the simplicity of behavior of the electronic admittance is such that similarities of behavior are far more striking than differences.

We have seen from Appendix I that at a frequency $\Delta\omega$ away from the resonant frequency ω_0 where $\Delta\omega \ll \omega_0$, the admittance at the gap may be expressed as:

$$Y_C = G_C + j2M\Delta\omega/\omega_0. \tag{7.1}$$

[6] Appendix IV discusses the variation of phase with frequency and repeller voltage. The variation of phase of electronic admittance with frequency is included in Section IX A.

Digitized by Google
Original from UNIVERSITY OF MICHIGAN
Generated on 2019-09-23 04:25 GMT / http://hdl.handle.net/2027/mdp.39015077775156
Public Domain, Google-digitized / http://www.hathitrust.org/access_use#pd-google

Here the quantity M is the characteristic admittance of the resonator, which depends on resonator shape and is unaffected by scaling from one frequency to another. G_c is the shunt conductance due to circuit and to load. Y_c as given by (7.1) represents to the degree of approximation required the admittance of any resonant circuit and load with only one resonance near the frequency of oscillation.

It is profitable to consider again in more detail a complex admittance plot similar to Fig. 4. In Fig. 12 the straight vertical line is a plot of (7.1).

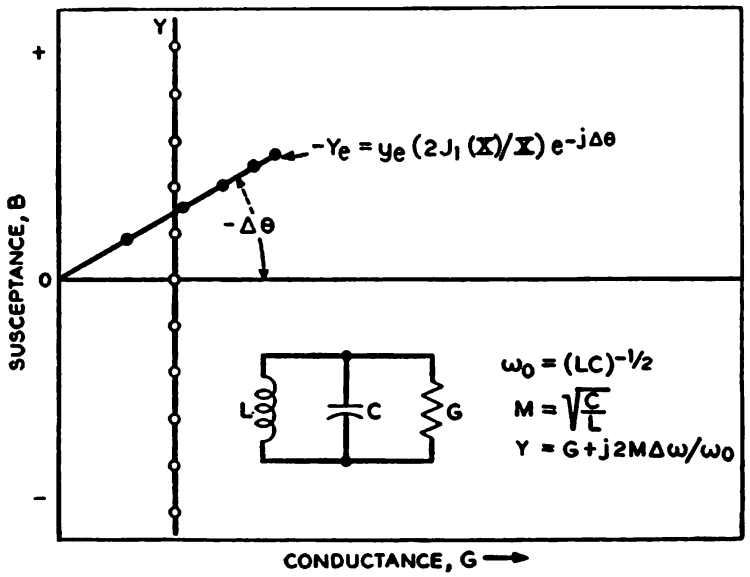

Fig. 12.—The resonator and its load can be represented as a shunt resonant circuit with a shunt conductance G. For frequencies near resonance, the conductance is nearly constant and the susceptance B is proportional to frequency, so that when susceptance is plotted vs conductance, the admittance Y is a vertical straight line. The circles mark off equal increments of frequency. The electronic admittance is little affected by frequency but much affected by amplitude. Tne negative of an electronic admittance Y_e having a constant phase angle $-\Delta\theta$ is shown in the figure. The dots mark off equal amplitude steps. Oscillation will occur at a frequency and amplitude specified by the intersection of the curves Y and $-Y_e$.

The circles mark equal frequency increments. Now if we neglect the variation of the electronic admittance with phase, then the negative of the small signal electronic admittance on this same plot will be a vector, the locus of whose termination will be a circle. The vector is shown in Fig. 12. The dots mark off admittance values corresponding to equal amplitude increments as determined by the data of Fig. 5.

Steady oscillation will take place at the frequency and amplitude represented by the intersection of the two curves. If the phase angle $\Delta\theta$ of the $-Y_e$ curve is varied by varying the repeller voltage, the point of intersection will shift on both the Y_c curve and the $-Y_e$ curve. The shift along the

Digitized by Google
Original from UNIVERSITY OF MICHIGAN
Generated on 2019-09-23 04:25 GMT / http://hdl.handle.net/2027/mdp.39015077775156
Public Domain, Google-digitized / http://www.hathitrust.org/access_use#pd-google

Y_c curve represents a change in frequency of oscillation; the shift along the $-Y_e$ curve represents a change in the amplitude of oscillation. If we know the variation of amplitude with position along the $-Y_e$ curve, and the variation of frequency with position along the Y_c curve, we can obtain both the amplitude and frequency of oscillation as a function of the phase of $-Y_e$, which is in turn a function of repeller voltage.

From (2.3) and (2.7) we can write $-Y_e$ in terms of the deviation of drift angle $\Delta\theta$ from $n + \frac{3}{4}$ cycles.

$$-Y_e = y_e(2J_1(X)/X)e^{j\Delta\theta}. \tag{7.2}$$

The equation relating frequency and $\Delta\theta$ can be written immediately from inspection of Fig. 12.

$$\begin{aligned} 2M\Delta\omega/\omega_0 &= -G_c \tan\Delta\theta \\ \Delta\omega/\omega_0 &= -(G_c/2M)\tan\Delta\theta \\ \Delta\omega/\omega_0 &= -(1/2Q)\tan\Delta\theta. \end{aligned} \tag{7.3}$$

Here Q is the loaded Q of the circuit.

The maximum value of $\Delta\theta$ for which oscillation can occur (at zero amplitude) is an important quantity. From Fig. 12 this value, called $\Delta\theta_0$, is obviously given by

$$\begin{aligned} \cos\Delta\theta_0 &= G_c/y_e = (G_c/M)(M/y_e) \\ &= (M/y_e)/Q. \end{aligned} \tag{7.4}$$

From this we obtain

$$\tan\Delta\theta_0 = \pm\,(Q^2(y_e/M)^2 - 1)^{\frac{1}{2}}. \tag{7.5}$$

By using (7.3) we obtain

$$(\Delta\omega/\omega_0)_0 = \pm\,(\tfrac{1}{2})\,(y_e/M)\,(1 - (M/y_eQ)^2)^{\frac{1}{2}} \tag{7.6}$$

or

$$(\Delta\omega/\omega_0)_0 = \pm(\tfrac{1}{2})\,(y_e/M)\,(1 - (G_c/y_e)^2)^{\frac{1}{2}}. \tag{7.7}$$

These equations give the electronic tuning from maximum amplitude of oscillation to zero amplitude of oscillation (extinction).

The equation relating amplitudes may be as easily derived from Fig. 12.

$$G_c^2 + (2M\Delta\omega/\omega)^2 = y_e^2\,(2J_1(X)/X)^2 \tag{7.8}$$

a'

$\Delta\omega = 0$ let $X = X_0$. Then

$$\Delta\omega/\omega_0 = (y_e/2M)\,((2J_1(X)/X)^2 - (2J_1(X_0)/X_0)^2)^{\frac{1}{2}}. \tag{7.9}$$

Digitized by Google
Original from UNIVERSITY OF MICHIGAN
Generated on 2019-09-23 04:26 GMT / http://hdl.handle.net/2027/mdp.39015077775156
Public Domain, Google-digitized / http://www.hathitrust.org/access_use#pd-google

It is of interest to have the value of $\Delta\omega/\omega_0$ at half the power for $\Delta\omega = 0$ At half power, $X = X_0/\sqrt{2}$, so

$$(\Delta\omega/\omega_0)_{\frac{1}{2}} = (y_e/2M)((2J_1(X_0/\sqrt{2})/(X_0/\sqrt{2}))^2 - (2J_1(X_0)/X_0)^2)^{\frac{1}{2}}. \quad (7.10)$$

For given values of modulation coefficient and V_0, X is a function of th *r-f* gap voltage V and also of drift angle and hence of $\Delta\theta$, or repeller voltage (see Appendix IV). For the fairly large values of θ typical of most reflex oscillators, we can neglect the change in X due directly to changes in $\Delta\theta$, and consider X as a direct measure of the *r-f* gap voltage V. Likewise y_e is a function of drift time whose variation with $\Delta\theta$ can and will be disregarded. Hence from (7.9) we can plot $(X/X_0)^2$ vs. $\Delta\omega/\omega_0$ and regard this as a representation of normalized power vs. frequency.

Let us consider now what (7.3) and (7.9) mean in connection with a given reflex oscillator. Suppose we change the load. This will change Q in (7.3) and X_0 in (7.9). From the relationship previously obtained for the condition for maximum power output, $G_R/y_e = J_0(X_0)$, we can find the value of X_0 that is, X at $\Delta\omega = 0$, for various ratios of G_R/y_e. For $G_R = 0$ (zero resonator loss) the optimum power value of X_0 is 2.4. When there is some resonator loss, the optimum total conductance for best power output is greater and hence the optimum value of X_0 is lower.

In Fig. 13 use is made of (7.3). $\Delta\omega/\omega_0$ is plotted vs. $\Delta\theta$ (which decreases as the repeller is made more negative) for several values of Q, and in Fig. 14, (7.9) is used to plot $(X/X_0)^2$ vs. $(2M/y_e)\Delta\omega/\omega_0$, which is a generalized electronic tuning variable, for several values of X_0. These curves illustrate typical behavior of frequency vs. drift angle or repeller voltage and power vs. frequency for a given reflex oscillator for various loads. In practice, the S shape of the frequency vs. repeller voltage curves for light loads (high Q) is particularly noticeable. The sharpening of the amplitude vs. frequency curves for light loads is also noticeable, though of course the cusp-like appearance for zero load and resonator loss cannot be reproduced experimentally. It is important to notice that while the plot of output vs. frequency for zero load is sharp topped, the plot of output vs. repeller voltage for zero load is not.

Having considered the general shape of frequency vs. repeller voltage curves and power vs. frequency curves, it is interesting to consider curves of electronic tuning to extinction $((\Delta\omega/\omega_0)_0)$ and electronic tuning to half power $((\Delta\omega/\omega_0)_{\frac{1}{2}})$ vs. the loading parameter, $(M/y_eQ) = G_C/y_e$. Such curves are shown in Fig. 15. These curves can be obtained using (7.7) and (7.10). In using (7.10) X can be related to G_C/y_e by the relation previously derived from $2J_1(X)/X = G_C/y_e$ and given in Fig. 5 as a function of X. It is to be noted that the tuning to the half power point, $(\Delta\omega/\omega_0)_{\frac{1}{2}}$, and the tuning to the extinction point, $(\Delta\omega/\omega_0)_0$, vary quite differently with loading.

Generated on 2019-09-23 04:26 GMT / http://hdl.handle.net/2027/mdp.39015077775156
Public Domain, Google-digitized / http://www.hathitrust.org/access_use#pd-google
Digitized by Google
Original from UNIVERSITY OF MICHIGAN

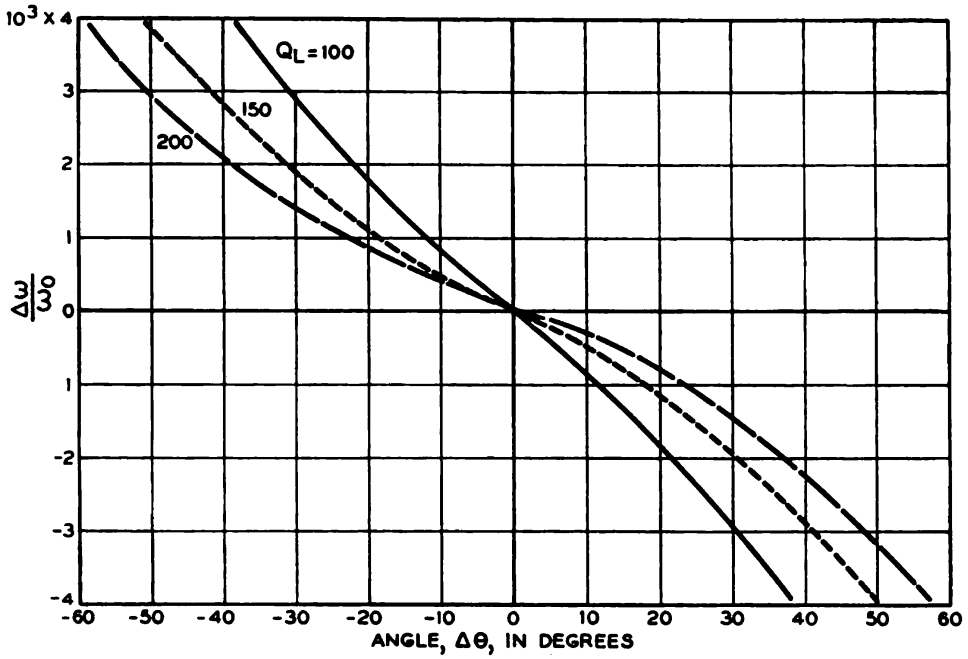

Fig. 13.—A parameter proportional to electronic tuning plotted vs deviation from optimum drift angle $\Delta\theta$ for various values of loaded Q. For lower values of Q, the frequency varies rapidly and almost linearly with $\Delta\theta$. For high values of Q, the frequency curve is S shaped and frequency varies slowly with $\Delta\theta$ for small values of $\Delta\theta$.

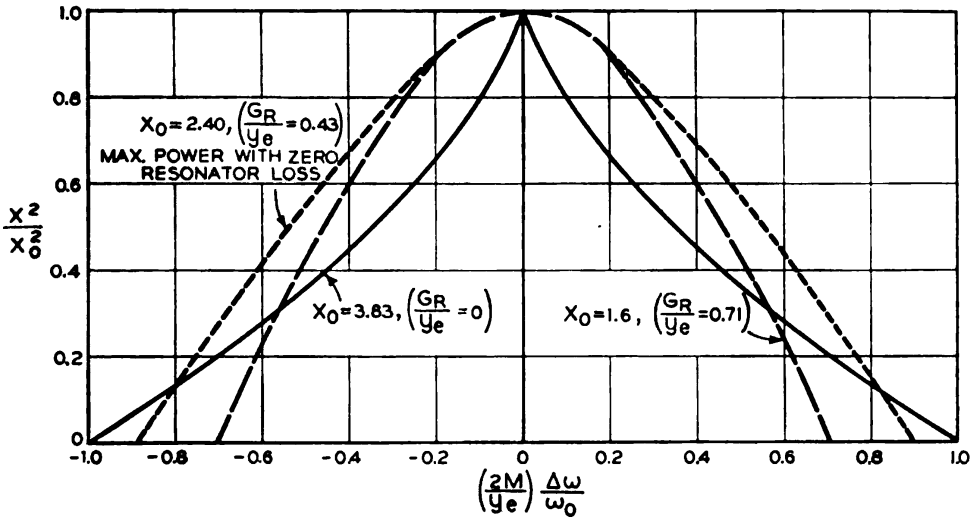

Fig. 14.—The relative power output vs a parameter proportional to the frequency deviation caused by electronic tuning, for various values of load. For zero loss and zero load, the curve is peaked. For zero loss and optimum load, the curve has its greatest width between half power points. For zero loss and greater than optimum load, the curve is narrow.

Generated on 2019-09-23 04:26 GMT / http://hdl.handle.net/2027/mdp.39015077775156
Public Domain, Google-digitized / http://www.hathitrust.org/access_use#pd-google
Digitized by Google
Original from UNIVERSITY OF MICHIGAN

The quantity

$$(\Delta\omega/\omega_0)_{\frac{1}{2}}$$

has a maximum value at $G_C/y_e = .433(X = 2.40)$, which is the condition for maximum power output when the resonator loss is zero.

In Fig. 11 we have a plot of G_C/y_e vs. G_R/y_e for optimum loading (that is loading to give maximum power for $\Delta\theta = 0$). This, combined with the

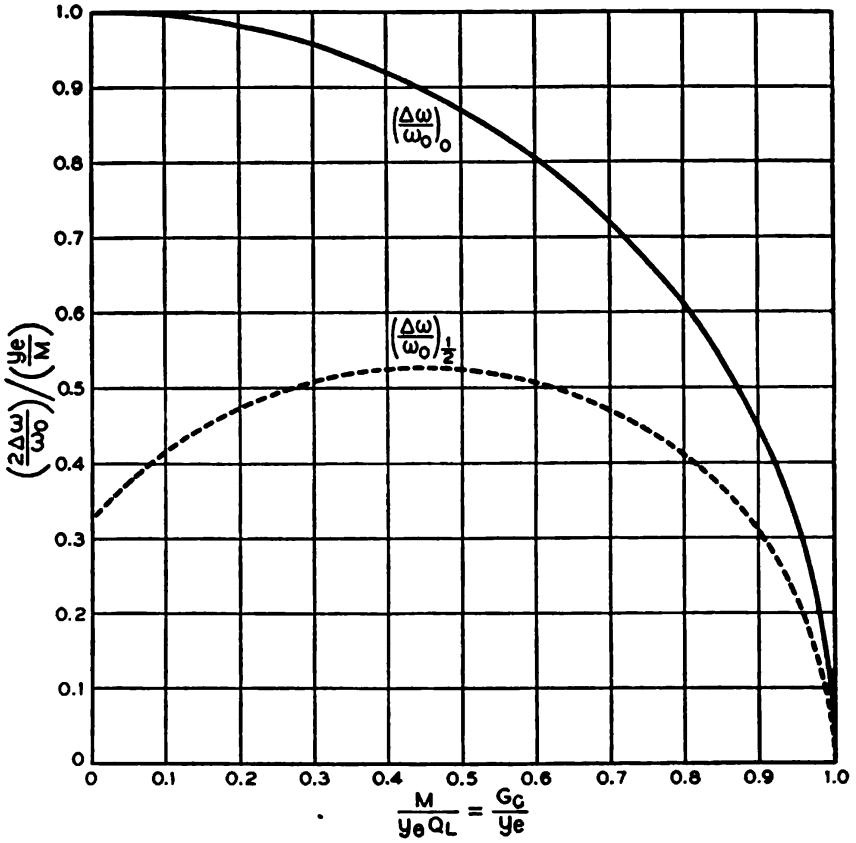

Fig. 15.—A parameter proportional to electronic tuning range vs the ratio of total circuit conductance and small signal electronic admittance. The electronic tuning to extinction $(\Delta\omega/\omega_0)_0$ is more affected by loading than the electronic tuning to half power points $(\Delta\omega/\omega_0)_{\frac{1}{2}}$.

curves of Fig. 15, enables us to draw curves in the case of optimum loading for electronic tuning as a function of the resonator loss. Such curves are shown in Fig. 16.

From Fig. 16 we see that with optimum loading it takes very large resonator losses to affect the electronic tuning range to half power very much, and that the electronic tuning range to extinction is considerably more affected by resonator losses. Turning back to Fig. 7, we see that power is affected even more profoundly by resonator losses. It is interesting to

Digitized by Google
Original from UNIVERSITY OF MICHIGAN
Generated on 2019-09-23 04:26 GMT / http://hdl.handle.net/2027/mdp.39015077775156
Public Domain, Google-digitized / http://www.hathitrust.org/access_use#pd-google

compare the effect of going from zero loss to a case in which the loss conductance is ½ of the small signal electronic conductance ($G_R = y_e/2$). The table below shows the fraction to which the power or efficiency, the elec-

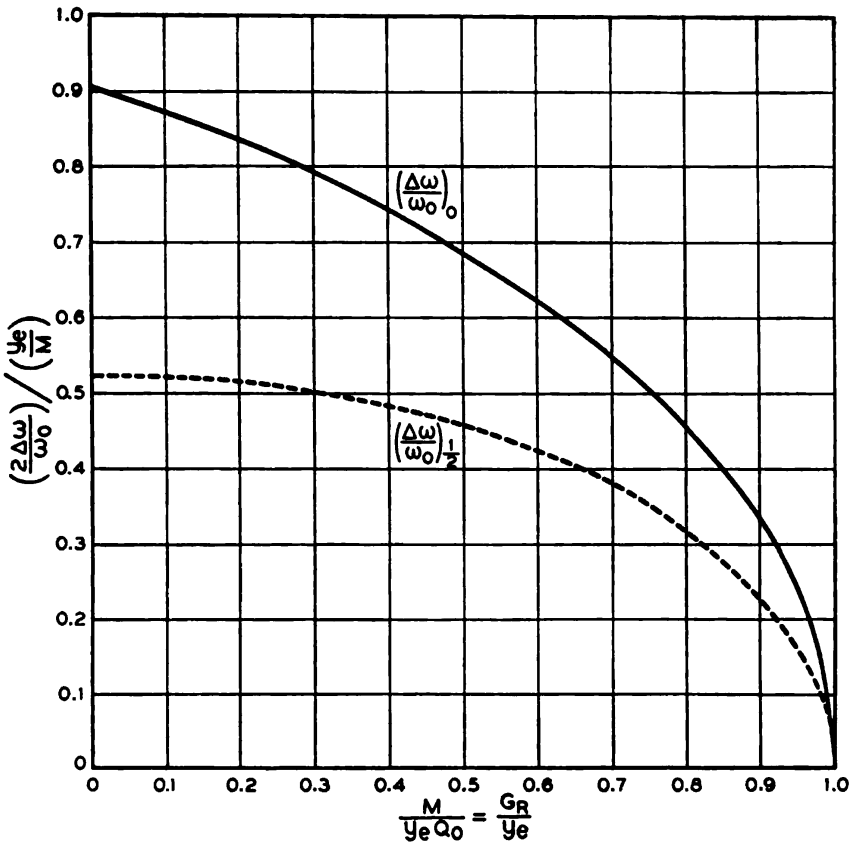

Fig. 16.—The effect of resonator loss on electronic tuning in an oscillator adjusted for optimum power output at the center of the electronic tuning range. A parameter proportional to electronic tuning is plotted vs the ratio of the resonator loss to small signal electronic admittance. The electronic tuning to extinction is more affected than the electronic tuning to half power as the loss is changed.

tronic tuning range to extinction, and the electronic tuning range to half power are reduced by this change.

Power, Efficiency (η)	Electronic Tuning to Extinction $(\Delta\omega/\omega_0)_0$	Electronic Tuning To Half Power $(\Delta\omega/\omega_0)_{\frac{1}{2}}$
.24	.76	.88

From this table it is obvious that efforts to control the electronic tuning by varying the ratio $\frac{G_R}{y_e}$ are of dubious merit.

Digitized by Google
Original from UNIVERSITY OF MICHIGAN
Generated on 2019-09-23 04:27 GMT / http://hdl.handle.net/2027/mdp.39015077775156
Public Domain, Google-digitized / http://www.hathitrust.org/access_use#pd-google

One other quantity may be of some interest; that is the phase angle of electronic tuning at half power and at extinction. We already have an expression involving $\Delta\theta_0$ (the value at extinction) in (7.4). By taking advantage of (3.10) and (3.8) (Figs. 5 and 11), we can obtain $\Delta\theta_0$ vs. G_C/y_e

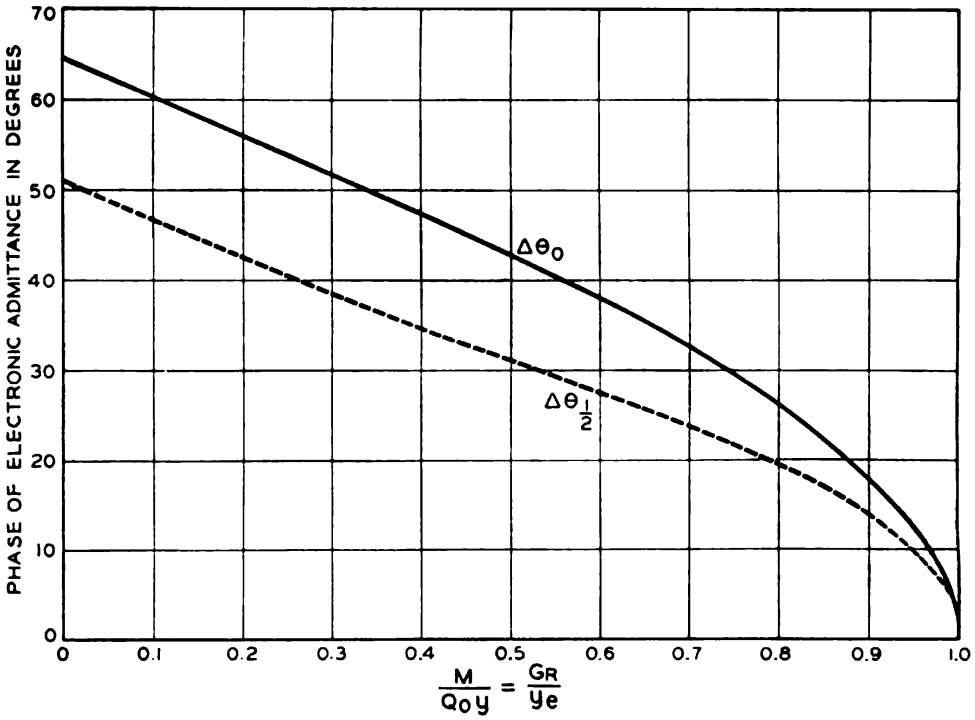

Fig. 17.—The phase of the drift angle for extinction and half power vs the ratio of resonator loss to small signal electronic admittance.

$(=M/Qy_e)$ for optimum loading. By referring to Fig. 12 we can obtain the relation for $\Delta\theta_{\frac{1}{2}}$ (the value at half power)

$$G_C = y_e\,[2J_1(X_0/\sqrt{2})/(X_0/\sqrt{2})]\cos\Delta\theta_{\frac{1}{2}}. \tag{7.11}$$

However, we have at $\Delta\theta = 0$

$$G_C = y_e\,[2J_1(X_0)/X_0]. \tag{7.12}$$

Hence

$$\cos\Delta\theta_{\frac{1}{2}} = \frac{J_1(X_0)}{\sqrt{2}J_1(X_0/\sqrt{2})}. \tag{7.13}$$

Again, from (3.8) we can express X_0 for optimum power at $\Delta\theta = 0$ in terms of G_R/y_e. In Fig. 17, $\Delta\theta_0$ and $\Delta\theta_{\frac{1}{2}}$ are plotted vs. G_R/y_e for optimum loading.

Digitized by Google
Original from UNIVERSITY OF MICHIGAN
Generated on 2019-09-23 04:27 GMT / http://hdl.handle.net/2027/mdp.39015077775156
Public Domain, Google-digitized / http://www.hathitrust.org/access_use#pd-google

VIII. Hysteresis

All the analysis presented thus far would indicate that if a reflex oscillator is properly coupled to a resistive load the power output and frequency will be single-valued functions of the drift time or of the repeller voltage, as illustrated in Fig. 18. During the course of the development in these laboratories of a reflex oscillator known as the 1349XQ, it was found that even if

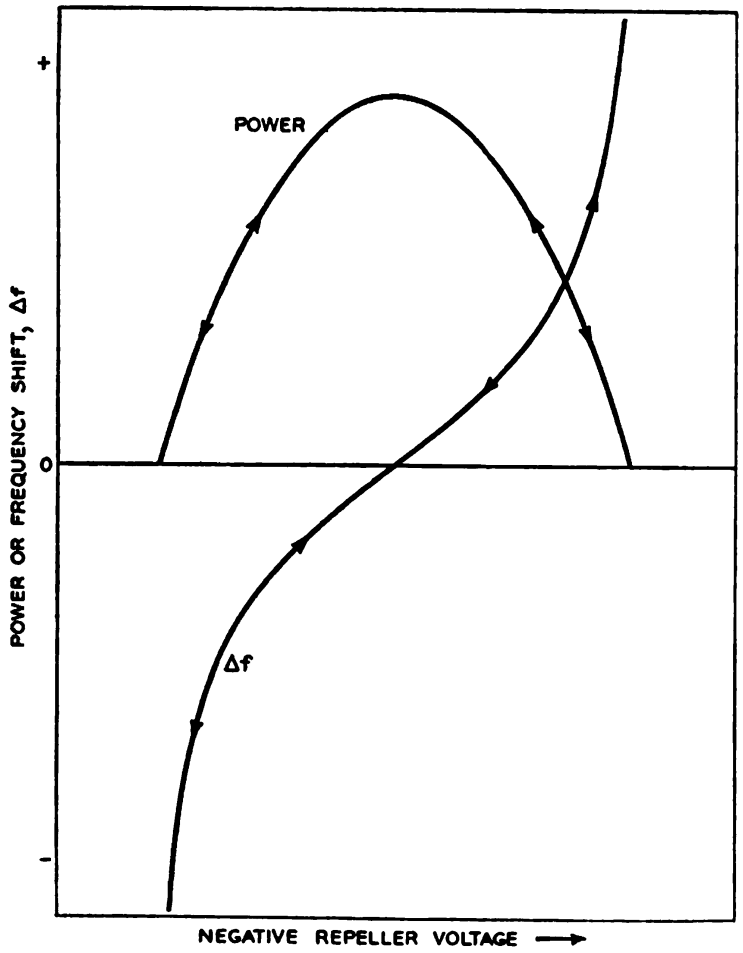

Fig. 18.—Ideal variation of power and frequency with repeller voltage, arbitrary units.

the oscillator were correctly terminated the characteristics departed violently from the ideal, as illustrated in Fig. 19. Further investigation disclosed that this departure was, to a greater or less degree, a general characteristic of all reflex oscillators in which no special steps had been taken to prevent it.

The nature of this departure from expected behavior is that the output is not a single valued function of the repeller voltage, but rather that at a given repeller voltage the output depends upon the direction from which the repel-

Generated on 2019-09-23 04:27 GMT / http://hdl.handle.net/2027/mdp.39015077775156
Public Domain, Google-digitized / http://www.hathitrust.org/access_use#pd-google
Digitized by Google
Original from UNIVERSITY OF MICHIGAN

ler voltage is made to approach the given voltage. Consider the case illustrated in Fig. 19. The arrows indicate the direction of repeller voltage variation. If we start from the middle of the characteristic and move toward more negative values of repeller voltage, the amplitude of oscillation varies continuously until a critical value is reached, at which a sudden decrease in

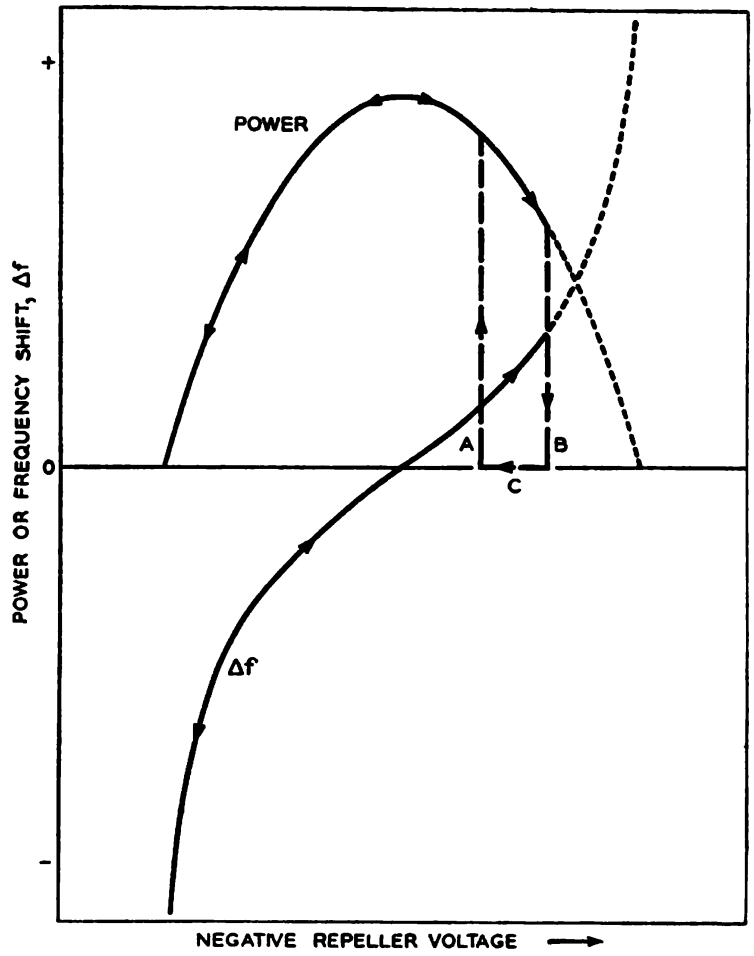

Fig. 19.—A possible variation of power and frequency with repeller voltage when there is electronic hysteresis. The arrows indicate the direction of variation of repeller voltage.

amplitude is observed. This drop may be to zero amplitude as shown or to a finite amplitude. In the latter case the amplitude may again decrease continuously as the repeller voltage is continuously varied to a new critical value, where a second drop occurs, etc. until finally the output falls to zero. In every observed case, even for more than one drop, the oscillation always dropped to zero discontinuously. Upon retracing the repeller voltage variation, oscillation does not restart at the repeller voltage at which it stopped but remains zero until a less negative value is reached, at which point the

Generated on 2019-09-23 04:27 GMT / http://hdl.handle.net/2027/mdp.39015077775156
Public Domain, Google-digitized / http://www.hathitrust.org/access_use#pd-google
Digitized by Google
Original from UNIVERSITY OF MICHIGAN

oscillation jumps to a large amplitude on the normal curve and then varies uniformly. The discontinuities occur sometimes at one end of the characteristic and sometimes at the other, and infrequently at both. It was first thought that this behavior was caused by an improper load,[7] but further investigation proved that the dependence on the load was secondary and the conclusion was drawn and later verified that the effect had its origin in the electron stream. For this reason the discontinuous behavior was called electronic hysteresis.

In any self-excited oscillator having a simple reasonant circuit, the oscillating circuit may be represented schematically as shown in Fig. 20. Here L and C represent the inductance and capacitance of the oscillator. G_R is a shunt conductance, representing the losses of the circuit, and G_L is the conductance of the load. Henceforth for the sake of convenience we

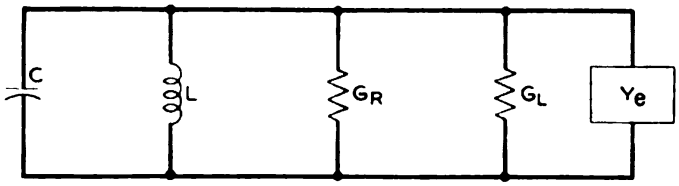

Fig. 20.—Equivalent circuit of reflex oscillator consisting of the capacitance C, inductance L, the resonator loss conductance G_R, the load conductance G_L and the electronic admittance Y_e.

will lump these and call the total G_L. Y_e represents the admittance of the electron stream. Such a circuit has a characteristic transient of the form

$$V = V_0 e^{-\alpha t} e^{j\omega t} \tag{8.1}$$

where

$$\alpha = \frac{G_e + G_L}{2C} \quad \text{and} \quad \omega \doteq \frac{1}{\sqrt{LC}}.$$

Oscillations will build up spontaneously if

$$G_{e0} + G_L < 0\,. \tag{8.2}$$

For stable oscillation at amplitude V we require

$$G_e[V] + G_L = 0 \tag{8.3}$$

(8.2) and (8.3) state that the amplitude of oscillation will build up until non-linearities in the electronic characteristics reduce the electronic conductance to a value equal and opposite to the total load plus circuit conductance. Thus, in general

$$Y_e = G_{e0}F_1(V) + jB_{e0}F_2(V) \tag{8.4}$$

[7] See Section IX.

Digitized by Google
Original from UNIVERSITY OF MICHIGAN
Generated on 2019-09-23 04:27 GMT / http://hdl.handle.net/2027/mdp.39015077775156
Public Domain, Google-digitized / http://www.hathitrust.org/access_use#pd-google

where

$$Y_e = G_{e0} + jB_{e0} \tag{8.5}$$

is the admittance for vanishing amplitude, which is taken as a reference value. The foregoing facts are familiar to any one who has worked with oscillators.

Now, condition (8.3) may be satisfied although (8.2) is not. Then an oscillator will not be self-starting, although once started at a sufficiently large amplitude its operation will become stable. An example in common experience is a triode Class C oscillator with fixed grid bias. In such a case

$$F(V_1) > F(0) \tag{8.6}$$

holds for some V_1.

As an example of normal behavior, let us assume that $F(V)$ is a continuous monotonically decreasing function of increasing V, with the reference value of V taken as zero. Then the conductance, $G_e = G_{e0}F(V)$ will vary with V as shown in Fig. 21. Stable oscillation will occur when the amplitude V_1 has built up to a value such that the electronic conductance curve intersects the horizontal line representing the load conductance, G_L. G_{e0} is a function of one or more of the operating parameters such as the electron current in the vacuum tube. If we vary any one of these parameters indicated as X_n the principal effect will be to shrink the vertical ordinates as shown in Fig. 21 and the amplitude of oscillation will assume a series of stable values corresponding to the intercepts of the electronic conductance curves with the load conductance. If, as we have assumed, $F(V)$ is a monotonically decreasing function of V, the amplitude will decrease continuously to zero as we uniformly vary the parameter in such a direction as to decrease G_{e0}. Zero amplitude will, of course, occur when the curve has shrunk to the case where $G_{e0} = G_L$. Under these conditions the power output, $\frac{1}{2}G_LV^2$, will be a single value function of the parameter as shown in Fig. 22 and no hysteresis will occur.

Suppose, however, that $F(V)$ is not a monotonically decreasing function of V but instead has a maximum so that $G_{e0}F(V)$ appears as shown in Fig. 23. In this case, if we start with our parameter $X = X_1$ and vary our parameter X in such a direction as to shrink the curve, the amplitude will decrease smoothly until the parameter arrives at a value of X_5 corresponding to amplitude V_5 at which the load line is tangent to the maximum of the conductance curve. Further variation of X in the same direction will cause the amplitude to jump to zero. Upon reversing the direction of the variation of the parameter, oscillation cannot restart until X arrives at a value X_4 such that the zero amplitude conductance is equal to the load conductance. When this occurs the amplitude will suddenly jump to the value V_4.

Digitized by Google
Original from UNIVERSITY OF MICHIGAN
Generated on 2019-09-23 04:28 GMT / http://hdl.handle.net/2027/mdp.39015077775156
Public Domain, Google-digitized / http://www.hathitrust.org/access_use#pd-google

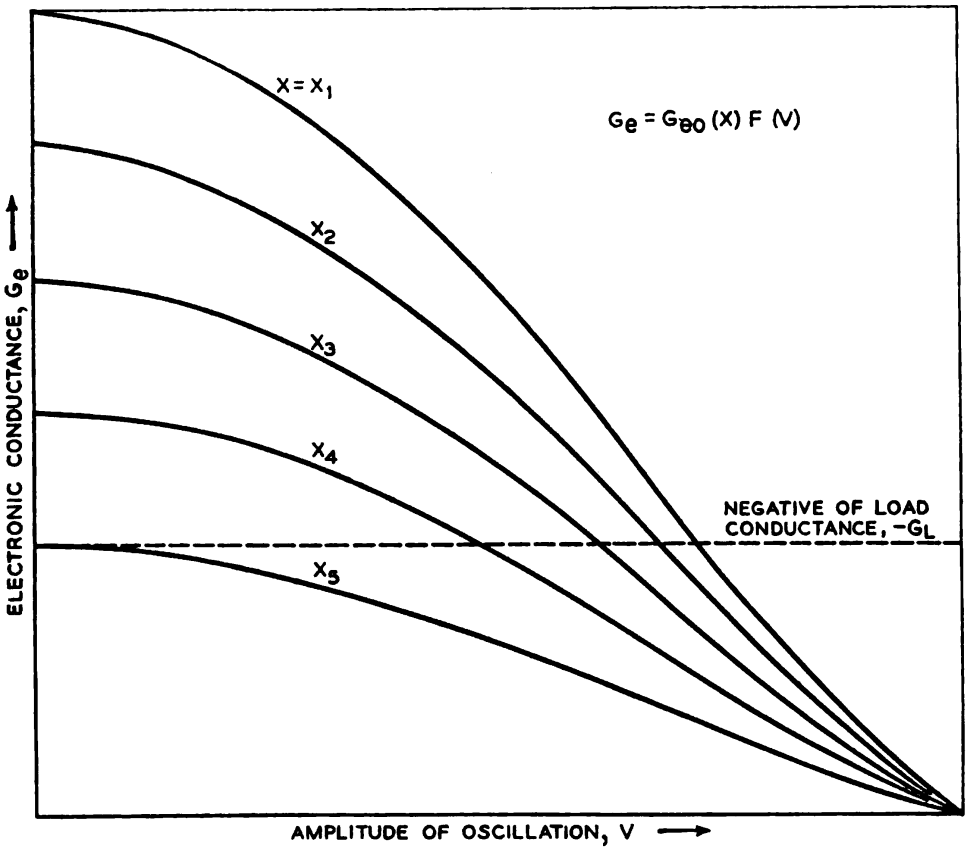

Fig. 21.—A possible variation of electronic conductance with amplitude of oscillation for the general case of an oscillator. Arbitrary units are employed. Different curves correspond to several values of a parameter X which determines the small signal values of the conductance. The load conductance is indicated by the horizontal line. Stable oscillation for any given value of the parameter X occurs at the intersection of the electronic conductance curve with the load line G_L.

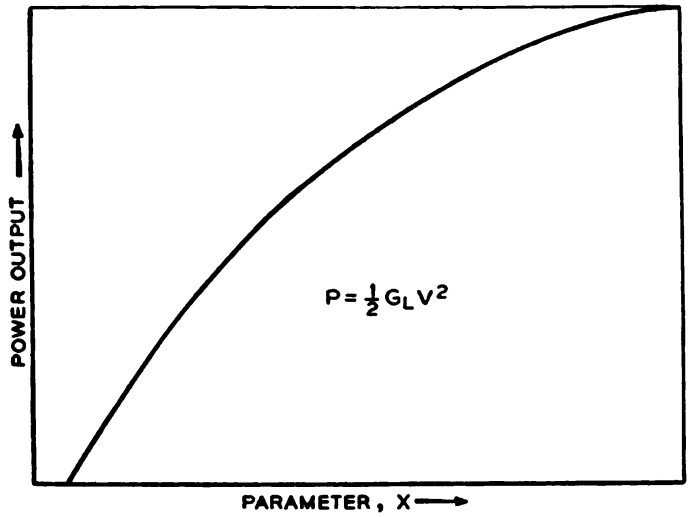

Fig. 22.—Variation of power output with the parameter X when the conditions of Fig. 21 apply.

Digitized by Google
Original from UNIVERSITY OF MICHIGAN
Generated on 2019-09-23 04:28 GMT / http://hdl.handle.net/2027/mdp.39015077775156
Public Domain, Google-digitized / http://www.hathitrust.org/access_use#pd-google

Under these conditions the power output will appear as shown in Fig. 24, in which the hysteresis is apparent.

Let us now consider the conditions obtaining in a reflex oscillator. Fig. 1 shows a schematic diagram of a reflex oscillator. This shows an electron gun which projects a rectilinear electron stream across the gap of a resonator.

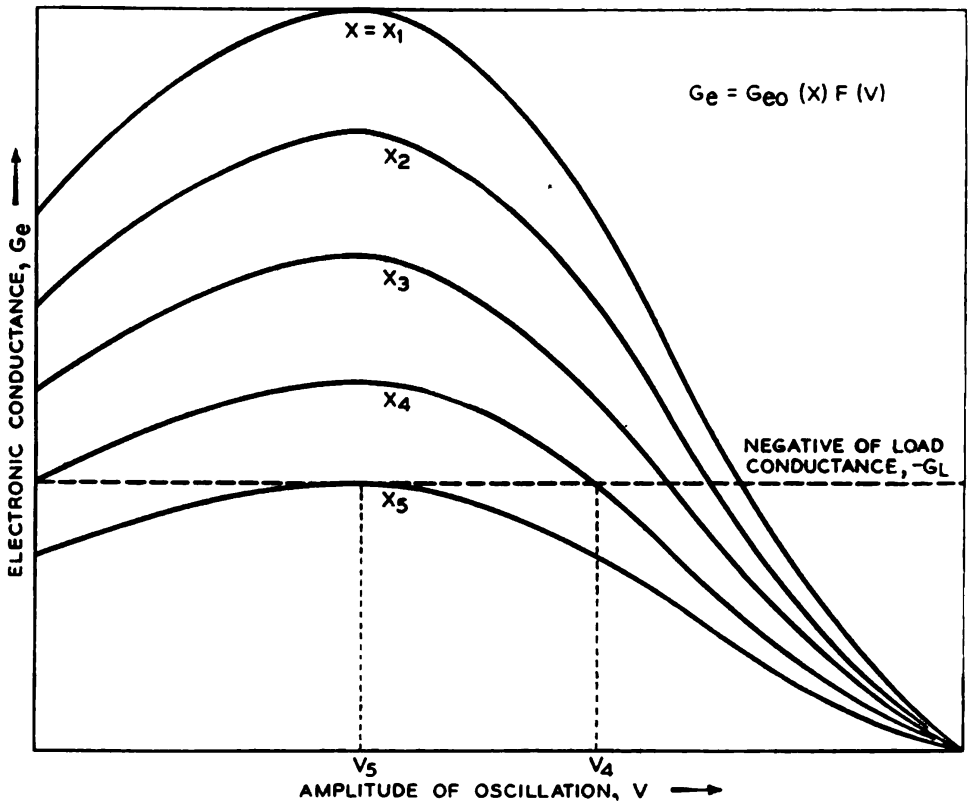

Fig. 23.—Variation of electronic conductance with amplitude of oscillation of a form which will result in hysteresis. The parameter X determines the small signal value of the conductance. The horizontal line indicates the load conductance.

After the beam passes through this gap it is retarded and returned by a uniform electrostatic field. If we carry out an analysis to determine the electronic admittance which will appear across the gap if the electrons make one round trip, we arrive at expression 2.2 which may be written

$$Y_e = \frac{I_0 \beta^2 \theta}{V_0} \frac{J_1(X)}{X} [\sin \theta + j \cos \theta] \tag{8.7}$$

where

$$X = \frac{\theta \beta V}{2V_0}.$$

Digitized by Google
Original from UNIVERSITY OF MICHIGAN
Generated on 2019-09-23 04:28 GMT / http://hdl.handle.net/2027/mdp.39015077775156
Public Domain, Google-digitized / http://www.hathitrust.org/access_use#pd-google

This admittance will be a pure conductance if $\theta = \theta_0 = (n + \frac{3}{4})\,2\pi$. As we have seen, in an oscillator designed specifically for electronic tuning, n usually has a value of 3 or greater and the variations $\Delta\theta$ from θ arising from

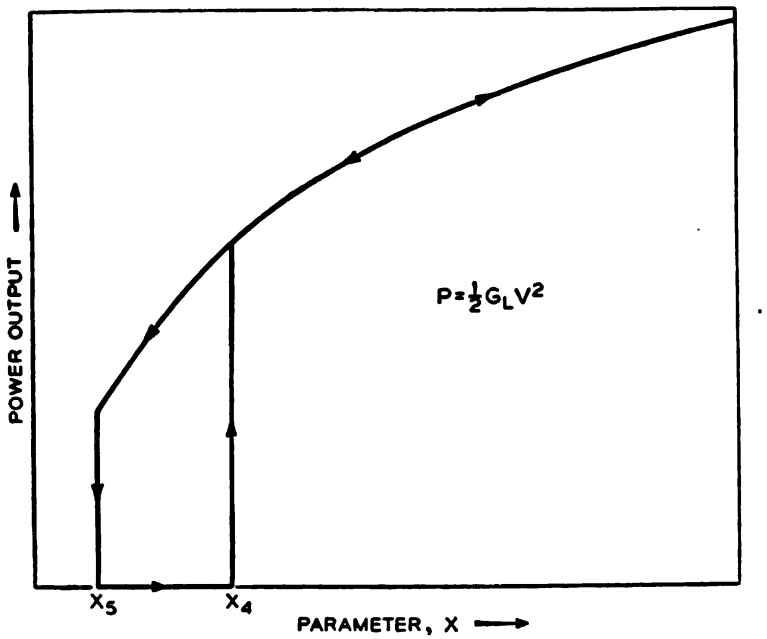

Fig. 24.—A curve of power output vs parameter X resulting from the conductance curves shown in Fig. 23 and illustrating hysteresis.

repeller voltage variation are sufficiently small so that the effect of $\Delta\theta$ in varying X may be neglected. In this case we may write

$$G_e = -y_e \frac{2J_1(CV)}{CV} \cos \Delta\theta$$

$$y_e = \frac{i_0 \beta^2 \theta_0}{2V_0} \tag{8.8}$$

$$C = \frac{\theta_0 \beta}{2V_0}.$$

The parameter which we vary in obtaining the repeller characteristic of the tube is $\Delta\theta$. The variation of this parameter is produced by shifting the repeller voltage V_R from the value V_{R0} corresponding to the transit angle θ_0. Since as is shown, Fig. 25a, $\frac{J_1(CV)}{CV}$ decreases monotonically as V increases, no explanation of hysteresis is to be found in this expression. Fig. 25b shows the smooth symmetrical variation of output with repeller voltage about the value for which $\Delta\theta = 0$ which is to be expected.

Generated on 2019-09-23 04:28 GMT / http://hdl.handle.net/2027/mdp.39015077775156
Public Domain, Google-digitized / http://www.hathitrust.org/access_use#pd-google
Digitized by Google
Original from UNIVERSITY OF MICHIGAN

Now suppose a second source of conductance G_{e2} exists whose amplitude function is of the form illustrated in Fig. 26a. Let us suppose that for the

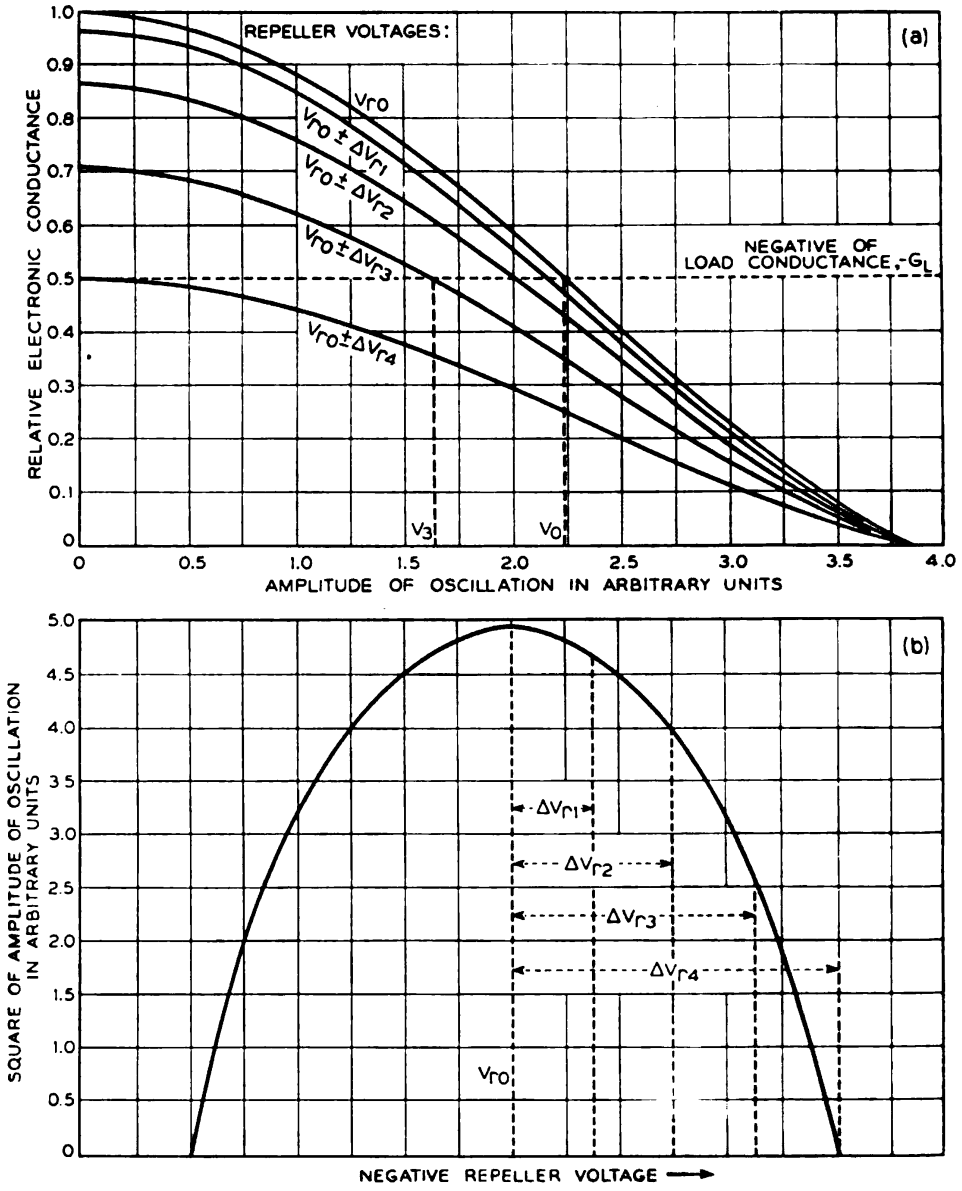

Fig. 25.—*a*. Variation of electronic conductance with amplitude of oscillation for an ideal oscillator. The parameter controlling the small signal electronic conductance is the repeller voltage which determines the transit angle in the repeller region. The horizontal line indicates the load conductance.

b. The variation of power output with the repeller voltage which results from the characteristics of Fig. 25a.

value of θ_0 assumed the phase of this conductance is such as to oppose G_{e1}. G_{e2} may or may not be a function of $\Delta\theta$. For the sake of simplicity let us assume that G_{e2} varies with $\Delta\theta$ in the same way as G_{e1}. The total conduc-

Digitized by Google
Original from UNIVERSITY OF MICHIGAN
Generated on 2019-09-23 04:28 GMT / http://hdl.handle.net/2027/mdp.39015077775156
Public Domain, Google-digitized / http://www.hathitrust.org/access_use#pd-google

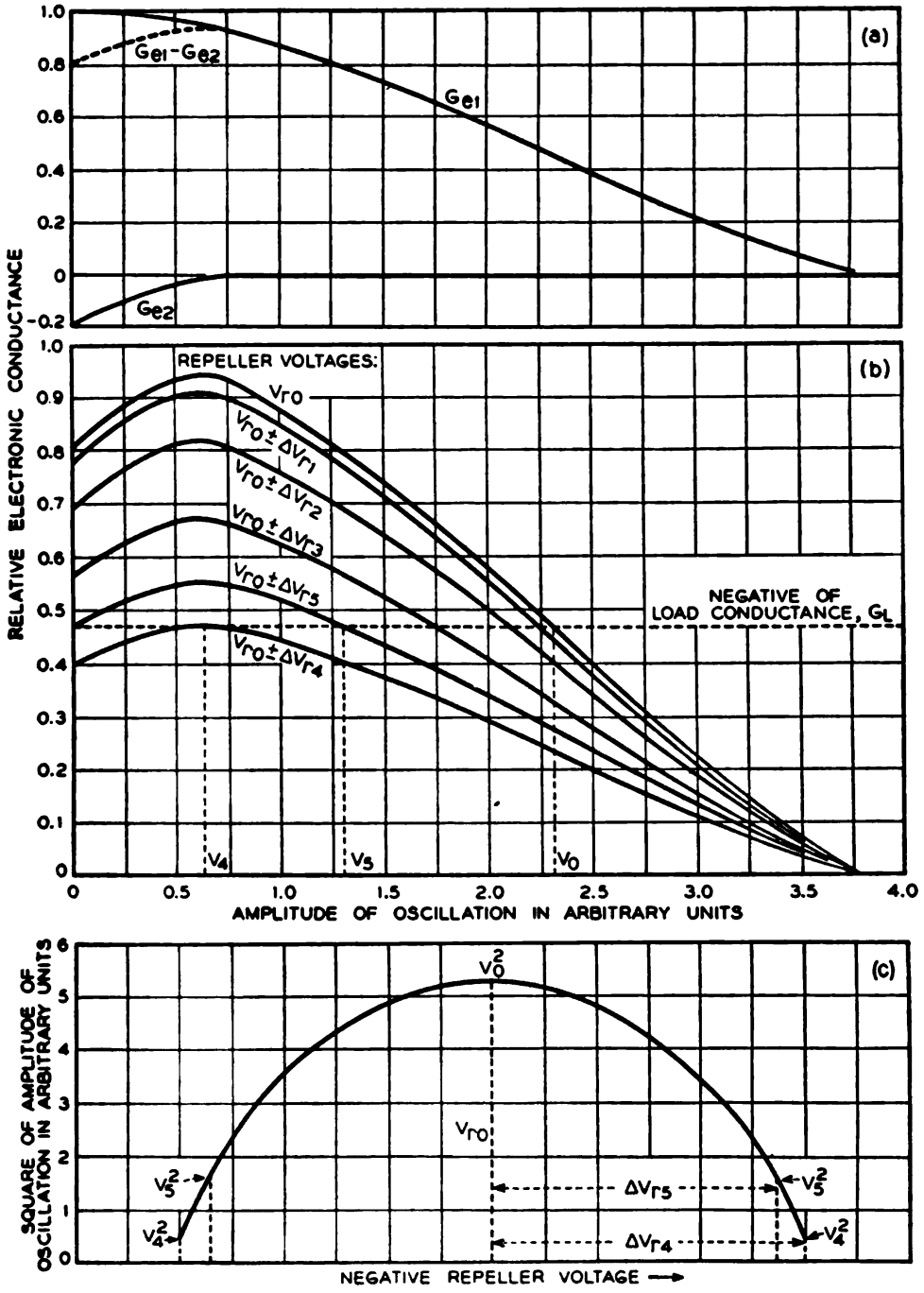

Fig. 26.—*a*. Curve G_{e1} shows the variation of electronic conductance with amplitude of oscillation for an ideal reflex oscillator. Curve G_{e2} represents the variation of a second source of electronic conductance with amplitude. The difference of these two curves indicated G_{e1}-G_{e2} shows the variation of the sum of these two conductance terms with amplitude.

b. Electronic conductance vs amplitude of oscillation when two conductance terms exist whose variation with repeller voltage is the same.

c. Power output vs repeller voltage for a reflex oscillator in which two sources of conductance occur varying with amplitude as shown in Fig. 26b.

Digitized by Google
Original from UNIVERSITY OF MICHIGAN
Generated on 2019-09-23 04:29 GMT / http://hdl.handle.net/2027/mdp.39015077775156
Public Domain, Google-digitized / http://www.hathitrust.org/access_use#pd-google

tance $G_e = G_{e1} - G_{e2}$ will appear as shown. As the repeller voltage is varied from the optimum value the conductance curve will shrink in proportion to $\cos \Delta\theta$, and the amplitude of oscillation for each value of $\Delta\theta$ will adjust itself to the value corresponding to the intersection of the load line and the conductance plot as shown in Fig. 26b. When the load line becomes tangent, as for amplitude V_4, further variation of the repeller voltage in the same direction will cause oscillation to jump from V_4 to zero amplitude. Correspondingly, on starting oscillation will restart with a jump to V_3. Hence, two sources of conductance varying in this way will produce conditions previously described, which would cause hysteresis as shown in Fig. 26c. The above assumptions lead to hysteresis symmetrically disposed about the optimum repeller voltage. Actually, this is rarely the case, but the explanation for this will be deferred.

Fig. 27 shows repeller characteristics for an early model of a reflex oscillator designed at the Bell Telephone Laboratories. The construction of this oscillator was essentially that of the idealized oscillator of Fig. 1 upon which the simple theory is based. However, the repeller characteristics of this oscillator depart drastically from the ideal. It will be observed that a double jump occurs in the amplitude of oscillation. The arrows indicate the direction of variation of the repeller voltage. The variation in the frequency of oscillation is shown, and it will be observed that this also is discontinuous and presents a striking feature in that the rate of change of frequency with voltage actually reverses its sign for a portion of the range. A third curve is shown which gives the calculated phase $\Delta\theta$ of the admittance arising from drift in the repeller field. This lends very strong support to the hypothesis of the existence of a second source of conductance, since this phase varies by more than 180°, so that for some part of the range the repeller conductance must actually oppose oscillation. The zero value phase is arbitrary, since there is no way of determining when the total angle is $(n + \frac{3}{4})2\pi$.

Having recognized the circumstances which can lead to hysteresis in the reflex oscillator, the problem resolves itself into locating the second source of conductance and eliminating it.

A number of possible sources of a second conductance term were investigated in the particular case of the 1349 oscillator, and most were found to be of negligible importance. It was found that at least one important second source of conductance arose from multiple transits of the gap made by electrons returning to the cathode region. In the case of the 1349 a design of the electron optical system which insured that the electron stream made only one outgoing and one return transit of the gap eliminated the hysteresis in accordance with the hypothesis.

Digitized by Google
Original from UNIVERSITY OF MICHIGAN
Generated on 2019-09-23 04:29 GMT / http://hdl.handle.net/2027/mdp.39015077775156
Public Domain, Google-digitized / http://www.hathitrust.org/access_use#pd-google

Inasmuch as multiple transits appear to be the most common cause for hysteresis in reflex oscillator design, it seems worthwhile to obtain a more detailed understanding of the mechanism in this case. Other possible

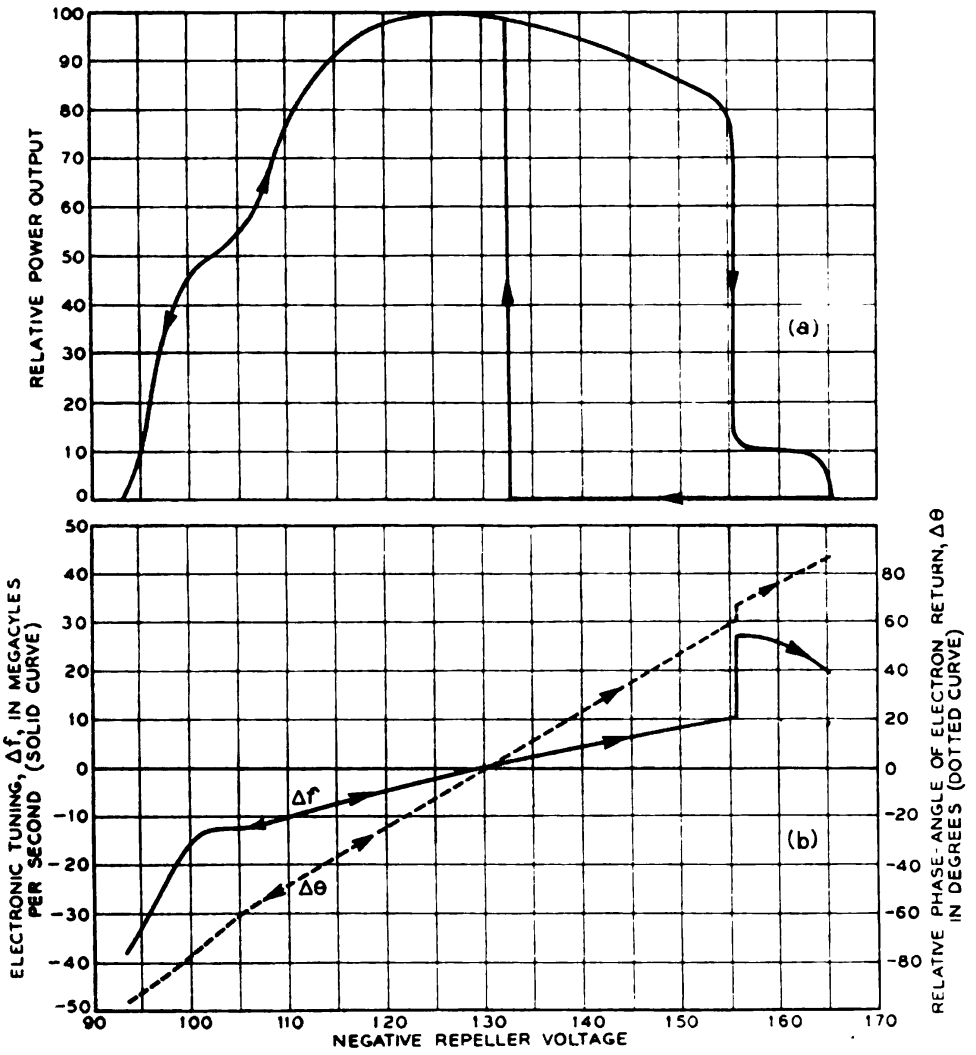

Fig. 27.—Amplitude, frequency and transit phase variation with the repeller voltage obtained experimentally for a reflex oscillator exhibiting electronic hysteresis. The arrows indicate the direction of variation of the repeller voltage.

mechanisms such as velocity sorting on the repeller will give rise to similar effects and can be understood from what follows.

In the first order theory, the electrons which have retraversed the gap are conveniently assumed to vanish. Actually, of course, the returning stream is remodulated and enters the cathode space. Unfortunately, the

Digitized by Google
Original from UNIVERSITY OF MICHIGAN
Generated on 2019-09-23 04:29 GMT / http://hdl.handle.net/2027/mdp.39015077775156
Public Domain, Google-digitized / http://www.hathitrust.org/access_use#pd-google

conditions in the cathode region are very complex, and an exact analysis would entail an unwarranted amount of effort. However, from an approximate analysis one can obtain a very simple and adequate understanding of the processes involved.

Let us examine the conditions existing after the electrons have returned through the gap of the idealized reflex oscillator. In the absence of oscillation, with an ideal rectilinear stream and ideally fine grids all the electrons which leave the cathode will return to it. When oscillation exists all electrons which experience a net gain of energy on the two transits will be captured by the cathode, while those experiencing a net loss will not reach it, but instead will return through the gap for a third transit, etc. In a practical oscillator even in the absence of oscillation only a fraction of the electrons which leave the cathode will be able to return to the cathode, because of losses in axial velocity produced by deflections by the grid wires and various other causes. As a result, it will not be until an appreciable amplitude of oscillation has been reached that a major proportion of the electrons which have gained energy will be captured by the cathode. On the other hand, there will be an amplitude of oscillation above which no appreciable change in the number captured will occur.

The sorting action which occurs on the cathode will produce a source of electronic admittance. Another contribution may arise from space charge interaction of the returning bunched beam with the outgoing stream. A third component arises from the continued bunching resulting from the first transit of the gap. From the standpoint of this third component the reflex oscillator with multiple transits suggests the action of a cascade amplifier. The situation is greatly complicated by the nature of the drift field in the cathode space. All three mechanisms suggested above may combine to give a resultant second source. Here we will consider only the third component. Consider qualitatively what happens in the bunching action of a reflex oscillator. Over one cycle of the r.f. field, the electrons tend to bunch about the electron which on its first transit crosses the gap when the field is changing from an accelerating to a decelerating value. The group recrosses the gap in such a phase that the field extracts at least as much energy from every electron as it gave up to any electron in the group. When we consider in addition various radial deflections, we see that very few of the electrons constituting this bunch can be lost on the cathode.

Although it is an oversimplification, let us assume that we have a linear retarding field in the cathode region and also that none of the electrons are intercepted on the cathode. To this order of approximation a modified cascade bunching theory would hardly be warranted and we will consider only that the initial bunching action is continued. Under these conditions,

Digitized by Google
Original from UNIVERSITY OF MICHIGAN
Generated on 2019-09-23 04:29 GMT / http://hdl.handle.net/2027/mdp.39015077775156
Public Domain, Google-digitized / http://www.hathitrust.org/access_use#pd-google

we can show that the admittance arising on the third transit of the gap will have the form

$$Y_e' = +I_0' \frac{\beta^2 \theta_t}{V_0} \frac{J_1\left(\frac{\theta_t \beta V}{2V_0}\right)}{\frac{\theta_t \beta V}{2V_0}} [\sin \theta_t + j \cos \theta_t] \tag{8.9}$$

where I_0' is the effective d.c. contribution to the third transit. $\theta_t = \theta + \theta_C$ is the total transit angle made up of the drift angle in the repeller space, θ, and the drift angle in the cathode space θ_C. As before, assume that the small changes in θ_t caused by the changing repeller voltage over the electronic tuning range exercise an appreciable effect only in changing the sine and cosine terms. Then we may write

$$Y_e' = G_e' + jB_e' = y_e' \frac{2J_1(C_2V)}{C_2V} [\sin \theta_t + j \cos \theta_t] \tag{8.10}$$

where

$$C_2 = \frac{\theta_{t0} \beta V}{2V_0}, \quad \text{and} \quad y_e' = \frac{\beta^2 I_0' \theta_{t0}}{2V_0}.$$

If $\Delta\theta = \theta_t - \theta_{t0}$

$$G_e' = y_e' \frac{2J_1(C_2V)}{C_2V} [\sin \theta_{t0} \cos \Delta\theta_t + \cos \theta_{t0} \sin \Delta\theta_t]. \tag{8.11}$$

Now

$$\begin{aligned} \Delta\theta &= \omega_0 \tau \frac{\Delta V_g}{V_g + V_0} + \Delta\omega\tau_0 \\ \Delta\theta_e &= \Delta\omega\tau_e \\ \Delta\theta_t &= \omega_0 \tau \frac{\Delta V_g}{V_g + V_0} + \Delta\omega\tau_0 + \Delta\omega\tau_e. \end{aligned} \tag{8.12}$$

We observe that the phase angle of the admittance arising on the third transit varies more rapidly with repeller voltage (i.e., frequency) than the phase angle of the second transit admittance. This is of considerable importance in understanding some of the features of hysteresis.

Let us consider (8.11) for some particular values of θ_C or θ_t. We remember that θ_t is greater than θ and hence $C_2 > C_1$. Since this is so, the limiting function $\frac{2J_2(C_2V)}{C_2V}$ will become zero at a lower value of V than $\frac{2J_1(C_1V)}{C_1V}$. We will consider two cases $\theta_t = (n + \frac{1}{4})2\pi$ and $\theta_t = (n + \frac{3}{4})2\pi$. These

Digitized by Google
Original from UNIVERSITY OF MICHIGAN
Generated on 2019-09-23 04:29 GMT / http://hdl.handle.net/2027/mdp.39015077775156
Public Domain, Google-digitized / http://www.hathitrust.org/access_use#pd-google

correspond respectively to a conductance aiding and bucking the conductance arising on the first return. In case 1 we have

$$G_e' = -y_e' \frac{2J_1(C_2V)}{C_2V} \cos \Delta\theta_t \tag{8.13}$$

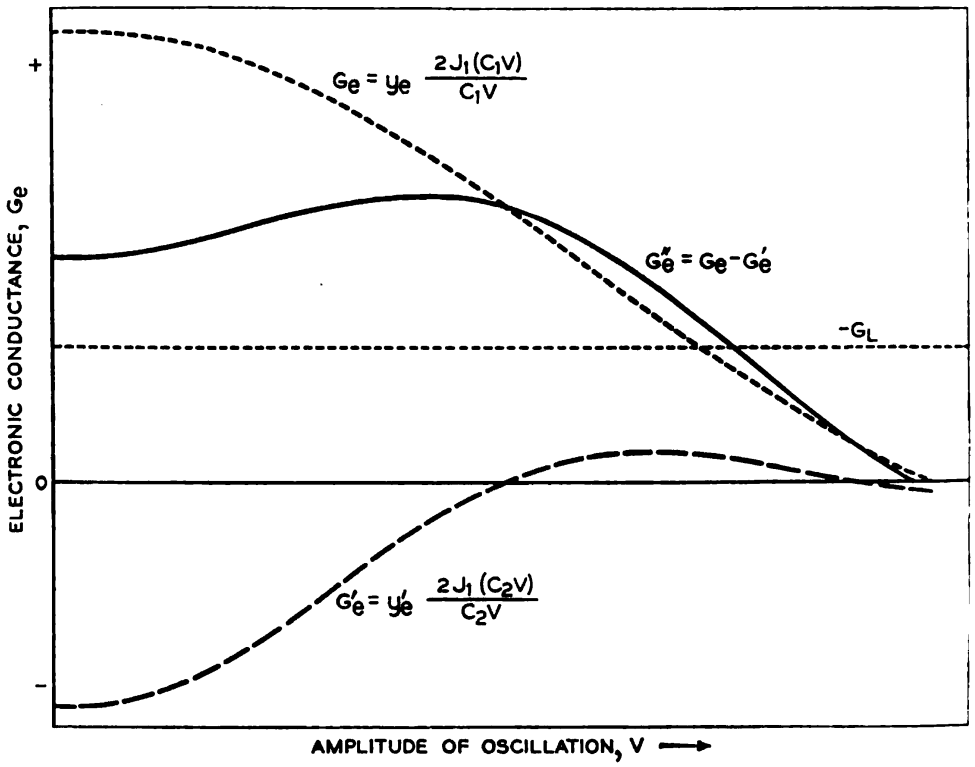

Fig. 28.—Theoretically derived variation of electronic conductance with amplitude of oscillation. Curve G_e represents conductance arising from drift action in the repeller space. Curve G_e' represents the conductance arising from continuing drift in the cathode region. G_e'' represents the conductance variation with amplitude which will result if G_e and G_e' are in phase opposition.

and case 2

$$G_e' = +y_e' \frac{2J_1(C_2V)}{C_2V} \cos \Delta\theta_t \,. \tag{8.14}$$

Figure 28 illustrates case (2) and Fig. 29 case (1). If $\cos \Delta\theta_t$ and $\cos \Delta\theta$ varied in the same way with repeller voltage, the resultant limiting function would shrink without change in form as the repeller voltage was varied, and it is apparent that Fig. 28 would then yield the conditions for hysteresis and Fig. 29 would result in conditions for a continuous characteristic. If Fig. 28 applied we should expect hysteresis symmetrical about the optimum repeller voltage. We recall, however, that in Fig. 27 hysteresis

Digitized by Google
Original from UNIVERSITY OF MICHIGAN
Generated on 2019-09-23 04:30 GMT / http://hdl.handle.net/2027/mdp.39015077775156
Public Domain, Google-digitized / http://www.hathitrust.org/access_use#pd-google

occurred only on one end of the repeller characteristic and was absent on the other. The key to this situation lies in the fact that $\Delta\theta_t$ and $\Delta\theta$ do not vary in the same way when the repeller voltage is changed and the frequency shifts as shown in (8.12). As a result, the resulting limiting function does not shrink uniformly with repeller voltage, since the contribution G_e' changes more rapidly than G_e. Hence we should need a continuous series of pictures of the limiting function in order to understand the situation completely.

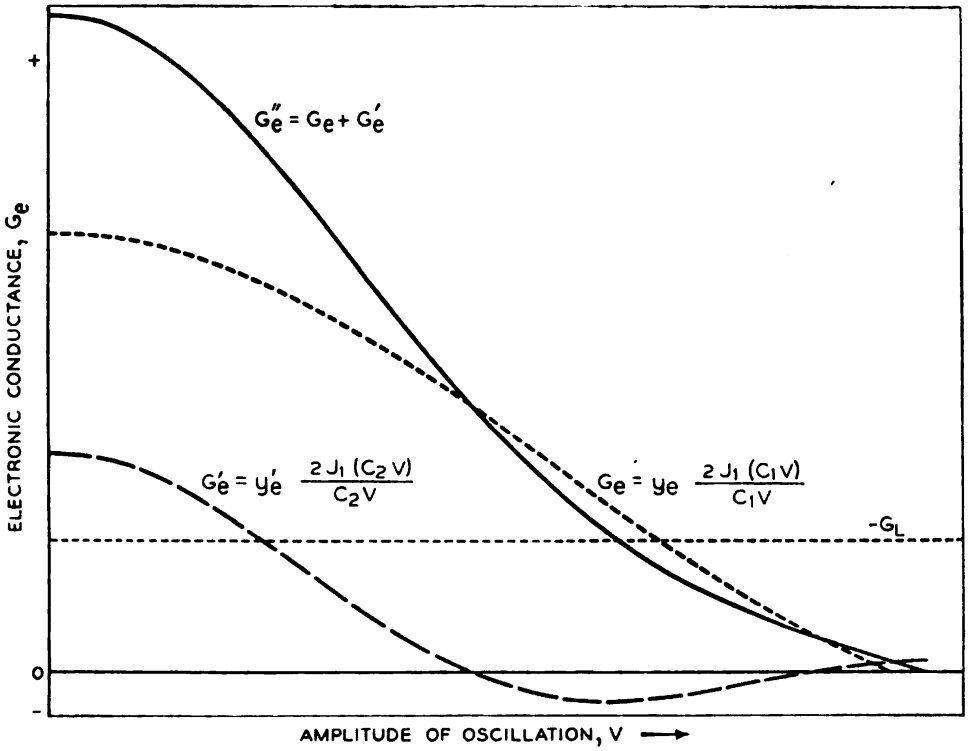

Fig. 29.—Theoretically derived curves of electronic conductance vs amplitude of oscillation. Curve G_e shows the variation of the resultant electronic conductance when the repeller space contribution and the cathode space contribution are in phase addition.

Suppose we consider Fig. 29 and again assume in the interests of simplicity that $\Delta\theta_t$ and $\Delta\theta$ vary at the same rate. In this case we observe that in a region the conductance varies very rapidly with amplitude. This would imply that in this region the output would tend to be independent of the repeller voltage. If we refer again to Fig. 27 we observe that the output is indeed nearly independent of the repeller voltage over a range.

We see that these facts all fit into a picture in which, because of the more rapid phase variation of θ_t than θ with repeller voltage, the limiting function at one end of the repeller voltage characteristic has the form of Fig. 28. accounting for the hysteresis, and at the other end has the form of Fig. 29,

Digitized by Google
Original from UNIVERSITY OF MICHIGAN
Generated on 2019-09-23 04:30 GMT / http://hdl.handle.net/2027/mdp.39015077775156
Public Domain, Google-digitized / http://www.hathitrust.org/access_use#pd-google

accounting for the relative independence of the output on the repeller voltage.

In what has been given so far we have arrived qualitatively at an explanation for the variation of the amplitude. There remains the explanation for the behavior of the frequency. In this case we plot susceptance as a function of amplitude and, as in the case of the conductance, there will be several contributions. The primary electronic susceptance will be given by

$$B_e = y_e \frac{2J_1(CV)}{CV} \sin \theta_e \tag{8.15}$$

Hence, as we vary the parameter $\Delta\theta$ by changing the repeller voltage the susceptance curve swells as the conductance curve shrinks. The circuit condition for stable oscillation is that

$$B_e + 2j\Delta\omega C = 0. \tag{8.16}$$

A second source of susceptance will arise from the continuing drift in the cathode space. Referring to equation (8.10) we see that this will have the form

$$B_e' = y_e' \frac{2J_1(C_2V)}{C_2V} \cos \theta_t \tag{8.17}$$

and corresponding to equation (8.11) we write

$$B_e' = y_e' \frac{2J_1(C_2V)}{C_2V} [\cos \theta_{t0} \cos \Delta\theta_t - \sin \theta_{t0} \sin \Delta\theta_t]. \tag{8.18}$$

Consider the functions given by (8.18) for values of $\theta_{t0} = (n + \frac{1}{4})2\pi$ and $(n + \frac{3}{4})2\pi$ as functions of V. These are the extreme values which we considered in the case of the conductance. The ordinates of these curves give the frequency shift as a function of the amplitude.
In case 1 we have

$$B_e' = -y_e' \frac{2J_1(C_2V)}{C_2V} \sin \Delta\theta_t \tag{8.19}$$

and case 2

$$B_e' = y_e' \frac{2J_1(C_2V)}{C_2V} \sin \Delta\theta_t . \tag{8.20}$$

The total susceptance will be the sum of the susceptance appearing across the gap as a result of the drift in the repeller space and the susceptance which appears across the gap as a result of the cascaded drift action in the repeller region and the cathode region. If $\sin \Delta\theta_t$ and $\sin \Delta\theta$ varied in the same way with the repeller voltage, the total susceptance would expand

Digitized by Google
Original from UNIVERSITY OF MICHIGAN
Generated on 2019-09-23 04:30 GMT / http://hdl.handle.net/2027/mdp.39015077775156
Public Domain, Google-digitized / http://www.hathitrust.org/access_use#pd-google

or contract without change in form as the repeller voltage was varied. In Figs. 30 and 31 a family of susceptance curves are shown corresponding respectively to cases 1 and 2 above for various values of $\Delta\theta_t$, assuming that $\Delta\theta_t$ and $\Delta\theta$ vary in the same way with the repeller voltage. As the

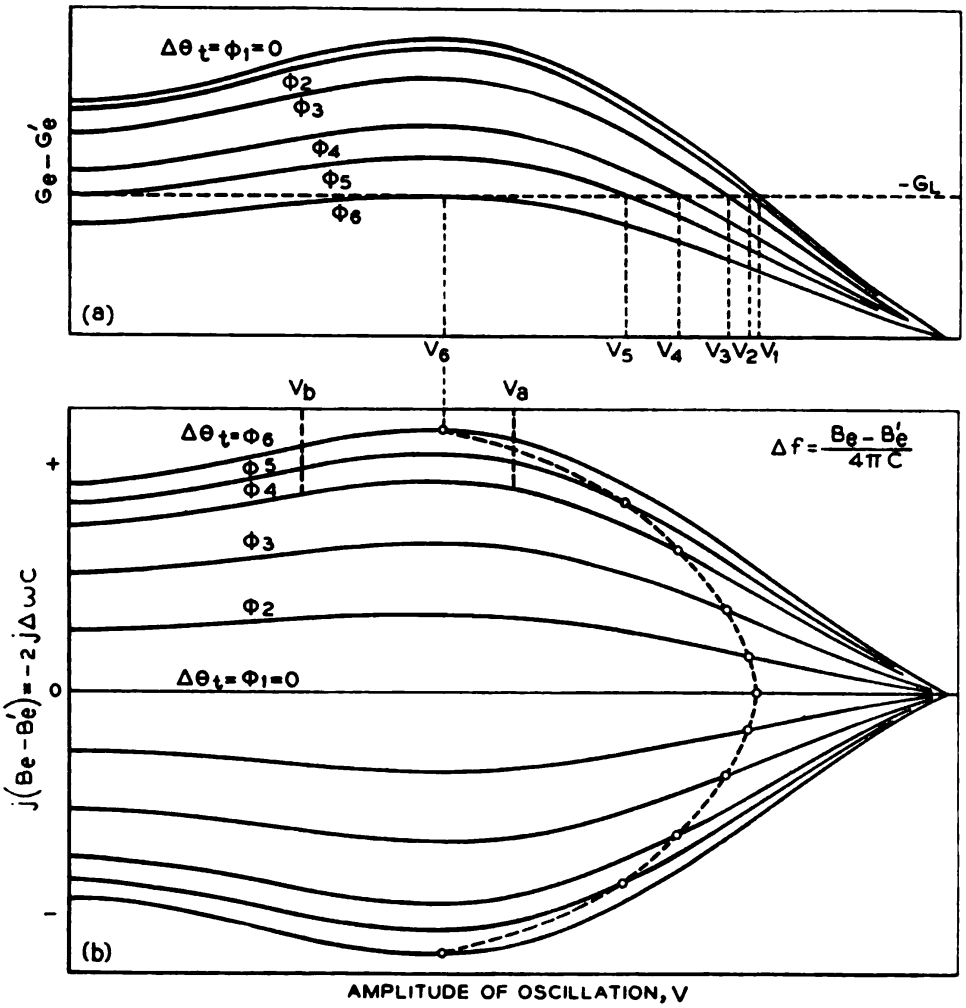

Fig. 30.—*a*. Theoretical variation of electronic conductance vs amplitude of oscillation in the case in which two components are in phase opposition. The parameter is the repeller transit phase. It is assumed that the two contributions have the same variation with this phase.

b. Susceptance component of electronic admittance as a function of amplitude for the case of phase opposition given in Fig. 30a. The parameter is the repeller phase. The dashed line shows the variation of amplitude with the susceptance shift.

repeller voltage is varied the amplitude of oscillation will be determined by the conductance limiting function. In the case of the susceptance we cannot determine the frequency from the intersection of the curve with a load line. The frequency of oscillation will be determined by the drift angle and the amplitude of oscillation. The amplitude variation with

Digitized by Google
Original from UNIVERSITY OF MICHIGAN
Generated on 2019-09-23 04:30 GMT / http://hdl.handle.net/2027/mdp.39015077775156
Public Domain, Google-digitized / http://www.hathitrust.org/access_use#pd-google

angle may be obtained from Fig. 30a, which gives the conductance family. This gives the frequency variation with angle indicated by the curve con-

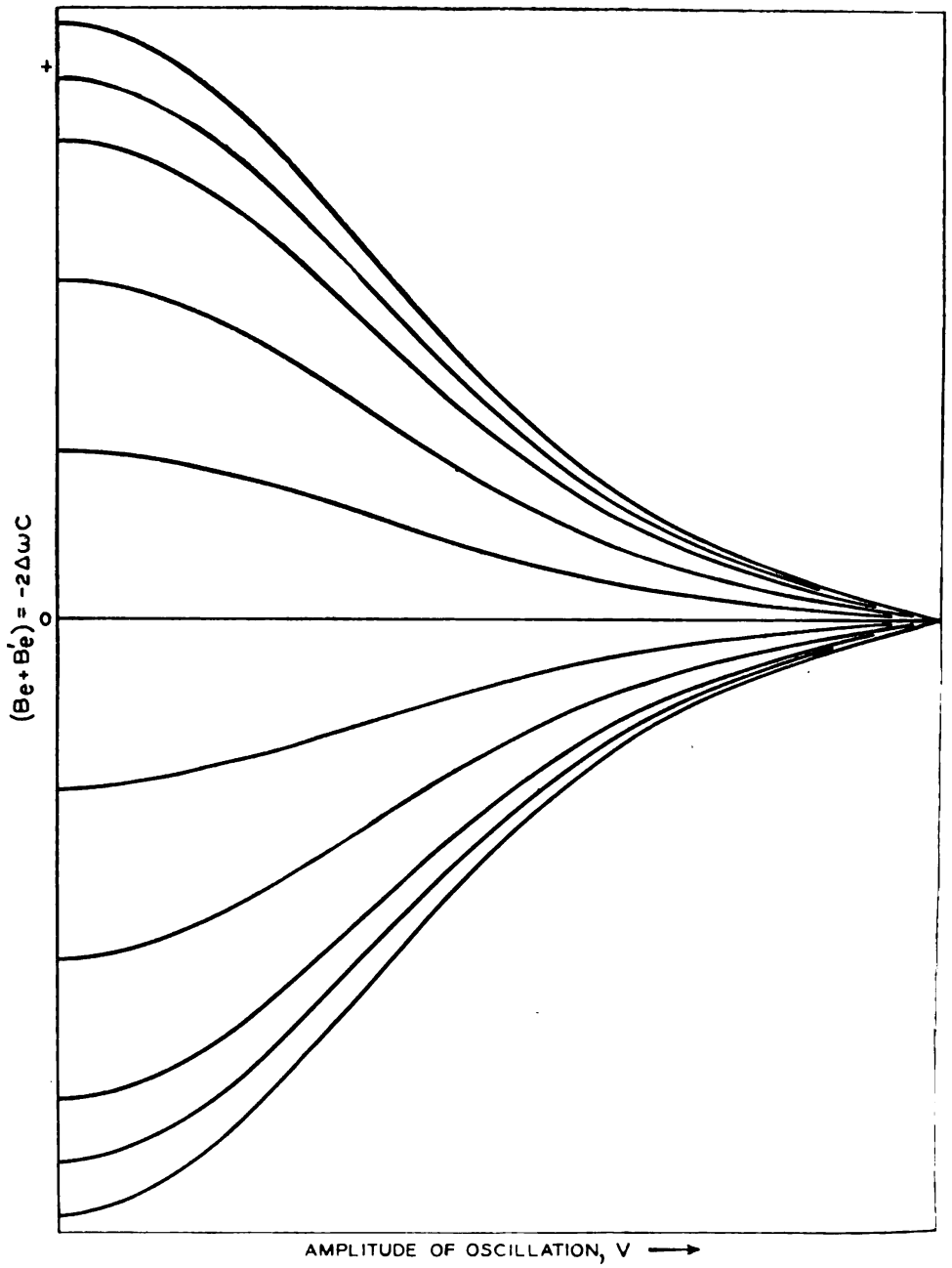

Fig. 31.—Theoretical variation of the susceptance components of electronic admittance vs amplitude of oscillation for the case in which two components of electronic susceptance are in phase addition.

necting the dots of Fig. 30b. On the assumption that $\Delta\theta_t$ and $\Delta\theta$ vary at the same rate with repeller voltage a symmetrical variation about $\Delta\theta = 0$ will occur as shown in Fig. 30b. However, from the arguments used con-

Digitized by Google
Original from UNIVERSITY OF MICHIGAN
Generated on 2019-09-23 04:30 GMT / http://hdl.handle.net/2027/mdp.39015077775156
Public Domain, Google-digitized / http://www.hathitrust.org/access_use#pd-google

cerning the conductance the actual case would involve a transition from the situation of Fig. 30b to that of Fig. 31. If a discontinuity in amplitude occurs in which the amplitude does not go to zero, it will be accompanied by a discontinuity in frequency, since the discontinuity in amplitude in general will cause a discontinuity in the susceptance. If this discontinuity in susceptance occurs between values of the amplitude such as V_a and V_b of Fig. 30, we observe that the direction of the frequency jump may be opposite to the previous variation. We also observe that if the rate of change of susceptance with amplitude is greater than the rate of change of susceptance with $\Delta\theta$, then in regions such as that lying between zero amplitude of V_b the rate of change of frequency with $\Delta\theta$ may reverse its direction.

One can see that because of the longer drift time contributing to the third transit the conductance arising on the third transit may be of the same order as that arising on the second transit. In oscillators in which several repeller modes, i.e., various numbers of drift angles, may be displayed, one finds that the hysteresis is most serious for the modes with the fewest cycles of drift in the repeller space. One might expect this, since for these modes the contribution from the cathode space is relatively more important.

Some final general remarks will be made concerning hysteresis. One thing is obvious from what has been said. With the admittance conditions as depicted, if all the electronic operating conditions are fixed and the load is varied hysteresis with load can exist. This was found to be true experimentally, and in the case of oscillators working into misterminated long lines it can produce disastrous effects. Where hysteresis is severe enough, it will be found that what we have chosen to call the sink margin will be much less than the theoretically expected value. An illustration of this is given in Fig. 109.

The explanation which we have given for the hysteresis in the reflex oscillator depends upon the existence of two sources of conductance. This was apparently a correct assumption in the case studied, since the elimination of the second source also eliminated the hysteresis. It is possible, however, to obtain hysteresis in a reflex oscillator with only a single source. This can occur if the phase of the electronic admittance is not independent of the amplitude. Normally, in adjusting the repeller voltage the value is chosen for the condition of maximum output. This means that the drift angle is set to a value to give maximum conductance for large amplitude. If the drift angle is then a function of the amplitude, this will mean that for small amplitude it will no longer be optimum. Thus, although the limiting function $\frac{J_1(CV)}{CV}$ tends to increase the electronic conductance as the amplitude declines, the phase factor will oppose this increase. If the phase factor depended sufficiently strongly on the amplitude, the decrease in G_e caused by

Digitized by Google
Original from UNIVERSITY OF MICHIGAN
Generated on 2019-09-23 04:31 GMT / http://hdl.handle.net/2027/mdp.39015077775156
Public Domain, Google-digitized / http://www.hathitrust.org/access_use#pd-google

the phase might outweigh the increase due to the function $\frac{J_1(C_1V)}{C_1V}$. As a result the conductance might have a maximum value for an amplitude greater than zero, leading to the conditions shown in Fig. 23, under which hysteresis can exist.

The first order theory for the reflex oscillator does not predict such an effect, since the phase is independent of amplitude. The second order theory gives the admittance as

$$Y_e = \frac{\beta_2 I_0 \theta}{2V_0} \cdot \frac{2J_1(X)}{X} e^{-j(\theta-(\pi/2))} \left(1 - \frac{1}{4\theta^2} \cdot \left[\tfrac{1}{2}X^2(X^2+1) - X^3\frac{J_0(X)}{X} - \frac{j}{2\theta}(2-X^2) - X\frac{J_0(X)}{J_1(X)}\right]\right) \tag{8.21}$$

The quantity appearing outside the brackets is the admittance given by the first order theory. The second order correction contains real and imaginary parts which are functions of X and hence of the amplitude of oscillation. Thus, for fixed d-c conditions the admittance phase depends upon the amplitude of oscillation and hence hysteresis might occur. It should be observed that the correction terms are important only for small values of the transit angle θ. In particular, this explanation would not suffice for the case described earlier since the design employed which eliminated the hysteresis left the variables of equation (8.21) unchanged.

IX. Effect of Load

So far we have considered the reflex oscillator chiefly from the point of view of optimum performance; that is, we have attempted chiefly to evaluate its performance when it is used most advantageously. There has been some discussion of non-optimum loading, but this has been incidental to the general purpose of the work. Oscillators frequently are worked into other than optimum loads, sometimes as a result of incorrect adjustment, sometimes through mistakes in design of equipment and quite frequently by intention in order to take advantage of particular properties of the reflex oscillator when worked into specific non-optimum loads.

In this section we will consider the effects of other than optimum loads on the performance of the reflex oscillator. We may divide this discussion into two major subdivisions classified according to the type of load. The first type we call fixed element loads, and the second variable element loads. The first type is constructed of arbitrary passive elements whose constants are independent of frequency. The second category includes loads constructed of the same type of elements but connected to the oscillator by lines of sufficient length so that the frequency variation of the load admittance is appreciably modified by the line.

Digitized by Google
Original from UNIVERSITY OF MICHIGAN
Generated on 2019-09-23 04:31 GMT / http://hdl.handle.net/2027/mdp.39015077775156
Public Domain, Google-digitized / http://www.hathitrust.org/access_use#pd-google

A. *Fixed Element Loads*

In this discussion it will be assumed initially that $\Delta\theta$, the phase angle of $-Y_e$, is not affected by frequency. The results will be extended later to account for the variation of $\Delta\theta$ with frequency. A further simplification is the use of the equivalent circuit of Fig. 118, Appendix I. Initially, the output circuit loss, R, will be taken as zero, so the admittance at the gap will be

$$Y_e = G_R + 2jM\Delta\omega/\omega + Y_L/N^2. \tag{9.1}$$[8]

Here, G_R is the resonator loss conductance, M is the resonator characteristic admittance, and Y_L is the load admittance.

We will now simplify this further by letting $G_R = 0$

$$Y_e = 2jM\Delta\omega/\omega + Y_L/N^2. \tag{9.2}$$

From Fig. 12 we see

$$G_L/N^2 = y_e[2J_1(X)/X] \cos\Delta\theta \tag{9.3}$$

$$\frac{B_L}{N^2} + \frac{2M\Delta\omega}{\omega} = -y_e[2J_1(X)/X] \sin\Delta\theta\,. \tag{9.4}$$

Now it is convenient to define quantities expressing power, conductance and susceptance in dimensionless form.

$$p = X^2G_L/2.5N^2y_e \tag{9.5}$$

$$G_1 = G_L/N^2y_e \tag{9.6}$$

$$B_1 = B_L/N^2y_e. \tag{9.7}$$

The power P produced by the electron stream and dissipated in G_L is related to p

$$P = \left(\frac{2.5I_0V_0}{\theta}\right)p. \tag{9.8}$$

In terms of p and G_1, (9.3) can be written

$$p = (1/1.25)(2.5p/G_1)^{-\frac{1}{2}}J_1[(2.5p/G_1)^{\frac{1}{2}}] \cos\Delta\theta. \tag{9.9}$$

By dividing (9.4) by (9.3), we obtain

$$\Delta\omega/\omega_0 = (-G_L/2N^2M) \tan\Delta\theta - B_L/2N^2M \tag{9.10}$$

$$-(2M/y_e)\Delta\omega/\omega_0 = G_1 \tan\Delta\theta + B_1. \tag{9.11}$$

[8] To avoid confusion on the reader's part, it is perhaps well to note that we are, for the sake of generality, changing nomenclature. Hitherto we have used Y_L to denote the load at the oscillator. Actually our load as the appendix shows is usually coupled by some transformer whose equivalent transformation ratio is $1/N^2$, so that the admittance at the gap will be Y_L/N^2.

Digitized by Google
Original from UNIVERSITY OF MICHIGAN
Generated on 2019-09-23 04:34 GMT / http://hdl.handle.net/2027/mdp.39015077775156
Public Domain, Google-digitized / http://www.hathitrust.org/access_use#pd-google

Equations (9.9) and (9.11) give the behavior of a reflex oscillator with zero output circuit loss as the load is changed. It is interesting to plot this behavior on a Smith chart.[9] Such a plot is known as a Rieke diagram or an impedance performance chart. Suppose we first make a plot for $\Delta\theta = 0$. This is shown in Fig. 32. Constant p contours are solid and, as

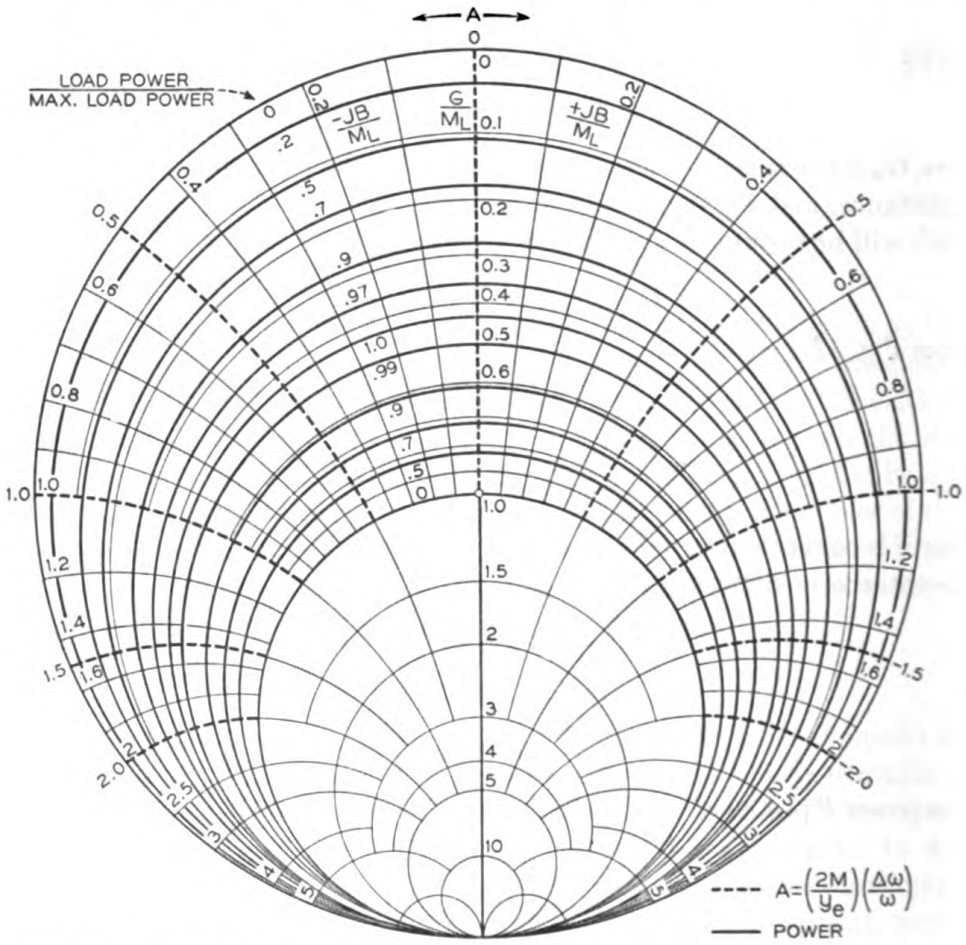

Fig. 32.—Theoretical Rieke diagram for a reflex oscillator operating with optimum drift angle. The resonator is assumed lossless. Admittances are normalized in terms of the small signal electronic admittance of the oscillator so that oscillation will stop for unity standing wave.

can be seen from the above, they will coincide with the constant conductance lines of the chart. Constant frequency curves are dashed and, for $\Delta\theta = 0$, they coincide with the locii of constant susceptance. The numbers on the frequency contours give values of $(2M/y_e)(\Delta\omega/\omega_0)$. The choice of units is such that $G_1 = 1$ means that the load conductance is just equal to small signal electronic conductance which, it will be recalled, is the starting condition for oscillation. Hence, the $G_1 = 1$ contour is a zero power contour. Any larger values of G_1 will not permit oscillation to start, so the G_1 contour

[9] P. H. Smith, "Transmission Line Calculator," *Electronics*, Jan. 1939, pp. 29-31.

Digitized by Google
Original from UNIVERSITY OF MICHIGAN
Generated on 2019-09-23 04:34 GMT / http://hdl.handle.net/2027/mdp.39015077775156
Public Domain, Google-digitized / http://www.hathitrust.org/access_use#pd-google

bounds a region of zero power commonly called the "sink," since all the frequency contours converge into it. The other zero power boundary is the outer boundary of the chart, $G_1 = 0$, which, of course, is an open circuit load. The power contours on this chart occur in pairs, except the maximum power contour which is single. These correspond to coupling greater than and less than the optimum.

The value of G_1 for any given power contour for $\Delta\theta = 0$ may be determined by referring to Fig. 9. We are assuming no resonator loss so we use the curve for which $G_R/y_e = 0$. From (9.5), if $p = 1$ we have $G_L/N^2y_e = 2.5/X^2$ which, substituted in (9.3), gives $XJ_1(X) = 1.25$. This is just the condition for maximum power output with no resonator loss. From this it can be seen that we have chosen a set of normalized coordinates. Hence, in using Fig. 9, we have $p = H/H_m$, where $H_m = .394$ is the maximum generalized efficiency. Thus, for any given value of p we let H in Fig. 9 have the value $.394p$ and determine the two values of G_1 corresponding to that contour.

From Fig. 32 we can construct several other charts describing the performance of reflex oscillators under other conditions. For instance, suppose we make $\Delta\theta$ other than zero. Such a condition commonly occurs in use either through erroneous adjustment of the repeller or through intentional use of the electronic tuning of the oscillator. We can construct a new chart for this condition using Fig. 32. Consider first the constant power contours. Suppose we consider the old contour of value p_n lying along a conductance line G_{1n}. To get a new contour, we can change the label from p_n to $p_m = p_n \cos\Delta\theta$, and we move the contour to a conductance line $G_n = G_m \cos\Delta\theta$. That this is correct can be seen by substituting these values in (9.9). Consider a given frequency contour lying along B_1. We shift each point of this contour along a constant conductance line G_{1n} an amount $B_m = G_{1n} \tan\Delta\theta$. It will be observed that this satisfied (9.11). In Fig. 33 this has been done for $\tan\Delta\theta = 1$, $\cos\Delta\theta = \sqrt{2}/2$.

Now let us consider the effect of resonator loss. Suppose we have a shunt resonator conductance G_R. Let

$$G_2 = G_R/y_e. \tag{9.12}$$

Then, if the total conductance is G_n, the fraction of the power produced which goes to the load is

$$f = (G_n - G_2)/G_n = G_1/(G_1 + G_2) \tag{9.13}$$

accordingly, we multiply each power contour label by the fraction f. Then we move all contour points along constant susceptance lines to new values

$$G_m = G_n - G_2 \tag{9.14}$$

In Fig. 34, this has been done to the contours of Fig. 32, for $G_2 = .3$.

Digitized by Google
Original from UNIVERSITY OF MICHIGAN
Generated on 2019-09-23 04:34 GMT / http://hdl.handle.net/2027/mdp.39015077775156
Public Domain, Google-digitized / http://www.hathitrust.org/access_use#pd-google

The diagrams so far obtained have been based on the assumption that $\Delta\theta$ has been held constant. To obtain such a diagram experimentally would be extremely difficult. It would require that, as the frequency changed through load pulling, and hence the total transit angle $\theta = 2\pi f\tau$ changed, an adjustment of the repeller voltage be made to correct the change. In actual practice, Rieke diagrams for a reflex oscillator are usually made holding the

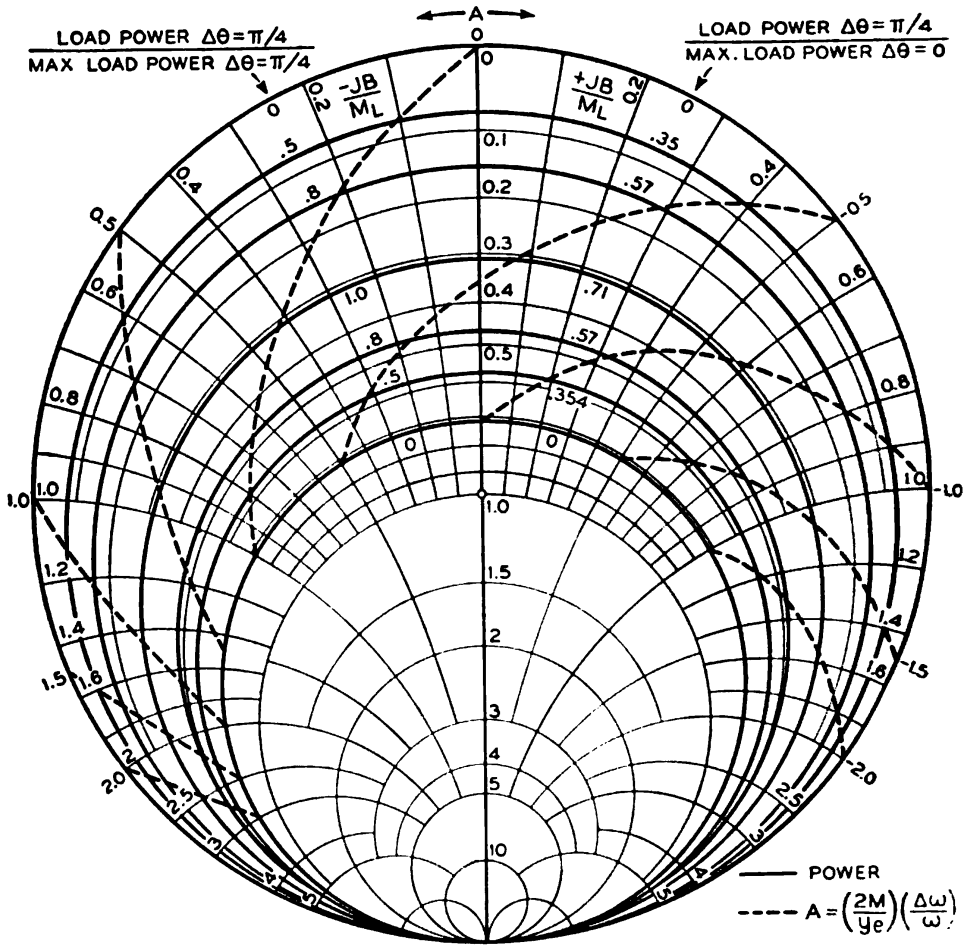

Fig. 33.—A transformation of the Rieke diagram of Fig. 32 showing the effect of shifting the drift angle away from the optimum by 45°.

transit time τ constant or in other words, with fixed operating voltages. What this does to the basic diagram of Fig. 32 is not difficult to discover, provided that $\delta\theta$ is sufficiently small so that we may ignore the variations of the Bessels functions with $\delta\theta$. We will first investigate the effect of fixed repeller voltage on the constant frequency contours. To do this we will rewrite (9.11), replacing $\Delta\theta$ by $\Delta\theta + \delta\theta$ and expand.

$$\delta\theta = \Delta\omega\tau = \frac{\Delta\omega}{\omega_0}\omega_0\tau \tag{9.15}$$

Digitized by Google
Original from UNIVERSITY OF MICHIGAN
Generated on 2019-09-23 04:34 GMT / http://hdl.handle.net/2027/mdp.39015077775156
Public Domain, Google-digitized / http://www.hathitrust.org/access_use#pd-google

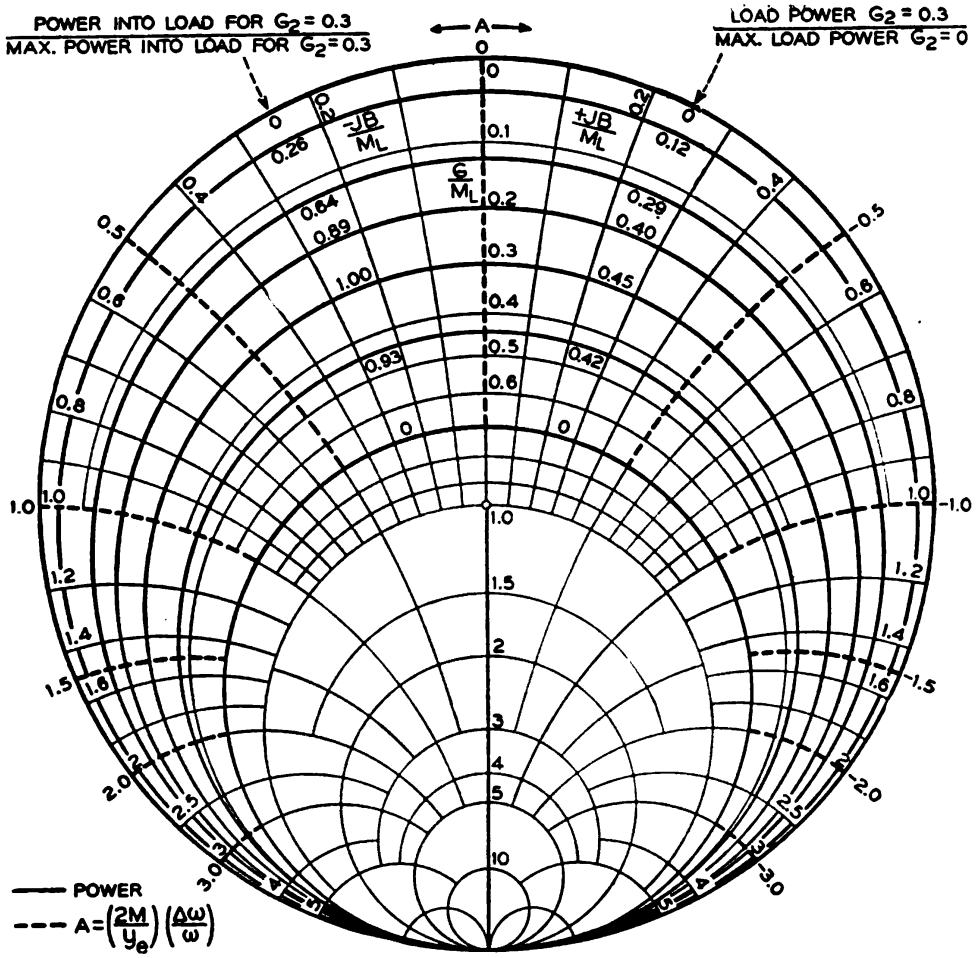

Fig. 34.—A transformation of the Rieke diagram of Fig. 32 to show the effect of the resonator loss if the phase angle is assumed to be optimum.

In rewriting (9.11) we will also replace G_1 by $G_1 + G_2$, to take resonator loss into account. We obtain for very small values of $\delta\theta$

$$-(2M/y_e)(\Delta\omega/\omega_0) = ((G_1 + G_2)\tan\Delta\theta + B_1)S \tag{9.16}$$

$$S = 1/(1 + (G_1 + G_2)\omega_0\tau/(2M/y_e)\cos^2\Delta\theta)$$

$$S = 1/(1 + \omega_0\tau/2Q\cos^2\Delta\theta). \tag{9.17}$$

Q is the loaded Q of the oscillator.

To obtain the new constant frequency contours in the case of $\Delta\theta = 0$ we shift each point of the old contour from its original position at a susceptance B_n along a constant conductance line G_n to a new susceptance line $B_m = B_n/S$. This neglects a second order correction. It will be observed that for small values of the conductance G_1 near the outer boundary, the frequency shifts will be practically unchanged, but near the sink where the

Digitized by Google
Original from UNIVERSITY OF MICHIGAN
Generated on 2019-09-23 04:35 GMT / http://hdl.handle.net/2027/mdp.39015077775156
Public Domain, Google-digitized / http://www.hathitrust.org/access_use#pd-google

conductance G_1 is large the effect is to shift the constant frequency contours along the sink boundary away from the zero susceptance line to larger susceptance values. Hence, the constant frequency contours no longer coincide with the constant susceptance contours, not even for $\Delta\theta = 0$.

The change in the power contours is considerably more marked. As the frequency of the oscillator changes the transit angle is shifted from the optimum value by an amount $\delta\theta = (\Delta\omega/\omega_0)\omega_0\tau$. Thus the electronic conductance is reduced in magnitude by a factor $\cos \frac{\Delta\omega}{\omega_0} \omega_0\tau$. In particular, for the sink contour where the load conductance is just equal to the electronic conductance we see that when the repeller voltage is held constant the 0 power contour lies not on the $G_1 = 1 - G_2$ contour but on the locus of values $G_1 = \cos \frac{\Delta\omega}{\omega_0} \omega_0\tau - G_2$.

In order to determine the power contours when the transit time rather than the transit angle is held constant we make use of (9.3) with addition of resonator loss. In normalized coordinates ((9.6) and (9.12)) and for a phase angle of electronic admittance $\delta\theta$ we have

$$G_1 + G_2 = \frac{2J_1(X)}{X} \cos \delta\theta . \tag{9.18}$$

From (9.5) and (9.13) we have for the power output

$$p = \frac{G_1}{G_1 + G_2} \frac{2XJ_1(X)}{2.5} \cos \delta\theta . \tag{9.19}$$

Along any constant frequency contour $\delta\theta$ is constant and has the value given by (9.15) in terms of ω_0 and $\omega_0\tau$. Hence, it will be convenient to plot $(G_1 + G_2)$ vs X for various values of $\delta\theta$ as a parameter. This has been done in Fig. 35. The angle $\delta\theta$ has been specified in terms of a parameter A which appears in the Rieke diagrams as a measure of frequency deviation.

$$A = \frac{2M}{y_e} \frac{\Delta\omega}{\omega_0} \tag{9.20}$$

In terms of the parameter A

$$\delta\theta = (y_e/2M)(\omega_0\tau)A . \tag{9.21}$$

Once we have the curves of Fig. 35 we can find the power for any point on the impedance performance chart. We may, for instance, choose to find the power along the constant frequency contours, for each of which A (or $\delta\theta$) has certain constant values. We assume some constant resonator loss G_2. Choosing a point along the contour is merely taking a particular value of G_1. Having $\delta\theta$, G_2 and G_1 we can obtain X from Fig. 35. Then, knowing X, we can calculate the power from (9.19).

Digitized by Google
Original from UNIVERSITY OF MICHIGAN
Generated on 2019-09-23 04:35 GMT / http://hdl.handle.net/2027/mdp.39015077775156
Public Domain, Google-digitized / http://www.hathitrust.org/access_use#pd-google

In constructing an impedance performance chart we want constant power contours. In obtaining these it is convenient to assume a given value of G_2. We will use $G_2 = .3$ as an example. Then we can use Fig. 35 and

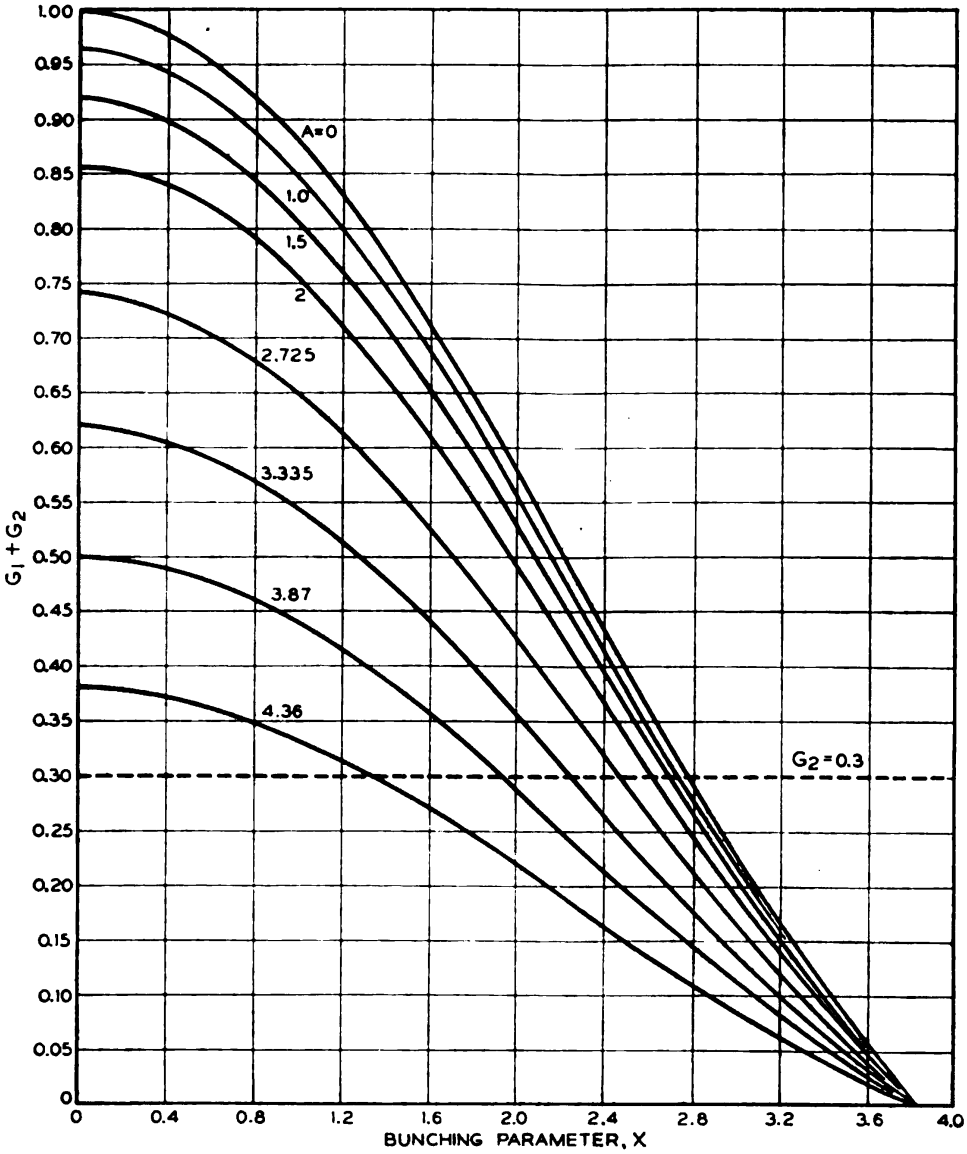

Fig. 35.—Curve of load plus loss conductance vs bunching parameter X for various values of a parameter A which gives the deviation in the drift time from the optimum time. The load and loss conductance are normalized in terms of the small signal electronic admittance. The horizontal line represents a loss conductance of $G_2 = .3$.

(9.19) to construct a family of curves giving p vs G_1 with A (or $\delta\theta$) as a parameter. In a particular case it was assumed that

$$M/y_e = 90$$

$$\omega_0\tau = 2\pi(7 + \tfrac{3}{4}).$$

Digitized by Google
Original from UNIVERSITY OF MICHIGAN
Generated on 2019-09-23 04:35 GMT / http://hdl.handle.net/2027/mdp.39015077775156
Public Domain, Google-digitized / http://www.hathitrust.org/access_use#pd-google

These values are roughly those for the 2K25 reflex oscillator. Figure 36 shows p vs G_1 for the particular parameters assumed above. The curves were obtained by assuming values of G_1 for an appropriate A and so obtaining values of X from Fig. 35. Then the power was calculated using (9.19) and so a curve of power vs G_1 for a particular value of A was constructed.

Figure 37 shows an impedance performance chart obtained from (9.16) and Fig. 36. In using Fig. 36 to obtain constant power contours, we need merely note the values of G_1 at which a horizontal line on Fig. 36 intersects the curves for various values of A. Each curve either intersects such a horizontal (constant power) line at two points, or it is tangent or it does not intersect. The point of tangency represents the largest value of A at which the power can be obtained, and corresponds to the points of the crescent shaped power contours of the impedance performance chart. The maximum power contour contracts to a point.

Along the boundary of the sink, for which $p = 0$, $X = 0$ and we have from (9.18)

$$G_1 = \cos \delta\theta - G_2 . \tag{9.22}$$

The results which we have obtained can be extended to include the case in which $\Delta\theta \neq 0$. Further, as we know from Appendix I, we can take into account losses in the output circuit by assuming a resistance in series with the load. In a well-designed reflex oscillator the output circuit has little loss. The chief effect of this small loss is to round off the points of the constant power contours.

In actually measuring the performance of an oscillator, output and frequency are plotted vs load impedance as referred to the characteristic impedance of the output line. Also, frequently the coupling is adjusted so that for a match (the center of the Smith chart) optimum power is obtained. We can transform our impedance performance chart to correspond to such a plot by shifting each point G, B on a contour to a new point

$$G_1 = G/G_{max}$$
$$B_1 = B/G_{max}$$

where G_{max} is the conductance for which maximum power is obtained. Such a transformation of Fig. 37 is shown in Fig. 38.

It will be noted in Fig. 38 that the standing wave ratio for 0 power, the sink margin, is about 2.3. This sink margin is nearly independent of the resonator loss for oscillators loaded to give maximum power at unity standing wave ratio, as has been discussed and illustrated in Fig. 10. If the sink margin must be increased or the pulling figure must be decreased[10] the coup-

[10] The pulling figure is arbitrarily defined as the maximum frequency excursion produced when a voltage standing wave ratio of $\sqrt{2}$ is presented to the oscillator and the phase is varied through 180°.

Digitized by Google
Original from UNIVERSITY OF MICHIGAN
Generated on 2019-09-23 04:35 GMT / http://hdl.handle.net/2027/mdp.39015077775156
Public Domain, Google-digitized / http://www.hathitrust.org/access_use#pd-google

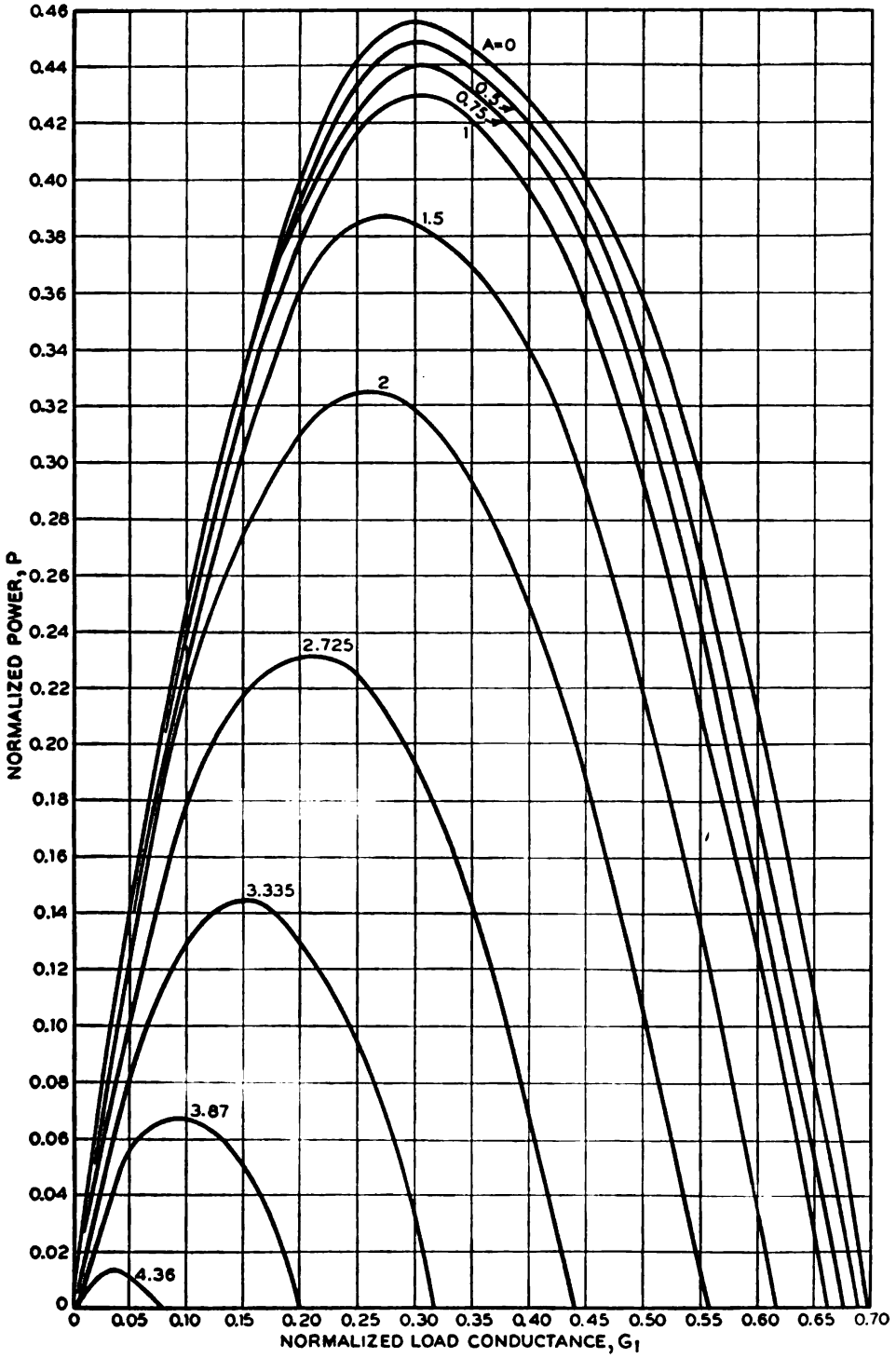

Fig. 36.—Normalized power vs normalized load conductance for various values of the parameter A which gives the deviation in drift time from the optimum drift time. These curves are computed for the case $G_2 = .3$. Optimum drift angle equal to 15.5 π radians and a ratio of characteristics resonator admittance to small signal electronic admittance of 90 is assumed.

Digitized by Google
Original from UNIVERSITY OF MICHIGAN
Generated on 2019-09-23 04:35 GMT / http://hdl.handle.net/2027/mdp.39015077775156
Public Domain, Google-digitized / http://www.hathitrust.org/access_use#pd-google

ling can be reduced so that for unity standing wave ratio the load conductance appearing at the gap is less than that for optimum power.

Finally, in making measurements the load impedance is usually evaluated at a point several wavelengths away from the resonator. If performance is plotted in terms of impedances so specified, the points on the contours of

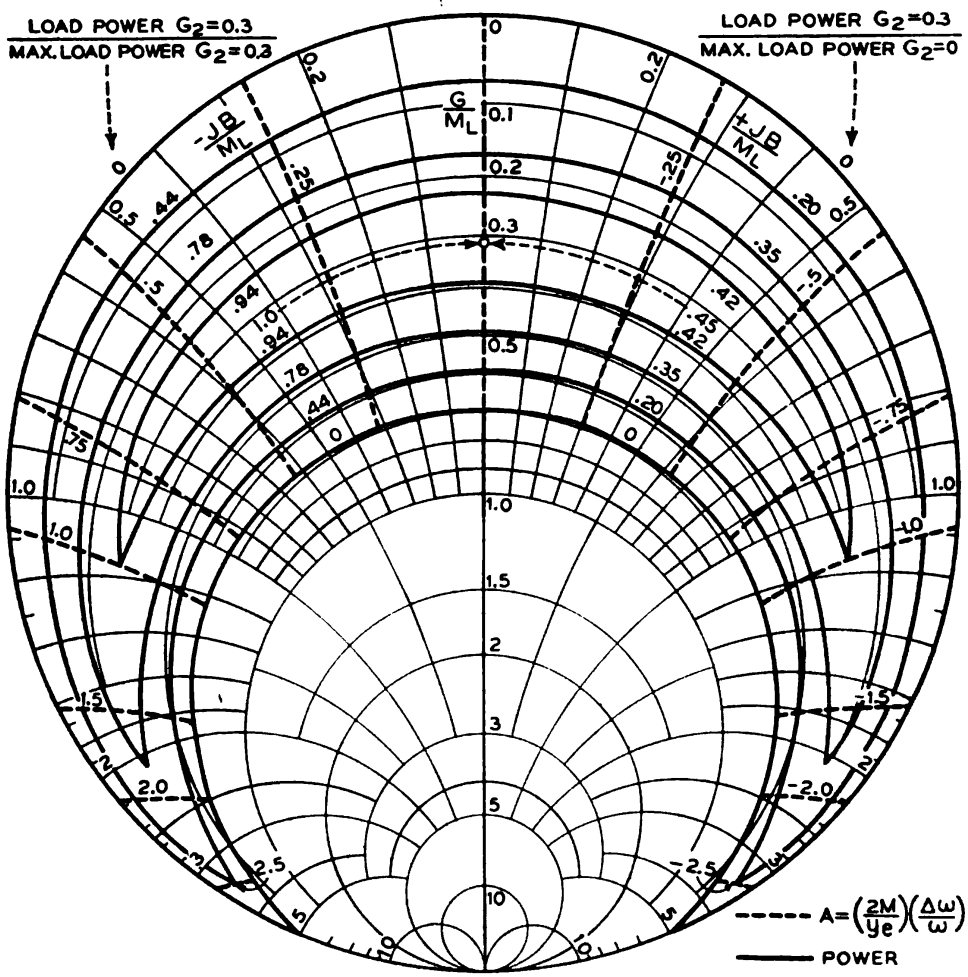

Fig. 37.—A Rieke diagram for a reflex oscillator having a lossy resonator, taking into account the variation of drift angle with frequency pulling. This results in closed power contours.

Fig. 38 appear rotated about the center. As the line length in wavelengths will be different for different frequencies, points on different frequency contours will be rotated by different amounts. This can cause the contours to overlap in the region corresponding to the zero admittance region of Fig 38. With very long lines, the contours may overlap over a considerable region. The multiple modes of oscillation which then occur are discussed in somewhat different terms in the following section.

Digitized by Google
Original from UNIVERSITY OF MICHIGAN
Generated on 2019-09-23 04:36 GMT / http://hdl.handle.net/2027/mdp.39015077775156
Public Domain, Google-digitized / http://www.hathitrust.org/access_use#pd-google

Figure 39 shows the performance chart of Fig. 38 as it would appear with the impedances evaluated at a point 5 wavelengths away from the resonator. Figure 71 of Section XIII shows an impedance performance chart for 2K25 reflex oscillator.

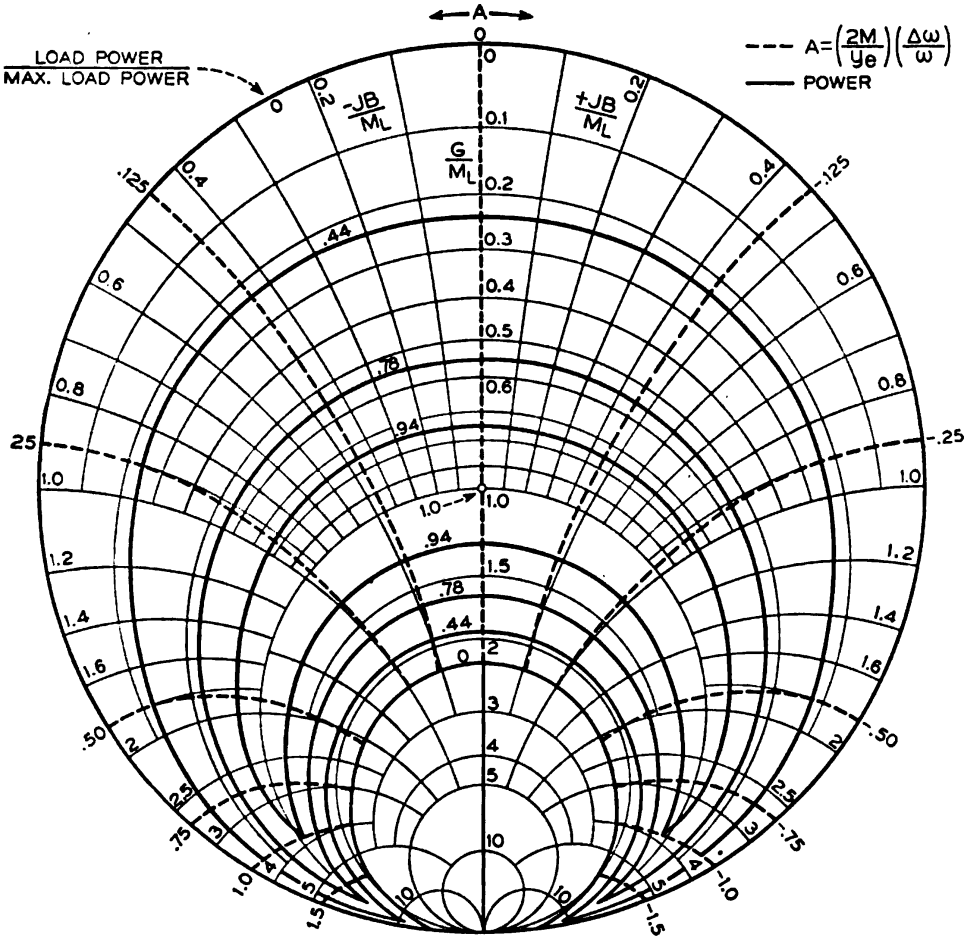

Fig. 38.—The Rieke diagram of Fig. 37 transformed to apply to the oscillator loaded for optimum power at unity standing wave.

B. *Frequency-Sensitive Loads—Long Line Effect*

When the load presented to a reflex oscillator consists of a long line mismatched at the far end, or contains a resonant element, the operation of a reflex oscillator, and especially its electronic tuning, may be very seriously affected.

For instance, consider the simple circuit shown in Fig. 40. Here M_R is the characteristic admittance of the reflex oscillator resonator as seen from the output line or wave guide and M_L is the characteristic impedance of a line load ℓ long, so terminated as to give a standing wave ratio, σ.

Digitized by Google
Original from UNIVERSITY OF MICHIGAN
Generated on 2019-09-23 04:36 GMT / http://hdl.handle.net/2027/mdp.39015077775156
Public Domain, Google-digitized / http://www.hathitrust.org/access_use#pd-google

In the simple circuit assumed there are essentially three variables; (1) the ratio of the characteristic admittance of the resonant circuit, M_R to

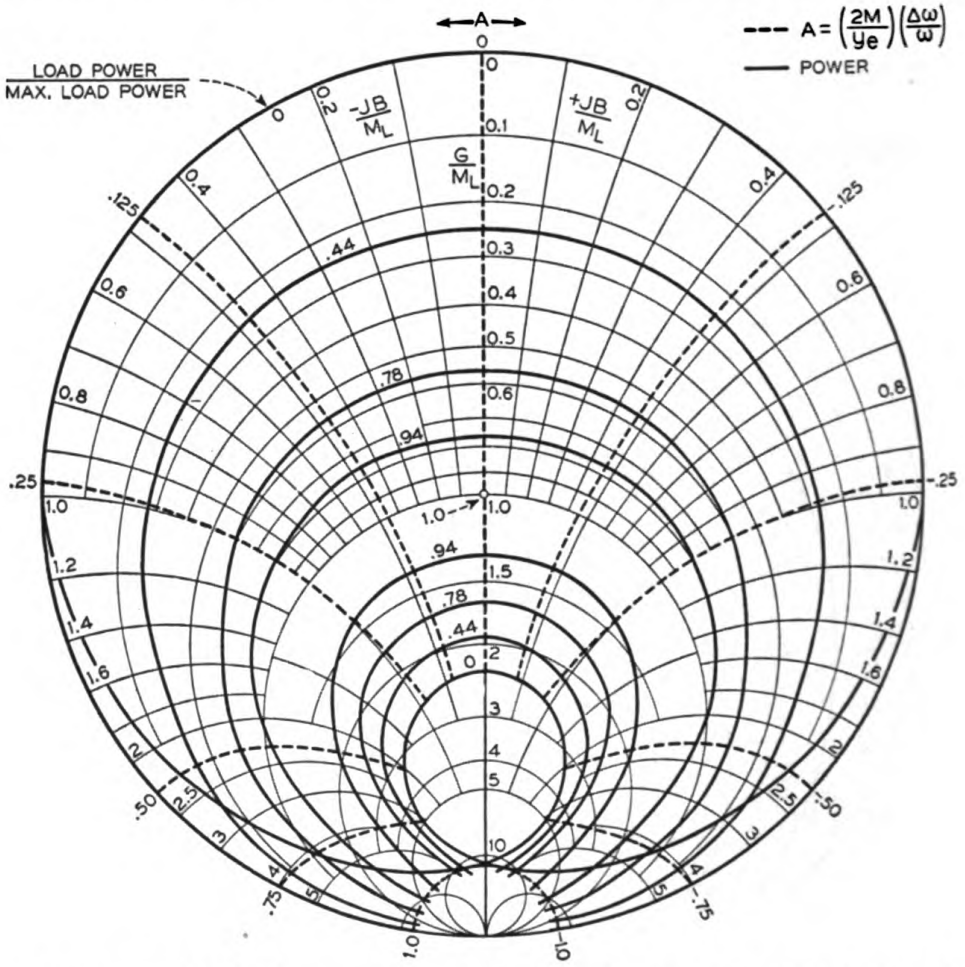

Fig. 39.—The Rieke diagram of Fig. 38 transformed to include the effect of a line five wave lengths long between the load and the oscillator.

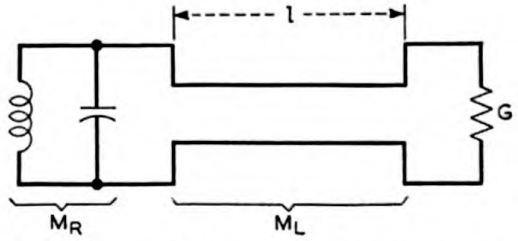

Fig. 40.—Equivalent circuit of a lossless resonator, a line and a mismatched load.

that of the line, M_L. This ratio will be called the external Q and signifid by Q_E

$$Q_E = M_R/M_L. \tag{9.23}$$

Digitized by Google
Original from UNIVERSITY OF MICHIGAN
Generated on 2019-09-23 04:36 GMT / http://hdl.handle.net/2027/mdp.39015077775156
Public Domain, Google-digitized / http://www.hathitrust.org/access_use#pd-google

For a lossless resonator and unity standing wave ratio, the loaded Q is equal to Q_E. For a resonator of unloaded Q, Q_0, and for unity standing wave ratio, the loaded Q, obeys the relation

$$1/Q = 1/Q_E + 1/Q_0 \tag{9.24}$$

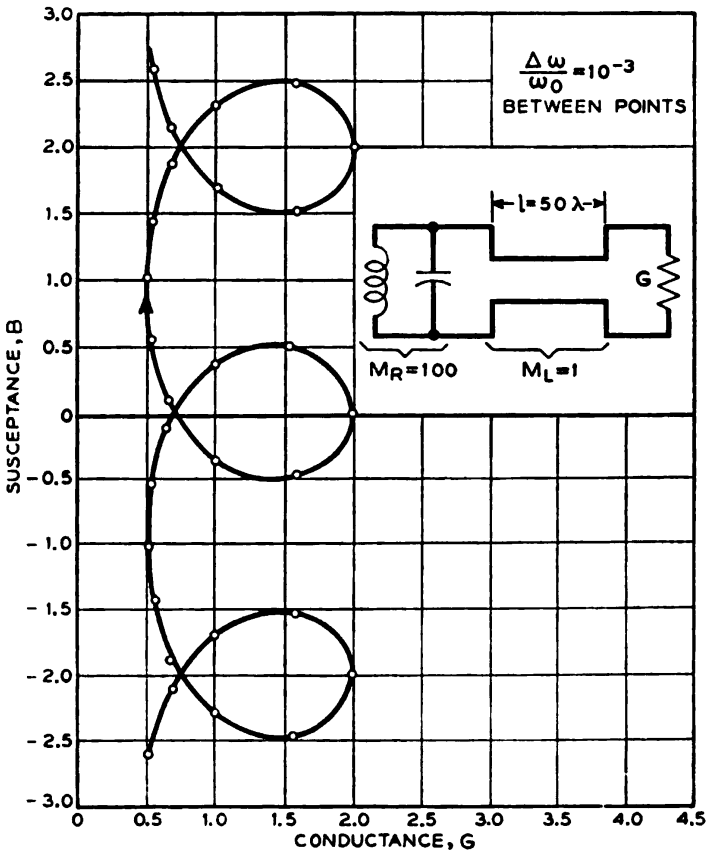

Fig. 41.—Susceptance vs conductance for a resonator coupled to a 50 wave length line terminated by a load having a standing wave ratio of 2. Characteristic admittance of the resonator is assumed to be equal to 100 in terms of a line characteristic admittance of unity. The circles mark off relative frequency increments

$$\frac{\Delta\omega}{\omega_0} = 10^{-3},$$

where ω_0 is the frequency of resonance.

(2) the length of the line called θ when measured in radians or n when measured in wavelengths, (3) the standing wave ratio σ.

Figures 41 and 42 show admittance plots for two resonant circuits loaded by mismatched lines of different lengths. The feature to be observed is the loops, which are such that at certain points the same admittance is achieved at two different frequencies. It is obvious that a line representing $-Y_s$

Digitized by Google
Original from UNIVERSITY OF MICHIGAN
Generated on 2019-09-23 04:36 GMT / http://hdl.handle.net/2027/mdp.39015077775156
Public Domain, Google-digitized / http://www.hathitrust.org/access_use#pd-google

may cut such a curve at more than one point: thus, oscillation at more than one frequency is possible. Actually, there may be three intersections per loop. The two of these for which the susceptance B is increasing with frequency represent stable oscillation; the intersection at which B is decreasing with frequency represents an unstable condition.

The loops are of course due to reactance changes associated with variation of the electrical length of the line with frequency. Slight changes in tuning of the circuit or slight changes in the length of the line shift the loops up or down, parallel to the susceptance axis. Thus, whether the electronic admittance line actually cuts a loop, giving two possible oscillating frequencies, may depend on the exact length of the line as well as on the existence of loops. The frequency difference between loops is such as to change the electrical length of the line by one-half wavelength.

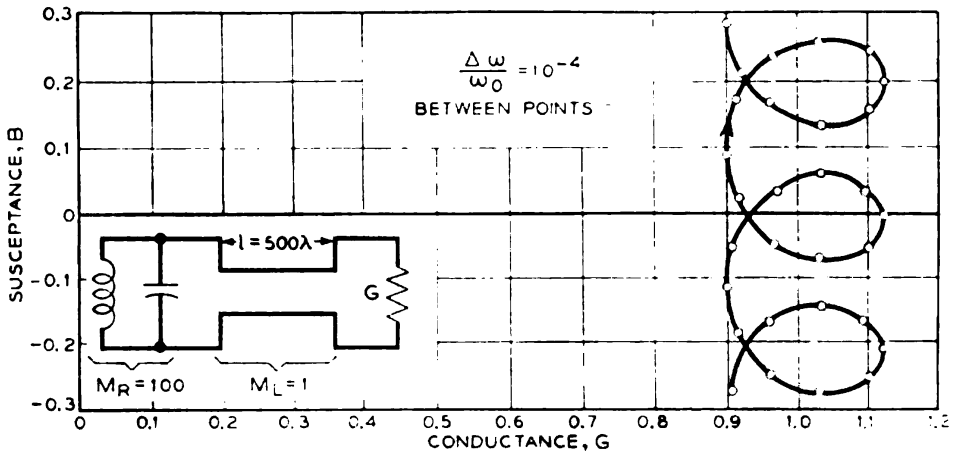

Fig. 42.—Susceptance vs conductance for line 500 wave lengths long terminated by a load having a standing wave ratio of 1.11. Circles mark off relative frequency increments of 10^{-4}. Characteristic admittance to the resonator equals 100.

The existence or absence of loops and their size depend on all three parameters. Things which promote loops are:

Low ratio of M_R/M_L or Q_R

Large n or θ

High σ

As any parameter is changed so as to promote the existence of loops, the Y curve first has merely a slight periodic variation from the straight line for a resistively loaded circuit. Further change leads to a critical condition in which the curve has cusps at which the rate of change of admittance with frequency is zero. If the electronic admittance line passes through a cusp,

Digitized by Google
Original from UNIVERSITY OF MICHIGAN
Generated on 2019-09-23 04:36 GMT / http://hdl.handle.net/2027/mdp.39015077775156
Public Domain, Google-digitized / http://www.hathitrust.org/access_use#pd-google

the frequency of oscillation changes infinitely rapidly with load. Still further change results in the formation of loops. Further change results in expansion of loops so that they overlap, giving more than three intersections with the electronic admittance line.

Loops may exist for very low standing wave ratios if the line is sufficiently long. Admittance plots for low standing wave ratio are very nearly cycloidal in shape; those for higher standing wave ratios are similar to cycloids in appearance but actually depart considerably from cycloids in exact form.

By combining the expression for the near resonance admittance of a tuned circuit with the transmission line equation for admittances, the expression for these admittance curves is obtained. Assuming the termination to be an admittance Y_T which at frequency ω_0 is θ_0 radians from the resonator,

$$Y = j2M_R\Delta\omega/\omega_0 + M_L\frac{(Y_T/M_L) + j\tan\theta_0(1 + \Delta\omega/\omega_0)}{1 + j(Y_T/M_L)\tan\theta_0(1 + \Delta\omega/\omega_0)}. \quad (9.25)$$

The critical relation of parameters for which a cusp is formed is important, for it divides conditions for which oscillation is possible at one frequency only and those for which oscillation is possible at two frequencies. This cusp corresponds to a condition in which the rate of change with frequency of admittance of the mismatched line is equal and opposite to that of the circuit. This may be obtained by letting Y_T be real.

$$Y_T/M_L > 1, \qquad \theta_0 = n\pi \text{ where } n \text{ is an integer.}$$

The standing wave ratio is then

$$\sigma = Y_T/M_L. \quad (9.26)$$

The second term on the right of (9.25) is then

$$Y_2 = M_L\left(\frac{\sigma + j\tan\theta_0\Delta\omega/\omega_0)}{1 + j\sigma\tan\theta_0\Delta\omega/\omega_0}\right). \quad (9.27)$$

For very small values of $\Delta\omega$ we see that very nearly

$$Y_2 = M_L[\sigma - j(\sigma^2 - 1)\theta_0\Delta\omega/\omega_0]. \quad (9.28)$$

Thus for the rate of change of total admittance to be zero

$$2M_R = M_L(\sigma^2 - 1)\theta_0$$

$$\theta_0 = 2(M_R/M_L)(\sigma^2 - 1)$$

$$= 2Q_E/(\sigma^2 - 1). \quad (9.30)$$

Thus, the condition for no loops, and hence, for a single oscillating frequency, may be expressed

$$\theta_0 < 2Q_E/(\sigma^2 - 1) \quad (9.31)$$

Digitized by Google
Original from UNIVERSITY OF MICHIGAN
Generated on 2019-09-23 04:37 GMT / http://hdl.handle.net/2027/mdp.39015077775156
Public Domain, Google-digitized / http://www.hathitrust.org/access_use#pd-google

or

$$\sigma < \sqrt{1 + 2Q_E/\theta_0}.$$

We will remember that θ_0 is the length of line in radians, σ is the standing wave ratio, measured as greater than unity, and Q_E is the external Q of the resonator for unity standing wave ratio.

Replacing a given length of line by the same length of wave guide, we find that the phase angle of the reflection changes more rapidly with frequency, and instead of (9.31) we have the condition for no loops as

$$\theta < 2Q_E(1 - (\lambda/\lambda_0)^2)/(\sigma^2 - 1) \tag{9.32}$$

$$\sigma < \sqrt{1 + 2Q_E(1 - (\lambda/\lambda_0)^2)/\theta_0}.$$

Here λ is the free space wavelength and λ_0 is the cutoff wavelength of the guide.

Equations (9.32) are for a particular phase of standing wave, that is, for relations of Y_T and θ_0 which produce a loop symmetrical above the G axis. Loops above the G axis are slightly more looped than loops below the G axis because of the increase of θ_0 with frequency. For reasonably long lines, (9.32) applies quite accurately for formation of loops in any position; for short lines loops are of no consequence unless they are near the G axis.

An imporant case is that in which the resonant load is coupled to the resonator by means of a line so short that it may be considered to have a constant electrical length for all frequencies of interest. The resonant load will be assumed to be shunted with a conductance equal to the characteristic admittance of the line. As the multiple resonance of a long mismatched line resulted in formation of many loops, so in this case we would rightly suspect the possibility of a single loop.

If the resonant load is $\frac{1}{4}$, $\frac{3}{4}$, etc. wavelengths from the resonator, and both resonate at the same frequency, a loop is formed symmetrical about the G axis. Figure 43 is an admittance curve for resonator and load placed $\frac{1}{4}$ wavelength apart. Tuning either resonator or load moves this loop up or down.

If the distance from resonator to resonant load is varied above or below a quarter wave distance, the loop moves up or down and expands. This is illustrated by an eighth wavelength diagram for the same resonator and load as of Fig. 43 shown in Fig. 44.

When the distance from the resonator to the resonant load, including the effective length of the coupling loop, is $\frac{1}{2}$, 1, $1\frac{1}{2}$, etc. wavelengths, for frequencies near resonance the resonant load is essentially in shunt with the resonator, and its effect is to increase the loaded Q of the resonator. An admittance curve for the case is shown in Fig. 45. In this case the loops

Generated on 2019-09-23 04:37 GMT / http://hdl.handle.net/2027/mdp.39015077775156
Public Domain, Google-digitized / http://www.hathitrust.org/access_use#pd-google
Digitized by Google
Original from UNIVERSITY OF MICHIGAN

have moved considerably away in frequency, and expanded tremendously. There are still recrossings of the axis near the origin, however, as indicated in this case by the dashed line which represents 2 crossings, in this case about 4% in frequency above and below the middle crossing if the length of the line ℓ is $\lambda/2$.

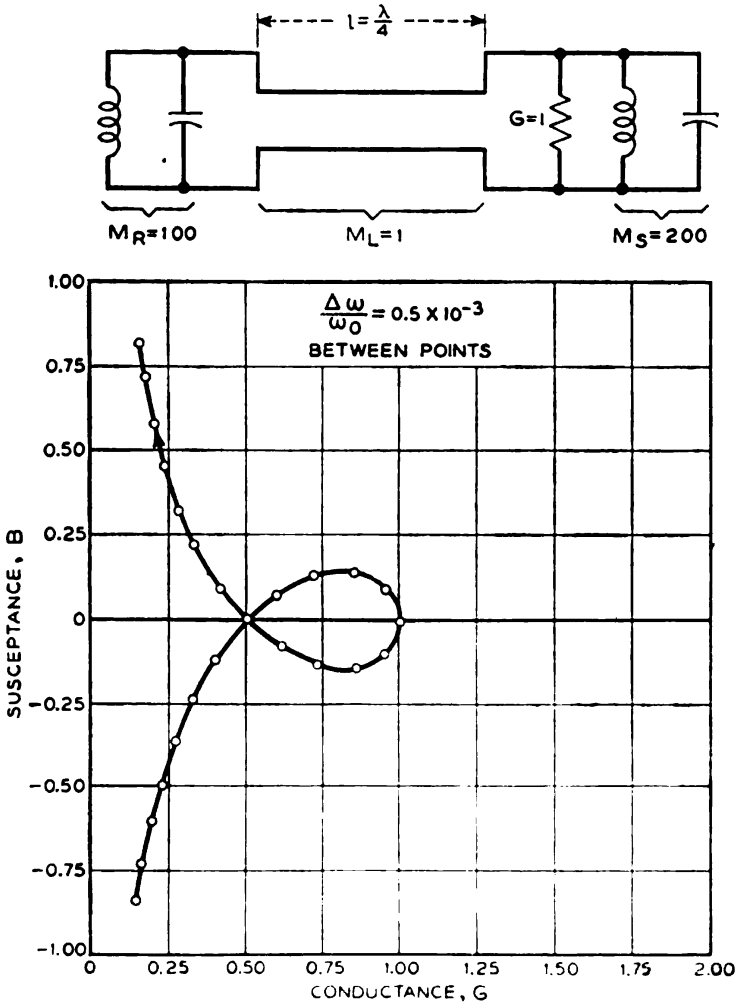

Fig. 43.—Susceptance vs conductance for two resonators coupled by a quarter wave line. The resonator at which the admittance is measured has a characteristic admittance of 100 in terms of a line characteristic admittance of unity. The other resonator has a characteristic admittance of 200 and a shunt conductance of unity. The circles mark off relative frequency increments of $\frac{1}{2} \times 10^{-3}$ in terms of the resonant frequency.

As a sort of horrible example, an admittance curve for a high Q load 50 wavelengths from the resonator was computed and is shown in Fig. 46. Only a few of the loops are shown.

Admittance curves for more complicated circuits such as impedance transformers can be computed or obtained experimentally.

Digitized by Google
Original from UNIVERSITY OF MICHIGAN
Generated on 2019-09-23 04:37 GMT / http://hdl.handle.net/2027/mdp.39015077775156
Public Domain, Google-digitized / http://www.hathitrust.org/access_use#pd-google

As has been stated, one of the most serious effects of such mismatched long line or resonant loads is that on the electronic tuning. For instance, consider the circuit admittance curve to be that shown in Fig. 47, and the minus electronic admittance curve to be a straight line extending from the origin. As the repeller voltage is varied and this is swung down from the $+B$ axis its extreme will at some point touch the circuit admittance line

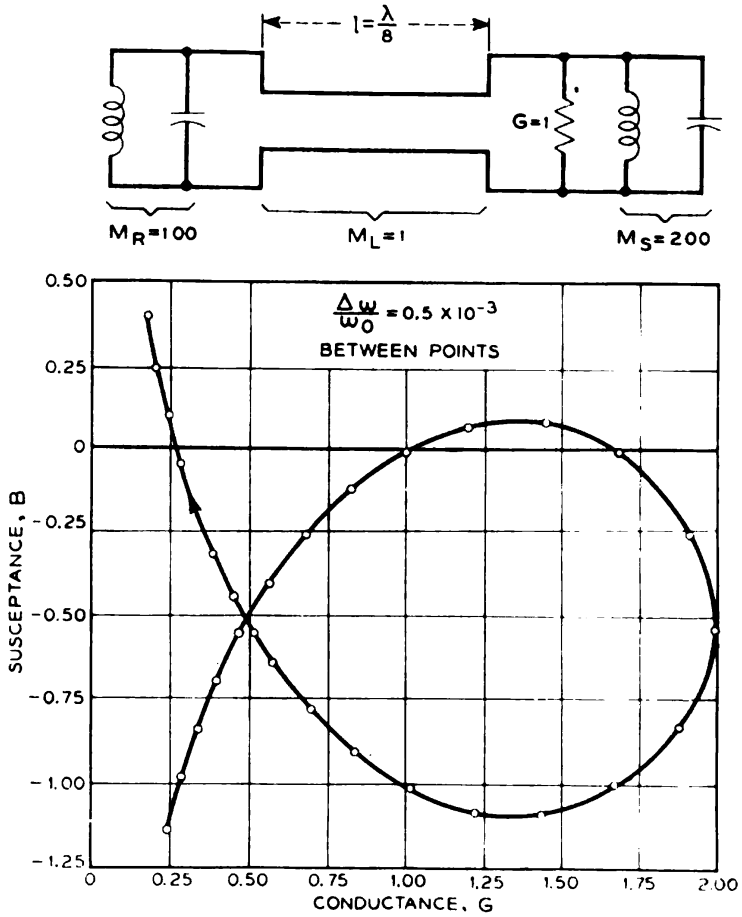

Fig. 44.—Susceptance vs conductance for the same resonators as of Fig. 43 coupled by a one-eighth wave line.

and oscillation will commence. As the line is swung further down, the frequency will decrease. Oscillation will increase in amplitude until the $-Y_e$ line is perpendicular to the Y line. From that point on oscillation will decrease in amplitude until the $-Y_e$ line is parallel to the Y curve on the down side of the loop. Beyond this point the intersection cannot move out on the loop, and the frequency and amplitude will jump abruptly to correspond with the other intersection. As the $-Y_e$ line rotates further,

Digitized by Google
Original from UNIVERSITY OF MICHIGAN
Generated on 2019-09-23 04:37 GMT / http://hdl.handle.net/2027/mdp.39015077775156
Public Domain, Google-digitized / http://www.hathitrust.org/access_use#pd-google

amplitude will decrease and finally go to zero when the end of the $-Y_e$ line touches the Y curve. If the $-Y_e$ line is rotated back, a similar phenomenon is observed. This behavior and the resulting electronic tuning characteristic are illustrated in Figs. 47 and 48. Such electronic tuning

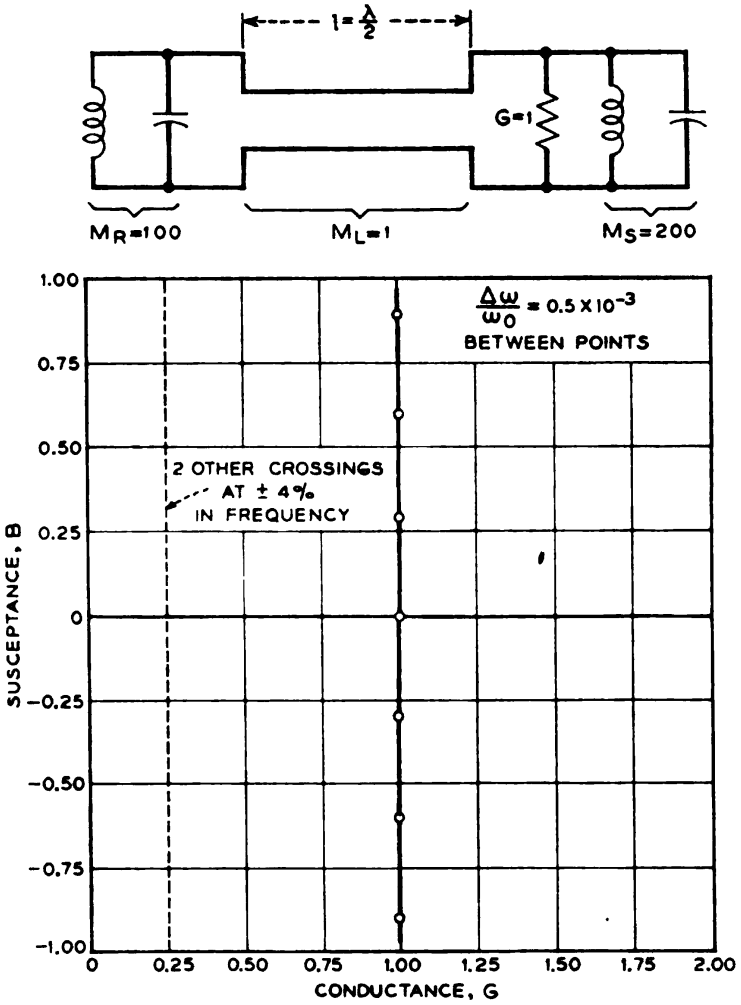

Fig. 45.—Susceptance vs conductance for the same resonators as of Fig. 43 coupled by a one-half wave line. The dash line indicates two other crossings of the 0 susceptance axis, at frequencies ±4% from the resonant frequency of the resonators.

characteristics are frequently observed when a reflex oscillator is coupled tightly to a resonant load.

C. *Effect of Short Mismatched Lines on Electronic Tuning*

In the foregoing, the effect of long mismatched lines in producing additional multiple resonant frequencies and possible modiness in operation has

Digitized by Google
Original from UNIVERSITY OF MICHIGAN
Generated on 2019-09-23 04:37 GMT / http://hdl.handle.net/2027/mdp.39015077775156
Public Domain, Google-digitized / http://www.hathitrust.org/access_use#pd-google

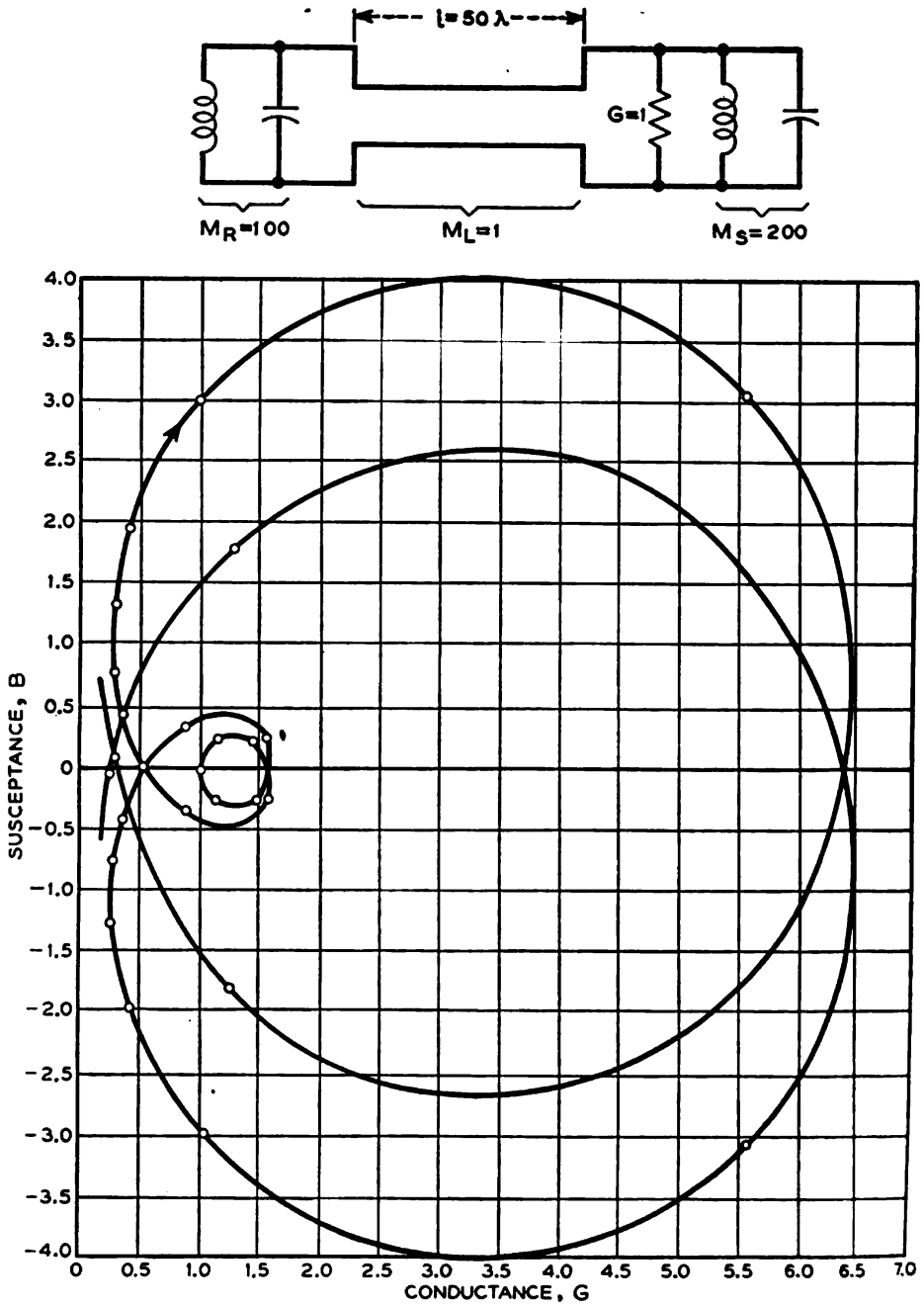

Fig. 46.—Susceptance vs conductance for the resonators of Fig. 43 coupled by a line 50 wave lengths long.

been explained. The effect of such multiple resonance on electronic tuning has been illustrated in Fig. 48.

If a short mismatched line is used as the load for a reflex oscillator, there

Digitized by Google
Original from UNIVERSITY OF MICHIGAN
Generated on 2019-09-23 04:38 GMT / http://hdl.handle.net/2027/mdp.39015077775156
Public Domain, Google-digitized / http://www.hathitrust.org/access_use#pd-google

may be no additional modes, or such modes may be so far removed in frequency from the fundamental frequency of the resonator as to be of little

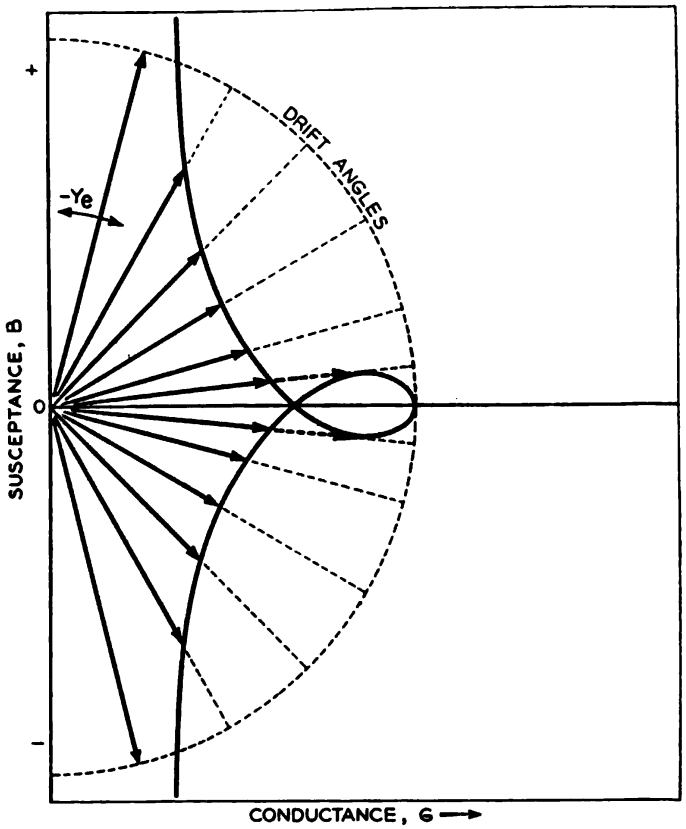

Fig. 47.—Behavior of the intersection between a circuit admittance line with a loop and the negative of the electronic admittance line of a reflex oscillator as the drift angle is varied (circuit hysteresis).

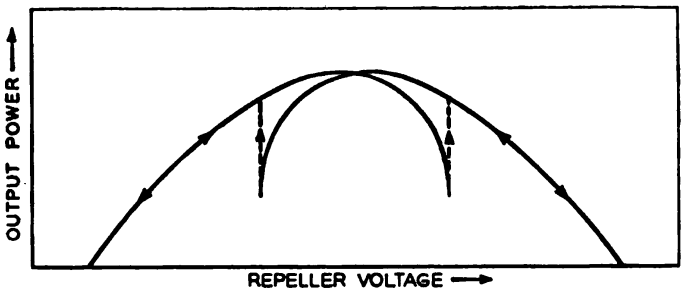

Fig. 48.—Output vs repeller voltage for the conditions obtaining in Fig. 47.

importance. Nonetheless, the short line will add a frequency-sensitive reactance in shunt with the resonant circuit, and hence will change the characteristic admittance of the resonator.

Digitized by Google
Original from UNIVERSITY OF MICHIGAN
Generated on 2019-09-23 04:38 GMT / http://hdl.handle.net/2027/mdp.39015077775156
Public Domain, Google-digitized / http://www.hathitrust.org/access_use#pd-google

Imagine, for instance, that we represent the resonator and the mismatched line as in shunt with a section of line N wavelengths or θ radians long misterminated in a frequency insensitive manner so as to give a standing wave ratio σ. If M_L is the characteristic admittance of the line, the admittance it produces at the resonator is

$$Y_L = M_L \frac{\sigma + j \tan \theta}{1 + j\sigma \tan \theta}. \tag{9.33}$$

Now, if the frequency is increased, θ is made greater and Y is changed.

$$\partial Y_L/\partial\theta = M_L \frac{j(1 - \sigma^2) \sec^2 \theta}{(1 + j\sigma \tan \theta)^2}. \tag{9.34}$$

We are interested in the susceptive component of change. If

$$Y_L = G_L + jB_L \tag{9.35}$$

we find

$$\partial B_L/\partial\theta = M_L \frac{(1 - \sigma^2)(1 - \sigma^2 \tan^2 \theta) \sec^2 \theta}{(1 + \sigma^2 \tan^2 \theta)}. \tag{9.36}$$

Now, if frequency is changed by an amount df, θ will increase by an amount $\theta(df/f)$ and B_L will change by an amount

$$dB_L = (\partial B_L/\partial\theta)(2\pi N)(df/f). \tag{9.37}$$

We now define a parameter M_M expressing the effect of the mismatch as follows

$$\pi(\partial B_L/\partial\theta) = M_M. \tag{9.38}$$

Then

$$dB_L = 2NM_M(df/f). \tag{9.39}$$

If the characteristic admittance of the resonator is M_R, then the characteristic admittance of the resonator plus the line is

$$M = M_R + NM_M. \tag{9.40}$$

If, instead of a coaxial line, a wave guide is used, and λ_0 and λ are the cutoff and operating wavelengths, we have

$$dB_L = 2NM_M(df/f)(1 - (\lambda/\lambda_0)^2)^{-\frac{1}{2}} \tag{9.41}$$

and

$$M = M_R + NM_M(1 - (\lambda/\lambda_0)^2)^{-\frac{1}{2}} \tag{9.42}$$

In Fig. 49 contour lines for M_M constant are plotted on a Smith Chart (reflection coefficient plane). Over most of the plane M_M has a moderate

Digitized by Google
Original from UNIVERSITY OF MICHIGAN
Generated on 2019-09-23 04:38 GMT / http://hdl.handle.net/2027/mdp.39015077775156
Public Domain, Google-digitized / http://www.hathitrust.org/access_use#pd-google

positive value tending to increase characteristic admittance and hence decrease electronic tuning. Over a very restricted range in the high admittance region M_M has large negative values and over a restricted range outside of this region M_M has large positive values.

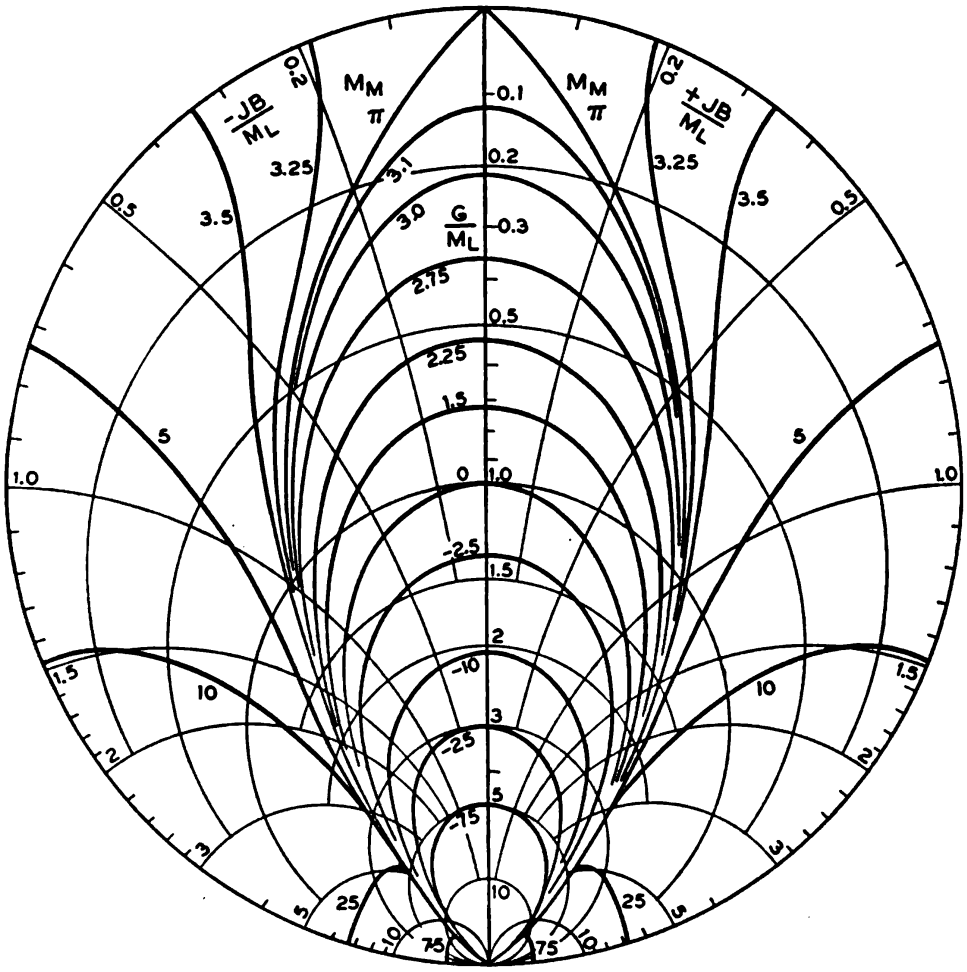

Fig. 49.—Lines of constant value of a parameter M_M shown on a chart giving the conductance and susceptance of the terminating admittance of a short line. The parameter plotted multiplied by the number of wave lengths in the line gives the additional characteristic admittance due to the resonant effects of the line. The parameter M_M is of course 0 for terminated lines (center of chart).

This is an appropriate point at which to settle the issue: what do we mean by a "short line" as opposed to a "long line." For our present purposes, a short line is one short enough so that M_M does not change substantially over the frequency range involved. Thus whether a line is short or not depends on the phase of the standing wave at the resonator (the position

Digitized by Google
Original from UNIVERSITY OF MICHIGAN
Generated on 2019-09-23 04:38 GMT / http://hdl.handle.net/2027/mdp.39015077775156
Public Domain, Google-digitized / http://www.hathitrust.org/access_use#pd-google

on the Smith Chart) as well as on the length of the line. M_M changes most rapidly with frequency in the very high admittance region.

As a simple example of the effect of a short mismatched line on electronic tuning between half power points, consider the case of a reflex oscillator with a lossless resonator so coupled to the line that the external Q is 100 and the electronic conductance is 3 in terms of the line admittance. Suppose we couple to this a coaxial line 5 wavelengths long with a standing wave ratio $\sigma = 2$, vary the phase, and compute the electronic tuning for various

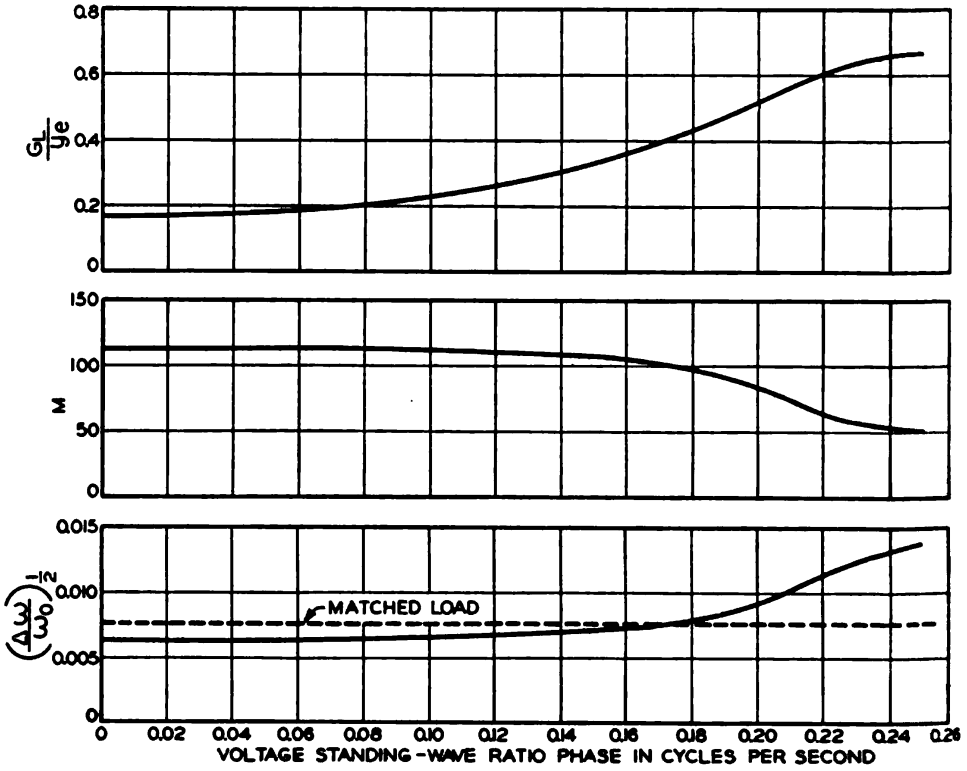

Fig. 50.—The normalized load conductance, the characteristic admittance of the resonator and the normalized electronic tuning range to half power plotted vs standing wave ratio phase for a particular case involving a short misterminated line. The electronic tuning for a matched line is shown as a heavy horizontal line in the plot of $(\Delta\omega/\omega_0)_{\frac{1}{2}}$.

phases. We can do this by obtaining the conductance and M_L from Fig. 49 and using Fig. 15 to btain $(\Delta\omega/\omega_0)_{\frac{1}{2}}$. In Fig. 50, the parameters G_L/y_e (the total characteristic admittance including the effect of the line), N, and, finally, $(\Delta\omega/\omega_0)_{\frac{1}{2}}$ have been plotted vs standing wave phase in cycles. $(\Delta\omega/\omega_0)_{\frac{1}{2}}$ for a matched load is also shown. This example is of course not typical for all reflex oscillators: in some cases the electronic tuning might be reduced or oscillation might stop entirely for the standing wave phases which produce high conductance.

Digitized by Google
Original from UNIVERSITY OF MICHIGAN
Generated on 2019-09-23 04:38 GMT / http://hdl.handle.net/2027/mdp.39015077775156
Public Domain, Google-digitized / http://www.hathitrust.org/access_use#pd-google

X. Variation of Power and Electronic Tuning with Frequency

When a reflex oscillator is tuned through its tuning range, the load and repeller voltage being adjusted for optimum efficiency for a given drift angle, it is found that the power and efficiency and the electronic tuning vary, having optima at certain frequencies.

When we come to work out the variation of power and electronic tuning with frequency we at once notice two distinct cases: that of a fixed gap spacing and variable resonator (707A), and that of an essentially fixed resonator and a variable gap spacing (723A etc.); see Section XIII. Here we will treat as an example the latter case only.

The simplest approximation of the tuning mechanism which can be expected to accord reasonably with facts is that in which the resonator is represented as a fixed inductance, a constant shunt "stray" capacitance and a variable capacitance proportional to $1/d$, where d is the gap spacing The validity of such a representation over the normal operating range has been verified experimentally for a variety of oscillator resonators. Let C_0 be the fixed capacitance and C_1 be the variable capacitance at some reference spacing d_1. Then, letting the inductance be L, we have for the frequency

$$\omega = (L(C_0 + C_1 d_1/d))^{\frac{1}{2}}. \tag{10.1}$$

Suppose we choose d_1 such that

$$C_0 = C_1. \tag{10.2}$$

Then, letting

$$d/d_1 = D \tag{10.3}$$

$$\omega_1 = (2LC_0)^{\frac{1}{2}} = 2\pi f_1 \tag{10.4}$$

$$\omega/\omega_1 = W. \tag{10.5}$$

We find

$$W = 2^{\frac{1}{2}}(1 + 1/D)^{-\frac{1}{2}}. \tag{10.6}$$

This relation is shown in Fig. 51, where D is plotted vs W. It is perfectly general (within the validity of the assumptions) for a proper choice of reference spacing d_1. We have, then, in Fig. 51 a curve of spacing D vs reduced frequency W.

The parameter which governs the power and efficency is G_R/y_e. We have

$$G_R/y_e = (G_R/\beta^2)(2V_0/I_0\theta). \tag{10.7}$$

As V_0, I_0 and θ will not vary in tuning the oscillator, we must look for variaton in G_R and β^2.

Digitized by Google
Original from UNIVERSITY OF MICHIGAN
Generated on 2019-09-23 04:39 GMT / http://hdl.handle.net/2027/mdp.39015077775156
Public Domain, Google-digitized / http://www.hathitrust.org/access_use#pd-google

For parallel plane grids, we have

$$1/\beta^2 = (\theta_g/2)^2/\sin^2(\theta_g/2) \tag{10.8}$$

where θ_g is the transit angle between grids. We see that in terms of W and D we can write

$$\theta_g = \theta_1 WD. \tag{10.9}$$

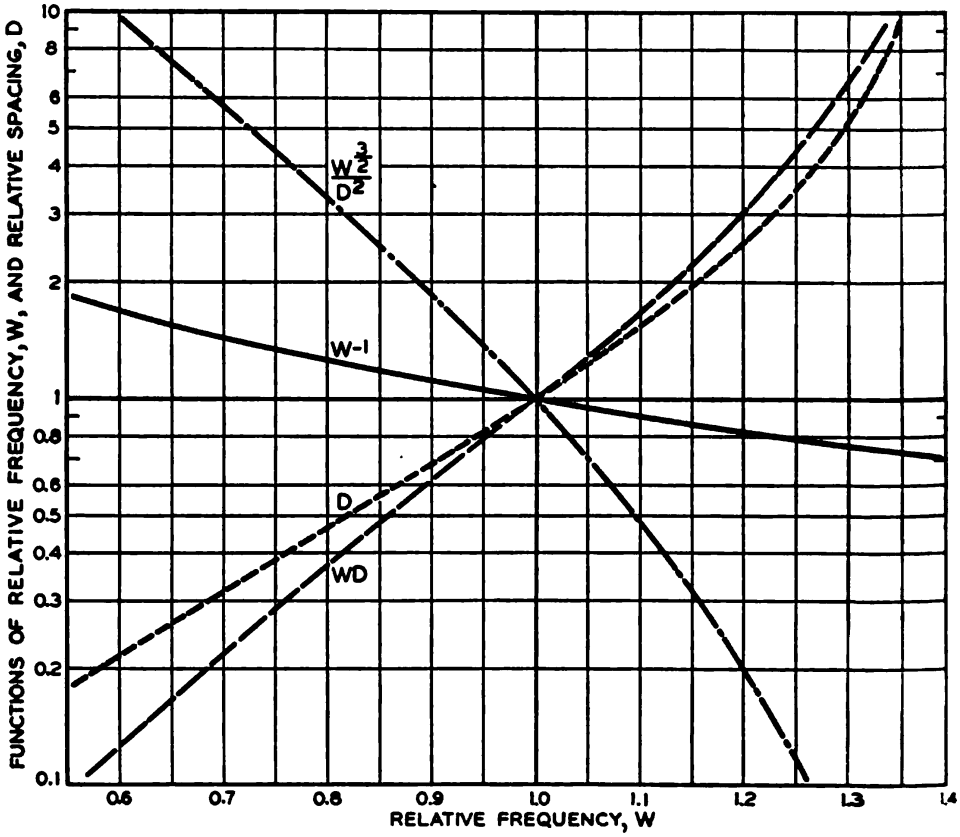

Fig. 51.—Various functions of relative frequency W and relative spacing D plotted vs relative frequency.

Here θ_1 is the gap transit angle at a spacing d_1 and a frequency W_1. So that we may see the effect of tuning on $1/\beta^2$, WD has been plotted vs W in Fig. 51 and $1/\beta^2$ has been plotted vs θ_g in Fig. 52.

We now have to consider losses. From (9.7) of Appendix IX we see that the grid loss conductance can be expressed in the form

$$G_g = G_{g1} W^{\frac{3}{2}}/D^2. \tag{10.10}$$

Here G_{g1} is the grid loss conductance at $d = d_1$ and $\omega = \omega_1$.

Finally, let us consider the resonator loss. If the resonator could be represented by an inductance L with a series resistance R, at high frequencies the conductance would be very nearly

Digitized by Google
Original from UNIVERSITY OF MICHIGAN
Generated on 2019-09-23 04:40 GMT / http://hdl.handle.net/2027/mdp.39015077775156
Public Domain, Google-digitized / http://www.hathitrust.org/access_use#pd-google

$$G_L = R/(\omega L)^2. \tag{10.11}$$

If R varies as $\omega^{\frac{1}{2}}$, we see that we could then write

$$G_L = G_{L1}W^{-\frac{1}{2}}. \tag{10.12}$$

Here G_{L1} is the conductance at a frequency ω_1.

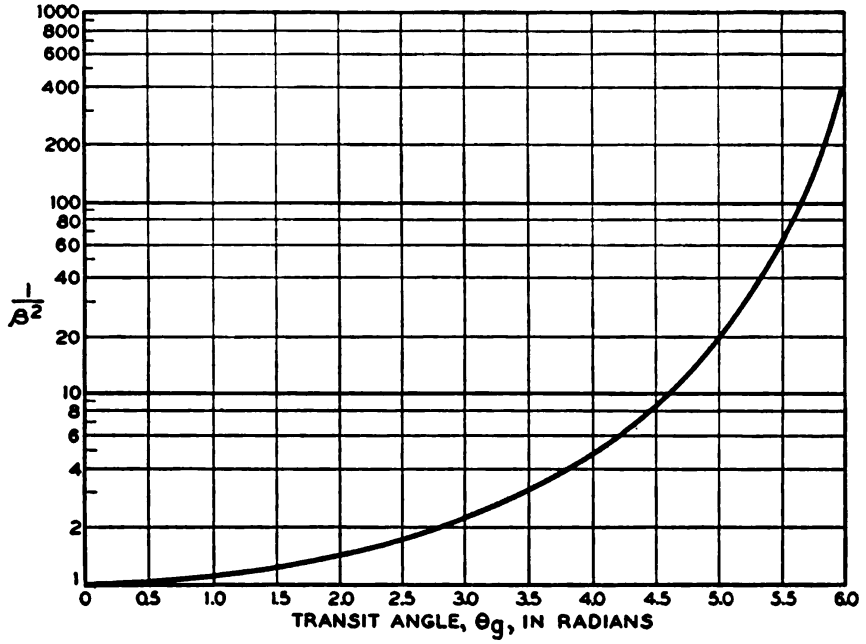

Fig. 52.—The reciprocal of the square of the modulation coefficient is a function of the gap transit angle in radians for the case of fine parallel grids.

As an opposite extreme let us consider the behaviour of the input conductance of a coaxial line. It can be shown that, allowing the resistance of such a line to vary as $\omega^{\frac{1}{2}}$, the input conductance is

$$G\ell = A\omega^{\frac{1}{2}} \csc^2 (\omega\ell/C). \tag{10.13}$$

Here ℓ is the length of the line and C is the velocity of propagation. If G_L given by (10.12) and $G\ell$ of 10.13 give the same value of conductance at some angular frequency ω_1 then it will be found that for values of ℓ typical of reflex oscillator resonators the variation of $G\ell$ with ω will be significantly less than that of G_L. Although typical cavities are not uniform lines (10.13) indicates that a slower variation than (10.12) can be expected. It will be found moreover that the shape of the power output vs frequency curves are not very sensitive to the variation assumed. Hence as a reasonable compromise it will be assumed that the resonator wall loss varies as

Digitized by Google
Original from UNIVERSITY OF MICHIGAN
Generated on 2019-09-23 04:45 GMT / http://hdl.handle.net/2027/mdp.39015077775156
Public Domain, Google-digitized / http://www.hathitrust.org/access_use#pd-google

$$G_S = G_{S1}W^{-1}. \tag{10.14}$$

In Fig. 51 W^{-1} has been plotted vs W.

Now let us take an actual example. Suppose that at $D = 1$, i.e. ($d = d_1$, $\omega = \omega_1$)

$$\theta = 2$$

$$G_{g1} = .270/y_e$$

$$G_{S1} = .095/y_e$$

The information above has been used in connection with Figs. 51 and 52 and ratio of resonator loss to small signal electronic admittance, G_R/y_e, has been plotted vs W in Fig. 53. A 2K25 oscillator operated at a beam

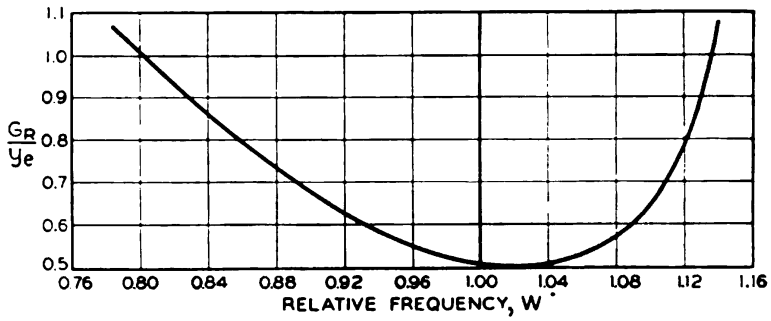

Fig. 53.—Computed variation of ratio of resonator loss to small signal electronic admittance vs relative frequency W for certain resonator parameters assumed to fit the characteristics of the 2K25.

voltage, V_0, of 300 volts had a total cathode current I_0 of 26 ma. This current passed three grids on the first transit and back through the third grid on the return transit. On a geometrical basis, 53% of the cathode current should make this second transit across the gap. Thus the useful beam power was about

$$P_0 = (.53)\ (300)\ (.026) = 4.1.$$

If we assume a drift effectiveness factor F of unity, then for the $7\frac{3}{4}$ cycle mode, the efficiency should be given by H_m divided by $7\frac{3}{4}$. H_m is plotted as a function of G_R/y_e in Fig. 7. Thus, we can obtain η, the efficiency, and hence the power output. This has been done and the calculated power output is plotted vs W in Fig. 54, where $W = 1$ has been taken to correspond to 9,000 mc. It is seen that the theoretical variation of output with frequency is much the same as the measured variation.

Generated on 2019-09-23 04:46 GMT / http://hdl.handle.net/2027/mdp.39015077775156
Public Domain, Google-digitized / http://www.hathitrust.org/access_use#pd-google
Digitized by Google
Original from UNIVERSITY OF MICHIGAN

Actually, of course, the parameters of the curve were chosen so that it corresponds fairly well to the experimental points. The upper value of W at which the tube goes out of oscillation is most strongly influenced by the value of θ_1 chosen. We see from Fig. 51 that as W is made greater than unity WD increases rapidly and hence, from Fig. 52, β^2 decreases rapidly, increasing G_R/y_e. On the other hand, as W is made smaller than unity, β^2 approaches unity but the grid loss term $W^{\frac{1}{2}}/D^2$ increases rapidly, and this term is most effective in adjusting the lower value of W at which oscillation will cease. Finally, the resonator loss term, varying as W^{-1}, does not change rapidly and can be used to adjust the total loss and hence the optimum value of G_R/y_e and the optimum efficiency.

It is clear that the power goes down at low frequencies chiefly because in moving the grids very close together to tune to low frequencies with a fixed nductance the resonator losses and especially the grid losses are increased.

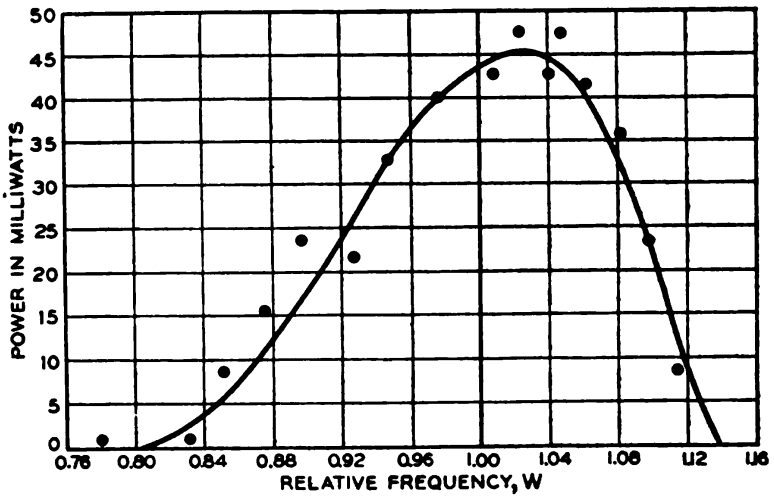

Fig. 54.—Computed curve of variation of power in milliwatts with relative frequency W for the parameters used in Fig. 53. The circles are experimental points. The curve has been fitted to the points by the choice of parameters.

In going to high frequencies the power decreases chiefly because moving the grids far apart to tune to high frequencies decreases β^2. Both of these effects are avoided if a fixed grid spacing is used and the tuning is accomplished by changing the inductance as in the case of the 707A. In such tubes there will be an upper frequency limit either because even with a fixed grid spacing β^2 decreases as frequency increases, or else there will be a limit at the resonant frequency of the smallest allowable external resonator, and there will be a lower frequency limit at which the repeller voltage for a given mode approaches zero; however, the total tuning range may be 3 to 1 instead of around 30% between extinction points, as for the 2K25.

Digitized by Google
Original from UNIVERSITY OF MICHIGAN
Generated on 2019-09-23 04:46 GMT / http://hdl.handle.net/2027/mdp.39015077775156
Public Domain, Google-digitized / http://www.hathitrust.org/access_use#pd-google

The total electronic tuning between half-power points at optimum loading, $2(\Delta f)_{\frac{1}{2}}$, can be expressed

$$2(\Delta f)_{\frac{1}{2}} = (fy_e/M)(2\Delta\omega/\omega_0)/(y_e/M). \tag{10.15}$$

We can obtain $(2\Delta\omega/\omega_0)/(y_e/M)$ from Fig. 16.

If we assume a circuit consisting of a constant inductance L and a capacitance, the characteristic admittance of the resonator is

$$M = 1/\omega L = \tfrac{1}{2}\pi f_1 W \tag{10.16}$$

and

$$2(\Delta f)_{\frac{1}{2}} = 2\pi W^2 f_1^2 L y_e (2\Delta\omega/\omega_0)/(y_e/M) \tag{10.17}$$

and we have

$$y_e = \beta^2 I_0 (2\pi N)/2V_0 . \tag{10.18}$$

Here N is the total drift in cycles.

A rough calculation estimates the resonator inductance of the 2K25 as $.30 \times 10^{-9}$ henries. Using the values previously assumed, $I_0 = (.53)(.026)$, $V_0 = 300$, $N = 7\frac{3}{4}$, and the values of $G_R/y_e\beta^2$ and f_1 previously assumed, we can obtain electronic tuning.

A curve for half power electronic tuning vs W has been computed and is shown in Fig. 55, together with experimental data for a 2K25. The experimental data fall mostly above the computed curve. This could mean that the inductance has been incorrectly computed or that the drift effectiveness is increased over that for a linear drift field, possibly by the effects of space charge. By choosing a value of the drift effectiveness factor other than unity we could no doubt achieve a better fit of the electronic tuning data and still, by readjusting G_{g1} and G_{s1}, fit the power data. This whole procedure is open to serious question. Further, it is very hard to measure such factors as G_{g1} for a tube *under operating conditions*, with the grids heated by bombardment. Indirect measurements involve many parameters at once, and are suspect. Thus, Figs. 54 and 55 are presented merely to show a qualitative correspondence between theory and experiment.

XI. Noise Sidebands in Reflex Oscillations

In considering power production, the electron flow in reflex oscillators can be likened to a perfectly smooth flow of charge. However, the discrete nature of the electrons, the cause of the familiar "shot noise" in electron flow engenders the production of a small amount of *r-f* power in the neighborhood of the oscillating frequency—"noise sidebands". Thus the energy spectrum of a reflex oscillator consists of a very tall central spike, the power output of the oscillator, and, superposed, a distribution of noise energy having its highest value near the central spike.

Digitized by Google
Original from UNIVERSITY OF MICHIGAN
Generated on 2019-09-23 04:47 GMT / http://hdl.handle.net/2027/mdp.39015077775156
Public Domain, Google-digitized / http://www.hathitrust.org/access_use#pd-google

Such noise or noise "sidebands" can be produced by any mechanism which causes the parameters of the oscillator to fluctuate with time. As the mean speed, the mean direction, and the convection current of the electron flow all fluctuate with time, possible mechanisms of noise production are numerous. Some of these mechanisms are:

(1) Fluctuation in mean speed causes fluctuation in the drift angle and hence can give rise to noise sidebands in the output through frequency modulation of the oscillator.

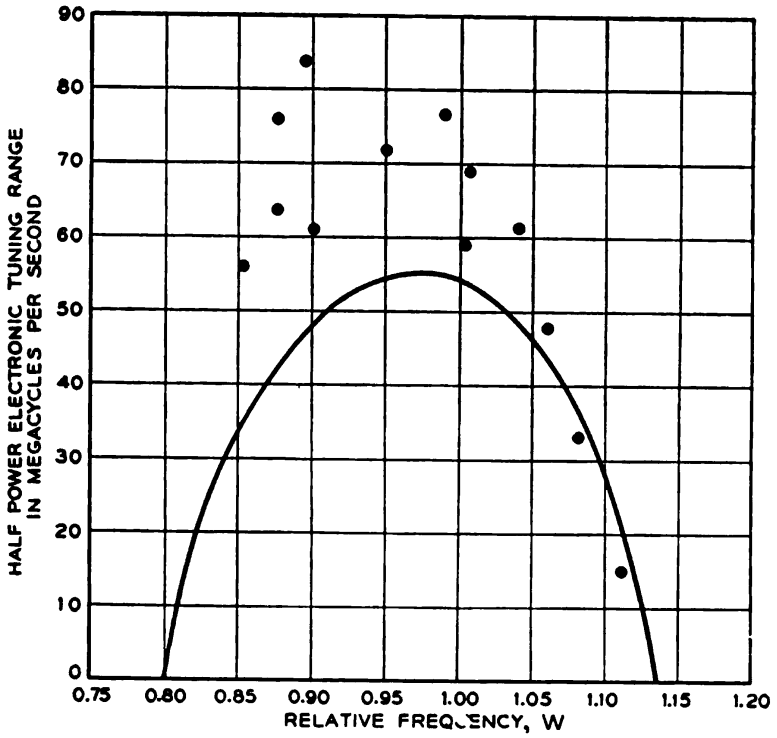

Fig. 55.—Computed variation of electronic tuning range in megacycles vs relative frequency W. The curve is calculated from the same data as that in Fig. 54 with no additional adjustment of parameters. Points represent experimental data.

(2) If the drift field acts differently on electrons differently directed, fluctuations in mean direction of the electron flow may cause noise sidebands through either amplitude or frequency modulation of the output.

(3) Low frequency fluctuations in the electron convection current may amplitude modulate the output, causing noise sidebands, and may frequency modulate the output when the oscillator is electronically tuned away from the optimum power point.

(4) High frequency fluctuations in the electron stream may induce high frequency noise currents in the resonator directly.

Mechanism (4) above, the direct induction of noise currents in the resonator by noise fluctuations in the electron stream, is probably most impor-

Generated on 2019-09-23 04:47 GMT / http://hdl.handle.net/2027/mdp.39015077775156
Public Domain, Google-digitized / http://www.hathitrust.org/access_use#pd-google
Digitized by Google
Original from UNIVERSITY OF MICHIGAN

tant, although (3) may be appreciable. An analysis of the induction of noise in the resonator is surprisingly complicated, for the electron stream acts as a non-linear load impedance to the noise power giving rise to a complicated variation of noise with frequency and with amplitude of oscillation. On the basis of analysis and experience it is possible, however, to draw several general conclusions concerning reflex oscillator noise.

First, it is wise to decide just what shall be the measure of noise. The noise is important only when the oscillator is used as a beating oscillator, usually in connection with a crystal mixer. A power P is supplied to the mixer at the beating oscillator frequency. Also, the oscillator supplies at signal frequency, separated from the beating oscillator frequency by the intermediate frequency, a noise power P_n proportional, over a small frequency range, to the band-width B. An adequate measurement of the noisiness of the oscillator is the ratio of P_n to the Johnson noise power, kTB. The general facts which can be stated about this ratio and some explanation of them follow:

(1) Electrons which cross the gap only once contribute to noise but not to power. Likewise, if there is a large spread in drift angle among various electron paths, some electrons may contribute to noise but not to power.

(2) The greater the separation between signal frequency and beating oscillator frequency (i.e., the greater the intermediate frequency) the less the noise.

(3) The greater the electronic tuning range, the greater the noise for a given separation between signal frequency and beating oscillator frequency. This is natural; the electronic tuning range is a measure of the relative magnitudes of the electronic admittance and the characteristic admittance of the circuit.

(4) The degree of loading affects the noise through affecting the bunching parameter X. The noise seems to be least for light loading.

(5) Aside from controlling the degree of loading, resonator losses do not affect the noise; it does not matter whether the unused power is dissipated inside or outside of the tube.

(6) When the tube is tuned electronically, the noise usually increases at frequencies both above and below the optimum power frequency, but the tube is noisier when electronically tuned to lower frequencies. At the optimum frequency, the phase of the pulse induced in the circuit when an electron returns across the gap lags the pulse induced on the first crossing by 270°. When the drift time is shortened so as to tune to a higher frequency, the angle of lag is decreased and the two pulses tend to cancel; in tuning electronically to lower frequencies the pulses become more nearly in phase.

An approximate theoretical treatment leads to the conclusion that aside from avoiding loss of electrons in reflection, or very wide spreads in transit

Digitized by Google
Original from UNIVERSITY OF MICHIGAN
Generated on 2019-09-23 04:47 GMT / http://hdl.handle.net/2027/mdp.39015077775156
Public Domain, Google-digitized / http://www.hathitrust.org/access_use#pd-google

time for various electrons, (see (1) above) and aside from narrowing the electronic tuning range, which may be inadmissible, the only way to reduce the noise is to increase the cathode current. This is usually inadmissible. Thus, it appears that nothing much can be done about the noise in reflex oscillators without sacrificing electronic tuning range.

The seriousness of beating oscillator noise from a given tube depends, of course, on the noise figure of the receiver without beating oscillator noise and on the intermediate frequency. Usually, beating oscillator noise is worse at higher frequencies, partly because higher frequency oscillators have greater electronic tuning (see (3) above). At a wavelength of around 1.25 cm, with a 60 mc I.F. amplifier, the beating oscillator noise may be sufficient so that were there no other noise at all the noise figure of the receiver would be around 12 db.

Beating oscillator noise may be eliminated by use of a sharply tuned filter between the beating oscillator and the crystal. This precludes use of electronic tuning. Beating oscillator noise may also be eliminated by use of a balanced mixer in which, for example, the signal is fed to two crystals in the same phase and the beating oscillator in opposite phases. If the I.F. output is derived so that the signal components from the two crystals add, the output due to beating oscillator noise at signal frequencies will cancel out. There is an increasing tendency for a number of reasons to use balanced mixers and thus beating oscillator noise has become of less concern.

XII. Build-up of Oscillation

In certain applications, reflex oscillators are pulsed. In many of these it is required that the *r-f* output appear quickly after the application of *d-c* power, and that the time of build-up be as nearly the same as possible for successive applications of power. In this connection it is important to study the mechanism of the build-up of oscillations.

In connection with build-up of oscillations, it is convenient to use complex frequencies. Impedances and admittances at complex frequencies are given by the same functions of frequency as those at real frequencies. Suppose, for instance, the radian frequency is

$$\omega = w - j\alpha \tag{12.1}$$

This means the oscillations are increasing in amplitude. The admittance of a conductance G at this frequency is

$$Y = G$$

The admittance of a capacitance C and the impedance of an inductance L are

$$Y = j\omega C = jwC + \alpha C \tag{12.2}$$

$$Z = j\omega L = jwL + \alpha L \tag{12.3}$$

Digitized by Google
Original from UNIVERSITY OF MICHIGAN
Generated on 2019-09-23 04:47 GMT / http://hdl.handle.net/2027/mdp.39015077775156
Public Domain, Google-digitized / http://www.hathitrust.org/access_use#pd-google

In other words, to an increasing oscillation reactive elements have a "loss" component of admittance or impedance. This "loss" component corresponds not to dissipation but to the increasing storage of electric or magnetic energy in the reactive elements as the oscillation increases in amplitude.

The admittance curves plotted in Figs. 41–46 may be regarded as contours in the admittance plane for $\alpha = 0$. If such a contour is known either by calculation or experiment, and it is divided into equal frequency increments, a simple construction will give a neighboring curve for $\omega = w - j\Delta\alpha$ where $\Delta\alpha$ is a small constant. Suppose that the change in Y for a frequency $\Delta\omega_1$ is ΔY_1. Then for a change $-j\Delta\alpha$

$$\Delta Y = -j \frac{\Delta Y_1}{\Delta\omega_1} \Delta\alpha. \tag{12.4}$$

Thus, to construct from a constant amplitude admittance curve an admittance curve for an increasing oscillation, one takes a constant fraction of each admittance increment between constant frequency increment points (a constant fraction of each space between circles in Figs. 41–46), rotates it 90 degrees clockwise, and thus establishes a point on the new curve.

This construction holds equally well for any conformal representation of the admittance plane (for instance, for the reflection coefficient plane represented on the Smith chart).

The general appearance of these curves for increasing oscillations in terms of the curve for real frequency can be appreciated at once. The increasing amplitude curve will lie to the right of the real frequency curve where the latter is rising and to the left where the latter is falling. Thus the loops will be diminished or eliminated altogether for increasing amplitude oscillations, and the low conductance portions will move to the right, to regions of higher conductance. This is consistent with the idea that for an increasing oscillation a "loss" component is added to each reactance, thus degrading the "Q", increasing the conductance, and smoothing out the admittance curve.

The oscillation starts from a very small amplitude, presumably that due to shot noise of the electron stream. For an appreciable fraction of the build-up period the oscillation will remain so small that nonlinearities are unimportant. The exponential build-up during this period is determined by the electronic admittance for very small signals.

As an example, consider a case in which the electronic admittance for small signals is a pure conductance with a value of $-y_e$. Here the fact that that the quantity is negative is recognized by prefixing a minus sign.

Assume also that the circuit admittance including the load may be expressed as in (a-22) of Appendix I, which holds very nearly in case there is only one resonance in resonator and load. Then for a complex frequency $w_e - j\alpha_e$ the circuit admittance will be

Digitized by Google
Original from UNIVERSITY OF MICHIGAN
Generated on 2019-09-23 04:48 GMT / http://hdl.handle.net/2027/mdp.39015077775156
Public Domain, Google-digitized / http://www.hathitrust.org/access_use#pd-google

$$Y_c = G_c + 2M\alpha_0/w_0 \tag{12.5}$$

Thus in this special case we have for oscillation

$$y_0 = G_c + 2M\alpha_0/w_0 \tag{12.6}$$

and

$$\alpha_0 = \frac{w_0}{2M}(Y_0 - G_c). \tag{12.7}$$

The amplitude, then, builds up initially according to the law

$$V = V_0 e^{\alpha_0 t}. \tag{12.8}$$

If the amplitude does not change too rapidly, the build-up characteristic of an oscillator can be obtained step-by-step from a number of contours for constant α and from a $-Y_0$ curve marked with amplitude points. The $-Y_0$ curve might, for instance, be obtained from a Rieke diagram and an admittance curve.

Consider the example shown in Fig. 56. Fig. 56a shows curves constructed for complex frequencies from the admittance curve for the resonant circuit for real frequency. In addition the negative of the electronic admittance is shown. Oscillation will start from some very small amplitude, $V = V_0$, and build-up at an average rate given by $\alpha = 2.5 \times 10^{-6}$ until $V = 1$. Let $V_0 = .1$. Then the interval to build-up from $V = .1$ to $V = 1$ is

$$\Delta t_1 = \frac{\ln\left(\frac{1}{.1}\right)}{2.5 \times 10^{-6}}$$

$$= .92 \times 10^{-6} \text{ seconds.}$$

From amplitude 1 to amplitude 2 the average value of α will be 1.5×10^{-6} and the time interval will be

$$\Delta t_2 = \frac{\ln\left(\frac{2}{1}\right)}{1.5 \times 10^{-6}}$$

$$= .46 \times 10^{-6} \text{ seconds.}$$

Similarly, from 2 to 3

$$\Delta t_3 = \frac{\ln\left(\frac{3}{2}\right)}{.5 \times 10^{-6}}$$

$$= .80 \times 10^{-6} \text{ seconds.}$$

The build-up curve is shown in Fig. 56b.

Similarly, from a family of admittance contours constructed from a cold impedance curve, and from a knowledge of frequency and amplitude vs time,

Digitized by Google
Original from UNIVERSITY OF MICHIGAN
Generated on 2019-09-23 04:48 GMT / http://hdl.handle.net/2027/mdp.39015077775156
Public Domain, Google-digitized / http://www.hathitrust.org/access_use#pd-google

Y_e can be obtained as a function of time. It may be that in many cases the real part of the frequency is nearly enough constant during build-up so that only the amplitude vs time need be known. As the input will commonly be a function of time for such experimental data, Y_e vs time will yield Y_e at vari-

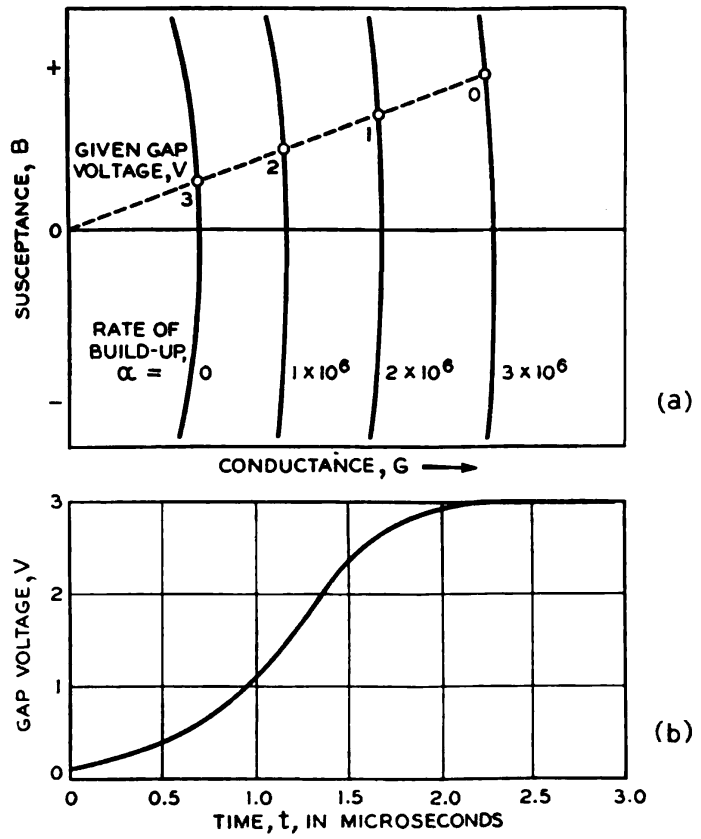

Fig. 56.—*a*. A plot of the circuit admittance (solid lines) for various rates of build-up specified by the parameters α. The voltage builds up as $e^{\alpha t}$. The circuit conductance is greater for large values of α. The negative of the electronic admittance is shown by the dashed lines. The circles mark off the admittance at which various amplitudes or voltages of oscillation occur. The intersections give the rates of build-up of oscillation at various voltages. By assuming exponential build up at a rate specified by α between the voltages at these intersections, an approximate build-up can be constructed.

b. A build up curve constructed from the data in Fig. 56a.

ous amplitudes and inputs. Curves for various rates of applying input will yield tables of Y_e as a function of both input and amplitude.

It will be noted that to obtain very fast build-up with a given electronic admittance, the conductance should vary slowly with α. This is the same as saying that the susceptance should vary slowly with ω, or with real frequency. For singly resonant circuits, this means that ω_o/M should be large.

Suppose the admittance curve for real frequency, i.e. $\alpha = 0$, has a single

Digitized by Google
Original from UNIVERSITY OF MICHIGAN
Generated on 2019-09-23 04:48 GMT / http://hdl.handle.net/2027/mdp.39015077775156
Public Domain, Google-digitized / http://www.hathitrust.org/access_use#pd-google

loop and is symmetrical about the G axis as shown in Fig. 57. Suppose the $-Y_e$ curve lies directly on the G axis. The admittance contours for increasing values of α will look somewhat as shown. Suppose build-up starts on Curve 2. When Curve 1 with the cusp is reached, the build-up can continue along either half as the loop is formed and expands, resulting either of the two possible frequencies of Curve 0. Presumably in this symmetrical

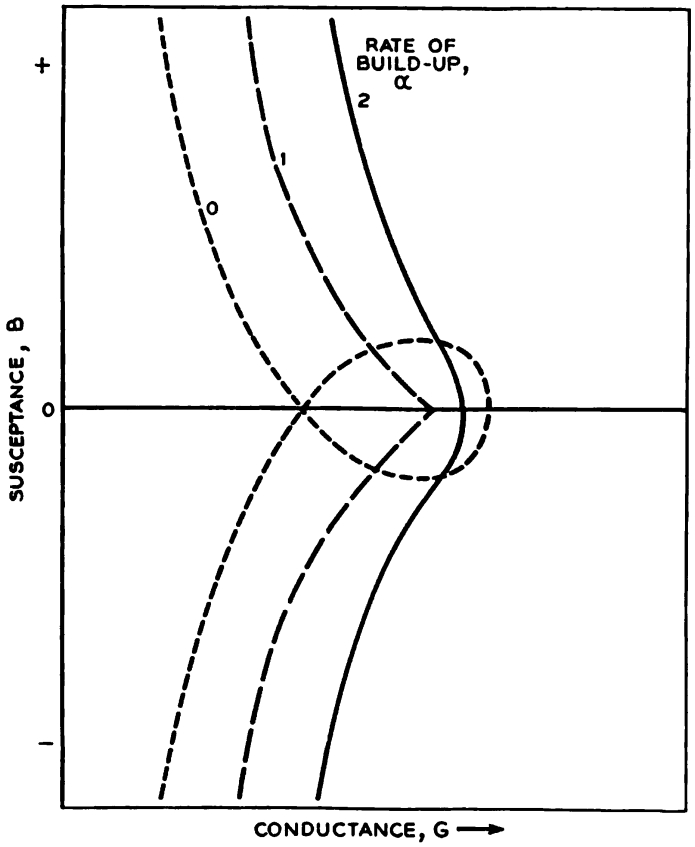

Fig. 57.—Circuit admittance vs circuit conductance in arbitrary units for different rates of build-up at turn-on. When the build-up is rapid ($\alpha = 2$) the admittance curve has no loop. As the rate of build-up decreases the curve sharpens until it has a cusp $\alpha = 1$. As the rate of build-up further decreases the curve develops a loop ($\alpha = 0$). There may be uncertainty as to which of the final intersections with the $\alpha = 0$ line will represent oscillation.

case, nonsynchronous fluctuations would result in build-up to each frequency for half of the turn-ons. If one frequency were favored by a slight dissymmetry, the favored frequency would appear on the greater fraction of turn-ons. For a great dissymetry, build-up may always be in one mode, although from the impedance diagram steady oscillation in another mode appears to be possible.

Digitized by Google
Original from UNIVERSITY OF MICHIGAN
Generated on 2019-09-23 04:48 GMT / http://hdl.handle.net/2027/mdp.39015077775156
Public Domain, Google-digitized / http://www.hathitrust.org/access_use#pd-google

In the absence of hum or other disturbances the build-up of oscillations starts from a randomly fluctuating voltage caused by shot noise.[11] Thus, from turn-on to turn-on some sort of statistical distribution may be expected in the time τ taken to reach a given fraction of the final amplitude. In unpublished work Dr. C. R. Shannon of these laboratories has shown that in terms of α_o, the initial rate of build-up, the standard deviation $\delta\tau$ and the root mean square deviation $(\overline{\delta\tau^2})^{1/2}$ are given by

$$\delta\tau = .38/\alpha_o \tag{12.9}$$

$$(\overline{\delta\tau^2})^{1/2} = .64/\alpha_o \tag{12.10}$$

Thus the "jitter" in the successive positions of the r-f pulses associated with evenly spaced turn-ons is least when the initial rate of build-up, given by α_o, is greatest.

Such conditions do not obtain on turn-off, and there is little jitter in the trailing edge of a series of r-f pulses. This is of considerable practical importance.

XIII. Reflex Oscillator Development at the Bell Telephone Laboratories

For many years research and development directed towards the generation of power at higher and higher frequencies have been conducted at the Bell Telephone Laboratories. An effort has been made to extend the frequency range of the conventional grid controlled vacuum tube as well as to explore new principles, such as those embodied in velocity variation oscillators. The need for centimeter range oscillators for radar applications provided an added impetus to this program and even before the United States entry into the war, as well as throughout its duration, these laboratories, cooperating with government agencies, engaged in a major effort to provide such power sources. The part of this program which dealt with high power sources for transmitter uses has been described elsewhere. This paper deals with low power sources, which are used as beating oscillators in radar receivers. In the following sections some of the requirements on a beating oscillator for a radar receiver will be outlined in order to show how the reflex oscillator is particularly well suited for such an application.

A. *The Beating Oscillator Problem*

The need for a beating oscillator in a radar system arises from the necessity of amplifying the very weak signals reflected from the targets. Immediate rectification of these signals would entail a very large degradation in signal to noise ratio, although providing great simplicity of operation. It would also lead to a lack of selectivity. Amplification of the signals at the

[11] See Appendix 10.

Digitized by Google
Original from UNIVERSITY OF MICHIGAN
Generated on 2019-09-23 04:48 GMT / http://hdl.handle.net/2027/mdp.39015077775156
Public Domain, Google-digitized / http://www.hathitrust.org/access_use#pd-google

signal frequency would require centimeter range amplifiers having good signal to noise properties. No such amplifiers existed for the centimeter range, and it was necessary to beat the signal frequency to an intermediate frequency for amplification before rectification. For a number of reasons, such intermediate frequency amplifiers operate in the range of a few tens of megacycles, so that the beating oscillator must generate very nearly the same frequency as the transmitter oscillator.

In radar receivers operating at frequencies up to several hundred megacycles, conversion is frequently achieved with vacuum tubes. For higher frequencies crystal converters have usually been employed. With few exceptions, the oscillators to be described were used with these crystal converters which require a small oscillator drive of the order of one milliwatt. In general it is desirable to introduce attenuation between the oscillator and the crystal to minimize effects due to variation of the load. Approximately 13 db is allowed for such padding so that a beating oscillator need supply about 20 milliwatts. Power in excess of this is useful in many applications but not absolutely necessary. Since the power output requirements are low, efficiency is not of prime importance and is usually, and frequently necessarily, sacrificed in the interest of more important characteristics.

The beating oscillator of a radar receiver operating in the centimeter range must fulfill a number of requirements which arise from the particular nature of the radar components and their manner of operation. The intermediate frequency amplifier must have a minimum pass band sufficient to amplify enough of the transmitter sideband frequencies so that the modulating pulse is reproduced satisfactorily. It is not desirable to provide much margin in band width above this minimum since the total noise increases with increasing band width. It is therefore necessary for best operation that the frequency of the beating oscillator should closely follow frequency variations of the transmitter, so that a constant difference frequency equal to the intermediate frequency is maintained.

This becomes more difficult at higher frequencies, inasmuch as all frequency instabilities, such as thermal drifts, frequency pulling, etc. occur as percentage variations. Some of the frequency variations occur at rapid rates. An example of this is the frequency variation which is caused by changes in the standing wave presented to the transmitter. Such variations may arise, for instance, from imperfections in rotating joints in the output line between the transmitter to the scanning antenna.

For correction of slow frequency drifts a manual adjustment of the frequency is frequently possible, but instances arise, notably in aircraft installations, in which it is not possible for an operator to monitor the frequency constantly. Rapid frequency changes, moreover, occur at rates in excess of the reaction speed of a normal man. Hence for obvious tactical reasons

Digitized by Google
Original from UNIVERSITY OF MICHIGAN
Generated on 2019-09-23 04:49 GMT / http://hdl.handle.net/2027/mdp.39015077775156
Public Domain, Google-digitized / http://www.hathitrust.org/access_use#pd-google

it is imperative that the difference frequency between the transmitter and the beating oscillator should be maintained by automatic means. As an illustration of the problem one may expect to have to correct frequency shifts from all causes, in a 10,000 megacycle system, of the order of 20 megacycles. Such correction may be demanded at rates of the order of 100 megacycles per second per second.

Although the frequency range of triode oscillators has since been somewhat extended, at the time that beating oscillators in the 10 centimeter range were first required the triode oscillators available did not adequately fulfill all the requirements. In general the tuning and feedback adjustments were complicated and hence did not adapt themselves to automatic frequency control systems. Velocity variation tubes of the multiple gap type which gave more satisfactory performance than the triodes existed in this range. These, however, generally required operating voltages of the order of a thousand volts and frequently required magnetic fields for focussing the electron stream. The tuning range obtainable by electrical means was considerably less than needed and, just as in the case of the triode oscillator, the mechanical tuning mechanism did not adapt itself to automatic control. These difficulties focussed attention on the reflex oscillator, whose properties are ideally suited to automatic frequency control. The feature of a single resonant circuit is of considerable importance in a military application, in which simple adjustments are of primary concern. The repeller control of the phase of the negative electronic admittance which causes oscillation provides a highly desirable vernier adjustment of the frequency, and, since this control dissipates no power, it is particularly suited to automatic frequency control. Furthermore, since the upper limit on the rate of change of frequency is set by the time of transit of the electrons in the repeller field and the time constant of the resonant circuit, both of which are generally very small fractions of a micro-second, very rapid frequency correction is possible.

As the frequency is varied with the repeller voltage, the amplitude of oscillation also varies in a manner previously described. The signal to noise performance of a crystal mixer depends in part on the beating oscillator level and has an optimum value with respect to this parameter. In consequence, there are limitations on how much the beating oscillator power may depart from this optimum value. This has a bearing on the oscillator design in that the amount of amplitude variation permitted for a given frequency shift is limited. The usual criterion of perfomance adopted has been the electronic tuning, i.e. the frequency difference, between points for a given repeller mode at which the power has been reduced to half the maximum value.

Reception of the wrong sideband by the receiver causes trouble in con-

Digitized by Google
Original from UNIVERSITY OF MICHIGAN
Generated on 2019-09-23 04:49 GMT / http://hdl.handle.net/2027/mdp.39015077775156
Public Domain, Google-digitized / http://www.hathitrust.org/access_use#pd-google

nection with automatic frequency control circuits in a manner too complicated for treatment here. In some cases this necessitates a restriction on the total frequency shift between extinction points for a given repeller mode. The relationship between half power and extinction electronic tuning has been discussed in Section VII.

In addition to the electrical requirements which have been outlined, military applications dictate two further major objectives. The first is the attainment of simple installation and replacement, which will determine, in part, the outward form of the oscillator. The second is low voltage operation, which fundamentally affects the internal design of the tubes. In some instances military requirements conflict with optimum electronic and circuit design, and best performance had to be sacrificed for simplicity of construction and operation. In particular, in some cases it was necessary to design for maximum flexibility of use and compromise to a certain extent the specific requirements of a particular need.

In the following section we will describe a number of reflex oscillators which were designed at the Bell Telephone Laboratories primarily to meet military requirements. These oscillators are described in approximate chronological order of development in order to indicate advances in design and the factors which led to these advances.

The reflex oscillators which will be described fall into two general classifications determined by the method employed in tuning the resonator. In one category are oscillators tuned by varying primarily the inductance of the resonator and in the other are those tuned by varying primarily the capacitance of the resonator. The second category includes two types in which the capacitance is varied in one case by external mechanical means and in the second case by an internal means using a thermal control.

B. *A Reflex Oscillator With An External Resonator—The 707*

The Western Electric 707A tube, which was the first reflex oscillator extensively used in radar applications, is characteristic of reflex oscillators using inductance tuning. It was intended specifically for service in radar systems operating at frequencies in a range around 3000 megacycles. Fig. 58 shows a photograph of the tube and Fig. 59 an x-ray view showing the internal construction. A removable external cavity is employed with the 707A as indicated by the sketch superimposed on the x-ray of Fig. 59. Such cavities are tuned by variation of the size of the resonant chamber. Such tuning can be considered to result from variation of the inductance of the circuit.

The form of this oscillator is essentially that of the idealized oscillator shown in Fig. 58. The electron gun is designed to produce a rectilinear cylindrical beam. The gun consists of a disc cathode, a beam forming elec-

Digitized by Google
Original from UNIVERSITY OF MICHIGAN
Generated on 2019-09-23 04:49 GMT / http://hdl.handle.net/2027/mdp.39015077775156
Public Domain, Google-digitized / http://www.hathitrust.org/access_use#pd-google

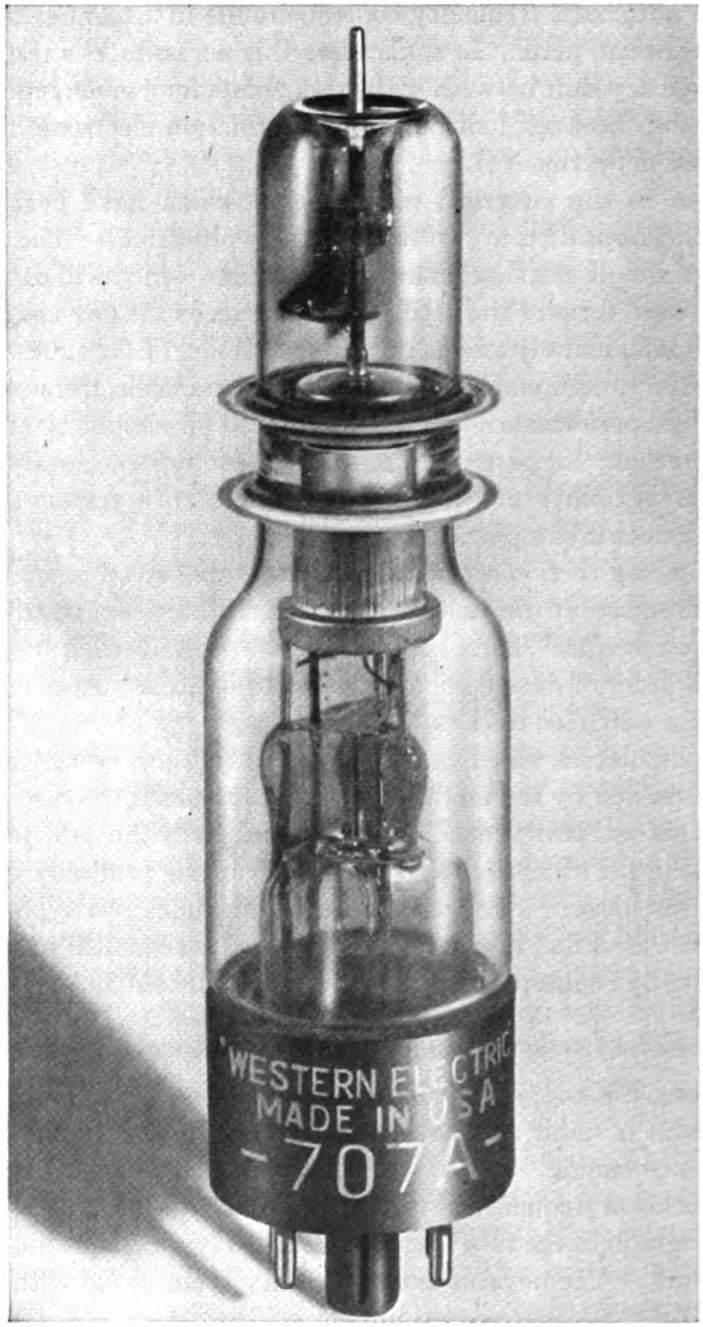

Fig. 58.—External view of the W.E. 707-A reflex oscillator tube. This tube is intended for use with an external cavity and was the first of a series of low voltage oscillators.

trode and an accelerating electrode G_1 which is a mesh grid formed on a radius. The gun design is based on the principle of maintaining boundary conditions such that a rectilinear electron beam will flow through the resonator gap. The resonator grids G_2 and G_3 are mounted on copper discs.

Digitized by Google
Original from UNIVERSITY OF MICHIGAN
Generated on 2019-09-23 04:49 GMT / http://hdl.handle.net/2027/mdp.39015077775156
Public Domain, Google-digitized / http://www.hathitrust.org/access_use#pd-google

One of these has a re-entrant shape to minimize stray capacitance in the resonant circuit. These discs are sealed to glass tubing which provides a

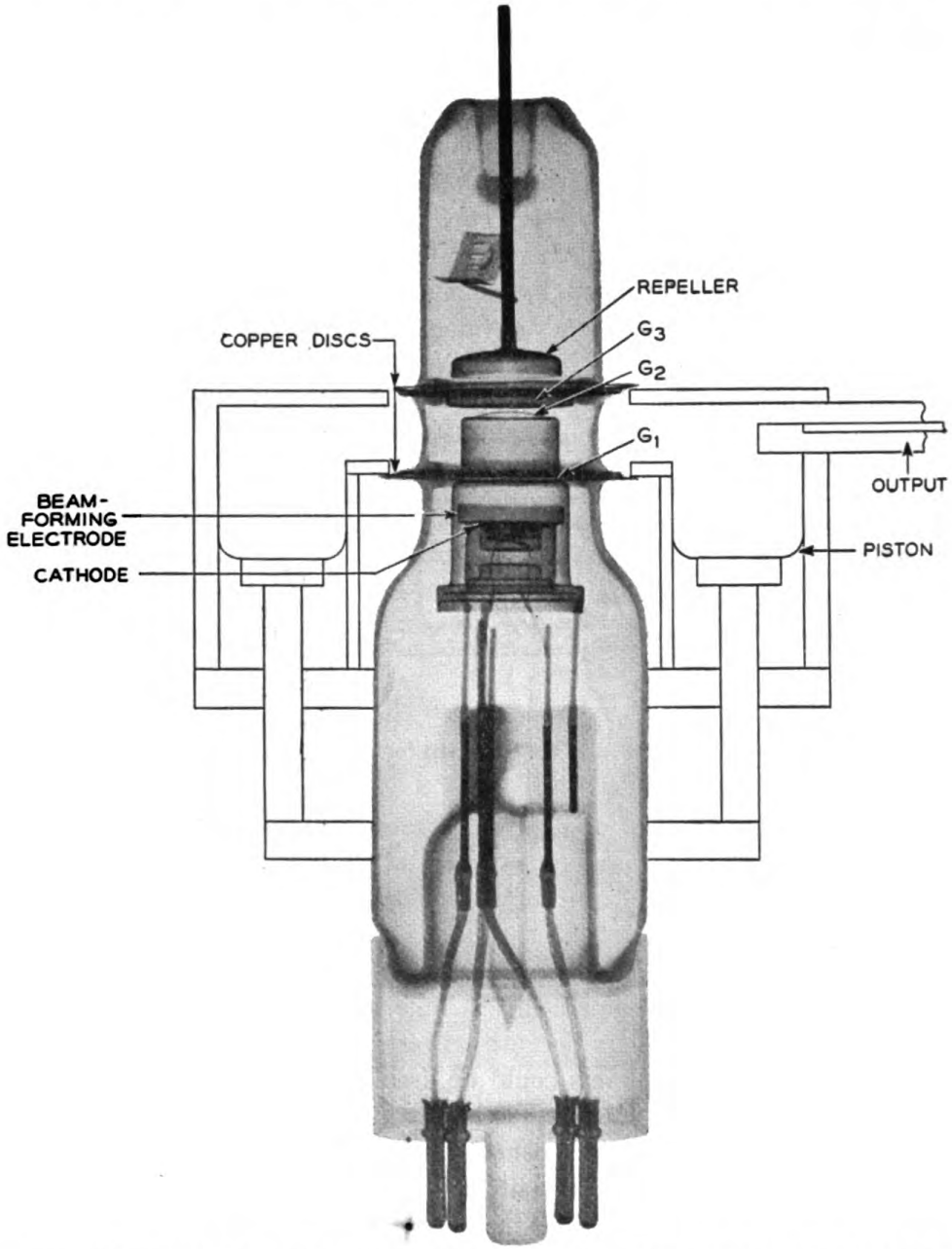

Fig. 59.—X-ray view of the W.E. 707-A shows the method of applying an external cavity tuned with a piston.

vacuum envelope. The discs extend beyond the glass to permit attachment to the external resonant chamber. The shape of the repeller is chosen

Digitized by Google
Original from UNIVERSITY OF MICHIGAN
Generated on 2019-09-23 04:49 GMT / http://hdl.handle.net/2027/mdp.39015077775156
Public Domain, Google-digitized / http://www.hathitrust.org/access_use#pd-google

to provide as nearly as possible a uniform field in the region into which the beam penetrates.

A wide variety of cavity resonators has been designed for use with this oscillator. An oscillator of this construction is fundamentally capable of oscillating over a much wider frequency range than tubes tunable by means of capacitance variation. The advantage arises from the fact that the interaction gap where the electron stream is modulated by the radio frequency field is fixed. As discussed in more detail in Section X, this results in a slower variation of the modulation coefficient with frequency and also a slower variation of cavity losses and gap impedance than in an oscillator in which tuning is accomplished by changing the gap spacing. A cavity designed for wide range frequency coverage using the 707A tube is shown in Fig. 60. Using such a cavity it is possible to cover a frequency range from 1150 to 3750 megacycles. The inductance of the circuit is varied by moving the shorting piston in the coaxial line. For narrow frequency ranges,

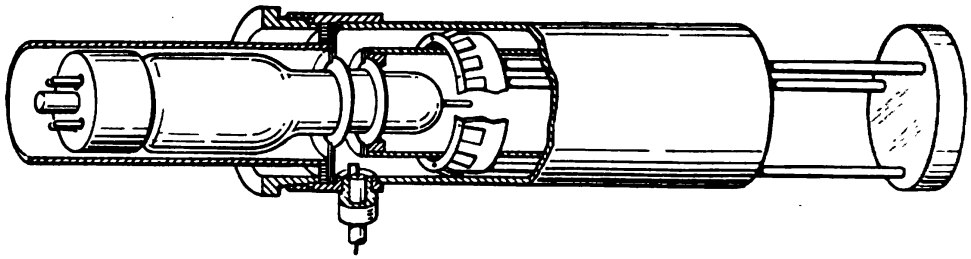

Fig. 60.—Sketch showing a piston tuned circuit for the W.E. 707-A which will permit operation from 1150 to 3750 mc.

cavities of the type shown in Fig. 61 are more suitable. In such cavities tuning is effected by means of plugs which screw into the cavity to change its effective inductance. Power may be extracted from the cavity by means of an adjustable coupling loop as shown in Fig. 61.

The 707A was the first reflex oscillator designed to operate at a low voltage i.e. 300 volts. This low operating voltage proved to be a considerable advantage in radar receivers because power supplies in this voltage range provided for the i.f. amplifiers could be used for the beating oscillator as well. Operation at this voltage was achieved by using an interaction gap with fine grids, which limits the penetration of high frequency fields. This results in a shorter effective transit angle across the gap for a given gap spacing and a given gap voltage than for a gap with coarse or no grids. Hence, for a given gap spacing a good modulation coefficient can be obtained at a lower voltage. Moreover, since drift action results in more efficient bunching at low voltages, a larger electronic admittance is obtained than with an open gap. This gain in admittance more than outweighs the

Generated on 2019-09-23 04:49 GMT / http://hdl.handle.net/2027/mdp.39015077775156
Public Domain, Google-digitized / http://www.hathitrust.org/access_use#pd-google
Digitized by Google
Original from UNIVERSITY OF MICHIGAN

greater capacitance of a gap with fine grids, so that a larger electronic tuning range is obtained than with an open gap. The successful low voltage operation of the 707A established a precedent which was followed in all the succeeding reflex oscillators designed for radar purposes at the Bell Tele-

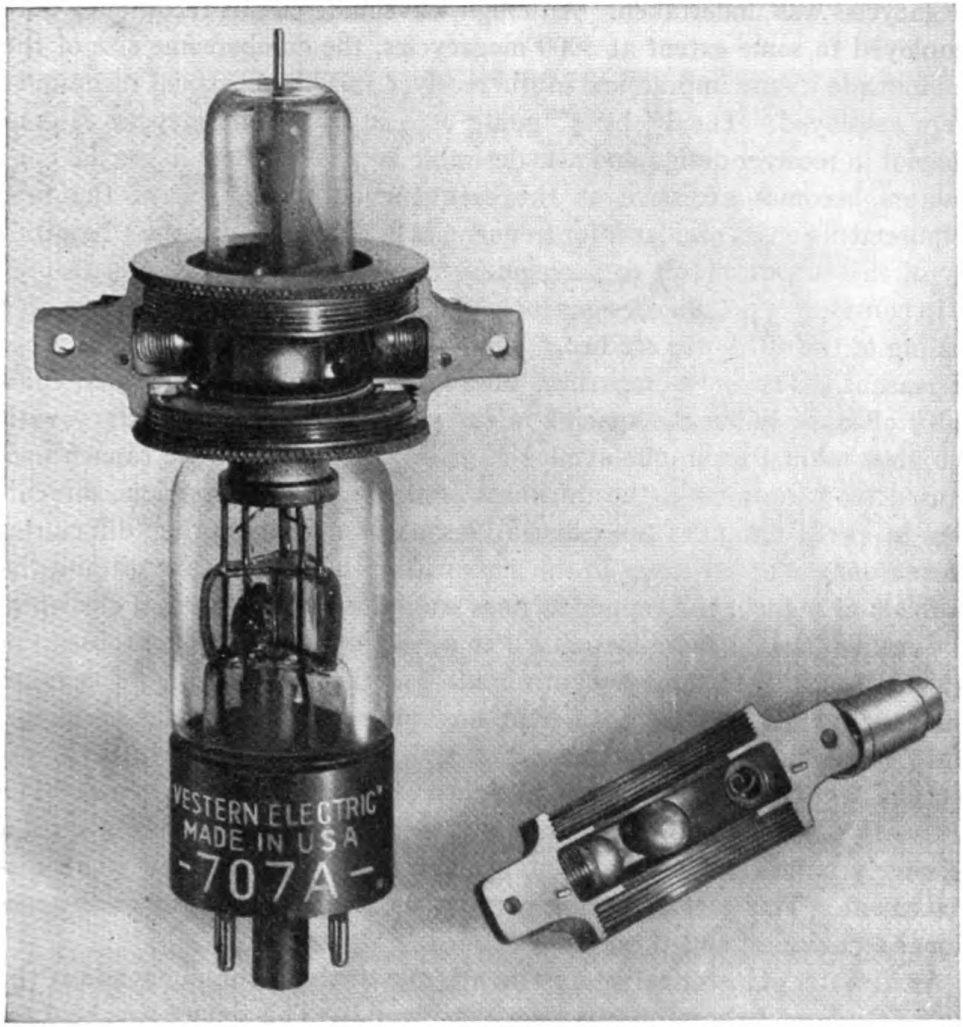

Fig. 61.—A narrow tuning range cavity for the W.E. 707-A of the type used in radar systems. The inductance of the cavity can be adjusted by moving screws into it. This view also shows the adjustable coupling loop.

phone Laboratories. The 707A is required to provide a minimum power output of 25 milliwatts and a half power electronic tuning of 20 megacycles near 3700 megacycles. The power output and the electronic tuning are in excess of this value over the range from 2500 megacycles to 3700 megacycles in a repeller mode having $3\frac{3}{4}$ cycles of drift.

Generated on 2019-09-23 04:50 GMT / http://hdl.handle.net/2027/mdp.39015077775156
Public Domain, Google-digitized / http://www.hathitrust.org/access_use#pd-google
Digitized by Google
Original from UNIVERSITY OF MICHIGAN

C. *A Reflex Oscillator With An Integral Cavity—The* 723

The need for higher definition in radar systems constantly urges operation at shorter wavelengths. Thus, while radar development proceeded at 3000 megacycles, a program of development in the neighborhood of 10,000 megacycles was undertaken. Although waveguide circuit techniques were employed to some extent at 3000 megacycles, the cumbersome size of the guide made its use impractical in the receiver and hence coaxial techniques were employed. The 1″ by ½″ guide used at 10,000 megacycles is convenient in receiver design and also desirable because the loss in coaxial conductors becomes excessive at this frequency. Hence, one of the first requirements on an oscillator for frequencies in this range was the adaptability of the output circuit to waveguide coupling.

In considering possible designs for a 10,000 megacycle oscillator the simple scaling of the 707A was studied. This appeared impractical for a number of reasons. The most important limitation was the constructional difficulty of maintaining the spacing in the gap with sufficient accuracy with the glass sealing technique available. Also, variations in the capacitance caused by variations in the thickness of the seals caused serious difficulties in predetermining an external resonator. Contributing difficulties arose from the power losses in the glass within the resonant circuit and the problem of making the copper to glass seals close to the internal elements.

Consideration of these factors led to a new approach to the problem, in which the whole of the resonant circuit was enclosed within the vacuum envelope. This required a different mechanism for tuning the resonator, since variation of the inductance of a cavity requires relatively large displacements which are difficult to achieve through vacuum seals. The alternative is to vary the capacitance of the gap. Since the gap is small a relatively large change in capacitance can be achieved with a small displacement. This sort of tuning permits the use of metal tube constructional techniques, and these were applied.

As a matter of historical interest an attempt at this technique made at the Bell Telephone Laboratories is shown in Fig. 62. This device was held together by a sealing wax and string technique and was not tunable in the first version. It oscillated successfully on the pumps, however, and a second version was constructed which was tuned by means of an adjustable coaxial line shunting the cavity resonator. Adjustment of this auxiliary line gave a tuning range of 7.5%. Such a tuning method is fraught with the complications outlined in Section IX.

An early reflex oscillator tube of the integral cavity type designed at the Bell Telephone Laboratories was the Western Electric 723A/B.

Generated on 2019-09-23 04:50 GMT / http://hdl.handle.net/2027/mdp.39015077775156
Public Domain, Google-digitized / http://www.hathitrust.org/access_use#pd-google
Digitized by Google
Original from UNIVERSITY OF MICHIGAN

This design was superseded later by the W.E. 2K25 which has a greater frequency range and a number of design refinements. From a constructional point of view the two types are closely similar, however, and to avoid duplication the later tube will be described to typify a construction which served as a basis for a whole series of oscillators in the range from 2500 to 10,000 Mc/s.

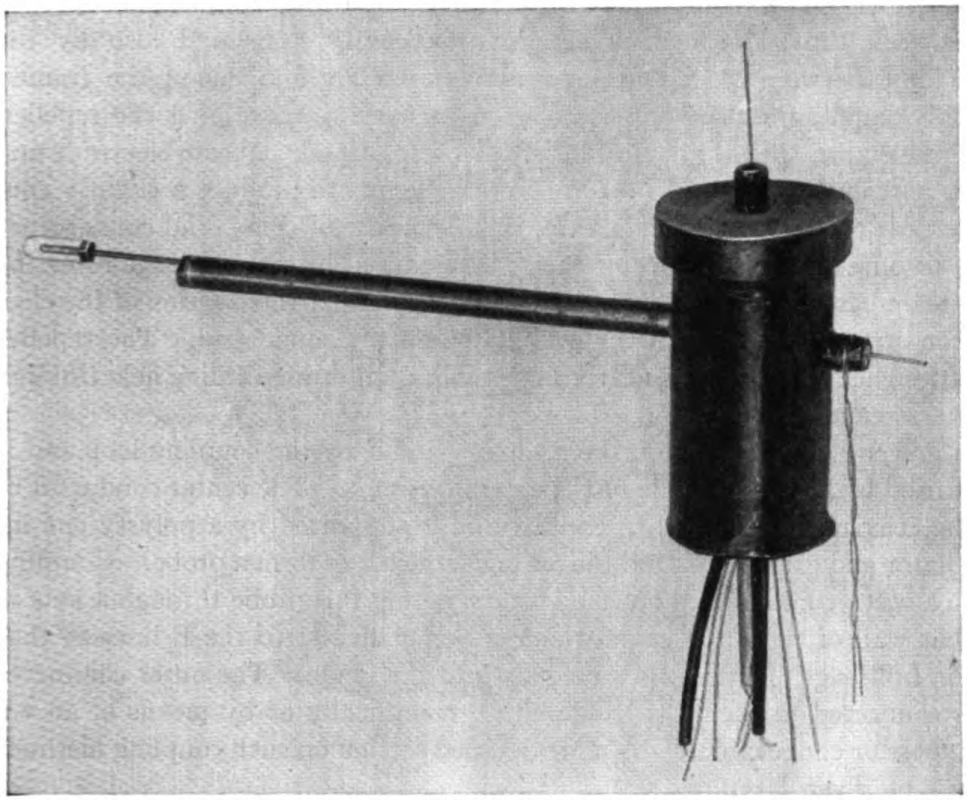

Fig. 62.—An early continuously pumped metal reflex oscillator tuned with an external line.

Before proceeding to a description of the 2K25 tube it seems desirable to recapitulate in more detail the design objectives from a mechanical point of view. These were:

1. To provide a design which would lend itself to large scale production and one sufficiently rugged as to be capable of withstanding the rough use inherent in military service.
2. To provide output means which permit coupling to a wave guide in such a manner that installation or replacement could be accomplished in the simplest possible manner.
3. To provide a tuning mechanism for the resonant circuit which, while simple, would give sufficiently fine tuning to permit setting and holding

Generated on 2019-09-23 04:50 GMT / http://hdl.handle.net/2027/mdp.39015077775156
Public Domain, Google-digitized / http://www.hathitrust.org/access_use#pd-google
Digitized by Google
Original from UNIVERSITY OF MICHIGAN

a frequency within one or two parts in 10,000. In addition, in order to avoid field installation it was desired to have the tuning mechanism cheap enough to be factory installed and discarded with each tube.

4. The oscillator was required to be compact and light in weight to facilitate its use in airborne and pack systems.

Figure 63 shows a cross-section view of the final design of the 2K25 reflex oscillator. The resonant cavity is formed in part by the volume included between the frames which support the cavity grids and also by the volume between the flexible vacuum diaphragm and one of the frames. This diaphragm also supports a vacuum housing containing the repeller. The electron optical system consists of a disc cathode, a beam electrode and an accelerating grid. These are so designed as to produce a slightly convergent outgoing electron stream. The purpose of this initial convergence is to offset the divergence of the stream caused by space charge after the stream passes the accelerating grid and to minimize the fraction of the electron stream captured on the grid frame on the round trip. The repeller is designed to provide as nearly as possible a uniform retarding field through the stream cross-section.

Power is extracted from the resonant circuit by the coupling loop and is carried by the coaxial line to the external circuit. The center conductor of the coaxial line external to the vacuum is supported by a polystyrene insulator and extends beyond the outer conductor to form a probe. Coupling to a wave guide is accomplished by projecting this probe through a hole in that wall of the wave guide which is perpendicular to the E lines so that the full length of the probe extends into the guide. The outer conductor is connected to the wave guide either metallically or by means of an r.f. bypass or choke circuit. A more detailed section on such coupling methods will be given later.

The tube employed a standard octal base modified to pass the coaxial line. Thus if a standard octal socket is similarly modified and mounted on the wave guide it is possible to couple the oscillator to the wave guide and power supply circuits simply by plugging it into the socket, just as with any conventional vacuum tube.

The tuning means for this type of oscillator tube presented a serious problem. This will be appreciated when it is realized that the mechanism must permit setting frequencies correctly to within one megacycle in a device in which the frequency changes at the rate of approximately 200 megacycles per thousandth of an inch displacement of the grids. In other words, the tuner was required to make possible the adjustment of the grid spacing to an accuracy of five millionths of an inch. The design of the mechanism adopted was originated by Mr. R. L. Vance of these Laboratories. The operation of the tuner can be seen from an examination of the cross-section

Digitized by Google
Original from UNIVERSITY OF MICHIGAN
Generated on 2019-09-23 04:51 GMT / http://hdl.handle.net/2027/mdp.39015077775156
Public Domain, Google-digitized / http://www.hathitrust.org/access_use#pd-google

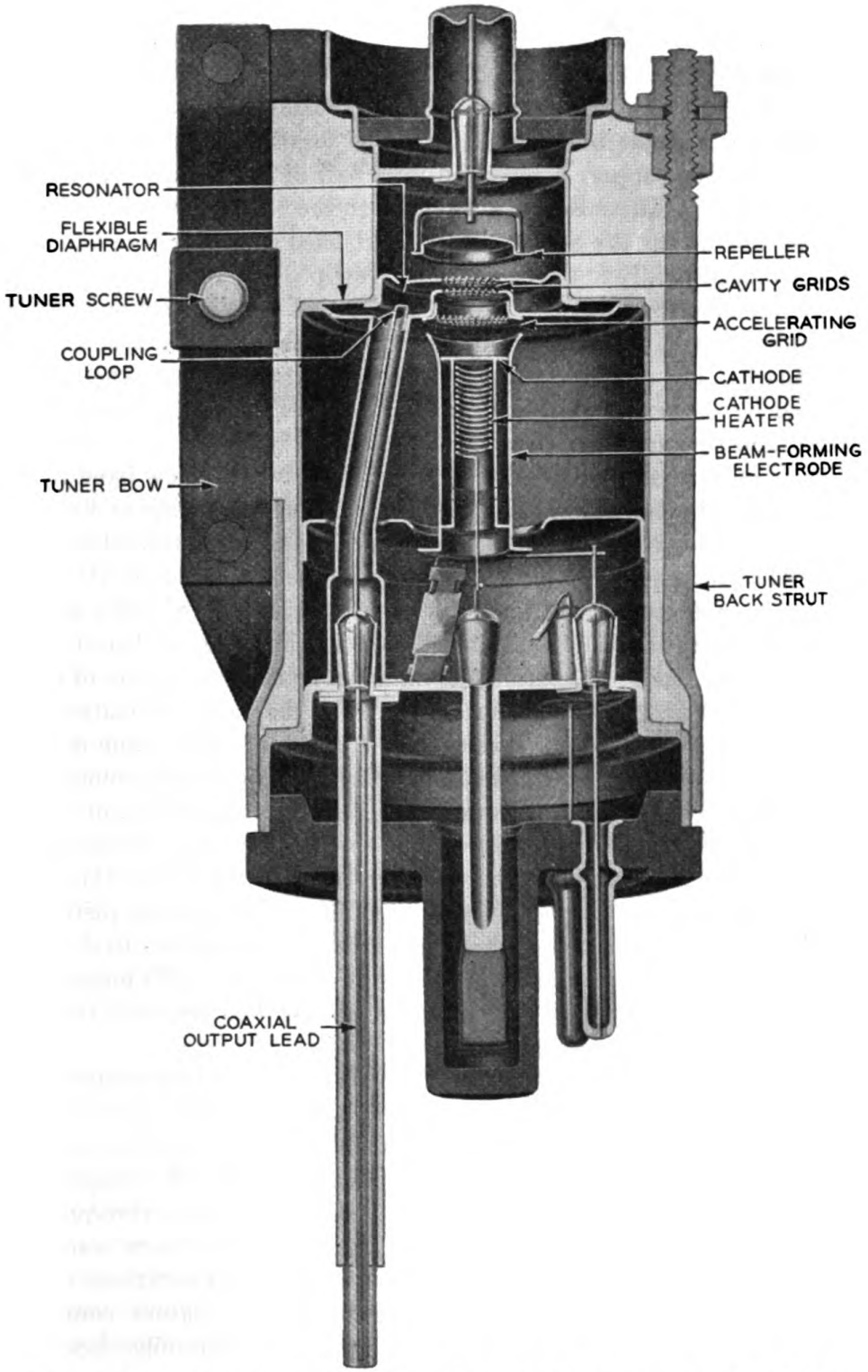

Fig. 63.—A 3 centimeter reflex oscillator with an internal resonator. This tube is a further development of the earliest internal resonator reflex oscillator designed at the Bell Telephone Laboratories.

Digitized by Google
Original from UNIVERSITY OF MICHIGAN
Generated on 2019-09-23 04:51 GMT / http://hdl.handle.net/2027/mdp.39015077775156
Public Domain, Google-digitized / http://www.hathitrust.org/access_use#pd-google

and external views of Figs. 63 and 67. On one side of the tube a strut extending from the base is attached to the repeller housing. This strut acts as a rigid vertical support but provides a hinge for lateral motion. On the opposite side the support is provided by a pair of steel strips. These are clamped together where they are attached to the vacuum housing support and also where they are attached to a short fixed strut near the base. A nut is attached rigidly to the center of each strip. One nut has a right and the other a left handed thread. A screw threaded right handed on one half and left handed on the other half of its length turns in these nuts and drives them apart. The mechanism is thus a toggle which, through the linkage provided by the repeller housing, serves to move the grids relative to one another and thus to provide tuning action.

The 723A/B was originally designed for a relatively narrow band in the vicinity of 9375 megacycles. It operates at a resonator voltage of 300 volts and the beam current of a typical tube would be approximately 24 milliamperes. The design was based on the use of repeller voltage mode which with the manufacturing tolerances lay between 130 and 185 volts at 9375 megacycles. It is difficult to establish with certainty the number of cycles of drift for this mode. Experimental data can be fitted by values of either $6\frac{3}{4}$ or $7\frac{3}{4}$ cycles and various uncertainties make the value calculated from dimensions and observed voltages equally unreliable. This value is, however, of interest principally to the designer and of no particular moment in application. The performance was specified for the output line of the oscillator coupled to a $\frac{5}{8}'' \times 1\frac{1}{4}''$ wave guide so that the probe projected full length into the guide through the wider wall and on the axis of the guide. With a matched load coupled in one direction and a shorting piston adjusted for an optimum in the other the oscillator was required to deliver a minimum of 20 milliwatts power output at a frequency of 9375 megacycles. Under the same conditions the electronic tuning was required to be at least 28 megacycles between half power points.

For reasons of continuity a more detailed description of the properties of the 3 centimeter oscillator will be given in a later section. The 723A/B oscillator served as the beating oscillator for all radar systems operating in the 3 centimeter range until late in the war when the 2K25 supplanted it. At the time that the 723A/B was developed the best techniques and equipment available were employed. In retrospect these were somewhat primitive and of course this resulted in a number of limitations of performance. Since the tubes designed as beating oscillators commonly served as signal generators in the development of ultra-high frequency techniques and equipment the wartime designer of such oscillators usually found himself in the position of lifting himself by his own bootstraps. In spite of these limitations the later modifications of the 723A/B which led to

Digitized by Google
Original from UNIVERSITY OF MICHIGAN
Generated on 2019-09-23 04:51 GMT / http://hdl.handle.net/2027/mdp.39015077775156
Public Domain, Google-digitized / http://www.hathitrust.org/access_use#pd-google

the 2K25 did not fundamentally change the design but were rather in the direction of extending its performance to meet the expanding requirements of the radar art. The incorporation of the resonant cavity within the vacuum envelope resulted in a major revision of the scope of the designer's problems. He assumed a part of the burden of the circuit engineer in that it became necessary for him to design an appropriate cavity and predetermine the correct coupling of the oscillator to the load. The latter transferred to the laboratory a problem which in the case of separate cavity oscillators had been left as a field adjustment.

D. *A Reflex Oscillator Designed to Eliminate Hysteresis—The 2K29*

As service experience with the external cavity type of reflex oscillator was gained a number of limitations of such a design became apparent. The difficulties arose primarily from the conditions of military application. A typical difficulty was the corrosion of cavities and copper flanges under the severe tropical conditions met in some service applications. The difficulty of maintaining a moistureproof seal in a cavity tuned by variation of the inductance made it very difficult to alleviate this condition. The success of the all metal technique in the three centimeter range suggested the application of the same principles to the design of a 10 centimeter oscillator and this was undertaken.

Mechanically, the problem was straightforward, but an extrapolation of the electrical design of the 723A/B to 10 centimeters suffered from a fatal defect. The difficulty, previously described in Section VIII, was the discontinuous and multiple valued character of the output as a function of the repeller voltage. Reference to Fig. 19 will indicate the operational problems which would arise in an oscillator in which the hysteresis existed in marked degree. The a.f.c. systems were such that in starting the repeller voltage would start from a value more negative than required for oscillation and decrease. As the repeller voltage decreased through the range where oscillation would occur the frequency would of course cover a range of values. When the repeller voltage reached a value such that the frequency of the oscillator had a value differing from the transmitter by the intermediate frequency the steady shift of the repeller voltage would be stopped and would then hunt over a limited range about the value required to maintain the difference frequency. When adjusted for operation this condition would pertain with the repeller voltage at a value such that the oscillator would be delivering maximum power. If under operating conditions the frequency required of the oscillator by the system drifted to that corresponding to the amplitude jump at B, any further drift of frequency could not be corrected. Thus, one effect of the hysteresis is to limit the electronic tuning range. As a second possibility, let us assume that the

Digitized by Google
Original from UNIVERSITY OF MICHIGAN
Generated on 2019-09-23 04:51 GMT / http://hdl.handle.net/2027/mdp.39015077775156
Public Domain, Google-digitized / http://www.hathitrust.org/access_use#pd-google

frequency has drifted so that the oscillator is operating in a range between A and B of Fig. 19. If now the operation of the system is momentarily interrupted the a.f.c. system will start hunting. This is done by returning to the non-oscillating repeller voltage just as when operation is initiated. When the hunting repeller voltage passes through the value between A and B from the non-oscillating state no oscillation occurs and hence the a.f.c. cannot lock in and the system becomes inoperative. Thus it is imperative that hysteresis be kept, as a minimum requirement, outside the useful electronic tuning range.

As indicated in Section VIII it was found that the electronic hysteresis occurred when the electron stream made more than two transits across the gap. Thus an added objective of the design of the 10 centimeter metal oscillator became the achievement of an electron optical system which would limit the number of transits to two while insuring that the maximum number of electrons leaving the cathode would make the two transits with a minimum spread in zero signal transit time.

Figure 64 shows a sectional view of the final design adopted. The electron optical structure differs from that of the 723A/B in a number of respects. The first grid of the 723A/B has been eliminated and one of the cavity grids now plays a dual role in simultaneously serving as an accelerating grid. The grids are curved towards the cathode, which has a central spike. This arrangement is intended to produce a hollow cylindrical electron stream. It will be observed that the second grid is larger in diameter than the first and that the repeller has a central spike. The design is such that the cylindrical beam entering the repeller region is caused to diverge radially, so that in re-traversing the gap after its reversal in direction it impinges on and is captured by the frame supporting the first grid.

The repeller design was determined by using an electrolytic trough to determine the potential plots for a number of trial configurations. Then by making point by point calculations of the electron paths the best configuration was chosen. A typical example of such path tracing is shown in Fig. 65. This figure shows the equipotential lines and the trajectories computed for electrons on the inner and outer boundaries of the outgoing stream. The method of calculating the trajectories has been described by Zworykin and Rajchman.[12] It assumes that space charge may be neglected. Fig. 65 shows that the repeller design is such that the cylindrical outgoing stream is focussed upon its return onto the frame supporting the first grid. The cathode spike prevents emission from the central portion of the cathode, since it would be difficult to prevent electrons from this portion from returning into the cathode space. A second requirement on

[12] V. K. Zworykin and J. A. Rajchman, *Proc. of I.R.E.*, Sept. 1939, Vol. 17, No. 9, pp. 558–566.

Digitized by Google
Original from UNIVERSITY OF MICHIGAN
Generated on 2019-09-23 04:51 GMT / http://hdl.handle.net/2027/mdp.39015077775156
Public Domain, Google-digitized / http://www.hathitrust.org/access_use#pd-google

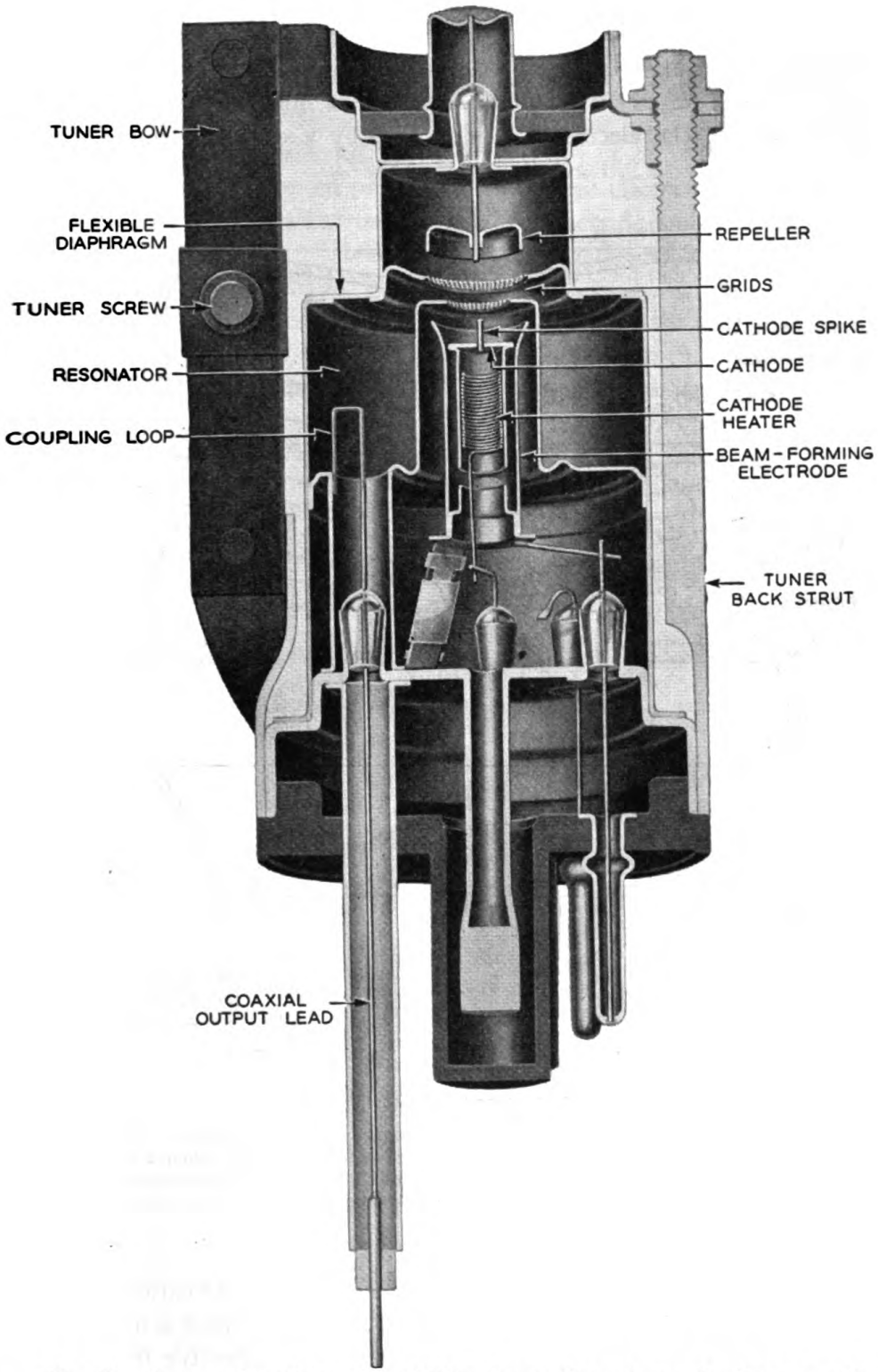

Fig. 64.—Section view of the W.E. 2K29 reflex oscillator shows the electron optical system used in eliminating hysteresis. (Fig. 65) This tube has an internal cavity and is designed for the frequency range from 3400 to 3960 mc/s.

Digitized by Google
Original from UNIVERSITY OF MICHIGAN
Generated on 2019-09-23 04:51 GMT / http://hdl.handle.net/2027/mdp.39015077775156
Public Domain, Google-digitized / http://www.hathitrust.org/access_use#pd-google

the design was that the spread in the transit angle for zero signal should be small. This requirement is not as stringent as might be expected. The contribution to the electronic conductance by a current element whose

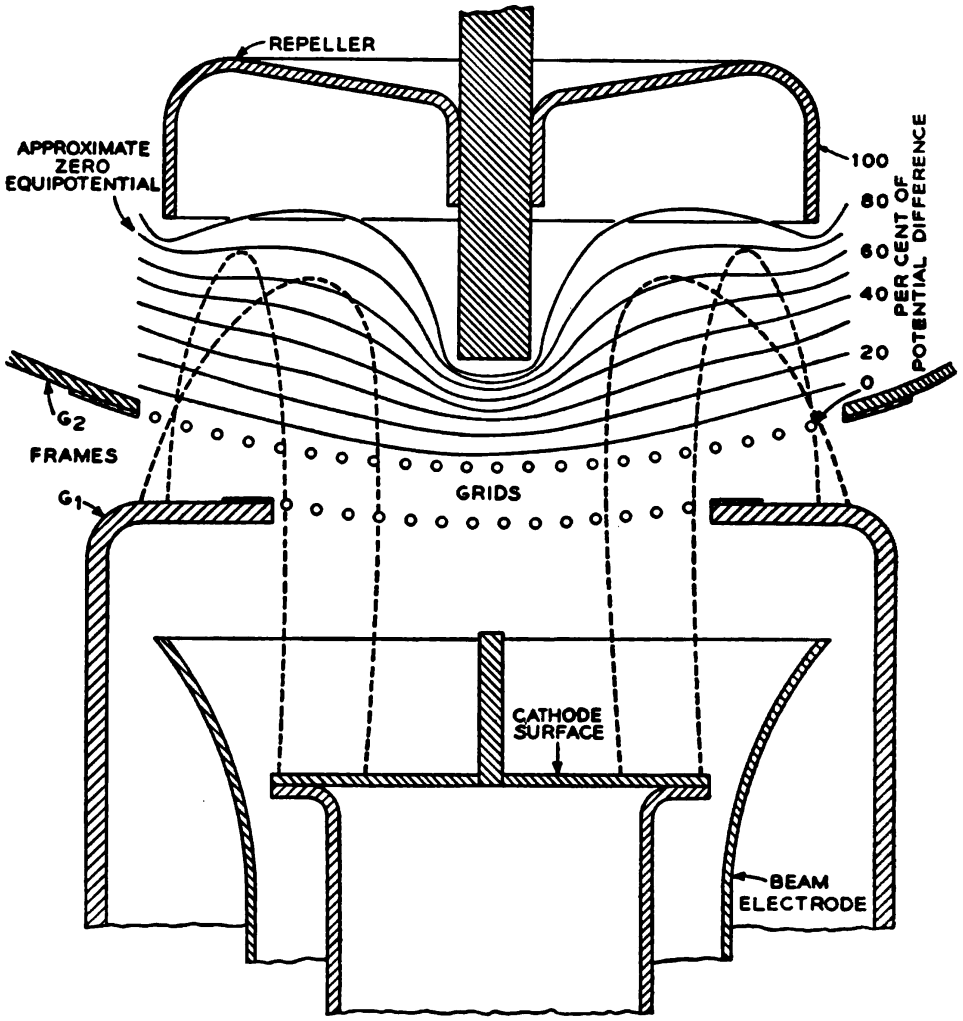

Fig. 65.—Repeller design for eliminating hysteresis in a reflex oscillator. The electrons make only two transits through the gap. The repeller does not return them to the cathode region but to the edge supporting one of the grids of the gap. Equipotentials determined from an electrolytic trough investigation are shown and the electron trajectories computed from these equipotentials.

transit angle deviates from the optimum by a small angle $\Delta\theta$ varies as $\cos \Delta\theta$, so that even for spreads in angle as great as $\pm$ 30° the effect is not serious.

The design illustrated in Fig. 64 was strikingly effective in reducing hysteresis. Fig. 66 shows repeller characteristics for the original design which was extrapolated from the 723A/B and for the design of Fig. 64.

Digitized by Google
Original from UNIVERSITY OF MICHIGAN
Generated on 2019-09-23 04:52 GMT / http://hdl.handle.net/2027/mdp.39015077775156
Public Domain, Google-digitized / http://www.hathitrust.org/access_use#pd-google

In addition to improving the electronic tuning characteristics the design was found to be more stable against variations in load, as would be expected from the discussion of Section VIII.

The arrangement adopted provided a prototype electron optical system which was used in a whole series of reflex oscillators designed for radar and communication systems. These tubes were the 726A, 726B and 726C, 2K29, 2K22, 2K23 and 2K56.

The output line of these tubes is intended to couple through an adapter to either a coaxial line or a wave guide. In the first case the adapter serves to couple the output line of the tube to the cable, in some instances through

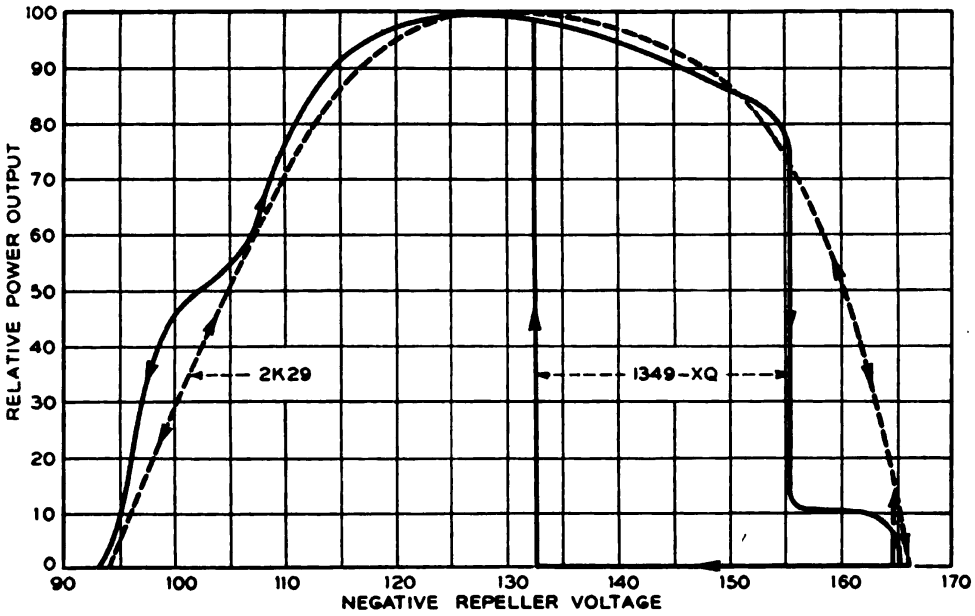

Fig. 66.—Use of the electron optical system shown in Fig. 65 eliminated the bad features of the repeller characteristics of the earlier 1349XQ in which the electrons were returned to the repeller region and gave the repeller characteristic of the final 2K29 (dashed line).

an impedance transformer and in some instances directly. As practice developed it became standard to design for optimum oscillator output characteristics with output line coupled to a 50 ohm resistive impedance. In the second case the adapter serves to couple the tube output line to the guide through a transducer.

A typical example of a reflex oscillator incorporating this construction is the 2K29. This tube is intended to cover the frequency range from 3400 to 3960 Mc/s. An external view of this tube is shown in Fig. 67. It will be observed that the center conductor of the output line extends beyond the polystyrene supporting bushing. Fig. 68 shows an adapting fitting which

Digitized by Google
Original from UNIVERSITY OF MICHIGAN
Generated on 2019-09-23 04:52 GMT / http://hdl.handle.net/2027/mdp.39015077775156
Public Domain, Google-digitized / http://www.hathitrust.org/access_use#pd-google

permits the oscillator to be coupled to a fifty ohm coaxial cable. The center conductor of the tube output line projects into the split chuck, while contact is made to the outer conductor of the tube output line by the spring contact fingers *F*. The coupling unit can be mounted in a standard octal socket so that the tube can be coupled simultaneously to the power supplies and the high frequency circuit by a simple plug in operation. It is frequently desirable to insulate the outer conductor of the oscillator from

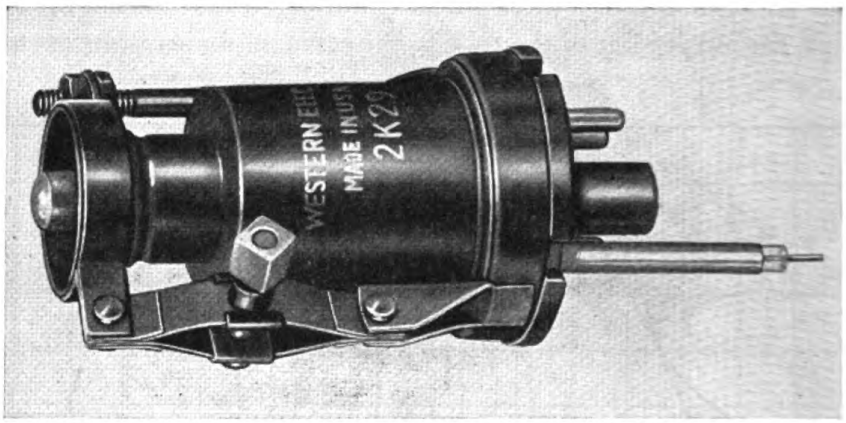

Fig. 67.—Metal reflex oscillator with enclosed resonator designed for operation from 3400 to 3960 mc/s.

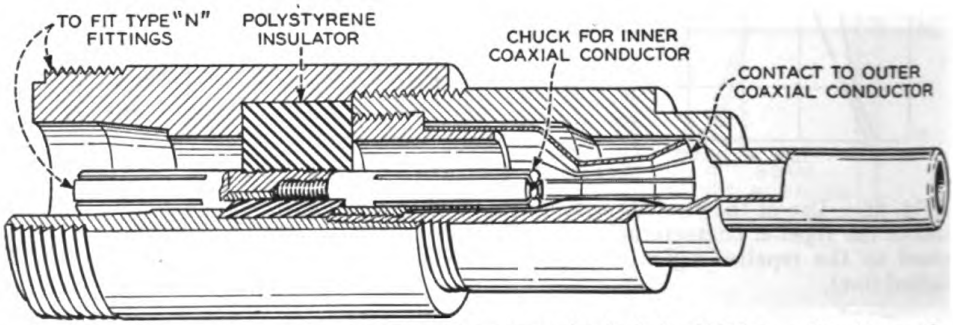

Fig. 68.—A transducer for connecting the output lead of the 2K29 to a 50 ohm cable.

the line for direct voltages while maintaining the high frequency contact. This can be accomplished with either an insulating sleeve of low capacitance or a modification of the design which incorporates a high frequency trap in the outer conductor. In some instances it is necessary to insulate the center conductor of the tube from the line for direct voltages. This can be done with a concentric condenser. The characteristic impedance of the section of the coupler may be made the same as that of the line by maintaining the proper ratio of the diameters of the condenser and the outer

Digitized by Google
Original from UNIVERSITY OF MICHIGAN
Generated on 2019-09-23 04:52 GMT / http://hdl.handle.net/2027/mdp.39015077775156
Public Domain, Google-digitized / http://www.hathitrust.org/access_use#pd-google

conductor or may be arranged so that the condenser serves simultaneously as an impedance transformer to transform the impedance of the line to that required for best performance of the oscillator. A general discussion of the problems involved in such coupling designs will be given in a later section.

One of the primary considerations in the design of a reflex oscillator is the choice of resonator characteristics. The various controlling factors have been outlined in previous sections. In Section X it was shown that the power output and the electronic tuning optimize at different gap transit

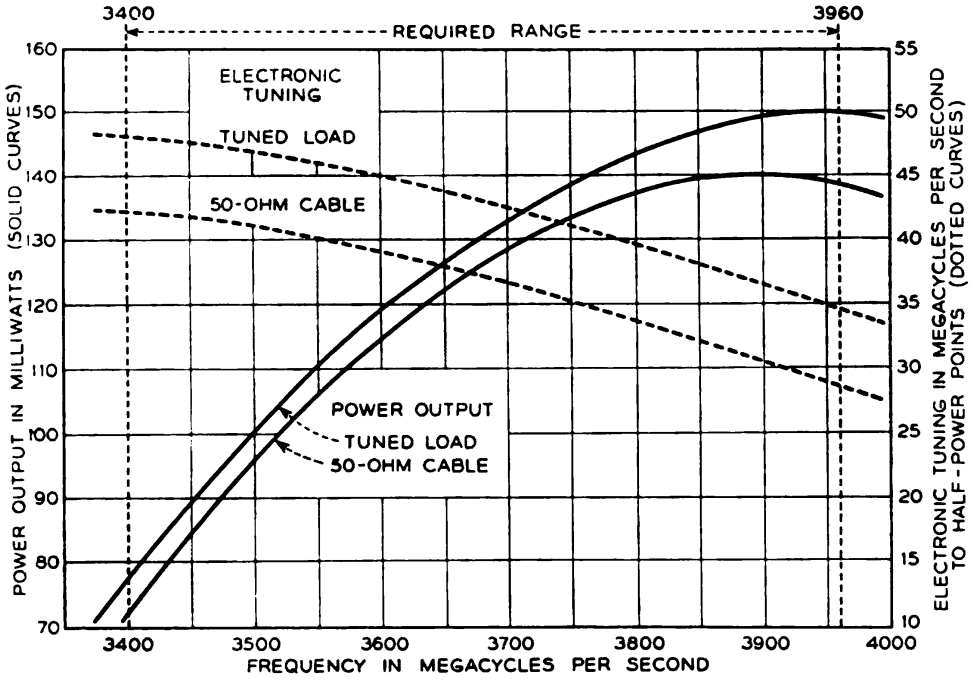

Fig. 69.—Power output and electronic tuning vs frequency for the 2K29 reflex oscillator. The solid lines give the performance into a load adjusted for optimum power output at each frequency. The dashed lines show the performance obtained when the tube is coupled to a 50 ohm load by means of the fitting of Fig. 68.

angles. It is therefore necessary to compromise with the ultimate use in mind. In a beating oscillator for a radar receiver, uniformity of the electronic tuning is of greater importance than uniformity of power output, since an adjustment of the coupling to the crystal permits some variation of the latter quantity. Hence, the resonator characteristics are chosen to provide as nearly uniform electronic tuning as possible. Fig. 69 shows the electronic tuning and power output characteristics for the Western Electric 2K29 tube. These are shown for two conditions. The solid lines show the power output and electronic tuning measured into an adjustable load which

Digitized by Google
Original from UNIVERSITY OF MICHIGAN
Generated on 2019-09-23 04:52 GMT / http://hdl.handle.net/2027/mdp.39015077775156
Public Domain, Google-digitized / http://www.hathitrust.org/access_use#pd-google

made it possible to present to the oscillator at each frequency the admittance into which the oscillator delivered maximum power output. The solid lines show the power output and electronic tuning over the band with the oscillator connected to a load presenting a resistive 50 ohm impedance to the coupling unit of Fig. 68. The problems involved in obtaining such performance will be outlined in the next section.

E. *Broad-Band Reflex Oscillators—The 2K25*

As experience with the design of radar systems and components developed and as a better understanding of the operation and limitations of the individual components was achieved, a great deal of effort was directed toward simplifying and making more reliable the number of adjustments required to optimize the performance of a system. As an illustration of this problem as related to the beating oscillator, the development problem of the 2K25 will be described. As the number of radar systems in the three centimeter range increased it became apparent that to avoid self-jamming it would be desirable to assign frequencies to various sets operating, for example, in a fleet unit. Secondarily, the over-all band of the three centimeter range was widened to cover from 8500 to 9660 Mc/s. Prior to this the 723A/B had been essentially a spot frequency oscillator and had been primarily tested as such. As was so frequently the case with tubes for military requirements, it was desired that the ultimate tube be interchangeable with an existing tube, in this case the 723A/B, and hence the improvements had to be effected within its framework.

Changes in the electronic design from that of the 723A/B produced an improved performance in the 2K25. These were a modification of the electron gun which increased the effectiveness of the electron stream and the elimination of a resonance of the region containing the electron gun which coupled with the resonant cavity and in some cases impaired the performance over the wide band. Beyond this the problem concerned the determination of an output coupling system which would provide the desired properties. This will be described in detail.

One of the most serious difficulties which occurred in early radar receivers arose from the general failure to appreciate the effect of the load impedance on the performance of an oscillator. This problem has been discussed in Section IX. In early radar receivers the method of coupling the beating oscillator to the crystal was dictated mainly by mechanical convenience rather than electrical considerations, and as a result most of the discontinuities of performance due to bad load conditions which are discussed in Section IX occurred at one time or another in most of the systems. For instance, users were much surprised to find that a beating oscillator which could be tuned to frequencies both above and below that required for

Digitized by Google
Original from UNIVERSITY OF MICHIGAN
Generated on 2019-09-23 04:52 GMT / http://hdl.handle.net/2027/mdp.39015077775156
Public Domain, Google-digitized / http://www.hathitrust.org/access_use#pd-google

reception of the signal might yet fail to oscillate at the desired frequency. The convenience of simple replaceability of the local oscillator became in this instance a cross for its designer, since an exchange of tube would frequently eliminate the effect. This led to the obvious conclusion on the part of the user that the oscillator was defective, in spite of the fact that the presumably defective tube had passed the test specifications and would operate satisfactorily in some other receiver. The plain fact, in the light of later knowledge, was that the tubes were being improperly used, so that the usual range of manufacturing variations was not tolerable.

The appreciation of this fact led to a new approach to the problem of coupling the beating oscillator to a waveguide. In early designs the oscillator was decoupled from the load by withdrawing the probe from the waveguide. This presented the oscillator with an uncontrolled admittance with disastrous results in many cases. The new approach, proposed by the group working with Dr. H. T. Friis at the Bell Telephone Laboratories, was that of designing the receiver so that the beating oscillator could be operated into an essentially fixed impedance. The crystal was in this case loosely coupled to form a part of this load, so that variations in its impedance and the impedance looking toward the TR tube were largely masked. A great many further refinements in the design of the receiver have since been proposed, but this basic principle of defining the load into which the oscillator is required to operate is fundamental to all. In the interests of simplicity of use it appeared to be desirable to endeavor to pre-plumb the coupling of the oscillator to the wave guide. The tube designer in this instance found himself perforce, as so frequently occurs in dealing with micro-waves, a circuit designer—an instructive and illuminating experience which might happily be reversed.

The wave guide coupling was made separate from the tube, both to preserve the plug in feature of the tube and to maintain its interchangeability with the 723A/B. As a further simplification it was desired that the coupling should require no adjustments. A convenient fixed load admittance to present to this coupler is the characteristic admittance of the wave guide, since this can readily be maintained fixed over a wide band. The problem, then, is the apparently straightforward one of transforming the guide admittance to the admittance which the oscillator requires for optimum performance. Actually, the problem is complicated by the fact that the optimum admittance will vary throughout the band. The electronic admittance varies with frequency even for a fixed drift angle, because the modulation coefficient of the gap varies as the oscillator is tuned. The losses of the resonator also vary with frequency, both because of skin effect, the depth of penetration of the high frequency currents changing with frequency, and because the circulating currents in the resonator are a function

Digitized by Google
Original from UNIVERSITY OF MICHIGAN
Generated on 2019-09-23 04:53 GMT / http://hdl.handle.net/2027/mdp.39015077775156
Public Domain, Google-digitized / http://www.hathitrust.org/access_use#pd-google

of the effective capacitance of the gap. As the capacitance increases in tuning to lower frequencies the I^2R losses therefore increase.

The objective of the coupling design may not be to obtain maximum power output at all points in the band but rather to obtain uniformity of electronic tuning and power output. An additional requirement in some cases is that a minimum sink margin as defined in section VIII should be maintained. This is equivalent to the problem arising in magnetron design of controlling the pulling figure.[13]

In designing an appropriate wave guide coupling a number of variables are at one's disposal. In the case of the W.E. 2K25 the variables available are, the length of the tube probe exposed within the guide, the offset of the probe from the axis of the guide, and the distance from the probe to the shorting piston in the guide. In addition, the characteristics of the output line of the tube are adjustable, and, finally, the coupling of the loop to the resonator can be adjusted. As one might expect, there is a large number of solutions with so many variables available. The most desirable solution is one which provides a low standing wave ratio in all parts of the coupling system. The method employed in the present case was to design a wave guide to coaxial transducer which would provide a smooth broad band transition from the wave guide characteristic admittance to the admittance of the coaxial line. In the ideal case, the characteristic admittance of the coaxial line to the loop should be maintained as uniform as possible. Structural considerations in the present case led to discontinuities which had to be appropriately balanced in the final transducer. Dr. W. E. Kock of the Bell Telephone Laboratories has given an expression which, for thin probes, relates the probe length, the offset and the distance of the backing piston when given the characteristic admittance of the coaxial line and the dimensions of the guide between which a match is required. Once such a transducer has been obtained, the admittances which must be presented to it in order to obtain maximum power from the oscillator are measured over the band. From such measurements it is then possible to determine the corrections in the loop size and in the transducer to obtain a given sink margin throughout the band. This last step actually involves a certain amount of cut and try in an effort to obtain satisfactory performance in all respects. Figure 70 illustrates the transducer developed for the W.E. 2K25 oscillator for use with 1″ by ½″ wave guide. All tests made on this tube are specified in terms of operation in this coupler and with a load having the characteristic impedance of the 1″ x ½″ guide presented to the coupler.

Figure 71 shows a performance diagram for a typical W.E. 2K25 oscillator operating in the coupler of Fig. 70. The reference plane for the diagram is

[13] J. B. Fisk, H. D. Hagstrum and P. L. Hartman, "The Magnetron as a Generator of Centimeter Waves". See pp. 56 ff.

Digitized by Google
Original from UNIVERSITY OF MICHIGAN
Generated on 2019-09-23 04:53 GMT / http://hdl.handle.net/2027/mdp.39015077775156
Public Domain, Google-digitized / http://www.hathitrust.org/access_use#pd-google

not the plane of the grids of the oscillator but is instead a more accessible reference plane external to the tube, in this instance the plane through the wave guide perpendicular to its axis which includes the tube probe. It will be observed that the sink margin in the case illustrated was equal to 5.5. At the frequency at which this diagram was obtained, the minimum sink margin permitted by the test specification is 2.5. The variation in this margin results from a variety of causes. As shown in Section III the sink margin is determined by the ratio of the total load conductance to the small signal electronic conductance. The total load conductance consists of the

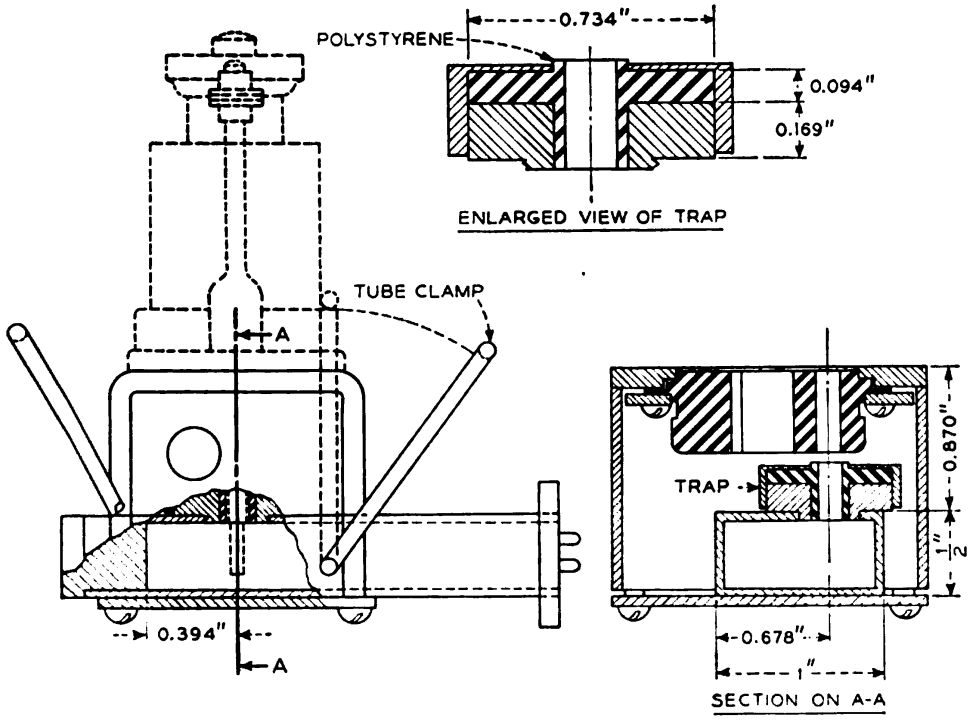

Fig. 70.—A broad band coupling designed to connect the 2K25 to a 1″ x ½″ wave guide

conductance representing the resonator losses and the conductance arising from the wave guide load transformed through the coupling system. Hence, the coupled load will be subject to variations in the loop dimensions, the characteristics of the coupling line and the transducer. The resonator loss will differ from tube to tube because of the variation in the heating of the grids and resonator by the electron stream, and there will be variations arising from other causes. The electronic conductance varies from tube to tube primarily because of the spread in beam current and secondarily as a result of such factors as variations in the modulation coefficient of the gaps, non-uniformities in the drift space causing a spread in the transit time and

Generated on 2019-09-23 04:53 GMT / http://hdl.handle.net/2027/mdp.39015077775156
Public Domain, Google-digitized / http://www.hathitrust.org/access_use#pd-google
Digitized by Google
Original from UNIVERSITY OF MICHIGAN

the like. The sum total of these variations necessitated the maintenance of an average sink margin of 6.7 times in order to insure a minimum of 2.5.

Figure 72 illustrates further characteristics of the 2K25 oscillator and coupling. These data are the results of standing wave measurements looking towards the coupler with the tube inoperative. From such "cold test"

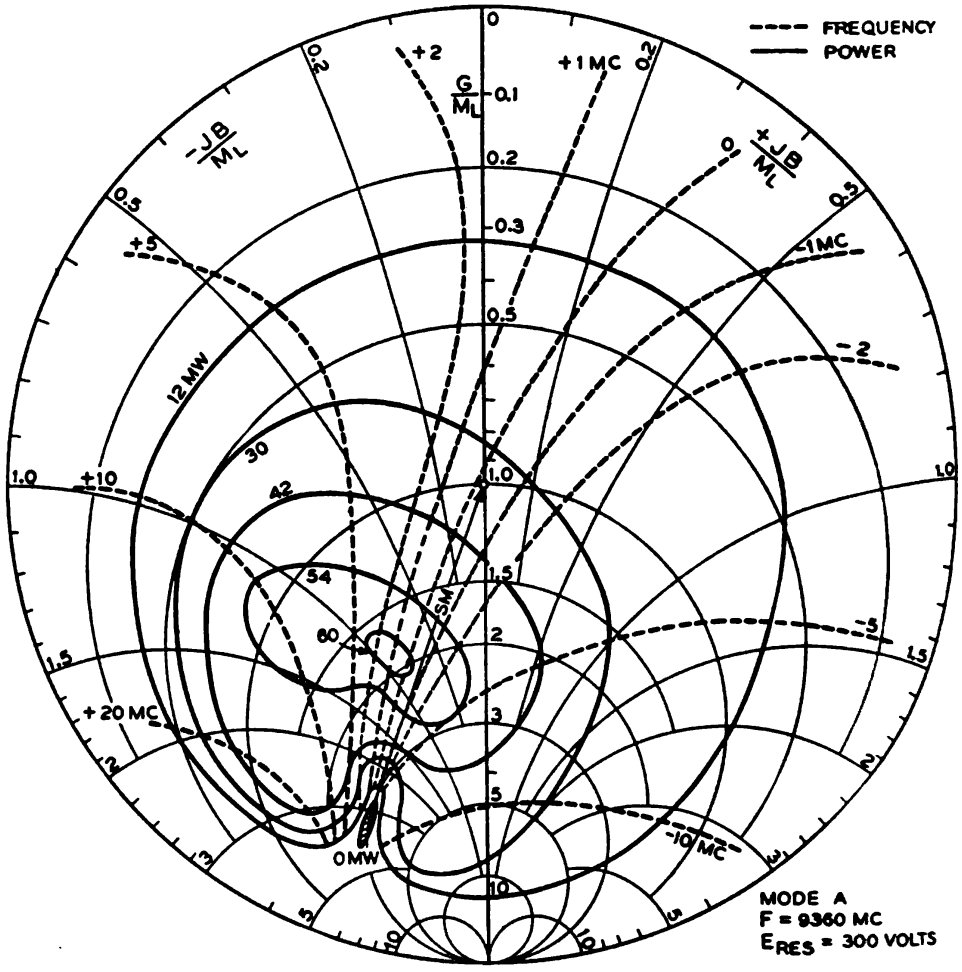

Fig. 71.—A Rieke diagram for the 2K25 connected to the load by the coupling of Fig. 70. This diagram was obtained for a repeller mode having a drift angle of 15.5 π radians at a nominal frequency of 9360 mc/s.

measurements one may determine the intrinsic Q_0 of the resonator and the external Q_E. The former is a measure of the resonator losses while the latter is a measure of the tightness of coupling of the oscillator to the load. The values of Q_0 measured from a cold test have little significance in an oscillator in which heating of the resonator and especially of the grids is appreciable. This is particularly true of oscillators tuned by variation of

Digitized by Google
Original from UNIVERSITY OF MICHIGAN
Generated on 2019-09-23 04:53 GMT / http://hdl.handle.net/2027/mdp.39015077775156
Public Domain, Google-digitized / http://www.hathitrust.org/access_use#pd-google

the capacitance of the interaction gap. It is possible to make hot tests in which the thermal conditions of operation are established without the interaction effects of the beam, but these measurements are not available for the 2K25. The external Q_E is not affected, at least to a first order, by thermal effects in the resonator. The third curve of Fig. 72 shows the ratio of the power delivered when a matched load is coupled to the coupler to the power delivered to a load which presents optimum impedance to the oscil-

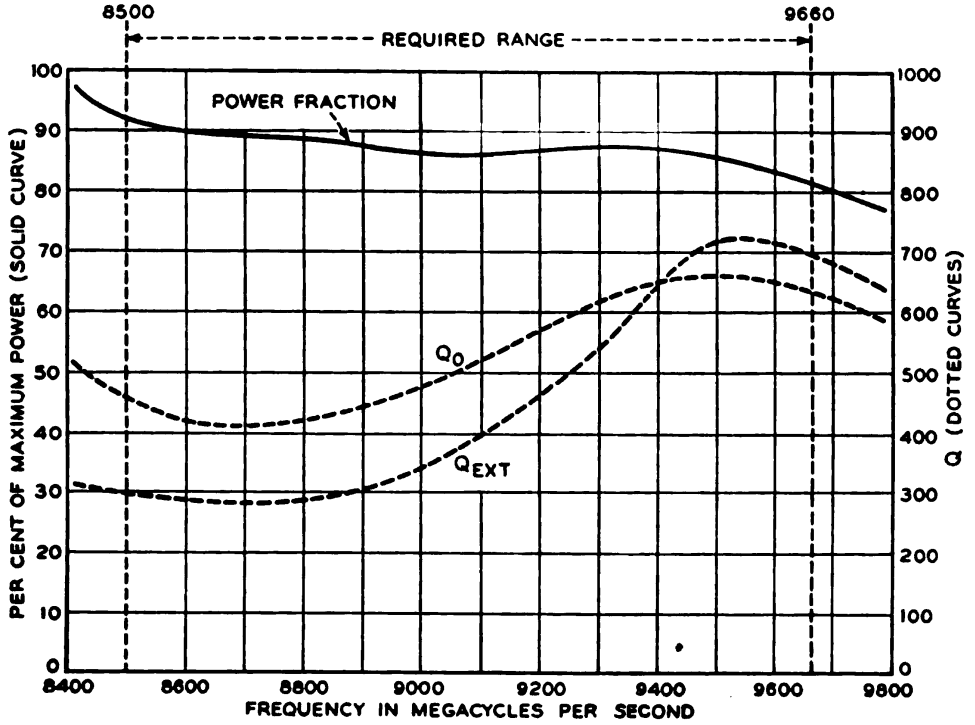

Fig. 72.—Variation of the percentage of maximum power output delivered, unloaded Q, Q_0, and external Q, Q_E, as functions of frequency for the 2K25 when coupled to the characteristic admittance of the 1″ x ½″ guide with the coupling of Fig. 70. The power variation is for a mode having 15.5 π radians drift.

lator. These data are given for the normal operating repeller mode as discussed below.

It was pointed out early in this work that the available power output and electronic tuning have a contrary variation with respect to the number of cycles of drift in the repeller space. Consequently, this is one of the most important and exasperating parameters of the tube. Fig. 73 is a diagram illustrating the characteristics of a typical W.E. 2K25 oscillator. The abscissa is the repeller-cathode voltage which, for a fixed resonator voltage, determines the drift angle. Thus, as this voltage is made increasingly negative, successive modes of oscillation appear, corresponding to consecu-

Generated on 2019-09-23 04:53 GMT / http://hdl.handle.net/2027/mdp.39015077775156
Public Domain, Google-digitized / http://www.hathitrust.org/access_use#pd-google
Digitized by Google
Original from UNIVERSITY OF MICHIGAN

tive decreasing values of n. Our best determination for the value of n for each mode is given. The base lines are displaced vertically on a uniform wavelength scale, so that the variation of repeller voltage with wavelength is indicated. The power output increases with decreasing values of n but the half power electronic tuning for each repeller mode has a contrary variation. The repeller mode chosen as providing the best compromise between power output and half power electronic tuning is the $7\frac{3}{4}$ cycle mode. The design of the coupling unit and all the primary characteristics of the tube are based on the use of this mode. It will be observed that repeller

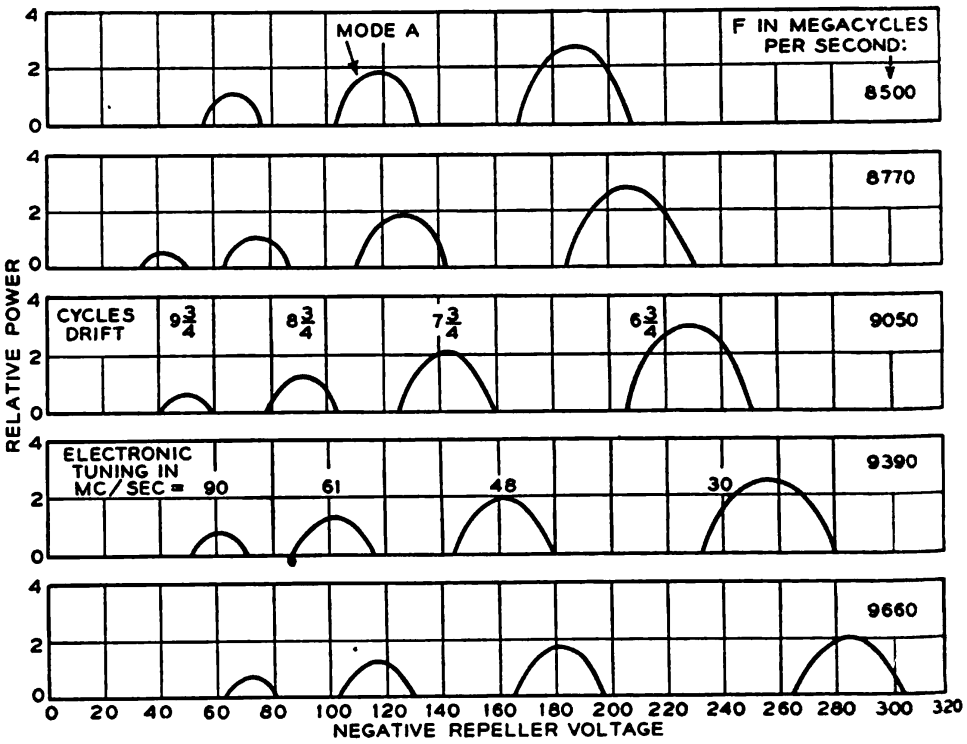

Fig. 73.—Operation of the 2K25 in various repeller modes and at various frequencies when connected to characteristic admittance of a 1" x ½" guide by the coupling of Fig. 70.

modes having n values less than 6 do not appear in Fig. 73. For values of n = to 0, 1, 2 and possibly 3, this is because the conductance representing the resonator losses is in excess of the electronic conductance. For the values of n = 4 and 5 the coupled load conductance plus the resonator loss conductance in the specified transducer are in excess of the electronic conductance. Conversely for modes having n values in excess of 7 the coupling is weaker than desired.

Fig. 74 illustrates the broad band characteristics for a typical W.E. 2K25 tube operating in the coupling of Fig. 70 into a matched load. In Fig. 74

Digitized by Google
Original from UNIVERSITY OF MICHIGAN
Generated on 2019-09-23 04:54 GMT / http://hdl.handle.net/2027/mdp.39015077775156
Public Domain, Google-digitized / http://www.hathitrust.org/access_use#pd-google

are shown the power output, half power electronic tuning, and sink margin as functions of frequency for the $7\frac{3}{4}$ cycle mode.

F. *Thermally Tuned Reflex Oscillators—The 2K45*

The trend toward the simplification of radar systems to the fewest possible adjustments, coupled with the ever present possibility of enemy jamming, led to the attempt to produce a system which was described as a single knob system. The ultimate objective of such a system was ability to shift the frequency of the transmitter at will with a single control. This puts the chief burden on the receiver, which must automatically track with the

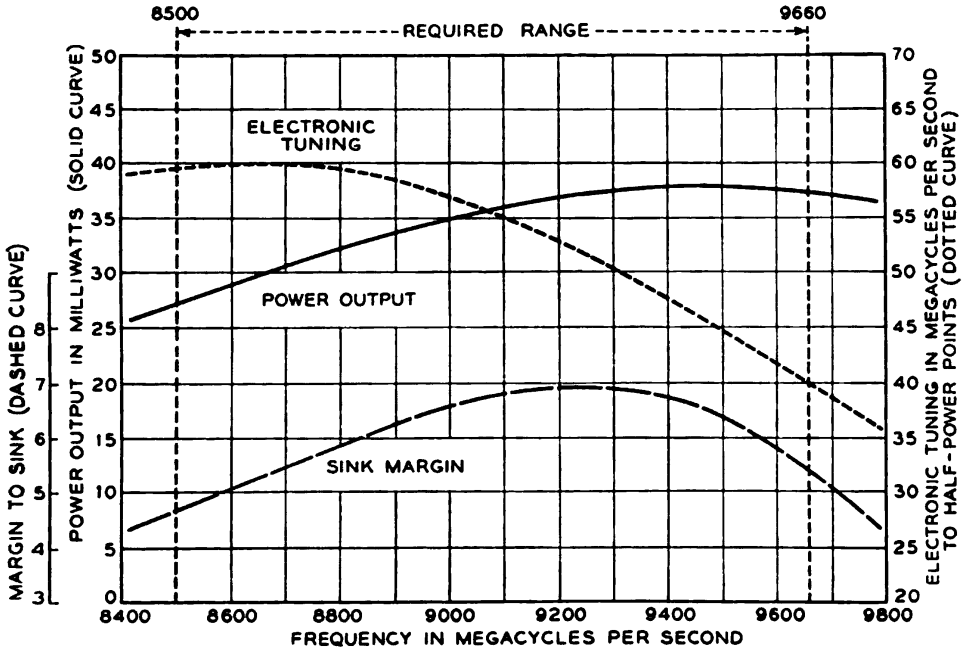

Fig. 74.—Variation of electronic tuning, power output and sink margin with frequency for the 2K25 in a repeller mode having 15.5 π radians drift. Characteristic admittance load and coupling of Fig. 70.

transmitter. The problem is much simplified by designing as many of the components as possible so that retuning is not required when the frequency is shifted within the requisite band. In the case of the beating oscillator it was necessary to devise a mechanism which would permit rapid automatic control over a frequency range of 1160 mc. This range was many times in excess of any immediately realizable electronic tuning range. It is of course apparent that such a method of tuning will also lend itself readily to use in many applications in which, although the transmitter frequency is nominally fixed, the system is required to operate under such extreme conditions that the sum total of the possible frequency deviations is in excess of the available

Digitized by Google
Original from UNIVERSITY OF MICHIGAN
Generated on 2019-09-23 04:55 GMT / http://hdl.handle.net/2027/mdp.39015077775156
Public Domain, Google-digitized / http://www.hathitrust.org/access_use#pd-google

electronic tuning range. Examples of such systems are installations in high altitude air craft, in which wide variations in temperature and pressure may be expected.

It was highly desirable to have the frequency control electrical. One means of obtaining such a control is through motion of the resonator grids produced by the thermal expansion of an element heated electrically. A step in this direction was taken in the Sperry Gyroscope Company 2K21 oscillator in which the resonator was tuned by the thermal expansion of a strut heated by passing a considerable current through it.

At the Bell Telephone Laboratories the design for a thermally tuned beating oscillator was based on a method which permitted the control of a small current at a high voltage. In general, controlled high voltages are easily available both from power supplies and from control circuits. Further, it seemed desirable that the control of the heating should require no power. These considerations suggested that the heating of the thermal tuning element be accomplished by electron bombardment. Through the use of a negative grid to regulate the bombardment, the tuning control became a pure voltage adjustment. The bombardment method made it possible to utilize configurations in the tuner which would have been less practical if resistance heating had been employed.

An early reflex oscillator incorporating these ideas was the Western Electric 2K45 vacuum tube. Fig. 75 shows an external view of the tube which, except for the output coaxial line, looks like a forshortened 6L6 vacuum tube. The plug-in feature of the earlier mechanically tuned oscillators was maintained in this oscillator, which was designed to couple to the waveguide circuit through the same transducer developed for the 2K25.

Figures 76 and 77 are cross-sectional views of the 2K45 made at right angles to each other. The thermal tuning mechanism is contained in the upper part of the structure. It is a bimetallic combination consisting of a U shaped channel and a multi-leaf bow. The channel is formed of a material with a large coefficient of expansion and a high resistance to slow permanent deformation or creep at elevated temperatures. At the ends of this channel, tabs bent down at right angles to the channel axis, provide rigid vertical support for the channel without interfering with axial expansion. These tabs are connected to the resonator, which in turn is supported by the vacuum envelope as closely as possible in order to minimize the thermal impedance of the path. This connection also serves to cool the channel ends. The multi-leaf bow is welded to the channel at its end. The leaves are made of a material having a low coefficient of expansion and, as they are fastened to the channel at its ends, they remain cool and do not expand appreciably as the channel is heated. The purpose of the multi-leaf con-

Generated on 2019-09-23 04:55 GMT / http://hdl.handle.net/2027/mdp.39015077775156
Public Domain, Google-digitized / http://www.hathitrust.org/access_use#pd-google
Digitized by Google
Original from UNIVERSITY OF MICHIGAN

struction of the bow is to reduce the internal stresses produced by bending during the tuning action.

A cathode, control grid and a pair of focussing wires are supported by micas in a position facing the open side of the U channel. The channel serves as an anode for the cathode current, which is controlled by the grid. The focussing wires beam the cathode current into the anode. The grid is proportioned so that under all operating conditions it remains negative, and the control system need supply no power to it.

The heating of the channel by the electron bombardment causes it to expand with a large differential with respect to the bow. As a result the bow flattens out and its center moves toward the channel. The purpose of this construction is to provide a magnification of the expansion of the

Fig. 75.—An external view of the W.E. 2K45—an early thermally tuned reflex oscillator designed by the Bell Telephone Laboratories.

channel which by itself would provide insufficient motion. The cross member welded to the center of the bow and the vertical struts transmit the motion of the bow to the diaphragm which supports one of the cavity grids. The action is illustrated in Fig. 78 which shows a series of X-ray views of an operating tube. Thus, the first view shows the conditions for no power applied to the tube, the second, for the tube operating but with the tuner grid biased to cut-off. The following views show the behavior with progressive increases in the power into the tuner channel.

The ramifications in the design of a thermal tuner are many and the possible configurations of the mechanism will depend greatly on the individual requirements of the application. It is possible, however, to lay down some basic principles. These are concerned with positiveness of action and speed of tuning. With regard to the first, it may seem anomalous to speak of

Generated on 2019-09-23 04:55 GMT / http://hdl.handle.net/2027/mdp.39015077775156
Public Domain, Google-digitized / http://www.hathitrust.org/access_use#pd-google
Digitized by Google
Original from UNIVERSITY OF MICHIGAN

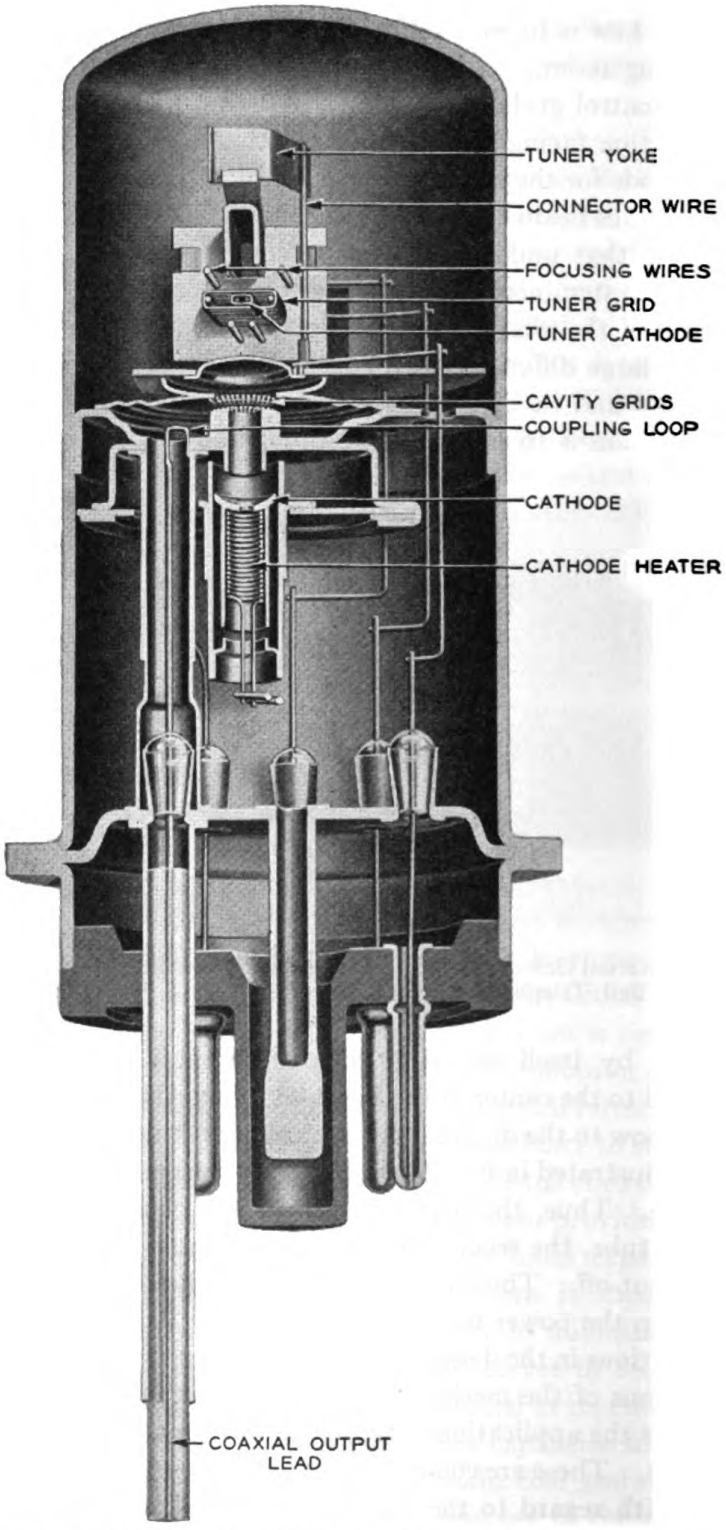

Fig. 76.—Internal features of the W.E. 2K45: section through the output lead and normal to the tuner cathode and strut.

Digitized by Google
Original from UNIVERSITY OF MICHIGAN
Generated on 2019-09-23 04:55 GMT / http://hdl.handle.net/2027/mdp.39015077775156
Public Domain, Google-digitized / http://www.hathitrust.org/access_use#pd-google

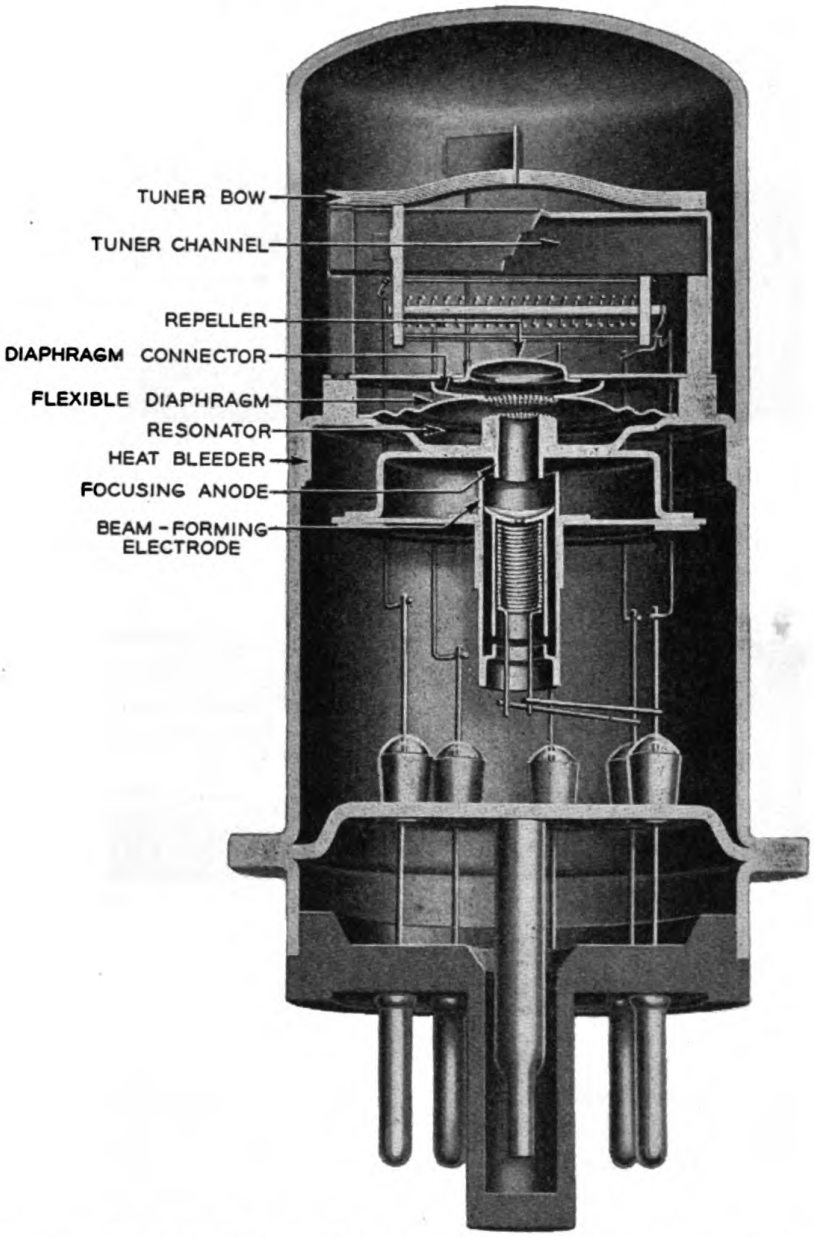

Fig. 77.—A section of the W.E. 2K45 cut parallel to the tuner cathode and strut.

positive action in a device which has thermal inertia. What is actually meant, however, may be best indicated by the following: Let us suppose that some power, P_a, must be dissipated in the tuner in order to hold the oscillator at a frequency, f_a. Now, suppose that the tube is operating with power less than P_a and that we are required to switch to frequency f_a. In order to switch rapidly, we apply power in excess of P_a to the tuner until the frequency has reached f_a, at which time we switch to the power P_a required

Digitized by Google
Original from UNIVERSITY OF MICHIGAN
Generated on 2019-09-23 04:55 GMT / http://hdl.handle.net/2027/mdp.39015077775156
Public Domain, Google-digitized / http://www.hathitrust.org/access_use#pd-google

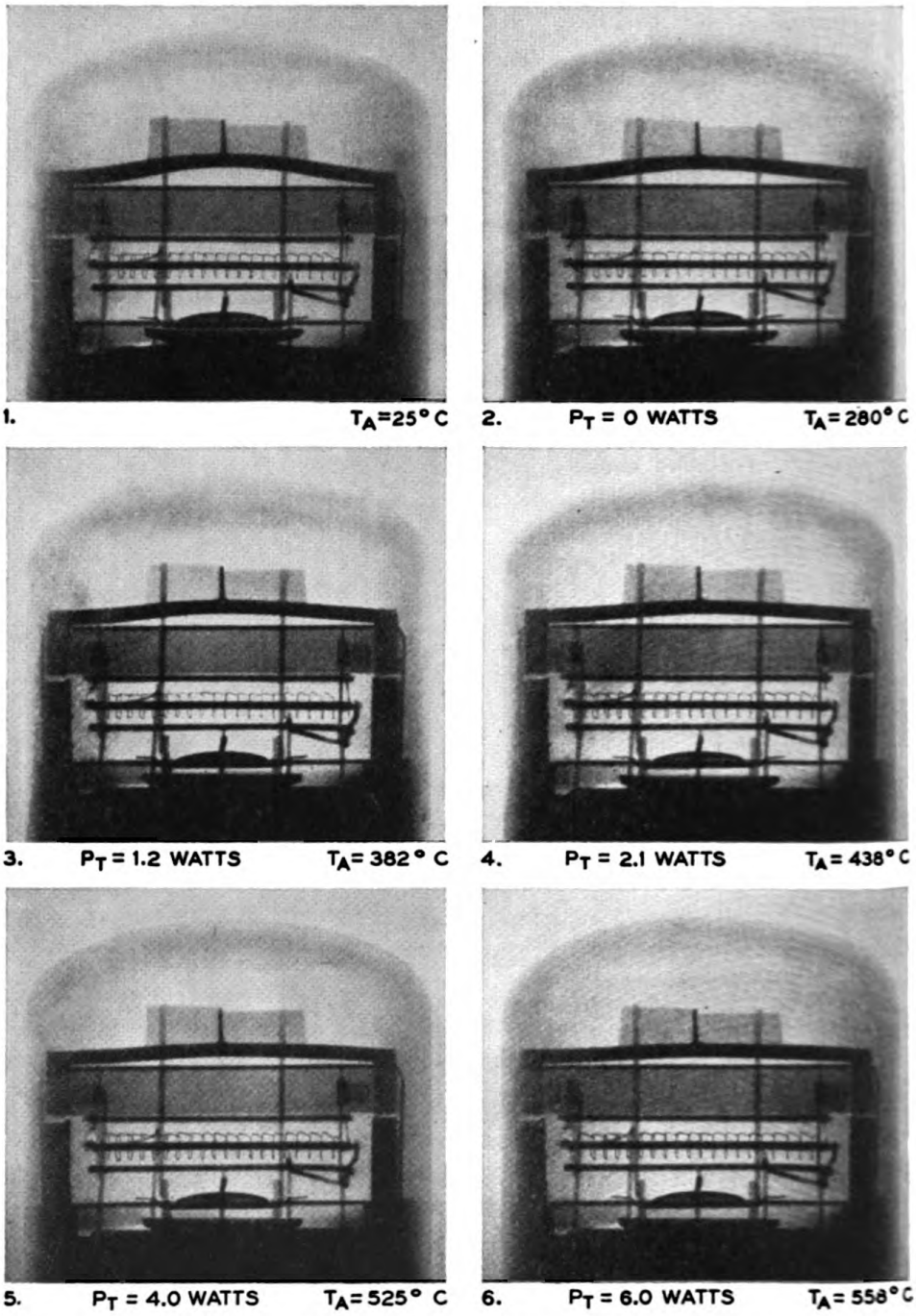

FIG. 78.—A series of x-ray photographs of the thermal tuning mechanism of an operating 2K45. These show the motion of the bows for successively increasing power inputs to the tuner channel.

to sustain f_a. We say that the control is positive if no overshoot occurs, i.e., if the frequency does not continue to change for a time and then return to

Digitized by Google
Original from UNIVERSITY OF MICHIGAN
Generated on 2019-09-23 04:56 GMT / http://hdl.handle.net/2027/mdp.39015077775156
Public Domain, Google-digitized / http://www.hathitrust.org/access_use#pd-google

f_a. We might equally well have illustrated this by an example in which the tuner was cooling. In order to avoid overshoot it is necessary that no thermal impedance exist between the heat source and the expanding element. Thus, as an example of a tuner in which overshoot will occur, one may cite an expanding strut in the form of a tube heated by a resistance heater internal to the tube. In order to transfer heat from the resistance heater to the tubing the former must of necessity operate at the higher temperature. Hence, in the example given above, when the power is switched to the sustaining value heat will continue to be transferred to the tubing until the heater and the tubing arrive at the same temperature. To minimize the thermal impedance the heat should be generated within the body of, or on the surface of, the expanding element. The resistance heating by current passing through the expanding element illustrates the first case and heating by electron bombardment the second.

The second principle is quite obvious when once stated. If a rapid shift in frequency is to be obtained at any point within the required tuning range, then the potential tuning range must be considerably in excess of that required. Thus, if the tube is operating near one of the required frequency limits and one demands that it go to the limit, the shift will progress very slowly in the absence of excess range. If, however, it is possible to overdrive the limit, the time required will be materially shortened. On the basis of actual tube design this requires that the safe maximum or full on power into the tuner must be considerably in excess of the power required to hold the tuner at the frequency band limit nearest the full on condition. The tuning mechanism must be capable of continuous operation under the full on condition in case this accidentally persists. Further, the power required to hold the tuner at the other end of its band must be considerably in excess of zero in order that rapid cooling may occur near this limit. It is not necessary that the tuner produce motion for power inputs outside the band limits; the essential condition is that the rates of heating and cooling near these limits should have values considerably greater than zero.

It is always possible to purchase heating speed by the expenditure of power in available over-drive. The cooling speed, on the other hand, is controlled by the temperature difference between the source and sink, the heat capacity of the tuner and the mechanism of cooling. Two methods of cooling are available, conduction and radiation. For small amounts of motion and in circumstances where large forces are not required, conduction cooling can provide a satisfactory answer. In cases in which a large amount of motion is required, as in the 2K45, conduction cooling imposes a number of serious restrictions. The expanding element must be made from a material having a large coefficient of expansion and necessarily must be long. Unfortunately, alloys having large expansion coefficients are very poor con-

Digitized by Google
Original from UNIVERSITY OF MICHIGAN
Generated on 2019-09-23 04:56 GMT / http://hdl.handle.net/2027/mdp.39015077775156
Public Domain, Google-digitized / http://www.hathitrust.org/access_use#pd-google

ductors of heat. In the case of conduction the cooling rate will depend on the ratio of the length times the heat capacity divided by the cross-section. For radiation cooling the rate depends on the heat capacity divided by the radiating area and is independent of the length except as the heat capacity depends upon this factor. Radiation cooling has the advantage that it permits more freedom of structural shape and the material may be chosen on the basis of strength. In the operating range of the 2K45 the heat radiated is approximately four times that conducted away.

The automatic frequency control circuits which have been used with thermally tuned beating oscillators in radar receivers have been of a full on or off type so that they do not continuously hold the frequency at a fixed reference difference from the transmitter frequency. The reason for this in part is that a pulse transmitter gives the required reference information only during the pulse. Thus with an on-off control circuit if at a given pulse a correction of frequency is demanded the power into the tuner is turned full on or off, depending on the direction of the correction, and left in this condition until the occurrence of the next pulse which again determines the direction of the control. The result is that the frequency of the beating oscillator continually hunts about the transmitter frequency. The control system must be designed to hold the hunting deviation within tolerable limits. It is of course possible to work within narrower limits than full on or off tuner power. One advantage of full on or off control is that it results in the minimum tuning time between required frequencies since the tuning rate is at all times held to the maximum possible value.

Under certain conditions the performance of a thermal tuner may be completely described by a time constant. In general, however, this is not the case and the information required in designing a control system is concerned first with initiation of operation and second with the factors determining the magnitude of the hunting deviation. For initiation of operation, one is concerned with the time required for the oscillator to reach the operating frequency. The quantities known as the cycling times give upper limits for this quantity. The cycling times are to a certain extent arbitrarily defined as indicated in the following. There are two band limit frequencies. f_c, the limit requiring the lesser power input, P_c, and corresponding to a tuner temperature, T_c, and f_h, the limit for which the power input will be P_h, and the temperature, T_h. The cycling time for heating, τ_h, is defined and measured in the following manner. The power input to the tuner is set to P_c and held at this value until equilibrium is established. The power input is then switched to the maximum allowed value, P_m and the time interval, τ_h, between the instant of switching and the instant at which the frequency of operation has reached f_h is measured. Correspondingly, the cycling time τ_c for cooling is measured by setting to P_h until equilibrium is

Digitized by Google
Original from UNIVERSITY OF MICHIGAN
Generated on 2019-09-23 04:56 GMT / http://hdl.handle.net/2027/mdp.39015077775156
Public Domain, Google-digitized / http://www.hathitrust.org/access_use#pd-google

established and then switching the tuner power off and measuring the interval, τ_c, until the operating frequency reaches f_c. These quantities are of importance in determining the "Out of Operation" time in case the frequency reference of the control system is momentarily lost, so that the control starts cycling in order to re-establish the reference.

While the cycling times can be taken to give an indication of the average speed of tuning, more detailed information is required to determine the hunting deviation. This demands a knowledge of the instantaneous tuning rates which will result at any point in the band when the power is switched full on or off. These rates vary through the band since the overdrive available, for example, on heating will decrease as the operating frequency approaches the limit nearest to the maximum drive.

In the following, an outline will be given of the factors which must be considered in designing a thermally tuned reflex oscillator. The 2K45 will be used as an illustration. Our first consideration concerns the time required for the tuner to heat and cool between given temperatures. In Appendix XI expressions are derived for the cycling times τ_h and τ_c. The expressions applicable to the 2K45 are:

$$\tau_h = \frac{CT_m}{2KT_m^4} [F_1(T_{rh}) - F_1(T_{rc})] \tag{13.1}$$

$$\tau_c = \frac{CT_0}{2KT_0^4} [F_2(T_{sc}) - F_2(T_{sh})] \tag{13.2}$$

where the symbols are defined in the appendix. The functions F_1 and F_2 are plotted in terms of the reduced temperatures, T_r and T_s in Figs. 79 and 80. In the analysis conduction cooling is neglected and it is assumed that the whole of the expanding element operates at the same temperature. Because of these limitations the theory is largely qualitative. It will be observed that the cycling time, τ_h, is proportional to the ratio of the heat energy stored in the tuner at the maximum equilibrium temperature to the rate of loss of energy at this temperature. It is therefore apparent that this equilibrium temperature should have the maximum possible value, and also that the heat capacity of the tuner should be kept to a minimum. Assuming for simplicity that the frequency of oscillation is proportional to the temperature, so that a given temperature difference is proportional to the frequency, one sees by examining the function F_1 that it is desirable to keep the reduced temperatures T_{rh} and T_{rc} small compared to 1. Under these circumstances, the cycling time τ_h will have its minimum value and will be more or less independent of the reduced temperatures. If we examine the expression for the cycling time for cooling, τ_c, we observe that this is proportional to the ratio of the heat stored in the tuner at the equilibrium

Digitized by Google
Original from UNIVERSITY OF MICHIGAN
Generated on 2019-09-23 04:56 GMT / http://hdl.handle.net/2027/mdp.39015077775156
Public Domain, Google-digitized / http://www.hathitrust.org/access_use#pd-google

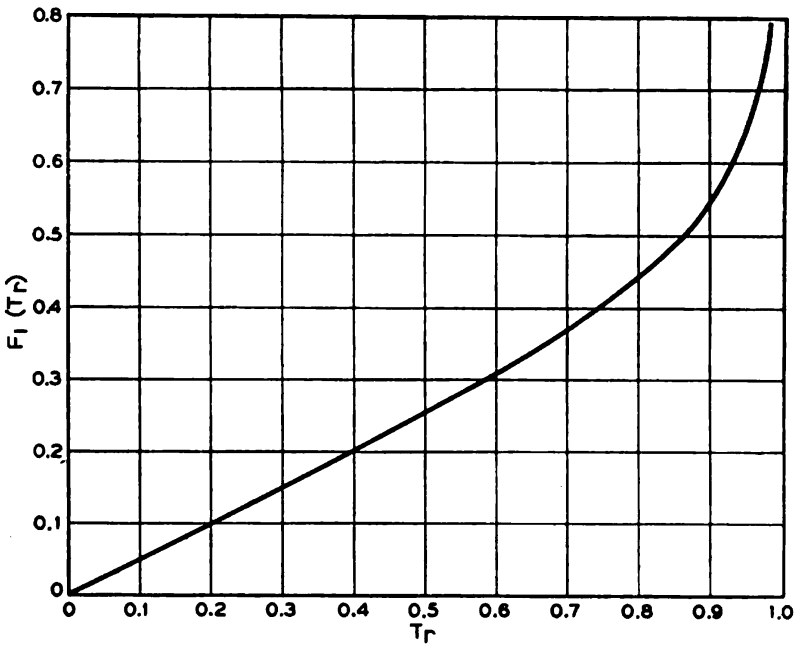

Fig. 79.—A plot of a function used in determining the time required for the temperature of a thermal tuner to rise between two given values when the tuner is cooled by radiation alone. The abscissae are given in terms of a reduced temperature.

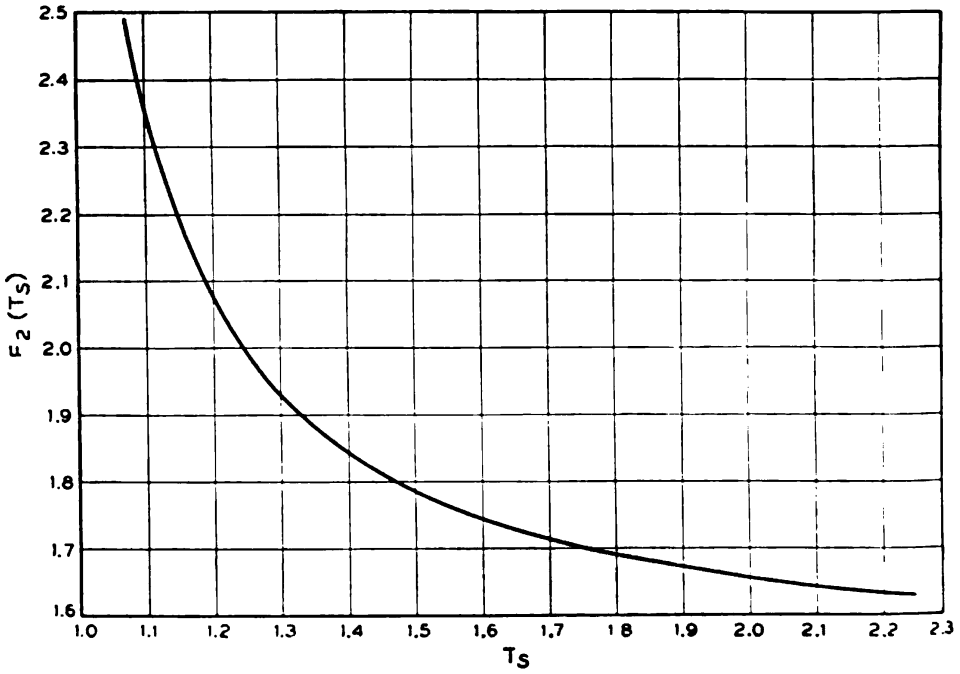

Fig. 80.—A plot of a function used in determining the time required for the temperature of a thermal tuner to fall between two given values when cooled by radiation alone. The abscissae are given in terms of a reduced temperature.

Digitized by Google
Original from UNIVERSITY OF MICHIGAN
Generated on 2019-09-23 04:56 GMT / http://hdl.handle.net/2027/mdp.39015077775156
Public Domain, Google-digitized / http://www.hathitrust.org/access_use#pd-google

temperature T_0 corresponding to zero bombardment power divided by the rate of heat loss at this temperature. This indicates a rather paradoxical result, that the temperature for zero bombardment power should be as high as possible. This arises from the dependence on radiation cooling. We are imited in setting the value of T_0 by the form of the function F_2, which requires that the reduced temperatures T_{sc} and T_{sh} should be very large compared to 1. Since the true temperatures corresponding to these reduced values must simultaneously be small compared to T_m, it is apparent that we are not completely free to make T_0 large, and a compromise must be worked out.

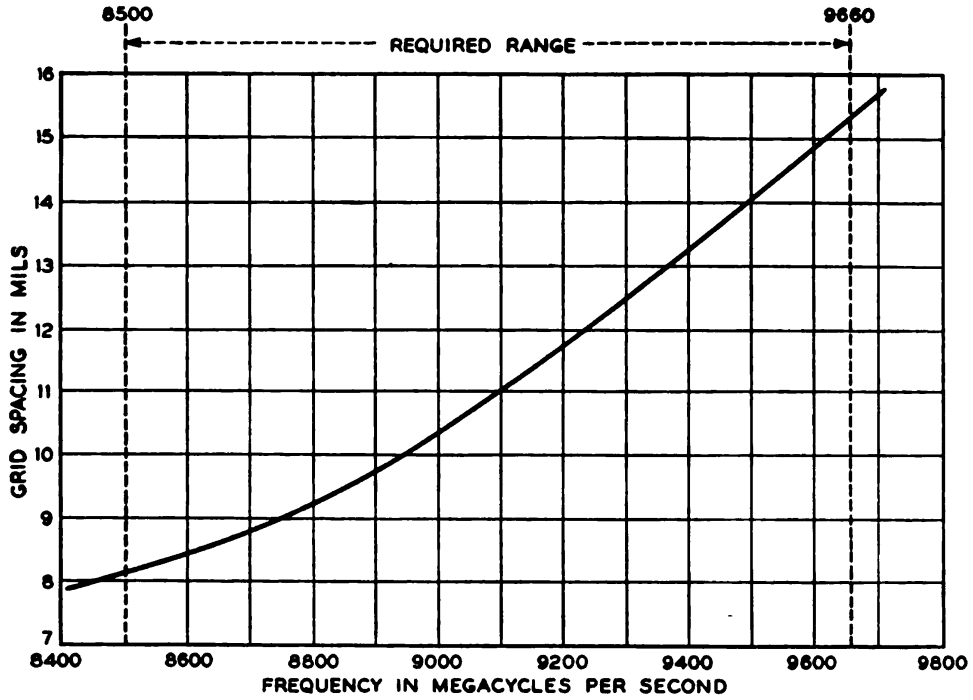

Fig. 81.—Variation of the frequency of resonance vs gap displacement for the W.E. 2K45 resonator. The vertical lines show the required tuning range.

In determining a practical design for a thermal tuner, the first characteristic which must be known is the variation of the resonant frequency of the oscillator cavity as a function of gap displacement. It is apparent that, for the highest speed of tuning, the rate of change of frequency with gap displacement should have the maximum possible value. However, this tuning characteristic is dictated by the performance requirements of the tube as an oscillator and hence is not available as a variable in the design. Fig. 81 shows the variation of frequency with gap displacement for the 2K45 resonator. The required range is indicated.

When the required motion is known a choice may be made of a mechanism

Digitized by Google
Original from UNIVERSITY OF MICHIGAN
Generated on 2019-09-23 04:57 GMT / http://hdl.handle.net/2027/mdp.39015077775156
Public Domain, Google-digitized / http://www.hathitrust.org/access_use#pd-google

for a tuner. There is a certain amount of arbitrariness in choosing the limiting dimensions of the tuner. If the expanding element is to be short it is necessary either to operate over a very wide range of temperatures or else use some mechanical means of amplifying the motion obtained over a more limited range. Since the more limited is the required temperature range the greater is the tuning speed, it is obviously advantageous to use mechanical amplification. As previously pointed out the electron bombardment method of heating and radiation cooling are especially suitable to such a mechanism because of the freedom of design they permit. Previous dis-

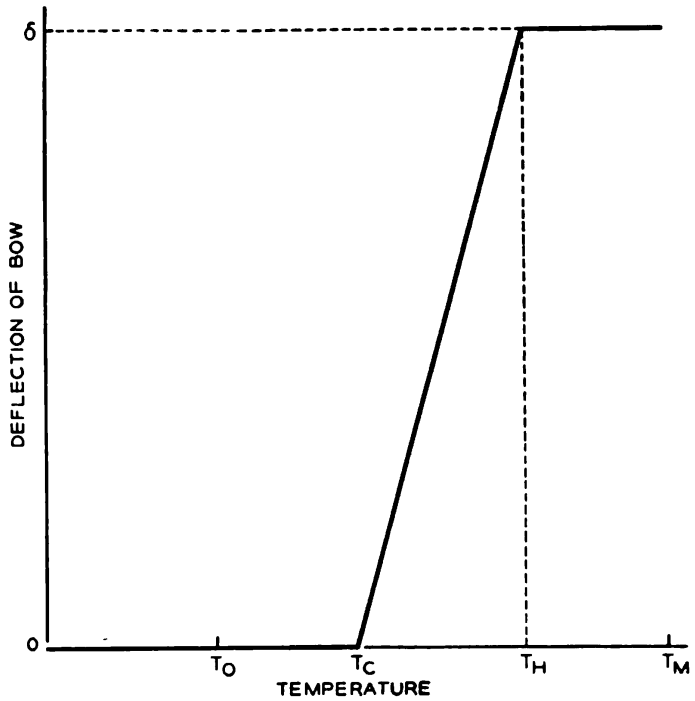

Fig. 82.—The ideal type of deflection vs temperature characteristic desired for a thermally tuned oscillator. The motion δ is that required to shift the resonant frequency of the cavity through its required band.

cussion has shown that the temperatures corresponding to zero and maximum power input must be separated by wide margins from the temperatures corresponding to the limits of the tuning range. Any motion which occurs in these margins is unnecessary and in general undesirable. Ideally, the tuning mechanism should have a characteristic as shown in Fig. 82. The type of tuning mechanism chosen for the 2K45 is a first approximation to such a characteristic, as is shown in Fig. 83, which gives a family of characteristics corresponding to various initial offsets of the bow for a given length of bow. The bows are formed to a sinusoidal shape. This structure gives

Digitized by Google
Original from UNIVERSITY OF MICHIGAN
Generated on 2019-09-23 04:57 GMT / http://hdl.handle.net/2027/mdp.39015077775156
Public Domain, Google-digitized / http://www.hathitrust.org/access_use#pd-google

a large mechanical amplification of the expansion of the tuner. The tuner is made as long as will fit conveniently into the tube envelope. Further arbitrary decisions are required with regard to the power which can be ex-

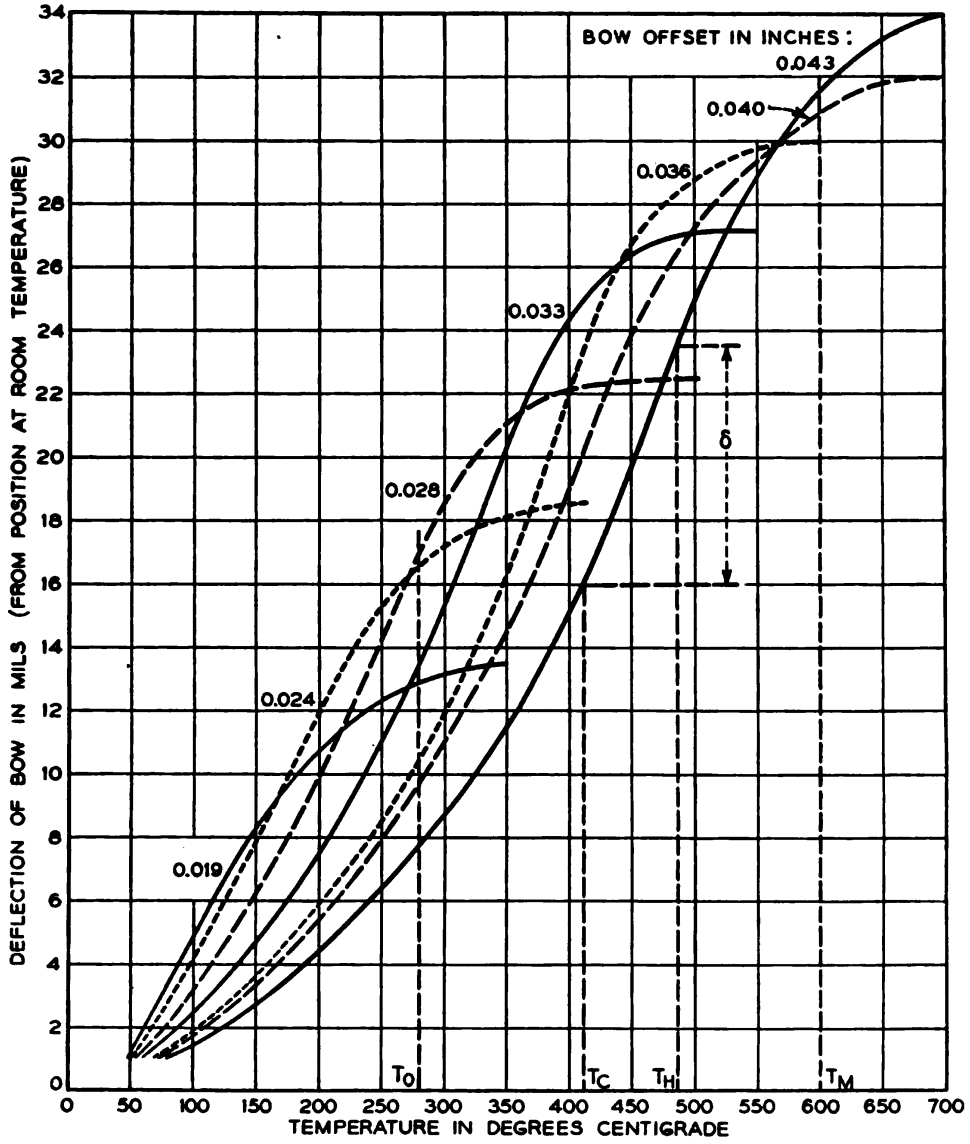

Fig. 83.—A family of deflection vs temperature characteristics for the type of tuning mechanism used in the W.E. 2K45. The parameter is the initial offset of the bows from the channel at room temperature.

pended in operating the tuner. With such decisions made, the tuner design can then be completed as a compromise of a great many variables. Limitations on the strength of the tuner materials at elevated temperatures deter-

Generated on 2019-09-23 04:57 GMT / http://hdl.handle.net/2027/mdp.39015077775156
Public Domain, Google-digitized / http://www.hathitrust.org/access_use#pd-google
Digitized by Google
Original from UNIVERSITY OF MICHIGAN

mine a maximum safe operating temperature. The anode material is chosen to have a large coefficient of expansion and resistance to "creep" at elevated temperatures. In choosing the form of the tuner it is necessary to keep constantly in mind the necessity of maintaining the minimum ratio of heat capacity to radiating surface. A minimum operating temperature of the tuner is determined by heat flow to it from extraneous sources. Figure 84 shows the temperature as a function of bombardment power input for the 2K45 tuner. It will be observed that the heat from sources other than bombardment produces a considerable rise in temperature. One principal source of uncontrolled heating is radiation from the tuner cathode. This

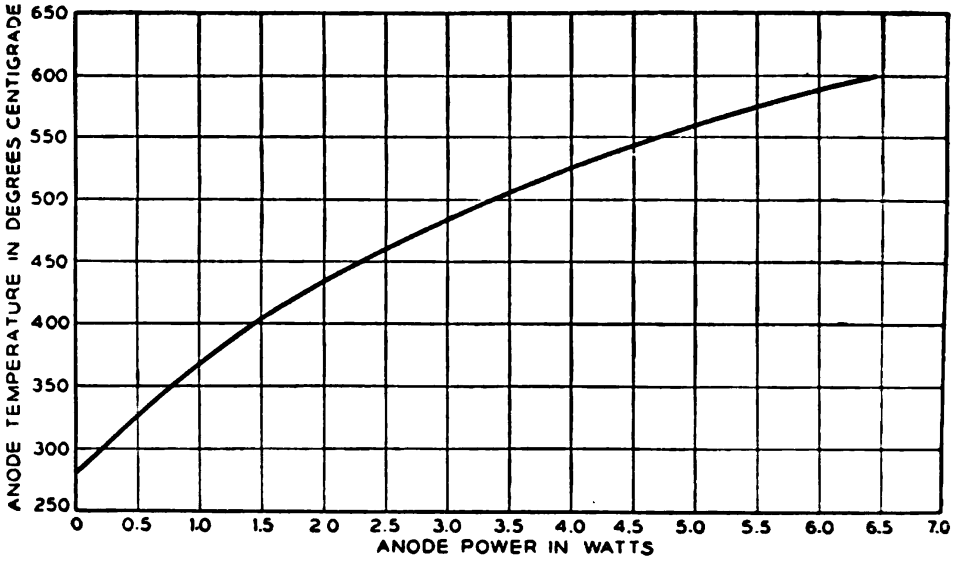

Fig. 84.—The tuner anode temperature as a function of the bombardment power. The temperature rise at zero bombardment power is caused by radiation from the thermal cathode and extraneous sources.

is minimized by keeping the cathode as remote from the anode as is consistent with the required electronic characteristics.

When the maximum and minimum operating temperatures and the length of the channel are determined the remaining problem is to determine and offset for the tuning bow which will provide the optimum tuning characteristics. We wish to obtain characteristics such that the heating time τ_h and the cooling time τ_c are approximately equal and of a minimum value. The choice of the bow offset also involves a choice of an initial gap spacing for the resonator. On Fig. 83 the boundary values for the limiting temperatures T_t and T_m are indicated by vertical lines. With any given bow offset which corresponds to a particular tuning characteristic a limit is set on the initial gap spacing by the requirement that the total motion of the bow between

Digitized by Google
Original from UNIVERSITY OF MICHIGAN
Generated on 2019-09-23 04:57 GMT / http://hdl.handle.net/2027/mdp.39015077775156
Public Domain, Google-digitized / http://www.hathitrust.org/access_use#pd-google

room temperature and T_m shall not exceed the initial gap spacing. From our previous analysis we know that to provide maximum tuning speed we desire to make the temperature intervals $T_c - T_0$ and $T_m - T_h$ as large as possible. For any given tuning characteristic these intervals may be adjusted by a variation of the initial gap spacing subject to the limitation just

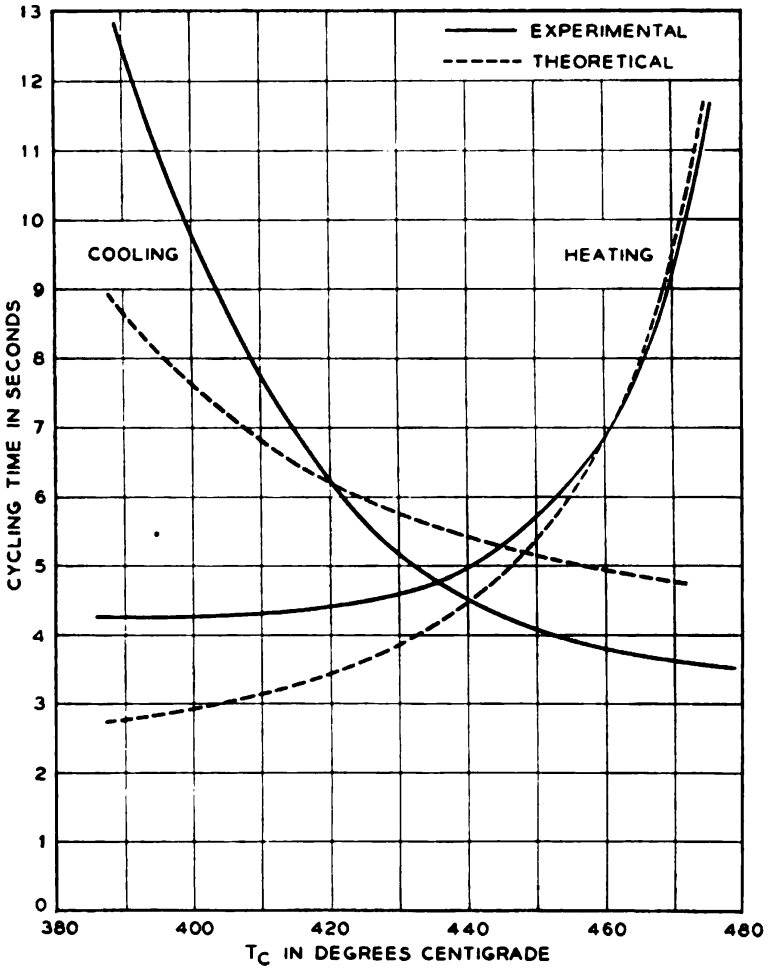

Fig. 85.—The cycling time of the W.E. 2K45 as a function of the temperature of the channel at the band frequency limit requiring the smaller tuner power. The solid lines are the experimental curves, the dashed lines are theoretical results. One point on the heating time is fitted in order to determine the heat capacity of the tuner.

imposed. Since T_c and T_h are interrelated for a given bow characteristic by the fact that they correspond to a specific increment of motion δ determined by the cavity design, we may study the effect of shifting the interval δ along the tuner characteristic by varying the initial gap offset. We may specify this in terms of value of T_c. The result of such a study is shown in Fig. 85. The optimum offset corresponds to the temperature at which the

Digitized by Google
Original from UNIVERSITY OF MICHIGAN
Generated on 2019-09-23 04:57 GMT / http://hdl.handle.net/2027/mdp.39015077775156
Public Domain, Google-digitized / http://www.hathitrust.org/access_use#pd-google

curves for τ_h and τ_c cross over. The optimum bow offset is then the value which provides the minimum value at the crossover. From the theory given earlier it is possible to compute these curves. If we had analytical expressions for the motion of the tuner with temperature and for the variation of frequency with gap spacing it should be possible to obtain completely theoretical curves.

As a test of the theory of heating and cooling it is sufficient to use the experimental curves for the motion of the tuner with temperature and the variation of frequency with gap spacing in conjunction with the heating and cooling curves of Figs. 79 and 80 calculated from equations (13.1) and (13.2). The value of K which must be determined in order to obtain numerical values from the curves of Figs. 79 and 80 may be determined from Fig. 84 by using the relationship

$$K = \frac{P_a - P_b}{T_a^4 - T_b^4}$$

where P_a and P_b are the bombardment power inputs corresponding to anode temperatures T_a and T_b. There is no ready means for directly determining the heat capacity C. However, if one point on either the heating or cooling curves is fitted to the experimental data the value of C may be determined and the remainder of the points computed. The results of such a computation are shown by the dashed lines in Fig. 85. In view of the restrictive assumptions of a uniform anode temperature and the neglect of all conduction cooling the agreement in general form is reasonably good.

The W.E. 2K45 includes a number of advances in reflex oscillator technique over the 2K25. It will be observed in Figs. 76 and 77 that the electron optical system employed in the gun differs from that used in the 2K25. In the 2K25 a gun producing a rectilinear beam was employed. In the 2K45 the gun consists of a concave cathode surrounded by a cylindrical electrode and a focussing anode. The design of this type of gun was originated by Messrs. A. L. Samuel and A. E. Anderson at these laboratories. The design is such as to produce a radial focus beam which converges into the cylindrical section of the focussing anode. After the beam enters the focussing anode its convergence is decreased by its own space charge, and the beam passes through the grids at approximately the condition of minimum diameter. Between the second grid and the repeller the beam continues to diverge radially on the outbound and return trips. The intention of the design is that the beam shall have diverged sufficiently so that the maximum possible fraction will recross the gap within a ring having an inner diameter equal to the first grid and outer diameter equal to the second grid. Under these conditions only a small fraction of the beam will return into the cathode region, the remainder being captured on the support of the first grid after the

Digitized by Google
Original from UNIVERSITY OF MICHIGAN
Generated on 2019-09-23 04:57 GMT / http://hdl.handle.net/2027/mdp.39015077775156
Public Domain, Google-digitized / http://www.hathitrust.org/access_use#pd-google

second transit of the gap. This tends to eliminate electronic tuning hysteresis and the repeller characteristic of the 2K45 is essentially free of this phenomenon. This gun design has the further advantage that it avoids the necessity for the first grid used in the 2K25. This eliminates the current interception on this grid with a resulting increase in the effective current crossing the gap. This type of gun also permits the design of a more efficient resonator by reducing the grid losses.

A second variation in design from the 2K25 is that in the 2K45 the second grid moves with reference to the repeller. This has the advantage of reducing the variation of the repeller voltage for optimum power with resonator tuning. The drift angle in a uniform repeller field is given by

$$\theta = \frac{k\sqrt{V_0}}{V_0 + V_R}\, \ell f \tag{13.3}$$

where ℓ is the spacing between the repeller and the second grid of the resonator. If the same drift angle θ is maintained at all frequencies in the band, then the repeller voltage must vary. If ℓ is fixed as f increases V_R must also increase in order to maintain a fixed fraction. If ℓ varies and increases as f decreases then a smaller variation in V_R is required and in the particular case that ℓ varies inversely with f the repeller variation may be made zero. Usually other requirements determine the variation of ℓ and it is not always possible to make the variation zero. In the case of the 2K45 the variation over the band is approximately half the amount which would occur if ℓ were fixed.

The output coupling and line of the 2K45 were designed so that the oscillator would provide the desired characteristics in the same waveguide adapter as designed for the 2K25. The power output as a function of frequency for a typical tube is shown in Fig. 86a. Curves A, B and C of Fig. 86 show the variation of power output with cavity tuning when the repeller voltage is set for an optimum at the indicated frequency and held fixed as the cavity tuning is varied. The frequency shift between half power points in this case is very much wider than with repeller tuning. This is a consequence of the fact that whereas in repeller tuning both the frequency and the drift time change in a direction to shift the transit angle away from the value for maximum power, with cavity tuning only the frequency changes. Moreover, the fact that the repeller to second grid spacing in this design varies with frequency tends to reduce the variation of the drift angle with frequency. The envelope of the curves A, B and C gives the power output as a function of frequency when the repeller voltage is adjusted to an optimum at each frequency.

Fig. 86b gives the half power electronic tuning as a function of frequency measured statically and also dynamically with a 60 cycle repeller sweep. The difference arises from thermal effects.

Digitized by Google
Original from UNIVERSITY OF MICHIGAN
Generated on 2019-09-23 04:58 GMT / http://hdl.handle.net/2027/mdp.39015077775156
Public Domain, Google-digitized / http://www.hathitrust.org/access_use#pd-google

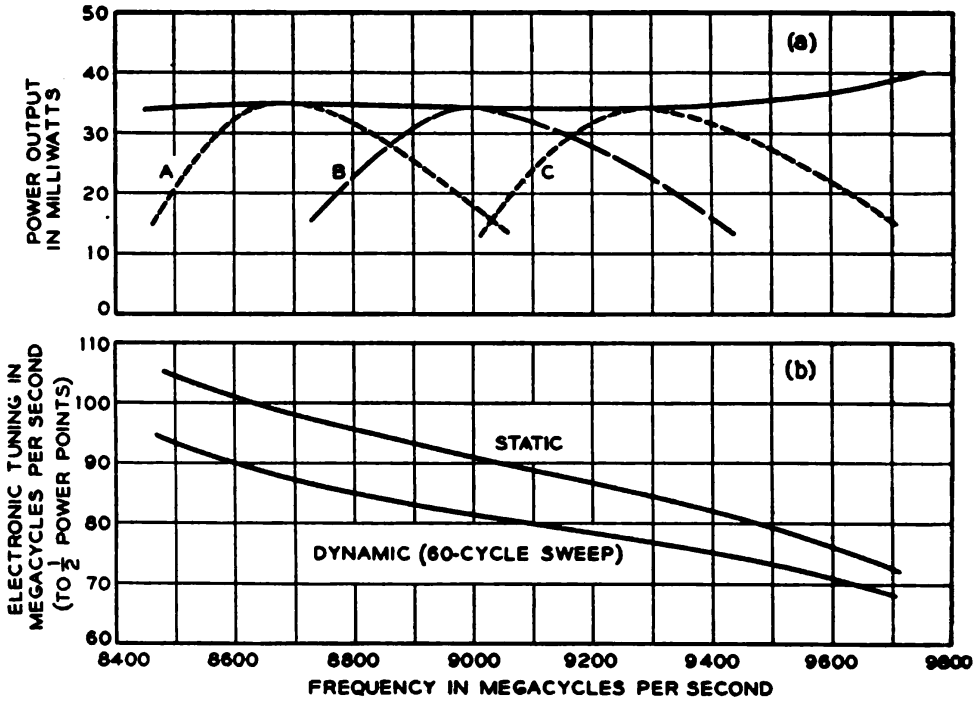

Fig. 86.—Characteristics of the W.E. 2K45 reflex oscillator. Fig. 86-a shows the variation of the power output as a function of frequency in two cases. The curves *A*, *B* and *C* illustrate the power variation with frequency when the repeller voltage is set for the optimum at the indicated frequency and held fixed as the cavity tuning is changed. The envelope of these curves shows the power variation with frequency when the repeller voltage is maintained at its optimum value for each frequency.

In Fig. 86b the electronic tuning is shown, in one case where the repeller voltage is shifted between half power points so slowly that thermal equilibrium exists at all times and in the dynamic case in which the repeller voltage is shifted at a 60 cycle rate.

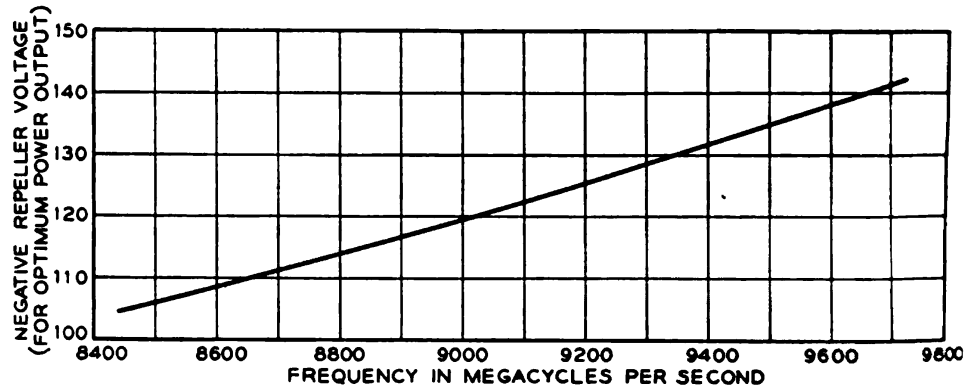

Fig. 87.—Repeller voltage for optimum power as a function of frequency for the W.E. 2K45 oscillator.

Fig. 87 shows the variation of repeller voltage for optimum power with frequency. This variation is so nearly linear that it has been proposed that

Digitized by Google
Original from UNIVERSITY OF MICHIGAN
Generated on 2019-09-23 04:58 GMT / http://hdl.handle.net/2027/mdp.39015077775156
Public Domain, Google-digitized / http://www.hathitrust.org/access_use#pd-google

a potentiometer properly ganged with the transmitter in radar systems would provide optimum output throughout the band. This is an advantage over electronic tuning, since the signal to noise performance of the receiver depends in part on the beating oscillator power into the crystal.

In a thermally tuned tube it is necessary to provide safeguards against excessive power input to the tuning strut since this might produce a permanent deformation and impair tuner operation. A simple method for obtaining such protection is to use low-frequency cathode feedback produced by a cathode resistor. With a cathode biasing resistor of 725 ohms the grid may be held 15 volts positive with respect to the more positive end of the cathode biasing resistor indefinitely without damage to the tuner when the normal plate voltage of 300 volts is applied.

The grid control characteristics for a typical 2K45 shown in Fig. 88 were obtained while using the cathode biasing resistor. These characteristics may be given in two ways. In one case the repeller voltage is held fixed and the characteristics are given over a range between half power points. It will be observed in this case that the characteristics are discontinuous because of the electronic tuning resulting from the repeller voltage shifts between ranges. For the other case the repeller voltage is maintained at its optimum value at each frequency.

In either case, one striking feature is the essential linearity of the variation of frequency with grid voltage. This is of considerable importance in many frequency stabilizing systems and represents an advantage of thermal tuning over electronic tuning. In the case of electronic tuning, as shown in Section VII, the rate of change of frequency with repeller voltage varies rapidly as the repeller voltage shifts away from the optimum value. Since frequency stabilization is essentially a feedback amplifier problem in which the rate of change of the frequency with the control voltage enters as one of the factors determining the feedback, it is apparent that the frequency stabilization will vary as the repeller voltage is shifted. In contrast, for the case of thermal tuning, because of the linearity of frequency with grid voltage, the stabilization will be independent of the frequency. It should not be for-

2K45 Operating Conditions

	Normal	Maximum
Heater Voltage	6.3	6.8 Volts
Resonator Voltage	300	350 Volts
Klystron Current	22	30 mA
Repeller Voltage Range	−60 to −175	−350 Volts
Tuner Current	0 to 25	mA
Tuner Power		7.0 Watts
τ_h (9660-8500 *Mc/s*)	6.0	9.0 Sec
τ_c (8500-9660 *Mc/s*)	6.0	9.0 Sec

Digitized by Google
Original from UNIVERSITY OF MICHIGAN
Generated on 2019-09-23 04:58 GMT / http://hdl.handle.net/2027/mdp.39015077775156
Public Domain, Google-digitized / http://www.hathitrust.org/access_use#pd-google

gotten, however, that thermal tuning is inherently slower in action than electronic tuning, since the latter is capable of frequency correction rates limited, for practical purposes, only by the control circuits, whereas in

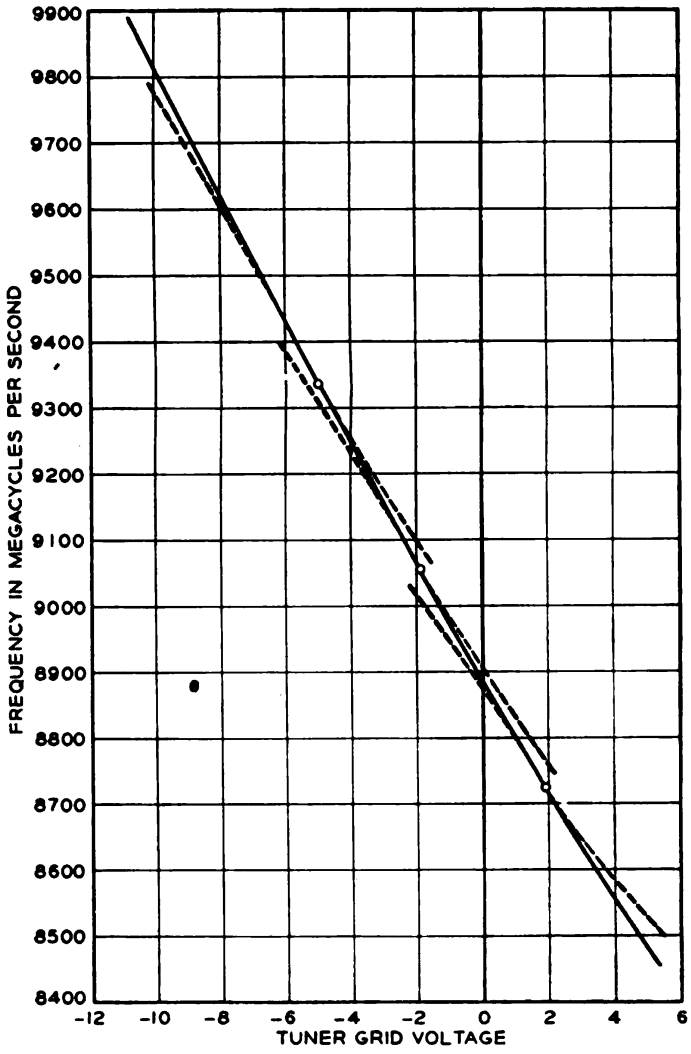

Fig. 88.—Frequency as a function of the grid voltage for the W.E. 2K45 oscillator. The dashed lines show the variation when the repeller voltage is held fixed for the mid-range value and the solid lines shows the variation with the repeller voltage maintained at its optimum value for each frequency. These characteristics apply when a 725 ohm biasing resistor is connected in series with the tuner cathode.

thermal tuning the thermal inertia of the tuning strut limits the tuning speed to rates of the order of 100 mc/sec^2 for the 2K45.

The operating conditions for the 2K45 are given in the table at the bottom of page 595.

Generated on 2019-09-23 04:58 GMT / http://hdl.handle.net/2027/mdp.39015077775156
Public Domain, Google-digitized / http://www.hathitrust.org/access_use#pd-google
Digitized by Google
Original from UNIVERSITY OF MICHIGAN

G. *An Oscillator With Waveguide Output—The 2K50*

Late in the war it became apparent that there was an urgent need for radar systems which would permit a very high degree of resolution. Such resolution requires the use of the shortest wavelengths possible, and as a practical step development work was undertaken in the neighborhood of 1 cm.

Work at these Laboratories led to a tube which produced over 20 milliwatts and was thermally tunable over the desired frequency range by means roughly similar to those employed in the 2K45. This tube had a wave guide output. It had no grids; a sharply focused beam passed through a .015″ aperture in the resonator. The tube operated at a cavity voltage of 750 volts.

Work by Dr. H. V. Neher at the M.I.T. Radiation Laboratory resulted in a design for an oscillator using grids which operated at a resonator voltage of 300 volts. At the request of the Radiation Laboratory, the Bell Telephone Laboratories undertook such development and modification as was necessary to make the design conform to standard manufacturing techniques. This work was carried out with the close cooperation of Dr. Neher.

Figure 89 shows an external view of the tube and Fig. 90 a cross sectional view of the final structure. There are two striking departures in this tube from the designs previously described. One of these is that the axis of symmetry is no longer parallel to the axis of the envelope but instead is perpendicular to it. This construction makes possible in part the other striking feature of the tube, which is the wave guide output. A number of factors combine to make this type of output desirable and practical. The resonant cavity for a wavelength near 1.25 cm. becomes extremely small. Were loop coupling used this would necessitate a very small coupling loop and also a very small diameter output line. The small dimensions with loop coupling would require tolerances extremely difficult to maintain with conventional vacuum tube techniques. On the other hand, the wave guide used at 1.25 cm. is of dimensions (.170″ x .420″) such that a wave guide output with a choke coupling can readily be incorporated in a standard vacuum tube envelope.

The wave guide coupling is accomplished by means of a tapered wave guide which couples to the cavity through a non-resonant iris. The guide tapers in the narrow dimension only, from the iris to a circular output window. The tapered guide couples to the window by means of a circular half wave choke. The VSWR introduced by the window is 1.1 or less. External to the tube, there is an insulating fitting which permits the tube to be coupled directly to the guide by means of a second choke coupling. This makes it possible to operate the shell of the tube at a different potential

Digitized by Google
Original from UNIVERSITY OF MICHIGAN
Generated on 2019-09-23 04:58 GMT / http://hdl.handle.net/2027/mdp.39015077775156
Public Domain, Google-digitized / http://www.hathitrust.org/access_use#pd-google

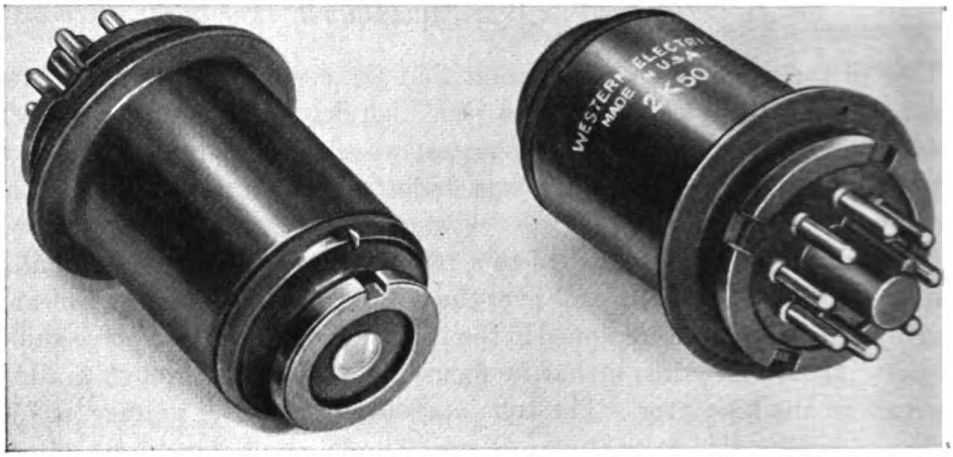

Fig. 89.—The 2K50—a reflex oscillator with thermal tuning and a wave guide output for operation in the 1 centimeter range.

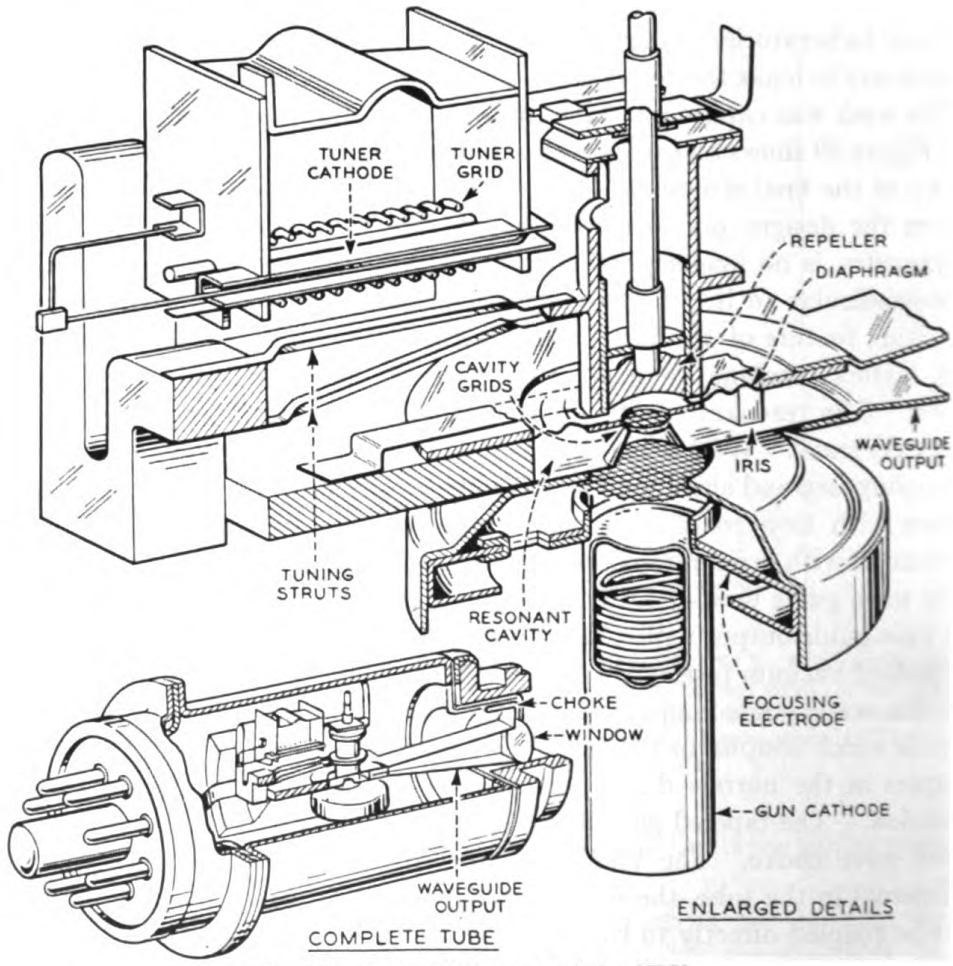

Fig. 90.—Internal features of the 2K50.

Digitized by Google
Original from UNIVERSITY OF MICHIGAN
Generated on 2019-09-23 04:59 GMT / http://hdl.handle.net/2027/mdp.39015077775156
Public Domain, Google-digitized / http://www.hathitrust.org/access_use#pd-google

than the guide. This is desirable in a radar receiver for circuit reasons, which require that the cathode of the oscillator be at ground potential.

The iris size is a compromise chosen to provide sufficient sink margin throughout the band. An iris coupling inherently varies with frequency and provides a weaker coupling at lower frequencies. Hence, since a suffi-

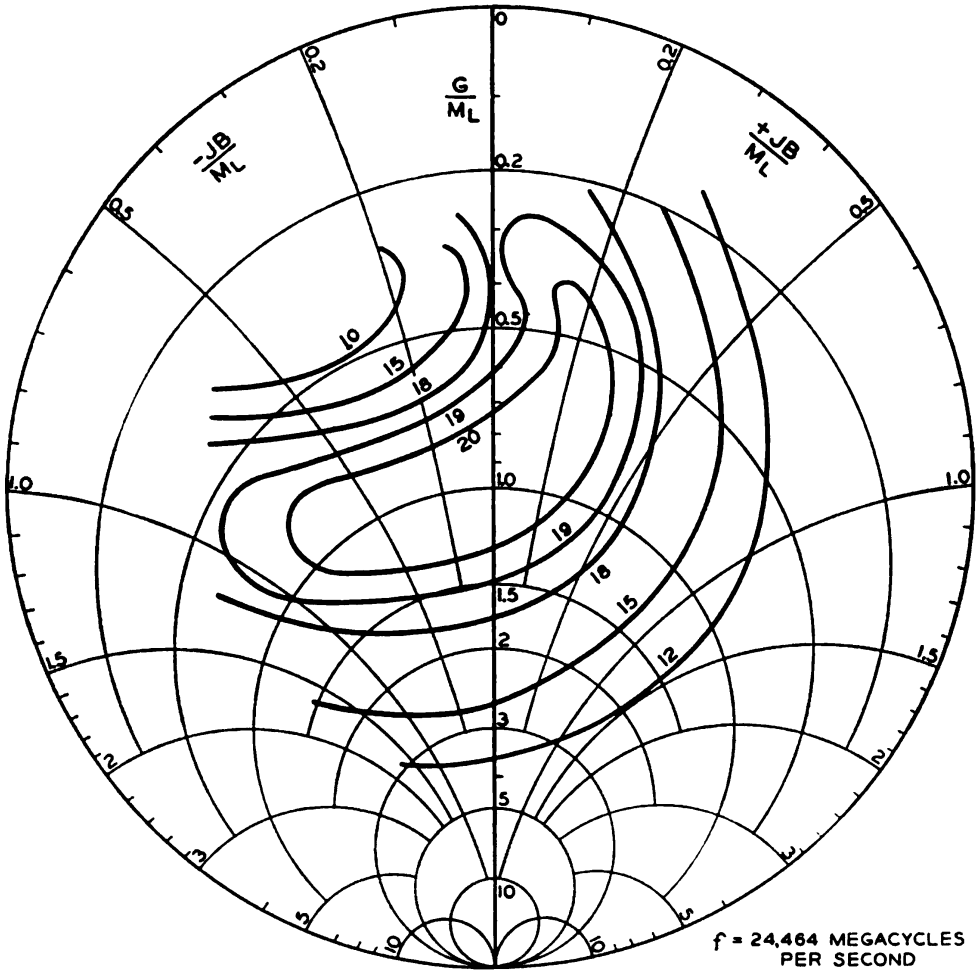

Fig. 91.—A performance diagram for the 2K50 at the high frequency band limit. This diagram shows loci of constant power as a function of the admittances presented at the plane of the tube window. Admittances are normalized in terms of the characteristic admittance of the wave guide.

cient sink margin must be provided at the wavelength where the coupling is a maximum, this means that an excess of sink margin exists at the low frequency end of the band. This is illustrated by the impedance performance diagrams of Figs. 91 to 93.

The 2K50 presented a difficult mechanical problem which will be appreciated when the minute dimensions of the resonant cavity are observed in

Digitized by Google
Original from UNIVERSITY OF MICHIGAN
Generated on 2019-09-23 04:59 GMT / http://hdl.handle.net/2027/mdp.39015077775156
Public Domain, Google-digitized / http://www.hathitrust.org/access_use#pd-google

Fig. 90. The electron optical system consists of a concave cathode, a cylindrical beam electrode, and a grid concave towards the cathode. This produces an electron beam which converges into a conical nose and through the cavity grids to the repeller space. The repeller, which returns the beam across the gap, is rigidly held in a mica supported in a cylindrical housing connected to a diaphragm which serves as one wall of the resonator. The

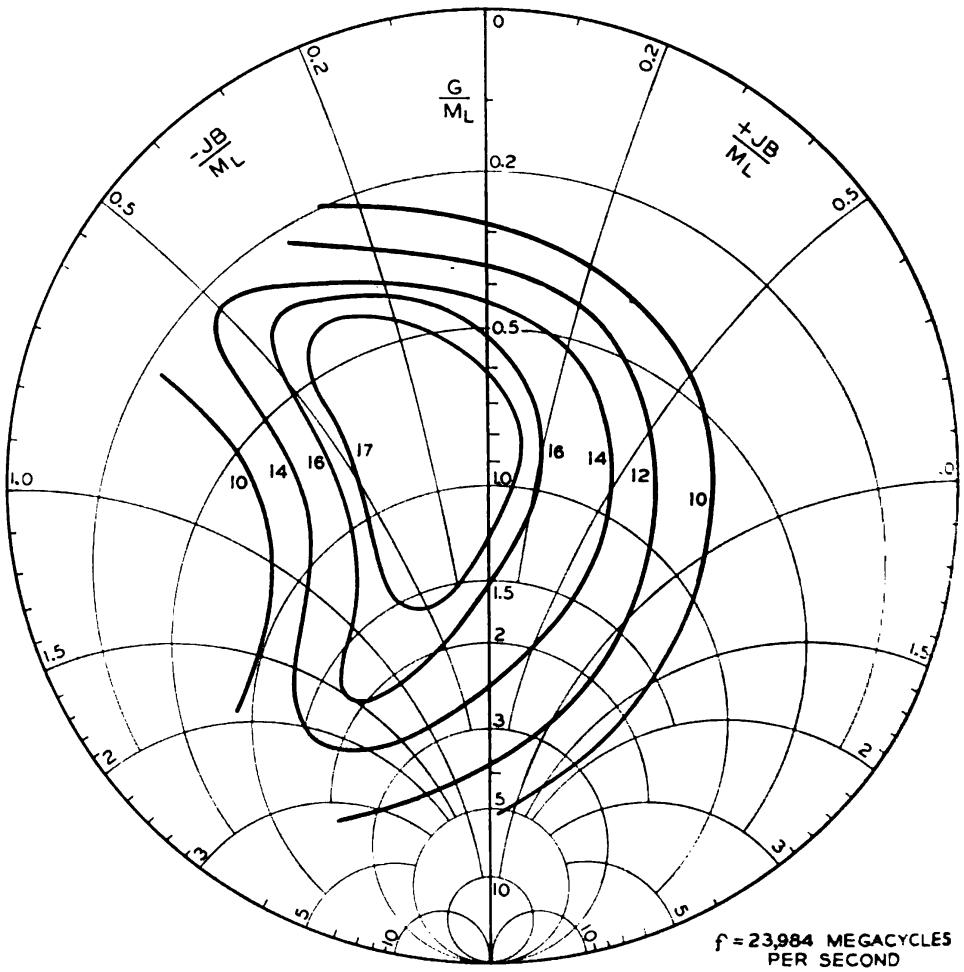

Fig. 92.—Performance diagram for the 2K50 at the mid-band frequency.

cylindrical housing is connected to a thermal tuning mechanism consisting of a simple framed structure in the shape of a right triangle. The base of the triangle is a heavy piece of metal brazed to the cavity block and a bleeder shoe which in turn is brazed to the bulb. One leg of the triangle can be heated by electron bombardment controlled, as in the 2K45, by a negative grid. The other leg is heated only by conduction. Since both legs are made from the same material, general heating of the structure will produce

Digitized by Google
Original from UNIVERSITY OF MICHIGAN
Generated on 2019-09-23 04:59 GMT / http://hdl.handle.net/2027/mdp.39015077775156
Public Domain, Google-digitized / http://www.hathitrust.org/access_use#pd-google

only a second order effect. Because of the small motion required to tune the 2K50 through its range, the tuner dimensions permit reliance on conduction cooling.

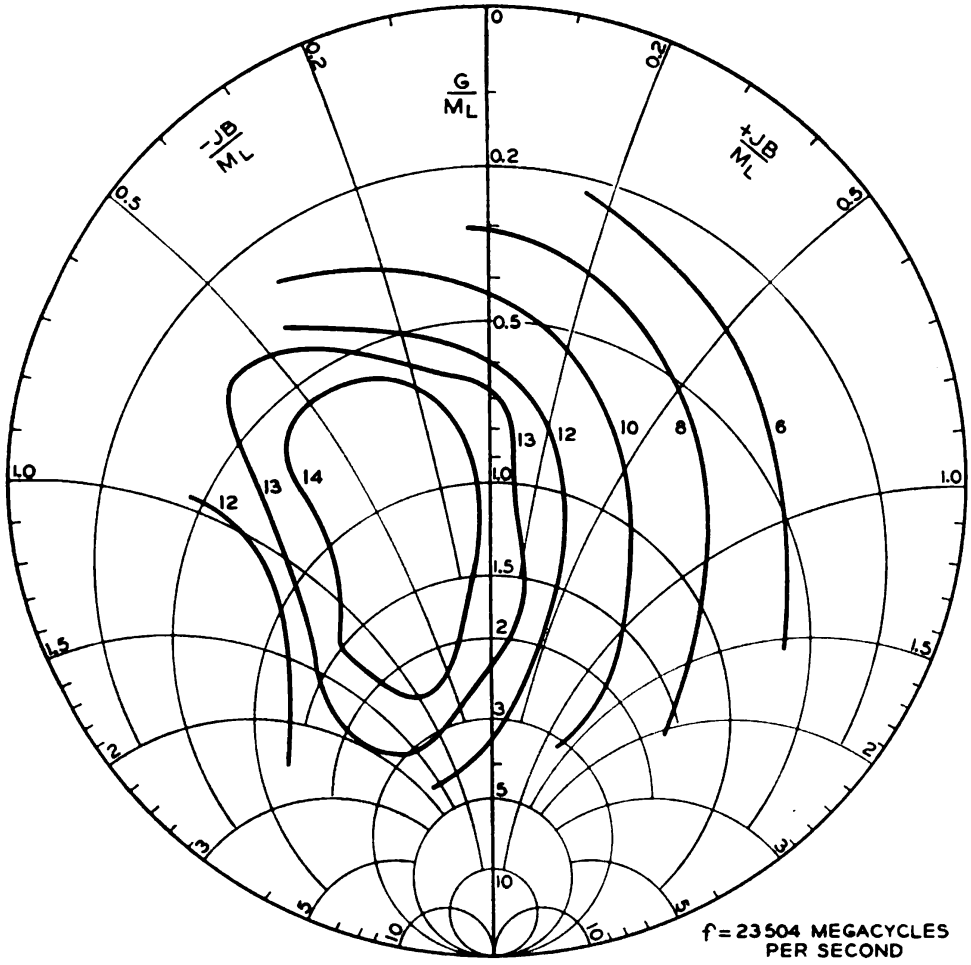

Fig. 93.—Performance diagram for the 2K50 at the low frequency band limit.

The characteristics of the thermal tuner of the 2K50 differ considerably from the 2K45. In Appendix XI expressions are given for the heating and cooling times as

$$\tau_h = \frac{c}{k} \log_e \frac{P_m - kT_c}{P_m - kT_h} \tag{13.4}$$

$$\tau_c = \frac{c}{k} \log_e \frac{T_h}{T_c}. \tag{13.5}$$

It is desirable that the cycling times should be equal. Equating (13.4) and (13.5) one obtains

$$P_m = k(T_h + T_c). \tag{13.6}$$

Digitized by Google
Original from UNIVERSITY OF MICHIGAN
Generated on 2019-09-23 04:59 GMT / http://hdl.handle.net/2027/mdp.39015077775156
Public Domain, Google-digitized / http://www.hathitrust.org/access_use#pd-google

This states that the maximum permitted temperature, $T_m = P_m/k$, shall exceed the temperature T_h by the same temperature difference as that by which T_c exceeds the sink temperature. From (13.4) and (13.5) it can be seen that to minimize the heating and cooling times the heat capacity should be small and the heat conductivity of the strut should be large. It is also evident that the ratio T_h/T_c should be as nearly unity as possible. This requires that the tuner should produce the required displacement in the smallest temperature interval possible. If a given temperature difference is required to produce the necessary motion, then from a speed standpoint it is desirable to make both T_h and T_c large in order that their ratio shall be nearly unity. The allowable temperature is usually limited by constructional considerations.

Over the normal tuning range of a reflex oscillator we have previously shown that the tuning characteristic may be represented by

$$\lambda = \alpha\sqrt{C_f + C(x)} \tag{13.7}$$

where α is a constant

C_f is a lumped fixed capacitance

$$C(x) = \frac{\beta}{x}$$

β is a constant.

Hence one can show that for small changes Δx from x_0

$$\Delta\lambda = -\frac{\frac{1}{2}\lambda_0\beta\Delta x}{x_0^2 C_0} \tag{13.8}$$

$$C_0 = C_f + C(x_0). \tag{13.9}$$

One may also show that for the type of tuner employed and the small motions involved in the 2K50 the displacement of the grids as a function of the temperature difference $T - T_0$ will be

$$x = x_0 - H(T - T_0) \tag{13.10}$$

whence

$$\Delta\lambda = \frac{\frac{1}{2}\lambda_0\beta H(T - T_0)}{x_0^2 C_0}. \tag{13.11}$$

If at time $t = 0$, $x = x_0$, $T = T_0$, $\lambda = \lambda_0$, we have for heating

$$\lambda' - \lambda_0 = \frac{\frac{1}{2}\lambda_0\beta H}{x_0^2 C_0}\left(\frac{P_i}{k} - T_0\right)(1 - e^{-(kt/c)}). \tag{13.12}$$

If we give P_i its maximum value P_m then at $t = \infty$ the temperature of the strut will be $\frac{P_i}{k} = T_m$, $\lambda = \lambda_m$

Digitized by Google
Original from UNIVERSITY OF MICHIGAN
Generated on 2019-09-23 04:59 GMT / http://hdl.handle.net/2027/mdp.39015077775156
Public Domain, Google-digitized / http://www.hathitrust.org/access_use#pd-google

and $$\Delta\lambda = \lambda_m - \lambda_0 = \frac{\frac{1}{2}\lambda_0 \beta H}{x_0^2 C_0} (T_m - T_0) \tag{13.13}$$

or $$\lambda - \lambda_0 = (\lambda_m - \lambda_0)(1 - e^{-(kt/c)}). \tag{13.14}$$

Thus the behavior of this type of tuner may be described by a time constant which is given by $\tau = \frac{c}{k}$. This has been verified experimentally for the 2K50, in which this constant has been found to have a typical value of 1.3 seconds.

The instantaneous tuning rates at a given wavelength based on full on-full off operation can be shown to be

$$\frac{df}{dt} = -\frac{1}{\tau}\frac{f}{f_m}(f - f_m) \quad \text{heating} \tag{13.15}$$

$$\frac{df}{dt} = \frac{1}{\tau}\frac{f}{f_0}(f_0 - f) \quad \text{cooling} \tag{13.16}$$

where f_0 is the frequency at zero tuner power

f_m is the frequency at maximum permitted drive.

Figure 94 shows the instantaneous tuning rate as a function of frequency on heating and cooling.

Typical power output versus frequency characteristics for the 2K50 are shown in Fig. 95. Curve A shows the power output with the repeller voltage optimized at each frequency while Curve B gives the variation when the repeller voltage is set for an optimum at the center of the band and held fixed as the frequency changes. For constructional reasons the spacing between the repeller and second cavity grid is fixed in the 2K50 so that on a proportional frequency basis the range between half power points with fixed repeller voltage is smaller for the 2K50 than for the 2K45.

Figure 96 shows the frequency vs. grid voltage characteristics for the 2K50. For normal operation with full on-full off operation the grid voltage is switched between zero and cutoff.

H. *A Millimeter Range Oscillator*

During the latter stages of work on the 2K50 development, work was started on an oscillator for a wavelength range around .625 cm. The design of this developmental tube known as the 1464XQ was undertaken.

There are several difficulties in going from 1.25 cm. to .625 cm. Greater accuracy of construction is required and the cathode must be operated at a higher current density. The greatest difficulty arises from the fact that the grids cannot be directly scaled in size from those used in tubes for longer wavelengths.

Digitized by Google
Original from UNIVERSITY OF MICHIGAN
Generated on 2019-09-23 04:59 GMT / http://hdl.handle.net/2027/mdp.39015077775156
Public Domain, Google-digitized / http://www.hathitrust.org/access_use#pd-google

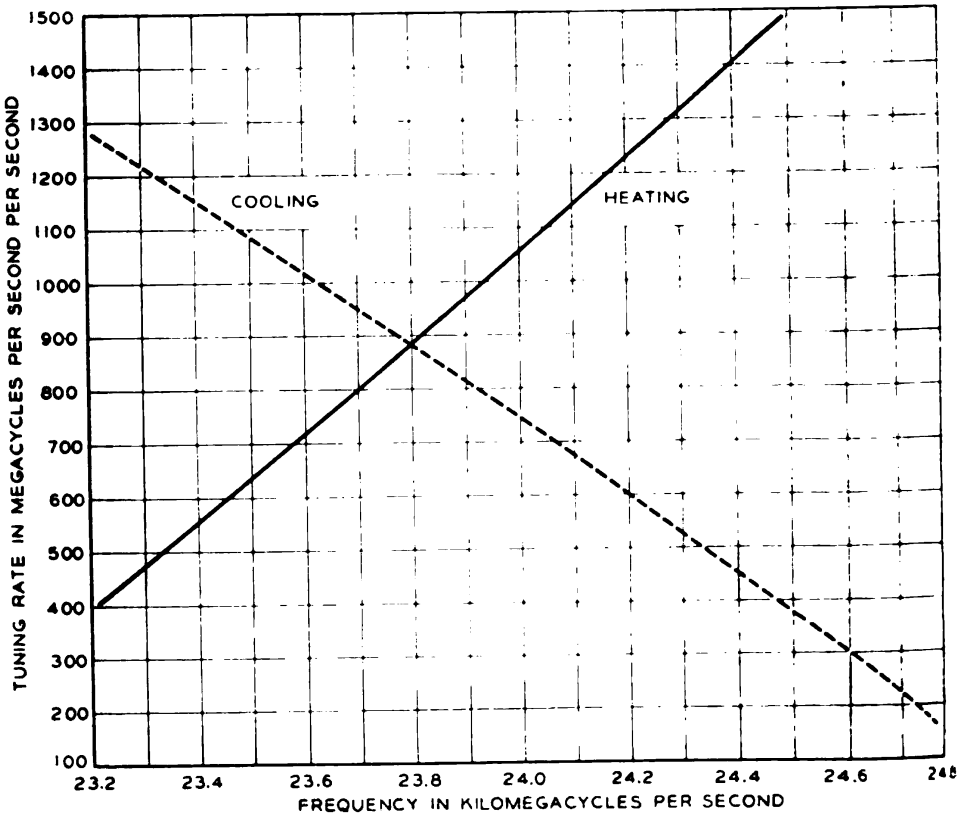

Fig. 94.—Computed instantaneous tuning rates on heating and cooling for the 2K50 oscillator. These results are based on a time constant of 1.3 seconds and on the assumption of "full on or off" operation.

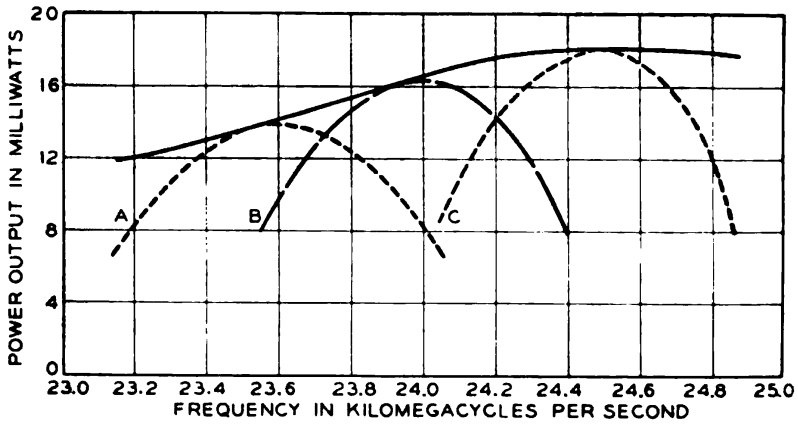

Fig. 95.—Power output characteristics of the 2K50 oscillator. Curves *A*, *B* and *C* illustrate the power variation with frequency when the repeller voltage is set for the optimum at the indicated frequency and held fixed as a cavity tuning is changed. The envelope of these curves shows the power variation with frequency when the repeller voltage is maintained at its optimum value for each frequency.

Generated on 2019-09-23 05:00 GMT / http://hdl.handle.net/2027/mdp.39015077775156
Public Domain, Google-digitized / http://www.hathitrust.org/access_use#pd-google
Digitized by Google
Original from UNIVERSITY OF MICHIGAN

Let us consider the factors involved in scaling from a tube operating at a given frequency to a smaller tube operating at a higher frequency. If the cathode is operated space-charge-limited and the anode voltage is the same as for the larger tube, the total electron current will be the same and each grid wire will intercept as much current and hence receive the same power to dissipate as in the larger tube. Suppose the length of a grid wire in the larger tube is l_0 and in the smaller tube the length of the corresponding wire is l_1. Suppose that all the other dimensions of the smaller tube, including

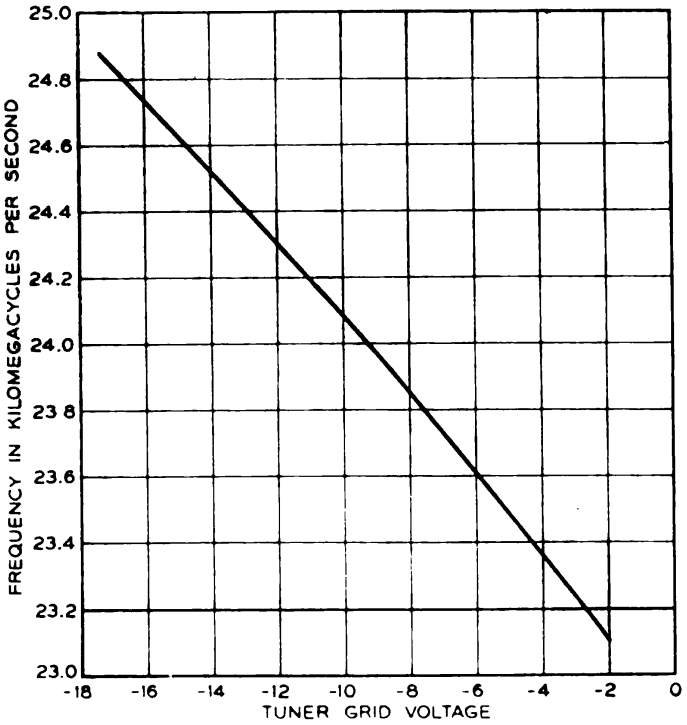

Fig. 96.—Frequency vs tuner grid voltage for the 2K50.

the diameter of the grid wire, are reduced in the ratio l_1/l_0. We do not know *a priori* whether or not the temperature distribution along the grid wires of the smaller tube will be the same as that for the larger tube; suppose, however, that it is. Then if T_0 is the temperature at some typical point, say, the hottest, on the grid wire of the larger tube, and T_1 is the temperature at the similar point on the smaller tube, the power the wire loses by radiation in the large tube, P_{r0} and in the small tube, P_{r1} are given by

$$P_{r0} = Al_0^2T_0^4 \tag{13.17}$$

$$P_{r1} = Al_1^2T_1^4. \tag{13.18}$$

Digitized by Google
Original from UNIVERSITY OF MICHIGAN
Generated on 2019-09-23 05:00 GMT / http://hdl.handle.net/2027/mdp.39015077775156
Public Domain, Google-digitized / http://www.hathitrust.org/access_use#pd-google

Here A is nearly constant for given tube geometry and materials. In radiation the power lost varies as the area, which varies as l^2, and as the temperature to the fourth power.

The power lost by end cooling, for the large and the small tube, P_{e0} and P_{e1} will be given by

$$P_{e0} = Bl_0T_0 \tag{13.19}$$

$$P_{e1} = Bl_1T_1. \tag{13.20}$$

Here B is another constant. These relations express the fact that the power lost by end cooling (thermal conduction) varies as cross sectional area divided by length and hence as l and as temperature difference, taken as proportional to T.

Now, in scaling the tube the power to be dissipated has been kept constant. Further, in making the tube small, the hottest point of the grid cannot be run hotter than the melting point of the wire; in fact, it cannot be run nearly this hot without unreasonable evaporation of metal. Suppose we let the grid in the smaller tube attain the maximum allowable temperature T_m and let the power the wire must dissipate be P. Then for the large tube

$$P = P_{r0} + P_{e0} = (Al_0T_0^3 + B)l_0T_0 \tag{13.21}$$

and for the smaller tube

$$P = P_{r1} + P_{e1} = (Al_1T_m^3 + B)l_1T_m. \tag{13.22}$$

Hence, the smallest value l_1 can have without running the grid too hot is given by the equation

$$l_1 = l_0 \frac{T_0}{T_m} \frac{(Al_0T_0^3 + B)}{(Al_1T_m^3 + B)}. \tag{13.23}$$

We see that if l_0 is very small,

$$\begin{aligned} Al_0T_m^3 &\ll B \\ Al_1T_m^3 &\ll B \end{aligned} \tag{13.24}$$

Numerical examples show that this is so for a tube such as the 2K50. This means that nearly all of the power dissipated by the grid is lost through end cooling, not radiation.[14] Further, in the 2K50 the grid is already operating near the maximum allowable temperature. Hence, nearly, $T_0 = T_m$ and the smallest ratio in which the tube can be scaled down without overheating the grids is approximately unity. This means that in making a tube for .625 cm. the grid wire cannot be made half the diameter of the wire used in

[14] The fact that one kind of dissipation predominates in both cases justifies the assumption of the same temperature distribution in both cases.

Digitized by Google
Original from UNIVERSITY OF MICHIGAN
Generated on 2019-09-23 05:00 GMT / http://hdl.handle.net/2027/mdp.39015077775156
Public Domain, Google-digitized / http://www.hathitrust.org/access_use#pd-google

the 2K50. In fact, the diameter of the grid wire can be made but little smaller. Thus, in the 1464XQ the grid is relatively coarse compared with that in the 2K50. This results in a reduced modulation coefficient and hence in less efficiency.

In going to .625 cm., resonator losses are of course greater. The surface resistivity of the resonator material varies as the square root of the frequency. Surface roughness becomes increasingly important in increasing resistance at higher frequencies. Further, in order to provide means for moving the diaphragm in tuning, it was necessary in the 1464XQ to use a second mode resonator (described later) and this also increases losses over those encountered at lower frequencies.

Development of the 1464XQ was stopped short of completion with the cessation of hostilities. However, oscillation in the range .625–.660 cm. had been obtained. The power output varied from 2–5 milliwatts between the short wave and long wave extremes of the tuning range. The cathode current was around 20 ma, the resonator voltage 400 volts. The tube operated in several repeller modes in a repeller voltage range 0 to −180 volts.

Figures 97 and 98 illustrate features of the 1464XQ oscillator. Figure 98 is a scale drawing of the resonator and repeller structure. The electron beam is shot through two apertures covered with grids of .6 mil tungsten wire. These grids are 80% open and are lined up. The aperture in the grid nearest the gun is 23 mils in diameter and the second aperture is 34 mils in diameter. The repeller is scaled almost exactly from the 723A 3 cm. reflex oscillator. A second mode resonator is used. The inner part, a, of Fig. 98 is about the size of a first mode resonator. This is connected to an outer portion, c, by a quarter wave section of small height, b, which acts as a decoupling choke. The resonator is tuned by moving the upper disk with respect to the lower part, thus changing the separation of the grids. The repeller is held fixed. Power is derived from the outer part, c, of the resonator by means of an iris and a wave guide, which may be seen in the section photograph Fig. 97. There is an internal choke attached to the end of the part of the wave guide leading from the resonator. This is opposed to a short section of wave guide connected to the envelope, and in the outer end of this wave guide there is a steatite and glass window of a thickness to give least reflection of power.

I. *Oscillators for Pulsed Applications—The 2K23 and 2K54*

All the reflex oscillators described in the preceding sections have been low power oscillators intended for beating oscillator or signal oscillator applications. Some limitation on the power capability of these oscillators in the form previously described is set by the power handling capacity of the grids. If the tubes are pulsed with pulse durations which are short compared with

Digitized by Google
Original from UNIVERSITY OF MICHIGAN
Generated on 2019-09-23 05:01 GMT / http://hdl.handle.net/2027/mdp.39015077775156
Public Domain, Google-digitized / http://www.hathitrust.org/access_use#pd-google

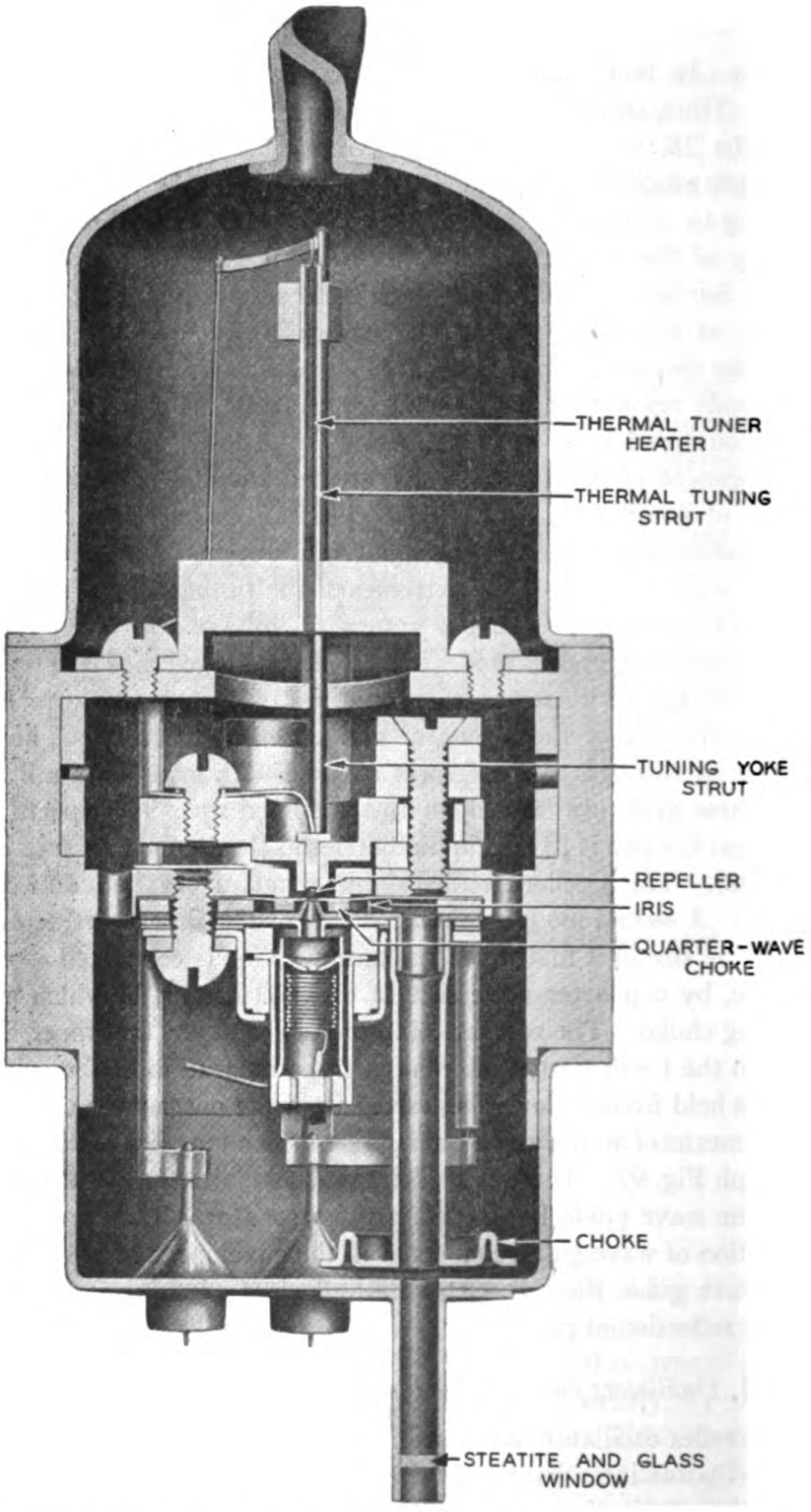

Fig. 97.—An experimental thermally tuned reflex oscillator, the 1464, designed for operation between the wave lengths of .6 and .7 cms.

Digitized by Google
Original from UNIVERSITY OF MICHIGAN
Generated on 2019-09-23 05:01 GMT / http://hdl.handle.net/2027/mdp.39015077775156
Public Domain, Google-digitized / http://www.hathitrust.org/access_use#pd-google

the thermal time constant of the grids, then the peak power input to the oscillators may be increased over the continuous limit by the duty factor, provided that the voltages applied are consistent with the insulation limits of the tubes and that the peak currents drawn from the cathode are not in excess of its capacity.

An application for a pulsed oscillator arose in the AN/TRC-6 radio system.[15] This was an ultra-high frequency military communication system using pulse position modulation to convey intelligence. With the high gain which may be achieved with antennas in the centimeter range, the power necessary in the transmitter for transmission over paths limited by line of sight is of the order of a few watts peak. In beating oscillator applications the power output is of secondary importance to electronic tuning, so that the reflex oscillators previously described were designed to operate with a drift time in the repeller space such as to provide the desired tuning. In a

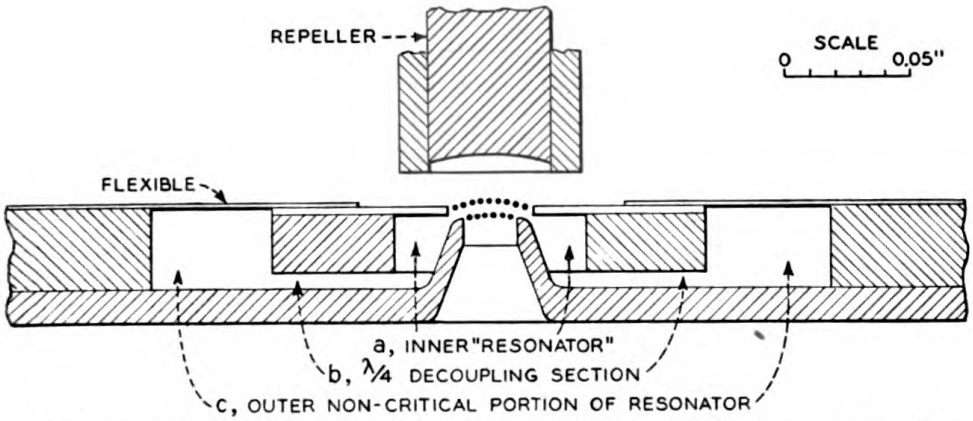

Fig. 98.—The resonator and repeller structures of the oscillator shown in Fig. 97.

pulsed transmitter electronic tuning is unnecessary and indeed undesirable, since it leads to frequency modulation on the rise and fall of the pulse. In section III it is shown that for maximum efficiency with a given resonator loss there will be an optimum value for the drift time. If there were no resonator loss this time would be $\frac{3}{4}$ cycles, which is the minimum possible. By utilizing the optimum drift angle and taking advantage of the higher peak power inputs permitted by pulsing it was possible to obtain peak power outputs of the order of several watts using the same structure as employed for the beating oscillators previously described without exceeding the power dissipating capability of such a structure. From the standpoint of military convenience this was a very desirable situation for reasons of simplicity of tuning and ease of installation.

[15] A Multi-channel Micro-wave Radio Relay System, H. S. Black, W. Beyer, T. J. Grieser, and F. A. Polkinghorn, *Electrical Engineering* Vol. 65, No. 12, pp. 798–806, Dec. 1946.

Digitized by Google
Original from UNIVERSITY OF MICHIGAN
Generated on 2019-09-23 05:01 GMT / http://hdl.handle.net/2027/mdp.39015077775156
Public Domain, Google-digitized / http://www.hathitrust.org/access_use#pd-google

The first tube designed for this service was the 2K23. It was based on the design employed in the 2K29 and operated with a drift time of $1\frac{3}{4}$ cycles in the repeller space. A severe limitation on the performance was set by by the requirement that a single oscillator should cover the frequency range from 4275 to 4875 Mc/s. It is shown in Section X that in an oscillator tuned by changing the capacitance of the gap the efficiency will vary considerably

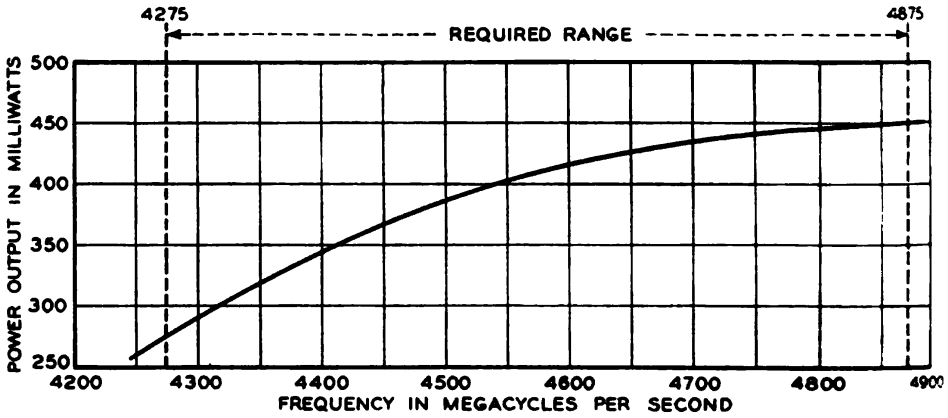

Fig. 99.—Variation of the peak power output vs frequency for the 2K23 reflex oscillator. This tube was designed for pulse operation with a duty factor of 10 in a repeller mode having 3.5 π radians drift.

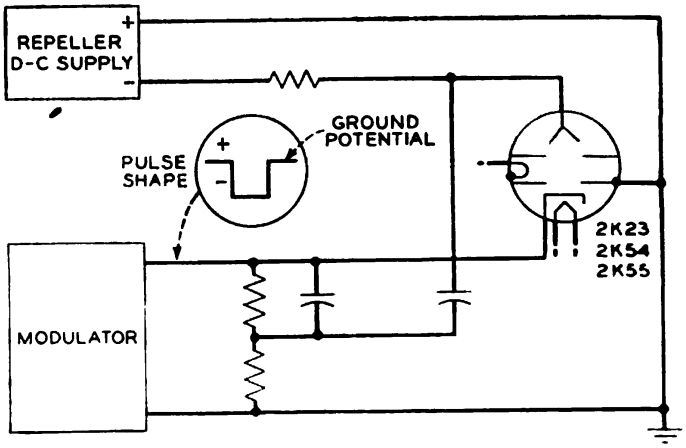

Fig. 100.—Modulator circuit for use in connection with reflex oscillators showing means for applying pulse voltage to the repeller to reduce frequency modulation during pulsing.

over such a tuning range. In the case of the 2K23 the variation of the peak power output with frequency is shown in Fig. 99. The duty factor at which the tube was used (the ratio of the time between pulses to the pulse length) was 10. In the AN/TRC-6 application the tube was operated on a fixed current basis; i.e., the pulse amplitude was adjusted to a value such that the average current drawn was 15 ma. The schematic of the circuit employed in pulsing oscillators in this way is shown in Fig. 100. The resonator

Digitized by Google
Original from UNIVERSITY OF MICHIGAN
Generated on 2019-09-23 05:02 GMT / http://hdl.handle.net/2027/mdp.39015077775156
Public Domain, Google-digitized / http://www.hathitrust.org/access_use#pd-google

of the oscillator is operated at ground and the cathode of the oscillator is pulsed negative with respect to this ground. The repeller voltage is referenced from the cathode and this reference is maintained during the pulse. Some frequency modulation occurs during the rise and fall of the pulse because of the changing electron velocity. This can be reduced in part by applying a part of the pulse in the repeller circuit proportioned in such a way as to tend to maintain the drift time independent of the cathode to resonator voltage. Satisfactory performance is achieved in this way.

As mentioned previously, the intelligence is conveyed by pulse position modulation. The AN/TRC-6 system uses time division multiplex to provide eight communication channels. The multiplexing is achieved by transmitting a four micro-second marker pulse which provides a time reference followed by eight one micro-second pulses. The time of each of the latter pulses is independently varied in position with reference to the marker pulse.

The time interval from the marker to each pulse could be measured to either the leading or trailing edge of the pulse. In Section XII it is shown that the leading edge of the r.f. pulse will be subject to what is commonly called "jitter" because of the random time of rise which will result if oscillation starts from shot or Johnson noise. Conceivably oscillation might be started by shock excitation of the resonant circuit by the pulsed beam current. However, in Appendix X it is shown that the initial excitation produced by shot noise in the beam exceeds that induced by the current transient by a factor of approximately 100. The trailing edge of the pulse will not be subject to this form of jitter provided two conditions are met. First, the pulse duration must be long enough so that oscillation builds up to full amplitude during the pulse. Second, the receiver must have a sufficient bandwidth so that the transient which occurs on reception of the leading edge has fallen to a small value by the time the trailing edge is received. Since these conditions were met in the AN/TRC-6 system, the trailing edge of the pulse was used.

In the latter stages of the development of the AN/TRC-6 system it was decided to remove the restriction that the required tuning range should be covered with a single transmitter tube. This made possible the achievement of a design which would provide an improved performance throughout the band. In order to improve the circuit efficiency of the resonator, the new designs were based on the oscillator structure which was employed in the 2K45. It has been pointed out previously that this makes possible a considerably higher resonant impedance of the cavity, partly because of the reduced gap capacitance and also because the smaller first and second grids reduce the resonator losses. These effects were reflected in the higher efficiency obtained in the 2K54 and 2K55.

Digitized by Google
Original from UNIVERSITY OF MICHIGAN
Generated on 2019-09-23 05:02 GMT / http://hdl.handle.net/2027/mdp.39015077775156
Public Domain, Google-digitized / http://www.hathitrust.org/access_use#pd-google

The three tubes, the 2K23, 2K54 and 2K55 were intended to couple to wave guide circuits. Although direct coupling to the guide through a wave guide output would have been desirable in some ways, it would have resulted in a very large and awkward structure. It seemed best, therefore, to retain the coaxial output feature of tubes designed for beating oscillator service. From a standpoint of convenience, it would have been desirable

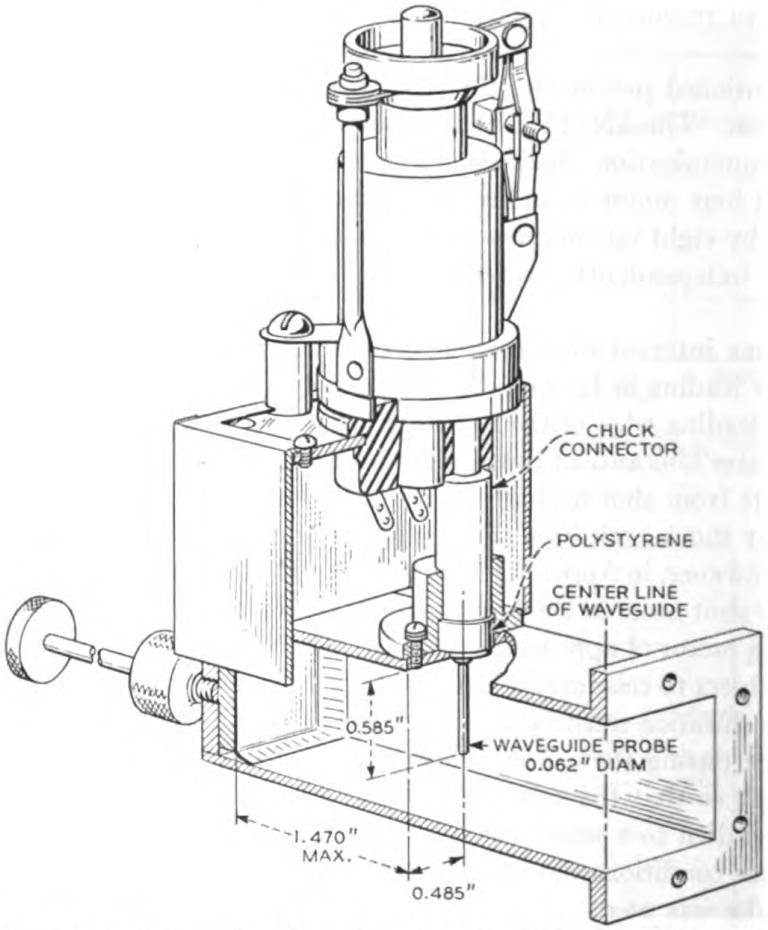

Fig. 101.—A transducer designed to adapt the 2K23, 2K54 and 2K55 oscillators to a terminated wave guide load. If the back piston of this coupling is set at a distance of 1.08″ from the center of the probe the impedance presented to the oscillator line is 50 ohms with a 1 db variation over the required frequency range.

to have had the wave guide probe an integral part of the tube, as is the case in the 2K25. However, the length of a quarter wave probe at the operating wave lengths of the AN/TRC-6 system made such a design hazardous. Because of this a transducer was developed into which the tube could be plugged. This is shown in Fig. 101. The central chuck extends the center conductor of the output coaxial of the tube into the guide. It had been

Digitized by Google
Original from UNIVERSITY OF MICHIGAN
Generated on 2019-09-23 05:02 GMT / http://hdl.handle.net/2027/mdp.39015077775156
Public Domain, Google-digitized / http://www.hathitrust.org/access_use#pd-google

originally intended to design this transducer so that all elements would be fixed. It was found, however, that an adjustable back piston setting permitted compensation for manufacturing tolerances in the tubes as well as permitting the presentation of a better impedance to the oscillator over the band than was attainable with a fixed transducer. This is illustrated in Fig. 102 which shows the power output versus frequency for a typical 2K54 and a typical 2K55 as a function of frequency for three cases. In one case, as shown by curve B, the power output is delivered at all frequencies into the optimum impedance, i.e. the impedance into which the oscillator will deliver maximum power. Curve *A* shows the power output delivered into

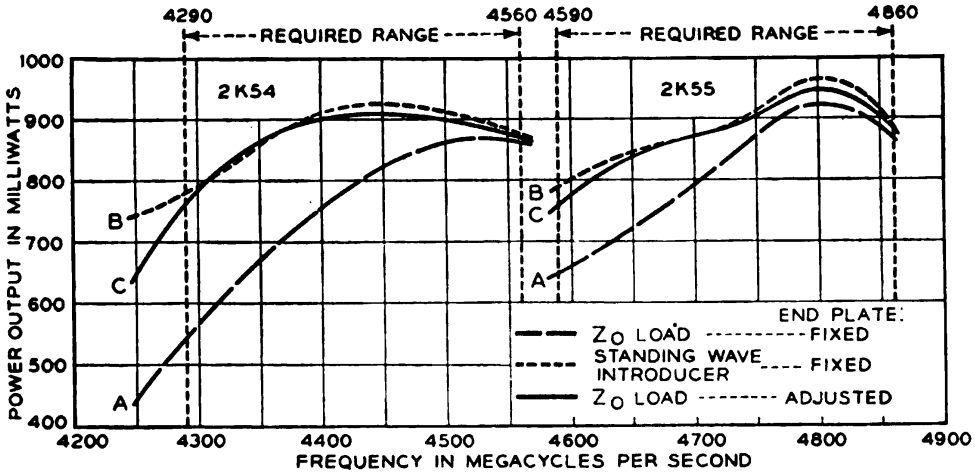

Fig. 102.—Peak power output vs frequency for the 2K54 and 2K55 oscillators for several load conditions. Curves *A* give the performance obtained when the tubes operate into a characteristic admittance load through the coupling of Fig. 101 with the end plate fixed so that the admittance presented to the tubes is constant to within 1 db over the frequency range. Curves *B* give the performance obtained when the optimum impedance s presented to the oscillators throughout the band. Curves *C* give the performance obtained when the tubes are coupled to a characteristic admittance load with the coupling unit of Fig. 101 and with a back piston adjusted to the best value at each frequency.

a transducer which has the back piston fixed at a distance from the probe, so chosen that the impedance seen by the oscillator is flat over the band to within 1 *db*. Curve *C* shows the power output when the back piston of the transducer is adjusted so that the tube delivers maximum power. It can be seen that the performance obtained under the latter circumstances is very nearly as good as that obtained when the optimum impedance is presented to the oscillator.

From Sections III and IX we would expect that, since the coupling system is such as to give maximum power throughout the band, the sink margin should be slightly greater than 2. Figures 103 to 106 give impedance performance diagrams for 2K54 and 2K55 at the four transmitting frequencies

Digitized by Google
Original from UNIVERSITY OF MICHIGAN
Generated on 2019-09-23 05:02 GMT / http://hdl.handle.net/2027/mdp.39015077775156
Public Domain, Google-digitized / http://www.hathitrust.org/access_use#pd-google

of the AN/TRC-6 system. From this it can be seen that the sink margin is approximately 2 at all frequencies. In a transmitter tube another factor, which is of small importance in a beating oscillator, becomes of interest. This factor is the pulling figure, which is defined as the maximum frequency

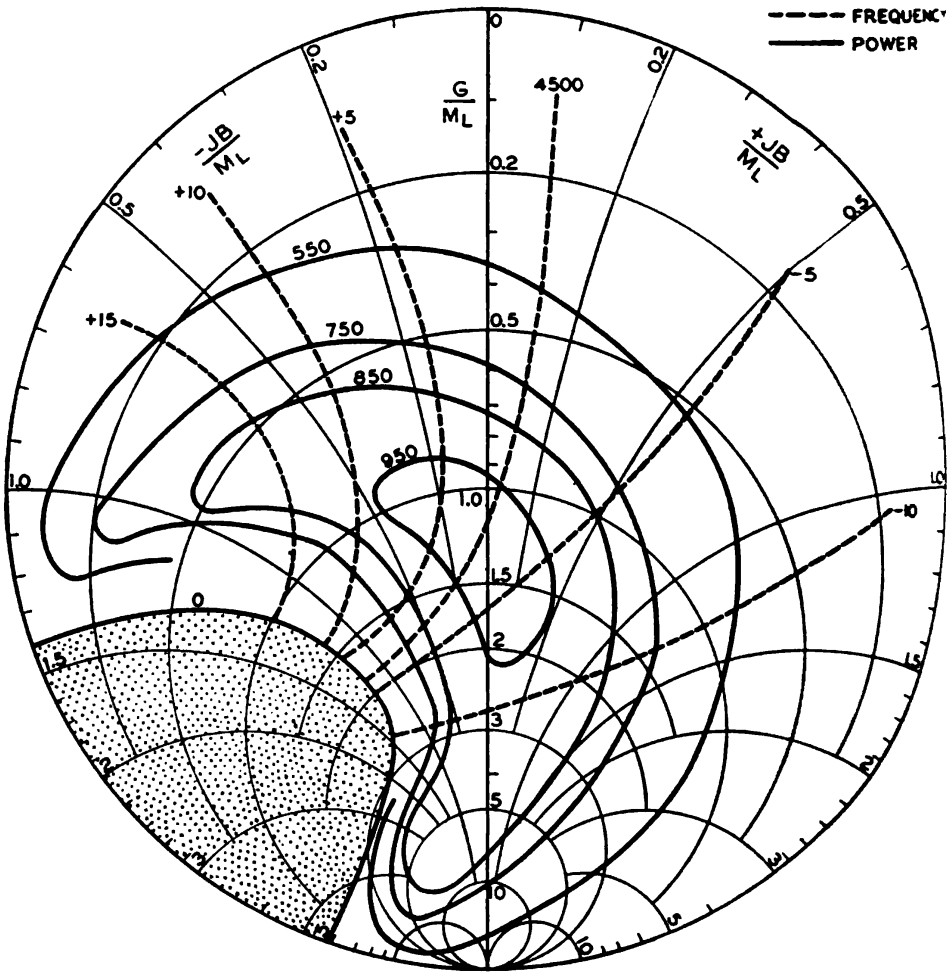

Fig. 103.—Rieke diagram for the 2K54 at a nominal frequency of 4500 megacycles. The point at the unity *vswr* condition is obtained by adjusting the repeller voltage and the back piston of the coupling of Fig. 101 to the values which gave maximum power. These conditions were then held fixed for the remainder of the chart.

excursion which will be produced when a VSWR of 3 *db* is presented to the transmitter and the phase is varied over 180°. Fig. 107 gives the pulling figure as a function of frequency for the 2K54 and 2K55. The requirements on the pulling figure for the 2K54 and 2K55 were not severe, since in the AN/TRC-6 system the tube is coupled to the antenna by a very short wave guide run and, furthermore, the antennas are fixed.

Digitized by Google
Original from UNIVERSITY OF MICHIGAN
Generated on 2019-09-23 05:02 GMT / http://hdl.handle.net/2027/mdp.39015077775156
Public Domain, Google-digitized / http://www.hathitrust.org/access_use#pd-google

Investigation of the pulling figure of early models of the 2K55 led, however, to the disclosure of one unforeseen pitfall arising from the existence of electronic hysteresis. It had at first been considered that electronic hysteresis would not be of importance in the transmitter tube, where the feature of electronic tuning was of no importance. This might be true in a CW oscilla-

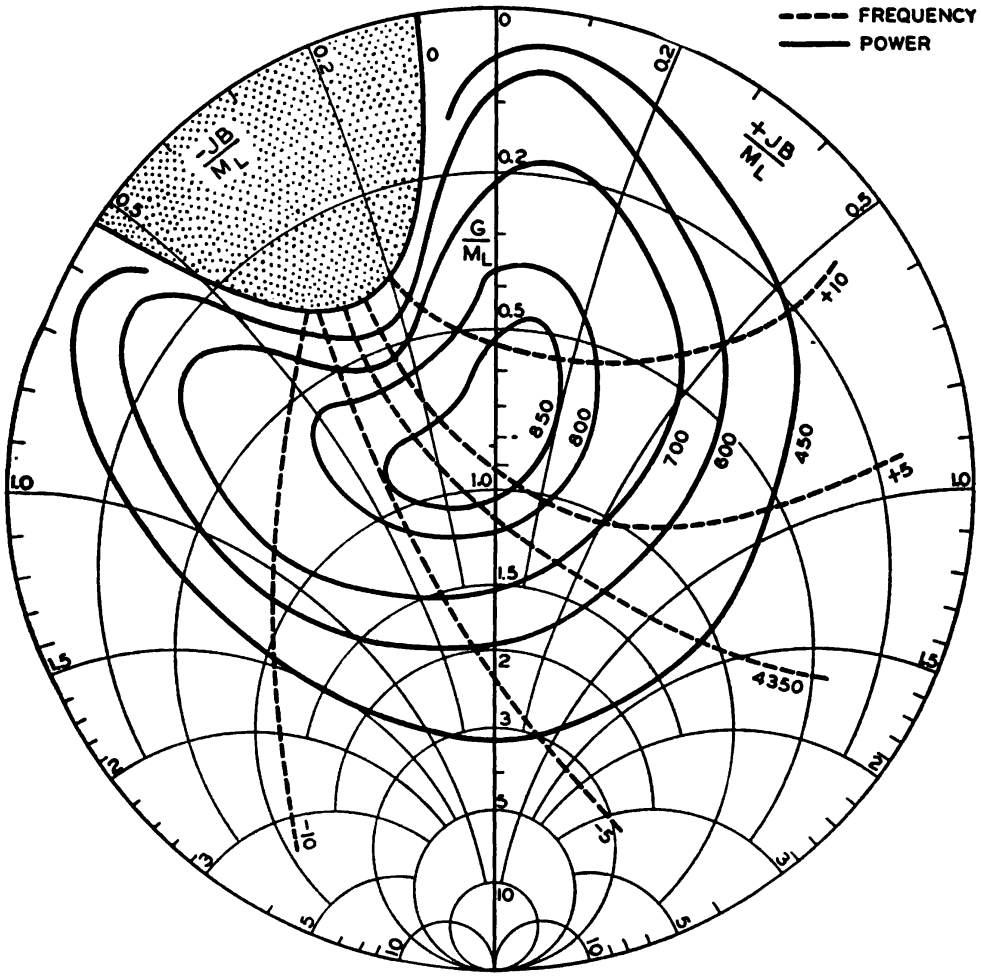

Fig. 104.—Rieke diagram for the 2K54 oscillator at a nominal frequency of 4350 megacycles. The unity *vswr* point was obtained as described in Fig. 103.

tor, but in a pulsed oscillator the existence of hysteresis resulted in an unforeseen reduction of the sink margin. Since the oscillator is being pulsed, for each pulse the oscillating conditions are being re-established. Although the cathode-repeller voltage need not vary during the pulsing, the fact that the cathode-resonator voltage is being changed means that for each pulse the drift angle in the repeller space varies on the rise and fall of the pulse. The effect during the rise of the pulse is the same as though the repeller

Digitized by Google
Original from UNIVERSITY OF MICHIGAN
Generated on 2019-09-23 05:02 GMT / http://hdl.handle.net/2027/mdp.39015077775156
Public Domain, Google-digitized / http://www.hathitrust.org/access_use#pd-google

voltage were made less negative. In other words, on the rise of each pulse the situation is equivalent to that in a *CW* oscillator when, for a fixed resonator voltage, one starts with a repeller voltage too negative to permit oscillation and then reduces the repeller voltage until oscillation occurs. Let us now suppose that the hysteresis is such that under these circumstances

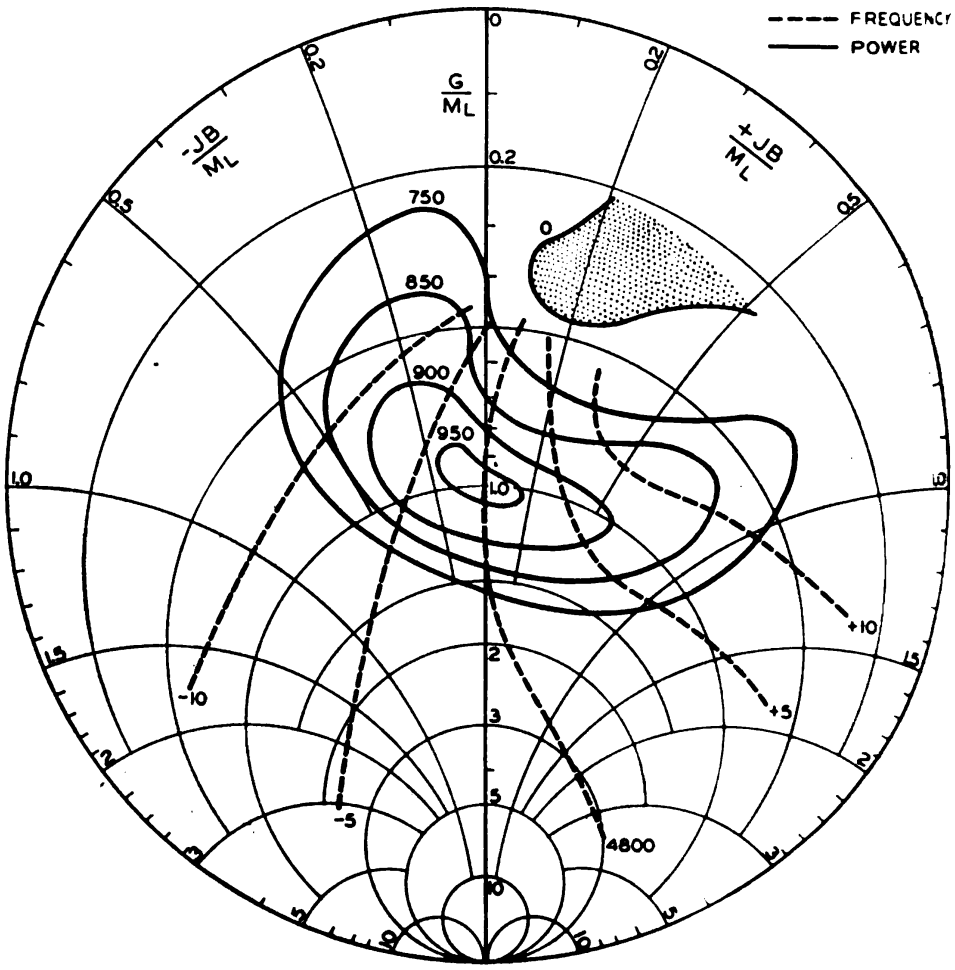

Fig. 105.—Rieke diagram for the 2K55 oscillator at a nominal frequency of 4800 megacycles. The unity *vswr* point was obtained as described in Fig. 103.

the amplitude of oscillation would suddenly jump to a large value. We would then obtain a variation of peak power output as a function of the repeller voltage shown in Fig. 108. Ordinarily, the repeller voltage would be adjusted so as to obtain maxmum power output as, for example, with the repeller voltage V_{R1}. Next, let us suppose that a variable impedance is presented to the oscillator with the repeller voltage held fixed at value V_{R1}, as would be done, for example, in obtaining an impedance performance

Digitized by Google
Original from UNIVERSITY OF MICHIGAN
Generated on 2019-09-23 05:03 GMT / http://hdl.handle.net/2027/mdp.39015077775156
Public Domain, Google-digitized / http://www.hathitrust.org/access_use#pd-google

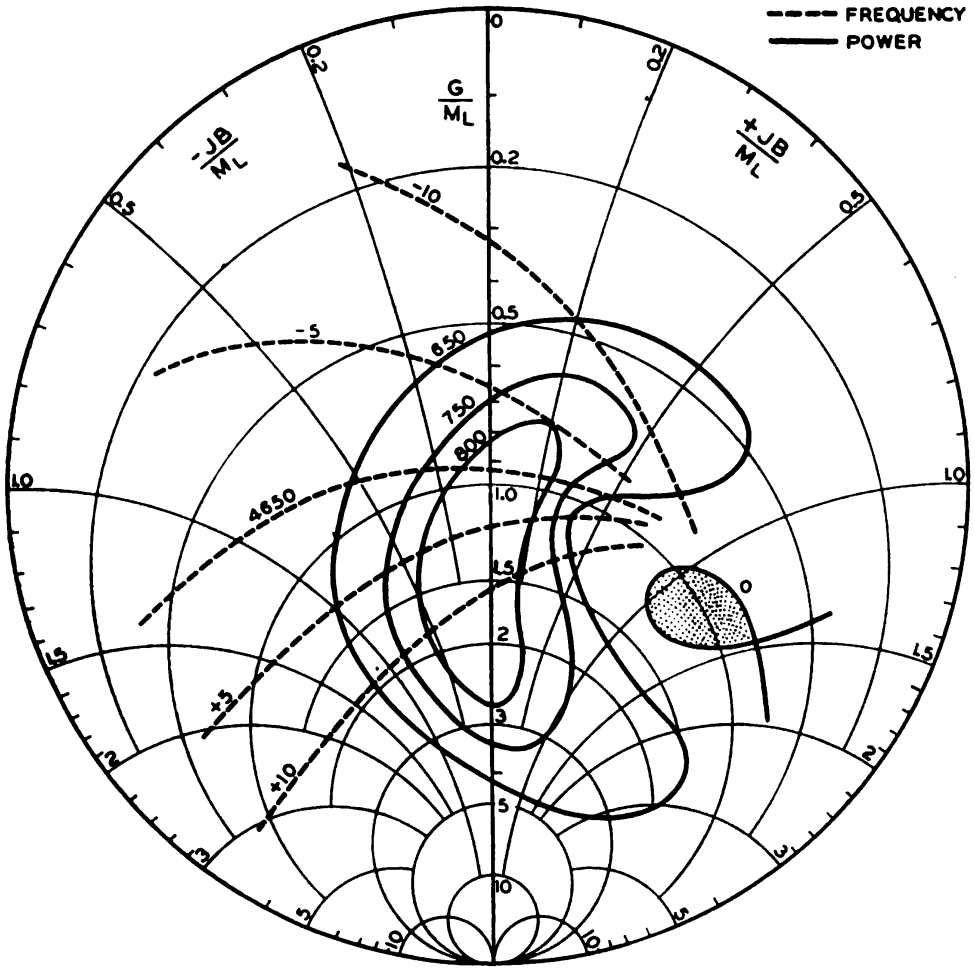

Fig. 106.—Rieke diagram for the 2K55 oscillator at a nominal frequency of 4650 megacycles. The unity *vswr* point was obtained as described in Fig. 103.

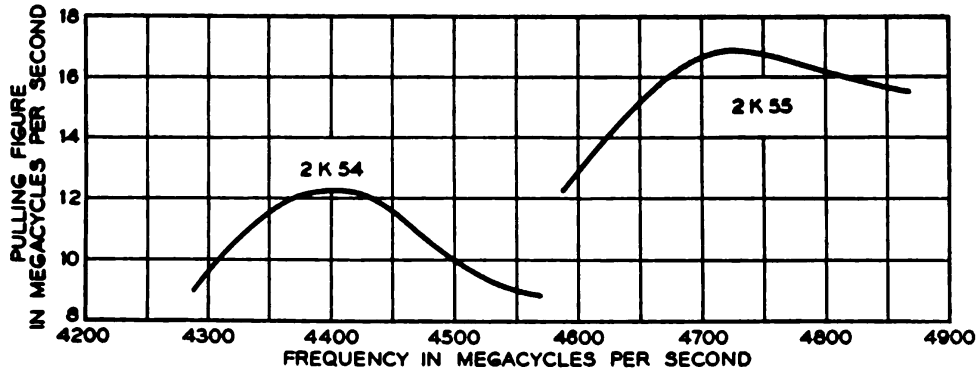

Fig. 107.—Pulling figures for the 2K54 and 2K55 reflex oscillators as functions of frequency. With a unity *vswr* load the repeller voltage and back piston of the coupling of Fig. 101 were adjusted for a maximum power and held fixed for the pulling figure measurements.

Digitized by Google
Original from UNIVERSITY OF MICHIGAN
Generated on 2019-09-23 05:03 GMT / http://hdl.handle.net/2027/mdp.39015077775156
Public Domain, Google-digitized / http://www.hathitrust.org/access_use#pd-google

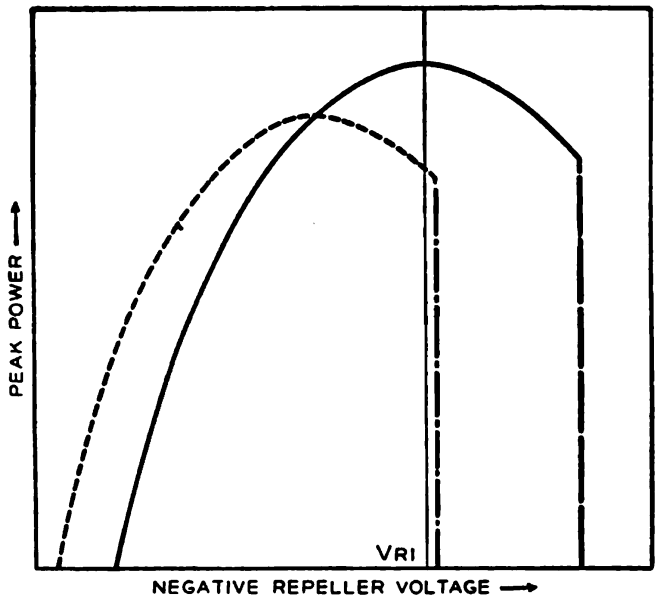

Fig. 108.—The variation of power output with repeller voltage for a pulsed reflex oscillator exhibiting hysteresis.

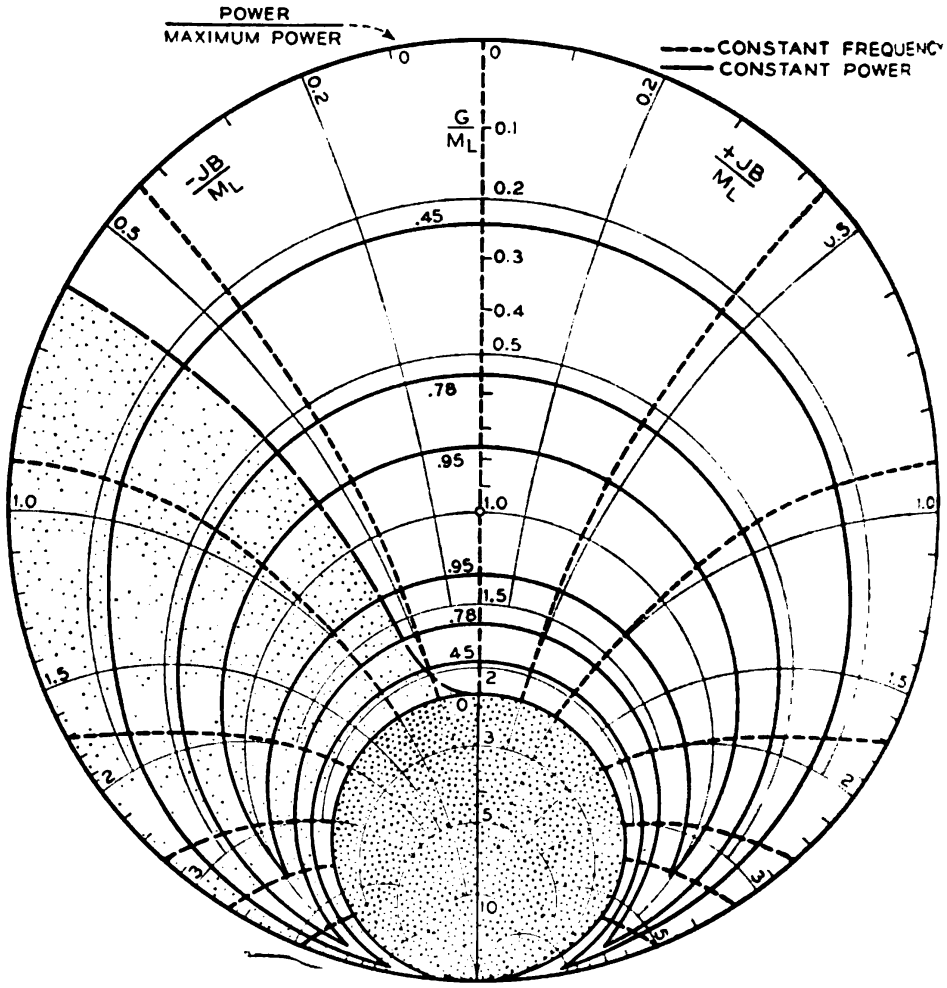

Fig. 109.—The effect of hysteresis on the Rieke diagram of a pulsed reflex oscillator. The hysteresis shown in Fig. 108 can result in failure of a pulsed oscillator to operate in the lightly shaded portion of the Rieke diagram as well as the heavily shaded portion corresponding to the normal sink.

Digitized by Google
Original from UNIVERSITY OF MICHIGAN
Generated on 2019-09-23 05:03 GMT / http://hdl.handle.net/2027/mdp.39015077775156
Public Domain, Google-digitized / http://www.hathitrust.org/access_use#pd-google

diagram. The effect of varying the impedance on the repeller characteristic in Fig. 108 is to shift the whole characteristic to the right or left, depending upon the phase of the impedance, as well as to change its general form as shown by the dotted curve. It can be seen from this that if the hysteresis is sufficiently bad and if the pulling figure exceeds a particular value, one

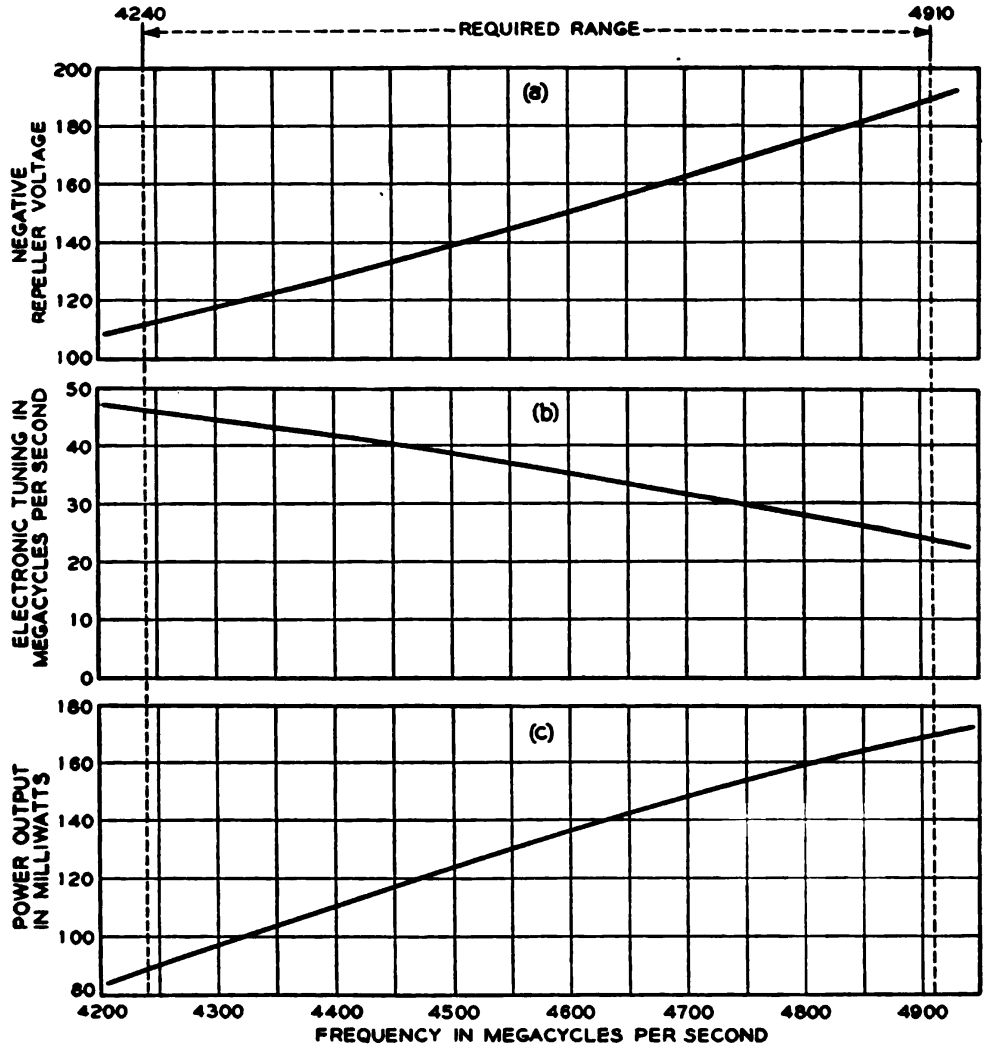

Fig. 110.—Performance characteristics of the 2K22 operated into a 50 ohm load.

effect of the hysteresis will be to reduce the sink margin, and this is found to be the case. Fig. 109 shows an impedance performance diagram obtained with pulsed operation for an early model of the 2K55 in which the hysteresis was excessive. From this it can be seen that the area of the sink on the diagram is very greatly increased and also that the sink margin is reduced from the theoretical value of somewhat in excess of 2 to a value of less than

Digitized by Google
Original from UNIVERSITY OF MICHIGAN
Generated on 2019-09-23 05:03 GMT / http://hdl.handle.net/2027/mdp.39015077775156
Public Domain, Google-digitized / http://www.hathitrust.org/access_use#pd-google

1.1 although maximum power occurs at unity VSWR. A modification in the design reduced the hysteresis and eliminated this effect as shown by Figs. 103 to 106.

In addition to the transmitter tube for the AN/TRC-6 system, it was necessary to design a beating oscillator. This tube is known as the Western Electric 2K22. Its design was scaled from the 2K29, previously described. The tube was designed to operate into a 50 ohm impedance and can be coupled by a coaxial adapter to a 50 ohm line or by means of the transducer of Fig. 101 to a wave guide. When the back piston of the transducer is set at a distance of 1.080″ from the probe center, the impedance presented to the oscillator is 50 ohms with approximately a 1 *db* variation over the frequency range. Fig. 110 gives the performance characteristics of the 2K22 operating into a 50 ohm load. The AN/TRC-6 system using these tubes provided a military communication system during the war. A description of this service has been given.[12] Also, models of the AN/TRC-6 system have been put into service to provide telephone communication between Cape Cod and Nantucket and also between San Francisco and Catalina Island.

J. *Scope of Oscillator Development at the Bell Telephone Laboratories*

The reflex oscillators discussed in the foregoing sections were developed primarily for beating oscillator service, and in one instance for a transmitter. Reflex oscillators also received wide application in test equipment. The best-known application of this type was in the spectrum analyzer, in which the electronic tuning characteristic of the oscillators made possible the display of output spectra, and especially of the spectra of magnetron oscillators, on an oscilloscope. This greatly facilitated the development of the magnetron. The reflex oscillator also was widely used as a signal generator, and the ease of frequency adjustment particularly suited it to this application. In some signal generators it was desired to pulse the reflex oscillator at low power levels. As an alternative to the method previously described, in which the voltage between the cathode and resonator was pulsed, it is possible to leave this voltage fixed and to pulse the voltage between the repeller and cathode. In this case the repeller-cathode voltage is set at a base value at which the tube will not oscillate and the pulse varies this voltage to the oscillating value.

The oscillators which have been described have been chosen to indicate various features of their development. In addition to these, a number of other oscillators were developed to meet various service needs. Figure 111 shows a chart giving the frequency ranges of these tubes. Of the eleven beating oscillators of the reflex oscillator type on the Army-Navy preferred

Digitized by Google
Original from UNIVERSITY OF MICHIGAN
Generated on 2019-09-23 05:03 GMT / http://hdl.handle.net/2027/mdp.39015077775156
Public Domain, Google-digitized / http://www.hathitrust.org/access_use#pd-google

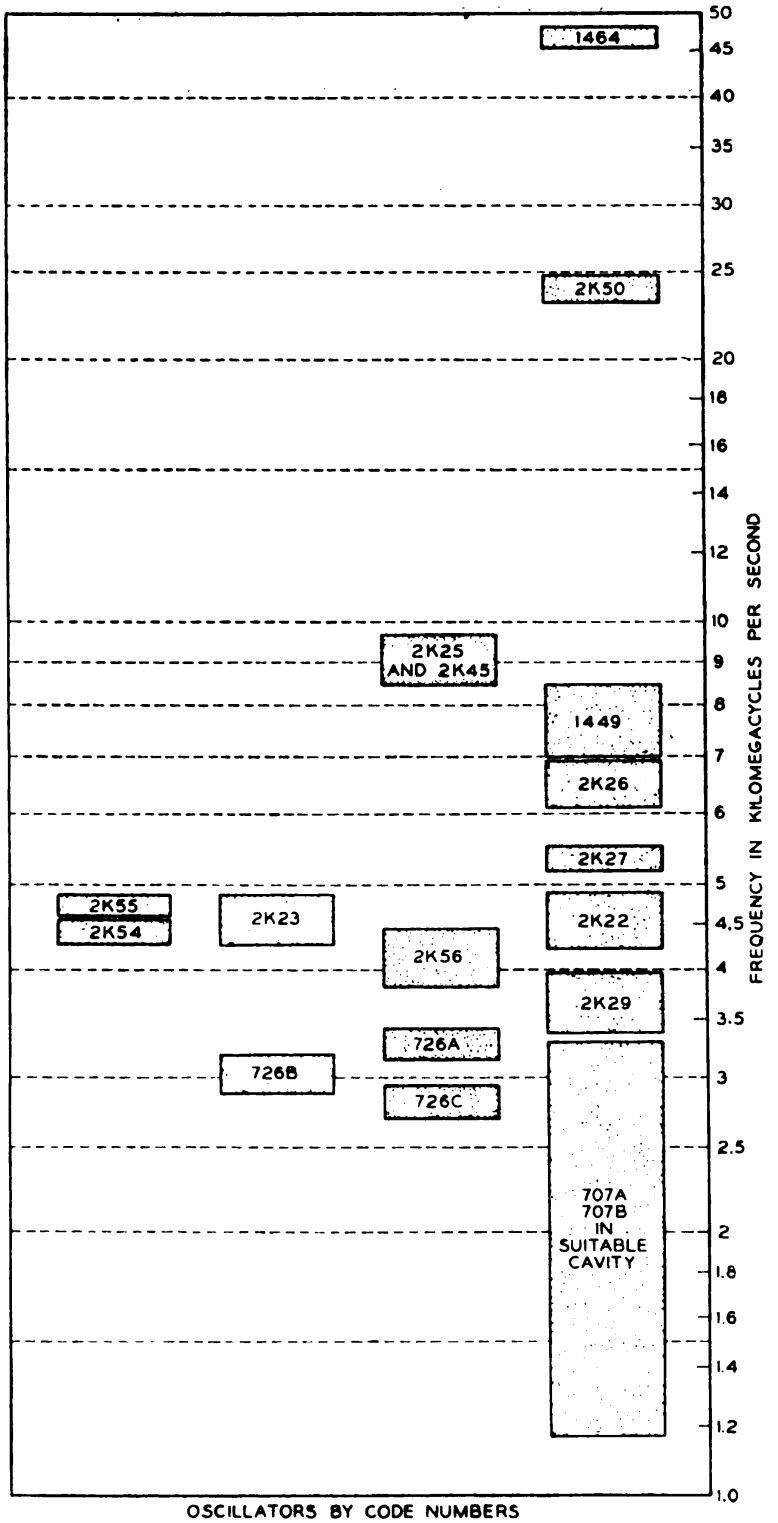

Fig. 111.—Reflex oscillators developed at the Bell Telephone Laboratories. The boxes around the tube numbers show the frequency range covered.

Generated on 2019-09-23 05:04 GMT / http://hdl.handle.net/2027/mdp.39015077775156
Public Domain, Google-digitized / http://www.hathitrust.org/access_use#pd-google
Digitized by Google
Original from UNIVERSITY OF MICHIGAN

list of electron tubes for 1945, nine were developed at the Bell Telephone Laboratories.

APPENDIX I

Resonators

In thinking about resonators it is important in order to avoid confusion to keep a few fundamental ideas in mind. One of the most important is that we must not use the notion of scalar potential in connection with fluctuating magnetic fields. Electric fields produced by fluctuating magnetic fields cannot be derived from a scalar potential, and in the presence of such fields to speak about the potential at a point is hopelessly confusing.[16]

The idea of voltage as the line integral of electric field along a given path between two points is useful, but it must be remembered that the voltage depends on the path chosen. Consider, for instance, an ordinary 60-cycle transformer with the secondary wound of copper tubing. For a path from one secondary terminal to the other through the center of the tubing the voltage (integral of field times distance) is zero. For a path between terminals outside of core and coil, the voltage between terminals is $d\psi/dt$, where ψ is the magnetic flux linkage of the path and the coil, counting each line of force as many times as the path encircles it.

If resistance drop is neglected the work done in moving a charge through a conductor is zero. The line integral of an electric field around a closed path is $d\psi/dt$. If part of the path is through a conductor, or through a space where there is no electric field, the voltage along the rest of the path (as between portions of the conductor) is $d\psi/dt$. For paths linking different amounts of flux, the voltage will be different. In the case of low frequency transformers, all paths linking the terminals and lying outside of the core and coil link practically the same amount of flux, and there is little ambiguity about the voltage. In reflex oscillators the electrons travel from one field free region to another along a certain path and this determines the path along which the voltage should be evaluated.

To review: the voltage between two points is the integral of the field along the path times distance, and refers to a certain path. If the path begins and ends in a field free region, the voltage is $d\psi/dt$, where ψ is the magnetic flux linking the chosen path and a return path through the field free region.

To this should be added that high frequency currents and fields penetrate the surface of metals only a fraction of a thousandth of an inch in the centimeter range,[17] so that the interior of a conductor is field free, and fields inside of a metal enclosed space cannot produce fields outside of that space.

[16] The electric field can, of course, be derived from a scalar and a vector potential.
[17] As an example, for copper the field is reduced to (1/2.72) of its value at the surface

Digitized by Google
Original from UNIVERSITY OF MICHIGAN
Generated on 2019-09-23 05:04 GMT / http://hdl.handle.net/2027/mdp.39015077775156
Public Domain, Google-digitized / http://www.hathitrust.org/access_use#pd-google

In considering resonators we should further note that the magnetic flux must be produced by a flow of current, either convection current or displacement current, around the lines of force. In a transformer this can be identified as the current flowing in the coils. In the resonators used in reflex oscillators it is the current flowing in the walls and, as displacement current, across the gap and from one face of the resonator to the other.

Two axially symmetrical resonators suitable for use in reflex oscillators are shown schematically in Figs. 112 and 113. The resonator in Fig. 112 has grids and might be used with a broad unfocused electron beam at a low d-c voltage; that shown in 113 has open apertures and might be used with a

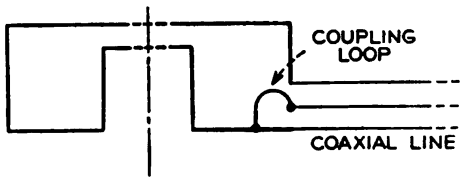

Fig. 112.—An oscillator cavity with grids and loop coupling to a coaxial line.

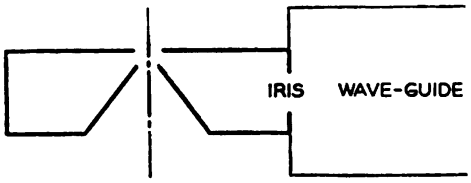

Fig. 113.—An oscillator cavity without grids and with iris coupling to a wave guide.

focused high voltage electron beam. In Fig. 112, the resonator is coupled to a coaxial line by means of a coupling loop or coil; in Fig. 113 the resonator is coupled to a wave guide by means of a small aperture or "iris."

Let us consider the resonator of Fig. 112 in the light of what we have just said. A magnetic field flows around the axis inside of the resonator. There is an electric field between the top and bottom inside surfaces of the resona-

---

at a depth.

$$\delta = 3.82 \times 10^{-6}\sqrt{\lambda} \qquad \text{(a1)}$$

Here λ is wavelength in centimeters. It may also be convenient to note that the surface resistivity of a centimeter square of resonator surface is, for copper,

$$R = .045/\sqrt{\lambda} \qquad \text{(a2)}$$

This means that if a current of I amperes flows on a surface over a width W and a length l, the power dissipation is

$$P = I^2Rl/W \qquad \text{(a3)}$$

For other non-magnetic metals, both δ and R are proportional to the square root of the resistivity with respect to that of copper.

Digitized by Google
Original from UNIVERSITY OF MICHIGAN
Generated on 2019-09-23 05:05 GMT / http://hdl.handle.net/2027/mdp.39015077775156
Public Domain, Google-digitized / http://www.hathitrust.org/access_use#pd-google

tor. There is no electric field outside of the resonator (except a very little that leaks out near the grids). To take a charge from one grid to another *outside* of the resonator requires no work. Thus the voltage across the gap is $d\psi/dt$, where ψ is the magnetic flux around the axis. Actually, there is a little magnetic flux between the grids, and hence the voltage near the edges of the grids is a little less than that at the center.

Current flows as a displacement current between the grids, and as convection current radially out around, and back along the inside of the resonator to the other grid. This current flow produces the magnetic field that links the axis.

Part of the magnetic flux links the coupling loop. If this part is ψ_ℓ and if the coupling loop is open-circuited, the voltage across the coupling loop will be $d\psi_\ell/dt$.

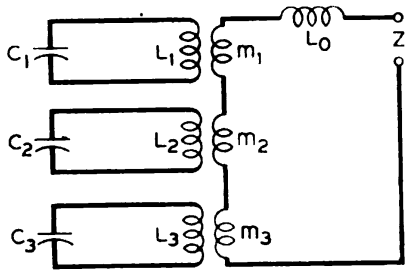

Fig. 114.—Equivalent circuit for a resonator having 3 modes of resonance.

In the resonator of Fig. 113, power leaks out through the iris into the wave guide. Part of the wall current in the resonator flows out through the hole into the guide; part of the magnetic flux in the resonator leaks out into the guide.

In dealing with resonators as resonant circuits of reflex oscillators, to which the electron stream and the load are coupled, we are interested in the gap and output impedances. For a clear and exact treatment, the reader is referred to a paper by Schelkunoff.[18] No exhaustive treatment of the problem will be given here, but a few important general results will be given.

If the resonator is lossless, the impedance looking into the loop may be represented exactly by an equivalent circuit indicated in Fig. 114. As coils used at low frequencies are really not simply ideal "inductances." (an idealized concept), but have many resonances (ascribed to distributed capacitance), so the resonator has many, in fact, an infinity of resonances. In the equivalent circuit shown in Fig. 114, only 3 of these are represented,

[18] S. A. Schelkunoff, Representation of Impedance Functions in Terms of Resonant Frequencies, *Proc. I.R.E.*, 32, 2, pp. 83–90, Feb., 1944.

Digitized by Google
Original from UNIVERSITY OF MICHIGAN
Generated on 2019-09-23 05:05 GMT / http://hdl.handle.net/2027/mdp.39015077775156
Public Domain, Google-digitized / http://www.hathitrust.org/access_use#pd-google

by the inductances L_1, L_2, L_3 and the capacitances C_1, C_2, C_3. These resonant circuits are coupled to the terminals by mutual inductances m_1, m_2, m_3. In series with these appears the inductance measured at very low frequencies L_0, the self inductance of the coupling loop. The circuit in Fig. 114 may be regarded as a symbolic representation to be used in evaluating Z, just as a mathematical expression may be a symbolic representation of the value of an impedance.

In practical cases, the resonances are usually considerably separated in frequency, and near a desired resonance the effect of others may be neglected. In addition, if the Q is high we may add a conductance G_R across the capacitance to represent resonator losses (Fig. 115). It would be equally legitimate to add a resistance in series with L. In Fig. 115 a load impedance Z_L has been added. Fig. 115 is a very accurate representation of a slightly ossy resonator, a low loss coupling loop, and a load impedance. The

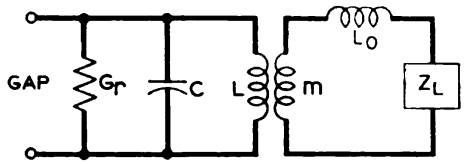

Fig. 115.—Equivalent circuit showing connection between the oscillator gap regarded as one pair of terminals and the oscillator load for an oscillator resonator having only one resonant frequency near the frequency of operation.

meaning of L and C will be made clearer a little later. We will now clarify the meaning of m. Suppose no current flows in the coupling loop ($Z = \infty$). Let the peak gap voltage be V. The peak voltage across m will be

$$V_m = mV/L \tag{a4}$$

In a resonator, if a peak voltage V across the gap produces a peak flux ψ_m linking the coupling loop when no current flows in the coupling loop, then

$$V_m = d\psi_m/dt = mV/L \tag{a5}$$

This defines m in terms of magnetic field, and L.

Figure 115 is also a quite accurate representation of Fig. 113. In this case the "terminals" are taken as located at the end of the wave guide. L_0 is the inductance of the iris, which will vary with frequency.

When we are interested in the impedance at the gap as a function of frequency, we may equally well use the equivalent circuit of Fig. 116. Here G_L represents conductance due to load; G_R represents conductance due to resonator loss. The total conductance, called G_G, is

$$G_G = G_R + G_L \tag{a6}$$

Digitized by Google
Original from UNIVERSITY OF MICHIGAN
Generated on 2019-09-23 05:06 GMT / http://hdl.handle.net/2027/mdp.39015077775156
Public Domain, Google-digitized / http://www.hathitrust.org/access_use#pd-google

The circuit of Fig. 116 does not tell us how G_L varies with variation in load impedance Z_L. Further, L and C in this circuit are changed in changing Z_L, and include a contribution from the inductance of the coupling loop (which should not be very large).

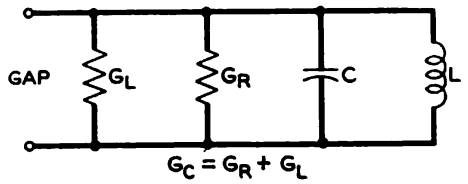

Fig. 116.—A simplified equivalent circuit of an oscillator resonator.

Several resonator parameters are vitally important in discussing reflex oscillators. These will be discussed referring to Fig. 116. G_L and G_R have already been defined. The resonant radian frequency ω_0 is of course

$$\omega_0 = (LC)^{-1/2} \tag{a7}$$

A very important quantity will be called the characteristic admittance M

$$M = (C/L)^{1/2} \tag{a8}$$

This quantity is important because at a frequency $\Delta\omega$ off resonance the admittance of the circuit is very nearly

$$Y = G + j2M\Delta\omega/\omega_0 \qquad \Delta\omega = \omega - \omega_0 \tag{a9}$$

The "loaded" Q of the circuit will be referred to merely as Q and is

$$Q = M/G_C \tag{a10}$$

The unloaded Q is

$$Q_0 = M/G_R \tag{a11}$$

A quantity which may be called the "external Q" is

$$Q_R = M/G_L \tag{a12}$$

We see

$$1/Q_0 + 1/Q_R = 1/Q \tag{a13}$$

The energy stored in the magnetic field at zero voltage across the resonator, and the energy stored in the electric field at the voltage maximum are both

$$W_s = (1/2)V^2C \tag{a14}$$

$$= (1/2)V^2M/\omega_0 \tag{a15}$$

Digitized by Google
Original from UNIVERSITY OF MICHIGAN
Generated on 2019-09-23 05:06 GMT / http://hdl.handle.net/2027/mdp.39015077775156
Public Domain, Google-digitized / http://www.hathitrust.org/access_use#pd-google

Here V is the peak gap voltage. Expressions (a14) and (a15) are valuable in making resonator calculations from exact or approximate field distributions. They define C, L and M in terms of electric and magnetic field. The energy dissipated per cycle is

$$W_L = \pi V^2 C/\omega_0 \tag{a16}$$

Hence, we might have written Q as

$$Q = 2\pi W_s/W_L \tag{a17}$$

This is one popular definition of Q.

In (a8)–(a17) we usually assume that there is no appreciable energy stored in the load or the field of the coupling loop, so that M is considered as unaffected by load. The effect of "high Q" loads with considerable energy storage is considered in a somewhat different manner in Sec. IXB.

It must be emphasized that the expressions given above are valid for high Q circuits only (a Q of 50 is high in this sense). Expression (a17) is often used as a general definition of Q, but it is not complete without an additional definition of the meaning of resonance in a low Q circuit with many modes. Schelkunoff uses another definition of Q. Unforced oscillations in a damped circuit can be represented as a combination of several terms

$$V_1 e^{p_1 t} + V_2 e^{p_2 t} + \cdots \tag{a18}$$

$$p_1 = \alpha_1 + j\omega_1 \tag{a19}$$

Schelkunoff takes the Q of the nth mode as

$$Q_n = \omega_n/\alpha_n \tag{a20}$$

This is at least a consistent and complete definition. The reader can easily see that it accords with the definitions given for high Q's in connection with the circuit of Fig. 116.

Sometimes there may be a complicated circuit between the gap and a coaxial line or wave guide. In this case, the circuits intervening between the gap and the line can be regarded as a 4 terminal transducer (Fig. 117). The constants of this transducer will vary with frequency. No further consideration of this generalized treatment will be given, as it is well covered in books on network theory. A particular representation of the transducer will be pointed out, however. If the impedance in the line is referred to a special point, one parameter can be eliminated, giving the equivalent circuit shown in Fig. 118. If the gap is short-circuited, the impedance is zero and the impedance at the special point to be chosen on the line is R; the special point may be chosen as the potential minimum with the gap shorted.

Digitized by Google
Original from UNIVERSITY OF MICHIGAN
Generated on 2019-09-23 05:06 GMT / http://hdl.handle.net/2027/mdp.39015077775156
Public Domain, Google-digitized / http://www.hathitrust.org/access_use#pd-google

N, the voltage ratio of a perfect transformer, is usually complex. The impedance ratio NN^* is real. If we are not interested in the relation of output phase to gap phase, we may disregard the phase angle of N, and deal only with the impedance ratio, the absolute value of N squared, which we will call N^2. Thus, using this equivalent circuit and disregarding the phase of N we can for our purposes reduce the number of independent parameters from the usual 6 for a passive 4 terminal network to 4. $Y(= G + jB)$, N^2 and R. This reduction can greatly simplify the algebra and arithmetic of microwave problems. The circuit of Fig. 118 has an additional advantage; if we choose our impedance reference point on the output line or guide to be the suitable point nearest to the actual output

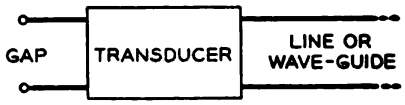

Fig. 117.—A 4-terminal transducer is the most general connection between the oscillator gap and a line or wave guide.

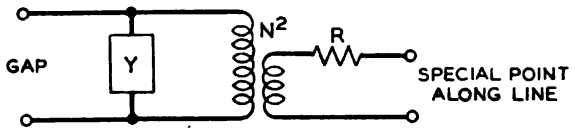

Fig. 118.—One circuit which will represent all the properties of a general 4-terminal transducer. This circuit consists of an admittance Y shunting the gap, a perfect transformer of complex ratio N and a series resistance R.

loop or iris, the circuit represents fairly accurately the frequency dependence of the output impedance if we merely take Y as

$$Y = G_R + j\omega(C - 1/\omega L) \tag{a21}$$

Near resonance we may use the simpler form.

$$Y = G_R + j2M\Delta\omega/\omega_0 \tag{a22}$$

Something has already been said in a general way about the evaluation of L and C in terms of the electric and magnetic field distribution in a resonator. It is completely outside of the scope of this paper to consider this subject at any length; the reader is referred to various books.[19, 20, 21] The discontinuity calculations of Whinnery and Jamieson[22] are also of great value in

[19] Electromagnetic Waves, S. A. Schelkunoff, Van Nostrand, 1943.
[20] Fields & Waves in Modern Radio, Ramo & Whinnery, Wiley, 1944.
[21] Microwave Transmission Data, Sperry Gyroscope Company, 1944.
[22] J. R. Whinnery and H. W. Jamieson, Equivalent Circuits for Discontinuities in Transmission Lines, *Proc. I.R.E.*, 32, 2, pp. 99–114.

Generated on 2019-09-23 05:06 GMT / http://hdl.handle.net/2027/mdp.39015077775156
Public Domain, Google-digitized / http://www.hathitrust.org/access_use#pd-google
Digitized by Google
Original from UNIVERSITY OF MICHIGAN

making resonator calculations. These can be profitably combined with disk transmission line formulae.[19, 20]

The writers would like to point out that in the present state of the art the testing of resonator calculations by models is important. Models need not be made of the size finally desired. If all dimensions are made N times as large, the wavelength will be N times as great. The characteristic admittance M will be unchanged. If the material is the same, and the surface is smooth and homogeneous, Q and $1/G_R$, the shunt resonant resistance, will be $\sqrt{N}$ times as great.

It is perhaps a needless caution to say that the accuracy of a method of resonator calculation cannot be judged by its mathematical complexity or the difficulty of using it. Methods of calculation which are simple and may seem to make unduly broad approximations are sometimes better founded than appears on the surface, and complicated methods, exact if carried far enough, may be so unsuited to the problem as to give very bad answers if used in obtaining approximate values.

APPENDIX II

Modulation Coefficient

In this appendix the effects of space charge are neglected.

The modulation coefficient β is defined as the peak energy in electron volts an electron can gain in passing through the field of a gap divided by the peak r-f voltage across the gap. If an electron were transported across the gap very quickly when the r-f voltage was at a maximum the energy in electron volts gained by the electron would be equal to the peak r-f voltage. Thus, the modulation coefficient can also be defined as the ratio of the peak energy actually gained to the energy which would be gained in a very quick transit at the time of maximum voltage.

In this appendix modulation coefficient will be considered only for r-f voltages small compared with the d-c accelerating voltage.

If an electron gains an energy β times the *r-f* voltage V across the gap, the work done on it is βeV electron volts. By the conservation of energy, an induced current must flow between the electrodes of the gap, transferring a charge-βe against the voltage V and hence taking an amount of energy βeV from the circuit. Pursuing this argument we see that the modulation coefficient β times the electron convection current in the beam, q, gives the current induced in the gap by electron flow. In a circuit sense, there is fed into the gap, as from an infinite impedance source, an induced current βq.

We will assume that the gap involves a region in which the field along the electron path rises from zero and falls to zero again. This region is assumed

Digitized by Google
Original from UNIVERSITY OF MICHIGAN
Generated on 2019-09-23 05:06 GMT / http://hdl.handle.net/2027/mdp.39015077775156
Public Domain, Google-digitized / http://www.hathitrust.org/access_use#pd-google

to be small compared with a wavelength and to have little a-c magnetic field in it, so that we can pretty accurately represent the field in this restricted region as the gradient of a potential. Along the path the potential is taken as the real part of

$$V(x)e^{j\omega t} \tag{b1}$$

For small gap voltages, to first order, the time that an electron reaches a given position may be taken as unaffected by the signal, so that

$$t = x/u_0 + t_0 \tag{b2}$$

Then the gradient along the path is

$$\frac{\partial V}{\partial x} = \text{Real } V'(x)e^{j(\omega x/u_0+\omega t_0)}. \tag{b3}$$

The change in momentum in passing through the field may be obtained by integrating the force on an electron times the time through the field. Let points a and b be in the field-free region to the left and right of the gap. Then we have

$$\Delta(\dot{x}) = \text{Real } \frac{\eta}{u_0}\int_a^b V'(x)e^{j(\omega x/u_0+\omega t_0)}\,dx \tag{b4}$$

$$\Delta(\dot{x}) = \text{Real } \frac{\eta e^{j\omega t_0}}{u_0}\int_a^b V'(x)e^{j\gamma x}\,dx \tag{b5}$$

$$\gamma = \omega/u_0\,. \tag{b6}$$

The integral will be a complex quantity. The exponential factor involving the starting time t_0 will rotate this. $\Delta(\dot{x})$ will have a maximum value when the rotation causes the vector to lie along the real axis, and this maximum value is thus the absolute value of the integral. Hence

$$\Delta(\dot{x})_{\max} = \frac{\eta}{u_0}\left|\int_a^b V'(x)e^{j\gamma x}\,dx\right|. \tag{b7}$$

For a-c voltages small compared with the voltage specifying the speed u_0, the energy change is proportional to the momentum change. For an electron transported instantly from one side of the gap to the other, the momentum change can be obtained by setting $\gamma = 0$.

$$\begin{aligned}\Delta(\dot{x})_0 &= \frac{\eta}{u_0}\int_a^b V'(x)\,dx \\ &= \frac{\eta}{u_0}V.\end{aligned} \tag{b8}$$

Digitized by Google
Original from UNIVERSITY OF MICHIGAN
Generated on 2019-09-23 05:06 GMT / http://hdl.handle.net/2027/mdp.39015077775156
Public Domain, Google-digitized / http://www.hathitrust.org/access_use#pd-google

Here V is the voltage between a and b. Hence, the modulation coefficient β is given for small signals by

$$\beta = (1/V)\left|\int_a^b V'(x)e^{j\gamma x}\,dx\right| \tag{b9}$$

$$V = V(b) - V(a) \tag{b10}$$

$$\gamma = \omega/u_0 \tag{b11}$$

$$u_0 = \sqrt{2\eta V_0} \tag{b12}$$

Thus u_0 is the electron velocity.

It is sometimes convenient to integrate by parts, giving the mathematical expression for β a different form

$$\beta = (1/V)\left|\frac{V'(x)e^{j\gamma x}}{j\gamma}\Big|_a^b - \frac{1}{j\gamma}\int_a^b V''(x)e^{j\gamma x}\,dx\right|$$

as $V'(x)$ is zero at a and b

$$\beta = (1/V)\left|\frac{1}{\gamma}\int_a^b V''(x)e^{j\gamma x}\,dx\right|. \tag{b13}$$

An interesting and important case is that of a uniform field between grids. Let the first grid be at $x = 0$ and the second at $x = d$. There is an abrupt transition to a gradient V/d at $x = 0$, and another abrupt transition to zero gradient at $x = d$. Thus, the integral (b13) is reduced to these two contributions, and we obtain

$$\beta = (1/V)\left|\frac{V}{\gamma d}\left(1 - e^{j\gamma d}\right)\right|. \tag{b14}$$

This is easily seen to be

$$\beta = \sin(\gamma\, d/2)/(\gamma\, d/2) \tag{b14}$$

This function, the modulation coefficient for fine parallel grids, is plotted in Fig. 119.

Sometimes apertures, as, circular apertures, or long narrow slits are used without grids. There are important relations between the modulation coefficient for a path on the axis and one parallel to the axis for such systems.[22]

In a two-dimensional gap system with axial symmetry, if the modulation coefficient for a path along the axis is β_0, the modulation coefficient for a path y away from the axis is

$$\beta_y = \beta_0 \cosh \gamma y \tag{b15}$$

[22] These relations first came to the attention of the writers through unpublished work of D. P. R. Petrie, C. Strachey and P. J. Wallis of Standard Telephones and Cables.

Digitized by Google
Original from UNIVERSITY OF MICHIGAN
Generated on 2019-09-23 05:12 GMT / http://hdl.handle.net/2027/mdp.39015077775156
Public Domain, Google-digitized / http://www.hathitrust.org/access_use#pd-google

In an axially symmetrical electrode system, if the modulation coefficient on the axis is β_0, the modulation coefficient at a radius r is

$$\beta_r = \beta_0 I_0 (\gamma r) \tag{b16}$$

Here I_0 is a modified Bessel function.

It is easy to see why (b15) and (b16) must be so. The field in the gap can be resolved by means of a Fourier integral into components which vary

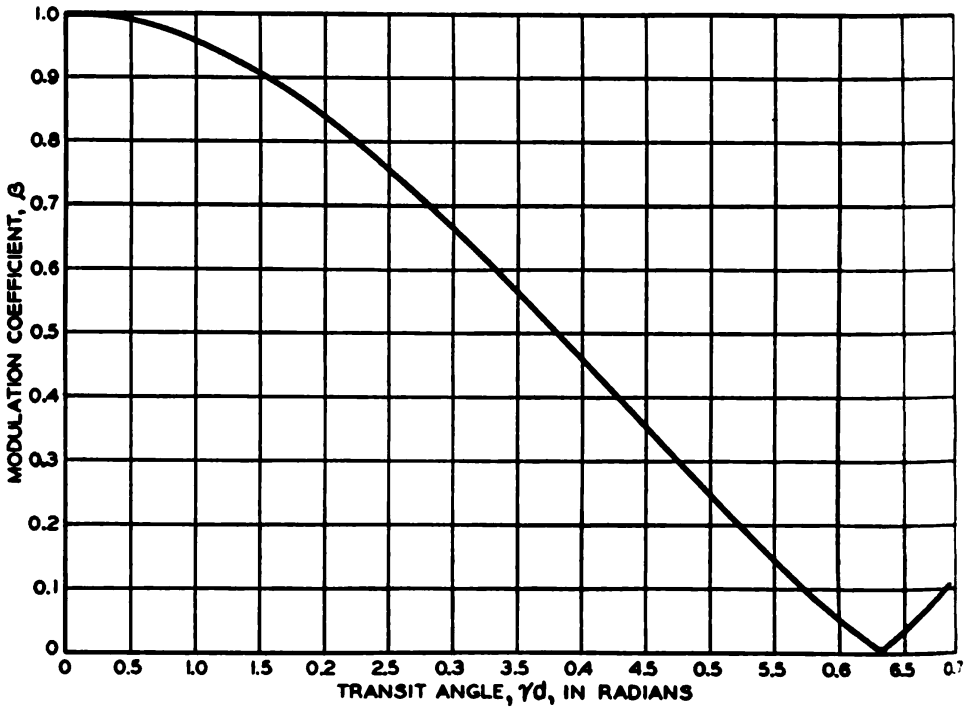

Fig. 119.—Modulation coefficient for fine parallel grids vs transit angle across the gap in radians.

$$\beta = |\sin(\gamma d/2)/(\gamma d/2)|, \qquad \gamma = \omega/u_0 = 3170/\lambda\sqrt{V_0}.$$

sinusoidally along the axis and as the hyperbolic cosine (in the two-dimensional case) of the same argument normal to the axis or as the modified Bessel function (in the axially symmetrical case) of the same argument radially. When the integration of (b9) is carried out, only that portion of the Fourier integral representation for which the argument is γx contributes to the result, and as that part contains as a factor cosh γy or $I_0(\gamma r)$ (b15) and (b16) are established.

The simple theory of velocity modulation presented in Appendix III makes no provision for variation of modulation coefficient across the beam. If we confine ourselves to very small signals, we find that the factor which appears is β^2. We may distinguish two cases: If the distance from the axis

Digitized by Google
Original from UNIVERSITY OF MICHIGAN
Generated on 2019-09-23 05:12 GMT / http://hdl.handle.net/2027/mdp.39015077775156
Public Domain, Google-digitized / http://www.hathitrust.org/access_use#pd-google

of symmetry were the same for both transits of the electron, we would do well to average β^2. If the electrons got thoroughly mixed up in position between their two transits, we would do well to average β and then square the average. We will present both average and r.m.s. values of β. The averaged value of β will be denoted as β_a, the r.m.s. value as β_s; the value on the axis will be called β_0.

From (b15) and (b16) we obtain by simple averaging for the two dimensional case,

$$\beta_a = \beta_0 \frac{\sinh \gamma y}{\gamma y} \tag{b17}$$

$$\beta_s = \beta_0 \left[\tfrac{1}{2} \left(\frac{\sinh 2\gamma y}{2\gamma y} + 1 \right) \right]^{\frac{1}{2}} \tag{b18}$$

and for an axially symmetrical case

$$\beta_a = \beta_0 2I_1(\gamma r)/(\gamma r) \tag{b19}$$

$$\beta_s = \beta_0 [I_0^2(\gamma r) - I_1^2(\gamma r)]^{1/2} \tag{b20}$$

It is convenient to rewrite these in a slightly different form, using (b15) and (b16).

$$\beta_a = \beta_y (\tanh \gamma y/\gamma y) \tag{b21}$$

$$\beta_s = \beta_y \left[\frac{\sinh 2\gamma y + 2\gamma y}{2\gamma y(\cosh 2\gamma y + 1)} \right]^{\frac{1}{2}} \tag{b22}$$

$$\beta_a = \beta_r 2I_1(\gamma r)/(\gamma r) I_0(\gamma r) \tag{b23}$$

$$\beta_s = \beta_r [1 - I_1^2(\gamma r)/I_0^2(\gamma r)]^{1/2} \tag{b24}$$

Now consider two similar cases: two pairs of parallel semi-infinite plates with a very narrow gap between them, and two semi-infinite tubes of the same diameter, on the same axis and with a very narrow gap between them (see Fig. 120). For electrons traveling very near the conducting surface, V' is zero save over a very short range at the gap, and the modulation coefficient is unity. Thus, by putting $\beta_y = \beta_r = 1$, we can use expressions (b15)–(b24) directly to evaluate β_a, β_s and β_0 for the configurations described. These quantities are shown in Figs. 121 and 122.

Suppose, now, that the gap between the plates or tubes is not very small. In this case, we need to know the variation of potential with distance across the space d long which separates the edges of the gap in order to get the modulation coefficient at the very edge of the gap, β_y or β_r.

If the tubing or plates surrounding the gap are thick, we might reasonably

Digitized by Google
Original from UNIVERSITY OF MICHIGAN
Generated on 2019-09-23 05:13 GMT / http://hdl.handle.net/2027/mdp.39015077775156
Public Domain, Google-digitized / http://www.hathitrust.org/access_use#pd-google

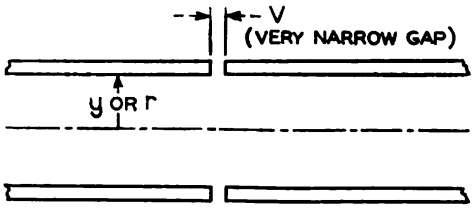

Fig. 120.—A gap consisting of pairs of semi-infinite planes or semi-infinite tubes.

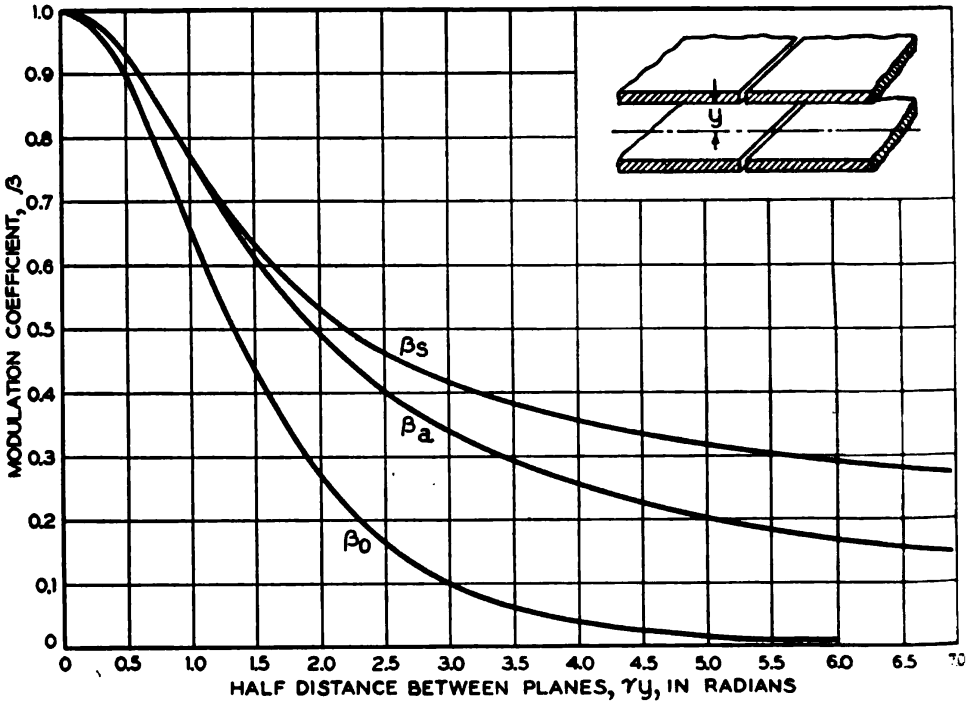

Fig. 121.—Modulation coefficient for two semi-infinite pairs of parallel planes with the edges very very close together, plotted vs the half distance between planes in radians. β_0 is the modulation coefficient for electrons travelling along the axis. β_a is the average modulation coefficient and β_s is the r.m.s. modulation coefficient. The separation of the planes is $2y$, $\beta_0 = 1/\cosh \gamma y$,

$$\beta_a = \tanh \gamma y/\gamma y, \qquad \beta_s = \left[\frac{\sinh 2\gamma y + 2\gamma y}{2\gamma y(\cosh 2\gamma y + 1)}\right]^{\frac{1}{2}}$$

assume a linear variation of potential with distance in the space between them. In this case, (b9) gives

$$\beta_y \text{ or } \beta_r = F_1(\gamma d) = \sin(\gamma d/2)/(\gamma d/2) \qquad \text{(b25)}$$

This is the same function shown in Fig. 119.

If the tube wall or plates are very thin, one may, following Petrie, Strachey and Wallis[22] assume a potential variation between the edges of the gap of

Digitized by Google
Original from UNIVERSITY OF MICHIGAN
Generated on 2019-09-23 05:13 GMT / http://hdl.handle.net/2027/mdp.39015077775156
Public Domain, Google-digitized / http://www.hathitrust.org/access_use#pd-google

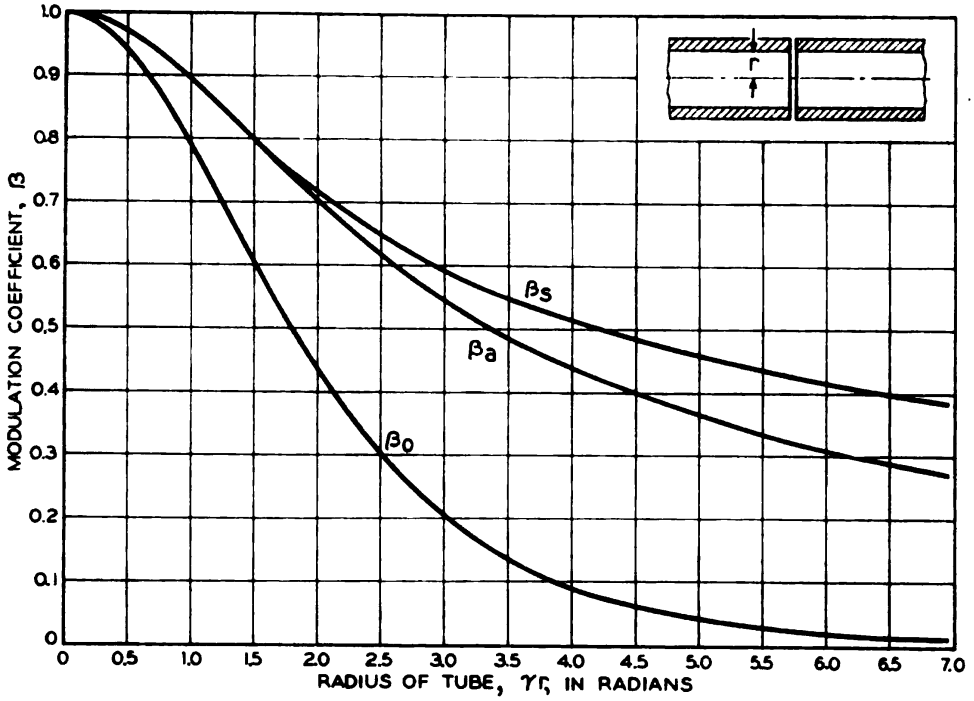

Fig. 122.—Modulation coefficient for two semi-infinite tubes separated by a very small distance, plotted vs the radius of the tube in radians. β_0 is the modulation coefficient on the axis, β_a is the average modulation coefficient and β_s is the root mean square modulation coefficient. r is the radius of the cylinders.

$$\beta_0 = 1/I_0(\gamma r), \qquad \beta_a = 2I_1(\gamma r)/\gamma r I_0(\gamma r),$$
$$\beta_s = [1 - I_1^2(\gamma r)/I_0^2(\gamma r)]^{\frac{1}{2}}$$

the form

$$V = \frac{1}{\pi} \sin^{-1} \frac{2x}{d} \tag{b26}$$

In this case, (b9) gives

$$\beta_y \text{ or } \beta_r = F_2(\gamma d) = J_0(\gamma d/2) \tag{b27}$$

Both $F_1(\gamma d)$ and $F_2(\gamma d)$ are plotted vs. γd in Fig. 123.

Figures 121, 122 and 123 cover fairly completely the case of slits and holes. The same methods may be used to advantage in making an approximate calculation taking into account the effect of grid pitch and wire size on modulation coefficient.

Assume we have a pair of lined up grids, as shown in Fig. 124. Approximately, the potential near the left one is given as

$$V = V_1' x/2 + (aV_1'/4\pi) \ln\left[2\left(\cosh\frac{2\pi x}{a} - \cos\frac{2\pi y}{a}\right)\right]. \tag{b28}$$

Digitized by Google
Original from UNIVERSITY OF MICHIGAN
Generated on 2019-09-23 05:13 GMT / http://hdl.handle.net/2027/mdp.39015077775156
Public Domain, Google-digitized / http://www.hathitrust.org/access_use#pd-google

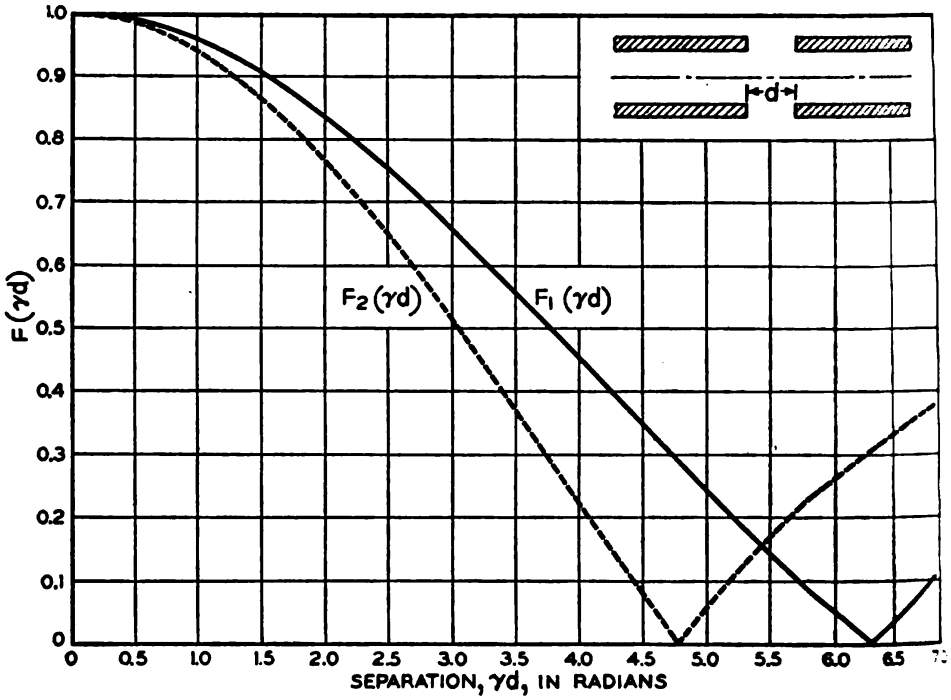

Fig. 123.—If the planes or tubes considered in Figs. 121 and 122 are separated by appreciable distance, the modulation coefficients given in those figures must be multiplied by a factor $F(\gamma d)$. In this figure, the multiplying factor is evaluated and plotted vs the separation in radians for two assumptions—that the gap has very blunt edges ($F_1(\gamma d)$) and that the gap has very sharp edges ($F_2(\gamma d)$).

This is zero far to the left and $V_1'x$ far to the right. This expression is useful only when the wire radius r is quite small compared with the separation a. Midway between wires,

$$V = V_1'x/2 + (a\,V_1'/2\pi)\ln\left[2\cosh\frac{\pi x}{a}\right] \tag{b29}$$

$$V'' = (V_1'\pi/2a)\,\mathrm{sech}^2\frac{\pi x}{a} \tag{b30}$$

If we use (b30) for each grid, the values of V'' for the two grids will overlap somewhat. However, let us neglect this overlap, apply (b30) at each grid and using (b13), integrate for each grid from $-\infty$ to $+\infty$, giving

$$\beta_0 = (1/V)(V_1'\pi/\gamma a)\,|\,1 - e^{j\gamma d}\,|\left|\int_{-\infty}^{\infty}\mathrm{sech}^2\frac{\pi x}{a}\,e^{j\gamma x}\,dx\right| \tag{b31}$$

$$= f\{\sin(\gamma d/2)/(\gamma d/2)\}G_0(\gamma a)$$

where

$$f = V_1'/(V/d) \tag{b32}$$

$$G_0(\gamma a) = \tfrac{1}{2}\left|\int_{-\infty}^{\infty}e^{(j\gamma a/\pi)u}\,\mathrm{sech}^2 u\,du\right| = (\gamma a/2)/\sinh(\gamma a/2) \tag{b33}$$

Digitized by Google
Original from UNIVERSITY OF MICHIGAN
Generated on 2019-09-23 05:13 GMT / http://hdl.handle.net/2027/mdp.39015077775156
Public Domain, Google-digitized / http://www.hathitrust.org/access_use#pd-google

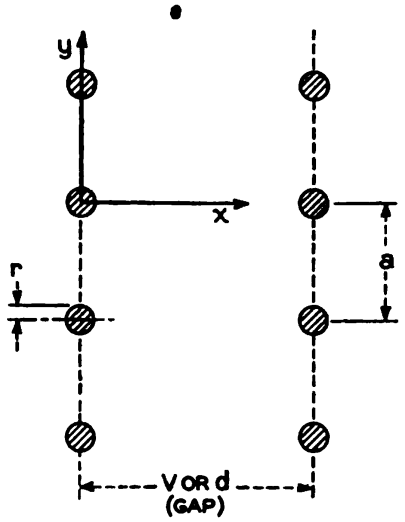

Fig. 124.—A gap consisting of lined up grids.

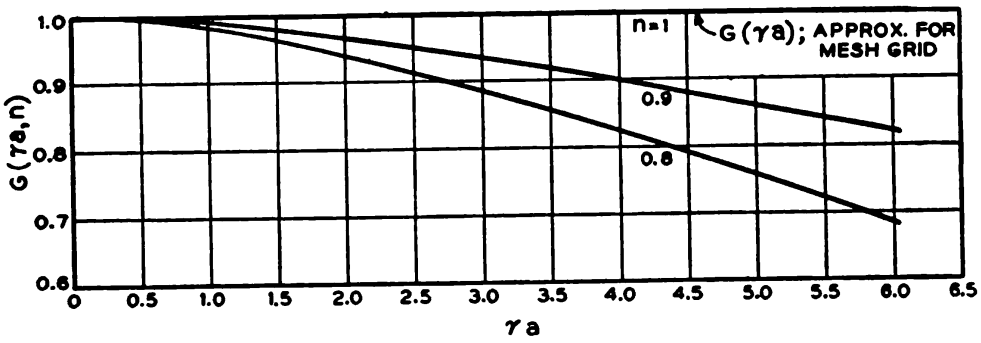

Fig. 125.—A factor used in obtaining the modulation coefficient of lined up grids vs the wire spacing in radians. n is the fraction open. The curve for $n = 1$ also applies approximately for a mesh grid.

Suppose we average over the open space of the grid. If the grid is a fraction n open, from (b17) we see that the average over the open space will be obtained by substituting for G_0 a quantity $G(\gamma a, n)$ given by

$$G(\gamma a,n) = \{\sinh (n\gamma a/2)/(n\gamma a/2)\}G_0(\gamma a) \tag{b34}$$

In Fig. 125, $G(\gamma a,n)$ is plotted vs. γa for $n = 1, .9, .8$. This about covers the useful range of values. It should be positively noted that the average is over the *open* area of the grid and applies to current getting through.

It remains to evaluate the factor f. Suppose $x = 0$. At the surface of the grid wire, $y = r$, the radius of the wire,

$$\delta V = (V_1' a/4\pi) \ln\left[2\left(1 - \cos\frac{2\pi r}{a}\right)\right] = (V_1' a/2\pi) \ln\left[2 \sin\frac{\pi r}{a}\right]$$

Digitized by Google
Original from UNIVERSITY OF MICHIGAN
Generated on 2019-09-23 05:13 GMT / http://hdl.handle.net/2027/mdp.39015077775156
Public Domain, Google-digitized / http://www.hathitrust.org/access_use#pd-google

As we have already assumed r is small, we may as well write

$$\delta V = (V_1' a/2\pi)2.3 \log_{10}\left(\frac{a}{2\pi r}\right) \tag{b35}$$

This emphasizes the sign of δV.

According to (b28), the grid plane appears from a distance to be at zero potential. Thus,

$$V_1' d - 2\delta V = V \tag{b36}$$

and from (b32)

$$f = \{1 + (a/\pi d)\ 2.3 \log_{10}(a/2\pi r)\}^{-1} \tag{b37}$$

If we go back over our results, we have for lined-up singly-wound grids, from (b31), (b34) and (b37), the average modulation coefficient

$$\beta_a = f\{\sin(\gamma a/2)/(\gamma a/2)\}G(\gamma a, n) \tag{b38}$$

The quantity $\sin(\gamma a/2)$ can be obtained from Fig. 119, $G(\gamma a,n)$ is plotted in Fig. 125, and f can be calculated from (b37) above.

It must be emphasized again that these expressions are good only for very fine wires ($r \ll a$), and get worse the closer the spacing compared with the wire separation. It is also important to note that $G(\gamma a,n)$ indicates little reduction of β_a even for quite wide wire separation. Now γd will be less than 2π, as $\beta_a = 0$ at $\gamma d = 2\pi$. As a approaches d in magnitude, the assumptions underlying the analysis, in which the integration around each grid was carried from $-\infty$ to ∞, become invalid and the analysis is not to be trusted.

It is very important to bear one point in mind. If we design a resonator assuming parallel conducting planes a distance L apart at the gap, and then desire to replace these planes with grids without altering the resonant frequency, we should space the grids not L apart but

$$d = fL \tag{b39}$$

apart to get the same capacitance and hence the same resonant frequency.

Mesh grids are sometimes used. To get a rough idea of what is expected, we may assume the potential about a grid to be

$$V = V_1' x/2 + (aV_1'/8\pi) \ln\left[2\left(\cosh\frac{2\pi x}{a} - \cos\frac{2\pi y}{a}\right)\right] + (aV_1'/8\pi) \ln\left[2\left(\cosh\frac{2\pi y}{a} - \cos\frac{2\pi z}{a}\right)\right] \tag{b40}$$

Digitized by Google
Original from UNIVERSITY OF MICHIGAN
Generated on 2019-09-23 05:13 GMT / http://hdl.handle.net/2027/mdp.39015077775156
Public Domain, Google-digitized / http://www.hathitrust.org/access_use#pd-google

Here the grid is assumed to lie in the y, z, plane. This gives a mesh of wires about squares a on a side, the wires bulging at the intersections. We take r to be the wire radius midway between intersections.

We see that β_0 will be the same in this case as in the case of a parallel wire grid. Thus the added wires, which intercept electrons, haven't helped us as far as this part of the expression goes.

As a further approximation, an averaging will be carried out as if the apertures had axial symmetry. Averaging will be carried out to a radius giving a circle of area a^2. The steps will not be indicated.

Further a factor analogous to f will be worked out. Again, the steps will not be indicated. The results are

$$\beta_a = g\{\sin(\gamma d/2)/(\gamma d/2)\}G_1(\gamma a) \tag{b41}$$

$$G_1(\gamma a) = 2I_1(\gamma a/\sqrt{\pi})/(\gamma a/\sqrt{\pi})G_0(\gamma a) \tag{b42}$$

$$g = 1 + (.365\ a/d)\ (\log_{10}(a/\pi r) - .69) \tag{b43}$$

The quantity $G_1(\gamma,a)$ is plotted in Fig. 125 for comparison with the parallel wire case. It should be emphasized that these expressions assume $r \ll a$, and that $G_1(\gamma a)$ is really only an estimate based on a doubtful approximation. The indications are, however, that the only beneficial affect of going from a parallel wire grid to a mesh with the same wire spacing lies in a small decrease in δV (a small increase in the mu of the grid), while by doubling the number of wires in the parallel wire grid, a can be halved, both raising mu and increasing $G(\gamma a,n)$.

APPENDIX III

Approximate Treatment of Bunching

We assume[24] that the conditions are as shown in Fig. 126 where the electron energy on first entering the gap is specified by the potential V_0. Across the gap there exists a radio frequency voltage, V sin ωt. The ratio of the energy gained by the electron in crossing the gap to the energy which it would gain if the transit time across the gap were zero is called the modulation coefficient and is denoted by a factor, β. We assume that the modulation coefficient is the same for all electrons. We also neglect the effects of space charge throughout. After leaving the gap the electrons enter an electrostatic retarding field of strength $E_0 = \dfrac{V_R + V_0}{l}$

[24] This analysis follows the method given by Webster, J. App. Phys. 10, July 1939, pp. 501–508.

Digitized by Google
Original from UNIVERSITY OF MICHIGAN
Generated on 2019-09-23 05:14 GMT / http://hdl.handle.net/2027/mdp.39015077775156
Public Domain, Google-digitized / http://www.hathitrust.org/access_use#pd-google

such that the stream flow is reversed and caused to retraverse the gap. The round trip transit time, τ_a, in the retarding field when a signal exists across the gap is then given by

$$\tau_a = \frac{2\sqrt{2\eta(V_0 + \beta V \sin \omega t_1)}}{\eta E_0} \tag{c1}$$

where $\eta = \frac{e}{m} \times 10^7 = 1.77 \times 10^{15}$ in practical units and t_1 is the time of first entry of the gap. The time of return to the gap will be

$$t_2 = t_1 + \tau_a \tag{c2}$$

More accurately t_1 and t_2 are measured from the central plane of the gap in which case a second term should be added to (c1) corresponding to motion at

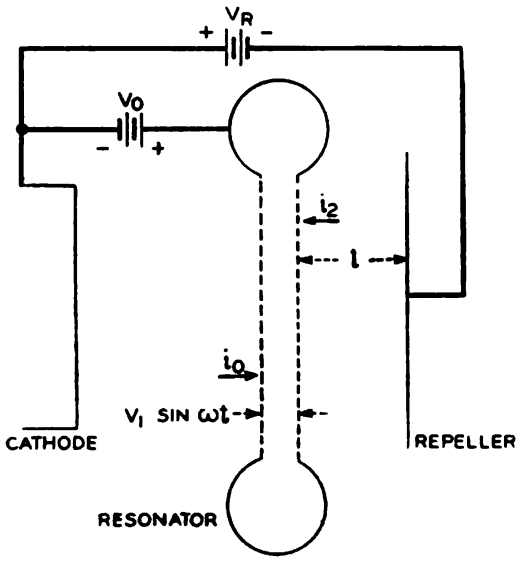

Fig. 126.—Diagram of a reflex oscillator showing quantities used in the treatment of bunching.

constant velocity. This term is, however, very small and will be neglected here. If i_2 is the current returning to the gap and I_0 the uniform current entering the gap on its first transit, then from conservation of charge one may write

$$I_0\, dt_1 = i_2\, dt_2 \tag{c3}$$

In what follows it will be first assumed that t_2 and t_1 are related by a single valued function. At the end of this appendix it will be shown that the analysis is also valid where the relating function is multiple valued.

We now make a Fourier series analysis of i_2 in order to determine the

Digitized by Google
Original from UNIVERSITY OF MICHIGAN
Generated on 2019-09-23 05:14 GMT / http://hdl.handle.net/2027/mdp.39015077775156
Public Domain, Google-digitized / http://www.hathitrust.org/access_use#pd-google

harmonic distribution. Thus

$$i_2 = a_0 + a_1 \cos(\omega t_2 + \varphi) + a_2 \cos 2(\omega t_2 + \varphi) + \cdots + b_1 \sin(\omega t_1 + \varphi) + b_2 \sin 2(\omega t_2 + \varphi) + \cdots \tag{c4}$$

where

$$a_n = \frac{1}{\pi}\int_{-\pi}^{\pi} i_2 \cos n(\omega t_2 + \varphi)\, d\omega t_2$$
$$b_n = \frac{1}{\pi}\int_{-\pi}^{\pi} i_2 \sin n(\omega t_2 + \varphi)\, d\omega t_2 \tag{c5}$$

Using (c1) to (c3) we change our variable to t_1 obtaining

$$a_n = \frac{1}{\pi}\int_{-\pi}^{\pi} I_0 \cos n\omega\left(t_1 + \frac{2\sqrt{2\eta(V_0 + \beta V \sin \omega t_1)}}{E_0} + \varphi\right) d\omega t_1 \tag{c6}$$

Let $\omega t_1 = \theta_1 \qquad \omega\tau_0 = \dfrac{2\omega\sqrt{2\eta V_0}}{E_0} = \theta \qquad X = \dfrac{\theta\beta V}{2V_0}$

$$a_n = \frac{1}{\pi}\int_{-\pi}^{\pi} I_0 \cos n\left(\theta_1 + \varphi + \theta\left[1 + \frac{X}{\theta}\sin\theta_1 - \tfrac{1}{2}\frac{X^2}{\theta^2}\sin^2\theta_1 + \cdots\right]\right) d\theta_1 \tag{c7}$$

(c7) cannot be evaluated in closed form without further restriction. The first order theory may be obtained by assuming that $\frac{1}{2}\dfrac{nX^2}{\theta} \ll \dfrac{\pi}{2}$. It is not sufficient to assume that $\dfrac{X^2}{\theta} \ll X$. The latter assumes that the third and higher terms of the expansion are small compared to the second. Let the integrand be denoted as $i_0 \cos nx$. The quantity to be evaluated is the argument of a trigonometric function where the total angle is of less importance than the difference $nx - 2m\pi$ where m is the largest integer for which the difference is positive. The condition first expressed requires that the contribution of the third and higher terms to the difference phase shall be small. The restriction requires that

$$n\left(\frac{\beta V}{2V_0}\right)^2 \omega\tau_0 \ll \pi \tag{c8}$$

This is a more stringent requirement than

$$\frac{X}{\theta} = \frac{\beta V_1}{2V_0} \ll 1 \tag{c9}$$

(c9) requires only a small modulation depth while (c8) imposes a restriction on both the modulation depth and the drift time.

Digitized by Google
Original from UNIVERSITY OF MICHIGAN
Generated on 2019-09-23 05:14 GMT / http://hdl.handle.net/2027/mdp.39015077775156
Public Domain, Google-digitized / http://www.hathitrust.org/access_use#pd-google

With the restriction (c8) imposed we obtain

$$a_n = \frac{1}{\pi}\int I_0 \cos n\left(\theta_1 + \varphi + \theta\left[1 + \frac{X}{\theta}\sin\theta_1\right]\right)d\theta_1 \qquad \text{(c10)}$$

If we let $\varphi = -\theta$ all coefficients b_n will be zero and

$$a_n = 2(-1)^n I_0 J_n(Xn), \qquad a_0 = I_0 \qquad \text{(c11)}$$

Thus the first order expansion for the current returning through the gap is

$$i_2 = I_0[(1 - 2J_1(X)\cos\omega(t_2 - \tau_0) + 2J_2(2X)\cos 2\omega(t_2 - \tau_0)\cdots] \qquad \text{(c12)}$$

Our principal interest is in the fundamental component, which in complex notation is given by

$$(i_2)_f = -2I_0J_1(X)e^{j\omega(t_2-\tau_0)} \qquad \text{(c13)}$$

It is shown in Appendix II that the circuit current induced in the gap will be given, if account is taken of the phase reversal of π resulting from the reversal of direction of the beam, by

$$I_2 = -\beta(i_2)_f$$

The gap voltage at the time of return will be $v = V\sin\omega t_2$ or in complex notation

$$v = Ve^{j(\omega t_2-(\pi/2))} \qquad \text{(c14)}$$

Hence the electronic admittance to the fundamental will be

$$Y_e = \frac{I_2}{v} = \frac{2I_0\beta}{V}J_1\left(\frac{\omega\tau_0\beta V}{2V_0}\right)e^{-j(\omega\tau_0-(\pi/2))} \qquad \text{(c15)}$$

In the foregoing it was assumed that t_2 was a single valued function of t_1. We may generalize by writing (c3) as

$$\sum I_0\,dt_1 = i_2\,dt_2 \qquad \text{(c16)}$$

For sufficiently large signals there may be several intervals dt_1 which contribute charge to a given interval dt_2 and hence we write a summation for the left hand side of (c16). When the Fourier analysis is made and the change in variable from t_2 to t_1 is made the single integral breaks up into a sum of integrals. In Fig. 127 we plot time t_1 on a vertical scale with the sine wave indicating the instantaneous gap voltage. Displaced to the right on a vertical scale we plot time t_2. The solid lines connect corresponding times in the absence of signal for increments of time dt_1 and dt_2. When sufficiently

Digitized by Google
Original from UNIVERSITY OF MICHIGAN
Generated on 2019-09-23 05:14 GMT / http://hdl.handle.net/2027/mdp.39015077775156
Public Domain, Google-digitized / http://www.hathitrust.org/access_use#pd-google

large signals are applied some of the electrons in the original interval dt_1 will gain or lose sufficient energy to be thrown outside the original corresponding interval dt_2 as for example as indicated by AB. If we consider a whole cycle of the gap voltage in time t_2 it is apparent that, under steady state conditions, for every electron which is thrown outside the corresponding cycle in t_2 another from a different cycle in t_1 is thrown in whose phase differs by a multiple of 2π as for example CD. In summing the effects of these charge increments the difference of 2π in starting phase produces no physical effect. This is of course also true mathematically in the Fourier analysis of a periodic function since in integrating over an interval 2π it is immaterial whether we integrate over a single interval or break it up into a

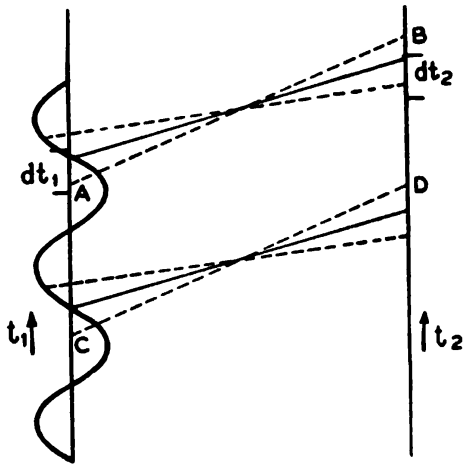

Fig. 127.—Diagram showing the relation between t_1, the time an electron crosses the gap for the first time, and t_2, the time the electron returns across the gap.

sum of integrals over intervals $-\pi$ to a, $2\pi n_1 + a$ to $2\pi n_1 + b$, $2\pi n_2 + b$ to $2\pi n_2 + c$, etc. where the subintervals sum up to 2π. Hence we conclude that the preceding analysis is also valid up to (c7) for signals sufficiently large so that t_2 and t_1 are related by a multiple valued function and is valid beyond that point provided that we do not violate (c8).

APPENDIX IV

Drift Angle as a Function of Frequency and Voltage

Let τ be the transit time in the drift space. Then the drift angle is

$$\theta = \omega\tau \tag{d1}$$

For changes in voltage (resonator or repeller), both τ and ω will change.

Digitized by Google
Original from UNIVERSITY OF MICHIGAN
Generated on 2019-09-23 05:14 GMT / http://hdl.handle.net/2027/mdp.39015077775156
Public Domain, Google-digitized / http://www.hathitrust.org/access_use#pd-google

Thus

$$\Delta\theta/\theta = \Delta\omega/\omega + \Delta\tau/\tau$$
$$= \Delta\omega/\omega + ((\partial\tau/\partial V)/\tau)\Delta V \tag{d2}$$

As shown in Appendix VI, the derivative of τ with respect to repeller voltage, $\partial\tau/\partial V_R$, is always negative, while the derivative of τ with respect to resonator voltage, $\partial\tau/\partial V_0$, may be either negative or positive. For a linear variation of potential in the drift region, $\partial\tau/\partial V_0$ is zero when $V_R = V_0$ and negative for smaller values of V_R.

APPENDIX V

Electronic Admittance—Non-Simple Theory

A closer treatment of the drift action in the repeller space follows, in which are considered the changes which occur as the voltage on the cavity becomes large.

The additional terms to be considered come from an evaluation in series of the higher-order terms of (c7), which were neglected in Appendix III. Only the fundamental component of current will be considered, although other terms could be included if desired. The integrals of interest may be rewritten from (c7), using the relation $\varphi = -\theta$, as follows:

$$a_1 = \frac{I_0}{\pi}\int_{-\pi}^{\pi}\cos\left(\theta_1 + X\sin\theta_1 - \frac{1}{2}\frac{X^2}{\theta}\sin^2\theta_1 + \frac{1}{2}\frac{X^3}{\theta^2}\sin^3\theta_1 + \cdots\right)d\theta_1 \tag{e1}$$

$$b_1 = \frac{I_0}{\pi}\int_{-\pi}^{\pi}\sin\left(\theta_1 + X\sin\theta_1 - \frac{1}{2}\frac{X^2}{\theta}\sin^2\theta_1 + \frac{1}{2}\frac{X^3}{\theta^2}\sin^3\theta_1 + \cdots\right)d\theta_1 \tag{e2}$$

We shall hereinafter neglect terms of higher order in $\frac{1}{\theta}$ than those explicitly shown here. With this neglect, we can expand the trigonometric functions, obtaining

$$a_1 = \frac{I_0}{\pi}\int_{-\pi}^{\pi}\cos(\theta_1 + X\sin\theta_1)\left[1 - \frac{1}{8}\frac{X^4}{\theta^2}\sin^4\theta_1 + \cdots\right]d\theta_1 - \frac{I_0}{\pi}\int_{-\pi}^{\pi}\sin(\theta_1 + X\sin\theta_1) \cdot \left[-\frac{1}{2}\frac{X^2}{\theta}\sin^2\theta_1 + \frac{1}{2}\frac{X^3}{\theta^2}\sin^3\theta_1 + \cdots\right]d\theta_1 \tag{e3}$$

Digitized by Google
Original from UNIVERSITY OF MICHIGAN
Generated on 2019-09-23 05:15 GMT / http://hdl.handle.net/2027/mdp.39015077775156
Public Domain, Google-digitized / http://www.hathitrust.org/access_use#pd-google

$$b_1 = \frac{I_0}{\pi}\int_{-\pi}^{\pi}\sin\,(\theta_1 + X\sin\theta_1)\left[1 - \frac{1}{8}\frac{X^4}{\theta^2}\sin^4\theta_1 + \cdots\right]d\theta_1$$
$$+ \frac{I_0}{\pi}\int_{-\pi}^{\pi}\cos\,(\theta_1 + X\sin\theta_1) \tag{e4}$$
$$\cdot\left[-\frac{1}{2}\frac{X^2}{\theta}\sin^2\theta_1 + \frac{1}{2}\frac{X^3}{\theta^2}\sin^3\theta_1 + \cdots\right]d\theta_1$$

Now of these terms, not all give contributions; some integrate to zero since the integrand is an odd function of θ_1. Rewriting with those terms omitted,

$$a_1 = \frac{I_0}{\pi}\int_{-\pi}^{\pi}\cos\,(\theta_1 + X\sin\theta_1)\left[1 - \frac{1}{8}\frac{X^4}{\theta^2}\sin^4\theta_1 + \cdots\right]d\theta_1$$
$$- \frac{I_0}{\pi}\int_{-\pi}^{\pi}\sin\,(\theta_1 + X\sin\theta_1)\left[\frac{1}{2}\frac{X^3}{\theta^2}\sin^3\theta_1 + \cdots\right]d\theta_1 \tag{e5}$$

$$b_1 = \frac{I_0}{\pi}\int_{-\pi}^{\pi}\cos\,(\theta_1 + X\sin\theta_1)\left[-\frac{1}{2}\frac{X^2}{\theta}\sin^2\theta_1 + \cdots\right]d\theta_1\,. \tag{e6}$$

Evaluation of these terms is formally simplified by the following relationships, each obtained by differentiation of the previous one:

$$-2J_1(X) = \frac{1}{\pi}\int_{-\pi}^{\pi}\cos\,(\theta_1 + X\sin\theta_1)\,d\theta_1 \tag{e7}$$

$$-2J_1'(X) = -\frac{1}{\pi}\int_{-\pi}^{\pi}\sin\,(\theta_1 + X\sin\theta_1)\sin\theta_1\,d\theta_1 \tag{e8}$$

$$-2J_1''(X) = -\frac{1}{\pi}\int_{-\pi}^{\pi}\cos\,(\theta_1 + X\sin\theta_1)\sin^2\theta_1\,d\theta_1\,. \tag{e9}$$

Continuation of this process gives all the terms of interest in (e5) and (e6). Hence

$$a_1 = I_0\left(-2J_1 + \frac{1}{4}\frac{X^4}{\theta^2}J_1^{iv} + \frac{X^3}{\theta^2}J_1''' + \cdots\right) \tag{e10}$$

$$b_1 = I_0\frac{X^2}{\theta}\,(-J_1'' + \cdots). \tag{e11}$$

Therefore the expression for the fundamental component of the beam current may be written as follows, passing to complex notation:

$$(i_2)_f \sim a_1\cos\,(\omega t_2 - \theta) + b_1\sin\,(\omega t_2 - \theta)$$
$$(i_2)_f = (a_1 - jb_1)e^{j(\omega t_2 - \theta)} \tag{e12}$$
$$= e^{j\omega t_2}e^{-j\theta}I_0\left(-2J_1 + j\frac{X^2}{\theta}J_1'' + \frac{1}{\theta^2}(X^3J_1''' + \tfrac{1}{4}X^4J_1^{iv})\right) + \cdots.$$

Digitized by Google
Original from UNIVERSITY OF MICHIGAN
Generated on 2019-09-23 05:15 GMT / http://hdl.handle.net/2027/mdp.39015077775156
Public Domain, Google-digitized / http://www.hathitrust.org/access_use#pd-google

Following usual conventions, the real part of the complex expression represents the physical situation, and the exponential time function will usually be omitted in what follows.

Similarly to Appendix III, the induced current in the gap is

$$I_2 = -\beta(i_2)_f$$

$$= e^{j\omega t}\beta e^{-j\theta} I_0\left(2J_1 - j\frac{X^2}{\theta}J_1'' - \frac{1}{\theta^2}(X^3 J_1''' + \tfrac{1}{4}X^4 J_1^{iv})\right). \quad \text{(e13)}$$

The gap voltage is still the same, viz.

$$v \backsim V\sin\omega t_2 \backsim Ve^{j(\omega t_2-(\pi/2))} = +\frac{2V_0}{\beta}\frac{X}{\theta}e^{j(\omega t_2-(\pi/2))}. \quad \text{(e14)}$$

Accordingly, the electronic admittance to the fundamental will be

$$Y_e = \frac{I_2}{v} = \frac{I_0}{V_0}\beta^2\frac{\theta}{X}e^{j((\pi/2)-\theta)}\left(J_1 - \frac{jX^2}{\theta 2}J_1'' - \frac{1}{\theta^2}\left(\frac{X^3}{2}J_1''' + \frac{X^4}{8}J_1^{iv}\right)\right) \quad \text{(e15)}$$

The argument of J_1 and its derivatives is understood to be X. The derivatives can be evaluated in terms of J_0 and J_1 by repeated use of the Bessel function recurrence relations (see Jahnke-Emde, Funktionentafeln, p. 144). The result is

$$Y_e = \frac{I_0}{V_0}\beta^2\frac{\theta}{X}e^{j((\pi/2)-\theta)}\left(J_1 - \frac{j}{\theta}\left[\left(1-\frac{X^2}{2}\right)J_1 - \frac{X}{2}J_0\right] - \frac{1}{\theta^2}\left[\tfrac{1}{8}(X^2+X^4)J_1 - \tfrac{1}{4}X^3 J_0\right] + \cdots\right). \quad \text{(e16)}$$

The real part of this will be of interest; it is

$$G_e = +\frac{I_0}{V_0}\beta^2\frac{\theta}{X}\sin\theta\left(J_1 + \frac{\cot\theta}{\theta}\left[\left(1-\frac{X^2}{2}\right)J_1 - \frac{X}{2}J_0\right] - \frac{1}{\theta^2}\left[\tfrac{1}{8}(X^2+X^4)J_1 - \tfrac{1}{4}X^3 J_0\right]\right). \quad \text{(e17)}$$

The power generated by the electron stream is given by

$$P = -\tfrac{1}{2}G_e V^2$$

$$= -I_0 V_0\frac{2X}{\theta}\left(\sin\theta\left[J_1 - \frac{1}{8\theta^2}((X^2+X^4)J_1 - 2X^3 J_0)\right] + \frac{\cos\theta}{\theta}\left[\left(1-\frac{X^2}{2}\right)J_1 - \frac{X}{2}J_0\right]\right) + \cdots. \quad \text{(e18)}$$

Digitized by Google
Original from UNIVERSITY OF MICHIGAN
Generated on 2019-09-23 05:15 GMT / http://hdl.handle.net/2027/mdp.39015077775156
Public Domain, Google-digitized / http://www.hathitrust.org/access_use#pd-google

Of this power, only a part is usefully delivered to the load admittance G_L, the rest being dissipated because of the circuit loss conductance G_R. The power lost in the circuit is

$$P_R = \tfrac{1}{2}G_R V^2 = \frac{2V_0^2 G_R}{\beta^2}\frac{X^2}{\theta^2} \tag{e19}$$

Accordingly, the useful power delivered to the load is

$$P_L = P - P_R \tag{e20}$$

A quantity of interest is the maximum useful power which can be obtained from the reflex oscillator; this is given by

$$\frac{\partial P_L}{\partial X} = 0 = \frac{\partial P_L}{\partial \theta} \tag{e21}$$

These two conditions are expressed by the next two equations.

$$2XJ_0 + \frac{1}{\theta}\cot\theta\,(-X^3J_0 - X^2J_1) + \frac{1}{\theta^2}\left((\tfrac{7}{4}X^3 - \tfrac{1}{4}X^5)J_0 + \left(-\frac{X^2}{2} - \tfrac{3}{2}X^4\right)J_1\right) + \frac{4V_0}{\beta^2 I_0}G_R\frac{X}{\theta\sin\theta} = 0 \tag{e22}$$

$$XJ_0 + (-4 + X^2)J_1 + \theta\cot\theta\cdot 2J_1 - \frac{\cot\theta}{\theta}((-\tfrac{1}{2}X^3 - 2X)J_0 + (4 - \tfrac{7}{4}X^2 + \tfrac{1}{4}X^4)J_1) + \frac{1}{\theta^2}(-\tfrac{3}{2}X^3J_0 + \tfrac{3}{4}(X^2 + X^4)J_1) - \frac{4V_0}{\beta^2 I_0}G_R\frac{X}{\theta\sin\theta} = 0 \tag{e23}$$

One may note that even if one sets $G_R = 0$ and neglects terms in $\frac{1}{\theta^2}$ the second of these equations is a little different from the corresponding one of Appendix III, so that a slightly different phase angle is predicted for maximum generated power. The result of Appendix III was

$$\theta\cot\theta = 1$$

predicting a phase angle θ slightly less than $\theta_n = (n + \frac{3}{4})2\pi$. However, the zero order result here is

$$\theta\cot\theta = 2 - \frac{X^2}{2} = -.892 \tag{e24}$$

predicting a phase angle a trifle larger than θ_n, in the approximation of Appendix III.

Digitized by Google
Original from UNIVERSITY OF MICHIGAN
Generated on 2019-09-23 05:15 GMT / http://hdl.handle.net/2027/mdp.39015077775156
Public Domain, Google-digitized / http://www.hathitrust.org/access_use#pd-google

The equations (e22) and (e23) may look as if drastic measures would now be needed, but a parametric solution is surprisingly easy; one need only solve (e22) for G_R, and substitute back into the power expression (e20). The results are

$$G_R = -\frac{I_0}{V_0}\frac{\beta^2}{4}\theta \sin\theta\left(2J_0 + \frac{\cot\theta}{\theta}\left[-X^2J_0 - XJ_1\right] + \frac{1}{\theta^2}\left[\left(\tfrac{1}{4}X^2 - \tfrac{1}{4}X^4\right)J_0 + \left(-\frac{X}{2} - \tfrac{3}{8}X^3\right)J_1\right] + \cdots\right) \tag{e25}$$

$$P_L = -I_0V_0\frac{X}{\theta}\sin\theta\left(2J_1 - XJ_0 + \frac{\cot\theta}{\theta}\left[\left(-X + \frac{X^3}{2}\right)J_0 + \left(2 - \frac{X^2}{2}\right)J_1\right] + \frac{1}{\theta^2}\left[\frac{X^4}{2}J_1 + \left(-\tfrac{3}{8}X^3 + \tfrac{1}{8}X^5\right)J_0\right]\right) \tag{e26}$$

$$G_L = -G_e - G_R = -\frac{I_0}{V_0}\beta^2\frac{\theta}{X}\sin\theta\left(J_1 - \tfrac{1}{2}XJ_0 + \frac{\cot\theta}{\theta}\cdot\left[\left(1 - \frac{X^2}{4}\right)J_1 + \left(-\frac{X}{2} + \frac{X^3}{4}\right)J_0\right] + \frac{1}{\theta^2}\left[\tfrac{1}{4}X^4J_1 + \left(-\tfrac{3}{16}X^3 + \tfrac{1}{16}X^5\right)J_0\right]\right) \tag{e27}$$

One further convolution is necessary, because the equations (e25) and (e26) are still subject to the optimum phase angle condition (e23). Since we are here carrying only terms as far as $\frac{1}{\theta^2}$, approximations are in order.

From (e24) we get the hint that $\theta \cot\theta$ is of the order of unity, so that terms in $\frac{\cot\theta}{\theta}$ are of the same order as those in $\frac{1}{\theta^2}$. Accordingly an approximate solution is obtainable by adding (e22) and (e23) and neglecting these small terms. The result is

$$\theta\cot\theta = 2 - \frac{X^2}{2} - \frac{3XJ_0}{2J_1} \equiv F(X) \tag{e28}$$

Therefore the optimum phase angle is given by

$$\theta = \theta_n - \frac{F(X)}{\theta_n}, \qquad \theta_n = (n + \tfrac{3}{4})2\pi \tag{e29}$$

$$\sin\theta = -1 + \frac{[F(X)]^2}{2\theta_n^2} \tag{e30}$$

Digitized by Google
Original from UNIVERSITY OF MICHIGAN
Generated on 2019-09-23 05:15 GMT / http://hdl.handle.net/2027/mdp.39015077775156
Public Domain, Google-digitized / http://www.hathitrust.org/access_use#pd-google

$$\frac{\sin\theta}{\theta} = -\frac{1}{\theta_n}\left[1 + \frac{1}{\theta_n^2}(F - F^2/2)\right] \tag{e31}$$

$$\frac{\cot\theta}{\theta} = \frac{1}{\theta_n^2}F(X) \tag{e32}$$

From computation it turns out that in the range of interest, the quantity $F(X)$ does not differ from (-1) by more than 20%.

The desired approximate solution comes now from substituting the explicit phase optimum (e29) to (e32) back into (e25)–(e27). The results are:

$$G_R = \frac{I_0}{V_0}\beta^2\frac{\theta_n}{2}\left(J_0 + \frac{1}{\theta_n^2}S_1(X)\right) \tag{e33}$$

$$P_L = I_0 V_0 \frac{X^2}{\theta_n}\left(\frac{2J_1}{X} - J_0 + \frac{1}{\theta_n^2}S_2(X)\right) \tag{e34}$$

$$G_L = \frac{I_0}{V_0}\beta^2\frac{\theta_n}{2}\left(\frac{2J_1}{X} - J_0 + \frac{1}{\theta_n^2}S_3(X)\right) \tag{e35}$$

The S-functions are given by

$$S_1(X) = \left(-F - \frac{F^2}{2} - \frac{X^2F}{2} + \frac{7}{8}X^2 - \frac{1}{8}X^4\right)J_0 + \left(-\frac{X^2}{2}F - \frac{X^2}{4} - \frac{3}{4}X^4\right)\frac{J_1}{X} \tag{e36}$$

$$S_2(X) = \left(-F^2 - F\frac{X^2}{2} + 4F + \frac{1}{2}X^4\right)\frac{J_1}{X} + \left(\frac{F^2}{2} + \frac{X^2F}{2} - 2F - \frac{3}{8}X^2 + \frac{1}{8}X^4\right)J_0 \tag{e37}$$

$$S_3(X) = \left(\frac{F^2}{2} + \frac{FX^2}{2} - \frac{3}{8}X^2 + \frac{1}{8}X^4\right)J_0 + \left(-F^2 - F\frac{X^2}{2} + \frac{1}{2}X^4\right)\frac{J_1}{X} \tag{e38}$$

The equations (e33)–(e35) have the following meaning: they presuppose that the load G_L has been adjusted for maximum useful power in the presence of circuit loss G_R, and that the drift angle is also optimum. Then the useful power is given parametrically in terms of the circuit conductance by equations (e33) and (e34), while (e35) gives the required optimum load conductance, also in terms of the parameter X.

The results may be expressed as a chart of useful power, plotted against the value of resonator loss conductance. This is done in Fig. 128.

One may also be interested in the maximum power which could be gen-

Generated on 2019-09-23 05:16 GMT / http://hdl.handle.net/2027/mdp.39015077775156
Public Domain, Google-digitized / http://www.hathitrust.org/access_use#pd-google
Digitized by Google
Original from UNIVERSITY OF MICHIGAN

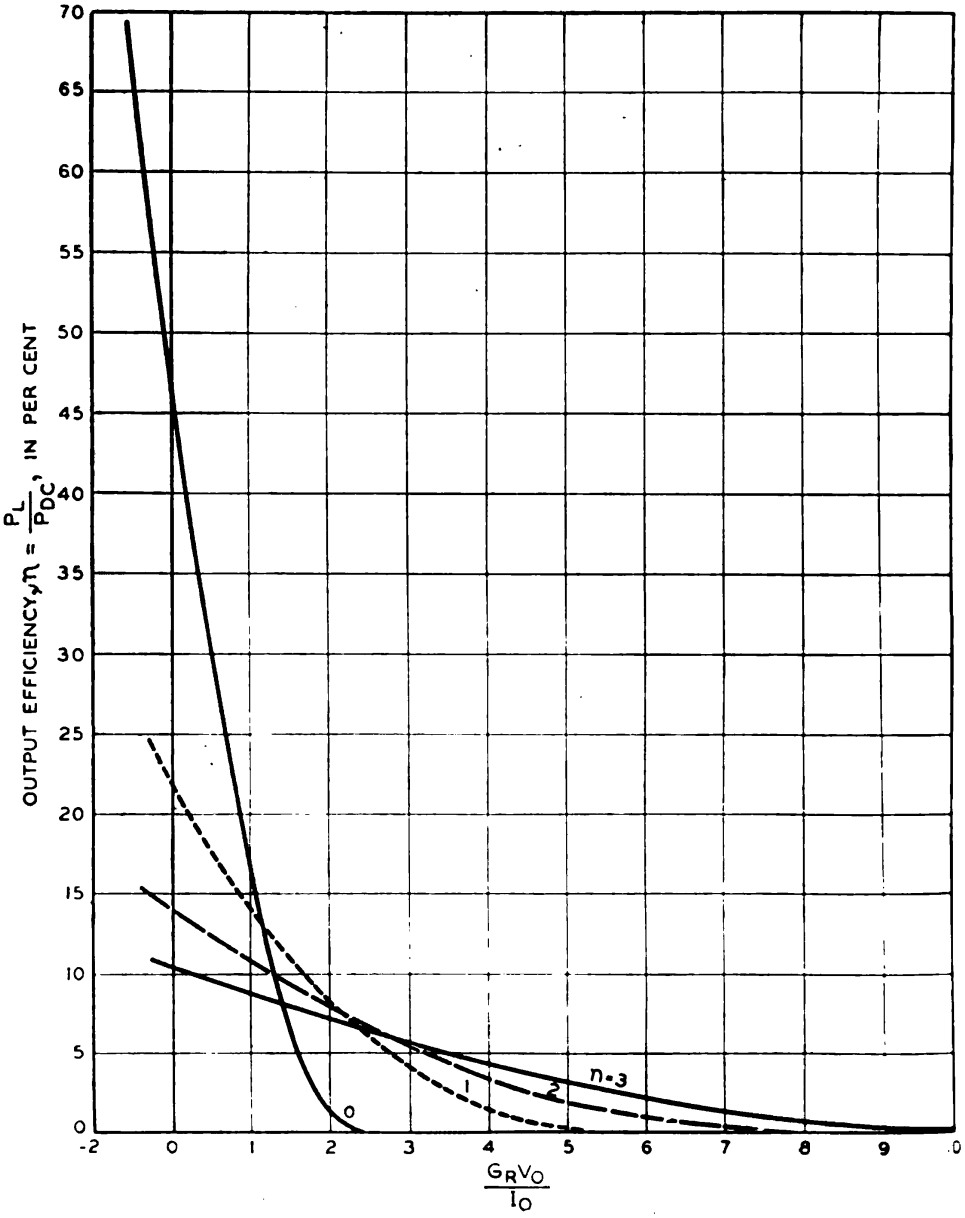

Fig. 128.—Plot of efficiency vs a parameter proportional to resonator loss for several repeller modes.

n	0	1	2	3
η	0.48	0.22	0.14	0.105

Fig. 129.—Maximum efficiency for several repeller modes.

erated if the resonator were perfect. This comes from setting $G_R = 0$ calculating the resulting value of useful power. The results are compared with the simpler theory in Fig. 129.

Digitized by Google
Original from UNIVERSITY OF MICHIGAN
Generated on 2019-09-23 05:16 GMT / http://hdl.handle.net/2027/mdp.39015077775156
Public Domain, Google-digitized / http://www.hathitrust.org/access_use#pd-google

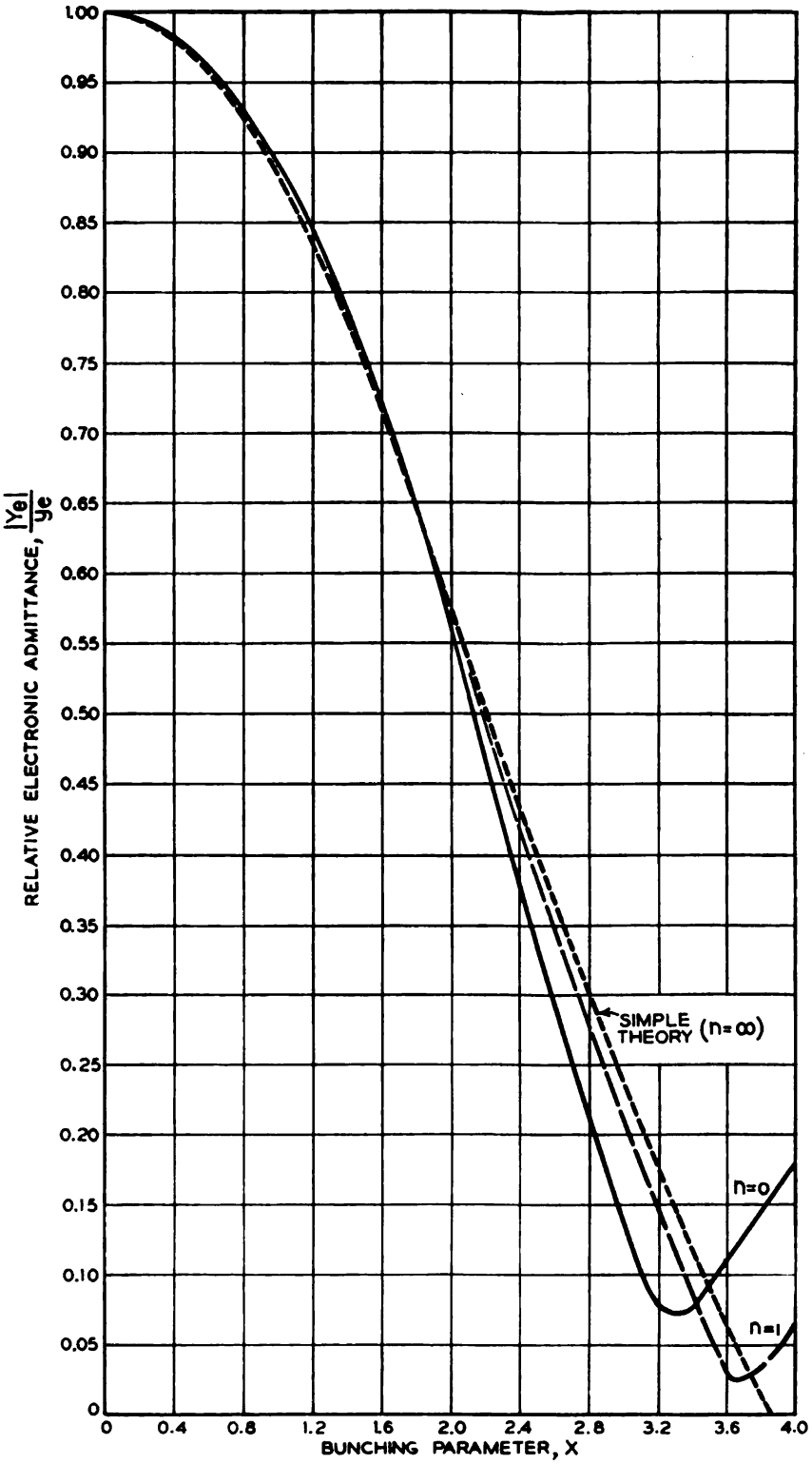

Fig. 130.—Relative electronic admittance vs bunching parameter for several repeller modes.

Digitized by Google
Original from UNIVERSITY OF MICHIGAN
Generated on 2019-09-23 05:16 GMT / http://hdl.handle.net/2027/mdp.39015077775156
Public Domain, Google-digitized / http://www.hathitrust.org/access_use#pd-google

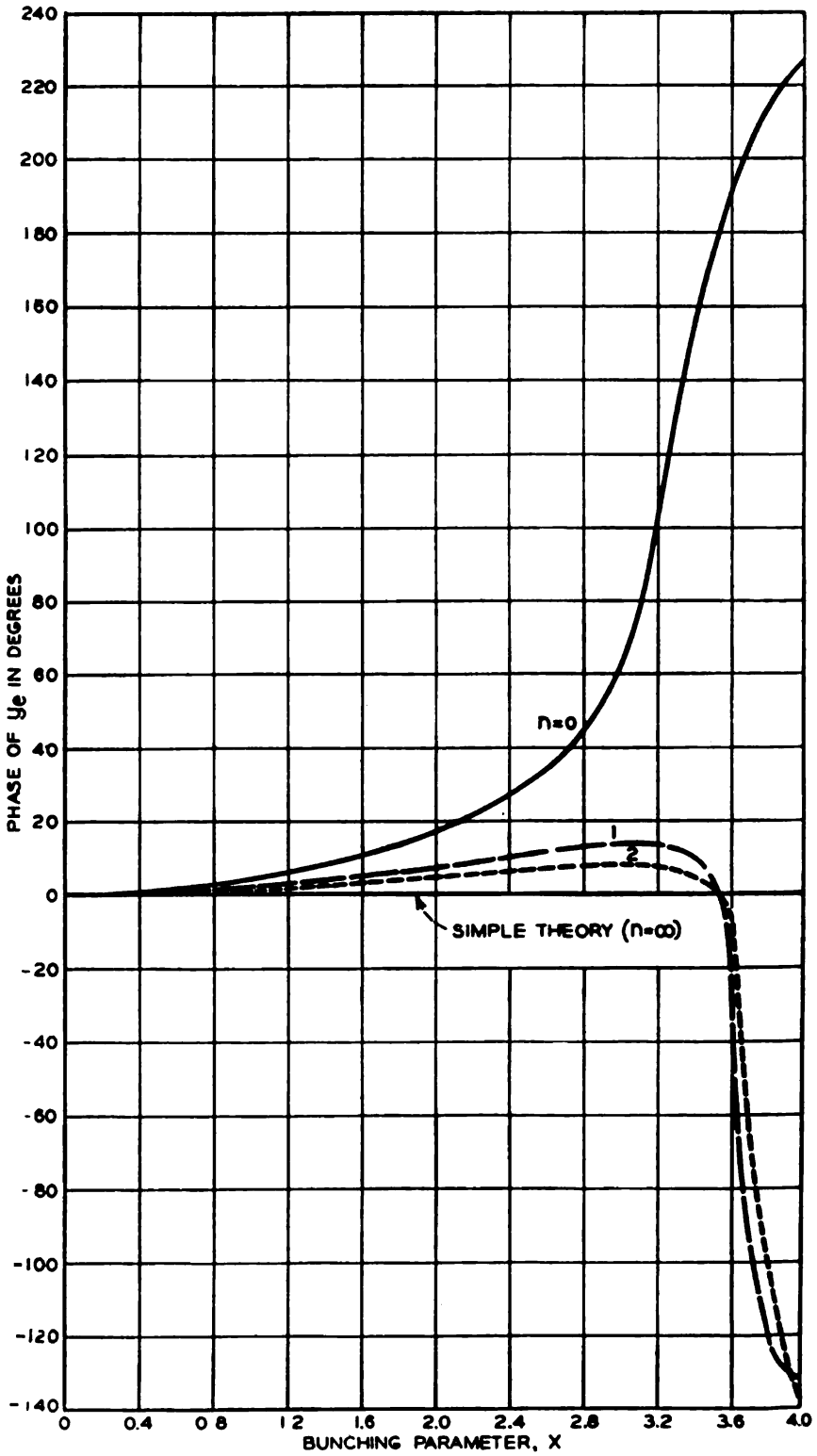

Fig. 131.—Phase of electronic admittance vs bunching parameter for several repeller modes.

Digitized by Google
Original from UNIVERSITY OF MICHIGAN
Generated on 2019-09-23 05:16 GMT / http://hdl.handle.net/2027/mdp.39015077775156
Public Domain, Google-digitized / http://www.hathitrust.org/access_use#pd-google

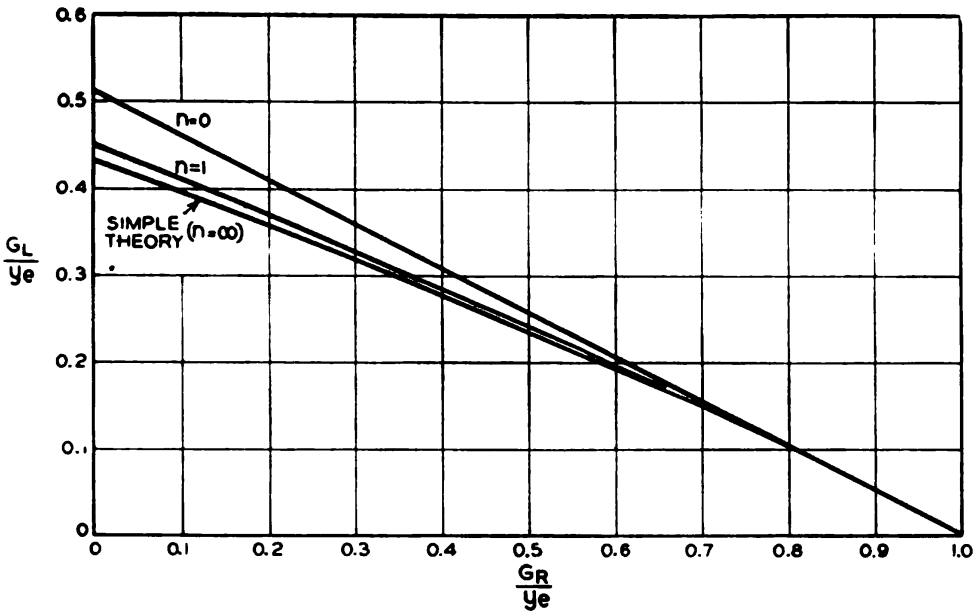

Fig. 132.—Optimum load conductance divided by small signal electronic admittance vs resonator loss conductance divided by small signal electronic admittance for several repeller modes.

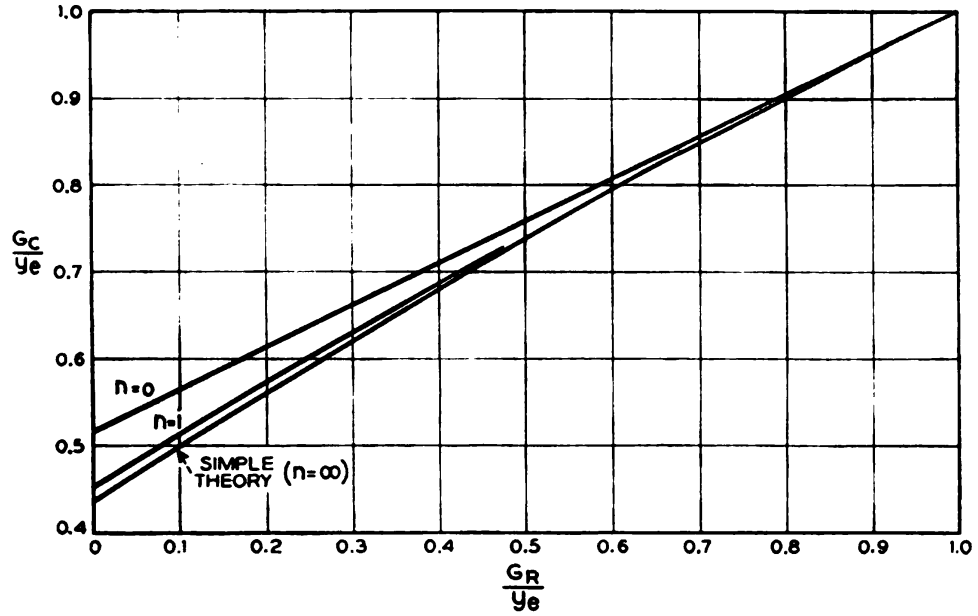

Fig. 133.—Optimum total circuit conductance divided by small signal electronic admittance vs resonator loss conductance divided by small signal electronic admittance for several repeller modes.

Further data which may be determined include the variation of the magnitude of the electronic admittance with gap voltage, in Fig. 130; also its phase, in Fig. 131. The optimum load conductance is plotted as a

Digitized by Google
Original from UNIVERSITY OF MICHIGAN
Generated on 2019-09-23 05:16 GMT / http://hdl.handle.net/2027/mdp.39015077775156
Public Domain, Google-digitized / http://www.hathitrust.org/access_use#pd-google

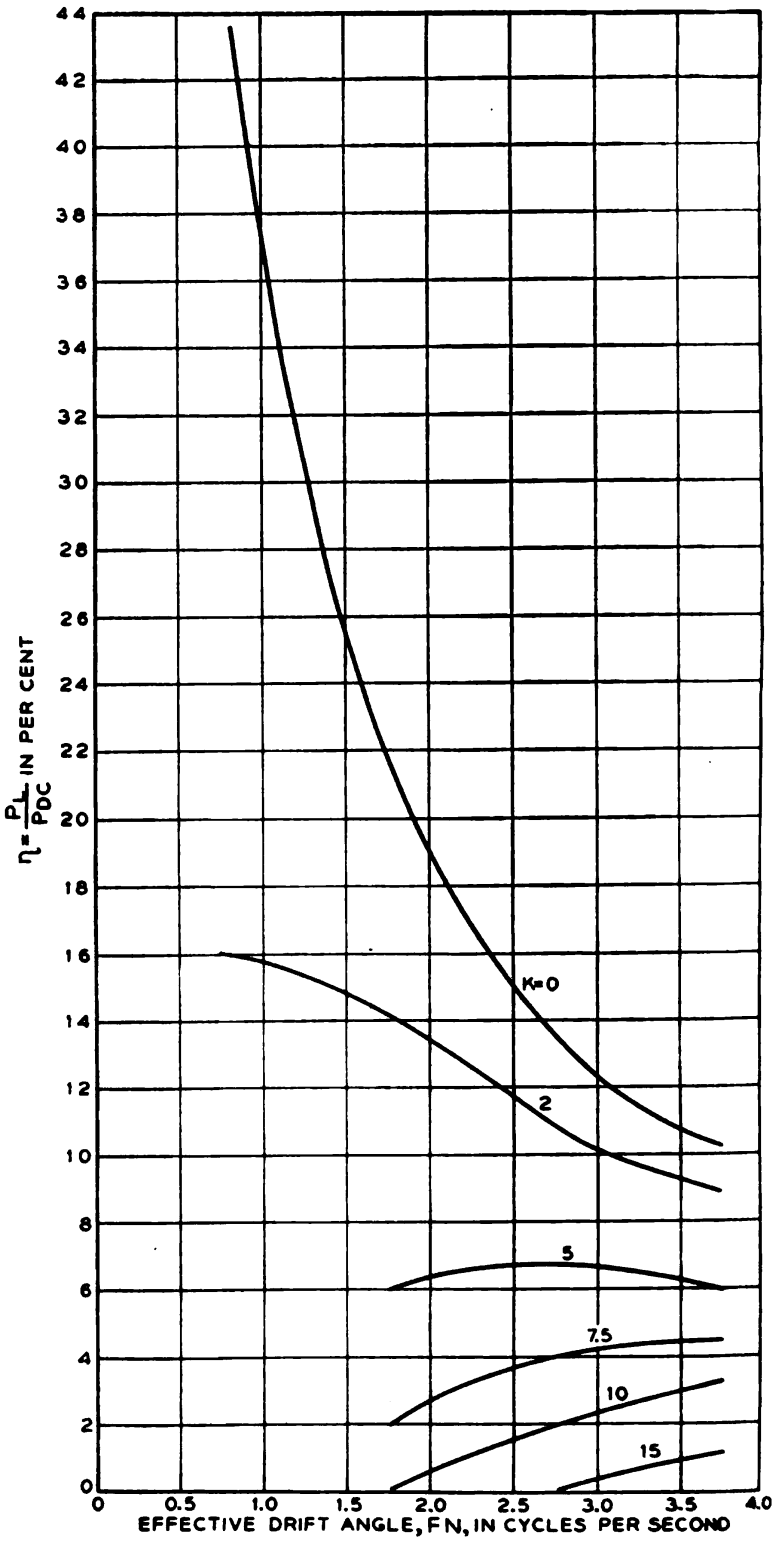

Fig. 134.—Efficiency vs effective drift angle for several degrees of resonator loss.

Digitized by Google
Original from UNIVERSITY OF MICHIGAN
Generated on 2019-09-23 05:17 GMT / http://hdl.handle.net/2027/mdp.39015077775156
Public Domain, Google-digitized / http://www.hathitrust.org/access_use#pd-google

function of resonator loss in Fig. 132, and the total conductance, load plus loss, in Fig. 133. The next Fig. 134, plots efficiency versus mode number

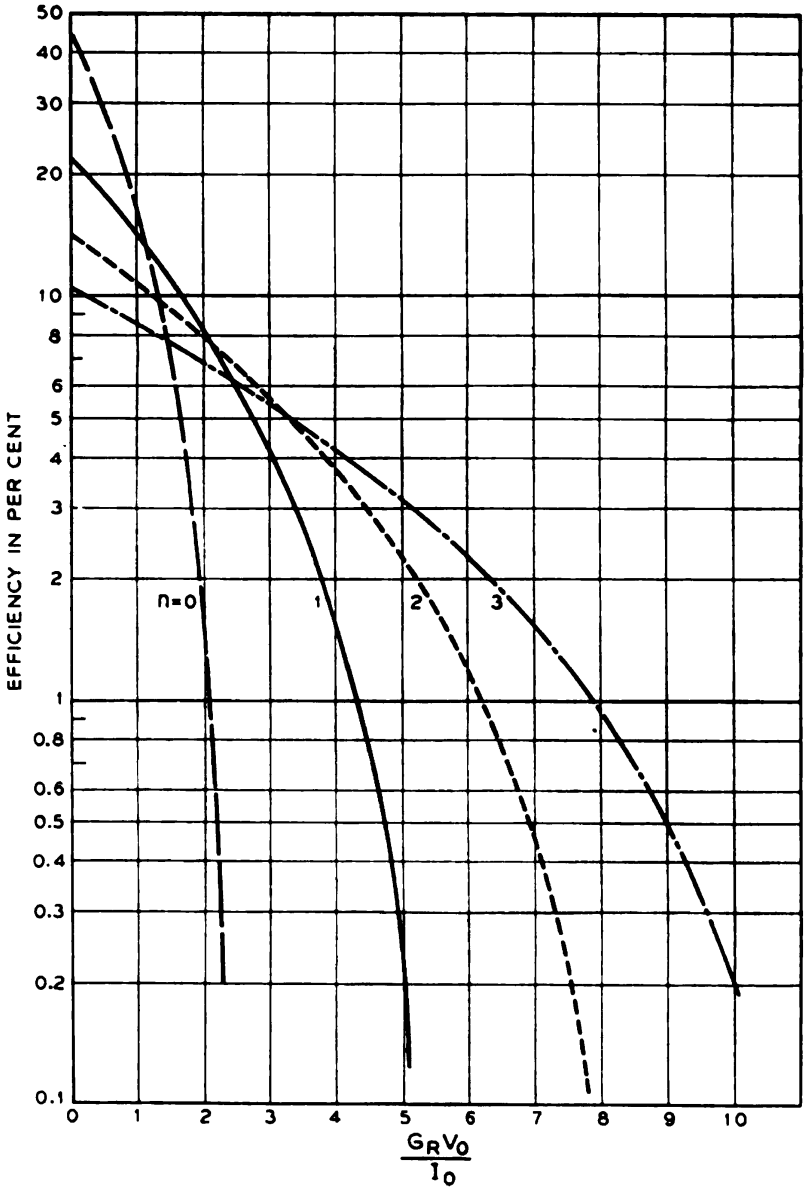

Fig. 135.—Efficiency vs a parameter proportional to resonator loss for several repeller modes.

with resonator loss as a parameter, while the next Fig. 135, plots efficiency versus resonator loss with mode number as a parameter.

Most of these graphs include for comparison the results of the simpler theory, and it can be seen that the deviations indicated by the second

Digitized by Google
Original from UNIVERSITY OF MICHIGAN
Generated on 2019-09-23 05:17 GMT / http://hdl.handle.net/2027/mdp.39015077775156
Public Domain, Google-digitized / http://www.hathitrust.org/access_use#pd-google

order theory are ordinarily rather small even for the first two modes of operation, and are quite negligible for higher modes.

APPENDIX VI

General Potential Variation in the Drift Space

Suppose that the potential of the drift space is given by $V(x)$, where $x = 0$ at zero potential and $x = \ell$ at the gap. Then the transit time from the gap to zero potential and back again is

$$\tau_0 = (2/\sqrt{2\eta}) \int_0^{\ell} \frac{dx}{(V(X))^{\frac{1}{2}}} \tag{f1}$$

Imagine now that the entire drift space is raised by a very small amount ΔV. The zero potential point will now occur at

$$x = -\Delta V/V'(0) \tag{f2}$$

where

$$V'(x) = dV/dx \tag{f3}$$

Hence the new transit time will be

$$\tau_0 + \Delta\tau = (2/\sqrt{2\eta}) \int_{-\Delta V/V'(0)}^{\ell} \frac{dx}{[V(x) + \Delta V]^{\frac{1}{2}}} \tag{f4}$$

Now let

$$z = x + \Delta V/V'(0) \tag{f5}$$

Then, including first order terms only, if $V(x)$ can be expanded in a Taylor's series about 0,

$$\begin{aligned} \tau_0 + \Delta\tau &= (2/\sqrt{2\eta}) \int_0^{\ell+\Delta V/V'(0)} \frac{dz}{[V(z) - [V'(z)/V'(0)]\Delta V + \Delta V]^{\frac{1}{2}}} \\ &= (2/\sqrt{2\eta}) \left(\int_0^{\ell} \frac{dz}{[V(z)]^{\frac{1}{2}}} + \Delta V \int_0^{\ell} \frac{[(V'(z)/V'(0)) - 1]\, dz}{2[V(z)]^{\frac{1}{2}}} \right. \\ &\qquad \left. + \frac{\Delta V}{V'(0)[V(\ell)]^{\frac{1}{2}}} \right) \end{aligned} \tag{f6}$$

Whence

$$\tau' = \frac{\Delta\tau}{\Delta V} = (2/\sqrt{2\eta}) \left(\frac{1}{V'(0)[V(\ell)]^{\frac{1}{2}}} + \int_0^{\ell} \frac{[(V'(z)/V'(0)) - 1]\, dz}{2[V(z)]^{\frac{1}{2}}} \right) \tag{f7}$$

In computing F it should be noted that by definition the gap voltage pre-

Digitized by Google
Original from UNIVERSITY OF MICHIGAN
Generated on 2019-09-23 05:17 GMT / http://hdl.handle.net/2027/mdp.39015077775156
Public Domain, Google-digitized / http://www.hathitrust.org/access_use#pd-google

viously referred to as V_0 is

$$V_0 = V(\ell) \tag{f8}$$

In the notation as it has been modified, the transit time is

$$\tau_0 = (2/\sqrt{2\eta}) \int_0^\ell \frac{dz}{(V(z))^{\frac{1}{2}}} . \tag{f9}$$

For a constant retarding field in the drift space of magnitude E_0, we can write

$$\eta E_0(\tau_1/2) = v = \sqrt{2\eta V} \tag{f10}$$

Here V is the total energy with which electrons are shot into the drift space. From (f10)

$$\tau_1 = \frac{2\sqrt{2\eta V}}{\eta E_0} \tag{f11}$$

$$\tau_1' = d\tau/dV = \frac{2\sqrt{2\eta V}}{\eta E_0}\left(\frac{1}{2V}\right) = \frac{\tau_0}{2V} . \tag{f12}$$

In the notation used earlier this is

$$\tau_1' = \frac{\tau_0}{2V(\ell)} . \tag{f13}$$

Now we will compare τ' from (f7) with τ_1', the rate of change of transit time for a linear field, taking τ_1' for the same resonator voltage $V(\ell)$ and the same transit time, given by (f1), as the nonlinear field. The factor F relating τ' and τ_1' will then be

$$F = \tau'/\tau_1'$$

$$= 2V(\ell)\left\{\frac{1}{V'(0)[V(\ell)]^{\frac{1}{2}}} + \int_0^\ell \frac{[V'(z)/V'(0) - 1]\, dz}{2[V(z)]^{\frac{1}{2}}}\right\}\left[\int_0^\ell \frac{dz}{[V(z)]^{\frac{1}{2}}}\right]^{-1} . \tag{f14}$$

If an electron is shot into the drift space with more than average energy, its greater penetration causes it to take longer to return, but it covers any element of distance in less time. Consider a case in which the gradient of the potential is small near the zero potential (much change in penetration for a given change in energy) and larger near the gap. The first term in the brackets of (f14) will be large, and the second is in this case positive. This means that in this type of field the increased penetration per unit energy and the effect of covering a given distance in less time with increased energy work together to give more drift action than in a constant field. However,

Digitized by Google
Original from UNIVERSITY OF MICHIGAN
Generated on 2019-09-23 05:17 GMT / http://hdl.handle.net/2027/mdp.39015077775156
Public Domain, Google-digitized / http://www.hathitrust.org/access_use#pd-google

we might have the gradient near the gap less than that at the zero potential. In that case the second term in the brackets would be negative. This means a diminution in drift action because the penetration changes little with energy while the electron travels faster over the distance it has to cover.

To show how large this effect of weakening the field near the zero potential point may be, we will consider a specific potential variation, one which approximates the field in a long hollow tubular repeller. The field considered will be that in which

$$V(z) = (e^z - 1)/e^l \tag{f15}$$

We obtain

$$F = (e^l - 1) + \frac{(e^l - 1)^{\frac{1}{2}}}{\tan^{-1}(e^l - 1)^{\frac{1}{2}}}. \tag{f16}$$

Now

$$V'(0) = e^{-l} \tag{f17}$$

$$V'(z) = 1 \tag{f18}$$

Hence

$$F = \left(\frac{1}{V'(0)} - 1\right) + \frac{\left(\frac{1}{V'(0)} - 1\right)^{\frac{1}{2}}}{\tan^{-1}\left(\frac{1}{V'(0)} - 1\right)^{\frac{1}{2}}}. \tag{f19}$$

This shows clearly how the effective drift angle is increased as the field at the zero potential point is weakened. For instance, if $V'(0) = \frac{1}{2}$, so that the field at the zero potential point is $\frac{1}{2}$ that at the gap, the drift effectiveness for a given number of cycles drift is more than doubled ($F = 2.27$).

There is another approach which is important in that it relates the variations of drift time obtained by varying various voltages. Suppose the gap voltage with respect to the cathode is V_0 and the repeller voltage with respect to the cathode is $-V_R$. Now suppose V_0 and V_R are increased by a factor α, so that the resonator and repeller voltages become αV_0 and $-\alpha V_R$. The zero voltage point at which the electrons are turned back will be at the same position and so the electrons will travel the same distance, but at each point the electrons will go $\alpha^{-\frac{1}{2}}$ times as fast. If, instead of introducing the factor α, we merely consider the voltages V_R and V_0 to be the variables, we see that the transit time can be written in the form

$$\tau = V_0^{-\frac{1}{2}} F(V_R/V_0) \tag{f20}$$

Digitized by Google
Original from UNIVERSITY OF MICHIGAN
Generated on 2019-09-23 05:18 GMT / http://hdl.handle.net/2027/mdp.39015077775156
Public Domain, Google-digitized / http://www.hathitrust.org/access_use#pd-google

The function $F(V_R/V_0)$ expresses the effect on τ of different penetrations of the electron into the drift field and the factor $V_0^{-\frac{1}{2}}$ tell us that if V_R and V_0 are changed in the same ratio, the drift time changes as one over the square root of either voltage.

We can differentiate, obtaining

$$\partial\tau/\partial V_R = V_0^{-\frac{1}{2}}F'(V_R/V_0) \tag{f21}$$

$$\partial\tau/\partial V_0 = -V_0^{-\frac{1}{2}}((V_R/V_0)F'(V_R/V_0) - (1/2)F(V_R/V_0)) \tag{f22}$$

If the electron gains an energy βV in crossing the gap, the effect on τ is the same as if V_0 were increased by βV and V_R were changed by an amount $-\beta V$, because in an acceleration of an electron in crossing the gap the electron gains energy with respect to both the resonator (where the energy is specified by V_0 for an unaccelerated electron) and with respect to the repeller ($-V_R$ for an unaccelerated electron). We may thus write

$$\partial\tau/\partial(\beta V) = \partial\tau/\partial V_0 - \partial\tau/\partial V_R$$

$$= -V_0^{-\frac{1}{2}}[(1 + V_R/V_0)F'(V_R/V_0) + \tfrac{1}{2}F(V_R/V_0)] \tag{f23}$$

This expression (f23) is for the same quantity as (f7). V_0 of (f23) is $V(\ell)$ of (f7). Expressions (f21), (f22) and (f23) compare the effects on drift time of changing the repeller voltage alone, as in electronic tuning, the resonator voltage alone, and of accelerating the electrons in crossing the gap. As making the repeller more negative always decreases the drift time, we see that the two terms of (f22) subtract, and usually $|\partial\tau/\partial V_0|$ will be less than $|\partial\tau/\partial V_R|$. In fact, for a linear variation potential in the drift space and for $V_0 = V_R$, $\partial\tau/\partial V_0 = 0$. Weak fields at the zero potential point make the absolute value of $F'(V_R/V_0)$ larger and hence tend to make both $|\partial\tau/\partial V_R|$ and $|\partial\tau/\partial(\beta V)|$ larger. However, these quantities are not changed in quite the same way.

The reader should be warned that (f14) and (f20)–(f23) apply only for fields not affected by the space charge of the electron beam. For instance, suppose we had a gap with a flat grid and a parallel plane repeller a long way off at zero potential. If edge effects and thermal velocities were neglected, we would have a Child's law discharge. The potential would be zero beyond a certain distance from the repeller, and we would have

$$V(z) = Az^{\frac{4}{3}}$$

According to (f14), F should be infinite. There is no reason to expect infinite drift action, however, for the drift field, which is affected by the fluctuating electron density in the beam, is a function of time, and (f14) does not apply.

Digitized by Google
Original from UNIVERSITY OF MICHIGAN
Generated on 2019-09-23 05:18 GMT / http://hdl.handle.net/2027/mdp.39015077775156
Public Domain, Google-digitized / http://www.hathitrust.org/access_use#pd-google

APPENDIX VII

Ideal Drift Field

The behavior of reflex oscillators has been analyzed on the basis of a uniform field in the drift space. It can be shown that this is not the drift field which gives maximum efficiency. The field which does give maximum efficiency under certain assumptions is described in this appendix.

Consider a reflex oscillator in which a voltage V appears across the gap. This voltage causes an energy change of $\beta V \cos \theta_1$ for the electron crossing the gap. Here θ_1 is the phase at which a given electron crosses the gap for the first time. The effect of the drift space is to cause the electron to return after an interval τ_a where τ_a is a function of this energy.

$$\tau_a = f(\beta V \cos \theta_1) \tag{g1}$$

Thus, each value of τ_a will occur twice every cycle (2π variation of θ_1). We will have

$$\theta_1 = \omega t_1 \tag{g2}$$

$$\begin{aligned} \theta_a &= \omega(t_1 + \tau_a) \\ &= \theta_1 + \varphi(\theta_1) \end{aligned} \tag{g3}$$

$$\varphi(\theta_1) = \omega \tau_a \tag{g4}$$

Here t_1 is the time at which an electron first crosses the gap and $(t_1 + \tau_a)$ is the time of return to the gap. θ_1 and θ_a are the phase angles of the voltage at first crossing and return.

The net work done by an electron in the two crossings is

$$W = \beta V e[-\cos \theta_1 + \cos (\theta_1 + \varphi(\theta_1))] \tag{g5}$$

If the beam current has a steady value I_0, the power produced will be

$$P = (\beta V I_0/2\pi) \int_{-\pi}^{\pi} [-\cos \theta_1 + \cos (\theta_1 + \varphi(\theta_1))]\, d\theta_1 . \tag{g6}$$

The integral of $\cos \theta_1$ is of course zero. Further, from (g4) we see that

$$\varphi(\theta_1) = \varphi(-\theta_1)$$

Hence

$$\begin{aligned} P &= (\beta V I_0/2\pi) \int_0^{\pi} [\cos (-\theta_1 + \varphi(\theta_1) + \cos (\theta_1 + \varphi(\theta_1))]\, d\theta_1 \\ &= (\beta V I_0/2\pi) \int_0^{\pi} \cos \varphi(\theta_1) \cos \theta_1\, d\theta_1 . \end{aligned} \tag{g7}$$

Digitized by Google
Original from UNIVERSITY OF MICHIGAN
Generated on 2019-09-23 05:18 GMT / http://hdl.handle.net/2027/mdp.39015077775156
Public Domain, Google-digitized / http://www.hathitrust.org/access_use#pd-google

As $\cos \varphi(\theta_1)$ cannot be greater than unity, it is obvious that this will have its greatest value if the following holds

$$0 < \theta_1 < \pi/2, \qquad \varphi(\theta_1) = 2n\pi, \qquad \cos \varphi(\theta_1) = +1 \tag{g8}$$

$$\pi/2 < \theta_1 < \pi, \qquad \varphi(\theta_1) = (2m + 1)\pi, \qquad \cos \varphi(\theta_1) = -1 \tag{g9}$$

These conditions are such that for a positive value of $\cos \varphi$ the gap voltage is accelerating giving a longer drift time than obtains for a negative value of $\cos \varphi(\theta_1)$ for which a retarding gap voltage is required. Thus, physically we must have

$$2n > 2m + 1 \tag{g10}$$

The simplest case is that for $n = 1$ and $m = 0$, so that in terms of the gap voltage

$$\begin{aligned} v < 0, \qquad & \varphi(\theta_1) = \pi \\ v > 0, \qquad & \varphi(\theta_1) = 2\pi \end{aligned} \tag{g11}$$

This sort of drift action is illustrated by the curve shown in Fig. 136.

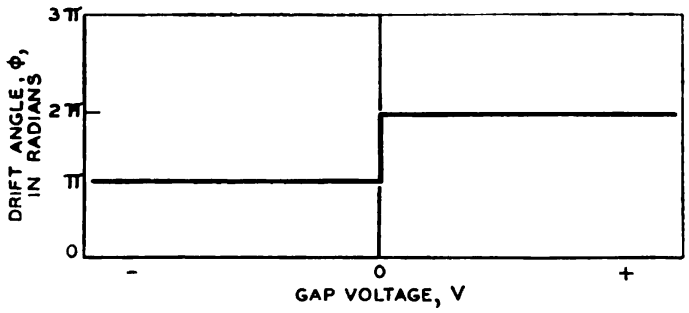

Fig. 136.—Ideal variation of drift time in the repeller region with resonator gap voltage.

The problem of finding the variation with distance which would give this result was referred to Dr. L. A. MacColl who gave the following solution:

Suppose V_0 is the voltage of the gap with respect to the cathode and Φ is the potential in the drift space. Let

$$x_0 = \sqrt{2\eta V_0}/\omega \tag{g12}$$

Here ω is the operating radian frequency. Let x be a measure of distance in the drift field.

$$\begin{aligned} \Phi &= V_0[1 - (x/x_0)^2], \qquad 0 < x < x_0 \\ \Phi &= V_0\{1 - [(x/x_0)^2 + 1]^2/4(x/x_0)^2\}, \qquad x > x_0 \end{aligned} \tag{g13}$$

This potential distribution is plotted in Fig. 137.

Digitized by Google
Original from UNIVERSITY OF MICHIGAN
Generated on 2019-09-23 05:18 GMT / http://hdl.handle.net/2027/mdp.39015077775156
Public Domain, Google-digitized / http://www.hathitrust.org/access_use#pd-google

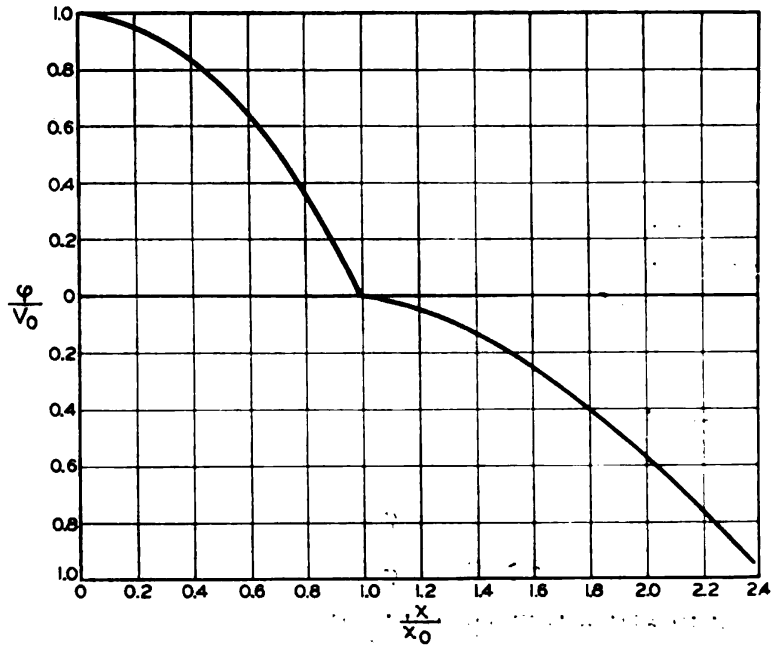

Fig. 137.—Variation of potential in the repeller region vs distance to give the characteristics shown in Fig. 7.1.

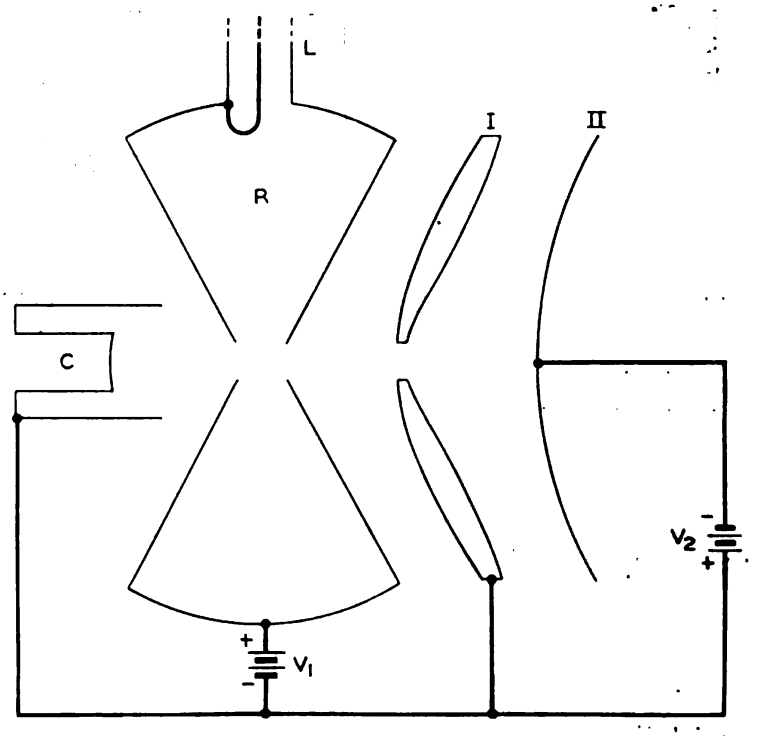

Fig. 138.—Electrodes to achieve approximately the potential variation in the drift region shown in Fig. 7.2.

Digitized by Google
Original from UNIVERSITY OF MICHIGAN
Generated on 2019-09-23 05:18 GMT / http://hdl.handle.net/2027/mdp.39015077775156
Public Domain, Google-digitized / http://www.hathitrust.org/access_use#pd-google

The shapes for electrodes to realize this field may be obtained analytically by known means or experimentally by measurements in a water tank. The general appearance of such electrodes and their embodiment in a reflex oscillator are shown in Fig. 138. Here C is the thermionic cathode forming part of an electron gun which shoots an electron beam through the apertures or gap in a resonator R. The beam is then reflected in the drift field formed by the resonator wall, zero potential electrode I and negative electrode II, which give substantially the axial potential distribution shown in Fig. 137. Small apertures in the resonator wall and in electrode I allow passage of the electron beam without seriously distorting the drift field. Voltage sources V_1 and V_2 maintain the electrodes at proper potentials. Either suitable convergence of the electron beam passing through the resonator from the gun or axial magnetic focusing will assure return of reflected electrons through the resonator aperture. In addition, the aperture in electrode I forms a converging lens which tends to offset the diverging action of the fields existing between the resonator wall and I, and between I and II. R-f power is derived from resonator R by a coupling loop and line L.

APPENDIX VIII

Electronic Gap Loading

If a measurement is made of gap admittance in the presence and in the absence of the electron beam passing across it once, it will be found that the electron stream gives rise to an admittance component Y. The susceptance is unimportant, but the conductance G can have a noticeable effect on the efficiency of an oscillator.

Petrie, Strachey and Wallis have provided an important expression for this gap conductance due to longitudinal fields when the r-f voltage is small compared with the beam voltage V_0.[25] In this analysis it is presumed that the fields in the beam are due to the voltages on the electrodes only and not to the space change in the beam.[26] This analysis is of such importance that it is of interest to reproduce it in a slightly modified form. We will first consider the general cases of interaction with longitudinal fields and will then consider transverse fields also

A. *Longitudinal Field*

Assume a stream of electrons flowing in the positive x direction, constituting a current $-I_0$, bunched to have an a-c convection current component

[25] These expressions were communicated to the writers through unpublished but widely circulated material by D. P. R. Petrie, C. Strachey and P. J. Wallis of Standard Telephones and Cables Valve Laboratory.

[26] The expressions are valid in the presence of space charge, but as the field is not known, they cannot be evaluated.

Digitized by Google
Original from UNIVERSITY OF MICHIGAN
Generated on 2019-09-23 05:19 GMT / http://hdl.handle.net/2027/mdp.39015077775156
Public Domain, Google-digitized / http://www.hathitrust.org/access_use#pd-google

i_1. Now if t_1 is the time a particle passes x_1 and t_2 the time the particle passes x_2, the convection current at x_2 will be

$$i_2 = (-I_0 + i_1)\frac{dt_1}{dt_2} + I_0. \tag{h1}$$

This merely states that the charge which passes x_1 in the time interval dt_1 will pass x_2 in the time interval dt_2. Suppose the electrons are accelerated at x_1 by a voltage

$$Ve^{j\omega t_1}$$

If V_0 is the voltage specifying the average speed of the electrons, the velocity will be

$$v = (2\eta V_0)^{\frac{1}{2}}(1 + (V/V_0)e^{j\omega t_1})^{\frac{1}{2}} \tag{h2}$$

We then have

$$\begin{aligned} t_2 &= t_1 + \tau(1 + (V/V_0)e^{j\omega t_1})^{-\frac{1}{2}} \\ \tau &= x(2\eta V_0)^{-\frac{1}{2}} \end{aligned} \tag{h3}$$

$$\frac{dt_2}{dt_1} = 1 - \frac{j\omega\tau(V/V_0)e^{j\omega t_1}}{2(1 + (V/V_0)e^{j\omega t_1})}. \tag{h4}$$

Now assume $(V/V_0) \ll 1$. If we neglect higher powers than the first we can replace t_1 by

$$t_1 = t_2 - \tau$$

and obtain

$$\frac{dt_1}{dt_2} = 1 + \frac{j\tau V e^{j\omega(t_1-\tau)}}{2V_0} \tag{h5}$$

and from (h1), neglecting products of two a-c quantities

$$i_2 = i_1 - \frac{j\omega\tau I_0}{2V_0} Ve^{j\omega(t_1-\tau)}. \tag{h6}$$

Suppose we consider an electron stream travelling through a longitudinal field of potential fluctuating as $e^{j\omega t}$ and of magnitude $V(x)$, where $V(x)$ may be complex. Then the current at x_2 due to the action of the field at x_1 is, omitting for convenience the factor $e^{j\omega t}$,

$$di_2 = \frac{jI_0 V'(x_1)}{2V_0}\gamma(x_2 - x_1)e^{-j\gamma(x_2-x_1)}\,dx_1 \tag{h7}$$

$$\gamma = \omega/u_0 \tag{h8}$$

$$u_0 = (2\eta V_0)^{\frac{1}{2}}. \tag{h9}$$

Digitized by Google
Original from UNIVERSITY OF MICHIGAN
Generated on 2019-09-23 05:19 GMT / http://hdl.handle.net/2027/mdp.39015077775156
Public Domain, Google-digitized / http://www.hathitrust.org/access_use#pd-google

Hence, the convection current at x_2 is

$$i_2 = \frac{-jI_0}{2V_0} \int_{-\infty}^{x_2} V'(x_1)\gamma(x_2 - x_1)e^{-j\gamma(x_2-x_1)}\,dx_1 . \tag{h10}$$

The power flow *from the electron stream to the circuit* is

$$P = \tfrac{1}{2} \int_{-\infty}^{\infty} V'(x_2)i_2^*\,dx_2 \tag{h11}$$

$$P = \frac{jI_0}{4V_0} \int_{-\infty}^{\infty} \int_{-\infty}^{x_2} V'(x_2)V'^*(x_1)\gamma(x_2 - x_1)e^{j\gamma(x_2-x_1)}\,dx_1\,dx_2 . \tag{h12}$$

We have in (h12) an expression, based on the physics of the picture, for power flow from the electron stream to the circuit. This expression is a product of the electron convection current, due to bunching, and the electric field, and the product is integrated from $x = -\infty$ to $x = +\infty$, which is merely a way of including all the a-c fields present. We could as well have integrated between two points a and b between which all a-c fields lie.

We will now go through some strictly mathematical manipulations of (h12), designed to transform it to a more handy form. In the following steps we may regard x_1 and x_2 as merely two different variables of integration, disregarding completely their physical significance.

Suppose in the x_1 x_2 plane, x_1 is measured + to the right and x_2, + upwards. Then the plane is divided into two portions by the line $x_2 = x_1$, and we are integrating over the upper left portion. If we reverse the order of integration we obtain

$$P = \frac{jI_0}{4V_0} \int_{-\infty}^{\infty} \int_{x_1}^{\infty} V'(x_2)V'^*(x_1)\gamma(x_2 - x_1)e^{j\gamma(x_2-x_1)}\,dx_2\,dx_1 . \tag{h13}$$

Let us (a) interchange the variables of integration x_2 and x_1 and (b) take the conjugate of P. We obtain

$$P^* = \frac{jI_0}{4V_0} \int_{-\infty}^{\infty} \int_{x_2}^{\infty} V'(x_2)V'^*(x_1)\gamma(x_2 - x_1)e^{j\gamma(x_2-x_1)}\,dx_1\,dx_2 . \tag{h14}$$

The real part of P is $\frac{1}{2}(P + P^*)$; hence

$$\text{Real} = \frac{jI_0}{8V_0} \int_{-\infty}^{\infty} \int_{-\infty}^{\infty} V'(x_2)V'^*(x_1)\gamma(x_2 - x_1)e^{j\gamma(x_2-x_1)}\,dx_1\,dx_2 . \tag{h15}$$

Let us consider the quantity

$$A = \int_{-\infty}^{\infty} V'(x)e^{j\gamma x}\,dx \tag{h16}$$

Digitized by Google
Original from UNIVERSITY OF MICHIGAN
Generated on 2019-09-23 05:19 GMT / http://hdl.handle.net/2027/mdp.39015077775156
Public Domain, Google-digitized / http://www.hathitrust.org/access_use#pd-google

$$|A|^2 = AA^* = \left(\int_{-\infty}^{\infty} V'(x_2)e^{j\gamma x_2}\,dx_2\right)\left(\int_{-\infty}^{\infty} V'^*(x_1)e^{-j\gamma x_1}\,dx_1\right)$$
$$= \int_{-\infty}^{\infty}\int_{-\infty}^{\infty} V'(x_2)V'^*(x_1)e^{j\gamma(x_2-x_1)}\,dx_1\,dx_2 \tag{h17}$$

$$\frac{\partial |A|^2}{\partial \gamma} = \frac{j}{\beta}\int_{-\infty}^{\infty}\int_{-\infty}^{\infty} V'(x_2)V'^*(x_1)\gamma(x_2 - x_1)e^{j\gamma(x_2-x_1)}\,dx_1\,dx_2\,. \tag{h18}$$

Hence, we see

$$\text{Real} = \frac{I_0}{8V_0}\,\gamma\,\frac{\partial |A|^2}{\partial \gamma}\,. \tag{h19}$$

B. *Transverse Field*

Suppose we consider the additional power transfer because of deflections. There will be two sources of energy transfer. First, imagine a fluctuating y component of velocity, $\dot{y}$. Let u_0 be the x component of velocity and $-I_0$ the convection current to the right. In a distance dx this will flow against the potential gradient in the y direction a distance

$$dy = (\dot{y}/u_0)dx \tag{h20}$$

and the power flowing to the field from the beam will be

$$dP = -\frac{I_0}{2}\frac{\partial V}{\partial y}\,(\dot{y}^*/u_0)\,dx. \tag{h21}$$

This is not the total power transfer, however. The beam will also suffer a displacement y in the y direction. Now the x component of field varies with displacement; hence the beam will encounter a varying field. We can write the instantaneous power transferred from the beam to the field. Let $(V)_i$ be the instantaneous value of V and $(y)_i$ be the instantaneous value of y. The instantaneous power will be

$$dp = -I_0\left(\frac{d(V)_i}{dx} + \frac{\partial^2(V)_i}{\partial x \partial y}\,(y)_i\right)dx. \tag{h22}$$

Let us compare this with the instantaneous power transferred from the beam to the field by a fluctuating convection current $(i)_i$

$$dp = \frac{\partial(V)_i}{\partial x}\,(i)_i\,. \tag{h23}$$

We see that according to our convention that

$$P = VI^* \tag{h24}$$

Digitized by Google
Original from UNIVERSITY OF MICHIGAN
Generated on 2019-09-23 05:19 GMT / http://hdl.handle.net/2027/mdp.39015077775156
Public Domain, Google-digitized / http://www.hathitrust.org/access_use#pd-google

we may write, from (h22)

$$dP = -\frac{I_0}{2}\frac{\partial^2 V}{\partial x\,\partial y}\,y^*\,dx. \tag{h25}$$

The y gradient of the potential at x_1 produces a velocity at x_2

$$\dot{y}_2 = \frac{\eta}{u_0}\int_{-\infty}^{x_2}\left(\frac{\partial V}{\partial y}\right)_1 e^{-j\gamma(x_2-x_1)}\,dx_1\,. \tag{h26}$$

It produces a displacement at x_2

$$y_2 = \frac{\eta}{u_0^2}\int_{-\infty}^{x_2}\left(\frac{\partial V}{\partial y}\right)_1 (x_2 - x_1)e^{-j\gamma(x_2-x_1)}\,dx_1\,. \tag{h27}$$

Writing the total power as

$$P = P_1 + P_2\,. \tag{h28}$$

We have the two contributions from (h22) and (h23) using (h9)

$$P_1 = \frac{-I_0}{4V_0}\int_{-\infty}^{\infty}\int_{-\infty}^{x_2}\left(\frac{\partial V}{\partial y}\right)_2\left(\frac{\partial V}{\partial y}\right)_1^* e^{j\gamma(x_2-x_1)}\,dx_1\,dx_2 \tag{h29}$$

and

$$P_2 = \frac{-I_0}{4V_0}\int_{-\infty}^{\infty}\int_{-\infty}^{x_2}\left(\frac{\partial^2 V}{\partial x\,\partial y}\right)_2\left(\frac{\partial V}{\partial y}\right)_1^* (x_2 - x_1)e^{j\gamma(x_2-x_1)}\,dx_1\,dx_2\,. \tag{h30}$$

Again, we will turn to mathematical manipulation disregarding the physical significance of the variables. If we change the order of integration, (h30) becomes

$$P_2 = \frac{-I_0}{4V_0}\int_{-\infty}^{\infty}\int_{x_1}^{\infty}\left(\frac{\partial^2 V}{\partial x\,\partial y}\right)_2\left(\frac{\partial V}{\partial y}\right)_1 (x_2 - x_1)e^{j\gamma(x_2-x_1)}\,dx_2\,dx_1\,. \tag{h31}$$

Integrating with respect to x_2 by parts we obtain

$$\begin{aligned} P_2 = -\frac{I_0}{4V_0}\Bigg(&\int_{-\infty}^{\infty}\left(\frac{\partial V}{\partial y}\right)_2\left(\frac{\partial V}{\partial y}\right)_1^* (x_2 - x_1)e^{j\gamma(x_2-x_1)}\,dx_1\Bigg|_{x_1}^{\infty} \\ &- j\int_{-\infty}^{\infty}\int_{x_1}^{\infty}\left(\frac{\partial V}{\partial y}\right)_2\left(\frac{\partial V}{\partial y}\right)_1^* \gamma(x_2 - x_1)e^{j\gamma(x_2-x_1)}\,dx_2\,dx_1 \\ &- \int_{-\infty}^{\infty}\int_{x_1}^{\infty}\left(\frac{\partial V}{\partial y}\right)_2\left(\frac{\partial V}{\partial y}\right)_1^* e^{j\gamma(x_2-x_1)}\,dx_2\,dx_1\Bigg). \end{aligned} \tag{h32}$$

The first term is zero because $\left(\frac{\partial V}{\partial y}\right)^*$ is zero at $x_1 = -\infty$ and $(x_2 - x_1)$ is

Digitized by Google
Original from UNIVERSITY OF MICHIGAN
Generated on 2019-09-23 05:19 GMT / http://hdl.handle.net/2027/mdp.39015077775156
Public Domain, Google-digitized / http://www.hathitrust.org/access_use#pd-google

zero at $x_2 = x_1$. Changing the order of integration, we obtain

$$P_2 = +j\frac{I_0}{4V_0}\int_{-\infty}^{\infty}\int_{-\infty}^{x_2}\left(\frac{\partial V}{\partial y}\right)_2\left(\frac{\partial V}{\partial y}\right)_1^*\gamma(x_2 - x_1)e^{j\gamma(x_2-x_1)}\,dx_1\,dx_2 + \frac{I_0}{4V_0}\int_{-\infty}^{\infty}\int_{-\infty}^{x_2}\left(\frac{\partial V}{\partial y}\right)_2\left(\frac{\partial V}{\partial y}\right)_1^* e^{j\gamma(x_2-x_1)}\,dx_1\,dx_2. \tag{h33}$$

From (h29) and (h30) we see that the total power is

$$P = j\frac{I_0}{4V_0}\int_{-\infty}^{\infty}\int_{-\infty}^{x_2}\left(\frac{\partial V}{\partial y}\right)_2\left(\frac{\partial V}{\partial y}\right)_1^*\gamma(x_2 - x_1)e^{j\gamma(x_2-x_1)}\,dx_1\,dx_2. \tag{h34}$$

By the same means resorted to in connection with (h12) we find

$$\text{Real} = \frac{I_0}{8V_0}\gamma\frac{\partial\,|B|^2}{\partial\gamma} \tag{h35}$$

$$B = \int_{-\infty}^{\infty}\frac{\partial V}{\partial y}e^{j\gamma x}\,dx. \tag{h36}$$

We can go a step further. We have

$$A = \int_{-\infty}^{\infty}\frac{\partial V}{\partial x}e^{j\gamma x}\,dx. \tag{h37}$$

Now

$$\frac{\partial A}{\partial y} = \int_{-\infty}^{\infty}\frac{\partial^2 V}{\partial x\partial y}e^{j\gamma x}\,dx. \tag{h38}$$

Integrating by parts

$$\frac{\partial A}{\partial y} = \frac{\partial V}{\partial y}e^{j\gamma x}\Big|_{-\infty}^{\infty} - j\gamma\int_{-\infty}^{\infty}\frac{\partial V}{\partial y}e^{j\gamma x}\,dx. \tag{h39}$$

The first term is zero, and we see that

$$|B|^2 = (|\partial A/\partial y|^2/\gamma^2) \tag{h40}$$

$$\text{Real} = \frac{I_0}{8V_0}\gamma\frac{\partial(|\partial A/\partial y|^2/\gamma^2)}{\partial\gamma}. \tag{h41}$$

C. *Electronic Gap Loading*

In (h19) and (h41) we have expressed the power flow from the electron stream to the circuit in rather general terms. What we want immediately is the quantity (conductance) giving the power flow from the circuit to the stream for a single gap. Assume we have a single gap with unit peak r-f voltage across it. The power absorbed by the electron stream can be

Digitized by Google
Original from UNIVERSITY OF MICHIGAN
Generated on 2019-09-23 05:20 GMT / http://hdl.handle.net/2027/mdp.39015077775156
Public Domain, Google-digitized / http://www.hathitrust.org/access_use#pd-google

attributed to a shunt conductance such that

$$P_R = GV^2/2 = G/2$$
$$G = 2P_R . \tag{h42}$$

Also, in this case $|A|$ is simply β, the modulation coefficient. Hence, the conductance due to action of the longitudinal fields is, from (h18), simply

$$G_1 = \frac{-I_0\gamma}{4V_0}\frac{\partial\beta^2}{\partial\gamma}. \tag{h43}$$

And, due to the action of transverse fields there is another conductance, from (h41)

$$G_2 = -\frac{I_0\gamma}{4V_0}\frac{\partial}{\partial\gamma}\left(\frac{1}{\gamma^2}\left(\frac{\partial\beta}{\partial y}\right)^2\right) \tag{h44}$$

$$G = G_1 + G_2 . \tag{h45}$$

These are surprisingly simple and very useful relations.

It is interesting to take an example which will indicate both effects. We have from (b24) for tubes of radius r_0 with a narrow gap between them

$$\beta_s^2 = \beta_r^2[1 - I_1^2(\gamma r_0)/I_0^2(\gamma r_0)]. \tag{h46}$$

Accordingly, the part of the conductance due to the longitudinal field is

$$G_L = F_L(\gamma r_0)I_0/4V_0 \tag{h47}$$

$$F_L(\gamma r_0) = -\gamma\partial\beta_s^2/\partial\gamma$$
$$= -2\left[\left(\frac{I_1(\gamma r_0)}{I_0(\gamma r_0)}\right)^2 - \gamma r_0\left(\frac{I_1(\gamma r_0)}{I_0(\gamma r_0)}\right) - \left(\frac{I_1(\gamma r_0)}{I_0(\gamma r_0)}\right)^2\right]. \tag{h48}$$

Similarly, the part of the conductance due to the transverse field is

$$G_T = F_T(\gamma r_0)I_0/4V_0 \tag{h49}$$

$$F_T(\gamma r_0) = -\gamma\frac{\partial}{\partial\gamma}\frac{1}{r_0^2}\int_0^{r_0}\left(\frac{1}{\gamma}\frac{\partial}{\partial r}\beta_r\right)^2 2r\,dr. \tag{h50}$$

From (b16) we obtain

$$\beta_r = I_0(\gamma r)/I_0(\gamma r_0) \tag{h51}$$

$$\frac{1}{\gamma}\frac{\partial\beta_r}{\partial r} = I_1(\gamma r)/I_0(\gamma r_0)\,\frac{1}{r_0^2}\int_0^{r_0}\left(\frac{1}{\gamma}\frac{\partial}{\partial r}\beta r\right)^2 2r\,dr$$
$$= \left[\frac{I_2(\gamma r_0)}{I_0(\gamma r_0)} - \frac{I_1^2(\gamma r_0)}{I_0^2(\gamma r_0)}\right]. \tag{h52}$$

Digitized by Google
Original from UNIVERSITY OF MICHIGAN
Generated on 2019-09-23 05:20 GMT / http://hdl.handle.net/2027/mdp.39015077775156
Public Domain, Google-digitized / http://www.hathitrust.org/access_use#pd-google

And from this we obtain

$$F(\gamma r_0) = -2\left[1 - \frac{2I_1(\gamma r_0)}{\gamma r_0 I_0(\gamma r_0)} + \gamma r_0\left(\frac{I_1(\gamma r_0)}{I_0(\gamma r_0)}\right) - \left(\frac{I_1(\gamma r_0)}{I_0(\gamma r_0)}\right)^3 - 2\left(\frac{I_1(\gamma r_0)}{I_0(\gamma r_0)}\right)^2\right]. \quad \text{(h53)}$$

The total conductance is

$$G = G_1 + G_2 = (F_L(\gamma r_0) + F_T(\gamma r_0))I_0/4V_0. \quad \text{(h54)}$$

In Fig. 139, (G_1V_0/I_0), (G_2V_0/I_0) and (GV_0/I_0) are plotted vs γr_0. It may be seen that while the conductance due to transverse fields may be negative, the total conductance is always positive.

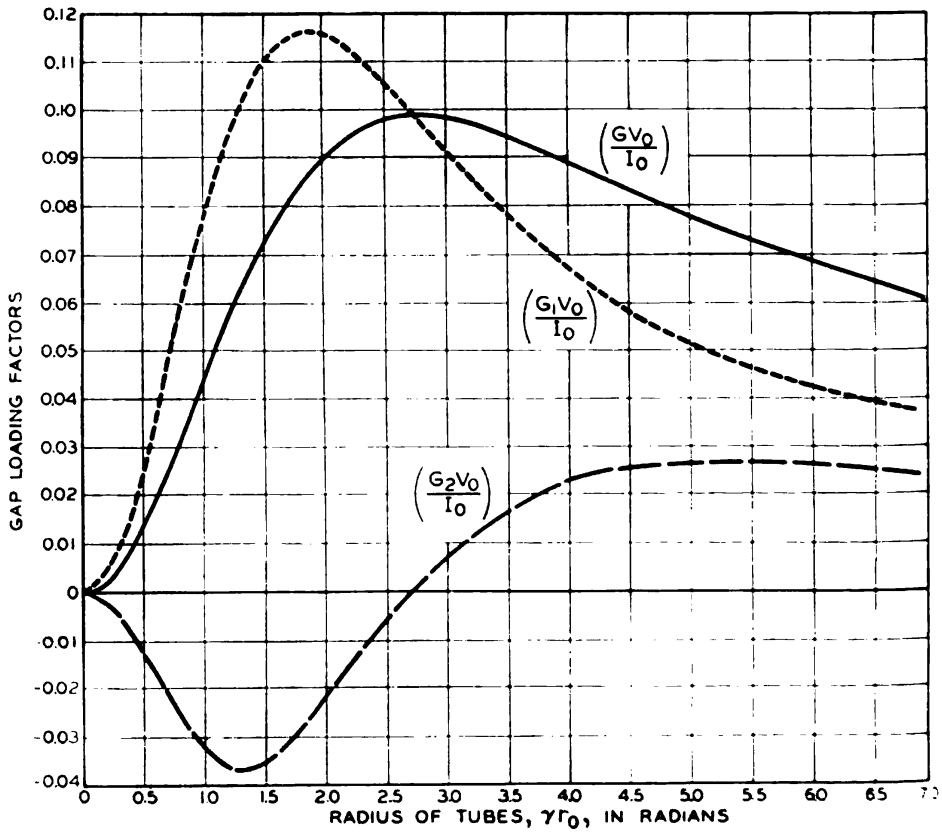

Fig. 139.—Gap loading factor vs radius of tubes forming gap measured in radians. The tubes are supposed to be filled with uniform electron flow. The curve involving G_1 is that for longitudinal effects, that involving G_2 is for transverse effects, and that involving G is for both combined.

This example tends to exaggerate the effects of transverse fields because the beam is assumed to fill the whole tube. In an actual case the beam

Digitized by Google
Original from UNIVERSITY OF MICHIGAN
Generated on 2019-09-23 05:20 GMT / http://hdl.handle.net/2027/mdp.39015077775156
Public Domain, Google-digitized / http://www.hathitrust.org/access_use#pd-google

would probably not fill the whole tube, and the effect of transverse fields would be less.

Perhaps a more useful expression is one involving longitudinal fields only; that for infinitely fine parallel grids. In this case, if the separation is ℓ

$$\beta^2 = \sin^2 (\gamma\ell/2)/(\gamma\ell/2)^2 \tag{h55}$$

and, from (h43)

$$G = \frac{I_0}{2V_0} \frac{\sin (\gamma\ell/2)}{(\gamma\ell/2)} \left[\frac{\sin (\gamma\ell/2)}{(\gamma\ell/2)} - \cos (\gamma\ell/2) \right]. \tag{h56}$$

In Fig. 140, (GV_0/I_0) is plotted vs $(\gamma\ell/2)$. The negative conductance region beyond $\gamma\ell = 2\pi$, familiar through Llewellyn's work with diode oscillators, is of less interest in connection with reflex oscillators.

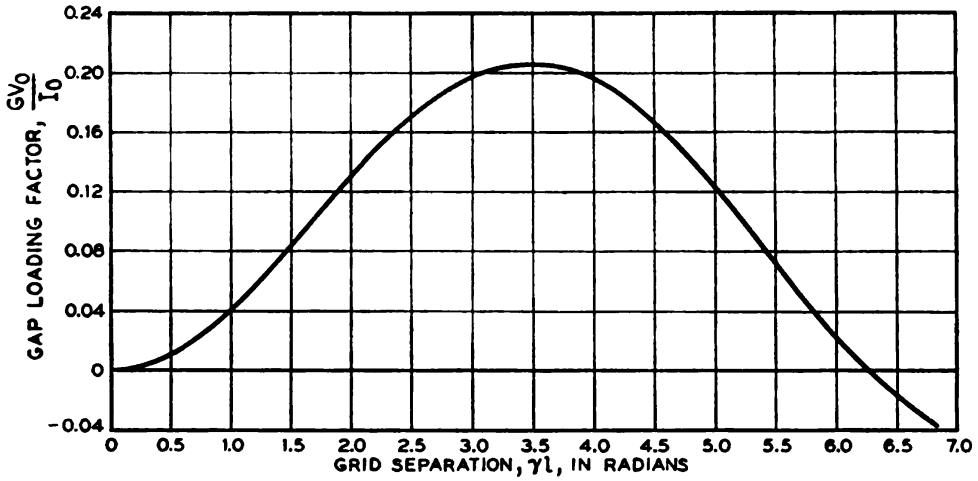

Fig. 140.—Gap loading factor for fine parallel grids vs grid separation in radians.

It is of some interest to compare the electronic gap loading with the small signal electronic conductance due to drift action. Assume, for instance, we have fine parallel plane grids for which $\gamma\ell = \pi$. From (h2) we get

$$(GV_0/I_0) = .202.$$

As the current crosses the gap twice we should count the current involved as twice the d-c beam current I_b

$$G = .404\, I_b/V_0\,.$$

From (2.1)

$$\beta = .633$$

$$\beta^2 = .400.$$

Digitized by Google
Original from UNIVERSITY OF MICHIGAN
Generated on 2019-09-23 05:20 GMT / http://hdl.handle.net/2027/mdp.39015077775156
Public Domain, Google-digitized / http://www.hathitrust.org/access_use#pd-google

If we assume 3.75 cycles of drift, then from (2.4) the magnitude of the small signal electronic admittance is

$$y_e = \beta^2 I_0 \theta / 2V_0 \qquad \text{(h57)}$$
$$= 4.71\, I_0/V_0 .$$

Thus, in this example, the gap loading is about 1/10 of the small signal electronic admittance.

D. *Bunching in the Gap*

An unbunched stream will become bunched due to a single transit across an excited gap. Expression (h10) gives us a means for calculating the extent of this bunching. As an example, we will consider the case of fine parallel grids separated by a distance ℓ. Then the gradient is given by

$$V'(x_1) = V/\ell \qquad \text{(h58)}$$

from $x_1 = 0$ to $x_1 = x_2 = \ell$, and by zero elsewhere. Thus

$$i_2 = \frac{jI_0 V}{2V_0 \ell} \int_0^\ell \gamma(\ell - x_1) e^{-j\gamma(\ell - x_1)}\, dx_1$$

$$i_2/V = (I_0/V_0)(1/2)[1 - (j/\gamma\ell)(1 - e^{j\gamma\ell})]e^{-j\gamma\ell}. \qquad \text{(h59)}$$

It should be noted that for large values of $\gamma\ell$

$$i_2/V = (1/2)(I_0/V_0)e^{-j\gamma\ell}. \qquad \text{(h60)}$$

For our previous example, if $\gamma\ell = \pi$,

$$i_2/V = .592\ (I_0/V_0)e^{-j3.53}. \qquad \text{(h61)}$$

If the current is referred to the center of the gap instead of the second grid, we obtain a current i such that

$$i/V = .592\ (I_0/V_0)e^{-j1.96}. \qquad \text{(h62)}$$

Now, the electrons constituting current i will drift 3.75 cycles and will return across the gap in the opposite direction. To get the induced circuit current I we take this into account and multiply by β

$$I/V = -\beta(i/V)e^{-j\pi(3.75)}$$
$$= -.375(I_0/V_0)e^{-j19\pi}. \qquad \text{(h63)}$$

This is very nearly of the same size as the electronic gap loading.

The general conclusion seems to be that for typical conditions encountered in reflex oscillators, gap loading and bunching in the gap are small and probably less important than various errors in the theory.

Generated on 2019-09-23 05:20 GMT / http://hdl.handle.net/2027/mdp.39015077775156
Public Domain, Google-digitized / http://www.hathitrust.org/access_use#pd-google
Digitized by Google
Original from UNIVERSITY OF MICHIGAN

APPENDIX IX

Losses in Grids

Although the general problem of resonator loss calculation is not treated in this paper, grids seem peculiar to vacuum tubes and losses in grids will be discussed briefly.

Assume that we have a pair of grids of some mesh or network material, parallel, circular, and of a diameter compared with the wavelength small enough so that variation of voltage over the grids may be neglected. The capacitance inside of a radius r is

$$\begin{aligned} C &= \epsilon\pi r^2/d \\ \epsilon &= 8.85 \times 10^{-14} \text{ farads/cm.} \end{aligned} \tag{i1}$$

Here d is the separation between the grids. For unit r.m.s. voltage across the grids, the power dissipated in the part of both grids lying in the range dr at r is

$$\begin{aligned} dP &= 2(\omega C)^2(R\,dr/2\pi r) \\ &= \omega^2\epsilon^2\pi R r^3\,dr/d^2. \end{aligned} \tag{i2}$$

Here R is the surface resistivity. The total power is equal to V^2G, where G is the conductance measured at the edge of the grids, and is

$$\begin{aligned} G = P &= \frac{\omega^2\epsilon^2\pi R}{d^2}\int_0^{D/2} r^3\,dr \\ &= \omega^2\epsilon^2\pi R D^4/64\,d^2. \end{aligned} \tag{i3}$$

It is interesting to express ω in terms of λ, the wavelength, c the velocity of light, and then to put in numerical values

$$G = (1/16)\pi^2c^2\epsilon^2RD^4/\lambda^2\,d^2 \tag{i4}$$

$$G = 1.39 \times 10^{-5}RD^4/\lambda^2\,d^2. \tag{i5}$$

Now for the copper, the surface resistivity is

$$R_c = .045/\sqrt{\lambda} \tag{i6}$$

where λ is measured in cm. Suppose the grid material is non-magnetic and has N times the low frequency resistivity of copper. Then for it, the surface resistivity will be $N^{\frac{1}{2}}$ times that given by (i6). Suppose that the diameter of the grid wires is $2r$ and the distance center to center is a. If current flowed on one half of the wire surface only, the surface resistivity parallel to the wires would be

$$R = N^{\frac{1}{2}}R_c(a/\pi r). \tag{i7}$$

Digitized by Google
Original from UNIVERSITY OF MICHIGAN
Generated on 2019-09-23 05:21 GMT / http://hdl.handle.net/2027/mdp.39015077775156
Public Domain, Google-digitized / http://www.hathitrust.org/access_use#pd-google

If we use this as the surface resistivity in (i5) we obtain

$$G = 1.99 \times 10^{-7} \left(\frac{a}{r}\right) \sqrt{N/\lambda}/D^4\lambda^2 d^2. \tag{i8}$$

It is a somewhat remarkable fact that if we work out the loss for a pair of grids with surface resistivity R in one direction and infinite resistivity in the other direction (parallel wire grids) we get just twice the conductance given by (i5). Thus, it appears to be roughly true that if we have a given parallel wire grid, adding wires between the original wires and adding wires perpendicular to the original wires should have about the same effect in reducing circuit loss.

APPENDIX X

Starting of Pulsed Reflex Oscillator

If a reflex oscillator is turned on gradually, the voltage from which the oscillations build up is certainly that due to shot noise in the electron stream. However, if the current is turned on as a pulse of short time of rise, it might be that the microwave voltage produced by the high frequency components of the pulse would be larger than the voltage produced by shot noise, and hence that oscillations would build up from the transient produced by the pulse and not from shot noise. This would be important because presumably the voltages produced by the pulse are always the same and related in the same manner to the time of application of the pulse; thus, in buildup from the transient of the pulse there would be no jitter.

In an effort to decide from which voltage the oscillations build up, we will consider Johnson noise and shot noise voltages.

Associated with a mode of oscillation of the resonator there is a mean stored energy kT. If L and C are the effective inductance and capacitance of the mode and $\overline{I^2}$ and $\overline{V^2}$ are the mean square current and voltage

$$kT = \overline{I^2}L/2 + \overline{V^2}C/2. \tag{j1}$$

On the average, half of the energy is in the capacitance and half in the inductance; thus

$$\begin{aligned} \overline{V^2} &= kT/C \\ &= kT\omega_0/M. \end{aligned} \tag{j2}$$

Here M is the characteristic admittance of the mode and ω_0 is the resonant radian frequency.

As an equivalent circuit for the mode we may use conductance G in shunt with an inductance L and a capacitance C. The impressed Johnson noise

Digitized by Google
Original from UNIVERSITY OF MICHIGAN
Generated on 2019-09-23 05:21 GMT / http://hdl.handle.net/2027/mdp.39015077775156
Public Domain, Google-digitized / http://www.hathitrust.org/access_use#pd-google

current for a bandwidth B is

$$\overline{I_t^2} = 4kTGB. \tag{j3}$$

Suppose the current crossing the gap is $2I_0$ (a current I_0 with two transits). If the current has full shot noise (no space charge reduction of noise) the impressed shot noise current per unit bandwidth will be

$$\begin{aligned} \overline{I_s^2} &= 2e(2I_0)B \\ &= 4eI_0B. \end{aligned} \tag{j4}$$

Thus, we see that the shot noise voltage will be the Johnson noise voltage times the factor

$$\begin{aligned} \overline{I_s^2} &= \frac{e}{kT}\frac{I_0}{G} \\ &= \frac{11{,}600}{T}\frac{I_0}{G}. \end{aligned} \tag{j5}$$

The conductance G is given by

$$G = M/Q.$$

Let us take reasonable values,

$$\begin{aligned} T &= 293^\circ \text{ K } (20^\circ \text{ C}) \\ I_0 &= .2 \text{ amperes} \\ M &= .06 \text{ mhos} \\ Q &= 400 \text{ (loaded } Q\text{)}. \end{aligned}$$

The values of M and Q are about right for the 2K23 pulsed reflex oscillator. We obtain

$$\frac{\overline{I_s^2}}{\overline{I_t^2}} = 5.3 \times 10^4. \tag{j6}$$

Thus, shot noise is very much more important than Johnson noise.

From (j2) and (j5) we see that the shot noise voltage squared may be expressed as

$$\overline{V_s^2} = \frac{e\omega_0 I_0 Q}{M^2}. \tag{j7}$$

In pulsing a reflex oscillator, the voltage and current will be raised simultaneously; however for the sake of simplicity in calculation, we will assume that the voltage is constant and the injected current is zero at $t = 0$, rises

Digitized by Google
Original from UNIVERSITY OF MICHIGAN
Generated on 2019-09-23 05:21 GMT / http://hdl.handle.net/2027/mdp.39015077775156
Public Domain, Google-digitized / http://www.hathitrust.org/access_use#pd-google

linearly with time to a value I_0 at a time Δt, and remains constant thereafter. There will be a return current across the gap, the negative of the injected current and delayed by the drift time τ with respect to the injected current.

In calculating the response to this applied current, loaded Q will be assumed to be infinite; actually, the shunt resistance will be positive when the current is small and negative when the current becomes large enough so that the electronic conductance is larger in magnitude than the circuit conductance. The assumption of zero conductance should, however, give us an idea of the transient which would be effective in starting the oscillator.

If a charge dq is put onto a capacitance $C = M/\omega_0$ forming part of a resonant circuit of frequency ω_0, the subsequent voltage across the circuit will be

$$dV = \frac{\omega_0}{M} e^{j\omega_0 t}\, dq. \tag{j8}$$

We see that for times late enough so that the injected and returned current are both constant, the voltage due to our assumed current will be

$$V = \frac{\omega_0}{M} I_0 \left(\int_0^{\Delta t} \frac{t_0}{\Delta t} e^{j\omega(t-t_0)}\, dt_0 + \int_{\Delta t}^{t} e^{j\omega(t-t_0)}\, dt_0 - \int_{\tau}^{\tau+\Delta t} \frac{t_0 - \tau}{\Delta t} e^{j\omega(t-t_0)}\, dt_0 - \int_{\tau+\Delta t}^{t} e^{j\omega(t-t_0)}\, dt_0 \right). \tag{j9}$$

Integrating, we find

$$V = \left(\frac{I_0}{M \Delta t\, \omega_0} \right) (1 - e^{-j\omega_0 \tau})(e^{-j\omega_0 \Delta t} - 1). \tag{j10}$$

If we have $n + 3/4$ cycle drift,

$$e^{-j\omega_0 \tau} = -j. \tag{j11}$$

The extreme value of $(e^{-j_0 \omega \Delta t} - 1)$ is -2. For this value we would obtain

$$|V|^2 = \frac{2I_0^2}{M^2 \Delta t^2 \omega_0^2}. \tag{j12}$$

From this and (j7) we obtain

$$\frac{\overline{V_s^2}}{|V|^2} = \frac{eQ\Delta t^2 \omega_0^3}{2I_0}. \tag{j13}$$

Taking the values

$$e = 1.59 \times 10^{-19} \text{ coulombs}$$
$$I_0 = .2 \text{ amperes}$$
$$Q = 400 \text{ (loaded } Q\text{)}$$
$$\Delta t = .2 \times 10^{-6} \text{ seconds}$$
$$\omega_0 = 25 \times 10^9 \text{ radians/second.}$$

Digitized by Google
Original from UNIVERSITY OF MICHIGAN
Generated on 2019-09-23 05:21 GMT / http://hdl.handle.net/2027/mdp.39015077775156
Public Domain, Google-digitized / http://www.hathitrust.org/access_use#pd-google

We obtain

$$\frac{\overline{V_s^2}}{|\overline{V}|^2} = 99.2. \tag{j14}$$

The indications are that oscillations will built up from shot noise rather than from the high frequency transients induced by the pulse.

The preceding analysis assumes that the full shot noise voltage will appear across the resonator soon enough to override the pulse. The shot noise voltage will reach full amplitude in a time after application of the current of the order of $Q/f_0 = 2\pi Q/\omega_0$. For the values given above

$$2\pi Q/\omega_0 = .05 \times 10^{-6}$$

as this is a considerably smaller time than the .2 microseconds allotted for the buildup of the pulse, the assumption of full shot noise voltage is presumably fairly accurate.

APPENDIX XI

Thermal Tuning

Two extreme conditions may exist

(1) Cooling is by radiation alone

(2) Cooling is by conduction alone.

(1) *Radiation Cooling*

The rate of change of temperature on heating will be given by

$$\frac{dT}{dt} = \frac{1}{C}[P_i - KT^4]. \tag{k1}$$

Where

T is the absolute temperature of the expanding element.

C is the heat capacity of the element.

K is the radiation loss in watts/(degree Kelvin)^4.

P_i is the power input to the tuner in watts.

It is assumed that the temperature of the surroundings is constant and the power radiated to the expanding element is included in P_i. Let

$$P_i = KT_e^4 \quad \text{and} \quad T_r = \frac{T}{T_e}. \tag{k2}$$

T_r is then a reduced temperature since T_e is the temperature which the expanding element would reach at equilibrium for a given power input, i.e $T_e = \left(\frac{P_i}{K}\right)^{1/4}$. T_r is then always less than 1.

Digitized by Google
Original from UNIVERSITY OF MICHIGAN
Generated on 2019-09-23 05:21 GMT / http://hdl.handle.net/2027/mdp.39015077775156
Public Domain, Google-digitized / http://www.hathitrust.org/access_use#pd-google

Upon substitution of ($k2$) in ($k1$)

$$\frac{dT_r}{dt} = \frac{K}{C} T_e^3[1 - T_r^4] \tag{k3}$$

which may be integrated to

$$\frac{C}{2KT_e^3} [\tan^{-1} T_r + \tanh^{-1} T_r] = t + t_0 \tag{k4}$$

where t_0 is a constant of integration. Let

$$F_1(T_r) = [\tan^{-1}T_r + \tanh^{-1}T_r]. \tag{k5}$$

This function is plotted in Fig. 79. In order to determine the cycling time for heating τ_h assume

At	$t = 0,$	$T_r = T_{rc}$	i.e. $T_{rc} = T_c/T_m$
	$t = \tau_h,$	$T_r = T_{rh}$	$T_{rh} = T_h/T_m$

where

T_m is the value of the temperature T_e corresponding to the maximum power input P_m.
T_h is the temperature corresponding to one band limit.
T_c is the temperature corresponding to the other band limit.
$T_h > T_c$.

The cycling time for heating τ_h is then

$$\tau_h = \frac{C}{2KT_m^3} [\tan^{-1} T_{rh} - \tan^{-1} T_{rc} + \tanh^{-1} T_{rh} - \tanh^{-1} T_{rc}] \tag{k6}$$

$$= \frac{C}{2KT_m^3} [F_1(T_{rh}) - F_1(T_{rc})] \tag{k7}$$

which gives the time required for the expanding element to rise in temperature from T_{rc} to T_{rh}, i.e. from T_c to T_h.

If we reduce the power input and wish to determine the cooling time the analysis is similar. If the power input from electron bombardment is reduced to zero there will still be power input to the tuner. The residual power which is kept to the minimum possible level comes from such sources as heat radiated from the cathode and general heating of the envelope by the oscillator section.

Let P_0 be the value of the reduced power input.

Digitized by Google
Original from UNIVERSITY OF MICHIGAN
Generated on 2019-09-23 05:22 GMT / http://hdl.handle.net/2027/mdp.39015077775156
Public Domain, Google-digitized / http://www.hathitrust.org/access_use#pd-google

Then $$-\frac{dT}{dt} = \frac{1}{C}(KT^4 - P_0) \tag{k8}$$

or $$\frac{dT_s}{dt} = -\frac{K}{C}T_0^3(T_s^4 - 1). \tag{k9}$$

Here $$T_s = \frac{T}{T_0} \quad \text{and} \quad P_0 = KT_0^4 \tag{k10}$$

where P_0 is the power from other sources than direct bombardment. In this case T_s is always greater than 1.
Integration yields

$$\frac{C}{2KT_0^3}[\tan^{-1} T_s + \operatorname{ctnh}^{-1} T_s] = t + t_0 . \tag{k11}$$

Let $$F_2(T_s) = [\tan^{-1}T_s + \operatorname{ctnh}^{-1}T_s]. \tag{k12}$$

This function is plotted in Fig. 80. To determine the cycling time for cooling assume

At time $t = 0$, $T_s = T_{sh}$ i.e. $T_{sh} = T_h/T_0$

$t = \tau_C$, $T_s = T_{sc}$ $T_{sc} = T_c/T_0$.

Then $$\tau_C = \frac{C}{2KT_0^3}[F_2(T_{sc}) - F_2(T_{sh})] \tag{k13}$$

giving the time for the contracting element to cool from temperature T_{sh} to T_{sc}; i.e. from T_h to T_c .

(2) *Conduction Cooling*

The rate of change of temperature on heating will be given by

$$\frac{dT}{dt} = \frac{1}{C}(P_i - kT) \tag{k14}$$

where

T is the temperature difference between the tuning strut and the heat sink.
C is the heat capacity of the strut.
k is the conduction loss in watts/°C.
P_i is the power into the tuner.

The solution of (k14) is then,

$$\frac{P_i}{k} - T = \left(\frac{P_i}{k} - T_0\right)e^{-(k/C)t} \tag{k15}$$

Digitized by Google
Original from UNIVERSITY OF MICHIGAN
Generated on 2019-09-23 05:22 GMT / http://hdl.handle.net/2027/mdp.39015077775156
Public Domain, Google-digitized / http://www.hathitrust.org/access_use#pd-google

where T_0 is the temperature difference at $t = 0$.

If

the temperature difference from the sink is $T_0 = T_c$ at the cooler limit of the band.

T_h is the temperature difference from the sink at the hotter limit of the band.

P_m is the maximum permitted input, then the cycling time for heating

$$\tau_h = \frac{C}{k} \log_e \frac{P_m - kT_c}{P_m - kT_h}. \tag{k16}$$

On cooling

$$\frac{dT}{dt} = -\frac{k}{C} t \tag{k17}$$

from which

$$T = T_0 e^{-(k/C)t} \tag{k18}$$

$$\tau_c = \frac{C}{k} \log_e \frac{T_h}{T_c}. \tag{k19}$$

Acknowledgments

A large number of people have contributed to the work described in this paper. The program was carried on under the general direction of J. R. Wilson whose support and advice are gratefully acknowledged. J. O. McNally gave more specific direction to these efforts and is responsible for many of the design features. We are greatly indebted to him for his close support and encouragement.

Members of the Bell Laboratories technical staff concerned with various portions of the developments were E. M. Boone, K. Cadmus, R. Hanson, C. A. Hedberg, P. Kusch, C. G. Matland, H. E. Mendenhall, R. M. Ryder and R. C. Winans. R. S. Gormley of the Western Electric Company made considerable contributions to the work on the 2K25.

The mechanical design, construction and specifications for manufacture were carried out by a group of engineers under the direction of V. L. Ronci. This group included D. P. Barry, F. H. Best, S. O. Ekstrand, G. B. Gucker. C. Maggs, W. D. Stratton, R. L. Vance and E. J. Walsh. L. A. Wooten and his associates cooperated in numerous chemical problems throughout this work.

The authors wish to make particular acknowledgement of the work of two technical assistants, Miss Z. Marblestone and F. P. Dreschler, whose

Generated on 2019-09-23 05:22 GMT / http://hdl.handle.net/2027/mdp.39015077775156
Public Domain, Google-digitized / http://www.hathitrust.org/access_use#pd-google
Digitized by Google
Original from UNIVERSITY OF MICHIGAN

diligent and painstaking efforts were a direct contribution to the successful completion of most of the designs described herein.

The NDRC Radiation Laboratories at the Massachusetts Institute of Technology extended very close cooperation both on problems of design and applications of the tubes. A. G. Hill and J. B. H. Kuper were particularly helpful with technical advice and support. H. V. Neher was responsible for the initial design of the 2K50 and assisted on its final development at the Bell Laboratories. G. Hobart assisted on the 2K50 at M.I.T. and also on the final development as a resident at Bell Laboratories.

Professor R. D. Mindlin on leave from Columbia University served as a consultant on vibration and stress analysis problems particularly on the design of diaphragms and mechanical and thermal tuning mechanisms.

In the preparation of the manuscript the authors are particularly indebted to R. M. Ryder for his extension of the simple bunching theory which is included as a part of this paper. L. A. MacColl provided the solution for several mathematical problems.

Generated on 2019-09-23 05:22 GMT / http://hdl.handle.net/2027/mdp.39015077775156
Public Domain, Google-digitized / http://www.hathitrust.org/access_use#pd-google
Digitized by Google
Original from UNIVERSITY OF MICHIGAN

Development of Silicon Crystal Rectifiers for Microwave Radar Receivers

By J. H. SCAFF and R. S. OHL

Introduction

TO THOSE not familiar with the design of microwave radars the extensive war use of recently developed crystal rectifiers[1] in radar receiver frequency converters may be surprising. In the renaissance of this once familiar component of early radio receiving sets there have been developments in materials, processes, and structural design leading to vastly improved converters through greater sensitivity, stability, and ruggedness of the rectifier unit. As a result of these developments a series of crystal rectifiers was engineered for production in large quantities to the exacting electrical specifications demanded by advanced microwave techniques and to the mechanical requirements demanded of combat equipment.

The work on crystal rectifiers at Bell Telephone Laboratories during the war was a part of an extensive cooperative research and development program on microwave weapons. The Office of Scientific Research and Development, through the Radiation Laboratory at the Massachusetts Institute of Technology, served as the coordinating agency for work conducted at various university, government, and industrial laboratories in this country and as a liaison agency with British and other Allied organizations. However, prior to the inception of this cooperative program, basic studies on the use of crystal rectifiers had been conducted in Bell Telephone Laboratories. The series of crystal rectifiers now available may thus be considered to be the outgrowth of work conducted in three distinct periods. First, in the interval from 1934 to the end of 1940, devices incorporating point contact rectifiers came into general use in the researches in ultra-high-frequency and microwave communications techniques then under way at the Holmdel Radio Laboratories of Bell Telephone Laboratories.

[1] A crystal rectifier is an assymmetrical, non-linear circuit element in which the seat of rectification is immediately underneath a point contact applied to the surface of a semiconductor. This element is frequently called "point contact rectifier" and "crystal detector" also. In this paper these terms are considered to be synonymous.

Digitized by Google
Original from UNIVERSITY OF MICHIGAN
Generated on 2019-09-23 05:26 GMT / http://hdl.handle.net/2027/mdp.39015077775156
Public Domain, Google-digitized / http://www.hathitrust.org/access_use#pd-google

At that time the improvement in sensitivity of microwave receivers employing crystal rectifiers in the frequency converters was clearly recognized, as were the advantages of rectifiers using silicon rather than certain well known minerals as the semi-conductor. In the second period, from 1941 to 1942, the advent of important war uses for microwave devices stimulated increased activity in both research and development. During these years the pattern for the interchange of technical information on microwave devices through government sponsored channels was established and was continued through the entire period of the war. With the extensive interchange of information, considerable international standardization was achieved. In view of the urgent equipment needs of the Armed Services emphasis was placed on an early standardization of designs for production. This resulted in the first of the modern series of rectifiers, namely, the ceramic cartridge design later coded through the Radio Manufacturers Association as type 1N21. In the third period, from 1942 to the present time, process and design advances accruing from intensive research and development made possible the coding and manufacture of an extensive series of rectifiers all markedly superior to the original 1N21 unit.

It is the purpose of this paper to review the work done in Bell Telephone Laboratories on silicon point contact rectifiers during the three periods mentioned above, and to discuss briefly typical properties of the rectifiers, several of the more important applications and the production history.

Crystal Rectifiers in the Early Microwave Research

The technical need for the modern crystal rectifier arose in research on ultra-high frequency communications techniques. Here as the frontier of the technically useful portion of the radio spectrum was steadily advanced into the microwave region, certain limitations in conventional vacuum tube detectors assumed increasing importance. Fundamentally, these limitations resulted from the large interelectrode capacitance and the finite time of transit of electrons between cathode and anode within the tubes. At the microwave frequencies (3000 megacycles and higher), they became of first importance. As transit time effects are virtually absent in point contact rectifiers, and since the capacitance is minute, it was logical that the utility of these devices should again be explored for laboratory use.

The design of the point contact rectifiers used in these researches was dictated largely, of course, by the needs of the laboratory. Frequently the rectifier housing formed an integral part of the electrical circuit design while other structures took the form of a replaceable resistor-like cartridge. A variety of structures, including the modern types, arranged in chronological sequence, are shown in the photograph, Fig. 1. In general, the

Digitized by Google
Original from UNIVERSITY OF MICHIGAN
Generated on 2019-09-23 05:26 GMT / http://hdl.handle.net/2027/mdp.39015077775156
Public Domain, Google-digitized / http://www.hathitrust.org/access_use#pd-google

principal requirements of the rectifiers for laboratory use were that the units be sensitive, stable chemically, mechanically, and electrically, and

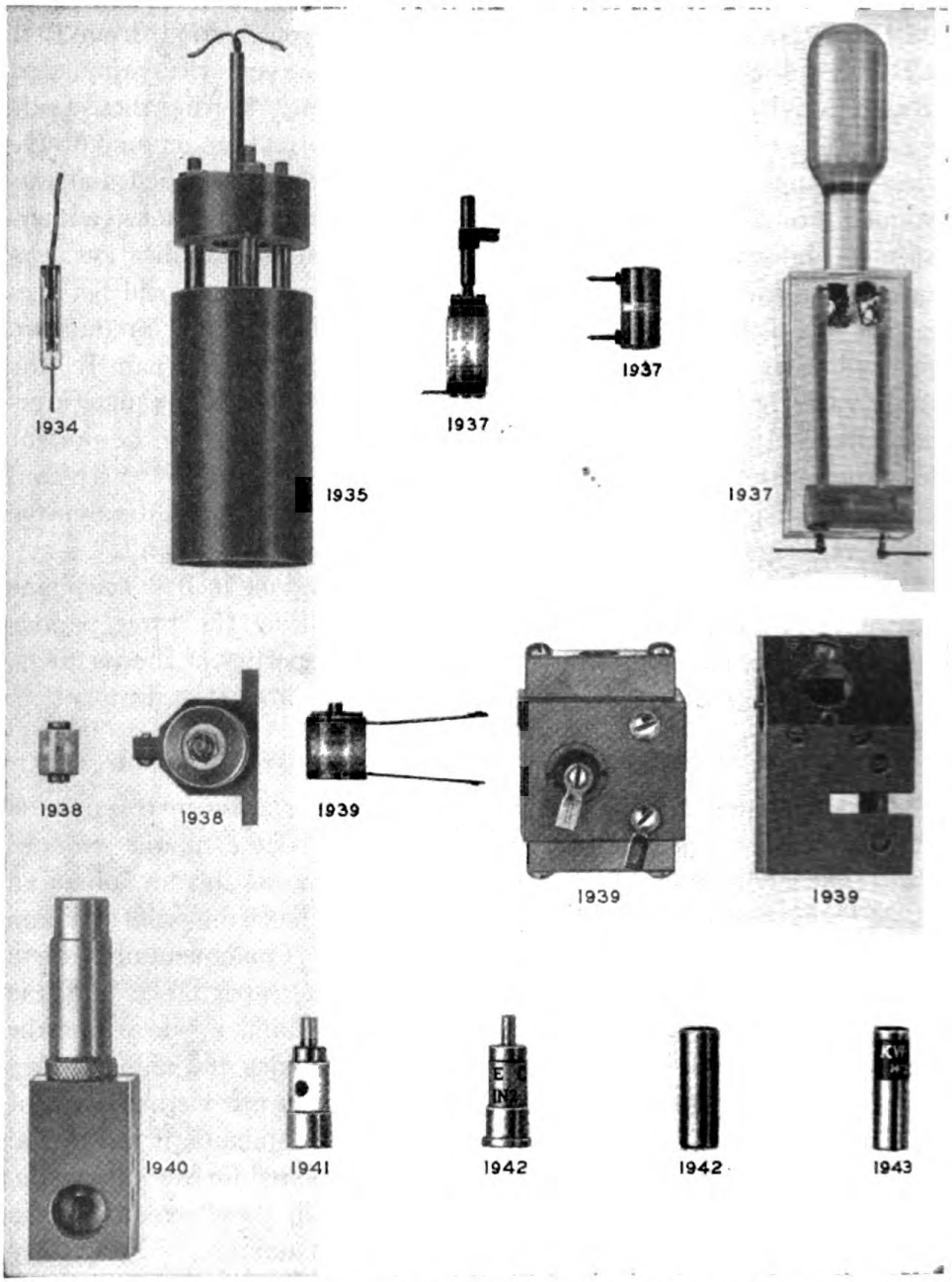

Fig. 1—Point contact rectifier structures. 1934–1943. Approximately $\frac{3}{8}$ actual size.

that they be easily adjusted. Considering the known vagaries of the device's historical counterpart, it was considered prudent to provide in the structures means by which the unit could be readjusted as frequently as might prove necessary or desirable.

Digitized by Google
Original from UNIVERSITY OF MICHIGAN
Generated on 2019-09-23 05:26 GMT / http://hdl.handle.net/2027/mdp.39015077775156
Public Domain, Google-digitized / http://www.hathitrust.org/access_use#pd-google

As the properties of various semi-conductors were known to vary widely, an essential part of the early work was a survey of the properties of a number of minerals and metalloids potentially useful as rectifier materials. There were examined and tested approximately 100 materials, including zincite, molybdenite, galena, iron pyrites, silicon carbide, and silicon. Of the materials investigated most were found to be unsuitable for one reason or another, and iron pyrites and silicon were selected as having the best overall characteristics. The subsequent studies were then directed toward improving the rectifying material, the rectifying surface, the point contact and the mounting structure.

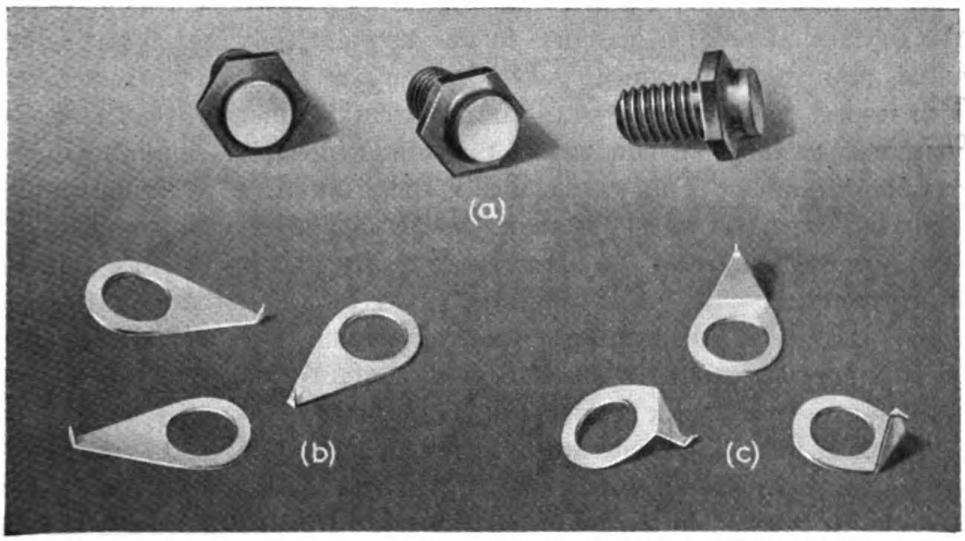

Fig. 2—Rectifier inserts and contact points for use in early 3000 megacycle converters. Overall length of insert $\frac{3}{16}$-inch approximately.

For use at frequencies in the region of 3000 megacycles standard demountable elements, consisting of rectifier "inserts" and contact points, were developed for use in various housings or mounting blocks, depending upon the particular circuit requirements. The rectifier "inserts" consisted of small wafers of iron pyrite or silicon, soldered to hexagonal brass studs as shown in Fig. 2a. In these devices the surface of the semi-conductor was prepared by grinding, polishing, and etching to develop good rectification characteristics. Our knowledge of the metallurgy of silicon had advanced by this time to the stage where a uniformly active rectifier surface could be produced and searching for active spots was not necessary. Furthermore, it was possible to prepare inserts of a positive or negative variety, signifying that the easy direction of current flow was obtained with the silicon positive with respect to the point or vice versa. Owing to a greater nonlinearity of the current voltage characteristic, the n-type or negative

Generated on 2019-09-23 05:27 GMT / http://hdl.handle.net/2027/mdp.39015077775156
Public Domain, Google-digitized / http://www.hathitrust.org/access_use#pd-google
Digitized by Google
Original from UNIVERSITY OF MICHIGAN

insert tended to give better performance as microwave converters while the p-type, or positive insert, because of greater sensitivity at low voltages, proved to be more useful in test equipment such as resonance indicators in frequency meters. In certain instances also, it was advantageous for the designer to be able to choose the polarity best suited to his circuit design. In contrast, however, to the striking uniformity obtained with the silicon processed in the laboratory, the pyrite inserts were very non-uniform. Active rectification spots on these natural mineral specimens could be found only by tediously searching the surface of the specimen. Moreover, rectifiers employing the pyrite inserts showed a greater variation in properties with frequency than those in which silicon was used.

In addition to providing a satisfactory semi-conductor, it was necessary also to develop suitable materials for use as point contacts. For this use metals were required which had satisfactory rectification characteristics with respect to silicon or pyrites and sufficient hardness so that excessive contact areas were not obtained at the contact pressures employed in the rectifier assembly. The metals finally chosen were a platinum-iridium alloy and tungsten, which in some cases was coated with a gold alloy. These were employed in the form of a fine wire spot welded to a suitable spring member. The spring members themselves were usually of a wedge shaped cantilever design and were made from coin silver to facilitate electrical connection to the spring. Several contact springs of two typical designs are shown in the photograph, Figs. 2b and 2c.

A typical mounting block arranged for use with the inserts and points is shown in Fig. 1 (1940) and in Fig. 3. This block was so constructed that it could be inserted in a 70 ohm coaxial line without introducing serious discontinuities in the line. The contact point of the rectifier was assembled in the block to be electrically connected to the central conductor of the coaxial radio frequency input fitting, while the crystal insert screwed into a tapered brass pin electrically connected to the central conductor of the coaxial intermediate frequency and d-c output fitting. The tapered pin fitted tightly into a tapered hole in a supporting brass cylinder, but was insulated from the cylinder by a few turns of polystyrene tape several thousandths of an inch thick. This central pin was thus one terminal of a coaxial high-frequency by-pass condenser. The capacitance of this condenser depended upon the general nature of the circuits in which the block was to be used, and was generally about 15 mmfs. The arrangement of the point, the crystal insert and their respective supporting members was such that the point contact could be made to engage the surface of the silicon at any spot and at the contact pressure desired and thereafter be clamped firmly in a fixed position by set screws. Typical direct current characteristics of the positive and negative silicon inserts and of pyrite inserts assembled and adjusted in this mounting block are shown in Fig. 4.

Digitized by Google
Original from UNIVERSITY OF MICHIGAN
Generated on 2019-09-23 05:27 GMT / http://hdl.handle.net/2027/mdp.39015077775156
Public Domain, Google-digitized / http://www.hathitrust.org/access_use#pd-google

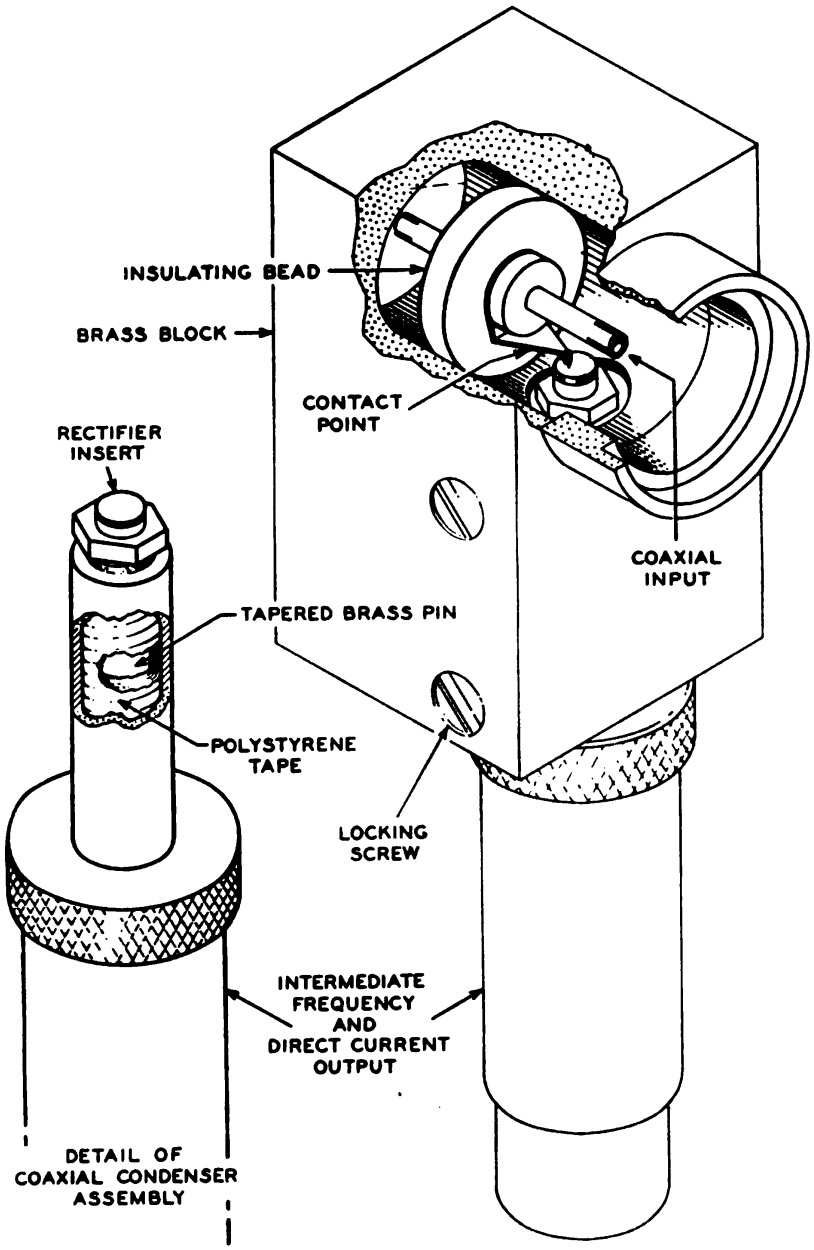

Fig. 3—Schematic diagram of one of the early crystal converter blocks.

The inserts and points in appropriate mounting blocks were widely used in centimeter wave investigations prior to 1940.[2] The principal laboratory uses were in frequency converter circuits in receivers, and as radio fre-

[2] G. C. Southworth and A. P. King, "Metal Horns as Directive Receivers of Ultra-Short Waves," *Proc. I. R. E.* v. 27, pp. 95–102, 1939; Carl R. Englund, "Dielectric Constants and Power Factors at Centimeter Wave Lengths," *Bell Sys. Tech. Jour.*, v. 23, pp. 114–129, 1944; Brainerd, Koehler, Reich, and Woodruff, "Ultra High Frequency Techniques," D. Van Nostrand Co., Inc., 250–4th Avenue, New York, 1942.

Digitized by Google
Original from UNIVERSITY OF MICHIGAN
Generated on 2019-09-23 05:27 GMT / http://hdl.handle.net/2027/mdp.39015077775156
Public Domain, Google-digitized / http://www.hathitrust.org/access_use#pd-google

quency instrument rectifiers. They were also used to a relatively minor extent in some of the early radar test equipment. Moreover, the availability of these devices and the knowledge of their properties as microwave converters tended to focus attention on the potentialities of radar designs employing crystal rectifiers in the receiver's frequency converter. Similarly, the techniques established for preparation of the inserts tended to orient subsequent manufacturing process developments. For example, the methods now generally used for preparing silicon ingots, for cutting the rectifying element from the ingot with diamond saws, and for forming the

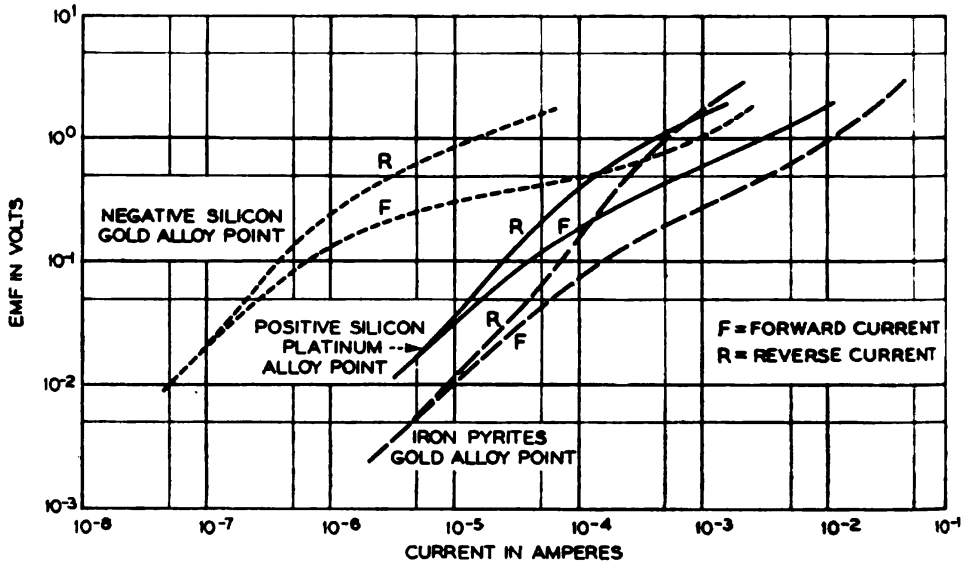

Fig. 4—Direct-current characteristics of silicon and iron pyrite rectifiers fabricated as inserts, 1939.

back contact to the rectifying element by electroplating procedures, are still essentially similar to the techniques used for preparing the inserts in 1939. As a contribution to the defense research effort, this basic information, with various samples and experimental assemblies, was made available to governmental agencies for dissemination to authorized domestic and foreign research establishments.

Development of the Ceramic Type Cartridge Structure

The block rectifier structure previously described was well adapted to various laboratory needs because of its flexibility, but for large scale utilization certain limitations are evident. Not only was it necessary that the parts be accurately machined, but also the adjustment of the rectifier in

Digitized by Google
Original from UNIVERSITY OF MICHIGAN
Generated on 2019-09-23 05:27 GMT / http://hdl.handle.net/2027/mdp.39015077775156
Public Domain, Google-digitized / http://www.hathitrust.org/access_use#pd-google

the block structure required considerable skill. With recognition of the military importance of silicon crystal rectifiers, effort was intensified in the development of standardized structures suitable for commercial production.

In the 1940–1941 period, contributions to the design of silicon crystal rectifiers were made by British workers as a part of their development of new military implements. For these projected military uses, the problem of replacement and interchangeability assumed added importance. The design trend was, therefore, towards the development of a cartridge type structure with the electrical adjustment fixed during manufacture, so that the unit could be replaced easily in the same manner as vacuum tubes.

In the latter part of 1941 preliminary information was received in this country through National Defense Research Committee channels on a rectifier design originating in the laboratories of the British Thomson-Houston Co., Ltd. A parallel development of a similar device was begun in various American laboratories, including the Radiation Laboratory at the Massachusetts Institute of Technology, and Bell Telephone Laboratories. In the work at Bell Laboratories, emphasis was placed both on development of a structure similar to the British design and on exploration and test of various new structures which retained the features of socket interchangeability but which were improved mechanically and electrically.

In the work on the ceramic cartridge, the external features of the British design were retained for reasons of mechanical standardization but a number of changes in process and design were made both to improve performance and to simplify manufacture. To mention a few, the position of the silicon wafer and the contact point were interchanged because measurements indicated that an improvement in performance could thereby be obtained. To obviate the necessity for searching for active spots on the surface of the silicon and to improve performance, fused high purity silicon was substituted for the "commercial" silicon then employed by the British. The rectifying element was cut from the ingots by diamond saws, and carefully polished and etched to develop optimum rectification characteristics. Similar improvements were made in the preparation of the point or "cats whisker", replacing hand operations by machine techniques. To protect the unit from mechanical shock and the ingress of moisture, a special impregnating compound was developed which was completely satisfactory even under conditions of rapid changes in temperature from $-40°$ to $+70°$C. All such improvements were directed towards improving quality and establishing techniques for mass production.

In this early work time was at a premium because of the need for prompt standardization of the design in order that radar system designs might in

Digitized by Google
Original from UNIVERSITY OF MICHIGAN
Generated on 2019-09-23 05:28 GMT / http://hdl.handle.net/2027/mdp.39015077775156
Public Domain, Google-digitized / http://www.hathitrust.org/access_use#pd-google

turn be standardized, and that manufacturing facilities might be established to supply adequate quantities of the device. The development and initial production of the device was accomplished in a short period of time. This was possible because process experience had been acquired in the insert development, and centimeter wave measurements techniques and facilities were then available to measure the characteristics of experimental units at the operating frequency. By December 1941, a pattern of manufacturing techniques had been established so that production by the Western Electric Company began shortly thereafter. This is believed to have been the first commercial production of the device in this country.

As a result of the basic information on centimeter wave measurements techniques which was available from earlier microwave research at the Holmdel Radio Laboratory, it was possible also, at this early date, to propose to the Armed Services that each unit be required to pass an acceptance test consisting of measurement of the operating characteristics at the intended operating frequency. This plan was adopted and standard test methods devised for production testing. Considering the complexity of centimeter wave measurements, this was an accomplishment of some magnitude and was of first importance to the Armed Services because it assured by direct measurement that each unit would be satisfactory for field use.

The cartridge structure resulting from these developments and meeting the international dimensional standards is shown in Fig. 5. It consists of two metal terminals separated by an internally threaded ceramic insulator. The rectifying element itself consists of a small piece of silicon (p-type) soldered to the lower metal terminal or base. The contact spring or "cats whisker" is soldered into a cylindrical brass pin which slides freely into an axial hole in the upper terminal and may be locked in any desired position by set screws. The spring itself is made from tungsten wire of an appropriate size, formed into an S shape. The free end of the wire, which in a finished unit engages the surface of the silicon and establishes rectification, is formed to a cone-shaped configuration in order that the area of contact may be held at the desired low value.

The silicon elements used in the rectifiers are prepared from ingots of fused high purity silicon. Alloying additions are made to the melt when required to adjust the electrical resistivity of the silicon to the value desired. The ingots are then cut and the silicon surfaces prepared and cut into small pieces approximately 0.05 inch square and 0.02 inch thick suitable for use in the rectifiers. The contact springs are made from tungsten wire, gold plated to facilitate soldering. Depending upon the application, the wires

Digitized by Google
Original from UNIVERSITY OF MICHIGAN
Generated on 2019-09-23 05:28 GMT / http://hdl.handle.net/2027/mdp.39015077775156
Public Domain, Google-digitized / http://www.hathitrust.org/access_use#pd-google

may be 0.005 inch, 0.0085 inch, or 0.010 inch in diameter. After forming the spring to the desired shape, the tip is formed electrolytically.

In assembling the rectifier cartridge, the two end terminals, consisting of the base with the silicon element soldered to it, and the top detail containing the contact spring, are threaded into the ceramic tube so that the free end of the spring does not engage the silicon surface. An adhesive

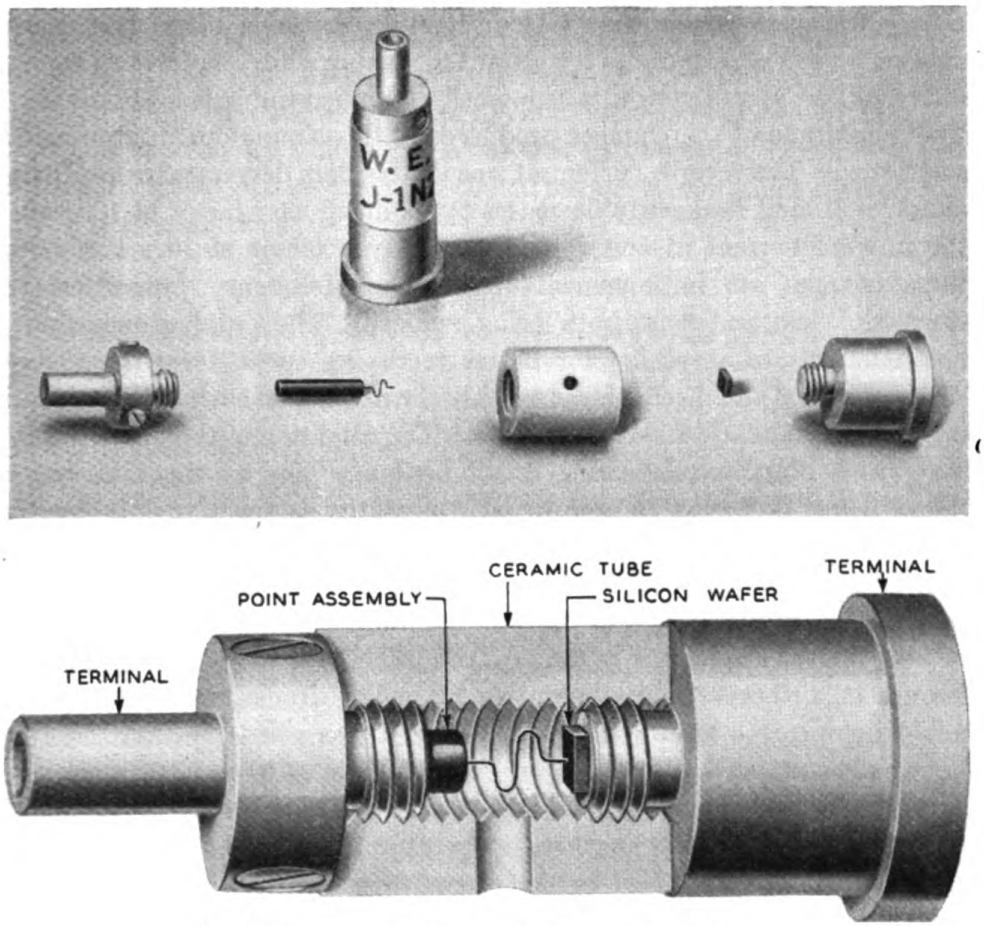

Fig. 5—Ceramic cartridge rectifier structure and parts.
Overall length of assembled rectifier is approximately $\frac{3}{4}$ inch.

is employed to secure the parts firmly to the ceramic. The rectifier is then "adjusted" by bringing the point into engagement with the silicon surface and establishing optimum electrical characteristics. Finally the unit is impregnated with a special compound to protect it from moisture and from damage by mechanical shock. Units so prepared are then ready for the final electrical tests.

The adjustment of the rectifier is an interesting operation for at this

Digitized by Google
Original from UNIVERSITY OF MICHIGAN
Generated on 2019-09-23 05:28 GMT / http://hdl.handle.net/2027/mdp.39015077775156
Public Domain, Google-digitized / http://www.hathitrust.org/access_use#pd-google

stage in the process the rectification action is developed, and to a considerable degree, controlled. If the point is brought into contact with the silicon surface and a small compressional deflection applied to the spring, direct-current measurements will show a moderate rectification represented by the passage of more current at a given voltage in the forward direction than in the reverse. If the side of the unit is now tapped sharply by means of a small hammer, the forward current will be increased, and, at the same time, the reverse current decreased.[3] With successive blows the reverse current is reduced rapidly to a constant low value while the forward current increases, but at a diminishing rate, until it also becomes relatively constant. The magnitude of the changes produced by this simple operation is rather surprising. The reverse current at one volt seldom decreases by less than a factor of 10 and frequently decreases by as much as a factor of 100, while the forward current at one volt increases by a factor of 10. Paralleling these changes are improvements in the high-frequency properties, the conversion loss and noise both being reduced. The tapping operation is not a haphazard searching for better rectifying spots, for with a given silicon material and mechanical assembly the reaction of each unit to tapping is regular, systematic and reproducible. The condition of the silicon surface also has a pronounced bearing on "tappability" for by modifications of the surface it is possible to produce, at will, materials sensitive or insensitive in their reaction to the tapping blows.

In the development of the compounds for filling the rectifier, special problems were met. For example, storage of the units for long periods of time under either arctic or tropical conditions was to be expected. Also, for use in air-borne radars operating at high altitudes, where equipment might be operated after a long idle period, it was necessary that the units be capable of withstanding rapid heating from very low temperatures. The temperature range specified was from $-40°$ to $+70°$C. Most organic materials normally solid at room temperature, as the hydrocarbon waxes, are completely unsuitable, as the excessive contraction which occurs at low temperatures is sufficient to shift the contact point and upset the precise adjustment of the spring. Nor are liquids satisfactory because of their tendency to seep from the unit. However, special gel fillers, consisting of a wax dispersed in a hydrocarbon oil, were devised in Bell Telephone Laboratories to meet the requirements, and were successfully applied by the leading manufacturers of crystal rectifiers in this country. Materials of a similar nature, though somewhat different in composition, were also used subsequently in Britain. Further improvements in these compounds have been made recently, extending the temperature range 10°C at low

[3] Southworth and King; loc. cit.

Digitized by Google
Original from UNIVERSITY OF MICHIGAN
Generated on 2019-09-23 05:28 GMT / http://hdl.handle.net/2027/mdp.39015077775156
Public Domain, Google-digitized / http://www.hathitrust.org/access_use#pd-google

temperatures and about 30°C at high temperatures in response to the design trend towards operation of the units at higher temperatures. The units employing this compound may, if desired, be repeatedly heated and cooled rapidly between −50°C and +100°C without damage.

Use of the impregnating compound not only improves mechanical stability but prevents ingress or absorption of moisture. Increase of humidity would subject the unit not only to changes in electrical properties such as variation in the radio frequency impedance, but also to serious corrosion, for the galvanic couple at the junction would support rapid corrosion of the metal point. In fact, with condensed moisture present in unfilled units corrosion can be observed in 48 hours. For this reason alone, the development of a satisfactory filling compound was an important step in the successful utilization of the units by the Armed Services under diverse and drastic field conditions.

TABLE I

Shelf Aging Data on Silicon Crystal Rectifiers of the Ceramic Cartridge Design

Storage Conditions	Initial Values		Values After Storage for 7 Months	
	Conversion Loss (Median) (L)	Noise Ratio (Median) (N_r)	Conversion Loss (median) (L)	Noise Ratio (median) (N_r)
	db	*db*	*db*	*db*
75°F. 65% Relative Humidity	6.8	3.9	6.7	4.3
110°F. 95% Relative Humidity	6.9	3.9	6.9	4.3
−40°C	7.0	3.9	6.8	3.9

The large improvement in stability achieved in the present device as compared with the older crystal detectors may be attributed to the design of the contact spring, correct alignment of parts in manufacture and to the practice of filling the cavity in the unit with the gel developed for this purpose. Considering the apparently delicate construction of the device, the stability to mechanical or thermal shock achieved by these means is little short of spectacular. Standard tests consist of dropping the unit three feet to a wood surface, immersing in water, and of rapidly heating from −40 to 70°C. None of these tests impairs the quality of the unit. Similarly the unit will withstand storage for long periods of time under adverse conditions. Table I summarizes the results of tests on units which were stored for approximately one year under arctic (−40°), tropical (114°F—95% relative humidity), and temperate conditions. Though minor changes in the electrical characteristics were noted in the accelerated tropical test, none of the units was inoperative after this drastic treatment.

Digitized by Google
Original from UNIVERSITY OF MICHIGAN
Generated on 2019-09-23 05:28 GMT / http://hdl.handle.net/2027/mdp.39015077775156
Public Domain, Google-digitized / http://www.hathitrust.org/access_use#pd-google

Development of the Shielded Rectifier Structure

Rectifiers of the ceramic cartridge design, though manufactured in very large quantities and widely and successfully used in military apparatus, have certain well recognized limitations. For example, they may be accidentally damaged by discharge of static electricity through the small point contact in the course of routine handling. If one terminal of the unit is held in the hand and the other terminal grounded, any charge which may have accumulated will be discharged through the small contact. Since such static charges result in potential differences of several thousand volts it is understandable that the unit might suffer damage from the discharge. Although damage from this cause may be avoided by following a few simple precautions in handling, the fact that such precautions are needed constitutes a disadvantage of the design.

Certain manufacturing difficulties are also associated with the use of the threaded insulator. The problem of thread fit requires constant attention. Lack of squareness at the end of the ceramic cylinder or lack of concentricity in the threaded hole tends to cause an undesirable eccentricity or angularity in the assembled unit which can be minimized only by rigid inspection of parts and of final assemblies. At the higher frequencies (10,000 megacycles), uniformity in electrical properties, notably the radio frequency impedance, requires exceedingly close control of the internal mechanical dimensions. In the cartridge structure where the terminal connections are separated by a ceramic insulating member, the additive variations of the component parts make close dimensional control inherently difficult.

To eliminate these difficulties the shielded structure, shown in Fig. 6, was developed. In this design the rectifier terminates a small coaxial line. The central conductor of the line, forming one terminal of the rectifier, is molded into an insulating cylinder of silica-filled bakelite, and has spot welded to it a 0.002-inch diameter tungsten wire spring of an offset C design. The free end of the spring is cone shaped. The rectifying element is soldered to a small brass disk. Both the disk, holding the rectifying element, and the bakelite cylinder, holding the point, are force-fits in the sleeve which forms the outer conductor of the rectifier. By locating the bakelite cylinder within the sleeve so that the free end of the central conductor is recessed in the sleeve, the unit is effectively protected from accidental static damage as long as the holder or socket into which the unit fits is so designed that the sleeve establishes electrical contact with the equipment at ground potential before the central conductor. The sleeve also shields the rectifying contact from effects of stray radiation.

The radio frequency impedance of the shielded unit can be varied within certain limits by modifying the diameter of the central conductor. For

Digitized by Google
Original from UNIVERSITY OF MICHIGAN
Generated on 2019-09-23 05:29 GMT / http://hdl.handle.net/2027/mdp.39015077775156
Public Domain, Google-digitized / http://www.hathitrust.org/access_use#pd-google

example, in the 1N26 unit, which was designed for use at frequencies in the region of 24,000 megacycles, a small metal slug fitting over the central conductor makes it possible to match a coaxial line having a 65-ohm surge impedance. For certain circumstances this modification in design is advantageous, while in others it is a disadvantage because the matching slug is effective only over a narrow range of frequencies.

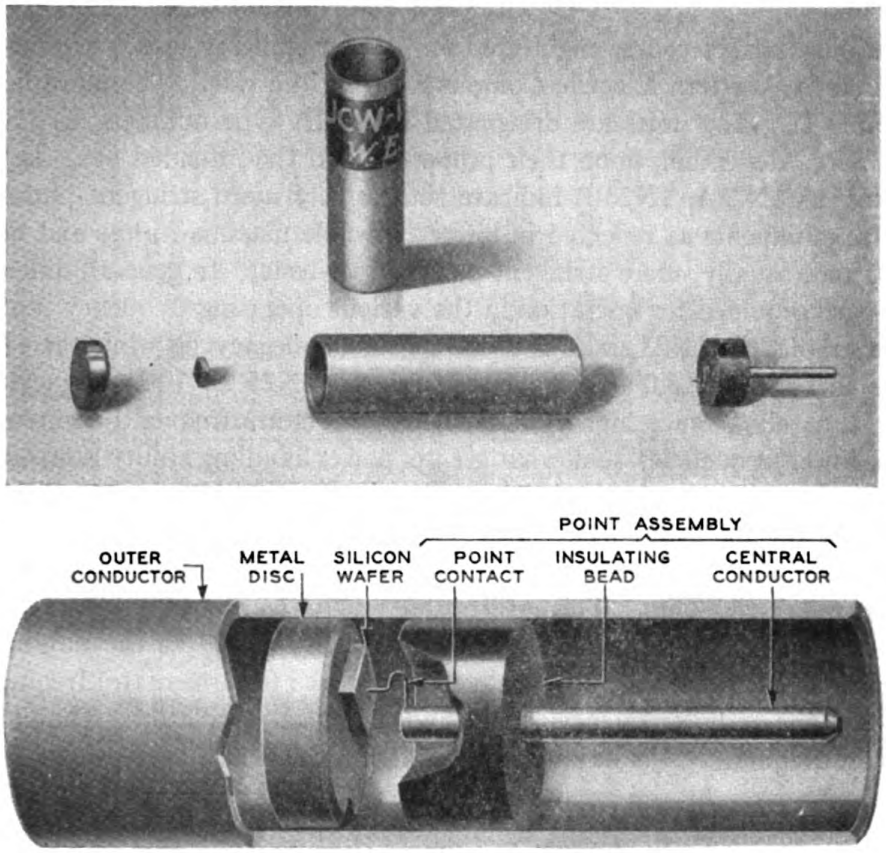

Fig. 6—Shielded rectifier structure and parts. Overall length of assembled rectifier is approximately $\frac{3}{4}$ inch.

The shielded structure was developed in 1942 and since it was of a simplified design with reduced hazard of static damage, it was proposed to the Armed Services for standardization in June of that year. However, because of the urgency of freezing the design of various radars and because the British had already standardized on the outline dimensions of the ceramic type cartridge, Fig. 5, the Services did not consider it advantageous to standardize the new structure when first proposed. In deference to this international standardization program, plans for the manufacture of this

Generated on 2019-09-23 05:29 GMT / http://hdl.handle.net/2027/mdp.39015077775156
Public Domain, Google-digitized / http://www.hathitrust.org/access_use#pd-google
Digitized by Google
Original from UNIVERSITY OF MICHIGAN

structure were held in abeyance during 1942 and 1943. However, an opportunity for realizing the advantages inherent in the shielded design was afforded later in the war and a sufficient quantity of the units was produced to demonstrate its soundness. As anticipated from the constructional features, marked uniformity of electrical properties was obtained.

Types, Applications, and Operating Characteristics

Various rectifier codes, engineered for specific military uses, were manufactured by Western Electric Company during the war. These are listed in Table II. The units are designated by RMA type numbers, as 1N21, 1N23, etc., depending upon their properties and the intended use. Letter suffixes, as 1N23A, 1N23B, indicate successively more stringent performance requirements as reflected in lower allowable maxima in loss and noise ratio, and, usually, more stringent power proof-tests. In general, different codes are provided for operation in the various operating frequency ranges. For example, the 1N23 series is tested at 10,000 megacycles while the 1N21 series is tested at 3,000 megacycles and the 1N25 at 1000 megacycles, approximately. Since higher transmitter powers are frequently employed at the lower frequencies, somewhat greater power handling ability is provided in units for operation in this range.

One of the more important uses of silicon crystal rectifiers in military equipment was in the frequency converter or first detector in superheterodyne radar receivers. This utilization was universal in microwave receivers. In this application the crystal rectifier serves as the non-linear circuit element required to generate the difference (intermediate) frequency between the radio frequency signal and the local oscillator. The intermediate frequency thus obtained is then amplified and detected in conventional circuits. As the crystal rectifier is normally used at that point in the receiving circuit where the signal level is at its lowest value, its performance in the converter has a direct bearing on the overall system performance. It was for this reason that continued improvements in the performance of crystal rectifiers were of such importance to the war effort.

For the converter application, the signal-to-noise properties of the unit at the operating frequency, the power handling ability, and the uniformity of impedance are important factors. The signal-to-noise properties are measured as conversion loss and noise ratio. The loss, L, is the ratio of the available radio frequency signal input power to the available intermediate frequency output power, usually expressed in decibels. The noise ratio, N_R, is the ratio of crystal output noise power to thermal (KTB) noise power. The loss and noise ratio are fundamental properties of the

Generated on 2019-09-23 05:29 GMT / http://hdl.handle.net/2027/mdp.39015077775156
Public Domain, Google-digitized / http://www.hathitrust.org/access_use#pd-google
Digitized by Google
Original from UNIVERSITY OF MICHIGAN

Generated on 2019-09-23 05:29 GMT / http://hdl.handle.net/2027/mdp.39015077775156
Public Domain, Google-digitized / http://www.hathitrust.org/access_use#pd-google

TABLE II

Performance Specifications—Silicon Crystal Rectifiers

Code	W.E. Spec. No.	Structure	Nominal Operating Frequency	Test Power	Max. Conversion Loss	Max. Noise Ratio[7]	Int. Freq. Impedance	Min. Figure of Merit	Low-Level Resistance	Proof Test Method, Note	Test Level	Normal Use
			mega-cycles	*milli-watts*	*db*		*ohms*		*ohms*			
1N21	D-163366	Cartridge	3000	0.4	8.5	4.0						Converter
1N21A	D-168355	"	"	0.4	7.5	3.0				5	0.3 erg	"
1N21B	D-169113	"	"	0.5	6.5	2.0	375[1]			5	2.0 ergs	"
1N23	D-168356	"	10000	1.0	10.0	3.0	"			5	0.3 erg	"
1N23A	D-169304	"	"	1.0	8.0	2.7	"			5	1.0 erg	"
1N23B	D-169305	"	"	1.0	6.5	2.7	"			5	0.3 erg	"
1N25	D-170247	"	1000	1.25	8.0	2.5	100–400[2]			6	12.5v[3] 6.ω[4]	"
1N26	D-168707	Shielded	24000	1.0	8.5	2.5	300–600[2]			5	0.1 erg	"
1N27	D-172981	Cartridge	3000	.005 max.				60	4000 max. at 1 mv			Low-Level Detector
1N28	D-168030	"	"	0.4	7.0	2.0	300[1]			5	5.0 erg	Converter
1N31	D-171936	Shielded	10000	.005 max.				55	6000–23,000 at 5 mv max. 20–25°C.	6	1.5v[3] 25.ω[4]	Low-Level Detector

[1] Average values under conditions of production test—not limited directly by specifications.
[2] Values limited by specifications.
[3] Pulse generator voltage.
[4] Pulse generator impedance.
[5] Single D.C. spike.
[6] Multiple square pulse.
[7] Numerical ratio.

Digitized by Google
Original from UNIVERSITY OF MICHIGAN

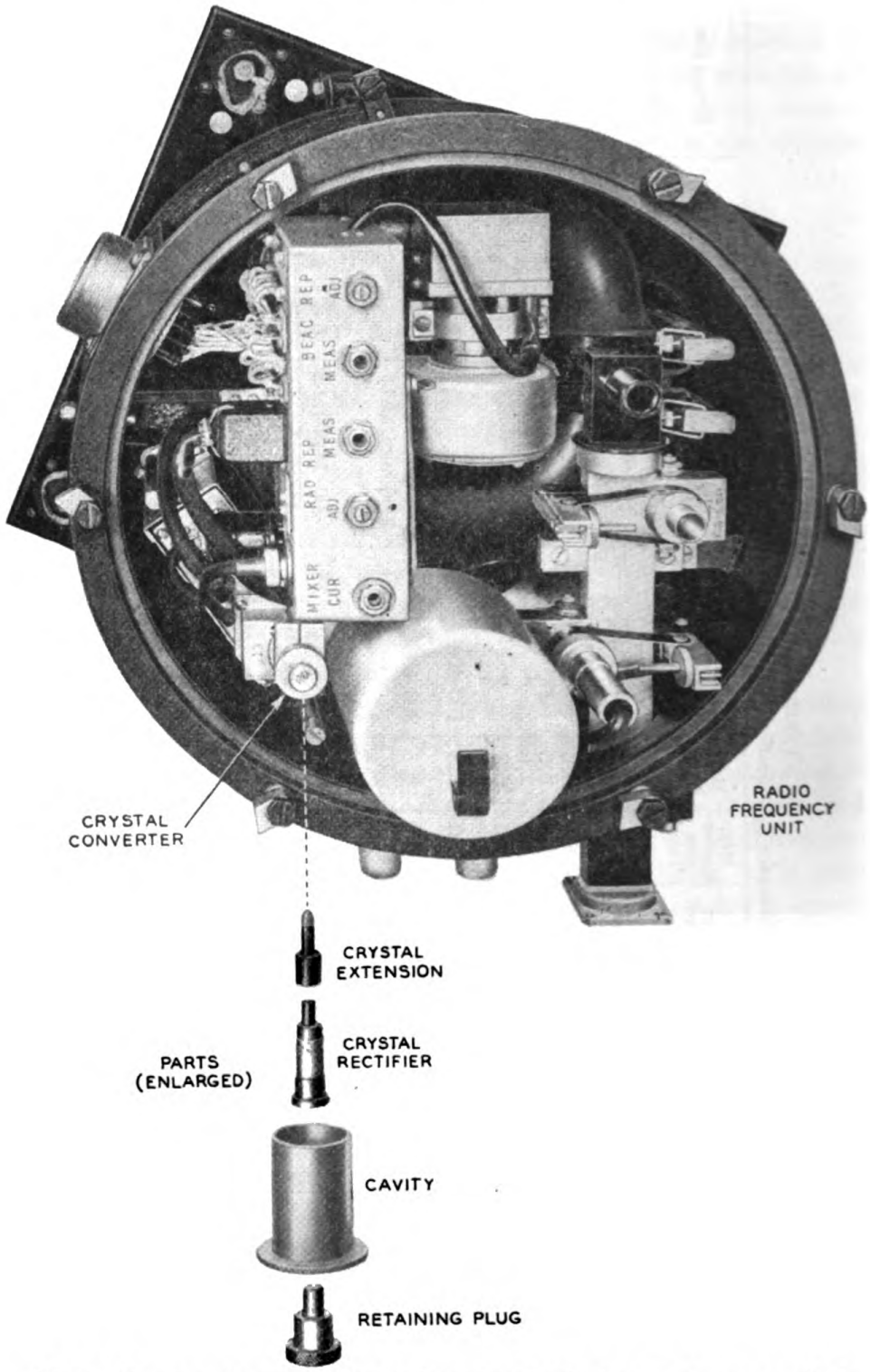

Fig. 7—Converter for wave guide circuits as installed in the radio frequency unit of the AN/APQ13 radar system. This was standard equipment in B-29 bombers for radar bombing and navigation.

Digitized by Google
Original from UNIVERSITY OF MICHIGAN
Generated on 2019-09-23 05:29 GMT / http://hdl.handle.net/2027/mdp.39015077775156
Public Domain, Google-digitized / http://www.hathitrust.org/access_use#pd-google

converter. From these data and other circuit constants, the designer may calculate[4] expected receiver performance.

For operation as converters,[5] crystal rectifiers are employed in suitable holders. These may be arranged for use with either coaxial line or wave guide circuits, depending upon the application. Figure 7 shows a converter for wave guide circuits installed in the radio frequency unit of an air-borne radar system. A typical converter designed for use with coaxial lines is shown in the photograph Fig. 8. A schematic circuit of this converter is shown in Fig. 9. In such circuits the best signal-to-noise ratio is realized when an optimum amount of beating oscillator power is supplied. The optimum power depends, in part, on the properties of the rectifier itself, and, in part, on other circuit factors as the noise figure of the intermediate

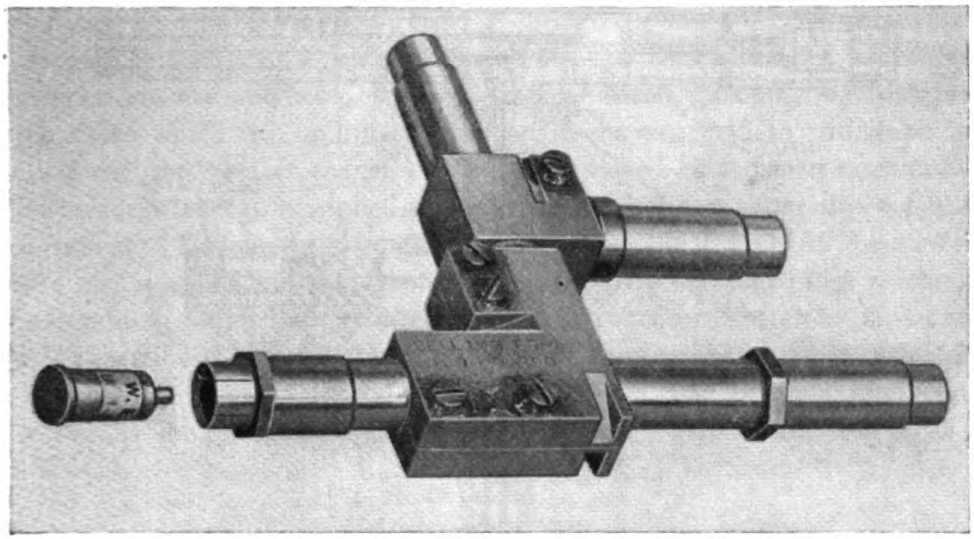

Fig. 8—Converter for use at 3000 megacycles. The crystal rectifier is located adjacent to its socket in the converter.

frequency amplifier. For a well designed intermediate frequency amplifier with a noise figure of about 5 decibels, the optimum beating oscillator power is such that between 0.5 and 2.0 milliamperes of rectified current flows through the rectifier unit. Under these conditions and with the unit matched to the radio frequency line, the beating oscillator power absorbed by the unit is about one milliwatt. For intermediate frequency amplifiers

[4] The quantities L and N_R are related to receiver performance by the relationship

$$F_R = L(N_R - 1 + F_{IF})$$

where F_R is the receiver noise figure and F_{IF} is the noise figure of the intermediate frequency amplifier. All terms are expressed as power ratios. A rigorous definition of receiver noise figure has been given by H. T. Friis "Noise Figures of Radio Receivers," *Proc. I. R. E.*, vol. 32, pp. 419–422; July, 1944.

[5] C. F. Edwards, "Microwave Converters," *Proc. I. R. E.*, Vol. 35, p. 1181; Nov. 1947.

Digitized by Google
Original from UNIVERSITY OF MICHIGAN
Generated on 2019-09-23 05:35 GMT / http://hdl.handle.net/2027/mdp.39015077775156
Public Domain, Google-digitized / http://www.hathitrust.org/access_use#pd-google

with poorer noise figures, the drive for optimum performance is higher than the figures cited above. Conversely, for intermediate frequency amplifiers with exceptionally low noise figures, optimum performance is obtained with lower values of beating oscillator drive. If desired, somewhat higher currents than 2.0 milliamperes may be employed without damage to the crystal.

The impedance at the terminals of a converter using crystal rectifiers, both at radio and intermediate frequencies, is a function not only of the rectifier unit, but also of the circuit in which the unit is used and of the

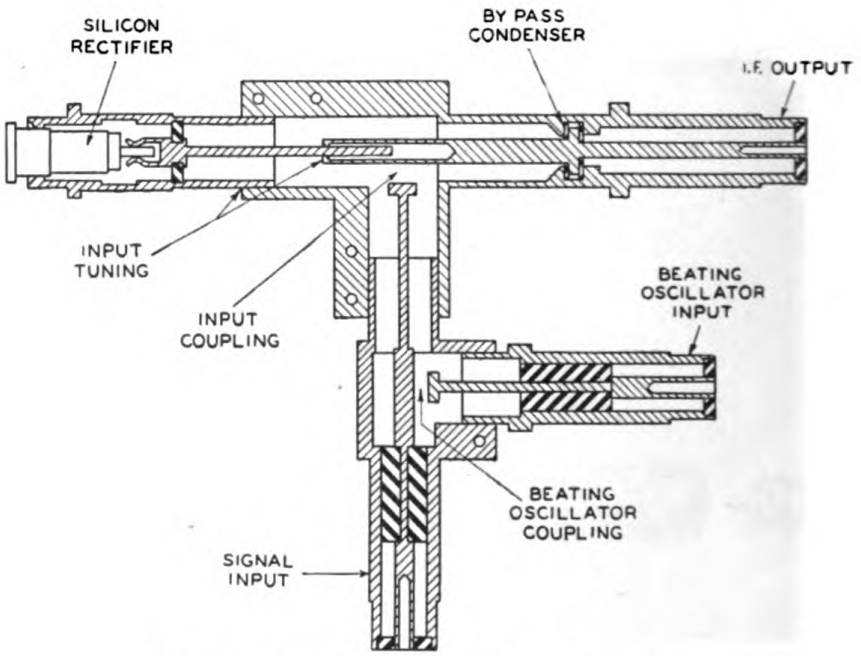

Fig. 9—Schematic diagram of crystal converter.

power level at which it is operated. Consequently the specification of an impedance for a crystal rectifier is of significance only in terms of the circuit in which it is measured. Since the converters used in the production testing of crystal rectifiers are not necessarily the same as those used in the field, and since in addition there are frequently several converter designs for the same type of unit, a specification of crystal rectifier impedance in production testing can do little more than select units which have the same impedance characteristic in the production test converter. The impedances at the terminals of two converters of different design but using the same crystal rectifier may vary by a factor of 3 or even more, with the intermediate frequency impedance generally varying more drastically than the radio frequency impedance. The variation is also a function of the con-

Generated on 2019-09-23 05:36 GMT / http://hdl.handle.net/2027/mdp.39015077775156
Public Domain, Google-digitized / http://www.hathitrust.org/access_use#pd-google
Digitized by Google
Original from UNIVERSITY OF MICHIGAN

version loss. Crystals with large conversion losses are less susceptible to impedance changes from reactions in the radio frequency circuit than are low conversion loss units.

The level of power to which the rectifiers can be subjected depends upon the way in which the power is applied. The application of an excessive amount of power or energy results in the electrical destruction of the unit by rupture of the rectifying material. Experimental evidence indicates that the electrical failure may be in one of three categories. The total energy of an applied pulse is responsible for the impairment when the pulse length is shorter than 10^{-7} seconds, the approximate thermal time constant of the crystal rectifier as given by both measurement and calculation. For pulse lengths of the order of 10^{-6} seconds the peak power in the pulse is the determining factor, and for continuous wave operation the limitation is in the average power.

In performance tests in manufacture all units for which burnout tolerances are specified are subjected to proof-tests at levels generally comparable with those which the unit may occasionally be expected to withstand in actual use, but greater than those to be employed as a design maximum. The power or energy is applied to the unit in one of two types of proof-test equipment. The multiple, long time constant (of the order of 10^{-6} seconds) pulse test is applied to simulate the plateau part of a radar pulse reaching the crystal through the gas discharge transmit-receive switch.[6] This test uses an artificial line of appropriate impedance triggered at a selected repetition rate for a determined length of time. The power available to the unit is computed from the usual formula,

$$P = \frac{V^2}{4Z},$$

where P is the power in watts, V is the potential in volts to which the pulse generator is charged, and Z is the impedance in ohms of the pulse generator. In general, where this test is employed, a line is used which matches the impedance of the unit under test at the specified voltage.

The second type of test is the single discharge of a coaxial line through the unit to simulate a radar pulse spike reaching the crystal before the transmit-receive switch fires. The pulse length is of the order of 10^{-9} second. The energy in the test spike may be computed from the relation

$$E = \frac{10^7}{2} CV^2,$$

where E is the energy in ergs, C the capacity of the coaxial line in farads, and V the potential in volts to which the line is charged.

[6] A. L. Samuel, J. W. Clark, and W. W. Mumford, "The Gas Discharge Transmit-Receive Switch". See pp. 310 ff.

Digitized by Google
Original from UNIVERSITY OF MICHIGAN
Generated on 2019-09-23 05:36 GMT / http://hdl.handle.net/2027/mdp.39015077775156
Public Domain, Google-digitized / http://www.hathitrust.org/access_use#pd-google

Specification proof-test levels are, of course, not design criteria. Since the units are generally used in combination with protective devices, such as the transmit-receive switch, it is necessary to conduct tests in the circuits of interest to establish satisfactory operating levels.

In general, however, the units may be expected to carry, without deterioration, energy of the order of a third of that used in the single d-c spike proof-test or peak powers of a magnitude comparable with that used in the multiple flat-top d-c pulse proof-test. The upper limit for applied continuous wave signals has not been determined accurately, but, in general, rectified currents below 10 milliamperes are not harmful when the self bias is less than a few tenths of a volt.

The service life of a crystal rectifier will depend completely upon the conditions under which it is operated and should be quite long when its ratings are not exceeded. During the war, careful engineering tests conducted on units operating as first detectors in certain radar systems revealed no impairment in the signal-to-noise performance after operation for several hundred hours. A small group of 1N21B units showed only minor impairments when operated in laboratory tests for 100 hours with pulse powers (3000 megacycles) up to 4 watts peak available to the unit under test.

Another important military application of silicon crystal rectifiers was as low-power radio frequency rectifiers for use in wave meters or other items of radar test equipment. Here the rectification properties of the unit at the operating frequency are of primary interest. Since units which are satisfactory as converters also function satisfactorily as high-frequency rectifiers special types were not required for this application.

Units were also used in military equipment as detectors to derive directly the envelope of a radio frequency signal received at low power levels. These signals were modulated usually in the video range. The low-level performance is a function of the resistance at low voltages and the direct-current output for a given low-power radio frequency input. These may be combined to derive a figure of merit which is a measure of receiver performance.[7]

Typical direct-current characteristics of the silicon rectifiers at temperatures of $-40°$, 25° and 70°C are given in Fig. 10. It will be noted in these curves that both the forward and reverse currents are decreased by reducing the temperature and increased by raising the temperature. The reverse current changes more rapidly with temperature than the forward current, however, so that the rectification ratio is improved by reducing the temperature, and impaired by raising the temperature. The data shown are for typical units of the converter type. It should be emphasized, however,

[7] R. Beringer, Radiation Laboratory Report No. 61–15, March 16, 1943.

Digitized by Google
Original from UNIVERSITY OF MICHIGAN
Generated on 2019-09-23 05:36 GMT / http://hdl.handle.net/2027/mdp.39015077775156
Public Domain, Google-digitized / http://www.hathitrust.org/access_use#pd-google

that by changes in processing routines the direct-current characteristics shown in Fig. 10 may be modified in a predictable manner, particularly with respect to absolute values of forward current at a particular voltage.

Modern Rectifier Processes

When the development of the type 1N21 unit was undertaken, the scientific and engineering information at hand was insufficient to permit intentional alteration or improvement in electrical properties of the rectifier. In these early units, the control of the radio frequency impedance, power handling ability and signal-to-noise ratio left much to be desired. Within a short time, some improvements in performance were realized by process improvements such as the elimination of burrs and irregularities from the point contact to reduce noise. Substantial improvements were not obtained,

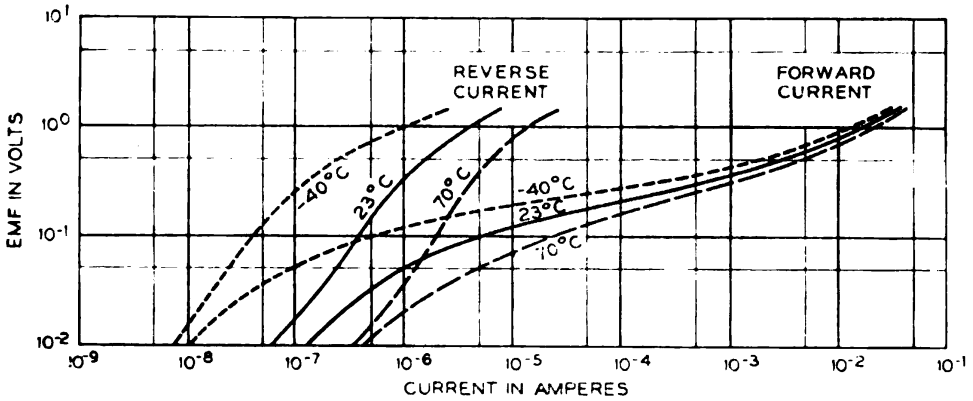

Fig. 10—Direct-current characteristics of P-type silicon crystal rectifier at various temperatures.

however, until certain improved materials, processes, and techniques were developed.

In the engineering development of improved crystal rectifier materials and processes, basic data have been acquired which make it possible to alter the properties of the rectifier in a predictable manner so that the units may now be engineered to the specific electrical requirements desired by the circuit designer in much the same manner as are modern electron tubes. This has led not only to improvements in performance but also to a diversification in types and applications.

The simplified equivalent circuit for the point contact rectifier, shown in Fig. 11, provides a basis for consideration of the various process features. In Fig. 11, C_B represents the electrical capacitance at the boundary between the point contact and the semi-conductor, R_B the non-linear resistance at this boundary, and R_S is the spreading resistance of the semi-conductor

Digitized by Google
Original from UNIVERSITY OF MICHIGAN
Generated on 2019-09-23 05:36 GMT / http://hdl.handle.net/2027/mdp.39015077775156
Public Domain, Google-digitized / http://www.hathitrust.org/access_use#pd-google

proper, that is the total ohmic resistance of the silicon to current through the point. The capacitance C_B being shunted across the rectifying boundary, decreases the efficiency of the device by its by-pass action because the current through it would be dissipated as heat in the resistance R_S. Losses from this source increase rapidly with increased frequency because of the enhanced by-pass action. It would appear, therefore, that to improve efficiency it would be important to minimize both R_S and C_B by some method such as reducing the area of the rectifying contact and lowering the body resistance of the silicon employed. For a given silicon material, the impedances desired for reasons of circuitry and considerations of mechanical stability place a limit on the extent to which performance may be improved by reducing the contact area. R_S may be reduced by using silicon of lower resistivity, but this generally results in poorer rectification. This impairment is due apparently to some subtle change in the properties of the rectifying junction resulting from decreasing the specific resistance of the silicon material.

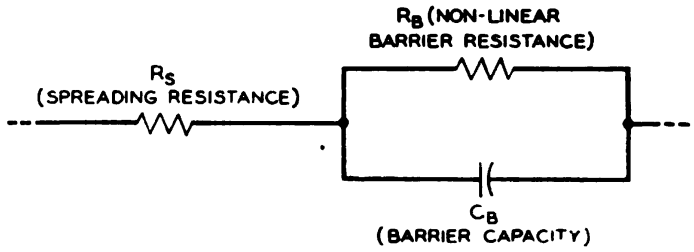

Fig. 11—Simplified equivalent circuit of crystal rectifier.

The answer to this apparent dilemma lies in the application of an oxidizing heat treatment to the surface of the semi-conductor. This process derives from researches conducted independently in this country and in Britain, though there was considerable interchange of information between various interested laboratories. In the oxidizing treatment, apparently the impurities in the silicon which contribute to its conductivity diffuse into the adhering silica film, thereby depleting impurities from the surface of the silicon. When the oxide layer is then removed by solution in dilute hydrofluoric acid, the underlying silicon layer is exposed and remains intact as the acid does not readily attack the silicon itself.

Since decreasing the impurity content of a semi-conductor increases its resistivity, the silicon surface has higher resistivity after the oxidizing treatment than before. Thus by oxidation of the surface of low resistance silicon it is possible to secure the enhanced rectification associated with the high resistance surface layer, while by virtue of the lower resistivity of the underlying material the I^2R losses through R_S are reduced.

Digitized by Google
Original from UNIVERSITY OF MICHIGAN
Generated on 2019-09-23 05:36 GMT / http://hdl.handle.net/2027/mdp.39015077775156
Public Domain, Google-digitized / http://www.hathitrust.org/access_use#pd-google

In actual practice the properties of the rectifier are governed by the resistivity of the silicon material, the contact area, and the degree of oxidation of the surface. By the controlled alteration of these factors units may be engineered for specific applications. The body resistance of the silicon is controlled by the kind and quantity of the impurities present. Aluminum, beryllium or boron may be added to purified silicon to reduce its resistivity to the desired level. Boron is especially effective for this purpose, the quantity added usually being less than 0.01 per cent. As little as 0.001 per cent has a very pronounced effect upon the electrical properties. The contact area is determined by the design of contact spring employed and the deflection applied to it in the adjustment of the rectifier. The degree of oxidation is controlled by the time and temperature of the treatment and the atmosphere employed.

In the development of the present rectifier processes, certain experimental relationships were obtained between the performance and the contact area on the one hand, and the power handling ability and contact area on the other. These show the manner in which the processes should be changed to produce a desired change in properties. For example, Fig. 12 shows the relationship between the spring deflection applied to a unit and the conversion loss at a given frequency. The apparent contact area, (i.e., the area of the flattened tip of the spring in contact with the silicon surface, as measured microscopically) also increases with increasing spring deflection. It will be seen in Fig. 12 that for a given silicon material, the conversion loss at 10,000 megacycles increases rapidly with the contact area. The curves tend to reach constant loss values at the higher spring deflections. It is believed that this may be ascribed to the fact that for a given spring size and form, the increment in contact area obtained by successive increments in spring deflection would diminish and finally become zero after the elastic limit of the spring is exceeded.

The losses plotted in Fig. 12 were measured on a tuned basis, that is, the converter was adjusted for maximum intermediate frequency output at a fixed beating oscillator drive for each measurement. Were these measurements made on a fixed tuned basis, that is, with the converter initially adjusted for maximum intermediate frequency output for a unit to which the minimum spring deflection is applied, and the units with larger deflections then measured without modification of the converter adjustment, even greater degradation in conversion loss than that shown in Fig. 12 would be observed. This results from the dependence of the radio frequency impedance upon the contact area. In loss measurements made on the tuned basis, changes in the radio frequency impedance occasioned by the changes in the contact area do not affect the values of mismatch loss obtained, while on the

Generated on 2019-09-23 05:37 GMT / http://hdl.handle.net/2027/mdp.39015077775156
Public Domain, Google-digitized / http://www.hathitrust.org/access_use#pd-google
Digitized by Google
Original from UNIVERSITY OF MICHIGAN

fixed tuned basis they would result in an increase in the apparent loss because of the mismatch of the radio frequency circuits.

While the conversion loss is degraded by increasing the contact area, the power handling ability[8] of the rectifiers is improved, as shown in Fig. 13.

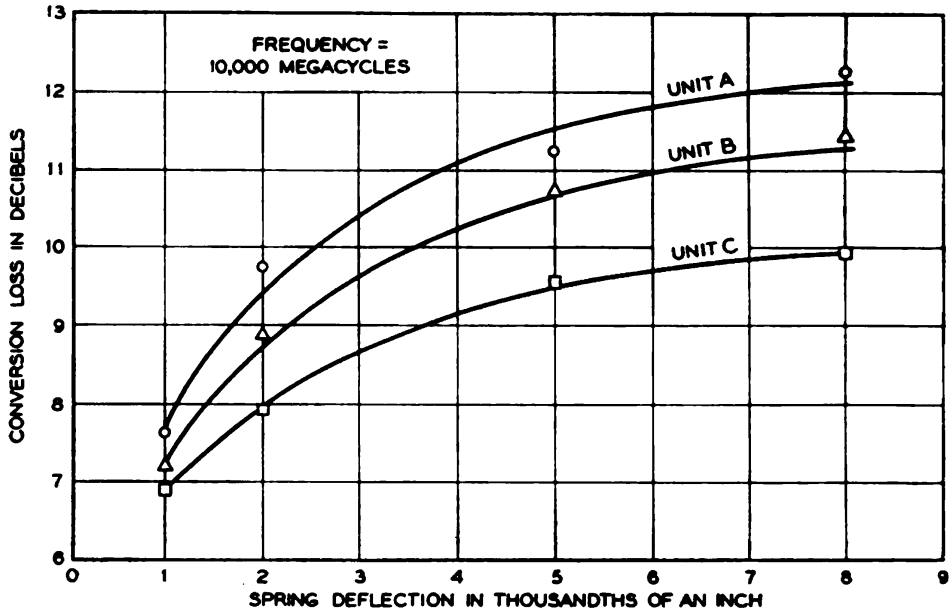

Fig. 12—Relationship between spring deflection and conversion loss in silicon crystal rectifiers.

This is not surprising because the larger area contact gives a wider current distribution and thus minimizes the localized heating effects near the contact. Generally, therefore, in the development of units for operation at a

[8] The measurement of power handling ability of crystal rectifiers by application of radio frequency power is complicated by the fact that the impedance of the unit under test varies with power level. If a unit is matched in a converter at a low-power level and power at a higher level is then applied, not all of the power available is absorbed by the unit but a portion of it is reflected (due to the change in impedance). This factor has been called the self protection of the unit and it necessitates the distinction between the power absorbed by and the power available to the unit under test. The data for Fig. 13 were acquired by first matching the unit in converters at low powers (about 0.3 milliwatts CW 3000 mcs) and then exposing it for a short period to successively higher levels of pulse power of square wave form of 0.5 microseconds width at a repetition rate of 2000 pulses per second, measuring the loss and noise ratio after each power application. The power handling ability is then expressed as the available peak power required to cause a 3 db impairment in the conversion loss or the receiver noise figure. This method was employed because in radar receivers the units are matched for low-power levels. In this respect the method simulates field operating conditions, but the "spike" of radar pulses is absent.

The increase in power handling ability with increasing area shown in Fig. 13 is confirmed by similar measurements with radio frequency pulse power with the unit matched at high-level powers, by direct-current tests, and by simple 60-cycle continuous wave tests. The magnitude of the increase depends, however, upon the particular method employed for measurement.

Generated on 2019-09-23 05:37 GMT / http://hdl.handle.net/2027/mdp.39015077775156
Public Domain, Google-digitized / http://www.hathitrust.org/access_use#pd-google
Digitized by Google
Original from UNIVERSITY OF MICHIGAN

given frequency, a compromise must be effected between these two important performance factors. Because of increased condenser by-pass action a smaller area must be used to obtain a given conversion loss at a higher frequency. For this reason the power handling ability of units designed for use at the higher frequencies is somewhat less than that of the lower-fre-

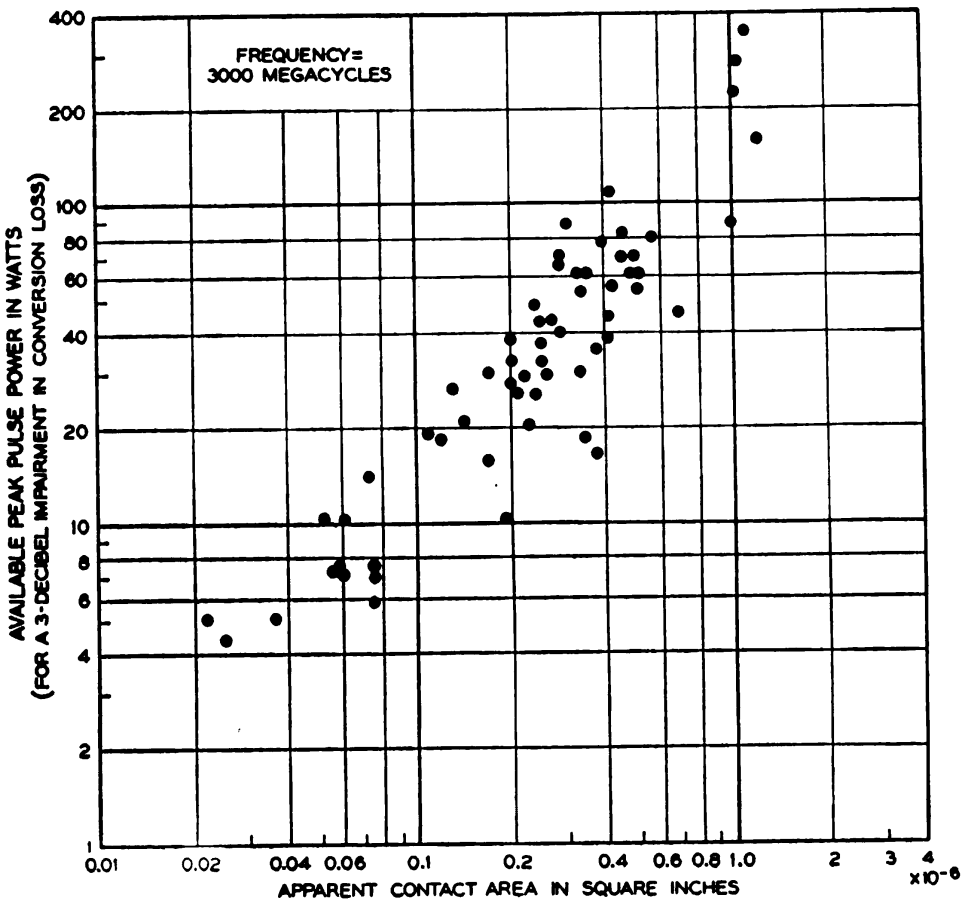

Fig. 13—Correlation between power handling ability measured with microsecond radio frequency pulses and contact area in silicon crystal rectifiers.

quency units because emphasis has been placed upon achieving a given signal-to-noise performance in each frequency band.

Use of the improved materials and processes produced rather large improvements in the d-c rectification ratio, conversion loss, noise, power handling ability, and uniformity. Typical direct-current rectification characteristics of units produced by both the old and the new processes are shown in Fig. 14. These curves show that reverse currents at one volt were decreased by a factor of about 20 while the forward currents were increased by

Digitized by Google
Original from UNIVERSITY OF MICHIGAN
Generated on 2019-09-23 05:37 GMT / http://hdl.handle.net/2027/mdp.39015077775156
Public Domain, Google-digitized / http://www.hathitrust.org/access_use#pd-google

a factor of approximately 2.5 giving a net improvement in rectification ratio of 50 to 1. The parallel improvement in receiver performance resulting from process improvements is shown in Fig. 15. A comparison in power handling

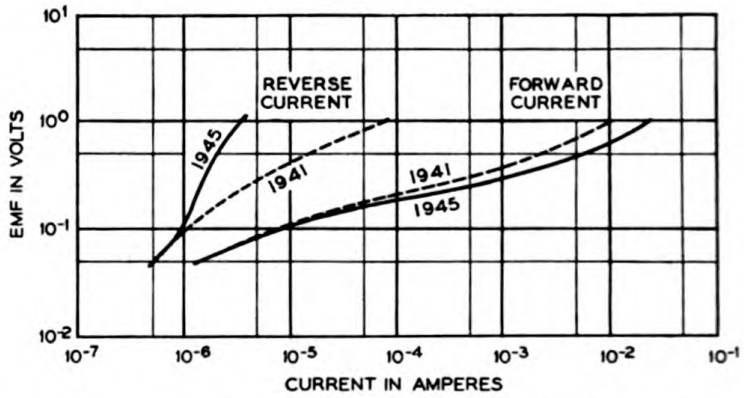

Fig. 14—Improvement in the direct-current rectification characteristics of silicon crystal rectifiers in a four-year period.

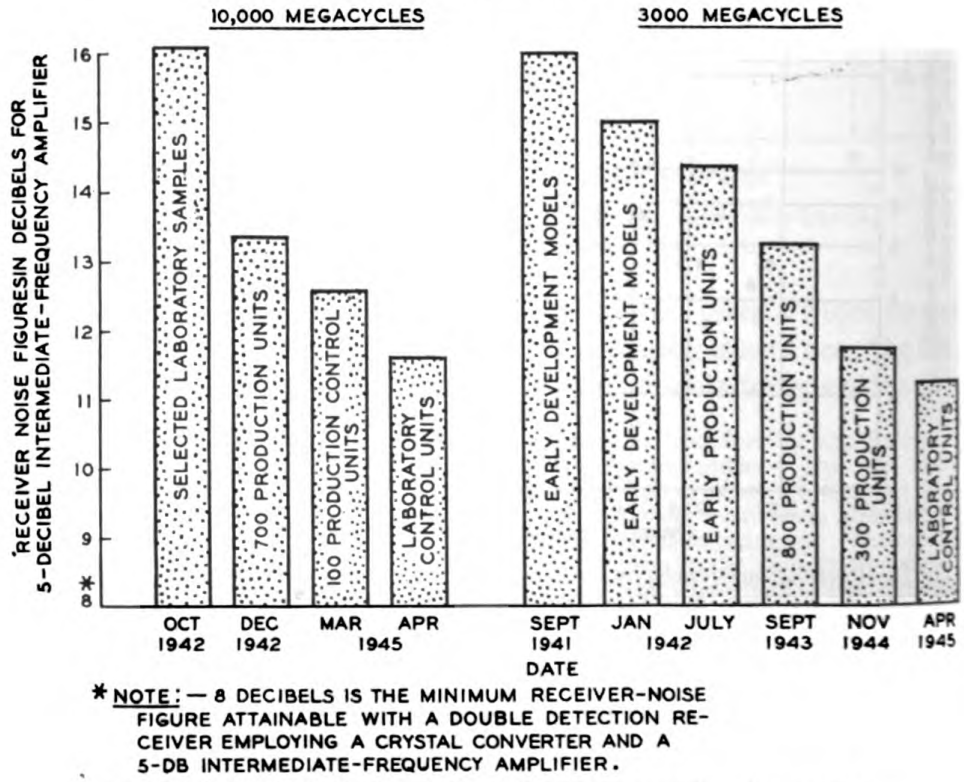

Fig. 15—Effect of continued improvement in the crystal rectifier on the microwave receiver performance. The noise figures plotted are average values.

ability of the 3000-megacycle converter types made by the improved procedures and the older procedures is shown in Fig. 16.

The flexibility of the processes may be illustrated by comparison of two

Digitized by Google
Original from UNIVERSITY OF MICHIGAN
Generated on 2019-09-23 05:37 GMT / http://hdl.handle.net/2027/mdp.39015077775156
Public Domain, Google-digitized / http://www.hathitrust.org/access_use#pd-google

very different units, the 1N26 and the 1N25. Though direct comparison of power handling ability is complicated by the fact that the burnout test methods employed in the development of the two codes were widely different, it may be stated conservatively that while the 1N26 would be damaged after absorbing something less than one watt peak pulse power, the 1N25 unit will withstand 25 watts peak or more. The 1N26 unit is, however, capable of satisfactory operation as a converter at a frequency of some 20 times that of the 1N25. These two units have been made by essentially the same procedures, the difference in properties being principally due to modification of alloy composition, heat treatment, and contact area.

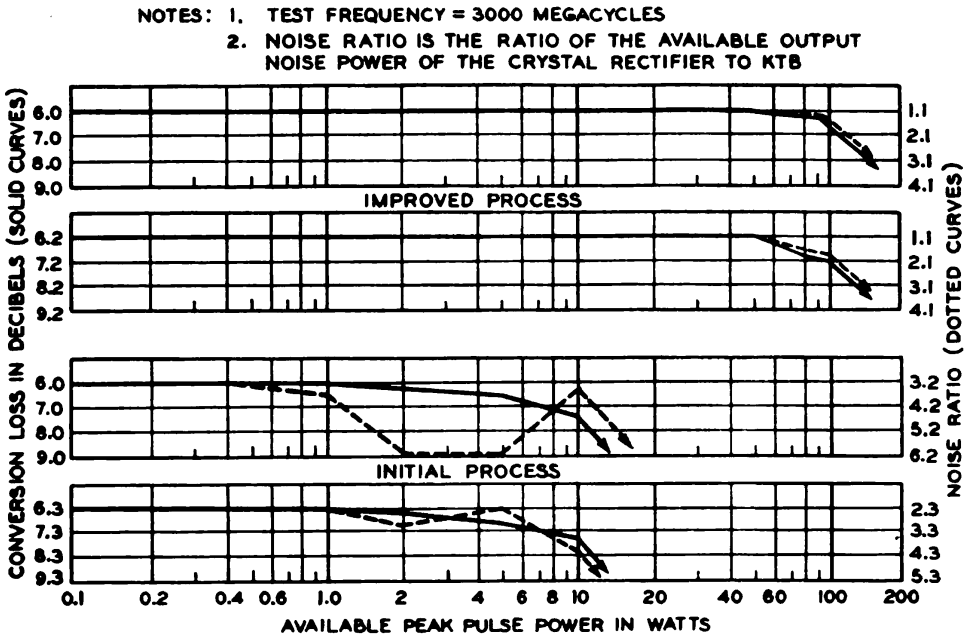

Fig. 16—Comparison of the radio frequency power handling ability of silicon crystal rectifiers prepared by different processes.

Prior to the process developments described above, in the interests of simplifying the field supply problem one general purpose unit, the type 1N21, had been made available for field use. However, it became obvious that the advantages of having but a single unit for field use could be retained only at a sacrifice in either power handling ability or high-frequency conversion loss. Since the higher power radar sets operated at the lower microwave frequencies, it seemed quite logical to employ the new processes to improve power handling ability at the lower microwave frequencies and to improve the loss and noise at the higher frequencies. A recommendation accordingly was made to the Services that different units be coded for operation at 3000 megacycles and at 10,000 megacycles. The decision in the matter was

Digitized by Google
Original from UNIVERSITY OF MICHIGAN
Generated on 2019-09-23 05:37 GMT / http://hdl.handle.net/2027/mdp.39015077775156
Public Domain, Google-digitized / http://www.hathitrust.org/access_use#pd-google

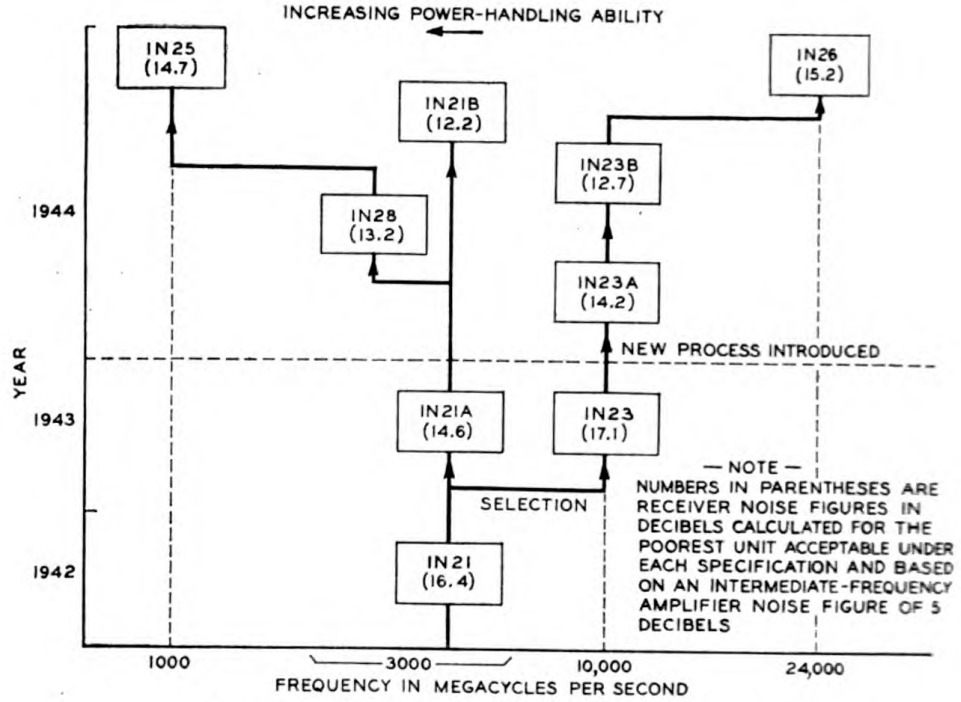

Fig. 17—Evolution of coded silicon crystal rectifiers.

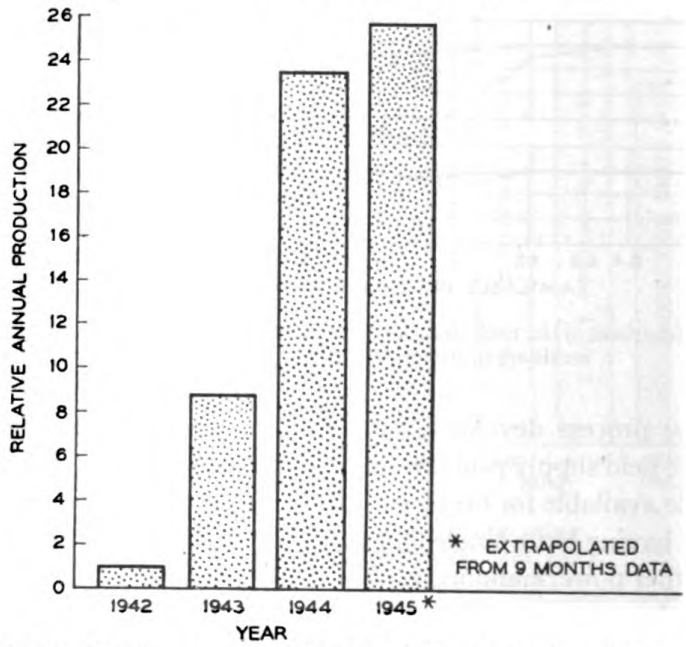

Fig. 18—Relative annual production of silicon crystal rectifiers at the Western Electric Company 1942–1945.

affirmative. The importance of this decision may be appreciated from the fact that it permitted the coding and manufacture of units such as the 1N21B and 1N28, high burnout units with improved performance at 3000

Digitized by Google
Original from UNIVERSITY OF MICHIGAN
Generated on 2019-09-23 05:38 GMT / http://hdl.handle.net/2027/mdp.39015077775156
Public Domain, Google-digitized / http://www.hathitrust.org/access_use#pd-google

megacycles, and the 1N23B unit which was of such great importance in 10,000 megacycle radars because of its exceptionally good performance. From this stage in the development the diversification in types was quite rapid. The evolution of the coded units, of increasing power handling ability for a given performance level at a given frequency, and of better performance at a given frequency is graphically illustrated in Fig. 17. The large improvements in calculated receiver performance are again evident, especially when it is considered that the receiver performances given are for the poorest units which would pass the production test limits.

Extent of Manufacture and Utilization

An historical resumé of the development of crystal rectifiers would be incomplete if some description were not given of the extent of their manufacture and utilization. Commercial production of the rectifiers by Western Electric Company started in the early part of 1942 and through the war years increased very rapidly. Figure 18 shows the increase in annual production over that of the first year. By the latter part of 1944 the production rate was in excess of 50,000 units monthly. Production figures, however, reveal only a small part of the overall story of the development. The increase in production rate was achieved simultaneously with marked improvements in sensitivity, the improvements in process techniques being reflected in manufacture by the ability to deliver the higher performance units in increasing numbers.

The recent experience with the silicon rectifiers has demonstrated their utility as non-linear circuit elements at the microwave frequencies, that they may be engineered to exacting requirements of both a mechanical and electrical nature, and that they can be produced in large quantities. The deficiencies of the detector of World War I, which limited its utility and contributed to its retrogression, have now been largely eliminated. It is a reasonable expectation that the device will now find an extensive application in communications and other electrical equipment of a non-military character, at microwave as well as lower frequencies, where its sensitivity, low capacitance, freedom from aging effects, and its small size and low-power consumption may be employed advantageously.

Acknowledgements

The development of crystal rectifiers described in this paper required the cooperative effort of a number of the members of the staff of Bell Telephone Laboratories. The authors wish to acknowledge these contributions and in particular the contributions made by members of the Metallurgical group and the Holmdel Radio Laboratory with whom they were associated in the development.

Digitized by Google
Original from UNIVERSITY OF MICHIGAN
Generated on 2019-09-23 05:38 GMT / http://hdl.handle.net/2027/mdp.39015077775156
Public Domain, Google-digitized / http://www.hathitrust.org/access_use#pd-google

Characteristics of Vacuum Tubes for Radar Intermediate Frequency Amplifiers

By G. T. FORD

1. Introduction

THE desired characteristics for vacuum tubes for use in broad-band intermediate frequency amplifiers are primarily high transconductance, low capacitances, high input resistance, and good noise figure. These characteristics determine the frequency bandwidth, amplification, and signal-to-noise ratio attainable with such an amplifier. The maximum operating frequency is generally limited by the input resistance of the tube which decreases as the frequency is increased, and, in some cases, by the tube noise which increases with increasing frequency. Three other characteristics which are also important are small physical size, low power consumption, and ruggedness. The present paper describes how these characteristics are related to the performance requirements for intermediate frequency (IF) amplifiers used in radar systems and shows how the requirements were met in the design of the Western Electric 6AK5 Vacuum Tube.

In a coaxial cable carrier telephone system of the type which was initially installed between Stevens Point, Wisconsin and Minneapolis, Minnesota[1] the upper frequency of the useful band is of the order of three megacycles per second (mc) and the bandwidth is of the same order. The Western Electric 386A tube was developed a number of years ago for amplifiers such as those used in this system. It is characterized by high transconductance and low capacitances. In radar receiving systems similar but more exacting requirements must be met for the IF amplifier. It is desirable to operate in many cases at a mid-band frequency of 60 mc, to have a bandwidth of the order of 2–10 mc, and to have as close to the ideal noise figure as possible. Additional considerations of great practical importance are low power consumption, small size, and ruggedness.

The choice of the mid-band frequency for the IF amplifier is influenced by considerations, a detailed discussion of which is outside the scope of this paper. For example, the characteristics of the beating oscillator and ite relation to the operation of the automatic frequency control (AFC) system, when AFC is used, are involved. The usual practice has been to

[1] "Stevens Point and Minneapolis Linked by Coaxial System," K. C. Black, *Bell Laboratories Record*, January 1942, pp. 127–132.
"Television Transmission Over Wire Lines," M. E. Strieby and J. F. Wentz, *Bell System Technical Journal*, January 1941, Vol. 20, p. 62.

Digitized by Google
Original from UNIVERSITY OF MICHIGAN
Generated on 2019-09-23 09:05 GMT / http://hdl.handle.net/2027/mdp.39015077775156
Public Domain, Google-digitized / http://www.hathitrust.org/access_use#pd-google

standardize on a mid-band frequency of 30 mc or 60 mc. The latter frequency has been used in most radars developed at the Bell Telephone Laboratories.

In pulsed radar systems the transmitter is turned on and off by the modulator in such a way that radio frequency energy is generated for a pulse duration τ seconds at a repetition rate which is usually several hundred per second. When the transmitter is modulated by a pulse which approaches that shown in Fig. 1(a), the energy-frequency distribution in the transmitted signal is as shown in Fig. 1(b). Although the maximum of the distribution

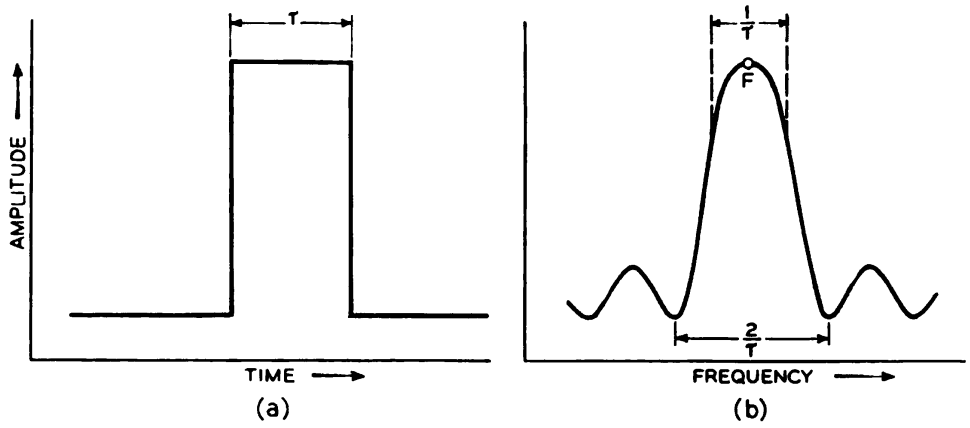

Fig. 1a—Modulating pulse
Fig. 1b—Amplitude—frequency distribution in transmitted RF pulse.

curve lies at the transmitter frequency F, there is considerable energy in the range $F \pm \frac{1}{2\tau}$ and the receiver usually has a bandwidth of at least $\frac{1}{\tau}$ in order to make as efficient use as possible of the energy in the echoes reflected by the target. For many radar applications, this requirement and the problems of transmitter and beating oscillator frequency stability result in the use of a bandwidth of as much as 10 mc for the IF amplifier.

The Western Electric 386A tube, Fig. 2(a), had characteristics which approached those needed to meet the IF amplifier requirements discussed above. It was therefore slightly modified in physical form for convenience of use and recoded the Western Electric 717A tube, Fig. 2(b). The 717A tube was used extensively in IF amplifiers in several radar systems. As the emphasis on small size and light weight for airborne radars increased, and, as the need for better characteristics became more pressing, further development was undertaken which resulted in the Western Electric 6AK5 tube, Fig. 3.

The importance of size and weight for radar systems to be used in airplanes is obvious. The use of miniature tubes in airborne equipment has

Digitized by Google
Original from UNIVERSITY OF MICHIGAN
Generated on 2019-09-23 09:05 GMT / http://hdl.handle.net/2027/mdp.39015077775156
Public Domain, Google-digitized / http://www.hathitrust.org/access_use#pd-google

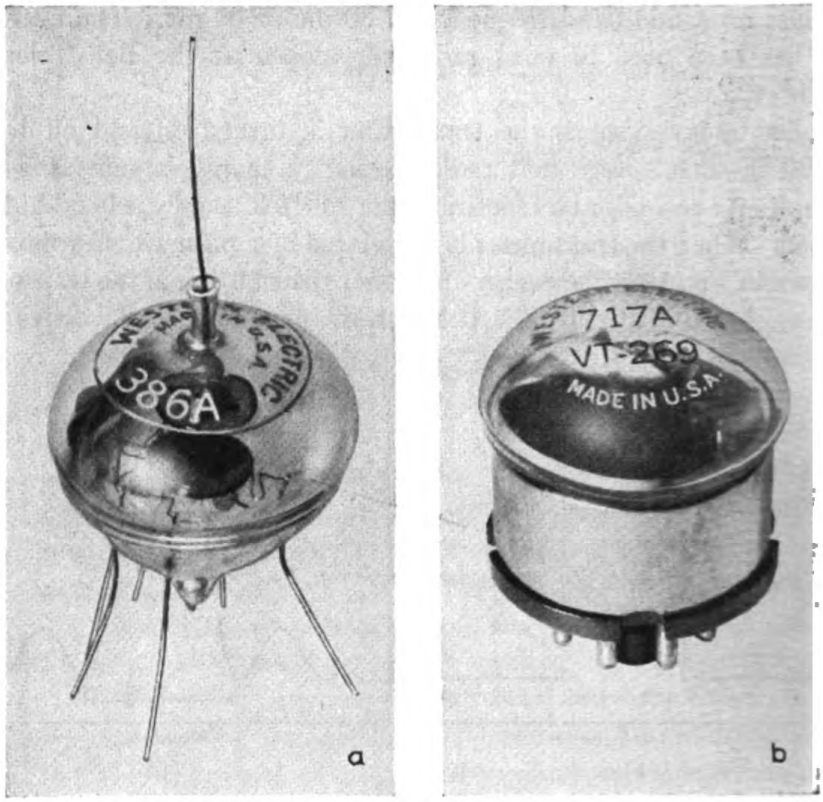

Fig. 2a—Western Electric 386A vacuum tube (full size).
Fig. 2b—Western Electric 717A vacuum tube (full size).

Fig. 3—Western Electric 6AK5 vacuum tube (full size).

been a consequence wherever their power handling capabilities are adequate to meet the performance requirements. The IF amplifier offers an ideal opportunity to effect substantial savings in both size and weight by using

Digitized by Google
Original from UNIVERSITY OF MICHIGAN
Generated on 2019-09-23 09:06 GMT / http://hdl.handle.net/2027/mdp.39015077775156
Public Domain, Google-digitized / http://www.hathitrust.org/access_use#pd-google

small tubes. When the IF frequency is as high as 30 mc or 60 mc, the circuit elements are physically small, so that the tube size is relatively important. The power level is low enough so that miniature tubes are applicable. The photograph shown in Fig. 4 illustrates the reduction in the size of the IF amplifier obtained by using 6AK5 tubes in place of 6AC7 tubes which were widely used previously. The larger amplifier weighs 2 lbs. 4 oz. while the smaller one weighs only 9 oz. Each of these amplifiers provides an over-all amplification of about 95 db at a mid-band frequency of 60 mc. The bandwidths of the two amplifiers are comparable. The amplifier using 6AC7 tubes requires 31.3 watts of power, while the 6AK5

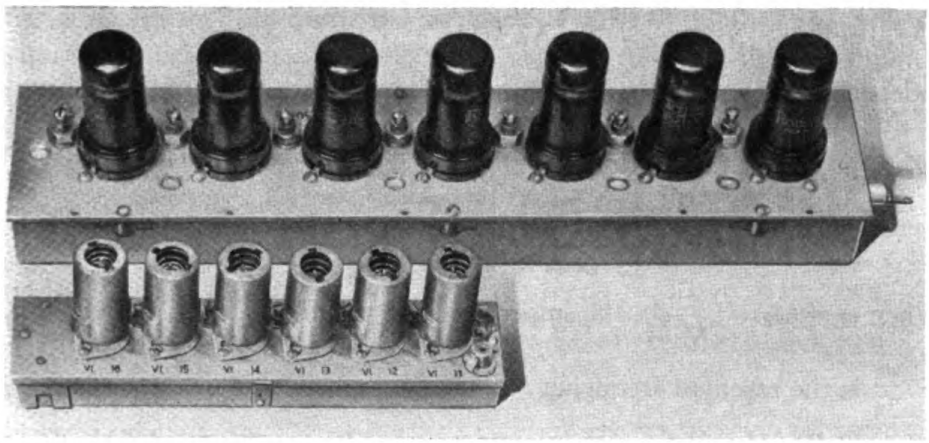

Fig. 4—60 Megacycle IF amplifiers (¼ full size).

amplifier requires 14.4 watts. The power savings possible with the 6AK5 tubes are not particularly important from the power economy standpoint, but rather because of the easier heat dissipation problem. In compact equipment such as airborne radar, the problem of keeping the operating temperatures of the various components within safe limits is formidable.

In the later years of the war the 6AK5 tube became the standard IF amplifier tube for radar systems and because of its superior properties was used for other applications in many other radio equipments.

2. Amplification and Bandwidth

The amplification that can be obtained with a given number of stages, and the useful bandwidth, are closely related. Within certain limits, one can be increased at the expense of the other. In fact, the product of the amplification per stage and the bandwidth is one important measure of the goodness of a particular tube and circuit design. A simple case will illustrate how this comes about. Assume the band-pass interstage shown in Fig. 5. L is the inductance of the coil, R is the shunt resistance equivalent to the

Digitized by Google
Original from UNIVERSITY OF MICHIGAN
Generated on 2019-09-23 09:06 GMT / http://hdl.handle.net/2027/mdp.39015077775156
Public Domain, Google-digitized / http://www.hathitrust.org/access_use#pd-google

load resistor and any loading effects due to high-frequency losses in the tubes or circuit elements, and C is the total shunt capacitance of the tubes, the circuit elements and the wiring. If it is assumed that R, L and C are

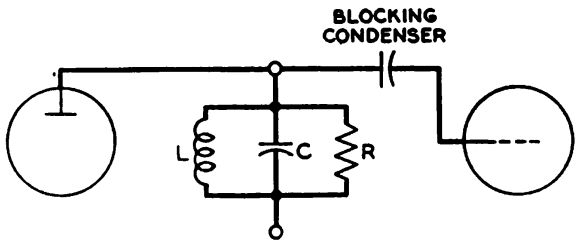

Fig. 5—Band-pass interstage.

independent of frequency, the magnitude of the impedance of this network is

$$|Z| = \frac{1}{\left[\left(\frac{1}{R}\right)^2 + \left(\omega C - \frac{1}{\omega L}\right)^2\right]^{1/2}} \quad (1)$$

When $\omega = \omega_0 = \frac{1}{\sqrt{LC}}$ the impedance is a maximum and the frequency $f_0 = \frac{\omega_0}{2\pi}$ is the resonant frequency. The maximum value of the impedance is $|Z_0| = R$. If this type of interstage is used in a grounded-cathode type of circuit employing a pentode tube, the small-signal voltage amplification A_v from the control grid of the tube to the plate is

$$A_v = G_m |Z| \quad (2)$$

where G_m is the grid-plate transconductance of the tube. It is assumed that $|Z|$ is small compared to the plate resistance of the pentode and that there is no feedback. The voltage amplification A_{v0} at the resonant frequency is then

$$A_{v0} = G_m R \quad (3)$$

If the bandwidth is defined as $\Delta F = f_1 - f_2$, where f_1 and f_2 are the two frequencies where $A_v = \frac{A_{v0}\sqrt{2}}{2}$, it can be shown that

$$\Delta F = f_1 - f_2 = \frac{1}{2\pi RC} \quad (4)$$

The product of the mid-band voltage gain times the bandwidth can be called the band merit, B_0, and we have

$$B_0 = (\Delta F)(A_{v0}) = \frac{1}{2\pi RC}(G_m R) = \frac{G_m}{2\pi C} \quad (5)$$

Digitized by Google
Original from UNIVERSITY OF MICHIGAN
Generated on 2019-09-23 09:06 GMT / http://hdl.handle.net/2027/mdp.39015077775156
Public Domain, Google-digitized / http://www.hathitrust.org/access_use#pd-google

This expression for band merit has been derived from the product of the bandwidth and the voltage amplification for a simple band-pass interstage. Higher band merits can be realized with a given tube by using more complicated coupling networks.

Another interpretation of band merit is to say that it is the frequency at which the voltage amplification is unity. This is the frequency at which the product of the transconductance and the reactance of the shunt capacitance is unity.

From the foregoing expression for band merit it is evident that, in general, the higher the band merit the fewer is the number of stages that are required to obtain a given gain and bandwidth. It is highly desirable to keep the number of stages small in order to save space, weight and power consumption and to avoid the use of unnecessary components which reduce the

TABLE I

Type	Heater Power	Plate Current	Total Power Consumption	Nominal Transconductance	Transconductance per Unit Plate Current	Band Merit
	watts	*ma*	*watts*	*umhos*	*umhos/ma*	*mc*
6AC7	2.84	10	4.7	9,000	900	89.5
6AG7	4.10	30	9.6	11,000	367	85.3
6AG5	1.89	7.2	3.0	5,100	708	90.0
717A	1.10	7.5	2.3	4,000	533	71.4
6AK5	1.10	7.5	2.3	5,000	667	117.

reliability in operation. In practice the total amplification in the receiver is made high enough so that the system noise, with no signal, produces a fair indication on the output device when the gain control is set for maximum gain. For a bandwidth of 5 mc, the equivalent *RF* input noise power level is of the order of 2×10^{-13} watt and the power level necessary for a suitable oscilloscope presentation in a radar is about 20 milliwatts. The net over-all gain needed is then about 110 *db*. Making an allowance of, say, 15 *db* for losses in the detectors and elsewhere, a total of about 125 *db* gain is required. A minimum of about 110 *db* of this is usually in the *IF* part of the receiver. With this amount of gain as a requirement it is easy to see the importance of high band merit, small size, and low power consumption in the *IF* tubes.

Table I, above, compares the salient characteristics of the 6AK5 with those of other similar types of tubes.

The tube design factors which determine the band merit will now be examined by considering an idealized case. For an idealized plane parallel triode structure in which edge effects are assumed to be negligible, the plate current can be related to the tube geometry and the applied voltages approximately as follows:[2]

[2] "Fundamentals of Engineering Electronics," W. G. Dow, pp. 44, 102, et seq.

Digitized by Google
Original from UNIVERSITY OF MICHIGAN
Generated on 2019-09-23 09:07 GMT / http://hdl.handle.net/2027/mdp.39015077775156
Public Domain, Google-digitized / http://www.hathitrust.org/access_use#pd-google

$$I_b = \frac{2.33 \times 10^{-6} A \left(E_{c1} + \frac{E_b}{\mu}\right)^{3/2}}{a^2 \left(1 + \frac{1}{\mu}\frac{a+b}{b}\right)^{3/2}} \quad \ldots\ldots\ldots\ldots (6)$$

It is assumed that the electrons leave the cathode with zero initial velocities. The failure to take into account the effects of initial velocities makes this equation only a fair approximation for close-spaced tubes, but it is still instructive to assume it is approximately correct for the purposes of the present discussion. "A" is the active area of the structure, "a" is the distance from the cathode to the plane of the grid, "b" is the distance from the plane of the grid to the plate, E_b is the plate voltage, E_{c1} is the effective grid voltage (including the effect of contact potential) and μ is the amplification constant. Dimensions are in cms. This stipulation is unnecessary for equation (6) but is necessary for some of the later equations. For a plane parallel tetrode or pentode, equation (6) is a good approximation if E_b is replaced by the screen voltage E_{c2}, μ is replaced by the "triode mu" μ_{12} (mu of control grid with respect to screen grid) and the coefficient M introduced, where M is the ratio of the plate current to the cathode current. The reason this approximation is good is that the field at the cathode, and therefore the cathode current, is determined almost entirely by the potentials of the first two grids. Because of the screening effect of these grids the potential of the plate has little effect on the cathode current. We have then

$$I_b = \frac{2.33 \times 10^{-6} MA \left(E_{c1} + \frac{E_{c2}}{\mu_{12}}\right)^{3/2}}{a^2 \left(1 + \frac{1}{\mu_{12}}\frac{a+b}{a}\right)^{3/2}} \quad \ldots\ldots\ldots\ldots (7)$$

The distance "b" is now the distance from the plane of the grid to the plane of the screen. This expression can be differentiated with respect to E_{c1} to get

$$G_m = \frac{dI_b}{dE_{c1}} = \frac{3}{2} \frac{2.33 \times 10^{-6} MA \left(E_{c1} + \frac{E_{c2}}{\mu_{12}}\right)^{1/2}}{a^2 \left(1 + \frac{1}{\mu_{12}}\frac{a+b}{a}\right)^{3/2}} \quad \ldots\ldots\ldots\ldots (8)$$

It is assumed that μ_{12} and M are independent of E_{c1}. If we let I_0 be the cathode current density, then substitute MI_0A for I_b in (7), and eliminate the expression $\left(E_{c1} + \frac{E_{c2}}{\mu_{12}}\right)$ between (7) and (8), we have

$$G_m = \frac{3}{2} \frac{(2.33 \times 10^{-6})^{2/3} MA I_0^{1/3}}{a^{4/3} \left(1 + \frac{1}{\mu_{12}}\frac{a+b}{a}\right)} \quad \ldots\ldots\ldots\ldots (9)$$

Digitized by Google
Original from UNIVERSITY OF MICHIGAN
Generated on 2019-09-23 09:07 GMT / http://hdl.handle.net/2027/mdp.39015077775156
Public Domain, Google-digitized / http://www.hathitrust.org/access_use#pd-google

Neglecting the stray capacitances between the lead wires and also the edge effects, the greater proportion of the cold capacitance (input plus output) in Farads can be approximated by

$$C_0 = .0885A\left(\frac{1}{a}+\frac{1}{b}+\frac{1}{c}\right)\times 10^{-12} \quad \ldots\ldots\ldots\ldots (10)$$

where "a" and "b" have the same meaning as in (7) and "c" is the spacing between the plate and the suppressor (or screen in the case of a tetrode). This is of course a highly idealized case. The cathode, the grids, and the plate, are each assumed to be plane conductors of infinitesimal thickness, each having an area equal to the active area of the structure.* The band merit then becomes.

$$B_0 = \frac{G_m}{2\pi C_0} = \frac{4.74\, M\, I_0^{1/2}\times 10^8}{a^{4/3}\left(\frac{1}{a}+\frac{1}{b}+\frac{1}{c}\right)\left(1+\frac{1}{\mu_{12}}\frac{a+b}{a}\right)} \quad \ldots\ldots (11)$$

With a given cathode current, the factor M increases as the screen current is reduced. The use of small wires for the screen grid is an important factor in obtaining minimum screen current.

I_0, the useful cathode current density, is limited by the emission capabilities of the cathode. In practice it is necessary to operate in a region considerably below the maximum available emission to avoid excessive changes in transconductance which would result from variations in cathode activity with time. Also, the shot noise will begin to rise when the region of temperature-limited operation is approached. It should be noted that B_0 is independent of the area A.

Taking reasonable values for M, I_0 and μ_{12}, ($M = 0.75$, $I_0 = 50\ ma/cm^2$, $\mu_{12} = 25$), equation (11) becomes

$$B_0 = \frac{1.31\times 10^8}{a^{4/3}\left(\frac{1}{a}+\frac{1}{b}+\frac{1}{c}\right)\left(1+.04\,\frac{a+b}{a}\right)} \quad \ldots\ldots\ldots (12)$$

The curves in Figs. 6, 7 and 8 show how B_0 varies with each of the variables "a", "b" and "c" when a constant value is assigned to the other two. The band merit shown on these curves is considerably greater than that which can be realized in an actual circuit of the simple band-pass type assumed because the stray capacitances in the tube, the socket, the circuit elements, and the wiring increase the total interstage capacitance substantially. Also, the grid-cathode capacitance is substantially higher under normal operating

* This assumption is obviously not true, particularly in the case of the suppressor grid, but, by simply regarding the effective suppressor-plate spacing as somewhat greater than the actual spacing, the assumption becomes useful.

Digitized by Google
Original from UNIVERSITY OF MICHIGAN
Generated on 2019-09-23 09:07 GMT / http://hdl.handle.net/2027/mdp.39015077775156
Public Domain, Google-digitized / http://www.hathitrust.org/access_use#pd-google

conditions, because of the presence of space charge, than when the tube is cold, as assumed in deriving equation (11). It has been assumed in making

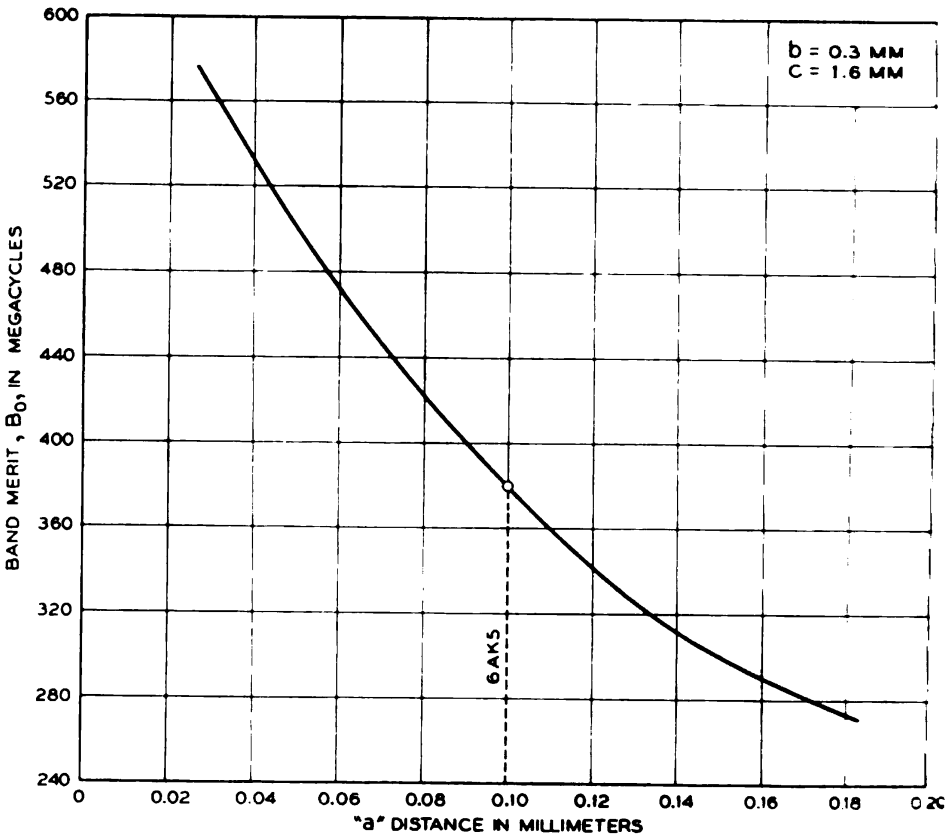

Fig. 6—Band merit vs. grid-cathode spacing.

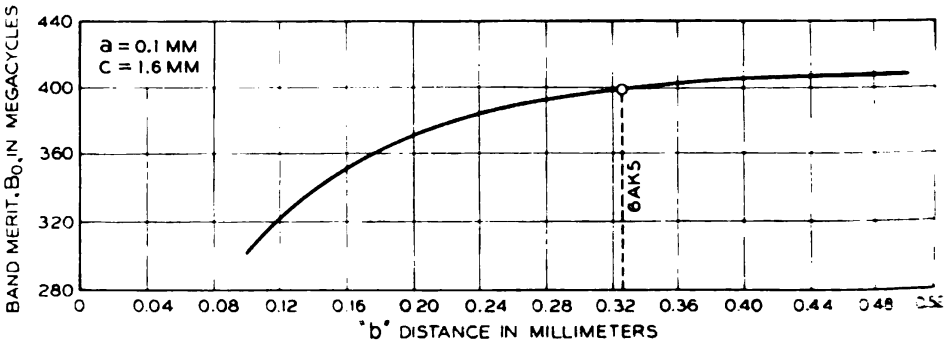

Fig. 7—Band merit vs. grid-screen spacing.

the calculations that the current density and the triode *mu* are held constant while "*a*", "*b*" and "*c*" are varied. In the cases of "*a*" and "*b*", this requires that the control grid and/or screen voltage be varied in such a fashion as to hold I_0 constant. The current density is nearly independent of "*c*" over a

Digitized by Google
Original from UNIVERSITY OF MICHIGAN
Generated on 2019-09-23 09:07 GMT / http://hdl.handle.net/2027/mdp.39015077775156
Public Domain, Google-digitized / http://www.hathitrust.org/access_use#pd-google

reasonable range provided "c" is not so large as to cause the formation of a virtual cathode in the screen-plate space.

Figure 6 shows that B_0 rises as "a" is reduced. Reducing "a" also has the advantage that a lower screen voltage is required with a given grid bias. The improvement in B_0 as "a" is reduced is quite rapid, but of course the mechanical difficulties involved in reducing "a" below about 0.10 mm become very great.

The curve in Fig. 7 shows that B_0 does not increase much if "b" is increased above about 0.30 mm, and increasing "b" has the disadvantage that higher screen voltage for a given grid bias is required.

The curve in Fig. 8 shows that B_0 increases very slowly if "c" is increased beyond about 1.50 mm, and increasing "c" has the disadvantage that the external dimensions of the structure become greater. Increasing "c" also means that the plate comes closer to any shield which is placed around the

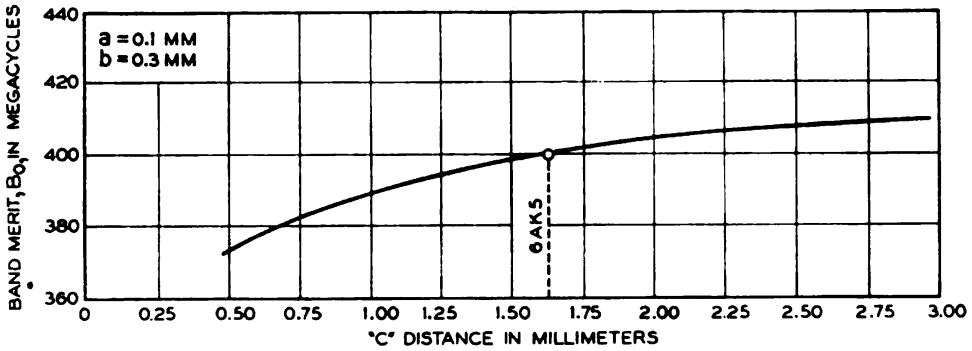

Fig. 8—Band merit vs. plate-suppressor spacing.

bulb of the tube, thus increasing the output capacitance and tending to cancel out any improvement obtained in the structure itself. Also, if "c" is made too large a virtual cathode may be formed in the screen-plate space under some conditions. This would interfere with the normal operation of the tube.

In order to take full advantage of the close grid-cathode spacing, the control-grid pitch should be no greater than about 1.5 times the spacing and the grid wires should be as small as possible. If the pitch is too large, the parts of the cathode directly opposite the grid wires will be cut off while space current is flowing from the sections opposite the spaces between grid wires. This state of affairs shows up in the characteristics as excessive variation of the triode amplification factor, μ_{12}, as the grid bias is varied, and results in a reduction of the transconductance. That is, when the grid is made more negative the amplification factor μ_{12} decreases so that the plate current does not decrease as much as it would if μ_{12} remained constant.

Generated on 2019-09-23 09:07 GMT / http://hdl.handle.net/2027/mdp.39015077775156
Public Domain, Google-digitized / http://www.hathitrust.org/access_use#pd-google
Digitized by Google
Original from UNIVERSITY OF MICHIGAN

When the grid is made more positive the plate current rise is reduced because μ_{12} increases. The grid wires should be as small as possible so as to block off no more of the area of the structure than is necessary. An ideal grid would be an infinitesimally thin conducting plane which offered no resistance to the passage of electrons through it except that due to its electrostatic potential (sometimes called a "physicist's grid"). In the 6AK5 tube the grid-cathode clearance is 0.089 mm (0.0035 inch), the control-grid pitch is 0.0127 mm (0.0050 inch), and the wire size is 0.0010 inch. Experiments have shown that substantially higher transconductance could have been realized, with the same spacing, if smaller wires and smaller pitch had been used, but the mechanical difficulties would have been much greater.

The way to achieve a high band merit from the tube design standpoint is thus to use as close grid-cathode clearance as practicable, to operate the tube at as high a current density as the emission capabilities of the cathode will permit, and to keep the stray capacitances as low as possible. It was noted above from (11) that B_0 is independent of A. However, if it were possible to maintain the same grid-cathode clearance with a large tube as it is with a small one, the larger tube would have the advantage that the stray capacitances in the tube would be a smaller fraction of the total capacitance so that the band merit for the tube would be higher. It would also be closer to what can be realized when the tube is used in an actual circuit because the capacitances added by the socket, the wiring and the circuit elements would be less important. However, the practical mechanical limitations controlling the minimum grid-cathode clearance have been such that the band merit is roughly independent of the tube size over a moderate range of sizes of high transconductance receiving tubes.

3. Input Conductance

Two factors tend to make the input conductance of tubes higher at high frequencies than at low frequencies. One is the effect of lead inductances and the other is the effect of transit time. If the loading produced by these effects is no more than that required to get the desired bandwidth, it may be no particular disadvantage for stages other than the first one in the amplifier. As will be seen later, however, this effect in the input tube increases the noise figure. The practical result of a consideration of these effects is that the leads are made as short as possible and that small tubes are used in order to use close grid-cathode clearances when the frequency at which the tubes are to be used is above about 10 mc. The expression derived by North[3] for

[3] "Analysis of the Effects of Space Charge on Grid Impedance," D. O. North, I. R. E. Proceedings, Vol. 24, No. 1, January, 1936.

Digitized by Google
Original from UNIVERSITY OF MICHIGAN
Generated on 2019-09-23 09:07 GMT / http://hdl.handle.net/2027/mdp.39015077775156
Public Domain, Google-digitized / http://www.hathitrust.org/access_use#pd-google

the input conductance of a tetrode or pentode can be re-written, neglecting the higher order terms, to give the approximate expression

$$G_{in} = \frac{5.0 \times 10^{-3} a^2 f^2 G_m}{V_1}\left[1 + 3.3\,\frac{b}{a\left(1 + \sqrt{\frac{V_2}{V_1}}\right)}\right] \quad \ldots\ldots(13)$$

where G_m is the triode-connected transconductance, a is grid-cathode spacing in cms, b is grid-screen spacing in cms, V_1 and V_2 are the effective grid-plane and screen-plane potentials in volts, and f is the frequency in mc. It is assumed that there are no lead inductances and that there is no potential minimum in the grid-cathode region. For a given transconductance, (13) shows that close spacings are necessary for minimum grid conductance.

If the lead inductances between the external circuit and the tube elements are appreciable, the input loading may be excessive even though the transit time through the tube structure is negligibly small. The general case taking account of the mutual and self inductances of all the leads of a pentode has been treated by Strutt and van der Ziel[4]. The equations are cumbersome even though only the first order terms in frequency are retained. If all of the lead inductances except that in series with the cathode are neglected, and transit time is assumed to be negligible, the input conductance of a pentode becomes approximately[5]

$$G_{in} = \omega^2 G_m L_k C_k \quad \ldots\ldots(14)$$

where L_k is the cathode lead inductance and C_k is the grid-cathode capacitance. It is further assumed that the plate-grid capacitance is negligible.

Work done at the Naval Research Laboratory includes data on the input conductance of 6AK5 tubes in the frequency range from 100 mc to 300 mc. Through the courtesy of the Naval Research Laboratory some of the data are reproduced in Fig. 9. It is of interest to check a point on this curve against equation (14). For the 6AK5, 0.02 micro-henry is the estimated* cathode lead inductance, $G_m = 5000 \times 10^{-6}$ mhos, and $C_k = 4 \times 10^{-12}$ farad. At a frequency of 250 mc we have a calculated conductance of 990 micromhos, which checks roughly with the value of 1110 micromhos from the curve in Fig. 9. Equation (13) can be used to obtain an approximate value for the loading due to transit time. Taking $a = 0.0089$ cm., $b = 0.032$ cm., $G_m = 6.7 \times 10^{-3}$ mhos, $f = 250$ mc, $V_1 = +2.3$ volts, and $V_2 = +120$ volts, a calculation gives $G_{in} = 177$ micromhos. These results

[4] "The Causes for the Increase of the Admittance of Modern High-Frequency Amplifier Tubes," M. J. O. Strutt and A. van der Ziel, *I. R. E. Proceedings*, Vol. 26, No. 8, August 1938.

[5] "Hyper and Ultra-High Frequency Engineering," Sarbacher and Edson, p. 435.

* This has been checked roughly by Q-meter measurements.

Digitized by Google
Original from UNIVERSITY OF MICHIGAN
Generated on 2019-09-23 09:08 GMT / http://hdl.handle.net/2027/mdp.39015077775156
Public Domain, Google-digitized / http://www.hathitrust.org/access_use#pd-google

show that the performance of the 6AK5 near the upper end of its present useful frequency range is probably limited to a considerable degree by the lead inductances rather than by transit time effects in the structure.

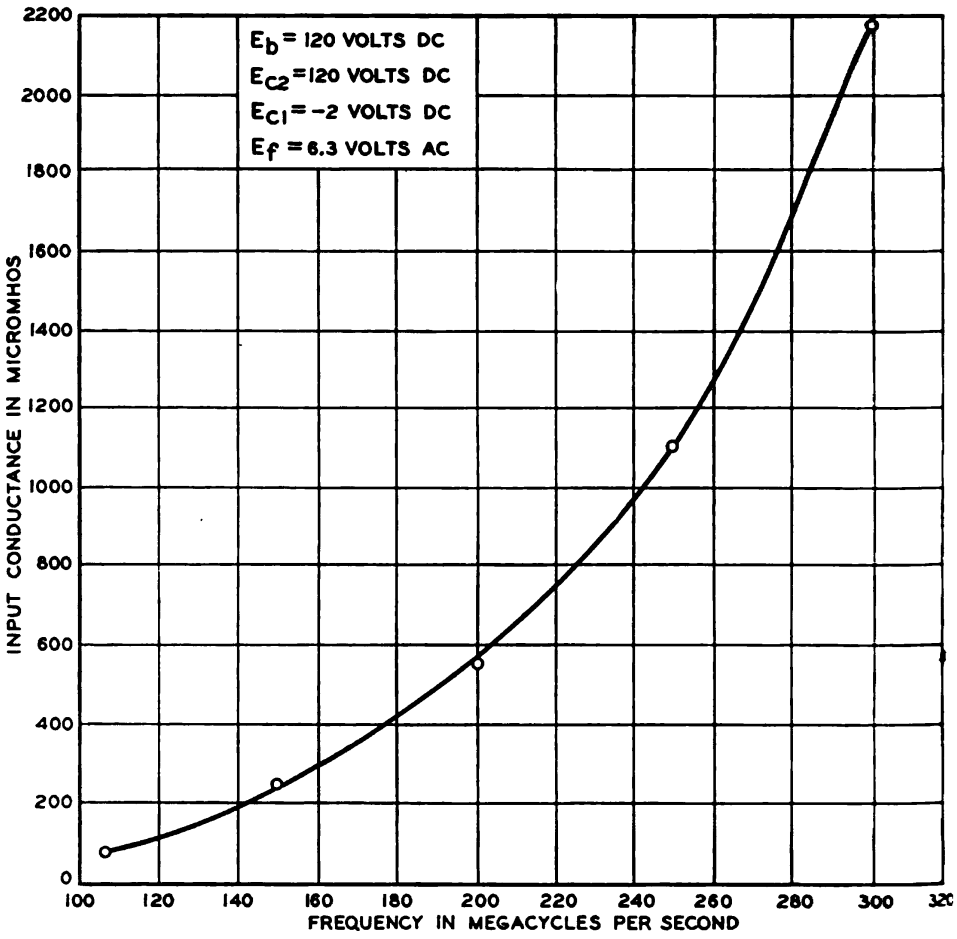

Fig. 9—Average input conductance vs. frequency for six 6AK5 tubes—courtesy of Naval Research Laboratory.

4. Noise

Although it may be possible to employ enough stages of IF amplification to provide the necessary gain and band-width we may still have a relatively insensitive receiver for weak signals. This comes about because there are inherent electrical disturbances in vacuum tubes and passive networks which give rise to random voltages. Since these disturbances may be of the order of the strength of the signal, they must be kept to a minimum in order to maintain a high signal-to-noise ratio. In a receiving system in which no RF amplification is used ahead of the first detector, the signal-to-noise ratio is limited to a large extent by the noisiness of the first detector and the first

Generated on 2019-09-23 09:08 GMT / http://hdl.handle.net/2027/mdp.39015077775156
Public Domain, Google-digitized / http://www.hathitrust.org/access_use#pd-google
Digitized by Google
Original from UNIVERSITY OF MICHIGAN

IF tube. The noise performance of the first IF stage will be discussed in some detail.**

A convenient method of expressing the departure from ideal performance is the use of the "noise figure" proposed by Friis.[6] The noise figure of a network or amplifier may be defined as follows:

$$NF = \frac{\text{Available output noise power}}{GKT\Delta f} \quad \ldots\ldots\ldots\ldots (15)$$

where G is the "available gain" which is defined as the ratio of the available signal power at the output terminals of the network or amplifier to the available signal power at the terminals of the signal generator. $KT\Delta f$ is the available noise power from a passive resistance, where K is Boltzmann's constant, T is absolute temperature and Δf is the incremental bandwidth. This follows from consideration of a noise generator of resistance R_0 working into a load resistance R_0. This is the condition for maximum power into the load, half of the noise voltage appearing across the source and half across the load. The open-circuit noise voltage appearing across the terminals of a resistance R_0 is

$$V^2 = 4KTR_0\Delta f \quad \ldots\ldots\ldots\ldots\ldots\ldots (16)$$

The noise power delivered to the load by the source resistance will be

$$P_n = \frac{V^2}{4R_0} = KT\Delta f \quad \ldots\ldots\ldots\ldots\ldots\ldots (17)$$

If there were no source of noise other than that of the resistance of the signal source itself, the noise figure would be unity. If the signal source works directly into a matched load resistance at the same temperature, the noise figure is 2 since the available output noise power is $KT\Delta f$ and the available gain is one-half.

The importance of the noise figure of the radar receiver is obvious since a reduction in the noise figure is equivalent to the same percentage increase in transmitter power. In recent radar systems the noise arising in the first IF stage constituted a substantial part of the total receiver noise.

If the first IF tube provides at least 15 db gain, noise introduced by its plate load impedance, and by anyother sources in the rest of the amplifier, is usually negligible. The departure of the noise figure of the IF amplifier from unity is then due to noise arising in the first tube and in its input circuit.

In the very high frequency (VHF) range, essentially all of the noise arising

** It will be assumed in all of the discussion about noise that there is no noise due to flicker effect, emission of positive ions, microphonics, sputter, ionization, secondary emission, or reflection of electrons from charged insulators.

[6] "Noise Figure of Radio Receivers," H. T. Friis, *I. R. E. Proceedings*, July 1944.

Digitized by Google
Original from UNIVERSITY OF MICHIGAN
Generated on 2019-09-23 09:08 GMT / http://hdl.handle.net/2027/mdp.39015077775156
Public Domain, Google-digitized / http://www.hathitrust.org/access_use#pd-google

in the tube itself is due to random fluctuations in the emission of electrons from the cathode. For a parallel plane diode in a circuit such as that shown in Fig. 10(*a*), the mean square noise current is[7]

$$i_k^2 = 2\Gamma^2 e I_k \Delta f \quad \text{(18}$$

where e is the electronic charge, I_k is the d-c cathode current, Δf is the incremental bandwidth, and Γ is a factor which takes into account the

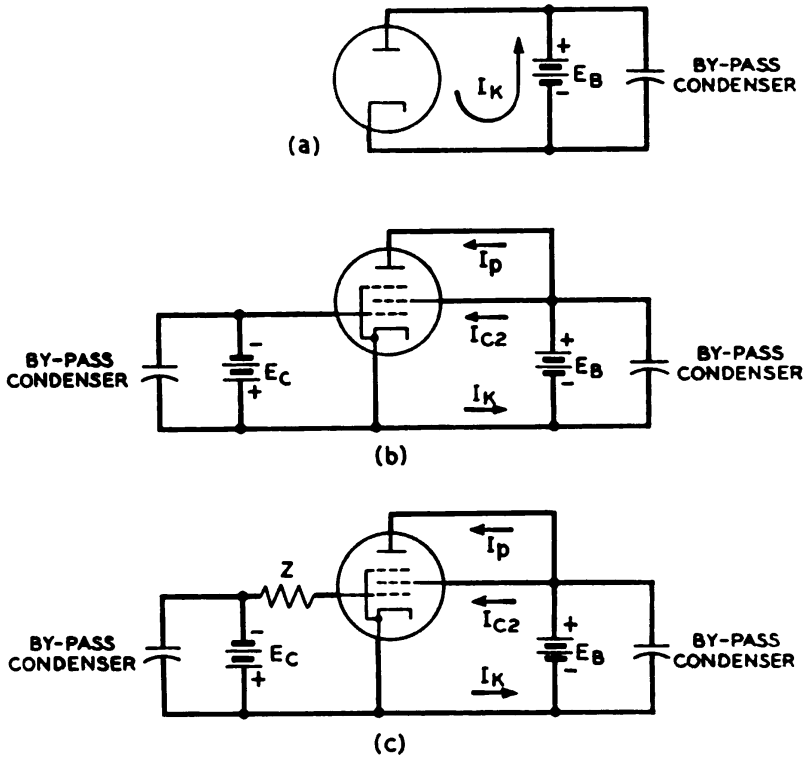

Fig. 10a—Diode, negligible circuit impedance.
Fig. 10b—Pentode, negligible circuit impedance.
Fig. 10c—Pentode, impedance in grid circuit.

"cushioning effect" of space charge. For anode-cathode spacings and operating conditions such that the transit time is not too large a faction of the period of the frequency involved, Γ is of the order of 0.20 when the zero-field emission is several times larger than I_k. Under temperature-limited conditions Γ is unity. That is, under favorable space-charge-limited conditions, the fluctuation noise component in I_k is only about 20% of the value for the same cathode current under temperature-limited conditions. Although the introduction of grids between the cathode and anode

[7] "Fluctuations in Space-Charge-Limited Currents at Moderately High Frequencies," B. J. Thompson, D. O. North, W. A. Harris, *R. C. A. Review*, October 1940, Vol. 5, p. 244.

Digitized by Google
Original from UNIVERSITY OF MICHIGAN
Generated on 2019-09-23 09:08 GMT / http://hdl.handle.net/2027/mdp.39015077775156
Public Domain, Google-digitized / http://www.hathitrust.org/access_use#pd-google

of the simple diode complicates the noise problem, the factor Γ remains of great importance. It is therefore desirable to control the tube processing in manufacture so as to insure adequate available emission in every tube. An "activity test" is made on completed tubes for this purpose. This test consists of reducing the heater voltage by an arbitrary amount (usually 10%) and observing the change in one of the tube characteristics which is sensitive to changes in available emission. The characteristic used for tubes like the 717A and 6AK5 is the transconductance. If the transconductance decreases by more than about 20% for a 10% reduction in heater voltage, with the other operating voltages held constant, insufficient available emission is indicated and Γ is higher than for more "active" tubes.

In the case of a pentode with negligible impedance in each of its leads, as shown in Fig. 10(b), the fluctuation in the cathode current is the same as that given in equation (18), but the noise component in the plate lead is larger. Thompson, North, and Harris[7] showed that it can be written as

$$i_p^2 = 2eI_p\Delta f\left[\frac{\Gamma^2 I_p + I_{c2}}{I_k}\right] \quad \ldots\ldots\ldots\ldots\ldots\ldots (19)$$

where I_p is the d-c plate current and I_{c2} is the d-c screen current. It was mentioned above that Γ can be made as low as 0.20 by providing adequate available emission. From the design standpoint, equation (19) also shows that the screen current should be as small as possible. For normal operating conditions in a pentode, the screen current is influenced by the screening fraction (fraction of area blocked off by grid wires) of the screen grid and by the amount of space current turned back to the screen in the screen-plate region. The way to get a minimum screening fraction and still obtain the desired function of the screen grid of reducing the plate-grid capacitance is to use wire of as small diameter as possible. The presence of a suppressor grid, at cathode potential, placed between the screen and the plate to prevent interchange of secondary electrons, causes a certain proportion of the space current which would otherwise go to the plate to be turned back to the screen. Here again, this effect is minimized by using as fine wire as possible for the suppressor grid. It was pointed out in an earlier section that fine wires are desired for the control grid. The ideal for each of the three grids in an IF pentode would be a conducting plane which offers no resistance to the passage of electrons other than the influence of its potential.

When impedances are connected in the various leads of a pentode the noise components discussed above will, in general, be different due to the influence of fluctuation voltages developed between the elements of the tube. In particular it is found experimentally in the VHF range of frequencies that when an impedance Z is introduced between the grid and cathode, as shown in Fig. 10(c), the noise component in the plate lead rises more than

Digitized by Google
Original from UNIVERSITY OF MICHIGAN
Generated on 2019-09-23 09:08 GMT / http://hdl.handle.net/2027/mdp.39015077775156
Public Domain, Google-digitized / http://www.hathitrust.org/access_use#pd-google

would be expected due to thermal noise from Z, because of the effect of grid noise. North and Ferris[8] showed that the grid noise can be taken into account by assuming that the input resistance of the tube is a resistance noise source whose absolute temperature is about 4.8 times ambient, if the input loading is due to transit time effects alone. One consequence of this input loading is that at high frequencies the best signal-to-noise ratio is usually obtained with an input circuit of lower impedance than that which would be used at low frequencies.

Actually, as was brought out in an earlier section, the loading in tubes like the 6AK5 is probably due largely to lead inductances between the active tube elements and the external circuit components up to a few hundred megacycles. According to Pierce[9] the effect of the cathode lead inductance feedback is to reduce the signal component in the output current while leaving the noise current due to screen interception noise unaffected. Input loading may be a limiting factor in tubes like the 717A and 6AK5 when the frequency is of the order of 100 mc or higher, both because of its effect on gain in some cases and because of its adverse effect on the signal-to-noise ratio for early stage use. There is good evidence that the 6AK5 structure would be useful at much higher frequencies than is the case at present if the circuit connections to the tube elements were improved by more advantageous mounting of the structure and the use of more suitable sockets or external connectors.

Noise measurements made by a number of workers at Bell Telephone Laboratories[10] indicate that an average noise figure of about 2.8 can be obtained with the 6AK5 at a midband frequency of 60 mc, with a well-designed input circuit, and bandwidths up to 10 mc. At a mid-band frequency of 30 mc the noise figure is about 2.4. At 100 mc it is about 3.6.

5. Description of the Design of the Western Electric 6AK5 Tube

In order that the reader may have a full appreciation of the dimensions and other requirements of design to meet the characteristics discussed above, a detailed description of the 6AK5 tube follows.

5.1 *Mechanical Description*

The 6AK5 tube is an indirectly heated cathode type pentode employing the 7-pin button stem and the T-5-1/2 size miniature bulb. The outline dimensions are shown in Fig. 11. A photograph of a mount ready to be sealed into a bulb is shown in Fig. 12. Figure 13 is a photograph of a transverse section through the tube at the middle of the structure in a plane

[8] "Fluctuations Induced in Vacuum Tube Grids at High Frequencies," D. O. North and W. R. Ferris, *I. R. E. Proceedings*, Vol. 29, No. 2, February 1941.
[9] Unpublished Technical Memorandum, J. R. Pierce.
[10] S. E. Miller, V. C. Rideout, R. S. Julian.

Digitized by Google
Original from UNIVERSITY OF MICHIGAN
Generated on 2019-09-23 09:09 GMT / http://hdl.handle.net/2027/mdp.39015077775156
Public Domain, Google-digitized / http://www.hathitrust.org/access_use#pd-google

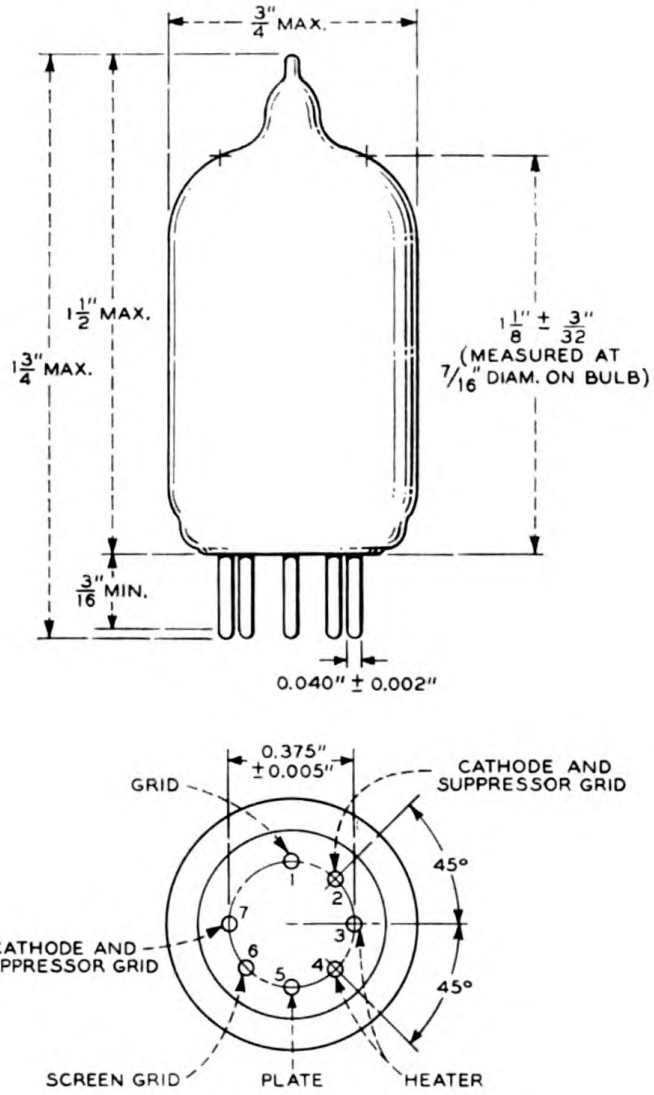

Fig. 11—6AK5 outline dimensions.

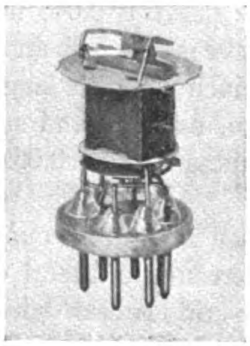

Fig. 12—6AK5 mount structure (full size).

Digitized by Google
Original from UNIVERSITY OF MICHIGAN
Generated on 2019-09-23 09:14 GMT / http://hdl.handle.net/2027/mdp.39015077775156
Public Domain, Google-digitized / http://www.hathitrust.org/access_use#pd-google

parallel to the stem or "base" of the tube. The magnification in Fig. 13 as reproduced is about 5½ times.

The heater is a conventional folded type with eight legs of coated tungsten wire. The wire diameter is 0.0014 inches and the unfolded length is 3 inches. The insulating coating consists of fired aluminum oxide and is about 0.0025 inch thick.

The cathode is of oval cross-section with the contours of the longer sides shaped to conform to the shape of the control grid. The major axis of the

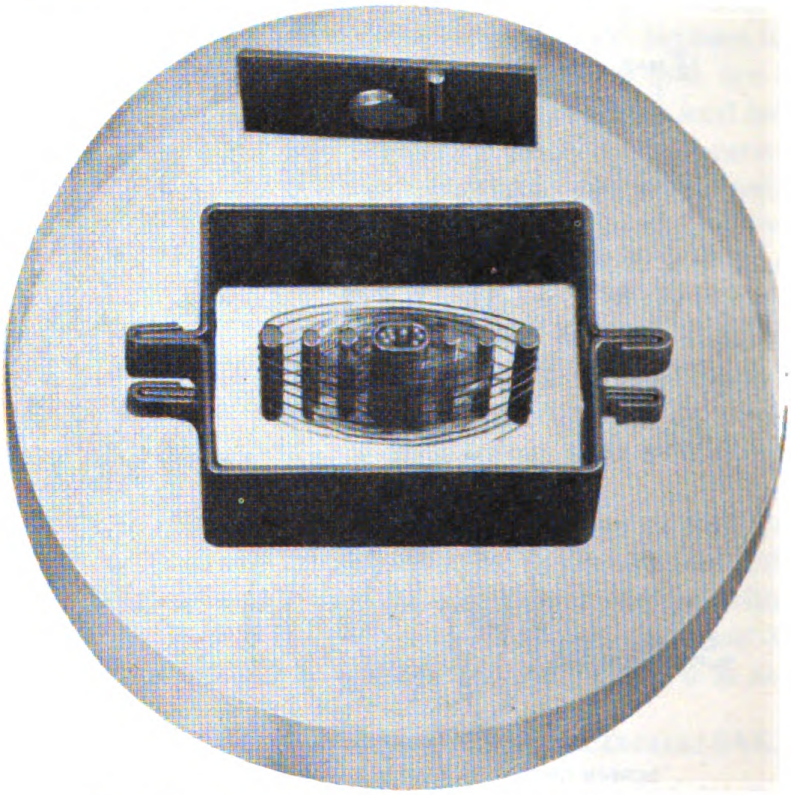

Fig. 13—Transverse section of 6AK5 tube (5½ times).

cross-section of the cathode sleeve is 0.048 inch. The minor axis is 0.025 inch. The length of the sleeve is 0.47 inch and it is coated over a centralized section which extends 0.28 inch along its length. The coating is the usual mixture of oxides of barium, calcium, and strontium. Before the tube is processed, the coating thickness is about 0.002 inch. After processing, it is about 0.001 inch thick.

The grids are oval-shaped and are wound with small diameter wires. The control-grid and the screen-grid lateral wires are 0.001 inch diameter tungsten. The suppressor-grid lateral wires are 0.002 inch diameter molybdenum. The control-grid wires are gold-plated in order to minimize primary emission of electrons from this grid.

Digitized by Google
Original from UNIVERSITY OF MICHIGAN
Generated on 2019-09-23 09:14 GMT / http://hdl.handle.net/2027/mdp.39015077775156
Public Domain, Google-digitized / http://www.hathitrust.org/access_use#pd-google

The plate has a rectangular transverse cross-section and is made of 0.005 inch thickness carbonized nickel. The carbonization increases the thermal emissivity of the plate surface so that a reasonable amount of power dissipation in the plate can be tolerated.

The end shields are made of nickel-plated iron. The reason for using this material instead of nickel, as is more often the case, is to prevent overheating of these shields during the exhaust process. At the temperatures used, the iron shields pick up less energy in the induction field during the out-gassing of the plate than do nickel shields. The function of the end shields is to minimize the stray capacitance between the plate and the control grid.

The insulators or spacers which hold the tube elements in proper disposition with respect to each other are of high grade mica. They are coated with magnesium oxide to minimize surface leakage effects.

The getter, which can be seen at the top of the structure in Fig. 12, contains barium which is flashed onto the inside surface of the bulb at the end of the exhaust process in order to take up residual gas evolving from the parts of the tube during operation.

Although the individual parts are extremely small and fragile, the completed tube is surprisingly rugged. The short supporting wires in the stem and the support provided by the bulb-contacting top insulator result in the stem, bulb, and mount structure being a relatively rigid unit. The small parts assembled into the mount are very light in weight and therefore exert relatively small forces on their supporting members under conditions of mechanical shock. Shock tests performed at the Naval Research Laboratory and at the Bell Laboratories show that the 6AK5 tube stands up satisfactorily under a steady vibration of rms acceleration 2.5 times gravity and withstands 1 millisecond shocks of over 300 times gravity.

The most important single geometrical factor in the tube is the spacing between the cathode and the control grid. In the 6AK5 tube this clearance is 0.0035 inch after processing. Before processing it is 0.0025 inch. The manufacturing difficulties involved in assembling the structure and maintaining such small clearances are obviously very great. However, as was seen from the discussion above, this close spacing is essential in order to obtain the desired high-frequency performance.

It can be observed that the close mounting of the structure on the stem provides very short lead lengths between the tube elements and the external pins. This is of importance at frequencies where the inductances of the lead wires become comparable in magnitude to the circuit reactances.

5.2 *Low Frequency Electrical Charatceristics*

The usual static characteristics are shown by the curves in Fig. 14. The ratings, nominal characteristics, and cold capacitances are given in Table II.

Generated on 2019-09-23 09:15 GMT / http://hdl.handle.net/2027/mdp.39015077775156
Public Domain, Google-digitized / http://www.hathitrust.org/access_use#pd-google
Digitized by Google
Original from UNIVERSITY OF MICHIGAN

5.3 *Fixed Tuning*

It is highly desirable to design the IF amplifier with fixed tuning in order to minimize the number of adjustments that need to be made when tubes

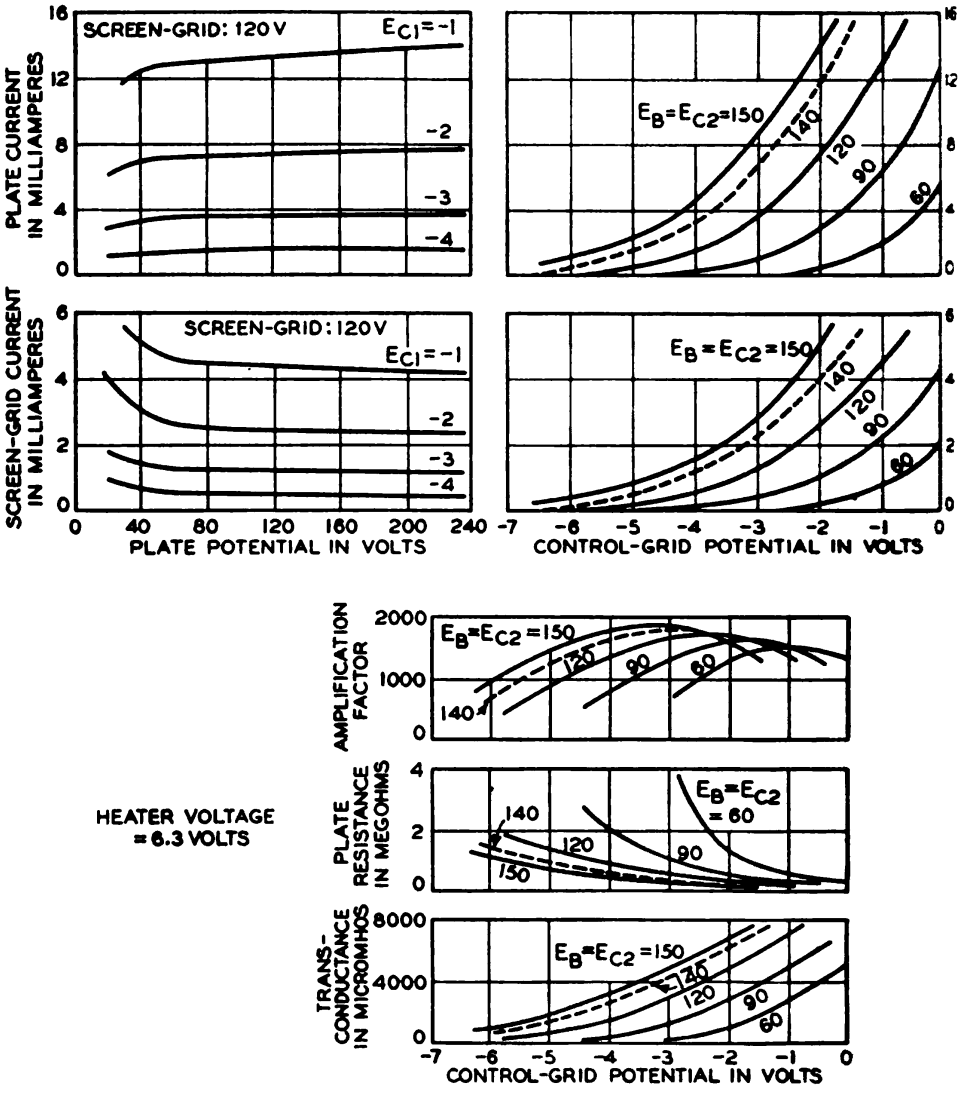

Fig. 14—Average 6AK5 characteristics.

are changed. The difficulty immediately arises that, since the tube capacitances are usually a large fraction of the total shunt capacitance of each coupling network, the variations in capacitance from one tube to another become very important. It is essential that, after the amplifier is lined up at the factory with standard tubes, any stock tubes taken at random shall give satisfactory performance in the amplifier. This requires close control

Digitized by Google
Original from UNIVERSITY OF MICHIGAN
Generated on 2019-09-23 09:15 GMT / http://hdl.handle.net/2027/mdp.39015077775156
Public Domain, Google-digitized / http://www.hathitrust.org/access_use#pd-google

of the capacitances. Not only must the capacitances be held within the limits of the test specification, but the product averages must be kept close to the design center values particularly in the cases of the input and output capacitances.

TABLE II

HEATER RATING			
Heater voltage			6.3 volts, a-c or d-c
Nominal heater current			0.175 ampere
Maximum Ratings (Design-center values)			
Maximum plate voltage			180 volts
Maximum screen voltage			140 volts
Maximum plate dissipation			1.7 watts
Maximum screen dissipation			0.5 watt
Maximum cathode current			18 milliamperes
Maximum heater-cathode voltage			90 volts
Maximum bulb temperature			120°C
OPERATING CONDITIONS AND CHARACTERISTICS			
Plate voltage	120	150	180 volts
Screen voltage	120	140	120 volts
Cathode-bias resistor	200	330	200 ohms
Plate current	7.5	7.0	7.7 milliamperes
Screen current	2.5	2.2	2.4 milliamperes
Amplification factor	1700	1800	3500
Plate resistance	0.34	0.42	0.69 megohms
Transconductance	5000	4300	5100 micromhos
INTERELECTRODE CAPACITANCES (*With JAN 1A No. 314 shield connected to cathode*)			
Control grid to heater, cathode, screen grid and suppressor grid			3.90 $\mu\mu$f
Plate to control grid			0.01 $\mu\mu$f
Plate to heater, cathode, screen grid and suppressor grid			2.85 $\mu\mu$f

6. CONCLUSION

The important factors to be considered in evaluating the suitability of a vacuum tube for broad band IF use in the VHF range are as follows:

1. Band merit
2. Noise figure
3. Input conductance
4. Power consumption
5. Physical size
6. Control of capacitances

We have seen that the tube design features which make a tube good on the basis of these requirements are close grid-cathode spacing, fine grid wires, short lead wires, and small elements. An important consideration from the manufacturing standpoint is the control of cathode emission for low noise. It has been possible to extend the useful frequency range of conventional receiving tubes up through the VHF range and somewhat higher by this line of attack.

Digitized by Google
Original from UNIVERSITY OF MICHIGAN
Generated on 2019-09-23 09:15 GMT / http://hdl.handle.net/2027/mdp.39015077775156
Public Domain, Google-digitized / http://www.hathitrust.org/access_use#pd-google

The 6AK5 tube is an outgrowth of the many years of development in this general field by the Electronics group of the Bell Telephone Laboratories. Contributions to the success of the development have been made by chemists, physicists, mechanical engineers and electrical engineers too numerous to mention individually and to whom the author is indebted for much of the material presented.

Generated on 2019-09-23 09:16 GMT / http://hdl.handle.net/2027/mdp.39015077775156
Public Domain, Google-digitized / http://www.hathitrust.org/access_use#pd-google
Digitized by Google
Original from UNIVERSITY OF MICHIGAN

Radar Antennas

By H. T. FRIIS and W. D. LEWIS

Introduction

RADAR proved to be one of the most important technical achievements of World War II. It has many sources, some as far back as the nineteenth century, yet its rapid wartime growth was the result of military necessity. This development will continue, for radar has increasing applications in a peacetime world.

In this paper we will discuss an indispensable part of radar—the antenna. In a radar system the antenna function is two-fold. It both projects into space each transmitted radar pulse, and collects from space each received reflected signal. Usually but not always a single antenna performs both functions.

The effectiveness of a radar is influenced decisively by the nature and quality of its antenna. The greatest range at which the radar can detect a target, the accuracy with which the direction to the target can be determined and the degree with which the target can be discriminated from its background or other targets all depend to a large extent on electrical properties of the antenna. The angular sector which the antenna can mechanically or electrically scan is the sector from which the radar can provide information. The scanning rate determines the frequency with which a tactical or navigational situation can be examined.

Digitized by Google
Original from UNIVERSITY OF MICHIGAN
Generated on 2019-09-23 09:17 GMT / http://hdl.handle.net/2027/mdp.39015077775156
Public Domain, Google-digitized / http://www.hathitrust.org/access_use#pd-google

Radar antennas are as numerous in kind as radars. The unique character and particular functions of a radar are often most clearly evident in the design of its antenna. Antennas must be designed for viewing planes from the ground, the ground from planes and planes from other planes. They must see ships from the shore, from the air, from other ships, and from submarines. In modern warfare any tactical situation may require one or several radars and each radar must have one or more antennas.

Radar waves are almost exclusively in the centimeter or microwave region, yet even the basic microwave techniques are relatively new to the radio art. Radar demanded antenna gains and directivities far greater than those previously employed. Special military situations required antennas with beam shapes and scanning characteristics never imagined by communication engineers.

It is natural that war should have turned our efforts so strongly in the direction of radar. But that these efforts were so richly and quickly rewarded was due in large part to the firm technical foundations that had been laid in the period immediately preceeding the war. When, for the common good, all privately held technical information was poured into one pool, all ingredients of radar, and of radar antennas in particular, were found to be present.

A significant contribution of the Bell System to this fund of technical knowledge was its familiarity with microwave techniques. Though Hertz himself had performed radio experiments in the present microwave region, continuous wave techniques remained for decades at longer wavelengths. However, because of its interest in new communication channels and broader bands the Bell System has throughout the past thirty years vigorously pushed continuous wave techniques toward the direction of shorter waves. By the middle nineteen-thirties members of the Radio Research Department of the Bell Laboratories were working within the centimeter region.

Several aspects of this research and development appear now as particularly important. In the first place it is obvious that knowledge of how to generate and transmit microwaves is an essential factor in radar. Many lower frequency oscillator and transmission line techniques are inapplicable in the microwave region. The Bell Laboratories has been constantly concerned with the development of generators which would work at higher and higher frequencies. Its broad familiarity with coaxial cable problems and in particular its pioneering work with waveguides provided the answers to many radar antenna problems.

Another telling factor was the emphasis placed upon measurement. Only through measurements can the planners and designers of equip-

Digitized by Google
Original from UNIVERSITY OF MICHIGAN
Generated on 2019-09-23 09:18 GMT / http://hdl.handle.net/2027/mdp.39015077775156
Public Domain, Google-digitized / http://www.hathitrust.org/access_use#pd-google

ment hope to evaluate performance, to chose between alternatives or to see the directions of improvement. Measuring techniques employing double detection receivers and intermediate frequency amplifiers had long been in use at the Holmdel Radio Laboratory. By employing these techniques radar engineers were able to make more sensitive and accurate measurements than would have been possible with single detection.

Antennas are as old as radio. Radar antennas though different in form are identical in principle with those used by Hertz and Marconi. Consequently experience with communication antennas provided a valuable background for radar antenna design. As an example of the importance of this background it can be recalled that a series of experi-

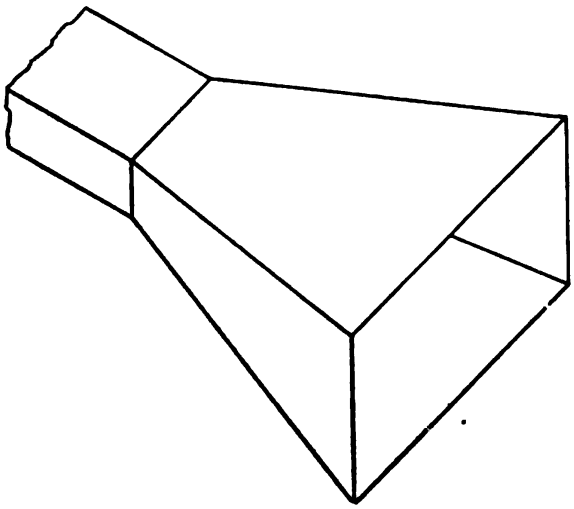

Fig. 1—An Electromagnetic Horn.

ments with short wave antennas for Transatlantic radio telephone service had culminated in 1936 in a scanning array of rhombic antennas. The essential principles of this array were later applied to shipborne fire control antenna which was remarkable and valuable because of the early date at which it incorporated modern rapid scanning features.

In addition to the antenna arts which arose directly out of communication problems at lower frequencies some research specifically on microwave antennas was under way before the war. Early workers in waveguides noticed that an open ended waveguide will radiate directly into space. It is not surprising therefore that these workers developed the electromagnetic horn, which is essentially a waveguide tapered out to an aperture (Fig. 1).

One of the first used and simplest radio antennas is the dipole (Fig.

Generated on 2019-09-23 09:18 GMT / http://hdl.handle.net/2027/mdp.39015077775156
Public Domain, Google-digitized / http://www.hathitrust.org/access_use#pd-google
Digitized by Google
Original from UNIVERSITY OF MICHIGAN

2). Current oscillating in the dipole generates electromagnetic waves which travel out with the velocity of light. A single dipole is fairly non-directive and consequently produces a relatively weak field at a distance. When the wave-length is short the field of a dipole in a

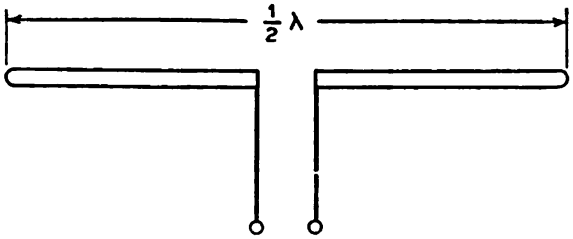

Fig. 2—A Microwave Dipole.

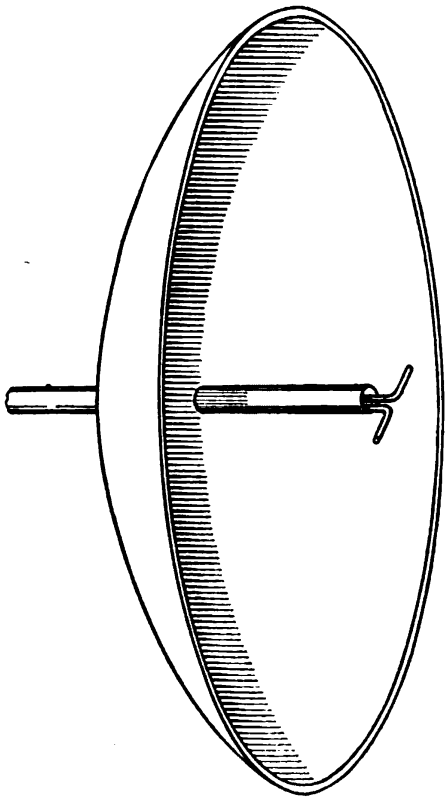

Fig. 3—A Dipole Fed Paraboloid.

chosen direction can be increased many times by introducing a reflector which directs or 'focusses' the energy.

In communication antennas the focussing reflector is most commonly a reflecting wire array. Even at an early date in radar the wavelength was so short that 'optical' reflectors could be used. These were

Digitized by Google
Original from UNIVERSITY OF MICHIGAN
Generated on 2019-09-23 09:18 GMT / http://hdl.handle.net/2027/mdp.39015077775156
Public Domain, Google-digitized / http://www.hathitrust.org/access_use#pd-google

sometimes paraboloids similar to those used in searchlights (Fig. 3). Sometimes they were parabolic cylinders as in the Mark III, an early shipborne fire control radar developed at the Whippany Radio Laboratory.

From these relatively simple roots, the communication antenna, the electromagnetic horn and the optical reflector, radar antennas were developed tremendously during the war. That this development in the Bell Laboratories was so well able to meet demands placed on it was due in large part to the solid foundation of experience possessed by the Research and Development groups of the Laboratories. Free interchange of individuals and information between the Laboratories and other groups, both in the United States and Great Britain, also contributed greatly to the success of radar antenna development.

Because of its accelerated wartime expansion the present radar antenna field is immense. It is still growing. It would be impossible for any single individual or group to master all details of this field, yet its broad outline can be grasped without difficulty.

The purpose of this paper is two-fold, both to provide a general discussion of radar antennas and to summarize the results of radar antenna research and development at the Bell Laboratories. Part I is a discussion of the basic electrical principles which concern radar antennas. In Part II we will outline the most common methods of radar antenna construction. Practical military antennas developed by the Bell Laboratories will be described in Part III.

The reader who is interested in general familiarity with the over all result rather than with technical features of design may proceed directly from this part to Part III.

PART I

ELECTRICAL PRINCIPLES

1. General

Radar antenna design depends basically on the same broad principles which underlie any other engineering design. The radar antenna designer can afford to neglect no aspect of his problem which has a bearing on the final product. Mechanical, chemical, and manufacturing considerations are among those which must be taken into account.

It is the electrical character of the antenna, however, which is connected most directly with the radar performance. In addition it is through attention to the electrical design problems that the greatest number of novel antennas have been introduced and it is from the electrical viewpoint that the new techniques can best be understood.

An antenna is an electromagnetic device and as such can be understood

Digitized by Google
Original from UNIVERSITY OF MICHIGAN
Generated on 2019-09-23 09:18 GMT / http://hdl.handle.net/2027/mdp.39015077775156
Public Domain, Google-digitized / http://www.hathitrust.org/access_use#pd-google

through the application of electromagnetic theory. Maxwell's equations provide a general and accurate foundation for antenna theory. They are the governing authority to which the antenna designer may refer directly when problems of a fundamental or baffling nature must be solved.

It is usually impracticable to obtain theoretically exact and simple solutions to useful antenna problems by applying Maxwell's Equations directly. We can, however, use them to derive simpler useful theories. These theories provide us with powerful analytical tools.

Lumped circuit theory is a tool of this sort which is of immense practical importance to electrical and radio engineers. As the frequency becomes higher the approximations on which lumped circuit theory is based become inaccurate and engineers find that they must consider distributed inductances and capacitances. The realm of transmission line theory has been invaded.

Transmission line theory is of the utmost importance in radar antenna design. In the first place the microwave energy must be brought to the antenna terminals over a transmission line. This feed line is usually a coaxial or a wave-guide. It must not break down under the voltage which accompanies a transmitted pulse. It must be as nearly lossless and reflectionless as possible and it must be matched properly to the antenna terminals.

The importance of a good understanding of transmission line theory does not end at the antenna terminals. In any antenna the energy to be transmitted must be distributed in the antenna structure in such a way that the desired radiation characteristics will be obtained. This may be done with transmission lines, in which case the importance of transmission line theory is obvious. It may be done by 'optical' methods. If so, certain transmission line concepts and methods will still be useful.

While it is true that transmission line theory is important it is not necessary to give a treatment of it in this paper. Adequate theoretical discussions can be found elsewhere in several sources.[1] It is enough at this point to indicate the need for a practical understanding of transmission line principles, a need which will be particularly evident in Part II, Methods of Antenna Construction.

We may, if we like, think of the whole radar transmission problem in terms of transmission line theory. The antenna then appears as a transformer between the feed line and transmission modes in free space. We cannot, however, apply this picture to details with much effectiveness unless we have some understanding of radiation.

In the sections to follow we shall deal with some theoretical aspects of radiation. We shall begin with a discussion of fundamental *transmission*

[1] See, for example, S. A. Schelkunoff, *Electromagnetic Waves*, D. Van Nostrand Co. Inc., 1943, in particular, Chapters VII and VIII, or F. E. Terman, *Radio Engineer's Handbook*, McGraw-Hill Book Co., Inc., 1943, Section 3.

Digitized by Google
Original from UNIVERSITY OF MICHIGAN
Generated on 2019-09-23 09:19 GMT / http://hdl.handle.net/2027/mdp.39015077775156
Public Domain, Google-digitized / http://www.hathitrust.org/access_use#pd-google

principles. This discussion is applicable to all antennas regardless of how they are made or used. When applied to radar antennas it deals chiefly with those properties of the antenna which affect the radar range.

Almost all microwave radar antennas are large when measured in wavelengths. When used as transmitting antennas they produce desired radiation characteristics by distributing the transmitted energy over an area or 'wave front'. The relationships between the phase and amplitude of electrical intensity in this wave front and the radiation characteristics of the antenna are predicted by *wave front analysis*. Wave front analysis is essentially the optical theory of diffraction. Although approximate it applies excellently to the majority of radar antenna radiation problems. We shall discuss wave front analysis in Section 3.

2. Transmission Principles

2.1 *Gain and Effective Area of an Antenna*

An extremely important property of any radar antenna is its ability to project a signal to a distant target. The *gain* of the antenna is a number which provides a quantitative measure of this ability. Another important property of a radar antenna is its ability to collect reflected power which is returning from a distant target. The *effective area* of the antenna is a quantitative measure of this ability. In this section these two quantities will be defined, and a simple relation between them will be derived. Their importance to radar range will be established.

Definition of Gain. When power is fed into the terminals of an antenna some of it will be lost in heat and some will be radiated. The *gain* G of the antenna can be defined as the ratio

$$G = P/P_0 \tag{1}$$

where P is the power flow per unit area in the plane linearly polarized electromagnetic wave which the antenna causes in a distant region usually in the direction of maximum radiation and P_0 is the power flow per unit area which would have been produced if all the power fed into the terminals had been radiated equally in all directions in space.

Definition of Effective Area. When a plane linearly polarized electromagnetic wave is incident on the receiving antenna, received power P_R will be available at the terminals of the antenna. The *effective area* of the antenna is defined, by the equation

$$A = P_R/P' \tag{2}$$

where P' is the power per unit area in the incident wave. In other words the received power is equal to the power flow through an area that is equal to the effective area of the antenna.

Digitized by Google
Original from UNIVERSITY OF MICHIGAN
Generated on 2019-09-23 09:19 GMT / http://hdl.handle.net/2027/mdp.39015077775156
Public Domain, Google-digitized / http://www.hathitrust.org/access_use#pd-google

2.2 *Relationship between Gain and Effective Area*

Figure 4 shows a radio circuit in free space made up of a transmitting antenna T and a receiving antenna R. If the transmitted power P_T had

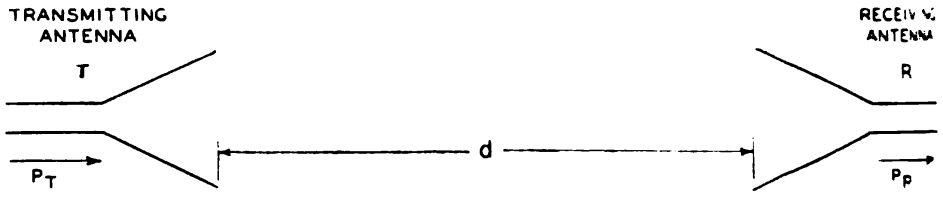

Fig. 4—Radio Circuit in Free Space.

been radiated equally in all directions, the power flow per unit area at the receiving antenna would be

$$P_0 = P_T \frac{1}{4\pi d^2} \tag{3}$$

Definition (1) gives, therefore, for the power flow per unit area at the receiving antenna

$$P = P_0 G_T = \frac{P_T G_T}{4\pi d^2} \tag{4}$$

and definition (2) gives for the received power

$$P_R = P A_R = \frac{P_T G_T A_R}{4\pi d^2} \tag{5}$$

From the law of reciprocity it follows that the same power is transferred if the transmitting and receiving roles are reversed. By (5) it is thus evident that

$$G_T A_R = G_R A_T$$

or

$$G_T/A_T = G_R/A_R \tag{6}$$

Equation (6) shows that the ratio of the gain and effective area has the same constant value for all antennas at a given frequency. It is necessary, therefore, to calculate this ratio only for a simple and well known antenna such as a small dipole or uniform current element.

2.3 *The Ratio G/A for a Small Current Element*

In Fig. 5 are given formulas[2] in M.K.S. units for the free space radiation from a small current element with no heat loss. We have assumed that

[2] See S. A. Schelkunoff, *Electromagnetic Waves*, D. Van Nostrand Co., Inc., 1943, p. 133

Digitized by Google
Original from UNIVERSITY OF MICHIGAN
Generated on 2019-09-23 09:19 GMT / http://hdl.handle.net/2027/mdp.39015077775156
Public Domain, Google-digitized / http://www.hathitrust.org/access_use#pd-google

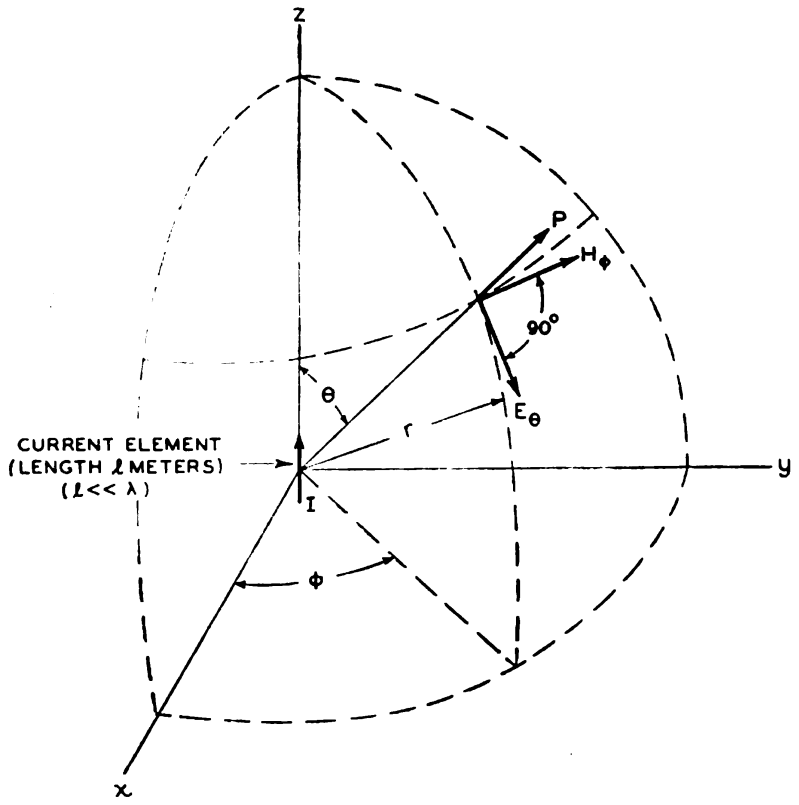

FOR $r \gg \lambda$:

$$\text{MAGNETIC INTENSITY} = H_\phi = i\frac{I\ell}{2\lambda r}e^{-i\frac{2\pi}{\lambda}r}\sin\theta \quad \frac{\text{AMPERES}}{\text{METER}} \qquad (1)$$

$$\text{ELECTRIC INTENSITY} = E_\theta = 120\pi H_\phi \quad \frac{\text{VOLTS}}{\text{METER}} \qquad (2)$$

$$\text{POWER FLOW} = P = |H_\phi E_\theta| = 30\pi\left[\frac{I\ell}{\lambda r}\right]^2 \sin^2\theta \quad \frac{\text{WATTS}}{\text{METER}^2} \qquad (3)$$

$$P \text{ IS MAXIMUM FOR } \theta = 90°. \textit{ i.e., } P_{MAX} = 30\pi\left[\frac{I\ell}{\lambda r}\right]^2 \frac{\text{WATTS}}{\text{METER}^2} \qquad (4)$$

POWER FLOW ACROSS SPHERE OF RADIUS r OR

$$\text{TOTAL RADIATION} = W = \int_0^\pi P\, 2\pi r \sin\theta\, r\,d\theta = 80\pi^2\left[\frac{I\ell}{\lambda}\right]^2 \text{WATTS} \qquad (5)$$

$$\text{RADIATION RESISTANCE} = R_{RAD} = \frac{W}{I^2} = 80\pi^2\left(\frac{\ell}{\lambda}\right)^2 \text{OHMS} \qquad (6)$$

$$\text{BY (4) AND (5)}: P_{MAX} = \frac{3}{8\pi r^2} W \quad \frac{\text{WATTS}}{\text{METER}^2} \qquad (7)$$

Fig. 5—Free Space Radiation from a Small Current Element with Uniform Current I Amperes over its Entire Length.

this element is centered at the origin of a rectangular coordinate system and that it lies along the Z axis. At a large distance r from the element

Digitized by Google
Original from UNIVERSITY OF MICHIGAN
Generated on 2019-09-23 09:19 GMT / http://hdl.handle.net/2027/mdp.39015077775156
Public Domain, Google-digitized / http://www.hathitrust.org/access_use#pd-google

the maximum power flow per unit area occurs in a direction normal to it and is given by

$$P_{max} = \frac{3W}{8\pi r^2} \frac{\text{watts}}{\text{meter}^2} \tag{7}$$

where W is the total radiated power. If W had been radiated equally in all directions the power flow per unit area would be

$$P_0 = \frac{W}{4\pi r^2} \frac{\text{watts}}{\text{meters}^2} \tag{8}$$

It follows that the gain of the small current element is

$$G_{dipole} = \frac{P_{max}}{P_0} = 1.5 \tag{9}$$

The effective area of the dipole will now be calculated. When it is used to receive a plane linearly polarized electromagnetic wave, the available output power is equal to the induced voltage squared divided by four times the radiation resistance. Thus

$$P_R = \frac{E^2 \ell^2}{4R_{rad}} \text{ Watts} \tag{10}$$

where E is the effective value of the electric field of the wave, ℓ is the length of the current element and R_{rad} is the radiation resistance of the current element. From Fig. 5 we see that $R_{rad} = \frac{80\pi^2\ell^2}{\lambda^2}$ ohms. Since the power flow per unit area is equal to the electric field squared divided by the impedance of free space, in other words $P_0 = \frac{E^2}{120\pi}$ we have

$$A_{dipole} = \frac{P_R}{P_0} = \frac{3\lambda^2}{8\pi} \text{ meter}^2 \tag{11}$$

We combine formulas (9) and (11) to find that

$$\frac{G_{dipole}}{A_{dipole}} = \frac{4\pi}{\lambda^2}$$

Since, as proved in 2.2 this ratio is the same for all antennas, it follows that for any antenna

$$\frac{G}{A} = \frac{4\pi}{\lambda^2} \tag{12}$$

Digitized by Google
Original from UNIVERSITY OF MICHIGAN
Generated on 2019-09-23 09:19 GMT / http://hdl.handle.net/2027/mdp.39015077775156
Public Domain, Google-digitized / http://www.hathitrust.org/access_use#pd-google

2.4 *The General Transmission Formula*

Transmission loss between transmitter and receiver through the radio circuit shown in Fig. 4 was given by equation (5). By substituting the relation (12) into (5) we can obtain the simple free space transmission formula:

$$P_R = P_T \frac{A_T A_R}{\lambda^2 d^2} \text{ watts} \tag{13}$$

Although this formula applies to free space only it is believed to be as useful in radio engineering as Ohm's law is in circuit engineering.

2.5 *The Reradiation Formula*

One further relation, the radar reflection formula is of particular interest. Consider the situation illustrated in Fig. 6. Let P_T be the power radiated

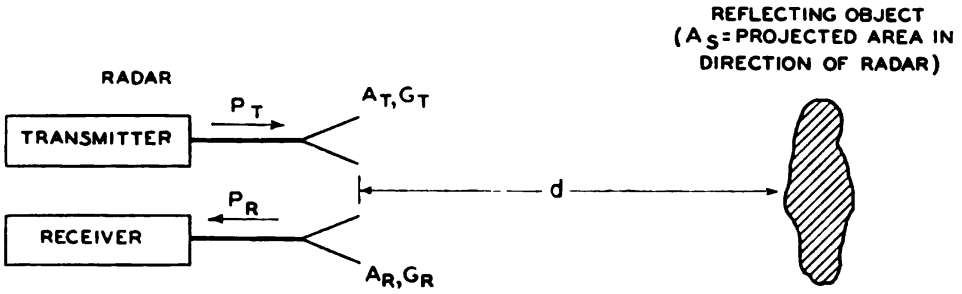

Fig. 6—Radar with Separate Receiving and Transmitting Antennas.

from an antenna with effective area A_T, A_S the area of a reflecting object at distance d from the antenna and P_R the power received by an antenna of effective area A_R. By equation (13) the power striking A_S is $\frac{P_T A_T A_S}{\lambda^2 d^2}$. If this power were reradiated equally in all directions the reflected power flow at the receiving antenna would be $\frac{P_T A_T A_S}{4\pi d^4 \lambda^2}$ but since the average reradiation is larger toward the receiving antenna, the power flow per unit area there is usually $K \frac{P_T A_T A_S}{4\pi d^4 \lambda^2}$ where $K > 1$. It follows from (2) that

$$P_R = K \frac{P_T A_T A_R A_S}{4\pi \lambda^2 d^4} \tag{14}$$

Formula (14) shows clearly why the use of large and efficient antennas will greatly increase the radar range.

Formula (14) applies to free space only. Application to other conditions

Digitized by Google
Original from UNIVERSITY OF MICHIGAN
Generated on 2019-09-23 09:19 GMT / http://hdl.handle.net/2027/mdp.39015077775156
Public Domain, Google-digitized / http://www.hathitrust.org/access_use#pd-google

may require corrections for the effect of the "ground", and for the effect of the transmission medium, which are beyond the scope of this paper.

2.6 *The Plane, Linearly Polarized Electromagnetic Wave*

In the foregoing sections we have referred several times to 'plane, linearly polarized electromagnetic waves'. These waves occur so commonly in antenna theory and practice that it is worth while to discuss them further here.

Some properties of linearly polarized, plane electromagnetic waves are illustrated in Fig. 7. At any point in the wave there is an electric field and a magnetic field. These fields are vectorial in nature and are at right angles to each other and to the direction of propagation. It is customary to give the magnitude of the electric field only.

If we use the M.K.S. system of units the magnitudes of the fields are expressed in familiar units. Electric intensity appears as volts per meter and magnetic intensity as amperes per meter. The ratio of electric to magnetic intensity has a value of 120π or about 377 ohms. This is the 'impedance' of free space. The power flow per unit area is expressed in watts per square meter. We see, therefore, that the electromagnetic wave is a means for carrying energy not entirely unlike a familiar two wire line or a coaxial cable.

Electromagnetic waves are generated when oscillating currents flow in conductors. We could generate a plane linearly polarized electromagnetic wave with a uniphase current sheet consisting of a network of fine wires backed up with a conducting reflector as shown in Fig. 7. This wave could be absorbed by a plane resistance sheet with a resistivity of 377 ohms, also backed up by a conducting sheet. The perfectly conducting reflecting sheets put infinite impedances in parallel with the current sheet and the resistance sheet, since each of these reflecting sheets has a zero impedance at a spacing of a quarter wavelength.

A perfectly plane electromagnetic wave can exist only under certain ideal conditions. It must be either infinite in extent or bounded appropriately by perfect electric and magnetic conductors. Nevertheless thinking in terms of plane electromagnetic waves is common and extremely useful. In the first place the waves produced over a small region at a great distance from any radiator are essentially plane. Arguments concerning receiving antennas therefore generally assume that the incident waves are plane. In the second place an antenna which has dimensions of many wavelengths can be analyzed with considerable profit on the basis of the assumption that it transmits by producing a nearly plane electromagnetic wave across its aperture. This method of analysis can be applied to the majority of microwave radar antennas, and will be discussed in the following sections.

Digitized by Google
Original from UNIVERSITY OF MICHIGAN
Generated on 2019-09-23 09:20 GMT / http://hdl.handle.net/2027/mdp.39015077775156
Public Domain, Google-digitized / http://www.hathitrust.org/access_use#pd-google

3. Wave Front Analysis

The fundamental design question is "How to get what we want?" In a radar antenna we want specified radiation characteristics; gain, pattern and polarization. Electromagnetic theory tells us that if all electric and magnetic currents in an antenna are known its radiation characteristics may be derived with the help of Maxwell's Equations. However, the essence of electromagnetic theory insofar as it is of use to the radar antenna

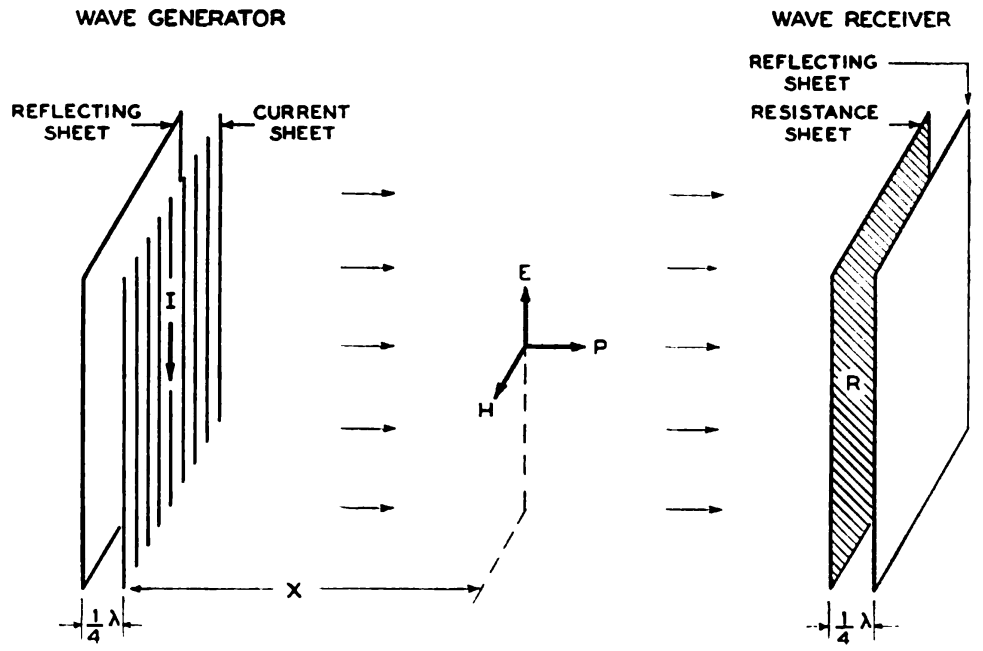

MAGNETIC INTENSITY = $H = Ie^{-i\frac{2\pi}{\lambda}x}$ $\frac{\text{AMPERES}}{\text{METER}}$

ELECTRIC INTENSITY = $E = 120\pi H$ $\frac{\text{VOLTS}}{\text{METER}}$

POWER FLOW = $P = EH$ $\frac{\text{WATTS}}{\text{METER}^2}$

CURRENT DENSITY = I $\frac{\text{AMPERES}}{\text{METER}}$

RESISTIVITY = $R = 120\pi$ OHMS

Fig. 7—Linearly Polarized Plane Electromagnetic Waves.

designer can usually be expressed in a simpler, more easily visualized and thus more useful form. This simpler method we call *wave front analysis*.

In a transmitting microwave antenna the power to be radiated is used to produce currents in antenna elements which are distributed in space. This distribution is usually over an area, it may be discrete as with a dipole array or it may be continuous as in an electromagnetic horn or paraboloid. These currents generate an advancing electromagnetic wave over the aperture of

Generated on 2019-09-23 09:25 GMT / http://hdl.handle.net/2027/mdp.39015077775156
Public Domain, Google-digitized / http://www.hathitrust.org/access_use#pd-google
Digitized by Google
Original from UNIVERSITY OF MICHIGAN

the antenna. The amplitude, phase and polarization of the electric intensity in portions of the wave are determined by the currents in the antenna and thus by the details of the antenna structure. This advancing wave can be called the 'wave front' of the antenna.

When the wave front of an antenna is known its radiation characteristics may be calculated. Each portion of the wave front can be regarded as a secondary or 'Huygens' source of known electric intensity, phase and polarization. At any other point in space the electric intensity, phase and polarization due to a Huygens source can be obtained through a simple expression given in the next section. The radiation characteristics of the antenna can be found by adding or integrating the effects due to all Huygens sources of the wave front.

This procedure is based on the assumption that the antenna is transmitting. A basic law of reciprocity assures us that the receiving gain and radiation characteristics of the antenna will be identical with the transmitting ones when only linear elements are involved.

This resolution of an antenna wave front into an array of secondary sources can be justified within certain limitations on the basis of the induction theorem of electromagnetic theory.[3] These limitations are discussed in a qualitative way in section 3.13.

3.1 *The Huygens Source*

Consider an elementary Huygens source of electric intensity E_0 polarized parallel to the X axis with area dS in the XY plane (Fig. 8). This can be thought of as an element of area dS of a wave front of a linearly polarized plane electromagnetic wave which is advancing in the positive z direction.[3] From Maxwell's Equations we can determine the field at any point of space due to this Huygens Source. The components of electric field, are found to be

$$\begin{aligned} E_r &= 0 \\ E_\theta &= i \frac{E_0\, dS}{2\lambda r} e^{-i(2\pi/\lambda)r} (1 + \cos\theta) \cos\phi \\ E_\phi &= -i \frac{E_0\, dS}{2\lambda r} e^{-i(2\pi/\lambda)r} (1 + \cos\theta) \sin\phi \end{aligned} \tag{15}$$

where λ is the wavelength.

We see at once that this represents a vector whose absolute magnitude at all points of space is given by

$$|E| = \frac{E_0\, dS}{2\lambda r} (1 + \cos\theta). \tag{16}$$

[3] S. A. Schelkunoff, Loc. Cit., Chap. 9.

Digitized by Google
Original from UNIVERSITY OF MICHIGAN
Generated on 2019-09-23 09:25 GMT / http://hdl.handle.net/2027/mdp.39015077775156
Public Domain, Google-digitized / http://www.hathitrust.org/access_use#pd-google

Here $\frac{E_0 dS}{\lambda}$ is an amplitude factor which depends on the wavelength, intensity and area of the elementary source and $1/r$ is an amplitude factor which specifies the variation of field with distance. $(1 + \cos\theta)$ is an amplitude factor which shows that the directional pattern of the elementary source is a cardioid with maximum radiation in the direction of propagation and no radiation in the reverse direction.

When we use the properties of the Huygens source in analyzing a micro-

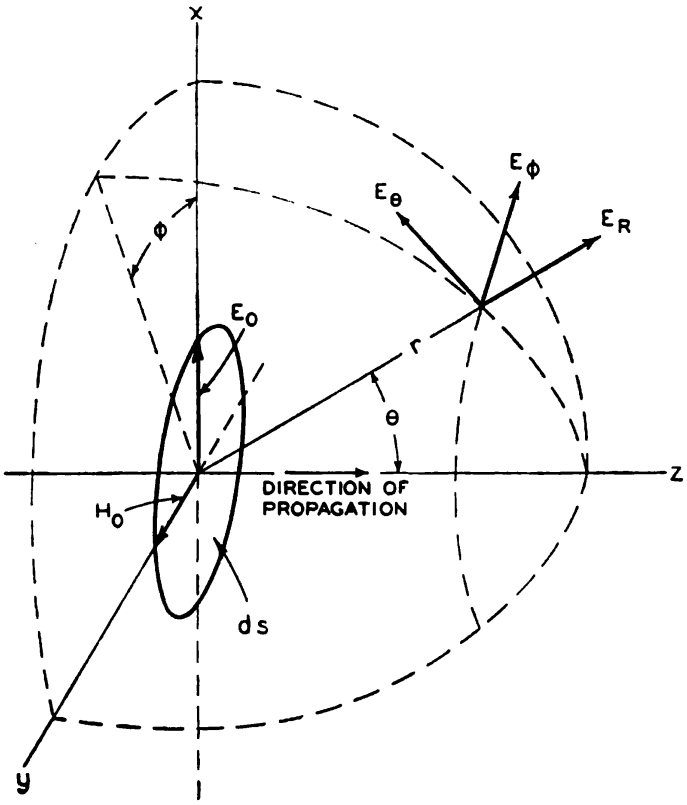

Fig. 8—The Huygens Source.

wave antenna we are usually concerned principally with radiation in or near the direction of propagation. For such radiation Equation 16 takes a particularly simple form in Cartesian Coordinates

$$E_x \cong i \frac{E_0 dS}{\lambda r} e^{-i(2\pi/\lambda)r}; \; E_y \cong 0; E_z \cong 0. \tag{17}$$

This represents an electric vector nearly parallel to the electric vector of the source. The amplitude is given by the factor $\frac{E_0 dS}{\lambda r}$ and the phase by the

Digitized by Google
Original from UNIVERSITY OF MICHIGAN
Generated on 2019-09-23 09:26 GMT / http://hdl.handle.net/2027/mdp.39015077775156
Public Domain, Google-digitized / http://www.hathitrust.org/access_use#pd-google

factor $i\, e^{-i(2\pi/\lambda)r}$. With this equation as a basis we will now proceed to study some relevant matters concerning radar antennas.

3.2 *Gain and Effective Area of an Ideal Antenna*

On the basis of (17) we can now determine the gain of an ideal antenna of area S ($S \gg \lambda^2$). This antenna is assumed to be free of heat loss and to transmit by generating an advancing wave which is uniform in phase and amplitude in the XY plane. Let the electric intensity in the wave front of

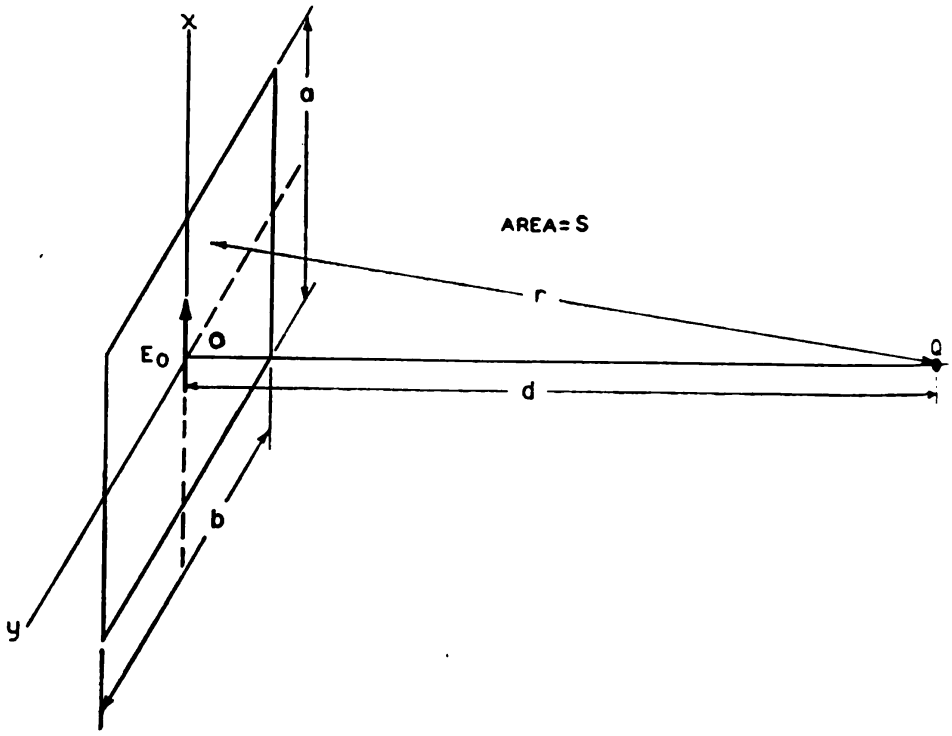

Fig. 9—An Ideal Antenna.

the ideal antenna be E_0 polarized parallel to the X axis (Fig. 9). The transmitted power P_T is equal to the power flow through S and is given by

$$P_T = \frac{E_0^2}{240\pi} S. \tag{18}$$

At a point Q on the Z axis the electric intensity is obtained by adding the effects of all the Huygens sources in S. If the distance of Q from O is so great that

$$r = d + \Delta$$

Digitized by Google
Original from UNIVERSITY OF MICHIGAN
Generated on 2019-09-23 09:26 GMT / http://hdl.handle.net/2027/mdp.39015077775156
Public Domain, Google-digitized / http://www.hathitrust.org/access_use#pd-google

where Δ is a negligibly small fraction of a wavelength for every point on S then we see from (17) that the electric vector at Q is given by

$$E_z = \int_S i \frac{E_0\, dS}{\lambda r} e^{-i(2\pi/\lambda)r} = i e^{-i(2\pi/\lambda)d} \frac{E_0 S}{\lambda d}; \; E_y = 0; \; E_z = 0. \tag{19}$$

The power flow per unit area at Q is therefore

$$P = \frac{1}{240\pi} \frac{E_0^2 S^2}{\lambda^2 d^2} = \frac{P_T S}{\lambda^2 d^2}$$

P_0 the power flow per unit area at Q when power is radiated isotropically from O is found by assuming that P_T is spread evenly over the surface of a sphere of radius d.

$$P_0 = \frac{P_T}{4\pi d^2} \tag{20}$$

The gain of a lossless, uniphase, uniamplitude, linearly polarized antenna is, by the definition of equation 1, the ratio of 19 and 20.

$$G_s = \frac{P_T S}{\lambda^2 d^2} \Big/ \frac{P_T}{4\pi d^2} = \frac{4\pi S}{\lambda^2}. \tag{21}$$

It follows from 12 that the effective area of the ideal antenna is

$$A = S \tag{22}$$

In other words in this ideal antenna the effective area is equal to the actual area. This is a result which might have been obtained by more direct arguments.

3.3 *Gain and Effective Area of an Antenna with Aperture in a Plane and with Arbitrary Phase and Amplitude*

Let us consider an antenna with a wave front in the XY plane which has a known phase and amplitude variation. Let the electric intensity in the wave front be

$$E(x, y) = E_0 a(x, y) e^{i\phi(x, y)} \tag{23}$$

polarized parallel to the x axis. The radiated power is equal to the power flow through S and is given by

$$P_{\text{rad}} = \frac{E_0^2 \int a^2(x, y)\, dS}{240\pi}. \tag{24}$$

The input power to the antenna is

$$P_T = P_{\text{rad}}/L. \tag{25}$$

Digitized by Google
Original from UNIVERSITY OF MICHIGAN
Generated on 2019-09-23 09:26 GMT / http://hdl.handle.net/2027/mdp.39015077775156
Public Domain, Google-digitized / http://www.hathitrust.org/access_use#pd-google

where L is a loss factor (<1). At a point Q on the Z axis the electric intensity is obtained by adding the effects of all the Huygens sources in S. If OQ is as great as in the above derivation for the gain of an ideal antenna then we see from 17 that the electric intensity at Q is

$$E_x = i \frac{e^{i(2\pi/\lambda)d}}{\lambda d} E_0 \int a(x, y) e^{i\phi(x,y)} dS; \; E_y = 0; \; E_z = 0. \tag{26}$$

The power flow per unit area at Q is given by

$$P = \frac{1}{240\pi} |E_x|^2 \tag{27}$$

and P_0 the power flow per unit area at Q when P_T is radiated isotropically is given by equation (3).

The power gain of the antenna, by definition 1 is therefore

$$G = \frac{P}{P_0} = \frac{|E_x|^2}{240\pi} \Big/ \frac{P_T}{4\pi d^2} = \frac{4\pi L}{\lambda^2} \frac{\left| \int_S a(x, y) e^{i\phi(x,y)} dS \right|^2}{\int_S a^2(x, y) \, dS}. \tag{28}$$

The gain expressed in *db* is given by

$$G_{db} = 10 \log_{10} G \tag{29}$$

We combine 12 and 28 to obtain

$$A = L \frac{\left| \int_S a(x, y) e^{i\phi(x,y)} dS \right|^2}{\int_S a^2(x, y) \, dS} \tag{30}$$

a formula for the effective area of the antenna.

3.4 *The Significance of the Pattern of a Radar Antenna*

The accuracy with which a radar can determine the directions to a target depends upon the ***beam widths*** of the radar antenna. The ability of the radar to separate a target from its background or distinguish it from other targets depends upon the beam widths and the ***minor lobes*** of the radar antenna. The efficiency with which the radar uses the available power to view a given region of space depends on the ***beam shape*** of the antenna. These quantities characterize the antenna pattern. In the following sections means for the calculation of antenna patterns in terms of wave front theory will be developed, and some illustrations will be given.

Generated on 2019-09-23 09:26 GMT / http://hdl.handle.net/2027/mdp.39015077775156
Public Domain, Google-digitized / http://www.hathitrust.org/access_use#pd-google
Digitized by Google
Original from UNIVERSITY OF MICHIGAN

3.5 *Pattern in Terms of Antenna Wave Front*

If the relative phase and amplitude in a wave front are given by

$$E(x, y) = a(x, y)e^{i\phi(x,y)} \tag{31}$$

the relative phase and amplitude at a distant point Q not necessarily on the Z axis (Fig. 10) in the important case where the angle QOZ between the direction of propagation and the direction to the point is small, is given from (17) by adding the contributions at Q due to all parts of the wave front. This gives

$$E_Q = \frac{i}{\lambda d}\int_S e^{-i(2\pi/\lambda)r} e^{i\phi(x,y)}\, a(x, y)\, dS. \tag{32}$$

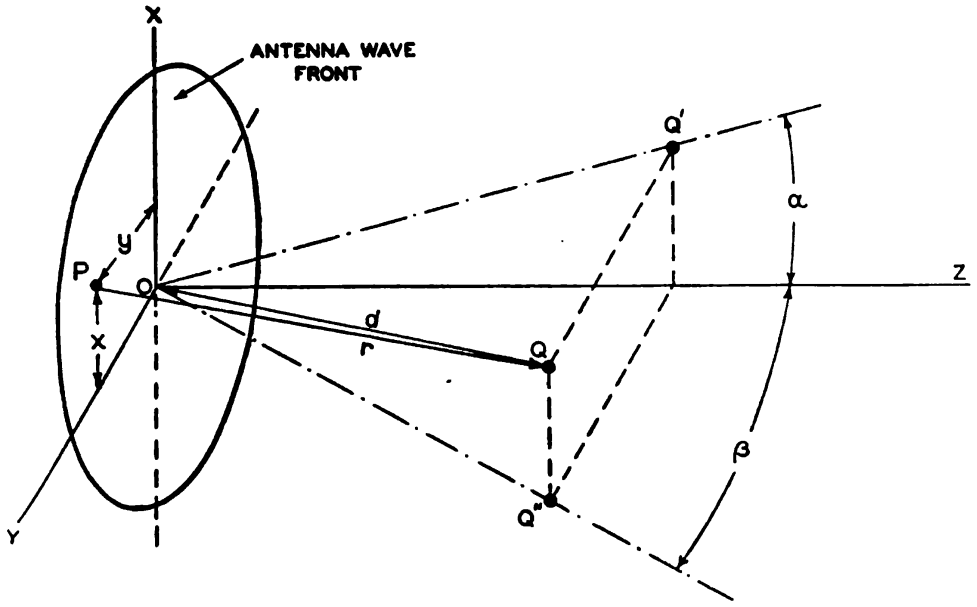

Fig. 10—Geometry of Pattern Analysis.

The quantity r in (32) is the distance from any point P with coordinates x, y, O, in the XY, plane to the point Q (Fig. 10). Simple trigonometry shows that when OQ is very large

$$r = d - x\sin\alpha - y\sin\beta \tag{33}$$

where d is the distance OQ, α is the angle ZOQ' between OZ and OQ' the projection of OQ on the XZ plane and β is similarly the angle ZOQ''. The substitution of 33 into 32 gives

$$E_Q = \frac{i\, e^{-i(2\pi/\lambda)d}}{\lambda d}\int_S e^{i(2\pi/\lambda)(x\sin\alpha + y\sin\beta) + i\phi(x,y)}\, a(x, y)\, dS. \tag{34}$$

Digitized by Google
Original from UNIVERSITY OF MICHIGAN
Generated on 2019-09-23 09:26 GMT / http://hdl.handle.net/2027/mdp.39015077775156
Public Domain, Google-digitized / http://www.hathitrust.org/access_use#pd-google

In most practical cases this equation can be simplified by the assumptions

$$\phi(x, y) = \phi'(x) + \phi''(y)$$

$$a(x, y) = a'(x)a''(y)$$

from which it follows that

$$| E_0 | = F(d)F(\alpha)F(\beta) \tag{35}$$

where $F(d)$ is an amplitude factor which does not depend on angle,

$$F(\alpha) = \int e^{i(2\pi/\lambda)x\sin\alpha + i\phi'(x)} a'(x)\, dx \tag{36}$$

is a directional factor which depends only on the angle α and not on the angle β or d, and $F(\beta)$ similarly depends on β but not on α or d. The pattern of an antenna can be calculated with the help of the simple integrals as in 36. and illustrations of such calculations will be given in the following sections.

3.6 *Pattern of an Ideal Rectangular Antenna*

Let the wave front be that of an ideal rectangular antenna of dimensions a, b; with linear polarization and uniform phase and amplitude. The dimensions a and b can be placed parallel to the X and Y axes respectively as sketched in Fig. 9. Equation 36 then gives

$$F(\alpha) = \int_{-a/2}^{a/2} e^{i(2\pi/\lambda)x\sin\alpha}\, dx = a\,\frac{\sin\psi}{\psi} \tag{37}$$

where $\psi = \dfrac{\pi a \sin\alpha}{\lambda}$.

Similarly

$$F(\beta) = b\,\frac{\sin\psi'}{\psi'} \tag{38}$$

where $\psi' = \dfrac{\pi b \sin\beta}{\lambda}$.

The pattern of the ideal rectangular aperture, in other words the distribution of electrical field in angle is thus given approximately by

$$F(\alpha)F(\beta) = ab\,\frac{\sin\psi}{\psi}\,\frac{\sin\psi'}{\psi'}. \tag{39}$$

The function $\dfrac{\sin\psi}{\psi}$ is plotted in Fig. 11. It is perhaps the most useful function of antenna theory, not because ideal antennas as defined above are particularly desirable in practice but because they provide a simple stand-

Digitized by Google
Original from UNIVERSITY OF MICHIGAN
Generated on 2019-09-23 09:27 GMT / http://hdl.handle.net/2027/mdp.39015077775156
Public Domain, Google-digitized / http://www.hathitrust.org/access_use#pd-google

ard with which more useful but more complex antennas can profitably be compared.

3.7 *Effect on Pattern of Amplitude Taper*

The $\frac{\sin\psi}{\psi}$ pattern which results from an ideal wave front has undesirably high minor lobes for most radar applications. These minor lobes will be reduced if the wave front of constant amplitude is replaced by one which retains a constant phase but has a rounded or 'tapered' amplitude distribution.

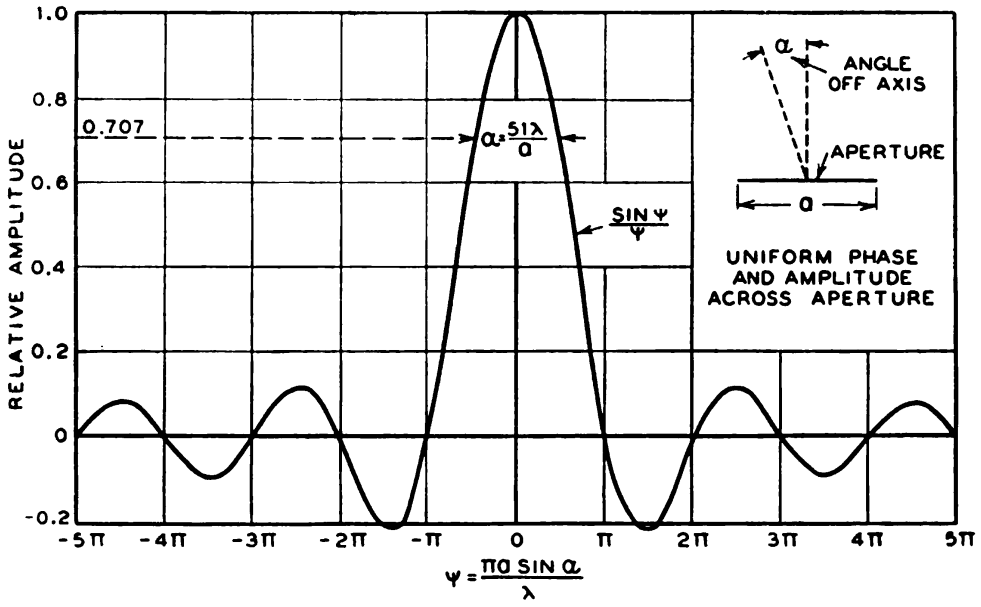

Fig. 11—Pattern of Ideal Rectangular Antenna.

If such an amplitude taper is represented analytically by the function

$$a'(x) = C_1 + C_2 \cos\frac{\pi x}{a} \tag{40}$$

then equation (36) is readily integrable. To integrate it we utilize the identity

$$\cos\frac{\pi x}{a} = \frac{e^{+i\pi x/a} + e^{-i\pi x/a}}{2}$$

upon which the integral becomes the sum of three simple integrals of the form

$$\int_{-a/2}^{a/2} e^{ikx}dx = a\left[\frac{\sin\frac{ka}{2}}{\frac{ka}{2}}\right] \tag{41}$$

Digitized by Google
Original from UNIVERSITY OF MICHIGAN
Generated on 2019-09-23 09:27 GMT / http://hdl.handle.net/2027/mdp.39015077775156
Public Domain, Google-digitized / http://www.hathitrust.org/access_use#pd-google

We therefore obtain

$$F(\alpha) = aC_1 \frac{\sin \psi}{\psi} + a \frac{C_2}{2} \left[\frac{\sin\left(\psi + \frac{\pi}{2}\right)}{\left(\psi + \frac{\pi}{2}\right)} + \frac{\sin\left(\psi - \frac{\pi}{2}\right)}{\left(\psi - \frac{\pi}{2}\right)} \right] \quad (42)$$

The patterns resulting from two possible tapers are given by substituting $C_1 = 0, C_2 = 1$ and $C_1 = 1/3, C_2 = 2/3$ in (42). These patterns are evidently calculable in terms of the known function $\frac{\sin \alpha}{\alpha}$. They are plotted in Figs. 12 and 13.

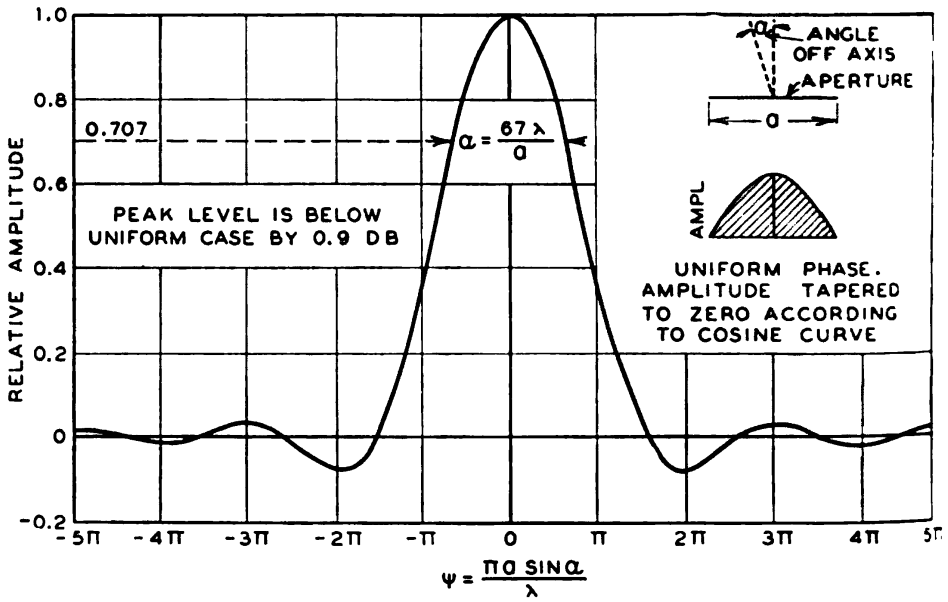

Fig. 12—Pattern of Tapered Rectangular Antenna.

It will be observed that minor lobe suppression through tapering is obtained at the expense of beam broadening. In addition to this the gain is reduced by tapering, as could have been calculated from 28. These undesirable effects must be contended with in any practical antenna design. The choice of taper must be made on the basis of the most desirable compromise between the conflicting factors.

3.8 *Effect on Pattern of Linear Phase Variation*

If we assume a constant amplitude and a linear phase variation

$$\phi'(x) = -k_1 x$$

Digitized by Google
Original from UNIVERSITY OF MICHIGAN
Generated on 2019-09-23 09:27 GMT / http://hdl.handle.net/2027/mdp.39015077775156
Public Domain, Google-digitized / http://www.hathitrust.org/access_use#pd-google

over an aperture $-a/2 < x < a/2$ then 36 becomes a simple integral of the form (41) and we obtain

$$F(\alpha) = a\frac{\sin \psi''}{\psi''} \quad \text{where} \quad \psi'' = \frac{\pi a}{\lambda}\sin \alpha - \frac{k_1 a}{2} \tag{43}$$

The physical interpretation of (43) is simply that the pattern is closely similar to the pattern of an antenna with constant amplitude and uniform phase but rotated through an angle θ where

$$\sin \theta = \frac{k_1 \lambda}{2\pi}$$

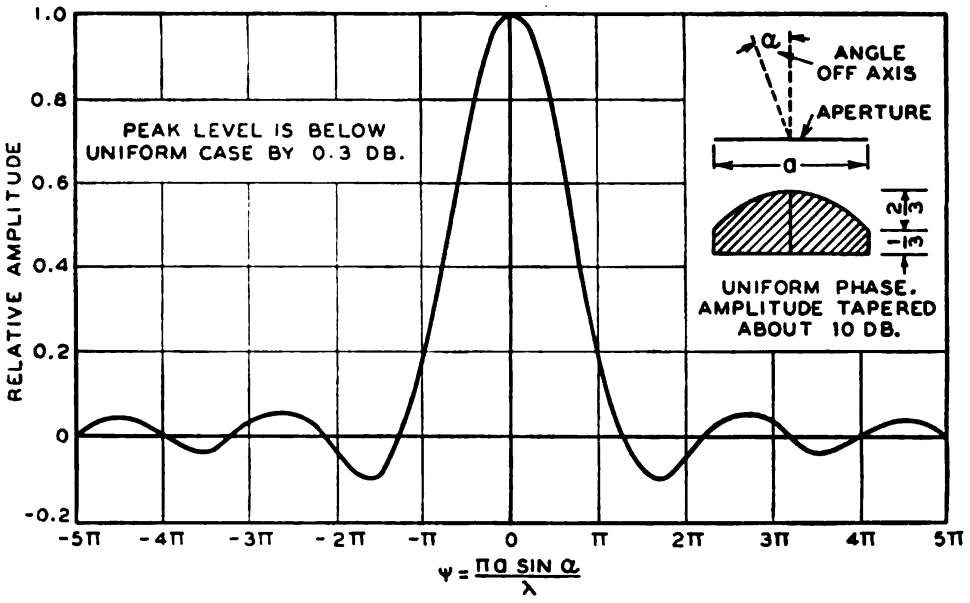

Fig. 13—Pattern of Tapered Rectangular Antenna.

Simple examination shows that the new direction of the radiation maximum is at right angles to a uniphase surface, as we would intuitively expect. This phenomenon has particular relevance to the design of scanning antennas.

3.9 *Effect on Pattern of Square Law Phase Variation*

If we assume a constant amplitude and a square law phase variation

$$\phi'(x) = -k_2^2 x^2$$

over the aperture $a/2 < x < a/2$ then the substitution

$$x = \frac{1}{k_2}\left[X + \frac{\frac{2\pi}{\lambda}\sin \alpha}{2k_2}\right] \tag{44}$$

Digitized by Google
Original from UNIVERSITY OF MICHIGAN
Generated on 2019-09-23 09:27 GMT / http://hdl.handle.net/2027/mdp.39015077775156
Public Domain, Google-digitized / http://www.hathitrust.org/access_use#pd-google

reduces (36) to the form

$$F(\alpha) = \frac{1}{k_2} e^{i\left(\frac{2\pi}{\lambda}\right)^2 \sin^2 \alpha / 4k_2^2} \int e^{-iX^2}\, dX \tag{45}$$

Equation (45) can be evaluated with the help of Fresnel's Integrals

$$\int \cos X^2\, dX, \qquad \int \sin X^2\, dX$$

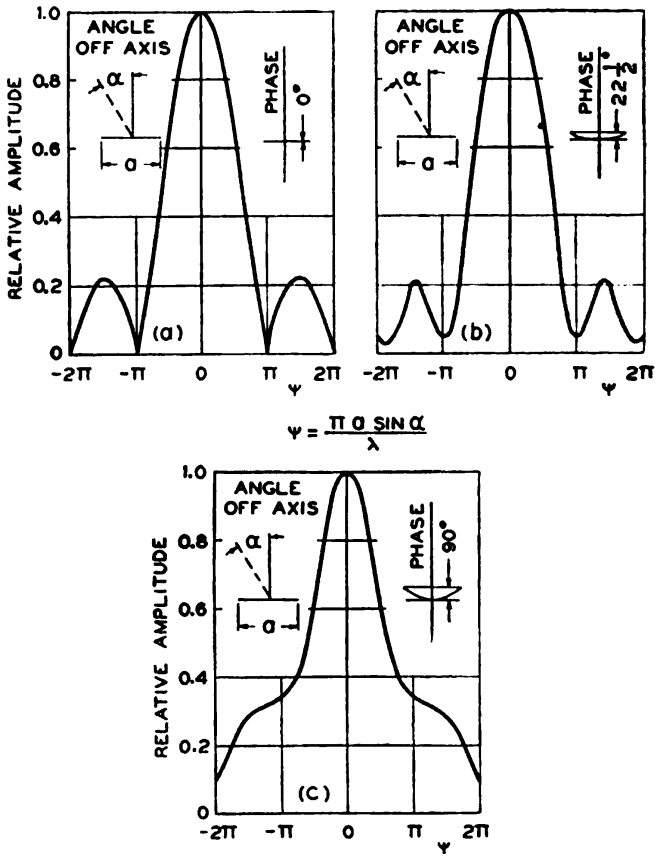

Fig. 14—Patterns of Rectangular Apertures with Square Law Phase Variation.

which are tabulated[4], or from Cornu's Spiral which is a convenient graphical representation of the Fresnel Integrals.

Typical computed patterns for apertures with square law phase variations are plotted in Fig. 14. These theoretical curves can be applied to the following important practical problems.

(1) The pattern of an electromagnetic horn.

[4] For numerical values of Fresnel's Integrals and a plot of Cornu's Spiral see Jahnke and Emde, *Tables of Functions* B. G. Teubner, Leipzig, 1933, or Dover Publications, New York City, 1943.

Generated on 2019-09-23 09:28 GMT / http://hdl.handle.net/2027/mdp.39015077775156
Public Domain, Google-digitized / http://www.hathitrust.org/access_use#pd-google
Digitized by Google
Original from UNIVERSITY OF MICHIGAN

(2) The defocussing of a reflector or lens due to improper placing of the primary feed.
(3) The defocussing of a zoned reflector or lens due to operation at a frequency off mid-band.

In addition to providing distant patterns of apertures with curved wave fronts (44) provides theoretical 'close in' patterns of antennas with plane wave fronts. This arises from the simple fact that a plane aperture appears as a curved aperture to close in points. The degree of curvature depends on the distance and can be evaluated by extremely simple geometrical considerations. When this has been done we find that Fig. 14 represents the so-called Fresnel diffraction field.

With this interpretation of square law variation of the aperture we can examine several additional useful problems. We can for instance justify the commonly used relation

$$D = \frac{2a^2}{\lambda}$$

for the minimum permissible distance of the field source from an experimental antenna test site. This distance produces an effective phase curvature of $\lambda/16$. We can examine optical antenna systems employing large primary feeds, in particular those employing parabolic cylinders illuminated by line sources.

3.10 *Effect on Pattern of Cubic Phase Variation*

If we assume a constant amplitude and a cubic phase variation $\phi'(x) = -k_3^3 x^3$ over the aperture from $-a/2 < x < a/2$ then equation (36) becomes

$$F(\alpha) = \int_{-a/2}^{a/2} e^{-ik_3^3 x^3} \cdot e^{i(2\pi/\lambda)x \sin\alpha} \cdot dx \tag{46}$$

If $k_3^3 x^3 \leq \frac{\pi}{2}$ then it is a fairly good approximation to write

$$e^{-ik_3^3 x^3} = 1 - ik_3^3 x^3 - \frac{k_3^6 x^6}{2} + \cdots \tag{47}$$

from which it follows that (46) can be integrated since it reduces to a sum of three terms each of which can be integrated.

Typical computed patterns for apertures with cubic phase variation are plotted in Figs. 15 and 16. Cubic phase distortions are found in practice when reflectors or lenses are illuminated by primary feeds which are off axis either because of inaccurate alignment or because beam lobing or scanning through feed motion is desired. The beam distortion due to cubic phase variation is known in optics as 'coma' and the increased unsymmetrical lobe which is particularly evident in Fig. 16 is commonly called a 'coma lobe'.

Digitized by Google
Original from UNIVERSITY OF MICHIGAN
Generated on 2019-09-23 09:28 GMT / http://hdl.handle.net/2027/mdp.39015077775156
Public Domain, Google-digitized / http://www.hathitrust.org/access_use#pd-google

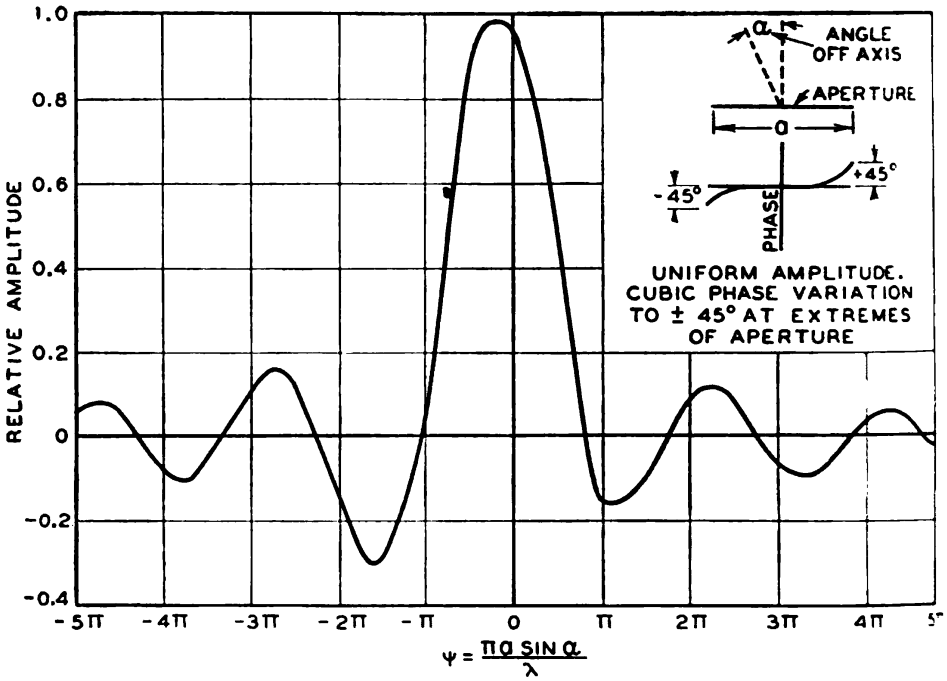

Fig. 15—Pattern of Rectangular Antenna with Cubic Phase Variation.

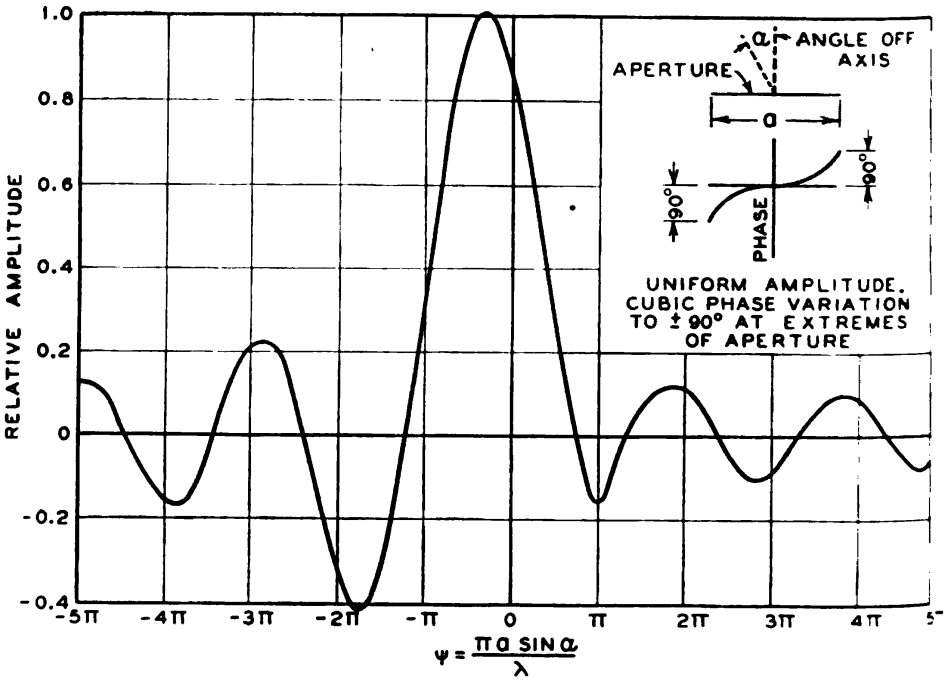

Fig. 16—Pattern of Rectangular Antenna with Cubic Phase Variation.

3.11 *Two General Methods*

In sections 3.7 and 3.8 we integrated (36) by expressing $a'(x)e^{i\phi'(x)}$ as a sum of terms of the form e^{ikx}. Since $a'(x)e^{i\phi'(x)}$ for finite amplitudes in a finite

Digitized by Google
Original from UNIVERSITY OF MICHIGAN
Generated on 2019-09-23 09:29 GMT / http://hdl.handle.net/2027/mdp.39015077775156
Public Domain, Google-digitized / http://www.hathitrust.org/access_use#pd-google

aperture can always be expressed as a Fourier sum of this form this solution can in principle always be found.

Alternatively in section 3.10 the integral was evaluated as a sum of integrals of the general type $\int x^n e^{ikx}\,dx$. Since $a'(x)e^{i\phi'(x)}$ for finite amplitudes in a finite aperture can always be expressed in terms of a power series, this solution can also in principle always be found.

3.12 *Arrays*

When the aperture consists of an array of component or unit apertures the evaluation of (36) must be made in part through a summation. When all of the elementary apertures are alike this summation can be reduced to the determination of an 'Array Factor'. The pattern of the array is given by multiplying the array factor by the pattern of a single unit.

The pattern of an array of identical units spaced equally at distances somewhat less than a wavelength can be proved to be usually almost equivalent to the pattern of a continuous wave front with the same average energy density and phase in each region.

3.13 *Limitations to Antenna Wave Front Analysis*

Through the analysis of antenna characteristics by means of wave front theory as based on equation (17) we have been able to demonstrate some of the fundamental theoretical principles of antenna design. The use of this simple approach is justified fully by its relative simplicity and by its applicability to the majority of radar antennas. Nevertheless it cannot always be used. It will certainly be inaccurate or inapplicable in the following cases:

(1) When any dimension of the aperture is of the order of a wavelength or smaller (as in many primary feeds).
(2) Where large variations in the amplitude or phase in the aperture occur in distances which are of the order of a wavelength or smaller (as in dipole arrays).
(3) Where the antenna to be considered does not act essentially through the generation of a plane wave front (as in an end fire antenna or a cosecant antenna).

When the wave front analysis breaks down alternative satisfactory approaches based on Maxwell's equation are sometimes but not always fruitful. Literature on more classical antenna theory is available in a variety of sources. For much fundamental and relevant theoretical work the reader is referred to Schelkunoff.[5]

[5] S. A. Schelkunoff, Loc. Cit.

Digitized by Google
Original from UNIVERSITY OF MICHIGAN
Generated on 2019-09-23 09:29 GMT / http://hdl.handle.net/2027/mdp.39015077775156
Public Domain, Google-digitized / http://www.hathitrust.org/access_use#pd-google

4. Application of General Principles

In the foregoing sections we have provided some discussion of what happens to a radar signal from the time that the pulse enters the antenna on transmission until the time that the reflected signal leaves the antenna on reception. We have for convenience divided the principles which chiefly concern us into three groups, transmission line theory, transmission principles and wave front theory.

With the aid of transmission line theory we can examine problems concerning locally guided or controlled energy. The details of the problems of antenna construction, such as those to be discussed in Part II frequently demand a grasp of transmission line theory. With it we can study local losses, due to resistance or leakage, which affect the gain of the antenna. We can examine reflection problems and their effect on the match of the antenna. Special antennas, such as those employing phase shifters or transmission between parallel conducting plates, introduce many special problems which lie wholly or partly in the transmission line field.

An understanding of the principles which govern transmission through free space aids us in comprehending the radar antenna field as a whole. Through a general understanding of antenna gains and effective areas we are better equipped to judge their significance in particular cases, and to evaluate and control the effects of particular methods of construction on them.

Wave front theory provides us with a powerful method of analysis through which we can connect the radiation characteristics produced by a given antenna with the radiating currents in the antenna. Through it we can examine theoretical questions concerning beam widths and shape, unwanted radiation and gain.

An understanding of theory is necessary to the radar antenna designer, but it is by no means sufficient. It is easy to attach too much importance to theoretical examination and speculation while neglecting physical facts which can 'make or break' an antenna design. Theory alone provides no substitute for the practical 'know how' of antenna construction. It cannot do away with the necessity for careful experiment and measurement. Least of all can it replace the inventiveness and aggressive originality through which new problems are solved and new techniques are developed.

PART II

METHODS OF ANTENNA CONSTRUCTION

5. General

Techniques are essential to technical accomplishment. An understanding of general principles alone is not enough. The designing engineer must have

Digitized by Google
Original from UNIVERSITY OF MICHIGAN
Generated on 2019-09-23 09:29 GMT / http://hdl.handle.net/2027/mdp.39015077775156
Public Domain, Google-digitized / http://www.hathitrust.org/access_use#pd-google

at his disposal or develop practical methods which can produce the results he requires. The effectiveness and simplicity of these methods are fair measures of the degree of technical development.

The study of methods of radar antenna construction is the study of the means by which radar antenna requirements are met. In a broader sense this includes an examination of mechanical structures, of the metals and plastics from which antennas are made, of the processes by which they are assembled, and of the finishes by which they are protected from their environment. It might include a study of practical installation and maintenance procedures. But these matters, which like the rest of Radar have unfolded widely during the war, are beyond the scope of this paper. An adequate discussion of them would have to be based on hundreds of technical reports and instruction manuals and on thousands of manufacturing drawings. The account of methods which is to follow will therefore be restricted to a discussion, usually from the electrical point of view, of the more useful and common radar antenna configurations.

6. Classification of Methods

During the history of radar, short as it is, many methods of antenna construction have been devised. To understand the details of all of these methods and the diverse applications of each is a task that lies beyond the ability of any single individual. Nevertheless most of the methods fall into one or another of a limited collection of groups or classifications. We can grasp most of what is generally important through a study of these groups.

In order to provide a basis for classification we will review briefly, from a transmitting standpoint, the action of an antenna. Any antenna is in a sense a transformer between a transmission line and free space. More explicitly, it is a device which accepts energy incident at its terminals, and converts it into an advancing electromagnetic wave with prescribed amplitude, phase and polarization over an area. In order to do this the antenna must have some kind of energy distributing system, some means of amplitude control and some means of phase control. The distributed energy must be suitably controlled in phase, amplitude and polarization.

All antennas perform these functions, but different antennas perform them by different means. Through an examination of the means by which they are performed and the differences between them we are enabled to classify methods of antenna construction.

To distribute energy over its aperture an antenna can use a branching system of transmission lines. When this is done the antenna is an array. Arrays are particularly common in the short wave communication bands, but somewhat less common in the microwave radar bands. In a somewhat simpler method the antenna distributes energy over an area by radiating it

Digitized by Google
Original from UNIVERSITY OF MICHIGAN
Generated on 2019-09-23 09:29 GMT / http://hdl.handle.net/2027/mdp.39015077775156
Public Domain, Google-digitized / http://www.hathitrust.org/access_use#pd-google

from an initial source or 'primary feed'. This distribution can occur in both dimensions at once, as from a point source. Alternatively the energy can be radiated from a primary source but be constrained to lie between parallel conducting plates so that it is at first distributed only over a long narrow aperture or 'line source'. Distribution over the other dimension occurs only after radiation from the line source.

In order to control the amplitude across the aperture of an array antenna we must design the branching junctions so that the desired power division occurs in each one. When the energy is distributed by radiation from a primary source we must control the amplitude by selecting the proper primary feed directivity.

We can control the phase of an array antenna by choosing properly the lengths of the branching lines. Alternatively we can insert appropriate phase changers in the lines.

When the energy is distributed by primary feeds, methods resembling those of optics can be used to control phase. The radiation from a point source is spherical in character. It can be 'focussed' into a plane wave by means of a paraboloidal reflector or by a spherical lens. The radiation from a point source between parallel plates or from a uniphase line source is cylindrical in character. It can be focussed by a parabolic cylinder or a cylindrical lens.

In Table A we have indicated a possible classification of methods of radar antenna construction. This classification is based on the differences discussed in the foregoing paragraphs.

TABLE A

CLASSIFICATION OF METHODS OF RADAR ANTENNA CONSTRUCTION

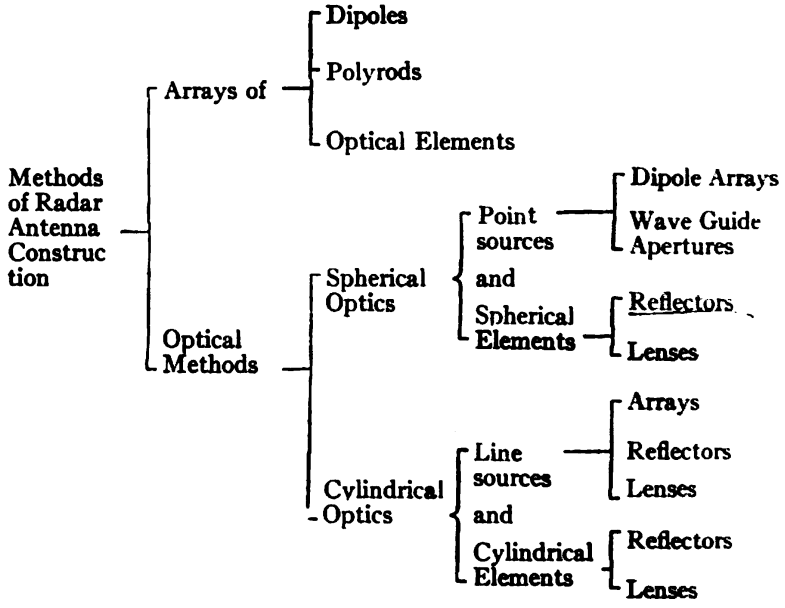

Digitized by Google
Original from UNIVERSITY OF MICHIGAN
Generated on 2019-09-23 09:29 GMT / http://hdl.handle.net/2027/mdp.39015077775156
Public Domain, Google-digitized / http://www.hathitrust.org/access_use#pd-google

7. Basic Design Formulation

Certain design factors are common to almost all radar antennas. Because of their importance it would be well to consider these factors in a general way before proceeding with a study of particular antenna techniques.

Almost every radar antenna, regardless of how it is made, has a well defined aperture or wave front. Through wave front analysis we can often examine the connections between the Huygens sources in the antenna aperture and the radiation characteristics of the antenna. We can, in other words, use wave front analysis to study the fundamental antenna design factors, provided the analysis does not violate one of the conditions of section 3.13.

7.1 *Dimensions of the Aperture*

The dimensions of the aperture of a properly designed antenna are related to its gain by simple and general approximate relations. If the aperture is uniphase and has an amplitude distribution that is not too far from constant the relation

$$G = \frac{4\pi A}{\lambda^2}$$

is useful in connecting the gain of an antenna with the area of its aperture. The effective area is related to the area of the aperture by the equation

$$A = \eta S$$

where η is an efficiency factor. In principle η could have any value but in practice for microwave antennas η has always been less than one. Its value for most uniphase and tapered amplitude antennas is between 0.4 and 0.7. In special cases, e.g. for cosecant antennas or for some scanners its value may be less than 0.4.

The necessary dimensions for the aperture may be determined from the required beam widths in two perpendicular directions. Beam widths are usually specified as half power widths, that is by the number of degrees between directions for which the one way response is 3 *db* below the maximum response. Figure 11 shows that for an ideal rectangular antenna with uniform phase, polarization and amplitude $\alpha_{P/2} = 51\frac{\lambda}{a}$ degrees where $\alpha_{P/2}$ = half power width in degrees, a = aperture dimension and λ = wavelength. The relation $\alpha_{P/2} = 65\frac{\lambda}{a}$ degrees is more nearly correct for the majority of practical antennas with round or elliptical apertures and with uniform phase and reasonably tapered amplitudes.

Digitized by Google
Original from UNIVERSITY OF MICHIGAN
Generated on 2019-09-23 09:34 GMT / http://hdl.handle.net/2027/mdp.39015077775156
Public Domain, Google-digitized / http://www.hathitrust.org/access_use#pd-google

7.2 *Amplitude Distribution*

Except where special, in particular cosecant, patterns are desired the principle factors affecting amplitude distribution are efficiency and required minor lobe level. The amplitude distribution or taper of an ideal uniphase rectangular wave front affects the minor lobe level as indicated by Figures 11, 12 and 13. Practical antennas tend to fall somewhat below this ideal picture because of non-uniform phase and because of variations from the ideal amplitude distribution due to discontinuities in the aperture and undesired leakage or spillover of energy. Nevertheless a commonly used rule of thumb is that minor lobes 20 *db* or more below the peak radiation level are tolerable and will not be exceeded with a rounded amplitude taper of 10 or 12 *db*.

7.3 *Phase Control*

Uniphase wave fronts are used whenever a simple pattern with prescribed gain, beam widths and minor lobes is to be obtained with minimum aperture dimensions. When special results are desired such as cosecant patterns or scanning beams the phase must be varied in special ways.

Mechanical tolerances in the antenna structure make it impossible to hold phases precisely to the desired values. The accuracy with which the phases can be held constant in practice varies with the technique, the antenna size and the wave length. Undesired phase variations increase the minor lobes and reduce the gain of an antenna. The extent to which phase variations can be expected to reduce the gain is indicated in Fig. 17.

8. Parabolic Antennas

The headlights of a car or the searchlights of an antiaircraft battery use reflectors to produce beams of light. Similarly the majority of radar antennas employ reflectors to focus beams of microwave energy. These reflectors may be exactly or approximately parabolic or they may have special shapes to produce special patterns. If they are parabolic they may be paraboloids which are illuminated by point sources and focus in both directions, or they may be parabolic cylinders which focus in only one direction. If they are parabolic cylinders they may be illuminated by line sources or they may be confined between parallel conducting plates and illuminated by point sources to produce line sources.

8.1 *Control of Phase*

A simple and natural way to distribute energy smoothly in space is to radiate it from a relatively nondirectional 'primary' source such as a dipole array or an open ended wave guide. This energy will be formed into a directive beam if a reflector is introduced to bring it to a plane area or wave front with constant phase. If the primary source is effectively a point as far as

Digitized by Google
Original from UNIVERSITY OF MICHIGAN
Generated on 2019-09-23 09:34 GMT / http://hdl.handle.net/2027/mdp.39015077775156
Public Domain, Google-digitized / http://www.hathitrust.org/access_use#pd-google

phase is concerned, that is if the radiated energy has the same phase for all points which are the same distance from a given point, then the reflector should be parabolic. This can be proved by simple geometrical means.

In Fig. 18 let the point source S coincide with the point $x = f$, $y = O$ of a coordinate system and let the uniphase wave front coincide with the line $x = f$. Let us assume that one point O of the reflector is at the origin. Then it can be shown that any other point of the reflector must lie on the curve

$$y^2 = 4fx$$

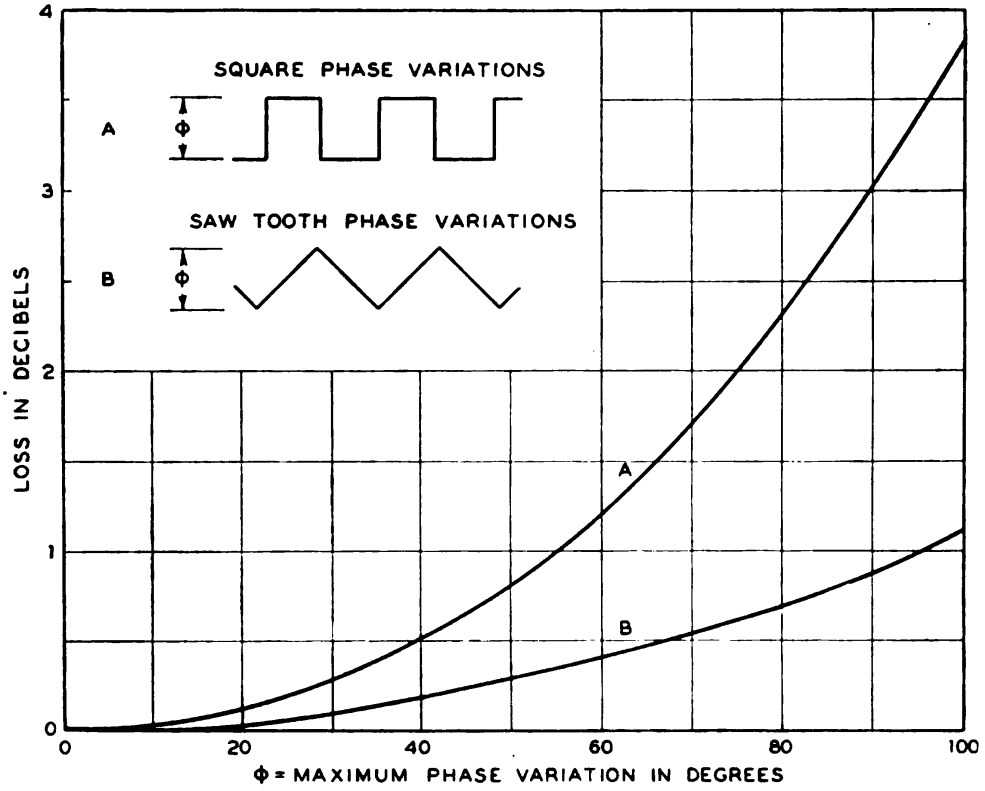

Fig. 17—Loss due to Phase Variation in Antenna Wave Front.

This is a parabola with focus at f, o and focal length f.

The derivation based on Fig. 18 is two dimensional and therefore in principle applies as it stands only to line source antennas employing parabolic cylinders bounded by parallel conducting planes (Fig. 24 and 25). If Fig. 18 is rotated about the X axis the parabola generates a paraboloid of revolution (Fig. 3). This paraboloid focusses energy spreading spherically from the point source at S in such a way that a uniphase wave front over a plane area is produced. Alternatively Fig. 18 can be translated in the Z direction perpendicular to the XY plane. The parabola then generates a

Digitized by Google
Original from UNIVERSITY OF MICHIGAN
Generated on 2019-09-23 09:35 GMT / http://hdl.handle.net/2027/mdp.39015077775156
Public Domain, Google-digitized / http://www.hathitrust.org/access_use#pd-google

parabolic cylinder and the point source S generates a line source at the focal line of the parabolic cylinder (Fig. 19). The energy spreading cylindrically from the line source is focussed by the parabolic cylinder in such a way that a uniphase wave front over a plane area is again produced. Parabolic cylinders and paraboloids are both used commonly in radar antenna practice.

In the discussion so far it has been assumed that the primary source is effectively a point source and that the reflector is exactly parabolic. If the primary source is not effectively a point source, in other words if it produces waves which are not purely spherical, then the reflector must be distorted from the parabolic shape if it is to produce perfect phase correction. When

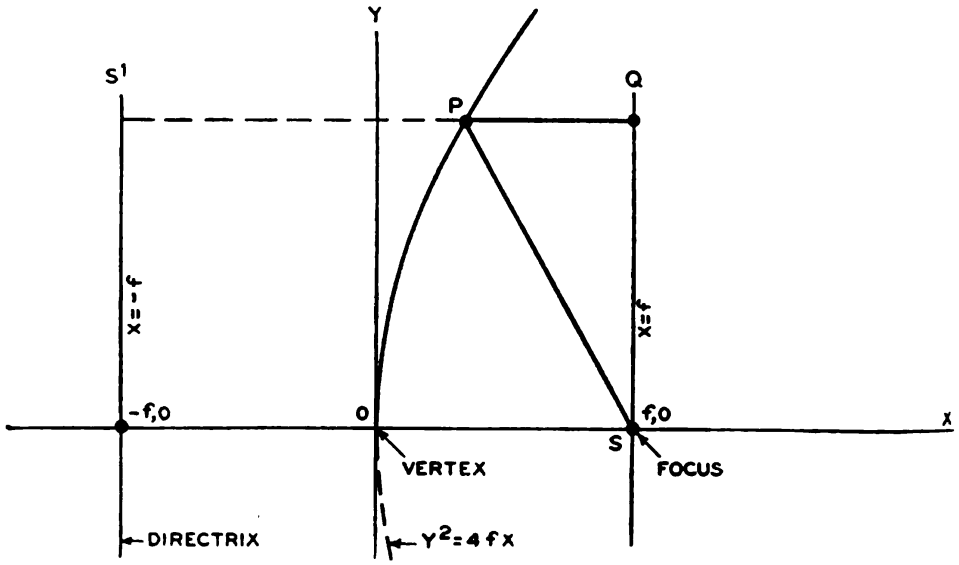

Fig. 18—Parabola.

this occurs the correct reflector shape is sometimes specified on the basis of an experimental determination of phase.

8.2 *Control of Amplitude*

When a primary source is used to illuminate a parabolic reflector there are two factors which affect the amplitude of the resulting wave front. One of these is of course the amplitude pattern of the primary source. The other is the geometrical or space attenuation factor which is different for different parts of the wave front. In most practical antennas each of these factors tends to taper the amplitude so that it is less at the edges of the antenna than it is in the central region. The effective area of the antenna is reduced by this taper.

In any finite parabolic antenna some of the energy radiated by the primary

Digitized by Google
Original from UNIVERSITY OF MICHIGAN
Generated on 2019-09-23 09:35 GMT / http://hdl.handle.net/2027/mdp.39015077775156
Public Domain, Google-digitized / http://www.hathitrust.org/access_use#pd-google

source will fail to strike the reflector. The effective area must also be reduced by the loss of this 'spill-over' energy.

The maximum effective area for a parabolic antenna is obtained by designing the primary feed to obtain the best compromise between loss due to taper and loss due to spill-over. It has been shown theoretically that this best compromise generally occurs when the amplitude taper across the aperture is about 10 or 12 *db* and that in the neighborhood of the optimum the efficiency is not too critically dependent on the taper.[6]

This theoretical result is well justified by experience and has been applied to the majority of practical parabolic antennas. It applies both when the reflector is paraboloidal so that taper in both directions must be considered

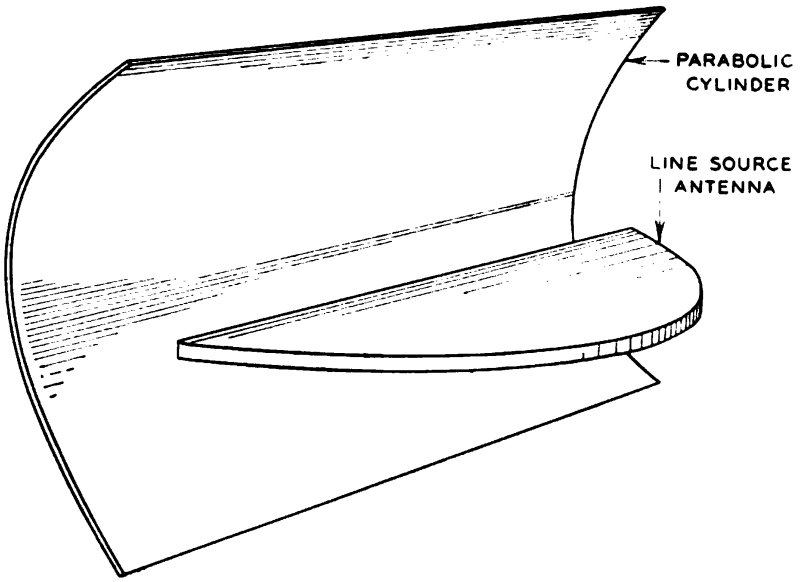

Fig. 19—A Parabolic Cylinder with Line Feed.

and when the reflector is a parabolic cylinder with only a single direction of taper. It is a fortunate by-product of a 10 or 12 *db* taper that it is generally sufficient to produce satisfactory minor lobe suppression.

8.3 *Choice of Configuration*

We have shown how a simple beam can be obtained through the use of a paraboloidal reflector with a point source or alternatively through the use of a reflecting parabolic cylinder and a line source. The line source itself can be produced with the help of a parabolic cylinder bounded by parallel conducting plates. We will now outline certain practical considerations. These considerations may determine which of the two reflector types will be

[6] C. C. Cutler, Parabolic Antenna Design for Microwaves, paper to be published in Proc. of the I. R. E.

Digitized by Google
Original from UNIVERSITY OF MICHIGAN
Generated on 2019-09-23 09:35 GMT / http://hdl.handle.net/2027/mdp.39015077775156
Public Domain, Google-digitized / http://www.hathitrust.org/access_use#pd-google

used for a particular job. They may help in choosing a focal length and in determining which finite portion of a theoretically infinite parabolic curve should be used. Finally they may assist in determining whether reflector technique is really the best for the purpose at hand or whether we could do better with a lens or an array.

In designing a parabolic antenna it must obviously be decided at an early stage whether a paraboloid or one or more parabolic cylinders are to be employed. This choice must be based on a number of mechanical and electrical considerations. Paraboloids are more common in the radar art than parabolic cylinders and are probably to be preferred, yet a categorical a priori judgment is dangerous. It will perhaps be helpful to compare the two alternatives by the simple procedure of enumerating some features in which each is usually preferable to the other.

Paraboloidal antennas

(a) are simpler electrically, since point sources are simpler than line sources.
(b) are usually lighter.
(c) are more efficient.
(d) have better patterns in the desired polarization.
(e) are more appropriate for conical lobing or spiral scanning.

Antennas employing parabolic cylinders

(a) are simpler mechanically since only singly curved surfaces are required.
(b) have separate electrical control in two perpendicular directions.

This last advantage of parabolic cylinders is important in special antennas, many of which will be described in later sections. It is useful where antennas with very large aspect ratios (ratio of dimensions of the aperture in two perpendicular directions) are desired. It is highly desirable where control in one direction is to be achieved through some special means, as in cosecant antennas, or in antennas which scan in one direction only.

Let us suppose that we have selected the aperture dimensions and have decided whether the reflector is to be paraboloidal or cylindrical. The reflector is not yet completely determined for we are still free in principle to use any portion of a parabolic surface of any focal length. In order to obtain economy in physical size the focal length is generally made between 0.6a and 0.25a where 'a' is the aperture. For the same reason a section of the reflecting surface which is located symmetrically about the vertex is often chosen (Figures 3 and 19).

When a symmetrically located section of the reflector is used certain difficulties are introduced. These difficulties, if serious enough so that their removal justifies some increase in size can be bypassed through the use of an

Digitized by Google
Original from UNIVERSITY OF MICHIGAN
Generated on 2019-09-23 09:35 GMT / http://hdl.handle.net/2027/mdp.39015077775156
Public Domain, Google-digitized / http://www.hathitrust.org/access_use#pd-google

offset section as shown in Fig. 20. We can comment on these difficulties as follows:

1. The presence of the feed in the path of the reflected energy causes a region of low intensity or 'shadow' in the wave front. The effect of this shadow on the antenna pattern depends on the size and shape of the feed and on the characteristics of the portion of the wave front where it is located. Its effect is to subtract from the undisturbed pattern a 'shadow pattern' component which is broad in angle. This decreases the gain and increases the minor lobes as indicated in Fig. 21.

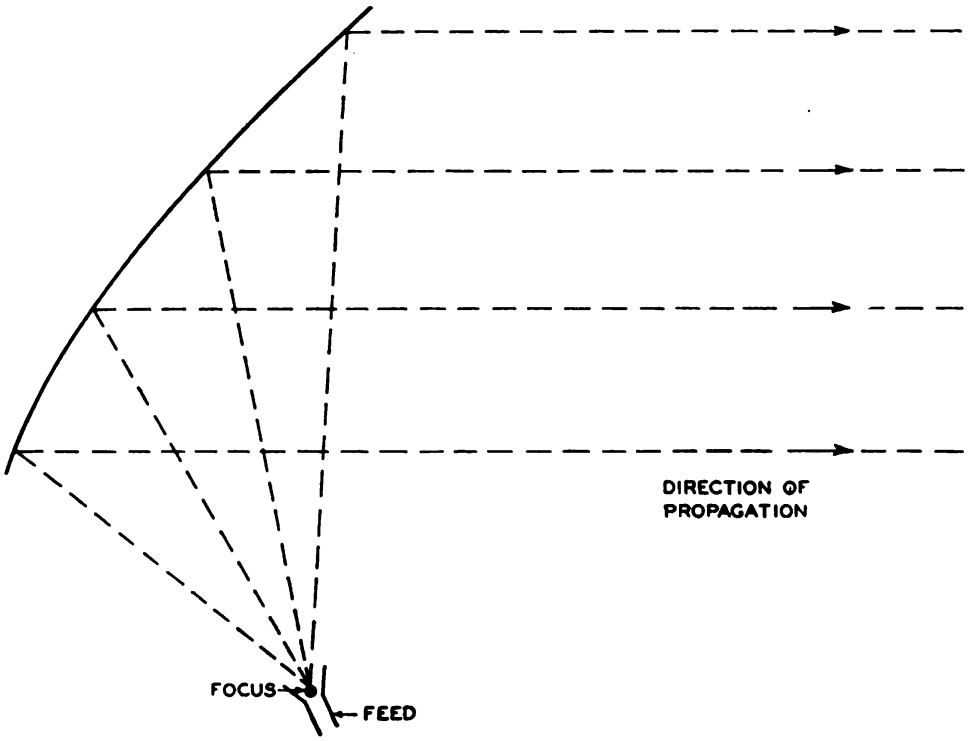

Fig. 20—Offset Parabolic Section.

2. Return of reflected energy into the feed introduces a standing wav of impedance mismatch in the feed line which is constant in amplitud but varies rapidly in phase as the frequency is varied. A mismatch a the feed which cancels the standing wave at one frequency will add to it at another frequency. A mismatch which will compensate over a band can be introduced by placing a raised plate of proper dimension at the vertex of the reflector as indicated in Fig. 22, but such a plate produces a harmful effect on the pattern. In an antenna which must operate over a broad band it is consequently usually better to match

[7] Figures 21, 22, and 23 are taken from C. C. Cutler, loc. cit.

Digitized by Google
Original from UNIVERSITY OF MICHIGAN
Generated on 2019-09-23 09:35 GMT / http://hdl.handle.net/2027/mdp.39015077775156
Public Domain, Google-digitized / http://www.hathitrust.org/access_use#pd-google

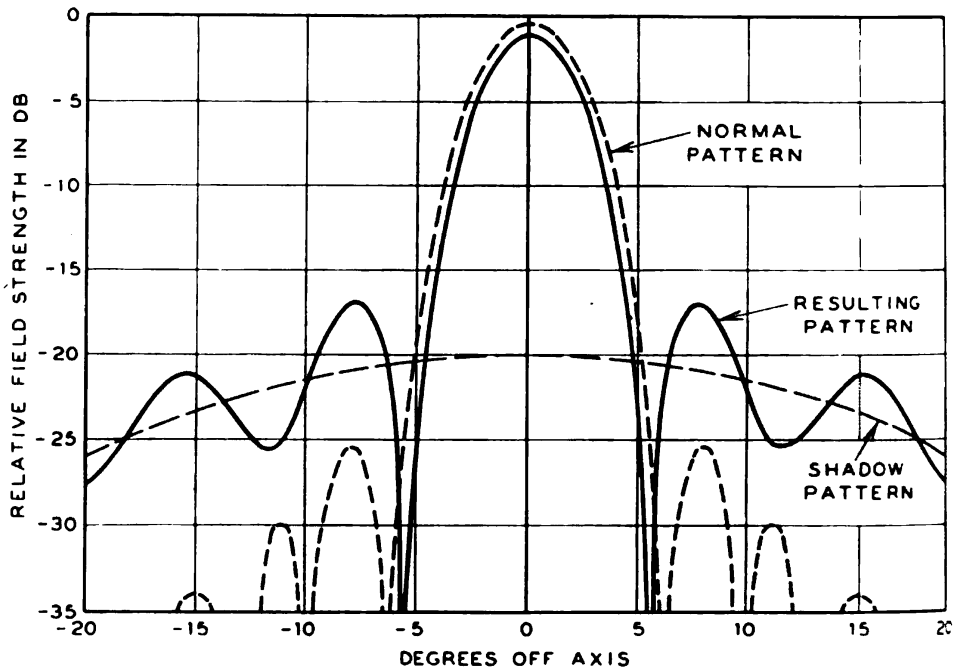

Fig. 21—Effect of Shadow on Paraboloid Radiation Pattern.

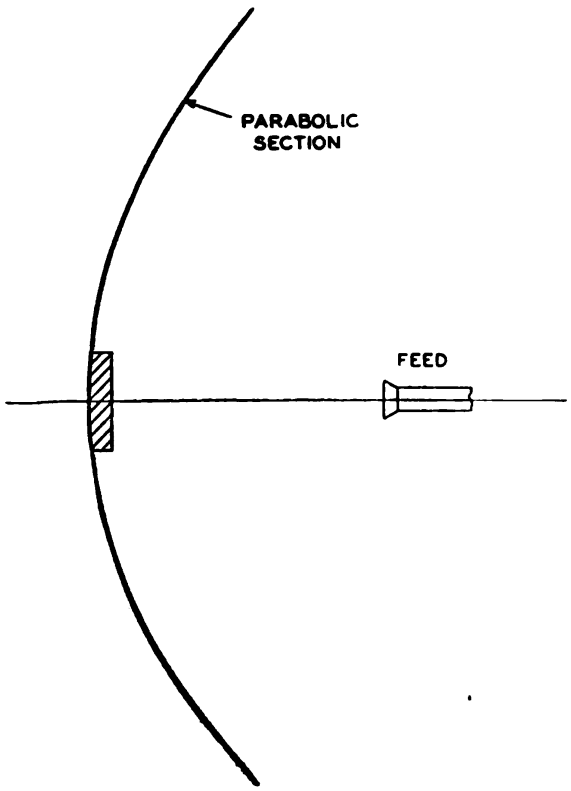

Fig. 22—Apex Matching Plate for Improving the Impedance Properties of a Paraboia

Digitized by Google
Original from UNIVERSITY OF MICHIGAN
Generated on 2019-09-23 09:36 GMT / http://hdl.handle.net/2027/mdp.39015077775156
Public Domain, Google-digitized / http://www.hathitrust.org/access_use#pd-google

the feed to space and accept the residual standing wave, or if this is too great to use an offset section of the parabolic surface.

8.4 *Feeds for Paraboloids*

We have seen that an antenna with good wave front characteristics and consequently with a good beam and pattern can be constructed by illuminating a reflecting paraboloid with a properly designed feed placed at its focus. In this section we will examine the characteristics which the feed should have and some of the ways in which feeds are made in practice.

A feed for a paraboloid should

a. be appropriate to the transmission line with which it is fed. This is sometimes a coaxial line but more commonly a waveguide.
b. Provide an impedance match to this feed line. This match should usually be obtained in the absence of the reflector but sometimes, for narrow band antennas, with the reflector present.
c. have a satisfactory phase characteristic. For a paraboloid the feed should be, as far as phase is concerned, a true point source radiating spherical waves. As discussed at the end of 8.1, if the wave front is not accurately spherical, a compensating correction in the reflector can be made.
d. have a satisfactory amplitude characteristic. According to 8.2 this means that the feed should have a major radiation lobe with its maximum striking the center of the reflector, its intensity decreasing smoothly to a value about 8 to 10 *db* below the maximum in the direction of the reflector boundaries and remaining small for all directions which do not strike the reflector.
e. have a polarization characteristic which is such that the electric vectors in the reflected wave front will all be polarized in the same direction.
f. not disturb seriously the radiation characteristics of the antenna as a whole. The shadow effect of the feed, the feed line and the necessary mechanical supports must be small or absent. Primary radiation from the feed which does not strike the reflector or reflected energy which strikes the feed or associated structure and is then reradiated must be far enough down or so controlled that the antenna pattern is as required.

In addition to the electrical requirements for a paraboloid feed it must of course be so designed that all other engineering requirements are met, it must be firmly supported in the required position, must be connected to the antenna feed line in a satisfactory manner, must sometimes be furnished with an air tight or water tight seal, and so forth.

Generated on 2019-09-23 09:36 GMT / http://hdl.handle.net/2027/mdp.39015077775156
Public Domain, Google-digitized / http://www.hathitrust.org/access_use#pd-google
Digitized by Google
Original from UNIVERSITY OF MICHIGAN

From the foregoing it is evident that a feed for a paraboloid is in itself a small relatively non-directive antenna. Its directivity is somewhat less than that obtained with an ordinary short wave array. It is therefore not surprising that dipole arrays are sometimes used in practice to feed paraboloids.

A simple dipole or half wave doublet can in itself be used to feed a paraboloid, but it is inefficient because of its inadequate directivity. It is preferable and more common to use an array in which only one doublet is excited directly and which contains a reflector system consisting of another doublet or a reflecting surface which is excited parasitically.

Dipole feeds although useful in practice have poor polarization characteristics and although natural when a coaxial antenna feed line is used are less convenient when the feed line is a waveguide. Since waveguides are more common in the microwave radar bands it is to be expected that waveguide feeds would be preferred in the majority of paraboloidal antennas.

The most easily constructed waveguide feed is simply an open ended waveguide. It is easy to permit a standard round or rectangular waveguide transmitting the dominant mode to radiate out into space toward the paraboloid. It will do this naturally with desirable phase, polarization and amplitude characteristics. It is purely coincidental, however, when this results in optimum amplitude characteristics. It is usually necessary to obtain these by tapering the feed line to form a waveguide aperture of the required size and shape. The aperture required may be smaller than a standard waveguide cross section so that its directivity will be less. In this case it may be necessary to 'load' it with dielectric material so that the power can be transmitted. It may be greater, in which case it is sometimes called an 'electromagnetic horn'. It may be greater in one dimension and less in the other, as when a paraboloidal section of large aspect ratio is to be illuminated.

If a single open ended waveguide or electromagnetic horn is used to feed a section of the paraboloid which includes the vertex, the waveguide feed line must partially block the reflected wave in order to be connected to the feed. To avoid this difficulty several rear waveguide feeds have been used. In this type of feed the waveguide passes through the vertex of the paraboloid and serves to support the feed at the focus. The energy can be caused to radiate back towards the reflector in any one of several ways, some of which involve reflecting rings or plates or parasitically excited doublets. The 'Cutler' feed[8] is perhaps the most successful and common rear feed. It operates by radiating the energy back towards the paraboloid through two apertures located and excited as shown in Fig. 23.

[8] C. C. Cutler, Loc. Cit.

Digitized by Google
Original from UNIVERSITY OF MICHIGAN
Generated on 2019-09-23 09:36 GMT / http://hdl.handle.net/2027/mdp.39015077775156
Public Domain, Google-digitized / http://www.hathitrust.org/access_use#pd-google

8.5 *Parabolic Cylinders between Parallel Plates*

In 8.0 we saw that parabolic cylinders may be illuminated by line sources or that they may be confined between parallel plates and illuminated by point sources to produce line sources. In either of these two cases the characteristics which the feed should have are specified accurately by the conditions stated at the beginning of 8.4 for paraboloidal feeds with the exceptions that condition *c* must be reworded so that it applies to cylindrical rather than to spherical optics.

We will first consider parabolic cylinders bounded by parallel plates because in doing so we describe in passing one form of feed for unbounded parabolic cylinders. Two forms of transmission between parallel plates are used in practice.

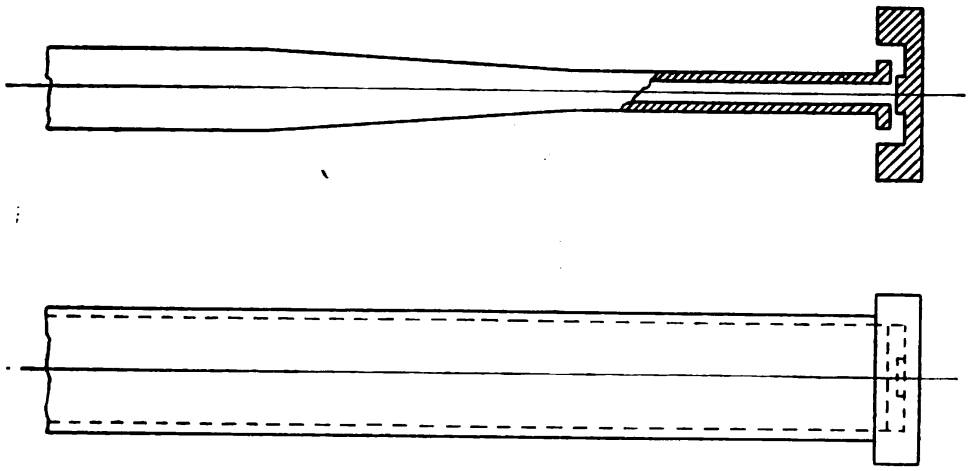

Fig. 23—Dual Aperture Rear Feed Horn.

a. The transverse electromagnetic (TEM) mode in which the electric vector is perpendicular to the plates. This is simply a slice of the familiar free space wave and can be propagated regardless of the spacing between the plates. It is the only mode that can travel between the plates if they are separated less than half a wavelength. Its velocity of propagation is independent of plate spacing.
b. The TE_{01} mode in which the electric vector is parallel to the plates. This mode is similar to the dominant mode in a rectangular waveguide and differs from it only in that it is not bounded by planes perpendicular to the electric vector. It can be transmitted only if the plate spacing is greater than half a wavelength, is the *only* parallel mode that can exist if the spacing is under a wavelength and is the only symmetrical parallel mode that can exist if the plate spacing is under three

Digitized by Google
Original from UNIVERSITY OF MICHIGAN
Generated on 2019-09-23 09:36 GMT / http://hdl.handle.net/2027/mdp.39015077775156
Public Domain, Google-digitized / http://www.hathitrust.org/access_use#pd-google

halves of a wavelength. Its phase velocity is determined by the plate spacing in a manner given by the familiar waveguide formula

$$V_p = \frac{c}{\sqrt{\epsilon - \left(\frac{\lambda}{2a}\right)^2}}$$

where 'c' is the velocity of light, ϵ is the dielectric constant relative to free space of the medium between the plates, λ is the wavelength in air and 'a' is the plate spacing.

The TEM mode between parallel plates can be generated by extending the central conductor of a coaxial perpendicularly into or through the wave space and backing it up with a reflecting cylinder as indicated in Fig. 24.

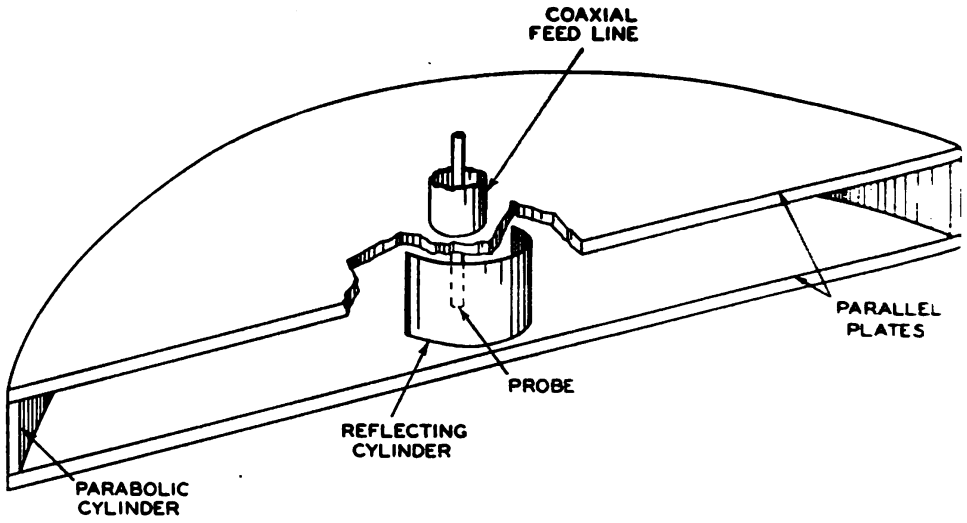

Fig. 24—Parabolic Cylinder Bounded by Parallel Plates. Probe Feed.

Alternatively this mode can be generated as indicated by Fig. 25 by a waveguide aperture with the proper polarization.

The TE_{01} mode, when used, is usually generated by a rectangular waveguide aperture set between the plates with proper polarization as indicated in Fig. 25. Care must be taken that only the desired mode is produced. The TEM mode will be unexcited if only the desired polarization is present in the feed. The next parallel mode is unsymmetrical and therefore even if it can be transmitted will be unexcited if the feed is placed symmetrically with respect to the two plates.

Parallel plate antennas as shown in figures 24 and 25 are useful where particularly large aspect ratios are required. The aperture dimension perpendicular to the plates is equal to the plate spacing and therefore small.

Generated on 2019-09-23 09:36 GMT / http://hdl.handle.net/2027/mdp.39015077775156
Public Domain, Google-digitized / http://www.hathitrust.org/access_use#pd-google
Digitized by Google
Original from UNIVERSITY OF MICHIGAN

It can be increased somewhat by the addition of flares. The other dimension can easily be made large.

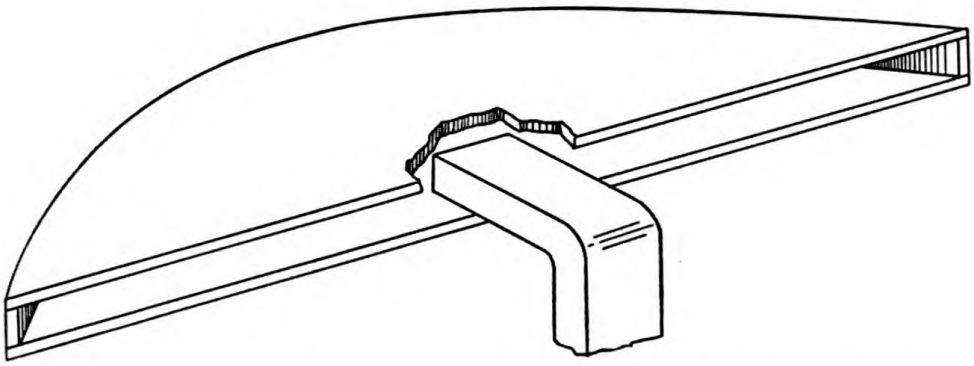

Fig. 25—Parabolic Cylinder Bounded by Parallel Plates. Wave Guide Feed.

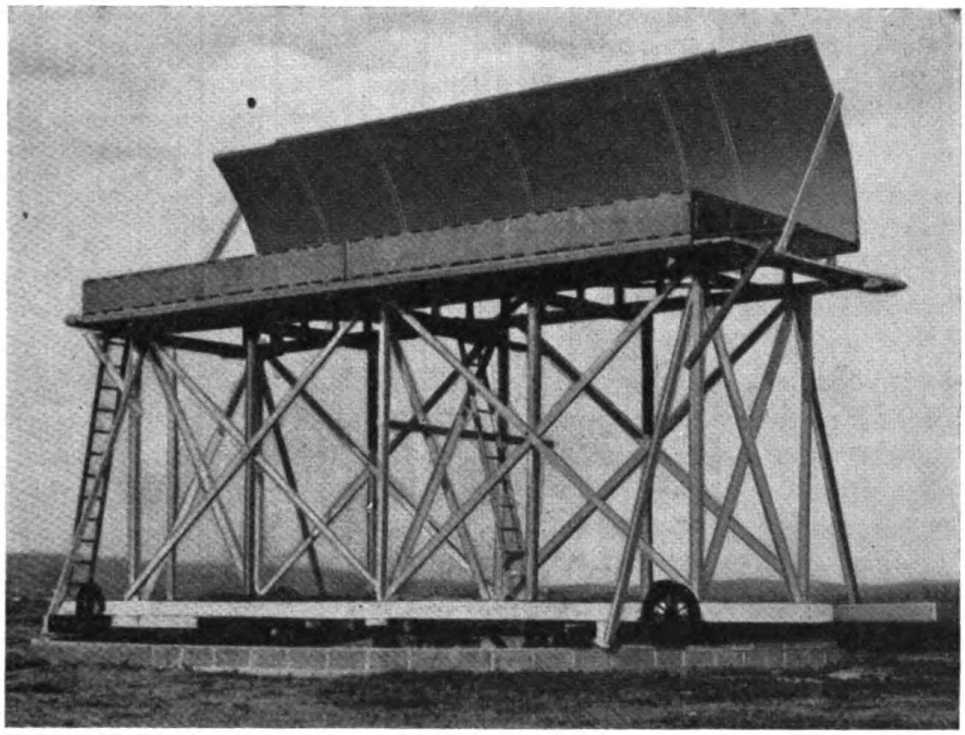

Fig. 26.—Experimental 7′ x 32′ Antenna.

8.6 *Line Sources for Parabolic Cylinders*

A line source for a parabolic cylinder is physically an antenna with a long narrow aperture. Any means for obtaining such an aperture can be used in producing a line source. Parallel plate systems as described in 8.5 have been used as line sources in several radar antennas. The large (7′ x 32′)

Digitized by Google
Original from UNIVERSITY OF MICHIGAN
Generated on 2019-09-23 09:37 GMT / http://hdl.handle.net/2027/mdp.39015077775156
Public Domain, Google-digitized / http://www.hathitrust.org/access_use#pd-google

experimental antenna shown in Fig. 26 was one of the first to illustrate the practicality of this design.

The horizontal pattern of the 7′ x 32′ antenna is plotted in Fig. 27. The horizontal beam width is seen to be of the order of 0.7 degrees.

The antenna illustrated in Fig. 26 is interesting in another way for it is a good example of a type of experimental construction which was extremely useful in wartime antenna development. Research and development engi-

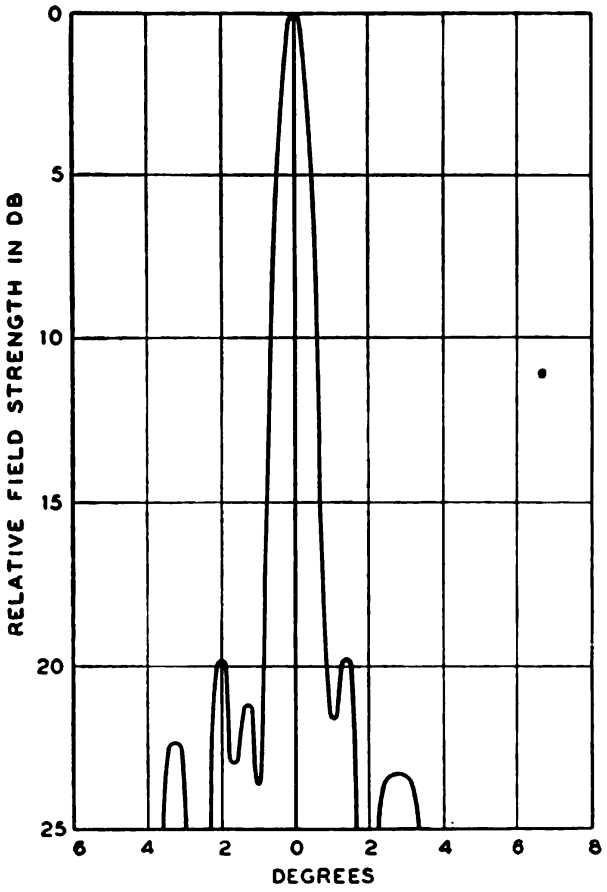

Fig. 27—7′ x 32′ Antenna, Horizontal Pattern.

neers found that they could often save months by constructing initial models of wood. Upon completion of a wooden model electrically important surfaces were covered with metal foil or were sprayed or painted with metal. Thus, where tolerances permitted, the carpenter shop could replace the relatively slow machine shop.

Another form of parallel plate line feed results when a plastic lens is placed between parallel plates and used as the focussing element. A linear array

Generated on 2019-09-23 09:38 GMT / http://hdl.handle.net/2027/mdp.39015077775156
Public Domain, Google-digitized / http://www.hathitrust.org/access_use#pd-google
Digitized by Google
Original from UNIVERSITY OF MICHIGAN

of elements excited with the proper phase and amplitude can also be used. Some discussion of alternative approaches will appear in the section on scanning techniques.

8.7 *Tolerances in Parabolic Antennas*

The question of tolerances will always arise in practice. Ideal dimensions are only approximated, never reached. The ease of obtaining the required accuracy is an important engineering factor.

The tolerances in paraboloidal antennas or in parabolic cylinders illuminated by line sources can be divided into three general classes:

(a) Tolerances on reflecting surfaces.
(b) Tolerances on spacial relationships of feed and reflector.
(c) Tolerances on the feed.

When the actual reflector departs from the ideal parabolic curve deviations in the phase will result. These will tend to reduce the gain and increase the minor lobes. The effects of such deviations on the gain can be estimated with the help of Fig. 17. We should recall that an error of σ in the reflector surface will produce an error of about 2σ in the phase front. Based on this kind of argument and on experience reflector tolerances are generally set in practice to about $\pm \frac{\lambda}{16}$ or $\pm \frac{\lambda}{32}$ depending on the amount of beam deterioration that can be permitted.

In Fig. 28 are compared some electrical characteristics of two paraboloidal antennas, one employing a precisely constructed paraboloidal searchlight mirror and the other a carefully constructed wooden paraboloidal reflector with the same nominal contour. This comparison is revealing for it shows the harm that can be done even by small defects in the reflector surface. Although the two patterns are almost identical in the vicinity of the main beam, the general minor lobe level of the wooden reflector remains higher at large angles and its gain is less.

It must not, however, be assumed that a solid reflecting surface is necessary to insure excellent results. Any reflecting surface which reflects all or most of the power is satisfactory provided that it is properly located. Perforated reflectors, reflectors of woven material and reflectors consisting of gratings with less than half wavelength spacing are commonly used in radar antenna practice. These reflectors tend to reduce weight, wind or water resistance and visibility. Many of them will be described in Part III of this paper.

The feed of a parabolic reflector should be located so that its phase center coincides with the focus of the reflector. If it is located at an incorrect dis-

Digitized by Google
Original from UNIVERSITY OF MICHIGAN
Generated on 2019-09-23 09:38 GMT / http://hdl.handle.net/2027/mdp.39015077775156
Public Domain, Google-digitized / http://www.hathitrust.org/access_use#pd-google

tance from the vertex a circular curvature of phase results and the system is said to be 'defocussed' (Sec. 3.9). As the feed is moved off the axis of the reflector the first effect is a shifting of the beam due to a linear variation of the phase (Sec. 3.8). For greater distances off axis a cubic component of phase error becomes effective (Sec. 3.10). Phase error, whether circular, cubic or more complex, results in a reduction in gain and usually in an increase of minor lobes. Although the effects of given amounts of phase curvature on the radiation characteristics of an antenna can be estimated by theoretical means, it is usually easier and quicker to find them experimentally.

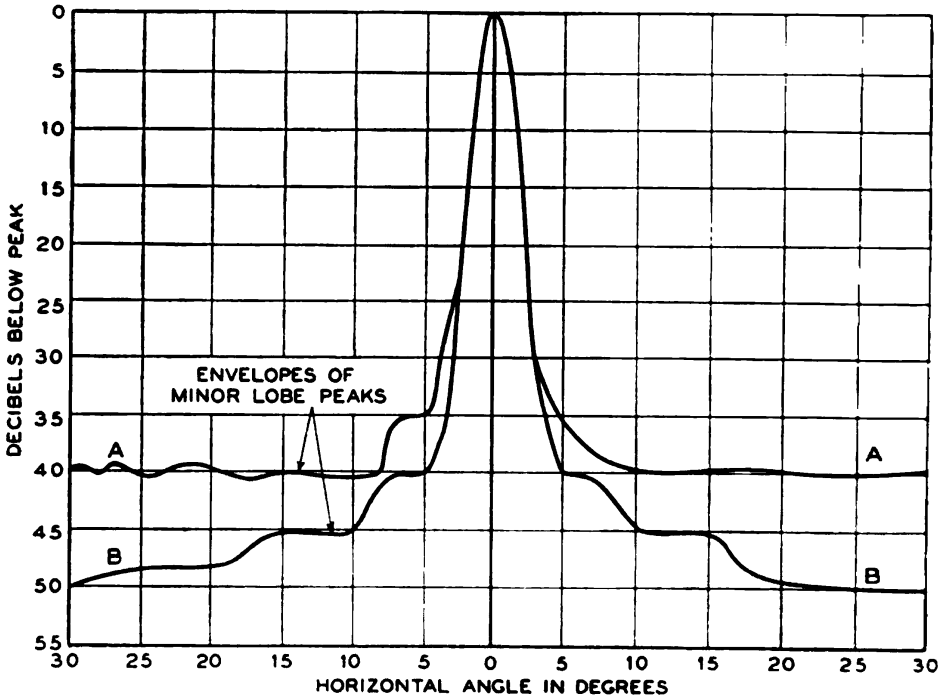

Fig. 28—Effect of Small Inaccuracies in Reflector.

The tolerances on the feed itself appear in various forms, many of which can be examined with the aid of transmission line theory and most of which are too detailed for discussion in this paper. It is generally true here also that experiment is a more effective guide than theory.

Experience has shown that when parallel plate systems are used, either as complete antennas or as line feeds for other elements, tolerances on the parallel conducting plates must be considered carefully. It is obvious that when the TE_{01} mode is used the plate spacing must be held closely, since the phase velocity is related to the spacing. This spacing can be controlled through the use of metallic spacers perpendicular to the plates. These

Generated on 2019-09-23 09:39 GMT / http://hdl.handle.net/2027/mdp.39015077775156
Public Domain, Google-digitized / http://www.hathitrust.org/access_use#pd-google
Digitized by Google
Original from UNIVERSITY OF MICHIGAN

spacers, if small enough in cross section, do not disturb things unduly. The velocity of the TEM mode is, on the other hand, almost independent of the plate spacing. This mode is, however, more likely to cause trouble by leaks through joints and cracks in the plates.

9. Metal Plate Lenses

At visible wavelengths lenses have, in the past, been far more common than in the microwave region, due chiefly to the absence of satisfactory lens materials. A solid lens of glass or plastic with a diameter of several feet is a massive and unwieldy object. By zoning, which will be discussed below, these difficulties can be reduced but they still remain.

A new lens technique, particularly effective in the microwave region was developed by the Bell Laboratories during the war.[9] It is evident that any material in which the phase velocity is different from that of free space can be used to make a phase correcting lens. The material which is used in this new technique is essentially a stack of equally spaced metal plates parallel to the electric vector of the wave front and to the direction of propagation. Lenses made from this material are called 'Metal Plate Lenses'.

When the spacing between neighboring plates is between $\lambda/2$ and λ only one mode with electric vector parallel to the plates can be transmitted. This is the TE_{01} mode for which the phase velocity is given in Sec. 8.5. When the medium between the plates is air this equation can be converted into the expression

$$N = \sqrt{1 - \left(\frac{\lambda}{2a}\right)^2}$$

for the effective index of refraction. Here λ is the wavelength in air and a is the plate spacing.

As a varies between $\lambda/2$ and λ, N varies as indicated in Fig. 29. In the neighborhood of $a = \lambda$, N is not far from 1 and as a approaches $\lambda/2$, N approaches 0. Since N is always less than 1 we see that there is an essential difference between metal plate lenses and glass or plastic lenses for which N is always greater than 1. This difference is seen in the fact that a glass lens corrects phases by slowing down a travelling wave front, while a metal lens operates in the reverse direction by speeding it up. This means that a convergent lens with a real focus must be thinner in the center than the edge, the opposite of a convergent optical lens (Fig. 30).

Unless the value of N is considerably different from 1 it is evident that very thick lens sections must be used to produce useful phase corrections. For this reason values of 'a' not far from $\lambda/2$ should be chosen. On the other hand values of 'a' too close to $\lambda/2$ would cause undesirably large reflections

[9] W. E. Kock, "Metal Lens Antennas", Proc. I. R. E., Nov., 1946.

Digitized by Google
Original from UNIVERSITY OF MICHIGAN
Generated on 2019-09-23 09:39 GMT / http://hdl.handle.net/2027/mdp.39015077775156
Public Domain, Google-digitized / http://www.hathitrust.org/access_use#pd-google

from the lens surfaces and impose severe restrictions on the accuracy of plate spacings. The compromises that have been used in practice are $N = 0.5$ for which $a = 0.577\lambda$ and $N = 0.6$ for which $a = 0.625\lambda$.

Even with $N = 0.5$ or 0.6 lenses become thick unless inconveniently long focal distances are used. Thick lenses are undesirable not only because they occupy more space and are heavier but also because the plate spacing must be held to a higher degree of accuracy if the phase correction is to be as

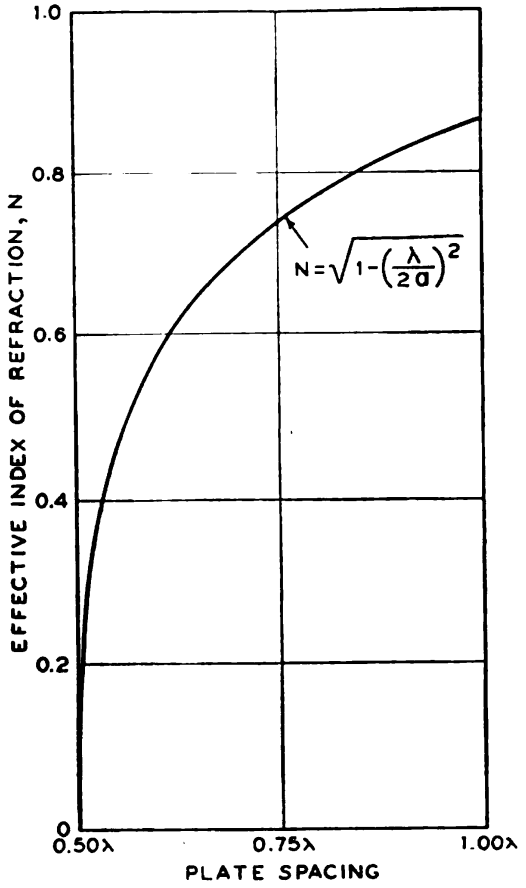

Fig. 29—Variation of Effective Index of Refraction with Plate Spacing in a Metal Plate Lens.

required. To get around these difficulties the technique of zoning is used.

Zoning makes use of the fact that if the phase of an electromagnetic vector is increased or decreased by any number of complete cycles the effect of the vector is unchanged. When applied to a metal plate lens antenna this means simply that wherever the phase correction due to a portion of the lens is greater than a wavelength this correction can be reduced by some integral number of wavelengths such that the residual phase correction is under one wavelength. If this is done it is evident that no portion of the

Digitized by Google
Original from UNIVERSITY OF MICHIGAN
Generated on 2019-09-23 09:39 GMT / http://hdl.handle.net/2027/mdp.39015077775156
Public Domain, Google-digitized / http://www.hathitrust.org/access_use#pd-google

lens needs to correct the phase by more than one wavelength. It follows that no portion of the lens need to be thicker than $\lambda/(1 - N)$.

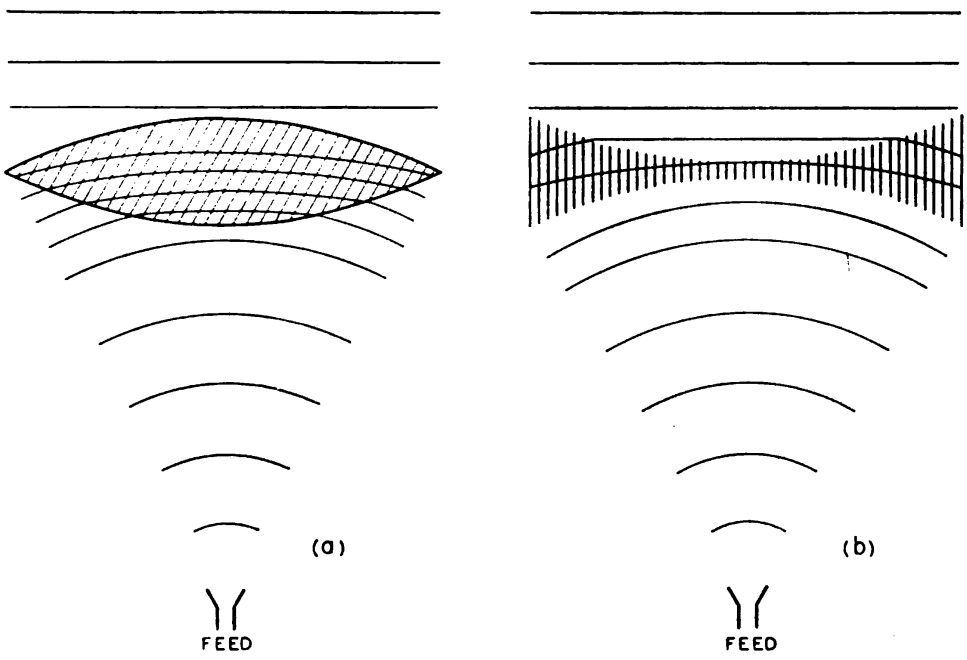

Fig. 30—Comparison of Dielectric and Metal Plate Lenses.

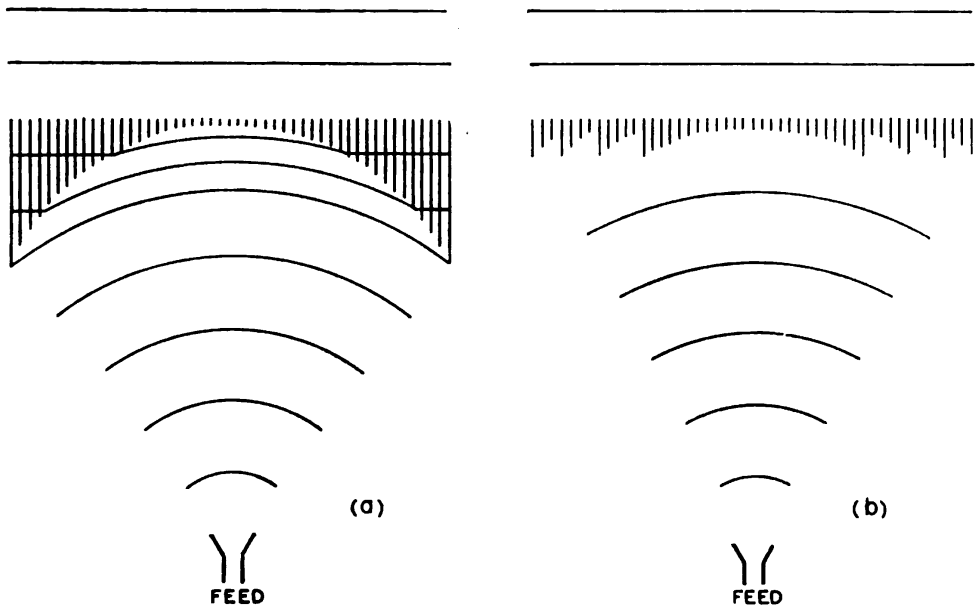

Fig. 31—Comparison of Unzoned and Zoned Metal Plate Lenses.

A cross section of a typical metal plate lens before and after zoning is illustrated in Fig. 31. This figure shows clearly why zoning reduces considerably the size and mass of a lens.

Digitized by Google
Original from UNIVERSITY OF MICHIGAN
Generated on 2019-09-23 09:44 GMT / http://hdl.handle.net/2027/mdp.39015077775156
Public Domain, Google-digitized / http://www.hathitrust.org/access_use#pd-google

Zoning is not without disadvantages. One disadvantage is obviously that a zoned lens which is designed for one frequency will not necessarily work well at other frequencies. It is in principle possible to design a broad band zoned metal plate lens corresponding to the color compensated lenses used in good cameras. So far, however, this has not been necessary since band characteristics of simple lenses have been adequate.

Another difficulty that zoning introduces is due to the boundary regions between the zones. The wave front in this region is influenced partly by one zone and partly by the other and may as a result have undesirable phase and amplitude characteristics. This becomes serious only if especially short focal distances are used.

9.1 *Lens Antenna Configurations*

Any of the configurations which are possible with parabolic reflectors have their analogues when metal plate lenses are used. Circular lenses illuminated by point sources and cylindrical lenses illuminated by line sources are not only theoretically possible but have been built and used. Since a lens has two surfaces there is actually somewhat more freedom in lens design than in reflector design. Metal Plate Lenses have usually been designed with one surface flat, but the possibility of controlling both surfaces is emerging as a useful design factor where special requirements must be met.

Feeds for lenses should fulfill most of the same requirements as feeds for reflectors. We find a difference in size in lens feeds in that they must generally be more directive because of greater ratios of focal length to aperture. A difference in kind occurs because the feed is located behind the lens where none of the focussed energy can enter the feed or be disturbed by it. As a result some matching and pattern problems which arise in parabolic antennas are automatically absent when lenses are used.

In choosing a design for a lens antenna system with a given aperture one must compromise between the large size which is necessary when a long focal length is used and the more zones which result if the focal length is made short. Most metal plate lenses so far constructed have had focal lengths somewhere between 0.5 and 1.0 times the greatest aperture dimension.

9.2 *Tolerances in Metal Plate Lenses*

It is not difficult to see that phase errors resulting from small displacements or distortions of a metal plate lens are much less serious than those due to comparable distortions of a reflector surface. This follows from the fact that the lens operates on a wave which passes through it. If a portion of the lens is displaced slightly in the direction of propagation it is still operating on roughly the same portion of the wave front and gives it the same phase correction. If a portion of a reflector were displaced in the same way the error in the wave front would be of the order of twice the

Digitized by Google
Original from UNIVERSITY OF MICHIGAN
Generated on 2019-09-23 09:45 GMT / http://hdl.handle.net/2027/mdp.39015077775156
Public Domain, Google-digitized / http://www.hathitrust.org/access_use#pd-google

displacement. Quantitative arguments show that less severe tolerances apply to all major structural dimensions of a metal lens antenna.

It is true of course that the dimensions of individual portions of the metal lens must be held with some accuracy. The metal plate spacing determines the effective index of refraction of the lens material. Where $N = 0.5$ it is customary to require that this be held to $\pm\lambda/75$, and where $N = 0.6$ to $\pm\lambda/50$. The thickness of the lens in a given region is less critical, and must be held to $\pm \dfrac{\lambda}{16\,(1-N)}$ where it is desired to hold the phase front to $\pm\lambda/16$.

Fig. 32 illustrates clearly the drastic way in which the location of a lens can be altered without seriously affecting the pattern. It shows, incidentally, how a lens may behave well when used as the focussing element in a moving feed scanning antenna.

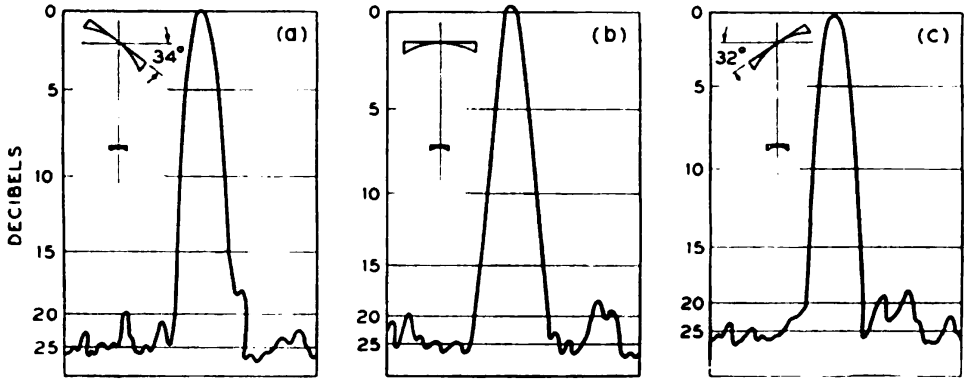

Fig. 32—Effect on Pattern of Lens Tilting.

9.3 *Advantages of Metal Plate Lenses*

On the basis of the above discussion we can see that metal plate lenses have certain considerable advantages. The most important of these is perhaps found in the practical matter of tolerances. It is a comparatively simple matter to hold dimensions of small objects to close tolerances but quite another thing to hold dimensions of large objects closely under the conditions of modern warfare. This advantage emerges with increasing importance as the wavelength is reduced.

Metal plate lenses have contributed a great degree of flexibility to radar antenna art. When they are used two surfaces rather than one may be controlled, and the dielectric constant can be varied within wide limits. Independent control in the two polarizations may be applied. We can confidently expect that they will become increasingly popular in the radar field.

10. Cosecant Antennas

One of the earliest uses of radar was for early warning against aircraft.

Generated on 2019-09-23 09:45 GMT / http://hdl.handle.net/2027/mdp.39015077775156
Public Domain, Google-digitized / http://www.hathitrust.org/access_use#pd-google
Digitized by Google
Original from UNIVERSITY OF MICHIGAN

The skies were searched for possible attackers with antennas which rotated continuously in azimuth. An equally important but later use appeared with the advent of great bombing attacks. Bombing radars 'painted' maps of the ground which permitted navigation and bombing during night and under even the worst weather conditions. In these radars also the antennas were rotated in azimuth, either continuously through 360° or back and forth through sectors.

The majority of radars designed to perform these functions provided vertical coverage by means of a special vertical pattern rather than a vertical scan. It can easily be seen that such a pattern would have to be 'special.' If we assume, for example, that a bombing plane is flying at an altitude of 10,000 feet, then the radar range must be 10,000 *csc* 60° = 11,500 feet if a target on the ground at a bomb release angle of 60° from the horizontal is to be seen. Such a range would by no means be enough to pick up the target at say 10° in time to prepare for bombing, for then a range of 10,000 csc 10° = 57,600 feet would be required. This range is far more than is necessary for the 60° angle. It appears then that in the most efficient design the radar range and therefore the radar antenna gain, must be different in different directions.

The required variation of gain with vertical direction could be specified in any one of several ways. It seems natural to specify that a given ground target should produce a constant signal as the plane flies towards it at a constant altitude. Neglecting the directivity of the target this will occur if the amplitude response of the antenna is given by $E = E_0 csc\theta$. This same condition will apply by reciprocity to an early warning radar antenna on the ground which is required to obtain the same response at all ranges from a plane which is flying in at a constant altitude.

This condition is not alone sufficient to specify completely the vertical pattern of an antenna. For one thing it can obviously not be followed when $\theta = 0$, for this would require infinite gain in this direction. Therefore a lower limit to the value of θ for which the condition is valid must be set. In addition an upper limit less than 90° is specified whenever requirements permit, since control at high angles is especially difficult. When the limits have been set it still remains to specify the magnitude of the constant E_0. This can be done by specifying the range in one particular direction. This specification must of course be consistent with all the factors that determine gain, including the reduction due to the required vertical spread of the pattern.

10.1 *Cosecant Antennas based on the Paraboloid*

It is evident that the standard paraboloidal antennas so far discussed will not produce cosecant patterns. These patterns being unsymmetrical will result only if the wave front phase and amplitude are especially controlled.

Digitized by Google
Original from UNIVERSITY OF MICHIGAN
Generated on 2019-09-23 09:45 GMT / http://hdl.handle.net/2027/mdp.39015077775156
Public Domain, Google-digitized / http://www.hathitrust.org/access_use#pd-google

on the other hand, because paraboloidal antennas are simple and common it is natural that many cosecant designs should be based on them. These designs can be classified into two groups, those in which the reflector is modified and those in which the feed is modified.

Some early cosecant antennas were made by introducing discontinuities in paraboloidal reflectors as illustrated in Fig. 33. These controlled the radiation more or less as desired over the desired cosecant pattern but pro-

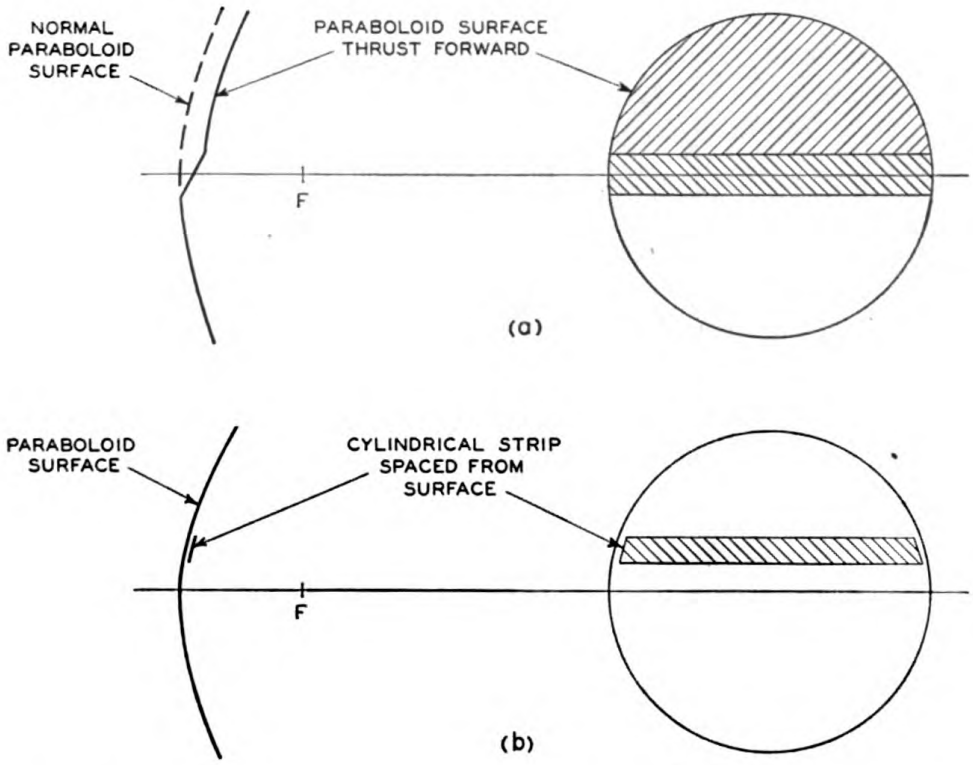

Fig. 33—Some Cosecant Antennas Based on the Paraboloid (Cosecant Energy Downward).

duced rather serious minor lobes elsewhere. This difficulty can be overcome through the use of a continuously distorted surface as illustrated in Fig 34. This reflector, first used at the Radiation Laboratories, is a normal paraboloid in the lower part whereas the upper part is the surface that would be obtained by rotating the parabola through the vertex of the upper part about its focal point.

Several types of feed have been used in combination with paraboloids to produce cosecant patterns. These are usually arrays which operate on the principle that each element is a feed which contributes principally to one

Digitized by Google
Original from UNIVERSITY OF MICHIGAN
Generated on 2019-09-23 09:45 GMT / http://hdl.handle.net/2027/mdp.39015077775156
Public Domain, Google-digitized / http://www.hathitrust.org/access_use#pd-google

region of the vertical pattern. The elements may be dipoles or waveguide apertures fed directly through the antenna feed line or they may be reflectors which reradiate reflected energy originating from a single primary source. No matter how excited they must be properly controlled in phase, amplitude and directivity.

Cosecant antennas based on the paraboloid are common and can sometimes fulfill all requirements with complete satisfaction. Nevertheless they

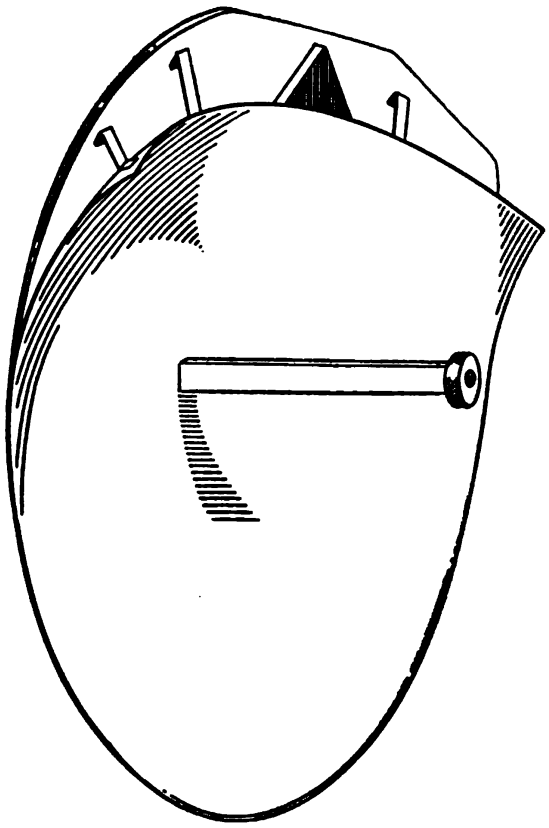

Fig. 34—Barrel Cosecant Antenna (Cosecant Energy Downward).

suffer from certain disadvantages. The most serious of these is that they lack resolution at high vertical angles, that is the beam is wider horizontally at high angles. This is to be expected for reasons of phase alone, for a paraboloidal reflector is, after all, designed to focus in only one direction. If phase difficulties were completely absent however, azimuthal resolution at high angles would still be destroyed because of cross polarized components of radiation. These components arise naturally from doubly curved reflectors, even simple paraboloids. They are sometimes overlooked when antennas are measured in a one way circuit with a linearly polarized test field, but must obviously be considered in radar antennas.

Generated on 2019-09-23 09:46 GMT / http://hdl.handle.net/2027/mdp.39015077775156
Public Domain, Google-digitized / http://www.hathitrust.org/access_use#pd-google
Digitized by Google
Original from UNIVERSITY OF MICHIGAN

10.2 *Cylindrical Cosecant Antennas*

Harmful cross polarized radiation is produced by doubly curved reflectors. This radiation is difficult to control and therefore undesirable where a closely controlled cosecant characteristic at high angles is required. Although not at first evident, it seems natural now to bypass polarization difficulties through the use of singly curved cylindrical reflectors. These reflectors if illuminated with a line source of closely controlled linear polarization provide a beam which is linearly polarized. This beam has also in azimuth approximately the directivity of the line source at all vertical angles. It is thus superior in two significant respects to cosecant beams produced by doubly curved reflecting surfaces.

A cylindrical cosecant antenna consists of a cylindrical reflector illuminated by a line source. Part of the cylinder is almost parabolic and contributes chiefly to the strong part of the beam which lies closest to the horizontal. This part is merged continuously into a region which departs considerably from the parabolic and contributes chiefly to the radiation at higher angles.

Although wave front principles can be used and certainly must not be violated, the principles of geometrical optics have been particularly effective in the determination of cosecant reflector shapes. The detailed application of these principles will not be discussed here. While applying the geometrical principles the designer must be sure that the over-all size and configuration of the antenna can produce the results he wants. He must design a line source with the desired polarization and horizontal pattern and a vertical pattern which fits in with the cosecant design. In addition he must take particular care to reduce sources of pattern distortion to a level at which they cannot interfere significantly with the lowest level of the cosecant 'tail'.

11. Lobing

In many of the tactical situations of modern war radar can be used to provide fire control information. Radar by its nature determines range and microwave radar with its narrow well defined beams is a natural instrument for finding directions to a target, whether the missile to be sent to that target is a shell, a torpedo or a bomb. In fire control radar, as opposed to search or navigational radar, two properties of the antenna deserve particular attention. These are the *accuracy* and the *rate* with which direction to a target can be measured.

Lobing is a means which utilizes to the fullest extent the accuracy available from a given antenna aperture and which increases, usually as far as is desired, the rate at which this information is provided and corrected.

Digitized by Google
Original from UNIVERSITY OF MICHIGAN
Generated on 2019-09-23 09:46 GMT / http://hdl.handle.net/2027/mdp.39015077775156
Public Domain, Google-digitized / http://www.hathitrust.org/access_use#pd-google

A lobing antenna which is to provide information concerng one angle only, azimuth for example, is capable of producing two beams, one at a time, and of switching rapidly from one to the other. This process is called *Lobe Switching*. The two beams are nearly coincident, differing in direction by about one beam width. When the signals from the two beams are compared, they will be equal only if the target lies on the bisector between the beams (Fig. 35). The two-signals can be compared visually on an indicator screen of the radar or they can be compared electrically and fed directly into circuits which control the direction of fire.

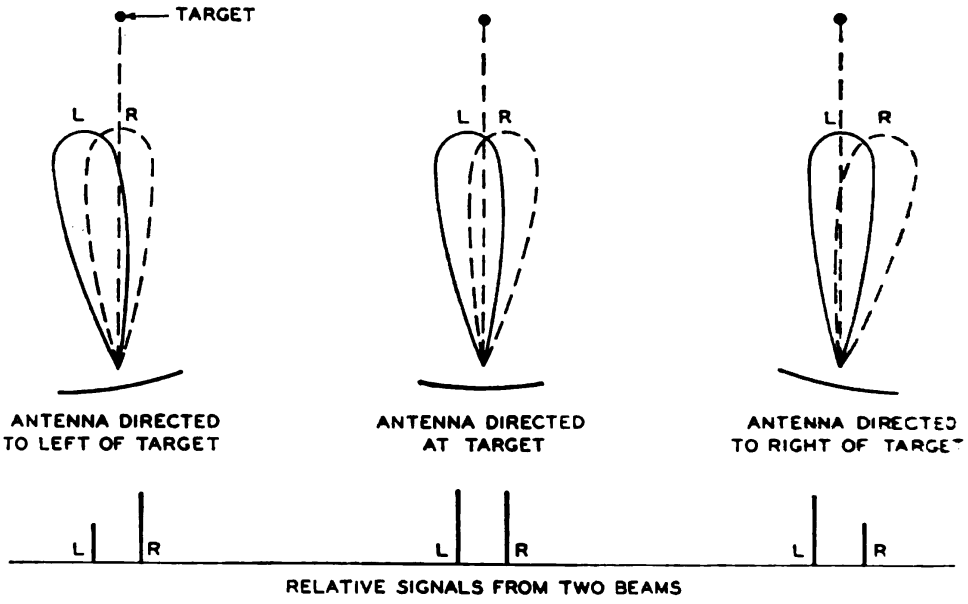

Fig. 35—Lobe Switching.

When two perpendicular directions are to be determined, such as the elevation and azimuth required by an anti-aircraft battery, four or in principle three discrete beams can be used. Radar antennas designed for solid angle coverage more commonly, however, produce a single beam which rotates rapidly and continuously around a small cone. This rotation is known as *conical lobing*. A comparison of amplitudes in a vertical plane can then be used to give the elevation of the target and a similar comparison in a horizontal plane to give its azimuth. Here too the electrical signals can be compared visually on an indicator screen, but an electrical comparison will provide continuous data which can be used to aim the guns and at the same time to cause the radar antenna to follow the target automatically.

11.1 *Lobe Switching*

Two methods of lobe switching are common. In one of these the lobing antenna is an array of two equally excited elements. Each of these ele-

Digitized by Google
Original from UNIVERSITY OF MICHIGAN
Generated on 2019-09-23 09:46 GMT / http://hdl.handle.net/2027/mdp.39015077775156
Public Domain, Google-digitized / http://www.hathitrust.org/access_use#pd-google

ments occupies one half of the final antenna aperture, and provides a uniphase front across this half. If the two elements were excited with the same phase the radiation maximum of the resulting antenna beam would occur in a direction at right angles to the combined phase front. If the phase of one element is made to lag behind that of the other by a small amount, 60° say, the phase of the combined aperture will of course be discontinuous with a step in the middle. This discontinuous phase front will approximate with a small error, a uniphase wave front which is tilted somewhat with respect to the wave fronts of the elements. The phase shift will therefore result in a slight shift of the beam away from the normal direction. When the phase shift is reversed the beam shift will be reversed. Two properly designed elementary antennas in combination with a means for rapidly changing the phase will therefore constitute a lobe switching antenna. Such an antenna is described more in detail in Sec. 14.6.

Another method of lobe switching is more natural for antennas based on optical principles. In this method two identical feeds are placed side by side in the focal region of the reflector. When one of these feeds illuminates the reflector a beam is produced which is slightly off the normal axial direction. Illumination by the other feed produces a second beam which is equally displaced in the opposite direction. The lobe of the antenna switches rapidly when the two feeds are activated alternately in rapid succession. The antenna must use some form of rapid switching appropriate to the antenna feed line. In several applications switches are used which depend on the rapid tuning and detuning of resonant cavities or irises.

11.2 *Conical Lobing*

A conically lobing antenna produces a beam which nutates rapidly about a fixed axial direction. This is usually accomplished by rotating or nutating an antenna feed in a small circle about the focus in the focal plane of a paraboloid or lens. This antenna feed can be a spinning asymmetrical dipole or a rotating or nutating waveguide aperture. It can result in a beam with linear polarization which rotates as the feed rotates, or preferably in a beam for which the polarization remains parallel to a fixed direction. The beam itself must be nearly circularly symmetric so that the radar response from a target in the axial direction will not vary with the lobing. The reflector or lens aperture is consequently usually circular.

When the antenna is small it is sometimes easier to leave the feed fixed and to produce the lobing by moving the reflector.

12. RAPID SCANNING

A lobing radar can provide range and angular information concerning a single target rapidly and accurately but these things are not always enough.

Digitized by Google
Original from UNIVERSITY OF MICHIGAN
Generated on 2019-09-23 09:46 GMT / http://hdl.handle.net/2027/mdp.39015077775156
Public Domain, Google-digitized / http://www.hathitrust.org/access_use#pd-google

It is sometimes necessary to obtain accurate and rapid information from all regions within an agular sector. It may be necessary to watch a certain region of space almost continuously in order to be sure of picking up fast moving targets such as planes. To accomplish any of these ends we must use a *rapid scanning* radar. A rapid scanning radar antenna produces a beam which scans continuously through an angular sector. The beam may sweep in azimuth or elevation alone or it may sweep in both directions to cover a solid angle. An azimuth or elevation scan may be sinusoidal or it may occur linearly and repeat in a sawtooth fashion. Solid angle scanning may follow a spiral or flower leaf pattern or it might be a combination of two one way scans. A combination of scanning in one direction and lobing in the other is sometimes used.

Scanning antennas must, unfortunately, be constructed in obedience to the same principles which regulate ordinary antennas. The same attention to phase, amplitude, polarization and losses is necessary if comparable results are to be obtained. When scanning requirements are added to these ordinary ones new problems are created and old ones made more difficult.

An antenna in order to scan in any specified manner must act to produce a wave front which has a constant phase in a plane which is always normal to the required beam direction. This can be done in several different ways. The simplest of these, electrically, is to rotate a fixed beam antenna as a whole in the required fashion. This can be called *mechanical scanning*. Alternatively an antenna array can be scanned if it is made up of suitable elements and the relative phases of these elements can be varied appropriately. This can be called *array scanning*. Thirdly, *optical scanning* can be produced by moving either the feed or the focussing element of a suitably designed optical antenna.

12.1 *Mechanical Scanning*

Electrical complexities of other types of rapid scanners are such that it is probably not going too far to say that the required scan should be accomplished by mechanical means wherever it is at all practical. This applies to radar antenna scans which occur at a slow or medium rate. Search antennas, whether they rotate continuously through 360° or back and forth over a sector are scanners in a sense but the scan is usually slow enough to be performed by rotating the antenna structure as a whole. As the scan becomes more rapid, mechanical problems become more severe and electrically scanning antennas appear more attractive.

Mechanical ingenuity has during the war extended the range in which mechanical scanners are used. One important and eminently practical mechanical rapid scanner, the 'rocking horse' is now in common use (Fig. 36). This antenna is electrically a paraboloid of elliptical aperture illu-

Digitized by Google
Original from UNIVERSITY OF MICHIGAN
Generated on 2019-09-23 09:46 GMT / http://hdl.handle.net/2027/mdp.39015077775156
Public Domain, Google-digitized / http://www.hathitrust.org/access_use#pd-google

minated by a horn feed, a combination which produces excellent electrical characteristics. The paraboloid and feed combination is made structurally strong and is pivoted to permit rotational oscillation in a horizontal plane. It is forced to oscillate by a rigid crank rod which is in turn driven by an eccentric crank on a shaft. The shaft is belt driven by an electric motor and its rotational rate is held nearly constant by a flywheel. The mechanical arrangement described so far would oscillate rotationally in an approximately sinusoidal fashion. Since every action has an equal and opposite reaction it would, however, react by producing an oscillatory torque on its

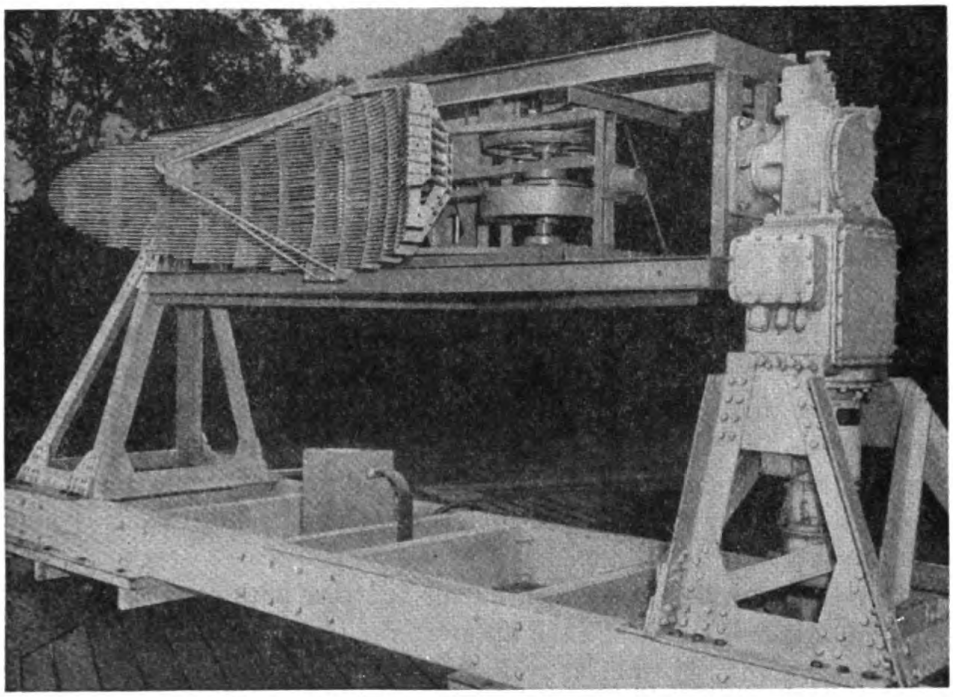

Fig. 36—Experimental Rocking Horse Antenna.

mounting. Since the antenna is large and the oscillation rapid this would produce a severe and undesirable vibration. To get around this difficulty an opposite and balancing rotating moment is introduced into the mechanical system. This appears in the form of a pivoted and weighted rod which is driven from the same eccentric crank by another and almost parallel crank arm.

Although not theoretically perfect the rotational 'dynamic' balancing described permits the antenna to scan without serious vibration. One form of this antenna will be described in a later section.

12.2 *Array Scanning*

During our discussion of general principles in Part II, we saw that an antenna wave front can be synthesized by assembling an array of radiating

Digitized by Google
Original from UNIVERSITY OF MICHIGAN
Generated on 2019-09-23 09:46 GMT / http://hdl.handle.net/2027/mdp.39015077775156
Public Domain, Google-digitized / http://www.hathitrust.org/access_use#pd-google

elements and distributing power to it through an appropriate transmission line network. If the radiation characteristics of the array are to be as desired the electrical drive of each element must have a specified phase and amplitude. In addition each element must in itself have a satisfactory characteristic and the elements must have a proper spacial relationship to each other.

Such array antennas have been extremely useful in the 'short wave' bands where wavelengths and antenna sizes are many times larger than at most radar wavelengths but for fixed beam radar antennas they have been largely superceded by the simpler optical antennas. Where a rapidly scanning beam is desired, however, they possess certain advantages which were put to excellent use in the war. These advantages spring from the possibility of scanning the beam of an array through the introduction of rapidly varying phase changes in its transmission line distributing system.

Let us first examine certain basic conditions that must be fulfilled if an array antenna is to provide a satisfactory scan. The pattern of any array is merely the sum of the patterns of its elements taking due account of phase, amplitude and spacial relationships. If all elements are alike and are spaced equally along a straight line it is not difficult to show that a mathematical expression for the pattern can be obtained in the form of a product of a factor which gives the pattern of a single element and an array factor. The array factor is an expression for the pattern of an array of elements each of which radiates equally in all directions. Since each of the elements is fixed in direction it is only through control of the array factor that the scan can be obtained.

If we excite all points of a continuous aperture with equal phase and a smoothly tapered amplitude the aperture produces a beam with desirable characteristics at right angles to itself and no comparable radiation elsewhere. Similarly if we excite all elements of an array of identical equally spaced circularly radiating elements with equal phase and a smoothly tapered amplitude the array will produce a beam with desirable characteristics at right angles to itself. It will also produce a beam in any *other* direction for which waves from the elements can add up to produce a wave front. Such other directions will exist whenever the array spacing is greater than one wavelength.

In order to see this more clearly let us examine Fig. 37, where line XX' represents an array of elements. From each element to the line AA' is a constant distance, so AA' is obviously parallel to a wave front when the elements are excited with equal phase. If we can find a line BB' to which the distance from each element is exactly one wavelength more or less than from its immediate neighbors then it too is parallel to a wavefront, for energy reaching it from any element of the array will have the same phase

Digitized by Google
Original from UNIVERSITY OF MICHIGAN
Generated on 2019-09-23 09:47 GMT / http://hdl.handle.net/2027/mdp.39015077775156
Public Domain, Google-digitized / http://www.hathitrust.org/access_use#pd-google

except for an integral number of cycles. The same will apply to a line CC', to which the distance from each element is exactly two wave lengths more or less than from its immediate neighbors, or to any other line where this difference is any integral number of wavelengths.

Now in no radar antenna do we desire two or more beams for they will result in loss of gain and probably in target confusion. The array must therefore be designed so that for all positions of scan all beams except one will be suppressed. This will automatically occur if the array spacing is somewhat less than one wavelength. If the array spacing is greater than one wavelength these extra beams will appear in the array factor; they

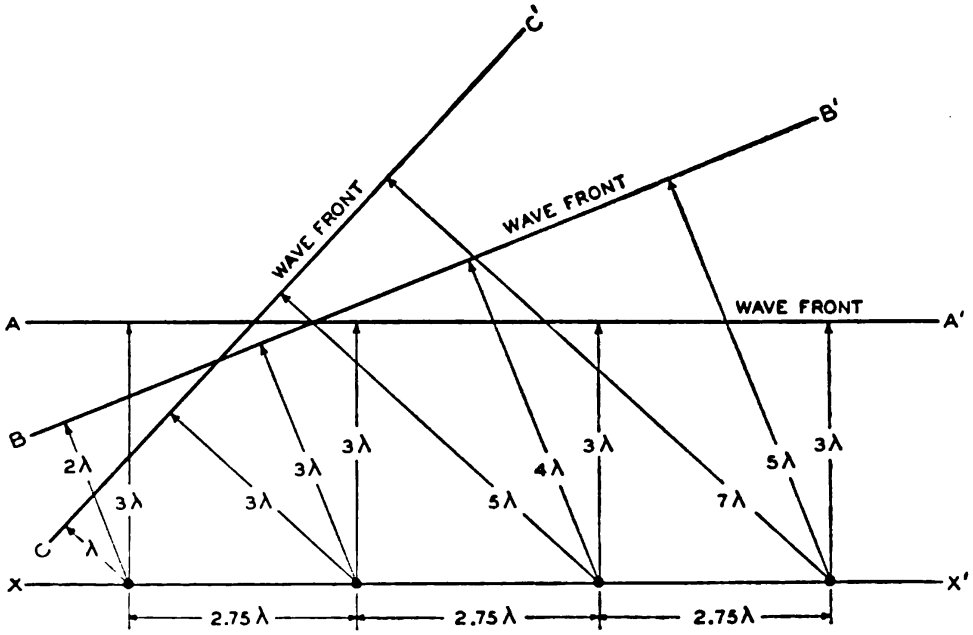

Fig. 37—Some Possible Wave Fronts of an Array of Elements Spaced 2.75 λ.

must therefore be suppressed by the pattern of a single element. The pattern of an element must in other words, have no significant components in any direction where an extra beam can occur.

Where elements with only side fire directivity are spaced more than a wavelength apart in a scanning array it is almost impossible to obtain adequate extra lobe suppression. If these elements are spaced by the minimum amount, that is by exactly the dimensions of their apertures and all radiate in phase they may indeed just manage to produce a desirable beam. A little analysis shows however that an appreciable phase variation from element to element, even though linear, will introduce a serious extra lobe. To get around this difficulty elements with some end fire directivity must be used.

Generated on 2019-09-23 09:47 GMT / http://hdl.handle.net/2027/mdp.39015077775156
Public Domain, Google-digitized / http://www.hathitrust.org/access_use#pd-google
Digitized by Google
Original from UNIVERSITY OF MICHIGAN

A simple end fire element, and one that has been used in practice, is the 'polyrod' (Fig. 38). A polyrod, is as its name implies, a rod of polystyrene. This rod, if inserted into the open end of a waveguide, and if properly proportioned and tapered, will radiate energy entering from the waveguide from points which are distributed continuously along its length. If the

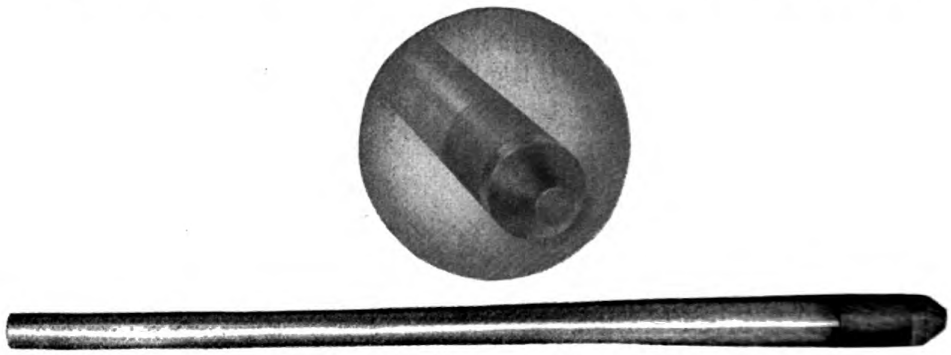

Fig. 38—A Polyrod.

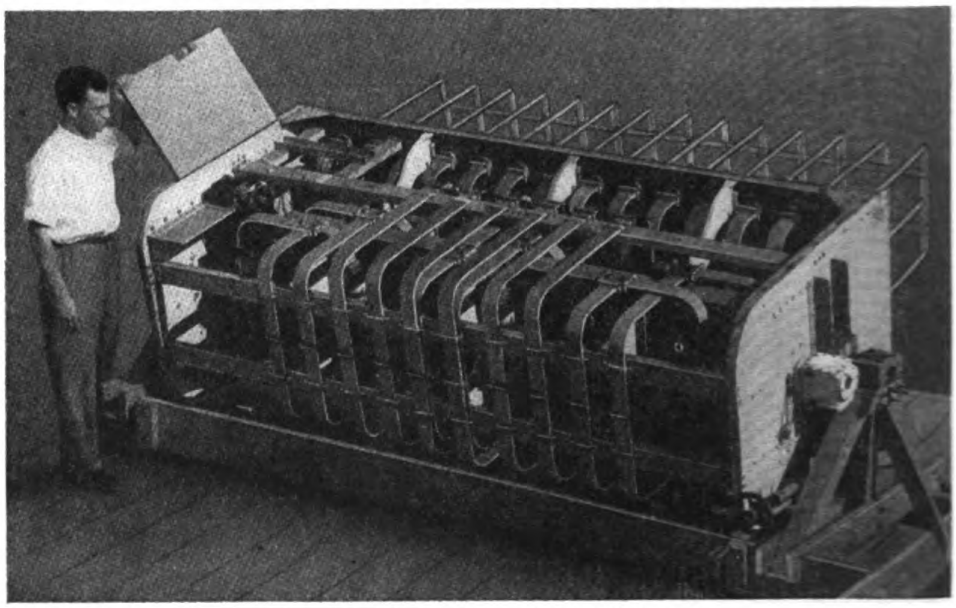

Fig. 39.—Experimental Polyrod Array.

wave in the polyrod travels approximately with free space velocity it will produce a radiation maximum in the direction of its axis. The radiation pattern of the polyrod will have a shape which is characteristic of end fire arrays, narrower and flatter topped than the pattern of a side fire array which occupies the same *lateral* dimension. This elementary pattern can be fitted in well with the array factor of a scanning array.

Such a scanning array is shown in Fig. 39 and will be described in

Digitized by Google
Original from UNIVERSITY OF MICHIGAN
Generated on 2019-09-23 09:47 GMT / http://hdl.handle.net/2027/mdp.39015077775156
Public Domain, Google-digitized / http://www.hathitrust.org/access_use#pd-google

greater detail in section 14.8. Each element of this array consists of a fixed vertical array of three polyrods. This elementary array provides the required vertical pattern and has appropriate horizontal characteristics. Fourteen of these elements are arranged in a horizontal array with a spacing between neighbors of about two wavelengths. Energy is distributed among the elements with a system of branching waveguides. Thirteen rotary phase changers are inserted strategically in the distributing system. Each phase change is rotating continuously and shifts the phase linearly from 0° to 360° twice for each revolution. As the phase changers rotate the array produces a beam which sweeps repeatedly linearly and continuously across the scanning sector.

When elements of a scanning array are spaced considerably less than one wavelength it is a very simple matter to obtain a suitable elementary pattern, for the array factor itself has only a single beam. This advantage is offset by the greater number of elements and the consequent greater complexity of distributing and phase shifting equipment. In one useful type of scanning antenna however distributing and phase shifting is accomplished in a particularly simple manner. Here the distributing system is merely a waveguide which can transmit only the dominant mode. The wide dimension of the guide is varied to produce the phase shifts required for scanning. The elements are dipoles. The center conductor of each dipole protrudes just enough into the guide to pick up the required amount of energy.

It is evident from the above discussion that such a waveguide fed dipole array will produce a single beam in the normal direction only if the dipoles are all fed in phase and are spaced less than a wavelength. It is therefore not satisfactory to obtain constant phase excitation by tapping the dipoles into the guide at successive guide wavelengths for these are greater than free space wavelengths. Consequently the dipoles are tapped in at successive half wavelengths in the guide and reversed successively in polarity to compensate for the successive phase reversals due to their spacing.

This type of array provides a line source which can be scanned by moving the guide walls. In order to leave these mechanically free suitable wave trapping slots are provided along the length of the array.

A practical antenna of this type will be described in Sec. 16.3.

12.3 *Optical Scanning*

With a camera or telescope all parts of an angular sector or field are viewed simultaneously. We would like to do the same thing by radar means, but since this so far appears impossible we do the next best thing by looking at the parts of the field in rapid succession. Nevertheless certain points of similarity appear. These points are emphasized by a survey of the fixed

Generated on 2019-09-23 09:47 GMT / http://hdl.handle.net/2027/mdp.39015077775156
Public Domain, Google-digitized / http://www.hathitrust.org/access_use#pd-google
Digitized by Google
Original from UNIVERSITY OF MICHIGAN

beam antenna field for there we find optical instruments in abundance, parabolic reflectors and even lenses.

It is not a very big step to proceed from an examination of optical systems to the suggestion that a scanning antenna can be provided by moving a feed over the focal plane of a reflector. Nevertheless experience shows that this will not be especially profitable unless done with due caution. The first effect of moving the feed away from the focus in the focal plane of a paraboloid is indeed a beam shift but before this process has gone far a third order curvature of the phase front is produced and is accompanied by a serious deterioration in the pattern and reduction in gain. This difficulty or aberration is well known in classical optical theory and is called coma. Coma is typified by patterns such as the one shown in Fig. 16. It is the first obstacle in the path of the engineer who wishes to design a good moving feed scanning antenna.

Coma is not an insuperable obstacle however. Its removal can be accomplished by the application of a very simple geometrical principle. This principle can be stated as follows: "The condition for the absence of coma is that each part of the focussing reflector or lens should be located on a circle with center at the focus."

This condition can be regarded as a statement of the spacial relationship required between the feed and all parts of the focussing element. It is a condition which insures that the phase front will remain nearly linear when the feed is moved in the focal plane. It can be applied approximately whether the focussing element is a reflector or a lens and to optical systems which scan in both directions as well as those which scan in one direction.

Coma is usually the most serious aberration to be reckoned with in a scanning optical system, but it is by no means the only one. Any defect in the phase and amplitude characteristic which arises when the feed is moved can cause trouble and must be eliminated or reduced until it is tolerable. Another defect in phase which arises is 'defocussing'. Defocussing is a square law curvature of phase and arises when the feed is placed at an improper distance from the reflector or lens. Its effect may be as shown in Fig. 14. It can in principle always be corrected by moving the feed in a correctly chosen arc, but this is not always consistent with other requirements on the system. In addition to troubles in phase an improper amplitude across the aperture of the antenna will arise when the feed is translated unless proper rotation accompanies this motion.

To combat the imperfections in an optical scanning system we can choose over-all dimensions in such a way that they will be lessened. Thus it is generally true that an increase in focal length or a decrease in aperture will increase the scanning capabilities of an optical system. This alone is usually not enough, however, we must also employ the degrees of free-

Digitized by Google
Original from UNIVERSITY OF MICHIGAN
Generated on 2019-09-23 09:47 GMT / http://hdl.handle.net/2027/mdp.39015077775156
Public Domain, Google-digitized / http://www.hathitrust.org/access_use#pd-google

dom available to us in the designing of the focussing element and the feed motion to improve the performance. If the degrees of freedom are not enough we must, if we insist on an optical solution introduce more. This could in principle result in microwave lenses similar to the four and five element glass lenses found in good cameras, but such complication has not as yet been necessary in the radar antenna art.

Since military release has not been obtained as this article goes to press we must omit any detailed discussion of optically scanning radar antenna techniques.

PART III

MILITARY RADAR ANTENNAS DEVELOPED BY THE BELL LABORATORIES

13. General

In the final part of this paper we will describe in a brief fashion the end products of radar antenna technology, manufactured radar antennas. Without these final practical exhibits the foregoing discussion of principles and methods might appear academic. By including them we hope to illustrate in a concrete fashion the rather general discussion of Parts I and II.

The list of manufactured antennas will be limited in several ways. Severe but obviously essential are the limitations of military security. In addition we will restrict the list to antennas developed by the Bell Laboratories. In cases where invention or fundamental research was accomplished elsewhere due credit will be given. Finally the list will include only antennas manufactured by contract. This last limitation excludes many experimental antennas, some initiated by the Laboratories and some by the armed forces.

It is worthwhile to begin with an account of the processes by which these antennas were brought into production. The initiating force was of course military necessity. The initial human steps were taken sometimes by members of the armed forces who had definite needs in mind and sometimes by members of the Laboratories who had solutions to what they believed to be military needs.

With a definite job in mind conferences between military and Laboratories personnel were necessary. Some of these dealt with legal or financial matters, others were principally technical. In the technical conferences it was necessary at an early date to bring military requirements and technical possibilities in line.

As a result of the conferences a program of research and development was often undertaken by the Laboratories. An initial contract was signed which

Generated on 2019-09-23 09:48 GMT / http://hdl.handle.net/2027/mdp.39015077775156
Public Domain, Google-digitized / http://www.hathitrust.org/access_use#pd-google
Digitized by Google
Original from UNIVERSITY OF MICHIGAN

called for the delivery of technical information, and sometimes for manufacturing drawings and one or more completed models. Usually the antenna was designed and manufactured as part of a complete radar system, sometimes the contract called for an antenna alone.

After preliminary work had been undertaken the status of the job was reviewed from time to time. If preliminary results and current military requirements warranted a manufacturing contract was eventually drawn up and signed by Western Electric and the contracting government agency. This contract called for delivery of manufactured radars or antennas according to a predetermined schedule.

Research and development groups of the Laboratories cooperated in war as in peace to solve technical problems and accomplish technical tasks. Under the pressure of war the two functions often overlapped and seemed to merge, yet the basic differences usually remained.

Members of the Research Department, working in New York and at the Deal and Holmdel Radio Laboratories in New Jersey were concerned chiefly with electrical design. It was their duty to understand fully electrical principles and to invent and develop improved methods of meeting military requirements. During the war it was usually their responsibility to prescribe on the basis of theory and experiment the electrical dimensions of each new radar antenna.

A new and difficult requirement presented to the Research Department was sometimes the cause of an almost personal competition between alternative schemes for meeting it. Some of these schemes were soon eliminated by their own weight, others were carried side by side far along the road to production. Even those that lost one race might reappear in another as a natural winner.

In the Development Groups working in New York and in the greatly expanded Whippany Radio Laboratory activity was directed towards coordination of all radar components, towards the establishment of a sound, well integrated mechanical and electrical design for each component and towards the tremendous task of preparing all information necessary for manufacture. It was the job of these groups also to help the manufacturer past the unavoidable snarls and bottlenecks which appeared in the first stages of production. In addition development personnel frequently tested early production models, sometimes in cooperation with the armed forces.

As we have intimated, research and development were indistinguishable at times during the war. Members of the research department often found themselves in factories and sometimes in aircraft and warships. Development personnel faced and solved research problems, and worked closely with research groups.

Generated on 2019-09-23 09:48 GMT / http://hdl.handle.net/2027/mdp.39015077775156
Public Domain, Google-digitized / http://www.hathitrust.org/access_use#pd-google
Digitized by Google
Original from UNIVERSITY OF MICHIGAN

For several years when pressure was high the effort was intense; at times feverish. Judging by military results it was highly effective. Some of the material results of this effort are described in the following pages.

14. Naval Shipborne Radar Antennas

14.1 *The SE Antenna*[10]

Very early in the war, the Navy requested the design of a simple search radar system for small vessels, to be manufactured as quickly as possible in order to fill the gap between design and production of the more complex search systems then in process of development. The proposed system was to be small and simple, to permit its use on vessels which otherwise would be unable to carry radar equipment because of size or power supply capability. This class of vessel included PT boats and landing craft.

The antenna designed for the SE system is housed as shown in Fig. 40. It was adapted for mounting on the top or side of a small ship's mast, and is rotated in azimuth by a mechanical drive, hand operated. The paraboloid reflector is 42 inches wide, 20 inches high, and is illuminated by a circular aperture 2.9 inches in diameter. In the interests of simplicity, the polarization of the radiated beam was permitted to vary with rotation of the antenna.

The SE antenna was operated at 9.8 cm, and fed by $1\frac{1}{2}$ x 3 rectangular waveguide. At the antenna base, a taper section converted from the rectangular waveguide to 3″ round guide, through a rotating joint directly to the feed opening.

Characteristics of the SE antenna are given below:

Wavelength	9.7 to 10.3 cm	
Reflector	42″ W x 20″ H	
Gain	25 db	
Horizontal Beam Width	6°	
Vertical Beam Width	12°, varying somewhat with polarization	
Standing Wave	9.7to10.0 cm	4.0 db
	10.0 to 10.3 cm	6.0 db

14.2 *The SL Radar Antenna*[11]

The SL radar is a simple marine search radar developed by Bell Telephone Laboratories for the Bureau of Ships. During the war, over 1000 of these radars were produced by the Western Electric Company and installed on Navy vessels of various categories. The principal field for installation was destroyer escort craft ("DE"s). Figure 41 shows an SL antenna installation aboard a DE. The antenna is covered, for wind and

[10] Written by R. J. Phillips.
[11] Written by H. T. Budenbom.

Digitized by Google
Original from UNIVERSITY OF MICHIGAN
Generated on 2019-09-23 09:48 GMT / http://hdl.handle.net/2027/mdp.39015077775156
Public Domain, Google-digitized / http://www.hathitrust.org/access_use#pd-google

weather protection, in a housing which can transmit 10 cm radiation. Visible also is the waveguide run down the mast to the r.f. unit.

The SL radar provides a simple non-stabilized PPI (Plan Position Indicator) display. The antenna is driven by a synchronous motor at 18 rpm. Horizontal polarization is used to minimize sea clutter. The

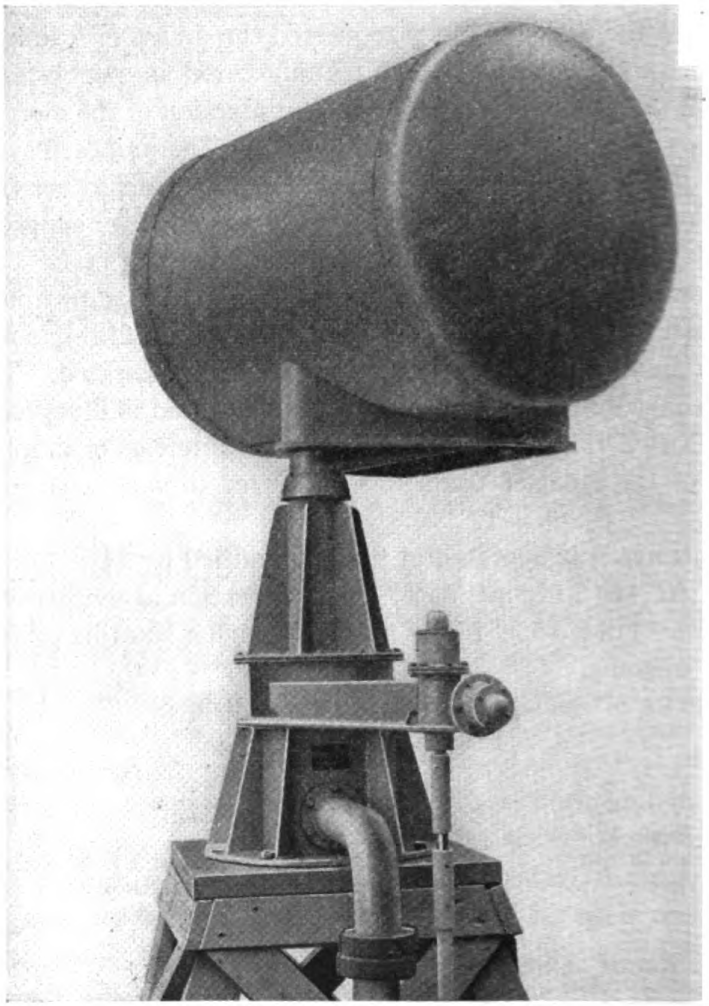

Fig. 40—SE Antenna.

radiating structure, shown in Figure 42, consists of a 20″ sector of a 42″ paraboloid. The resulting larger beam width in the vertical plane is provided in order to improve the stability of the pattern under conditions of ship roll. Figure 43 illustrates the path of the transmitted wave from the SL r.f. unit to the antenna. It also illustrates the manner in which horizontally polarized radiation is obtained. The diagram shows the position of

Digitized by Google
Original from UNIVERSITY OF MICHIGAN
Generated on 2019-09-23 09:48 GMT / http://hdl.handle.net/2027/mdp.39015077775156
Public Domain, Google-digitized / http://www.hathitrust.org/access_use#pd-google

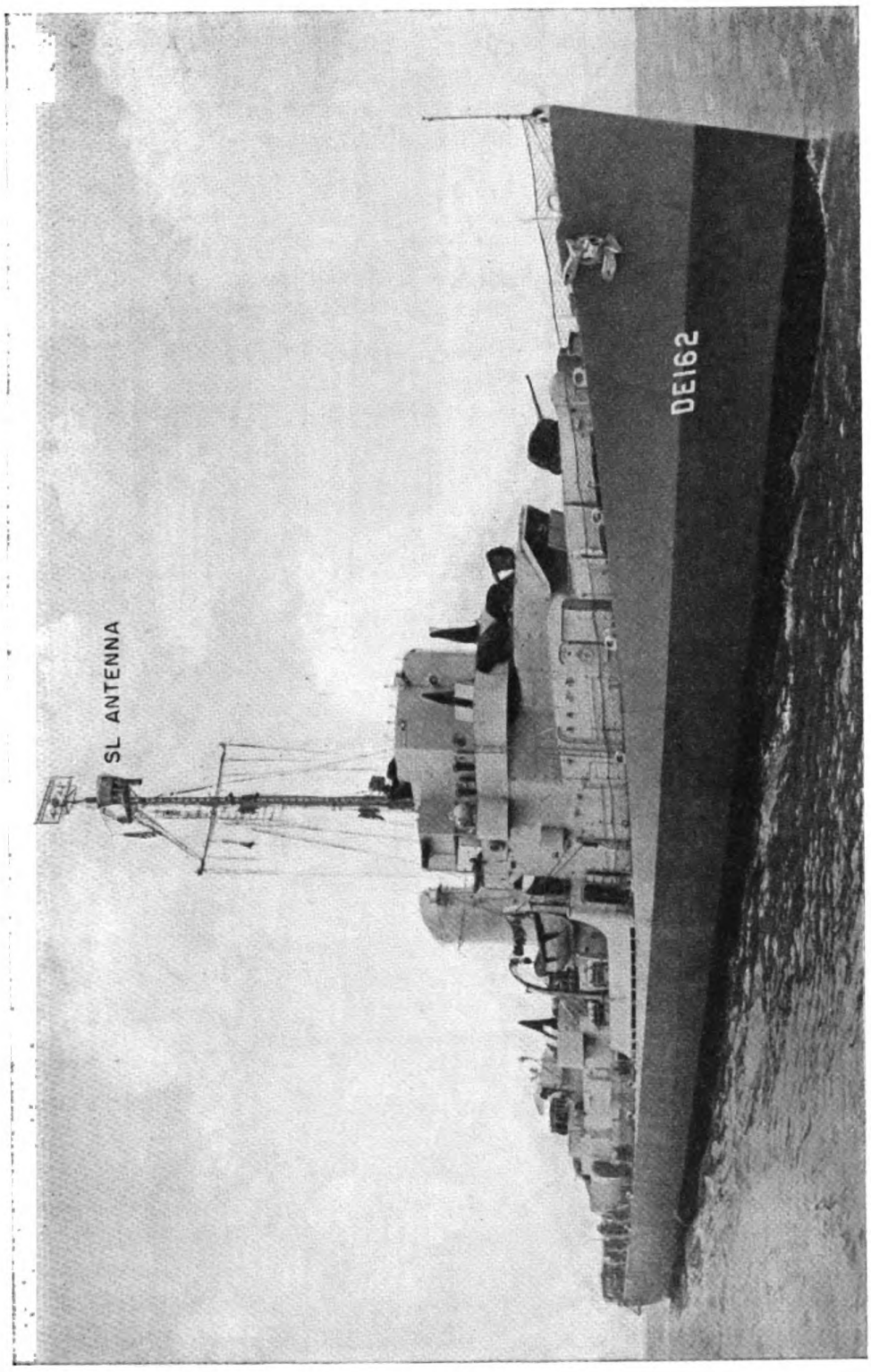

Fig. 41—SL Antenna Aboard DE.

Generated on 2019-09-23 09:48 GMT / http://hdl.handle.net/2027/mdp.39015077775156
Public Domain, Google-digitized / http://www.hathitrust.org/access_use#pd-google
Digitized by Google
Original from UNIVERSITY OF MICHIGAN

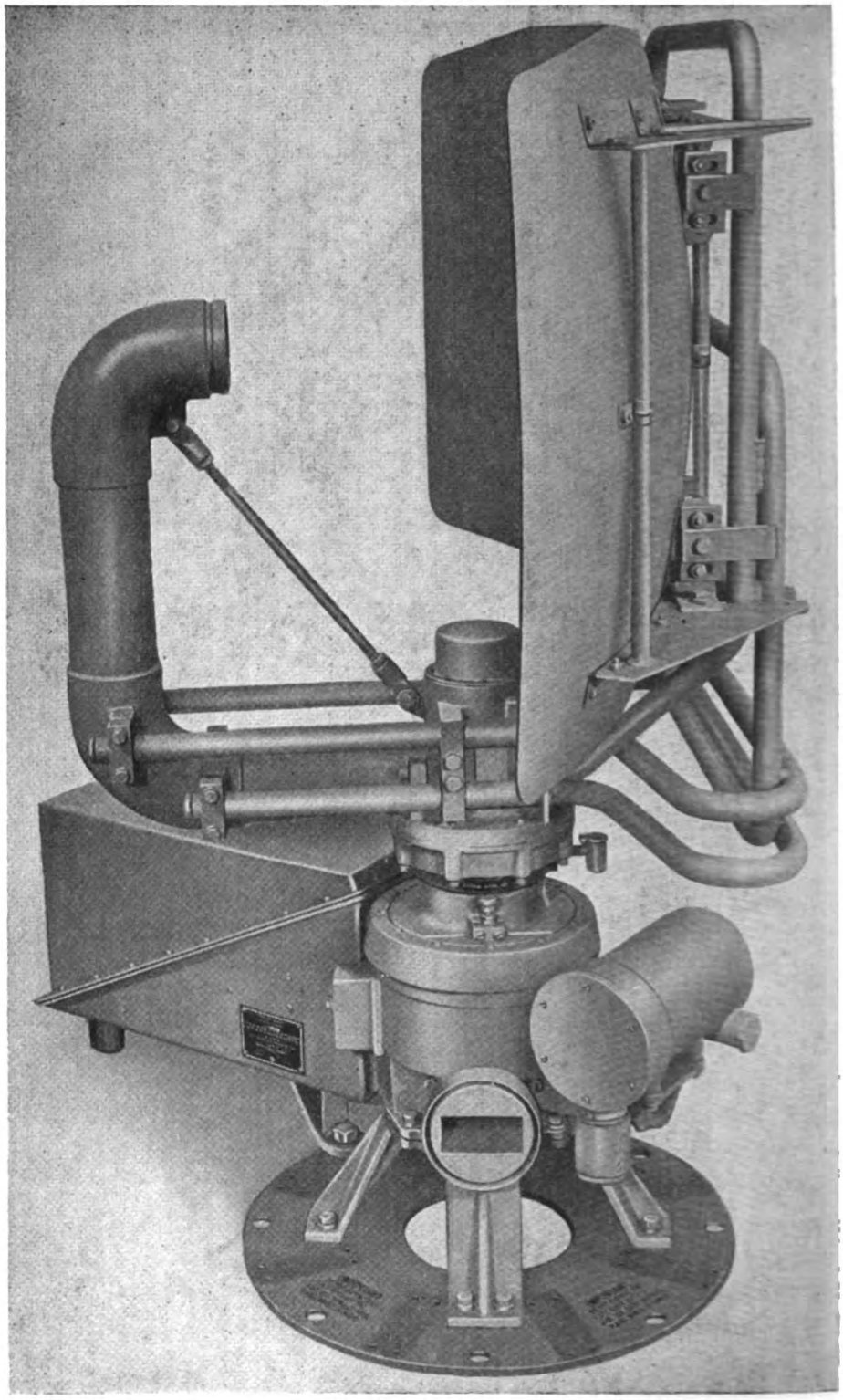

Fig. 42—SL Antenna.

Digitized by Google
Original from UNIVERSITY OF MICHIGAN
Generated on 2019-09-23 09:49 GMT / http://hdl.handle.net/2027/mdp.39015077775156
Public Domain, Google-digitized / http://www.hathitrust.org/access_use#pd-google

the electric force vector in traversing the waveguide run. The path from the r.f. unit is in rectangular guide ($TE_{1,0}$ mode) through the right angle bend, to the base of the rotary joint. A transducer which forms the base portion of the joint converts to the TM_{01} mode in circular pipe. For this mode, the electric field has radial symmetry, much as though the waveguide were a coaxial line of vanishingly small inner conductor diameter.

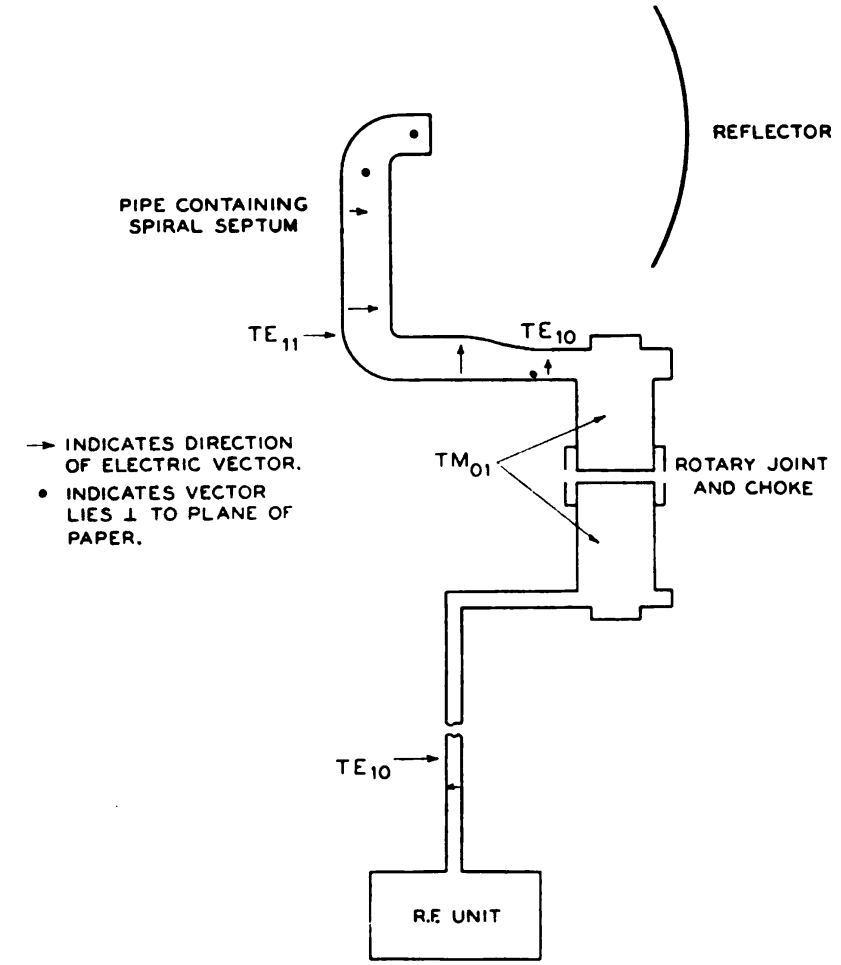

Fig. 43—SL Radar Antenna—Wave Guide Path.

The energy passes the rotary joint in this mode; choke labyrinths are provided at the joint to minimize radio frequency leakage. The energy then flows through another transducer, from TM_{01} mode back to TE_{10} mode. The lower horizontal portion of the feed pipe immediately tapers to round guide, the mode being now TE_{11}. Next the energy transverses a 90° elbow, which is a standard 90° pipe casting, and enters the vertical section im-

Generated on 2019-09-23 09:49 GMT / http://hdl.handle.net/2027/mdp.39015077775156
Public Domain, Google-digitized / http://www.hathitrust.org/access_use#pd-google
Digitized by Google
Original from UNIVERSITY OF MICHIGAN

mediately below the feed aperture. The E vector is in the plane of the paper at this point. However, the ensuing vertical section is fitted with a spiral septum. This gradually rotates the plane of polarization until at the top of this pipe the E vector is perpendicular to the plane of the paper. Thus, after transversing another 90° pipe bend, the energy emerges horizontally polarized, to feed the main reflector.

Specific electrical characteristics of the SL antenna are:

Polarization—Horizontal
Horizontal Half Power Beamwidth—6°
Vertical Half Power Beamwidth—12°
Gain—about 22 db.

14.3 *The SJ Submarine Radar Antenna*

It had long been expected that one of the early offensive weapons of the war would be the submarine. It was therefore natural that early in the history of radar the need for practical submarine radars was felt. The principal components of this need were twofold, to provide warning of approaching enemies and to obtain torpedo fire control data. The SJ Submarine Radar was the first to be designed principally for the torpedo fire control function.

Work on the SJ system was under way considerably before Pearl Harbor. When this work was initiated the advantages of lobing fire control systems were clearly recognized, but no lobing antennas appropriate for submarine use had been developed. Requirements on such an antenna were obviously severe, for in addition to fulfilling fairly stringent electrical conditions, it would have to withstand very large forces due to water resistance and pressure.

The difficulties evident at the outset of the work were overcome by an ingenious adaptation of the simple waveguide feed. It was recognized that a shift of the feed in the focal plane of a reflector would cause a beam shift. Why not, then, use two waveguide feeds side by side to produce the two nearly coincident beams required in a lobing antenna? When this was tried it was found to work as expected.

It remained to devise a means of switching from one waveguide feed to the other with the desired rapidity. This in itself was no simple problem, but was solved by applying principles learned through work on waveguide filters. The switch at first employed was essentially a branching filter at the junction of the single antenna feed line and the line to each feed aperture. Both branches of this filter were carefully tuned to the same frequency, that of the radar. The switching was performed by the insertion of small rapidly rotating pins successively into the resonant cavities of the

Generated on 2019-09-23 09:49 GMT / http://hdl.handle.net/2027/mdp.39015077775156
Public Domain, Google-digitized / http://www.hathitrust.org/access_use#pd-google
Digitized by Google
Original from UNIVERSITY OF MICHIGAN

two filters (Fig. 44). Presence of the pins in one of the filters detuned it and therefore prevented power from flowing through it. Rotation of the pins accordingly produced switching as desired.

In a later modification of this switch the same general principles were used but resonant irises rather than resonant cavities were employed.

The SJ Submarine Radar was in use at a comparatively early date in the war and saw much service with the Pacific submarine fleet. Despite some early doubts, submarine commanders were soon convinced of its powers.

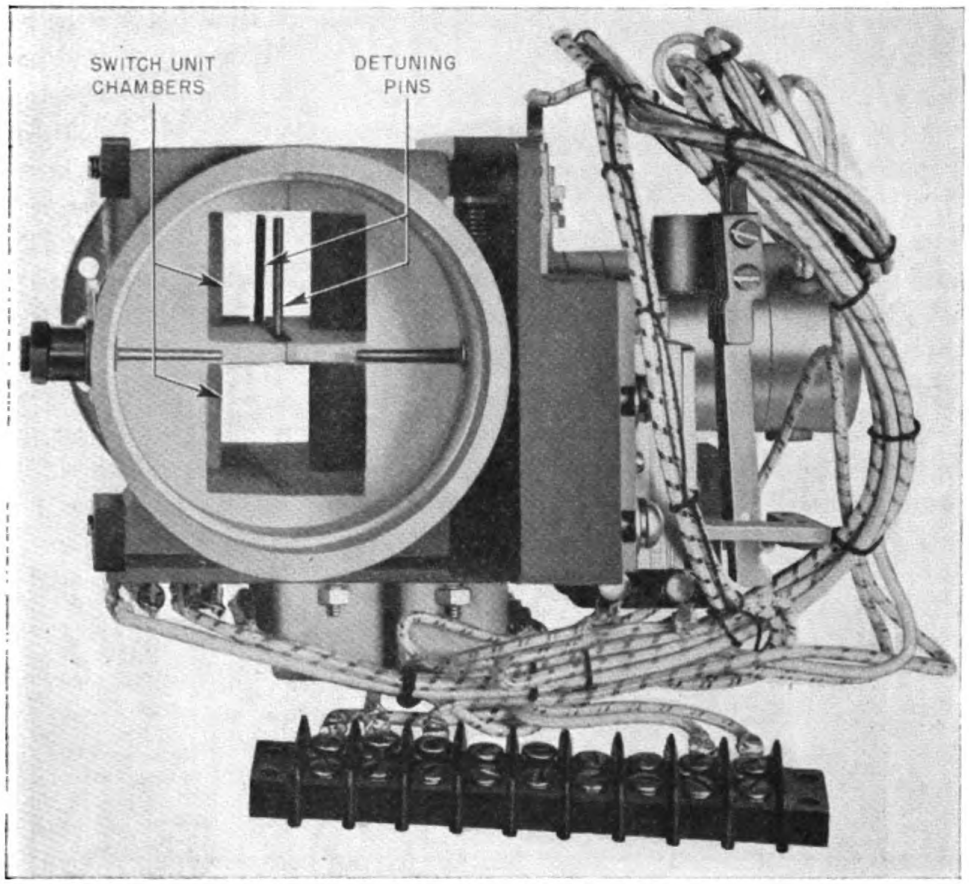

Fig. 44—The SJ Tuned Cavity Switch.

It is believed that in the majority of cases it replaced the periscope as the principle fire control instrument. In addition it served as a valuable and unprecedented aid to navigation.

It is interesting and relevant to quote from two letters to Laboratories engineers concerning the SJ. One dated October 3, 1943, from the radar officer of a submarine stated that there were twenty "setting sun" flags painted on the conning tower and asked the engineer to "let your mind dwell on the fact that you helped to put more than 50% of those flags there".

Digitized by Google
Original from UNIVERSITY OF MICHIGAN
Generated on 2019-09-23 09:49 GMT / http://hdl.handle.net/2027/mdp.39015077775156
Public Domain, Google-digitized / http://www.hathitrust.org/access_use#pd-google

The commander of another submarine wrote in a similar vein, "You can rest assured that we don't regard your gear as a bushy-brain space taker, but a very essential part of our armament".

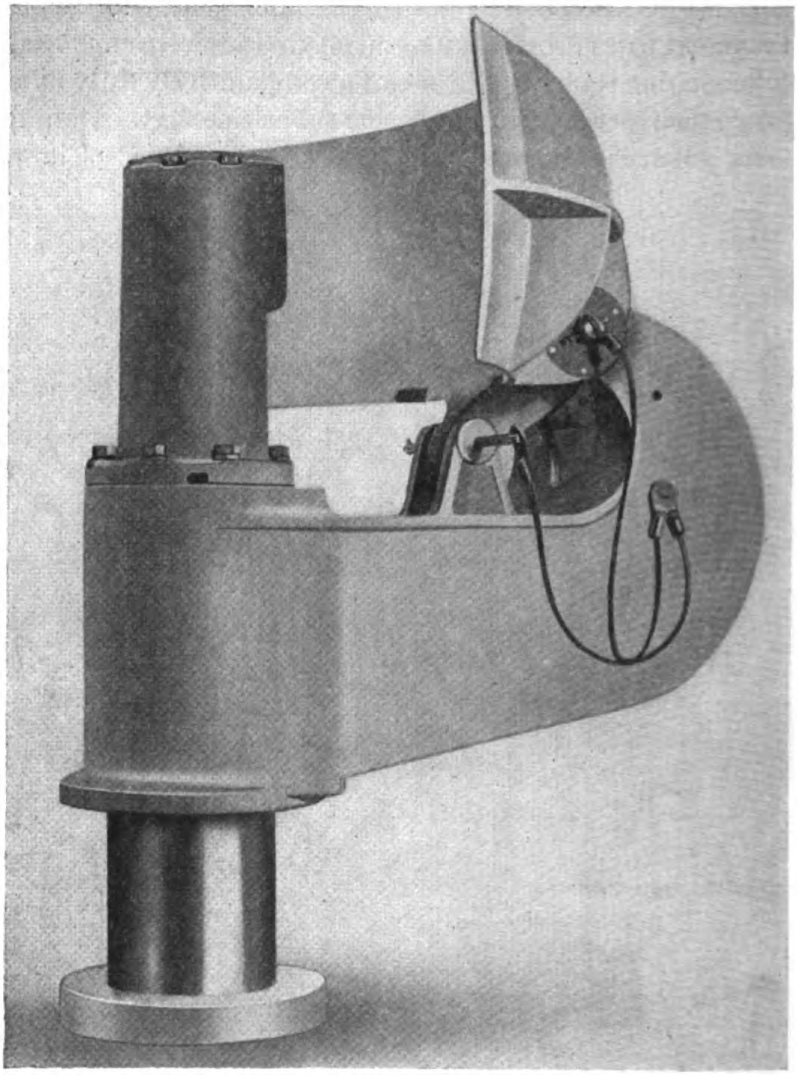

Fig. 45—The SJ Submarine Radar Antenna.

Figure 45 is a photograph of an SJ antenna. Its principal electrical characteristics are as follows:

Gain > 19 db
Horizontal Half Power Beamwidth 8°
Vertical Half Power Beamwidth 18°
Vertical Beam Character—Some upward radiation
Lobe Switching Beam Separation—approximately 5°
Gain reduction at beam cross-over < 1 db
Polarization—Horizontal

Digitized by Google
Original from UNIVERSITY OF MICHIGAN
Generated on 2019-09-23 09:50 GMT / http://hdl.handle.net/2027/mdp.39015077775156
Public Domain, Google-digitized / http://www.hathitrust.org/access_use#pd-google

14.4 *The Modified SJ/Mark 27 Radar Antenna*

The SJ antenna described above performed a remarkable and timely fire control job as a lobing antenna but was found to be unsatisfactory when rotated continuously to produce a Plan Position Indicator (PPI) presentation. In the PPI method of presentation range and angle are presented as radius and angle on the oscilloscope screen. Consequently a realistic map of the strategic situation is produced. This map is easily spoiled by false signals due to large minor lobes of the antenna.

Since it had been established that the PPI picture was valuable for navigation and warning as well as for target selection it was decided to modify the antenna in a way that would reduce these undesirably high minor lobes. These were evidently due principally to the shadowing effect of the massively built double primary feed. Accordingly a new reflector was designed which in combination with a slightly modified feed provided a much improved pattern.

The new reflector was different in configuration principally in that it was a partially offset section of a paraboloid. The reflector surface was also markedly different in character since it was built as a grating rather than a solid surface. This reduced water drag on the antenna. In addition the grating was less visible at a distance, an advantage that is obviously appreciable when the antenna is the only object above the water.

This modified antenna was used not only on submarines as part of the SJ-1 radar but also on surface vessels as the Mark 27 Radar Antenna. Figure 46 shows one of these antennas. Its electrical characteristics are as follows:

Gain > 20 db
Horizontal Half Power Beamwidth = 8°
Vertical Half Power Beamwidth = 17°
Vertical Beam Character—Some upward radiation
Lobe Switching Beam Separation—approximately 5°
Gain reduction at beam cross-over < 1 db
Polarization—Horizontal

14.5 *The SH and Mark 16 Antenna*[12]

The antennas designed for the SH and Mark 16 Radar Equipments are practically identical. The SH system was a shipborne combined fire control and search system, and the Mark 16 its land based counterpart was used by the Marine Corps for directing shore batteries.

These systems operated at 9.8 cm. The requirement that the system, operate as a fire control as well as a search system imposed some rather stringent mechanical requirements on the antenna. For search purposes, the antenna was rotated at 180 rpm, and indications were presented on a plan position indicator. For fire control data, slow, accurately controlled motion was required. Bearing accuracy is attained by lobe switching in

[12] Written by R. J. Philipps.

Digitized by Google
Original from UNIVERSITY OF MICHIGAN
Generated on 2019-09-23 09:50 GMT / http://hdl.handle.net/2027/mdp.39015077775156
Public Domain, Google-digitized / http://www.hathitrust.org/access_use#pd-google

much the same manner as in the SJ and SJ-1 antennas previously described.

The antenna is illustrated in Fig. 47. With the SH system, the unit is mast mounted; for the Mark 16, the unit is mounted atop a 50 foot steel

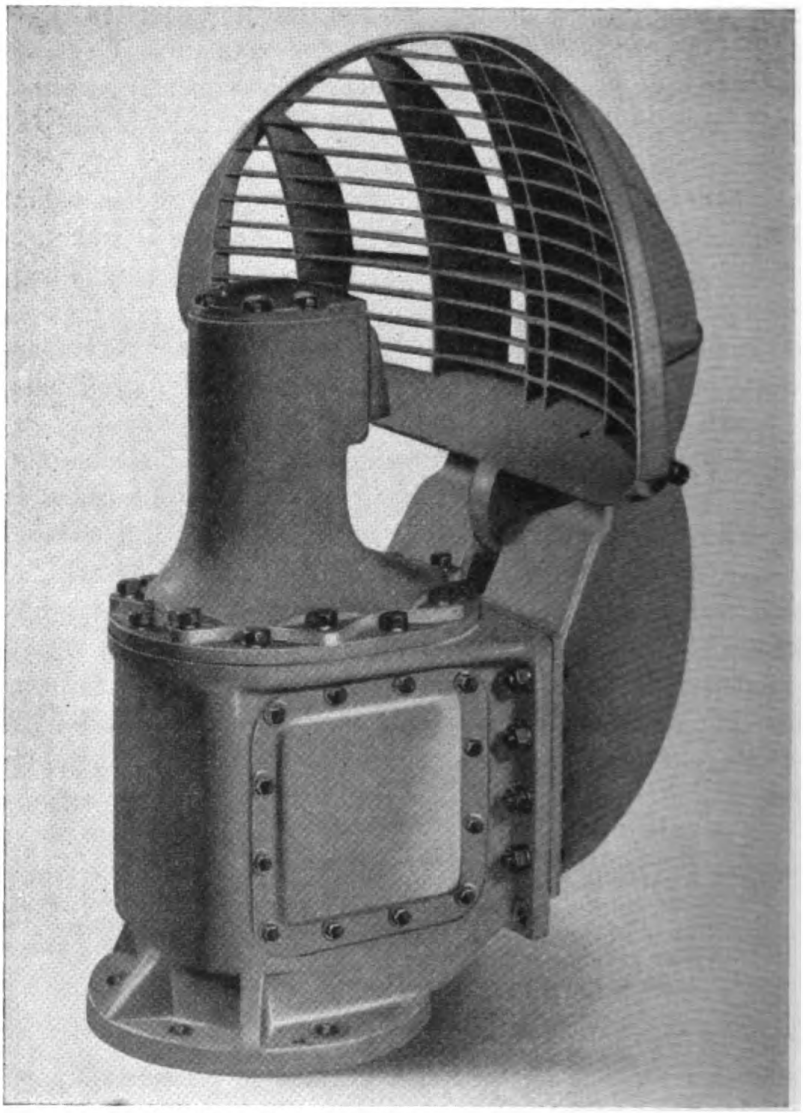

Fig. 46—The SJ-1/Mark 27 Submarine Radar Antenna.

tower which can be erected in a few hours with a minimum of personnel. The electrical characteristics are as follows:

Gain—21. db
Reflector Dimensions 30″ W x 20″ H
Horizontal beam width—7.5°
Vertical beam width—12°
Lobe separation—5° approximately
Loss in gain at lobe crossover—1 db approximately
Scan—(1) 360°, at 180 rpm for PPI operation
(2) 360°, at approximately 1 rpm for accurate azimuth readings, with lobe switching

Digitized by Google
Original from UNIVERSITY OF MICHIGAN
Generated on 2019-09-23 09:50 GMT / http://hdl.handle.net/2027/mdp.39015077775156
Public Domain, Google-digitized / http://www.hathitrust.org/access_use#pd-google

SH systems were most successfully used in invasion operations in the Aleutians. They were installed on landing craft, and the use of the high

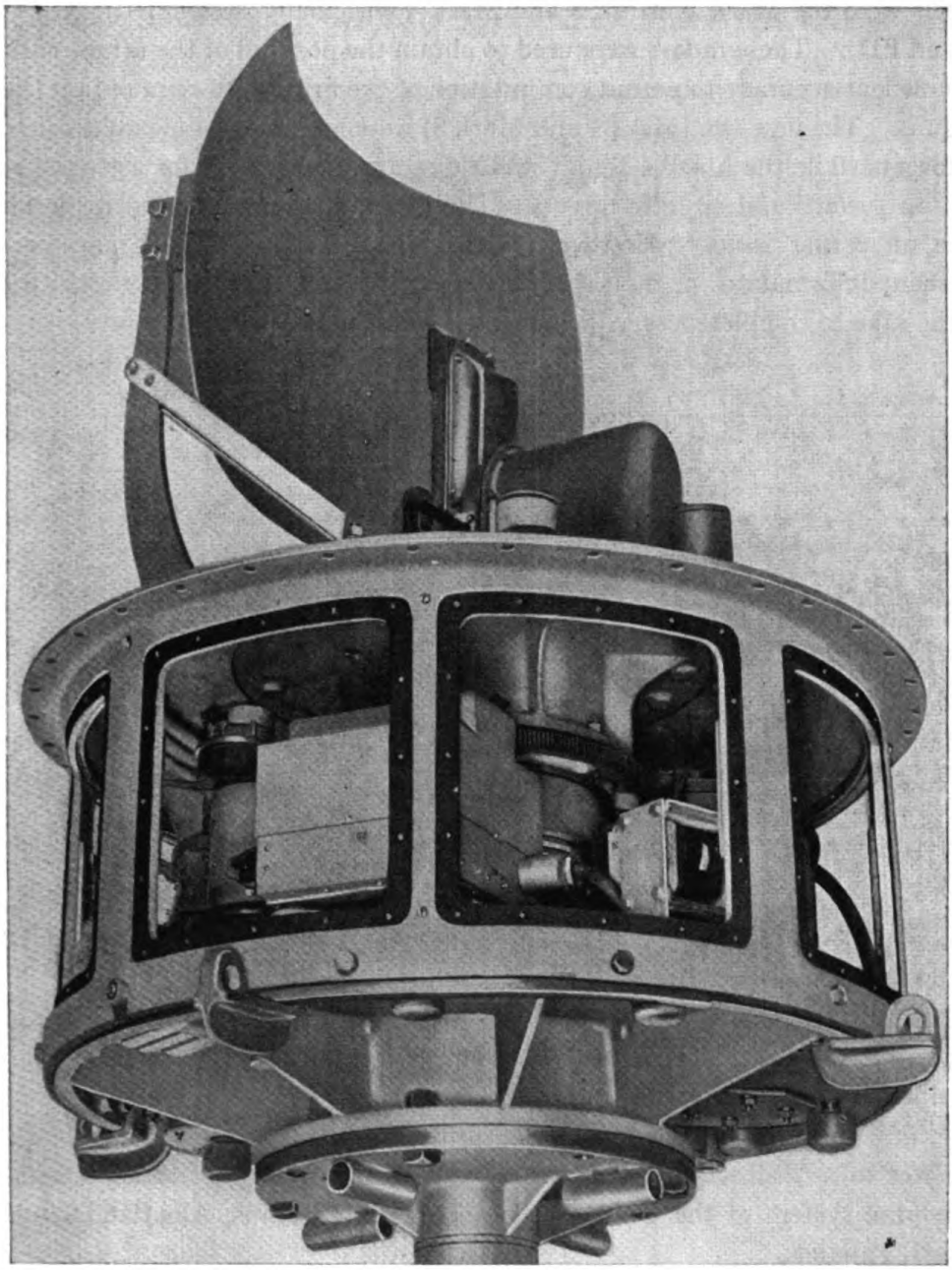

Fig. 47—SH Antenna.

speed scan enabled the craft to check constantly their relative positions in the dense fogs encountered during the landing operations.

Digitized by Google
Original from UNIVERSITY OF MICHIGAN
Generated on 2019-09-23 09:50 GMT / http://hdl.handle.net/2027/mdp.39015077775156
Public Domain, Google-digitized / http://www.hathitrust.org/access_use#pd-google

14.6 *Antennas for Early Fire Control Radars*[13]

The first radars to be produced in quantity for fire control on naval vessels were the Mark 1, Mark 3 and Mark 4 (originally designated FA, FC and FD). These radars were used to obtain the position of the target with sufficient accuracy to permit computation of the firing data required by the guns. The first two (Mark 1 and Mark 3) were used against enemy surface targets while the Mark 4 Radar was a dual purpose system for use against both surface and aircraft targets. These radars were described in detail in an earlier issue.[14] However, photographs of the antennas and pertinent information on the antenna characteristics are repeated herein for the sake of completeness. (See Table B and Figures 48, 49 and 50.)

TABLE B

	Radar			
	Mark 1	Mark 3		Mark 4
Dimensions	6′ x 6′	3′ x 12′	6′ x 6′	6′ x 7′
Operating Frequency	500 or 700 MC	680–720 MC		680–720 MC
Beam Width in Degrees (Between half power points one way.)				
Azimuth	12°	6°	12°	12°
Elevation	14°	30°	14°	12°
Antenna Gain	22 db	22 db	22 db	22.5 db.
Beam Shift in Degrees				
Azimuth	0°	±1.5°	±3°	±3°
Elevation	0°	0°	0°	±3°

An antenna quite similar to the Mark 3, 6 ft. x 6 ft. antenna, was also used on Radio Set SCR-296 for the Army. This equipment was similar to the Mark 3 in operating characteristics but was designed mechanically for fixed installations at shore points for the direction of coast artillery gun fire. For these installations the antenna was mounted on an amplidyne controlled turntable located on a high steel tower. The entire antenna and turntable was housed within a cylindrical wooden structure resembling a water tower. Equipments of this type were used as a part of the coastal defense system of the United States, Hawaiian Islands, Aleutian Islands and Panama.

[13] Written by W. H. C. Higgins.
[14] "Early Fire-Control Radars for Naval Vessels," W. C. Tinus and W. H. C. Higgins. See pp. 9 ff.

Generated on 2019-09-23 09:50 GMT / http://hdl.handle.net/2027/mdp.39015077775156
Public Domain, Google-digitized / http://www.hathitrust.org/access_use#pd-google
Digitized by Google
Original from UNIVERSITY OF MICHIGAN

14.7 *A Shipborne Anti-Aircraft Fire Control Antenna*[15]

A Shipborne Anti-Aircraft Fire Control Antenna is shown in Fig. 51. This antenna consists of two main horizontal cylindrical parabolas in each

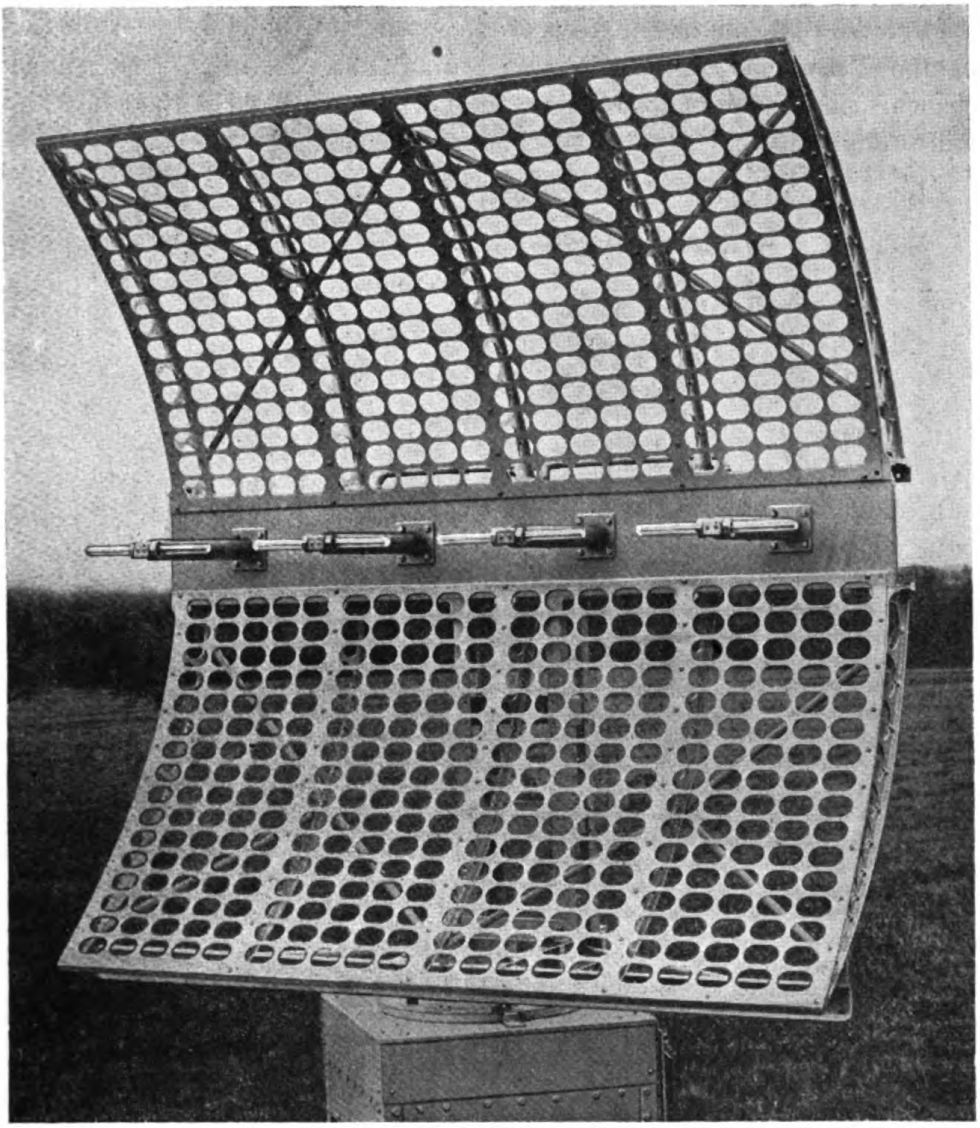

Fig. 48—Mark 1 Antenna.

of which two groups of four half-wave dipoles are mounted with their axes in a horizontal line at the focus of the parabolic reflectors. The four groups of dipoles are connected by coaxial lines on the back of the antenna to a lobe

[15] Written by C. A. Warren.

Digitized by Google
Original from UNIVERSITY OF MICHIGAN
Generated on 2019-09-23 09:51 GMT / http://hdl.handle.net/2027/mdp.39015077775156
Public Domain, Google-digitized / http://www.hathitrust.org/access_use#pd-google

switcher, which is a motor driven capacitor that has a single rotor plate and four stator plates, one for each group of dipoles. The phase shift introduced into the four feed lines by the lobe switching mechanism causes the antenna beam to be "lobed" or successively shifted to the right, up, left and down as the rotor of the capacitor turns through 360 degrees.

Mounted centrally on the front of the antenna at the junction of the two parabolic antennas is a smaller auxiliary antenna consisting of two dipole elements and a parabolic reflector, the purpose of which is to reduce the minor lobes that are present in the main antenna beam. The auxiliary

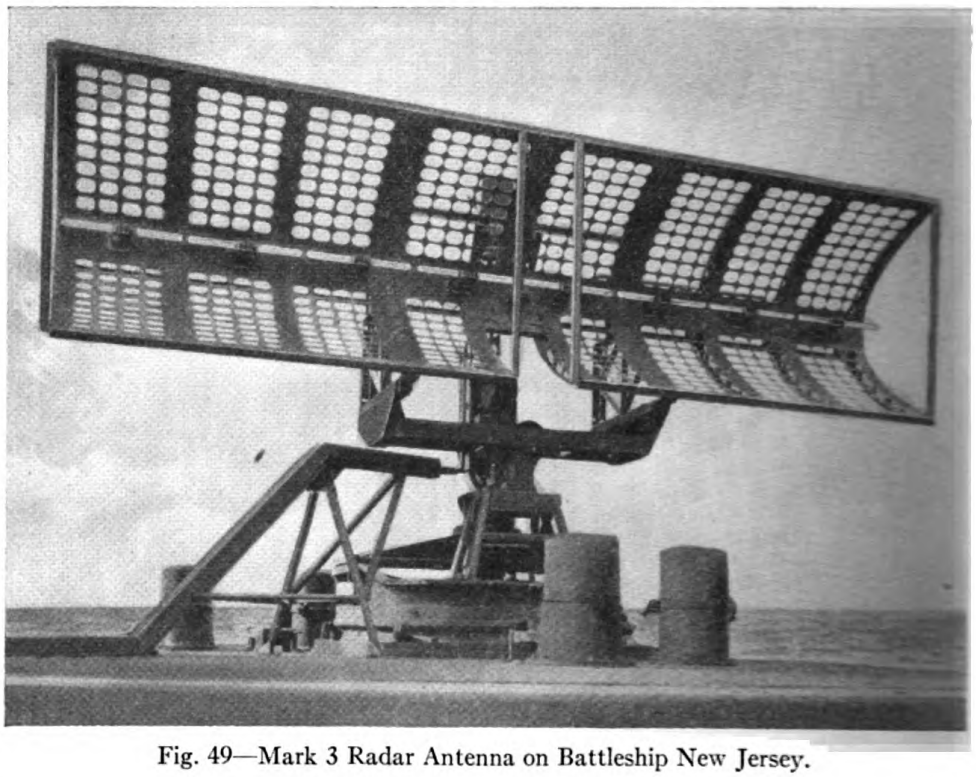

Fig. 49—Mark 3 Radar Antenna on Battleship New Jersey.

antenna beam is not lobe switched and is sufficiently broad in both the horizontal and vertical planes to overlap both the main antenna beam and the first minor lobes. The auxiliary antenna feed is so designed that its field is in phase with the field of the main beam of the main antenna. This causes the feed of the auxiliary antenna to "add" to the field of the main antenna in the region of its main beam, but to subtract from the field in the region of its first minor lobes. This occurs because the phase of the first minor lobes differs by 180 degrees from that of the main beam. As a result, the field of the main beam is increased and the first minor lobes are greatly

Generated on 2019-09-23 09:51 GMT / http://hdl.handle.net/2027/mdp.39015077775156
Public Domain, Google-digitized / http://www.hathitrust.org/access_use#pd-google
Digitized by Google
Original from UNIVERSITY OF MICHIGAN

reduced. By reducing these minor lobes to a low value, the region around the main beam is free of lobes, thus greatly reducing the possibility of false tracking due to "cross overs" between the main beam and the minor lobes.

14.8 *The Polyrod Fire Control Antenna*

The Polyrod Fire Control antenna is an array scanner employing essentially the same principles as those used in the multiple unit steerable antenna

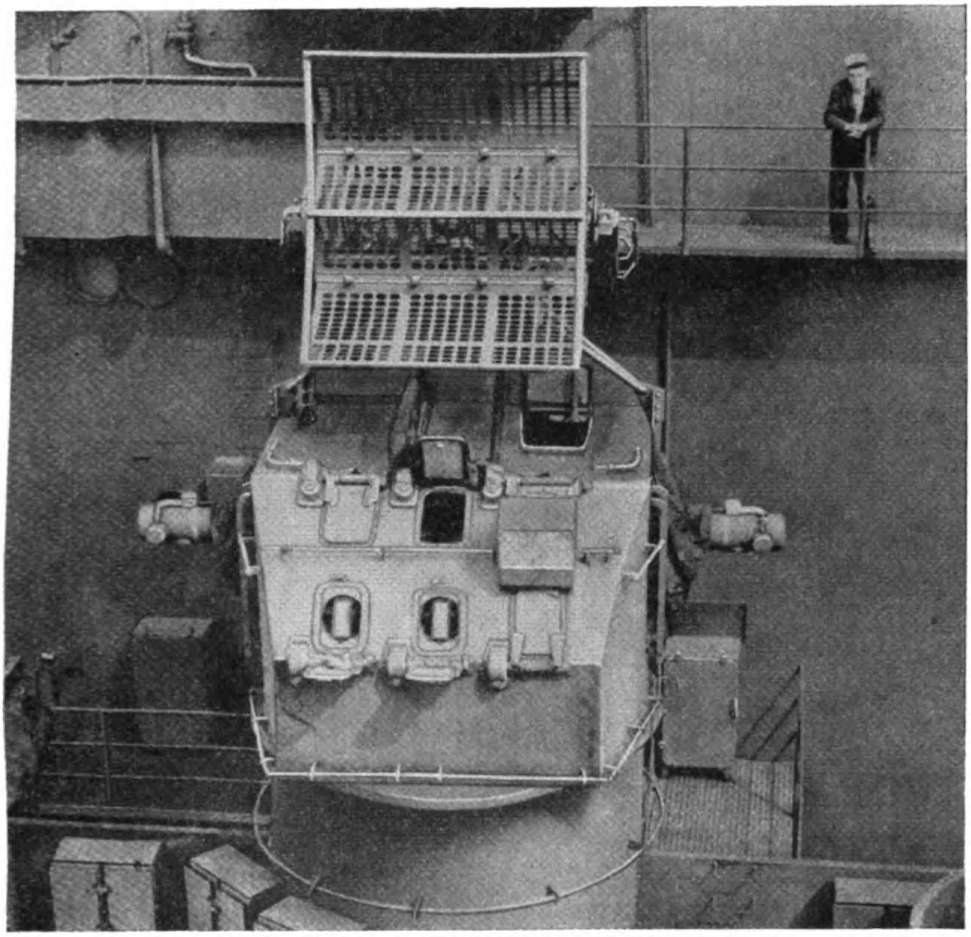

Fig. 50—Mark 4 Radar Antenna on Battleship Tennessee.

system (MUSA) developed before the war for short-wave transatlantic telephony. Some of these principles have been discussed in Sec. 12.2. That they could be applied with such success in the microwave region was due to a firm grounding in waveguide techniques, to the invention of the polyrod antenna and the rotary phase changer, and especially to excellent technical work on the part of research, development and production personnel. It is perhaps one of the most remarkable achievements of wartime

Digitized by Google
Original from UNIVERSITY OF MICHIGAN
Generated on 2019-09-23 09:51 GMT / http://hdl.handle.net/2027/mdp.39015077775156
Public Domain, Google-digitized / http://www.hathitrust.org/access_use#pd-google

radar that the polyrod antenna emerged to fill the rapid scanning need a early and as well developed as it did.

The Polyrod Fire Control antenna is a horizontal array of fourteen identical fixed elements, each element being a vertical array of three polyrods. Energy is distributed to the elements through a waveguide manifold. The phase of each element is controlled and changed to produce the desired scan by means of thirteen rotary phase changers. These phase shifters are

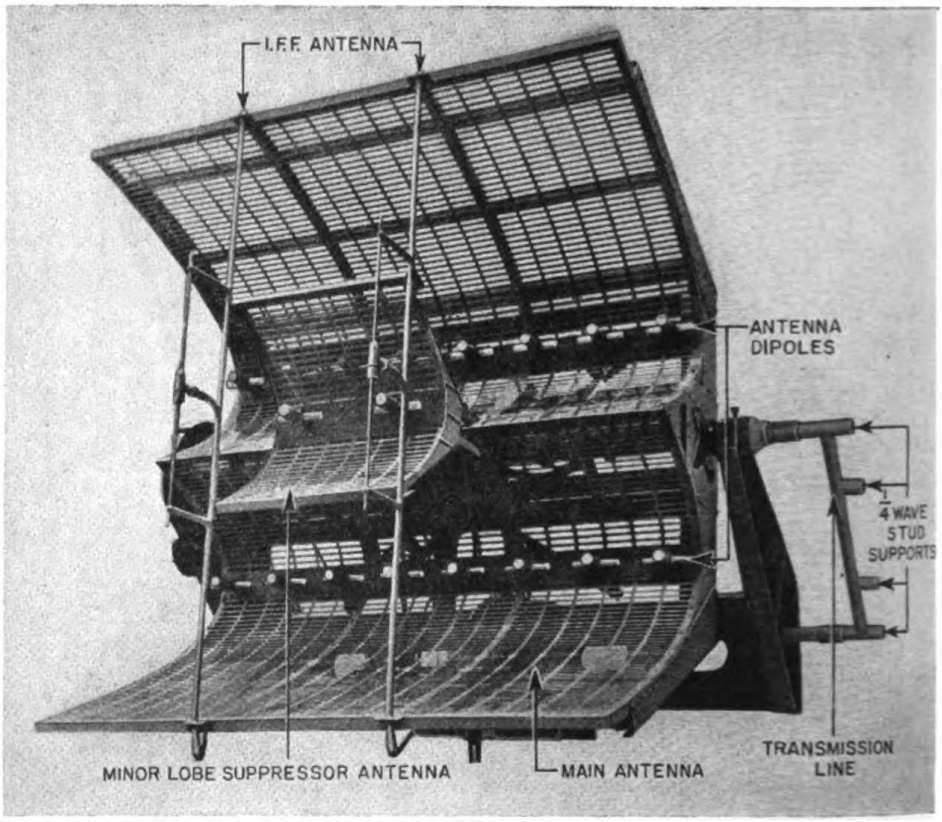

Fig. 51.—Shipborne Anti-Aircraft Fire Control Antenna

geared together and driven synchronously. Figure 52 is a schematic diagram of the waveguide and phase changer circuits.

Figure 39 shows an experimental polyrod antenna under test at Holmdel. Figure 53 is another view of the Polyrod antenna.

14.9 *The Rocking Horse Fire Control Antenna*

It was long recognized that an important direction of Radar development lay towards shorter waves. This is particularly true for fire control antennas where narrow, easily controlled beams rather than great ranges are needed. The Polyrod antenna had pretty thoroughly demon-

Digitized by Google
Original from UNIVERSITY OF MICHIGAN
Generated on 2019-09-23 09:51 GMT / http://hdl.handle.net/2027/mdp.39015077775156
Public Domain, Google-digitized / http://www.hathitrust.org/access_use#pd-google

strated the value of rapid scanning, yet the problem of producing a rapid scanning higher frequency antenna of nearly equal dimensions was a new and different one.

Several possible solutions to this problem were known. The array technique applied so effectively to the polyrod antenna could have been applied here also, but only at the expense of many more elements and greater complexity.

After much preliminary work it was finally concluded that a mechanically scanning antenna, the "rocking horse," provided the best solution to the higher frequency scanning problem. This solution is practical and relatively simple.

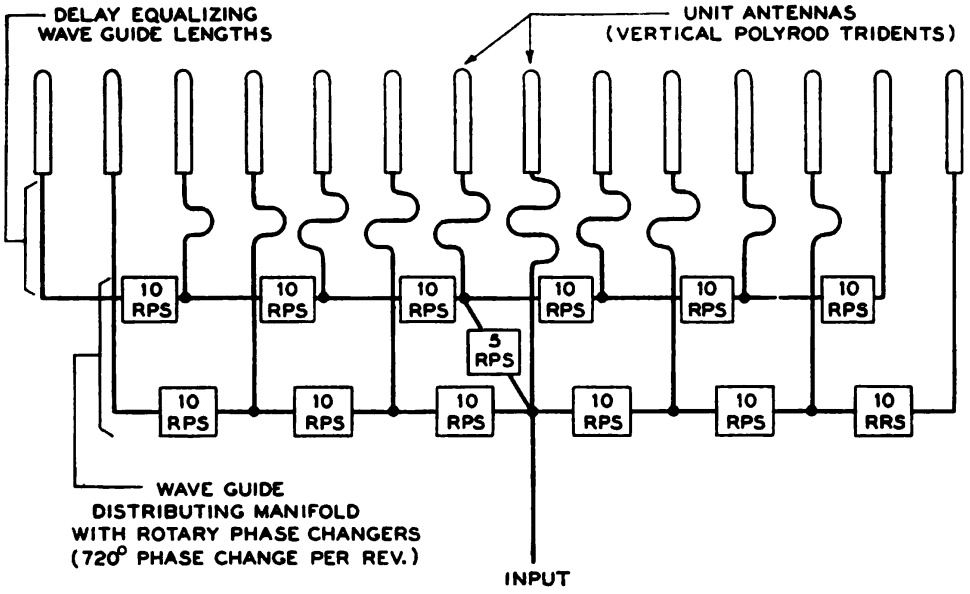

Fig. 52.—Schematic Diagram of Polyrod Fire Control Antenna.

The operation of the rocking horse is described in Sec. 12.1. It is essentially a carefully designed and firmly built paraboloidal antenna which oscillates rapidly through the scanning sector. Its oscillation is dynamically balanced to eliminate undesirable vibration.

Figure 54 is a photograph of a production model of the rocking horse antenna.

14.10 *The Mark 19 Radar Antenna*[16]

In Anti-aircraft Fire Control Radar Systems for Heavy Machine Guns it is necessary to employ a highly directive antenna and to obtain continuous rapid comparison of the received signals on a number of beam positions

[16] Sections 14.10, 14.11 and 14.12 were written by F. E. Nimmcke.

Digitized by Google
Original from UNIVERSITY OF MICHIGAN
Generated on 2019-09-23 09:52 GMT / http://hdl.handle.net/2027/mdp.39015077775156
Public Domain, Google-digitized / http://www.hathitrust.org/access_use#pd-google

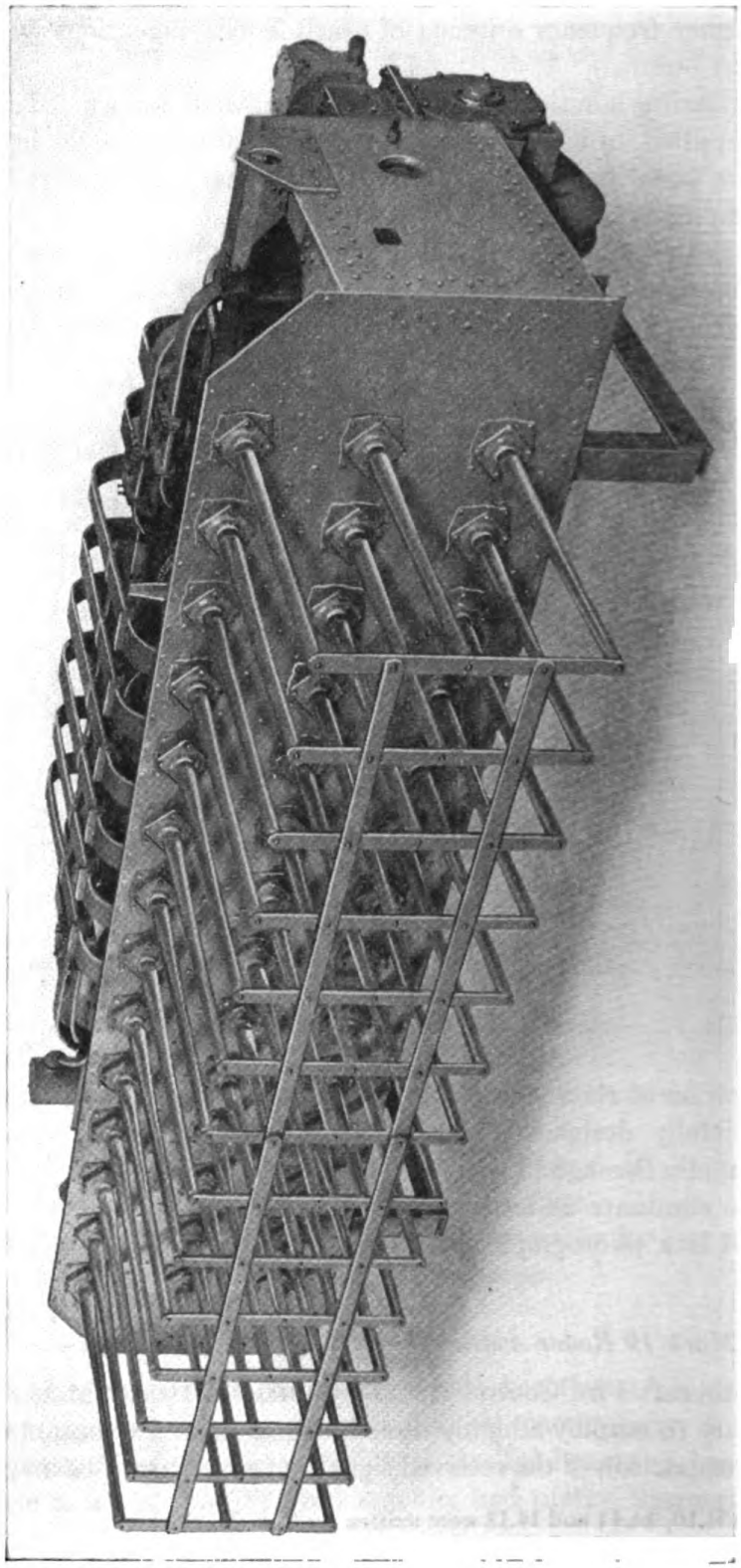

Fig. 53.—Polyrod Fire Control Antenna.

Digitized by Google
Original from UNIVERSITY OF MICHIGAN
Generated on 2019-09-23 09:52 GMT / http://hdl.handle.net/2027/mdp.39015077775156
Public Domain, Google-digitized / http://www.hathitrust.org/access_use#pd-google

as discussed in Section 11.2. Such an antenna is also required to obtain the high angular precision for anti-aircraft fire control. These requirements are achieved by the use of a conical scanning system. The beam from the antenna describes a narrow cone and the deviation of the axis of the cone from the line of sight to the target can be determined and measured by the phase difference between the amplitude modulated received signal and the frequency of the reference generator associated with the

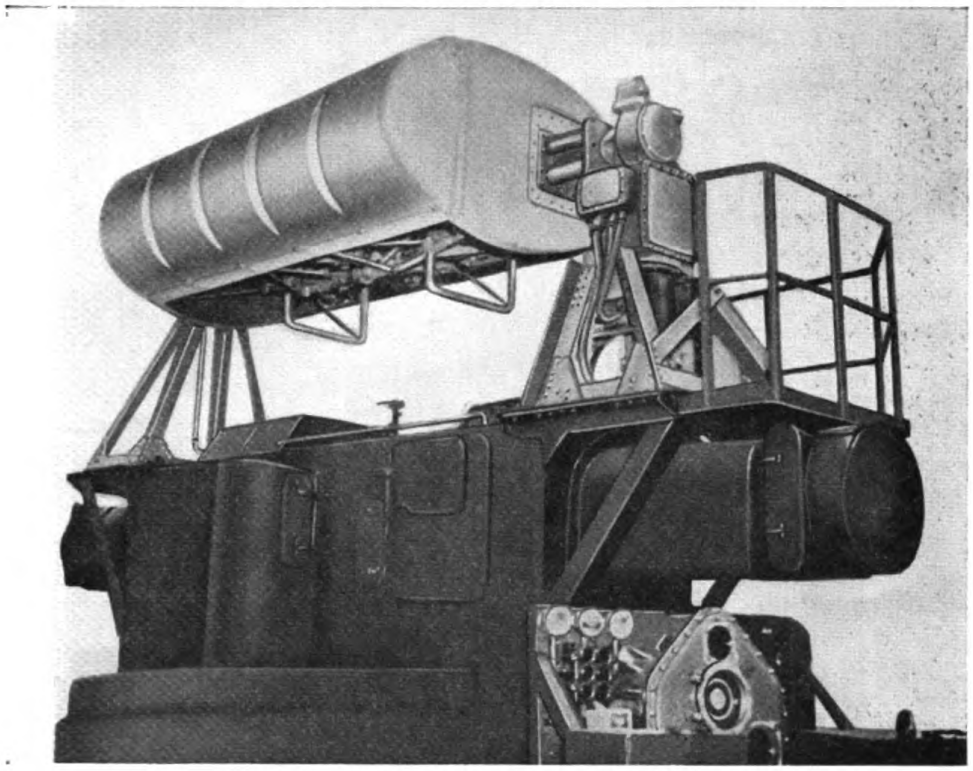

Fig. 54.—Rocking Horse Fire Control Antenna.

antenna. This information is presented to the pointer-trainer at the director in the form of a wandering dot on an oscilloscope.

The antennas described in sections 14.10, 14.11 and 14.12 were all designed by the Bell Laboratories as anti-aircraft fire control radar systems, particularly for directing heavy machine guns. They were designed for use on all types of Naval surface warships.

In Radar Equipment Mark 19, the first system to be associated with the control of 1.1 inch and 40 mm anti-aircraft machine guns, the antenna was designed for operation in the 10 cm region. This antenna consisted of a spinning half dipole with a coaxial transmission line feed. The antenna

Generated on 2019-09-23 09:52 GMT / http://hdl.handle.net/2027/mdp.39015077775156
Public Domain, Google-digitized / http://www.hathitrust.org/access_use#pd-google
Digitized by Google
Original from UNIVERSITY OF MICHIGAN

was driven by 115-volt, 60 cycle, single phase motor to which was coupled a two-phase reference voltage generator. The motor rotated at approximately 1800 rpm which resulted in a scanning rate of 30 cycles per second. This antenna was used with a 24-inch spun steel parabolic reflector which provided, at the 3 db point, a beam width of approximately 11° and a beam shift of 8.5° making a total beam width of approximately 20° when scanning. The minor lobes were down more than 17 db (one way) from the maximum; and the gain of this antenna was 21 db. This antenna assembly

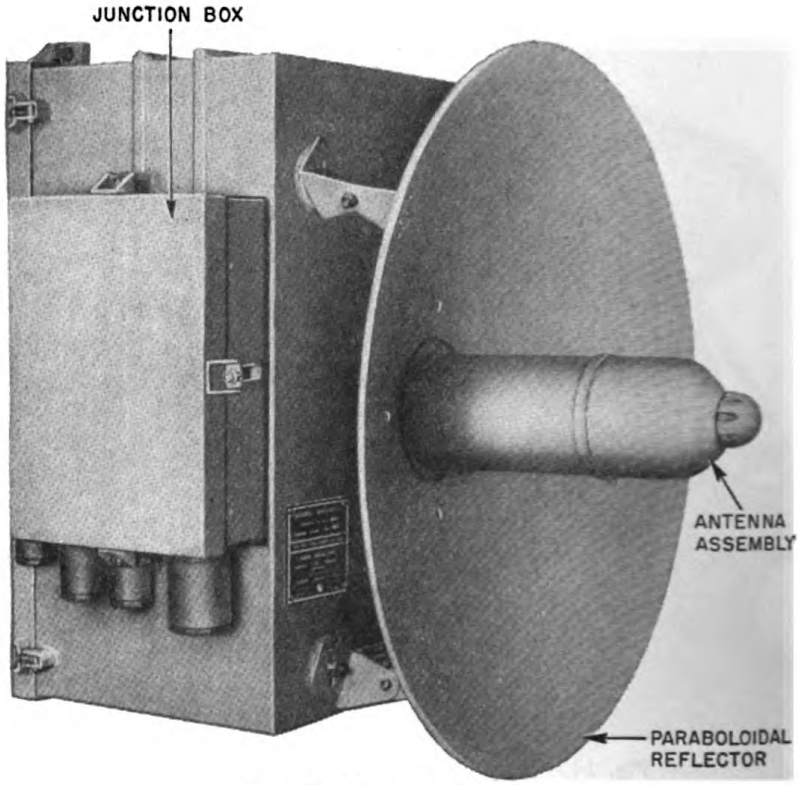

Fig. 55—Mark 19 Antenna.

was integral with a transmitter-receiver (Fig. 55) which was mounted on the associated gun director. Consequently, the size of the reflector was limited by requirements for unobstructed vision for the operators in the director. As a matter of fact, for this type of radar system serious consideration must be given to the size and weight of the antenna and associated components.

14.11 *The Mark 28 Radar Antenna*

The beam from the antenna used in Radar Equipment Mark 19 was relatively broad and to improve target resolution, the diameter of the

Generated on 2019-09-23 09:53 GMT / http://hdl.handle.net/2027/mdp.39015077775156
Public Domain, Google-digitized / http://www.hathitrust.org/access_use#pd-google
Digitized by Google
Original from UNIVERSITY OF MICHIGAN

reflector for the antenna in Mark 28 was approximately doubled. The Mark 28 is a 10 cm system and employs a conical scanning antenna similar to that described for Mark 19. The essential difference is that the spun steel parabolic reflector is 45 inches in diameter which provides a beam width of approximately 6.5° and a beam shift of 4.5° making a total of 11°.

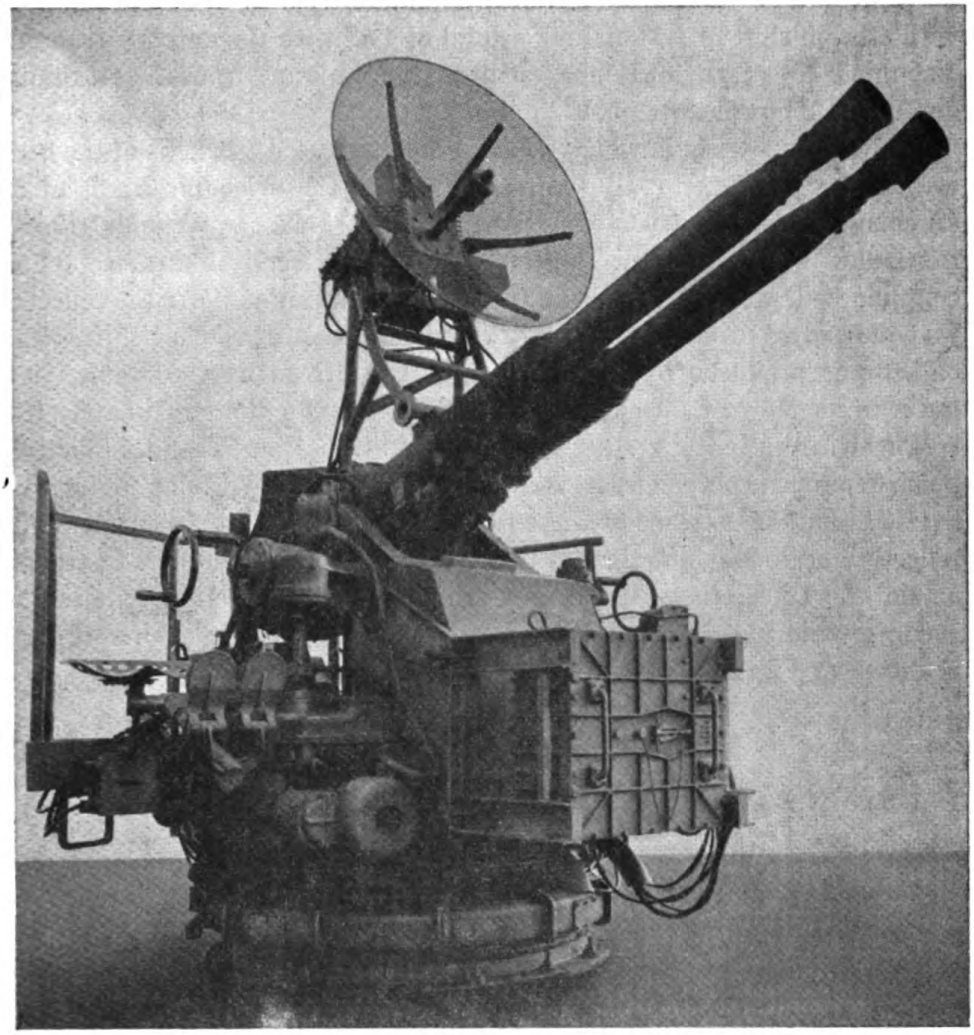

Fig. 56—Mark 28 Antenna Mounted on 40 MM Gun.

The minor lobes are down more than 17 db (one way) from the maximum; and the gain of this antenna is 26 db. It was found necessary to perforate the reflector of this dimension in order to reduce deflection caused by gun blast and by wind drag on the antenna assembly. The antenna assembly for Radar Equipment Mark 28 is shown in Fig. 56. This assembly is shown mounted on a 40 mm Gun.

Digitized by Google
Original from UNIVERSITY OF MICHIGAN
Generated on 2019-09-23 09:53 GMT / http://hdl.handle.net/2027/mdp.39015077775156
Public Domain, Google-digitized / http://www.hathitrust.org/access_use#pd-google

14.12 *A 3 CM Anti-Aircraft Radar Antenna.*

To obtain greater discrimination between a given target and other targets, or between a target and its surroundings, the wavelength was reduced to the 3 cm region. An antenna for this wavelength was designed to employ the conical scan principle. In this case the parabolic reflector was 30 inches in diameter and transmitted a beam approximately 3° wide at the 3db point with a beam shift of 1.5° making a total of 4.5° with the antenna scanning. The minor lobes are down more than 22 db (one way) from the maximum and the gain of this antenna is 35 db.

In the 3 cm system in which a Cutler feed was used, the axis of the beam was rotated in an orbit by "nutation" about the mechanical axis of the antenna. This was accomplished by passing circular waveguide through the hollow shaft of the driving motor. The rear end of the feed (choke coupling end) was fixed in a ball pivot while the center (near the reflector) was off set the proper amount to develop the required beam shift. This off set was produced by a rotating eccentric driven by the motor. The latter was a 440 volt, 60 cycle, 3 phase motor rotating at approximately 1800 rpm which resulted in a scanning rate of 30 cycles per second. The two-phase reference voltage generator was integral with the driving motor.

It was found necessary at these radio frequencies to use a cast aluminum reflector and to machine the reflecting surface to close tolerances in order to attain the consistency in beam width and beam direction required for accurate pointing. An antenna assembly for the 3 cm anti-aircraft radar is shown in Fig. 57.

15. Land Based Radar Antennas

15.1 *The SCR-545 Radar "Search" and "Track" Antennas*[17]

The SCR-545 Radar Set was developed at the Army's request to meet the urgent need for a radar set to detect aircraft and provide accurate target tracking data for the direction of anti-aircraft guns.

This use required that a narrow beam tracking antenna be employed to achieve the necessary tracking accuracy, furthermore, a narrow beam antenna suitable for accurate tracking has a very limited field of view and requires additional facilities for target acquisition. This was provided by the search antenna which has a relatively large field of view and is provided with facilities for centering the target in its field of view. These two antennas are integrated into a single mechanical structure and both radar axes coincide.

The "Search" antenna operates in the 200 mc band and is com-

[17] Section 15.1 was written by A. L. Robinson.

Digitized by Google
Original from UNIVERSITY OF MICHIGAN
Generated on 2019-09-23 09:53 GMT / http://hdl.handle.net/2027/mdp.39015077775156
Public Domain, Google-digitized / http://www.hathitrust.org/access_use#pd-google

posed of an array of 16 quarter wave dipoles spaced 0.1 wave-length in front of a flat metal reflector. All feed system lines and impedance matching devices are made up of coaxial transmission line sections. The array is divided into four quarters, each being fed from the lobe switching mechanism. This division is required to permit lobe switching in both horizontal and vertical planes. The function of the lobe switching mecha-

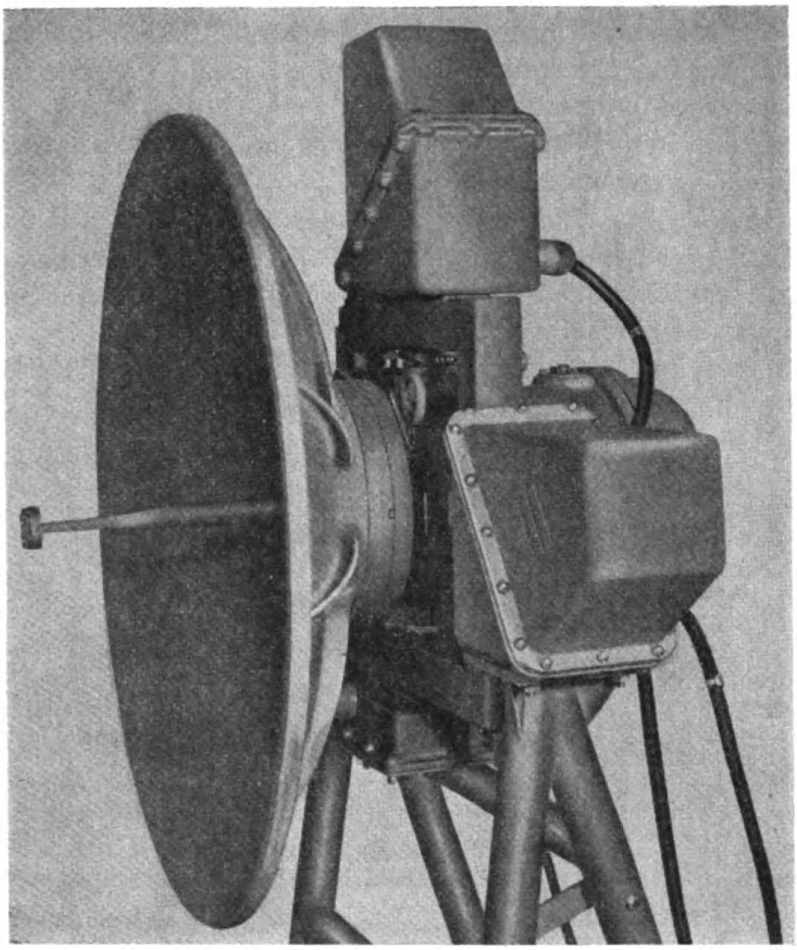

Fig. 57.—3CM Anti-Aircraft Radar Antenna.

nism is to introduce a particular phase shift in the excitation of the elements of one half of the antenna with respect to the other half. The theory of this type of lobe switching is discussed in section 11.1. The antenna beam spends approximately one quarter of a lobing cycle in each one of the four lobe positions. Each of the four lobe positions has the same radiated field intensity along the antenna axis and therefore when a target is on axis equal signals will be received from all four lobe positions.

Digitized by Google
Original from UNIVERSITY OF MICHIGAN
Generated on 2019-09-23 09:53 GMT / http://hdl.handle.net/2027/mdp.39015077775156
Public Domain, Google-digitized / http://www.hathitrust.org/access_use#pd-google

The "Track" antenna operates in the 10 cm. region and consists of a reflector which is a parabola or revolution, 57 inches in diameter, illuminated by a source of energy emerging from a round waveguide in the lobing mechanism. Conical lobing is achieved by rotating the source of energy around the parabola axis in the focal plane of the parabola. Conical lobing is discussed in section 11.2. The round waveguide forming the source is filled with a specially shaped polystyrene core to control the illumination of the parabola and to seal the feed system against the weather. The radio frequency power is fed through coaxial transmission line to a coaxial-waveguide transition which is attached to the lobing mechanism.

The "Search" and "Track" antenna lobing mechanisms are synchronized and driven by a common motor.

The radio frequency power for both antennas is transmitted through a single specially constructed coaxial transmission line to the common antenna structure, where a coaxial transmission line filter separates the power for each antenna.

Figure 58 is a photograph of a production model of the SCR-545 Radar Set. The principal electrical characteristics of the antennas are tabulated below:

	Antennas	
	Search	Track
Gain	14.5 db	30 db
Horizontal Beamwidth	23.5°	5°
Vertical Beamwidth	25.5°	5°
Polarization	Horizontal	Vertical
Type of Lobing	Lobe switching	Conical lobing
Angle between lobe positions	10°	3°
Lobing rate	60 cycles/sec.	60 cycles/sec.

The SCR-545 played an important part in the Italian campaign, particularly in helping to secure the Anzio Beach Head area, as well as combating the "V" bombs in Belgium. However the majority of SCR-545 equipments were sent to the Pacific Theater of Operations and played an important part in operations on Leyte, Saipan, Iwo Jima, and Okinawa.

15.2 *The AN/TPS-1A Portable Search Antenna*[18]

In order to provide early warning information for advanced units, a light weight, readily transportable radar was designed under Signal Corps contract.

[18] Written by R. E. Crane.

Digitized by Google
Original from UNIVERSITY OF MICHIGAN
Generated on 2019-09-23 09:53 GMT / http://hdl.handle.net/2027/mdp.39015077775156
Public Domain, Google-digitized / http://www.hathitrust.org/access_use#pd-google

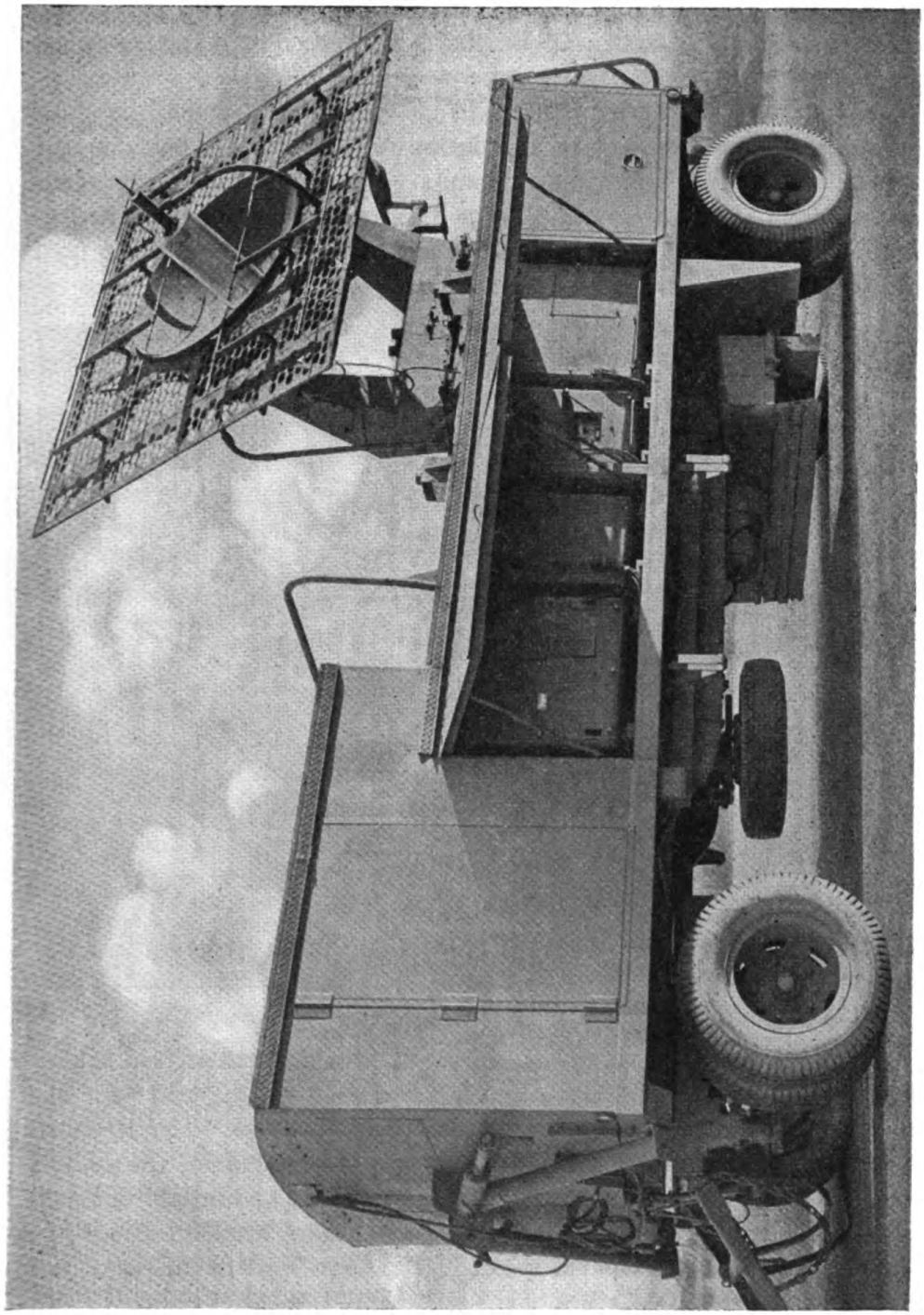

Fig. 58—SCR/545 Antenna.

Digitized by Google
Original from UNIVERSITY OF MICHIGAN
Generated on 2019-09-23 09:53 GMT / http://hdl.handle.net/2027/mdp.39015077775156
Public Domain, Google-digitized / http://www.hathitrust.org/access_use#pd-google

The objective was to obtain as long range early warning as possible with moderate accurracy of location. Emphasis was placed on detection of low flying planes.

The objectives for the set indicated that the antenna should be built as large as reasonable and placed as high as reasonable for a portable set. Some latitude in choice of frequency was permitted at first. For ruggedness and reliability reasons which seemed controlling at the time, the frequency was pushed as high as possible with vacuum tube detectors and R.F. amplifiers. This was finally set at 1080 mc.

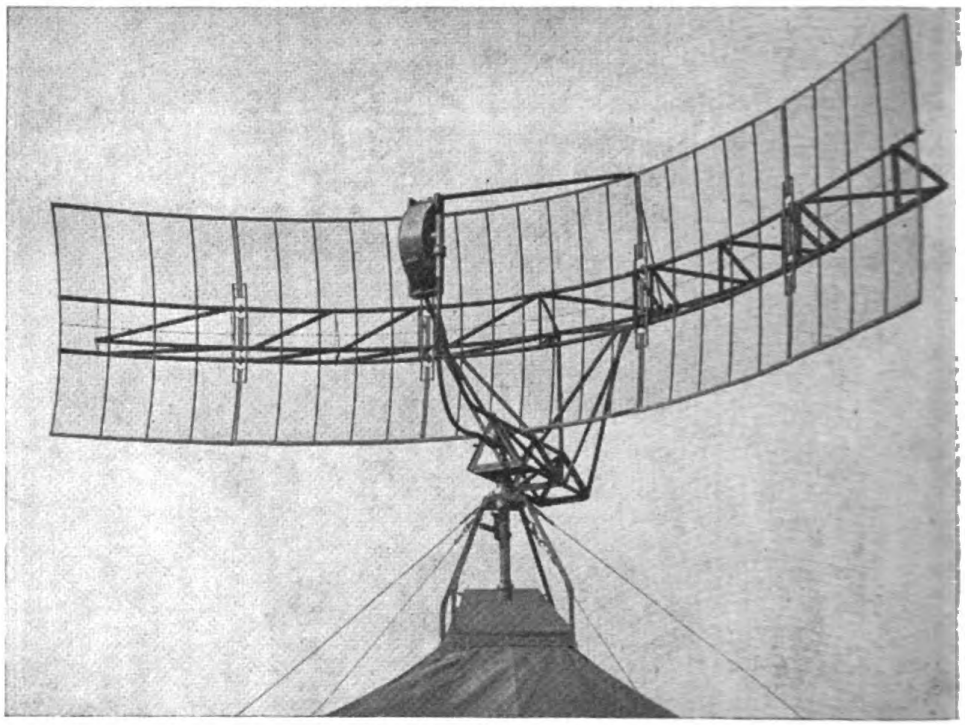

Fig. 59—AN/TPS-1A Antenna.

The antenna as finally produced was 15 ft. in width and 4 ft. in height. The reflecting surface was paraboloidal. The mouth of the feed horn was approximately at the focus of the generating parabola. The feedhorn was excited by a probe consisting of the inner conductor of the coaxial transmission line extended through the side of the horn and suitably shaped. To reduce side lobes and back radiation the feedhorn was dimensioned to taper the illumination so that it was reduced about 10 db in the horizontal and vertical planes at the edges of the reflector. Dimensions of probe and exact location of feed, etc. were determined empirically to secure acceptable impedance over the frequency band needed. This band, covered by spot frequency magnetrons, was approximately $\pm 2.5\%$ from mid frequency.

Figure 59 shows the antenna in place on top of the set.

Digitized by Google
Original from UNIVERSITY OF MICHIGAN
Generated on 2019-09-23 09:54 GMT / http://hdl.handle.net/2027/mdp.39015077775156
Public Domain, Google-digitized / http://www.hathitrust.org/access_use#pd-google

The characteristics of this antenna are summarized below:

Gain	27.3 db.
Horizontal Half Power Beamwidth	4.4°
Vertical Half Power Beamwidth	12.6°
Vertical Beam Characteristic	Symmetrical
Polarization	Horizontal
Impedance (SWR over ±2.5% band)	<4.0 db

16. Airborne Radar Antennas

16.1 *The AN/APS-4 Antenna*[19]

AN/APS-4 was designed to provide the Navy's carrier-based planes with a high performance high resolution radar for search against surface and airborne targets, navigation and interception of enemy planes under conditions of fog and darkness. For this service, weight was an all important consideration and throughout a production schedule that by V-J day was approaching 15,000 units, changes to reduce weight were constantly being introduced. In late production the antenna was responsible for 19 lbs. out of a total equipment weight of 164 lbs. The military requirements called for a scan covering 150° in azimuth ahead of the plane and 30° above and below the horizontal plane in elevation. To meet this requirement a Cutler feed and a parabolic reflector of 6.3″ focal length and 14½″ diameter was selected. Scanning in azimuth was performed by oscillating reflector and feed through the required 150° while elevation scan was performed by tilting the reflector. Beam pattern was good for all tilt angles. In early flight tests the altitude line on the B scope due to reflection from the sea beneath was found to be a serious detriment to the performance of the set. To reduce this, a feed with elongated slots designed for an elliptical reflector was tried and found to give an improvement even when used with the approximately round reflector. The elliptical reflector was also tried, but did not improve the performance sufficiently to justify the increased size.

As will be noted in Fig. 60, the course of the mechanical development brought the horizontal pivot of the reflector to the form of small ears projecting through the parabola. No appreciable deterioration of the beam pattern due to this unorthodox expedient was noted.

The equipment as a whole was built into a bomb-shaped container hung in the bomb rack on the underside of the wing. Various accidents resulted in this container being torn off the wing in a crash landing in water or dropped on the deck of the carrier. After these mishaps, the equipment was frequently found to be in good working order with little or no repair required.

[19] Written by F. C. Willis.

Digitized by Google
Original from UNIVERSITY OF MICHIGAN
Generated on 2019-09-23 09:54 GMT / http://hdl.handle.net/2027/mdp.39015077775156
Public Domain, Google-digitized / http://www.hathitrust.org/access_use#pd-google

Gain	28 db
Beamwidth	6° approx. circular
Polarization	Horizontal
Scan	Mechanical
Scanning Sector—Azimuth	150°
Scanning Sector—Elevation	60°
Scanning Rate	one per sec.
Total weight	19 lbs.

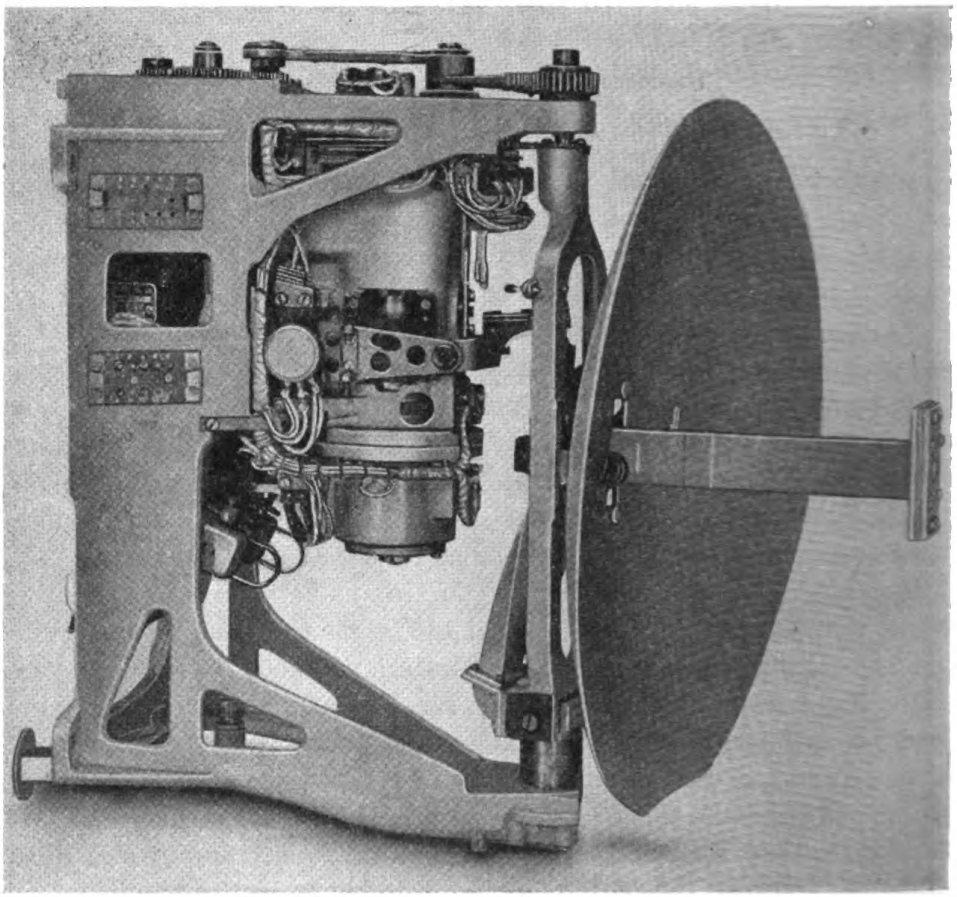

Fig. 60—AN/APS-4 Antenna.

16.2 *The SCR-520, SCR-717 and SCR-720 Antennas*[20]

The antenna shown in Fig. 61 is typical of the type used with the SCR-520 and SCR-720 aircraft interception (night fighter) airborne radar equipment, as well as the SCR-717 sea search and anti-submarine airborne radar equipment. The parabolic reflector is 29 inches in diameter and produces a radiation beam about 10° wide. The absolute gain is approximately 25 db. RF energy is supplied to a pressurized emitter through a pressurized transmission line system which includes a rotary joint located on the ver-

[20] Written by J. F. Morrison.

Digitized by Google
Original from UNIVERSITY OF MICHIGAN
Generated on 2019-09-23 09:54 GMT / http://hdl.handle.net/2027/mdp.39015077775156
Public Domain, Google-digitized / http://www.hathitrust.org/access_use#pd-google

tical axis and a tilt joint on the horizontal axis. Either vertical or horizontal polarization can be used by rotating the mounting position of the emitter. Vertical polarization is preferred for aircraft interception work and horizontal polarization is preferred for sea search work.

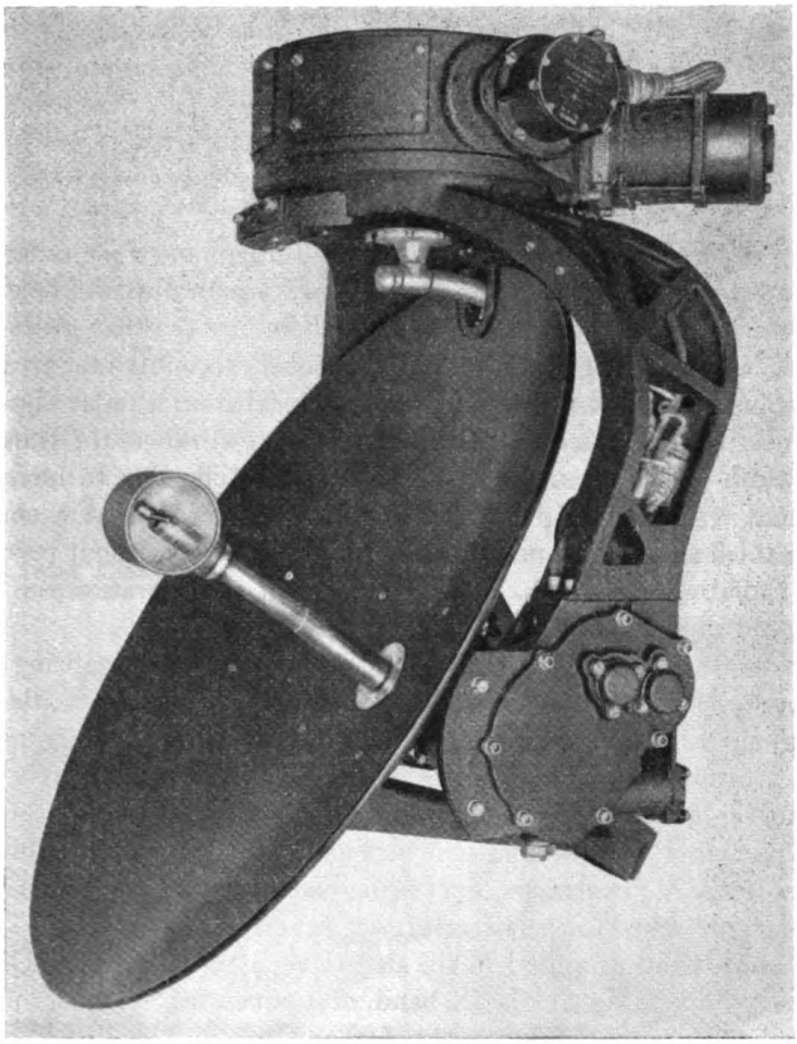

Fig. 61—SCR-520 Antenna.

For aircraft interception the military services desired to scan rapidly a large solid angle forward of the pursuing airplane, i.e. 90° right and left, 15° below and 50° above the line of flight. The data is presented to the operator in the form of both "B" and "C" presentations and for this purpose potentiometer data take-offs are provided on the antenna. The reflector is spun on a vertical axis at a rate of 360 rpm and at the same time it is

Digitized by Google
Original from UNIVERSITY OF MICHIGAN
Generated on 2019-09-23 09:54 GMT / http://hdl.handle.net/2027/mdp.39015077775156
Public Domain, Google-digitized / http://www.hathitrust.org/access_use#pd-google

made to nod up and down about its horizontal axis by controllable amounts up to a total of 65° and at a rate of 30° per second.

In the sea search SCR-717 equipment, selsyn azimuth position data take-offs are provided which drive a PPI type of indicator presentation. The rotational speed about the vertical axis in this case is either 8 or 20 rpm as selected by the operator. The reflector can also be tilted about its horizontal axis above or below the line of flight as desired by the operator.

It will be noted that the emitter moves with the reflector and accordingly it is always located at the focal point throughout all orientations of the antenna.

16.3 *The AN/APQ-7 Radar Bombsight Antenna*[21]

Early experience in the use of bombing-through-overcast radar equipment indicated that a severe limitation in performance was to be expected as the result of the inadequate resolution offered by the then available airborne radar equipments. This lack of resolution accounted for gross errors in bombing where the target area was not ideal from a radar standpoint.

To meet this increased resolution requirement in range, the transmitted pulse width was shortened considerably. In attempting to increase the azimuthal resolution, higher frequencies of transmission were employed. This enabled an improvement in azimuthal resolution without resorting to larger radiating structures, a most important consideration on modern high speed military aircraft.

To extend the size of the radiating structure without penalizing the aircraft performance, the use of a linear scanning array which would exhibit high azimuthal resolution was considered. This array was originally conceived in a form suitable to mount within the existing aircraft wing and transmit through the leading edge. As development proceeded, the restrictions imposed on the antenna structure as well as the aircraft wing design resulted in the linear array scanner being housed in an appropriate separate air foil and attached to the aircraft fuselage (Fig. 62).

The above study resulted in the development of the AN/APQ-7 radar equipment, operating at the X-band of frequencies.[22] This equipment provided facilities for radar navigation and bombing.

The AN/APQ-7 antenna consisted of an array of 250 dipole structures spaced at $\frac{1}{2}$ wavelength intervals and energized by means of coupling probes extending into a variable width waveguide. The vertical pattern was arranged to exhibit a modified $\csc^2$ distribution by means of accurately shaped "flaps" attached to the assembly.

[21] Written by L. W. Morrison.

[22] A large part of the antenna development was carried out at the M. I. T. Radiation Laboratory.

Digitized by Google
Original from UNIVERSITY OF MICHIGAN
Generated on 2019-09-23 09:55 GMT / http://hdl.handle.net/2027/mdp.39015077775156
Public Domain, Google-digitized / http://www.hathitrust.org/access_use#pd-google

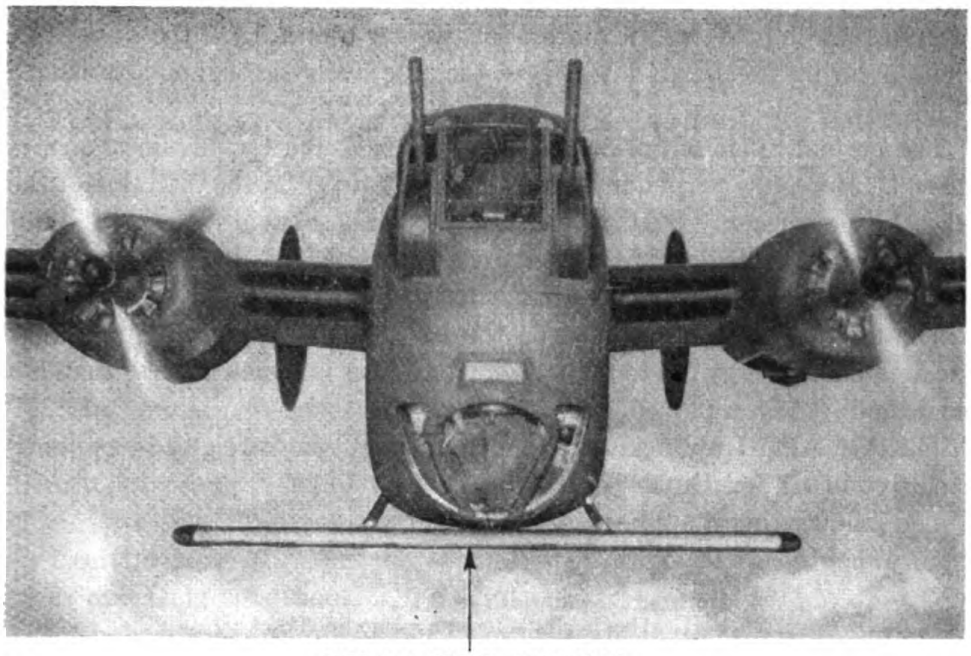

Fig. 62—AN/APQ-7 Antenna Mounted on B24 Bomber.

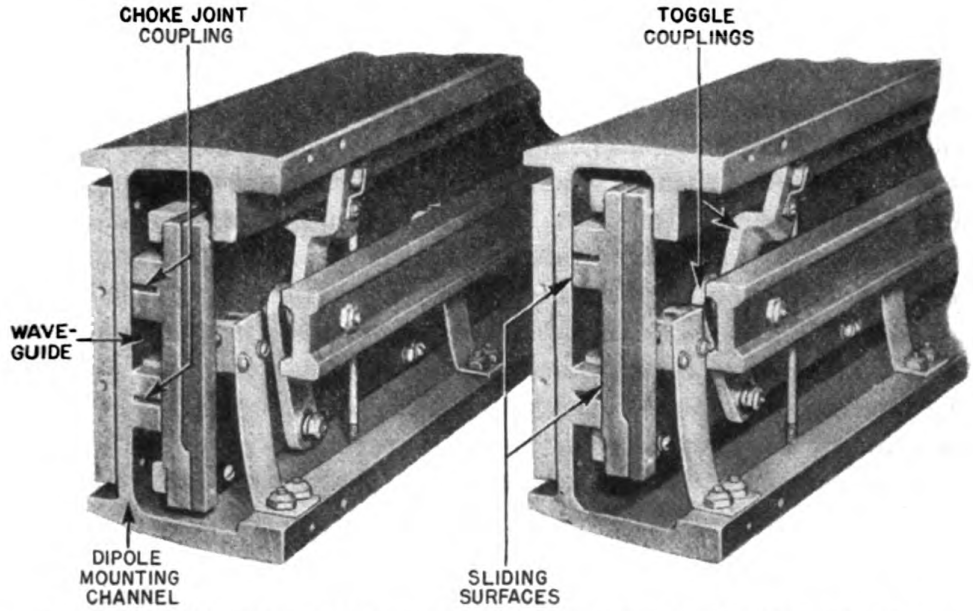

Fig. 63—AN/APQ-7 Antenna. Left—Contracted Wave Guide Assembly. Right—Expanded Wave Guide Assembly.

The scanning of the beam is accomplished by varying the width of the feed waveguide. This is accomplished by means of a motor driven actuated cam which drives a push rod extending along the waveguide assembly back

Digitized by Google
Original from UNIVERSITY OF MICHIGAN
Generated on 2019-09-23 09:55 GMT / http://hdl.handle.net/2027/mdp.39015077775156
Public Domain, Google-digitized / http://www.hathitrust.org/access_use#pd-google

and forth. Toggle arms are attached to this push rod at frequently spaced intervals which provides the motion for varying the width of the waveguide while assuring precise parallelism of the side walls throughout its length (Fig. 63).

The normal range of horizontal scanning exhibited by this linear array extends from a line perpendicular to the array to 30° in the direction of the feed. By alternately feeding each end, a total scanning range of ±30° from the perpendicular is achieved. Appropriate circuits to synchronize the indicator for this range are included.

The use of alternate end feed on the AN/APQ-7 antenna requires that the amount of energy fed to the individual dipoles is somewhat less than if a single end feed is employed.

The AN/APQ-7 antenna is 16½ feet in length and weighs 180 pounds exclusive of air foil housing.

The following data applies:

Gain = 32.5 db
Horizontal beamwidth = 0.4°
Vertical beam characteristic = modified $\csc^2$
Scan—Array scanning
Scanning Sector—± 30° Horizontal
Scanning Rate = 45°/second

ACKNOWLEDGMENTS

Contributors to the research and development of the radar antennas described in this paper included not only the great number of people directly concerned with these antennas but also the many people engaged in general research and development of microwave components and measuring techniques. A complete list of credits, therefore, will not be attempted.

In addition to the few individuals mentioned in footnotes throughout the paper, the authors would like to pay special tribute to the following co-workers in the Radio Research Department: C. B. H. Feldman who with the assistance of D. H. Ring made an outstanding contribution in the development of the polyrod array antenna; W. A. Tyrrell for his work on lobe switches; A. G. Fox, waveguide phase changers; A. P. King, paraboloids and horn antennas; A. C. Beck, submarine antennas; G. E. Mueller, polyrods.

Generated on 2019-09-23 09:55 GMT / http://hdl.handle.net/2027/mdp.39015077775156
Public Domain, Google-digitized / http://www.hathitrust.org/access_use#pd-google
Digitized by Google
Original from UNIVERSITY OF MICHIGAN

Techniques and Facilities for Microwave Radar Testing*

By E. I. GREEN, H. J. FISHER, J. G. FERGUSON

Methods and devices are described for testing microwave radars in the radio frequency range from about 500 mc to 25,000 mc, and at associated video frequencies. In general, the same instruments and techniques are applicable also in testing microwave communication systems.

Introduction

THAT radars are marvels of ingenuity has long since become common knowledge. This ingenuity is reflected, however, in complexity of circuits. A rough index of this is found in the number of vacuum tubes, which for a single radar may range from 50 to 250. Notwithstanding the most careful design, it is easy for the radar performance to become impaired under operating conditions.

Not only is radar complex, but its performance criteria are less tangible than those of conventional communication systems. Ordinary radio is to some extent self-testing in that reception of intelligible speech or signals frequently constitutes a sufficient check of satisfactory performance. With radar, the greater the range coverage and the more accurate the data, the more valuable the information is likely to be. However, the working range may fall to a fraction of the possible maximum or some other degradation or malfunctioning may occur, with nothing in the operation of the radar to tell that this has happened. Since lack of maximum performance may have serious military results, measurement of performance assumes the utmost importance in radar work.

The new techniques and new frequency ranges employed for radar necessitated the wartime development of a wide variety of new types of test equipment. A large part of this development work was concentrated at Bell Laboratories and at the N.D.R.C.'s Radiation Laboratory at M.I.T., working in close coordination with one another and with the technical services of the Army and Navy. In the manufacture of radar test equipment, Western Electric took a major part. This article discusses the techniques of radar testing and describes the types of test gear developed by Bell Laboratories and manufactured by Western Electric. These cover the radio frequency range from about 500 megacycles to 25,000 megacycles, together with associated video frequencies.

Because of its importance during the war, emphasis has been placed on

* Presented at A.I.E.E. Winter Convention, New York, N. Y., January 21–25, 1946. Published by *Elec'l. Engg., Trans. Sec.*, May 1946.

Digitized by Google
Original from UNIVERSITY OF MICHIGAN
Generated on 2019-09-23 09:56 GMT / http://hdl.handle.net/2027/mdp.39015077775156
Public Domain, Google-digitized / http://www.hathitrust.org/access_use#pd-google

the testing of microwave radars. However, similar methods and instruments have also been employed in the testing of microwave communication systems and such applications can be expected to increase. In this situation the developers and users of microwave communication systems are fortunate in that almost all of the techniques and devices developed for radar testing are equally applicable to communication systems. This is even true of the video units, which are useful in connection with pulse modulated telephone systems and AM or FM television systems.

So many persons, both within and outside Bell Laboratories, have contributed to the developments described that the authors have reluctantly reached the conclusion that the assignment of individual credit should not be attempted.

Requirements

Operation of Typical Radar

Subsequent discussion may be simplified by first reviewing briefly the operation of a somewhat typical radar, as shown in Fig. 1. Under the control of d.c. or so-called video pulses from the modulator, short pulses of radio frequency energy are delivered by the magnetron transmitter to a highly directive antenna, ordinarily arranged to scan a section of space. Energy reflected from an object or "target" in the path of the beam is intercepted by the same antenna. The received pulses or echoes are converted to an intermediate frequency by heterodyning against a local oscillator, the frequency of which may be automatically controlled.

To enable the same antenna to serve for both transmitting and receiving, a TR tube or transmit-receive switch is usually provided. This consists of a partially evacuated resonant cavity containing a spark gap which breaks down during the transmitted pulse, thus preventing the transmitted power from injuring the sensitive receiver. An RT tube, consisting of a similar resonant cavity and spark gap, may be provided to prevent absorption of the received signal by the transmitter. After amplification and detection of the received signal, the resultant video pulses are applied to an indicator which may present information in any of several different ways. Customarily the direction of the target (determined by antenna orientation) and its range (determined by reflection interval, 10.7 microseconds per mile) are shown. The system may be used merely for searching, or for fire control, bomb direction, or other functions, with additional equipment as required.

Types of Tests and Test Sets

Figure 2 shows an early assemblage of radar test equipment for the 10 cm range, initially produced in 1942, which has seen wide usage.

Digitized by Google
Original from UNIVERSITY OF MICHIGAN
Generated on 2019-09-23 09:57 GMT / http://hdl.handle.net/2027/mdp.39015077775156
Public Domain, Google-digitized / http://www.hathitrust.org/access_use#pd-google

The more important types of tests required in radar work, either at radar operating locations or at centralized service points, are: (1) Over-all Performance (Range Capability), (2) Transmitter Power, (3) Receiver Sensitivity, (4) Transmitter Frequency, (5) Transmitter Spectrum, (6) Standing Wave Ratio, (7) R. F. Envelope, (8) Receiver Recovery, (9) AFC Tracking, (10) I.F. Alignment, (11) Video Wave Shapes, (12) Range Calibration and (13) Computer Calibration.

The principal types of test sets required for carrying out the above are: (1) Signal Generators, (2) Echo Boxes, (3) Frequency and Power Meters (separate or combined), (4) Standing Wave Meters, (5) R.F. Loads, (6)

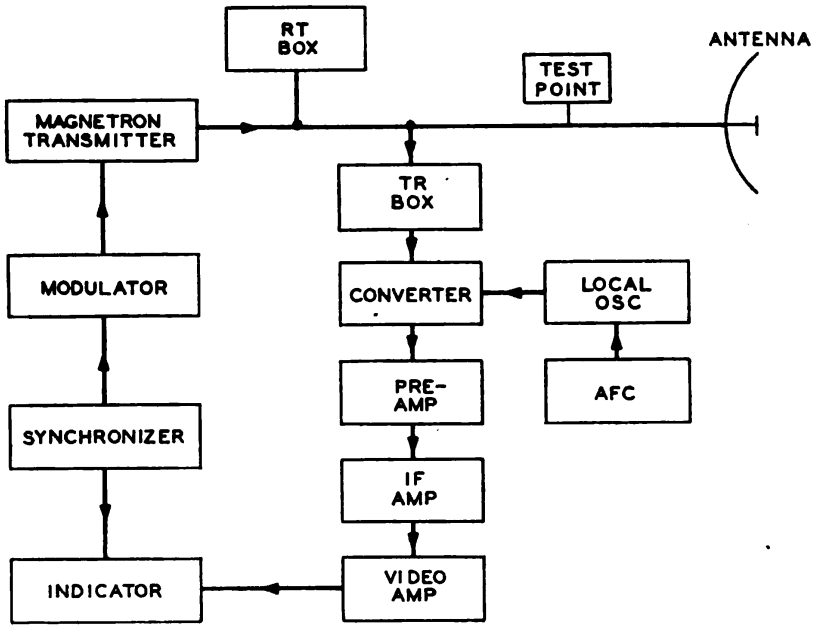

Fig. 1—Diagram of typical radar.

Oscilloscopes, (7) Video Dividers and Loads, (8) Range Calibrators, (9) Computer Test Sets and (10) Spectrum Analyzers. Various auxiliary testing instruments are also employed, including vacuum tube testers, I.F. signal generators, audio oscillators, flux meters, etc. Before discussing the above tests and devices individually, some of the requirements for radar test equipment, especially those resulting from military usage, will be summarized.

Generality of Application

Radars perform a great variety of functions, including search and surveillance, gun laying and fire control, bomb direction, and navigation. They are used in the air, on shipboard, and on the ground, in attack and in de-

Digitized by Google
Original from UNIVERSITY OF MICHIGAN
Generated on 2019-09-23 09:57 GMT / http://hdl.handle.net/2027/mdp.39015077775156
Public Domain, Google-digitized / http://www.hathitrust.org/access_use#pd-google

fense, in combat zones and in rear areas. To realize the advantages of different parts of the frequency spectrum, avoid interference, and keep ahead of enemy countermeasures, it has been necessary for radar to exploit many different frequency bands and sub-bands. These diversities have

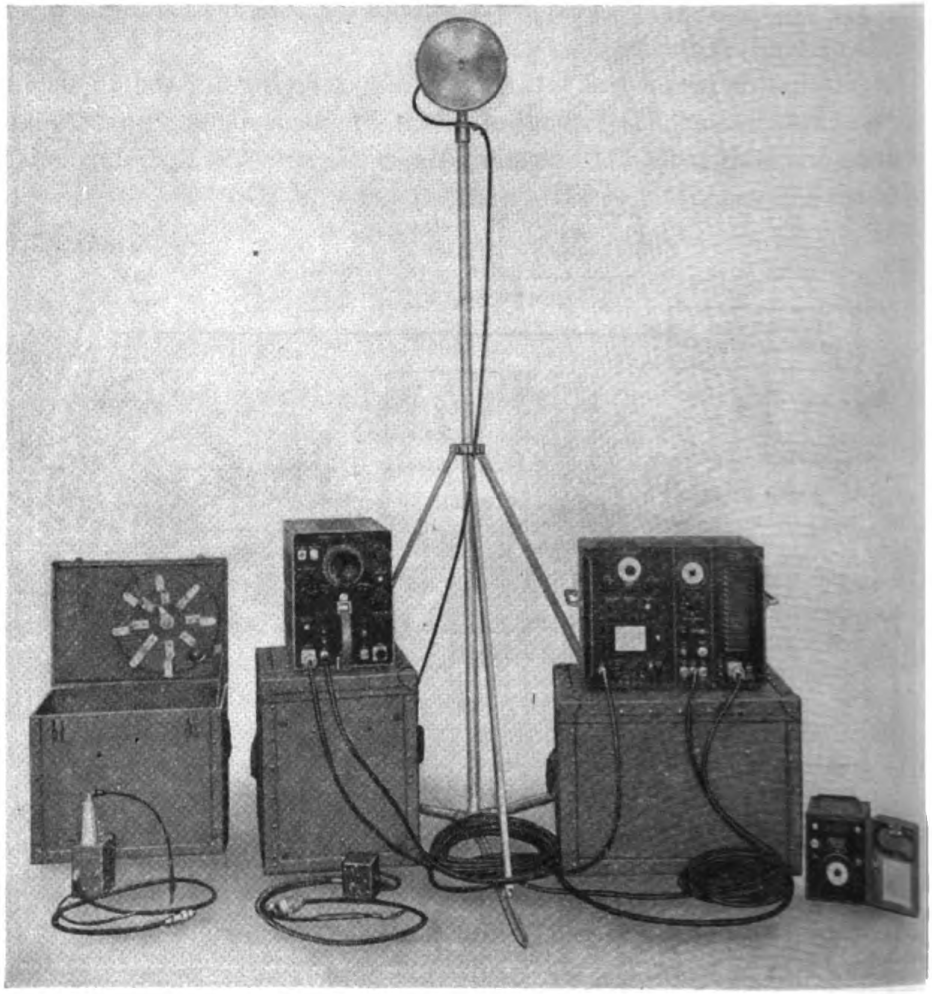

Fig. 2—Early radar test set for 3000 mc range—includes signal generator, oscilloscope, power meter, test antenna and auxiliary units.

bred a multiplicity of types of radar, with a corresponding variety of testing problems and requirements.

Maintenance and testing of radars must be performed at many different locations. In the Army these locations, known as echelons, include (a) the operating unit, (b) central service points, either fixed or mobile, for a number of operating units, and (c) large depots either in the military theatres or in the United States. Navy maintenance and testing are carried out on board the fighting ships or auxiliaries, and at advance and overhaul bases.

Digitized by Google
Original from UNIVERSITY OF MICHIGAN
Generated on 2019-09-23 09:57 GMT / http://hdl.handle.net/2027/mdp.39015077775156
Public Domain, Google-digitized / http://www.hathitrust.org/access_use#pd-google

In developing test equipment, an offhand approach might have been to provide specialized equipment for testing each radar under specific conditions. Since this would have made the total burden of development, manufacture and field maintenance well nigh intolerable, a coordinated plan was followed whereby (with minor exceptions) each test set was made capable of widespread application in testing as many radars under as varied conditions as possible.

Broadbanding

Generality of application required the designing of test equipment for broad frequency bands, bands as a rule much wider than those of the radars themselves. It was necessary, therefore, not only to develop new microwave testing techniques, but to advance the art still further to render the testing components as far as possible insensitive to frequency.

Precision

A radar itself is an instrument of considerable precision. The test equipment used for checking the radar performance in the field has to have still higher accuracy. It is noteworthy that the measuring accuracy realized throughout the microwave range is comparable with that obtainable at lower frequencies where many years of background exist.

Packaging—Size and Weight

Light weight and compactness are of paramount importance where a test set has to be carried any distance by the maintenance man, where it is used in cramped quarters in a plane, truck or submarine, or where it has to be taken up ship ladders or through small hatchways. To permit portable use under such conditions, the design objective was established of a weight not exceeding about 30 lbs. (exclusive of transit case), combined with a ruggedness adequate for all conditions of use. Through rigorous attention to both mechanical and electrical design, this objective has been realized (in many cases with considerable margin) except for a few sets intended primarily for bench use. Figure 3 illustrates the use of lightweight test equipment in maintaining airborne radars.

Environmental Influences

Military usage requires that the test equipment be capable of efficient operation at any ambient temperature between a minimum of the order of $-40°$ to $-55°$ C and a maximum of the order of $+65°$ to $+70°$ C, as well as at any relative humidity up to 95%. In addition the set must withstand continued exposure to driving rain, dust storms and all other conditions encountered in tropical, desert or arctic climates. Often the test set in its

Digitized by Google
Original from UNIVERSITY OF MICHIGAN
Generated on 2019-09-23 09:57 GMT / http://hdl.handle.net/2027/mdp.39015077775156
Public Domain, Google-digitized / http://www.hathitrust.org/access_use#pd-google

transit case must be capable of submergence under water without ill effects. Fungus-proofing with a fungicidal lacquer is a standard requirement.

Simplicity, Reliability, Accessibility

Not only must the functioning of the test set be reliable, stable and trouble-free, but the set must make minimum demands for special skill or tech-

Fig. 3—Portable units used in checking airborne radars at Boca Raton, Fla.

nique on the part of the maintenance man. Access for maintenance purposes, while important in radar test sets, is not as controlling as in the radars themselves and sometimes has to be sacrificed in part for compactness.

Ruggedness

For general application, the test equipment must be capable of withstanding airplane vibration, the shock of heavy guns, depth charges and

Digitized by Google
Original from UNIVERSITY OF MICHIGAN
Generated on 2019-09-23 09:58 GMT / http://hdl.handle.net/2027/mdp.39015077775156
Public Domain, Google-digitized / http://www.hathitrust.org/access_use#pd-google

near misses, and the combinations of shock and vibration connoted by the requirement of "transportation over all types of terrain in any Army vehicle." Test and experience have made it possible to translate these general requirements into two specific requirements, namely the ability to withstand (1) vibration at frequencies from 10 to 33 cycles per second with $\frac{1}{16}''$ excursion for 30 minutes in each of three axes and (2) the shock produced by a 400 lb. hammer falling through distances of 1, 2 and 3 ft. in each of three axes, and striking an anvil to which the set is attached. These requirements have been met without using shock and vibration mounts, which are undesirable in test sets because they increase size and weight.

Range Capability

The range capability of a radar, like that of any radio system, depends upon three things; the transmitted power, the loss in the medium, and the minimum perceptible received signal. Two of these can be combined by taking the ratio of the radiated signal to the minimum perceptible received signal. This ratio, ordinarily expressed as a level difference in db, is variously termed the "system performance," "over-all performance" or merely the "level difference." It may be determined by separate measurement of transmitter power and receiver sensitivity, or by a single overall measurement. With the powers and sensitivities commonly employed in radar, the level difference is of the order of 150 to 180 db.

The actual range that can be spanned for a given performance ratio varies considerably. For a given transmitted power, the echo power received by a radar theoretically varies inversely as the fourth power of the range. The reason for this is simple. In free space the power intercepted by a target which is small in comparison with the area of the radar beam in its vicinity will vary according to the inverse square of the distance from the radar. Similarly, that fraction of the energy reflected from the target which is intercepted by the receiving antenna will vary as the inverse square law. Since the received power involves the product of these two factors, the relation becomes:

$$P_r = K\frac{P_t}{R^4}, \quad \text{or}, \quad R = \left(K\frac{P_t}{P_r}\right)^{\frac{1}{4}} \tag{1}$$

where P_t and P_r represent, respectively, the transmitted and received power, R the range and K a constant determined by antenna design, character of target, etc.

Under operating conditions considerable departure from the above relationship may be experienced, due to such factors as (1) the curvature of the earth, (2) interference between the direct beam and single or multiple reflections, and (3) attenuation due to atmospheric absorption. Except under

Digitized by Google
Original from UNIVERSITY OF MICHIGAN
Generated on 2019-09-23 09:58 GMT / http://hdl.handle.net/2027/mdp.39015077775156
Public Domain, Google-digitized / http://www.hathitrust.org/access_use#pd-google

conditions of severe attenuation such as may occur at the very short wavelengths, the received power commonly varies somewhere between the inverse fourth power and the inverse 16th power of distance. To state it another way, the change in effective range is somewhere between the fourth and the sixteenth root of the change in system performance. The former condi-

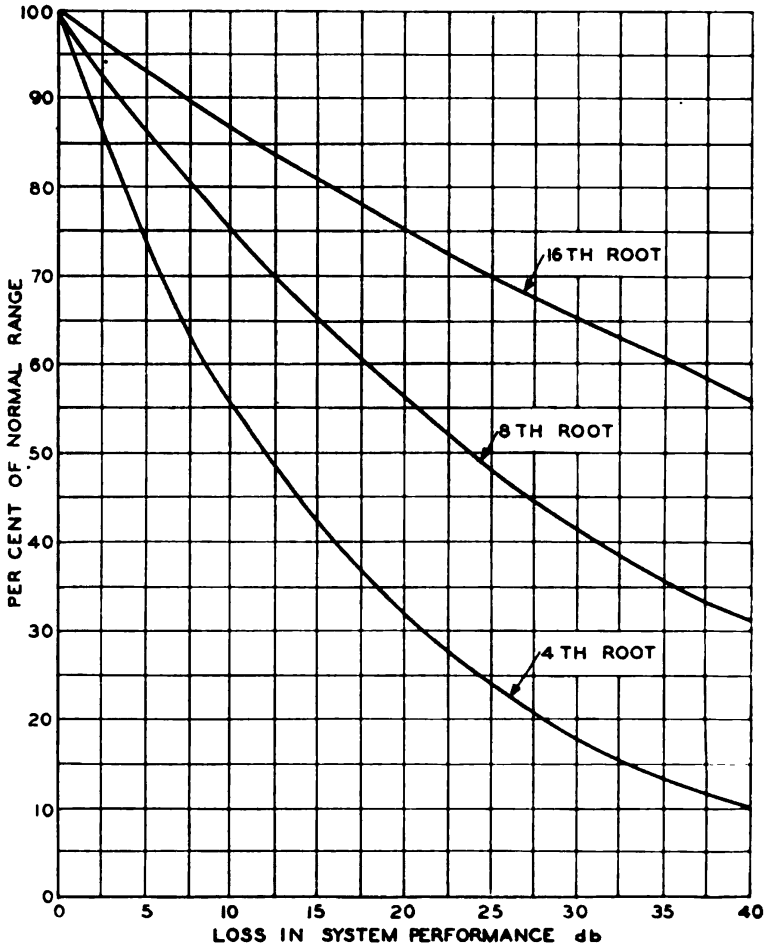

Fig. 4—Effect of reduction in system performance on radar range.

tion might hold for high angle plane-to-ship search in clear weather, the latter for ship-to-ship search in fog. The loss of range resulting from a given degradation of system performance is shown for 4th, 8th and 16th root laws by the curves of Fig. 4. Whatever the propagation law, reduction in performance always means loss of range.

Field surveys have shown that when test equipment is not available or not used, radars in the field are likely to give no more than $\frac{1}{2}$ to $\frac{1}{4}$ of the maximum range of which they are capable. Hence it is necessary to know

Digitized by Google
Original from UNIVERSITY OF MICHIGAN
Generated on 2019-09-23 09:58 GMT / http://hdl.handle.net/2027/mdp.39015077775156
Public Domain, Google-digitized / http://www.hathitrust.org/access_use#pd-google

with good accuracy the over-all performance. Known, or so-called standard, targets have often been used in the field for checking performance. Because of wide variations in transmission due to many factors, results obtained from such targets are frequently misleading.

Signal Generators

Signal generators for radar work deliver one or more different types of test signals, which may serve a variety of functions. More important among these functions are tuning or alignment of the radar components (TR and RT boxes, converter, beat oscillator, AFC, etc.), measurement of receiver sensitivity, checking TR and receiver recovery, measurement of loss, detection of frequency pulling, check of AFC following, measurement of IF bandwidth, check of automatic range tracking, measurement of standing wave ratio and check of video "gating" circuits. Many signal generators include means for measuring the power and frequency of the test signal, and also of an incoming signal.

Types of Signals

The test signals delivered by a signal generator may be CW, pulsed, or frequency-modulated. Occasionally square wave or sine wave modulation is provided.

Pulsed signal generators deliver a succession of single RF pulses or pulse trains, either of these generally synchronous with the pulses of the radar under test. Multivibrator or trigger techniques[1] are used to generate the pulses for modulating the microwave generator. The trigger pulse for synchronizing the pulsing circuits is commonly produced by rectifying RF pulses from the radar transmitter, thus avoiding a separate video connection to the radar. To avoid possible difficulties in video response, the RF test pulses should be of comparable width to those of the radar under test. For observing the test signals, either the radar indicator or an auxiliary oscilloscope may be used. With the single pulse method, provision is usually made for varying the delay of the test pulse with respect to the radar pulse. The width of the test pulse may also be adjustable or variable.

If the frequency of the signal generator is swept over a sufficiently wide frequency band, the IF output of the radar traces the curve of IF selectivity, thus producing a kind of pulse. With a suitable rate of frequency sweep, this pulse becomes comparable in width to the transmitter pulse, and when synchronized with the radar it can be used for test purposes. Since the pulse is produced in the radar, comparison of the shapes of receiver input and output pulses is not possible. The nominal duration of the pulse in the IF output is

$$T = B/\gamma \tag{2}$$

Digitized by Google
Original from UNIVERSITY OF MICHIGAN
Generated on 2019-09-23 09:58 GMT / http://hdl.handle.net/2027/mdp.39015077775156
Public Domain, Google-digitized / http://www.hathitrust.org/access_use#pd-google

where B is the width of IF band in cycles per second (for this purpose conveniently measured between 6 db points) and γ is the speed of frequency sweep in cycles per second per second. For best results this nominal width should be similar to the width of transmitter pulse for which the IF and video circuits are designed. This means that the scanning speed should be in the neighborhood of $B^2/2$.

A CW input of the same frequency as the transmitter produces in the output of the IF detector merely a direct current to which the video amplifier and radar indicator do not respond. However, CW test signals may be utilized by observing on a d.c. meter (built into the radar or separate) the change produced in detector current or converter current.

Receiver Sensitivity

Just as in radio, the sensitivity of a radar receiver is defined as the minimum received signal that is perceptible in the presence of set noise.* At microwave frequencies atmospheric disturbances are usually negligible, so that unless accidental or deliberate interfering signals are present, the operating sensitivity is the same as the intrinsic sensitivity of the receiver.

Receiver sensitivity is commonly stated as the minimum perceptible signal power in db referred to a milliwatt, (abbreviated as dbm). In practice, the receiver sensitivity depends upon the noise figure of the converter, the conversion loss, and the noise figure of the IF amplifier. If an RF amplifier is used, as is the practice at lower microwave frequencies, its noise figure is likely to be controlling. By noise figure in each case is meant the noise power in comparison with the thermal noise. The thermal noise in watts delivered to a load is kTB, where k is Boltzmann's constant, T is absolute temperature in degrees K, and B is the frequency bandwidth. Thus for a 4 mc band at 25° C the thermal noise is -108 dbm. With good design the over-all receiver noise is of the order of 10 to 15 db higher than thermal noise. The minimum detectable signal is usually not equal to the receiver noise but depends on the type of indicator, particularly on whether the presence of an echo is indicated by spot deflection or spot modulation.

With a CW signal generator, receiver sensitivity is measured by determining the minimum input power necessary to produce a perceptible change in meter reading. This affords a satisfactory relative measure of receiver performance, but since the radar indicator usually permits better visual discrimination against noise, the minimum input as read with the meter ordinarily differs from the minimum pulse input for barely discernible indicator response

* The term noise is commonly used even though the disturbances are observed on a cathode-ray screen.

Digitized by Google
Original from UNIVERSITY OF MICHIGAN
Generated on 2019-09-23 09:58 GMT / http://hdl.handle.net/2027/mdp.39015077775156
Public Domain, Google-digitized / http://www.hathitrust.org/access_use#pd-google

RF Oscillators

Beat oscillator tubes for radars deliver (with sufficient decoupling or isolation to prevent undue frequency pulling) a power of the order of milliwatts. This power being adequate for most test purposes, such tubes are well adapted for use as signal generators.

Throughout the greater part of the microwave range, reflex velocity-modulated tubes,[2] both the type with built-in cavity (Pierce-Shepherd) tuned mechanically or thermally, and that with external cavity (McNally) tuned by plugs, vanes or adjustment of dimensions, have been used. The former is more convenient for general use but the latter usually permits wider frequency coverage. Oscillation occurs when the repeller voltage is adjusted so that the round trip transit time corresponds to an odd number of quarter wavelengths. Ordinarily there are several different ranges of repeller voltage, corresponding to different numbers of quarter waves, each of which supports oscillation over a range of frequencies, called a mode of oscillation. Pulsing or frequency modulation is accomplished by applying a pulse or sawtooth wave to the repeller.

At the longer microwaves, a triode with closely spaced electrodes, or so-called "lighthouse" tube[3], has been employed in a tuned-plate tuned-grid oscillator of the positive grid type. Two coaxial lines, conveniently placed one inside the other, provide the tuning, with the feedback through interelectrode capacitances supplemented by loop coupling. The inner cavity (between plate and grid) controls the frequency of oscillation, while the outer cavity (between grid and cathode) provides a suitably high grid impedance. Mechanical arrangements are provided for tracking the tuning of the two cavities over a wide frequency range.

Some Design Principles

Standard signal generators which have been employed in the past for measuring the sensitivity of radio receivers usually deliver a known voltage across a low impedance. This voltage is applied in series with a dummy antenna to the receiver under test. In the microwave range this technique is inconvenient, and signal generators are designed to deliver test power on a matched impedance basis. Receiver sensitivity is stated in terms of power (dbm) instead of volts.

The components of a signal generator or other test unit are commonly arranged along a microwave transmission line. The wave guide type of line possesses certain advantages over a coaxial line in affording a lower loss, facilitating attenuator design as discussed in a subsequent section, etc. Hence the wave guide type of line is used in test equipment for those wavelengths where its size is not excessive, i.e. from about 4,000 mc upwards, and coaxial line for lower frequencies.

Digitized by Google
Original from UNIVERSITY OF MICHIGAN
Generated on 2019-09-23 09:58 GMT / http://hdl.handle.net/2027/mdp.39015077775156
Public Domain, Google-digitized / http://www.hathitrust.org/access_use#pd-google

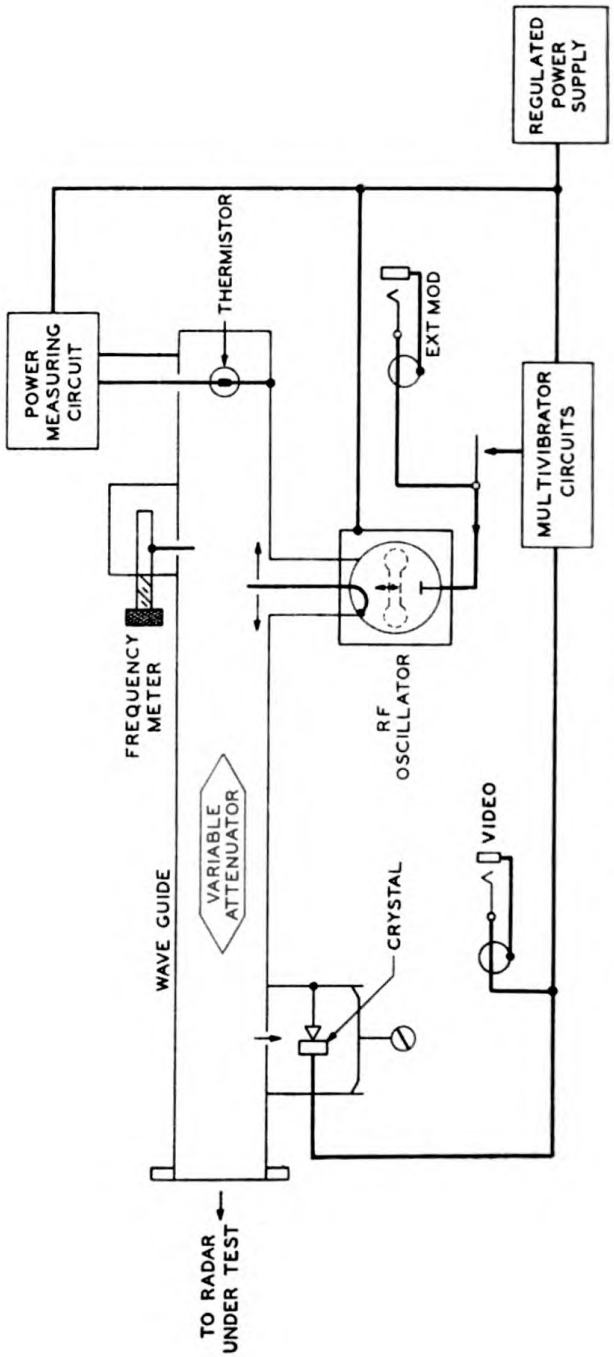

Fig. 5—Block diagram of TS-35A/AP signal generator.

Digitized by Google
Original from UNIVERSITY OF MICHIGAN
Generated on 2019-09-23 09:58 GMT / http://hdl.handle.net/2027/mdp.39015077775156
Public Domain, Google-digitized / http://www.hathitrust.org/access_use#pd-google

A major problem in the design of microwave signal generators is the provision of shielding adequate to reduce leakage signals due to unwanted couplings or stray fields well below the minimum signal required for receiver testing. This minimum level may be as low as −70 or −80 dbm, depending on the coupling loss in the test connection.

A Pulsed and FM Signal Generator

To illustrate the functioning of a signal generator, there is shown in Fig. 5 a block schematic of a design (Army-Navy type TS-35A/AP) which covers a 12% frequency band in the vicinity of 9000 mc. An RF connection to the radar is established with a wave guide flange coupling. The frequency and power of the radar transmitter are measured by means of a coaxial-type frequency meter and thermistor power measuring circuit as described in subsequent sections. The attenuator and pad are adjusted to reduce the incoming average power to about 1 milliwatt, which gives a suitable deflection on the indicating meter. The thermistor is mounted across the wave guide.

An RF pulse train is employed in many tests. To produce this the RF oscillator output is modulated by a multi-vibrator which pulses continuously except when being synchronized. Synchronizing pulses are derived by crystal rectification of the RF pulses from the radar transmitter. The result is an initial RF pulse of 7 microseconds followed by an off period of about 10 microseconds followed by a train of RF pulses each 2 microseconds wide and recurring every 8 microseconds until resynchronization occurs at the next radar pulse.

Using the pulse train, the radar system components can be tuned for maximum sensitivity by maximizing the signal on the indicator. To check receiver sensitivity the CW power is first adjusted so that a power of 1 milliwatt is delivered to the pad and attenuator. Then with the set in the pulsed condition the amplitude of the test signal is adjusted by means of the attenuator and pad until the signal on the radar indicator is barely discernible. It is necessary for this test that the frequency of the test signal be equal to the magnetron frequency. The frequency meter is provided as part of the signal generator for this purpose.

The receiver recovery, i.e. the time required by the receiver to recover after disablement by the transmitter pulse, determines the minimum range at which a radar can be used. With this test set the receiver recovery characteristic is indicated by the amplitude of the test pulses in the interval immediately following the transmitter pulse.

The set is also adapted to serve as an FM signal generator. A sawtooth wave applied to the repeller gives a succession of frequency sweeps, each

Generated on 2019-09-23 09:59 GMT / http://hdl.handle.net/2027/mdp.39015077775156
Public Domain, Google-digitized / http://www.hathitrust.org/access_use#pd-google
Digitized by Google
Original from UNIVERSITY OF MICHIGAN

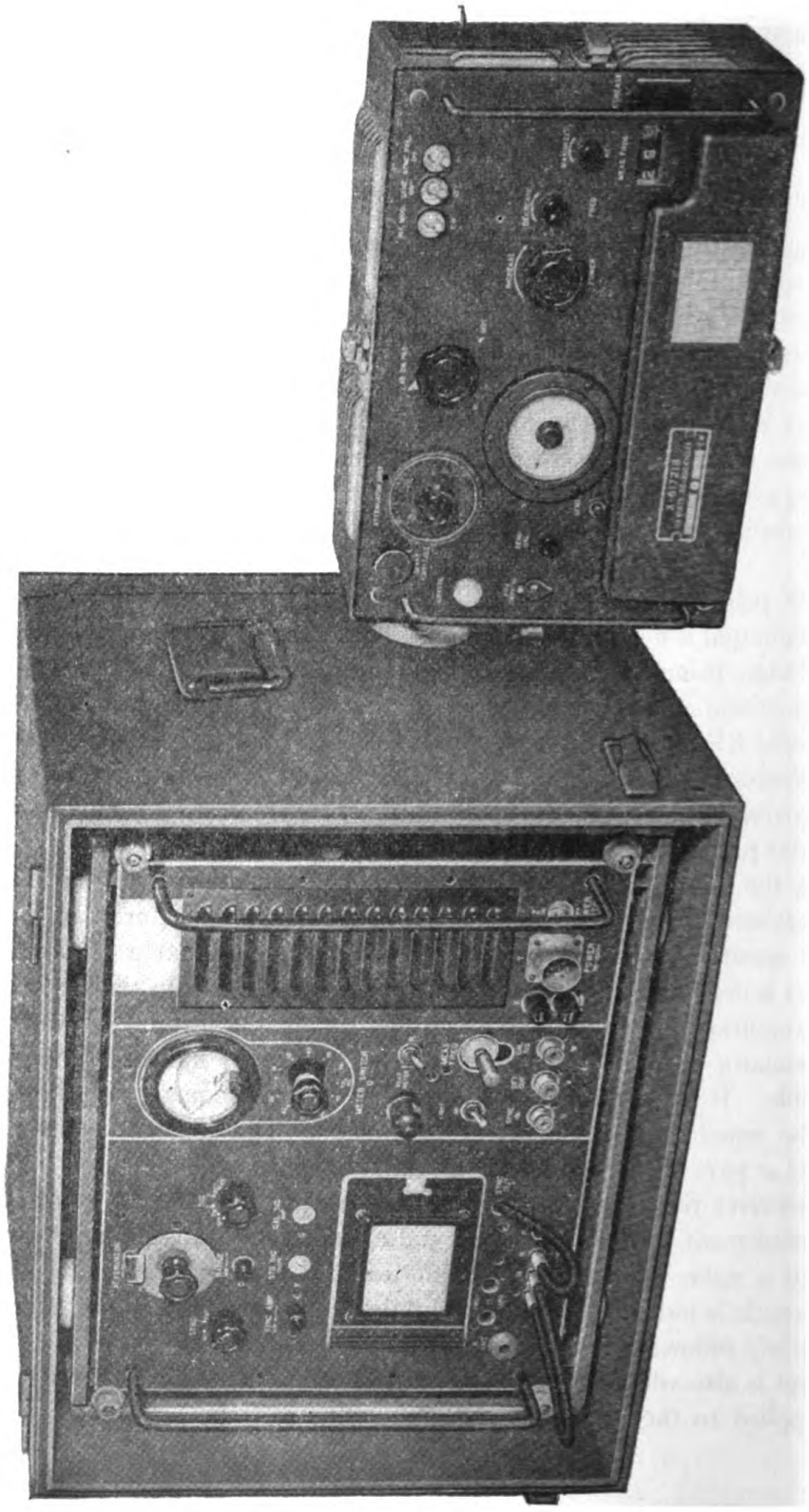

Fig. 6 1942 model signal generator compared with one produced in 1945.

Digitized by Google
Original from UNIVERSITY OF MICHIGAN
Generated on 2019-09-24 06:24 GMT / http://hdl.handle.net/2027/mdp.39015077775156
Public Domain, Google-digitized / http://www.hathitrust.org/access_use#pd-google

about 20 mc wide, and lasting about 6 microseconds. With this frequency modulated signal the width of receiver response may be observed on a Class A oscilloscope (i.e. one showing signal amplitude vs. time). However, with non-adjustable IF strips such measurement is seldom required. Failure of the radar AFC to follow frequency changes due to antenna scanning or other causes is indicated by a change in the indicator presentation. Pulling of the magnetron frequency due to changes in load impedance can be detected by turning off the AFC.

Signal Generator Designs

Designs of signal generators developed for the military arms during the war are interesting as landmarks of progress. The signal generator of the IE30 test set, deliveries of which began in May 1942, delivered pulsed RF signals in the 10 cm range, using sine wave synchronization. Following only three months later was the signal generator of the Army IE57A and Navy LZ test sets (Fig. 6), which covered a then very broad frequency band of 20% in the vicinity of 10 cm, and was designed to be triggered by the incoming RF pulse from the radar instead of by a separate synchronizing connection. This set and a redesigned version of it have seen wide usage in testing Army, Navy and Marine Corps radars.

Delivery of a test set for the 3 cm range, designated TS-35/AP, started in the fall of 1943. This set furnished both a train of pulses and a train of FM signals, both of which features have proved valuable. It covered a 9% frequency band with no tuning adjustment except for the oscillator. An improved design known as TS-35A (see Fig. 6) covered a 12% band.

Progress in reducing the size and weight of the test units is indicated by the fact that the IE30 signal generator weighed 121 lbs., IE57 74 lbs., whereas TS-35 and TS-35A weigh approximately 30 lbs.

Frequency Measurement

Usually a radar need not operate at a precise frequency. Accurate measurements are required in the field, however, to keep the operating frequency within limits, to set the local oscillator, to check the measuring frequency, etc. In the laboratory, accurate frequency measurement is fundamental.

Frequency measurement in the microwave range is ordinarily accomplished by (1) a resonant coaxial line or (2) a resonant cavity, generally cylindrical. These types are illustrated in Fig. 7. Sometimes a combination of the two, referred to as a hybrid or transition type resonator, is employed. The measurement is actually one of wavelength, with the scale calibrated in frequency or a conversion chart provided. Some specific designs of frequency meters are shown in Fig. 8.

Digitized by Google
Original from UNIVERSITY OF MICHIGAN
Generated on 2019-09-24 06:25 GMT / http://hdl.handle.net/2027/mdp.39015077775156
Public Domain, Google-digitized / http://www.hathitrust.org/access_use#pd-google

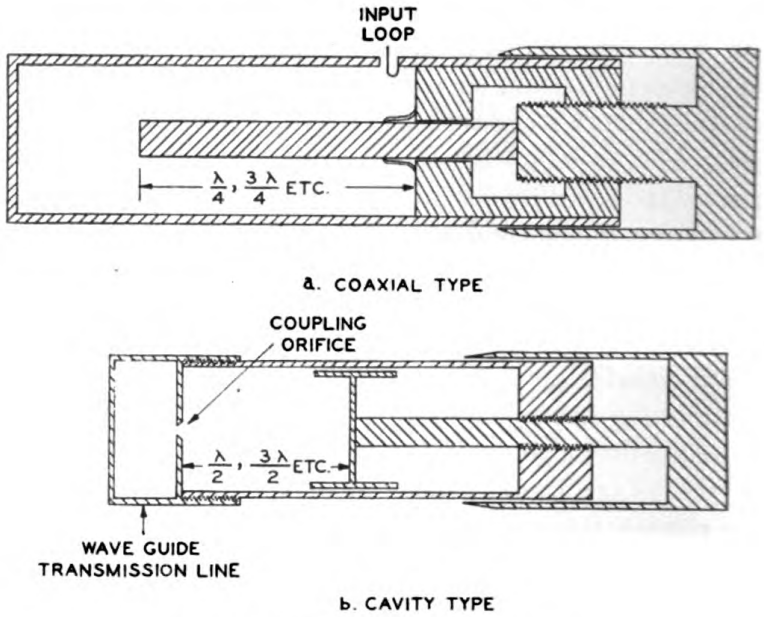

Fig. 7—Types of frequency meters.

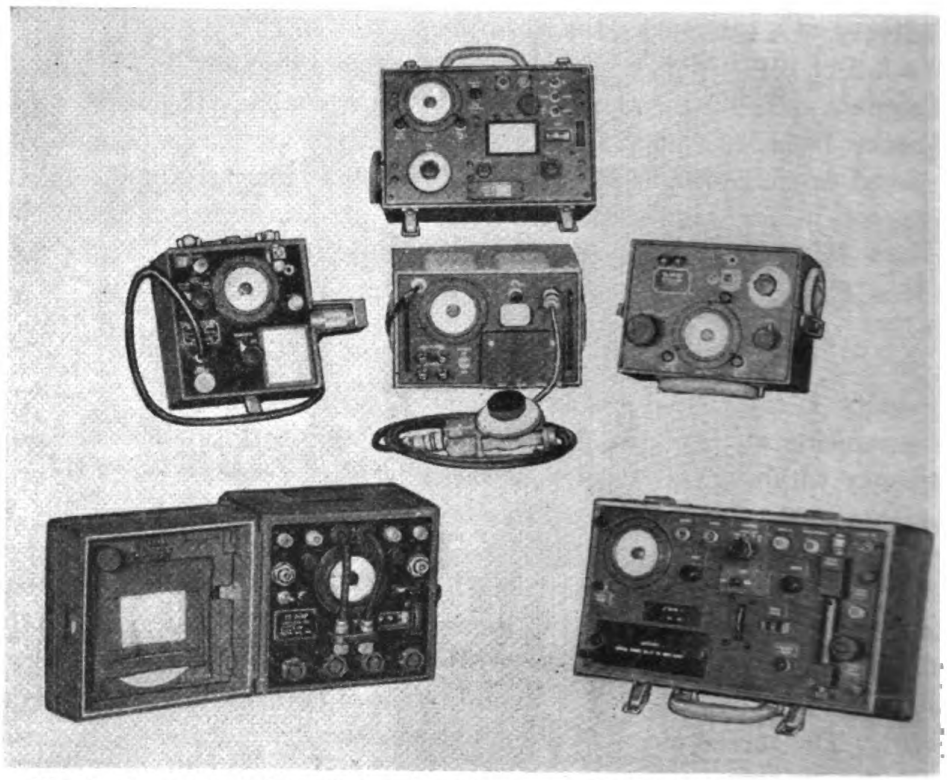

Fig. 8—A group of frequency and power meters designed for various bands in the frequency range 500 to 25,000 mc.

Digitized by Google
Original from UNIVERSITY OF MICHIGAN
Generated on 2019-09-24 06:25 GMT / http://hdl.handle.net/2027/mdp.39015077775156
Public Domain, Google-digitized / http://www.hathitrust.org/access_use#pd-google

Coaxial Wavemeters

A coaxial wavemeter is formed of a section of coaxial transmission line of small enough diameter so that only the coaxial mode (in wave guide notation $TM_{0,0,n}$) can exist. Usually the line is short-circuited at one end and open at the other, in which case resonance occurs at the odd quarter wavelengths $\lambda/4$, $3\lambda/4$ etc.). The open circuit is obtained merely by terminating the inner coaxial conductor, the continuing outer conductor acting as a wave guide below cutoff. Sometimes the line is short-circuited at both ends, giving resonance at the even quarter-wavelengths ($\lambda/2$, λ, etc.).

Cylindrical Cavity Wavemeters

A cylindrical cavity wavemeter is merely a section of cylindrical wave guide transmission line[4] whose length is varied. In order to avoid confusion with other modes, it is preferable to use the dominant mode (described in wave guide notation, $TE_{1,1,n}$*) i.e. the mode with the lowest cutoff frequency. The cutoff wavelength (λ_c) of this mode is $1.706D$, where D is the diameter in meters. For a higher Q it may be necessary to use the circular electric mode $TE_{0,1,n}$. The cutoff wavelength for this mode is .82D. No useful purpose is served by using modes with l and m subscripts above unity. TM modes are often used for fixed frequency cavities, but for variable cavities TE modes are preferable since these have zero current at the inner wall of the cylinder and thus obviate moving contact difficulty. If any mode higher than the dominant one is used, suppression of unwanted modes may be required.

The accuracy of a wavemeter is dependent on its resolving power. This in turn depends upon Q, which is an index of the decrement of the resonant circuit, and is equal to $f/\Delta f$, where Δf is the distance between 3 *db* points on the resonance curve.

In a coaxial wavemeter, maximum Q for a given inner diameter is obtained with a diameter ratio of about 3.6[5] The basic Q of a coaxial wavemeter, assuming copper of standard conductivity, is roughly[6]

$$Q_0 = 0.042D\sqrt{f} \tag{3}$$

This expression neglects end effects and hence gives somewhat too high a value of Q.

The basic Q's for $TE_{1,1,n}$ and $TE_{0,1,n}$ cylindrical cavity resonators employing copper of standard conductivity are, respectively,

* *TE* and *TM* represent, respectively, transverse electric and transverse magnetic. The subscripts l, m, n denote, respectively, the number of wavelengths around any concentric circle in the cross section, the number of wavelengths across a diameter, and the number of half wavelengths along the length of the cylinder.

Digitized by Google
Original from UNIVERSITY OF MICHIGAN
Generated on 2019-09-24 06:25 GMT / http://hdl.handle.net/2027/mdp.39015077775156
Public Domain, Google-digitized / http://www.hathitrust.org/access_use#pd-google

$$Q_0 = 0.0937 \times 10^{10} \frac{A^3}{\sqrt{f}} \frac{1}{1 + B^2\left(0.826 \frac{B}{n} + 0.295\right)} \tag{4}$$

$$Q_0 = 0.2762 \times 10^{10} \frac{A^3}{\sqrt{f}} \frac{1}{1 + B^2\left(2.439 \frac{B}{n}\right)} \tag{5}$$

with $A = \frac{\lambda_c}{\lambda}$, $B^2 = A^2 - 1$, and f is in cycles per second.

The value of Q which determines accuracy is not the basic Q, but the loaded or working Q, herein designated Q_L.

The resolving power of a wavemeter used for measuring a single frequency can be made considerably better than f/Q_L. With a sensitive meter it is readily possible to detect differences less than 1 db, which corresponds to a frequency interval of $f/2Q_L$.

The required accuracy in a wavemeter is generally absolute rather than a percentage. Hence increasingly large values of Q_L are required at the higher frequencies. Thus for a resolution of 1 mc, assuming 1 db discrimination, the values of Q_L required for different frequencies are:

Frequency	Q_L	Frequency	Q_L
1,000 mc	500	10,000 mc	5,000
3,000 mc	1,500	25,000 mc	12,500

An unnecessarily high value of Q_L has the disadvantage of making it more difficult to find the desired frequency.

Linearity

The displacement of the coaxial plunger of a coaxial type wavemeter for resonance is substantially a direct linear function of free space wavelength and if an ordinary centimeter micrometer drive is used it is possible to read wavelength differentials directly. Over bandwidths less than 20 per cent, displacement vs. frequency is also quite linear which is of considerable advantage for some uses.

For the cavity type wavemeter the displacement is a variable function of free space wavelength and becomes very non-linear as the cutoff frequency of the guide or cavity is approached. This is evident from the relation between wavelength in the guide, λ_g, wavelength in free space, λ, and cutoff wavelength, λ_c:

$$\lambda_g = \frac{\lambda}{\sqrt{1 - \frac{\lambda^2}{\lambda_c^2}}} \tag{6}$$

A cam or mechanical linkage may be employed to obtain a linear scale.

Digitized by Google
Original from UNIVERSITY OF MICHIGAN
Generated on 2019-09-24 06:26 GMT / http://hdl.handle.net/2027/mdp.39015077775156
Public Domain, Google-digitized / http://www.hathitrust.org/access_use#pd-google

Frequency Coverage

Increasing the length of a wavemeter is desirable because this gives a larger mechanical displacement for a given frequency interval. The permissible increase is limited, however, by ambiguity with the next lower mode in going toward the upper end of the frequency scale and with the next higher mode in going toward the lower end. This means that, if ambiguity is to be avoided, the ratio of top to bottom frequency cannot exceed $(n + 2)/n$ for a coaxial line of n quarterwaves. For a cylindrical cavity resonator the ratio for the $0,1,n$ mode must be less than $n + 1)/n$, the exact limit depending on proximity to cutoff.

Guideposts

The following guideposts are suggested for choosing the type of wavemeter in the microwave range. Where limitations of size and Q permit, the coaxial quarter-wave type should be used because of its greater linearity. If this type is inapplicable, the cavity type with $TE_{1,1,n}$ should be used unless its Q is inadequate, in which case $TE_{0,1,n}$ should be employed.

Couplings

A loop, orifice or probe may be used for coupling to a wavemeter. Coupling to a coaxial wavemeter is generally effected by a loop placed near a short-circuited end so as to be in the maximum magnetic field. For coupling to a cylindrical cavity wavemeter, an orifice in or near the base of the cavity is usually employed. The coupling to the wavemeter is kept small enough to avoid serious reduction of loaded Q.

Types of Detectors

Various types of detectors may be associated with a wavemeter, the most commonly used being (1) a crystal rectifier and microammeter, or (2) a thermistor bolometer. When a crystal rectifier is employed with a cavity or coaxial wavemeter a circuit similar to that shown in Fig. 9 is used. Important items in such a circuit are the "RF by-pass" condenser, and the "video" condenser. The latter, by providing a low-impedance path to the video signals, improves rectification efficiency when the input signal is pulsed. The quarter-wave stub shown in the figure is used when the input or coupling circuit does not provide DC and video paths. When the signal is pulsed at a low duty cycle, high peak currents through the crystal are obtained even though the average current through the meter is small, and it is possible to impair or burn out the crystal unless extreme care is taken. The use of a thermistor, which is self-protecting for large overloads, avoids this danger. Another expedient is to limit the crystal current to a small value and employ a video amplifier and oscilloscope.

Digitized by Google
Original from UNIVERSITY OF MICHIGAN
Generated on 2019-09-24 06:26 GMT / http://hdl.handle.net/2027/mdp.39015077775156
Public Domain, Google-digitized / http://www.hathitrust.org/access_use#pd-google

Methods of Use

A wavemeter may be used as either a transmission or a reaction instrument. In the former case (Fig. 10a) it is inserted directly in the transmission path, so that substantially no through transmission occurs except at resonance. In the latter case (Fig. 10b) the wavemeter is coupled to the transmission path or a branch circuit. When the meter is tuned off resonance it presents such a high impedance to the main path that its effect is negligible. At resonance, however, it offers a lower impedance which reflects energy in the main line so that less power reaches the detector and

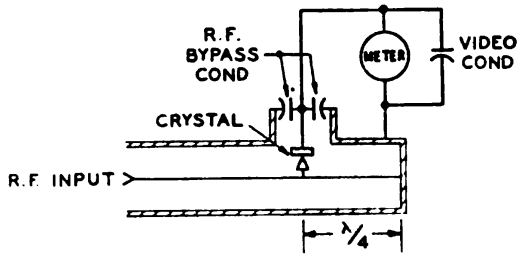

Fig. 9—Crystal detector for pulsed RF signals.

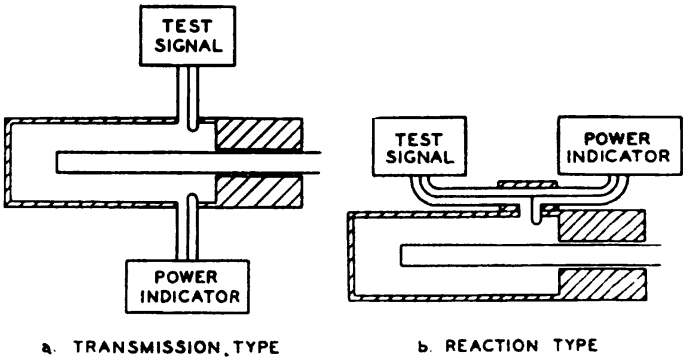

Fig. 10—Types of frequency meter circuits.

a dip in the reading occurs. For most applications the reaction arrangement is preferable since the power transmitted when the wavemeter is off tune may serve various purposes. For analysis of frequency spectrum the transmission method is necessary. This method requires two couplings to the wavemeter, which lowers the Q as compared with the reaction type.

Drive and Scale

A direct drive with a precision lead screw of the micrometer type is frequently used. Accuracy of reading is insured by spring loading to minimize backlash and by specifying close tolerances for threads and for concentricity of plunger and cavity. The scale on a wavemeter must be fine enough to permit utilization of the resolving power. The conventional micrometer

Digitized by Google
Original from UNIVERSITY OF MICHIGAN
Generated on 2019-09-24 06:26 GMT / http://hdl.handle.net/2027/mdp.39015077775156
Public Domain, Google-digitized / http://www.hathitrust.org/access_use#pd-google

type of scale sometimes makes accurate reading difficult in a small compact meter. Scale mechanisms which have been used include counter types, clock face or expanded drum types with gearing between vernier and coarse scales, and a single direct reading scale with divisions arranged in a spiral for compactness.

Effect of Temperature and Humidity

To minimize the effects of temperature on the accuracy of readings, invar has been employed for elements whose dimensions affect the wavelength. For accurate work, the scale reading must be corrected for temperature. A rough approximation is that the scale reading varies in accordance with the coefficient of expansion of the metal.

Water vapor included in the air dielectric of a wavemeter has an appreciable effect on the dielectric constant and hence on the resonant frequency.[7] Thus, for example, in going at sea level from 25° C, and 60% humidity to 50° C, and 90% humidity, the scale reading should be reduced by .03%. Correction can be made by means of a chart, a convenient form of which has been prepared by Radiation Laboratory.

Calibration

Frequency meters are calibrated against sub-standards which in turn are calibrated against a multiplier from lower frequencies for which a high order of accuracy can be obtained. Such multipliers have been made available at Radiation Laboratory and the National Bureau of Standards. The accuracy obtained at interpolation frequencies is of course less than at exact multiples of the base frequency. In the microwave range the accuracy is believed to be of the order of one part in 100,000.

Power Measurement

There are two needs for power measurement in radar maintenance, namely (1) in evaluating transmitter performance and (2) in standardizing test signals. Power output is, of course, only one factor in transmitter performance, others being (a) frequency and (b) spectral distribution or shape of RF envelope. Ability to measure absolute power is desirable to permit interchangeable use of test sets in the field.

Measurement of Pulse Power

The transmitter power as used in Formula (1) is the average power during the pulse. The relationship of pulse to (long) average power is

$$\frac{P_t \text{ av.}}{P_t \text{ pulse}} = Tf_r \tag{7}$$

Digitized by Google
Original from UNIVERSITY OF MICHIGAN
Generated on 2019-09-24 06:26 GMT / http://hdl.handle.net/2027/mdp.39015077775156
Public Domain, Google-digitized / http://www.hathitrust.org/access_use#pd-google

T is the pulse duration in seconds and f_r is the pulse recurrence frequency (P. R. F.) in cycles per second. The product Tf_r is the duty cycle. (Sometimes the reciprocal of this number is referred to as the duty cycle. The magnitude is usually such that no ambiguity arises.)

During the early days of radar it was the practice to measure pulse power. The test equipment was coupled to the radar by a path of known loss. The RF envelope was derived by means of a crystal rectifier and applied to an oscilloscope. With the aid of an RF attenuator the level applied to the crystal rectifier and oscilloscope was held constant. Calibration was obtained by using a signal generator whose output was standardized, prior to pulsing, with an averaging type of power meter. The procedure was rather involved, with several sources of possible error. Since it is much simpler to measure (long) average power, field measurement of pulse power was soon abandoned. Though the pulse power can be computed from average power if the pulse width, pulse shape and repetition rate are known, it soon became the practice to specify field performance requirements in terms of average power.

Thermistor Power Meters

A number of devices have been used for measuring average power in the microwave range. Those suitable for handling the small amounts of power normally involved in field tests include (1) thermistors, (2) platinum wire and (3) thermocouples. In each case the RF power to be measured is absorbed in the measuring element. The measurement consists in observing the resistance change in the thermistor or platinum wire, or the thermoelectric voltage from the thermocouple. By analogy with devices used for measuring minute quantities of radiant heat, either a thermistor or a platinum wire instrument is sometimes referred to as a bolometer. The platinum wire device has also been termed a barretter.

A thermistor for microwave power measurement is a tiny bead (about 5 mils in diameter) composed of a mixture of oxides of manganese, cobalt, nickel and copper, constituting a resistor with a very high negative temperature coefficient.[8]

The thermistor has a number of advantages for microwave work, namely: (1) resistance is highly sensitive to change of heating power, which obviates any need for amplification or a super-sensitive meter, and makes it possible to use a rugged d.c. meter; (2) reactance is low compared with RF resistance, which makes it possible to incorporate the thermistor in a power absorbing termination which matches the impedance of a microwave transmission line over a wide band; (3) resistance change is the same function of electrical heating power at any frequency, which permits direct comparison of the unknown microwave power with easily measurable d.c. power; (4) sensitivity

Digitized by Google
Original from UNIVERSITY OF MICHIGAN
Generated on 2019-09-24 06:26 GMT / http://hdl.handle.net/2027/mdp.39015077775156
Public Domain, Google-digitized / http://www.hathitrust.org/access_use#pd-google

to damage and burn-out is inherently low, and added protection results from impedance mismatch during overload. Because of these characteristics thermistors have been far more widely used than other detectors for microwave power measurement. Broad-band thermistor mounts have been designed to match both wave guide and coaxial transmission lines, the latter not only in the microwave range but also down to low frequencies. Some of the test sets specifically intended for power measurement or for combined power and frequency measurement are shown in Fig. 8.

The change in the thermistor resistance due to RF heating current is determined by placing the thermistor in one arm of a d.c. bridge. By noting the d.c. power necessary to balance the bridge with and without RF power in the thermistor, the magnitude of the RF power may be determined. For most purposes, however, a direct reading power meter is preferable. This can be obtained over a moderate range of power levels by employing an unbalanced bridge. The bridge is balanced for d.c. only and the measurement consists in noting the meter deflection when RF power is added.

The resistance of a thermistor is a highly sensitive function not only of electrical heating power but also of ambient temperature. For convenient field measurement, the effect of ambient temperature must be cancelled out in the indicator circuit so that the indication depends only on RF power.

Water Loads

A method which has been used in the laboratory and factory for measuring high-level microwave power consists in terminating the RF transmission line in a water load arranged as a continuous flow calorimeter. This method can be made quite accurate but is cumbersome. More recent practice is to terminate the RF line in a solid load of a type described later in this article, and to couple a thermistor power meter to the line by means of a directional coupler (described below) of known loss. Very close correlations have been obtained between the two methods over the entire microwave band.

Echo Boxes

A device unique to radar testing is a high Q resonant cavity, known as an "echo box" or "ring box." The cavity is coupled to the radar transmission line or antenna as indicated in Fig. 11. During the transmitted pulse, microwave energy is stored in the cavity. In the period immediately thereafter, energy is returned to the radar over the same path, producing a signal on the radar indicator. The energy in the cavity builds up exponentially to an amplitude dependent on the radar power. At the end of the pulse the returned energy decays exponentially, disappearing into the noise at a point determined by receiver sensitivity. The time interval between the

Digitized by Google
Original from UNIVERSITY OF MICHIGAN
Generated on 2019-09-24 06:26 GMT / http://hdl.handle.net/2027/mdp.39015077775156
Public Domain, Google-digitized / http://www.hathitrust.org/access_use#pd-google

end of the transmitted pulse and the point where the signal on the radar indicator disappears into the background noise, called the "ring time," therefore measures the over-all performance of the radar.

An echo box is a particularly useful instrument for radar testing because it measures over-all performance directly, because it permits a rapid tune-up, and because it utilizes the radar transmitter as its only source of power and therefore can be made extremely portable. Figure 12 shows typical ring-time patterns on different types of indicators. In actual practice the ring-time is read in miles on the radar range scale and hence is measured from

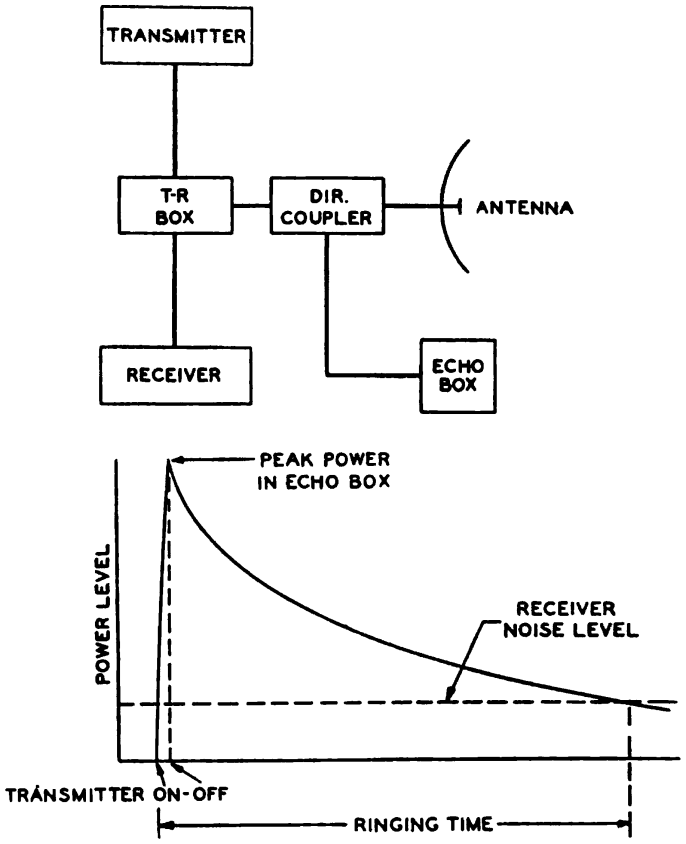

Fig. 11—Radar test with echo box.

the beginning of the transmitted pulse rather than the end. The difference is unimportant, however, since standard and limiting values of ringtime are established for operating conditions. It will be noted that the echo box does not return a true echo to the radar, so that the name "echo box" is not entirely appropriate.

Types and Uses

Echo boxes are of two general types, tuned and untuned. A tuned echo box is designed to resonate in a single mode adjustable over the operating

Digitized by Google
Original from UNIVERSITY OF MICHIGAN
Generated on 2019-09-24 06:27 GMT / http://hdl.handle.net/2027/mdp.39015077775156
Public Domain, Google-digitized / http://www.hathitrust.org/access_use#pd-google

frequency range. An untuned echo box is a fixed cavity of a size sufficient to support a very large number of modes within the working range. Tuned echo boxes are more versatile and more widely used than untuned boxes.

The most common type of tuned echo box is designed for hand tuning. While other shapes are possible, the most convenient one is a right cylinder whose length is adjusted by a movable piston. The $TE_{0,1,n}$ mode gives

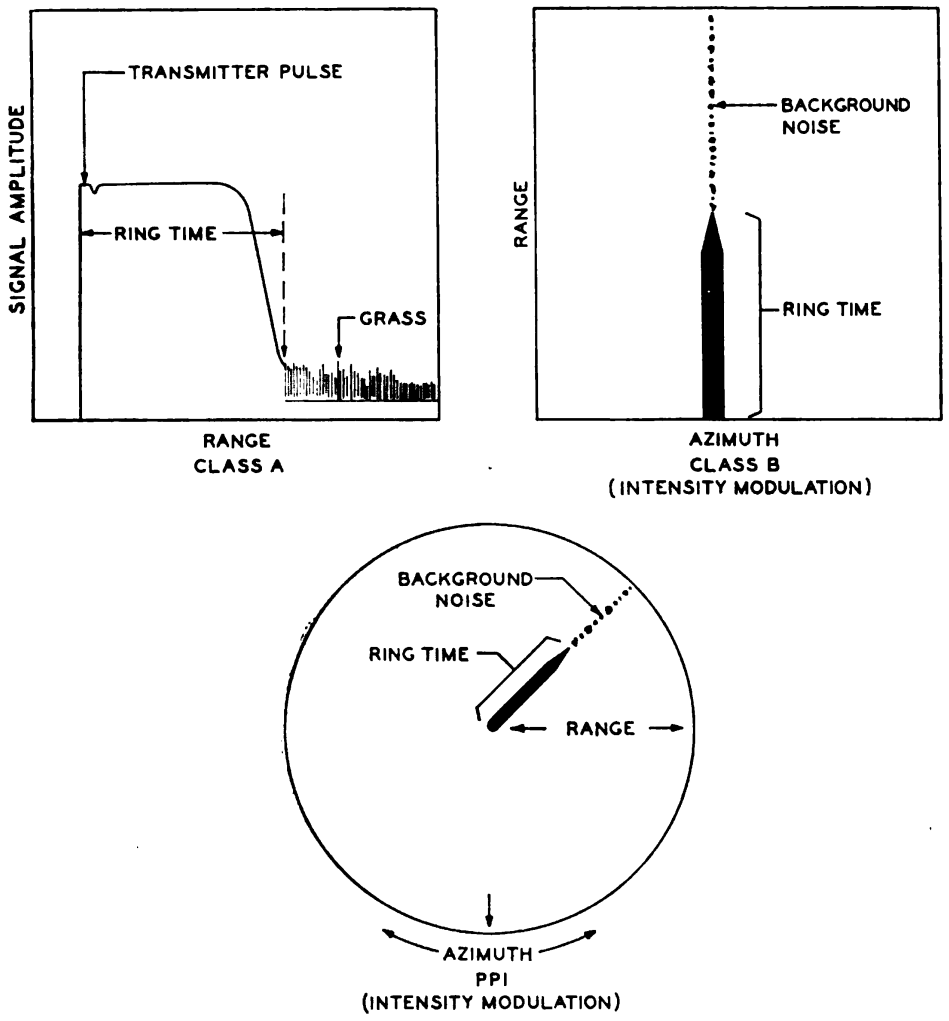

Fig. 12—Typical ringtime patterns on radar indicators.

maximum Q for a given volume and minimizes the number of unwanted modes present within the desired band. The value of n is determined by the desired value of Q (see formula 5). Unwanted modes can be partially avoided by choice of design parameters. However, for high values of Q, and especially for broad frequency bands, the suppression of unwanted modes involves design problems of the highest order.

Digitized by Google
Original from UNIVERSITY OF MICHIGAN
Generated on 2019-09-24 06:27 GMT / http://hdl.handle.net/2027/mdp.39015077775156
Public Domain, Google-digitized / http://www.hathitrust.org/access_use#pd-google

As indicated in Fig. 13, a tuned echo box cavity is usually provided with two couplings. One of these is to the radar pick-up; the other to an attenuating device, crystal rectifier, and meter, which serve for tuning the cavity and for other purposes. With such an instrument, not only can the radar be tuned up and its over-all performance determined, but many other tests can be made, to wit: (1) the setting of the plunger at resonance indicates the transmitter frequency or wavelength; (2) calibration of the crystal affords a rough measure of output power; (3) since the Q required for adequate ringtime is so high that the cavity selects only a narrow segment of the transmitter spectrum, a spectrum analysis can be made by plotting frequency versus crystal current reading; (4) slow recovery of TR box and receiver after the transmitted pulse can be detected by noting the behavior of the ringtime pattern at short ranges as the echo box is detuned; (5)

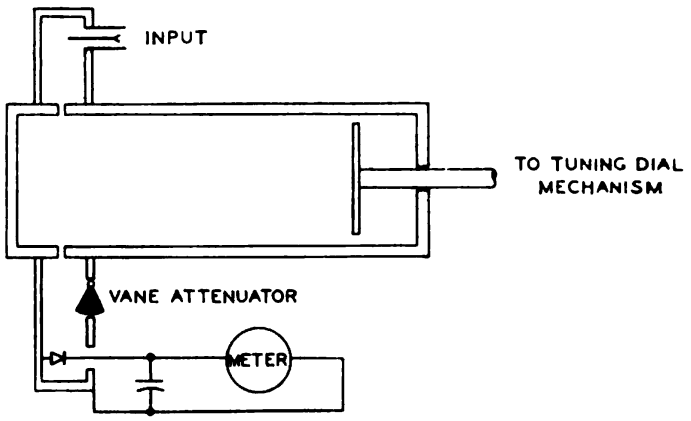

Fig. 13—Functional schematic of tuned echo box.

inability of the receiver to recover promptly after a strong signal (the result of imperfect d.c. reinsertion in the video amplifier or of overloading of the I.F. amplifier) is indicated by a blank following the end of the ring; (6) improper pulsing (e.g. double moding or misfiring) can be determined with a class A oscilloscope; (7) the frequency and power of the local oscillator can be measured. In tuned echo boxes, requirements for extreme fineness of tuning control and precise resettability have given rise to interesting problems in the design of the mechanical drive and indicating mechanism.

In another type of echo box, hand tuning is supplemented by motor-driven tuning or so-called "wobbling" over a frequency range wide enough to embrace expected variations in transmitter frequency. Operation is controlled by a single push-button which energizes the motor and actuates the cavity coupling. Such an instrument may be permanently installed in a plane and used to check the radar during flight.

Generated on 2019-09-24 06:27 GMT / http://hdl.handle.net/2027/mdp.39015077775156
Public Domain, Google-digitized / http://www.hathitrust.org/access_use#pd-google
Digitized by Google
Original from UNIVERSITY OF MICHIGAN

For an untuned or multi-resonant echo box, rectangular shape is convenient. The box should be large enough to make it highly probable that over the operating band one or more modes will be present within any frequency interval of width equal to the main concentration of the transmitter spectrum. For a given rectangular volume a cube gives the largest number of modes. The total number of modes up to a frequency of wave length λ is

$$N_M = 8.38\ V/\lambda_0^3 \tag{8}$$

where V is the volume. However, because of the cubical shape many different modes tend to coincide in wavelength, a condition referred to as

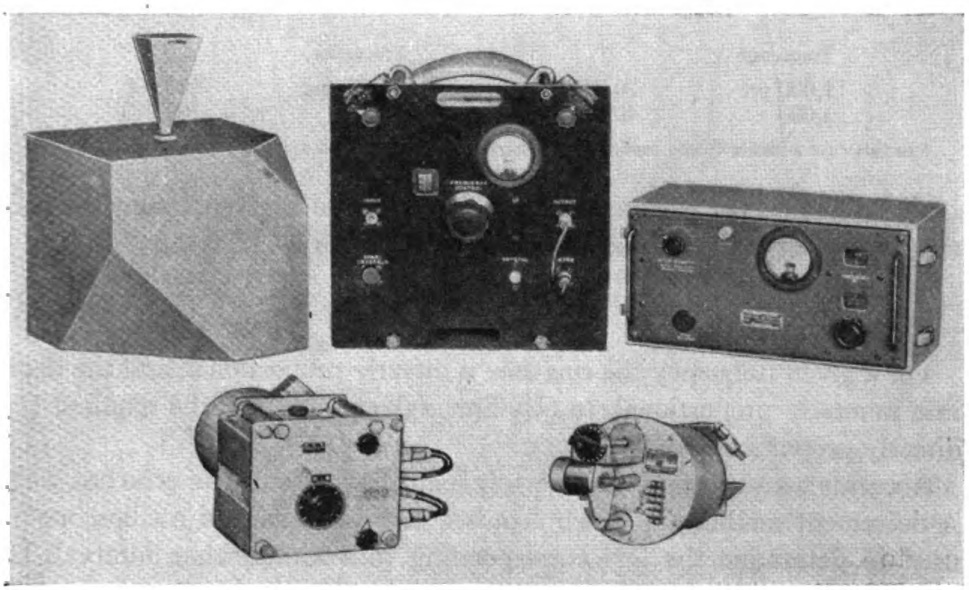

Fig. 14—A group of echo boxes of various types.

degeneracy. To spread out the modes, the box is made slightly off cube and one or more corners sliced off. At the longer microwaves the size of box is determined by the number of modes, and the size becomes quite awkward. For the shorter microwaves the size is determined by the required value of Q. Hence the use of untuned echo boxes has been limited to the frequency range from about 9000 mc upwards with sizes of the order of 12 to 24 inches on a side. Even with an extraordinarily high probability of finding modes within the radar band, substantial differences in response are found for relatively small changes in frequency. Accordingly untuned echo boxes are more useful for rough tune-up than for precise measurement.

A number of specific designs of echo boxes for different microwave bands are shown in Fig. 14.

Generated on 2019-09-24 06:27 GMT / http://hdl.handle.net/2027/mdp.39015077775156
Public Domain, Google-digitized / http://www.hathitrust.org/access_use#pd-google
Digitized by Google
Original from UNIVERSITY OF MICHIGAN

Q and Ring Time

For satisfactory measurement the ringtime must extend beyond nearby echoes which would obscure the test signal. For most radars a ringtime of 20 to 30 microseconds (about 2 to 3 miles) has been found satisfactory although considerably higher values have sometimes been provided. Even apart from echoes, a long ringtime is desirable since this gives a lower decay rate and a more sensitive measurement.

Computation will show that an extremely high value of Q is necessary to obtain the desired ringtime. For maximum ringtime the cavity coupling should be such as to make the working Q (Q_L) about 90 per cent of the non-loaded Q. Values of working Q which have been provided in different frequency ranges are approximately as follows:

Frequency	Q_L	Frequency	Q_L
1,000 mc	70,000*	10,000 mc	100,000
3,000	40,000	24,000	200,000

* In this case a higher Q was needed for a long range ground search system.

The difference in performance corresponding to a given change in ringtime can be determined from the decay rate which is

$$d = 27.3 f/Q_L \ db/\text{microsecond} \tag{9}$$

For a given frequency the ringtime is directly proportional, and the decay rate inversely proportional, to Q. For a given ringtime, the required Q is directly proportional to frequency.

Accurate measurement of extremely high Q's is essential in echo box work. A decrement method, in which a pulsed RF oscillator and oscilloscope are used to determine the loss corresponding to a known time interval, has proved most satisfactory.

Spectrum Analysis

The frequency components of a non-repetitive rectangular d-c. pulse may be determined by well known methods using Fourier integral analysis. The envelope of amplitudes is of the form $(\sin x)/x$ where $x = \pi fT$. This envelope is shown by the right-hand side of the curve of Fig. 15a, f_0 being assumed to represent zero frequency. The first zero occurs at the frequency $f = 1/T$.

Similarly the envelope of the spectrum of a rectangular a-c. pulse is given by the complete curve of Fig. 15a, f_0 in this case being the carrier frequency. For a non-repetitive pulse all frequencies are present in amplitude as shown by the envelope. When a stable carrier frequency is pulsed at uniform intervals and in precise phase relation, only harmonics of the repetition

Generated on 2019-09-24 06:27 GMT / http://hdl.handle.net/2027/mdp.39015077775156
Public Domain, Google-digitized / http://www.hathitrust.org/access_use#pd-google
Digitized by Google
Original from UNIVERSITY OF MICHIGAN

frequency are present under the envelope. In radar practice conditions are, as a rule, not sufficiently stable for this to occur.

Because of its bandwidth, an echo box cannot reproduce the ideal spectrum envelope of Fig. 15a. Instead the curve for a good spectrum may resemble that of Fig. 15b, while spectrum irregularities detrimental to radar performance may be revealed by curves such as those of Fig. 15c and 15d. Broadening of the spectrum is undesirable because less energy falls within the receiver band. Energy removed from the main concentration may result from double moding or from the occurrence of a different frequency during the rise or fall of the pulse. Frequency modulation due to a sloping

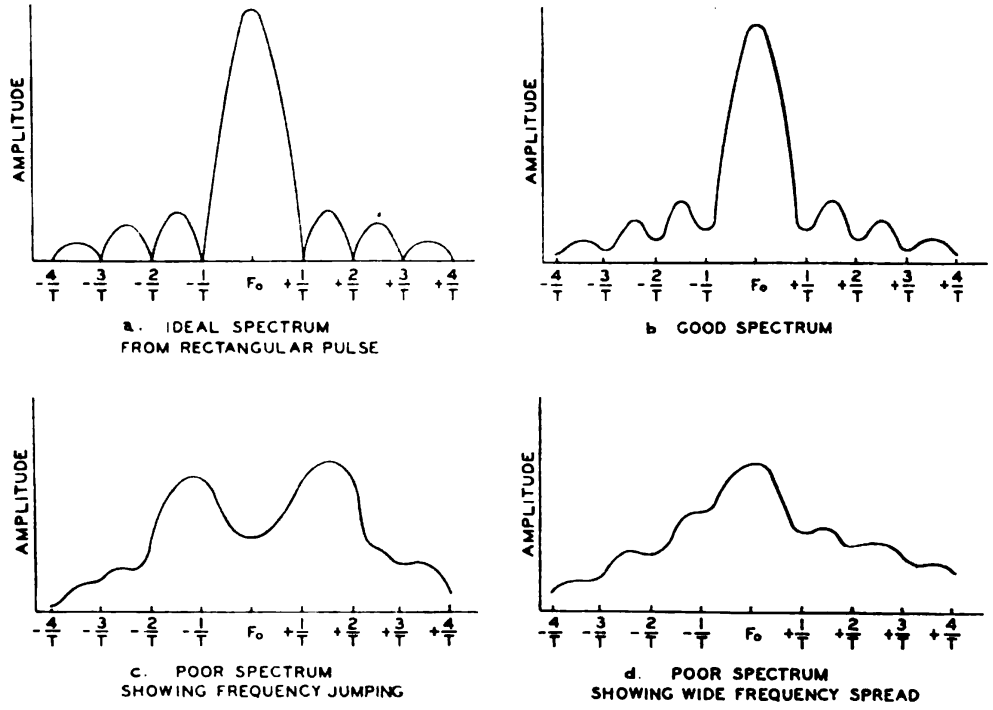
AMPLITUDE
a. IDEAL SPECTRUM FROM RECTANGULAR PULSE
b GOOD SPECTRUM
c. POOR SPECTRUM SHOWING FREQUENCY JUMPING
d. POOR SPECTRUM SHOWING WIDE FREQUENCY SPREAD

Fig. 15—Radar spectrum analysis with echo box.

or spiked input pulse produces a non-symmetrical spectrum, not infrequently characterized by a high side lobe. Frequency jump in the middle of the pulse, due to line reflection, may produce two distinct maxima.

Another device widely used for this purpose is the "Spectrum Analyzer" as developed by Radiation Laboratory, which provides an oscilloscope presentation of spectrum component amplitudes versus frequency.

Standing Wave Measurements

Theory

The expression for the distribution of current or voltage along a misterminated line of appreciable electrical length yields two terms which

Digitized by Google
Original from UNIVERSITY OF MICHIGAN
Generated on 2019-09-24 06:27 GMT / http://hdl.handle.net/2027/mdp.39015077775156
Public Domain, Google-digitized / http://www.hathitrust.org/access_use#pd-google

may be considered as representing two waves transmitted in opposite directions, one (the incident wave) from the generator toward the load, the other (the reflected wave) from the load toward the generator. The summation is a standing wave pattern. The standing wave ratio (SWR) is defined as the ratio of the wave amplitude at a maximum point (anti-node) to that at a minimum point (node). If the standing wave ratio is stated as a number it is necessary to specify whether it applies to voltage (VSWR) or power (PSWR). Possibility of ambiguity is avoided by stating the ratio in db.

The ratio of the reflected current to the incident current is the *reflection coefficient*, here designated as ρ. The value of the reflection coefficient is given both in magnitude and phase by

$$\rho = \frac{Z_0 - Z}{Z_0 + Z} \qquad (10)$$

where Z_0 is the characteristic impedance of the line and Z is the load impedance. The reflection coefficient is related to the standing wave ratio as follows:

$$VSWR = \sigma = \frac{1 + \rho}{1 - \rho}, \quad \text{or,} \quad \rho = \frac{\sigma - 1}{\sigma + 1} \qquad (11)$$

Plots of the relationships are shown in Fig. 16.

The reduction of radiated power due to reflection losses in a radar transmission line, while important, is usually less serious than other effects of impedance irregularities. Since the load impedance reacts on the oscillator circuit, the frequency and output of most transmitter tubes are quite sensitive to load impedance. If the line is electrically long, so that its impedance varies rapidly with frequency, marked instability of oscillator frequency may occur, a condition referred to as "long line effect."

Since radar transmission lines contain many potential sources of impedance discontinuity, including not only the antenna but a variety of couplings, bends, wobble joints, rotating joints, switches, etc., measurements of standing wave ratio are frequently required. The need for such measurements depends in part on whether the line is "preplumbed" or is provided with field adjustments.

Devices

Standing waves may be detected and measured by several different types of devices, including (1) a slotted line, (2) a squeeze section, (3) a directional coupler and (4) a hybrid T. All of these furnish information on the magnitude of the standing wave ratio. In some cases phase information may be obtained also, which permits determination of impedance,[9] but this knowledge, while useful in the laboratory, is seldom required in field work.

Generated on 2019-09-24 06:28 GMT / http://hdl.handle.net/2027/mdp.39015077775156
Public Domain, Google-digitized / http://www.hathitrust.org/access_use#pd-google
Digitized by Google
Original from UNIVERSITY OF MICHIGAN

A block diagram of an arrangement employing a slotted line for measuring standing waves is shown in Fig. 17. The oscillator source is commonly followed by a pad or attenuator to prevent frequency pulling. The slotted section may be either a coaxial or a wave guide line employing a mode which is not disturbed by the presence of the slot (e.g. normal coaxial mode; $TE_{1,0}$ in rectangular wave guide; $TM_{0,1}$ in round wave guide). A traveling pick-up probe or loop projects through the slot and couples energy from the line into a detector which delivers d-c. or audio-frequency to the indicator. The

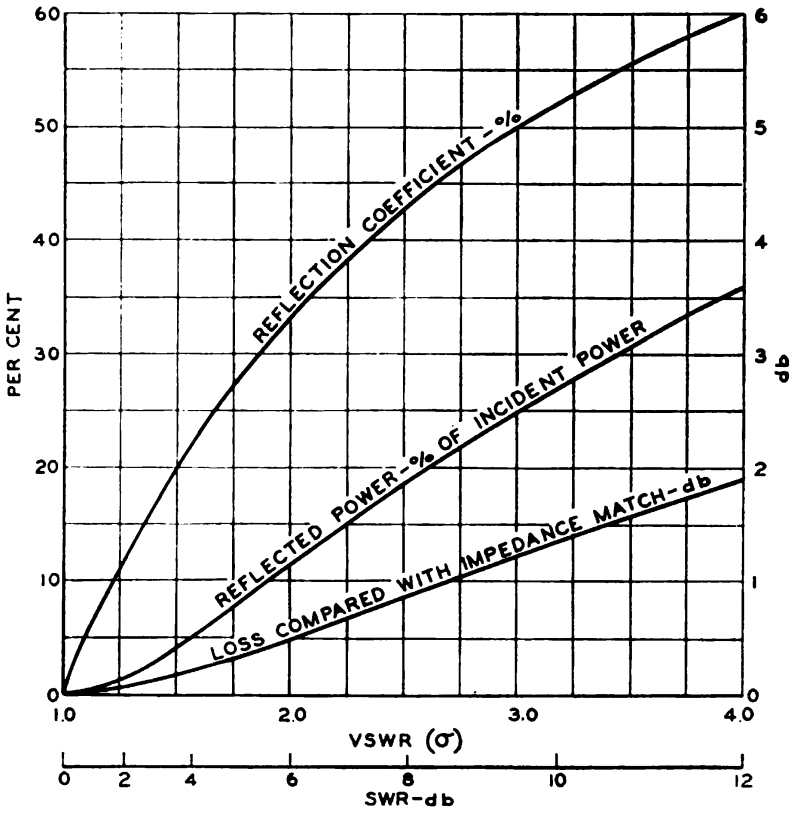

Fig. 16—Relations in mismatched transmission lines.

probe is moved longitudinally to find points of maximum and minimum field strength. To avoid distortion of the field within the line, the probe should be small and should project only a short distance inside the slot. For accurate results extreme care must be exercised in design and construction to avoid variation in depth of immersion as the probe is moved. Several slotted lines employed for standing wave measurements are shown in Fig. 18.

A squeeze section consists of a section of rectangular guide with slots milled in the center of both broad faces so that the width of the guide can be varied by external deforming means. This changes the wave length in

Digitized by Google
Original from UNIVERSITY OF MICHIGAN
Generated on 2019-09-24 06:28 GMT / http://hdl.handle.net/2027/mdp.39015077775156
Public Domain, Google-digitized / http://www.hathitrust.org/access_use#pd-google

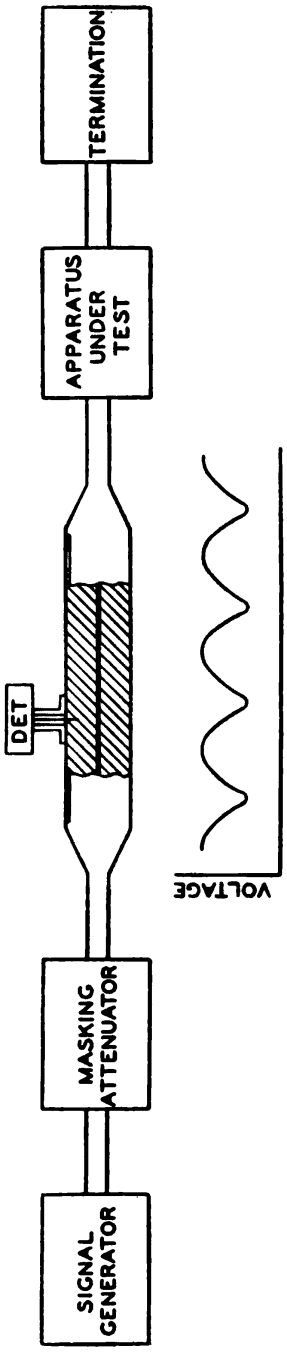

Fig. 17—Standing wave measurement.

Digitized by Google
Original from UNIVERSITY OF MICHIGAN
Generated on 2019-09-24 06:28 GMT / http://hdl.handle.net/2027/mdp.39015077775156
Public Domain, Google-digitized / http://www.hathitrust.org/access_use#pd-google

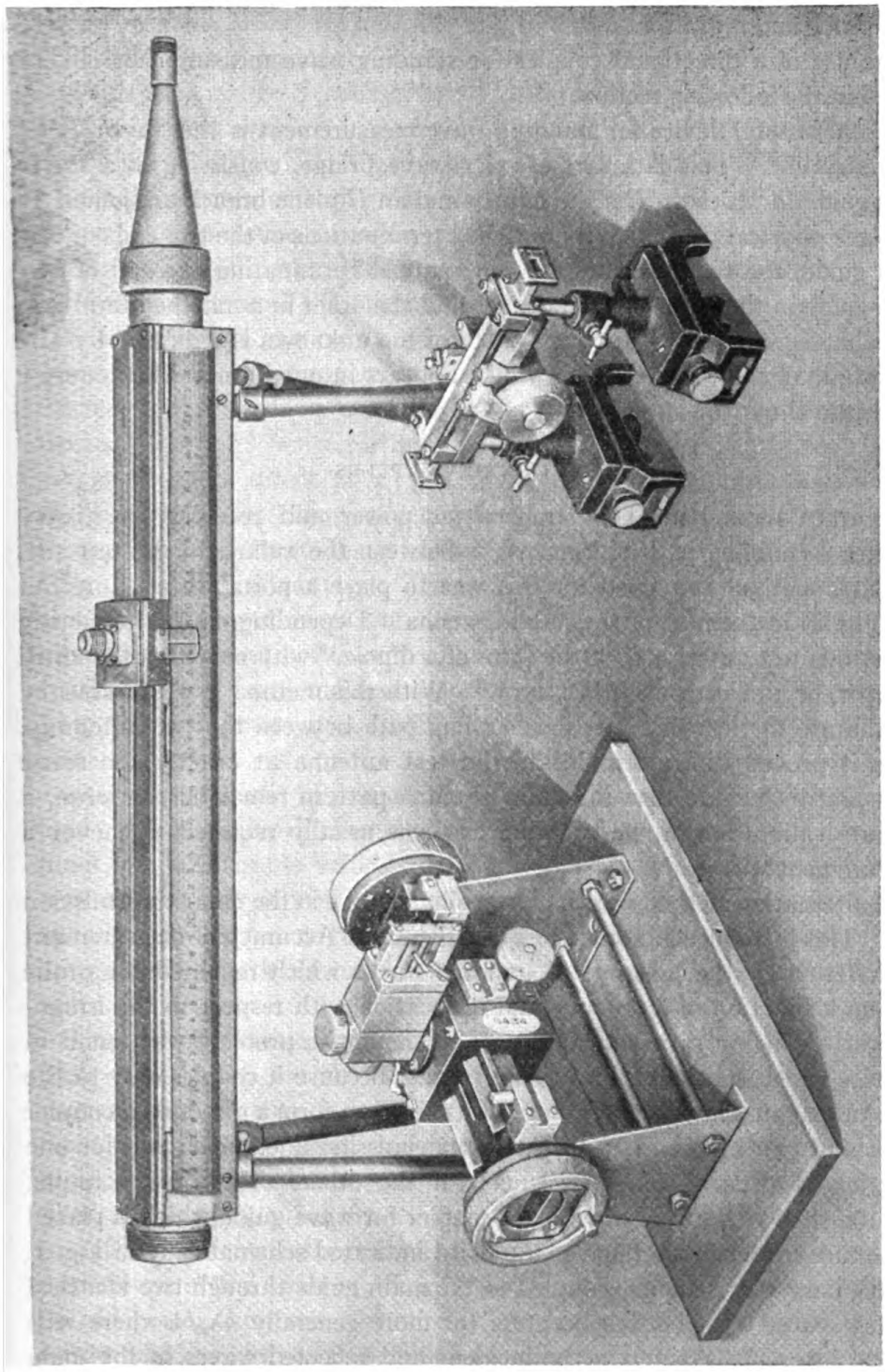

Fig. 18—Standing wave detectors used on coaxial and wave guide transmission lines.

Digitized by Google
Original from UNIVERSITY OF MICHIGAN
Generated on 2019-09-24 06:28 GMT / http://hdl.handle.net/2027/mdp.39015077775156
Public Domain, Google-digitized / http://www.hathitrust.org/access_use#pd-google

the guide, so that maximum and minimum values may be determined by a fixed probe and indicator.

The use of a directional coupler for standing wave measurement is discussed in the following section.

Another useful device for standing wave measurement is the "hybrid T" or "magic T". This is a sort of microwave bridge, consisting of a main wave guide to which an *E* plane branch and an *H* plane branch are joined in the same physical plane. With matched terminations of the two ends of the main guide, the two branches are conjugate. Terminating one end of the main guide in the unknown impedance and the other in a matched termination, the degree of impedance mismatch of the unknown is indicated by the magnitude of the reflected wave which appears in one branch when energy is fed into the other.

Directional Couplers

Accurate measurement of transmitter power and receiver sensitivity requires a coupling path of known loss between the radar and the test set. The first method employed for this was to place a portable test antenna (see Fig. 2) in the field of the radar antenna. Depending on the frequency range, this test antenna took the form of a dipole,[10] with or without a small reflector, or an electromagnetic horn.[11] With this method it was necessary to calibrate the loss of the space coupling path between the two antennas. Since it proved difficult to locate the test antenna at exactly the same point and to be sure that the main antenna pattern remained the same, a separate calibration of the coupling loss was usually required whenever a measurement was made.

An alternative method was to place a single probe in the radar transmission line. This introduced another sort of difficulty. Accuracy of measurement was vitiated by the presence of standing waves which rendered the probe pick-up a function of frequency and of location with respect to the irregularities. A highly satisfactory answer to the entire problem was found in a device which is called a directional coupler because it couples only to the wave propagated in one direction. In its simplest form a directional coupler consists of two couplings to the main transmission line, which add for one direction of transmission and cancel for the other. Thus, for example, Fig. 10a shows a form of directional coupler for wave guide which is placed in the radar transmission line at the point indicated schematically in Fig. 1. An auxiliary wave guide is coupled to the main guide through two identical orifices spaced $\lambda_g/4$ between centers (or more generally $n\lambda_g/4$ where n is an odd integer). Assuming the incident and reflected waves in the main guide to be directed as shown, and the auxiliary guide to be terminated on

Digitized by Google
Original from UNIVERSITY OF MICHIGAN
Generated on 2019-09-24 06:29 GMT / http://hdl.handle.net/2027/mdp.39015077775156
Public Domain, Google-digitized / http://www.hathitrust.org/access_use#pd-google

one end, a test circuit connected to the other end will be coupled to the incident wave, while theoretically the two couplings to the reflected wave will differ by $\lambda/2$ and therefore cancel one another.

With such a device measurements may be made of the characteristics of the incident wave independently of reflections. If the coupling to the main line is not too close there is no appreciable effect on the incident wave, and continuous monitoring can be had. Conversely, test signals applied through the directional coupler will travel in the main guide in the proper direction for testing the radar receiver.

If the locations of the termination and the test connection point in Fig. 19a are reversed, the couplings to the main transmission line are also reversed. Such an arrangement therefore permits measurement of the reflected power which in turn makes it possible to adjust for minimum reflected power and hence for minimum SWR. Comparison of the reflected power with the direct power determines the SWR. For convenience in measurement, two directional couplers pointed in opposite directions are frequently used, the combination being referred to as a bi-directional coupler (Fig. 19b). One advantage of this arrangement is that the ability to measure the reflected power from the antenna and that part of transmission line beyond the coupler provides means for detecting trouble in that part of the system. Directional couplers may be applied to any type of transmission line. Figure 19c shows a simple form of directional coupler for a coaxial line.

One characteristic of importance in a directional coupler is the coupling loss. A small value of coupling loss affords increased sensitivity of measurement, while a sizable value is desirable to minimize reaction on the main transmission line as well as for other reasons. A loss of around 20 db has usually been found a good compromise. It is now the practice to incorporate a directional coupler in every radar to obtain a test connection point.

Due to unavoidable imperfections, a directional coupler never gives complete cancellation for the undesired direction of transmission. The departure from ideality is indicated by the directivity (also referred to as front-to-back ratio) which is defined as the scalar ratio of the two powers measured at the test connection point when the same amount of power is applied to the main guide, first in one direction and then in the other. For measurements of the direct wave and of receiver characteristics, a moderate directivity, of the order of 15 db or better, is sufficient. In measuring reflected power, however, the directivity determines the amount of direct power which appears at the point of measurement and therefore controls accuracy. The chart of Fig. 20 will facilitate determination of the maximum

Digitized by Google
Original from UNIVERSITY OF MICHIGAN
Generated on 2019-09-24 06:29 GMT / http://hdl.handle.net/2027/mdp.39015077775156
Public Domain, Google-digitized / http://www.hathitrust.org/access_use#pd-google

Generated on 2019-09-24 06:29 GMT / http://hdl.handle.net/2027/mdp.39015077775156
Public Domain, Google-digitized / http://www.hathitrust.org/access_use#pd-google

Digitized by Google

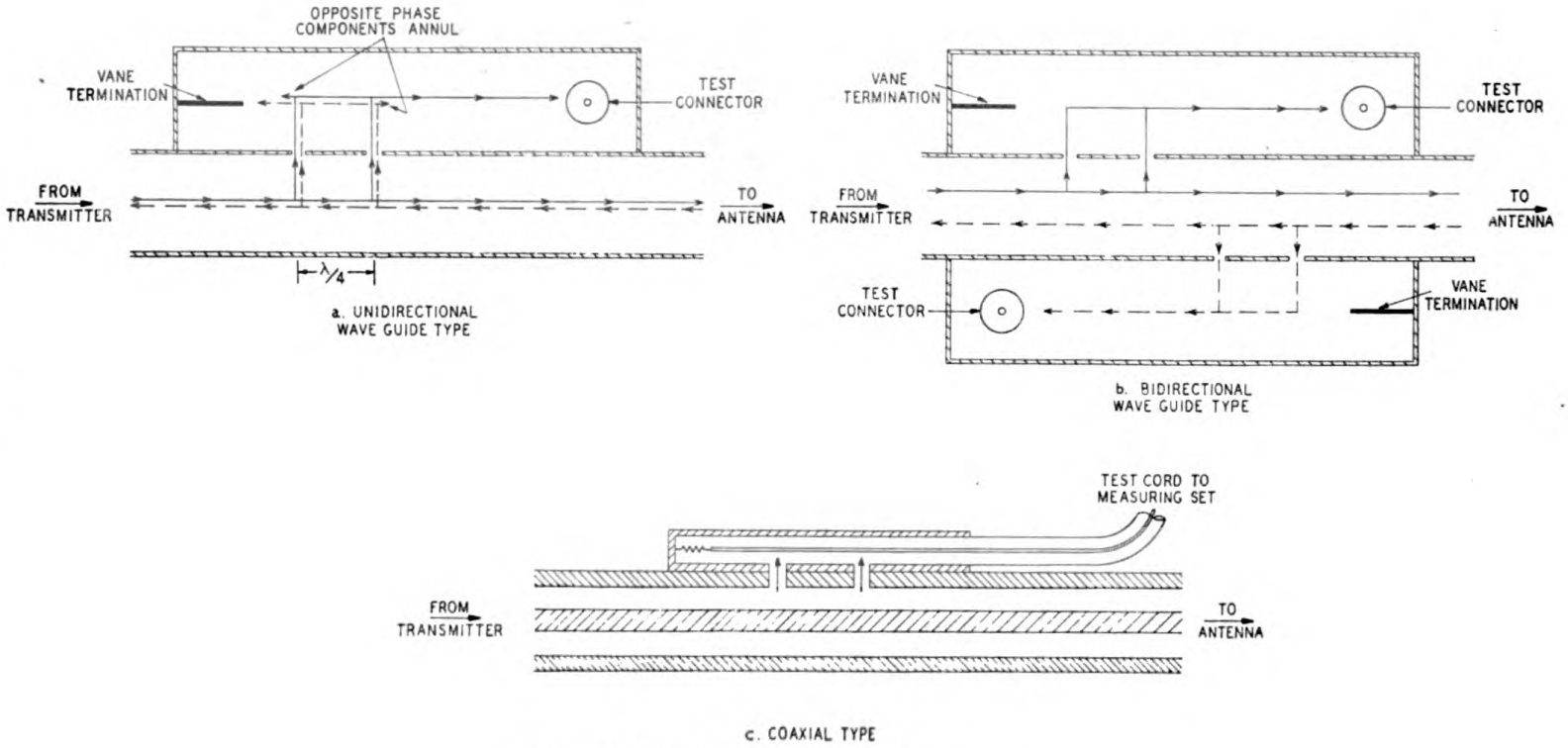

Fig. 19—Directional coupler arrangements.

Original from UNIVERSITY OF MICHIGAN

error that may occur in measuring different values of SWR with various assumed directivities.

With a simple two-hole coupler, the directivity deteriorates rapidly as the frequency departs from that corresponding to quarter-wave spacing.

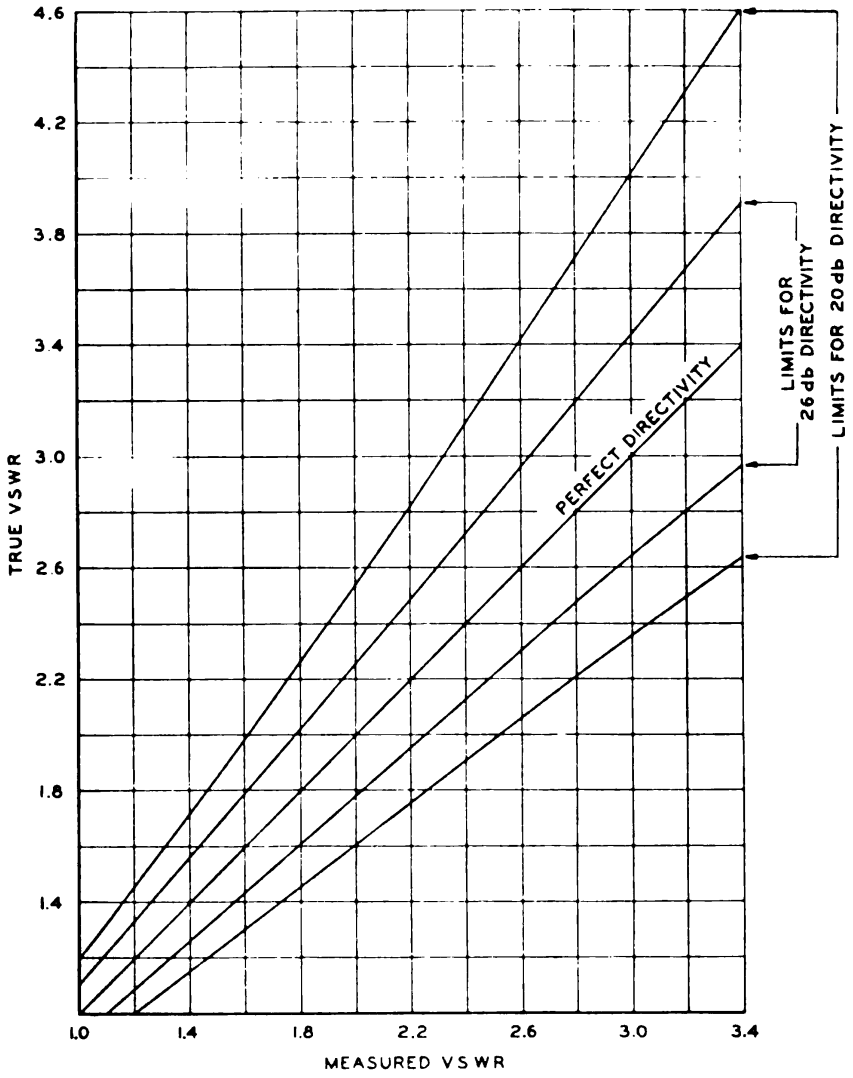

Fig. 20—Error in standing wave measurements caused by directivity of directional coupler.

By providing additional couplings suitably spaced, the residuals from different sets of couplings can also be cancelled against one another and the directivity versus frequency characteristic can be materially broadened. With multiple hole couplings a minimum directivity of 26 to 30 db over a frequency band of 10 to 20% is readily practicable in quantity production,

Generated on 2019-09-24 06:29 GMT / http://hdl.handle.net/2027/mdp.39015077775156
Public Domain, Google-digitized / http://www.hathitrust.org/access_use#pd-google
Digitized by Google
Original from UNIVERSITY OF MICHIGAN

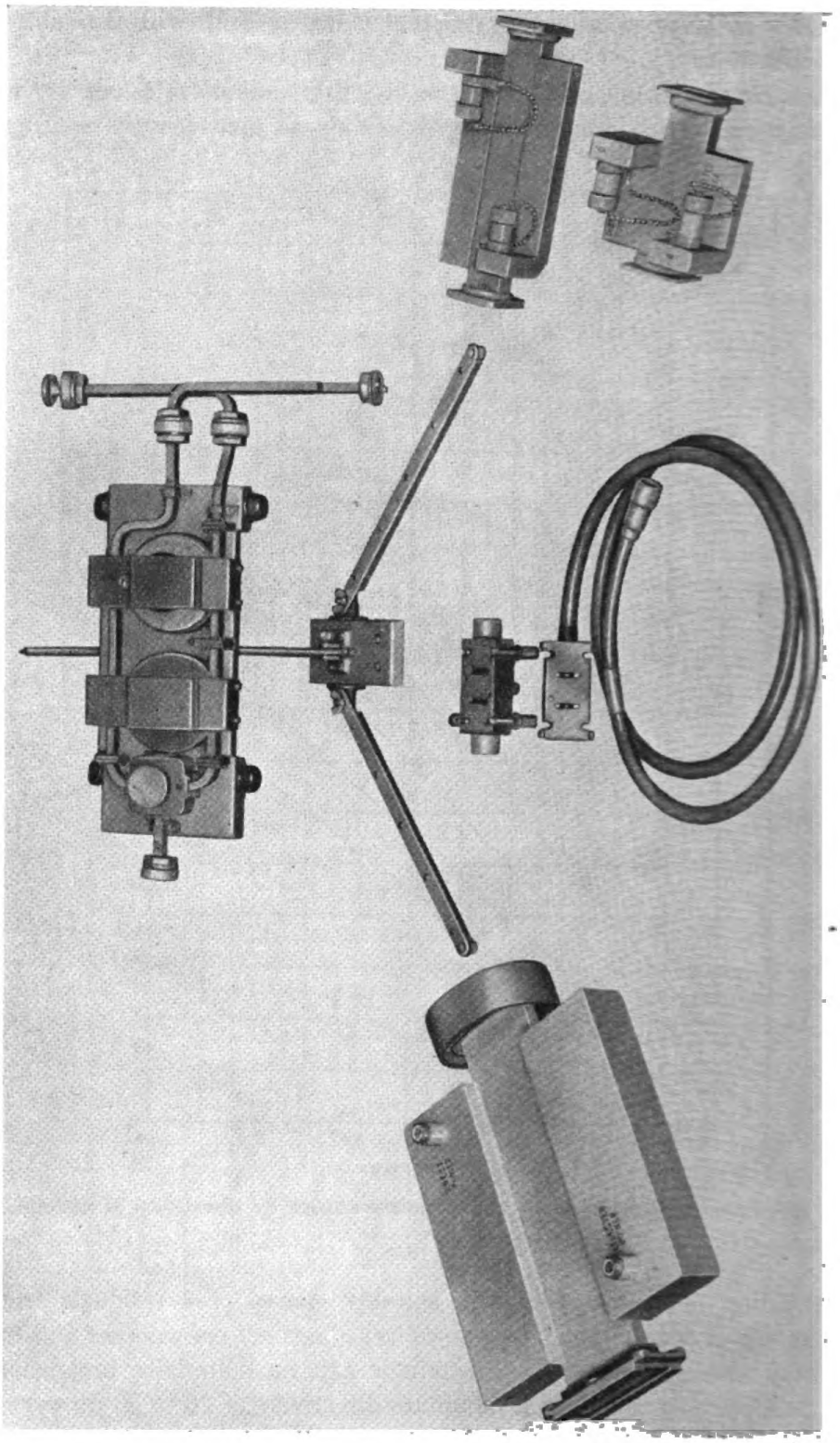

Fig. 21. A group of microwave directional couplers together with a directional coupler test set.

Digitized by Google
Original from UNIVERSITY OF MICHIGAN
Generated on 2019-09-24 06:29 GMT / http://hdl.handle.net/2027/mdp.39015077775156
Public Domain, Google-digitized / http://www.hathitrust.org/access_use#pd-google

and much better values are obtained in the laboratory. Some of the numerous designs of directional couplers developed for association with operating radars are shown in Fig. 21.

Because they are more convenient than slotted lines and can be made more accurate, directional couplers have been extensively used for SWR measurement in the laboratory. A number of special arrangements have been devised to improve both accuracy and convenience. A directional coupler arrangement which has been provided for field measurement of SWR in the vicinity of 25,000 mc is also illustrated in Fig. 21. In this the direct power is brought to equality with the reflected power by an attenuator whose dial is calibrated directly in SWR. A wave guide switch facilitates the power comparison.

Auxiliaries and Components

RF Loads

An RF load (or dummy antenna) which will absorb the radar power in an impedance which matches the transmission line is very useful in radar work. Such a device permits testing the radar in operating condition without actual radiation which might give information to the enemy or interfere with other radars. It also makes it possible to test the radar in locations where reflections from the ground or nearby objects would otherwise hamper or prevent a test. RF loads for microwave work usually consist of a section of transmission line (either coaxial or wave guide, depending on wavelength) containing a high-loss dielectric. The impedance of such a load is necessarily low and must be matched to the radar line by tapering the dielectric over a distance of several wave lengths.[10] Moreover, if the line is to handle high power, tapering over a considerable length is necessary to distribute the heat.

A coaxial load is preferably tapered from outer conductor to inner conductor, since this both reduces the voltage gradient and facilitates heat dissipation. A dielectric consisting of a mixture of bakelite, silica and graphite, molded in place, has been found satisfactory. For wave guides a ceramic containing carbon may be preformed, with taper in one or two dimensions, and cemented in place.

Figure 22 shows a number of RF loads developed for different frequency bands. One of these, TS-235/UP, provides an excellent impedance match over the frequency range from 500 mc to above 3,000 mc. When equipped with a blower designed for uniform transverse ventilation, it will handle a peak power of the order of 750 kw with a duty cycle of about .001.

Microwave Attenuators and Pads

RF attenuators and pads are cornerstones of microwave testing. Attenuators are used to adjust unknown signals to levels suitable for measure-

Digitized by Google
Original from UNIVERSITY OF MICHIGAN
Generated on 2019-09-24 06:30 GMT / http://hdl.handle.net/2027/mdp.39015077775156
Public Domain, Google-digitized / http://www.hathitrust.org/access_use#pd-google

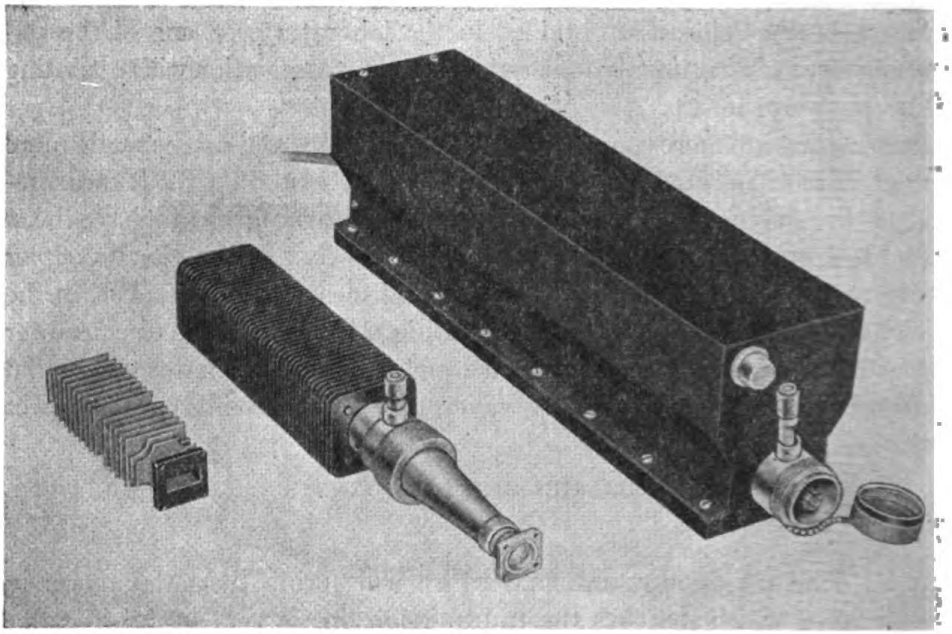

Fig. 22—RF loads for different bands in the microwave frequency range.

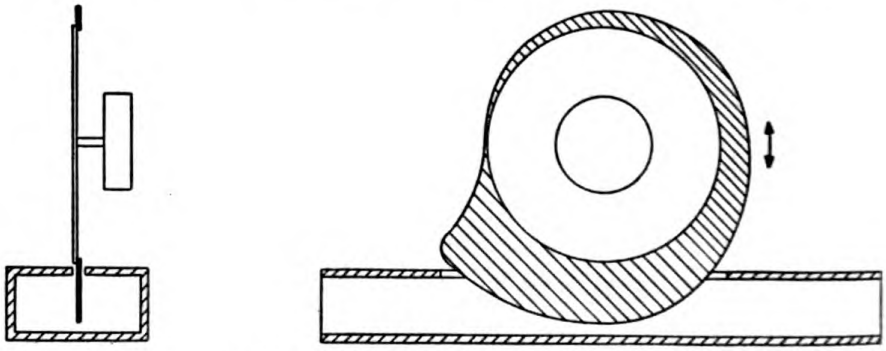

a. STRIP MOVING VERTICALLY IN GUIDE

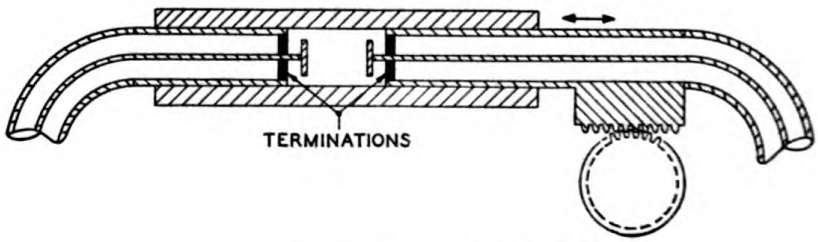

b. WAVE GUIDE BELOW CUTOFF

Fig. 23—Microwave attenuators.

ment and to obtain the minute test signals required for measuring receiver characteristics. Pads serve to change levels and to prevent interaction

Digitized by Google
Original from UNIVERSITY OF MICHIGAN
Generated on 2019-09-24 06:30 GMT / http://hdl.handle.net/2027/mdp.39015077775156
Public Domain, Google-digitized / http://www.hathitrust.org/access_use#pd-google

between testing components. Microwave attenuators and pads are of two general types (a) those which employ dissipative elements to absorb power and (b) non-dissipative devices which introduce propagation or coupling loss.

For the shorter microwaves the most convenient form of attenuator is of the dissipative type, employing a strip or vane of dielectric coated with a resistance material, as for example, carbon-coated bakelite. This is placed in rectangular wave guide with its plane paralleling the side of the guide. The attenuation is varied by varying the depth to which the vane is inserted in the guide (Fig. 23a) or by changing its position in the guide. A valuable feature of such attenuators is that the minimum loss can be made substantially zero. For good impedance match the strip must be tapered. By using two strips the over-all length of the attenuator can be reduced. Extremely satisfactory attenuators of this type covering a frequency range of 8 to 12%, with loss variable from 0 to 35 or 40 db, have been obtained in the frequency range 4,000 to 24,000 mc.

For the longer microwaves, where wave guides are inconveniently large, attenuators of the wave guide-below-cutoff type are very useful. These consist of a section of round wave guide whose diameter is small compared with wavelength and whose length is adjusted by telescoping (see Fig. 23b). The $TM_{0,1}$ mode has been found very satisfactory, and $TE_{1,1}$ has also been used. Connection is made to the attenuator by a coaxial circuit at each end, with disk excitation for the $TM_{0,1}$ mode and loop coupling for $TE_{1,1}$. The attenuation formulas are:[12]

$$TM_{0,1}. \qquad A = \frac{41.8}{D}\sqrt{1 - \left(\frac{1.31D}{\lambda}\right)^2}\ db/\text{meter} \tag{12}$$

$$TE_{1,1}. \qquad A = \frac{32.0}{D}\sqrt{1 - \left(\frac{1.71D}{\lambda}\right)^2}\ db/\text{meter} \tag{13}$$

where D = diameter of wave guide in meters. Because of the effect of other modes when the coupling is close, a minimum loss of 20 to 30 db is required before the attenuation becomes linear with displacement. The attenuation differentials are substantially independent of frequency. Attenuators of this type present a large impedance mismatch at either end, the effect of which may be alleviated by padding or by a termination.

Types of pads employed in microwave work include the following:

(1) Flexible coaxial cable, usually with high resistance inner conductor.
(2) Coaxial π with carbon coated rod and discs.
(3) Coaxial with carbon coated rod as inner conductor.
(4) Resistance strip in wave guide.
(5) Directional coupler.

Digitized by Google
Original from UNIVERSITY OF MICHIGAN
Generated on 2019-09-24 06:30 GMT / http://hdl.handle.net/2027/mdp.39015077775156
Public Domain, Google-digitized / http://www.hathitrust.org/access_use#pd-google

In calibrating microwave attenuators and pads, comparison with an accurately calibrated IF attenuator, using a heterodyne test set, has been found to give excellent results.

RF Cables and Connectors

Flexible RF cables for connecting test equipment to equipment under test are an important adjunct of field testing. At frequencies of 10,000 mc and below, flexible coaxial cables of about .4″ over-all diameter with solid or stranded inner conductor, solid low-loss dielectric (polyethylene) and braided outer conductor have been used satisfactorily, although in the upper part of this range special measures have been necessary to prevent attenuation change due to flexure and aging. Over most of this range coaxial jack and plug connections have been found satisfactory but wave guide connectors are preferable at the upper end. In the range above 10,000 mc, coaxial

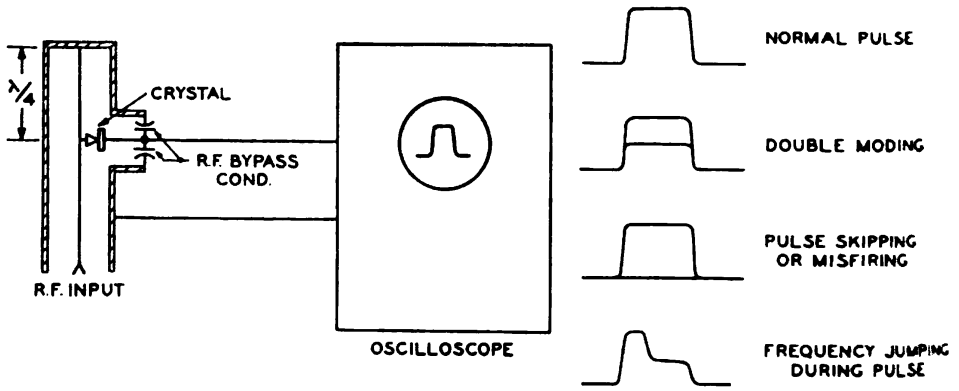

Fig. 24—Radar pulse envelopes.

cables of requisite stability have not yet been obtained and rubber covered wave guide with soldered articulated joints is the best form of flexible cable now available.

Oscilloscopes

Oscilloscopes are used extensively in radar maintenance (a) for examination of video waves and (b) for viewing RF envelopes. Satisfactory radar performance depends on a variety of video wave shapes which may include trapezoidal or triangular pulses, sawtooth waves, square waves or combinations of these. Observation of these wave shapes, supplemented if necessary by measurements of amplitude and duration, helps in diagnosing many troubles.

Examination of the envelope of the RF pulse is a convenient but less informative alternative to spectrum analysis. The envelope should be a clean, single trace of good shape. Figure 24 shows traces sometimes experi-

Generated on 2019-09-24 06:30 GMT / http://hdl.handle.net/2027/mdp.39015077775156
Public Domain, Google-digitized / http://www.hathitrust.org/access_use#pd-google
Digitized by Google
Original from UNIVERSITY OF MICHIGAN

enced. Double moding, i.e., oscillating at different frequencies on different pulses, is shown by a double trace. Frequency jumping during a pulse is shown by a break in the envelope. Misfiring gives a base line under the envelope. Other abnormalities in the RF envelope may result from incorrect video wave shape. Observation of the RF envelope requires a rectifier, usually a crystal, together with a suitable video amplifier. Since limitation of the scope to video functions permits general application to radars of all frequencies, the rectifier is generally provided externally.

The oscilloscopes available before the war did not meet the requirements of radar. Fast sweeps were necessary to permit viewing of pulses ranging from several microseconds to a fraction of a microsecond. Amplifiers were required for such pulses with low phase and amplitude distortion over a broad frequency band. Existing methods of synchronizing and phasing sweeps were also inadequate. The progress of the oscilloscope art during the war is illustrated in the successive designs of field test oscilloscopes shown in Fig. 25.

The BC910A oscilloscope, gotten out as a "stop gap" not long after the attack on Pearl Harbor, incorporates fast sweeps and broad-band amplification. Following close upon this was the BC1087A (Navy code CW60AAY) which replaced sine wave synchronization by a start-stop sweep triggered by the incoming pulses. This feature made it possible to superpose the erratic pulses produced by spark wheel and similar pulsers and at the same time avoided external synchronizing connections. A valuable feature conjoined with the start-stop sweep was a delay network in the main transmission path which gave the sweep time to start before the pulse reached the cathode-ray tube. This oscilloscope in original and modified form has seen wide service in all theaters. However, its weight of more than 60 pounds was a handicap for many uses.

Further advances in oscilloscope circuitry and in weight limitation resulted in TS-34/AP, weighing only 25 pounds. This combined the short pulse features of the previous design with those of the conventional oscilloscope for viewing slower waves. A schematic diagram is shown in Fig. 26. A redesign, coded as TS-34A/AP, incorporated variable start-stop sweeps and improved mechanical design. These two oscilloscopes, TS-34 and TS-34A, were produced to a total of some 12,000 and universally used by all branches of the service for both radar and radio testing. Toward the end of the war the trend toward shorter pulses, coupled with the need for precise measurement of wave amplitude and duration, led to a new design, TS-239/UP, which embodied wide advances over TS-34A in performance and versatility but with an increase in weight.

In association with different oscilloscopes, other video devices have been

Digitized by Google
Original from UNIVERSITY OF MICHIGAN
Generated on 2019-09-24 06:30 GMT / http://hdl.handle.net/2027/mdp.39015077775156
Public Domain, Google-digitized / http://www.hathitrust.org/access_use#pd-google

Generated on 2019-09-24 06:31 GMT / http://hdl.handle.net/2027/mdp.39015077775156
Public Domain, Google-digitized / http://www.hathitrust.org/access_use#pd-google

Digitized by Google

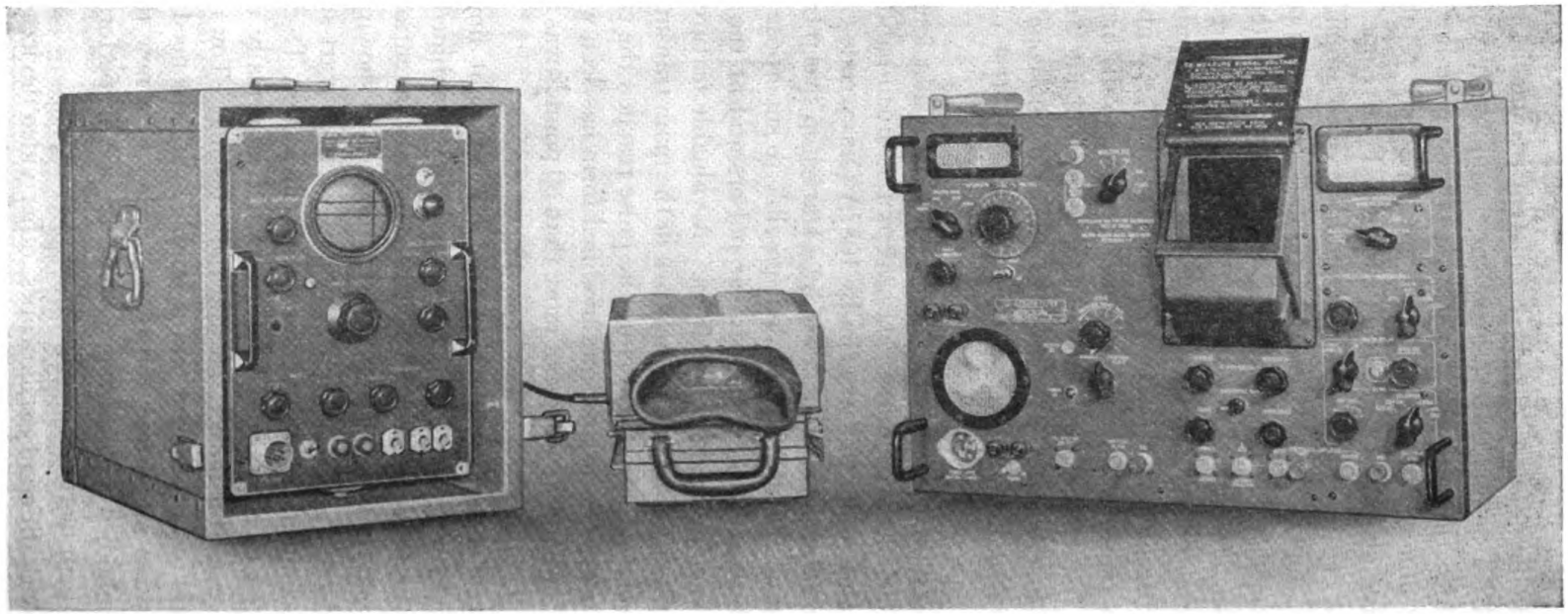

Fig. 25—Test oscilloscopes for viewing wave forms in radars. Left to right: BC-910-A (1942), TS-34A/AP (1944) and TS-239/Up (1945).

Original from UNIVERSITY OF MICHIGAN

employed. The amplitude of pulse applied to the magnetron is thousands of volts. To derive a voltage suitable for application to the oscilloscope, a voltage divider of the condenser type is used (TS-89/AP). Suitable video terminations, dividers, and loads, sometimes of high voltage and power capacity, are required to obtain proper test conditions and provide convenient test points (TS-98/AP, TS-390/TPM-4, TS-90/AP, TS-234/UP). Originally a high-impedance connection to the oscilloscope was effected by a single-stage amplifier unit (BC1167A), but a simple divider type of probe was later found more satisfactory for this purpose.

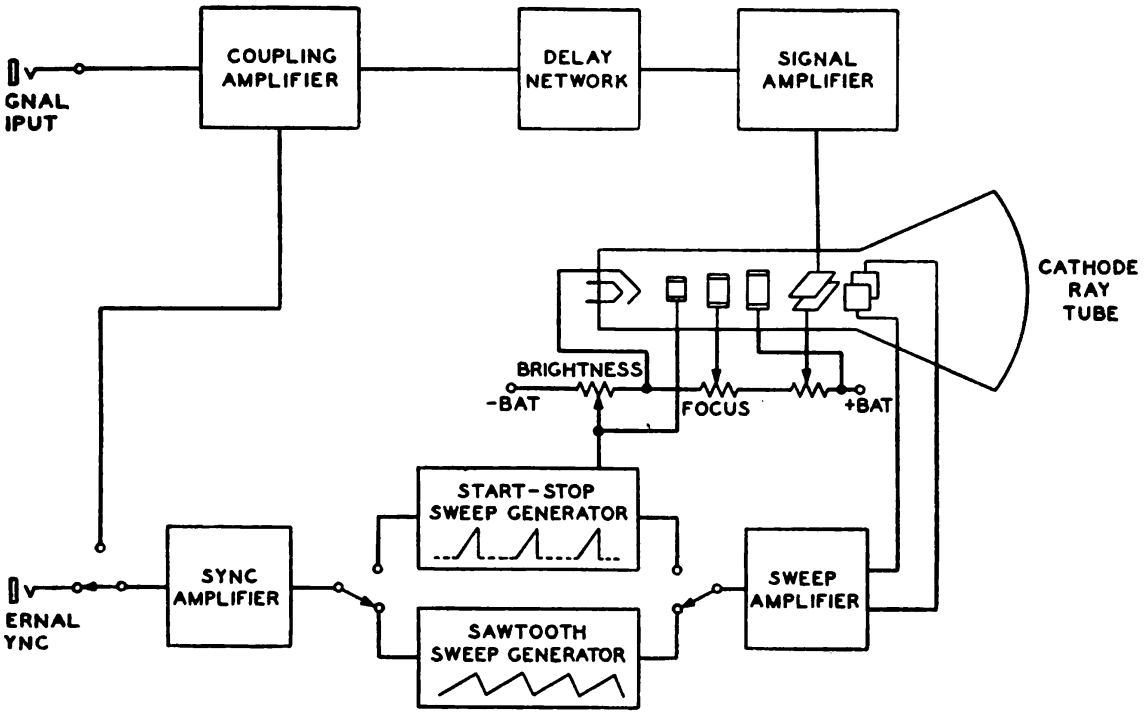

Fig. 26—Block diagram of TS-34/AP and TS-34A/AP oscilloscopes.

Range Calibration

Types of timing circuits used for radar range determination include (a) multi-vibrators, (b) coil and condenser oscillators (generally without but sometimes with temperature control) and occasionally (c) quartz crystal oscillators. The first two depend for their accuracy on condensers, resistances, coils and other elements which are subject to error due to aging, temperature, humidity, mechanical damage and the like. Nor is the quartz crystal oscillator wholly immune to error. Consequently, portable range calibrators are required for field maintenance.

Generated on 2019-09-24 06:31 GMT / http://hdl.handle.net/2027/mdp.39015077775156
Public Domain, Google-digitized / http://www.hathitrust.org/access_use#pd-google
Digitized by Google
Original from UNIVERSITY OF MICHIGAN

TS-102A/AP (Fig. 27) and its predecessors TS-102 and TS-19 are precision calibrators which have been extensively used for checking a large

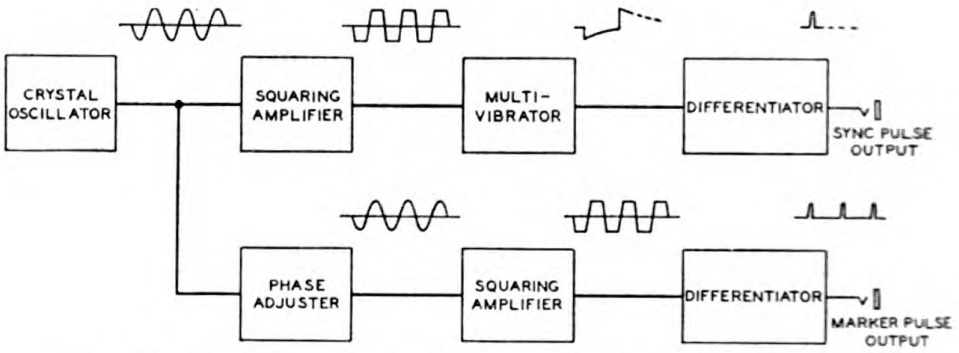

Fig. 27—Block diagram of TS-102/AP and TS-102A/AP range calibrators.

Fig. 28—Two test sets for checking the computers used in bombsight and fire control radars.

number of different airborne bombing and gunlaying radars and shipborne fire control and search radars. These sets deliver accurately spaced marker

Digitized by Google
Original from UNIVERSITY OF MICHIGAN
Generated on 2019-09-24 06:31 GMT / http://hdl.handle.net/2027/mdp.39015077775156
Public Domain, Google-digitized / http://www.hathitrust.org/access_use#pd-google

pulses, derived from a quartz crystal oscillator, for checking the radar range pulses. A trigger pulse derived from a multi-vibrator synchronized with the quartz oscillator is also provided for actuating the radar timing circuits. With certain radars the calibration procedure requires an oscilloscope as well. Extreme stability of marker pulses, better than $\pm.02$ microsecond, is obtained. A stop watch is included in these sets for checking rate of change in range.

Less precision is required in range calibration of search radars. For this purpose the TS-5/AP calibrator provides marker pulses of $\frac{1}{4}$, 1, 5 or 10 nautical or statute miles, derived from a coil and condenser oscillator with closely controlled temperature coefficients. This calibrator is designed to be triggered by the radar or some other external source.

Computer Test Sets, Etc.

A number of radars are equipped with computers which receive the data on location of target and its direction and rate of change, together with essential related information on such factors as wind velocity, ground speed, altitude, etc., and deliver the solution of the ballistic problem in the form of a voltage which releases bombs, points the guns or serves other purposes. Means for checking the accuracy of these computing devices are generally required. The type of test set needed depends upon the computer design, which has taken different forms according to the nature of the problem and the state of the art.

Two types of computer test set are shown in Fig. 28. TS-158/AP, designed for use with certain airborne bombing radars, furnishes to the computer a signal representing a target approaching at known speed and checks the accuracy of bomb release. TS-434/UP, designed for several airborne and ground radars, is an accurate instrument for determining the voltage ratios at various points in a computer and thus checking its performance.

Conclusion

More than 200 different designs of test sets were developed during the war by Bell Laboratories to meet the exacting requirements of radar field maintenance. These differed radically from previous art. Outstanding features were portability, precision and generality of application. The large number of designs is due partly to the varied functions of radar and to the varied conditions of use. Largely, however, it results from the fact that the frequency band that can be handled in any one set is limited, whereas many frequency ranges and subranges had to be covered in all.

Altogether more than 75,000 radar test sets were manufactured by Western Electric Company and these were used in all theatres of war by the

Generated on 2019-09-24 06:31 GMT / http://hdl.handle.net/2027/mdp.39015077775156
Public Domain, Google-digitized / http://www.hathitrust.org/access_use#pd-google
Digitized by Google
Original from UNIVERSITY OF MICHIGAN

United Nations forces. The production rate at the end of the war exceeded 5,000 test sets a month. In numerous cases, moreover, small preproduction quantities of test equipment were built on a "crash" basis for special missions and for training purposes. The test equipment produced for the field had to be more precise than the radars, and the equipment used in the factory and laboratory to test the field test equipment had to be still more precise.

Trends of development at war's end were toward (a) further broad-banding, simplification and precising, and (b) coverage of new frequency ranges.

References

(1) "Ultra-High Frequency Techniques," by J. G. Brainard, G. Koehler, H. J. Reich, and L. F. Woodruff, D. Van Nostrand, 1942.
(2) "Reflex Oscillators," by J. R. Pierce. See pp 488 ff.
(3) "The Lighthouse Tube," by E. D. McArthur and E. F. Peterson, *Proceedings of National Electronics Conference*, Vol. I, 1944, p. 38.
(4) "Electromagnetic Waves," by S. A. Schelkunoff, D. Van Nostrand, 1943.
(5) "The Proportioning of Shielded Circuits," by E. I. Green, F. A. Leibe and H. E Curtis, *Bell System Technical Journal*, Vol. 15, April 1936, p. 248.
(6) "Resonant Lines in Radio Circuits," by F. E. Terman, *Electrical Engineering*, Vol. 53, July 1934, p. 1046.
(7) "Ultra-Short-Wave Transmission Phenomena," by C. R. Englund, H. T. Crawford and W. W. Mumford, *Bell System Technical Journal*, Vol. 14, July 1935, p. 369.
(8) "Thermistors in Electronic Circuits," by R. R. Batcher, *Electronic Industries*, Vol. 4, Jan. 1945, p. 76.
(9) "An Impedance Transmission Line Calculator," by P. H. Smith, *Electronics*, Jan. 1944.
(10) "Microwave Transmission," by J. C. Slater, McGraw-Hill, 1942.
(11) "Theory of the Electromagnetic Horn," by W. L. Barrow and L. J. Chu, *Proc. I.R.E.*, Vol. 27, Jan. 1939, p. 51.
(12) "Attenuation of Electromagnetic Fields in Pipes Smaller Than Critical Size," by E. G. Lindner, *Proc. I.R.E.*, Vol. 30, Dec. 1942, p. 554.

Generated on 2019-09-24 06:31 GMT / http://hdl.handle.net/2027/mdp.39015077775156
Public Domain, Google-digitized / http://www.hathitrust.org/access_use#pd-google
Digitized by Google
Original from UNIVERSITY OF MICHIGAN

High Q Resonant Cavities for Microwave Testing

By I. G. WILSON, C. W. SCHRAMM and J. P. KINZER

Formulas and charts are given which aid the design of right circular cylinder cavity resonators operating in the $TE\ 01n$ mode, which yields the highest Q for a given volume. The application of these to the design of an echo box radar test set is shown, and practical considerations arising in the construction of a tunable cavity are discussed.

Introduction

A TUNABLE high Q resonant cavity is a particularly useful tool for determining the over-all performance of a radar quickly and easily[1].* Further, since it uses the radar transmitter as its only source of power, it can be made quite portable. When a high Q cavity is provided with two couplings, one for the radar pickup and the other to an attenuating device, crystal rectifier and meter which serve for tuning the cavity not only can an indication of over-all performance be obtained but other useful information as well. For example, the transmitter frequency can be measured; calibration of the crystal affords a rough measure of the transmitter power; and an analysis of the spectrum can be made by plotting frequency versus crystal current. This information is of particular importance in radar maintenance.

The Q required for this purpose is quite high, comparable to that obtained from quartz crystals in the video range. For this reason, such cavities have many additional possibilities for use in microwave testing equipment and microwave systems. For example, they may form component parts of a narrow band filter, or be used as discriminators for an oscillator frequency control.

Resonant cavities are of two general types—tuned and untuned. A tuned cavity is designed to resonate in a single mode adjustable over the radar frequency range. An untuned cavity is of a size sufficient to support a very large number of modes within the working range. Both are useful, but the tuned variety can give more information about the radar and hence has been more widely used.

While a tuned cavity may be a cylinder, parallelepiped or sphere (or even other shapes), the first of these has been most thoroughly explored by us. It offers the possibility of utilizing the anomalous circular mode, described by Southworth[2] in his work on wave guides, which permits the attainment of high Q's in quite a small size. In addition, it is easier to construct a variable length cylinder than a variable sized sphere.

* Superscripts refer to bibliography.

Digitized by Google
Original from UNIVERSITY OF MICHIGAN
Generated on 2019-09-24 06:34 GMT / http://hdl.handle.net/2027/mdp.39015077775156
Public Domain, Google-digitized / http://www.hathitrust.org/access_use#pd-google

Due to their interesting properties the history of resonators of the cavity type in which a dielectric space is enclosed by a conducting material, goes back many years. In 1893 J. J. Thompson[3] derived expressions for resonant frequencies of the transverse electric modes in a cylinder. Lord Rayleigh[4] published a paper in 1897 dealing with such resonant modes. The early work was almost entirely theoretical but some experiments were carried out in 1902 by Becker[5] at 5 and 10 centimeters. In recent years, the subject has been fairly thoroughly investigated (at least theoretically) for several simple shapes.

However, many of the presentations are highly mathematical with considerable space devoted to proofs; the results which would be most useful to an engineer are thus sometimes obscured. The purpose of this paper is to present certain engineering results together with information upon the application of the tunable cylindrical cavity to radar testing.

Definitions and Fundamental Formulas

Modes

By fundamental and general considerations, every cavity resonator, regardless of its shape, has a series of resonant frequencies, infinite in number and more closely spaced as the frequency increases. The total number N of these having a resonant frequency less than f is given approximately by:[4]

$$N = \frac{8\pi}{3c^3} Vf^3 \tag{1}$$

in which

V = volume of cavity in cubic meters.
c = velocity of electromagnetic waves in the dielectric in meters per second.
f = frequency in cycles per second.

With each resonance there is associated a particular standing wave pattern of the electromagnetic fields, which is identified by the term "mode."

In right cylinders (ends perpendicular to axis) the modes fall naturally into two groups, the transverse electric (TE) and the transverse magnetic (TM). In the TE modes, the electric lines everywhere lie in planes perpendicular to the cylinder axis, and in the TM modes, the magnetic lines so lie. Further identification of a specific mode is accomplished by the use of indices.

The MS Factor

With the cylinder further restricted to a loss-free dielectric and a nonmagnetic surface, there is associated with each mode a value of Q (quality factor)[7] which depends on the conductivity of the metallic surface, on the

Digitized by Google
Original from UNIVERSITY OF MICHIGAN
Generated on 2019-09-24 06:34 GMT / http://hdl.handle.net/2027/mdp.39015077775156
Public Domain, Google-digitized / http://www.hathitrust.org/access_use#pd-google

frequency and on the shape of the cylinder, e.g. whether it is circular or elliptical, and whether it is slender or stubby. The quantity $\frac{Q\delta}{\lambda}$, however, depends only upon the mode and shape of the cylinder and has been referred to as the mode-shape (MS) factor. In this formula, δ refers to skin depth as customarily defined[8], and λ is wavelength in the dielectric, as given by $\lambda = \frac{c}{f}$; both δ and λ are in meters.

Fundamental Formulas

Expressions for standing wave patterns and $Q\frac{\delta}{\lambda}$ are given in Table I, for right rectangular, circular and full coaxial cylinders*. The table is virtually self-explanatory, but a few remarks on mode designation are needed. The mode indices are l, m, n following the notation of Barrow and Mieher.[9] In the rectangular prism they denote the number of half-wavelengths along the coordinate axes. For the other two cases they have an analagous physical significance with l related to the angular coordinate, m to the radial and n to the axial.

In the elliptical cylinder, a further index is needed to distinguish between modes which differ only in their orientation with respect to the major and minor axes; these paired modes are termed even and odd, and have slightly different resonant frequencies.[10] In the circular cylinder they have the same frequency, a condition which is referred to as a degeneracy (in this case, double); that is, in the circular cylinder, odd and even modes are distinguishable only by a difference in their orientation within the cylinder with reference to the origin of the angular coordinate. In Table I, the field expressions are given for the even modes; those for the odd modes are obtained by changing $\cos l\theta$ to $\sin l\theta$ and $\sin l\theta$ to $\cos l\theta$ everywhere.

The value of N in the table is based on counting this degeneracy as a single mode; counting even and odd modes as distinct will nearly double the value of N, thus bringing it into agreement with the general equation (1). The distinction between even and odd modes is of limited importance in practical applications, and will not be further mentioned.

In Table I, the *mks* system of units is implied. The notation is in general accordance with that used in prior developments of the subject. For engineering applications, it is advantageous to reduce the results to units in ordinary use and to change the notation wherever this leads to a more obvious association of ideas. For these reasons, in what follows attention

* The elliptic cylinder (closely allied to the circular cylinder of which it is a generalization) is omitted as the necessary functions are not widely known or easily available.

Digitized by Google
Original from UNIVERSITY OF MICHIGAN
Generated on 2019-09-24 06:34 GMT / http://hdl.handle.net/2027/mdp.39015077775156
Public Domain, Google-digitized / http://www.hathitrust.org/access_use#pd-google

is confined to the circular cylinder, with changes in units and notation as specified later.

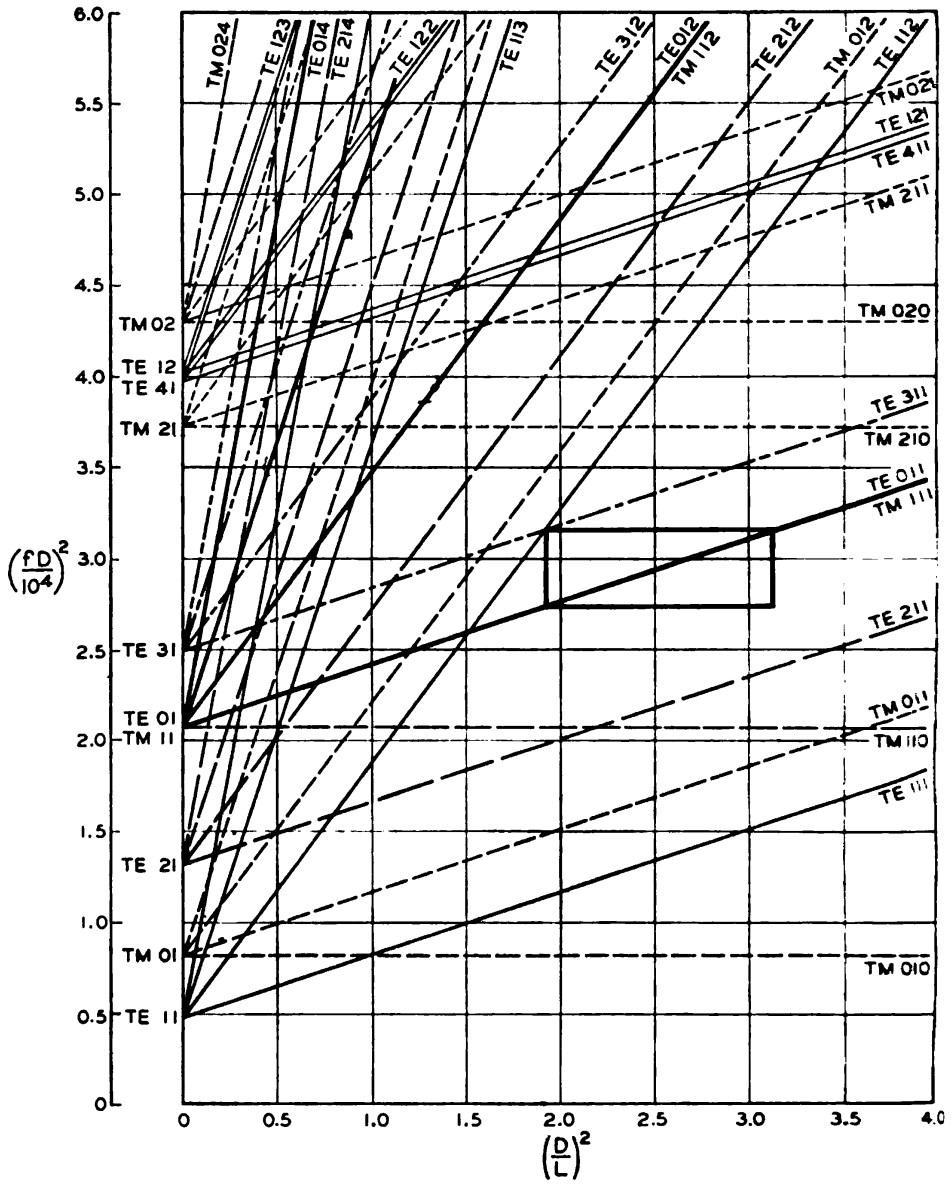

Fig. 1—Mode chart for right circular cylinder resonant cavity.

The Mode Chart

The formula relating the resonant frequency to the mode, shape and dimensions of the cylinder is of prime interest. It may be simply written as

$$(fD)^2 = A + Bn^2\left(\frac{D}{L}\right)^2$$

Digitized by Google
Original from UNIVERSITY OF MICHIGAN
Generated on 2019-09-24 06:35 GMT / http://hdl.handle.net/2027/mdp.39015077775156
Public Domain, Google-digitized / http://www.hathitrust.org/access_use#pd-google

TYPE OF CAVITY & CO-ORDINATE SYSTEM	MODE	FIELD EQUATIONS *	DEFI
RECTANGULAR PRISM 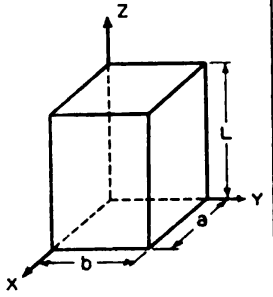	TM	$E_x = \sqrt{\frac{\mu}{\epsilon}}\frac{k_1k_3}{k^2}\cos k_1x \sin k_2y \sin k_3z$ $E_y = \sqrt{\frac{\mu}{\epsilon}}\frac{k_2k_3}{k^2}\sin k_1x \cos k_2y \sin k_3z$ $E_z = -\sqrt{\frac{\mu}{\epsilon}}\frac{k_1^2+k_2^2}{k^2}\sin k_1x \sin k_2y \cos k_3z$ $H_x = -\frac{k_2}{k}\sin k_1x \cos k_2y \cos k_3z$ $H_y = \frac{k_1}{k}\cos k_1x \sin k_2y \cos k_3z$ $H_z = 0$	$k_1 = \frac{\ell\pi}{a}$ k_2: $k^2 = k_1^2+k_2^2+k$ ℓ,m,n = INT IDENTIFYING 1 ASSUME THE JECT TO RES IN ADJOINING
	TE	$E_x = -\sqrt{\frac{\mu}{\epsilon}}\frac{k_2}{k}\cos k_1x \sin k_2y \sin k_3z$ $E_y = \sqrt{\frac{\mu}{\epsilon}}\frac{k_1}{k}\sin k_1x \cos k_2y \sin k_3z$ $E_z = 0$ $H_x = \frac{k_1k_3}{k^2}\sin k_1x \cos k_2y \cos k_3z$ $H_y = \frac{k_2k_3}{k^2}\cos k_1x \sin k_2y \cos k_3z$ $H_z = -\frac{k_1^2+k_2^2}{k^2}\cos k_1x \cos k_2y \sin k_3z$	
CIRCULAR CYLINDER 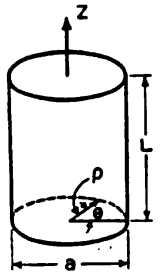	TM	$E_\rho = -\sqrt{\frac{\mu}{\epsilon}}\frac{k_3}{k}J'_\ell(k_1\rho)\cos\ell\theta \sin k_3z$ $E_\theta = \sqrt{\frac{\mu}{\epsilon}}\ell\frac{k_3}{k}\frac{J_\ell(k_1\rho)}{k_1\rho}\sin\ell\theta \sin k_3z$ $E_z = \sqrt{\frac{\mu}{\epsilon}}\frac{k_1}{k}J_\ell(k_1\rho)\cos\ell\theta \cos k_3z$ $H_\rho = -\ell\frac{J_\ell(k_1\rho)}{(k_1\rho)}\sin\ell\theta \cos k_3z$ $H_\theta = -J'_\ell(k_1\rho)\cos\ell\theta \cos k_3z$ $H_z = 0$	$k_1 = \frac{2r_{\ell m}}{a}$ $k^2 = k_1^2+k_3^2$ ℓ,m,n = DE RECTANGULA $r_{\ell m}$ = m^{th} ZE FOR T $r_{\ell m}$ = m^{th} ZE FOR T
	TE	$E_\rho = -\sqrt{\frac{\mu}{\epsilon}}\ell\frac{J_\ell(k_1\rho)}{k_1\rho}\sin\ell\theta \sin k_3z$ $E_\theta = -\sqrt{\frac{\mu}{\epsilon}}J'_\ell(k_1\rho)\cos\ell\theta \sin k_3z$ $E_z = 0$ $H_\rho = \frac{k_3}{k}J'_\ell(k_1\rho)\cos\ell\theta \cos k_3z$ $H_\theta = -\ell\frac{k_3}{k}\frac{J_\ell(k_1\rho)}{k_1\rho}\sin\ell\theta \cos k_3z$ $H_z = \frac{k_1}{k}J_\ell(k_1\rho)\cos\ell\theta \sin k_3z$	
FULL COAXIAL 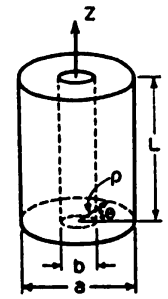 $\frac{b}{a} = \eta$	TM	SAME AS FOR CIRCULAR CYLINDER, BUT SUBSTITUTE: $Z_\ell(k_1\rho)$ FOR $J_\ell(k_1\rho)$ $Z'_\ell(k_1\rho)$ FOR $J'_\ell(k_1\rho)$ WHERE $Z_\ell(k_1\rho) = J_\ell(k_1\rho) - AY_\ell(k_1\rho)$ $Z'_\ell(k_1\rho) = J'_\ell(k_1\rho) - AY'_\ell(k_1\rho)$	SA CIRCULAR CY $r_{\ell m}$ = m $[J_\ell(\eta x)\ Y_\ell(x$ A = FOR T $r_{\ell m}$ = m $[J'_\ell(\eta x)\ Y'_\ell(x$ A = FOR T
	TE		

SOURCES: HANSEN, JNL. APP. PHYS., 9, P. 654 BORGNIS, ANN. d. PHYS., 35, P. 359 BORGNIS, HOCHF: TECH u. ELEK: AKUS., 56, P. 47 BARROW & MIEHER, PROC. I.R.E., 26, P. 184 *

Digitized by Google Original from UNIVERSITY OF MICHIGAN
Generated on 2019-09-24 06:35 GMT / http://hdl.handle.net/2027/mdp.39015077775156
Public Domain, Google-digitized / http://www.hathitrust.org/access_use#pd-google

Generated on 2019-09-24 06:35 GMT / http://hdl.handle.net/2027/mdp.39015077775156
Public Domain, Google-digitized / http://www.hathitrust.org/access_use#pd-google

Digitized by Google

Original from
UNIVERSITY OF MICHIGAN

where

f = frequency in megacycles per second.
D = diameter of cavity in inches.
L = length of cavity in inches.
A = a constant depending upon the mode. Values of A are given in Table II for the lowest 30 modes. Values of Bessel function roots are given in Table III for the first 180 modes.
B = a constant depending upon the velocity of electromagnetic waves in the dielectric. For air at 25°C and 60% relative humidity, $B = 0.34799 \times 10^8$.
n = third index defining the mode, i.e., the number of half wavelengths along the cylinder axis.

TABLE II.—*Constants for Use in Computing the Resonant Frequencies of Circular Cylinders*

$$(fD)^2 = \left(\frac{cr}{\pi}\right)^2 + \left(\frac{cn}{2}\right)^2 \left(\frac{D}{L}\right)^2 = A + B n^2 \left(\frac{D}{L}\right)^2$$

$B = 0.34799 \times 10^8$ $\quad c = 1.17981 \times 10^{10}$ inches/second

Mode	r	A
TM 01	2.40483	0.81563×10^8
02	5.52008	4.2975
03	8.65373	10.5617
11	3.83171	2.0707
12	7.01559	6.9415
13	10.17347	14.5970
21	5.13562	3.7197
22	8.41724	9.9923
31	6.38016	5.7410
32	9.76102	13.4374
41	7.58834	8.1212
51	8.77148	10.8511
61	9.93611	13.9238
TE 01	3.83171	2.0707
02	7.01559	6.9415
03	10.17347	14.5970
11	1.84118	0.47810
12	5.33144	4.0088
13	8.53632	10.2770
21	3.05424	1.3156
22	6.70613	6.3426
23	9.96947	14.0175
31	4.20119	2.4893
32	8.01524	9.0606
41	5.31755	3.9879
42	9.28240	12.1520
51	6.41562	5.8050
61	7.50127	7.9359
71	8.57784	10.3772
81	9.64742	13.1265

ue of c is for air at 25°C. and 60% relative humidity. D and L in inches; f in rcles.

Digitized by Google
Original from UNIVERSITY OF MICHIGAN
Generated on 2019-09-24 06:37 GMT / http://hdl.handle.net/2027/mdp.39015077775156
Public Domain, Google-digitized / http://www.hathitrust.org/access_use#pd-google

Formula (2) represents a family of straight lines, when $(D/L)^2$ and $(fD)^2$ are used as coordinates, and leads directly to the easily constructed and highly useful "Mode Chart" of Fig. 1.

It will be noted from Table II that the TE $0mn$ and the TM $1mn$ modes have the same frequency of resonance. This is a highly important case of degeneracy. In the design of practical cavities it is necessary to take measures to eliminate this degeneracy, as the TM mode (usually referred to as the companion of its associated TE mode) introduces undesirable effects. This is discussed more at length later.

Choice of Operating Mode

Turning now to the expressions for $Q\frac{\delta}{\lambda}$ these are seen to be of a rather complicated nature. For some of the lower order modes, their values are plotted in Figs. 2, 3 and 4. Examination of these leads to the question of which mode has the highest Q for a given volume. It is desirable to keep the volume a minimum, since, as shown by (1), the total number of resonances is a function of the volume. Analysis of the problem is somewhat involved, but leads to the conclusion that operation in the TE $01n$ mode* gives the smallest volume for an assigned Q, and also leads to specific values of n and D/L which give this result. In fact, for maximum Q/V in the TE $01n$ mode,

$$(fD)^2\left(\frac{D}{L}\right) = 3.11 \times 10^8 \tag{3}$$

which permits easy plotting on a mode chart of the locus of the operating points for best Q/V ratio.

Extraneous or Unwanted Modes

In echo boxes for radar testing, where high Q is of the utmost importance, the TE $01n$ mode has been used. The values of n vary from 1 at frequencies around 1 *kmc* to 50 at about 25 *kmc*.

All other modes are then regarded as unwanted or extraneous. The great utility of the mode chart lies in that it permits a quick determination of the most favorable operating area. We consider this now in detail.

Figure 5 shows a portion of a mode chart. It is clear that the sensible way to construct a tunable cylinder is to keep the diameter fixed and vary the length. With fixed diameter, the coordinates of the mode chart are essentially f^2 and $\left(\frac{1}{L}\right)^2$ and it is convenient to refer to them loosely as fre-

* Unimportant exceptions occur for values of $Q\frac{\delta}{\lambda} < 1.2$.

Digitized by Google
Original from UNIVERSITY OF MICHIGAN
Generated on 2019-09-24 06:39 GMT / http://hdl.handle.net/2027/mdp.39015077775156
Public Domain, Google-digitized / http://www.hathitrust.org/access_use#pd-google

quency and length. With this understanding, if the frequency band to be covered by the tunable cavity extends from f_1 to f_2 then the length must be adjustable from L_1 to L_2. Responses to frequencies within the band, but

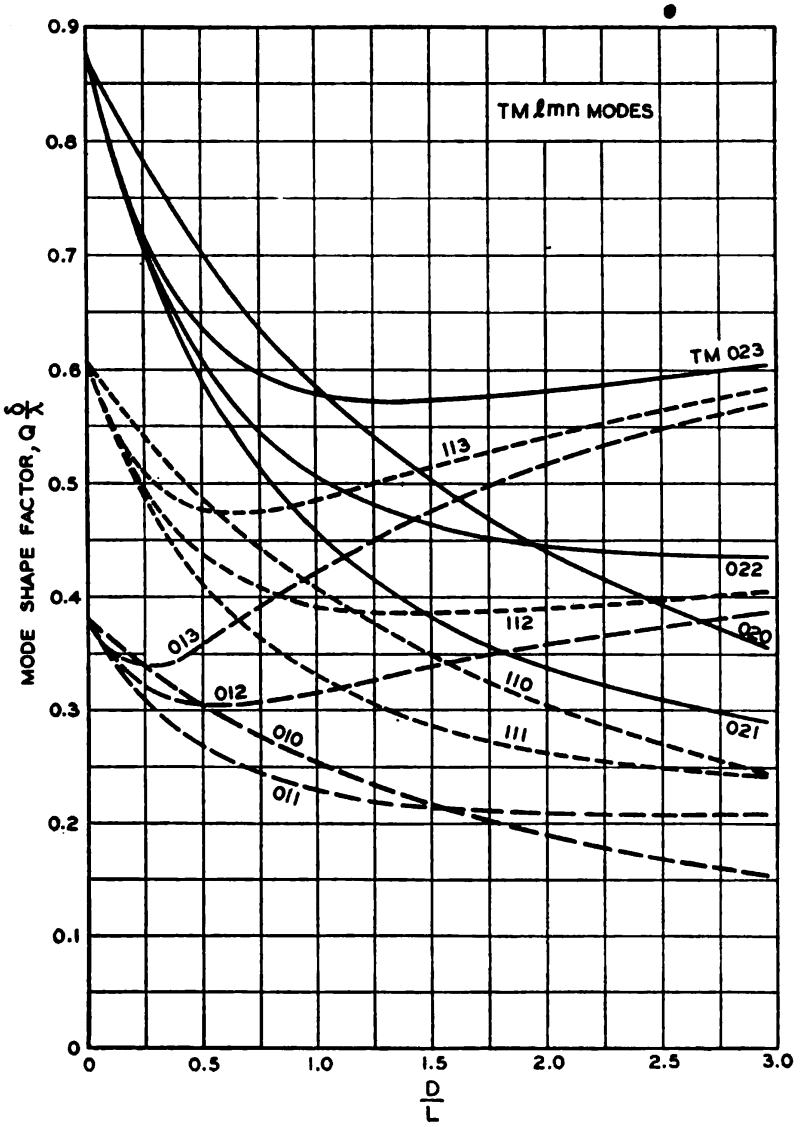

Fig. 2—Mode-shape factors $\left(Q\frac{\delta}{\lambda}\right)$ as a function of diameter to length ratio $\left(\frac{D}{L}\right)$ for circular cylinder resonator—*TM* modes.

which demand lengths outside the range L_1 to L_2 are of little interest because mechanical stops prohibit other lengths. On the assumption that the applied frequency will always lie within the operating band f_1 to f_2, responses to frequencies below f_1 or above f_2 are likewise of little interest. Therefore,

Digitized by Google
Original from UNIVERSITY OF MICHIGAN
Generated on 2019-09-24 06:39 GMT / http://hdl.handle.net/2027/mdp.39015077775156
Public Domain, Google-digitized / http://www.hathitrust.org/access_use#pd-google

major consideration need be given only to those modes which lie within the rectangle of which the desired TE 01n mode forms the diagonal.

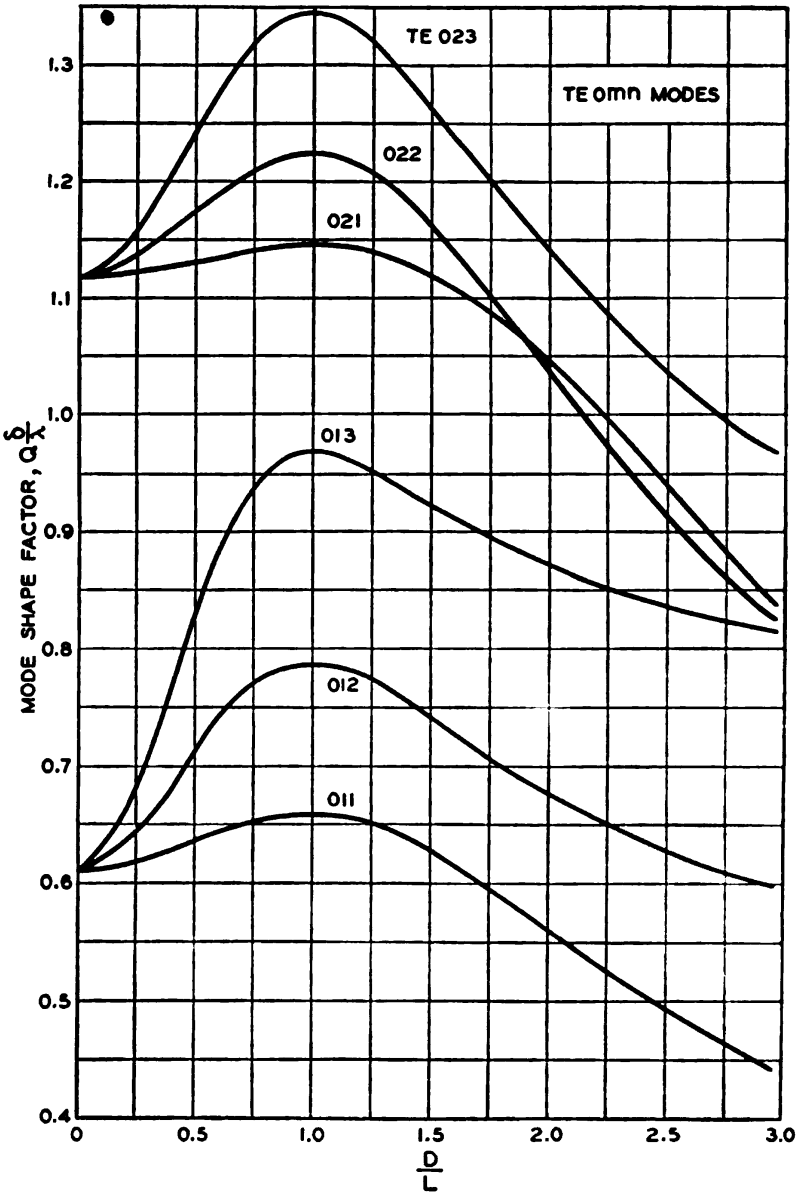

Fig. 3—Mode-shape factors $\left(Q\frac{\delta}{\lambda}\right)$ as a function of diameter to length ratio $\left(\frac{D}{L}\right)$ for circular cylinder resonator — TE modes with $l = 0$.

Any nondiagonal mode is an extraneous mode. Those which do not cross the desired mode within the frame are called interfering modes. They act to give responses at more than one tuning point when the applied fre-

Digitized by Google
Original from UNIVERSITY OF MICHIGAN
Generated on 2019-09-24 06:40 GMT / http://hdl.handle.net/2027/mdp.39015077775156
Public Domain, Google-digitized / http://www.hathitrust.org/access_use#pd-google

quency is held fixed, or alternatively to give responses at more than one frequency when the tuning is held fixed. In either event they lead to ambiguity and confusion, and their effects must be reduced to the point where this cannot occur.

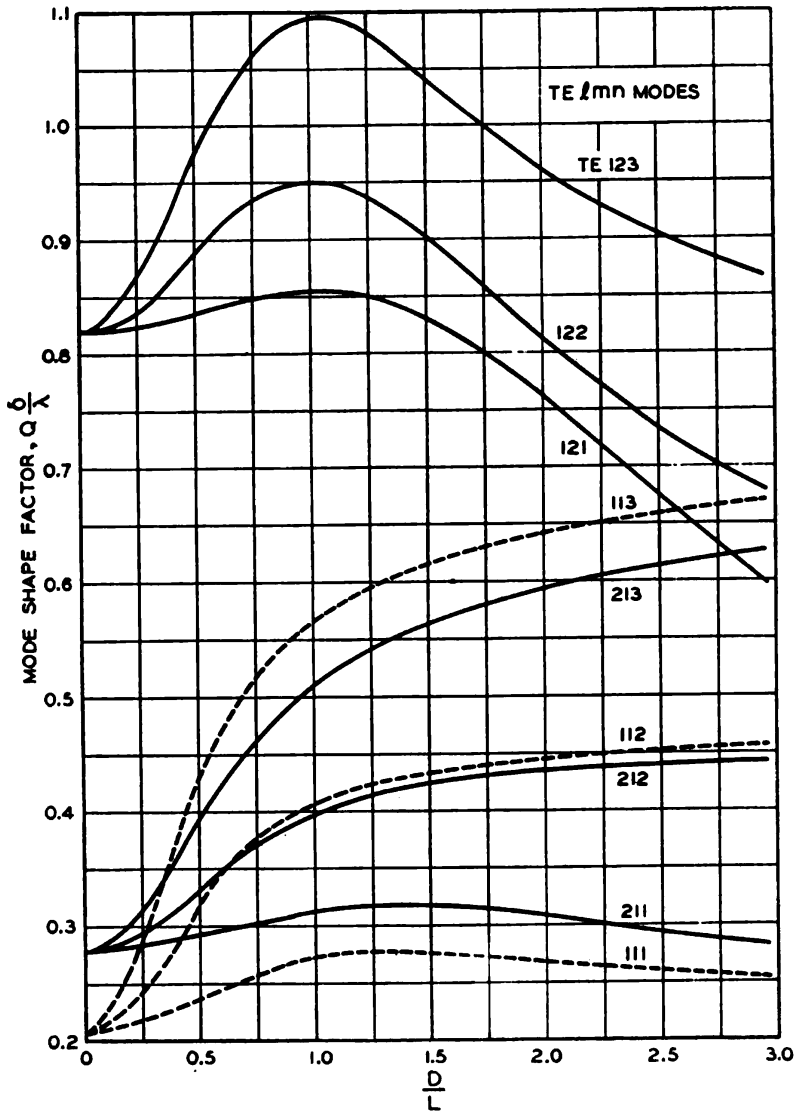

Fig. 4—Mode-shape factors $\left(Q\frac{\delta}{\lambda}\right)$ as a function of diameter to length ratio $\left(\frac{D}{L}\right)$ for circular cylinder resonator — TE modes with $l > 0$.

A special type of interfering mode is the $TE\ 01(n+1)$ mode. In the nature of things, it is virtually impossible to suppress this mode without likewise suppressing the desired $TE\ 01n$ mode. The width of the operating

Digitized by Google
Original from UNIVERSITY OF MICHIGAN
Generated on 2019-09-24 06:40 GMT / http://hdl.handle.net/2027/mdp.39015077775156
Public Domain, Google-digitized / http://www.hathitrust.org/access_use#pd-google

band is thus strictly limited, if ambiguity is to be avoided. This effect, termed self-interference, becomes an important factor as n increases, since

$$\frac{f_2}{f_1}\,(\text{maximum}) = \frac{n+1}{n}$$

This maximum value cannot be realized because it is incompatible with other requirements.

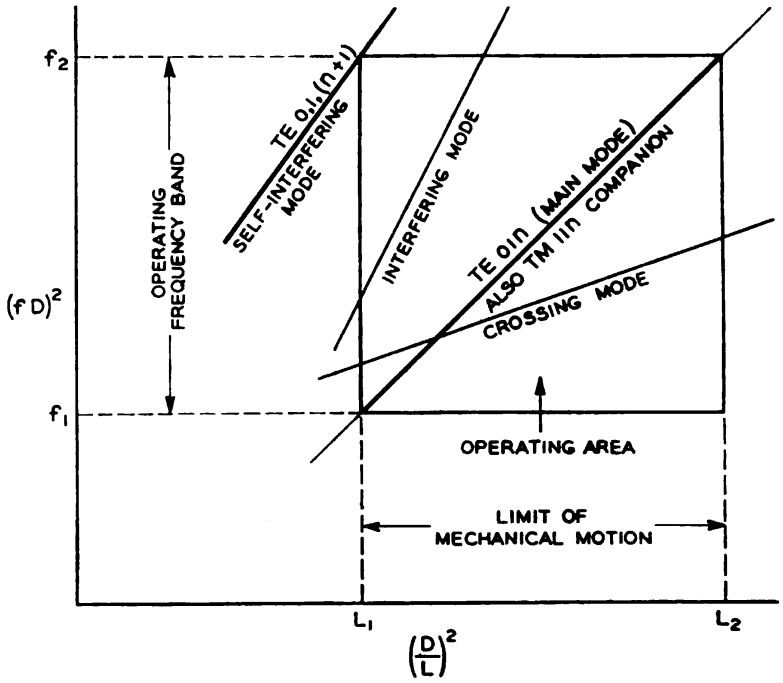

Fig. 5—Mode chart illustrating meaning of crossing and interfering modes and of operating area.

When an undesired mode crosses the main mode within the rectangle it is called a crossing mode. Except in a region close to the crossing point, it acts only to cause ambiguity as already discussed. In the immediate region of the crossing point, however, the cavity is simultaneously resonant in both modes. Violent interaction effects which may seriously degrade the cavity Q frequently occur at such a crossing.

Methods of Minimizing Effects of Unwanted Modes

A major problem in the design of a high Q cavity for radar test purposes in which the Q and frequency range are set by radar system considerations, is to reduce the effects of all the undesired modes without seriously degrading the main TE $01n$ mode. Among those to be suppressed is the companion TM $11n$ mode which is inherently of the same frequency.

Digitized by Google
Original from UNIVERSITY OF MICHIGAN
Generated on 2019-09-24 06:40 GMT / http://hdl.handle.net/2027/mdp.39015077775156
Public Domain, Google-digitized / http://www.hathitrust.org/access_use#pd-google

TABLE III.—*Values of the Bessel Function Zero (r_{lm}) for the First 180 Modes in a Circular Cylinder Resonator*

	r_{lm}	Mode*		r_{lm}	Mode*		r_{lm}	Mode*		r_{lm}	Mode*
1	1.8412	E 1-1	46	13.0152	M 3-3	91	18.4335	M 10-2	136	22.6716	E 2-7
2	2.4048	M 0-1	47	13.1704	E 2-4	92	18.6374	E 6-4	137	22.7601	M 1-7
3	3.0542	E 2-1	48	13.3237	M 1-4	93	18.7451	E 12-2	138	22.7601	E 0-7
4	3.8317	M 1-1	49	13.3237	E 0-4	94	18.9000	M 14-1	139	22.9452	M 8-4
5	3.8317	E 0-1	50	13.3543	M 9-1	95	18.9801	M 5-4	140	23.1158	M 14-2
6	4.2012	E 3-1	51	13.5893	M 6-2	96	19.0046	E 9-3	141	23.2548	E 21-1
7	5.1356	M 2-1	52	13.8788	E 12-1	97	19.1045	E 17-1	142	23.2568	M 18-1
8	5.3176	E 4-1	53	13.9872	E 5-3	98	19.1960	E 4-5	143	23.2643	E 16-2
9	5.3314	E 1-2	54	14.1155	E 8-2	99	19.4094	M 3-5	144	23.2681	E 7-5
10	5.5201	M 0-2	55	14.3725	M 4-3	100	19.5129	E 2-6	145	23.2759	M 11-3
11	6.3802	M 3-1	56	14.4755	M 10-1	101	19.5545	M 8-3	146	23.5861	M 6-5
12	6.4156	E 5-1	57	14.5858	E 3-4	102	19.6159	M 1-6	147	23.7607	E 10-4
13	6.7061	E 2-2	58	14.7960	M 2-4	103	19.6159	E 0-6	148	23.8036	E 5-6
14	7.0156	M 1-2	59	14.8213	M 7-2	104	19.6160	M 11-2	149	23.8194	E 13-3
15	7.0156	E 0-2	60	14.8636	E 1-5	105	19.8832	E 13-2	150	24.0190	M 4-6
16	7.5013	E 6-1	61	14.9284	E 13-1	106	19.9419	E 7-4	151	24.1449	E 3-7
17	7.5883	M 4-1	62	14.9309	M 0-5	107	19.9944	M 15-1	152	24.2339	M 9-4
18	8.0152	E 3-2	63	15.2682	E 6-3	108	20.1441	E 18-1	153	24.2692	M 15-2
19	8.4172	M 2-2	64	15.2867	E 9-2	109	20.2230	E 10-3	154	24.2701	M 2-7
20	8.5363	E 1-3	65	15.5898	M 11-1	110	20.3208	M 6-4	155	24.2894	E 22-1
21	8.5778	E 7-1	66	15.7002	M 5-3	111	20.5755	E 5-5	156	24.3113	E 1-8
22	8.6537	M 0-3	67	15.9641	E 4-4	112	20.7899	M 12-2	157	24.3382	M 19-1
23	8.7715	M 5-1	68	15.9754	E 14-1	113	20.8070	M 9-3	158	24.3525	M 0-8
24	9.2824	E 4-2	69	16.0378	M 8-2	114	20.8269	M 4-5	159	24.3819	E 17-2
25	9.6474	E 8-1	70	16.2235	M 3-4	115	20.9725	E 3-6	160	24.4949	M 12-3
26	9.7610	M 3-2	71	16.3475	E 2-5	116	21.0154	E 14-2	161	24.5872	E 8-5
27	9.9361	M 6-1	72	16.4479	E 10-2	117	21.0851	M 16-1	162	24.9349	M 7-5
28	9.9695	E 2-3	73	16.4706	M 1-5	118	21.1170	M 2-6	163	25.0020	E 14-3
29	10.1735	M 1-3	74	16.4706	E 0-5	119	21.1644	E 1-7	164	25.0085	E 11-4
30	10.1735	E 0-3	75	16.5294	E 7-3	120	21.1823	E 19-1	165	25.1839	E 6-6
31	10.5199	E 5-2	76	16.6982	M 12-1	121	21.2116	M 0-7	166	25.3229	E 23-1
32	10.7114	E 9-1	77	17.0038	M 6-3	122	21.2291	E 8-4	167	25.4170	M 16-2
33	11.0647	M 4-2	78	17.0203	E 15-1	123	21.4309	E 11-3	168	25.4171	M 20-1
34	11.0864	M 7-1	79	17.2412	M 9-2	124	21.6415	M 7-4	169	25.4303	M 5-6
35	11.3459	E 3-3	80	17.3128	E 5-4	125	21.9317	E 6-5	170	25.4956	E 18-2
36	11.6198	M 2-3	81	17.6003	E 11-2	126	21.9562	M 13-2	171	25.5094	M 10-4
37	11.7060	E 1-4	82	17.6160	M 4-4	127	22.0470	M 10-3	172	25.5898	E 4-7
38	11.7349	E 6-2	83	17.7740	E 8-3	128	22.1422	E 15-2	173	25.7051	M 13-3
39	11.7709	E 10-1	84	17.7887	E 3-5	129	22.1725	M 17-1	174	25.7482	M 3-7
40	11.7915	M 0-4	85	17.8014	M 13-1	130	22.2178	M 5-5	175	25.8260	E 2-8
41	12.2251	M 8-1	86	17.9598	M 2-5	131	22.2191	E 20-1	176	25.8912	E 9-5
42	12.3386	M 5-2	87	18.0155	E 1-6	132	22.4010	E 4-6	177	25.9037	M 1-8
43	12.6819	E 4-3	88	18.0633	E 16-1	133	22.5014	E 9-4	178	25.9037	E 0-8
44	12.8265	E 11-1	89	18.0711	M 0-6	134	22.5827	M 3-6	179	26.1778	E 15-3
45	12.9324	E 7-2	90	18.2876	M 7-3	135	22.6293	E 12-3	180	26.2460	E 12-4

* Nomenclature after Barrow & Mieher, "Natural Oscillations of Electrical Cavity Resonators" IRE Proceedings, April 1940, p. 184. M modes take zeros of $J_l(x)$; E modes take zeros of $J_l'(x)$. Number directly following E or M is l; number after hyphen is number of root.

Values less than 16.0 are abridged from six-place values and are believed to be correct; values more than 16.0 are abridged from five-place values and may be in error by one unit in fourth decimal place. **5** in fourth place indicates that higher value is to be used in rounding off to fewer decimals.

One solution, of limited application, is to choose an operating rectangle free from extraneous responses. An alternative solution is to design the cavity in a manner such that the undesired responses are reduced or sup-

Digitized by Google
Original from UNIVERSITY OF MICHIGAN
Generated on 2019-09-24 06:40 GMT / http://hdl.handle.net/2027/mdp.39015077775156
Public Domain, Google-digitized / http://www.hathitrust.org/access_use#pd-google

pressed to a point where their presence does not interfere with the normal operation of the cavity. In this latter case, the amount of suppression is naturally dependent upon the use to which the cavity is to be put, and is conceivably different for a high Q cavity used as a frequency meter, for example, and one used as a selective filter.

Experience has shown that certain families of modes are much more difficult to suppress than others, and are to be avoided, if at all possible. The feasibility of doing this can be determined by sliding the operating area (a suitable opening in a sheet of paper) around on a large mode chart until the most favorable operating region, consistent with other requirements, has been found.

Once a suitable operating area has been chosen, the cavity diameter is fixed and length and frequency scales added to the mode chart make it read directly in quantities readily measured.

Cavity Couplings

To be useful the cavity must be coupled to external circuits. The problem here is to get the correct coupling to the main mode and as little coupling as possible to all others. Since the electric field is zero everywhere at the boundary surface of the cavity for the TE 01n mode, coupling to it must be magnetic. This may be obtained either by a loop at the end of a coaxial line or by an orifice connecting the cavity with a wave guide.

The location for maximum coupling to the main mode is on the side of the cavity, an odd number of quarter-guide wavelengths from the end, or on the end about halfway (48%) out from the center to the edge. Correct orientation of loop or wave guide is achieved when the magnetic fields are parallel. This requires the axis of the loop to be parallel to the axis of the cylinder for side wall feed and to be perpendicular to the cylinder axis for end feed. Wave guide orientation is shown in Table IV.

The theory of coupling loops and orifices is not at present precise enough to yield more than approximate dimensions. Exact sizes of loops and holes have therefore been obtained experimentally for all designs.

On the basis of rather severely limiting assumptions,[11] coupling formulas for a round hole connecting a rectangular wave guide and a TE 01n cavity are given in Table IV. The assumptions are that the orifice is in a wall of negligible thickness, its diameter is small compared to the wavelength, it is not near any surface discontinuity, and that the wave guide propagates only its principal (gravest) mode and is perfectly terminated. In echo box applications, this theory leads to a computed diameter that is somewhat smaller than experiment shows to be correct.

The coupling to other modes can be analyzed, at least qualitatively, from the field expressions of Table I. This has been of value in making final

Generated on 2019-09-24 06:40 GMT / http://hdl.handle.net/2027/mdp.39015077775156
Public Domain, Google-digitized / http://www.hathitrust.org/access_use#pd-google
Digitized by Google
Original from UNIVERSITY OF MICHIGAN

Generated on 2019-09-24 06:41 GMT / http://hdl.handle.net/2027/mdp.39015077775156
Public Domain, Google-digitized / http://www.hathitrust.org/access_use#pd-google

	CASE 1A	1B	2A	2B	3A	3B
COUPLING METHOD	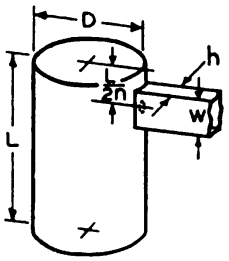	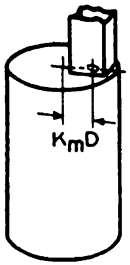	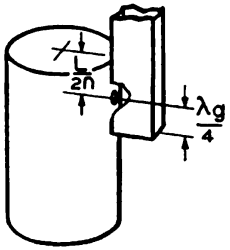	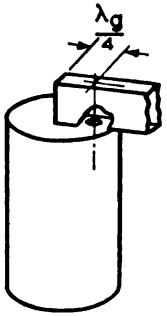	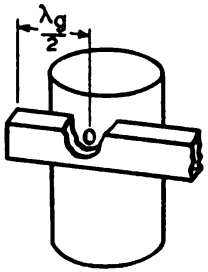	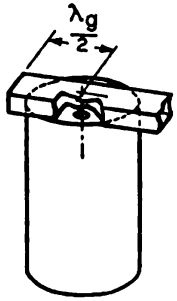
CIRCULAR ORIFICE	$\frac{\Delta f}{f} = -K_c \frac{\lambda^2 d^3}{D^4 L}$ $W_a = K_w \frac{\lambda^2 d^6}{\lambda_g w h D^4 L}$	$\frac{\Delta f}{f} = -K_c \frac{n^2 \lambda^2 d^3}{D^2 L^3}$ $W_a = K_w \frac{n^2 \lambda^2 d^6}{\lambda_g w h D^2 L^3}$	$\frac{\Delta f}{f}$ SAME AS 1A $W_a = K_w \frac{\lambda_g \lambda^2 d^6}{w^3 h D^4 L}$	$\frac{\Delta f}{f}$ SAME AS 1B $W_a = K_w \frac{n^2 \lambda_g \lambda^2 d^6}{w^3 h D^2 L^3}$	$\frac{\Delta f}{f}$ SAME AS 1A W_a SAME AS 1A	$\frac{\Delta f}{f}$ SAME AS 1B W_a SAME AS 1B
CONSTANTS	K_c K_w TE 01n 0.316 1.322 TE 02n 1.058 4.43 TE 03n 2.225 9.32	K_c K_w K_m 0.1107 0.464 0.2403 0.1995 0.836 0.1312 0.288 1.207 0.0905	K_w 0.331 1.108 2.330	K_w 0.1159 0.2089 0.302		

NOTATION: λ = FREE SPACE WAVELENGTH OF CAVITY RESONANCE; λ_g = GUIDE WAVELENGTH; d = DIAMETER OF ORIFICE; $W_a = \frac{1}{Q_a}$ = CAVITY LOADING

NOTE: FOR FEED LIKE CASES 2 AND 3, BUT WITH WAVEGUIDE TERMINATED IN BOTH DIRECTIONS, DIVIDE W_a BY 2

TABLE IV.—*Orifice Coupling of Wave Guide (TE 10 Mode) to Cylindrical Cavity (TE 0mn Mode)*

Digitized by Google
Original from UNIVERSITY OF MICHIGAN

small relocations of the coupling points to discriminate against a residual undesired mode.

Principle of Similitude

One other theorem generally applicable to all cavities has been useful in design. It is the principle of similitude, which may be stated as follows[11]:

> A reduction in all the linear dimensions of a cavity resonator by a factor $1/m$ (if accompanied by an increase in the conductivity of the walls by a factor m) will reduce the wavelengths of the modes by a factor $1/m$.

The condition given in parentheses is necessary for strict validity; for high Q cavities, it need not be considered.

Application of Theory

An illustration of an engineering application of the basic information just presented, is the design of an echo box test set for use in radar maintenance.

The test set has a number of components, but only the cavity proper and its couplings will be considered at this time.

Design Requirements

The basic design requirements of the cavity set by the radar are: (1) the working decrement, and (2) the tunable frequency limits (f_1 and f_2). Service use of these test sets in the 3 *kmc* and 9 *kmc* bands has shown that a working decrement of about 3 *db* per microsecond gives satisfactory results.

As seen in the discussion above, Q is a more useful design parameter for the resonant cavity than decrement, d. Hence the conversion

$$Q = \frac{27.3f}{d} \tag{4}$$

where d is expressed in *db* per microsecond, and f is in megacycles, gives the loaded or working Q to be realized.

Determining the Theoretical Q Required

For design purposes, however, there are several factors which dictate the use of a value for theoretical Q which is somewhat higher than the loaded Q just computed. The input and output couplings reduce the theoretical Q of the cavity due to their loadings. The coupling factor, s, expressed as the ratio of loaded to unloaded Q, has values for echo boxes of about 0.90 for the input coupling and from 0.90 to 0.99 for the output coupling. In addition, other factors such as the means used for mode suppression may degrade

Digitized by Google
Original from UNIVERSITY OF MICHIGAN
Generated on 2019-09-24 06:41 GMT / http://hdl.handle.net/2027/mdp.39015077775156
Public Domain, Google-digitized / http://www.hathitrust.org/access_use#pd-google

the Q. But, in simple designs, these may be negligible. Therefore, it is expedient to design for a theoretical Q of about 15 to 25 per cent in excess of the working Q to be realized.

The working Q's of a number of echo box designs are cited here to indicate the order of magnitude required at several frequencies:

1 *kmc*	70,000*
3	40,000
9	100,000
25	200,000

Finding the Cavity Dimensions

With the frequency and theoretical Q known, the dimensions of the cavity can be evaluated but the formulas of Table I require some simplification for engineering use.

The mode-shape (MS) factor, $Q\frac{\delta}{\lambda}$, may also be termed its selectivity which for the $TE\,01n$ modes may be expressed as follows:

$$Q\,\frac{\delta}{\lambda} = 0.610\,\frac{\left[1 + 0.168\left(\frac{D}{L}\right)^2 n^2\right]^{3/2}}{1 + 0.168\left(\frac{D}{L}\right)^3 n^2} \tag{5}$$

where:

δ = the skin depth in cm. $= \frac{1}{2\pi}\sqrt{\frac{10^9\rho}{f}}$

ρ = the resistivity in ohm-cm.

The skin depth is a factor which recognizes the dissipation of energy in the walls and ends of the cylinder. With increase of resistivity of these surfaces the currents penetrate deeper and the resulting Q is lower.

A comparison of the relative Q's computed from the resistivity of several metals will show the importance of this factor:

Silver	1.03
Copper	1.00
Gold	0.84
Aluminum	0.78
Brass	0.48

Therefore, a brass cavity will have about one-half of the Q that a similar cavity would have if made of copper. Similarly, the silverplating of a copper cavity will gain about 3 per cent in Q.

Equation 5 may be made more convenient for calculations by combining

* This value reflects the higher Q required on ground radars.

Digitized by Google
Original from UNIVERSITY OF MICHIGAN
Generated on 2019-09-24 06:41 GMT / http://hdl.handle.net/2027/mdp.39015077775156
Public Domain, Google-digitized / http://www.hathitrust.org/access_use#pd-google

terms which are a function of frequency and by assuming the conductivity of copper* for the cylinder walls. It then becomes

$$\frac{Q\sqrt{f}}{10^6} = 2.77 \frac{\left[1 + 0.168\left(\frac{D}{L}\right)^2 n^2\right]^{3/2}}{1 + 0.168\left(\frac{D}{L}\right)^3 n^2} \tag{6}$$

for $TE\ 01n$ modes; f is in megacycles.

Thus, it is seen that for the design parameters Q and f, selected values of n now define tentative useful points on the mode chart in terms of D/L and n.

Selection of Operating Area on Mode Chart

This will be more evident upon examination of Fig. 6, which is a basic design chart for cylindrical cavity resonators using $TE\ 01n$ modes. The coordinates of $(fD)^2$ and $(D/L)^2$ will be recognized from the previous discussion of the mode chart (Fig. 1) although in this case the range has been expanded by the use of logarithmic coordinates. Mode identification is obtained from equation 2; which, for $TE\ 01n$ modes becomes

$$(fD)^2 \times 10^{-8} = 2.0707 + 0.3480\, n^2\, (D/L)^2 \tag{7}$$

with D and L in inches and f in megacycles.

A family of $TE\ 01n$ modes has been drawn on the chart for selected values of n. To aid in designing for minimum volume a line labelled Max. $\frac{Q}{V}$ has been added (Equation 3). Lines of constant $Q\sqrt{f}$ are also shown as a series of dashed lines.

A tentative operating area on this chart may be selected on the basis of the required $Q\sqrt{f}$. Using mid-frequency for f, the intersection of the $Q\sqrt{f}$ line and the minimum volume line will define the operating mode, n, and also locate the center of the operating rectangle.

An enlarged plot of this area as in Fig. 7 will show all modes possible in the cavity. Some adjustment of the precise location of this area may then be desirable to eliminate certain types or numbers of unwanted modes. For example, it is extremely difficult to suppress $TE\ 02$ modes without affecting the $TE\ 01$ mode, because of the very close resemblance of the field configurations. On the other hand, most TM modes are easy to handle.

It may be possible to select an operating area such as the rectangle blocked out in Fig. 1 in which all extraneous responses (with the exception of the companion TM 111) are avoided. The largest rectangle which can be inscribed here is limited by the TE 311 and TE 112 modes. This will

* $\rho = 1.7241 \times 10^{-6}$ ohm-cm—the International Standard value for copper.

Digitized by Google
Original from UNIVERSITY OF MICHIGAN
Generated on 2019-09-24 06:41 GMT / http://hdl.handle.net/2027/mdp.39015077775156
Public Domain, Google-digitized / http://www.hathitrust.org/access_use#pd-google

permit a ±3.6 per cent frequency range. Several designs of 3 *kmc* echo boxes have been based on this area.

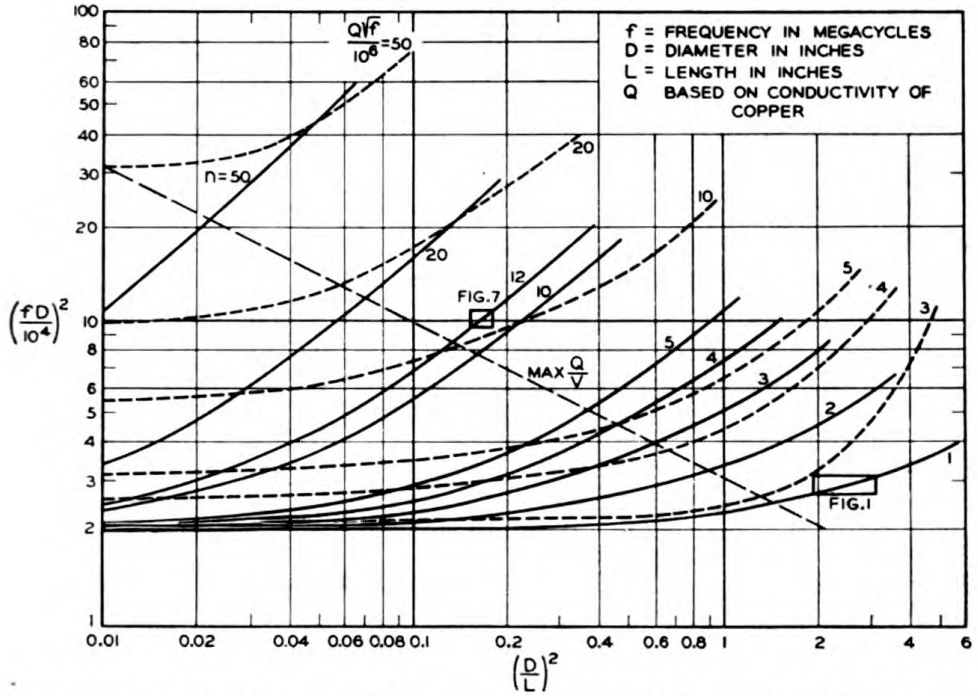

Fig. 6—Design chart for cylindrical cavity resonators operating in the *TE* 01*n* modes.

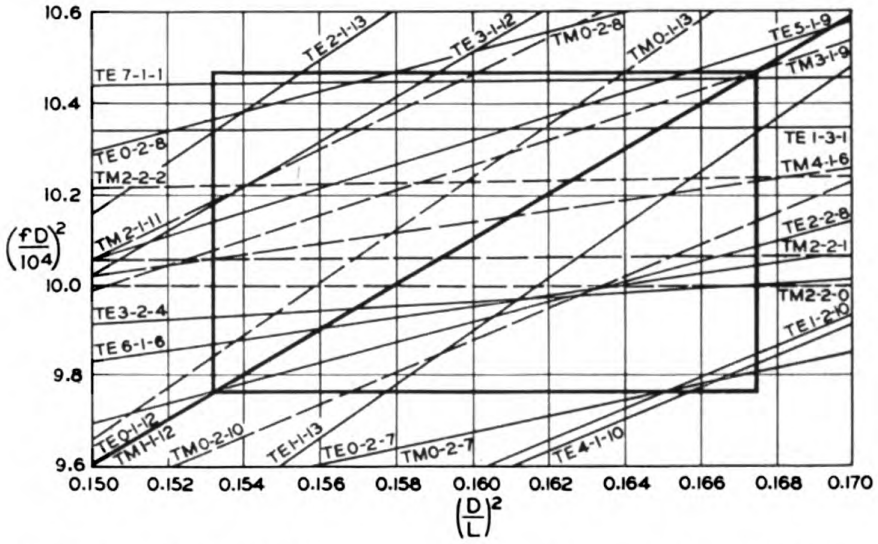

Fig. 7—Expanded mode chart covering the operating area of a 9 *kmc* echo box.

This type of solution is quite adequate for many of the simpler designs; but as the required Q becomes larger or the frequency coverage becomes

Digitized by Google
Original from UNIVERSITY OF MICHIGAN
Generated on 2019-09-24 06:41 GMT / http://hdl.handle.net/2027/mdp.39015077775156
Public Domain, Google-digitized / http://www.hathitrust.org/access_use#pd-google

greater it is generally not possible to locate such areas. An operating area for 9 *kmc* is shown on Fig. 7. Nine crossing modes and twelve interfering modes exist. For 25 *kmc* the crossing modes run into the forties with hundreds of interfering modes.

Suppression of the undesired modes requires a thorough knowledge of their field configurations and a number of effective techniques which may be applied on a practical engineering basis. Several examples are cited in later sections.

Since decrement is an important characteristic of these cavities, especially when applied to radar test sets, the uniformity of the decrement over the frequency range or "flatness of response" may be a significant design requirement. It will be seen from Fig. 3, that the MS factor of the wanted mode is not constant with varying D/L. In fact, if it were, the decrement would increase as the 3/2 power of frequency.

There are at least three attacks on this "flatness" problem: (1) to operate on the sloped portion of the MS curve in such a manner that its characteristic will tend to be complementary to the change with frequency; (2) to obtain compensation by varying the coupling with frequency—generally accomplished by selecting an appropriate coupling point along the side wall of the cavity; and (3) to overplate a portion of the cylinder's interior surface with a material of higher resistivity such as cadmium. For this third method, the formulas for $Q\frac{\delta}{\lambda}$ of Table I are no longer applicable since they assume a uniform resistivity of the cavity walls.

Thus, it will be seen that the final design of a cavity resonator is a compromise between a number of desired characteristics:

a) A cavity of minimum volume for a given Q.
b) A cavity having a minimum of extraneous responses of types difficult to suppress.
c) A cavity with compensation for flatness of decrement.

Engineering judgment is required to weigh the emphasis on each of these requirements which at times may be mutually exclusive.

Some Practical Considerations

Physically realizing the theoretical characteristics just described to obtain a satisfactory cavity brings forth a host of practical design problems. A number of these will be discussed in this section.

Description of Echo Box Test Sets

The schematics (Figs. 8 and 9) and photographs (Figs. 12 to 14) show the components and various construction methods of echo boxes in the 3 and 9 *kmc* bands. The cavity itself may be spun, drawn or turned of material

Digitized by Google
Original from UNIVERSITY OF MICHIGAN
Generated on 2019-09-24 06:42 GMT / http://hdl.handle.net/2027/mdp.39015077775156
Public Domain, Google-digitized / http://www.hathitrust.org/access_use#pd-google

such as brass or aluminum which will give mechanical stability without excessive weight.

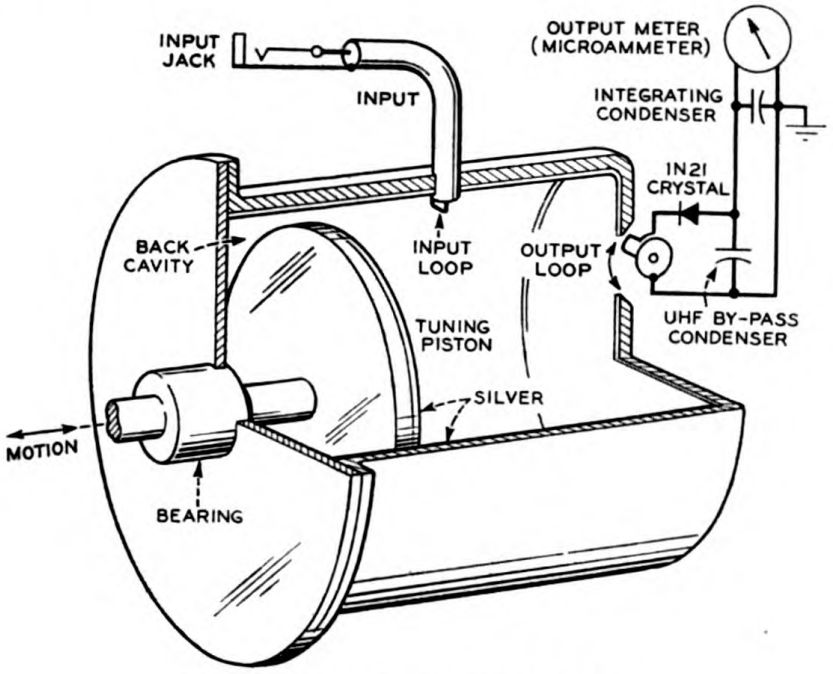

Fig. 8—Schematic of a 3 *kmc* echo box.

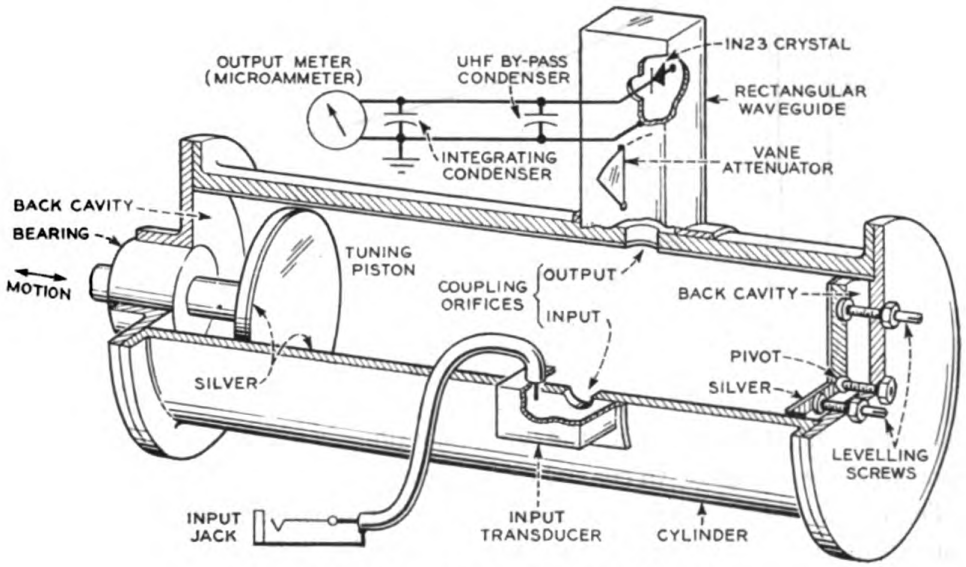

Fig. 9—Schematic of a 9 *kmc* echo box.

The movable plate is driven by the piston which operates in a close-fitting bearing. The drive mechanism translates the rotary motion of the tuning

Digitized by Google
Original from UNIVERSITY OF MICHIGAN
Generated on 2019-09-24 06:42 GMT / http://hdl.handle.net/2027/mdp.39015077775156
Public Domain, Google-digitized / http://www.hathitrust.org/access_use#pd-google

knob into linear motion of the piston through a crank and connecting rod assembly. Coupled to the drive shaft is an indicating dial to register frequency.

Silverplating is indicated on all interior surfaces of the cavity for minimum resistance to currents in the walls and ends of the cylinder.

For the 3 *kmc* bands, the input coupling is in the form of a loop protruding into the cavity and connected by coaxial microwave cable to the radar under

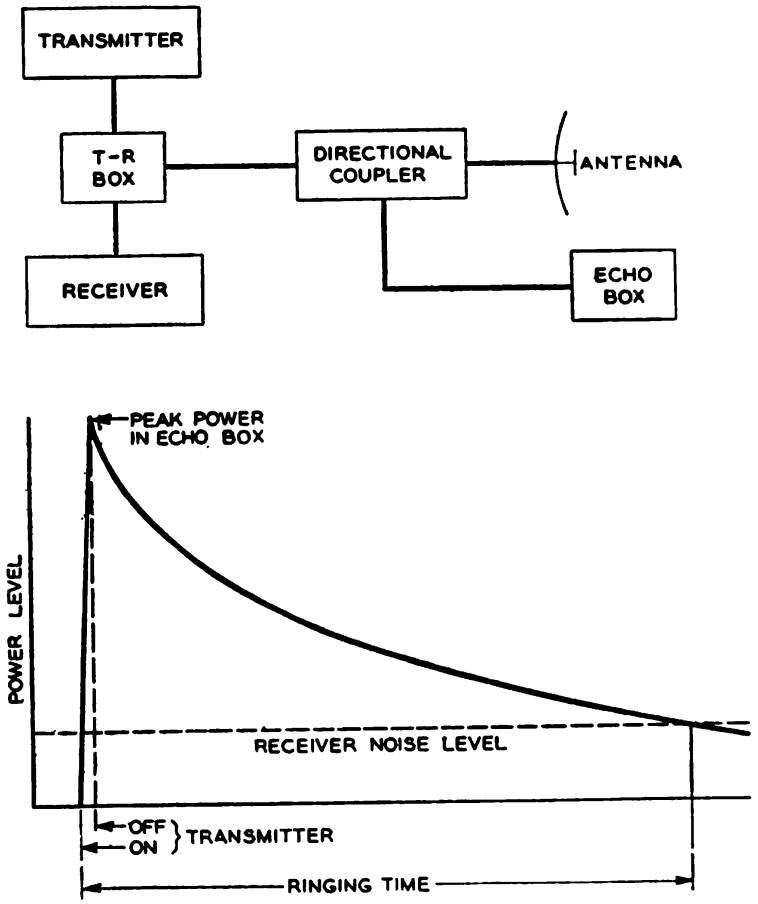

Fig. 10—Radar test with echo box.

test. For the 9 *kmc* bands, the input coupling is an orifice with which is associated a wave guide to coaxial cable transducer.

The output couplings for the two frequency bands also differ in construction. For the 3 *kmc* bands, the variable coupling is achieved by rotating the output loop before an aperture in the cavity. In this rotary mount is housed the rectifying crystal and by-pass condenser. An orifice is used for the 9 *kmc* band output coupling which feeds a crystal mounted in a wave guide. Amplitude control is by a vane attenuator in the wave guide. In

Digitized by Google
Original from UNIVERSITY OF MICHIGAN
Generated on 2019-09-24 06:45 GMT / http://hdl.handle.net/2027/mdp.39015077775156
Public Domain, Google-digitized / http://www.hathitrust.org/access_use#pd-google

all cases an integrating condenser is required to smooth out the *d-c* pulses delivered by the crystal to give output indication on the *d-c* microammeter.

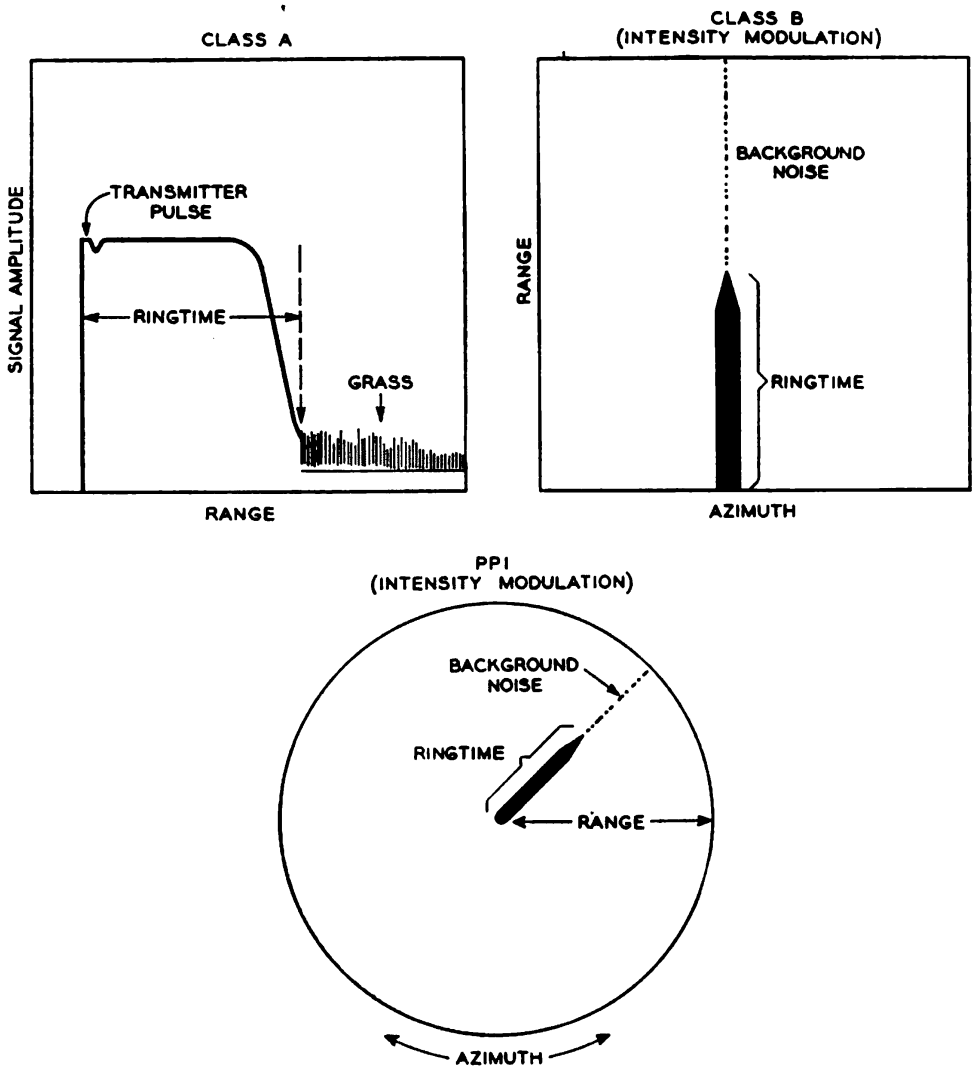

Fig. 11.—Typical ringtime patterns on radar indicators.

The cylinder in the 9 *kmc* band is an assembly of a tube and two end plates. One of these is driven by the piston as described and the other is adjustable for "levelling" i.e., parallelism of the two plates.

End Plate Gaps

The wanted *TE* mode is paired with a companion unwanted *TM* as described above. The fact that the *TM* mode has a Q substantially less than that of the *TE* makes the realization of the higher Q difficult. A method is

Digitized by Google
Original from UNIVERSITY OF MICHIGAN
Generated on 2019-09-24 06:45 GMT / http://hdl.handle.net/2027/mdp.39015077775156
Public Domain, Google-digitized / http://www.hathitrust.org/access_use#pd-google

needed of suppressing the *TM* in the presence of the *TE*. Since the resonant cavity is a cylinder, of variable length, the movable end plate (or reflector)

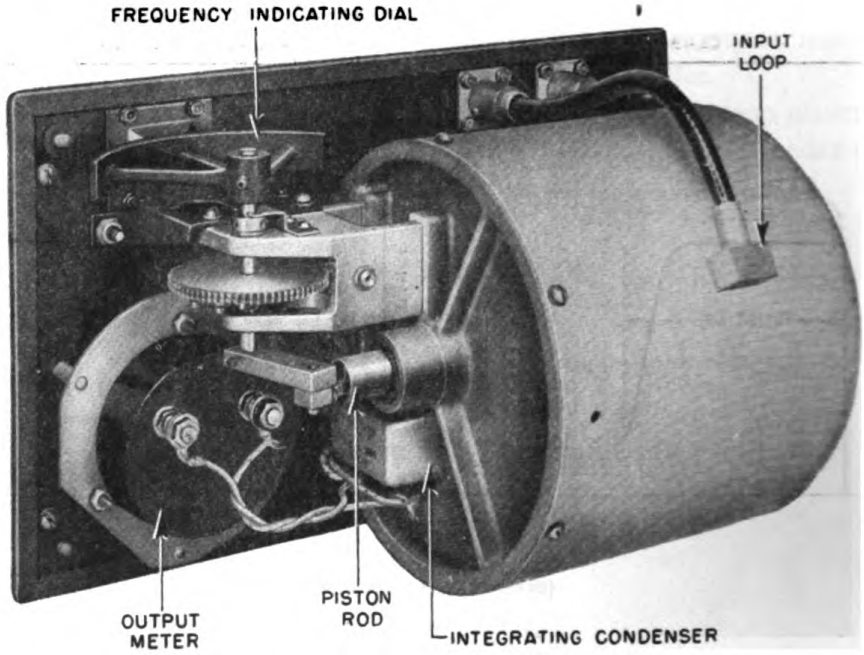

Fig. 12—Type of construction in a 3 *kmc* echo box.

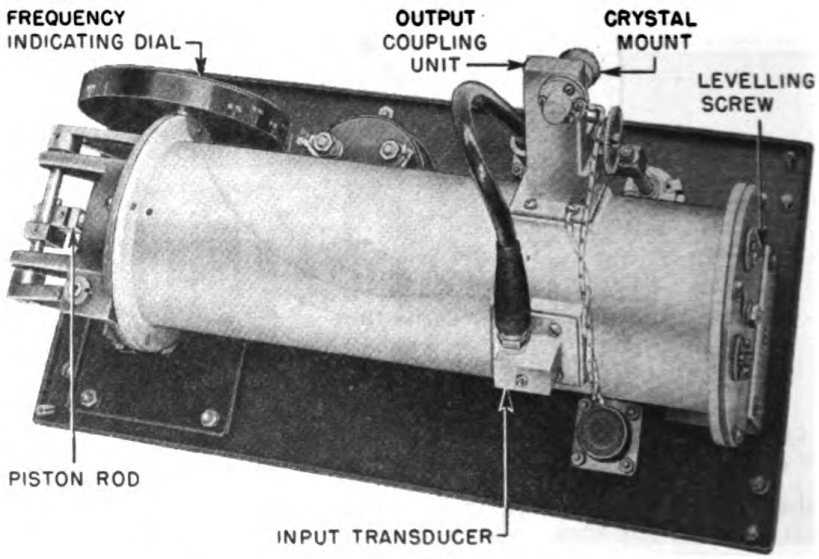

Fig. 13—Type of construction in a 9 *kmc* echo box.

can be modified to include a gap at its periphery. The gap perturbs the resonant frequencies of the two modes by different amounts so that they

Digitized by Google
Original from UNIVERSITY OF MICHIGAN
Generated on 2019-09-24 06:45 GMT / http://hdl.handle.net/2027/mdp.39015077775156
Public Domain, Google-digitized / http://www.hathitrust.org/access_use#pd-google

become separated. Secondly, the peripheral gap cuts through the surface currents at points of high density for *TM* modes and minimum density of *TE 0mn* modes and hence is a form of mode suppression. Thirdly, the gap greatly simplifies the mechanical design of a movable end plate by eliminating the need of physical contact with the side wall of the cylinder.

A similar gap may be used at the other end. This facilitates "levelling" of a false bottom in the cavity.

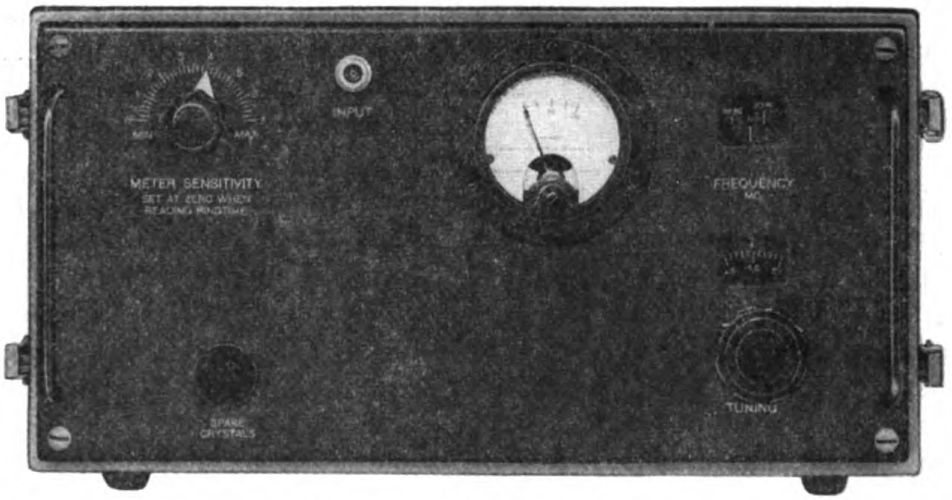

Fig. 14—Panel view of a 9 *kmc* echo box.

Back Cavity Effects

The cavity with a peripheral gap may give rise to further spurious resonances in the region behind the reflecting surface (known as the back cavity) if these responses are not damped. The addition of a lossy material such as bakelite or carbon loaded neoprene in the back cavity is a successful suppression method.

Cylinder Tolerances

The geometry of the structure is very important in realizing the potential Q of the cavity. The theoretical computations are based on a perfect right circular cylinder which in practice is seldom achieved. Distortions occur in various forms: e.g., the cylinder instead of being round may be elliptical; the ends may not be perpendicular to the axis of the cylinder or not parallel to each other; surface irregularities may be present causing field distortions within the cavity. Many of these effects have been minimized by requiring adherence to close dimensional tolerances.

For some designs, the requirement on the parallelism of the end plates is greater than can be commercially produced. An adjustable mechanism for

Digitized by Google
Original from UNIVERSITY OF MICHIGAN
Generated on 2019-09-24 06:45 GMT / http://hdl.handle.net/2027/mdp.39015077775156
Public Domain, Google-digitized / http://www.hathitrust.org/access_use#pd-google

levelling is a practical solution. Tilt adjustments in the order of 0.001 inch at the edge of the plate (about 3-inch diameter) are required in the 9 *kmc* band. Experience in the 25 *kmc* band shows evidence of the need for even finer control.

Plating

In addition, adequate control of the conductivity of the interior surfaces of the cavity is necessary to achieve a uniform manufactured product. This requires attention not only to the thickness and uniformity of the plating but also to the purity of the plating baths and the avoidance of introduction of foreign matter during buffing processes.

Couplings

The type and location of the coupling means can be used to discriminate between wanted and unwanted modes. Hence, this is a fertile field for mode suppression techniques. For example, since *TM* modes have $H_z = 0$, orifice coupling to the main mode at the side wall of the types shown in Table IV, cases 1A and 2A, will not couple to any *TM* modes. Again, if end coupling is used in a cavity which will support both the *TE* 01 and *TE* 02 modes, by locating this coupling at the point where $H_\rho = 0$ for the *TE* 02 mode (about 54% of the way out from the center), it will not be excited and coupling to the *TE* 01 will be only slightly below maximum.

For echo box test sets the magnitude of the input coupling to the wanted mode is a compromise between the incomplete buildup of the fields within the cavity during the charging interval and the loading of the cavity Q on discharge. This is carried on by varying the coupling and observing the "ringtime" (the echo box indication on the radar scope). Optimum coupling is achieved when ringtime is made a maximum.

Output couplings for echo boxes are made so that just enough energy is withdrawn from the cavity to give an adequate meter reading.

Drive Mechanism

The objective of the design of the tuning mechanism is to provide a smooth, fine control with a minimum of backlash. An illustration of the mechanical perfection required can be cited in a 9 *kmc* band design where $\frac{1}{4}$ inch of travel covered 200 megacycles in frequency. Hence, for frequency settings to be reproducible to within $\frac{1}{4}$ mc the mechanical backlash of the moving parts had to be held to about 0.0003 inches or 0.3 mil. To realize this in commercial manufacture and to maintain it after adverse operating conditions such as vibration and shock was a major mechanical design problem.

In the design of this drive mechanism it should be recognized that equal

Digitized by Google
Original from UNIVERSITY OF MICHIGAN
Generated on 2019-09-24 06:45 GMT / http://hdl.handle.net/2027/mdp.39015077775156
Public Domain, Google-digitized / http://www.hathitrust.org/access_use#pd-google

increments of cavity length will not produce uniform increments in frequency. The mode chart indicates graphically that a straight-line relationship exists between $(f)^2$ and $\left(\frac{1}{L}\right)^2$. Uniformly spaced markings on a dial reading directly in frequency can be realized by the use of such mechanisms as an eccentric operating on a limited arc. Adjustments are customarily provided to bring the cavity resonance and dial indication into agreement at some frequency of test. Frequency departures of the drive mechanism referred to this point are held commercially to about one part in 5000.

Application of Similitude

Echo box developments have often been undertaken at frequencies where adequate test equipment was not available. This has been especially true as the radar art progressed to higher and higher frequencies.

The principle of similitude has been utilized in the construction and test of models at the frequency of existing test facilities. The models have then been scaled to the assigned frequency band. This has been found to be a very practical expedient.

Use of Cavities For Radar Testing

The high Q resonant cavity when appropriately connected to a radar system returns to it a signal which may be used to judge the over-all performance of the radar. Its operation is as follows: During the transmitted pulse, microwave energy from the radar is stored in the cavity in the electromagnetic field. The charge of the cavity increases exponentially during this interval but fails to reach saturation for the cavity by a substantial margin because the pulse is too short. At the end of the pulse, the decay of this field supplies a signal of the same frequency as that of the radar transmitter (when the echo box is in tune) which is returned to the radar receiver as a continuous signal diminishing exponentially in amplitude.

The time interval between the end of the transmitted pulse and the point where the signal on the radar disappears into the background noise is the "ringtime." The term is used somewhat loosely since, in actual practice, the ringtime is measured on indicators whose range markings are generally in miles or yards referred to the beginning rather than the end of the pulse. The difference, of course, is small. It is customary to include the pulse length in all ringtime figures on operating radar systems. Typical ringtime patterns on radar indicators and a schematic of a radar test with an echo box are shown in Figs. 10 and 11.

As the output power of the radar either increases or decreases corresponding changes in the "charge" of the cavity will be reflected directly in ringtime changes. Similarly as the noise level of the radar receiver varies the

Digitized by Google
Original from UNIVERSITY OF MICHIGAN
Generated on 2019-09-24 06:46 GMT / http://hdl.handle.net/2027/mdp.39015077775156
Public Domain, Google-digitized / http://www.hathitrust.org/access_use#pd-google

merging point of the cavity signal and the noise will show proportional changes in ringtime. Hence, the ringtime indication measures these two factors on which the radar's ability to discern real targets so largely depends.

The exponential buildup and decay of the charge in the cavity occur at a rate determined by the working decrement of the cavity. As mentioned previously, a decrement of about 3 *db* per microsecond is a satisfactory value for the 3 *kmc* and 9 *kmc* bands. A one microsecond change in ringtime (roughly one-tenth mile) would, therefore, represent a change in system performance of 3 *db*.

Uniformity Control and Expected Ringtime

By introducing an adjustment for the working Q of the cavities it is now possible to control the uniformity of the manufactured product to very close limits. Other improvements have also been incorporated which insure that boxes which have been made alike as to Q will similarly give uniform ringtime indications on a test radar. If the test sets are all alike as to ringtime, it is then possible to quote an "expected ringtime" for each of the various radars to be serviced by the echo box. Initially a measuring tool indicating relative changes in day to day operation of the radars, the uniformity provision with its "expected ringtime" has made the echo box test set an absolute measuring instrument of moderate precision.

Other Uses

In addition to its use as a measure of over-all performance of a radar, a significant number of diagnostic tests may be performed when trouble develops, which aid in rapidly locating the source. One such test is spectrum analysis. The extreme selectivity of the high Q cavity permits examination of the spectrum of the pulsed wave and from this may be deduced characteristics of the pulse, including pulse length. Multiple-moding of the magnetron circuit is easily shown by this analysis.

The meter of the test set gives a relative indication of the output power of the radar and this in itself assists greatly in segregating transmitter troubles from receiver troubles.

Also of importance is the use of the echo box as a frequency meter. The high Q of the cavity plus the fine control of the drive mechanism and the direct reading dial give excellent results (comparable to that of a wavemeter).

Acknowledgement

The design of resonant cavities is a difficult and complex art. In bringing it to the present state, the number of individuals who have made significant mathematical, theoretical, engineering and mechanical contributions is so

Digitized by Google
Original from UNIVERSITY OF MICHIGAN
Generated on 2019-09-24 06:46 GMT / http://hdl.handle.net/2027/mdp.39015077775156
Public Domain, Google-digitized / http://www.hathitrust.org/access_use#pd-google

large that it is impossible to give them due credit by name. To them, however, the authors wish to acknowledge their indebtedness and to express their appreciation.

BIBLIOGRAPHY

1. E. I. Green, H. J. Fisher and J. G. Ferguson, "Techniques and Facilities for Microwave Radar Testing". See pp. 861 ff.
2. G. C. Southworth, "Hyper-Frequency Wave Guides—General Considerations and Experimental Results," B. S. T. J., 15, pp. 284–309 (1936).
3. J. J. Thompson, "Notes on Recent Researches in Electricity and Magnetism," Oxford, 1893.
4. Lord Rayleigh, "On the passage of electric waves thru tubes or the vibration of dielectric cylinders," *Phil. Mag.*, 43, pp. 125–132 (1897).
5. A. Becker, "Interferenzrohren fur electrische Wellen," *Ann. d. Phys.*, 8, pp. 22–62 (1902).
6. F. K. Richtmyer and E. H. Kennard, "Introduction to Modern Physics," pp. 184–189, McGraw Hill, 1942.
7. R. I. Sarbacher and W. A. Edson, "Hyper and Ultra-high Frequency Engineering," p. 377, Wiley, 1943.
8. H. A. Wheeler, "Formulas for the Skin Effect," *Proc. I. R. E.*, 30, pp. 412–424 (1942).
9. W. L. Barrow and W. W. Mieher, "Natural Oscillations of Electrical Cavity Resonators," *Proc. I. R. E.*, 28, pp. 184–191 (1940).
10. L. J. Chu, "Electromagnetic Waves in Elliptical Hollow Pipes of Metal," *Jour. App. Phys.*, 9, pp. 583–591 (1938).
11. H. A. Bethe, M.I.T. Radiation Laboratory Reports V-15-S, 43–22, 43–26, 43–27, and 43–30.
12. H. Konig, "The Laws of Similitude of the Electromagnetic Field, and Their Application to Cavity Resonators," *Hochf:tech u. Elek:akus*, 58, pp. 174–180 (1941). Also *Wireless Engr.*, 19, pp. 216–217, No. 1304 (1942).

Generated on 2019-09-24 06:47 GMT / http://hdl.handle.net/2027/mdp.39015077775156
Public Domain, Google-digitized / http://www.hathitrust.org/access_use#pd-google
Digitized by Google
Original from UNIVERSITY OF MICHIGAN

End Plate and Side Wall Currents in Circular Cylinder Cavity Resonator

By J. P. KINZER and I. G. WILSON

Formulas are given for the calculation of the current streamlines and intensity in the walls of a circular cylindrical cavity resonator. Tables are given which permit the calculation to be carried out for many of the lower order modes.

The integration of $\int_0^x \frac{J_\ell(x)}{J'_\ell(x)}\,dx$ is discussed; the integration is carried out for $\ell = 1, 2$ and 3 and tables of the function are given.

The current distribution for a number of modes is shown by plates and figures.

Introduction

In waveguides or in cavity resonators, a knowledge of the electromagnetic field distribution is of prime importance to the designer. Representations of these fields for the lower modes in rectangular, circular and elliptical waveguide, as well as coaxial transmission line, have frequently been described.

For the most part, however, these representations have been diagrammatic or schematic, intended only to give a general physical picture of the fields. In actual designs, such as high Q cavities for use as echo boxes,[1] accurately made plates of the distributions were found necessary to handle adequately problems of excitation of the various modes and of mode suppression.

One use of the charts is to determine where an exciting loop or orifice should be located and how the field should be oriented for maximum coupling to a particular mode. Optimum locations for both launchers and absorbers can be found. Naturally, when attention is concentrated on a single mode these will be located at the maximum current density points. If, however, two or more modes can coexist, and only one is desired, compromise locations can sometimes be found which minimize the unwanted phenomena.

Also, in a cylindrical cavity resonator of high Q with diameter large compared with the operating wavelength, there are many high order modes of oscillation whose resonances fall within the design frequency band. Some of these are undesired and one of the objectives of a practical design is to reduce their responses to a tolerable amount. This process is termed

[1] "High Q Resonant Cavities for Microwave Testing," Wilson, Schramm, Kinzer. See pp. 909 ff.

Digitized by Google
Original from UNIVERSITY OF MICHIGAN
Generated on 2019-09-24 06:47 GMT / http://hdl.handle.net/2027/mdp.39015077775156
Public Domain, Google-digitized / http://www.hathitrust.org/access_use#pd-google

"suppression of the extraneous modes". In this process, an exact knowledge of the distribution of the currents in the cavity walls has been found highly useful.

For example, it has been found experimentally that annular cuts in the end plates of the cylinder give a considerable amount of suppression to many types of extraneous modes with very little effect on the performance of the desired TE 01n mode. These cuts are narrow slits concentric with the axis of the cylinder and going all the way through the metallic end plates into a dielectric beyond.[2] The physical explanation is that an annular slit cuts through the lines of current flow of the extraneous modes, and thereby interrupts the radial component of current and introduces an impedance which damps, or suppresses, the mode. For the TE 01n mode, the slits

	TE Modes	TM Modes
End Plates	$H_\rho = \frac{k_3}{k_1} J_\ell'(k_1\rho) \cos \ell\theta$ $H_\theta = -\ell \frac{k_3}{k_1} \frac{J_\ell(k_1\rho)}{k_1\rho} \sin \ell\theta$	$H_\rho = \ell \frac{J_\ell(k_1\rho)}{k_1\rho} \sin \ell\theta$ $H_\theta = J_\ell'(k_1\rho) \cos \ell\theta$
Side Walls	$H_\theta = \left[-\ell \frac{k_3}{k_1} \frac{J_\ell(k_1 D/2)}{k_1 D/2}\right] [\sin \ell\theta \cos k_3 z]$ $H_z = J_\ell(k_1 D/2) \cos \ell\theta \sin k_3 z$	$H_\theta = J_\ell'(k_1 D/2) \cos \ell\theta \cos k_3 z$ $H_z = 0$

$$k = \frac{2\pi}{\lambda} = k_1^2 + k_3^2$$

$$k_1 = \frac{2r}{D} \qquad k_3 = \frac{n\pi}{L}$$

$r = m^{th}$ root of $J_\ell(x) = 0$ for TM Modes.

$= m^{th}$ root of $J_\ell'(x) = 0$ for TE Modes.

D = cavity diameter

L = cavity length

Fig. 1—Components of H vector at walls of circular cylinder cavity resonator.

are parallel to the current streamlines and there is no such interruption; presumably there is a slight increase in current density alongside the slit,

[2] Similar cuts through the side wall of the cylinder in planes perpendicular to the cylinder axis are also beneficial, but are more troublesome mechanically.

Generated on 2019-09-24 06:47 GMT / http://hdl.handle.net/2027/mdp.39015077775156
Public Domain, Google-digitized / http://www.hathitrust.org/access_use#pd-google
Digitized by Google
Original from UNIVERSITY OF MICHIGAN

as the current formerly on the surface of the removed metal crowds over onto the adjacent metal, but this is a second-order effect.

To determine the best location of such cuts, therefore, it is necessary to know the vector distributions of the wall currents for the various modes. This current vector, I, is proportional to and perpendicular to the magnetic vector, H, of the field at the surface. Expressions for the components of the H-vector at the surfaces of the end plates and side walls are given in Fig. 1.

END PLATE: *Contour Lines*

At the end plates, the magnitude of the H-vector at any point is given by:

$$H^2 = H_\rho^2 + H_\theta^2. \tag{1}$$

Now substitute values of H_ρ and H_θ from Fig. 1 into (1); drop any constant factors common to H_ρ and H_θ as these can be swallowed in a final proportionality constant; introduce the new variable x:

$$x = k_1 \rho = r \frac{\rho}{R}. \tag{2}$$

where $R = D/2$ = cavity radius. Thus is obtained:

$$H^2 = [J'_\ell(x) \cos \ell\theta]^2 + \left[\frac{\ell}{x} J_\ell(x) \sin \ell\theta\right]^2. \tag{3}$$

Now J_ℓ and J'_ℓ, are expressed in terms of $J_{\ell-1}$ and $J_{\ell+1}$ and a further reduction leads to:

$$H^2 = (J_{\ell-} \cos \ell\theta)^2 + (J_{\ell+} \sin \ell\theta)^2 \tag{4}$$

where

$$J_{\ell-} = J_{\ell-1}(x) - J_{\ell+1}(x) \tag{5}$$

and

$$J_{\ell+} = J_{\ell-1}(x) + J_{\ell+1}(x) \tag{6}$$

The formulas (4) to (6) apply to both TE and TM modes. The values obtained depend on r, which is different for each mode.

When $\theta = 0$, I is proportional to $J_{\ell-}$ and when $\theta = \pi/2\ell$, I is proportional to $J_{\ell+}$. Relative values of I are thus easily calculated for these cases, once tables of J_ℓ are available. Such tables have been prepared and are attached. For TE modes, when $\theta = 0$, $H_\theta = 0$, and the currents are all in the θ direction. For TM modes, when $\theta = 0$, $H_\rho = 0$, and the currents are all in the ρ-direction. When $\theta = \pi/2\ell$, the converse holds.

Figures 3 to 18 are a set of curves showing the relative magnitude of H (or I) for several of the lower order TE and TM modes. The abscissae

Digitized by Google
Original from UNIVERSITY OF MICHIGAN
Generated on 2019-09-24 06:49 GMT / http://hdl.handle.net/2027/mdp.39015077775156
Public Domain, Google-digitized / http://www.hathitrust.org/access_use#pd-google

are relative radius, i.e., ρ/R; the ordinates are relative magnitude referred to the maximum value. The drawings also give $r = \pi D/\lambda_c$ for each mode, where λ_c is the cutoff wavelength in a circular guide of diameter D. Values for any point of the surface of the end plate can be calculated by using these curves in conjunction with equation (4).

In general, for each mode there are certain radii at which the current flow is entirely radial, ($I_\theta = 0$). At these radii, which correspond to zeros of $J_\ell(x)$ or $J'_\ell(x)$, the annular cuts mentioned in the introduction are quite effective. However, the maxima of I_ρ do not coincide with the zeros of I_θ; and a more sophisticated treatment gives the best radius as that which maximizes ρI_ρ^2. Values of the relative radius for this last condition are given in Table IV.

Contour lines of equal relative current intensity are obtained by setting H^2 constant in (4), which then expresses a relation between x and θ. The easiest and quickest way to solve (4) is graphically, by plotting H vs. x for different values of θ.

END PLATE: *Current Streamlines*

It is easy to show that the equations of the current streamlines are given by the solutions of the differential equation

$$\frac{d\rho}{d\theta} = -\rho \frac{H_\theta}{H_\rho}. \tag{7}$$

In the case of the TE modes, (7) is easily solved by separation of the variables, leading to the final result:

$$J_\ell(x) \cos \ell\theta = C \tag{8}$$

in which C is a parameter whose value depends on the streamline under consideration. In the TE modes, the E-lines in the interior of the cavity also satisfy (8), hence a plot of the current streamlines in the end plate serves also as a plot of the E lines.

In the case of the TM modes, (7) is not so easily solved. Separation of the variables leads to:

$$-\log \sin \ell\theta = \int \frac{\ell^2 J_\ell(x)}{x^2 J'_\ell(x)}\, dx. \tag{9}$$

The right-hand side of (9) can be reduced somewhat, yielding

$$-\log \sin \ell\theta = \log [xJ'_\ell(x)] + \int \frac{J_\ell(x)}{J'_\ell(x)}\, dx \tag{10}$$

but no further reduction is possible. The remaining integral represents a new function which must be tabulated. Its evaluation is discussed at

Digitized by Google
Original from UNIVERSITY OF MICHIGAN
Generated on 2019-09-24 06:49 GMT / http://hdl.handle.net/2027/mdp.39015077775156
Public Domain, Google-digitized / http://www.hathitrust.org/access_use#pd-google

length in the Appendix, where it is denoted by $F\ell(x)$. Table II of the Appendix gives its values (for $\ell = 1, 2$ and 3) and also those of $G\ell(x)$ where

$$F\ell(x) = -\log G\ell(x) \tag{11}$$

Thus (10) becomes

$$-\log \sin \ell\theta = \log [x J'\ell(x)/G\ell(x)] + C' \tag{12}$$

and the final equation for the current streamlines is

$$[xJ'\ell(x)/G\ell(x)] \sin \ell\theta = C \tag{13}$$

where C is a parameter as before.

It is not difficult to show that $G\ell(x)/J'\ell(x)$ has zeros at the zeros of $J'\ell(x)$. For these values of x, $\sin \ell\theta = 0$ whatever the value of C, and all streamlines converge on (or diverge from) $2\ell m$ points on the end plate.

The flow lines of (13) are orthogonal to the family (8) and could readily be drawn in this manner. However, better accuracy is obtained by plotting (13).

END PLATE: *Distributions*

The 32 attached plates show the distribution of current in the end plates of a circular cylinder cavity resonator for a number of modes.

In the first set of 21, the scaling is such that the diameters of the figures are proportional to those of circular waveguides which would have the same cutoff frequency. This group is of particular interest to the waveguide engineer.

In a second group of 11, the scaling is such as to make the outside diameters of the cylinders uniform. This group is of particular interest to a cavity designer.

This distribution is a vector function of position; that is, at each point in the end plate the surface current has a different direction of flow and a different magnitude or intensity. The variation in current intensity is represented by ten degrees of background shading. The lightest indicates regions of least current intensity and the darkest greatest intensity. The direction of current flow is shown by streamlines. Streamlines are lines such that a tangent at any point indicates the direction of current flow at that point.

The modes represented are the

TE 01, 02, 03	*TM* 01, 02, 03
TE 11, 12, 13	*TM* 11, 12, 13
TE 21, 22, 23	*TM* 21, 22
TE 31, 32	*TM* 31, 32

Digitized by Google
Original from UNIVERSITY OF MICHIGAN
Generated on 2019-09-24 06:49 GMT / http://hdl.handle.net/2027/mdp.39015077775156
Public Domain, Google-digitized / http://www.hathitrust.org/access_use#pd-google

in the nomenclature which has become virtually standard. In this system, *TE* denotes transverse electric modes, or modes whose electric lines lie in planes perpendicular to the cylinder axis; *TM* denotes transverse magnetic modes, or modes whose magnetic lines lie in transverse planes. The first numerical index refers to the number of nodal diameters, or to the order of the Bessel function associated with the mode. The second numerical index refers to the number of nodal circles (counting the resonator boundary as one such) or to the ordinal number of a root of the Bessel function associated with the mode. On the end plates, the distribution does not depend upon the third index (number of half wavelengths along the axis of the cylinder) used in the identification of resonant modes in a cylinder. This considerably simplifies the problem of presentation. The orientation of the field inside the cavity and hence the currents in the end plate depend on other things; thus the orientation of the figures is to be considered arbitrary.

The plates also apply to the corresponding modes of propagation in a circular waveguide as follows: The background shading represents the instantaneous relative distribution of energy across a cross section of guide. For *TE* modes, the current streamlines depict the *E* lines; for the *TM* modes, they depict the projection of the *E* lines on a plane perpendicular to the cylinder axis.

SIDE WALL:

The current distribution in the side walls is easily obtained from the field equations of Fig. 1. For *TM* modes, the currents are entirely longitudinal; their magnitudes vary as $\cos \ell\theta \cos n\pi z/L$. This distribution is so simple as not to require plotting.

For *TE* modes, the situation is more complicated, since both H_z and H_θ exist along the side wall. The current streamlines are given by the solutions of the differential equation

$$\frac{dz}{d\theta} = -\frac{DH_\theta}{2H_z}. \tag{14}$$

By separation of the variables, the solution is found to be

$$\log (C \cos \ell\theta) = \left[\frac{k_1}{k_3}\right]^2 \log \cos k_3 z. \tag{15}$$

Contour lines of constant magnitude of the current are given by

$$\left(\frac{2k_3\ell}{k_1^2 D} \sin \ell\theta \cos k_3 z\right)^2 + (\cos \ell\theta \sin k_3 z)^2 = K^2. \tag{16}$$

In the above, C and K are parameters, different values of which correspond to different streamlines or contour lines, respectively.

Digitized by Google
Original from UNIVERSITY OF MICHIGAN
Generated on 2019-09-24 06:49 GMT / http://hdl.handle.net/2027/mdp.39015077775156
Public Domain, Google-digitized / http://www.hathitrust.org/access_use#pd-google

Since both streamlines and contours are periodic in z and θ, it is not essential to represent more than is covered in a rectangular piece of the side wall corresponding to quarter periods in z and θ. These are covered in a length $\frac{L}{2n}$ along the cavity and in a distance $\frac{\pi D}{4\ell}$ around the cavity. If such a piece of the surface be rolled out onto a plane it forms a rectangle of proportions $\frac{\pi nD}{2\ell L}$.

The difficulty in depicting the side wall currents of TE modes, as compared with the end plate currents, is now apparent. For the end plate, the "proportions" are fixed as being a circle. Furthermore, for a given ℓ, as m increases the effect is merely to add on additional rings to the previous streamline and contour plots. Here, however, the proportions of the rectangle are variable, in the first place. And for a given rectangle the streamlines and contours both change as ℓ and m are varied. Another way of expressing the same idea is that for end plates the current distribution does not depend upon the mode index n, and varies only in an additive way with the index m, whereas for the side walls the distribution depends in nearly equal strength on ℓ, m and n.

Some simplification of the situation is accomplished by introducing two new parameters, the "shape" and the "mode" parameters, defined by:

$$S = \frac{\pi nD}{2\ell L} \qquad M = \frac{\ell}{r} \tag{17}$$

and two new variables

$$Z = k_3 z \qquad \phi = \ell\theta. \tag{18}$$

Substitution of the above, and also the expressions for k_1 and k_3 (see Fig. 1) into (15) and (16) yields

$$\cos Z = C(\cos\phi)^{S^2M^2} \quad \text{(streamlines)} \tag{19}$$

$$\cos Z = \left[\frac{K^2 - \cos^2\phi}{(S^2M^4\sin^2\phi - \cos^2\phi)}\right]^{1/2} \cdot \quad \text{(contours)}. \tag{20}$$

For given proportions S, one can calculate the streamlines and contours for various values of M. Thus a "square array" of side wall currents can be prepared, such as shown on Fig. 2.

The mode parameter, M, in the physical case takes on discrete values which depend on the mode. Some of its values are given in the following table. They all lie between 0 and 1 and there are an infinite number of them.

Digitized by Google
Original from UNIVERSITY OF MICHIGAN
Generated on 2019-09-24 06:49 GMT / http://hdl.handle.net/2027/mdp.39015077775156
Public Domain, Google-digitized / http://www.hathitrust.org/access_use#pd-google

M =

M = 0

Digitized by Google
Original from UNIVERSITY OF MICHIGAN
Generated on 2019-09-24 06:51 GMT / http://hdl.handle.net/2027/mdp.39015077775156
Public Domain, Google-digitized / http://www.hathitrust.org/access_use#pd-google

Generated on 2019-09-24 06:51 GMT / http://hdl.handle.net/2027/mdp.39015077775156
Public Domain, Google-digitized / http://www.hathitrust.org/access_use#pd-google

Digitized by Google

Original from
UNIVERSITY OF MICHIGAN

VALUE OF $M = \ell/r$ FOR TE MODES

ℓ	1	2	3	4	5	6	10	15	20
$m = 1$	.5432	.6549	.7141	.7522	.7793	.8000	.8495	.8813	.9001
2	.1875	.2982	.3743	.4309	.4753	.5113	.6080	.6774	
3	.1172	.2006	.2644	.3154	.3575	.3930	.4945	.5730	
4	.0854	.1519	.2057	.2506	.2888	.3219	.4209		

For any given mode in any given cavity, the values of S and M can be calculated from (17). In general, these values will not coincide with those which have been plotted, but by the same token, they will lie among a group of four combinations which have been plotted. Since the changes in distribution are smooth, mental two-way interpolation will present no difficulty.

ACKNOWLEDGMENT

The final plates depicting the current distributions are the result of the efforts of many individuals in plotting, spray tinting of the background, inking of the streamlines on celluloid overlay, and photographing. Special mention must be made, however, of the contribution of Miss Florence C. Larkey, who carried out all the lengthy calculations of the tables hereto attached and of the necessary data for the plotting.

Generated on 2019-09-24 06:51 GMT / http://hdl.handle.net/2027/mdp.39015077775156
Public Domain, Google-digitized / http://www.hathitrust.org/access_use#pd-google
Digitized by Google
Original from UNIVERSITY OF MICHIGAN

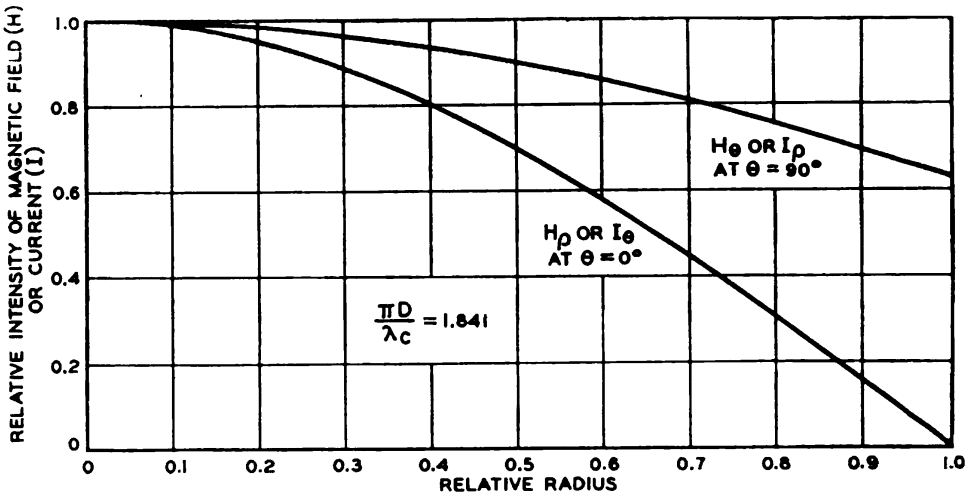
RELATIVE INTENSITY OF MAGNETIC FIELD (H) OR CURRENT (I)
RELATIVE RADIUS
H_θ OR I_ρ AT $\theta = 90°$
H_ρ OR I_θ AT $\theta = 0°$
$\frac{\pi D}{\lambda_c} = 1.841$

Fig. 3—End plate currents in TE 11 mode.

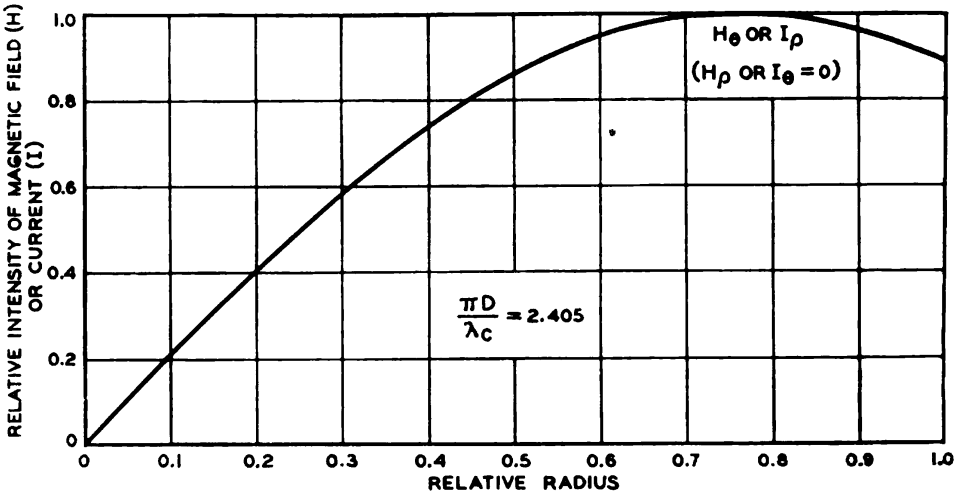
RELATIVE INTENSITY OF MAGNETIC FIELD (H) OR CURRENT (I)
RELATIVE RADIUS
H_θ OR I_ρ (H_ρ OR $I_\theta = 0$)
$\frac{\pi D}{\lambda_c} = 2.405$

Fig. 4—End plate currents in TM 01 mode.

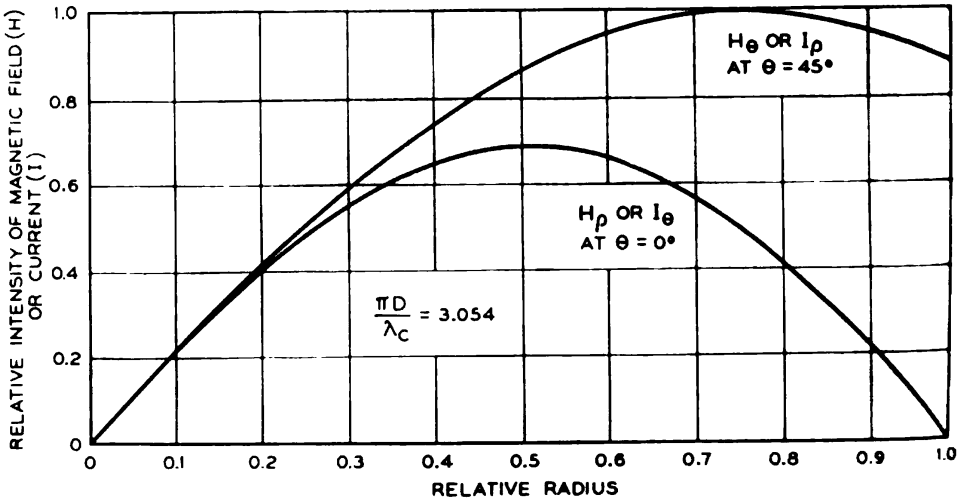
RELATIVE INTENSITY OF MAGNETIC FIELD (H) OR CURRENT (I)
RELATIVE RADIUS
H_θ OR I_ρ AT $\theta = 45°$
H_ρ OR I_θ AT $\theta = 0°$
$\frac{\pi D}{\lambda_c} = 3.054$

Fig. 5—End plate currents in TE 21 mode.

Digitized by Google
Original from UNIVERSITY OF MICHIGAN
Generated on 2019-09-24 06:52 GMT / http://hdl.handle.net/2027/mdp.39015077775156
Public Domain, Google-digitized / http://www.hathitrust.org/access_use#pd-google

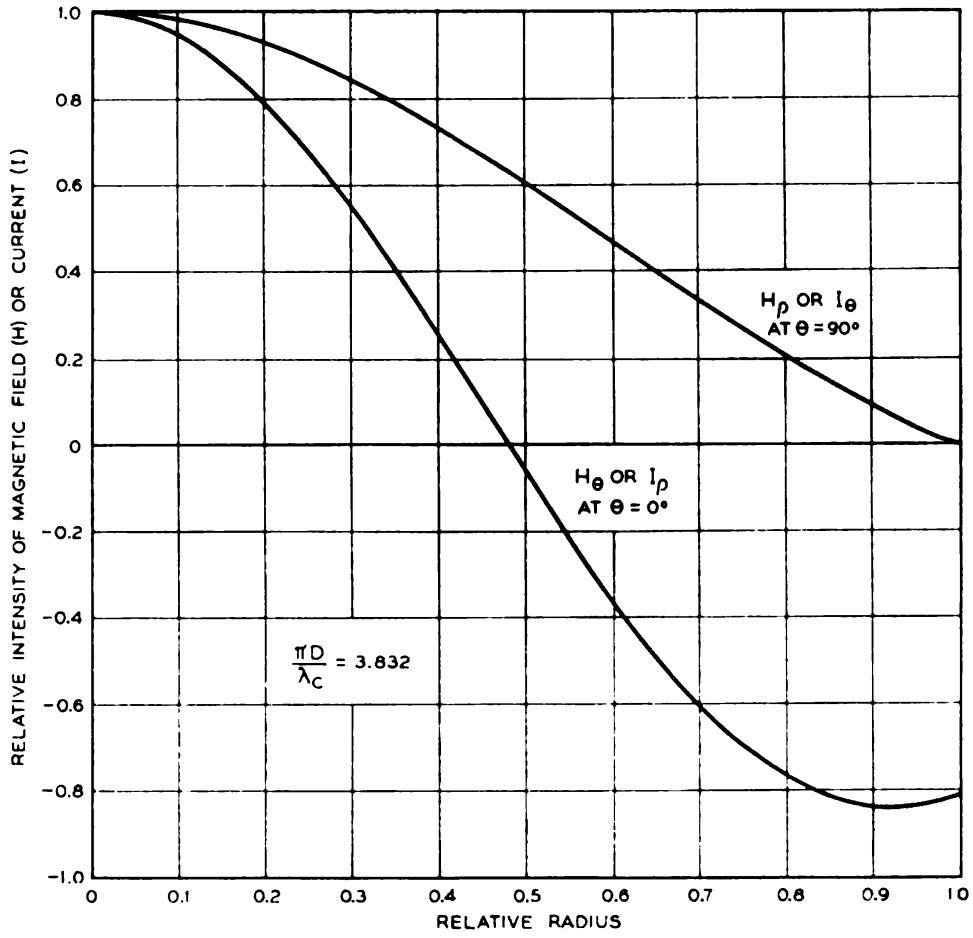

Fig. 6—End plate currents in TM 11 mode.

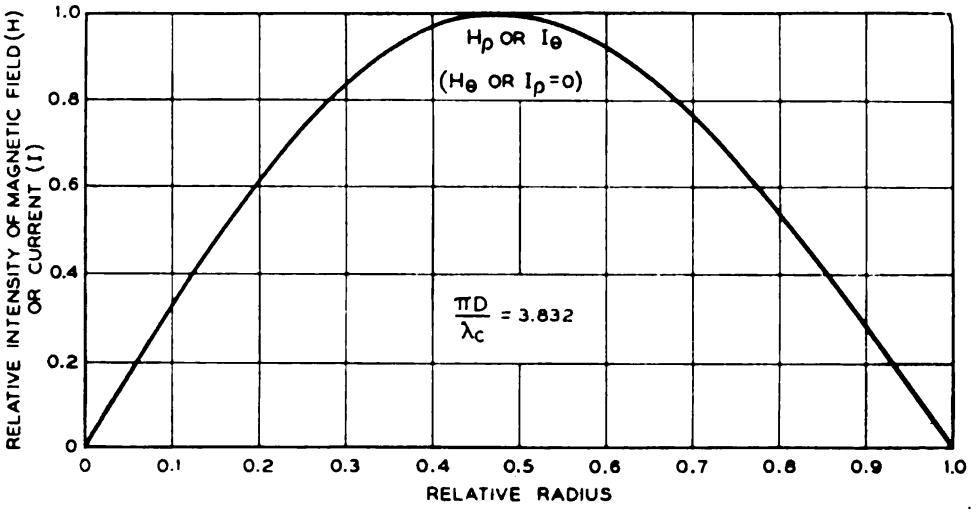

Fig. 7—End plate currents in TE 01 mode.

Digitized by Google
Original from UNIVERSITY OF MICHIGAN
Generated on 2019-09-24 06:52 GMT / http://hdl.handle.net/2027/mdp.39015077775156
Public Domain, Google-digitized / http://www.hathitrust.org/access_use#pd-google

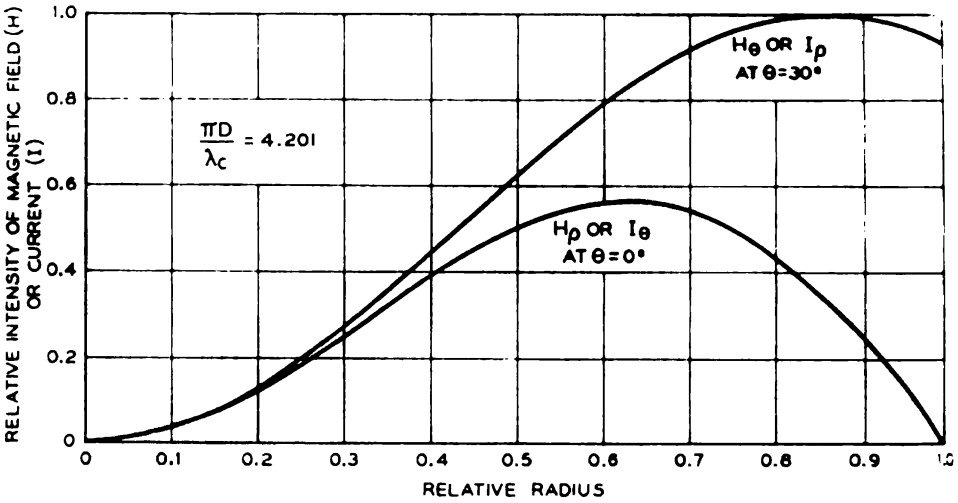
RELATIVE INTENSITY OF MAGNETIC FIELD (H) OR CURRENT (I)
RELATIVE RADIUS
H_θ OR I_ρ AT θ=30°
H_ρ OR I_θ AT θ=0°
$\frac{\pi D}{\lambda_c}$ = 4.201

Fig. 8—End plate currents in TE 31 mode.

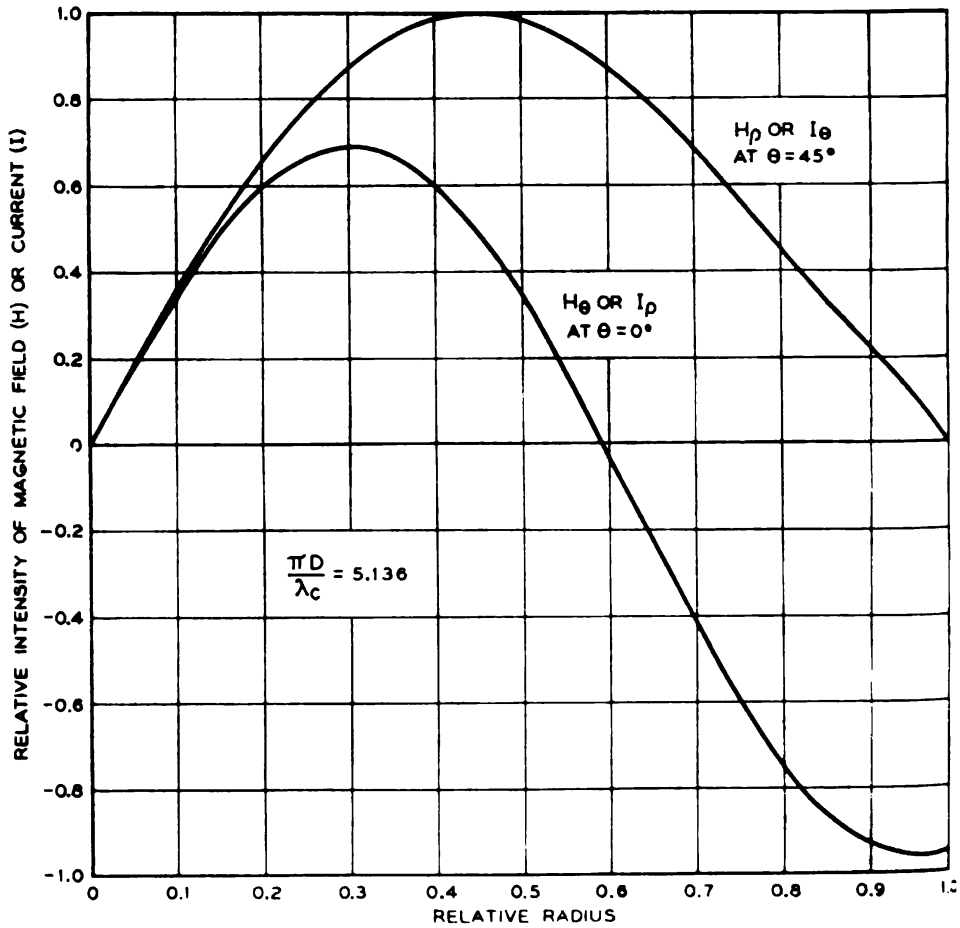
RELATIVE INTENSITY OF MAGNETIC FIELD (H) OR CURRENT (I)
RELATIVE RADIUS
H_ρ OR I_θ AT θ=45°
H_θ OR I_ρ AT θ=0°
$\frac{\pi D}{\lambda_c}$ = 5.136

Fig. 9—End plate currents in TM 21 mode.

Digitized by Google
Original from UNIVERSITY OF MICHIGAN
Generated on 2019-09-24 06:52 GMT / http://hdl.handle.net/2027/mdp.39015077775156
Public Domain, Google-digitized / http://www.hathitrust.org/access_use#pd-google

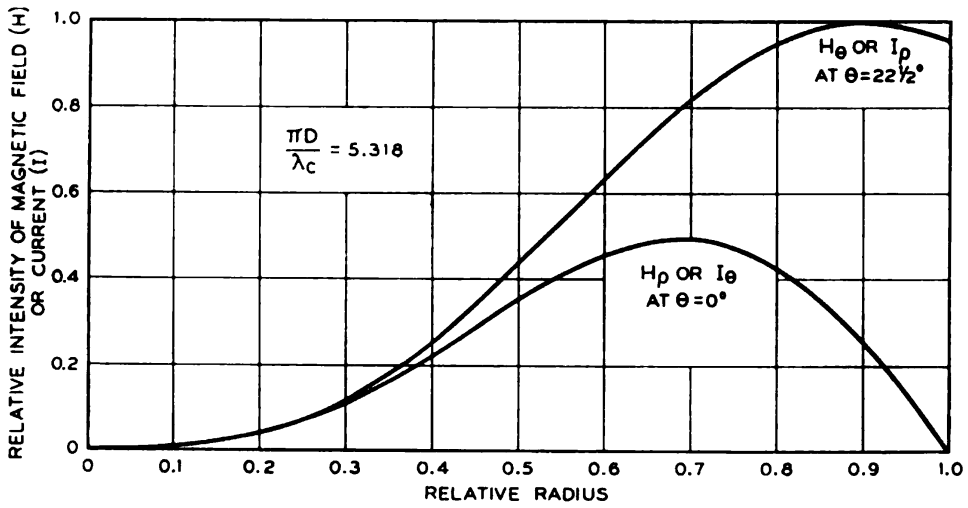
RELATIVE INTENSITY OF MAGNETIC FIELD (H) OR CURRENT (I)
RELATIVE RADIUS
$\frac{\pi D}{\lambda_c} = 5.318$
H_θ OR I_ρ AT $\theta = 22\frac{1}{2}°$
H_ρ OR I_θ AT $\theta = 0°$

Fig. 10—End plate currents in TE 41 mode.

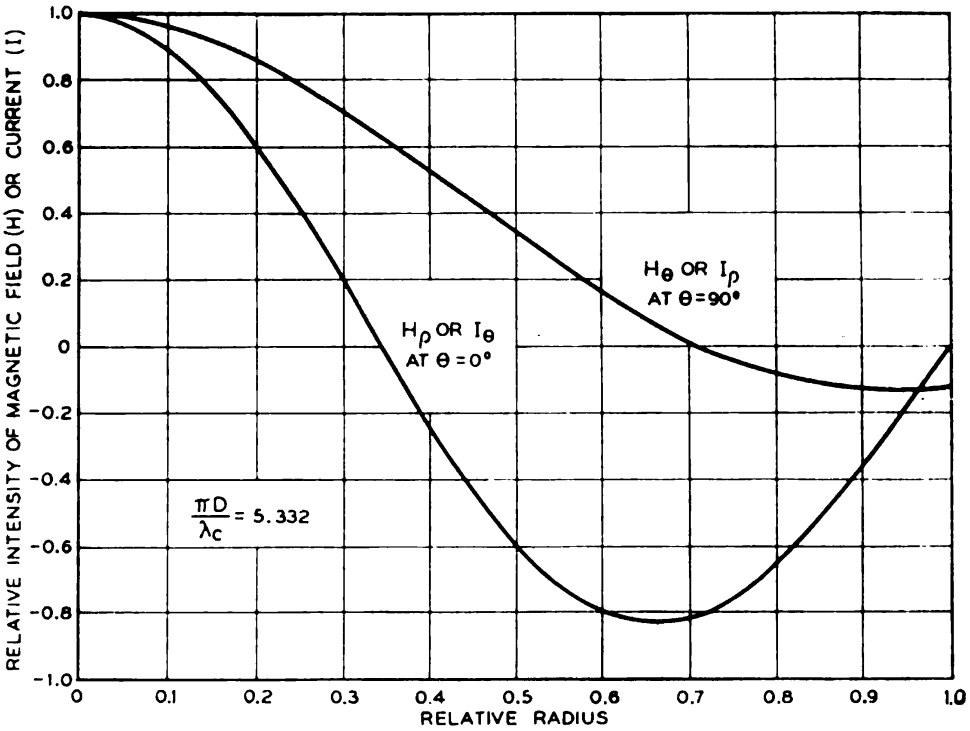
RELATIVE INTENSITY OF MAGNETIC FIELD (H) OR CURRENT (I)
RELATIVE RADIUS
$\frac{\pi D}{\lambda_c} = 5.332$
H_θ OR I_ρ AT $\theta = 90°$
H_ρ OR I_θ AT $\theta = 0°$

Fig. 11—End plate currents in TE 12 mode.

Digitized by Google
Original from UNIVERSITY OF MICHIGAN
Generated on 2019-09-24 06:52 GMT / http://hdl.handle.net/2027/mdp.39015077775156
Public Domain, Google-digitized / http://www.hathitrust.org/access_use#pd-google

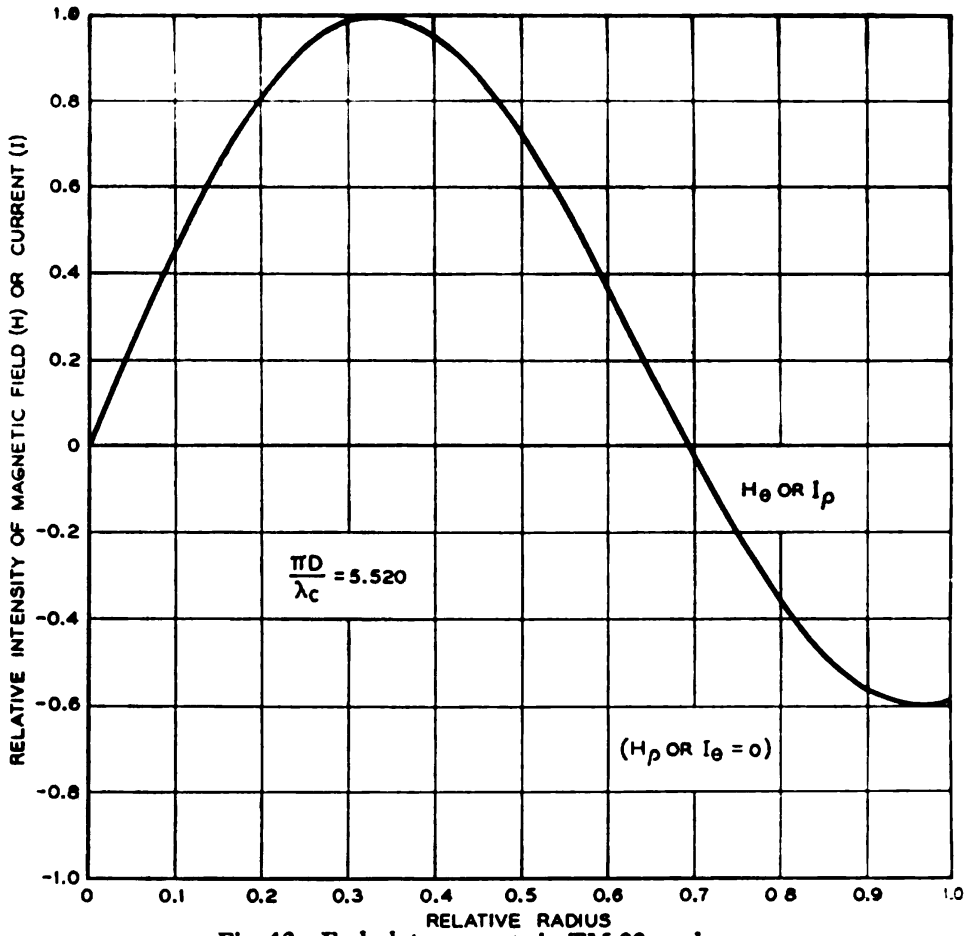
RELATIVE INTENSITY OF MAGNETIC FIELD (H) OR CURRENT (I)
RELATIVE RADIUS
H_θ OR I_ρ
$\frac{\pi D}{\lambda_c} = 5.520$
(H_ρ OR $I_\theta = 0$)

Fig. 12—End plate currents in TM 02 mode.

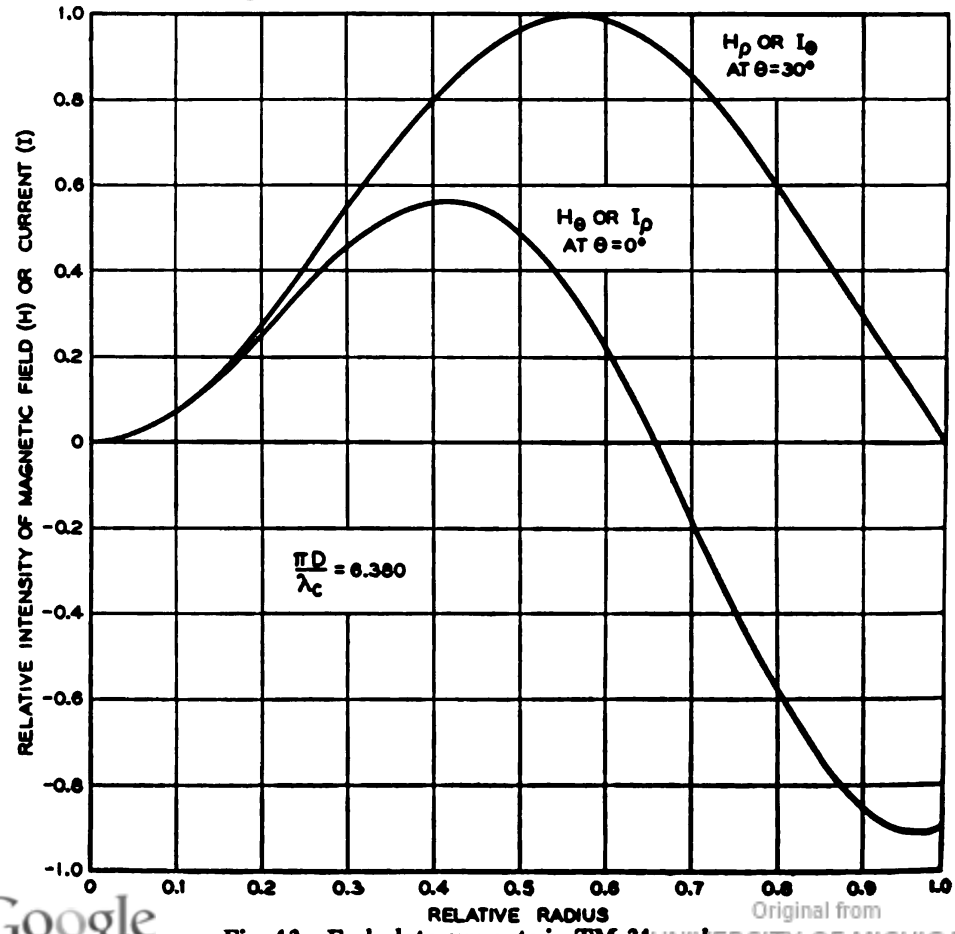
RELATIVE INTENSITY OF MAGNETIC FIELD (H) OR CURRENT (I)
RELATIVE RADIUS
H_ρ OR I_θ AT $\theta = 30°$
H_θ OR I_ρ AT $\theta = 0°$
$\frac{\pi D}{\lambda_c} = 6.380$

Fig. 13—End plate currents in TM 31 mode.

Digitized by Google
Original from UNIVERSITY OF MICHIGAN
Generated on 2019-09-24 06:52 GMT / http://hdl.handle.net/2027/mdp.39015077775156
Public Domain, Google-digitized / http://www.hathitrust.org/access_use#pd-google

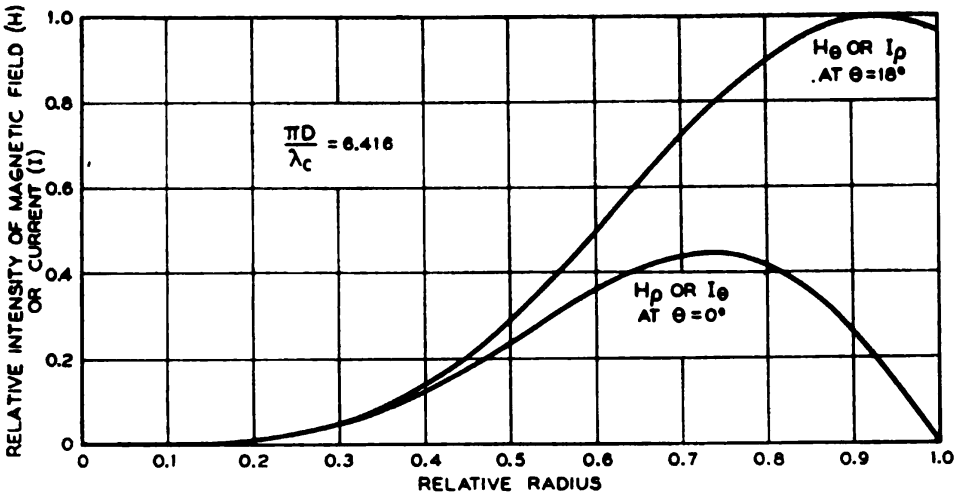

Fig. 14—End plate currents in TE 51 mode.

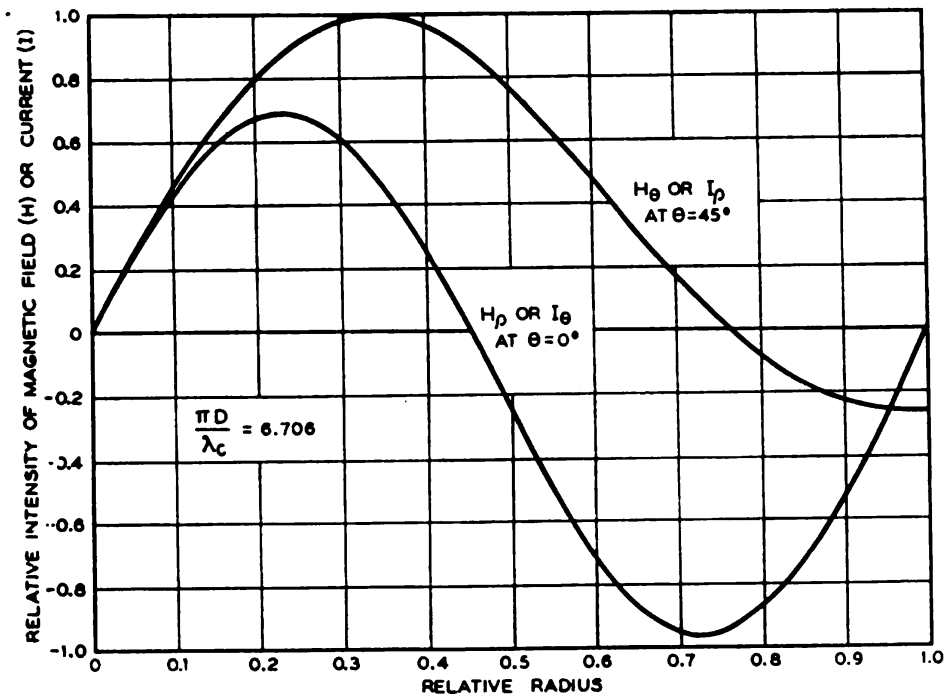

Fig. 15—End plate currents in TE 22 mode.

Generated on 2019-09-24 06:53 GMT / http://hdl.handle.net/2027/mdp.39015077775156
Public Domain, Google-digitized / http://www.hathitrust.org/access_use#pd-google
Digitized by Google
Original from UNIVERSITY OF MICHIGAN

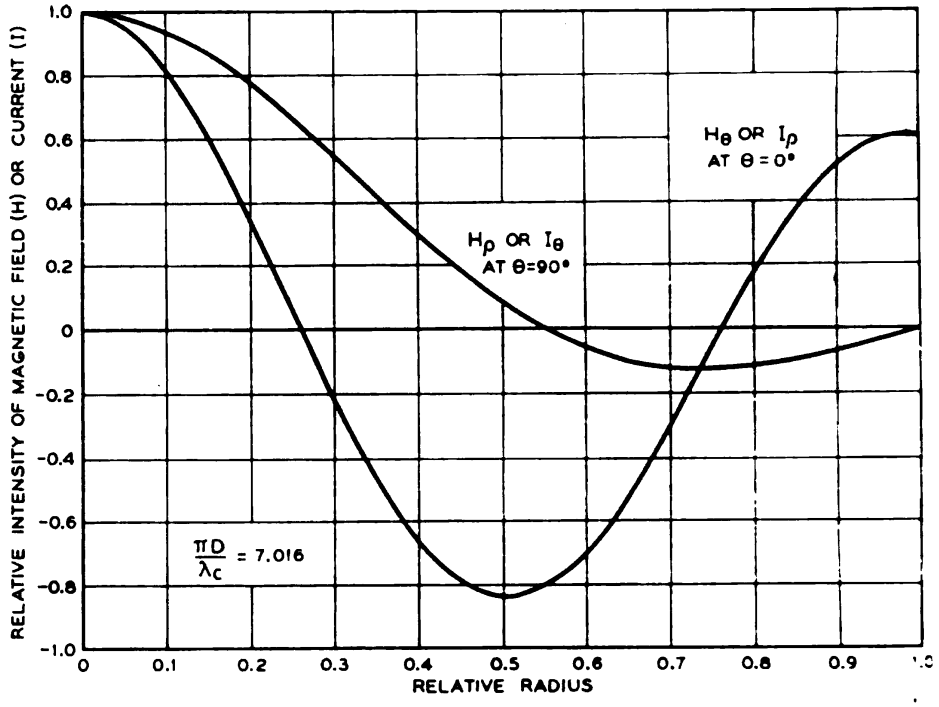
RELATIVE INTENSITY OF MAGNETIC FIELD (H) OR CURRENT (I)
RELATIVE RADIUS
H_θ OR I_ρ AT $\theta = 0°$
H_ρ OR I_θ AT $\theta = 90°$
$\frac{\pi D}{\lambda_c} = 7.016$

Fig. 16—End plate currents in TM 12 mode.

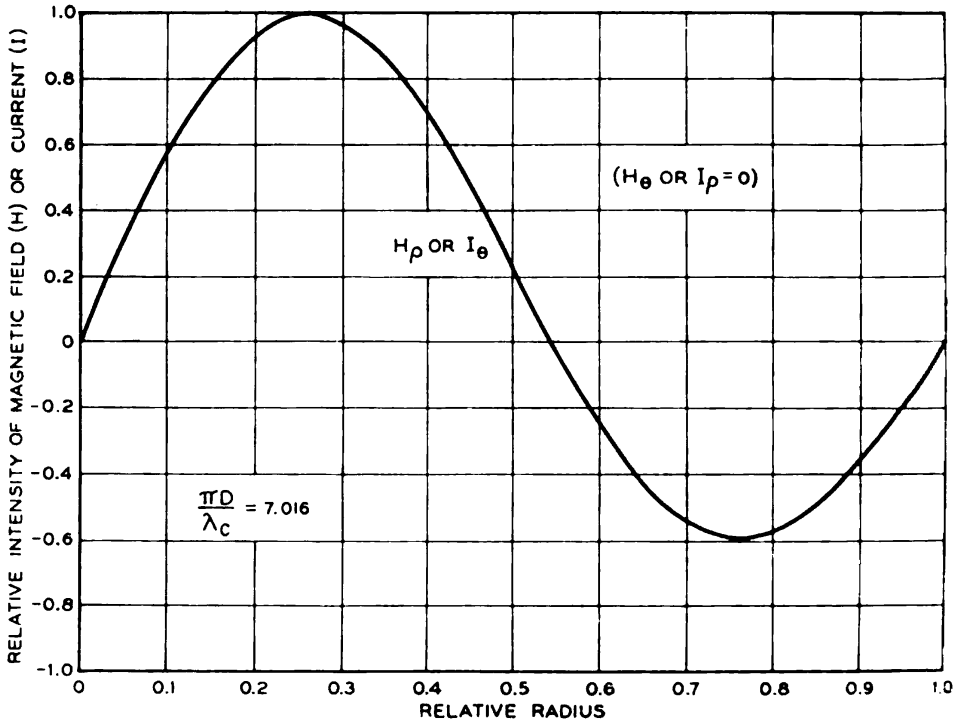
RELATIVE INTENSITY OF MAGNETIC FIELD (H) OR CURRENT (I)
RELATIVE RADIUS
(H_θ OR $I_\rho = 0$)
H_ρ OR I_θ
$\frac{\pi D}{\lambda_c} = 7.016$

Fig. 17—End plate currents in TE 02 mode.

Digitized by Google
Original from UNIVERSITY OF MICHIGAN
Generated on 2019-09-24 06:53 GMT / http://hdl.handle.net/2027/mdp.39015077775156
Public Domain, Google-digitized / http://www.hathitrust.org/access_use#pd-google

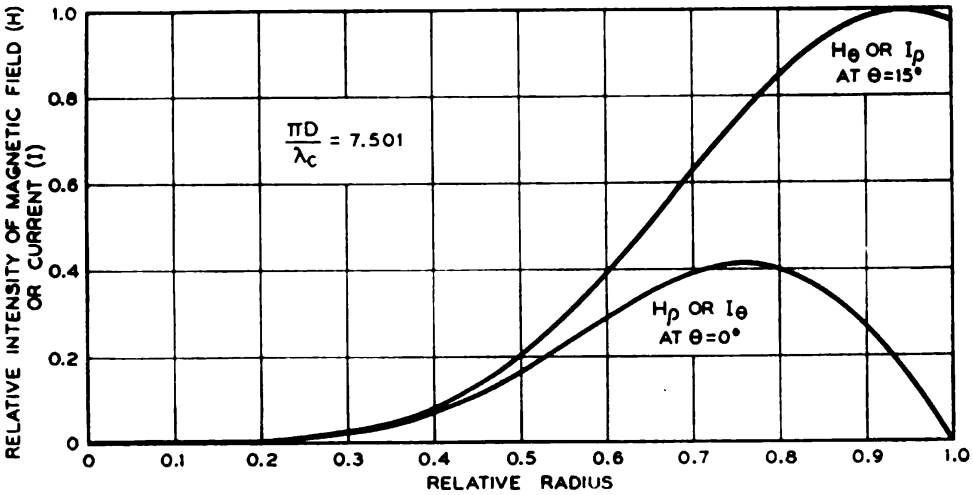

Fig. 18—End plate currents in TE 61 mode.

Digitized by Google
Original from UNIVERSITY OF MICHIGAN
Generated on 2019-09-24 06:53 GMT / http://hdl.handle.net/2027/mdp.39015077775156
Public Domain, Google-digitized / http://www.hathitrust.org/access_use#pd-google

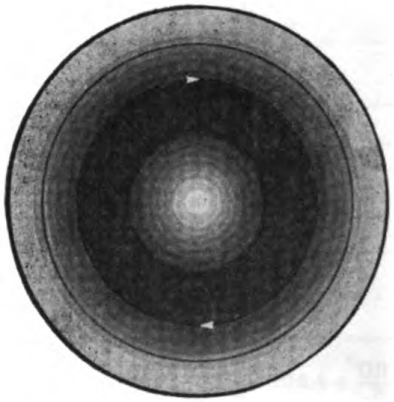

Fig. 19—TE 01 mode.

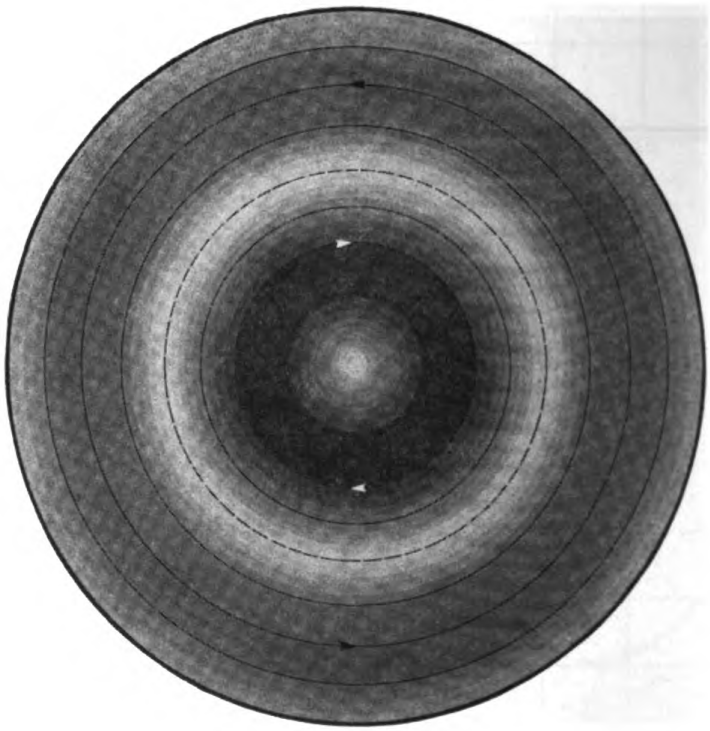

Fig. 20—TE 02 mode.

Digitized by Google
Original from UNIVERSITY OF MICHIGAN
Generated on 2019-09-24 06:53 GMT / http://hdl.handle.net/2027/mdp.39015077775156
Public Domain, Google-digitized / http://www.hathitrust.org/access_use#pd-google

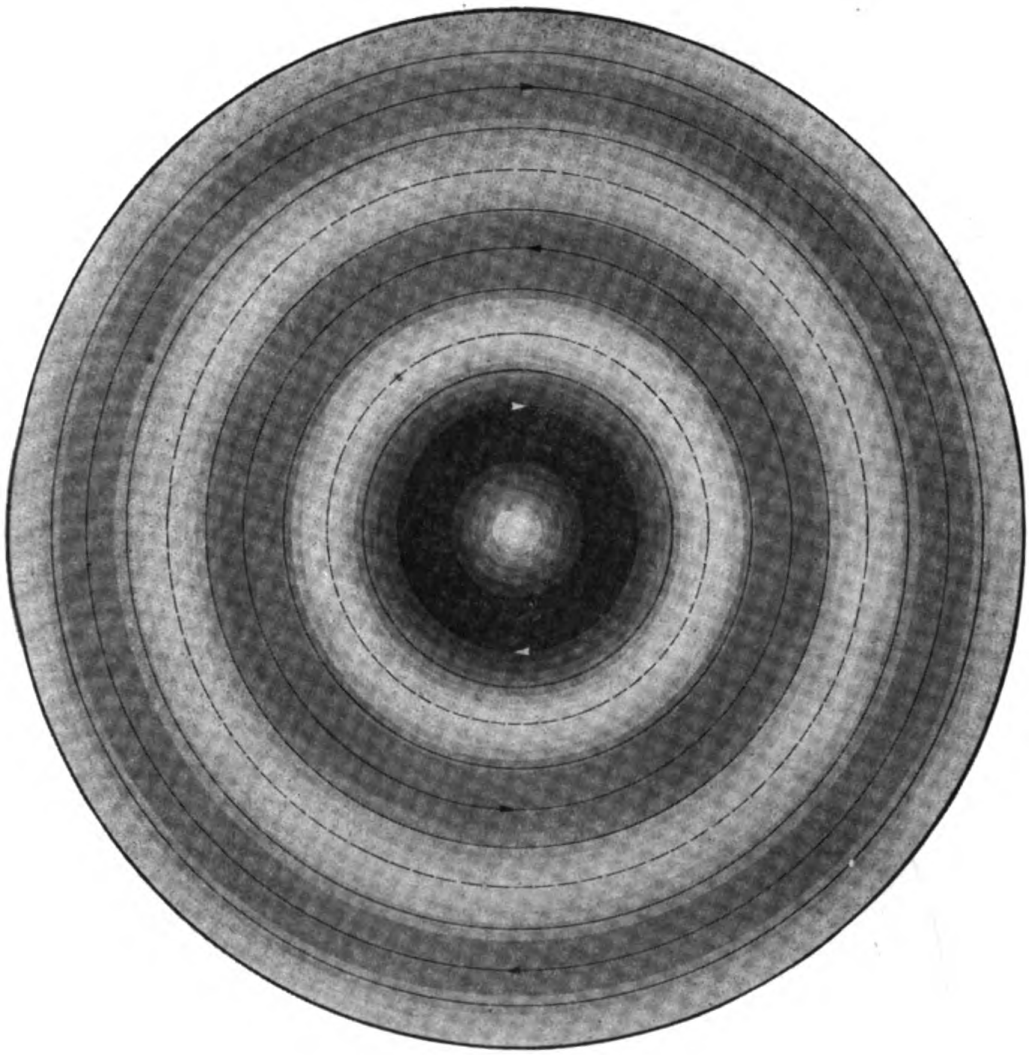

Fig. 21—TE 03 mode.

Fig. 22—TE 11 mode.

Digitized by Google
Original from UNIVERSITY OF MICHIGAN
Generated on 2019-09-24 06:53 GMT / http://hdl.handle.net/2027/mdp.39015077775156
Public Domain, Google-digitized / http://www.hathitrust.org/access_use#pd-google

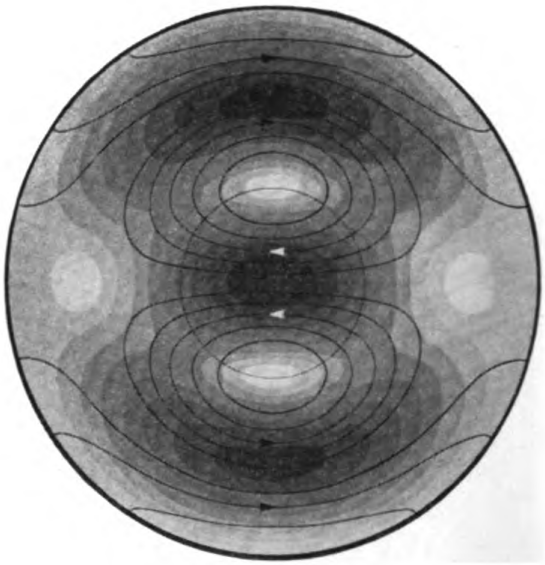

Fig. 23—TE 12 mode.

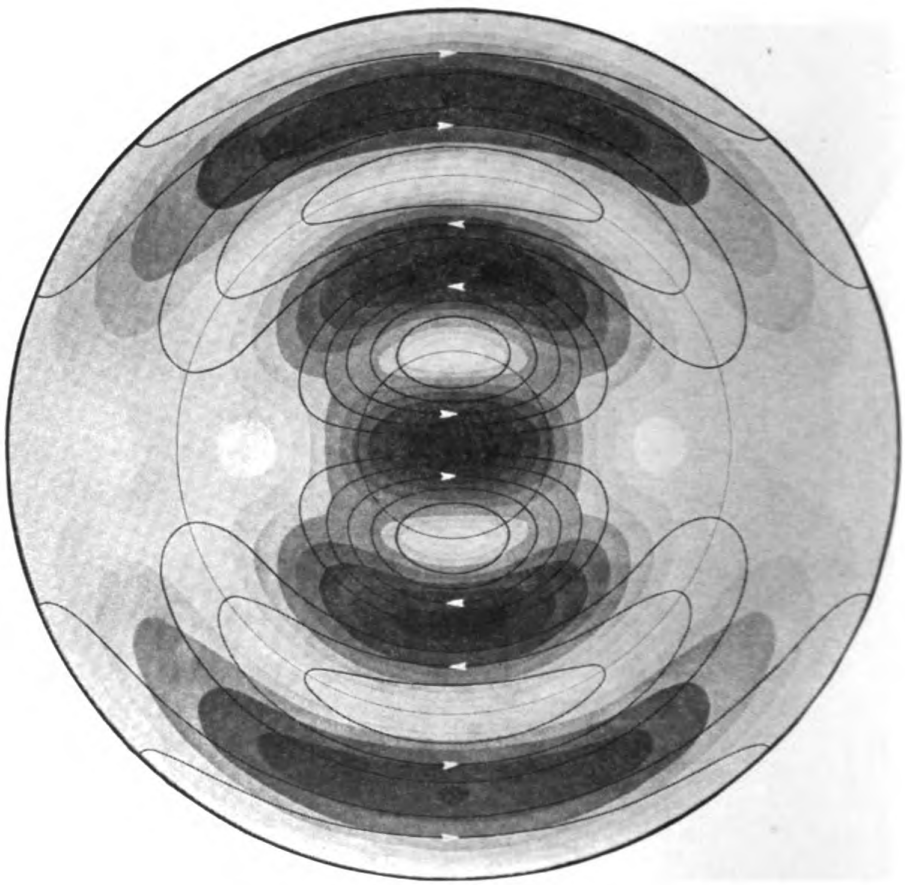

Fig. 24—TE 13 mode.

Digitized by Google
Original from UNIVERSITY OF MICHIGAN
Generated on 2019-09-24 06:54 GMT / http://hdl.handle.net/2027/mdp.39015077775156
Public Domain, Google-digitized / http://www.hathitrust.org/access_use#pd-google

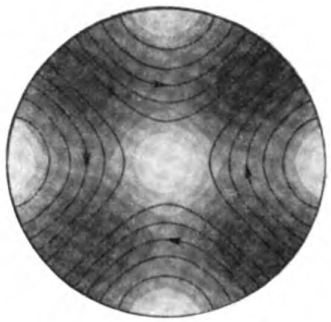

Fig. 25—TE 21 mode.

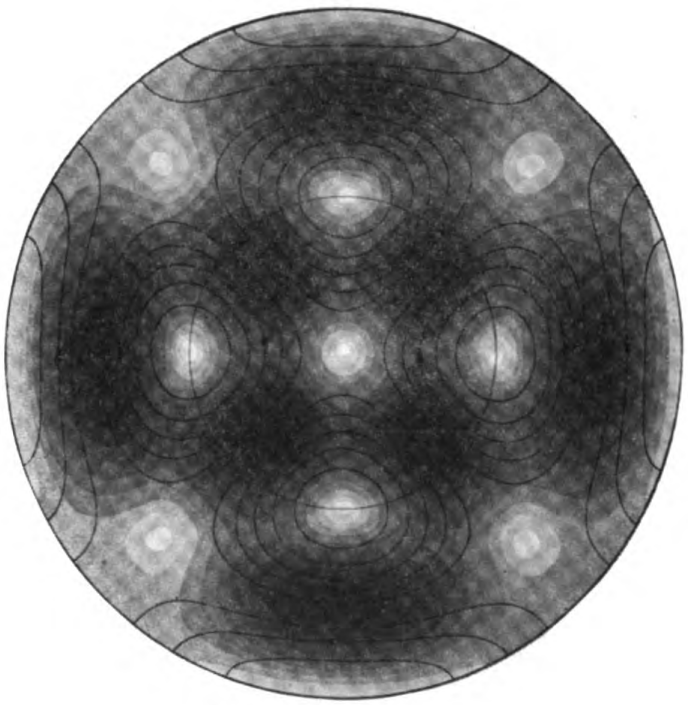

Fig. 26—TE 22 mode.

Generated on 2019-09-24 06:54 GMT / http://hdl.handle.net/2027/mdp.39015077775156
Public Domain, Google-digitized / http://www.hathitrust.org/access_use#pd-google
Digitized by Google
Original from UNIVERSITY OF MICHIGAN

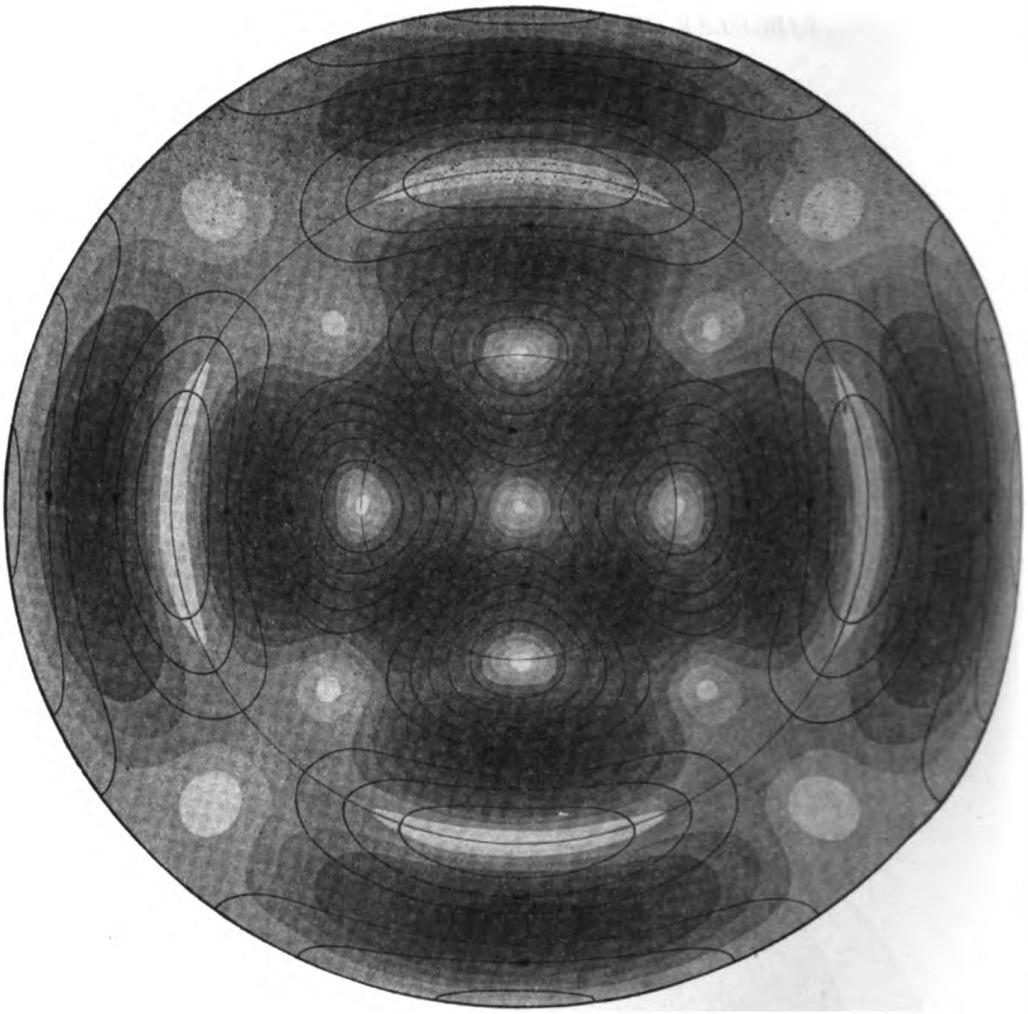

Fig. 27—TE 23 mode.

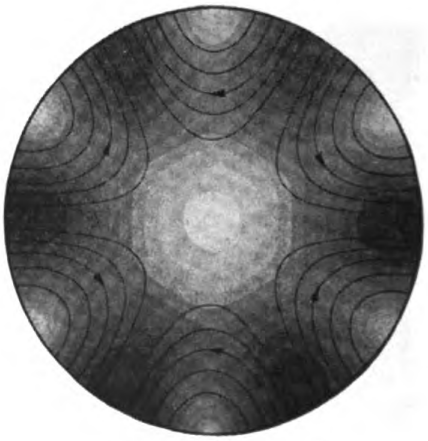

Fig. 28—TE 31 mode.

Digitized by Google
Original from UNIVERSITY OF MICHIGAN
Generated on 2019-09-24 06:54 GMT / http://hdl.handle.net/2027/mdp.39015077775156
Public Domain, Google-digitized / http://www.hathitrust.org/access_use#pd-google

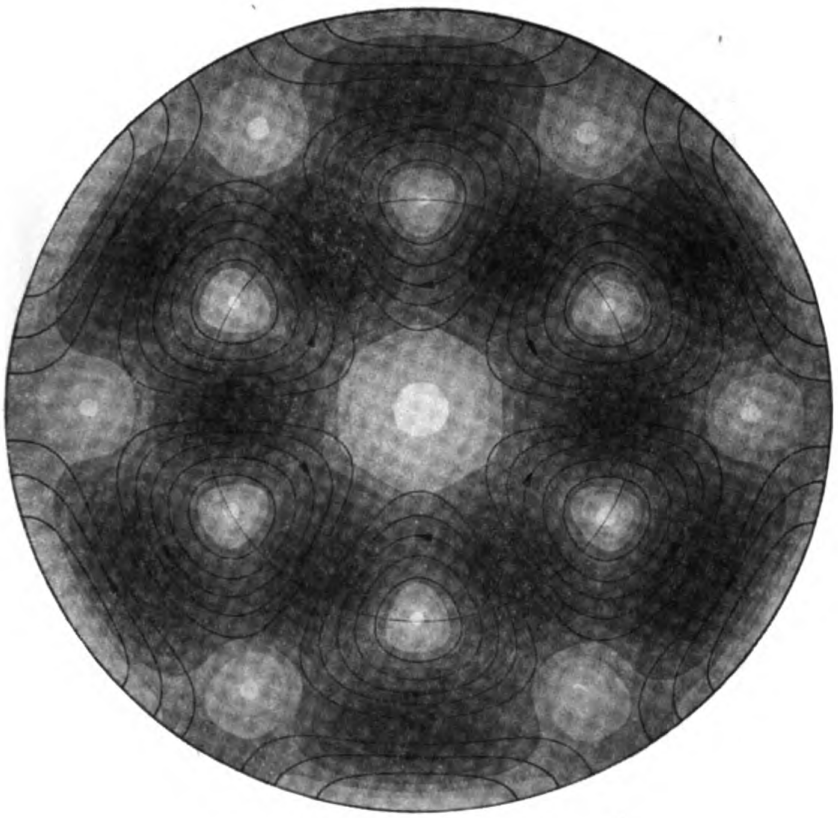

Fig. 29—TE 32 mode.

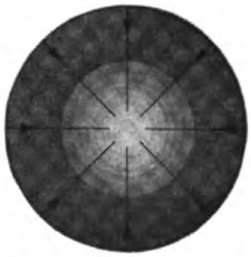

Fig. 30—TM 01 mode.

Generated on 2019-09-24 06:54 GMT / http://hdl.handle.net/2027/mdp.39015077775156
Public Domain, Google-digitized / http://www.hathitrust.org/access_use#pd-google
Digitized by Google
Original from UNIVERSITY OF MICHIGAN

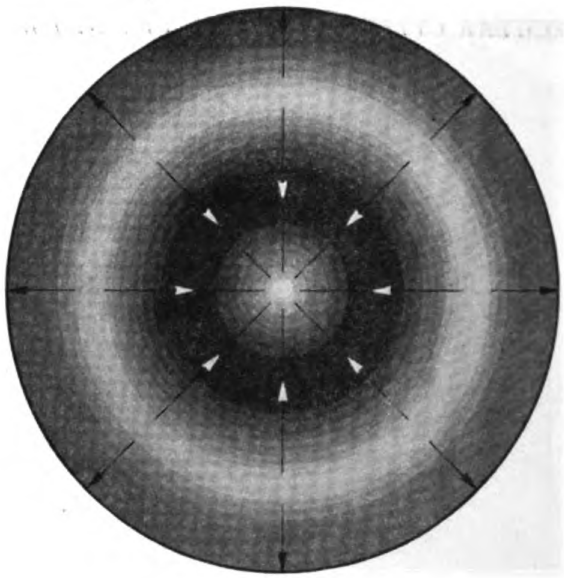

Fig. 31—TM 02 mode.

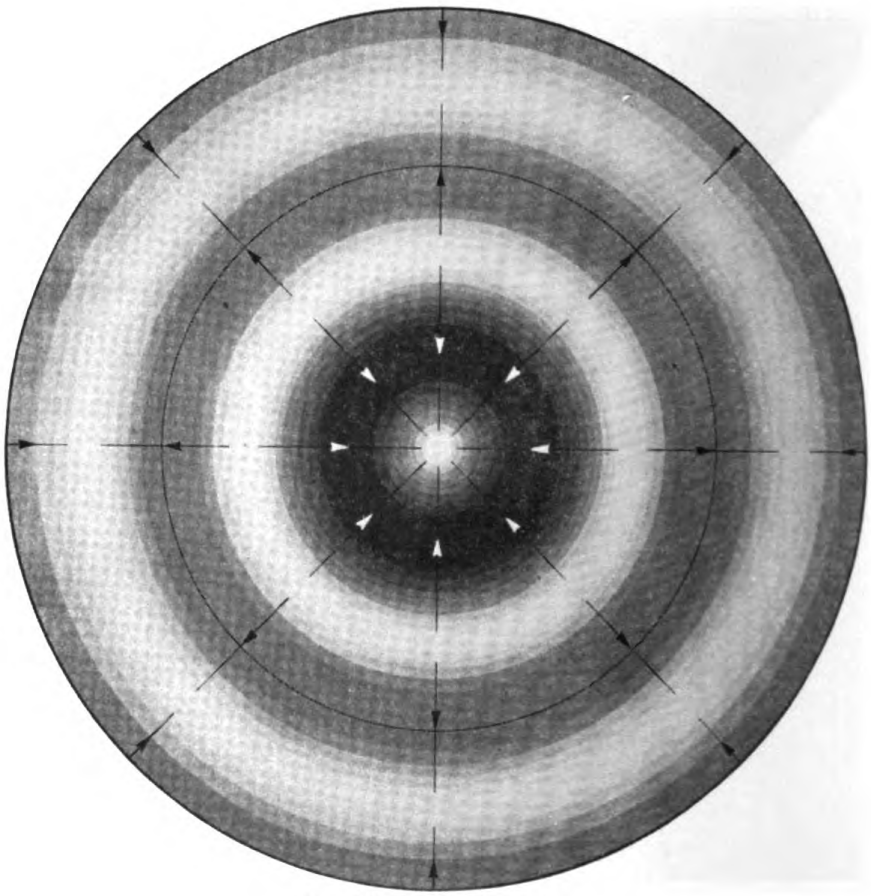

Fig. 32—TM 03 mode.

Digitized by Google
Original from UNIVERSITY OF MICHIGAN
Generated on 2019-09-24 06:54 GMT / http://hdl.handle.net/2027/mdp.39015077775156
Public Domain, Google-digitized / http://www.hathitrust.org/access_use#pd-google

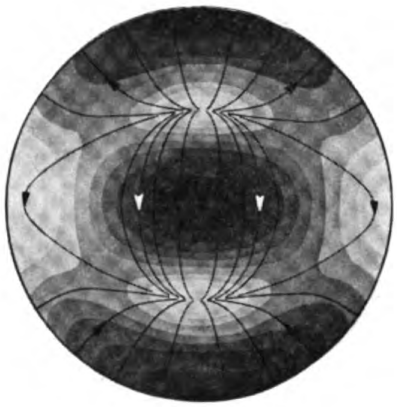

Fig. 33—TM 11 mode.

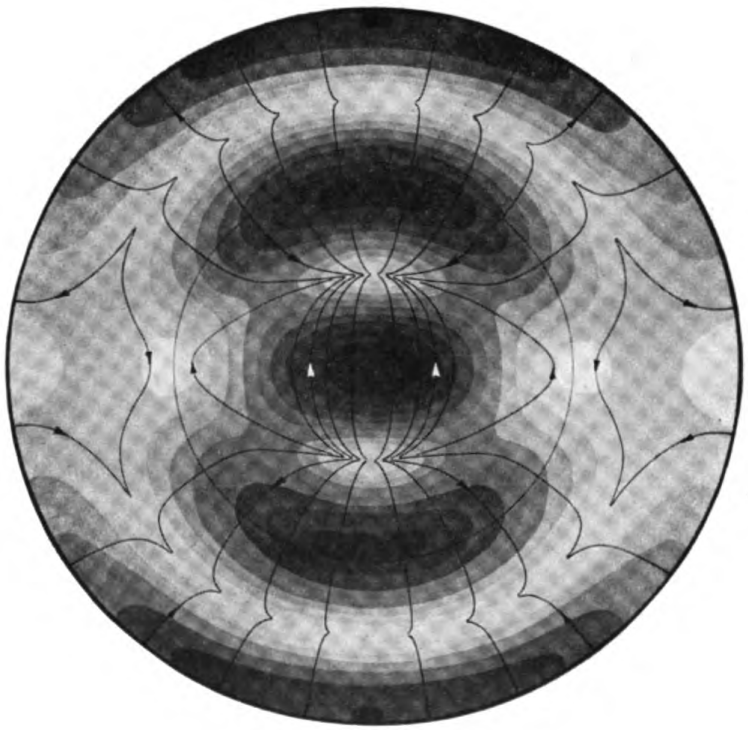

Fig. 34—TM 12 mode.

Digitized by Google
Original from UNIVERSITY OF MICHIGAN
Generated on 2019-09-24 06:55 GMT / http://hdl.handle.net/2027/mdp.39015077775156
Public Domain, Google-digitized / http://www.hathitrust.org/access_use#pd-google

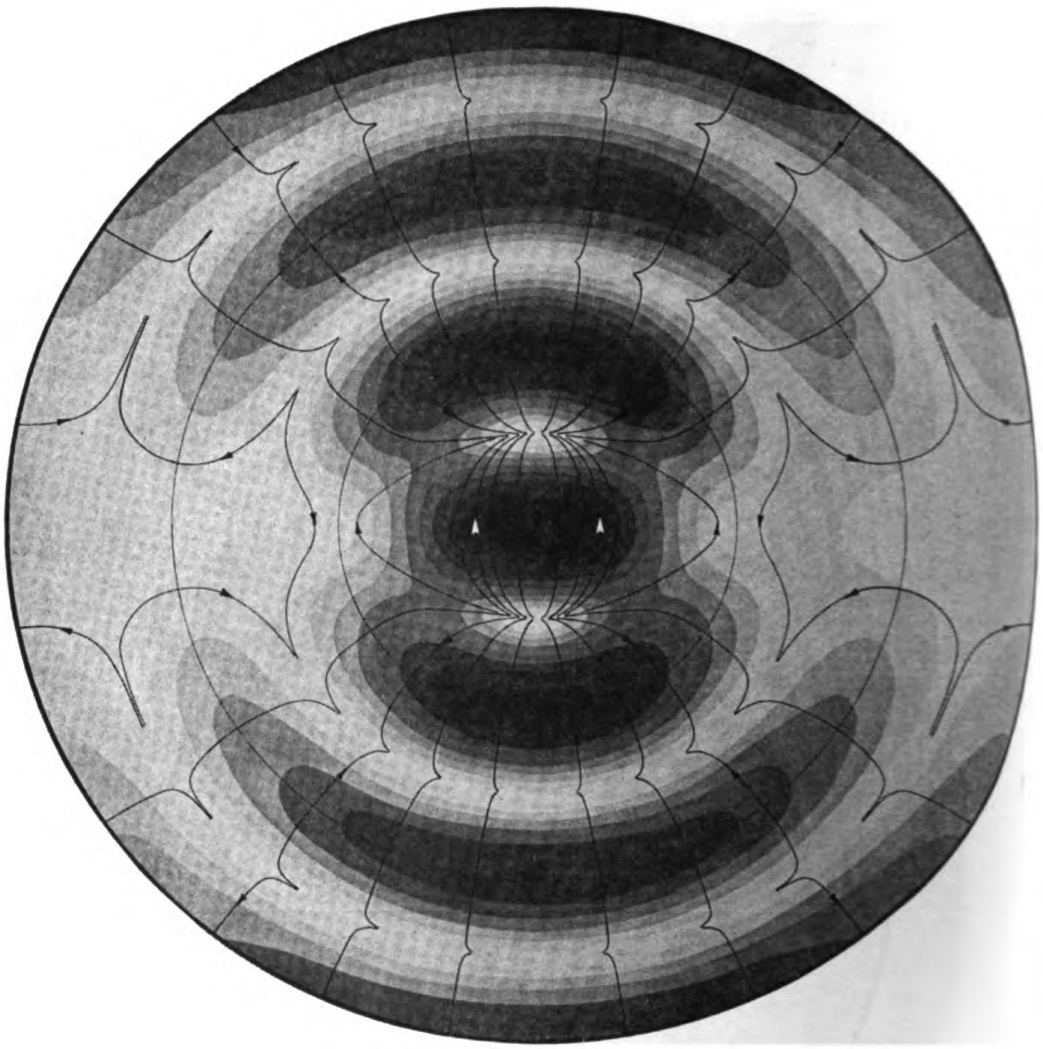

Fig. 35—TM 13 mode.

Digitized by Google
Original from UNIVERSITY OF MICHIGAN
Generated on 2019-09-24 06:55 GMT / http://hdl.handle.net/2027/mdp.39015077775156
Public Domain, Google-digitized / http://www.hathitrust.org/access_use#pd-google

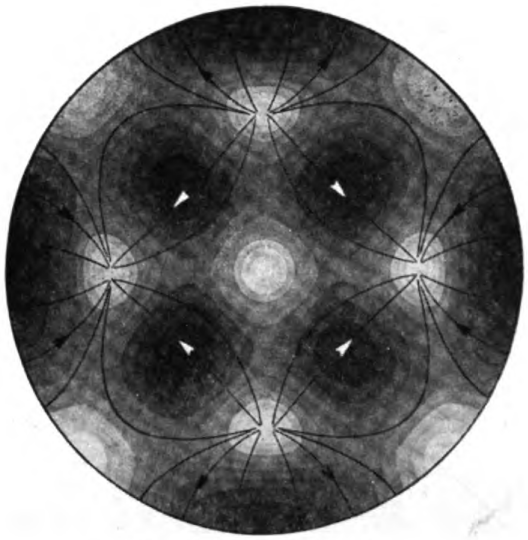

Fig. 36—TM 21 mode.

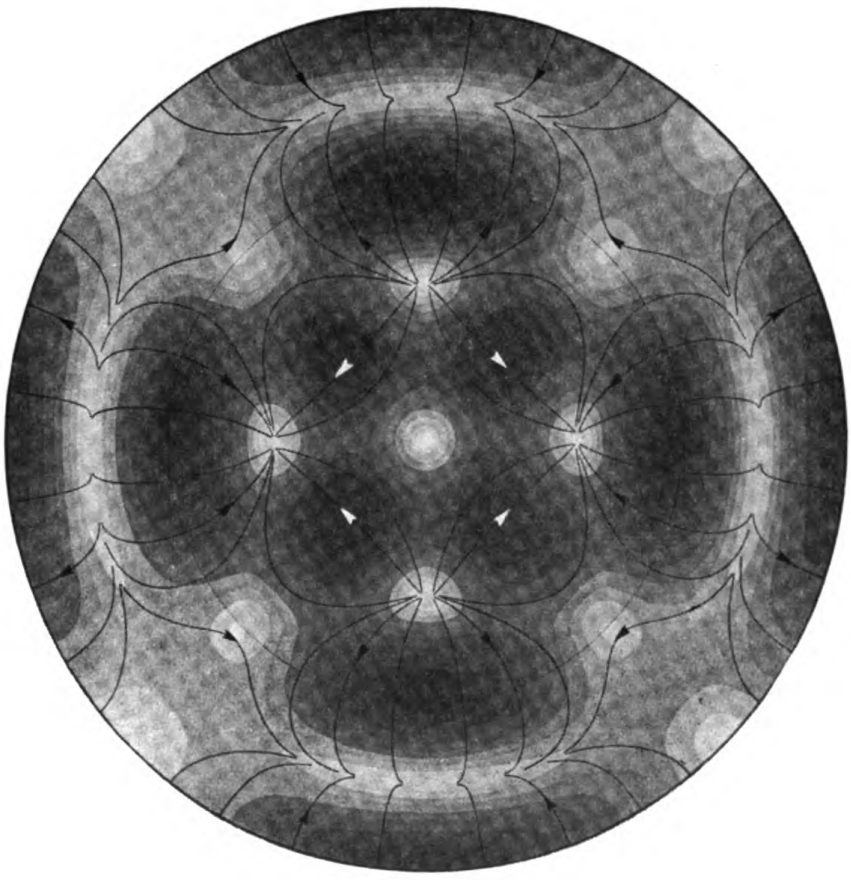

Fig. 37—TM 22 mode.

Digitized by Google
Original from UNIVERSITY OF MICHIGAN
Generated on 2019-09-24 06:55 GMT / http://hdl.handle.net/2027/mdp.39015077775156
Public Domain, Google-digitized / http://www.hathitrust.org/access_use#pd-google

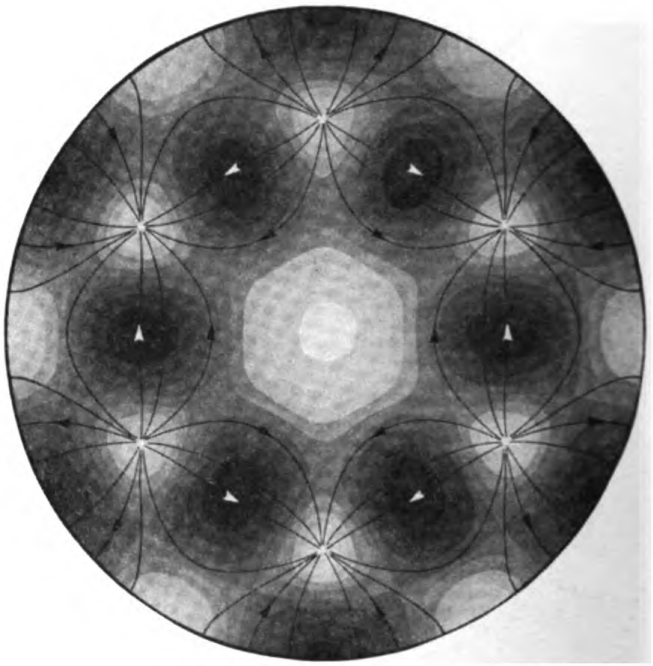

Fig. 38—TM 31 mode.

Generated on 2019-09-24 06:55 GMT / http://hdl.handle.net/2027/mdp.39015077775156
Public Domain, Google-digitized / http://www.hathitrust.org/access_use#pd-google
Digitized by Google
Original from UNIVERSITY OF MICHIGAN

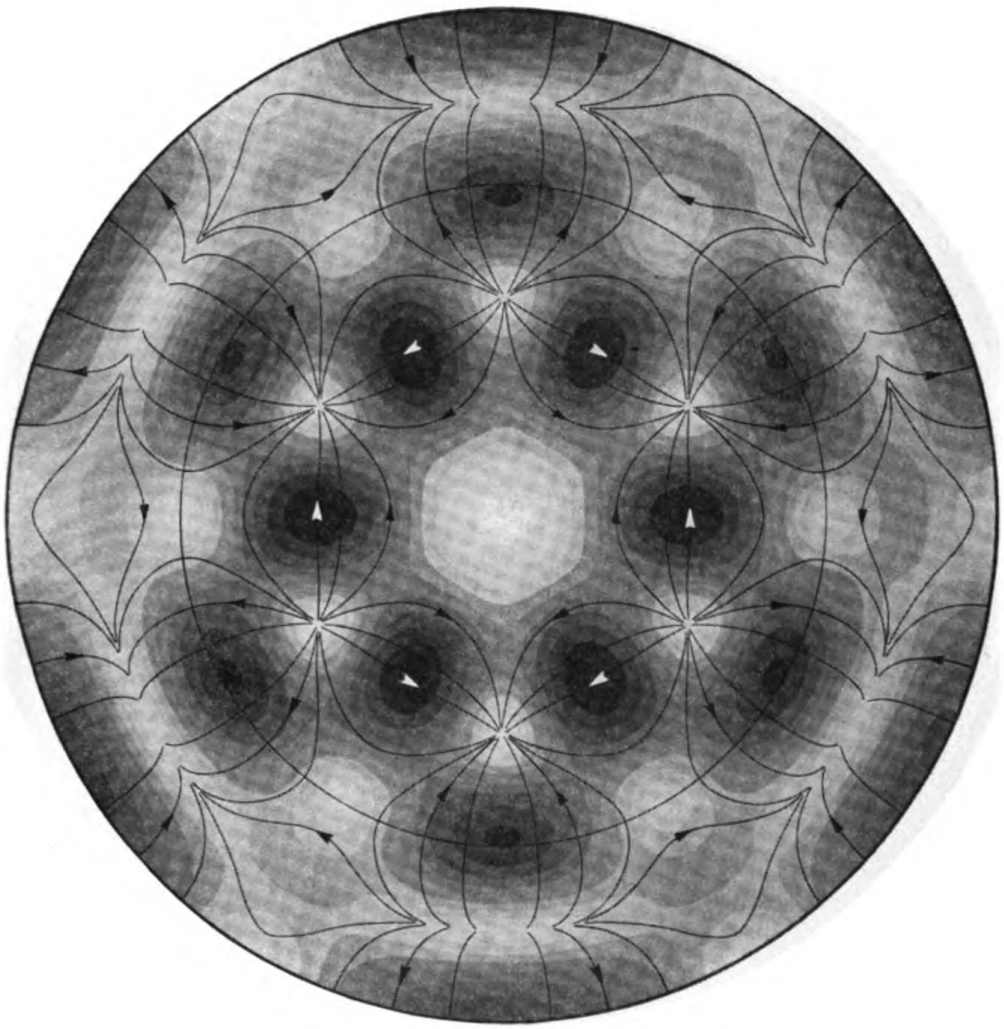

Fig. 39—TM 32 mode.

Generated on 2019-09-24 06:56 GMT / http://hdl.handle.net/2027/mdp.39015077775156
Public Domain, Google-digitized / http://www.hathitrust.org/access_use#pd-google
Digitized by Google
Original from UNIVERSITY OF MICHIGAN

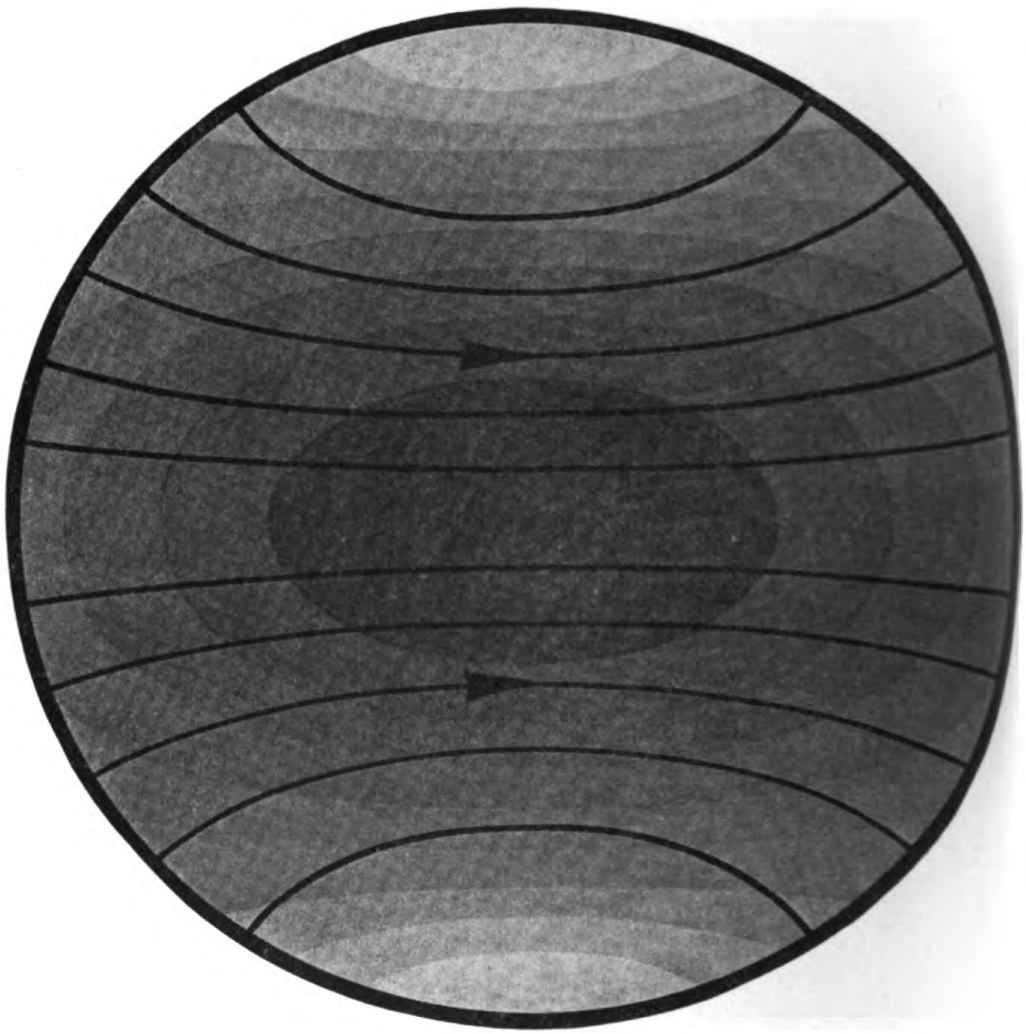

Fig. 40—TE 11 mode.

Generated on 2019-09-24 06:56 GMT / http://hdl.handle.net/2027/mdp.39015077775156
Public Domain, Google-digitized / http://www.hathitrust.org/access_use#pd-google
Digitized by Google
Original from UNIVERSITY OF MICHIGAN

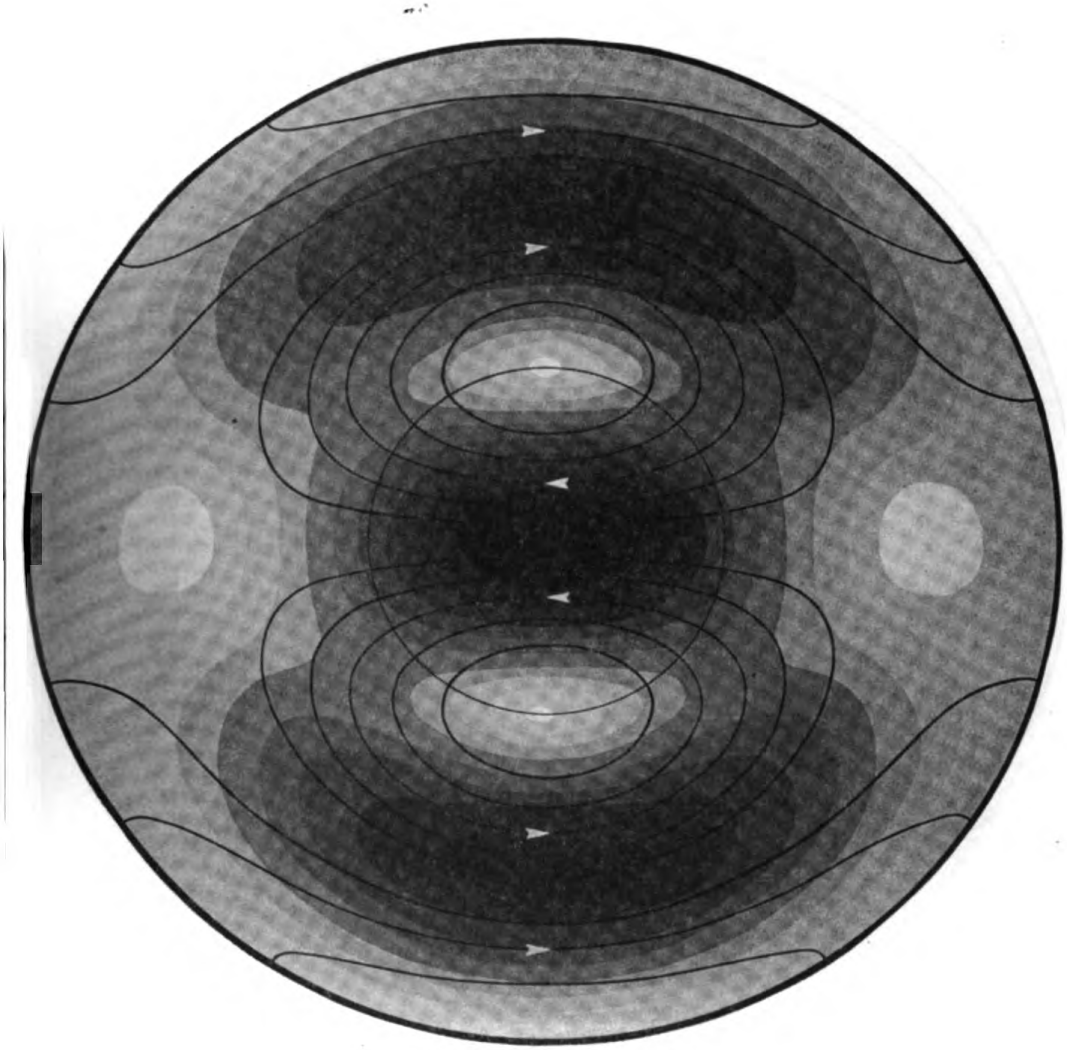

Fig. 41—TE 12 mode.

Generated on 2019-09-24 06:56 GMT / http://hdl.handle.net/2027/mdp.39015077775156
Public Domain, Google-digitized / http://www.hathitrust.org/access_use#pd-google
Digitized by Google
Original from UNIVERSITY OF MICHIGAN

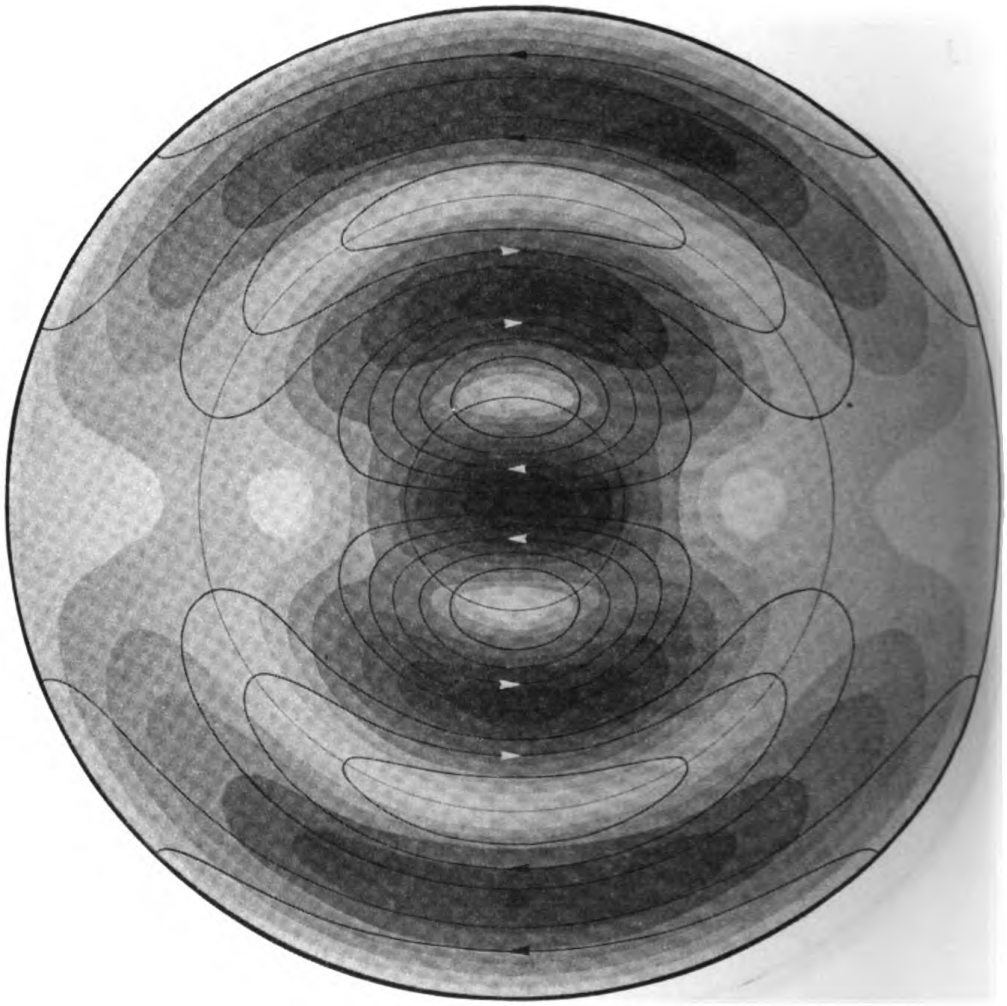

Fig. 42—TE 13 mode.

Generated on 2019-09-24 06:56 GMT / http://hdl.handle.net/2027/mdp.39015077775156
Public Domain, Google-digitized / http://www.hathitrust.org/access_use#pd-google
Digitized by Google
Original from UNIVERSITY OF MICHIGAN

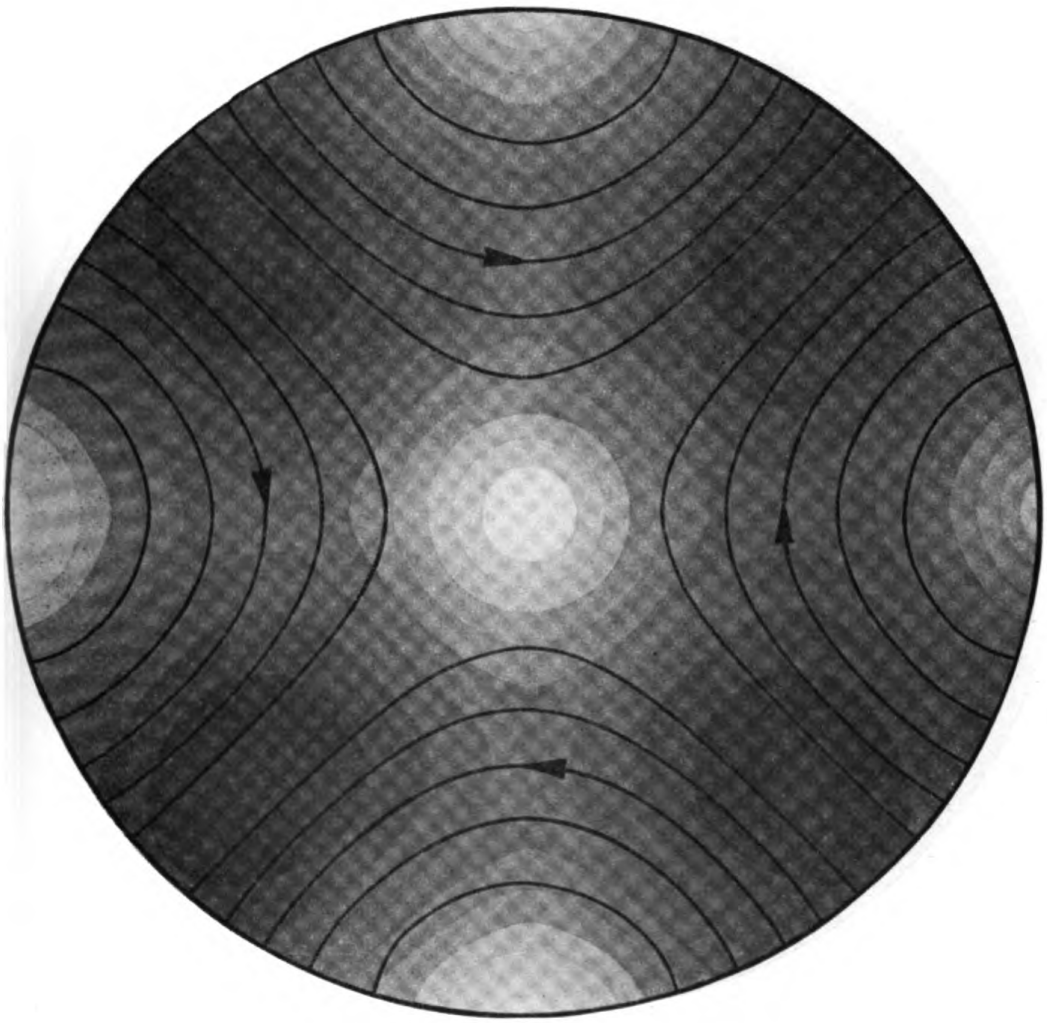

Fig. 43—TE 21 mode.

Generated on 2019-09-24 06:56 GMT / http://hdl.handle.net/2027/mdp.39015077775156
Public Domain, Google-digitized / http://www.hathitrust.org/access_use#pd-google
Digitized by Google
Original from UNIVERSITY OF MICHIGAN

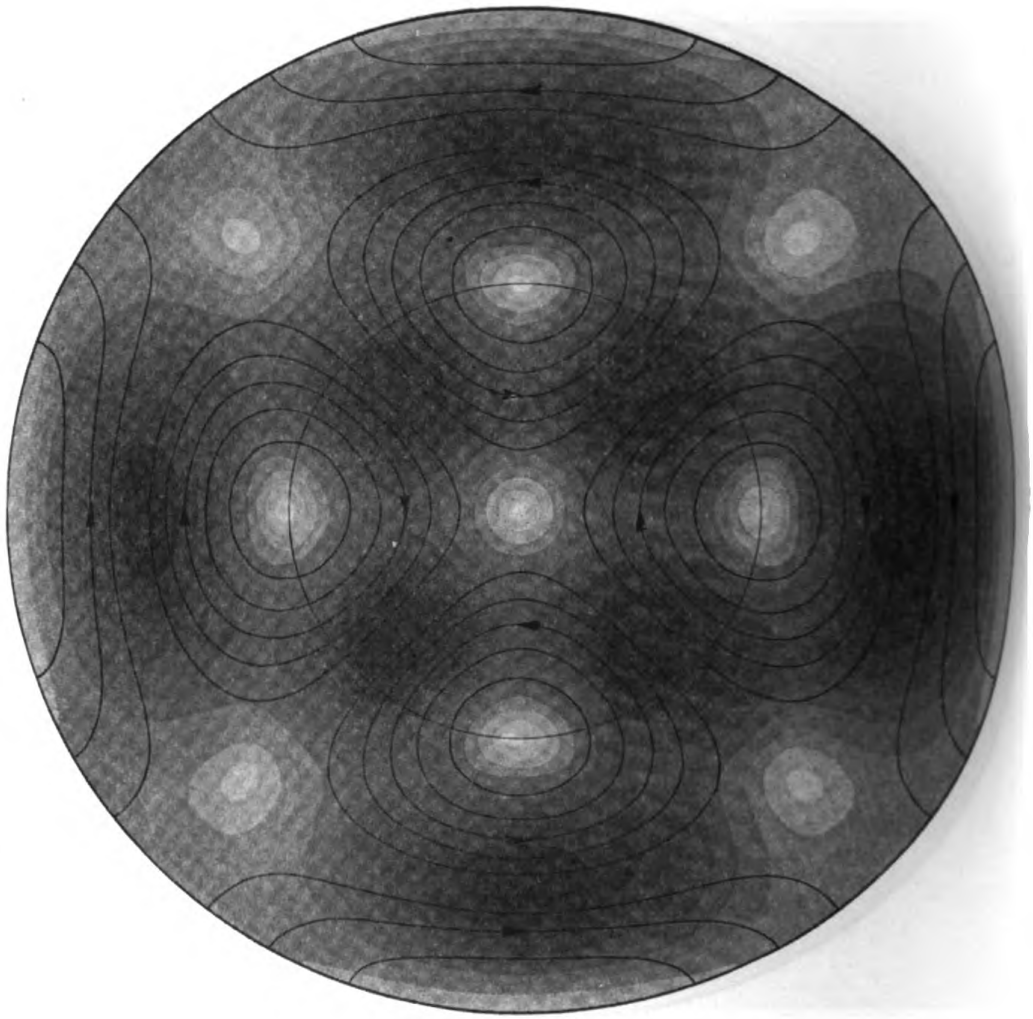

Fig. 44—TE 22 mode.

Digitized by Google
Original from UNIVERSITY OF MICHIGAN
Generated on 2019-09-24 06:57 GMT / http://hdl.handle.net/2027/mdp.39015077775156
Public Domain, Google-digitized / http://www.hathitrust.org/access_use#pd-google

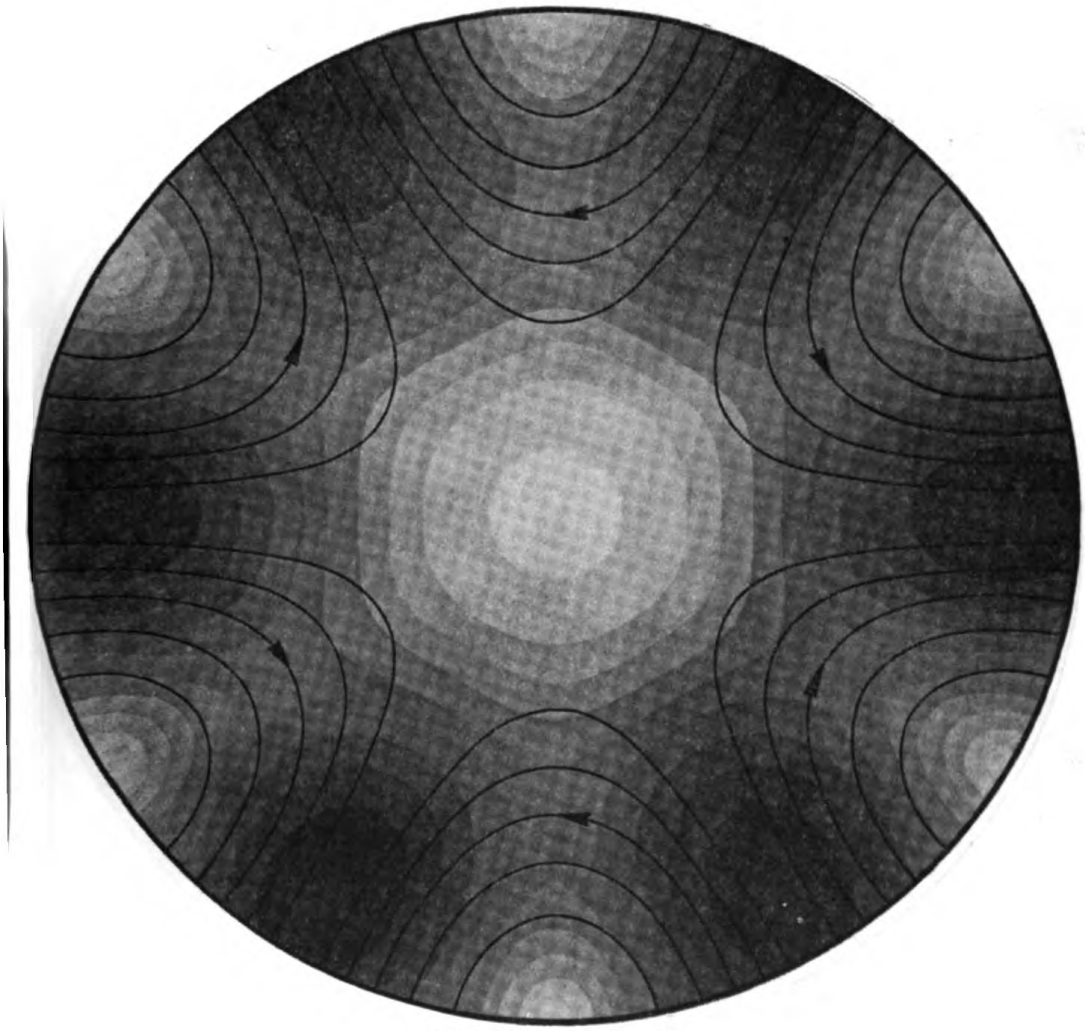

Fig. 45—TE 31 mode.

Digitized by Google
Original from UNIVERSITY OF MICHIGAN
Generated on 2019-09-24 06:57 GMT / http://hdl.handle.net/2027/mdp.39015077775156
Public Domain, Google-digitized / http://www.hathitrust.org/access_use#pd-google

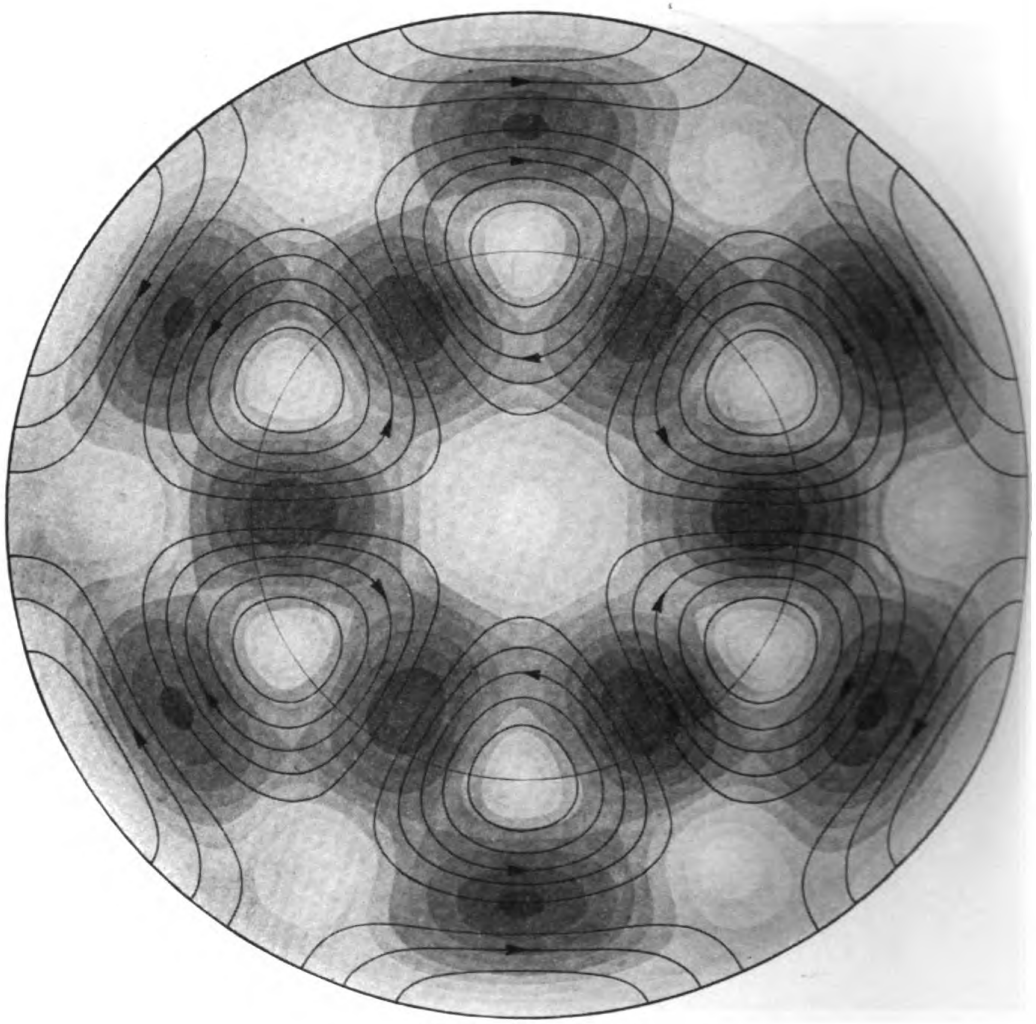

Fig. 46—TE 32 mode.

Generated on 2019-09-24 06:57 GMT / http://hdl.handle.net/2027/mdp.39015077775156
Public Domain, Google-digitized / http://www.hathitrust.org/access_use#pd-google
Digitized by Google
Original from UNIVERSITY OF MICHIGAN

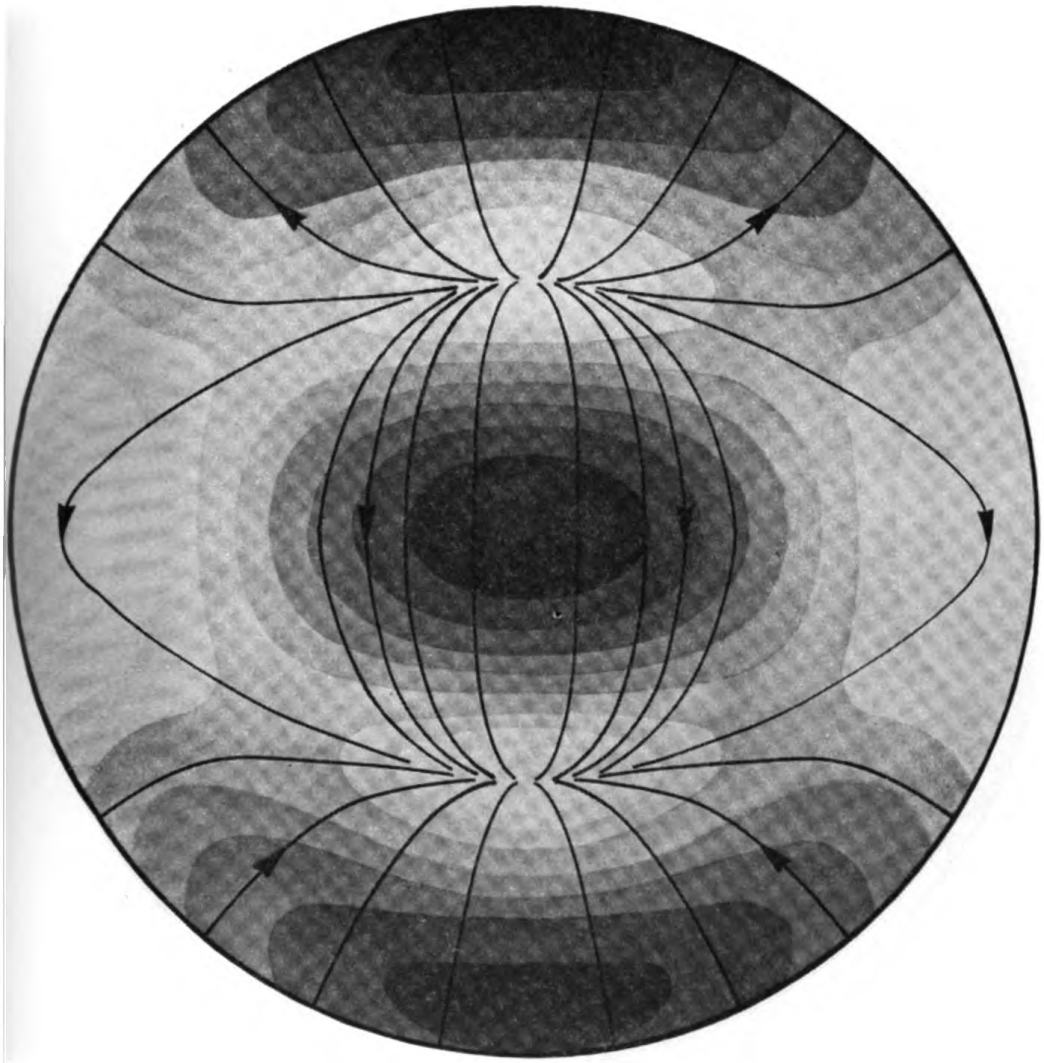

Fig. 47—TM 11 mode.

Generated on 2019-09-24 06:57 GMT / http://hdl.handle.net/2027/mdp.39015077775156
Public Domain, Google-digitized / http://www.hathitrust.org/access_use#pd-google
Digitized by Google
Original from UNIVERSITY OF MICHIGAN

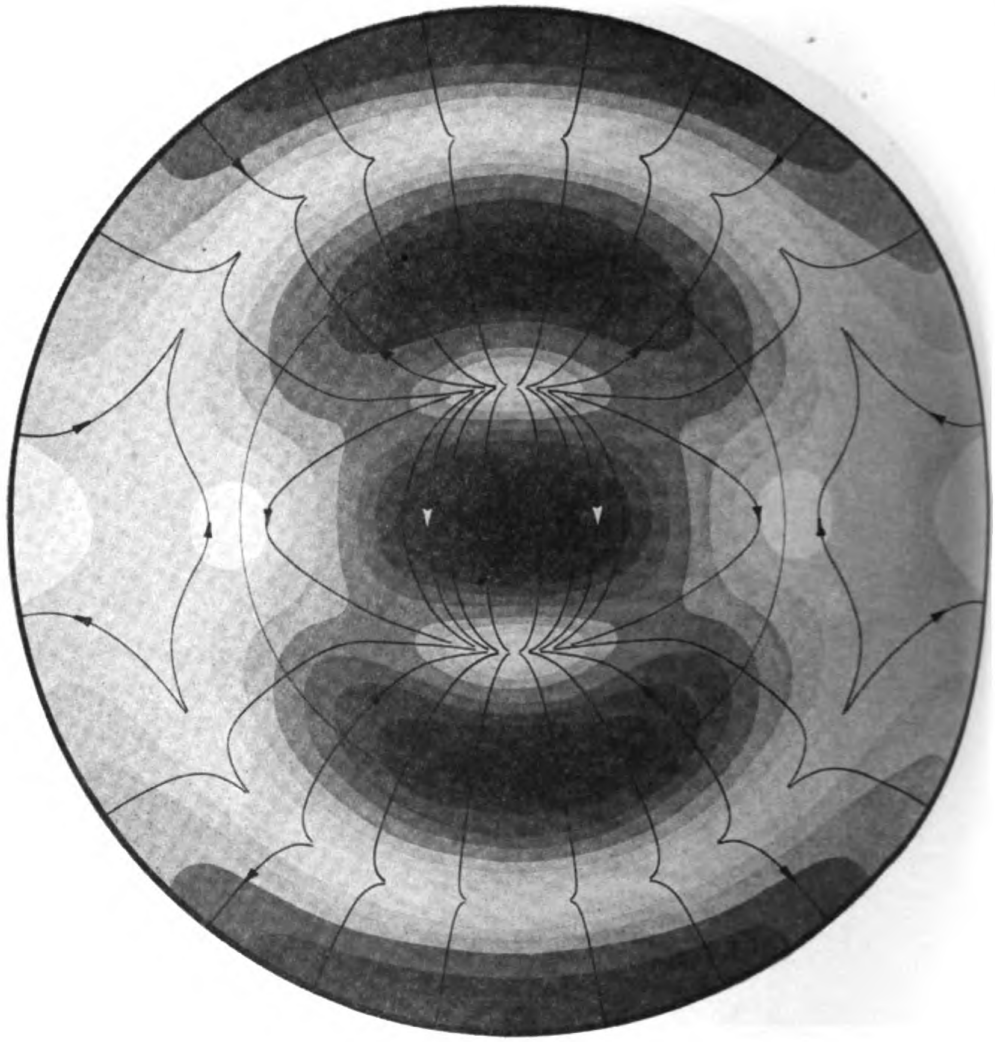

Fig. 48—TM 12 mode.

Generated on 2019-09-24 06:58 GMT / http://hdl.handle.net/2027/mdp.39015077775156
Public Domain, Google-digitized / http://www.hathitrust.org/access_use#pd-google
Digitized by Google
Original from UNIVERSITY OF MICHIGAN

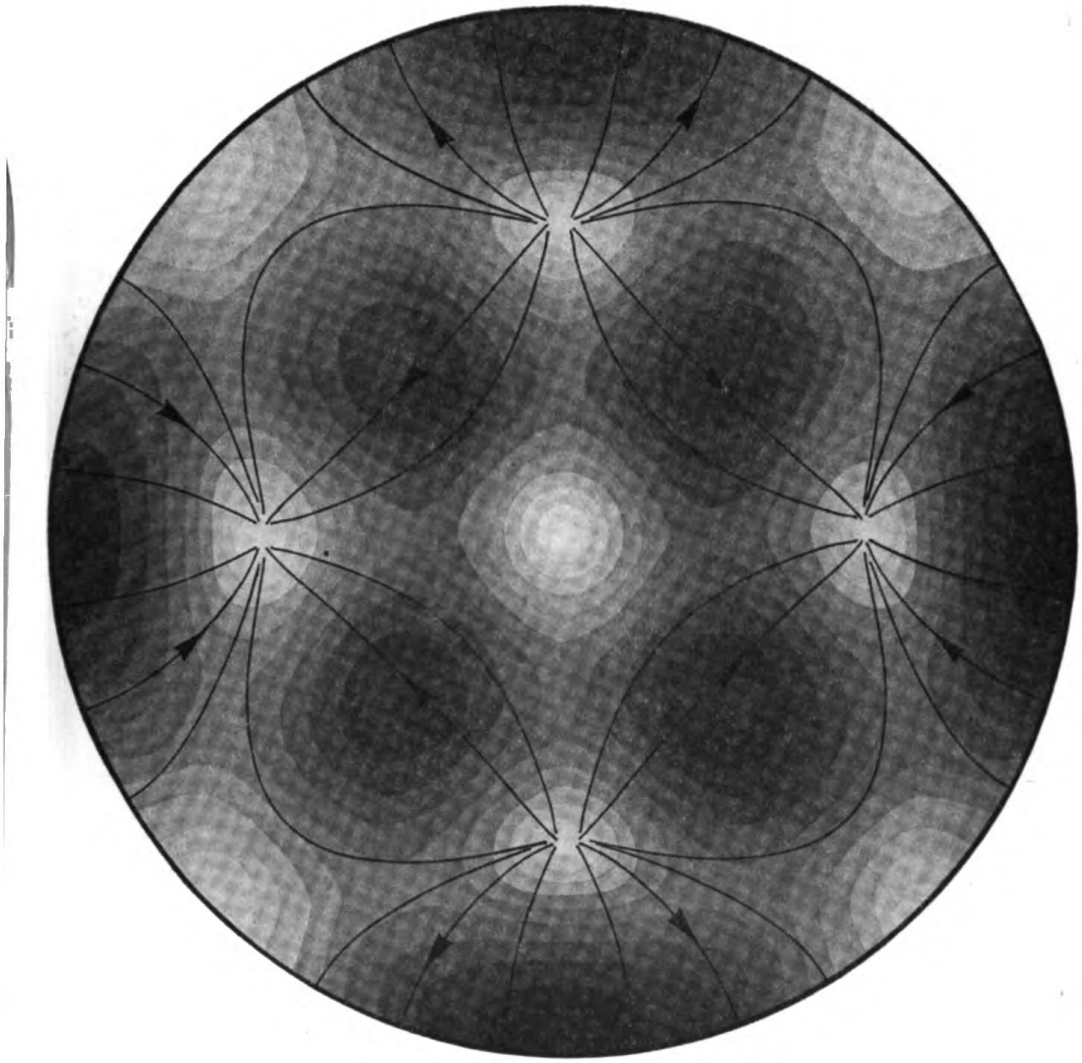

Fig. 49—TM 21 mode

Generated on 2019-09-24 06:58 GMT / http://hdl.handle.net/2027/mdp.39015077775156
Public Domain, Google-digitized / http://www.hathitrust.org/access_use#pd-google
Digitized by Google
Original from UNIVERSITY OF MICHIGAN

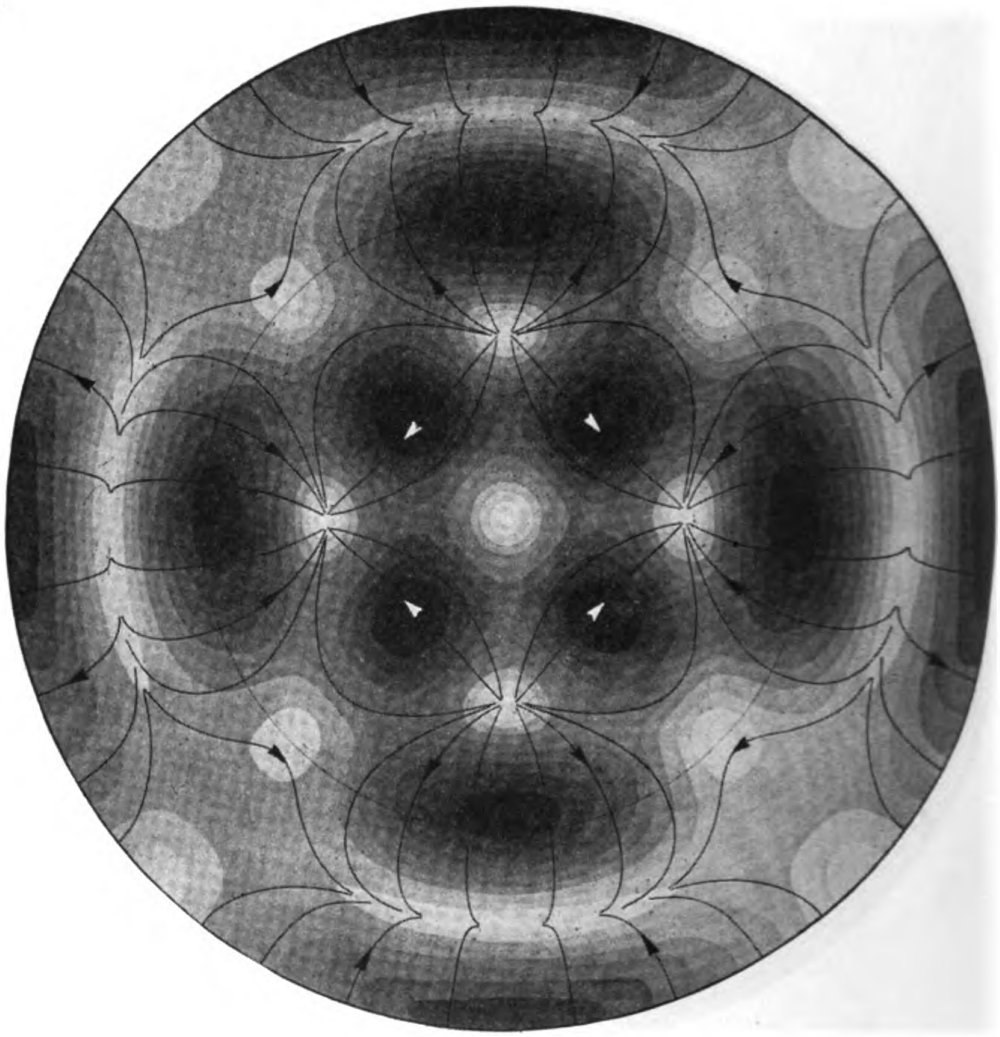

Fig. 50—TM 22 mode.

Generated on 2019-09-24 06:58 GMT / http://hdl.handle.net/2027/mdp.39015077775156
Public Domain, Google-digitized / http://www.hathitrust.org/access_use#pd-google
Digitized by Google
Original from UNIVERSITY OF MICHIGAN

APPENDIX

INTEGRATION OF $\int_0^x \frac{J_\ell(x)}{J'_\ell(x)}\,dx$

The discussion here is concerned only with integral values of $\ell > 0$. The integral is not simply expressible in terms of known (i.e., tabulated) functions, hence what amounts to a series expansion is used. The method follows Ludinegg[1] who gives the details for $\ell = 1$.

The value of the integrand at $x = 0$ is first discussed. For $\ell = 1$, $J_1(0) = 0$ and $J'_1(0) = 0.5$, hence the integrand has the value zero. For $\ell > 1$, both numerator and denominator are zero, hence the value is indeterminate. Evaluation by $(\ell - 1)$ differentiations of numerator and denominator separately leads to the result that the integrand (and the integral also) is zero at $x = 0$ for all ℓ.

We now introduce a constant $p\ell$ and a function $\phi\ell(x)$ which are such that the following equation is satisfied, at least for a certain range of values of x:

$$J_\ell = -p\ell\left(J''_\ell - \frac{(\ell - 1)J'_\ell}{x}\right) + \phi\ell J'_\ell. \tag{1}$$

Denote the desired integral by $F\ell(x)$, i.e.:

$$F\ell(x) = \int_0^x \frac{J_\ell(x)}{J'_\ell(x)}\,dx. \tag{2}$$

Then substitution of (1) into (2) yields:

$$F_\ell = -p\ell\left[\log \frac{J'_\ell}{x^{(\ell-1)}}\right]_0^x + \int_0^x \phi\ell\,dx. \tag{3}$$

For $x = 0$, $J'_\ell/x^{(\ell-1)}$ is indeterminate, but evaluation by differentiating numerator and denominator separately $(\ell - 1)$ times gives the value $1/2^\ell(\ell - 1)!$

If we can now arrange matters so that $\phi\ell$ remains finite in the range $(0, x)$, its integration can be carried out, a) by expansion into a power series and integration term-by-term, or, b) by numerical integration.

Solving (1) for $\phi\ell$ one obtains

$$\phi\ell = \frac{J_\ell + p\ell\left(J''_\ell - \dfrac{(\ell - 1)J'_\ell}{x}\right)}{J'_\ell}. \tag{4}$$

Equation (4) becomes indeterminate at $x = 0$, when $\ell > 1$. Evaluation by differentiating numerator and denominator separately ℓ times shows $\phi\ell(0) = 0$.

[1] *Hochfrequenztech. u. Elektroak.*, V. 62, pp. 38–44, Aug. 1943.

Digitized by Google
Original from UNIVERSITY OF MICHIGAN
Generated on 2019-09-24 07:00 GMT / http://hdl.handle.net/2027/mdp.39015077775156
Public Domain, Google-digitized / http://www.hathitrust.org/access_use#pd-google

At the first zero of J'_ℓ (the value of x at a zero of J'_ℓ will be denoted by r), ϕ_ℓ is held finite by choice of the value of p_ℓ. It is clear that (4) becomes indeterminate at $x = r$, if

$$p_\ell = -\frac{J_\ell(r)}{J''_\ell(r)}. \tag{5}$$

Since J_ℓ satisfies the differential equation

$$J''_\ell + \frac{1}{x} J'_\ell + (1 - \ell^2/x^2) J_\ell = 0 \tag{6}$$

and $J'_\ell(r) = 0$, one has by substitution

$$p_\ell = \frac{r^2}{r^2 - \ell^2}. \tag{7}$$

Values of p for several cases are:

ℓ =	1	2	3	4		1		1
r_1 =	1.841	3.054	4.201	5.318	r_2 =	5.331	r_3 =	8.536
p_ℓ =	1.418	1.751	2.040	2.303		1.036		1.014
$\phi_\ell(r)$ =	−0.126	−0.286	−0.446	−0.604		−0.180		−0.115

Evaluation of $\phi_\ell(r)$ by the usual process[2] gives:

$$\phi_\ell(r) = \frac{-r\ell(r^2 - \ell^2 - 2\ell)}{(r^2 - \ell^2)^2} \tag{8}$$

Values of $\phi_\ell(r)$ are given in the preceding table.

Since ϕ_ℓ is finite at the origin and at the first zero of J'_ℓ, it may be expanded into a Maclaurin series whose radius of convergence does not, however, exceed the value of x at the second zero of J'_ℓ. Alternatively, by choosing p_ℓ to keep ϕ_ℓ finite at the second (or k^{th}) zero of J'_ℓ it may be expanded into a Taylor series about some point in the interval between the first (or $(k-1)^{th}$) and third (or $(k+1)^{th}$) zeros. Expansions about the origin are given in Table I.

Unfortunately, the convergence of these power series is so slow that they are not very useful. Instead, equation (4) is used to calculate ϕ_ℓ and $\int \phi_\ell \, dx$ is obtained by numerical integration.

With p_ℓ fixed to hold ϕ_ℓ finite at the first root, r_1, of J'_ℓ, it is soon found that ϕ_ℓ becomes infinite at the higher roots. This is because different values

[2] Substitute (6) into (4) to eliminate J''_ℓ; differentiate numerator and denominator separately; use (6) to eliminate J_ℓ; allow $x \to r$, using $J'_\ell(r) = 0$ and value of p_ℓ from (7).

Digitized by Google
Original from UNIVERSITY OF MICHIGAN
Generated on 2019-09-24 07:00 GMT / http://hdl.handle.net/2027/mdp.39015077775156
Public Domain, Google-digitized / http://www.hathitrust.org/access_use#pd-google

of p are required at the different roots, as shown for $\ell = 1$ in the table above. A logical extension would therefore be to make p a function of x such that it takes on the required values at $r_1, r_2, r_3, \cdots$. When this is done and $p_\ell(x)$ is introduced into (1) and (2), one has to integrate

$$\int \frac{p(x)J''(x)}{J'(x)}\,dx$$

and this is intractable.[3]

Hence $p(x)$ is made a discontinuous function, such that p has the value p_1 corresponding to r_1 for values of x from zero to a point b_1 between r_1 and r_2; the value p_2 corresponding to r_2 for values of x from b_1 to a point b_2 between r_2 and r_3; and so forth. This introduces discontinuities in ϕ. No discontinuities exist, however, in the function

$$G_\ell = e^{-r}\ell \tag{9}$$

which is given in Table II. The calculations were made by Miss F. C. Larkey; numerical integration was according to Weddle's rule.

Within the limits of this tabulation, then, G_ℓ and F_ℓ are now considered to be known functions.

TABLE I

POWER SERIES EXPANSIONS OF $\phi_\ell(x)$

$$\phi_1(x) = \left(1 - \frac{3p}{4}\right)x + \left(\frac{1}{4} - \frac{17p}{96}\right)x^3 + \left(\frac{7}{96} - \frac{79p}{1536}\right)x^5 + \cdots$$

$$= -0.063813x - 0.001178x^3 - 0.0000358x^5 - \cdots$$

$$\phi_2(x) = \left(\frac{1}{2} - \frac{p}{3}\right)x + \left(\frac{1}{24} - \frac{7p}{288}\right)x^3 + \left(\frac{5}{1152} - \frac{169p}{17280}\right)x^5 + \cdots$$

$$= +0.15451x + 0.01648x^3 - 0.00580x^5 - \cdots$$

$$\phi_3(x) = \left(\frac{1}{3} - \frac{5p}{24}\right)x + \left(\frac{1}{72} - \frac{41p}{5760}\right)x^3 + \left(\frac{13}{17280} - \frac{103p}{276480}\right)x^5 + \cdots$$

$$= +0.12210x + 0.00667x^3 + 0.00375x^5 - \cdots.$$

[3] Unless $p = b + cJ'$ (b and c constants), which is not of any use.

Digitized by Google
Original from UNIVERSITY OF MICHIGAN
Generated on 2019-09-24 07:00 GMT / http://hdl.handle.net/2027/mdp.39015077775156
Public Domain, Google-digitized / http://www.hathitrust.org/access_use#pd-google

TABLE II

VALUES OF $F_1(x) = \int_0^x \frac{J_1(x)}{J_1'(x)}\,dx$; $G_1(x) = e^{-F_1}$

$F_1(x)$

x	0	.1	.2	.3	.4	.5	.6	.7	.8	.9
0	0	0050	0201	0455	0816	1291	1887	2616	3493	4539
1	5782	7261	9036	1.1192	1.3874	1.7336	2.2103	2.9577	4.6961	4.1846
2	2.7727	2.0801	1.6199	1.2775	1.0073	7864	6018	4454	3117	1970
3	0987	0147	−0564	−1157	−1640	−2018	−2296	−2475	−2556	−2537
4	−2416	−2188	−1845	−1377	−0769	0	+0960	2153	3646	5549
5	8060	1.1595	1.7307	3.2014	2.3851	1.4478	9635	6373	3939	2024
6	0470	−0812	−1879	−2768	−3506	−4111	−4594	−4966	−5233	−5398
7	−5463	−5429	−5292	−5049	−4693	−4214	−3598	−2826	−1868	−0655
8	+0789	2657	5107	8530	1.3992	2.7313	2.1565	1.1974	7154	3942
9	1562	−0300	−1802	−3034	−4053	−4897	−5590	−6150	−6591	−6921

$G_1(x)$

x	0	.1	.2	.3	.4	.5	.6	.7	.8	.9
0	1.0000	9950	9801	9555	9216	8789	8280	7698	7052	6351
1	5609	4838	4051	3265	2497	1766	1097	0519	0091	0152
2	0625	1249	1979	2787	3652	4555	5478	6406	7322	8212
3	9060	9854	1.0580	1.1226	1.1781	1.2236	1.2581	1.2808	1.2912	1.2888
4	1.2733	1.2445	1.2026	1.1476	1.0799	1.0000	9085	8063	6945	5741
5	4467	3136	1772	0407	0921	2351	3816	5287	6744	8168
6	9541	1.0846	1.2067	1.3190	1.4200	1.5084	1.5831	1.6432	1.6877	1.7157
7	1.7269	1.7209	1.6976	1.6568	1.5989	1.5241	1.4331	1.3265	1.2054	1.0709
8	9241	7667	6001	4261	2468	0613	1157	3020	4890	6742
9	8554	1.0304	1.1974	1.3545	1.4998	1.6318	1.7489	1.8497	1.9330	1.9978

Generated on 2019-09-24 07:00 GMT / http://hdl.handle.net/2027/mdp.39015077775156
Public Domain, Google-digitized / http://www.hathitrust.org/access_use#pd-google
Digitized by Google
Original from UNIVERSITY OF MICHIGAN

VALUES OF $F_2(x) = \int_0^x \frac{J_2(x)}{J_2'(x)}\,dx$; $G_2(x) = e^{-F_2}$

$F_2(x)$

x	0	.1	.2	.3	.4	.5	.6	.7	.8	.9
0	0	0025	0100	0226	0403	0632	0914	1251	1645	2097
1	2612	3192	3840	4563	5365	6253	7236	8323	9528	1.0866
2	1.2357	1.4008	1.5913	1.8061	2.0541	2.3456	2.6972	3.1380	3.7263	4.6110
3	6.4527	6.7644	4.7528	3.8572	3.2808	2.8597	2.5316	2.2658	2.0451	1.8590
4	1.7002	1.5641	1.4470	1.3466	1.2607	1.1881	1.1275	1.0783	1.0396	1.0112
5	9928	9843	9858	9974	1.0196	1.0530	1.0985	1.1573	1.2311	1.3223
6	1.4345	1.5726	1.7447	1.9640	2.2555	2.6743	3.3910	6.5119	3.5122	2.7144
7	2.2595	1.9432	1.7034	1.5131	1.3579	1.2294	1.1223	1.0328	.9586	.8977
8	.8490	.8115	.7846	.7679	.7612	.7645	.7779	.8020	.8372	.8845
9	.9452	1.0212	1.1149	1.2301	1.3725	1.5512	1.7817	2.0950	2.5660	3.4864

$G_2(x)$

x	0	.1	.2	.3	.4	.5	.6	.7	.8	.9
0	1.0000	9975	9900	9777	9605	9388	9127	8824	8483	8108
1	7701	7267	6811	6336	5848	5351	4850	4350	3856	3373
2	2906	2459	2036	1643	1282	0958	0674	0434	0241	0099
3	0017	0012	0086	0211	0376	0573	0795	1037	1294	1558
4	1826	2093	2353	2601	2834	3048	3238	3402	3536	3638
5	3705	3737	3731	3688	3607	3489	3334	3143	2920	2665
6	2383	2075	1747	1403	1048	0690	0337	0015	0298	0662
7	1044	1432	1821	2202	2572	2925	3255	3560	3834	4075
8	4278	4442	4563	4640	4671	4656	4593	4484	4329	4129
9	3886	3602	3280	2923	2535	2120	1683	1231	0768	0306

Generated on 2019-09-24 07:01 GMT / http://hdl.handle.net/2027/mdp.39015077775156
Public Domain, Google-digitized / http://www.hathitrust.org/access_use#pd-google
Digitized by Google
Original from UNIVERSITY OF MICHIGAN

VALUES OF $F_3(x) = \int_0^x \frac{J_3(x)}{J_3'(x)}\,dx$; $G_3(x) = e^{-F_3}$

$F_3(x)$

x	0	.1	.2	.3	.4	.5	.6	.7	.8	.9
0	0	0017	0067	0152	0268	0420	0604	0826	1081	1373
1	1703	2070	2476	2922	3410	3942	4518	5141	5814	6539
2	7319	8158	9060	1.0028	1.1070	1.2192	1.3401	1.4706	1.6118	1.7650
3	1.9321	2.1150	2.3165	2.5402	2.7908	3.0752	3.4034	3.7905	4.2624	4.8692
4	5.7117	7.1373	16.2303	7.2383	5.8409	5.0409	4.4852	4.0643	3.7292	3.4543
5	3.2239	3.0282	2.8605	2.7160	2.5913	2.4838	2.3914	2.3128	2.2467	2.1922
6	2.1487	2.1156	2.0927	2.0798	2.0768	2.0838	2.1012	2.1293	2.1685	2.2208
7	2.2864	2.3674	2.4664	2.5868	2.7340	2.9159	3.1460	3.4491	3.8790	4.5950
8	6.9408	4.9414	4.0348	3.5348	3.1912	2.9324	2.7276	2.5608	2.4227	2.3074
9	2.2108	2.1302	2.0637	2.0097	1.9676	1.9361	1.9147	1.9036	1.9025	1.9115

$G_3(x)$

x	0	.1	.2	.3	.4	.5	.6	.7	.8	.9
0	1.0000	9983	9933	9849	9734	9589	9413	9208	8975	8717
1	8434	8130	7806	7466	7110	6742	6365	5980	5591	5200
2	4810	4423	4041	3668	3305	2955	2618	2298	1995	1712
3	1448	1206	0986	0789	0614	0462	0333	0226	0141	0077
4	0033	0008	0000	0007	0029	0065	0113	0172	0240	0316
5	0398	0484	0572	0661	0749	0834	0915	0990	1057	1117
6	1166	1206	1233	1250	1253	1244	1223	1189	1143	1086
7	1016	0937	0849	0753	0650	0542	0430	0318	0207	0101
8	0010	0071	0177	0292	0411	0533	0654	0772	0887	0996
9	1096	1188	1270	1340	1398	1443	1474	1490	1492	1479

Generated on 2019-09-24 07:01 GMT / http://hdl.handle.net/2027/mdp.39015077775156
Public Domain, Google-digitized / http://www.hathitrust.org/access_use#pd-google
Digitized by Google
Original from UNIVERSITY OF MICHIGAN

Table III

Bessel Functions of The First Kind

$J_0(x)$

x	.0	.1	.2	.3	.4	.5	.6	.7	.8	.9
0	+1.0	9975	9900	9776	9604	+9385	9120	8812	8463	8075
1	+7652	7196	6711	6201	5669	+5118	4554	3980	3400	2818
2	+2239	1666	1104	0555	0025	−0484	0968	1424	1850	2243
3	−2601	2921	3202	3443	3643	−3801	3918	3992	4026	4018
4	−3971	3887	3766	3610	3423	−3205	2961	2693	2404	2097
5	−1776	1443	1103	0758	0412	−0068	+0270	+0599	+0917	+1220
6	+1506	1773	2017	2238	2433	+2601	2740	2851	2931	2981
7	+3001	2991	2951	2882	2786	+2663	2516	2346	2154	1944
8	+1717	1475	1222	0960	0692	+0419	0146	−0125	−0392	−0653
9	−0903	1142	1367	1577	1768	−1939	2090	2218	2323	2403

$J_1(x)$

x	.0	.1	.2	.3	.4	.5	.6	.7	.8	.9
0	+0	0499	0995	1483	1960	+2423	2867	3290	3688	4059
1	+4401	4709	4983	5220	5419	+5579	5699	5778	5815	5812
2	+5767	5683	5560	5399	5202	+4971	4708	4416	4097	3754
3	+3391	3009	2613	2207	1792	+1374	0955	0538	0128	−0272
4	−0660	1033	1386	1719	2028	−2311	2566	2791	2985	3147
5	−3276	3371	3432	3460	3453	−3414	3343	3241	3110	2951
6	−2767	2559	2329	2081	1816	−1538	1250	0953	0652	0349
7	−0047	+0252	+0543	+0826	+1096	+1352	1592	1813	2014	2192
8	+2346	2476	2580	2657	2708	+2731	2728	2697	2641	2559
9	+2453	2324	2174	2004	1816	+1613	1395	1166	0928	0684

$J_2(x)$

x	.0	.1	.2	.3	.4	.5	.6	.7	.8	.9
0	+0	0012	0050	0112	0197	0306	0437	0588	0758	0946
1	+1149	1366	1593	1830	2074	2321	2570	2817	3061	3299
2	+3528	3746	3951	4139	4310	4461	4590	4696	4777	4832
3	+4861	4862	4835	4780	4697	4586	4448	4283	4093	3879
4	+3641	3383	3105	2811	2501	2178	1846	1506	1161	0813
5	+0466	0121	−0217	−0547	−0867	−1173	1464	1737	1990	2221
6	−2429	2612	2769	2899	3001	3074	3119	3135	3123	3082
7	−3014	2920	2800	2656	2490	2303	2097	1875	1638	1389
8	−1130	0864	0593	0320	0047	+0223	0488	0745	0993	1228
9	+1448	1653	1840	2008	2154	2279	2380	2458	2512	2542

$J_3(x)$

x	.0	.1	.2	.3	.4	.5	.6	.7	.8	.9
0	+0	0	0002	0006	0013	0026	0044	0069	0102	0144
1	+0196	0257	0329	0411	0505	0610	0725	0851	0988	1134
2	+1289	1453	1623	1800	1981	2166	2353	2540	2727	2911
3	+3091	3264	3431	3588	3734	3868	3988	4092	4180	4250
4	+4302	4333	4344	4333	4301	4247	4171	4072	3952	3811
5	+3648	3466	3265	3046	2811	2561	2298	2023	1738	1446
6	+1148	0846	0543	0240	−0059	−0353	0641	0918	1185	1438
7	−1676	1896	2099	2281	2442	2581	2696	2787	2853	2895
8	−2911	2903	2869	2811	2730	2626	2501	2355	2190	2007
9	−1809	1598	1374	1141	0900	0653	0403	0153	+0097	+0343

Digitized by Google
Original from UNIVERSITY OF MICHIGAN
Generated on 2019-09-24 07:01 GMT / http://hdl.handle.net/2027/mdp.39015077775156
Public Domain, Google-digitized / http://www.hathitrust.org/access_use#pd-google

$J_4(x)$

x	.0	.1	.2	.3	.4	.5	.6	.7	.8	.9
0	+0	0	0	0	0001	0002	0003	0006	0010	0016
1	+0025	0036	0050	0068	0091	0118	0150	0188	0232	0283
2	+0340	0405	0476	0556	0643	0738	0840	0950	1067	1190
3	+1320	1456	1597	1743	1892	2044	2198	2353	2507	2661
4	+2811	2958	3100	3236	3365	3484	3594	3693	3780	3853
5	+3912	3956	3985	3996	3991	3967	3926	3866	3788	3691
6	+3576	3444	3294	3128	2945	2748	2537	2313	2077	1832
7	+1578	1317	1051	0781	0510	0238	−0031	−0297	−0557	−0810
8	−1054	1286	1507	1713	1903	2077	2233	2369	2485	2581
9	−2655	2707	2736	2743	2728	2691	2633	2553	2453	2334

$J_5(x)$

x	.0	.1	.2	.3	.4	.5	.6	.7	.8	.9
0	+0	0	0	0	0	0	0	0	0001	0001
1	+0002	0004	0006	0009	0013	0018	0025	0033	0043	0055
2	+0070	0088	0109	0134	0162	0195	0232	0274	0321	0373
3	+0430	0493	0562	0637	0718	0804	0897	0995	1098	1207
4	+1321	1439	1561	1687	1816	1947	2080	2214	2347	2480
5	+2611	2740	2865	2986	3101	3209	3310	3403	3486	3559
6	+3621	3671	3708	3731	3741	3736	3716	3680	3629	3562
7	+3479	3380	3266	3137	2993	2835	2663	2478	2282	2075
8	+1858	1632	1399	1161	0918	0671	0424	0176	−0070	−0313
9	−0550	0782	1005	1219	1422	1613	1790	1953	2099	2229

$J_6(x)$

x	.0	.1	.2	.3	.4	.5	.6	.7	.8	.9
0	0	0	0	0	0	0	0	0	0	0
1	0	0	0001	0001	0002	0002	0003	0005	0007	0009
2	0012	0016	0021	0027	0034	0042	0052	0065	0079	0095
3	0114	0136	0160	0188	0219	0254	0293	0336	0383	0435
4	0491	0552	0617	0688	0763	0843	0927	1017	1111	1209
5	1310	1416	1525	1637	1751	1868	1986	2104	2223	2341
6	2458	2574	2686	2795	2900	2999	3093	3180	3259	3330
7	3392	3444	3486	3516	3535	3541	3535	3516	3483	3436
8	3376	3301	3213	3111	2996	2867	2725	2571	2406	2229
9	2043	1847	1644	1432	1215	0993	0768	0540	0311	0082

$J_7(x)$

x	.0	.1	.2	.3	.4	.5	.6	.7	.8	.9
0	0	0	0	0	0	0	0	0	0	0
1	0	0	0	0	0	0	0	0001	0001	0001
2	0002	0002	0003	0004	0006	0008	0010	0013	0016	0020
3	0025	0031	0038	0047	0056	0067	0080	0095	0112	0131
4	0152	0176	0202	0232	0264	0300	0340	0382	0429	0479
5	0534	0592	0654	0721	0791	0866	0945	1027	1113	1203
6	1296	1392	1491	1592	1696	1801	1908	2015	2122	2229
7	2336	2441	2543	2643	2739	2832	2919	3001	3076	3145
8	3206	3259	3303	3337	3362	3376	3379	3371	3351	3319
9	3275	3218	3149	3068	2974	2868	2750	2620	2480	2328

Digitized by Google
Original from UNIVERSITY OF MICHIGAN
Generated on 2019-09-24 07:02 GMT / http://hdl.handle.net/2027/mdp.39015077775156
Public Domain, Google-digitized / http://www.hathitrust.org/access_use#pd-google

$J_1'(x)$

x	.0	.1	.2	.3	.4	.5	.6	.7	.8	.9
0	+5000	4981	4925	4832	4703	4539	4342	4112	3852	3565
1	+3251	2915	2559	2185	1798	1399	0992	0581	0169	−0241
2	−0645	1040	1423	1792	2142	2472	2779	3060	3314	3538
3	−3731	3891	4019	4112	4170	4194	4183	4138	4059	3948
4	−3806	3635	3435	3210	2962	2692	2404	2100	1782	1455
5	−1121	0782	0443	0105	+0227	+0552	0867	1168	1453	1721
6	+1968	2192	2393	2568	2717	2838	2930	2993	3027	3032
7	+3007	2955	2875	2769	2638	2483	2307	2110	1896	1666
8	+1423	1169	0908	0640	0369	0098	−0171	−0435	−0692	−0940
9	−1176	1398	1604	1792	1961	2109	2235	2338	2417	2472

$J_2'(x)$

x	.0	.1	.2	.3	.4	.5	.6	.7	.8	.9
0	+0	0250	0497	0739	0974	1199	1412	1610	1793	1958
1	+2102	2226	2327	2404	2457	2485	2487	2463	2414	2339
2	+2239	2115	1968	1799	1610	1402	1178	0938	0685	0422
3	+0150	−0128	−0409	−0691	−0971	−1247	1516	1777	2026	2261
4	−2481	2683	2865	3026	3165	3279	3368	3432	3469	3479
5	−3462	3419	3349	3253	3132	2988	2821	2632	2424	2199
6	−1957	1702	1436	1161	0879	0592	0305	0018	+0266	+0544
7	+0814	1074	1321	1553	1769	1967	2144	2300	2434	2543
8	+2629	2689	2725	2734	2719	2679	2614	2526	2415	2283
9	+2131	1961	1774	1572	1358	1133	0899	0659	0416	0170

$J_3'(x)$

x	.0	.1	.2	.3	.4	.5	.6	.7	.8	.9
0	+0	0006	0025	0056	0098	0152	0217	0291	0374	0465
1	+0562	0665	0772	0881	0991	1102	1210	1315	1415	1508
2	+1594	1671	1737	1792	1833	1861	1875	1873	1855	1821
3	+1770	1703	1619	1519	1403	1271	1125	0965	0793	0609
4	+0415	0212	0003	−0213	−0432	−0653	0874	1094	1310	1520
5	−1723	1918	2101	2272	2429	2570	2695	2801	2889	2956
6	−3003	3028	3031	3013	2973	2911	2828	2724	2600	2457
7	−2296	2118	1925	1719	1500	1270	1033	0789	0540	0289
8	−0038	+0211	+0457	+0696	+0928	+1150	1360	1557	1739	1904
9	+2052	2180	2288	2376	2441	2485	2507	2506	2483	2438

$J_4'(x)$

x	.0	.1	.2	.3	.4	.5	.6	.7	.8	.9
0	+0	0	0001	0003	0007	0013	0022	0034	0051	0071
1	+0097	0126	0161	0201	0246	0296	0350	0409	0473	0539
2	+0610	0682	0757	0833	0909	0985	1060	1133	1203	1269
3	+1330	1385	1434	1475	1508	1532	1545	1549	1541	1522
4	+1490	1447	1391	1323	1243	1150	1045	0929	0802	0665
5	+0518	0363	0200	0030	−0145	−0324	0506	0690	0874	1057
6	−1237	1412	1582	1745	1900	2045	2178	2299	2407	2500
7	−2577	2638	2683	2709	2718	2708	2679	2633	2568	2485
8	−2385	2267	2134	1986	1824	1649	1462	1265	1060	0847
9	−0629	0408	0184	+0039	+0261	+0480	0694	0900	1098	1286

Digitized by Google
Original from UNIVERSITY OF MICHIGAN
Generated on 2019-09-24 07:02 GMT / http://hdl.handle.net/2027/mdp.39015077775156
Public Domain, Google-digitized / http://www.hathitrust.org/access_use#pd-google

$J_5'(x)$

x	.0	.1	.2	.3	.4	.5	.6	.7	.8	.9
0	+0	0	0	0	0	0001	0002	0003	0005	0008
1	+0012	0018	0025	0034	0045	0058	0073	0092	0113	0137
2	+0164	0194	0228	0265	0305	0348	0394	0443	0494	0548
3	+0603	0660	0718	0777	0836	0895	0952	1008	1062	1113
4	+1160	1203	1242	1274	1301	1321	1333	1338	1335	1322
5	+1301	1270	1230	1180	1120	1050	0970	0881	0782	0675
6	+0559	0435	0304	0166	0023	−0126	0278	0433	0591	0749
7	−0907	1064	1217	1368	1513	1652	1783	1906	2020	2123
8	−2215	2294	2360	2412	2449	2472	2479	2470	2446	2405
9	−2349	2277	2190	2088	1972	1842	1700	1546	1382	1208

$J_6'(x)$

x	.0	.1	.2	.3	.4	.5	.6	.7	.8	.9
0	+0	0	0	0	0	0	0	0	0	0001
1	+0001	0002	0003	0004	0006	0009	0012	0016	0021	0027
2	+0034	0043	0053	0065	0078	0094	0111	0130	0152	0176
3	+0202	0231	0262	0295	0331	0368	0408	0450	0493	0538
4	+0585	0632	0680	0728	0776	0823	0870	0916	0959	1000
5	+1039	1074	1105	1132	1155	1172	1183	1188	1187	1179
6	+1163	1139	1108	1069	1022	0967	0904	0833	0753	0666
7	+0572	0470	0362	0247	0127	0002	−0128	−0261	−0397	−0535
8	−0674	0813	0952	1088	1222	1352	1478	1597	1710	1816
9	−1912	2000	2077	2143	2198	2240	2270	2287	2290	2279

TABLE IV

RELATIVE RADIUS FOR MAXIMUM OF ρI_p^2

Mode			
TE 11	.737		
12	.982	.254	
13	.993	.613	.159
21	.894		
22	.988	.407	
23	.995	.664	.274
31	.937		
32	.991	.491	
41	.956		
42	.993	.548	
51	.967		
61	.974		
TM 01	.901		
02	.983	.393	
03	.993	.627	.250
11	.961		
12	.989	.525	
13	.995	.682	.362
21	.977		
22	.992	.596	
31	.984		
32	.994	.643	
41	.988		
51	.990		
61	.992		

Generated on 2019-09-24 07:02 GMT / http://hdl.handle.net/2027/mdp.39015077775156
Public Domain, Google-digitized / http://www.hathitrust.org/access_use#pd-google
Digitized by Google
Original from UNIVERSITY OF MICHIGAN

Some Results on Cylindrical Cavity Resonators

By J. P. KINZER and I. G. WILSON

Certain hitherto unpublished theoretical results on cylindrical cavity resonators are derived. These are: an approximation formula for the total number of resonances in a circular cylinder; conditions to yield the minimum volume circular cylinder for an assigned Q; limitation of the frequency range of a tunable circular cylinder as set by ambiguity; resonant frequencies of the elliptic cylinder; resonant frequencies and Q of a coaxial resonator in its higher modes; and a brief discussion of fins in a circular cylinder.

The essential results are condensed in a number of new tables and graphs.

Introduction

THE subject of wave guides and the closely allied cavity resonators was of considerable interest even prior to 1942, as shown in the bibliography. it is believed that this bibliography includes virtually everything published up to the end of 1942. During the war, many applications of cavity resonators were made. Among these was the use of a tunable circular cylinder cavity in the $TE\ 01n$ mode as a radar test set; this has been treated in previous papers.[1,2] During this development, a number of new theoretical results were obtained; some of these have been published.[2] Here we give the derivation of these results together with a number of others not previously disclosed.

In the interests of brevity, an effort has been made to eliminate all material already published. For this reason, the topics are rather disconnected, and it is also assumed that the reader has an adequate background in the subject, such as may be obtained from a study of references 3 to 7 of the bibliography, or a text such as Sarbacher and Edson.[3]

A convenient reference and starting point is afforded by Fig. 1, taken from the Wilson, Schramm, Kinzer paper.[2] This figure also explains most of the notation used herein.

Acknowledgement

In this work, as in any cooperative scientific development, assistance and advice were received from many individuals and appropriate appreciation therefor is herewith extended. In some cases, explicit credit for special contributions has been given.

Contents

1. Approximation formula for number of resonances in a circular cylindrical cavity resonator.
2. Conditions for minimum volume for an assigned Q.

Digitized by Google
Original from UNIVERSITY OF MICHIGAN
Generated on 2019-09-24 07:03 GMT / http://hdl.handle.net/2027/mdp.39015077775156
Public Domain, Google-digitized / http://www.hathitrust.org/access_use#pd-google

3. Limitation of frequency range of a tunable cavity in the $TE\,01n$ mode as set by ambiguity.
4. Resonant frequencies of an elliptic cylinder.
5. Resonant frequencies and Q of higher order modes of a coaxial resonator.
6. Fins in a circular cylinder.

Approximation Formula for Number of Resonances in a Circular Cylinder

From Fig. 1, the resonant frequencies of the cylindrical cavity are obtained from the equation:

$$(fa)^2 = \left(\frac{cr}{\pi}\right)^2 + \left(\frac{cna}{2L}\right)^2 \tag{1}$$

in which r is written in place of $r_{\ell m}$, to simplify the equations. The distribution of the resonant frequencies, starting with the lowest, can be approximated by a continuous function

$$N \approx F(f_0) \approx G(\lambda_0)$$

where N represents the total number of resonances up to a frequency f_0 or a wavelength λ_0. This is bound to be an approximation, since the true function F is discontinuous (or stepped) by virtue of the resonances being a series of discrete values. For practical purposes, if F fits the stepped curve so that the steps fluctuate above and below F, it will be a useful approximation.

Derivation of such a formula as applied to the acoustic resonances of a rectangular box has recently been a subject of investigation by Bolt[9] and Maa.[10] Only slight modifications of their method need be made to apply to the present situation.

Multiply (1) thru by $\left(\frac{\pi}{c}\right)^2$:

$$\left(\frac{\pi af}{c}\right)^2 = r^2 + \left(\frac{\pi an}{2L}\right)^2.$$

Hence, if a point $\left(r, \frac{\pi an}{2L}\right)$ is plotted on the XY plane the distance from the origin to this point will be $\frac{\pi af}{c}$ and hence a measure of the resonant frequency. If all such points are plotted, they will form a lattice representing all the possible modes of resonance. The problem, then, is to find the number of lattice points in a quadrant of a circle with radius, $R = \frac{\pi af_0}{c}$.

Digitized by Google
Original from UNIVERSITY OF MICHIGAN
Generated on 2019-09-24 07:22 GMT / http://hdl.handle.net/2027/mdp.39015077775156
Public Domain, Google-digitized / http://www.hathitrust.org/access_use#pd-google

... FOR R OF TM) λ_0	FORMULAS FOR $Q\frac{\delta}{\lambda}$		DEFINITIONS
$\frac{p}{\lambda_0}$	$\frac{abL}{4}\cdot\frac{(p^2+q^2)(p^2+q^2+r^2)^{\frac{1}{2}}}{p^2b(a+L)+q^2a(b+L)}$	$n>0$	$p=\frac{\ell}{a}$ $q=\frac{m}{b}$ $r=\frac{n}{L}$
	$\frac{abL}{2}\cdot\frac{(p^2+q^2)^{\frac{3}{2}}}{p^2b(a+2L)+q^2a(b+2L)}$	$n=0$	
—	$\frac{abL}{4}\cdot\frac{(p^2+q^2)(p^2+q^2+r^2)^{\frac{3}{2}}}{aL\left[p^2r^2+(p^2+q^2)^2\right]+bL\left[q^2r^2+(p^2+q^2)^2\right]+abr^2(p^2+q^2)}$	$\ell m>0$	
	$\frac{abL}{2}\cdot\frac{(q^2+r^2)^{\frac{3}{2}}}{q^2L(b+2a)+r^2b(L+2a)}$	$\ell=0$	
	$\frac{abL}{2}\cdot\frac{(p^2+r^2)^{\frac{3}{2}}}{p^2L(a+2b)+r^2a(L+2b)}$	$m=0$	
$09\frac{S}{\lambda_0^2}$	$\frac{r_{\ell m}}{2\pi}\left[1+p^2R^2\right]^{\frac{1}{2}}\cdot\frac{1}{1+R}$	$n>0$	$R=\frac{a}{L}$ $p=\frac{n\pi}{2r_{\ell m}}$
	$\frac{r_{\ell m}}{\pi}\frac{1}{2+R}$	$n=0$	
	$\frac{r_{\ell m}}{2\pi}\left[1+p^2R^2\right]^{\frac{3}{2}}\frac{1-\left(\frac{\ell}{r_{\ell m}}\right)^2}{1+p^2R^3+p^2(1-R)R^2\left(\frac{\ell}{r_{\ell m}}\right)^2}$		
$\frac{3}{3}$	$\frac{r_{\ell m}}{2\pi}\left[1+p^2R^2\right]^{\frac{1}{2}}\frac{(1-\eta^2H')}{(1+\eta H')+R(1-\eta^2H')}$	$n>0$	$R=\frac{a}{L}$ $p=\frac{n\pi}{2r_{\ell m}}$
	$\frac{r_{\ell m}}{\pi}\cdot\frac{(1-\eta^2H')}{2(1+\eta H')+R(1-\eta^2H')}$	$n=0$	
OUBT = THE T	THESE EXPRESSIONS ARE NOT VALID FOR SMALL η WHEN $\ell=0$		
	$\frac{r_{\ell m}}{2\pi}\cdot\frac{\left[1+p^2R^2\right]^{\frac{3}{2}}M}{(1+\eta H)+p^2R^2\frac{\ell^2}{r_{\ell m}^2}\left(1+\frac{H}{\eta}\right)+p^2R^3M}$ WHERE $M=\left(1-\frac{\ell^2}{r_{\ell m}^2}\right)-\eta^2H\left(1-\frac{\ell^2}{\eta^2r_{\ell m}^2}\right)$		$H'=\left[\frac{Z'_\ell(\eta r_{\ell m})}{Z'_\ell(r_{\ell m})}\right]^2$ $H=\left[\frac{Z_\ell(\eta r_{\ell m})}{Z_\ell(r_{\ell m})}\right]^2$

sm, circular cylinder and full coaxial.

Digitized by Google
Original from UNIVERSITY OF MICHIGAN
Generated on 2019-09-24 07:22 GMT / http://hdl.handle.net/2027/mdp.39015077775156
Public Domain, Google-digitized / http://www.hathitrust.org/access_use#pd-google

Generated on 2019-09-24 07:23 GMT / http://hdl.handle.net/2027/mdp.39015077775156
Public Domain, Google-digitized / http://www.hathitrust.org/access_use#pd-google

Digitized by Google

Original from
UNIVERSITY OF MICHIGAN

The values of the Bessel zero, r, are not evenly spaced along the X axis; indeed the density, or number per unit distance, increases as r increases. Let the density be $p(x)$. Then the problem becomes one of finding the weight of a quadrant of material whose density varies as $p(x)$.

Suppose the expression for M, the number of zeros r less than some value x, is of the form

$$M = Ax^2 + Bx$$

whence, by differentiation,

$$p(x) = 2Ax + B.$$

The weight, W, of the quadrant of a circle of radius R is then, by integration,

$$W = \frac{2}{3} AR^3 + \frac{\pi}{4} BR^2.$$

Since there are $\frac{2L}{\pi a}$ lattice points per unit distance along the Y axis, $\frac{2LW}{\pi a}$ is apparently the total number of points in the quadrant. However, there are two small corrections to consider. First is that in this procedure a lattice point is represented by an area and for the points along the X axis half the area, i.e., a strip $\frac{\pi a}{4L}$ wide lying in the adjacent quadrant, has been omitted. Second is that the restriction $n > 0$ for TE modes eliminates half the points along the X axis. As it happens, these corrections just cancel each other. Thus we have

$$N = \frac{16\pi A}{3} \frac{V}{\lambda_0^3} + \frac{\pi B}{2} \frac{S}{\lambda_0^2}$$

in which

$$V = \frac{\pi a^2 L}{4} \qquad S = \pi aL \qquad \lambda_0 = \frac{c}{f_0}.$$

From a tabulation[11] of the first 180 values of r, the empirical values $A = 0.262$, $B = 0$ were obtained. This gives

$$N = 4.39 \frac{V}{\lambda_0^3}.$$

Subsequently, from an analysis of over a thousand modes in a "square cylinder" ($a = L$), Dr. Alfredo Baños, formerly of M.I.T. Radiation Laboratory, has calculated the empirical formula

$$N = 4.38 \frac{V}{\lambda_0^3} + 0.089 \frac{S}{\lambda_0^2} \tag{2}$$

Digitized by Google
Original from UNIVERSITY OF MICHIGAN
Generated on 2019-09-24 07:23 GMT / http://hdl.handle.net/2027/mdp.39015077775156
Public Domain, Google-digitized / http://www.hathitrust.org/access_use#pd-google

from which $A = 0.262$, $B = 0.057$. These values give better agreement with the 180 tabulated values of r.

There is a two-fold degeneracy in a circular cylinder for modes with $\ell > 0$, which is removed, for example, when the cylinder is made elliptical. The total number of modes, then, counting degeneracies twice, is about $2N$, which brings (2) in line with the general result that, in any cavity resonator, the total number of modes is of the order $\frac{8\pi}{3}\frac{V}{\lambda_0^3}$.

Minimum Volume of Circular Cylinder for Assigned Q

In practical applications of resonant cavities, the conditions of operation may require high values of Q which can be attained only by the use of high order modes. The total number of modes, most of which are undesired, can then be reduced only by making the cavity volume as small as possible, consistent with meeting the requirement on Q.

It will be shown that, for a cylinder, operation in the $TE\ 01n$ mode very probably gives the smallest volume for an assigned Q.

Statement of Problem

When the relative proportions (the shape) of a cavity and the mode of oscillation are fixed, both the Q and the volume, V, of the cavity are functions of the operating wavelength, λ. Since we are primarily interested in the relationship between Q and V, with λ fixed, some simplification can be made by eliminating λ as a parameter. This may be done by a change of variables to $Q\frac{\delta}{\lambda}$ and $\frac{V}{\lambda^3}$, respectively; to simplify the typography, these quantities will be denoted by single symbols:

$$P \equiv Q\frac{\delta}{\lambda}$$

$$W \equiv \frac{V}{\lambda^3}.$$

We are, consequently, interested in the following specific problem:

In a circular cylindrical resonator, which is the optimum mode family and what is the corresponding shape to obtain the smallest value of W for a preassigned value of P?

A rigorous solution cannot be obtained by the methods of elementary calculus, since P is not a continuous function of the mode of oscillation. However, a possible procedure is to assume continuity, and examine the relation between P and W under this assumption. If sufficiently positive results are obtained, the conclusions may then be carried over to the discontinuous (i.e., the physical) case with reasonable assurance that, except

Generated on 2019-09-24 07:25 GMT / http://hdl.handle.net/2027/mdp.39015077775156
Public Domain, Google-digitized / http://www.hathitrust.org/access_use#pd-google
Digitized by Google
Original from UNIVERSITY OF MICHIGAN

perhaps for special values, the correct answer is obtained. We proceed on this basis.

Solution

To permit a more coherent presentation of the arguments, only their general outline follows. More mathematical details are given later.

We start with the formulas for $Q\frac{\delta}{\lambda}$ $(= P)$ as given in Fig. 1.

The first operation is to show that, under comparable conditions, i.e., λ, r, n fixed, the TE $0mn$ modes give the highest values of P. That this is plausible can be seen in a general manner from the equations as they stand. For the TE modes, if $\ell = 0$, the numerator of the fraction is largest. Also, P simplifies, and the denominator roughly reduces the expression in square brackets to the 1/2 power. Now compare this expression with those for the TM modes. That for the TM modes ($n > 0$) is smaller because of the factor $(1 + R)$ in the denominator. Finally, that for the TM modes ($n = 0$) is still smaller, because $1 < (1 + p^2R^2)^{1/2}$.

This leaves only the TE $0mn$ modes to be considered, and the next step is to show that $m = 1$ is the most favorable value. Since the relation between P and W is complicated, a parameter φ is introduced, with φ defined by

$$\tan \varphi = pR. \tag{3}$$

The resulting parametric equations are:

$$P = \frac{r}{2\pi} \frac{1}{\cos^3 \varphi + \frac{1}{p} \sin^3 \varphi} \tag{4}$$

$$W = \frac{pr^3}{4\pi^2} \frac{1}{\cos^2 \varphi \sin \varphi}. \tag{5}$$

For each of the discrete values of r and n (n is related to p) then, plots of P vs W can be prepared as shown in Fig. 2 for the TE $01n$ modes.

Inspection of Fig. 2 shows that the best value of Q does not correspond to a minimum of W or a maximum of P for a given value of n, but rather to a point on the "envelope" of the curves. To get the envelope, we assume p to be continuous and proceed in the standard manner. It turns out that, by solving (4) for p in terms of P, r and φ, substituting the resulting expression in W, and setting $\frac{\partial W}{\partial \varphi} = 0$ an equation is obtained which, when solved for φ, gives the values of φ which lie on the envelope.

Digitized by Google
Original from UNIVERSITY OF MICHIGAN
Generated on 2019-09-24 07:25 GMT / http://hdl.handle.net/2027/mdp.39015077775156
Public Domain, Google-digitized / http://www.hathitrust.org/access_use#pd-google

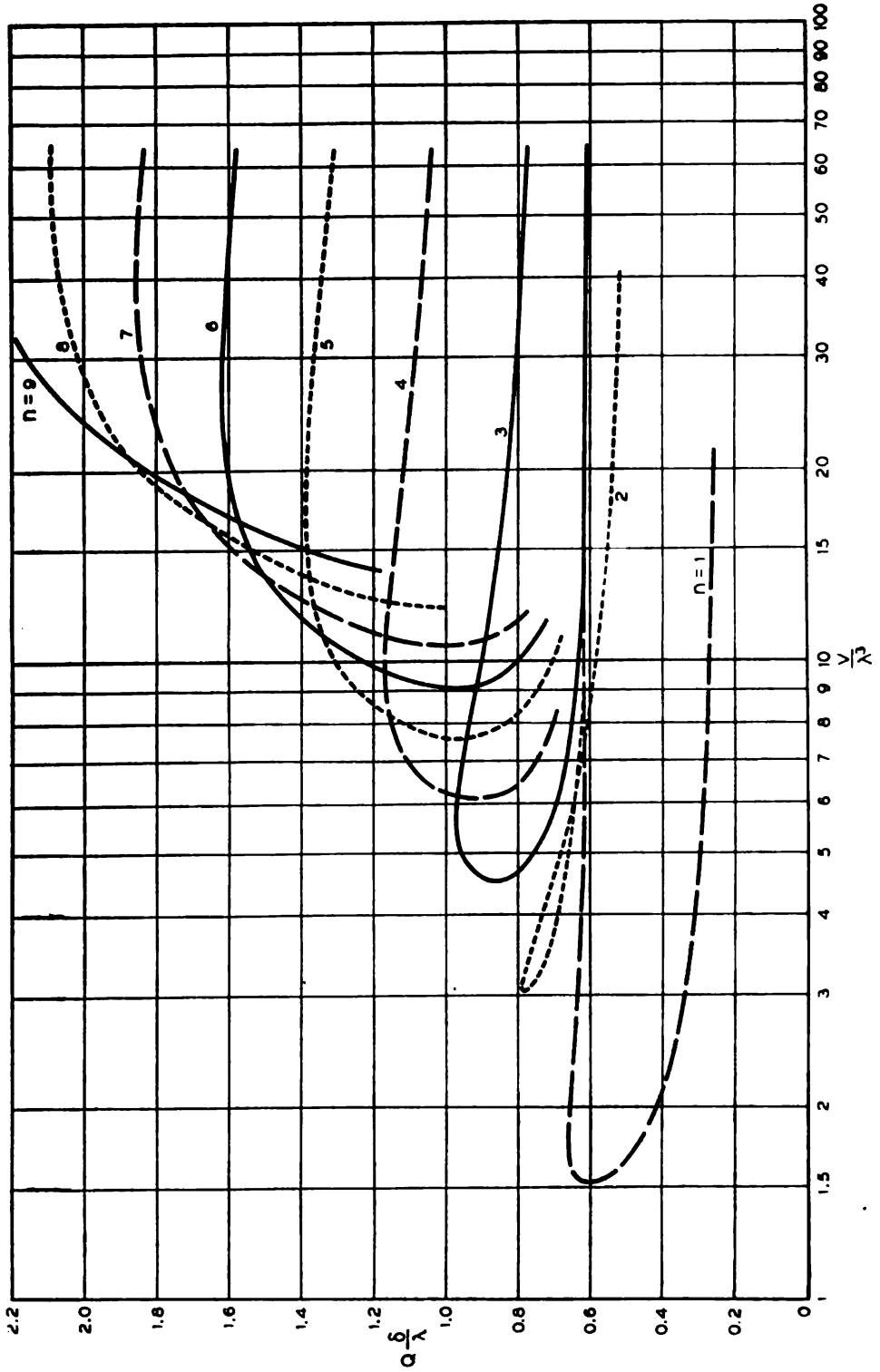

Fig. 2—Relation between $Q\frac{\delta}{\lambda}$ (= P) and $\frac{V}{\lambda^3}$ (= W) in cylindrical cavity resonator operating in TE $01n$ mode.

Digitized by Google
Original from UNIVERSITY OF MICHIGAN
Generated on 2019-09-24 07:25 GMT / http://hdl.handle.net/2027/mdp.39015077775156
Public Domain, Google-digitized / http://www.hathitrust.org/access_use#pd-google

We next substitute this expression for φ in W and calculate $\frac{\partial W}{\partial r}$ assuming now that r is continuous, and find that W has no minimum. Practically, this means that the smallest value of r should be used, i.e., the $TE\,01n$ mode.

Finally, since from Fig. 2 it is seen that the envelope is reasonably smooth for values of $Q\frac{\delta}{\lambda} > 1$, the expression for φ derived on the assumption of continuous p is used to obtain a simple relation of great utility in practical cavity design.

Details of solution

In (3), since R must be finite for a physical cylinder, $0 < \tan\varphi < \infty$, $0 < \sin\varphi < 1$, and $0 < \cos\varphi < 1$. Hence we may always divide by $\sin\varphi$ or $\cos\varphi$. Note that φ ranges between 0° and 90°.

From Fig. 1,

$$k = \frac{2r(1 + p^2R^2)^{1/2}}{a}$$

whence

$$k\sin\varphi = \frac{2prR}{a} \tag{6}$$

$$k\cos\varphi = \frac{2r}{a}. \tag{7}$$

We define W by:

$$W \equiv \frac{V}{\lambda^3} = \frac{\pi a^3}{4R}\,\frac{k^3}{8\pi^3}. \tag{8}$$

Substituting (6) and (7) in (8),

$$W = \frac{pr^3}{4\pi^2}\,\frac{1}{\cos^2\varphi\sin\varphi}. \tag{5'}$$

Substitution of (3) into the expression for $Q\frac{\delta}{\lambda}$ $(= P)$ for the TE modes as given in Fig. 1 yields, after some manipulation

$$P = \frac{r}{2\pi}\cdot\frac{1 - (\ell/r)^2}{\cos^3\varphi + \frac{1}{p}\sin^3\varphi + \left(\cos\varphi - \frac{1}{p}\sin\varphi\right)(\ell/r)^2\sin^2\varphi}.$$

Digitized by Google
Original from UNIVERSITY OF MICHIGAN
Generated on 2019-09-24 07:25 GMT / http://hdl.handle.net/2027/mdp.39015077775156
Public Domain, Google-digitized / http://www.hathitrust.org/access_use#pd-google

To show that any value of $\ell > 0$ reduces P below its value when $\ell = 0$, let

$$a = \cos^3 \varphi + \frac{1}{p} \sin^2 \varphi$$

$$b = \left(\cos \varphi - \frac{1}{p} \sin \varphi\right) \sin^2 \varphi$$

$$c = (\ell/r)^2.$$

It suffices to show that

$$\frac{1}{a} > \frac{1 - c}{a + bc}$$

where the question is in doubt because b may take on negative values. If the inequality is to be valid, it is necessary only that $(b + a) > 0$, that is, $\cos \varphi > 0$. Hence, for the TE modes, only $\ell = 0$ needs be considered. For this case, the expression for P simplifies to

$$P = \frac{r}{2\pi} \frac{1}{\cos^3 \varphi + \frac{1}{p} \sin^3 \varphi}. \tag{4'}$$

For the TM modes, there is similarly obtained

$$P = \frac{r}{2\pi} \frac{1}{\cos \varphi + \frac{1}{p} \sin \varphi} \qquad n > 0 \tag{9}$$

$$P = \frac{r}{2\pi} \frac{\cos \varphi}{\cos \varphi + \frac{1}{2p} \sin \varphi} \qquad n = 0. \tag{10}$$

It is easy to show, since $\cos \varphi < 1$ and $\sin \varphi < 1$, that both (9) and (10) are less than (4').

Hence we have shown that, under comparable conditions, i.e., r and p constant, the TE $0mn$ modes have higher values of P than any others. There is one flaw in the argument, viz., r takes on discrete values and cannot be made the same for all modes. It is conceivable, therefore, that for some specific values of P, a mode other than the TE $0mn$ can be found which gives a smaller W than either of the two "adjacent" TE $0mn$ modes, one having a value of r higher, the other lower, than the supposed high-P mode. This situation requires further refinement, and hence complication, in the analysis; we pass over this point.

Having so far indicated that the TE $0mn$ modes are the best, our next objective is find the best value of m, if possible.

Digitized by Google
Original from UNIVERSITY OF MICHIGAN
Generated on 2019-09-24 07:26 GMT / http://hdl.handle.net/2027/mdp.39015077775156
Public Domain, Google-digitized / http://www.hathitrust.org/access_use#pd-google

By use of the parametric equations (4) and (5), Fig. 2 has been plotted for $r = 3.83$ (TE 01n modes) and values of n from 1 to 9. This drawing shows that, for each discrete value of r, minimum W/P is given by points on the "envelope" of the family of curves.

The standard method of obtaining the envelope is to express W as a function of P with n as parameter (r is assumed fixed, for the moment), i.e., $W = F(P, n)$, and then set $\frac{\partial F}{\partial n} = 0$. However, in this case it is easier to express $W = G(P, \varphi)$ and $\varphi = H(n)$, whence

$$\frac{\partial F}{\partial n} = \frac{\partial G}{\partial \varphi} \cdot \frac{\partial \varphi}{\partial n}$$

and the envelope is obtained by setting $\frac{\partial G}{\partial \varphi} = 0$ provided $\frac{\partial \varphi}{\partial n} \neq 0$. We proceed, therefore, as follows.

Assume p is continuous, and solve (4) for p, obtaining:

$$p = \frac{\sin^3 \varphi}{\frac{r}{2\pi P} - \cos^3 \varphi}. \tag{11}$$

Now substitute (11) in (5). This gives W as a function of P and φ:

$$W = \frac{r^3}{4\pi^2}\left[\frac{\sin^2 \varphi}{\cos^2 \varphi\left(\frac{r}{2\pi P} - \cos^3 \varphi\right)}\right]. \tag{12}$$

To solve $\frac{\partial W}{\partial \varphi} = 0$, we differentiate and simplify. This yields

$$5 \cos^3 \varphi - 3 \cos^5 \varphi = \frac{r}{\pi P}. \tag{13}$$

Substituting (13) back into (11) yields

$$p = \frac{2 \sin \varphi}{3 \cos^3 \varphi} \tag{14}$$

The situation so far is that, with P and r assigned, W lies on the envelope and is a minimum when φ satisfies (13); p is then given by (14). Obviously, for (13) to hold, it is necessary that

$$\frac{r}{2\pi P} < 1.$$

To obtain the best value of r, the procedure is to differentiate $W_{\min}$ with respect to r, assuming now that r is continuous, and examine for a mini-

Digitized by Google
Original from UNIVERSITY OF MICHIGAN
Generated on 2019-09-24 07:26 GMT / http://hdl.handle.net/2027/mdp.39015077775156
Public Domain, Google-digitized / http://www.hathitrust.org/access_use#pd-google

mum. We can, however, first differentiate (12) by setting

$$\frac{dW}{dr} = \frac{\partial W}{\partial r} + \frac{\partial W}{\partial \varphi} \cdot \frac{\partial \varphi}{\partial r}$$

and then substitute from (13). However, when (13) is satisfied, $\frac{\partial W}{\partial \varphi} = 0$. This process yields

$$\frac{dW}{dr} = \frac{r^2}{\pi^2} \frac{(2 - 3\cos^2\varphi)}{9\sin^2\varphi\cos^5\varphi}.$$

This shows $\frac{dW}{dr}$ to be positive, when $\cos^2\varphi < \frac{2}{3}$. Hence $\frac{dW}{dr} = 0$ corresponds to a maximum, rather than a minimum.* If $\cos^2\varphi < \frac{2}{3}$, that is, $\varphi > 35°16'$, then r should be as small as possible. The smallest r is 3.83, for the TE $01n$ modes. For $r = 3.83$, and $\varphi > 35°$, from (13) there is obtained $P > 0.75$.

The analysis thus indicates that, for values of $P = Q\frac{\delta}{\lambda}$ greater than 0.75, the TE $01n$ mode yields the smallest ratio W/P or V/Q.

An interesting and simple relation between fa and R for minimum W/P can easily be derived from the foregoing equations. Substitute (14) back into (6), thereby obtaining

$$k = \frac{4Rr}{3a\cos^2\varphi}. \tag{15}$$

Now use (7) with (15) to eliminate $\cos\varphi$, replace k by $2\pi/\lambda$, and r by 3.83, its numerical value for the TE $01n$ modes. This gives

$$\left(\frac{a}{\lambda}\right)^2 R = 2.23$$

or by substituting $\lambda = \frac{c}{f}$, $c = 3 \times 10^{10}$,

$$(fa)^2 R = 20.1 \times 10^{20}.$$

This useful relation was first discovered by W. A. Edson.

Some further discussion is of interest. It is realized that a number of points have not been taken care of in a manner entirely satisfactory mathematically, but nevertheless important practical results have been obtained. As an example, since p and r can assume only discrete values, there are

* It is for this reason that the determination of the stationary values of $W(r, p, \varphi)$, subject to the constraint $P(r, p, \varphi) =$ constant, by La Grange multipliers fails to yield the desired least value of W/P.

Digitized by Google
Original from UNIVERSITY OF MICHIGAN
Generated on 2019-09-24 07:26 GMT / http://hdl.handle.net/2027/mdp.39015077775156
Public Domain, Google-digitized / http://www.hathitrust.org/access_use#pd-google

specific situations where some mode other than the $TE\ 01n$ gives a smaller W/P. For example, it may be shown that for P between 0.97 and 1.14 the TE 021 mode yields a smaller W than the TE 013 or TE 014 modes. However, the margin is small, and for larger P, the $TE\ 02n$ modes become progressively poorer.

Limitation on Frequency Range of Tunable Cavity as Set by Ambiguity

In the design of a tunable cylindrical resonant cavity intended for use in the $TE\ 01n$ mode, the requirements on Q may dictate a diameter large enough to sustain $TE\ 02n'$ or $TE\ 03n'$ modes. Also, the range of variation of cavity length may be such that the $TE\ 01(n+1)$ mode is supported. As the cavity is required to tune over a certain range of frequency, the maximum frequency range possible in the $TE\ 01n$ mode without interference from the $TE\ 01(n+1)$† or any $TE\ 02$ or $TE\ 03$ modes is of interest. The interference from the $TE\ 01(n+1)$ limits the useful range of the $TE\ 01n$ by the presence of extraneous responses at more than one dial setting for a given frequency or more than one frequency for a given dial setting. In applications so far made, it has been possible to eliminate extraneous responses from the $TE\ 02$ and $TE\ 03$ modes, but crossings of these modes with the main $TE\ 01n$ mode have not been permitted. No designs have had diameters sufficiently large to support $TE\ 04$ modes.

The desired relations are easily obtained by simple algebraic manipulation of equation (1). For simplicity in presentation of the results, we introduce some symbols applicable to this section only:

$$A = \left[\frac{cr_{l,m}}{\pi}\right]^2 \qquad B = \left[\frac{c}{2}\right]^2 = 2.247 \times 10^{20}$$

A_0 = value of A for $TE\ 01n$ modes $= 13.371 \times 10^{20}$

$t = A/A_0$

$\dot{x}_0 = (a/L)^2$ at low frequency end of useful range of $TE\ 01n$ mode

F = frequency range ratio $= \dfrac{\text{maximum } f}{\text{minimum } f}$.

The values of A and t depend upon the interfering mode under consideration. For the $TE\ 02n$ modes, $A = 44.822 \times 10^{20}$, $t = 3.3522$.

The two typical cases of interest are shown on Fig. 3. For case I, am-

† It is easy to show that the extraneous response from the $TE\ 01(n-1)$ mode is not limiting. The proof depends on the inequality $n^2 > (n+1)(n-1)$.

Digitized by Google
Original from UNIVERSITY OF MICHIGAN
Generated on 2019-09-24 07:26 GMT / http://hdl.handle.net/2027/mdp.39015077775156
Public Domain, Google-digitized / http://www.hathitrust.org/access_use#pd-google

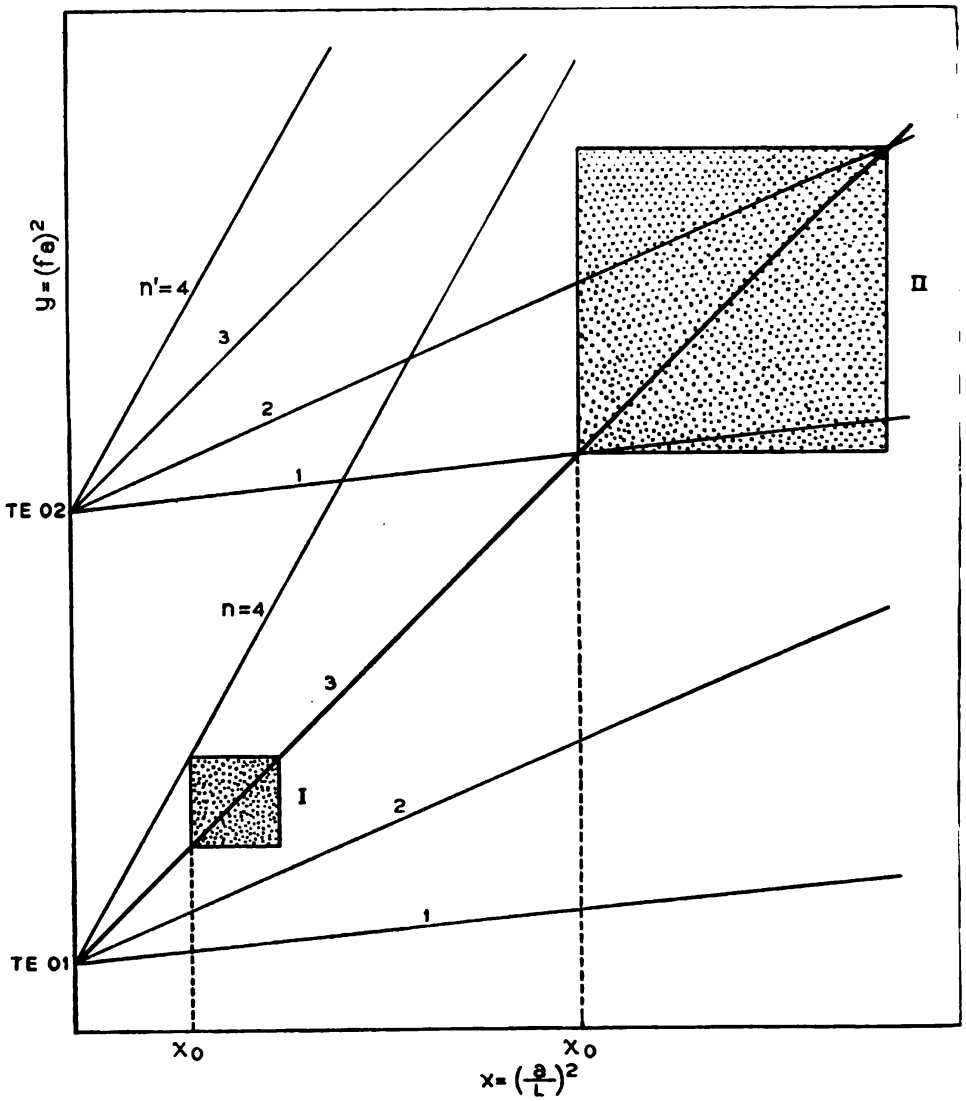

Fig. 3—Mode chart illustrating types of interference with $TE\ 01n$ mode.

biguity from $TE\ 01(n+1)$ mode, it is found that

$$F^2 = \frac{A_0 + B(n+1)^2 x_0}{A_0 + Bn^2 x_0}.$$

Curves of F for this case are shown on Fig. 4.

The maximum value of F is obtained when $x_0 = \infty$ and is

$$F_{max} = \frac{n+1}{n}.$$

Digitized by Google
Original from UNIVERSITY OF MICHIGAN
Generated on 2019-09-24 07:26 GMT / http://hdl.handle.net/2027/mdp.39015077775156
Public Domain, Google-digitized / http://www.hathitrust.org/access_use#pd-google

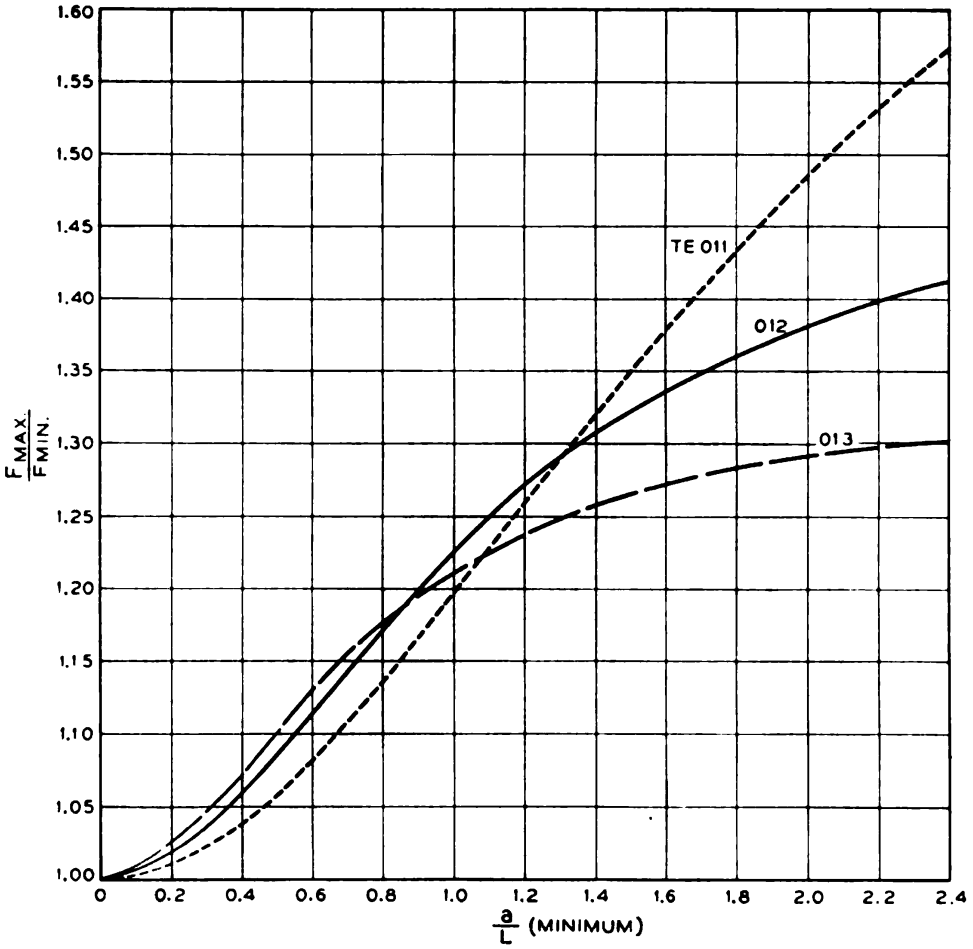

Fig. 4—Curves showing maximum value of frequency ratio without interference from $TE\ 01(n+1)$ mode (case I of Fig. 3).

TABLE I.—*Case II: Maximum Frequency Range Ratio, F, for TE 01n Mode when Limited by Mode Crossings with TE 02n' and TE 02(n'+1) Modes.*

n'	$n = 3$		$n = 4$		$n = 12$	
	F	$(a/L)_{\min}$	F	$(a/L)_{\min}$	F	$(a/L)_{\min}$
1	1.198	1.323	1.086	0.966	1.008	0.313
2			1.242	1.080	1.013	0.316
3					1.019	0.322
4					1.027	0.331
5					1.037	0.343
6					1.051	0.360
7					1.071	0.384
8					1.104	0.418
9					1.168	0.471
10					1.345	0.564

Digitized by Google
Original from UNIVERSITY OF MICHIGAN
Generated on 2019-09-24 07:27 GMT / http://hdl.handle.net/2027/mdp.39015077775156
Public Domain, Google-digitized / http://www.hathitrust.org/access_use#pd-google

For case II, range limited by mode crossings, it is found that

$$x_0 = \frac{A - A_0}{B(n^2 - n'^2)}$$

$$F^2 = \frac{(n^2 - n'^2)[n^2 t - (n' + 1)^2]}{(n^2 t - n'^2)[n^2 - (n' + 1)^2]}.$$

Some values for this case are given in Table I.

The formulas above are general and may be used for any pair of mode types by using the appropriate values for A and t.

The Elliptic Cylinder

In the design of high Q circular cylinder cavity resonators operating in the TE 01n mode, it is desirable to know how much ellipticity is tolerable, so that suitable manufacturing limits may be set. The elliptical wave guide has already been studied, notably by Brillouin[12] and Chu,[13] but the results are not in suitable form or of adequate precision for the present purposes. More recently tables[14] have become available which permit the calculation of some of the properties of the elliptical cylindrical resonator.

The elliptical cavity involves Mathieu functions, which are considerably more complicated than Bessel functions.[16] The tables give the numerical coefficients of series expansions, in terms of sines, cosines, and Bessel functions, of the Mathieu functions up to the fourth order. These tables have been used for the calculation of some quantities of interest in connection with elliptical deformations of a circular cylinder in the TE 01n mode.

The Ellipse

All mathematical treatments of the ellipse (including the tables mentioned above) use the eccentricity, e, as the quantity describing the amount of departure from the circular form. The eccentricity is the ratio

$$e = \frac{\text{distance between foci}}{\text{major axis}}.$$

This is not a quantity subject to direct measurement, hence we here introduce and use throughout the ellipticity, E, defined as

$$E = \frac{\text{difference between major and minor diameters}}{\text{major diameter}}.$$

It is clear that the ellipticity is easily obtained directly.

Again, many results are given in terms of the major diameter. Since we are interested in deformations from circular, and in such deformations the

Digitized by Google
Original from UNIVERSITY OF MICHIGAN
Generated on 2019-09-24 07:27 GMT / http://hdl.handle.net/2027/mdp.39015077775156
Public Domain, Google-digitized / http://www.hathitrust.org/access_use#pd-google

perimeter remains constant, while the major diameter changes, we have expressed our results in terms of an average diameter, defined as

$$D = \frac{\text{perimeter}}{\pi}.$$

Figure 5 shows the ellipse and various relations of interest.

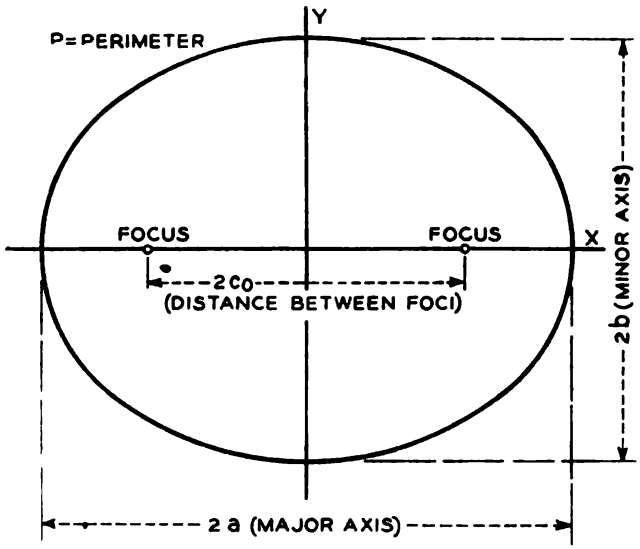

e = ECCENTRICITY = $\frac{c_0}{a}$

E = ELLIPTICITY = $\frac{(a-b)}{a}$

A = AREA = πab

D = "AVERAGE" DIAMETER = $\frac{P}{\pi}$

$b = a\sqrt{1-e^2} = a(1-E)$

$A = \pi a^2\sqrt{1-e^2} = \pi a^2(1-E)$

Fig. 5—The ellipse

Elliptic Coordinates and Functions

The elliptic coordinate system is shown on Fig. 6. Following Stratton,[15] we have used ξ in place of the table's z, since we wish to use z as the coordinate along the longitudinal axis. Stratton also uses $\eta = \cos\varphi$ as the angular coordinate; this is frequently convenient.

Analogous to $\cos \ell\theta$ and $\sin \ell\theta$ in the circular case, there are even and odd* angular functions, denoted by

$$^{e}S_{\ell}(c, \cos\varphi) \text{ and } ^{o}S_{\ell}(c, \cos\varphi)$$

which reduce to $\cos \ell\theta$ and $\sin \ell\theta$ respectively when $c \to 0$. Similarly, there are even and odd* radial functions, denoted by

$$^{e}J_{\ell}(c, \xi) \text{ and } ^{o}J_{\ell}(c, \xi)$$

* For $\ell = 0$, only even functions exist.

Digitized by Google
Original from UNIVERSITY OF MICHIGAN
Generated on 2019-09-24 07:27 GMT / http://hdl.handle.net/2027/mdp.39015077775156
Public Domain, Google-digitized / http://www.hathitrust.org/access_use#pd-google

which both reduce to $J_\ell(k_1\rho)$ when $c \to 0$. In the above, c is a parameter related to the ellipticity.* The tables do not give values of the functions, but rather give numerical coefficients

$$D_n^\ell \text{ and } F_n^\ell$$

of expansions in series of cosine, sine and Bessel functions, which permit one to calculate the elliptic cylinder functions. The coefficients, of course,

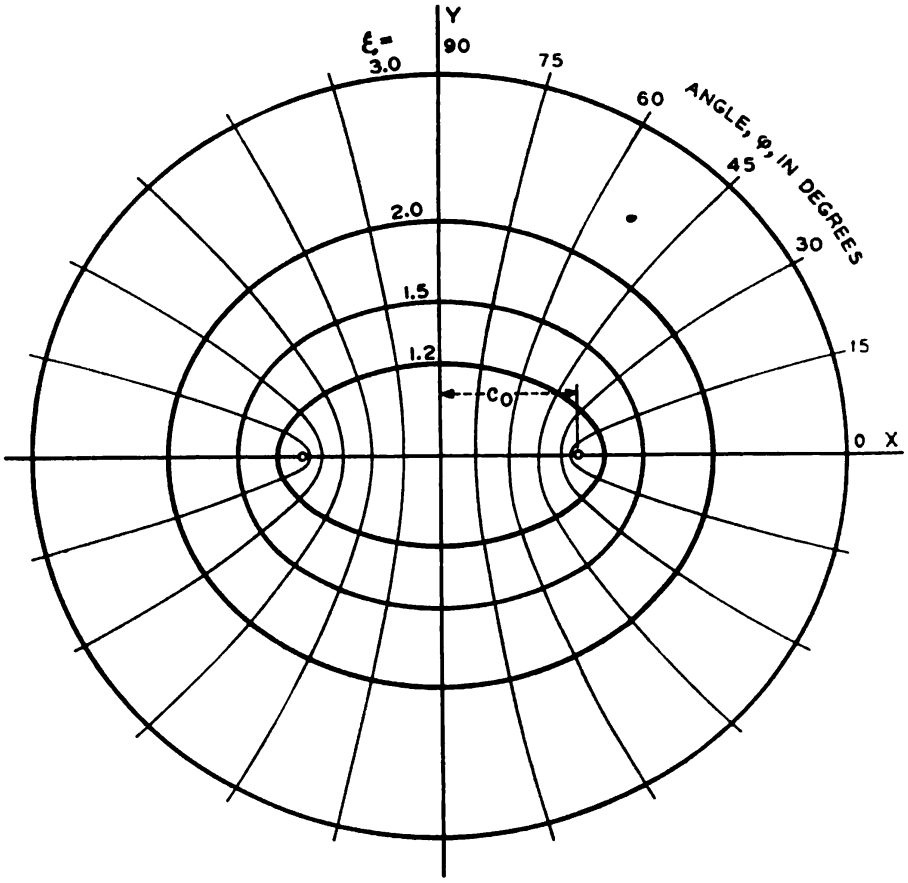

Fig. 6—Elliptic coordinate system

depend on the parameter c; the largest value of c in the tables is 4.5, which corresponds to an ellipticity of 39% in a cylinder operating in the TE $01n$ mode.** For this case, Bessel functions up to $J_{12}(x)$ and $J'_{12}(x)$ are needed for calculating the radial function. It is clear that calculations on elliptic cylinders have not been put on a simple basis.

* Not to be confused with c = velocity of electromagnetic waves; the symbol c is here carried over from the published tables.

** An ellipticity of 39% means that the difference between maximum and minimum diameters is 39% of the maximum diameter. For a given c, the ellipticity depends on the mode.

Digitized by Google
Original from UNIVERSITY OF MICHIGAN
Generated on 2019-09-24 07:27 GMT / http://hdl.handle.net/2027/mdp.39015077775156
Public Domain, Google-digitized / http://www.hathitrust.org/access_use#pd-google

Field Equations

The equations for the fields are easily obtained from section 6.12 of Stratton's book, and are given in Table II, which is self-explanatory, except for the quantity c, which we now proceed to discuss.

Resonant Frequencies

The elliptic cylinder has the major diameter, $2a$, and the focal distance, $2c_0$. The equation of its surface is then expressed by $\xi = \frac{a}{c_0} = \alpha$. On this surface, E_η must vanish. This requires that ${}^{eo}J'_\ell(c, \alpha) = 0$ for TE modes and that ${}^{eo}J_\ell(c, \alpha) = 0$ for TM modes. The series expansions are in terms of $c\xi$ as variable. Let $c\alpha = r'_{\ell m}$ or $r_{\ell m}$ be the roots of the above equations. Then $\frac{c}{c_0} = \frac{r}{a}$ (dropping the subscripts ℓ, m). Now, in working out the solution of the differential equations, it turned out that $c = c_0 k_1$. Here k_1 is one component of the wave number, k†. Hence $k_1 = \frac{r}{a}$. Furthermore, the eccentricity is $e = \frac{c_0}{a} = \frac{c}{r}$. The indicated procedure is: 1) choose a value of c; 2) find the various values of r for which the radial function or its derivative is zero; 3) then calculate the corresponding eccentricity and resonant frequency. Notice that for a given value of c, the values of r will depend on the mode, and hence so will the eccentricity.

We now wish to express our results in terms of the ellipticity and the average diameter. To convert eccentricity to ellipticity, we use

$$E = 1 - \sqrt{1 - e^2}.$$

The perimeter of the ellipse is given by $P = 4aE(e)$ where $E(e)$ is the complete elliptic integral of the second kind.††
In terms of the average diameter we find

$$k_1 = \frac{2}{D}\left[\frac{2rE(e)}{\pi}\right]$$

or calling the quantity in brackets s, $k_1 = \frac{2s}{D}$. This is now in the same form as k_1 for a circular cylinder of diameter D. The quantity s is the reciprocal of Chu's $\frac{\lambda_c}{S}$.

† It is recalled that

$$k = \frac{2\pi}{\lambda} = \sqrt{k_1^2 + k_3^2}; \qquad k_1 = \frac{r}{a}; \qquad k_3 = \frac{n\pi}{L}.$$

†† This is tabulated as $E(\alpha)$ in Jahnke & Emde, p. 85, with $\alpha = \sin^{-1}e$.

Digitized by Google
Original from UNIVERSITY OF MICHIGAN
Generated on 2019-09-24 07:34 GMT / http://hdl.handle.net/2027/mdp.39015077775156
Public Domain, Google-digitized / http://www.hathitrust.org/access_use#pd-google

We have calculated and give in Table III values of r, e, E and s for several values of c and for a few modes of special interest. For three cases, $^eTE\,01$, $^eTM\ 11$ and $^oTM\ 11$, we have determined an empirical formula to fit the calculated values of s. These are also given in Table III.

TABLE II. ELLIPTIC CYLINDER FIELDS

TE Modes

$$E_\xi = -k\sqrt{\frac{\mu}{\epsilon}}\frac{\sqrt{1-\eta^2}}{q}S_\ell'(c,\eta)J_\ell(c,\xi)\sin k_3 z\cos\omega t$$

$$E_\eta = k\sqrt{\frac{\mu}{\epsilon}}\frac{\sqrt{\xi^2-1}}{q}S_\ell(c,\eta)J_\ell'(c,\xi)\sin k_3 z\cos\omega t$$

$$H_\xi = k_3\frac{\sqrt{\xi^2-1}}{q}S_\ell(c,\eta)J_\ell'(c,\xi)\cos k_3 z\sin\omega t$$

$$H_\eta = k_3\frac{\sqrt{1-\eta^2}}{q}S_\ell'(c,\eta)J_\ell(c,\xi)\cos k_3 z\sin\omega t$$

$$H_z = k_1^2 S_\ell(c,\eta)J_\ell(c,\xi)\sin k_3 z\sin\omega t$$

TM Modes

$$E_\xi = -k_3\frac{\sqrt{\xi^2-1}}{q}S_\ell(c,\eta)J_\ell'(c,\xi)\sin k_3 z\cos\omega t$$

$$E_\eta = -k_3\frac{\sqrt{1-\eta^2}}{q}S_\ell'(c,\eta)J_\ell(c,\xi)\sin k_3 z\cos\omega t$$

$$E_z = k_1^2 S_\ell(c,\eta)J_\ell(c,\xi)\cos k_3 z\cos\omega t$$

$$H_\xi = -k\sqrt{\frac{\epsilon}{\mu}}\frac{\sqrt{1-\eta^2}}{q}S_\ell'(c,\eta)J_\ell(c,\xi)\cos k_3 z\sin\omega t$$

$$H_\eta = k\sqrt{\frac{\epsilon}{\mu}}\frac{\sqrt{\xi^2-1}}{q}S_\ell(c,\eta)J_\ell'(c,\xi)\cos k_3 z\sin\omega t$$

Notes:
Derivatives are with respect to ξ and η.
S_ℓ and J_ℓ carry prefixed superscripts, e or o, since they may be either even or odd.

$$q = c_0\sqrt{\xi^2-\eta^2} \qquad c = c_0 k_1$$

$$k_1 = \frac{r_{\ell,m}}{a} \qquad k_3 = \frac{n\pi}{L} \qquad k^2 = k_1^2 + k_3^2$$

$2c_0$ is distance between foci of ellipse.
a is the semi major diameter of the ellipse.
$r_{\ell,m}$ is the value of $c\xi$ that makes

$$J_\ell(c,\xi) = 0 \text{ for } TM \text{ modes}$$

$$J_\ell'(c,\xi) = 0 \text{ for } TE \text{ modes.}$$

Digitized by Google
Original from UNIVERSITY OF MICHIGAN
Generated on 2019-09-24 07:35 GMT / http://hdl.handle.net/2027/mdp.39015077775156
Public Domain, Google-digitized / http://www.hathitrust.org/access_use#pd-google

TABLE III ROOT VALUES OF RADIAL ELLIPTIC CYLINDER FUNCTIONS

Mode	c	r	e	E	s
*TE 01	0	3.8317	0	0	3.8317
	0.2	3.8343	0.05216	0.001361	3.8317
	0.4	3.8423	0.10410	0.005434	3.8318
	0.6	3.8558	0.15561	0.012181	3.8324
	0.8	3.8753	0.20643	0.021539	3.8337
	1.0	3.9015	0.25631	0.033406	3.8366
	1.2	3.9349	0.30496	0.047636	3.8417
	1.4	3.9763	0.35209	0.064033	3.8500
	1.6	4.0264	0.39738	0.082346	3.8624
	2.0	4.154	0.4814	0.12351	3.902
	3.0	4.634	0.6474	0.2378	4.101
	4.0	5.29	0.756	0.346	4.42
	4.5	5.66	0.795	0.393	4.62
		$s = 3.8317 + 4.33\,E^2 + 1.9E^3$			
*TM 11	0	3.8317	0	0	3.8317
	0.2	3.8330	0.05218	0.001362	3.8304
	0.4	3.8370	0.10425	0.005449	3.8265
	0.6	3.8436	0.15610	0.012259	3.8201
	0.8	3.8532	0.20762	0.021791	3.8113
	1.0	3.8658	0.25868	0.034036	3.8003
	1.2	3.8818	0.30913	0.048981	3.7874
	1.4	3.9015	0.35884	0.066599	3.7727
	1.6	3.9253	0.40761	0.086844	3.7568
	4.5	5.13	0.878	0.520	3.91
		$s = 3.8317 - 0.96E + 1.1E^2$			
*TM 11	0	3.8317	0	0	3.8317
	0.2	3.8356	0.05214	0.001361	3.8330
	0.4	3.8474	0.10397	0.005419	3.8370
	0.6	3.8670	0.15516	0.012111	3.8436
	0.8	3.8944	0.20542	0.021326	3.8530
	1.0	3.9298	0.25446	0.032918	3.8654
	1.2	3.9731	0.30203	0.046701	3.8809
	1.4	4.0243	0.34788	0.062462	3.8997
		$s = 3.8317 + 0.95E + 2.2E^2$			
*TE 22	0	6.706	0	0	6.706
	0.4	6.712	0.0596	0.00178	6.706
	0.8	6.729	0.1189	0.00709	6.705
	1.2	6.756	0.1776	0.01590	6.702
	1.6	6.788	0.2357	0.02817	6.693
	2.0	6.826	0.2930	0.04389	6.677
*TE 22	0	6.706	0	0	6.706
	0.4	6.712	0.0596	0.00178	6.706
	0.8	6.730	0.1189	0.00709	6.706
	1.2	6.762	0.1775	0.01587	6.708
	1.6	6.810	0.2350	0.02799	6.715
	2.0	6.877	0.2908	0.04323	6.729

Generated on 2019-09-24 07:35 GMT / http://hdl.handle.net/2027/mdp.39015077775156
Public Domain, Google-digitized / http://www.hathitrust.org/access_use#pd-google
Digitized by Google
Original from UNIVERSITY OF MICHIGAN

Mode	c	r	e	E	s
^{e}TE 32	0	8.015	0	0	8.015
	0.4	8.020	0.0499	0.00124	8.015
	0.8	8.035	0.0996	0.00497	8.015
	1.2	8.059	0.1489	0.01115	8.014
	1.6	8.093	0.1977	0.01974	8.013
	2.0	8.135	0.2459	0.03070	8.010
^{o}TE 32	0	8.015	0	0	8.015
	0.4	8.020	0.0499	0.00124	8.015
	0.8	8.035	0.0996	0.00497	8.015
	1.2	8.060	0.1489	0.01115	8.015
	1.6	8.097	0.1976	0.01972	8.018
	2.0	8.146	0.2455	0.03061	8.022
^{e}TM 01	0	2.4048	0		
	0.2	2.4090	0.08302		
	0.4	2.4216	0.16518		
	0.6	2.4431	0.24559		
	0.8	2.4739	0.32337		
	1.0	2.5149	0.39762		
^{e}TE 11	0	1.8412	0		
	0.2	1.8416	0.10860		
	0.4	1.8430	0.21704		
	0.6	1.8452	0.32516		
	0.8	1.8484	0.43280		
	1.0	1.8527	0.53975		

Notes:

Superscripts e and o on mode designation signify even and odd.

c is parameter used in the Tables (Stratton, Morse, Chu, Hutner, "Elliptic Cylinder and Spheroidal Wave Functions")

r is the value of the argument which, for TM modes, makes the radial function zero and, for TE modes, makes its derivative zero.

e is the eccentricity of the ellipse;

$$e = \frac{\text{distance between foci}}{\text{major diameter}}$$

E is the ellipticity of the ellipse;

$$E = \frac{\text{difference between major and minor diam.}}{\text{major diameter}}$$

s is the root value, referred to the "average diameter"; it is related to r by:

$$s = \frac{r}{\pi}\frac{\text{perimeter}}{\text{major diameter}}$$

The quantity s is also related to the cutoff wavelength in an elliptical wave guide according to:

$$s = \frac{\text{perimeter of guide}}{\text{cutoff wavelength}}$$

Resonator Q

Although the calculation of the root values is straightforward and not overly laborious, the same cannot be said for the integrations involved in the determination of resonator Q. The procedure is obvious: The field

Digitized by Google
Original from UNIVERSITY OF MICHIGAN
Generated on 2019-09-24 07:36 GMT / http://hdl.handle.net/2027/mdp.39015077775156
Public Domain, Google-digitized / http://www.hathitrust.org/access_use#pd-google

equations are given; it is only necessary to integrate $H^2 d\tau$ over the volume and $H^2 d\sigma$ over the surface and get Q from

$$Q = \frac{2}{\delta} \frac{\int H^2 d\tau}{\int H^2 d\sigma} \tag{16}$$

with δ = skin depth, a known constant. Unfortunately the integrations cannot at present be expressed in closed form. A numerical solution can be obtained by a combination of integration in series and of numerical integration.

The calculations have been made for the TE 01 mode with $c = 2.0$, for which $r = 4.154$. This value of c corresponds in this case to an ellipticity of about 12%; in a 4″ cylinder this would amount to 1/2″ difference between largest and smallest diameters. Evaluation* of the integrals yields:

$$\int_V H^2 \, d\tau = 12.307 \, k_3^2 L + 12.294 \, k_1^2 L$$

$$\int_S H^2 \, d\sigma = 49.228 \, k_3^2 + 0.1619 \, k_1 k_3^2 L + 6.6847 \, k_1^3 L$$

Substituting $k_1 = \frac{7.804}{D}$ and $k_3 = \frac{\pi n}{L}$, one obtains, finally

$$Q\delta = 0.471 \, D \left(\frac{1 + 0.1622 \, n^2 R^2}{1 + 0.0039 \, n^2 R^2 + 0.1529 \, n^2 R^3} \right).$$

For a circular cylinder,

$$Q_c \delta = 0.5 \, D \left(\frac{1 + 0.1681 \, n^2 R^2}{1 + 0.1681 \, n^2 R^3} \right).$$

Comparison of these two formulas for $Q\delta$ shows that the losses in the end plates (n^2R^3 term) are less with respect to the side wall losses in the elliptical cylinder. The net loss in $Q\delta$, as described by the reduction in the multiplier from 0.5 to 0.471, is thus presumably ascribable to an increase in side wall losses (stored energy assumed held constant). The additional term in n^2R^2 in the denominator is responsible for the difference in the attenuation-frequency behavior of elliptical vs circular wave guide as shown by Chu, Fig. 4. Incidentally, these results agree numerically with those of Chu.

* Numerical integration was by Weddle's rule; intervals of 5° in φ and 0.1 in x were used. The calculations were made by Miss F. C. Larkey.

Digitized by Google
Original from UNIVERSITY OF MICHIGAN
Generated on 2019-09-24 07:36 GMT / http://hdl.handle.net/2027/mdp.39015077775156
Public Domain, Google-digitized / http://www.hathitrust.org/access_use#pd-google

Corresponding expressions for the resonant wavelength are

$$\lambda = \frac{\pi D}{s\sqrt{1 + \left(\frac{\pi n D}{2sL}\right)^2}} = \frac{0.805\, D}{\sqrt{1 + 0.1622\, n^2 R^2}}$$

$$\lambda_c = \frac{0.820\, D}{\sqrt{1 + 0.1681\, n^2 R^2}}.$$

As an example, take $n = 1$, $R = 1$, then

(Circular)	$Q_c\delta = 0.500\, D$	$\lambda_c = 0.759\, D$
(Elliptical)	$Q\delta = 0.473\, D$	$\lambda = 0.747\, D$
	Ratio = 0.946	Ratio = 0.984.

Conclusions

The mathematics of the elliptic cylinder have not yet been developed to the point where the design of cavities of large ellipticity could be undertaken. On the other hand, sufficient results have been obtained to indicate that the ellipticity in a cavity intended to be circular, resulting from any reasonable manufacturing deviations, would not have a noticeable effect on the resonant frequencies or Q values, at least away from mode crossings.

Full Cylindrical Coaxial Resonator

The full coaxial resonator has been of some interest because of various suggestions for the use of a central rod for moving the tuning piston in a *TE* 01*n* cavity.

The cylindrical coaxial resonator, with the central conductor extending the full length of the resonator, has modes similar to the cylinder. In fact, the cylinder may be considered as a special case of the coaxial. The indices ℓ, m, n have much the same meaning and the resonant frequencies are determined by the same equation (1). However, now the value of r depends in addition (see Fig. 1) upon η, where

$$\eta = \frac{\text{diameter inner conductor}}{\text{diameter outer conductor}} = \frac{b}{a}.$$

The problem now arises of how best to represent the relations between f, a, b and L. The r's depend on η; so one possibility is to determine their values for a given η and then construct a series of mode charts, one for each value of η.

A more flexible arrangement is to plot the values of r vs η and allow the user to construct graphs suitable for the particular purpose in hand. An equivalent scheme has been used by Borgnis.[18]

It turns out that as $\eta \to 1$, $r(1 - \eta) \to m\pi$, for the *TM* modes and the

Digitized by Google
Original from UNIVERSITY OF MICHIGAN
Generated on 2019-09-24 07:36 GMT / http://hdl.handle.net/2027/mdp.39015077775156
Public Domain, Google-digitized / http://www.hathitrust.org/access_use#pd-google

TE 0*mn* modes, and $r(1 - \eta) \rightarrow (m - 1)\pi$ for all other *TE* modes. For the former modes, r becomes very large as $\eta \rightarrow 1$, that is, as the inner conductor fills the cavity more and more, the frequency gets higher and higher. For the *TE* $\ell 1n$ modes, however, as the inner conductor grows, the frequency falls to a limiting value. This is discussed in more detail by Borgnis.[18]

Figure 7 shows $r(1 - \eta)$ vs η, for a few of the lower modes; the scale for η between 0.5 and 1.0 is collapsed since this region does not appear to be of great engineering interest. A different procedure is used for the roots of the *TE* $\ell 1n$ modes. Figure 8 is a direct plot of r vs η for a few of the lower modes. In this case, $r \rightarrow \ell$ as $\eta \rightarrow 1$.

Distribution of Normal Modes

The calculation of the distribution of the resonant modes for the coaxial case follows along the lines of that for the cylinder, as given previously. The difference lies in the distribution of the roots r, which now depend upon the parameter η. The determination of this latter distribution offers difficulties. There is some evidence, however, that the normal modes will follow, at least to a first approximation, the same law as the cylinder, viz.:

$$N = 4.4 \frac{V}{\lambda_0^3}$$

with some doubt regarding the value of the coefficient.

$Q\frac{\delta}{\lambda}$ *in Coaxial Resonator*

The integrations needed to obtain this factor are relatively straightforward, but a little complicated. The final results are given in Fig. 1.

The defining equation is (16); the components of H are given in Fig. 1. The integrations can be done with the aid of integrals given by McLachlan[17] and the following indefinite integral:

$$\int \left[\ell \frac{2Z_\ell^2(x)}{x^2} + Z_\ell'^2(x) \right] x\, dx = \frac{x^2}{2}\left[Z_\ell'^2(x) + \frac{2Z_\ell(x)Z_\ell'(x)}{x} + Z_\ell^2(x)\left(1 - \frac{\ell^2}{x^2}\right)\right]$$

which can be verified by differentiation, remembering that $y = Z_\ell(x)$ is a solution of $y'' + \frac{1}{x}y' + \left(1 - \frac{\ell^2}{x^2}\right)y = 0$.

Digitized by Google
Original from UNIVERSITY OF MICHIGAN
Generated on 2019-09-24 07:36 GMT / http://hdl.handle.net/2027/mdp.39015077775156
Public Domain, Google-digitized / http://www.hathitrust.org/access_use#pd-google

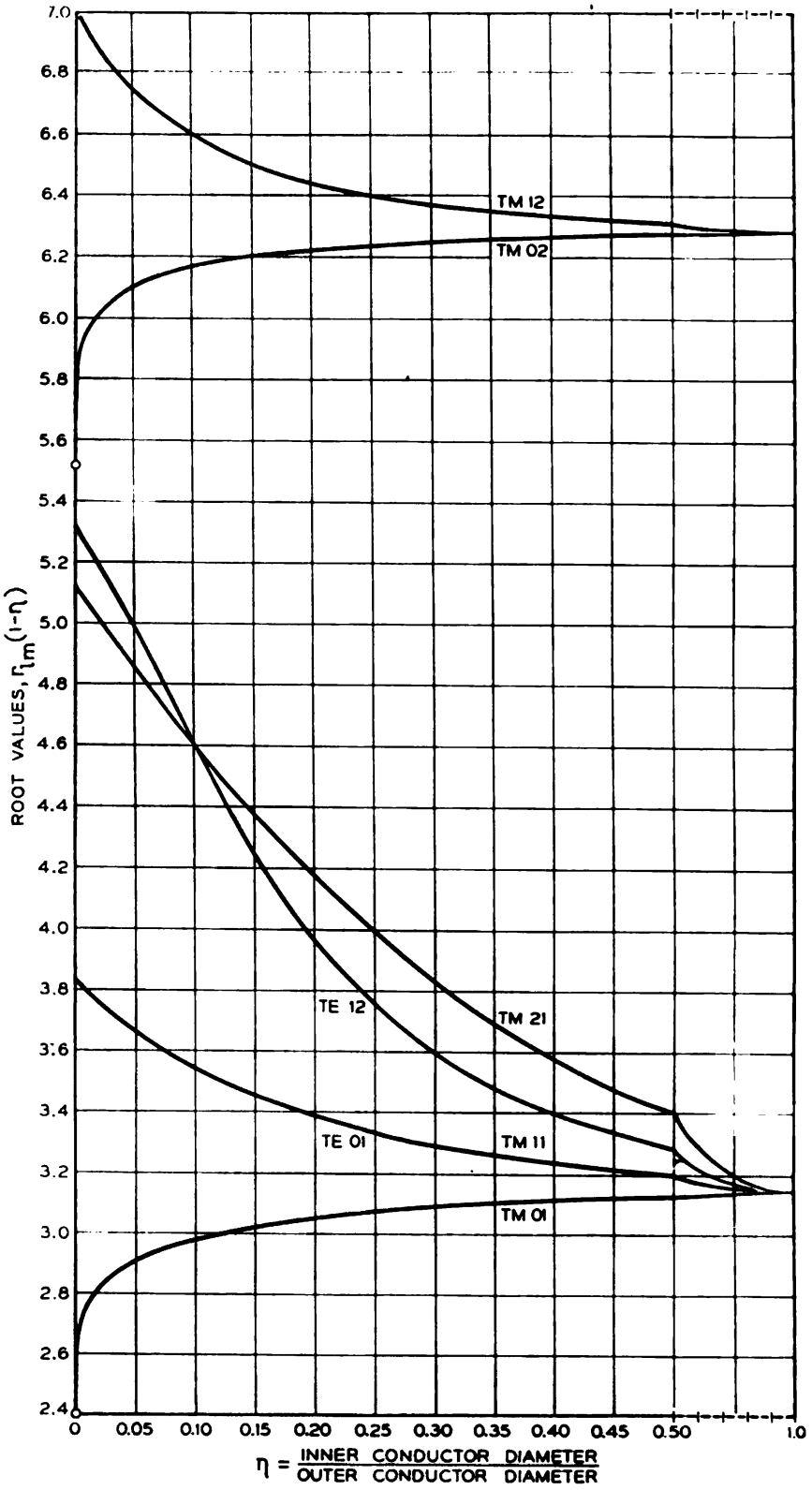

Fig. 7—Full coaxial resonator root values $r_{\ell m}(1-\eta)$

Digitized by Google
Original from UNIVERSITY OF MICHIGAN
Generated on 2019-09-24 07:36 GMT / http://hdl.handle.net/2027/mdp.39015077775156
Public Domain, Google-digitized / http://www.hathitrust.org/access_use#pd-google

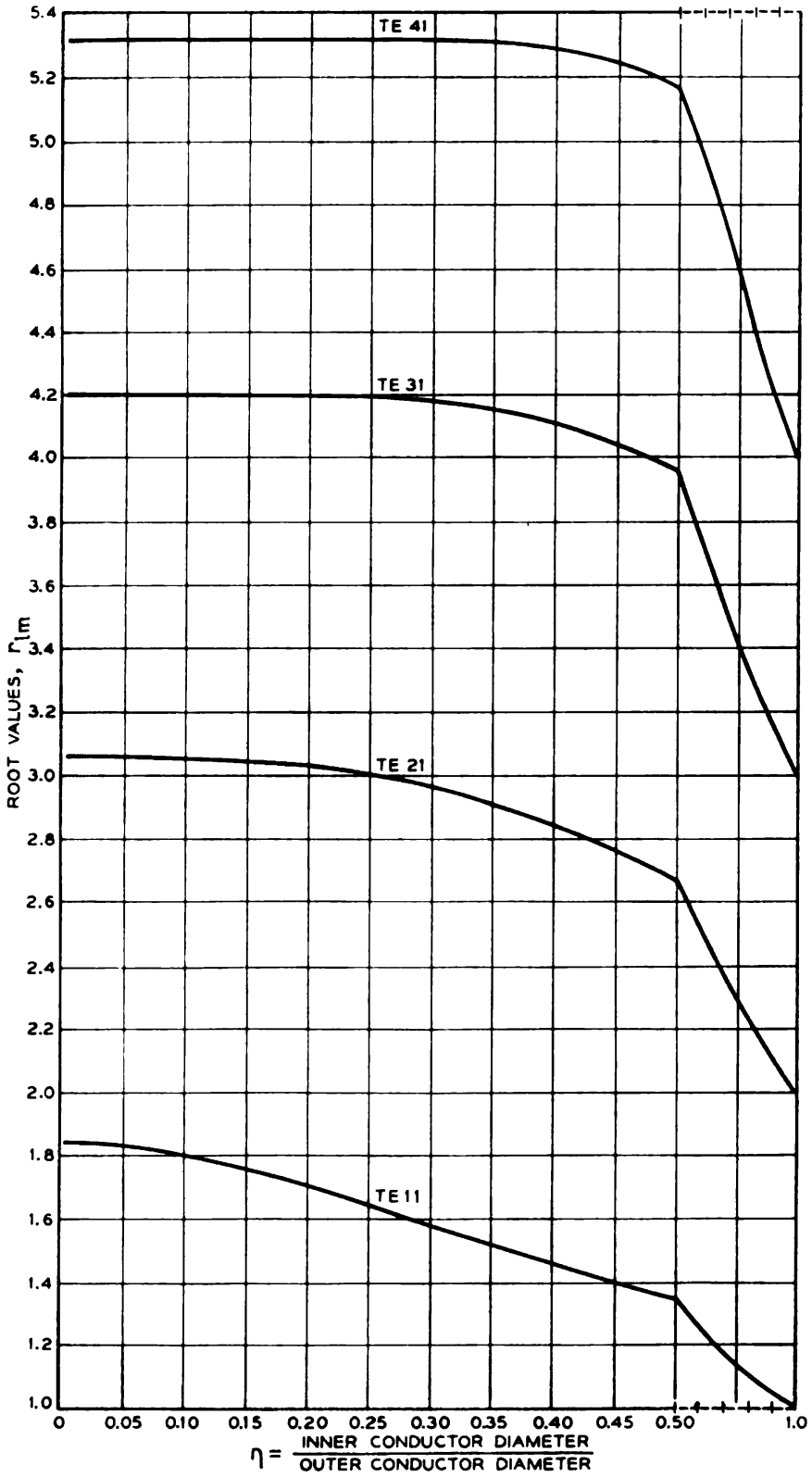

Fig. 8—Full coaxial resonator root values $r_{\ell m}$

Digitized by Google
Original from UNIVERSITY OF MICHIGAN
Generated on 2019-09-24 07:37 GMT / http://hdl.handle.net/2027/mdp.39015077775156
Public Domain, Google-digitized / http://www.hathitrust.org/access_use#pd-google

An investigation needs to be made of the behavior of the formulas as $\eta \to 0$ before any conclusion may be drawn regarding their blending into those for the cylinder. For *TE* modes with $\ell = 0$, the term involving $\frac{H}{\eta}$ disappears, hence no question arises. Consider then $\ell > 0$, and let $x = \eta r$ for the discussion following. From expansions given in McLachlan, it is easy to show that, for small x

$$Y_\ell(x) \approx -\frac{(\ell-1)!}{\pi}\left(\frac{2}{x}\right)^\ell \qquad Y'_\ell(x) \approx \frac{\ell!}{\pi}\left(\frac{2}{x}\right)^\ell \frac{1}{x}$$

$$J_\ell(x) \approx \frac{x^\ell}{2^\ell \ell!} \qquad J'_\ell(x) \approx \frac{x^{\ell-1}}{2^\ell(\ell-1)!}.$$

Since, from Fig. 1,

$$A = \frac{J'_\ell(r)}{Y'_\ell(r)} = \frac{J'_\ell(\eta r)}{Y'_\ell(\eta r)} = \frac{J'_\ell(x)}{Y'_\ell(x)}$$

it is found, upon substitution of the approximations given above:

$$Z_\ell(x) \approx \frac{2x^\ell}{2^\ell \ell!}.$$

That is, $Z_\ell(x) \sim x^\ell$ and hence $\to 0$ as $x \to 0$. Furthermore $Z_\ell(r)$ remains finite as $\eta \to 0$. Hence $H \sim x^{2\ell}$ and $\frac{H}{\eta} \sim x^{2\ell-1}$. Therefore, for $\ell > 0$, $\frac{H}{\eta} \to 0$ as $\eta \to 0$.

Hence, the expression for $Q\frac{\delta}{\lambda}$ for the coaxial structure reduces to that for the cylinder, for any value of ℓ, in the *TE* modes.

For the *TM* modes, and for $\ell > 0$, an entirely similar argument shows that H' remains finite as $\eta \to 0$. Hence, the expression for $Q\frac{\delta}{\lambda}$ or these modes also reduces to that for the cylinder.

For the *TM* modes, and with $\ell = 0$, we have

$$Z'_0(x) = -J_1(x) + J_0(x)\frac{Y_1(x)}{Y_0(x)}.$$

For $x \to 0$, $J_1(x) \to 0$ and $J_0(x) \to 1$, hence for small x,

$$Z'_0(x) \sim \frac{Y_1(x)}{Y_0(x)}.$$

Digitized by Google
Original from UNIVERSITY OF MICHIGAN
Generated on 2019-09-24 07:37 GMT / http://hdl.handle.net/2027/mdp.39015077775156
Public Domain, Google-digitized / http://www.hathitrust.org/access_use#pd-google

Now substitute the approximate values of the Y for small x. The result is

$$Z_0'(x) \sim \frac{1}{x \log \frac{x}{2}}.$$

Since $Z_0'(r)$ is finite, it follows that

$$\eta H' \sim \frac{1}{x\left(\log \frac{x}{2}\right)^2}$$

and it is easily shown that $\eta H' \to \infty$ as $\eta \to 0$. On the other hand, $\eta^2 H' \to 0$ as $\eta \to 0$. Hence, $Q\frac{\delta}{\lambda} \to 0$ as $\eta \to 0$. On the other hand, for $\eta = 0$, a

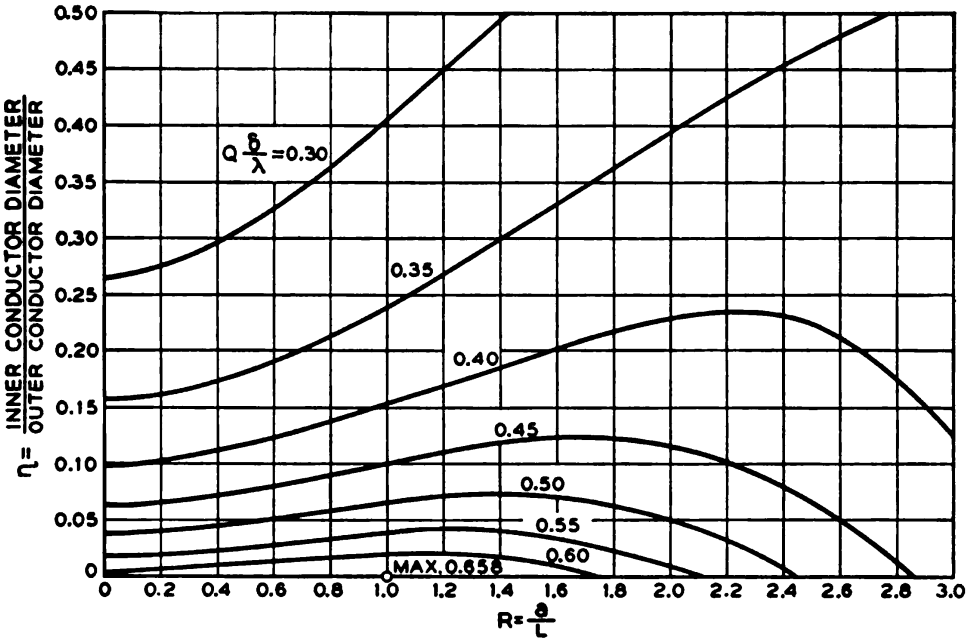

Fig. 9—Coaxial resonator. TE 011 mode Contour lines of $Q\frac{\delta}{\lambda}$

perfect cylinder exists whose $Q\frac{\delta}{\lambda}$ is not zero. It is concluded that the expression for $Q\frac{\delta}{\lambda}$ does not apply for small η for the TM modes with $\ell = 0$.

Thus it is seen that the expressions for the factor $(Q\frac{\delta}{\lambda})$ reduce to those given for the cylinder, when $\eta = 0$, except for TM modes with $\ell = 0$. For these latter cases, the factor approaches zero as η approaches zero, because $\eta H'$ increases without limit. This means that an assumption

Digitized by Google
Original from UNIVERSITY OF MICHIGAN
Generated on 2019-09-24 07:37 GMT / http://hdl.handle.net/2027/mdp.39015077775156
Public Domain, Google-digitized / http://www.hathitrust.org/access_use#pd-google

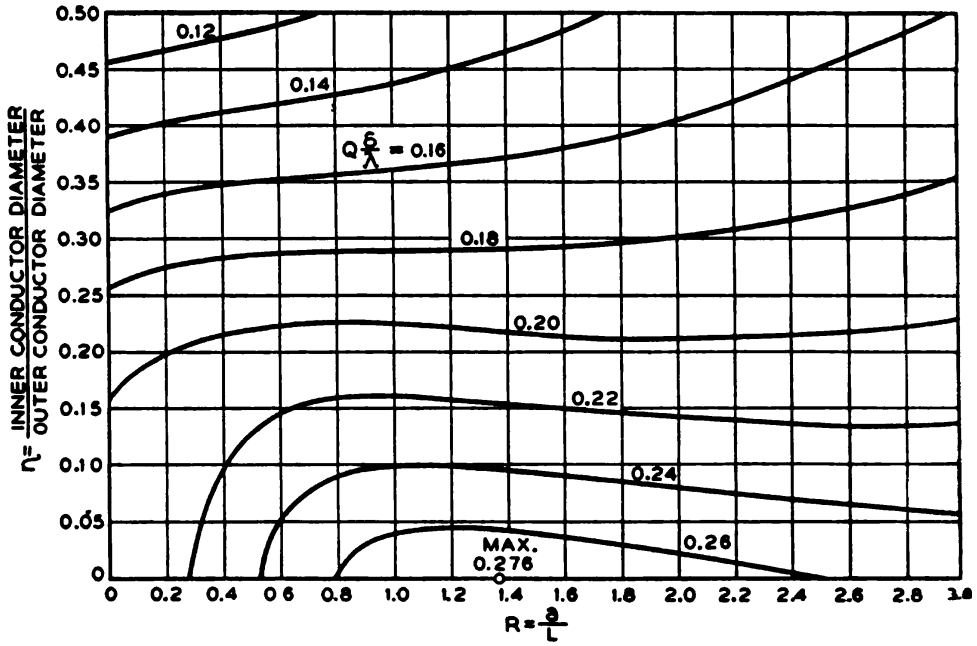

Fig. 10—Coaxial resonator. *TE* 111 mode Contour lines of $Q\frac{\delta}{\lambda}$

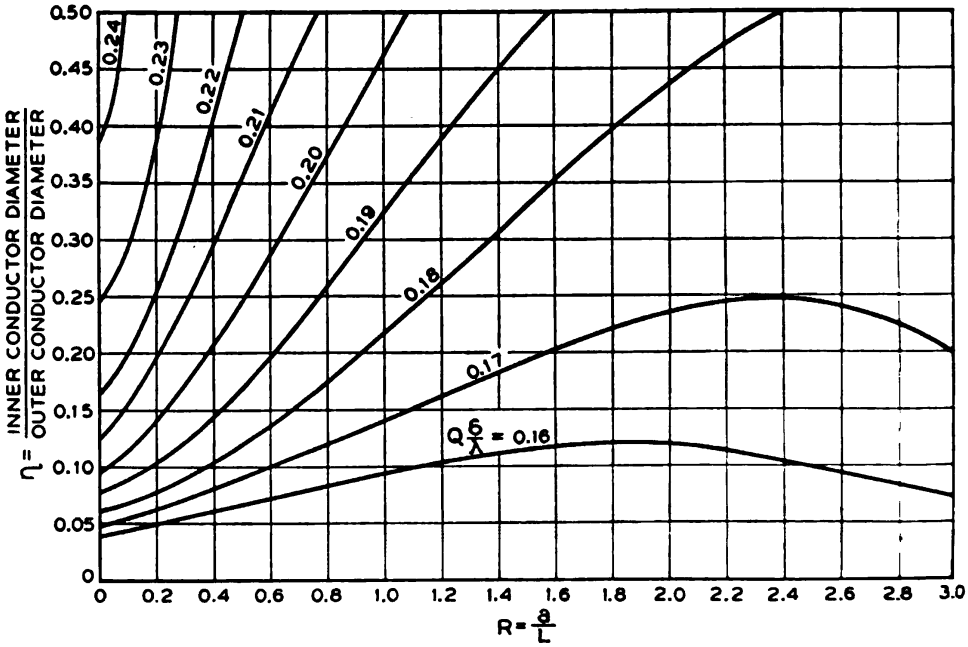

Fig. 11—Coaxial resonator. *TM* 011 mode Contour lines of $Q\frac{\delta}{\lambda}$

Digitized by Google
Original from UNIVERSITY OF MICHIGAN
Generated on 2019-09-24 07:38 GMT / http://hdl.handle.net/2027/mdp.39015077775156
Public Domain, Google-digitized / http://www.hathitrust.org/access_use#pd-google

which was made in the derivation of the Q values is not valid for small η; that is, the fields for the dissipative case are not the same as those derived on the basis of perfectly conducting walls.

The expressions for the factor are rather complicated, as it depends on several parameters. When a given mode is chosen, the number of parameters reduces to two, η and R. Contour diagrams of $Q\frac{\delta}{\lambda}$ vs η and R are given on Figs. 9, 10, 11 and 12 for the *TE* 011, *TE* 111, *TM* 011 and *TM* 111

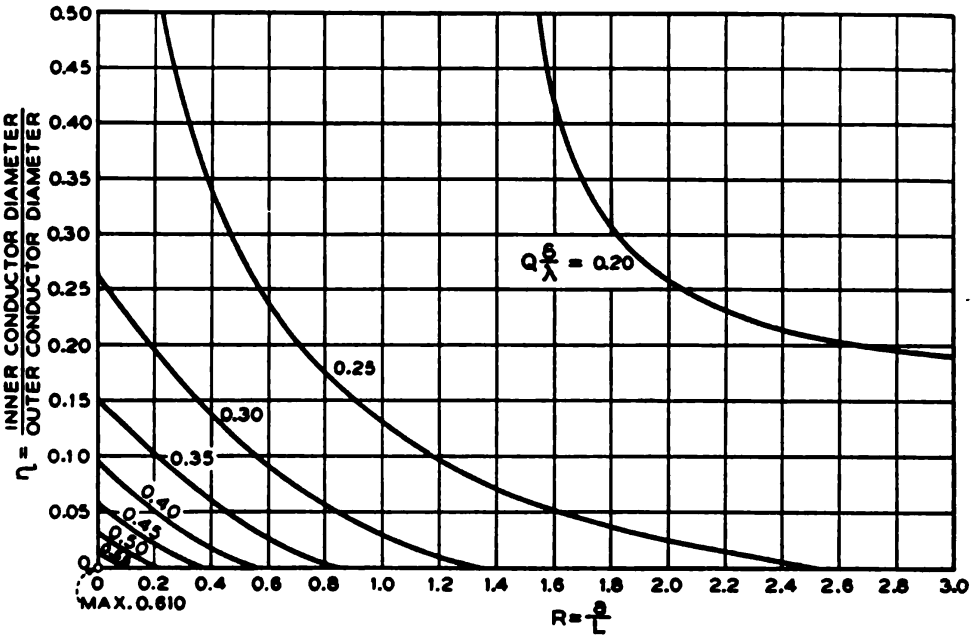

Fig. 12—Coaxial resonator. *TM* 111 mode Contour lines of $Q\frac{\delta}{\lambda}$

modes. As mentioned above, the true behavior of $Q\frac{\delta}{\lambda}$ for the *TM* 011 mode for small η is not given by the above formula, so this contour diagram has been left incomplete.

Fins in a Cavity Resonator

The suppression of extraneous modes is always an important problem in cavity design. Among the many ideas advanced along these lines is the use of structures internal to the cavity.

It is well known that if a thin metallic fin or septum is introduced into a cavity resonator in a manner such that it is everywhere perpendicular to the *E*-lines of one of the normal modes, then the field configuration and

Digitized by Google
Original from UNIVERSITY OF MICHIGAN
Generated on 2019-09-24 07:38 GMT / http://hdl.handle.net/2027/mdp.39015077775156
Public Domain, Google-digitized / http://www.hathitrust.org/access_use#pd-google

frequency of that particular mode are undisturbed. For example, Fig. 13 shows the *E*-lines in a *TE* 11*n* mode in a circular cylinder. If the upper half of the cylinder wall is replaced by a new surface, shown dotted, the field and frequency in the resulting flattened cylinder will be the same as

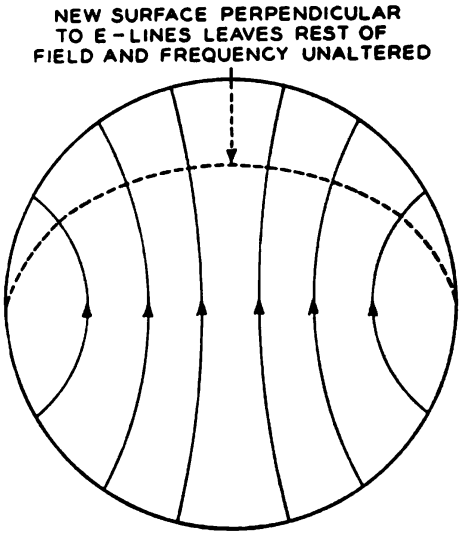

Fig. 13—*E* Lines in *TE* 11*n* mode

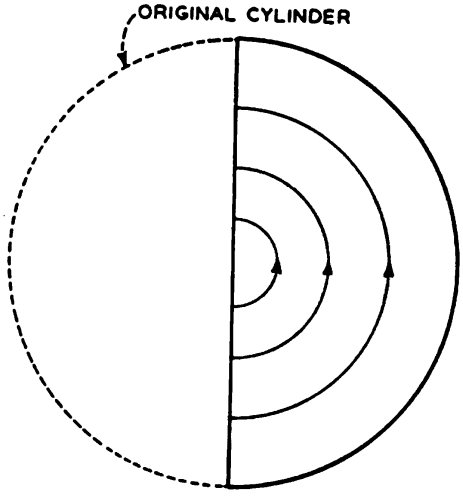

Fig. 14—"*TE* 01*n*" mode in half-cylinder

before. Indeed, they will also be the same in the crescent-shaped resonator indicated in the figure.

Except for isolated cases, all the other modes of the original cylinder will be perturbed in frequency since the old fields fail to satisfy the boundary conditions over the new surface. Furthermore, if the original cylinder was

Digitized by Google
Original from UNIVERSITY OF MICHIGAN
Generated on 2019-09-24 07:38 GMT / http://hdl.handle.net/2027/mdp.39015077775156
Public Domain, Google-digitized / http://www.hathitrust.org/access_use#pd-google

circular, its inherent double degeneracy will be lost and each of the original modes (with minor exceptions) will split into two.

Although the frequency and fields of the undisturbed mode are the same, the Q is not necessarily so. For example, Fig. 14 shows a "*TE* 01*n* mode" in a half cylinder.*

It is easy to calculate $Q\frac{\delta}{\lambda}$ for this case. The result is

$$Q\frac{\delta}{\lambda} = \frac{r}{2\pi} \cdot \frac{(1 + p^2R^2)^{3/2}}{1 + p^2R^2 + K_1 + K_2p^2R^2} \tag{17}$$

in which

$$K_1 = 1.290 \qquad K_2 = 0.653.$$

Here K_1 and K_2 are constants which account for the resistance losses in the flat side. For the full cavity, shown dotted in Fig. 14, eq. (17) holds with $K_1 = K_2 = 0$. If the circular cavity has a partition extending from the center to the rim along the full length, (17) holds with the values of K_1 and K_2 halved. If a fin projects from the rim partway into the interior, still other values of K_1 and K_2 are required. It is a simple matter to compute these for various immersions; Fig. 15 shows curves of K_1 and K_2. The following table gives an idea of the magnitudes involved:

MODE: *TE* 0,1,12 $R = 0.4$

Fin, % a	$Q\frac{\delta}{\lambda}$	Ratio
0%	2.573	1.0
10	2.536	.985
20	2.479	.965
50	2.04	.79
100	1.47	.57

The question now is asked, "Suppose a longitudinal fin were used, small enough to cause only a tolerable reduction in the Q. Would such a fin ameliorate the design difficulties due to extraneous modes?"

Some of the effects seem predictable. All modes with $\ell > 0$ will be split to some extent, into two modes of different frequencies. Consider the *TE* 12*n* mode, for example. There will be one mode, of the same frequency as the original whose orientation must be such that its E-lines are perpendicular to the fin. The Q of this mode would be essentially unchanged. There will be a second mode, oriented generally 90° from the first, whose E-lines will be badly distorted (and the frequency thereby lowered) in the vicinity

* Solutions for a cylinder of this cross-section are known and all the resonant frequencies and Q values could be computed, if they had any application.

Digitized by Google
Original from UNIVERSITY OF MICHIGAN
Generated on 2019-09-24 07:38 GMT / http://hdl.handle.net/2027/mdp.39015077775156
Public Domain, Google-digitized / http://www.hathitrust.org/access_use#pd-google

of the fin. It would be reasonable to expect the Q of this mode to be appreciably lowered because of the concentrated field there. If two fins at 90° were present, there would be no orientation of the original TE $12n$ mode which would satisfy the boundary conditions. In this case both new modes

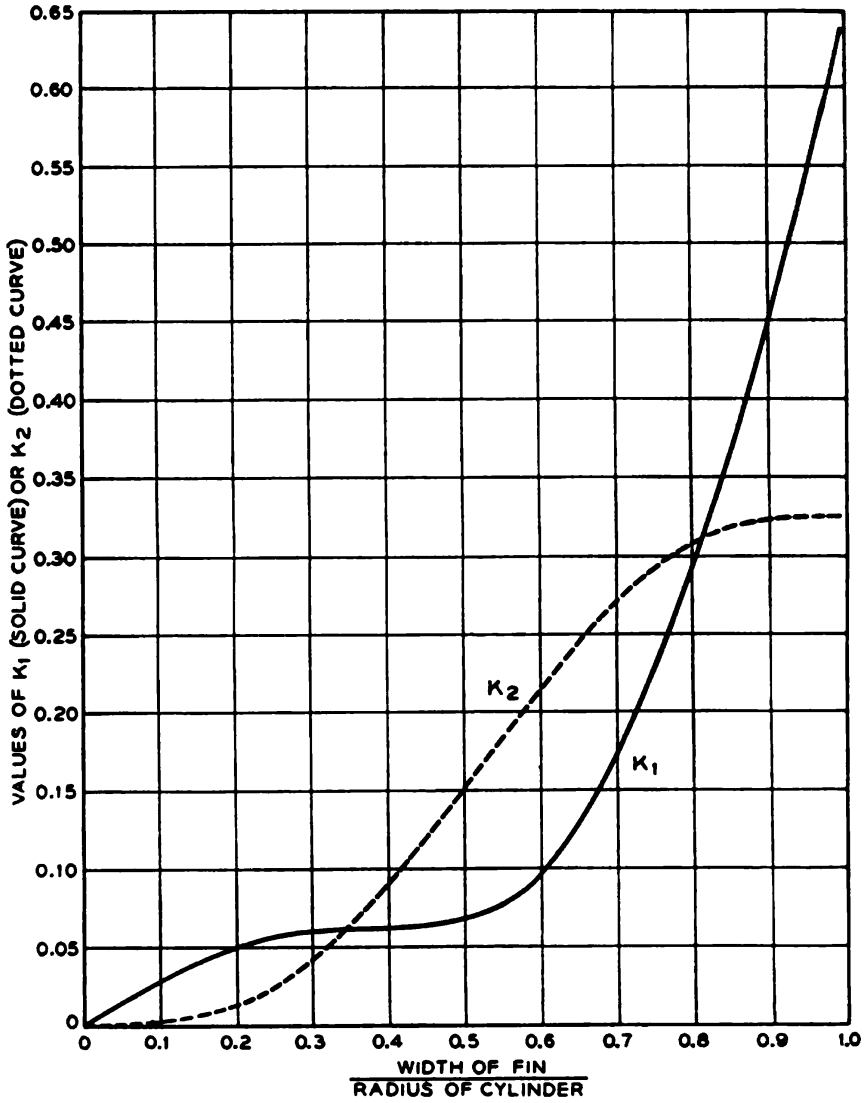

Fig. 15—Constants for calculation of Q of TE $01n$ mode in cylinder with longitudina fin.

would be perturbed in frequency from the original value. If both fins were identical, the perturbations would be equal and a double degeneracy ensue. Similar effects would happen to the other types of modes.

The major advantage derivable from such effects would appear to be in extraneous transmissions. The fin serves to orient positively the fields in

Digitized by Google
Original from UNIVERSITY OF MICHIGAN
Generated on 2019-09-24 07:38 GMT / http://hdl.handle.net/2027/mdp.39015077775156
Public Domain, Google-digitized / http://www.hathitrust.org/access_use#pd-google

the cavity, and the input and output coupling locations can then be appropriately chosen. On the basis that internal couplings are responsible for mode crossing difficulties, one might hazard a guess that a real fin would increase such couplings.

Another application of fins might be in a wave guide feed in which it is desired to establish only a $TE\,0m$ wave. In this case, Q is not so important and larger fins can be used. If these extended virtually to the center and x of them were present (with uniform angular spacing) all types of wave transmission having ℓ less than $x/2$, x even or ℓ less than x, x odd, would be suppressed. This use of fins is an extension of the wires that have been proposed in the past.

Bibliography

1. E. I. Green, H. J. Fisher, J. G. Ferguson, "Techniques and Facilities for Radar Testing." See pp. 861 ff.
2. I. G. Wilson, C. W. Schramm, J. P. Kinzer, "High Q Resonant Cavities for Microwave Testing". See pp. 909 ff.
3. J. R. Carson, S. P. Mead, S. A. Schelkunoff, "Hyper-Frequency Wave Guides—Mathematical Theory," *B.S.T.J.*, 15, pp. 310–333 (1936).
4. G. C. Southworth, "Hyperfrequency Wave Guides—General Considerations and Experimental Results," *B.S.T.J.*, 15, pp. 284–309 (1936).
5. W. W. Hansen "A Type of Electrical Resonator," *Jour. App. Phys.*, 9, pp. 654–663 (1938).—A good general treatment of cavity resonators. Also deals briefly with coupling loops.
6. W. W. Hansen and R. D. Richtmyer, "On Resonators Suitable for Klystron Oscillators," *Jour. App. Phys.*, 10, pp. 189–199 (1939).—Develops mathematical methods for the treatment of certain shapes with axial symmetry, notably the "dimpled sphere," or hour glass.
7. W. L. Barrow and W. W. Mieher, "Natural Oscillations of Electrical Cavity Resonators," *Proc. I.R.E.*, 28, pp. 184–191 (1940). An experimental investigation of the resonant frequencies of cylindrical, coaxial and partial coaxial (hybrid) cavities.
8. R. Sarbacher and W. Edson, "Hyper and Ultrahigh Frequency Engineering," John Wiley and Sons, (1943).
9. R. H. Bolt, "Frequency Distribution of Eigentones in a Three-Dimensional Continuum," *J.A.S.A.*, 10, pp. 228–234 (1939)—Derivation of better approximation formula than the asymptotic one; comparison with calculated exact values.
10. Dah-You Maa, "Distribution of Eigentones in a Rectangular Chamber at Low-Frequency Range," *J.A.S.A.*, 10, pp. 235–238 (1939)—Another method of deriving an approximation formula.
11. I. G. Wilson, C. W. Schramm, J. P. Kinzer, "High Q Resonant Cavities for Microwave Testing". See pp. 909 ff.
12. L. Brillouin, "Theoretical Study of Dielectric Cables," *Elec. Comm.*, 16, pp. 350–372 (1938)—Solution for elliptical wave guides.
13. L. J. Chu, "Electromagnetic Waves in Elliptic Hollow Pipes of Metal," *Jour. App. Phys.*, 9, pp. 583–591 (1938).
14. Stratton, Morse, Chu, Hutner, "Elliptic Cylinder and Spheroidal Wave Functions," M.I.T. (1941).

Generated on 2019-09-24 07:39 GMT / http://hdl.handle.net/2027/mdp.39015077775156
Public Domain, Google-digitized / http://www.hathitrust.org/access_use#pd-google
Digitized by Google
Original from UNIVERSITY OF MICHIGAN

15. J. A. Stratton, "Electromagnetic Theory," McGraw-Hill, (1941).
16. F. Jahnke and E. Emde, "Tables of Functions," pp. 288–293, Dover Publications (1943).
17. N. W. McLachlan, "Bessel Function for Engineers," Clarendon Press, Oxford (1934).
18. F. Borgnis, "Die konzentrische Leitung als Resonator," *Hochf: tech u. Elek:akus.*, 56, pp. 47–54, (1940).—Resonant modes and Q of the full coaxial resonator. For long abstract, see *Wireless Engineer*, 18, pp. 23–25, (1941).

ADDITIONAL BIBLIOGRAPHY

19. J. J. Thomson, "Notes on Recent Researches in Electricity and Magnetism," Oxford, Clarendon Press, 1893,—§300 gives the resonant frequencies of the TE modes in a cylinder with $a/L = 0$; §315–316 consider two concentric spheres; §317–318 treat of the Q of the spherical cavity.
20. Lord Rayleigh, "On the passage of electric waves through tubes or the vibrations of dielectric cylinders" *Phil. Mag.;* 43, pp. 125–132 (1897).—Considers rectangular and circular cross-sections.
21. A. Becker, "Interferenzröhren für elektrische Wellen," *Ann. d. Phys.*, 8, pp. 22–62 (1902)—Abstract in *Sci. Abs.*, 5, No. 1876 (1902)—Experimental work at 5 cm, and 10 cm.
22. R. H. Weber, "Elektromagnetische Schwingungen in Metallröhren," *Ann. d. Phys.* 8, pp. 721–751 (1902)—Abstract in *Sci. Abs.*, 6A, No. 96 (1903).
23. A Kalähne, "Elektrische Schwingungen in ringförmigen Metallröhren," *Ann. d. Phys.*, 18, pp. 92–127 (1905).—Abstract in *Sci. Abs.*, 8A, No. 2247 (1905).
24. G. Mie, "Beiträge zur Optik trüber Medien, speziell kolloidaler Metallösungen," *Ann. d. Phys.*, 25, pp. 337–445 (1908)—A part of this article deals with the solution of the equations for the sphere; also shown are the E and H lines for the lowest eight resonant modes.
25. H. W. Droste, "Ultrahochfrequenz-Ubertragung längs zylindrischen Leitern und Nichtleitern," *TFT*, 27, pp. 199–205, 273–279, 310–316, 337–341 (1931)—Abstract in *Wireless Engr.*, 15, p. 617, No. 4209 (1938).
26. W. L. Barrow, "Transmission of Electromagnetic Waves in Hollow Tubes of Metal," *Proc. I.R.E.*, 24, pp. 1298–1328 (1936)—A development of the equations of propagation together with a discussion of terminal connections.
27. S. A. Schelkunoff, "Transmission Theory of Plane Electromagnetic waves," *Proc. I.R.E.*, 25, pp. 1457–1492 (1937)—Treats waves in free space and in cylindrical tubes of arbitrary cross-section; special cases; rectangle, circle, sector of circle and ring.
28. L. J. Chu, "Electromagnetic Waves in Elliptic Hollow Pipes of Metal," *Jour. App. Phys.*, 9, pp. 583–591 (1938)—A study of field configurations, critical frequencies, and attenuations.
29. G. Reber, "Electric Resonance Chambers," *Communications*, Vol. 18, No. 12, pp. 5–8 (1938).
30. F. Borgnis, "Electromagnetische Eigenschwingungen dielektrischer Räume," *Ann. d. Phys.*, 35, pp. 359–384 (1939). Solution of Maxwells equations for rectangular prism, circular cylinder, sphere; also derivations of stored energy and Q values.
31. W. W. Hansen, "On the Resonant Frequency of Closed Concentric Lines," *Jour. App. Phys.*, 10, pp. 38–45 (1939).—Series approximation method for TM $OO\rho$ mode.
32. R. D. Richtmyer, "Dielectric Resonators," *Jour. App. Phys.*, 10, pp. 391–398 (1939).
33. H. R. L. Lamont, "Theory of Resonance in Microwave Transmission Lines with Discontinuous Dielectric," *Phil. Mag.*, 29, pp. 521–540 (1940).—With bibliography covering wave guides, 1937–1939.
34. E. H. Smith, "On the Resonant Frequency of a Type of Klystron Resonator," *Phys. Rev.*, 57, p. 1080 (1940).—Abstract.
35. W. C. Hahn, "A New Method for the Calculation of Cavity Resonators," *Jour. App. Phys.*, 12, pp. 62–68 (1941).—Series approximation method for certain circularly symmetric resonators.
36. E. U. Condon, "Forced Oscillations in Cavity Resonators," *Jour. App. Phys.*, 12 pp. 129–132 (1941).—Formulas for coupling loop and capacity coupling.
37. W. L. Barrow and H. Schaevitz, "Hollow Pipes of Relatively Small Dimensions," *A.I.E.E. Trans.*, 60, pp. 119–122 (1941).—Septate coaxial wave guide and cavity resonator, based on bending a flat rectangular guide into a cylinder.

Digitized by Google
Original from UNIVERSITY OF MICHIGAN
Generated on 2019-09-24 07:43 GMT / http://hdl.handle.net/2027/mdp.39015077775156
Public Domain, Google-digitized / http://www.hathitrust.org/access_use#pd-google

38. H. König, "The Laws of Similitude of the Electromagnetic Field, and Their Application to Cavity Resonators," *Wireless Engr.*, 19, p. 216–217, No. 1304 (1942). "The law of similitude has strict validity only if a reduction in dimensions by the factor $1/m$ is accompanied by an increase in the conductivity of the walls by the factor m." Original article in *Hochf; tech u. Elek:akus*, 58, pp. 174–180 (1941).
39. S. Ramo, "Electrical Concepts at Extremely High Frequencies," *Electronics*, Vol. 9, Sept. 1942, pp. 34–41, 74–82. A non-mathematical description of the physical phenomena involved in vacuum tubes, cavity resonators, transmission lines and radiators.
40. J. Kemp, "Wave Guides in Electrical Communication," *Jour. I.E.E.*, V. 90, Pt. III, pp. 90–114 (1943).—Contains an extensive listing of U. S. and British patents.
41. H. A. Wheeler, "Formulas for the Skin Effect," *Proc. I.R.E.*, 30, pp. 412–424 (1942)—Includes: a chart giving the skin depth and surface resistivity of several metals over a wide range of frequency; simple formulas for H.F. resistance of wires, transmission lines, coils and for shielding effect of sheet metal.
42. R. C. Colwell and J. K. Stewart, "The Mathematical Theory of Vibrating Membranes and Plates," *J.A.S.A.*, 3, pp. 591–595 (1932)—Chladni figures for a square plate.
43. R. C. Colwell, "Nodal Lines in A Circular Membrane" *J.A.S.A.*, 6, p. 194 (1935)—Abstract.
44. R. C. Colwell, "The Vacuum Tube Oscillator for Membranes and Plates," *J.A.S.A.*, 7, pp. 228–230 (1936)—Photographs of Chladni figures on circular plates.
45. R. C. Colwell, A. W. Friend, J. K. Stewart, "The Vibrations of Symmetrical Plates and Membranes," *J.A.S.A.*, 10, pp. 68–73 (1938).
46. J. K. Stewart and R. C. Colwell, "The Calculation of Chladni Patterns," *J.A.S.A.*, 11, pp. 147–151 (1939).
47. R. C. Colwell, J. K. Stewart, H. D. Arnett, "Symmetrical Sand Figures on Circular Plates," *J.A.S.A.*, 12, pp. 260–265 (1940).
48. V. O. Knudsen, "Resonance in Small Rooms," *J.A.S.A.*, 4, pp. 20–37 (1932)—Experimental check on the values of the eigentones.
49. H. Cremer & L. Cremer, "The Theoretical Derivations of the Laws of Reverberation," *J.A.S.A.*, 9, pp. 356–357 (1938)—Abstract of Akustische Zeits., 2, pp. 225–241, 296–302 (1937)—Eigentones in a rectangular chamber.
50. H. E. Hartig and C. E. Swanson, "Transverse Acoustic Waves in Rigid Tubes," *Phys. Rev.*, 54, pp. 618–626 (1938)—Experimental verification of the presence of acoustic waves in a circular duct, corresponding to the *TE* and *TM* electromagnetic waves; shows an agreement between calculated and experimental values of the resonant frequencies, with errors of the order of $\pm$ 1%.
51. D. Riabouchinsky, *Comptes Rendus*, 207, pp. 695–698 (1938) and 269, pp. 664–666 (1939). Also in Science Abstracts A42, #364 (1939) and A43, #1236 (1940).—Treats of supersonic analogy of the electromagnetic field.
52. F. V. Hunt, "Investigation of Room Acoustics by Steady State Transmission Measurements," *J.A.S.A.*, 10, pp. 216–227 (1939).
53. R. Bolt, "Standing Waves in Small Models," *J.A.S.A.*, 10, p. 258 (1939).
54. L. Brillouin, "Acoustical Wave Propagation in Pipes," *J.A.S.A.*, 11, p. 10 (1939)—Analogy with *TE* waves.
55. P. E. Sabine, "Architectural Acoustics: Its Past and Its Possibilities," *J.A.S.A.*, 11 pp. 21–28, (1939).—Pages 26–28 give an illuminating review of the theoretical work in acoustics.
56. R. H. Bolt, "Normal Modes of Vibration in Room Acoustics: Angular Distribution Theory," *J.A.S.A.*, 11, pp. 74–79 (1939).—Eigentones in rectangular chamber.
57. R. H. Bolt, "Normal Modes of Vibration in Room Acoustics: Experimental Investigations in Non-rectangular Enclosures," *J.A.S.A.*, 11, pp. 184–197 (1939).
58. L. Brillouin, "Le Tuyau Acoustique comme Filtre Passe-Haut," *Rev. D'Acous.*, 8, pp. 1–11 (1939).—A comparison with *TM* waves; some historical notes, tracing the inception of the theory back to 1849.
59. E. Skudrzyk, "The Normal Modes of Vibration of Rooms with Non-Planar Walls," *J.A.S.A.*, 11, pp. 364–365 (1940).—Abstract of Akustische Zeits., 4, p. 172 (1939).—Considers the equivalent of the *TM* OOp mode.
60. G. M. Roe, "Frequency Distribution of Normal Modes," *J.A.S.A.*, 13, pp. 1–7 (1941).—A verification of Maa's result for a rectangular room, and an extension to the cylinder, sphere and several derived shapes, which leads to the result that the number of normal modes (acoustic) below a given frequency is the same for all shapes.

Digitized by Google
Original from UNIVERSITY OF MICHIGAN
Generated on 2019-09-24 07:43 GMT / http://hdl.handle.net/2027/mdp.39015077775156
Public Domain, Google-digitized / http://www.hathitrust.org/access_use#pd-google

61. R. S. Bolt, H. Feshbach, A. M. Clogston, "Perturbation of Sound Waves in Irregular Rooms," *J.A.S.A.*, 14, pp. 65–73 (1942)—Experimental check of eigentones in a trapezoid vs calculated values.

ABSTRACTS OF FOREIGN LANGUAGE ARTICLES IN WIRELESS ENGINEER

62. H. Gemperlein, "Measurements on Acoustic Resonators," 16, p. 200, No. 1504 (1939).
63. M. Jouguet, "Natural Electromagnetic Oscillations of a Cavity," 16, p. 511, No. 3873, (1939).
64. M. S. Neiman, "Convex Endovibrators," 17, p. 65, No. 455, (1940).
65. F. Borgnis, "The Fundamental Electric Oscillations of Cylindrical Cavities," 17, p. 112, No. 905, (1940). See also Sci. Abs., B43, No. 343 (1940).
66. H. Buchholz, "Ultra-Short Waves in Concentric Cables, and the "Hollow-Space" Resonators in the Form of a Cylinder with Perforated-Disc Ends," 17, p. 166, No. 1301 (1940).
67. J. Müller, "Investigation of Electromagnetic Hollow Spaces," 17, p. 172, No. 1379 (1940).—Sci. Abs., B43, No. 857 (1940).
68. V. I. Bunimovich, "An Oscillating System with Small Losses," 17, p. 173, No. 1380 (1940).
69. M. S. Neiman, "Convex Endovibrators," 17, p. 218, No. 1743 (1940).
70. M. S. Neiman, "Toroidal Endovibrators," 17, p. 218, No. 1744 (1940).
71. H. Buchholz, "The Movement of Electromagnetic Waves in a Cone-Shaped Horn," 17, p. 370, No. 3009 (1940).—Cavity formed by cone closed by spherical cap.
72. O. Schriever, "Physics and Technique of the Hollow-Space Conductor," 18, p. 18 No. 2, (1941).—Review of history.
73. F. Borgnis, "Electromagnetic Hollow-Space Resonators in Short-Wave Technique," 18, p. 25, No. 61, (1941).
74. T. G. Owe Berg, "Elementary Theory of the Spherical Cavity Resonator," 18, p. 287, No. 1843 (1941).
75. F. Borgnis, "A New Method for measuring the Electric Constants and Loss Factors of Insulating Materials in the Centimetric Wave Band," 18, p. 514, No. 3435 (1941).—An application of the cylindrical cavity resonator.
76. V. I. Bunimovich, "The Use of Rectangular Resonators in Ultra-High-Frequency Technique," 19, p. 28, No. 65 (1942). Use in 17 cm oscillator.
77. V. I. Bunimovich, "A Rectangular Resonator used as a Wavemeter for Decimetric and Centimetric Waves," 19, p. 37, No. 176 (1942).
78. M. Watanabe, "On the Eigenschwingungen of the Electromagnetic Hohlraum," 19, p. 166, No. 927 (1942).
79. F. Borgnis, "The Electrical Fundamental Oscillation of the Cylindrical Two-Layer Cavity," 19, p. 370, No. 2306 (1942). Considers cylindrical resonator with two concentric internal cylinders of different dielectric constant.
80. W. Ludenia, "The Excitation of Cavity Resonators by Saw-Tooth Oscillations," 19, p. 422–423, No. 2641 (1942).
81. Ya. L. Al'pert, "On the Propagation of Electromagnetic Waves in Tubes," 19, p. 520, No. 3181 (1942).—Calculation of losses in a cylindrical wave guide.
82. V. I. Bunimovich, "The Propagation of Electromagnetic Waves along Parallel Conducting Planes," 19, p. 520, No. 3182 (1942).—Equations for Z_0 and attenuation of rectangular wave guide, and resonant frequency and Q of rectangular cavity.
83. C. G. A. von Lindern & G. de Vries, "Resonators for Ultra-High Frequencies," 19, p. 524, No. 3206 (1942).—Discusses transition from solenoid to toroidal coil to "single turn" toroid, i.e., toroidal cavity resonator.

ABSTRACTS IN SCIENCE ABSTRACTS

84. L. Bouthillon, "Coordination of the Different Types of Oscillations," A39, No. 1773 (1936).—General theory of mechanical, acoustic, optical and electric oscillations.
85. Bürck, Kotowski, and Lichte, "Resonance Effects in Rooms, their Measurement and Stimulation," A39, No. 5226 (1936).
86. G. Jäger, "Resonances of Closed and Open Rooms, Streets and Squares," 40A, No 306 (1937).
87. K. W. Wagner, "Propagation of Sound in Buildings," A40, No. 2199(1937).—Transmission through a small hole in a wall.
88. M. Jouguet, "Natural Electromagnetic Oscillations of a Spherical Cavity," 42A, No. 3822 (1939).
89. H. R. L. Lamont, "Use of the Wave Guide for Measurement of Micro-wave Dielectric Constants," 43A, No. 2684 (1940).

Digitized by Google
Original from UNIVERSITY OF MICHIGAN
Generated on 2019-09-24 07:44 GMT / http://hdl.handle.net/2027/mdp.39015077775156
Public Domain, Google-digitized / http://www.hathitrust.org/access_use#pd-google

Index

Aamodt, T., 237
Absolute Sensitivity of Radio Receivers, The (ref.), 378
Absorbent, copper impregnated activated carbon, 275
Activity test on vacuum tubes, 755
Adams, N. I., (ref.), 95
Admittance, average electronic, definition of, 61
AGC (automatic gain control), 479–480
Ahearn, A. J., 236
Alekseieff, N. T., (ref.), 71
Allison, H. W., 236
Altio, C. J., 237
Amplification and band width, 743–750
Amplifier, direct coupled pulse, 13
Analysis of the Effects of Space Charge on Grip Impedance, (ref.), 750
Anderson, Captain A. Eugene, 352, 620
A New Type of High Power Tube, (ref.), 344
Antenna, action of, 791–792
  amplitude distribution, 794
  amplitude taper, effect on pattern, 783–784, **784**, **785**
  aperture dimensions, 793
  aperture in a plane and with arbitrary phase and amplitude, gain and effective area of, 779–780
  array factor, 789
  arrays, 789
  beam width vs. aperture, **12**
  characteristics, Mark 3 and 4, table, 38
  coma, 826
  cosecant, 813–817
  cosecant, based on the paraboloid, 814–816, **815**, **816**
  cosecant, cylindrical, 817
  CXAS, **15**
  cylindrical parabolic reflector, 15
  defocussing, 826
  dipole, microwave, **766**
  effective area, definition of, 769
  electromagnetic horn, **765**
Antenna—*Cont.*
  gain and effective area, relationship between, 770–772
  gain, definition of, 769
  gain vs. aperture, **12**
  Huygens source, 776–778, **777**
  ideal, diagram of, **778**
  ideal, gain and effective area of, 778–779
  lens, metal plate, 809–813
    configurations of, 812
    effective index of refraction vs. plate spacing in, **810**
    zoning in, 810–812
  lens tilting, effect on pattern, **813**
    advantages of, 813
  lenses, comparison of metal plate and dielectric types, **811**
    comparison of zoned and unzoned types, **811**
    tolerances in, 812–813
  lobe switching, 31
  loss due to phase variation in wave front, **795**
  Mark 3, **31**, **32**, **33**, **34**, **35**
  Mark 4 installation on U.S.S. Tennessee, **50**, **51**
  Mark 4, on gun director, **49**
  parabolic, 794–809
    amplitude control, 796–797
    apex matching plate for improving impedance properties of, **800**
    configuration, choice of, 797–801
    phase control, 794–796
    tolerances in, 807–809
  parabolic cylinders between parallel plates, 803–805, **804**, **805**
  parabolic cylinders, line sources for, 805–807
  parabolic cylinder with line feed, **797**
  parabolic section, offset, **799**
  paraboloid, dipole-fed, **766**
    feeds for, 801–802
    paraboloidal, features of, 798
  pattern, horizontal, **806**
    analysis, geometry of, **781**
    effect of shadow on, **800**

Digitized by Google
Original from UNIVERSITY OF MICHIGAN
Generated on 2019-09-24 07:44 GMT / http://hdl.handle.net/2027/mdp.39015077775156
Public Domain, Google-digitized / http://www.hathitrust.org/access_use#pd-google

Antenna, pattern—*Cont.*
in terms of antenna wave front, 781–782
phase control, 794
phase variation, cubic, effect on pattern, 787, **788**
linear, effect on pattern, 784–785
square law, effect on pattern, 785–787, **786**
radiation, free space, from small current element with no heat loss, **771**
radio circuit for free space, **770**
rectangular, ideal, pattern of, 782, **783**
reflector, effect of small inaccuracies in, **808**
symmetrically located section of, difficulties in use of, 798–801
reflector wings, 24
Mark 2 and 3, **36**
schematic, Mark 4, **50**
single, conditions for operation, 310
development of (England), 6
successful employment of, 6
size, 11
TE_{01} mode, 803
TEM mode, 803
transmission between two parallel plates, forms of, 803–804
wave front analysis, limitations, 789
wave fronts of an array of elements, **823**
Antenna, radar, construction, 790–827
airborne, 855–860
anti-aircraft 3-CM, 850, **851**
AN/APQ-7, for bombing through overcast, 858–860, **859**
AN/APS-4, 855–856, **856**
AN/TPS-1A portable search, 852–855, **854**
construction methods, classification of, 792
design formulation, basic, 793–794
electrical characteristics of various types, 829, 834, 836, 837, 838, 840, 852, 855, 856, 860
electrical principles, 767–790
lobe switching, 818–819, **818**
lobing, 817–818
conical, 819
Antenna, radar—*Cont.*
Mark 1, (FA), 840, **841**
Mark 3, (FC), 840, **842**
Mark 4, (FD), 840, **843**
Mark 16, 837–839
Mark 19, 845–848, **848**
Mark 27, 837, **838**
Mark 28, 848–849, **849**
military, developed by Bell Laboratories, 827–860
MUSA, 843
naval shipborne types, 829–850, **831**, **842**, **843**
nutation, 850
pattern, significance of, 780
polyrod array, 824–825, **824**
polyrod fire control, 843–844, **845**, **846**
receiving and transmitting, separate, 773
reradiation formula, 773
rocking-horse type, **821**
fire control, 844–845, **847**
scanning, rapid, 819–827
array, 821–825, **823**, **824**
mechanical, 820–821, **821**
optical, 825–827
shipborne, anti-aircraft fire control, 841–843, **844**
SCR-296 radio set, army, 840
SCR-520, 856–858, **857**
SCR-545 search and track, 850–852, **853**
SCR-717, 856–858
SCR-720, 856–858
SE, 829, **830**
SH, 837–839, **839**
SJ submarine type, 834–836, **836**
SJ tuned cavity switch, **835**
SF-1, 837, **838**
SL, 829–834, **831**, **832**, **833**
transmission formula, free space, 773
transmission line theory, importance of, 768
wave front analysis, 775–789
waveguide path for SL type, **833**
Army and Navy laboratories, 9
ATR (anti-T-R tube), 318–323, **322**
ATR box analysis of, 360–363

Generated on 2019-09-24 07:44 GMT / http://hdl.handle.net/2027/mdp.39015077775156
Public Domain, Google-digitized / http://www.hathitrust.org/access_use#pd-google
Digitized by Google
Original from UNIVERSITY OF MICHIGAN

ATR box—*Cont.*
constant power loss vs. transmitting branch impedance, **341**
low-level in-tune input impedance, 342
low-level loss component, 340–343
low level loss vs. magnetron impedance, **342**
recovery effect, **329**
Attentuation of Electromagnetic Fields in Pipes Smaller than Critical Size, (ref.), 908

Baker, D. I., 237
Band merit, 744
vs. grid-cathode spacing, **748**
vs. grid-screen spacing, 748
vs. plate-suppressor spacing, **749**
Band-pass interstage, **744**
Banos, Dr. Alfredo, 987
Barrow, W. L., (ref.), 908, 911, 919, 935, 1017
Barry, D. P., 237, 708
Batcher, R. R., (ref.), 908
Beam width, 11
Mark 3 and 4, table, 38
Beat oscillator tube, desirable characteristics of, 391–392
Beating oscillator problem, 578–581
Beck, A. C., 860
Becker, A., (ref.), 910, 935
Bennett, W. R., 269
Beringer, R., (ref.), 730
Bessel Function for Engineers, (ref.), 1018
Bessel functions of the first kind, tables of, 981–984
Best, F. H., 237, 708
Bethe, H. A., (ref.), 935
Black, K. C., (ref.), 740
Blazier, C., 237
Blocking oscillator pulse generator, **449**
Bolt, R. H., (ref.), 986, 1017
Boone, E. M., 708
Borgnis, F., (ref.), 1006, 1018
Bowen, D. B., 236
Bowen, Dr. E. G., 5
Bozorth, R. M., 269
Brainerd, J. G., (ref.), 95, 715, 908
Bridge, phase measuring, patent, (ref.), 42
Brillouin, L., (ref.), 998, 1017
Brooklyn Navy Yard, 26
Budenbom, H. T., 829
Buncher and catcher, 61
Bureau of Ordnance, 4

Cadmus, K., 708
Cahoon, B. B., 236
Calbick, C. J., 236
Carson, J. R., (ref.), 1017
Causes for the Increase of the Admittance of Modern High Frequency Amplifier Tubes, (ref.), 751
Cavity, external, tuned with piston, method of applying, **583**
Cavity, narrow tuning range, for W. E. 707A, **585**
Chu, L. J., (ref.), 908, 935, 998, 1017
Cioffi, P. P., 237
Circuit, piston-tuned, for W. E. 707A, (1150–3750 MC), **584**
Clark, J. E., 237
Clark, J. W., (ref.), 45
Class A sweep, 19
application of, 39
Cleeton, C. E., (ref.), 70
Cockcroft, Professor J. D., 5
Colton, R., (ref.), 256
Communication Networks, (ref.), 95
Communication Networks, vol. II, (ref.), 126
Computers, use of, 27
Considerations in the Design of Centimeter-Wave Radar Receivers, (ref.), 477
Considerations in the design of a Radar IF Amplifier, (ref.), 406
Control and indicator, Mark 2-4, **28**
Coomes, E. A., (ref.), 256
Cornu's Spiral, 786
Corona points on rotary gap, **274**
Coulton, Maj. Gen. Roger B., (ref.), 9
Coupling, broad band, for connecting W. E. 2K25 to wave guide, **601**
Coupling window, **317**
Crandell, C. F., 352
Crane, R. E., 852
Crawford, A. B., 353

Digitized by Google
Original from UNIVERSITY OF MICHIGAN
Generated on 2019-09-24 07:44 GMT / http://hdl.handle.net/2027/mdp.39015077775156
Public Domain, Google-digitized / http://www.hathitrust.org/access_use#pd-google

Crawford, H. T., (ref.), 908
Crump, E. E., (ref.), 265
Crystal rectifier, definition of, 710
ceramic cartridge structure and parts, **719**
ceramic cartridge type, development of, 717–721
conversion loss, 724
converter, **726**, **727**, **728**
equivalent circuit of, **732**
improvement in, effect of, 735, **736**, **737**
inserts and contact points used in early 3,000-MC converters, **713**
insulator, threaded, manufacturing difficulties, 722
iron pyrites, d-c characteristics of, **716**
modern processes, 731–739
mounting block for, early type, **715**
noise ratio, 724
performance specifications, table of, 725
performance tests for, 729–730
shielded structure and parts, **723**
shielded structure, development of, 722–724
silicon, development of, **386**
ceramic cartridge, shelf aging data, 721
ceramic cartridge, standard tests for, 721
conversion loss vs. spring deflection, **734**
d-c characteristics of, **716**
d-c rectification characteristics, improvement of, **736**
evolution of, **738**
power handling ability, measurement of, 734
power handling ability vs. contact area, **735**
P-type, d-c characteristics at various temperatures, **731**
relative annual production of, **738**
voltage-current characteristics, **384**
type 1N21, 711, 725
type 1N21A, 725
type 1N21B, 725
type 1N23, 725
Crystal rectifier—*Cont.*
type 1N23A, 725
type 1N23B, 725
type 1N25, 725
type 1N26, 723, 725
type 1N27, 725
type 1N28, 725
type 1N31, 725
types (1934–1943), **712**
use in early microwave research, 711–716
Curtis, H. E., (ref.), 908
Cutler, C. C., (ref.), 797
Cutler feed, 802, **803**
Cut-off relation between critical anode potential and magnetic field, 65
CXAS radar, 15–26
antenna, **15**
antenna schematic, **17**
characteristics of, table, 25
dipoles, **16**
high voltage rectifier, **24**
indicator desk, **18**
main unit, **20**
modulation or pulse generator, **21**
power control panel, **23**
range mark system, **19**
receiver, **22**
rotary joint and transmission line fittings, **17**
transmitter, **23**

Data transmitters, synchro, use of, 27
Dbm, 870
Depew, C., 309
Die konzentriche Leitung als Resonator, (ref.), 1018
Dielectric Constants and Power Factors at Centimeter Wave Lengths, (ref.), 715
Dillinger, J. R., (ref.), 290
Diode circuit, with negligible circuit impedance, **754**
Dipoles, half-wavelength, 15
CXAS, **16**
Discontinuities in Transmission Lines, Equivalent Circuits for, (ref.), 656
Distribution of Eigentones in a Rectangular Chamber at Low-Frequency Range, (ref.), 1017

Digitized by Google
Original from UNIVERSITY OF MICHIGAN
Generated on 2019-09-24 07:44 GMT / http://hdl.handle.net/2027/mdp.39015077775156
Public Domain, Google-digitized / http://www.hathitrust.org/access_use#pd-google

Doherty, W. H., 269
Dow, W. G., (ref.), 745
Downing, H. L., 255
Dreschler, F. P., 708
"Duo-tone" nonlinear circuit arrangement, 422
Duplex tubes, cavity type, (English), 311
Duplexing technique, 13, 21, 45

Eberhardt, G. M., 353
Echo box designs, working Q's of, 923
Edson, W. A., (ref.), 95, 751, 935, 985, 994, 1017
Edwards, C. F., (ref.), 387, 727
Ekstrand, S. O., 708
Electrical Resonator, A Type of, (ref.), 1017
Electromagnetic Theory, (ref.), 1018
Electromagnetic wave, plane, linearly polarized, 774, **775**
Electromagnetic Waves, (ref.), 95, 656, 768, 908
Electromagnetic Waves in Elliptic Hollow Pipes of Metal, (ref.), 935, 1017
Electron, cycloidal path of, **63**
  cyclotron frequency of, 63
  induction by the space charge cloud, 83
  lines of electric force on, **82**
  mean angular velocity of, 85
  motion, perturbation of, 93
    in electric and magnetic fields, 62
    in crossed electric and magnetic fields, equations of, 64
  moving in a magnetic field, force on, 62
  orbits for negative resistance oscillator, **68**
  orbit in cyclotron frequency oscillator, **69**, **70**
  orbit of, gaining energy from RF field in a type III magnetron oscillator, **80**
    leaving cathode in different phases, **84**
    losing energy to RF field in a Type III magnetron oscillator, **80**
    which transfer energy to RF field, **89**
Electron—*Cont.*
  paths in a cylindrical DC magnetron, 65
  phase focusing, 81
  "reverse" mode, 76
  space charge configurations, 82
Electronic admittance, 495–498
Ellipse, the, 998–999, **999**
  average diameter of, 999
  eccentricity of, 998
  ellipticity of, 998
Elliptic Cylinder and Spheroidal Wave Functions, (ref.), 1017
Elliptic coordinates and functions, 999–1000, **1000**
  cylinder fields, 1002
  cylinder functions, radial, root values of, 1003–1004
Emission, "enhanced" primary, 146
End sparking tube, 282, **284**, **286**
  life vs. peak current and gap spacing, **287**
Englund, C. R. (ref.), 715, 908
Equivalent circuits, use of, 61
Everhart, E., 236

FA Radio Ranging Equipment, 26
Feldman, C. B. H., 860
Ferris, W. R., (ref.), 756
Field, L. M., 236, 237
Fields and Waves in Modern Radio, (ref.), 656
Fire control, definition of, 10
  program, ship radar, 4
Fisk, Dr. J. B. (ref.), 5, 43
Fluctuations Induced in Vacuum Tube Grids at High Frequencies, (ref.), 756
Fluctuations in Space-Charge-Limited Currents at Moderately High Frequencies, (ref.), 754
Force on electron moving in a magnetic field, 62
Formulas for the Skin Effect, (ref.), 935
Fourier transform, 142
Fowler, Professor R. H., 5
Fox, A. G., 860
Fracassi, R. D., 236

Digitized by Google
Original from UNIVERSITY OF MICHIGAN
Generated on 2019-09-24 07:45 GMT / http://hdl.handle.net/2027/mdp.39015077775156
Public Domain, Google-digitized / http://www.hathitrust.org/access_use#pd-google

Frequency Distribution of Eigentones in a Three-Dimensional Continuum, (ref.), 1017
Frequency range, 40 megacycles, 24
200 megacycles, 3
500–700 megacycles, 3, 13
1000 megacycles, 7
3000 megacycles, 5, 43
Fresnel's Integrals, 786
Friis, H. T., (ref.), 378, 599, 727, 753
Fundamentals of Engineering Electronics, (ref.), 745

Gaps, spark, rotary, fixed, sealed, 6
Gas Discharge Transmit-Receive Switch, the, (ref.), 45
Given, F. J., 269
Glass, M. S., 236
Gormley, R. S., 708
Goucher, F. S., (ref.), 290
Graphical Methods for Analysis of Velocity Modulation Bunching, (ref.), 508
Green, E. I., (ref.), 908
Grid, ideal, 750
Grid keyed oscillators, 13
Griest, R. H., 237
Gucker, G. B., 708
Guillemin, E. A., (ref.), 95, 126

Habann, (ref.), 67
Hagstrum, H. G., (ref.), 43
Hale, D. A. S., 237
Hall, N. L., 275
Hansen, R. K., 236
Hansen, W. W., (ref.), 1017
Hanson, R., 708
Harris, W. A., (ref.), 754
Harrison, A. E., (ref.), 508
Hartman, P. L., (ref.), 43
Hartree, (ref.), 86
Hartree harmonics, 78, 79, 104
Hartree line, 86
Haynes, J. R., (ref.), 290
Hebenstreit, W. B., 236, 237
Hedberg, C. A., 708
Henderson, F. B., 237
Herriger, (ref.), 67, 71
Hertz, 764
Higgins, W. H. C., 840
High Power Series Gaps Having Sintered Iron Sponge-Mercury Cathode, (ref.), 290
Hill, Dr. A. G., 352, 709
Hobart, G., 709
Hochfrequenztech. u. Elektroak., (ref.), 973
Hold in characteristics of AFC circuit, 476–477
Hopper, Andrew L., (ref.), 406
Hubbing technique, 224
Hull, A. W., (ref.), 62, 67
Hulster, F., (ref.), 67, 71
Hussey, L. W., 269
Hutchinson, F., 236
Hutner, (ref.), 1017
Hyper and Ultra-High Frequency Engineering, (ref.), 95, 751, 935, 1017
Hyper-Frequency Wave Guides—General Considerations and Experimental Results, (ref.), 935, 1017
Hyper-Frequency Wave Guides—Mathematical Theory, (ref.), 1017

IF amplifier, 60-megacycle, 743
IF amplifier, fixed tuning considerations, 760–761
Impedance Functions in Terms of Resonant Frequencies, Representation of, (ref.), 652
Impedance Transmission Line Calculator, (ref.), 908
Ingram, Dr. S. B., 309
Input conductance of tubes, 750–752
average, vs. frequency for six 6AK5 tubes, 752
of tetrode or pentode, approximate expression for, 751
Interferenzrohren fur electrische Wellen, (ref.), 935
Interstage band width and over-all gain of multistage IF amplifiers, 411
Introduction to Modern Physics, (ref.), 935

Jahnke-Emde, Funktionentafalen, (ref.), 674, 1018
Jamieson, H. W., (ref.), 656

Digitized by Google
Original from UNIVERSITY OF MICHIGAN
Generated on 2019-09-24 07:45 GMT / http://hdl.handle.net/2027/mdp.39015077775156
Public Domain, Google-digitized / http://www.hathitrust.org/access_use#pd-google

Johnson, J. B., 237
Johnson noise, 378
Joint Board on Scientific Information, (ref.), 3
Julian, R. S., (ref.), 756

Kelly, M. J. 237
Kennard, E. H., (ref.), 935
Kersta, L. G., (ref.), 265
Kilgore, G. R., (ref.), 67
King, A. P., (ref.), 715, 860
Knoop, W., 237
Kock, Dr. W. E., 600, 809
Koehler, G., (ref.), 95, 715, 908
Konig, H. (ref.), 935
Kovar cup, 195
Kuper, J. B. H., 709
Kusch, P., 708

Laico, J. P., 237
Larkey, Miss F. C., 943, 977, 1005
Laws of Similitude of the Electromagnetic Field, and Their Application tion to Cavity Resonators, The, (ref.), 935
Leibe, F. A., (ref.), 908
Leveridge, W. J., 237
Lighthouse Tube, The, (ref.), 908
Lindner, E. G., (ref.), 908
Line tuning section, 151
Little, J. B., 237
Llewellyn, 699
Lobe crossover, 38
Lobe switching, principle of, **36**
  antenna, 31
  capacitor, 37
  two plane, 48
Lobes, minor, 11
  side, unwanted, 11
Lobing antles, Mark 3 and 4, table, 38
Long line effect, 890
Ludi, F., (ref.), 110
Ludinegg, 975

Maa, Dah-You, (ref.), 986, 1017
MacColl, Dr. L. A., 689, 709
Maggs, C., 237, 708
Magic Tee, 389, 390
Magnetic Generation of a group of Harmonics, (ref.), 40, 257
Magnetron, equivalent circuit of, 124
  anode potential waves, π mode, **72**
  anode structure, multicavity, 102
  arcing during life, curves of, (725A), **235**
  British, general features of, 159
    reproduction of, 159
    10-cm. oscillator, 71
  cathode, 145, 231–236
    axial, construction, **222**
    end disks, 720A-E, **193**
    mesh, 196
    molybdenum, 218
    oxide coated, use of, 147
    requirements for, 147
    sintered nickel matrix type, 218
    structure of, 4J50, 4J52, and 4J78, 217
    structures, **232**
    surface, back bombardment of, 146
    tungsten, 225
    voltage, DC, peak, measurement of, 148
  cavity, stabilizing, **228**
  centimeter wave, resonator blocks of, **154**
  characteristics and operating data, 3-cm., table, 202
    10-cm., table, 188
    20–45 cm., table, 163
  choke coupling, **167**
  circuit parameters, 128
  cold start, 230
  contour of constant frequency transform to contour of constant power (Rieke diagram), **129**
  criterion for bunching in proper phase, 75
  criterion for oscillation, 74
  current, DC, average, 149
    peak, measurement of, 149
  current pulses, shaped, **267**
  CVD Magnetron Reports (British), 58
  cylindrical D-C, (ref.), 62
  cylindrical DC, current vs. magnetic field, **66**
    electron orbits at different magnetic fields, **66**
  efficiency of operation, over-all, 151

Generated on 2019-09-24 07:45 GMT / http://hdl.handle.net/2027/mdp.39015077775156
Public Domain, Google-digitized / http://www.hathitrust.org/access_use#pd-google
Digitized by Google
Original from UNIVERSITY OF MICHIGAN

Magnetron—*Cont.*
electronic efficiency of, 89
vs. load conductance, **91**
electronic interaction at anode gaps, 71
electronic mechanism of, 71
electrons, mean angular velocity, 76
field configurations for the modes of, **107**
flashover, 173
frequency characteristics, **136**
frequency, effect of temperature of resonator block on, 140
electronic effects on, 140
"pushing", 141
stabilization, 134
frequency of oscillation, determination of, 151
frequency-sensitive loads, 134
halo type loop, 121, 200, **203**
interaction field, 77
iris, decoupling, circular, **228**
load frequency and phase, relation between, 135
load impedance, determination of, 151
magnetic circuit, 148
magnetic field, DC, measurement of, 148
measurements, 148
laboratory arrangement for, **150**
mode, failure, π, 182
frequencies, determination of, 152
frequency separation, 78
frequency vs. tuner position, 5J26, **185**
identification, 152
locking straps, 111
non-oscillating, arrangement of apparatus for measurements on, 151
impedance measurements, 152
resistance and reactance vs. frequency, **131**
oscillator, analogy to other oscillators, 59
Bell Laboratories work on, 153
centimeter wave, schematic diagram, **59**
cyclotron frequency, type II, 68
equivalent circuit of, **60**

Magnetron, oscillator—*Cont.*
equivalent RF circuit of, **125**
fixed frequency, **155**
general description, 58
negative resistance, type I, 67
RF circuits of, 94
10 cm., British, x-ray photograph of, **159**
traveling wave, type III, 70
type III, necessary conditions for oscillation, 85
tunable, **156**
oscillation during buildup, necessary condition for, **143**
output circuit, 121
coaxial, schematic duagram, **167**
coaxial wave guide junction, **201**
waveguide, **122**
output couplings, **122**
direct, 121
electrostatic, 121
magnetic, 121
output line, load admittance, 123
output power and frequency, dependence on load, 132
"packaged" types, 153, 158
3-cm, 207
performance chart, 87, 152, **173**
dynamic, **145**, 149
of 720A-E, **195**
of 725A and 730A, **205**
power, average input, 149
average output, measurement of, 149
peak input, 149
peak output, calculation of, 149
pulling figure *PF*, 132, 152
pulse duration, measurement of, 149
recurrence rate, measurement of, 149
pulse shapes, DC voltage, plots of, **142**
voltage and current, importance of, 149
pulsed, duty cycle, measurement of, 149
frequency spectrum of, 141, 152
oscillation buildup, **142**
pushing figure, 152
resonator block, 700 A-B, **154**

Digitized by Google
Original from UNIVERSITY OF MICHIGAN
Generated on 2019-09-24 07:46 GMT / http://hdl.handle.net/2027/mdp.39015077775156
Public Domain, Google-digitized / http://www.hathitrust.org/access_use#pd-google

Magnetron, resonator block—*Cont.*
706AY-GY, **154**
720A-E, **154**
725A, **154**
3J21, **154**
4J21-30, **154**
4J50, **154**
5J26, **154**
resonator, hole and slot type, 98
"serpentine", 110
simple single frequency, 94
slot type, 98
strip type, 98
cavities, **99**
"turbator", (ref.), 110
two-coupled, 100
vane type, 98
resonator systems, 100
asymmetries in strapping, effects of, 115
British strapping, 115
coupling loop, disturbance caused by, 104
higher order modes, 109
modes, 103
degeneracy of, 104
frequencies, separation of, 110
strongly-coupled, 109
wavelength vs. mode number, **118**
perturbation, effect of, 104
rising sun, 116, 228
strapping, 111
breaks, effect of, 115
change in frequency caused by, 114
schemes, diagram of, **112**
shielding, 115
tightness, 114
unstrapped, mode frequency distribution of, **113**
Rieke diagram, 127, 128, **129**, **130**
rising sun type, **117**
advantages and disadvantages, 119
electric field component independent of angle, **120**
resonator system, performance chart for, **93**
scaling, cathode problems, 146
theory of, 91
Magnetron—*Cont.*
standing wave component of anode potential wave, **73**
strapping, echelon, **170**
straps, double ring, recessed, **172**
transformer, quarter wavelength, **222**
traveling anode potential wave, **74**
traveling wave picture, 78
tuners, symmetrical, 175
tuning, 137
element, "cookie", 176
schemes, **138**
V-I plots, **145**
dynamic, 149
voltage overshoot, 193
waveguide output, 122
window construction, **222**
10-cm., with eight resonators, V-B plot for, **87**
V-I plot or performance chart for, **88**
characteristics of, 86
20–45 centimeters, 160
Magnetron as a Generator of Centimeter Waves, (ref.), 43
Magnetron Oscillations of Ultra Short Wavelengths, (ref.), 67
Maliaroff, D. E., (ref.), 71
Manley, J. M., (ref.), 40, 257, 269
Marblestone, Miss Z., 708
M. I. T. Radiation Laboratory Reports V-15-S, 43-22, 43-26, 43-27, and 43-30, (ref.), 935
Mathieu functions, 998
Matland, C. G., 708
Maxwell's equations, 91, 100, 775, 776
McArthur, E. D., 379, 908
McLachlan, N. W., (ref.), 1007, 1018
McMillan Jr., F. L., 327
McNally, J. O., 708, 871
McRae, Colonel J. W., 352
Meacham, L. A., patent, (ref.), 42
Mead, S. P., (ref.), 1017
Measuring angles, problem of, 31
Megaw, E. C. S., (ref.), 67, 68
Mendenhall, H. E., 708
Metal Horns as Directive Receivers of Ultra-Short Waves, (ref.), 715
Metal Lens Antennas, (ref.), 809
Microwave Converters, (ref.), 387, 727
Microwave Transmission, (ref.), 95, 908

Digitized by Google
Original from UNIVERSITY OF MICHIGAN
Generated on 2019-09-24 07:46 GMT / http://hdl.handle.net/2027/mdp.39015077775156
Public Domain, Google-digitized / http://www.hathitrust.org/access_use#pd-google

Microwave Transmission Data, Sperry Gyroscope Company, (ref.), 656
Mieher, W. W., (ref.), 911, 919, 935, 1017
Miller, J. A., 237
Miller, Stewart E., (ref.), 406, 477, 756
Mindlin, Professor R. D., 709
Modulator, circuit, line, with fixed gap switch, **277**, **278**
with rotary spark gap switch, **272**
line type, 270
switch, fixed gap, 275–308
hydrogen-argon aluminum cathode gap, 279–287, **280**, **281**
Molybdenum permalloy tape, 258, **259**
Moore, G. E., 236, 237
Morrison, J. F., 856, 858
Morse, (ref.), 1017
Mueller, G. E., 860
Mumford, W. W., (ref.), 45, 908

N. D. R. C., group, 5
National Defense Research Committee, 3
Natural Oscillations of Electrical Cavity Resonators, (ref.), 919, 935, 1017
Naval Research Laboratory, 3, 10, 13
Negative Grid Triode Oscillator and Amplifier for Ultra High Frequencies, (ref.), 13
Neher, Dr., H. V., 625, 709
Nimmcke, F. E., 845
Noise, 752–756
"Noise figure," of a network, 378, 753
for point-contact silicon crystal rectifier and GL2C40, **380**
vs. signal source impedance, **406**
Noise Figures of Radio Receivers, (ref.) 378, 727, 753
Non-linear coil, 5, 6
pulse generator, 40
structures, 258–259, **259**
Nordsieck, A. T., 236, 237
North, D. O., (ref.), 378, 750, 754, 756

Okabe, K., (ref.), 67, 69
Operation of Sintered Iron Sponge-Mercury Cathode Type Series Gaps at S. C. I., A. E. W., and 5 Microsecond Conditions, (ref.), 290
Optical range finder, limitations of, 11
Optics and radar, coordination of, 27
Oscillators, grid keyed, 13
Output voltage vs. frequency characteristic, AFC circuit, **476**

Page, L., (ref.), 95
Page, Dr. R. M., 10, 311
Parabola, **796**
Parabolic Antenna Design for Microwaves, (ref.), 797
Passage of Electric Waves Thru Tubes or the Vibration of Dielectric Cylinders, On the, (ref.), 935
Pedestal pulse, 42
Pentode circuit, with impedance in grid circuit, **754**
with negligible circuit impedance, **754**
Permendur, 217
Petersen, E., (ref.), 40
Peterson, (ref.), 257
Peterson, E. F., (ref.), 379
Peterson, E. F., (ref.), 908
Petrie, D. P. R., (ref.), 659
Phase measuring bridge, patent, (ref.), 42
Phillips, R. J., 829, 837
Pierce, J. R., 237, 756, 871, 908
Poisoning of Oxide Cathodes, The, (ref.), 256
Posthumus, K., (ref.), 67, 70, 86, 230
Potter, J. G., 236
Preplumbing, 167
Principles of Electricity, (ref.), 95
Proportioning of Shielded Circuits, The, (ref.), 908
PSWR, 890
Pull in range of AFC circuit, 476–477
Pulse, generating methods, 5
envelope, rectangular, amplitude-time and energy-frequency relationships, **402**
generator, non-linear coil, 40
modulating, and amplitude-frequency distribution in transmitted RF pulse, **741**
shaping, 266–268
sweep trigger, 42
widths, 6
Pulse modulator, circuits, **240**
design considerations, 239–241
tube requirements, 238–239

Digitized by Google
Original from UNIVERSITY OF MICHIGAN
Generated on 2019-09-24 07:46 GMT / http://hdl.handle.net/2027/mdp.39015077775156
Public Domain, Google-digitized / http://www.hathitrust.org/access_use#pd-google

Pulse modulator—*Cont.*
tubes, 238–256
cathode emission, 255
cathode sparking, 254–255
current and voltage relationships, **239**
grid emission, primary, 255
Pulsed-power generation, British, 5
Pulsed Properties of Oxide Cathodes, The, (ref.), 256
Pulser, box, 268
load circuit, 264–265
low level, 259–261
low level coil, circuit, **260**
magnetic bias, 265
power, 261–264,
circuit diagram of, **262**
power, network, **268**
transformer coupling, 265
Pulsing rates, 6
Purinton, R. M., 353

Radar—A Report of Science at War (ref.), 3
Radar, airborne, ASH, 301 airborne,
airborne, AN/APS-4, 301
army, SCR268, 238
costs, 2
diagram of, **863**
level difference, 867
military application, England, 10
Germany, 10
Japan, 10
operation of, 862
over-all performance, 867
prewar development, 2
range capability, 867–869
range, effect of reduction in system performance on, **868**
RF oscillators, 871
system performance, 867
tests, types of, 862–863
Radar equipment, AN/APQ-5, **443**, **483**
AN/APQ-7, 414, **415**, **442**, 477–479, **478**, **479**, **483**
AN/APQ-13, 414, **415**, **442**, **726**
AN/APS-4, **369**, **397**, **400**, **401**, 417 **418**, 477
AN/TRC-639-648
CXAS, 13
FD (Mark 4), 48
Radar—*Cont.*
indicator viewing and photographic attachment, **442**
Mark 1, 3, 4, 13, 26
Mark 2, 26
Mark 3, 3, 4, 9, 27, 46
main unit on U. S. S. New Jersey, **52**
receiver with improved r-f amplifier, **47**
Mark 4, 3, 4, 9, 48
application and use of, 52
main unit on U. S. S. New Jersey, **52**
trainer and pointer operator's position on U. S. S. Barton, **54**
on U. S. S. Saratoga, **53**
Mark 20, **367**
receiver protection, 324–325
receiver self-protection, 332–333
SCR-545, 316, **317**
SH Naval fire control, **444**
SJ submarine radar, **368**
SL, **321**
SL-Naval Search Radar, **464**
Radar in the U. S. Army, (ref.), 9, 256
Radar receiver, function of, 366–368
AFC (automatic frequency control), 470–479, **474**, **478**, **479**
circuit design, 474–479
operation of, **476**
A-type display, 429
B-type display, 431, 443
C-type display, 431
GPI type display, 429
J-type display, 430
K-type display, 430
MS-type display, 432
PPI type display, 429
bearing marker circuits, electronic, 460–462, **461**
beat oscillator, 391–395, **392**
"blooming", 422
cathode-ray tube, 432–437
magnetic focus and deflection coil designs, **437**, **439**
electrostatic deflection type, **433**
fluorescent screen characteristics, 435
magnetic deflection type, **434**
permanent magnet focusing, **440**

Digitized by Google
Original from UNIVERSITY OF MICHIGAN
Generated on 2019-09-24 07:46 GMT / http://hdl.handle.net/2027/mdp.39015077775156
Public Domain, Google-digitized / http://www.hathitrust.org/access_use#pd-google

Radar receiver—*Cont.*
cavity structures, **398**
composition of, 373–376
converter, 382–391, **383**, **401**
and IF preamplifier (10,000 MC), **400**, **415**
balanced, **390**
crystal, (3000 MC), **387**, **388**
(10,000 MC), **389**
vacuum tube, (1000 MC), **385**
display types, classification of, 427–432
display types, military, **428**
IF amplifier, 401–419
band width, 401–403
component designs, 413–419
equipment designs, 416, 417, 418
equivalent input circuit, **406**
gain characteristics, 403–404
input circuit design, 405
intermediate midband frequency, 404
interstage circuits, **410**
interstage circuit design, 409–413
second detector, 405
second detector design, 413
tubes, characteristics of, 408
IF preamplifier, **415**
indicator, 427
input circuit, 376–400
designs, 395–400, **397**, **399**
input noise considerations, 377–379
input signal, characteristics of, 368–371, 377
liquid delay tank variable range unit, 465–467, **465**, **466**
magnetic deflection structures, voltage-current-time relationships, **456**
military, principal components of, **374**
multivibrator, 446–449
circuits, basic, **447**
Eccles-Jordan, 446
one-shot type, 447
free-running type, 448
output character, 371–373
output power, and frequency deviation vs. repeller voltage for 2K25 reflex oscillator, **396**
modes vs. repeller voltage for 2K25 reflex oscillator, **395**
pedestal generator, 461
Radar receiver—*Cont.*
phase shifter precision variable range unit, 467–470, **471**, **468**
condenser, **470**
timing wave generator circuit of, **469**
power supplies, 480–487, **482**, **483**, **486**
primary power sources, 480–481
Radio frequency amplifier design, (1000 MC), 379–382, **382**
range and bearing measurements, circuits for, 459–470
range marker circuits, 462–463
fixed, **462**
variable, **463**
range sweep stop pulser circuit, **459**
reflex oscillator, velocity modulated, 393–395, **394**
sweep amplifier, 454–459, **455**, **458**
sweep circuit, 443–459
functions, 445
start-stop type, 451
sweep generator circuits, **452**
sweep wave form, hyperbolic, development of, **453**
generation of, **454**
improving linearity of, **452**
timing wave, circuits, 449–451, **450**
form generator, 446
transformers, power, **485**
transmitter-indicator assembly, **464**
video amplifier, 419–427
circuits, 425–427, **426**
d-c restoration methods, 423–425
d-c restorer circuits, **424**
gain - frequency considerations, 419–421
gain - amplitude considerations, 421–423
gain vs. frequency, **420**
video frequency transformers, **426**
Radar systems, military, classification of, 365–366
Radiation Laboratory, N. D. R. C., 8
M. I. T., 3
Radiation Laboratory Report No. 61-15, (ref.), 730
Radio Engineer's Handbook, (ref.), 768
Rajchman, J. A., (ref.), 592

Digitized by Google
Original from UNIVERSITY OF MICHIGAN
Generated on 2019-09-24 07:46 GMT / http://hdl.handle.net/2027/mdp.39015077775156
Public Domain, Google-digitized / http://www.hathitrust.org/access_use#pd-google

Ramo, S., (ref.), 656
Range mark system, CXAS, **19**
Range, measuring system, Mark 3 and 4, **41**
measurement, methods of, 39
"notch", 39
operator's position, Mark 3, **29**
presentation, Mark 3 and 4, **40**
readings, accuracy, 19
tracking, 39
unit, Mark 2-4, **29**
Rayleigh, Lord, (ref.), 910, 935
Receiver, CXAS, **22**
Recent Researches in Electricity and Magnetism, Notes on, (ref.), 935
Rectifier, high voltage, CXAS, **24**
silicon-crystal point-contact, 7
Reflection coefficient, and SWR, relations between, **891**
definition of, 890
Reflection, surface, effect of on elevation beam, **25**
Reflector, cylindrical parabolic, 15
minimizing wind resistance of, 15
Reflex Oscillators, (ref.), 908
3-cm., with internal resonator, (2K-25), **589**
admittance plots for resonators coupled to various loads, **553, 554, 557, 558, 559, 560**
analysis, effect of approximations on, 507–508
beating oscillator noise, elimination of, 573
broad-band, 598–605
bunching, approximate treatment of, 667–671, **668, 671**
cavity, with grids and loop coupling to a coaxial line, **651**
without grids with iris coupling to a wave guide, **651**
characteristics, broad band, for W. E. 2K25 coupled into matched load, **605**
conductance, and susceptance of terminating admittance of a short line, **563**
electronic, susceptance components of, vs. amplitude of oscillation, **538**
Reflex Oscillators, electronic—*Cont.*
vs. amplitude of oscillation, general case, **525, 528, 529, 534, 535, 537**
vs. amplitude of oscillation, resulting in hysteresis, **526**
giving power flow from the circuit to the electron stream for a single gap, 696–700
optimum, vs. resonator loss, **681**
total circuit, optimum vs. resonator loss, **681**
cycling time vs. temperature of channel at band frequency limit requiring smaller tuner power, **619**
design objectives, mechanical, 587–588
development of, at Bell Laboratories, 578–650
drift angle, as a function of frequency and voltage, 671–672
for extinction, phase of, vs. ratio of resonator loss to small signal electronic admittance, **520**
drift field, ideal, 688–691
special, 508–510
drift time, ideal variation of, in repeller region with resonator gap voltage, **689**
efficiency, effect of losses on, 501
factor vs. ratio of resonator loss conductance to the small signal electronic admittance, **503**
of resonator, 501
maximum, for several repeller modes, **678**
parameter vs. ratio of load conductance to magnitude of small signal electronic admittance, **505**
vs. effective drift, **504**
vs. effective drift angle for several degrees of resonator loss, **682**
vs. parameter proportional to resonator loss for several repeller modes, **678, 683**
electrodes providing potential distribution resulting in maximum efficiency, **691**
electron current, RF, and RF power produced vs. RF RF gap voltage, **499**

Digitized by Google
Original from UNIVERSITY OF MICHIGAN
Generated on 2019-09-24 07:46 GMT / http://hdl.handle.net/2027/mdp.39015077775156
Public Domain, Google-digitized / http://www.hathitrust.org/access_use#pd-google

Reflex Oscillators—*Cont.*
electron optical system used in eliminating hysteresis, (W. E. 2K29), **593**
electronic admittance, non simple theory, 672–684
phase of, vs. bunching parameter for several repeller modes, **680**
relative amplitude of, vs. bunching parameter, **497**
relative, vs. bunching parameter for several repeller modes, **679**
electronic gap loading, 691–700
electronic tuning, effect of resonator loss on, **519**
equivalent circuit of, **523**
frequency, relative, functions of, and relative spacing vs. relative frequency, **566**
frequency vs. drift angle or repeller voltage and power vs. frequency, **517**
vs. gap displacement for W. E. 2K45, **615**
vs. grid voltage for W. E. 2K45, **624**
vs. tuner grid voltage for W. E. 2K50, **633**
gap, bunching in the, 700
loading, electronic, 510–512
factor for fine parallel grids vs. grid separation, **699**
vs. radius of tubes forming gap, **698**
voltage vs. time, **494**
grids, losses in, 701–702
hysteresis, electronic, 523
idealized, with grids, **492**
load conductance for optimum power, **506, 507**
half as great as that required to stop oscillation, **506**
load, effect of, 540–565
external, effect on performance, 503
frequency-sensitive, effect of, 551–559
plus loss conductance vs. bunching parameter X, **547**
lossless resonator plus line plus mismatched load, equivalent circuit of, **552**
Reflex Oscillators—*Cont.*
metal, continuously pumped, tuned with external line, **587**
millimeter range type, 631–635
modulation coefficient considerations, 657–667
effect of grid pitch and wire size on, 663–667, **665**
effect of slits and holes on, 661–663, **662, 663, 664**
for fine parallel grids, **660**
reciprocal of the square of, vs. gap transit angle, for case of fine parallel grids, **567**
modulator circuit for use with, **638**
motions of electrons in repeller space, **493**
noise, measure of, 572
production, mechanisms of, 571
sidebands, 570–573
operating conditions for 2K45, table, 623
operation in various repeller nodes and at various frequencies, (2K25), **604**
oscillation, build-up of, 573–579, **576, 577**
performance diagrams for W. E. 2K50, **627, 628, 629**
potential distribution in repeller region to give maximum efficiency, **690**
potential variation in the drift space, 684–687
power and electronic tuning, variation with frequency, 565–570
power and frequency variation with repeller voltage, ideal, **521**
with repeller voltage, with electronic hysteresis, **522**
power dissipated in resonator, 500
power flow from electron stream travelling through a longtitudinal field, 691–694
through a transverse field, 694–696
power-frequency characteristics for W. E. 2K25, **603**
power, normalized, vs. normalized load conductance, **549**
power output and electronic tuning vs. frequency for W. E. 2K29, **597**

Digitized by Google
Original from UNIVERSITY OF MICHIGAN
Generated on 2019-09-24 07:47 GMT / http://hdl.handle.net/2027/mdp.39015077775156
Public Domain, Google-digitized / http://www.hathitrust.org/access_use#pd-google

Reflex Oscillators—*Cont.*
power output characteristics of W. E. 2K50, **632**
power output of resonator, 501
power output, peak, vs. frequency for W. E. 2K23, **638**
peak, vs. frequency for 2K54 and 2K55 under varying load conditions, **641**
vs. parameter X, 525
vs. parameter X, with hysteresis, **527**
vs. repeller voltage, **528**, **529**
power produced by electron stream, 500
power vs. relative frequency, **569**
pulling figures for 2K54 and 2K55 vs. frequency, **645**
pulsed applications, 635–648
pulsed, exhibiting hysteresis, power output vs. repeller voltage, **646**
starting of, 702–705
repeller characteristic of 1349XQ and 2K29, **595**
of early model of, **531**
repeller design for eliminating hysteresis, **594**
repeller voltage vs. optimum power for W. E. 2K45, **622**
resonator, fundamental considerations on, 650–657
having 3 modes of resonance, equivalent circuit for, **652**
simplified equivalent circuit of, **654**
slightly lossy, with low loss coup ling loop and load impedance, equivalent circuit for, **653**
resonator loss, ratio of, to small signal electronic admittance vs. relative frequency, **568**
Rieke diagram for, under various operating conditions, **542**, **544**, **545**, **550**, **551**, **552**
susceptance vs. conductance, **496**, **514**
thermal tuner, conduction cooling of, 707–708
positiveness of action, 607–611
speed of, 611
radiation cooling of, 705–707
time for temperature rise and fall between two given values when cooled by radiation alone, **614**
Reflex Oscillators—*Cont.*
thermally-tuned, 605–624
AFC circuits for, 612–613
design considerations, 613–620
ideal deflection-temperature characteristic, **616**
W. E. 2K45 deflection-temperature characteristics, **617**
tuner, W. E. 2K45, anode temperature vs. anode power, **618**
tuning, electronic, 512–520
effect of resonant loads on, **561**
effect of short mismatched lines on, 559–565, **564**
to extinction vs. loading parameter, **518**
to half power vs. loading parameter, **518**
tuning mechanism, thermal, 606–607, **608**, **609**, **610**
tuning range, electronic, vs. relative frequency, **571**
tuning rates, instantaneous, computed, for W. E. 2K50, **632**
types developed at Bell Laboratories, including frequency ranges, chart of, **649**
waveguide output type, 625–631
Reich, H. J., (ref.), 95, 715, 908
Reiling, P. A., 269
Representation of Impedance Functions in Terms of Resonant Frequencies, (ref.), 353
Resonant cavities, back cavity effects, 931
coaxial, contour lines of special Q-factor for various modes:
TE 011, **1011**
TE 111, **1012**
TM 011, **1012**
TM 111, **1013**
coaxial, modes, normal, distribution of, 1007
root value plot for lower modes, **1008**, **1009**
couplings, 920–922, **921**, 932
cylindrical, circular, constants used in computing resonant frequencies of, 913
elliptic cylinder, the, 998–1006
end plate contour lines, 938–939

Digitized by Google
Original from UNIVERSITY OF MICHIGAN
Generated on 2019-09-24 07:47 GMT / http://hdl.handle.net/2027/mdp.39015077775156
Public Domain, Google-digitized / http://www.hathitrust.org/access_use#pd-google

Resonant cavities, cylindrical—*Cont.*
end plate current distributions, 940–941
end plate current distribution for various modes:
TE 01, **945**, **952**
TE 02, **950**, **952**
TE 03, **953**
TE 11, **944**, **953**, **964**
TE 12, **947**, **954**, **965**
TE 13, **954**, **966**
TE 21, **944**, **955**, **967**
TE 22, **949**, **955**, **968**
TE 23, **956**
TE 31, **946**, **956**, **969**
TE 32, **957**, **970**
TE 41, **947**
TE 51, **949**
TE 61, **951**
TM 01, **944**, **957**
TM 02, **948**, **958**
TM 03, **958**
TM 11, **945**, **959**, **971**
TM 12, **950**, **959**, **972**
TM 13, **948**, **960**
TM 21, **946**, **961**, **973**
TM 22, **961**, **974**
TM 31, **962**
TM 32, **963**
end plate current streamlines, 939–940
fin, metallic, thin, effect on E lines in TE 11n mode, **1014**
fins, 1013–1017
frequency range ratio for TE 01n mode when limited by mode crossings with TE 02n′ and TE 02 (n′ + 1) modes, maximum, **997**
frequency ratio, without interference from TE 01 (n + 1) mode, maximum value of, **997**
H vector at walls of, components of, 937
half cylinder, "TE 01n" mode in, **1014**
integration of a Bessel function divided by its derivative between the limits of zero and x, 975–984
Resonant cavities, cylindrical, end plate current streamlines—*Cont.*
tables of values, 978, 979, 980
minimum volume of for assigned Q, 988-995
mode chart showing types of interference with TE 01n mode, **996**
mode parameter for TE modes, 943
mode-shape factors vs. diameter to length ratio, TM modes, **915**
mode-shape factors vs. diameter to length ratio, TE modes, **916**, **917**
Q for elliptic cylinder resonator, 1004–1006
Q of TE 01n mode in cylinder with longitudinal fin, constants for, **1016**
relations between a function proportional to Q and a function proportional to volume of, **990**
resonances in, number of, approximation formula for, 986–988
side wall current distribution, 941–943
side wall current distribution for TE modes, diagram facing, **942**
tunable, limitation on frequency range of, as set by ambiguity, 995–998
values of Bessel function zero for the first 180 modes in, 919
cylindrical coaxial, full, 1006–1013
cylindrical, operating in the TE 01n modes, design chart for, **925**
cylinder tolerances, 931–932
dimensions of, finding, 923–924
drive mechanism, 932–933
formulas, 911–912
formulas, chart facing 911
formulas for, fields, resonant frequencies, and mode shape factors for rectangular prism, circular cylinder, and full coaxial, chart facing, **986**
gaps, end plate, 929–931
mode chart, 912–914, **912**

Digitized by Google
Original from UNIVERSITY OF MICHIGAN
Generated on 2019-09-24 07:53 GMT / http://hdl.handle.net/2027/mdp.39015077775156
Public Domain, Google-digitized / http://www.hathitrust.org/access_use#pd-google

Resonant cavities, mode chart—*Cont.*
expanded, covering operation area of a 9-KMC echo box, **925**
selection of operating area on, 924–926
showing meaning of crossing and interfering modes and of operating area, **918**
mode, extraneous or unwanted, 914–918
operating, choice of, 914
mode shape (MS) factor, 910–911
modes, 910
unwanted, methods of minimizing effects of, 918–920
plating, 932
Q's, relative, computed from resistivity of several metals, 923
Q required, theoretical, determination of, 922–923
similitude, application of, 933
principle of, 922
uniformity control and expected ringtime, 934
use of, for radar testing, 933–934
Resonant Lines in Radio Circuits, (ref.), 908
Resonators, linear array of, **102**
with distributed constants, 98
with lumped constants losses of, 96
Q-parameters of, 95
Resonators Suitable for Klystron Oscillators, On, (ref.), 1017
Richtmyer, F. K., (ref.), 935
Richtmyer, R. D., (ref.), 1017
Rideout, V. C., 353, 756
Rieke diagram, explanation of, 151
for pulsed reflex oscillator, effect of hysteresis on, **646**
for 2K25 with broad band coupling, **602**
for 2K54, **642**, **643**
for 2K55, **644**, **645**
Ring, D. H., 860
Robinson, A. L., 850
Ronci, V. L., 237, 708
Roschke, E. M., 269
Rothstein, J., (ref.), 256
Rudin, R., 236
Ryder, E. J., (ref.), 290
Ryder, R. M., 508, 708
Samuel, A. L., (ref.), 13, 45, 71, 620
Sarbacher, R. I., (ref.), 95, 751, 935, 985, 1017
Saw tooth sweep wave, 42
Schelkunoff, S. A., (ref.), 95, 353, 652, 656, 768, 789, 908
SCR-268 Radar, The, (ref.), 256
Schafer, J. P., 353
Schumacher, E. E., 269
Series branching circuits, 316–318, **317**, **319**
Sheperd, 871
Shockley, W., 258
Shunt branching circuit, 313–314, **314**
Side sparking tube, 286
life vs. peak current and gap spacing, **287**
Signal Corps, 39
Signal Corps Laboratories at Fort Monmouth, 9
Silicon-crystal point-contact rectifier, 7
Sintered iron sponge mercury cathode unit gap, **288**, **289**
Slater, J. C., (ref.), 86, 95, 236, 908
Slater line, 86
Smith, P. H., (ref.), 542, 908
Smith transmission line chart, **341**
Soderstrom, H. W., 237
Southworth, G. C., (ref.), 715, 909, 935, 1017
Spark gap, anode deposits, **283**, **286**
cathode loss vs. pulse duration, **285**
dissipation, 298–301
vs. pulse duration, **300**
calorimetric study of, 299
erosion problem, 275
corrosion problem, 275
fixed, dependability, 309
operating voltage range, 309
peak current, 308
peak power output, 308
pulse duration, 308
pulse repetition rate, 309
simplicity of manufacture, 309
switch voltage, 308
switching efficiency, 309
time jitter, 309
trigger requirements, 309
ratings, 308
maximum operating voltage vs. pulse repetition rate, **296**

Digitized by Google
Original from UNIVERSITY OF MICHIGAN
Generated on 2019-09-24 07:53 GMT / http://hdl.handle.net/2027/mdp.39015077775156
Public Domain, Google-digitized / http://www.hathitrust.org/access_use#pd-google

Spark gap—*Cont.*
mercury cathode, 287–290, 288
operating voltage, **291**
pulse characteristics, **297**
starting and operating charcteristics, 290–298
starting switch voltage, 293
starting voltage, 291
switching efficiency, 298–301
3-unit, operating voltage vs. time, **282**
voltage vs. time for starting and for operation at minimum switch voltage, **292**
for normal operating switch voltage and for operation at maximum switch voltage, **294**
Spark gaps in series, triggering, 276–279
Spectrum analyzer, 152
Standing wave detector, use of, 151
Standing wave introducers, 152
Steven Point and Minneapolis Linked by Coaxial System, (ref.), 740
Strachey, C., (ref.), 659
Stratton, 999
Stratton, J. A., (ref.), 1017, 1018
Stratton, W. D., 708
Strieby, M. E., (ref.), 740
Strutt, M. J. O., (ref.), 751
Stubner, F. W., 237
Sutton tube, 311
Sweep trigger pulse, 42
Sweep wave, saw tooth, 42
Switches, rotary spark gap, 271–275
experimental model, **273**
drawing of, **274**
SWR, definition of, 890
Synchro data transmitters, use of, 27

Tables of Functions, (ref.), 1018
Target angle sensitivity, 38
Taylor, Dr. A. Hoyt, 3, 10
Television Transmission Over Wire Lines, (ref.), 740
Terman, F. E., (ref.), 768, 908
Test equipment, application, generality of, 863–865
attenuators for microwaves, 899–901, **900**
BC910A oscilloscope, 903, **904**
BC1087A oscilloscope, 903
Test equipment—*Cont.*
broadbanding, 865
CW60AAY oscilloscopy (navy), 903
computer test sets, **906**, 907
directional coupler, errors in standing wave measurements caused by directivity of, **897**
for measuring standing waves, 894–899, **896**, **898**
dummy antenna, 899
early unit for 3,000-MC range, **864**
echo boxes, 883–888, **884**, **886**, **887**, **889**
Q and ringtime, relation between, 888
test on a radar, **928**
test sets, 926–929, **927**, **930**, **931**
tuned, **886**
environmental influences on, 865–866
frequency measurement, 875–881
frequency meters, 876
circuits, **880**
hybrid T for measuring standing waves, 894
IE30 test set, 875
IE57A army test set, 875, **874**
LZ navy test set, 875, **874**
magic T for measuring standing waves, 894
oscilloscopes, 902–905, **904**, **905**
packaging, 865
pads for microwaves, 901–902
portable units for airborne radar, **866**
power measurement, 881–883
precision of, 865
pulse, power measurement of, 881–882
range calibrators, 905–907, **906**
receiver sensitivity measurement, 870
requirements for, 862–867
RF cables and connectors, 902
RF load, 899, **900**
ring box, 883
ring time, 884
patterns on radar indicators, **885**, **929**
ruggedness of, 866–867
signal generators, 869–875, **872**, **874**
design principles, 871–873
pulsed and FM, 873–875
simplicity, reliability, and accessibility requirements, 866

Digitized by Google
Original from UNIVERSITY OF MICHIGAN
Generated on 2019-09-24 07:54 GMT / http://hdl.handle.net/2027/mdp.39015077775156
Public Domain, Google-digitized / http://www.hathitrust.org/access_use#pd-google

Test equipment—*Cont.*
slotted line for measuring standing waves, 891, **892**, **893**
spectrum analysis, 888–889, **889**
squeeze section for measuring standing waves, 891–894
standing wave measurements, 889–899
standing wave detectors used on coaxial and wave guide transmission lines, **893**
test signals, types of, 869–870
thermistor power meters, 882–883
TS-5/AP range calibrator, 907
TS-34/AP oscilloscope, 903, **905**
TS-34A/AP oscilloscope, 903, **904**, **905**
TS-35/AP test set, 875
TS-35A test set, 875, **874**
TS-35A/AP signal generator, **872**
TS-89/AP voltage divider for oscilloscope, 905
TS-102/AP range calibrator, **906**
TS-102A/AP range calibrator, **906**
TS-158/AP computer test set, **906**, 907
TS-235/UP RF load, 899, **900**
TS-239/UP oscilloscope, 903, **904**
TS-434/UP computer test set, **906**, 907
types, 862–863
water loads, 883
Test equipment, wavemeter, calibration of, 881
coaxial, 877, **876**
couplings, 879
cylindrical cavity, 877–878, **876**
detectors for, 879, **880**
drive and scale, 880–881
effect of temperature and humidity on, 881
frequency coverage, 879
linearity of, 878
methods of use, 880
QL required for different frequencies, 878
The Lighthouse Tube, (ref.), 379
Theoretical Study of Dielectric Cables, (ref.), 1017
Theory of the Electromagnetic Horn, (ref.), 908
Thermistor, 882
Thermistors in Electronic Circuits, (ref.), 908
Thompson, B. J., (ref.), 754
Thompson, J. J., (ref.), 910, 935
Tizard Mission, 5
TR boxes, 311
cavity parameters, relations between, table of, 358
copper-disc seal manufacturing and testing, 349–352, **350**, **351**
copper-to-glass disc seal, setup for, **348**
crystal gate, 327
design considerations, 343–345
direct coupling, 331–332
equivalent circuit including an ATR box, **361**
referred to the TR cavity, **355**
flat leakage power, 329–331
vs. gap length, 332
vs. gas pressure, **329**
"g" parameters, derived, 357
"g" parameters of windows, experimental determination of, 359–360
gas discharge parameter, 329
gas discharge power, 340
vs. low level loss adjustment, **325**
high-level, loss 333
operation, 356–357
idealized, analysis of, 383–359
igniter, the, 326
input standing wave ratio, 340
leakage power, 340
average, vs. average magnetron power, **362**
average, vs. pulse duration, **362**
average, vs. repetition rate, **361**
data, analysis of, 363
measurement, 333
pulse, shape of, **325**
vs. low level loss adjustment, **324**
vs. water vapor pressure, **331**
low-level loss, 337–340
transmission, 355–356
minimum leakage power vs. frequency, **330**
off-resonance analysis, 357–359
performance parameters, 323–324
recovery time, 333–337
recovery time characteristic, **334**, **335**

Digitized by Google
Original from UNIVERSITY OF MICHIGAN
Generated on 2019-09-24 07:54 GMT / http://hdl.handle.net/2027/mdp.39015077775156
Public Domain, Google-digitized / http://www.hathitrust.org/access_use#pd-google

TR boxes—*Cont.*
recovery time vs. ambient temperature, **337**
recovery time vs. life, **338**
recovery time vs. gas content, **338**
spike, the, 325–329, **325**
energy vs. gas pressure, **328**
vs. low level loss adjustment, **328**
vs. pulse repetition rate, **327**
temperature compensated discs, **347**
tube design, 345–349
turn on effect, 326
window width vs. window conductance, **360**
TR cavity, **317, 318, 320**
Train indicator, Mark 2-4, **30**
Train meter, zero center type, use of, 30
Transducer for adapting 2K23, 2K54 and 2K55 oscillators to a terminated wave guide load, **640**
for connecting output lead of 2K29 to 50-ohm cable, **596**
4-terminal, general, circuit representing all properties of, **656**
lossless, 124
Transmission Line Calculator, (ref.), 542
Transmission line, coaxial feed system, 15
duplexing, 24
gas-line system, 16
uniform, lossless, admittance of, 98
weatherproofing of, 16
Transmitter, CXAS, **23**
developments, magnetron, 43
Mark 3 and 4, **44**
Trigatrons (British), 279
Tube types, close spaced power tetrode, 4
doorknob, 13
Eimac 100-TH, 13
gas discharge, 6
gas discharge "T-R", 4
GL-466 (lighthouse tube), 46
GL-2C40, 379, **380, 381**
lighthouse, 7
magnetrons, 700 megacycle, 5
resonant-cavity magnetron, 4
Tube types—*Cont.*
single-cavity reflex oscillator, 7
vacuum, for ultra-short waves, **14**
700-type magnetron, **43**
1449, **649**
1464, **649**
316A (doorknob tube), 46
350A, 241
356A, 13
386A, 740–743, **742**
426XQ, development of, 253–254, **251**
characteristics of, **252–253**
table of ratings of, 244
700A-D, **162**
development of, 160–165
table of characteristics, 163
701-A, 44
development of, 241–244, **242**
characteristics of, **243**
table of ratings of, 244
702A-TR, **45**
702A, 311, **313**
706A-C, 184–187
table of characteristics, 188
707A, 581–585, **582, 583, 584, 585, 649**
709A, 311, **312, 313**
712A, 311
714A, 184–187
table of characteristics, 188
715A, **245**
characteristics of, **246–247**
development of, 244–249
table of ratings of, 244
717A, 414, 741, **742**, 745
characteristics of, 408
720A-E, **155, 157**
cathode, **232**
development of, 191–196, **192, 193**
performance chart of, **195**
table of characteristics, 188
721A, 313, **314, 321, 347**
723A/B, 586–591
724B, 313, **314, 322**
725A, **157, 201, 203**
cathode, **232, 234**
development of, 196–206
table of characteristics, 202
performance chart of, **205**

Digitized by Google
Original from UNIVERSITY OF MICHIGAN
Generated on 2019-09-24 07:54 GMT / http://hdl.handle.net/2027/mdp.39015077775156
Public Domain, Google-digitized / http://www.hathitrust.org/access_use#pd-google

Tube types—*Cont.*
726A, **649**
728A-J, **168**
development of, 165–168
table of characteristics, 163
703A, **204**
development of, 196–206
table of characteristics, 202
performance chart of, **205**
706AY-GY, **190**, **191**
cathode, **232**
development of, 187–191
table of characteristics, 188
714AY, 187–191
table of characteristics, 188
718AY-EY, 187–191
table of characteristics, 188
707B, **649**
715B, **248**
development of, 249–250
table of ratings of, 244
720B-D, 196
726B, **649**
726C, **649**
1349XQ, 521, 530
1464XQ, 631–635, **636**, **637**
1B22, **291**, **292**, **294**, **296**, **297**, **300**, 301–303, **302**
table of ratings, 308
1B23, 313, **314**, **319**, **320**
1B29, 303, **304**
table of ratings, 308
1B31, 304–305, **305**
table of ratings, 308
1B42, 305–307, **306**
table of ratings, 308
5D21, **249**, 265
development of, 250–253
current and voltage relations in, **250**
table of ratings of, 244
2J21, 197–201
2J48, 206–207
2J48–50, table of characteristics, 202
2J49, 206–207
2J50, 206–207
2J51, **208**, **209**
characteristics of, **212**
development of, 208–213, **208**, **209**

Tube types, 2J51—*Cont.*
2J51 magnetron, **156**
2J51, table of characteristics, 202
2J53/725A, 206–207
2J55, **207**
2J55-56, table of characteristics, 202
2J56, 207
3J21, cathode, **232**
3J21, **227**, **228**
development of, 223–231
characteristics of, 229
3J21 magnetron, **155**
3J30, 223
3J31, 223
4J21-25, performance chart of, **173**
4J21-25, table of characteristics, 163
4J21-30, **172**
cathode, **232**
development of, 169–174
magnetron, **155**
4J26-30, table of characteristics, 163
4J28, **171**
4J42, 176, **177**
magnetron, **156**
table of characteristics, 163
4J45-47, 196
table of characteristics, 188
4J50, 207, **220**
cathode, **232**
development of, 213–221
table of characteristics, 202
4J51, **156**
development of, 177, **178**
power output and mode frequency vs. tuner position, **180**
table of characteristics, 163
tuning member, **179**
4J52, **155**, 207, **221**, **222**
development of, 213–221
table of characteristics, 202
4J78, **220**
development of, 213–221
table of characteristics, 202
5J23, **170**
development of, 168–169
table of characteristics, 163
5J26, **156**
cathode, **232**
development of, 178–184, **181**, **182**, **185**

Digitized by Google
Original from UNIVERSITY OF MICHIGAN
Generated on 2019-09-24 07:54 GMT / http://hdl.handle.net/2027/mdp.39015077775156
Public Domain, Google-digitized / http://www.hathitrust.org/access_use#pd-google

Tube types—*Cont.*
2K22, **647**, **648**, **649**
2K23, 635–648, **638**, **640**, **649**
2K25, 393–395, **394**, **395**, **396**, 587–591, **589**, 598–605, **601**, **602**, **603**, **604**, **605**, **649**
2K26, **649**
2K27, **649**
2K29, 591–598, **593**, **595**, **596**, **597**, **649**
2K45, 605–624, **607**, **608**, **609**, **610**, **615**, **617**, **618**, **619**, **622**, **623**, **624**, **649**
2K50, 625–631, **626**, **627**, **628**, **629**, **632**, **633**, **649**
2K54, 635–648, **640**, **641**, **642**, **643**, **645**, **649**
2K55, **640**, **641**, **644**, **645**, **649**
2K56, **649**
6AC7, 743, 745
characteristics of, 408
6AG5, 745
characteristics of, 408
6AG7, 745
characteristics of, 408
6AK5, 7, 741–743, **742** 745, **752**, 756–761, **757**, **758**, **760**, 761
characteristics of, 408
Turbator, The, (ref.), 110
Tyrell, W. A., 860

Ultra High Frequency Techniques, (ref.), 95, 715, 908
Ultra-Short Wave Transmission Phenomena, (ref.), 908
U.S.S. Barton, **54**
Boise, 54, 313
Dakota, 54
Honolulu, Mark 3 antenna installation, **31**
New Jersey, **52**
Mark 3 antenna installation on, **34**
Pennsylvania, Mark 3 antenna installation, **33**
Philadelphia, 48
Porter, Mark 3 antenna installation, **32**
U. S. S.—*Cont.*
Roe, 49
San Francisco, 54
Mark 3 antenna installation on, **35**
Saratoga, **53**
Tennessee, **50**, **51**
Wichita, 26

Vance, R. L., 588, 708
van der Ziehl, A., (ref.), 751
VSWR, 890

Wallis, P. J., (ref.), 659
Walker, L. R., 236
Walsh, E. J., 708
Warren, C. A., 841
Wave guide system, **321**, **322**, **323**
Wax, N., 236, 237
Webster, (ref.), 667
Weddle's rule, 977, 1005
Wehe, H. G., 236
Weinhart, H. W., 309
Wentz, J. F., (ref.), 740
West, J. W., 255
Wheeler, H. A., (ref.), 935
Whinnery, J. R., (ref.), 656
Whippany radar laboratories, 5
table of characteristics, 163
Whitcomb, A. E., 236
Wiesner, J. B., 327
Williams, N. H., (ref.), 70
Willis, F. C., 855
Wilson, J. R., 237, 708
Wilson, W., (ref.), 344
Winans, R. C., 708
Witcher, C. M., 236
Wolfe, J. E., 255
Woodruff, L. F., (ref.), 95, 715, 908
Wooten, L. A., 237, 708
Wrathall, L. R., (ref.), 40, 257, 269

Yagi, H., (ref.), 70
Young, L. C., 10

Zacek, A., (ref.), 68
Zacharias, Dr. J. R., 352
Zirconium getter, use of, 229
Zworykin, V. K., (ref.), 592

Generated on 2019-09-24 07:54 GMT / http://hdl.handle.net/2027/mdp.39015077775156
Public Domain, Google-digitized / http://www.hathitrust.org/access_use#pd-google
Digitized by Google
Original from UNIVERSITY OF MICHIGAN

Generated on 2019-09-24 07:55 GMT / http://hdl.handle.net/2027/mdp.39015077775156
Public Domain, Google-digitized / http://www.hathitrust.org/access_use#pd-google
Digitized by Google
Original from UNIVERSITY OF MICHIGAN